4-13-2018

Steric Effects on the Formation of Manganese Oxide Clusters and 2-Dimensional Ammonium Formate Architectures

Carl Oberle
cdoy7d@mail.umsl.edu

Steric Effects on the Formation of Manganese Oxide Clusters and 2-Dimensional Ammonium Formate Architectures

By

Carl D. Oberle

B.S., Biochemistry, Saint Louis University

M.S., Chemistry, University of Missouri - St. Louis

A DISSERTATION

Submitted to the Graduate School of the

UNIVERSITY OF MISSOURI - ST. LOUIS

In Partial Fulfillment of the Requirements for the Degree

DOCTOR OF PHILOSOPHY

In

CHEMISTRY

With an Emphasis in Inorganic Chemistry

May 2018

Advisory Committee

Alicia M. Beatty, Ph. D.,

Chairperson

Stephen Holmes, Ph.D.

Nigam Rath, Ph.D.

Janet Braddock-Wilking, Ph.D.

ABSTRACT

Steric Effects on the Formation of Manganese Oxide Clusters and

2-Dimensional Ammonium Formate Architectures

(May 2018)

Carl D. Oberle

B.S., Biochemistry, Saint Louis University

M.S., Chemistry, University of Missouri - St. Louis

Chair of Committee: Dr. Alicia M. Beatty

It has been demonstrated by the Beatty group that altering the identity of the *ortho*-substituent of a dianiline counterion affects the assembly and dimensionality of a cadmium-chloride layer from 2-D to 0-D. This work seeks to extend this finding to metal oxide and organic hydrogen-bonded materials. By systematically increasing the *ortho*-substituent's size on the benzoate building block of reported manganese oxide clusters, of formula $Mn_xO_y(O_2C\text{-}\mathbf{R})_zL_w$ (where **R** = Alkyl, L = neutral monodentate ligand), we aim to impact the self-assembly of these materials relative to their parent forms; establishing a structure/function relationship of each material through measurement of their magnetization. The formation of 2-dimensional hydrogen-bonded ammonium formate layers will be investigated in the same manner. By maintaining the formate anion, but altering the identity of the ammonium cation, typically a substituted benzylamine, a novel series of 2-D layered structures will be closely compared in order to determine the impact of substituents on the formation of these lamellar materials. With respect to the ammonium formate compounds, the size of the *ortho*-substituent is considered as well as the position of substituent around the ring. Additionally, these ammonium formate compounds will also be compared to analogous ammonium-3,5-pyrazoledicarboxylate structures (HPzDCA) to evaluate the impacts of the anion on the formation of these layered materials.

We have found that with metal oxides, solvothermal methods, in addition to a bulky *ortho*-phenyl substituted benzoate, were required to alter the crystal structure of the Mn_{12}-type complex to a Mn_{13}-supercubane-type structure. We also found that lowering the site-specific symmetry of distorted Mn^{III} ions impacted the magnetization of the Mn_{12}-type substituted compounds. With ammonium formates, we have found that, by modifying the substituent in a series of benzylamines, the shape and orientation of the layer sheets and the interlayer pillars are drastically altered as per hydrogen bonding, and CH/π interactions. When compared to analogous HPzDCA compounds, the size of the anion (the mono-anion of 3,5-pyrazoledicarboxylic acid versus the formate ion) influences the shape of the layer. The smaller formate ion allows for enhanced flexibility in the hydrophilic sheet, as well as increased packing density of the ammonium cation.

Dedication

This dissertation is dedicated to my wonderful family; their love, support, and presence in my life were instrumental in getting me to this moment. Especially so Mom and Dad; thank you infinitely for never giving up on me and always believing in me, despite the innumerable curve-balls that I was so incredibly, jaw-droppingly, effective at throwing your way. My brother Paul, for always being a source of positivity, excitement, and generally good advice. And my sister Laura for being my scholastic role model, who got me interested in challenging myself through tough coursework; and brightening all of our lives with Carly. I would also like to dedicate this work to my great friend, Phil Ferko, who has been side-by-side with me during the entire process as my proverbial brother-in-arms. And finally, to Kathy Castulik who improved my wellbeing by introducing me to the wonderful world of health and fitness.

Acknowledgements

None of the work within would have been possible without the unwavering support and patience of Dr. Alicia Beatty, who served as my research advisor and mentor. She has been an indispensable conduit of information during my graduate career and has provided me with a great number of opportunities to share my research at conferences and seminars, as well as teaching and volunteer opportunities. Additionally, Dr. Beatty graciously supplied grant money in order to fund portions of my research career.

I owe many thanks to my committee members: Dr. Stephen Holmes, Dr. Nigam Rath, and Dr. Janet Wilking. During my time at UMSL they each served as course instructors as well as research mentors, and their lessons provided an invaluable platform to becoming a knowledgeable and productive chemist. Each member of my committee has offered valuable insight as well as research advice and instrument training, and were always readily available to help when needed.

Additionally, Dr. Bruce Hamper and Dr. Cynthia Dupureur have served as great role models and sources of inspiration for me during graduate school. Dr. Dupureur and Dr. Hamper have been incredibly supportive and encouraging, and have granted me a number of excellent opportunities to become more involved with the department, and with extracurricular teaching opportunities and STEM outreach programs. Being able to participate in demonstrations and tours for a wide range of audiences, as well as serving as a STARS Chemistry Advisor, has been great fun and a wonderful experience!

Certainly, I must acknowledge my family once again for their unending support during this long journey through school.

Table of Contents

Table of Figures

Table of Schemes

Table of Tables

References

1. Leeson, H. B., CCVII. On Crystallography, with a Description of a New Goniometer and Crystallonome. *Mem. Proc. Chem. Soc.* **1845,** *3*, 486-560.
2. Röntgen, W. C., Ueber eine neue Art von Strahlen. Vorläufige Mitteilung. *Aus den Sitzungsberichten der Würzburger Physik.-medic. Gesellschaft Würzburg* **1895**, 137-147.
3. Guntlin, C. P.; Ochsenbein, S. T.; Wörle, M.; Erni, R.; Kravchyk, K. V.; Kovalenko, M. V., Popcorn-Shaped FexO (Wüstite) Nanoparticles from a Single-Source Precursor: Colloidal Synthesis and Magnetic Properties. *Chem. Mater.* **2018**.
4. Gatteschi, D.; Sessoli, R.; Villain, J., *Molecular Nanomagnets*. Oxford University Press: 2006.
5. Hein, R. A., ac magnetic susceptibility, Meissner effect, and bulk superconductivity. *Phys. Rev. B.* **1986,** *33* (11), 7539-7549.
6. Tsai, H.-L.; Eppley, H. J.; de Vries, N.; Folting, K.; Christou, G.; Hendrickson, D. N., "Superparamagnetic-like properties of the valence-trapped $Mn^{II}Mn^{III7}Mn^{IV4}$ anion in the salt $(PPh_4)[Mn_{12}O_{12}(O_2CEt)_{16}(H_2O)_4]$". *Chem. Commun.* **1994**, 1475-1746.
7. Christou, G.; Gatteschi, D.; Hendrickson, D. N.; Sessoli, R., "Single-Molecule Magnets". *MRS Bulletin* **2000,** *25* (11), 66-71.
8. Bailey, M., The Crystal Structure of Terephthalic Acid. *Acta Cryst.* **1967,** *22*, 387-391.
9. Derissen, J. L., Isophthalic Acid. *Acta Cryst.* **1974,** *B30*, 2764-2765.
10. Vishweshwar, P.; Beauchamp, D. A.; Zaworotko, M. J., An Acetic Acid Solvate of Trimesic Acid That Exhibits Triple Inclined Interpenetration and Mixed Supramolecular Homosynthons. *Crystal Growth & Design.* **2006,** *6* (11), 2429-2431.
11. Saied, O.; Maris, T.; Wuest, J. D., Deformation of porous molecular networks induced by the exchange of guests in single crystals. *J. Am. Chem. Soc.* **2003,** *125* (49), 14956-14957.
12. Lee, S.; Mallik, A. B.; Xu, Z.; Lobkovsky, E. B.; Tran, L., Small Amphiphilic Organics Coordination Extended Solids and Constant Curvature Structures. *Acc. Chem. Res.* **2005,** *28*, 251-261.
13. Russell, V. A.; Etter, M. C.; Ward, M. D., Layered Materials by Molecular Design: Structural Enforcement by Hydrogen Bonding in Guanidinium Alkane-and Arenesulfonates. *J. Am. Chem. Soc.* **1994,** *116* (5), 1941-1952.
14. Lis, T., "Preparation, Structure, and Magnetic Properties of a Dodeeanuelear Mixed-Valence Manganese Carboxylate". *Acta Cryst.* **1980,** *B36*, 2042-2046.
15. Sessoli, R.; Tsai, H.-L.; Schake, A. R.; Wang, S.; Vincent, J. B.; Folting, K.; Gatteschi, D.; Christou, G.; Hendrickson, D. N., "High-Spin Molecules: "$Mn_{12}O_{12}(O_2CR)_{16}(H_2O)_4$". *J. Am. Chem. Soc.* **1993,** *115*, 1804-1816.
16. Sun, Z.; Ruiz, D.; Dilley, N. R.; Soler, M.; Ribas, J.; Folting, K.; Maple, B. M.; Christou, G.; Hendrickson, D. N., The origin of the second relaxation process in the [Mn12O12(O2CR)16(H2O)4] single-molecule magnets: 'Jahn–Teller isomerism' in the [Mn12O12] core. *Chem. Commun.* **1999**, 1973-1974.
17. Soler, M.; Rumberger, E.; Folting, K.; Hendrickson, D. N.; Christou, G., Synthesis, Characterization and magnetic properties of [Mn30O24(OH)8(O2CCH2C(CH3)3)32(H2O)2(CH3NO2)4]: The largest Manganese carboxylate cluster. *Polyhedron.* **2001,** *20*, 1365-1369.
18. Tasiopoulos, A. J.; Vinslava, A.; Wernsdorfer, W.; Abboud, K. A.; Christou, G., "Giant single-molecule magnets: a [Mn84] torus and its supramolecular nanotubes". *Angew. Chem. Int. Ed.* **2004,** *43* (16), 2117-21.
19. Eppley, H. J.; Tsai, H.-L.; de Vries, N.; Folting, K.; Christou, G.; Hendrickson, D. N., "High-Spin Molecules: Unusual Magnetic Susceptibility Relaxation Effects in $[Mn_{12}O_{12}(O_2CEt)_{16}(H_2O)_4]$ (S = 9) and the One-Electron Reduction Product $(PPh4)[Mn_{12}O_{12}(O_2CEt)_{16}(H_2O)_4]$ (S = 19/2)". *J. Am. Chem. Soc.* **1995,** *117*, 301-317.

20. Aubin, S. M. J.; Sun, Z.; Guzei, I. L.; Rheingold, A. L.; Christou, G.; Hendrickson, D. N., "Single-molecule magnets: isomeric $[Mn_{12}O_{12}(O_2CC_6H_4Me\text{-}4)_{16}(H_2O)_4]$ complexes exhibiting different rates of resonant magnetization tunnelling". *Chem. Commun.* **1997**, 2239-2240.
21. Sun, Z.; Ruiz, D.; Rumberger, E.; Incarvito, C. D.; Folting, K.; Rheingold, A. L.; Christou, G.; Hendrickson, D. N., "Isomeric Forms of $[Mn_{12}O_{12}(O_2CR)_{16}(H_2O)_4]$ Single-Molecule Magnets". *Inorg. Chem.* **1998,** *37* (4758-4759).
22. Sun, Z.; Gantzel, P. K.; Hendrickson, D. N., Supercubane Mixed-Valence Tridecanuclear Manganese Complex. *Inorg. Chem.* **1996,** *35*, 6640-6641.
23. Sessoli, R.; Gatteschi, D.; Caneschi, A.; Novak, M. A., "Magnetic bistability in a metal-ion cluster". *Nature* **1993,** *365*, 141-143.
24. de Campos, N. R.; Ribeiro, M. A.; Oliveira, W. X.; Reis, D. O.; Stumpf, H. O.; Doriguetto, A. C.; Machado, F. C.; Pinheiro, C. B.; Lloret, F.; Julve, M.; Cano, J.; Marinho, M. V., Magneto-structural versatility of copper(II)-3-phenylpropionate coordination polymers with N-donor coligands. *Dalton. Trans.* **2016,** *45*, 172-189.
25. Ferguson, A.; Thomson, K.; Parkin, A.; Cooper, P.; Milios, C. J.; Brechin, E. K.; Murrie, M., "Synthesis and characterisation of a mixed-valence Mn_{13} complex with S_6 symmetry by using 2-phenoxybenzoate". *Dalton Trans.* **2007,** (7), 728-730.
26. Vincent, J. B.; Chang, H.-R.; Folting, K.; Huffman, J. C.; Christou, G.; Hendrickson, D. N., "Preparation and Physical Properties of Trinuclear Oxo-Centered Manganese Complexes of the General Formulation $[Mn_3O(O_2CR)_6L_3]^{0,+}$ (R = Me or Ph; L = a Neutral Donor group) and the Crystal Structures of $[Mn_3O(O_2CMe)_6(pyr)_3(pyr)$ and $[Mn_3O(O_2CPh)_6(pyr)_2(H2O)]\cdot 0.5MeCN$". *J. Am. Chem. Soc.* **1987,** *109*, 5703-5711.
27. Lampropoulos, C.; Stamatatos, T. C.; Abboud, K. A.; Christou, G., A convenient MnIII starting material for the synthesis of homo- and heterometallic manganese carboxylate clusters: Mn9 and Mn10−xFex complexes. *Polyhedron* **2009,** *28* (9-10), 1958-1964.
28. Odendal, J. A.; Bruce, J. C.; Koch, K. R.; Haynes, D. A., Packing motifs in organic ammonium carboxylate salts: extension of the ring-stacking and ring-laddering concepts. *CrystEngComm.* **2010,** *12* (8), 2398-2408.
29. Smith, G., Two-dimensional hydrogen-bonded polymers in the crystal structures of the ammonium salts of phen-oxy-acetic acid, (4-fluoro-phen-oxy)acetic acid and (4-chloro-2-methyl-phen-oxy)acetic acid. *Acta Cryst.* **2014,** *E70* (12), 528-532.
30. Smith, G., Coordination polymeric structures in the sodium salt of 4-chloro-3-nitrobenzoic acid and the sodium and potassium salts of 4-nitroanthranilic acid. *Acta Cryst. C.* **2013,** *69* (12), 1472-1477.
31. Yuge, T.; Sakai, T.; Kai, N.; Hisaki, I.; Miyata, M.; Tohnai, N., Topological Classification and Supramolecular Chirality of 21-Helical Ladder-Type Hydrogen-Bond Networks Composed of Primary Ammonium Carboxylates: Bundle Control in 21-Helical Assemblies. *Chem. Eur. J.* **2008,** *14* (10), 2984-2993.
32. Li, Z.; Fowler, F. W.; Lauher, J. W., Weak Interactions Dominating the Supramolecular Self-Assembly in a Salt: A Designed Single-Crystal-to-Single-Crystal Topochemical Polymerization of a Terminal Aryldiacetylene. *J. Am. Chem. Soc.* **2009,** *131* (2), 634-643.
33. Djinovic, K.; Golic, L.; Leban, I., Structures of benzylammonium hydrogen malonate (I) and 4-picolinium hydrogen malonate (II). *Acta Cryst.* **1990,** *C46* (2), 281-286.
34. Barnes, J., Benzylammonium hydrogen oxalate hemihydrate. *Acta Cryst.* **2003,** *E59* (7), 931-933.
35. Matsumoto, A.; Odani, T.; Chikada, M.; Sada, K.; Miyata, M., Crystal-Lattice Controlled Photopolymerization of Di(benzylammonium) (Z,Z)-Muconates. *J. Am. Chem. Soc.* **1999,** *121* (48), 11122-11129.
36. Parshad, H.; Frydenvang, K.; Liljefors, T.; Sorensen, H. O.; Larsen, C., Aqueous solubility study of salts of benzylamine derivatives and p-substituted benzoic acid derivatives

using X-ray crystallographic analysis. *International Journal of Pharmaceutics* **2004,** *269* (1), 157-168.
37. Aakeröy, C. B.; Hughes, D. P.; Nieuwenhuyzen, M., The Oxamate Anion: A Flexible Building Block of Hydrogen-Bonded Architectures for Crystal Engineering. *J. Am. Chem. Soc.* **1996,** *118* (42), 10134-10140.
38. Bish, D. L., RIETVELD REFINEMENT OF THE KAOLINITE STRUCTURE AT 1.5 K. *Clay and Clay Minerals* **1993,** *41* (6), 738-744.
39. Yuge, T.; Miyata, M.; Tohnai, N., Novel Design of Tunable Organic Clay Mimic Structures Based on the Connection of One-Dimensional Supramolecular Synthons. *Crystal Growth & Design* **2006,** *6* (6), 1271-1273.
40. Beatty, A. M.; Granger, K. E.; Simpson, A. E., Crystal Engineering of Organic Clay Mimics from 3,5-Pyrazoledicarboxylic Acid and Amines. *Chem. Eur. J.* **2002,** *8* (14), 3254-3259.
41. Nahringbaurer, I., Hydrogen bond studies. XIV. The crystal structure of ammonium acetate. *Acta Cryst.* **1967,** *23*, 956-965.
42. Kuppers, H.; Jessen, S. M., Ammonium hydrogen carobnate. *Zeitschrift fur Kristallographie* **1993,** *203*, 167.
43. Chowdhury, M.; Kariuki, B. M., Supramolecular Assembly in Cinnamate Structures: The Influence of the Ammonium Ion and Halogen Interactions. *Crystal Growth & Design* **2014,** *6*, 774.
44. Hunter, C. A.; Sanders, J. K. M., The Nature of π-π Interactions. *J. Am. Chem. Soc.* **1990,** *112* (14), 5525-5534.
45. Aakeröy, C. B.; Nieuwenhuyzen, M., Hydrogen bonding in crystal engineering: two-dimensional layers of hydrogen l-malate anions. *Journal of Molecular Structure* **1996,** *374* (1), 223-239.
46. Christou, G., Manganese Carboxylate Chemistry and Its Biological Relevance. *Acc. Chem. Res.* **1989,** *22*, 328-335.

Chapter 1

Introduction

1.1 Overview of Research Goals

This dissertation work focuses primarily on the investigation of how systematically modifying starting materials and molecular synthons will influence the self-assembly of various materials in two separate chemical venues: firstly, in manganese oxide clusters; and secondly, in 2-dimensional hydrogen-bonded ammonium formate complexes.

Recently, much of the literature research focusing on metal oxide materials is concerned with the development of new complexes featuring interesting properties and potential applications. Instead, our focus is structural and concerns the generation of new metal oxide materials by altering the synthetic routes to existing, published, metal oxide materials. We seek to accomplish this by systematically changing one of the starting materials, growing crystals and solving crystal structures of the new material, then comparing the new and parent complexes. Comparing the physical structure and properties of the newly generated material to the parent compound allows us to establish an effective structure/function relationship, i.e., how physical structure, geometry, coordination environment, etc., changes the original material's properties. Do the properties change? Are they enhanced, or diminished? We seek to answer this question.

Our work with 2-dimensional lamellar materials, *via* the study of novel ammonium formates and the comparison of these to analogous 2-D materials, is strictly on a structural basis. This research focuses on the solid-state, structural assembly ramifications from pairing formic acid with a selection of systematically varied primary amine building blocks. By designing a series of ammonium formates which differ by the amine identity, size, and position of the substituents, can we evaluate the structural differences in this series and link the structural outcome with separate molecular synthons? In other words, can we select and evaluate two molecular building blocks and accurately predict how they will assemble and interact in the solid-state? We seek to investigate this research interest.

1.1.1 Specific Objectives

The specific objectives of this work are described as follows:

I. Synthesize a common manganese oxide cluster, Mn_{12}-Acetate, and exchange the peripheral acetate groups with systematically bulkier *ortho*-substituted benzoic acids *via* reported **substitution** routes.
    a. Grow crystals and solve the crystal structures of Mn_{12}-**R** substituted materials; identifying structural differences between the new Mn_{12}-**R** compound and the Mn_{12}-Acetate parent cluster.
    b. Explore new routes to different types of clusters *via* the transformation of newly synthesized Mn_{12}-**R** compounds by utilizing **solvothermal** methods.

II. Modify existing literature synthetic routes to manganese oxide clusters featuring **'ground-up'** preparation methods; where a manganese source and carboxylate source, are separately introduced into a reaction vessel, by swapping the intended carboxylate with systematically bulky *ortho*-substituted benzoates.
    a. Grow crystals and solve the crystal structures of new MnO-type clusters, identifying structural differences observed between the new materials and the published literature structures, establishing a connection between the product formed and the specific benzoate.

III. Synthesize organic 2-D hydrogen-bonded ammonium formate complexes featuring systematically substituted arene-containing primary amines, and other closely related amines.
    a. Grow crystals and solve crystal structures of these 2-D lamellar structures, establishing a relationship between amine identity and layer assembly, within the ammonium carboxylate family.

b. Compare crystal structures of ammonium formate complexes with analogous ammonium HPzDCA (the mono-anion of 3,5-pyrazoledicarboxylic acid) complexes previously synthesized in the Beatty lab; focusing on layer type, interdigitation, hydrogen bonding, π-interactions and CH/π interactions.

1.2 Introductory Notes from the Author

What follows is an evaluation and analysis of many new materials which reflect two different structural and material classes: discrete metal oxide clusters and 2-dimensional hydrogen-bonded networks. Indeed, each of the compounds reported herein fall within specific subclasses of their parent subclasses, and those subclasses may be even further divided.

Each of the two respective parent classes represents large fields of chemistry that offer limitless potential and unique chemistry in a rapidly expanding and developing scientific world. To help express their significance to chemistry I wish to communicate the following. Firstly, I would like to bring to attention, and offer a brief description of the related separate historic work and scientific advancement which led up to, and fully enabled the development of these two separate fields. Secondly, I seek to offer sufficient (and brief) description of the fields themselves. Ultimately, I hope to not only sufficiently brief the reader on these topics, but to spark the reader's curiosity towards these interesting fields. Many layers of information must be shed sequentially in order to reach the core of each focal point. So, we start at the beginning, where critical developments and discoveries were made, which enabled all of the work that is presented henceforth.

Certainly, it is impossible to include *all* detailed information in this single chapter; so, I hope that the reader's curiosity is piqued to not only read ahead, but to explore other undiscussed facets of this worthy chemistry. We now move to set the stage and move the pieces for the discussion and chapters to follow.

1.3 History, Crystallography, and Invisible Rays

To begin, we must first acknowledge the incredible work done in the *separate* fields of crystallography and X-ray radiation, prior to their eventual marriage.

It is hard to imagine a world without X-ray crystallography, it is additionally hard to imagine the two operating independently. When one hears the word crystallography today, it is likely their thoughts immediately shift to famous scientists such as Bragg (and Bragg), von Laue, and Perutz, specifically with respect to X-ray crystallography.[1-3] Certainly, the application of X-rays to crystalline materials was the major driving force behind advancing crystallography as a noteworthy method;[4] but initially, the field of crystallography once existed independently as a valid, however often overlooked, domain of research. The very definition of crystallography is simply "the branch of science concerned with the structure and properties of crystals."[5-6] It should come as no surprise that "the study of the structure and properties of crystals" started out the old-fashioned way; through physical inspection and manipulation,[7] leading to a standardized classification and measurement system.

1.3.1 Some Origins of Crystallography

Likely following in the footsteps of Louis Pasteur, who exhaustively studied the crystals of tartaric acid, separating enantiomers, *by hand*;[7] another pioneering crystallographer hoped to establish a set of standards in equipment, measurement, and classification of crystals in hopes of uniting and advancing the field of crystallography. One the earliest reports of crystallography, decoupled from X-ray radiation, is found as early as 1845 from Dr. H. B. Leeson. Leeson proposed to the Chemical Society the importance of a standardized classification and ordering system for crystalline materials; amid scrutiny and during a time where many researchers discounted the practical, and potential, advantage of crystallography.[8]

In his address to the Society, Leeson (somewhat irritably) states, "Discriminative chemical researchers have not received that assistance from crystallography which might have been reasonably anticipated from the natural distinction of form peculiar to various substances whose atoms are free to assume that symmetrical arrangement which is the natural result of certain attractive and repulsive forces pertaining to them. Many difficulties have concurred to deter persons from devoting greater attention to this branch of science, and to induce a belief that the advantages to be obtained therefrom are not sufficient to compensate the requisite amount of study and labour. Greater facility in the practical determination of crystalline forms will, it is believed, result from the use of the instruments herewith submitted to the Society; and it is also hoped that the principles of classification now proposed will obviate many of those difficulties consequent on the want of uniform and simple rules whereby to refer a given crystal to its appropriate class and order."

Leeson proposed in his report, through various figures, two designs for a crystallonome and goniometer (**Figure 1.3.1**), as well as the measurement methods for classifying the various shapes of sizes of crystals. These three pillars of his crystallography defense would be used to specify and standardize the measurement, orientation, viewing, and the calculations involved in describing the physical nature of crystals.

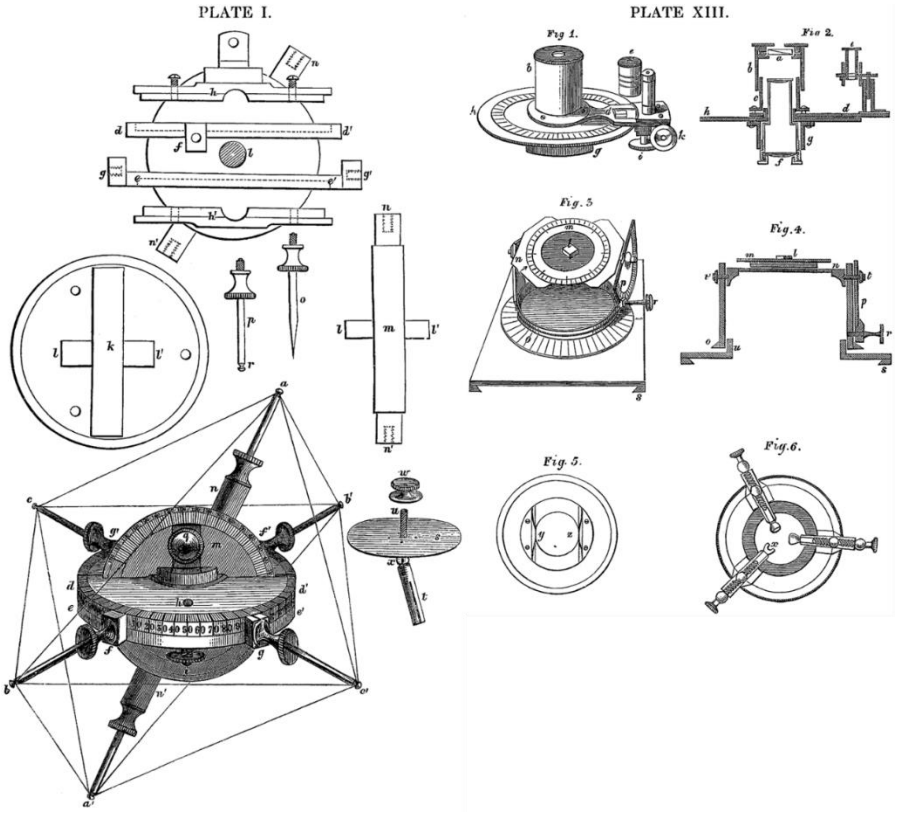

Figure 1.3.1 Proposed designs for a standardized crystallonome, Plate I *left*, and a goniometer, Plate XIII *right*. Figure adapted from reference 8.

1.3.2 Invisible Rays

Independently, and 50 years later, Wilhelm Röntgen made a discovery. Röntgen applied some high voltage to a covered, air-evacuated, gas-filled, glass tube, and a distant platinobarium screen spontaneously became illuminated![9] Röntgen attributed this glowing to the action of 'invisible rays' which he coined X-rays, or unknown-rays. Based on a series of follow-up experiments, Röntgen discovered that these putative invisible rays could be reflected by a prism, and that certain materials could absorb the rays (**Figure 1.3.2**). These insights and observations were quickly implemented into, and greatly accelerated physics and medical research. Within just one year of their discovery; various reliable sources,[10-11] potential applications,[12-13] and the acute

effects of X-ray radiation[14] were being explored and described. Röntgen's discovery was critical for the eventual merger with crystallography.

Hand des Anatomen Geheimrath von Kölliker. Im Physikalischen Institut der Universität Würzburg mit X-Strahlen aufgenommen von Professor Dr. *W. C. Röntgen.*

Figure 1.3.2 Röntgen's wife, Bertha's hand. This demonstrated to Röntgen how X-rays may pass through some materials. Figure adapted from reference 9.

1.3.3 Coalescence of Crystals and Light

Based on the principles of the delicate handling and mounting of crystals as well as the discovery that X-rays may be reflected by a prism, X-ray crystallography started to become a reality. These two fields of science would begin to coalesce in harmony as scientists such as

Friedrich, Knipping, Laue, Allen, Lorentz, Bragg (and Bragg), and others, began to discuss the diffraction of X-rays with respect to crystalline material.[2-3, 15-16] Much of the introductory work was presented in 1912 by Friedrich, Knipping, and Laue, where the interference of Röntgen's rays was probed and investigated.[3] In this important report, the source, diffraction, and experimental examples of the diffraction of Röntgen's rays by a crystalline material were discussed (**Figure 1.3.3**). These are truly the beginnings of modern crystallography!

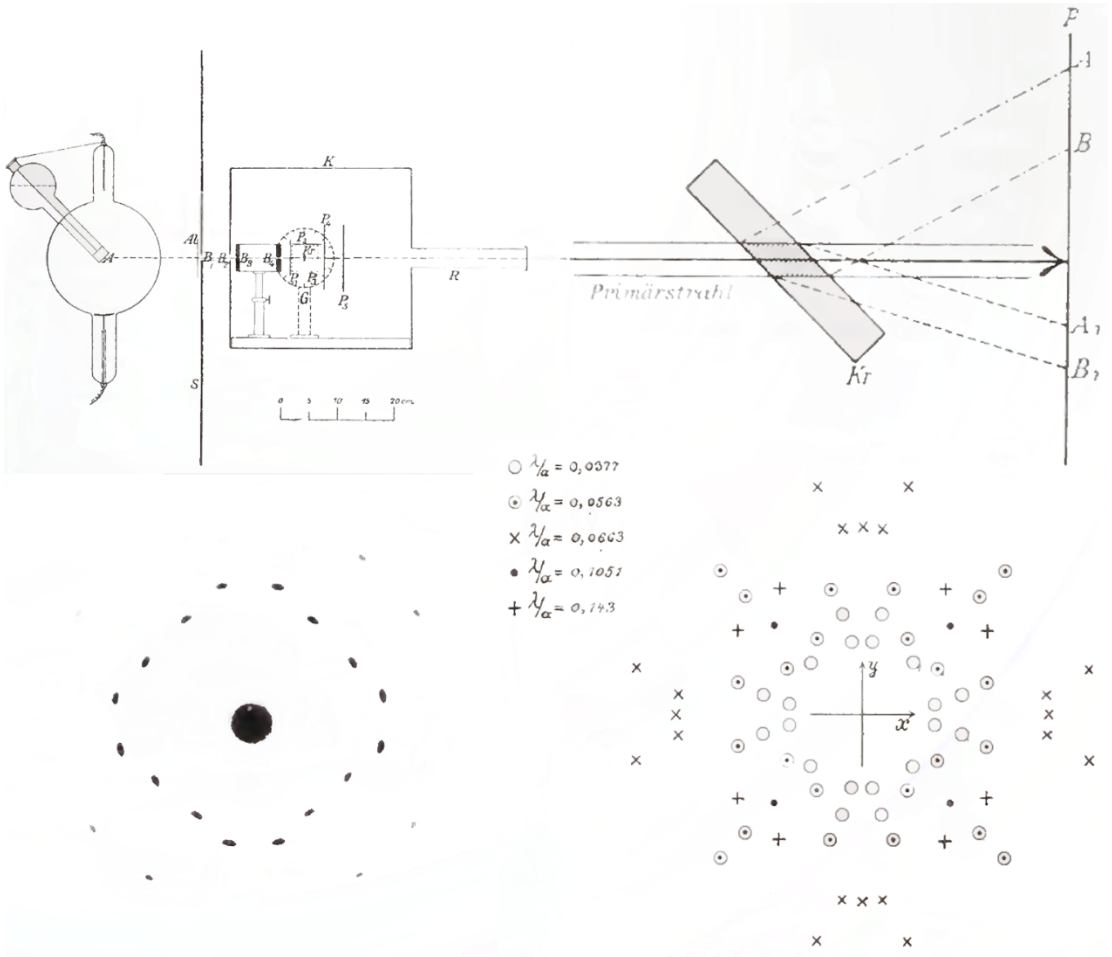

Figure 1.3.3 Friedrich, Knipping, and Laue's investigative work regarding X-ray interference.[3] *Top left*, the generation and direction of X-rays. *Top right*, on describing the diffractive nature of the X-rays. *Bottom left*, single diffraction frame from a mounted crystal. *Bottom right*, symmetry generation of the diffraction peaks. Reproduced from reference 3.

Researchers were thrilled by these discoveries, and efforts towards understanding and harnessing the effects were well underway. Just one year later in 1913, father and son, Sir William Laurence Bragg and William Henry Bragg, would go on to study and report the diffraction patterns of a plethora of crystals.[15-16] While considering Friedrich, Laue, and Knipping's findings, W. L. Bragg developed the Bragg Equation, $n\lambda = 2d\sin\Theta$, which gives the angle for coherent, in phase, reflections that can be used to calculate the d-spacing between atoms (**Figure 1.3.4**). This equation may be used to calculate the positions of atoms relative to each other. Indeed it was used for this very purpose; a mere 21 days after his report to Nature regarding the "Reflection of X-rays by Crystals",[16] father and son Bragg triumphantly reported the first X-ray crystallographic structure; that of diamond.[1]

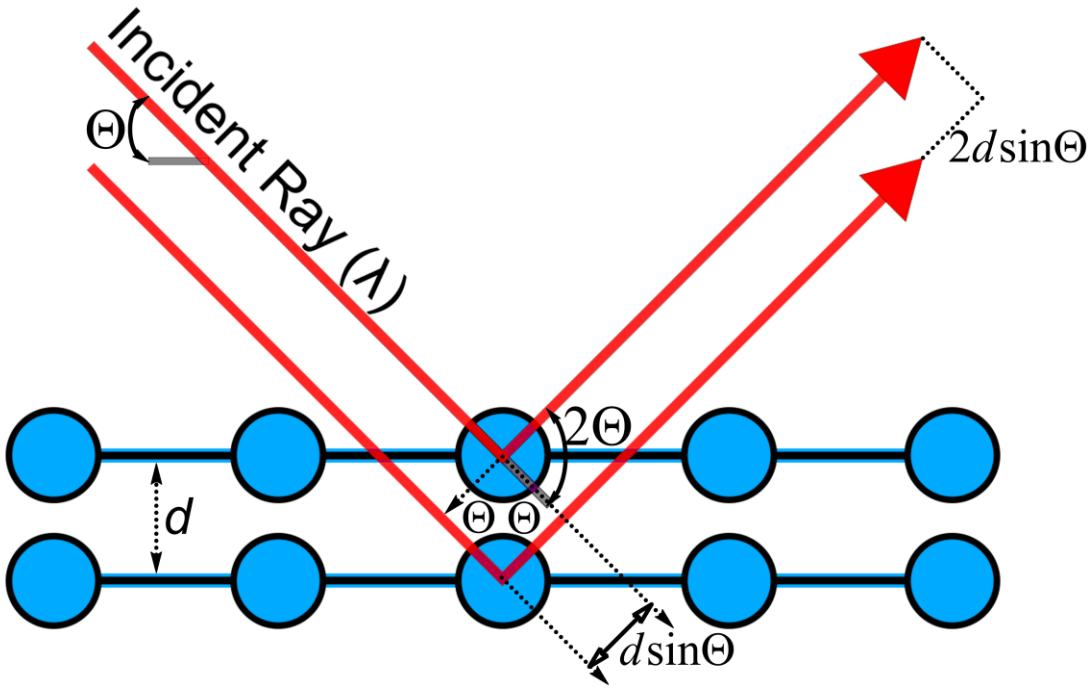

Figure 1.3.4 Braggs Law demonstrated on an ordered crystalline material where the blue balls represent atoms in a crystal lattice.

The reporting of the structure of diamond represented the first of now nearly 1 million total crystal structures recorded in the Cambridge Structural Database (CSD) to date.[17-18] The structures that were solved initially were of simple salts, but the structure solutions of much more complicated molecules of incredible importance would soon be uncovered. 40 years after the ordered, and repeating, structure of diamond was described, the structure of DNA would be solved by teams of researchers: Franklin and Gosling,[19-20] Pauling and Corey,[21] and Watson and Crick.[22-23] Ironically, in Watson and Crick's report to nature in 1953, *On the Molecular Structure of Nucleic Acids*, their comment on the structure of DNA follows, "This structure has novel features which are of considerable biological interest."[23] Considerable biological interest indeed! X-ray crystallography is highly responsible for extremely productive research avenues in chemistry and physics, and has managed to change how modern researchers fundamentally approach scientific interests.

1.4 Metal Oxides

Metal oxides represent another very important field in chemistry that has enjoyed considerable development and discovery since the development of X-ray crystallographic methods. Their classification is broad; any metal bound to any oxygen identifiable as O^{2-}. These are the most abundant materials in the Earth's crust and include metal oxides of the alkali and alkaline earth metals, the metalloids, those of the lanthanide and actinide series, and of course, the transition metal oxides.[4]

1.4.1 Transition Metal Oxides

The transition metal oxides offer limitless potential with respect to structural variability and function.[24] Their structures may be small infinitely repeating units of metal and oxygen in 2-D, or 3-D molecular inorganic coordination compounds; they may be composed of one or more type of metal ion, and may feature a variety of oxidation states within a discrete molecule (**Figure**

1.4.1).[25] These materials are frequently referred to as binary, ternary, quaternary, and even quinary elemental oxides of formula M_xO_y, where M is any transition metal (e.g., Mn_xO_y, Co_xO_y, Zn_xO_y), that is broadly representative of the oxides of that particular metal.[26] For example, an iron oxide, FeO, is a ubiquitous term which could refer to iron(III) oxide specifically, or any variety of iron oxide Fe_xO_y compounds.[4] Additionally, frequently cited metal oxide compounds may be given codenames. For example, in Chapter 2 we will discuss a popular dodecanuclear MnO compound often referred to as 'Mn-Acetate'.[27]

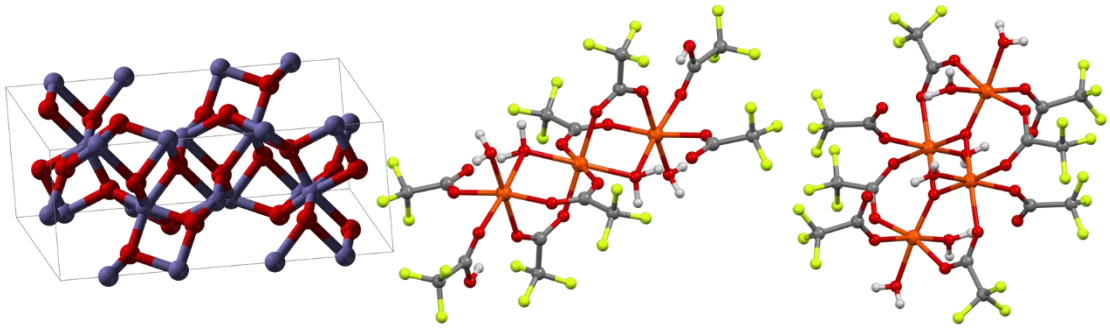

Figure 1.4.1 Some examples of iron oxides. *Left*, a simple repeating unit iron (III) oxide (Fe^{3+} represented by slate spheres) Fe_2O_3, hematite (rust). *Middle*, a trinuclear iron (II) oxide coordination complex. *Right*, a tetranuclear iron (II) oxide coordination complex.[25] *Note: in the crystal structures to follow, atoms are represented by tubes or spheres: dark grey represents carbon atoms, light grey represents hydrogen atoms, orange represents iron, blue spheres represent nitrogen atoms, red spheres represent oxygen atoms, beige represents silicon, yellow represents sulfur*.

In particular, transition metal oxide chemistry has enjoyed a spike in interest over the past four decades. Spectroscopic, analytic methods, and fundamental techniques have advanced rapidly since the 1980's, progress which has served to enhance the reliable characterization of metal oxide materials. General technologic advancement has provided the tools to effectively crack open the potential of metal oxide chemistry.[28] Metal oxide structures vary widely from

material to material and, in particular, the development of X-ray crystallography has contributed profoundly in the revelation of their secrets. Near limitless potential as nanostructures/materials,[29] photovoltaics,[30-31] electronics,[32] storage[33] and intercalation,[34] catalysis,[35-37] biomimetics,[38] redox reactions,[39] molecular magnetism,[40] and beyond,[41] wreaths this field of chemistry in constant interest.

1.5 Magnetism, Uncompensated Spin

Magnetism is a classically interesting topic that has preoccupied mathematicians and physicists since the first Greeks encountered magnetite. At its root, this force is derived from electric currents and magnetic moments of elementary particles. Generally, due to the electronic density and (dis)configuration of most materials, the overall magnetic moment in a solid is zero; cancelled out by competing and randomized spins throughout the structure with no preference in vector.[4] Based upon what cancels the effect, logically, the very foundation of magnetic forces must be directly attributed to the ordered, uncompensated electronic spins of atoms.

1.5.1 Basic Types of Magnetism and Exchange Interactions

The primary forms of magnetism can be divided into six different classes: diamagnetism, paramagnetism (and superparamagnetism), ferro and antiferromagnetism, and ferrimagnetism.[4] Briefly, diamagnets are those materials with no unpaired electrons, but will experience classical magnetization ordering in the direction opposite some applied field (i.e., in NMR experiments); and paramagnets are those materials with one or more unpaired electron in any number of molecular orbitals, whose spins align with the direction of an external applied field. Ferromagnets are materials in which each of the magnetic ions of a material align and provide a constructive contribution to the net magnetization, these strong fields can be felt without the use of sensitive detectors or instruments. Antiferromagnets have exactly equal amounts of ions in constructive and deconstructive alignment, resulting in zero net magnetic moment. No intrinsic field is

produced by these materials; these are very rare, and typically only accessed through very low temperatures.[4] Finally, *ferri*magnets are antiferromagnetic-*like*, but one of the two magnetic moment vectors, either up or down, is of lesser magnitude than the other; so a strong field may be felt by a ferrimagnetic material depending on its physical orientation (**Figure 1.5.1**).[4]

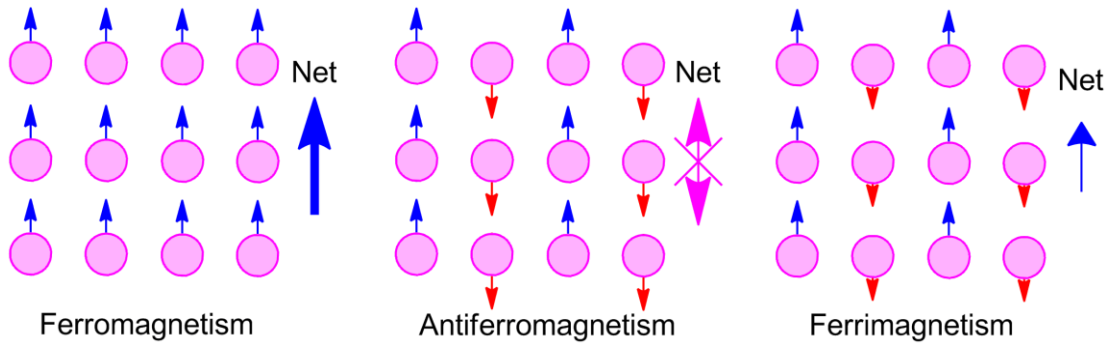

Figure 1.5.1 Illustration of spin alignment in different magnetic systems. *Left*, ferromagnetism, all spins align. *Middle*, antiferromagnetism, equal and opposite spins, no net magnetic moment. *Right*, ferrimagnetism, unequal and opposite spins, net magnetic moment in slight favor of the stronger vector. Pink balls represent ions.

The coupling of spins is not restricted to environments where metal ions are in direct proximity. The electronic spin coupling of two ions will occur through an intermediary atom, non-magnetic in nature, often oxygen; this is known as a magnetic superexchange interaction.[42] This effect allows for metal oxide materials in particular to become potentially useful materials in magnetism, apart from common bulk magnetic materials. However, depending on the electronic configuration of the metal ions present, the orbital occupancy of the superexchange coupling atom will either be vacant, half-filled, or fully occupied; as a result, the exchange interaction will either be ferromagnetic or antiferromagnetic.[4] Additionally, the angle of the M-O-M bond will also influence the type of coupling between ions, ferro- or antiferromagnetic.[42] These principles of superexchange are what have generated so much interest in manganese oxides, particularly

those of Mn^{III} where the high-spin singly filled dz^2 orbitals antiferromagnetically couple through the p_z orbital of the adjacent μ_2-oxo moiety.[43]

1.5.2 Crossing into Quantum Territory

It has been shown that moving from bulk materials to nano-, and femto-sized particles, has an effect on the total number of spins and the number of magnetic domains in a given magnetic material (**Figure 1.5.2**).[44] As the total number of spins approaches 1, and the total number of magnetic domains approaches a single domain, the classical behavior of magnetic materials blurs with quantum level magnetic behavior (**Figure 1.5.3**).[44] These discoveries were important in accessing and revealing various quantum topics such as quantum tunneling of magnetization (QTM).

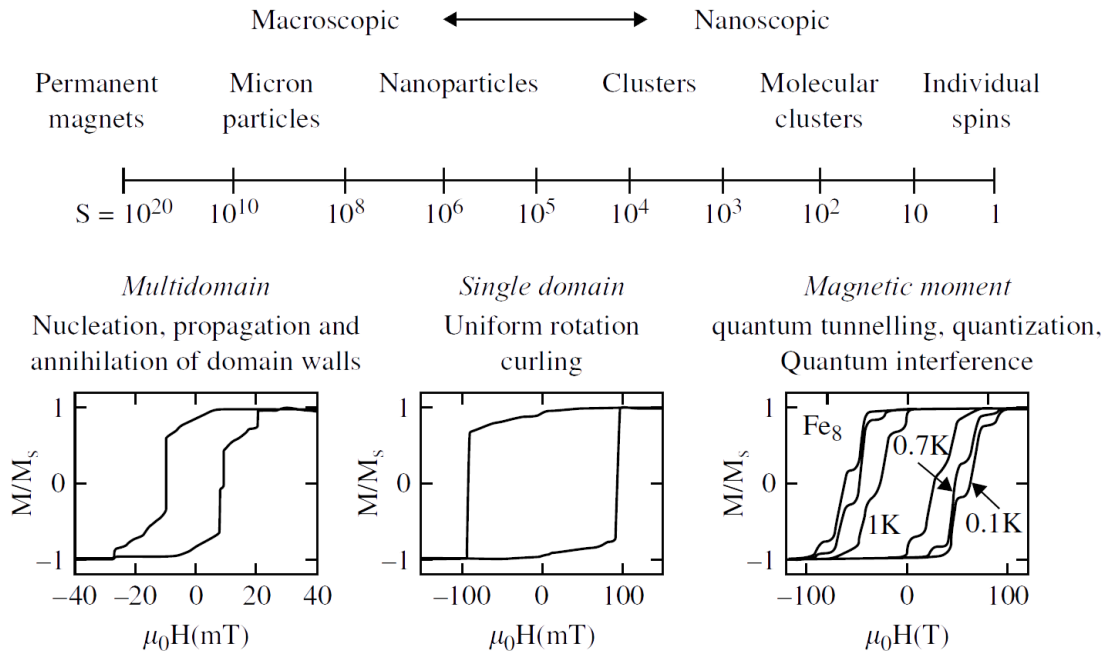

Figure 1.5.2 The appearance of new features in the magnetic hysteresis loop for nanosized particles and below. As the number of spins, S, approaches 1, quantum level properties (e.g., quantum tunneling) emerge in the material. *Right*, these quantized steps in the hysteresis loop for nanoscopic materials exposes these quantum level features. Figure adapted from reference 44.

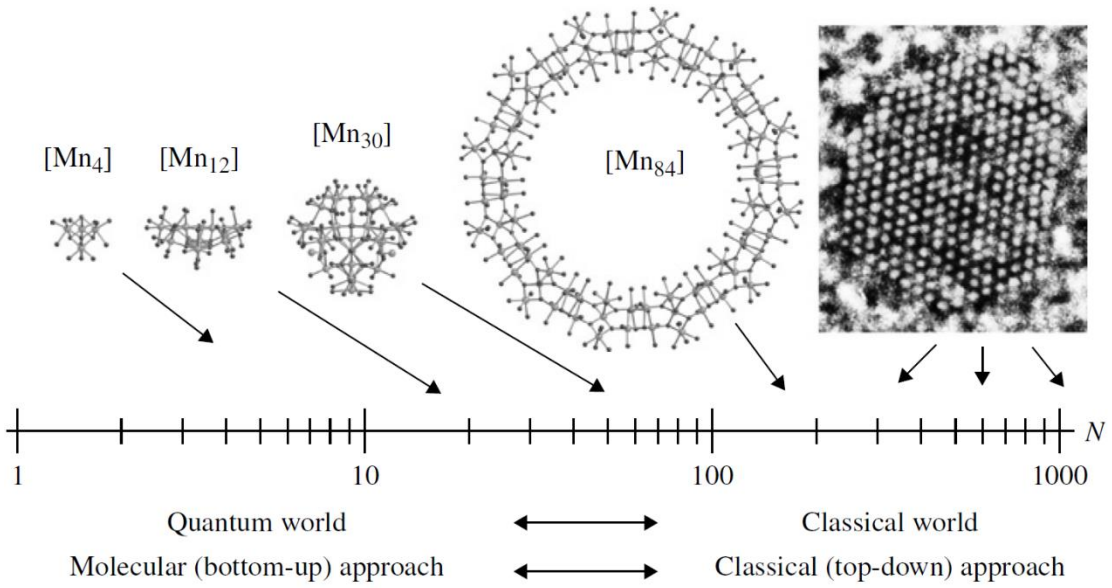

Figure 1.5.3 Bridging the gap between quantum and classical magnetic effects by adding more magnetic metal ion centers to the material. Figure adapted from reference 44.

1.5.3 Superparamagnetic 'Quantum Magnets'

Superparamagnetic materials represent a specialized class of magnetism that is unique to paramagnetically active particles that are 50 nanometers in diameter, and below, in size.[44] As per the effect of particle size on the magnetization, as the physical size decreases, the magnetic behavior of a material can enter what is known as the superparamagnetic state (SPM) (**Figure 1.5.4**).[45]

For small magnetic nanomaterials, the direction of its magnetization can randomly flip in response to temperature. The time between two state flippages is known as the Néel Relaxation time. If the states flip faster than the rate of measurement, in the absence of a magnetic field, the measured magnetization will be zero and the material is said to be in a superparamagnetic state. Within the SPM, an external field will align the particles as expected; but the total magnetic susceptibility and magnetic moment of the material will be much greater than a typical paramagnetic material (**Figure 1.5.5**).[46]

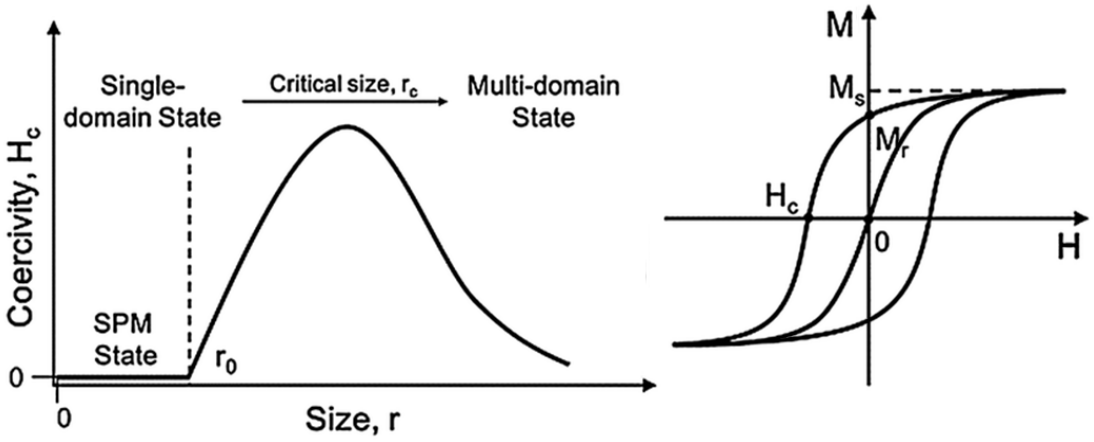

Figure 1.5.4 How critical size affects the number of magnetic domains in a material, and how materials in the SPM state show zero coercivity. *Left*, the relation of particle size and entrance into the SPM state. *Right*, coercivity of a truly single domain material, the curve that crosses the origin; and that of a larger superparamagnet, outer curve.[47]

In the superparamagnetic state an important parameter known as coercivity is brought to essentially zero (**Figure 1.5.4**). This parameter expresses the requisite magnitude of an external applied field to reduce the magnetization to zero after the material has been magnetically saturated. The higher the coercivity, the higher the required magnitude of the applied field is to demagnetize the material.[44] High coercivity materials function as permanent magnets, and those of low coercivity are referred to as soft magnets and are used for a number of flexible-state applications, e.g., data storage.[44]

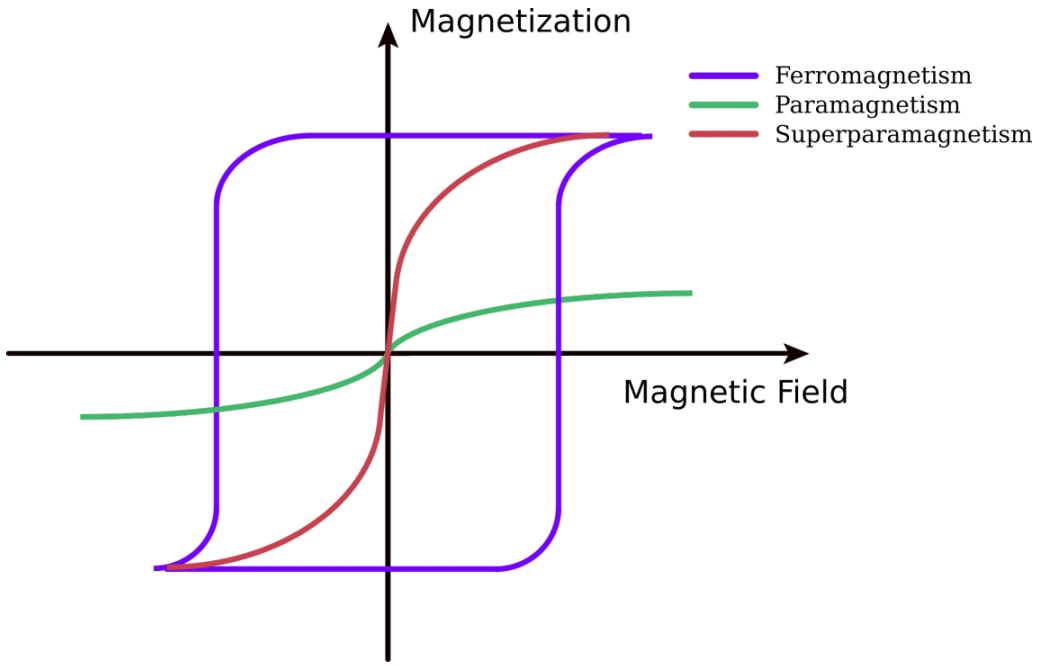

Figure 1.5.5 Showing the magnetization with respect to the magnetic field. The magnetization of superparamagnets can approach that of ferromagnets under a strong enough magnetic field. This force is much more significant than a typical paramagnet.[45]

These superparamagnetic conditions and parameters serve as the basis and foundation to explore a related and unique class of nanomagnets, the single-molecule magnet.

1.5.4 Single-Molecule Magnets

Single-molecule magnets (SMMs), or molecular nanomagnets, are a prodigious class of materials whose discovery and exploration has been revelatory in the fields of quantum physics and chemistry.[44, 48-56] Through their characterization, phenomenon such as quantum tunneling, have enjoyed closer inspection and understanding which has subsequently led to the proposal of advanced application candidates, such as quantum computers,[57] spintronics,[58] and information storage.[59] Generally, SMMs are described as iso-oriented, superexchange coupled metal ions, where at low temperature, below the blocking temperature T_B, the enormous extent of the coupling interactions is such that the entire molecule forms a ground-state that can be described

by a single net spin, S, which maintains its magnetization for some time, τ, after the applied field is removed (**Figure 1.5.6**).[44, 50, 54, 60] Unique to SMMs is that the magnetic hysteresis at this temperature is purely molecular in origin.[61]

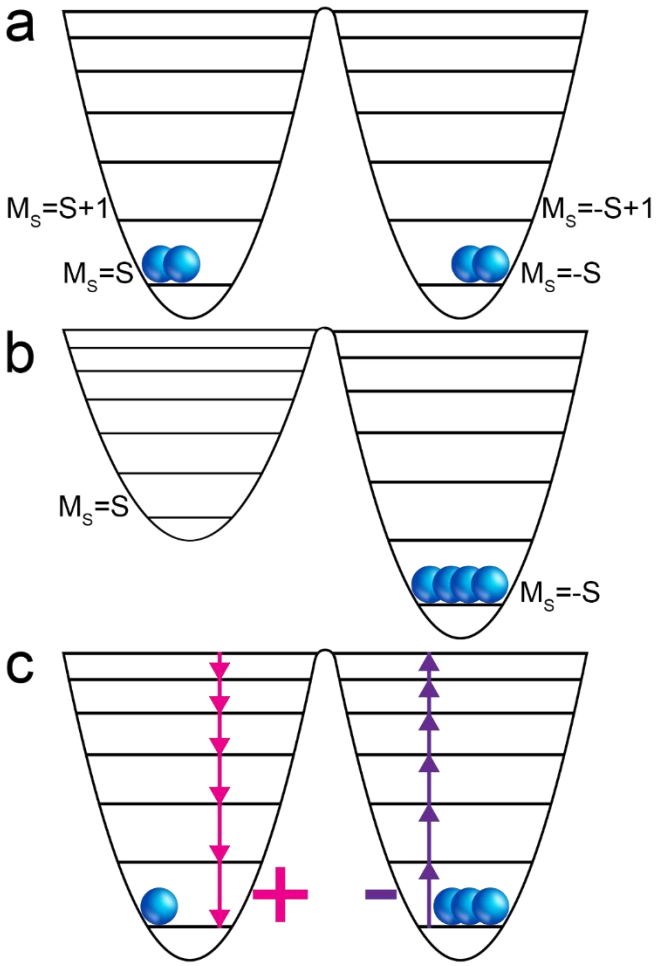

Figure 1.5.6 Illustration of energy levels and spin states of a SMM with magnetic anisotropy. **a)** the distribution of spins in zero-field: both wells are equally populated. **b)** When and external field is applied, one well is fully populated as all spins align in the direction (+\-) of the applied magnetic field. **c)** Upon removal of the applied magnetic field, ground state energies return, and spins return to equilibrium over time. Spin crossover represents the magnetic relaxation parameter, and the height of the well is proportional to the barrier to remagnetization, U_{eff}.

1.5.4.1 SMM Physical Parameters and Measurement

The major physical parameters of SMMs that cooperate are the ground spin state value, S, and uniaxial magnetic anisotropy, D; which serve to induce magnetic hysteresis and slow magnetic relaxation below what is referred to as the blocking temperature, T_B.[60, 62] The spin state values of individual ions are calculated by adding +1/2 per unpaired electron (as per the crystal field splitting arrangement), and the total spin value for the molecule is calculated by adding the individual ground spin states values of each coupled ion. These spin states will be either positive or negative as per the experimental determination of the material's overall ferromagnetic or antiferromagnetic ordering.[63] The D value, given in units cm^{-1}, for the material may be approximated mathematically,[64] but is typically determined *via* instrumental methods and computational line fitting.[65]

High-field magnetization, high-field EPR, and AC susceptibility are imperative for the close examination of SMM materials.[64, 66] DC susceptibility measurements are performed at low temperature with and without an external applied field (field-cooled (FC) and zero-field-cooled (ZFC)).[67] The temperature at the peak of a measured and plotted ZFC curve determines the T_B. EPR, usually W-band, is an important tool to utilize for determination of the axial zero-field splitting term, D;[68] though careful analysis of the quantized steps of the magnetic hysteresis loop also assists in determining this term.[69] Finally, AC susceptibility measurements can be used to determine the temperature of maximum χ_M'', the so-called imaginary part of the magnetic susceptibility, at which the spin relaxation frequency coincides with the external magnetic field frequency, ν.[51] This data can be manipulated into an Arrhenius plot in order to determine the value of the effective barrier to magnetization relaxation, U_{eff}, given in units kelvin, (**Figure 1.5.6**).[70] This term is generally accepted as the de facto parameter with which to evaluate and compare SMM performance, especially those SMMs within the same class of molecules.[56]

Single-molecule magnet materials show a clear hysteresis loop as the applied magnetic field is swept from one direction to the other.[61] Unlike the hysteresis loops observed in a bulk magnet, the hysteresis loops in a SMM shows regular, strongly temperature dependent, 'steps' in the magnetization at defined fields Hn = n0.4T where n = 0, 1, 2, etc., (**Figure 1.5.7**).[71] These 'steps' occur between spin-up and spin-down states during measurement and are a fingerprint of the material.[61-62, 72-73] Originally, this level of magnetic ordering was indicative of quantum tunneling of the magnetization (**Figure 1.5.8**),[69, 74-75] *especially* with respect to the temperature dependence, where total reversibility decreases with increasing temperature.[64] These hysteresis loop observations were paramount in exposing this concert of classical and quantum behavior present in these extremely unique materials; and subsequently formed the basis for their advanced applications which challenge energy as the upper limit for speed.[71, 76-78]

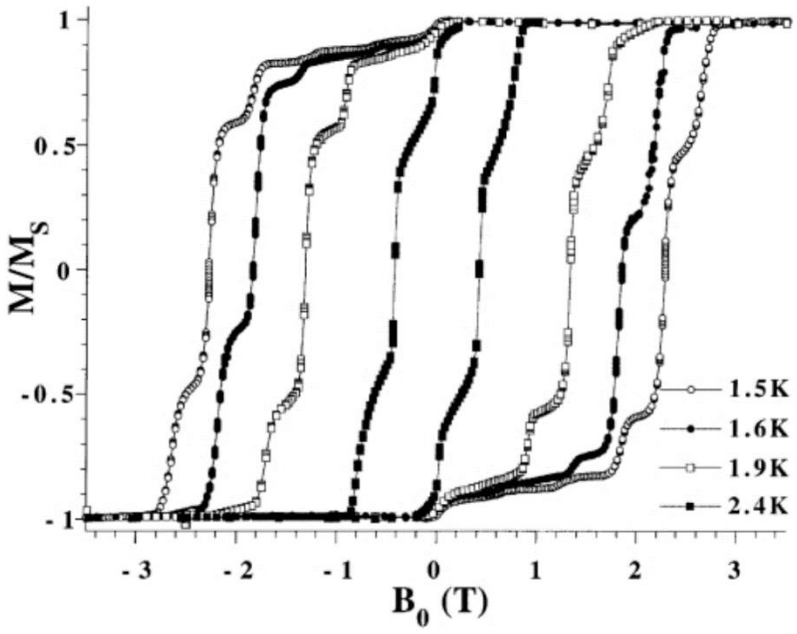

Figure 1.5.7 Example hysteresis loop of magnetization for a MnO-type SMM. Figure adapted from reference 79. *Note: The X-axis is sometimes given in units Oersted; however, effectively, the X-axis simply indicates the relative direction and magnitude of the applied magnetic field.*

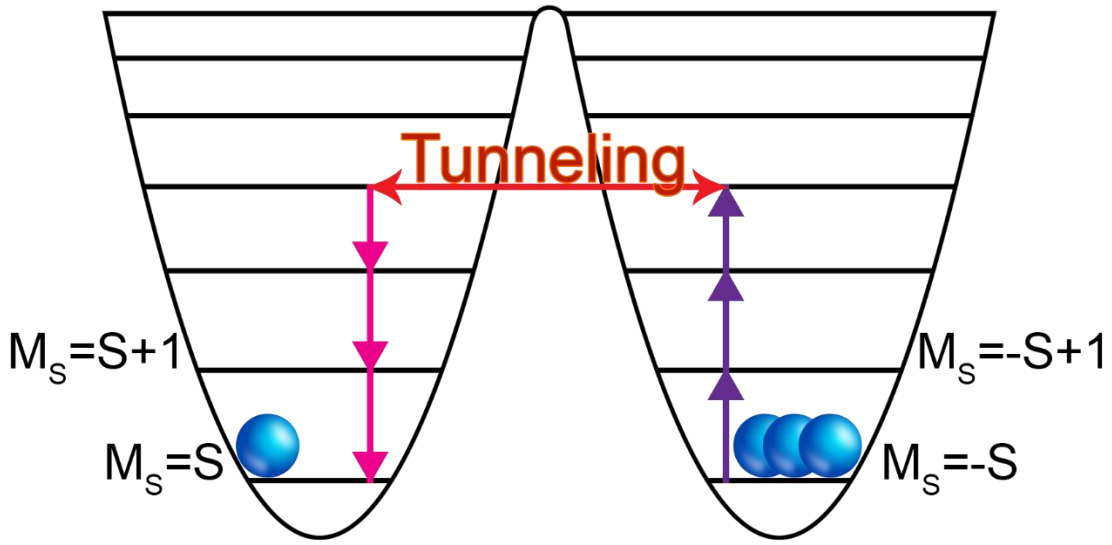

Figure 1.5.8 Quantum Tunneling of Magnetization. A potential shortcut to magnetic relaxation *via* thermally activated energy states.

Indeed, fastidious and complex instrumental analysis is essential for carefully and fully characterizing such magnetic behavior that is both temperature and field dependent, and molecular in nature.

1.5.4.2 SMM Hamiltonian Mechanics

Although individually important, no singular parameter (e.g., ground-state spin value, magnetic anisotropy, tunneling, spin phonon coupling, etc.) is solely responsible for completely defining a SMM's behavior. Each parameter must be considered as part of a whole when discussing a SMM's magnetic behavior.[65, 80] The total description of a SMM's magnetization is accomplished by relating each functional parameter *via* Hamiltonian mechanics.[81] Granted, each single-molecule magnet material is best described by a Hamiltonian function specifically designed for that individual system;[82-86] however, a generalized Hamiltonian will help in describing its basic and contemporary principles. The description of single-molecule magnets *via* the use of Hamiltonian mechanics has evolved throughout the years as the understanding of

magnetization has evolved; modern thought characterizes SMM magnetization as a Hamiltonian of *separate* Hamiltonian functions to as close to an approximation as possible:[87]

$$\hat{\mathrm{H}} = \hat{\mathrm{H}}_Z + \hat{\mathrm{H}}_A + \hat{\mathrm{H}}_{sp} + \hat{\mathrm{H}}_T \text{ (1)}$$

The beginning of this total function involves the Zeeman term, $\hat{H}_Z$, which is one of the original, and simplest methods of describing the spin-coupled magnetization in a single-molecule magnet:[88]

$$\hat{\mathrm{H}}_Z = g\mu_B \hat{\mathrm{H}}_Z \cdot \hat{\mathrm{S}}_Z \text{ (2)}$$

Where g is the magnetic field tensor, μ_B is the Bohr magneton, H is the applied magnetic field and S is the spin operator. The next term in this generalized Hamiltonian are the axial, or longitudinal, zero-field interactions, $\hat{H}_A$, which can be further detailed by their own Hamiltonian:[89]

$$\hat{\mathrm{H}}_A = D\hat{\mathrm{S}}_Z^2 - B\hat{\mathrm{S}}_Z^4 \text{ (3)}$$

Where D is the magnetic anisotropy, S is the spin operator, and B is the material's own perpendicular field. The third term in the series is the spin-phonon coupling parameter, $\hat{H}_{sp}$,[90] described as:

$$\hat{\mathrm{H}}_{sp} = g_i\left(\epsilon_{x,y,z} - \epsilon_{x,y,z}\right) * (\hat{\mathrm{S}}_{x,y,z}^2 - \hat{\mathrm{S}}_{x,y,z}^2) \text{ (4)}$$

Where g_i is the spin-phonon coupling constant along i = 1, 2, 3, or 4 symmetric elements, ϵ is the linear strain tensor along axes x, y, and z, and S is the spin vector.[91] The final term in the series represents the transverse interactions, which equates the rate of magnetization tunneling, $\hat{H}_T$,[68] given as:

$$\hat{\mathrm{H}}_T = g\mu_B \hat{\mathrm{H}}_x * \hat{\mathrm{S}}_x + E\left(\hat{\mathrm{S}}_x^2 - \hat{\mathrm{S}}_y^2\right) - B_4(\hat{\mathrm{S}}_+^4 + \hat{\mathrm{S}}_-^4) \text{ (5)}$$

Where g is the magnetic tensor, μ_B is the Bohr magneton, $\hat{H}_x$ is the transverse magnetic field, $E(\hat{S}_x^2 - \hat{S}_y^2)$ is the rhombic zero-field operator, and $B_4(\hat{S}_+^4 + \hat{S}_-^4)$ is the fourth-order quartic field operator for two different states of S (+ or -).[92] It is generally understood that there is still considerable research needed to understand the tunneling phenomenon.[93]

The description, characterization, and rationalization of SMM magnetization is an ongoing discussion in mathematics, physics, and chemistry. As the research progresses, more parameters, conditions, and coupling interactions continue to be considered and expressed in various Hamiltonian mechanics intent on describing the behavior of these unique materials.

1.6 The Hydrogen Bond

As it is almost impossible to overstate its importance, suffice it to say hydrogen bonding has a far-reaching effect on a huge variety of materials.[94-99] Certainly, some of the most famous examples of hydrogen bonding are the intricate interactions found in DNA,[21-22, 100] and the unique behavior of water.[101-105] The effects and chemistry of hydrogen bonding are far reaching and must be considered in a wide variety of established fields such as supramolecular chemistry,[106-108] physics,[109-110] astrochemistry,[111-112] biological science,[113-114] energy,[115] and computational simulations.[116]

1.6.1 Hydrogen Bonding Description

According to IUPAC specifications, the hydrogen bond is defined as an attractive interaction between a hydrogen atom with δ^+ character, and an atom or group of atoms in the same or different molecule with more δ^- character.[117-118] A typical hydrogen bond is depicted as X-H···Y. Where X-H represents the hydrogen bond donor and the three dots represent the putative hydrogen bond to Y, the hydrogen bond acceptor; typically an atom with δ^- character, either a negatively polarized atom or an ion.[119]

From a purely hydrogen donor/acceptor standpoint, the H···Y distance may range from 1.2 Å, all the way to 3.0 Å. If the donor site contains a *highly* polarizable atom (e.g., F-H, a very δ^+ H atom), and the acceptor is a *highly* anionic species (e.g., F^-), one can expect a F-H···F distance of 1.2 to 1.5 Å. If the donor is slightly polarizing the hydrogen atom (e.g., N-H), and the acceptor is also slightly anionic, such as a carbonyl, one can expect N-H···O=C hydrogen bond distances of around 1.5 to 2.2 Å. Alternatively, if the overall donor/acceptor polarization is weak, i.e., a C-H donor and a neutral oxygen acceptor, the hydrogen bond distance C-H···O will be around 2.0 to 3.0 Å.[120] These distances can extend further, upwards of 3.6 Å, when considering specially charged and substituted hydrogen bond acceptors and donors.[121-123]

1.6.2 Evaluating Hydrogen Bonds

Because the interaction is weak, its determination is handled differently than stronger forces such as covalent and ionic bonding interactions. Evidence for hydrogen bonding can be acquired *via*: crystallographic methods, theoretical methods (i.e., DFT and modeling), or spectroscopically (i.e., FT-IR, Raman). A checklist of criteria and characteristics regarding the expected behavior of the bond may be used when evaluating a potential hydrogen bond. The more guidelines that are satisfied, the more reliable the assignment will be. These criteria (1-6) and characteristics (A-E) are generally ascribed as:[117]

1. The forces are of electrostatic origin.
2. The X-H covalent bond is polarized.
3. The X-H···Y angle is 180°.
4. X-H peak red shifting indicates X-H···Y bonding.
5. X-H···Y bonding leads to H deshielding, observable in NMR experiments.
6. For experimental detection, ΔG_f for the hydrogen bond must be greater than the thermal energy of the system.

A. The pK_a of X-H and pK_b of Y-R correlates with the energy of the hydrogen bond.
B. H-bonds involved in proton transfer may be considered partially activated precursors.
C. Networks of hydrogen bonds show cooperativity of properties (e.g., DNA).
D. Hydrogen bonds show directional preference, and influence packing modes.
E. The extent of charge transfer between donor and acceptor is proportional to H-bond interaction energy.
F. A bond path can be connected between H and Y.

1.6.3 Etter's Rules on Hydrogen Bonding

Following extensive research and exhaustive study of databases of materials, a massive contribution from Etter and coworkers,[124] to the field of hydrogen bonding and molecular design, came in the form of a rule set to guide the design of solids through these weak forces. The rules, known as 'Etter's Rules' read as follows:

1. "All good proton donors and acceptors are involved in hydrogen bonding."
2. "Six-membered ring intramolecular hydrogen bonds form in preference to intermolecular hydrogen bonds."
3. "The best proton donor and acceptor remaining after intramolecular hydrogen bond formation will form intermolecular hydrogen bonds."

Additional rules follow in specific cases with regards to nitroanilines, carboxylic acid cocrystals with 2-aminopyrimidine, and nucleotide base cocrystals; however, these extended and specific rules will not be elaborated on unless specifically required.

1.6.4 Hydrogen Bond Geometry and Orientation

The hydrogen bond is an incredibly adaptable type of weak interaction that can be found in a wide variety of orientations and scenarios (**Figure 1.6.1**). One will find hydrogen bonds

stabilizing oxy-ions, involved in side-on interactions with π clouds of electrons, in strong charge assisted interactions, as complementary 'puzzle pieces,' and serving as bridges.[125] These types of bonds are capable of achieving directionality and chemical specificity that is comparable to covalent bonds.[126] Clearly a type of bonding interaction with such freedom and unique variability enables limitless potential as a useful property; we move forward to explore and discuss one of the hydrogen bond's most important uses.

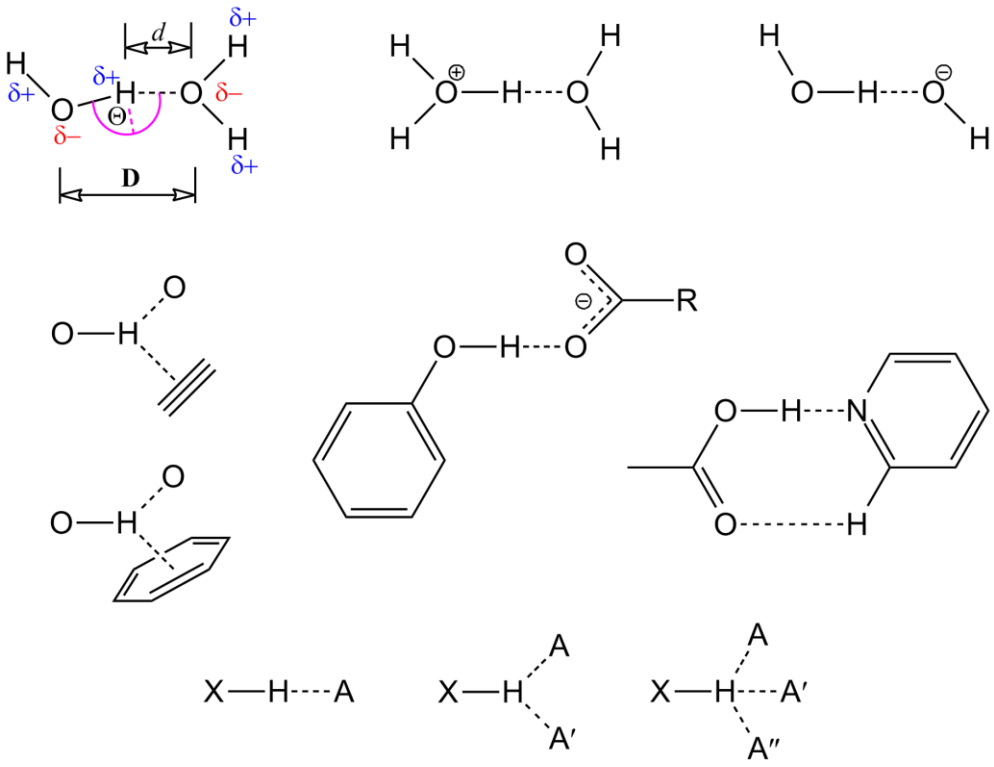

Figure 1.6.1 A brief cartography of hydrogen bonding. *Top row*, a series of hydrogen bonds of O and H derived species. *Middle row*) *left*, hydrogen interactions with π electron density, *middle*, charge assisted hydrogen bond, *right*, complementary two-degree discrete hydrogen bond. *Bottom row*, various modes of H-bond bridging between hydrogen bond acceptors. D = overall O-H⋯O distance, *d* = H⋯O bond distance, A is any hydrogen acceptor.

1.7 Supramolecular Chemistry, Hydrogen-Bonded Super Structures

Apart from being a 'simple' weak intermolecular force, hydrogen bonding has an important role and utility as it applies to the field of supramolecular chemistry and molecular design. As alluded to above, these bonds show a directional preference and influence molecular packing modes; critical parameters when considering molecular design.

Hydrogen bonding is both a tool and robust 'material'; a tool for use in the logical development of supramolecular structures,[127] and an attractive 'adhesive' material for use in the rational engineering and design of solids.[5] The development of this school of thought gave rise to the world of supramolecular chemistry. Supramolecular chemistry is perhaps best described by Jean-Marie Lehn as "chemistry beyond the molecule,"[127] and strongly focuses on the weak forces of non-covalent intermolecular interactions, especially those of hydrogen bonds (4-120 kJ/mol), but also includes: ion-ion (100-350 kJ/mol), ion-dipole (50-200 kJ/mol), dipole-dipole (5-50 kJ/mol), ion-π (5-80 kJ/mol), π-π (0-50 kJ/mol), and van der Waals forces (<5 kJ/mol).[5-6, 127-130]

1.7.1 Hydrogen Bonds: Construction Materials

Part of the very core of the utility of hydrogen bonding is based on the complementarity of the involved species, or synthons, which also drives much of the design philosophy behind supramolecular solids. The complementarity of hydrogen bonding is key in supramolecular synthons and can be divided into two general classes: homomeric, also referred to as self-complementary, and heteromeric complementary interactions. Homomeric synthons are those molecules that hydrogen bond cooperatively *strictly* through one type of functional group such as, but not limited to, carboxylic acids, amides, and pyridones (**Figure 1.7.1a**). Conversely, heteromeric synthons will demonstrate a combination of differing compatible functional groups, such as a carboxylic acid and amine, carboxylic acid and pyridine, or an amide and pyridone (**Figure 1.7.1b**).

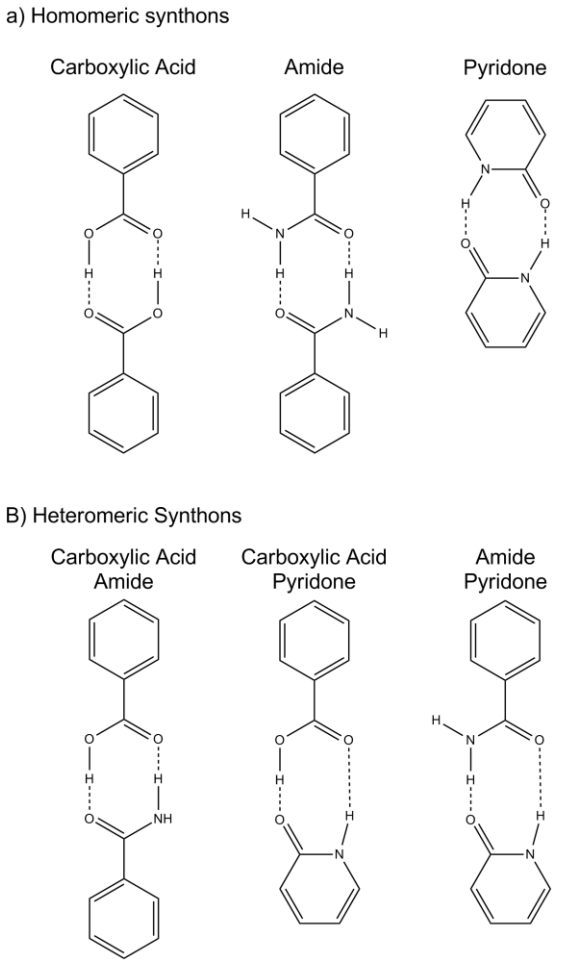

Figure 1.7.1 A few examples of self-complementary homomeric and complementary heteromeric supramolecular synthons.

In addition to these classes, the *degree* of complementarity may increase to triple,[131] quadruple,[132] or quintuple,[133] which will have an impact on the selectivity and strength of the hydrogen bonding, e.g., the three degrees of complementarity in some DNA base pairs (**Figure 1.7.2**).

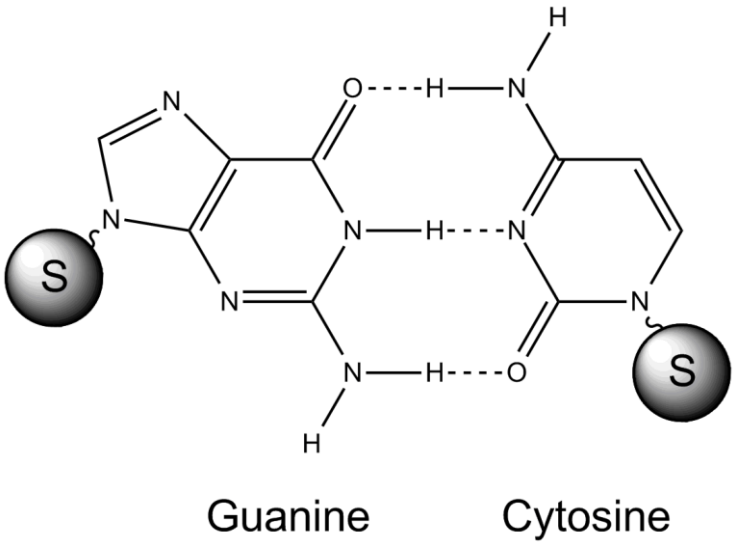

Figure 1.7.2 3 degrees of complementarity (and above) increases selectivity, i.e., G-C DNA base pairs.

1.7.2 Synthons: Designing Dimensionality in Hydrogen-Bonded Structures

Hydrogen bonding is sometimes referred to the most important of all directional intermolecular interactions.[118] Depending on the number, orientation, and position of suitable hydrogen-bonding substituents in a particular molecule, discrete 0-D, or extended dimensional hydrogen-bonded architectures, from 1-D to 3-D, will be generated.

1.7.2.1 Synthons: 0-Dimensions

If a certain set of molecules contains just *one* attached functional group that may hydrogen bond, these molecules usually hydrogen bond as a discrete pair. These discrete 0-D interactions are best described by those homomeric hydrogen bonding compounds, where the hydrogen bonding is localized between two molecules and cannot extend to other molecules infinitely. The compounds shown above in **Figure 1.7.2** illustrate this discrete, 0-dimensional, hydrogen-bonding interaction clearly. But what occurs as the number of active hydrogen bonding substituents in a molecule is increased?

1.7.2.2 Synthons: 1-Dimension

If a set of molecules contains *two* attached functional groups that are suitable for hydrogen bonding, with the appropriate spacing between the two, a 1-dimensional infinitely hydrogen-bonded chain will be generated. An infinite chain is always guaranteed when the substituents are appropriately separated, however, the degree of spacing between the two functional groups of the molecule will impact the shape of the 1-D hydrogen-bonded chain.

A direct example of this concept is demonstrated through the comparison of simple aryl dicarboxylic acids. Isophthalic acid and terephthalic acid are dicarboxylic acids that differ by a 60° deviation with respect to the relative positioning of their dicarboxylic acid functionalities. As it stands in these two molecules, the difference between a 120° and 180° offset of the two carboxylic acid functionalities results in either a zig-zag or a linear chain (**Figure 1.7.3**). It should be noted here that this degree of structural change results in an overall impact on the molecular packing of the synthons, and as a result the physical nature of the crystal.

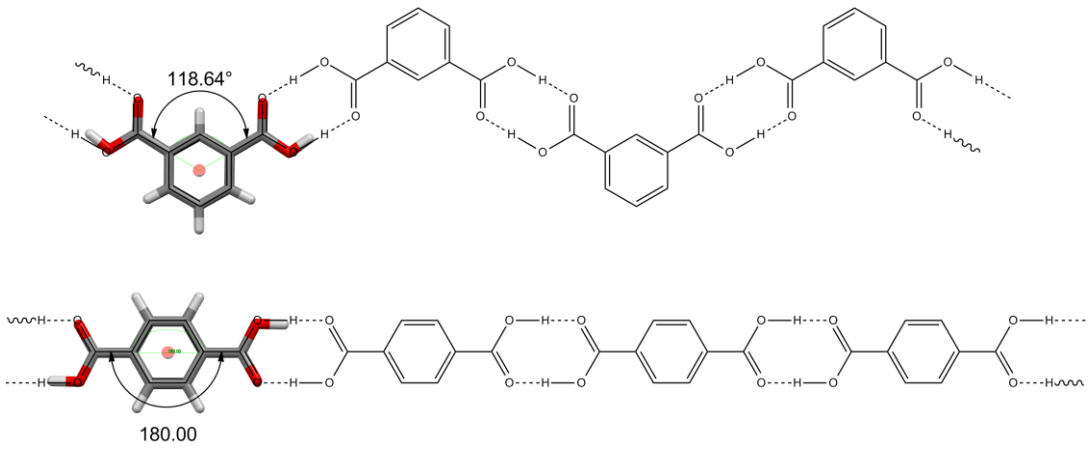

Figure 1.7.3 Structural outcome of 120° vs 180° orientation of the dicarboxylic acid functionality. *Top*, 120° angle in the isophthalic acid synthon results in zig-zag chains (Refcode: BENZDC01).[134] *Bottom*, 180° angle in the terephthalic acid synthon results in straight, linear chain (Refcode: TEPHTH).[135]

1.7.2.3 Synthons: 2-Dimensions

Likewise, if a set of molecules contains *three* attached functional groups which are suitable for hydrogen bonding, minding appropriate spacing between the active functionalities, a 2-dimensional infinitely hydrogen-bonded chain will be generated. Trimesic acid clearly demonstrates this concept, from its three carboxylic acid moieties positioned equidistantly, 120° apart (**Figure 1.7.4**).

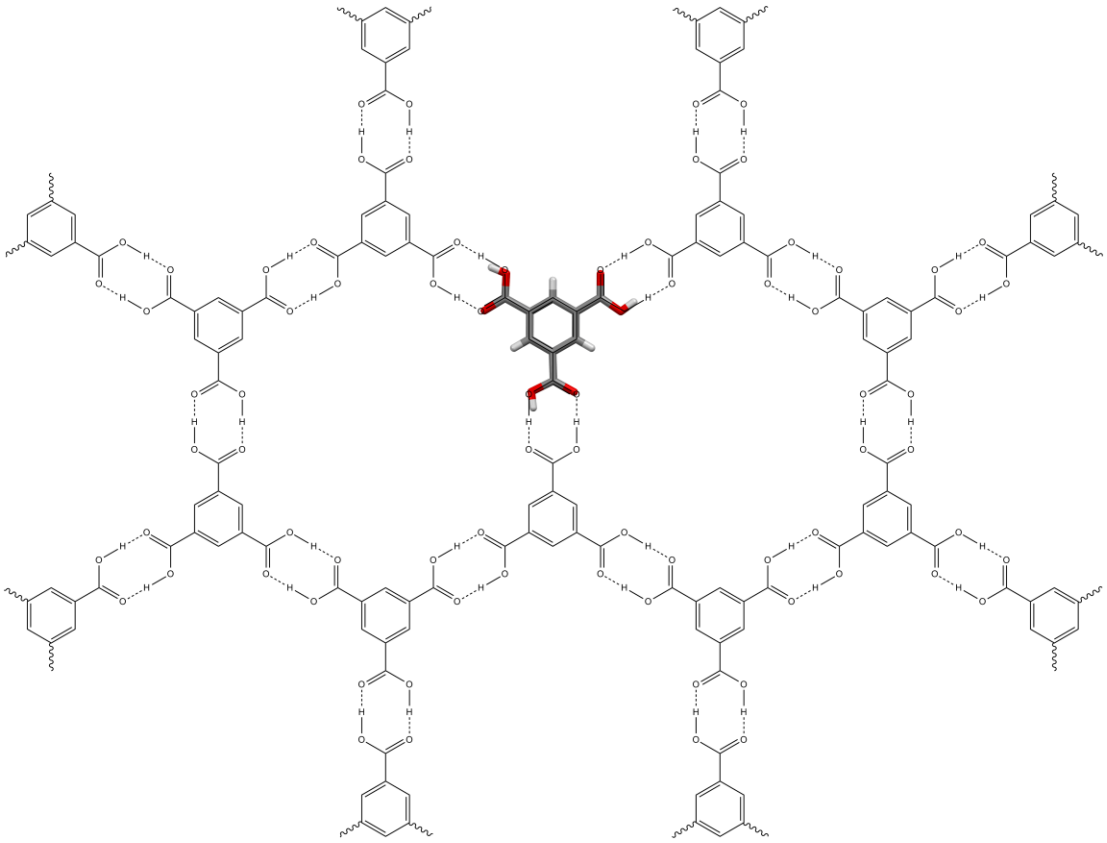

Figure 1.7.4 Trimesic acid's carboxylic acid functional groups hydrogen bond together, which infinitely links the molecules together in a 2-dimensional 'chicken-wire' super molecule (Refcode: LERSAD).[136]

1.7.2.4 Synthons: 3rd Dimension

If the previous dimensionality logic remains consistent, the engineering of a 3-dimensional hydrogen-bonded network shall require at least *four* attached functional groups which may participate in the hydrogen bonding interaction. Also, at least one of these functional groups must also be present in the 3rd dimension, otherwise a 2-D sheet would be generated instead. Indeed, this is demonstrated in a tetra-coordinated silicon molecule (**Figure 1.7.5**).

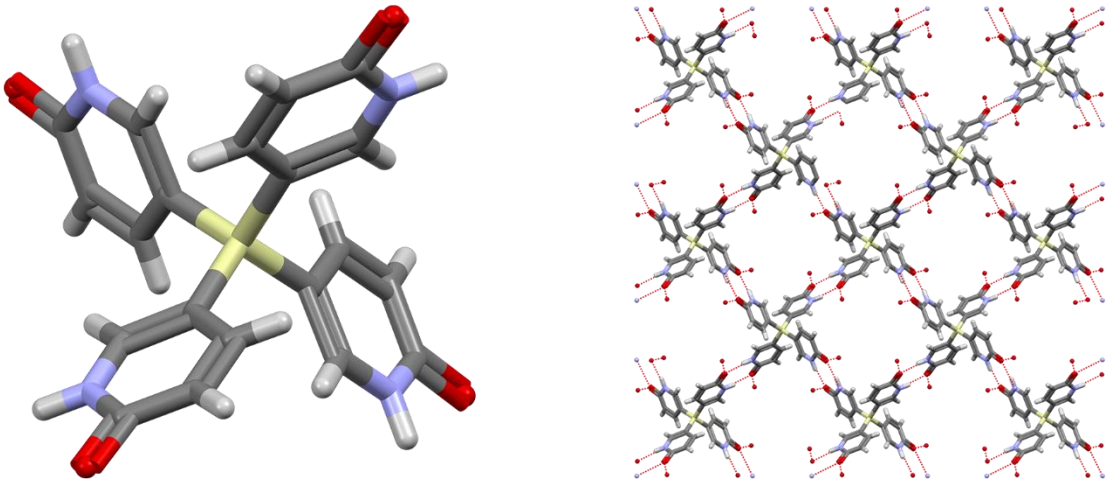

Figure 1.7.5 A 3-dimensional synthon (Refcode: INUJUW).[137] *Left*, a single synthon, showing the tetrahedral coordination environment around the central silicon atom. Right, packed structure, showing the grid-shaped arrangement of the molecules.

1.7.3 Rational Design of Supramolecular Structures

These hydrogen-bonded molecular synthons interact and chain like repeating puzzle pieces; this is the basis of molecular design and supramolecular chemistry. One can estimate from these simple examples, that as the complexity of the molecule and amount of active hydrogen bonding substituents increases, coupled with the careful consideration of how the position of these substituents will alter the structural outcome, that the number of potential novel supramolecular structures is essentially as vast as the library of compatible chemical synthons.

The manner in which these molecules interlink and chain into rank and file is the basis of supramolecular chemistry (**Figure 1.7.6**). Any change in the physical geometry and layout of molecules as they pack together inevitably impacts the structure, and the very physical appearance of the crystal; hence the term 'crystal engineering.'

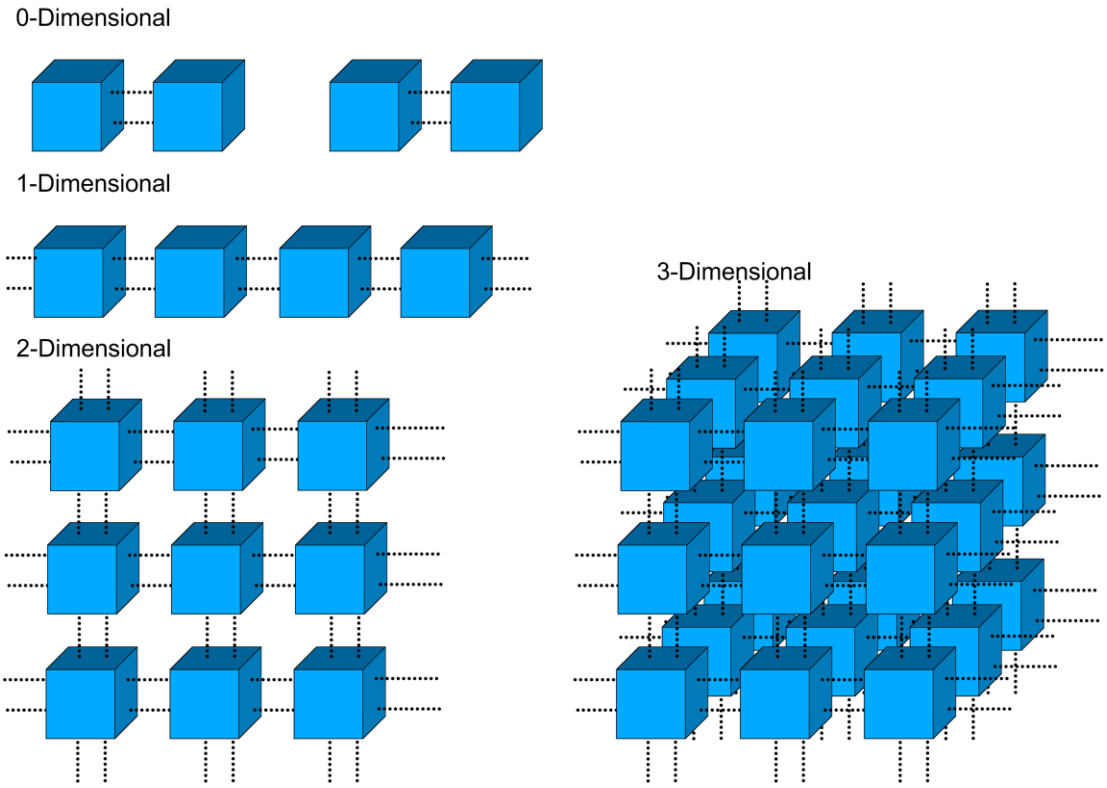

Figure 1.7.6 The assembly of supramolecular synthons into 0-, 1-, 2-, and 3-dimensional structures forms the basis of supramolecular chemistry.

1.8 Crystal Engineering

The above principles of hydrogen bonding have been applied *via* a multitude of synthons to establish the hydrogen bond as a reliable tool in supramolecular chemistry.[138-142] As a result, this tool has become deeply rooted and extensively utilized in the field of crystal engineering.[143-149] One of the most prolific crystal engineers, Gautam R. Desiraju, states that "...[crystal engineering] is the synthesis of functional solid-state structures from neutral or ionic building

blocks, using intermolecular interactions in the design strategy. Hydrogen bonds, coordination bonds, and other less directed interactions define sub-structural patterns, referred to as supramolecular synthons and secondary building units."[145]

The goal of crystal engineering is to synthesize functional materials that are tunable. For example, these functions frequently revolve around the intercalation of guest molecules into a scaffolded-porous system (i.e., host/guest systems),[150] which leads to functionalized materials intended for applications such as gas storage, catalysis, and photovoltaics, etc.[151-152] Certainly the goals of this field of science are vast, but in the end are primarily focused on developing an understanding of the relationship between structure and function.[153]

Generally, the synthesis of these dimensional materials involves the combination of two different building blocks (e.g., synthons), and by changing one of the building materials to a closely analogous synthon, a different analogous structure may be generated. Likewise, the crystal structures of the two systems may then be compared and functional differences can be explained by identifying physical changes in the crystal structure.

1.8.1 Common Crystal Topologies

As shown by extensive work conducted by Stephen Lee's group, some of the most abundant and common crystal topologies of supramolecular networks are: spherical (s), columnar (c), and lamellar (l) structural assemblies (**Figure 1.8.1**).[154] While structurally distinct, these three motifs share a common feature in that they are similarly composed of unique domains that are separated by an interface which is formed by the contact of two immiscible components; typically one hydrophobic and the other hydrophilic. The space between these two domains is usually where interesting intercalation chemistry will occur. These are important features for these structures in that the generation of supramolecular structures, and in turn engineered crystals, generally involves the utilization of a single or a pair of synthons with a non-polar region,

separating the hydrogen-bonding constituents, which are already polar by nature. Variation in the non-polar region of the synthons, has a direct impact on the supramolecular structure.

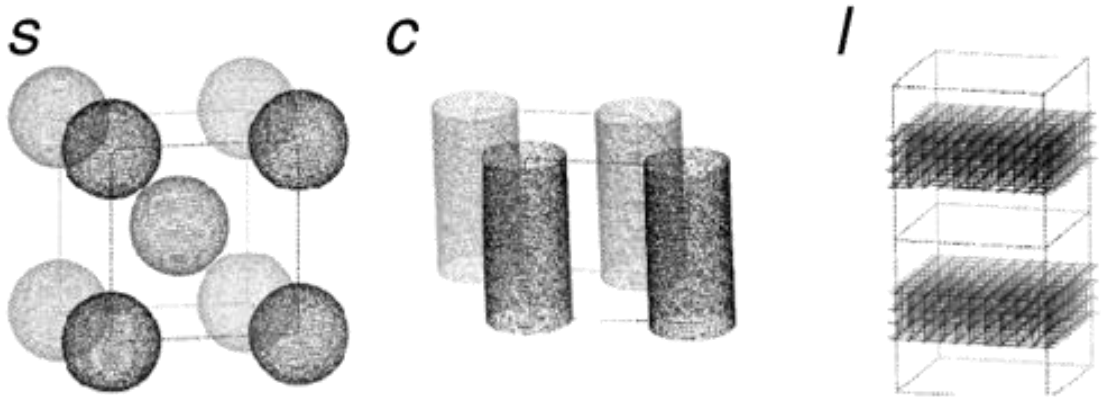

Figure 1.8.1 Prototypical examples of spherical (s), *left*, columnar (c), *middle*, and lamellar (l), *right*, materials. Figure adapted from reference 154.

Of the three primary structural topologies, 2-dimensional lamellar materials are of important interest in the field of supramolecular chemistry and crystal engineering due to their ability to intercalate guest molecules between the rigid 2-D ionic sheets. For lamellar-type materials, their structure is described as 2-dimensional solids that are typically comprised of a flat sheet, or substrate, and an additional component, often vertical and orthogonal to the substrate, situated between the sheets, within the interlayer space. For hydrogen-bonded structures, the lamellar sheets are often strengthened by charge-assisted hydrogen bonds, which are enhanced by an additional electrostatic effect.[155-161]

Based on the formation methodology of lamellar materials, the simple self-assemblage of two molecular subunits forming a crystalline solid, a tremendous amount of variability is observed in these structures. Properties such as layering type and interdigitation (expressed in greater detail in Chapter 4) play a critical role in determining the overall physical properties of these materials, such as porosity, and are decisive characteristics for qualitatively describing the

visual appearance of lamellar structures. These properties may be *directly* influenced by the identity of the two subunit synthons (e.g., through sterics); permitting a plethora of research avenues in this field.

1.8.2 Instrumental Methods Enable Crystal Engineering

Two notable developments with respect to X-ray crystallography are primarily responsible for fueling crystal engineering's rise in popularity. Coupled with the normal progression and improvements in computational power in accordance with Moore's Law; the ease and efficiency of solving crystal structures, through powerful programs such as SHELX,[162] as well as the development of a vast library of crystal structural data, the Cambridge Structural Database (CSD),[17, 163] allowed the possibility of solving and comparing crystal data effectively and accessibly. Grand databases of information on various crystal structures, including bond lengths and angles, close contacts, and packing allowed for a standardized and directed method for comparing multiple crystal structures. Thus, is one of the pillars of crystal engineering; where one material's functional parameters may differ from an analogous one, and the comparison of discrete physical crystal data, from a vast database, may be used to determine the structural effect behind the functional difference.

1.9 Atomic and Molecular Steric Considerations

According to Bruice, sterics will generally be encountered in two avenues; steric strain, and steric hinderance.[164] The very effects of sterics arise from the basic principle that any atom in a particular molecule takes up space. It is simply a matter of atomic radius, as the size of the atom, or substituent increases, the amount of potential steric impact on its surroundings also increases. Additionally, for substituents that are connected to a molecule by an appendaged joint (e.g., and ethoxy molecule tethered to benzene at some position), the steric effects will be

enhanced due to the rotational activity of the substituent, effectively permitting the substituent to block more physical space as it spins on its axis.[165]

1.9.1 Visualizing Sterics

As atoms are brought closer together, there is an energy cost associated with the overlapping of electronic clouds, represented and described by Pauli interactions or Born repulsions. These energetic implications affect how two molecules may interact. A qualitative look at an atom's or a molecule's steric properties can be estimated *via* a space filling model. Taking benzene into consideration; looking at a representative wire frame model of the molecule might lead one to assume that there is space in the middle of the carbon spine. However, when presented with the space-filling model of the molecule, it is clear to see that the atomic radius (and indeed other electrostatic properties, further detailed in Chapter 5) of the carbon spine effectively blocks what would be a pore (**Figure 1.9.1**).

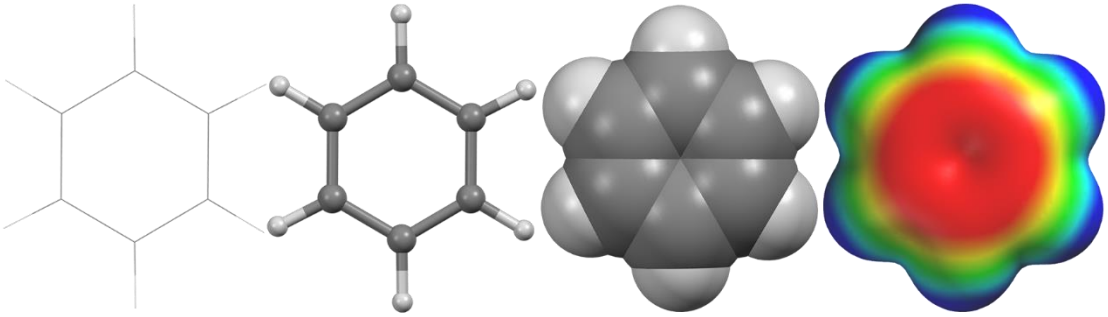

Figure 1.9.1 A transition in the viewing style of a benzene molecule revealing the actual spatial properties of atoms. From *left* to *right*: wireframe, ball and stick, space-filling model (Refcode: BENZEN), and electrostatic model.

1.9.2 The Role of Sterics in Chemistry

Steric effects have been shown to impact the chemistry of materials from organic chemistry to crystal engineering. For example, in organic chemistry, these effects may influence

reaction rate, or potentially physically block reaction pathways. Access to specific coordination sites on metals can also be physically blocked for certain ligands due to electrostatic repulsions; and as a result, materials may assemble and molecules interact differently based on steric conditions. Steric-induced blocking for example has a huge impact in biochemistry when considering enzymatic systems; where substrate-binding pockets typically rely on strict physical allowances, and physical blockage of that site from a particular metabolite serves as effective inhibition.[166] Certainly, steric effects are far reaching in many fields of chemistry.

1.9.2.1 Sterics in Organic Chemistry

In organic chemistry, steric effects will influence the kinetics of a reaction. For example, for alkyl halides, their reactivity is generally linked to steric hinderance; where the reaction rate will follow the general trend: methyl halide > 1° alkyl halide > 2° alkyl halide > 3° alkyl halide. Here not only is the type of alkyl group important, but also the number of atoms surrounding a given reaction site is also important for the reaction rates.

Additional kinetic influences within specific classes of alkyl halides also exist, such as the identity of what is bound to the α-carbon in a 1° alkyl halide affecting reaction rate. A popular example of this is the reaction of neopentyl bromide with a primary alcohol, compared to the same reaction with an unhindered, standard 1° alkyl halide. The *tert*-butyl group of neopentyl bromide drastically slows the reaction rate by inhibiting the accessibility of the bromide by the methoxy molecule (**Figure 1.9.2**).

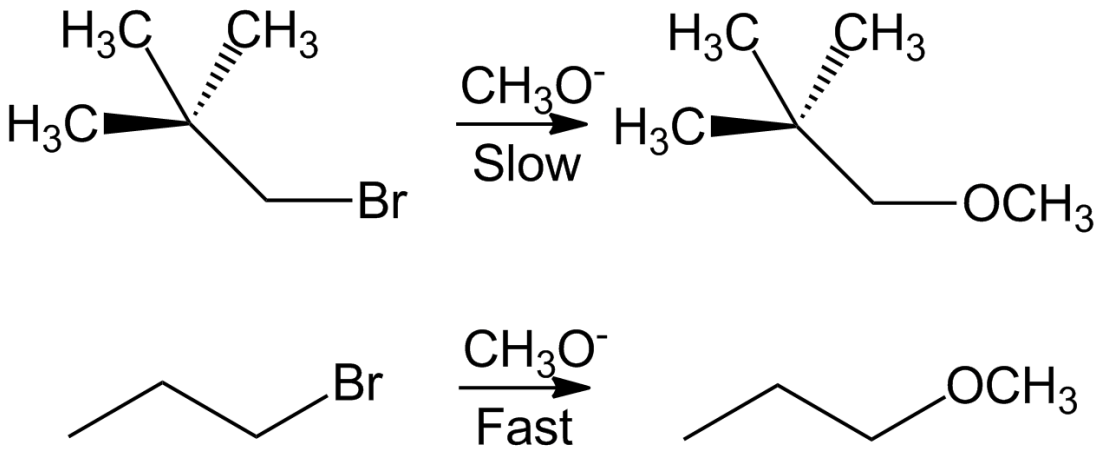

Figure 1.9.2 Two 1° alkyl halides, *top*, neopentyl bromide, *bottom*, alkyl bromide. Size of *tert*-butyl group inhibits the accessibility to bromide, slowing reaction rate relative to the straight alkyl chain version.

Regioselectivity is also important to consider alongside sterics. Essentially, as two large molecules come together, they shall react where the total physical steric hinderance is at a minimum. A common example of this is the regioselective dimethoxytritylation of the 5'-hydroxyl group of thymidine (**Figure 1.9.3**).[167] Here, the top route is more accessible because it maintains a more favorable distance between the trityl moiety and the ribose ring. This route is much more accessible than the bottom route, which brings the two reactants too close together, and repulsion dominates instead of reaction. Thus, the regioselectivity of this reaction is influenced by sterics.

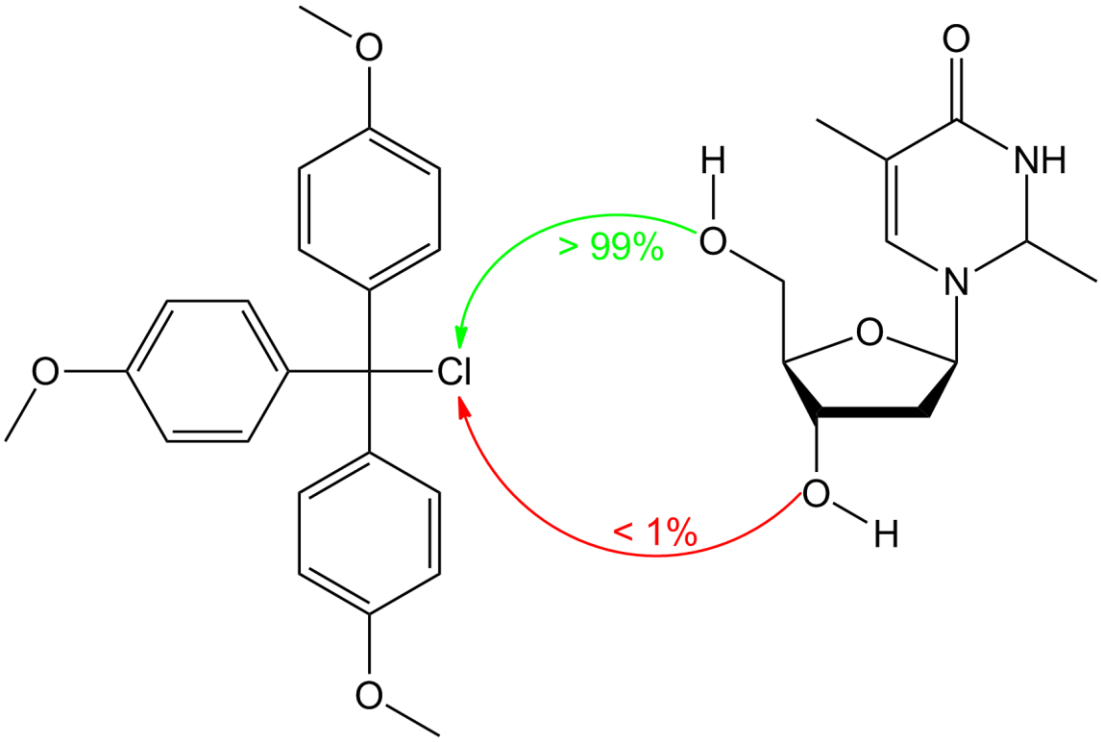

Figure 1.9.3 The tritylation of the primary 5'-hydroxyl group of thymidine. The *top* route is 99% favorable due to the space afforded between the trityl and ribose moieties. The *bottom* route will bring the two too close together, and is unfavorable.

1.9.2.2 Sterics in Inorganic Chemistry

In inorganic chemistry, the steric properties of atoms will influence the coordination environment of metal compounds. For example, transition metals contain 9 accessible valence orbitals for bonding, representing the maximum number of coordinated ligands. In instances where the coordinated ligand is very small (e.g., a hydride), each coordination site could potentially be occupied. An example of this is the nona-coordinated rhenium (VII) compound potassium nonahydridorhenate,[4] $[ReH_9]^{2-}$ $[K_2]^{+}$. As the size of the ligands increase from hydride and coordination sites on the metal are physically blocked, more typical transition metal coordination environments such as octahedral and tetrahedral are encountered, as steric hinderance increases.

1.9.2.3 Sterics in Crystal Engineering

In crystal engineering, sterics will impact the topology and layered assembly of crystals. A great example of this is through work conducted by Michael Ward's group concerning lamellar guanidinium sulfonates, $C(NH_2)_3^+ {}^-O_3S\mathbf{R}$, where **R** constitutes a wide variety of alkane- and arenesulfonates, $(CH_2)_xCH_3$ (x = 0-3), 10-camphor, benzene, 1-naphthalene, and 2-naphthalene. In his report, Ward described the spatial effects of the interlayer moieties as they related to length and width of the pillar (**Figure 1.9.4**)

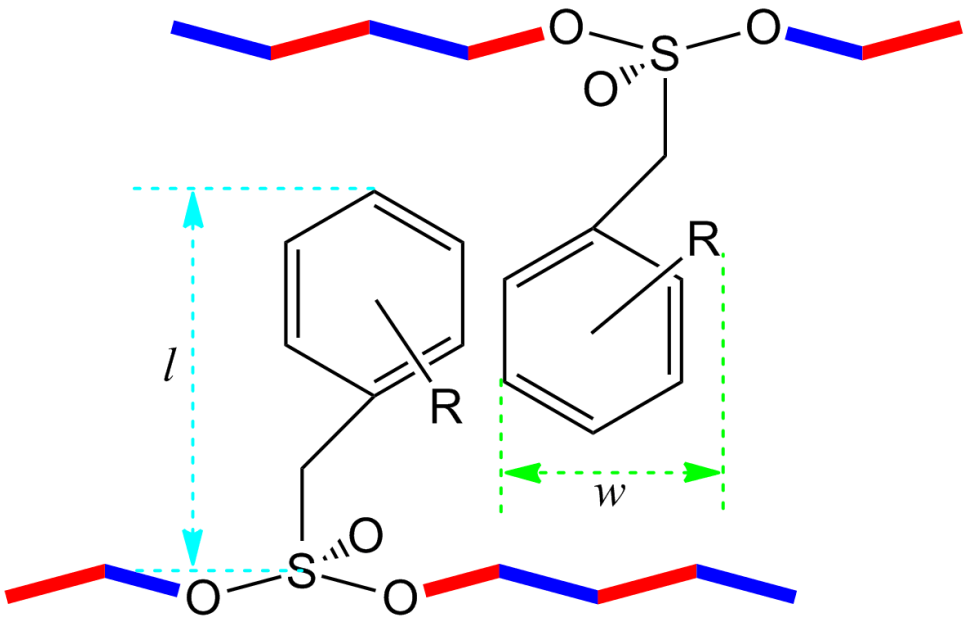

Figure 1.9.4 Demonstrating the measurement standard for determining length and width of the pillar moiety of the cation. Length, *l*, spans the sulfur component of the substrate to the tip of the pillar. Width, *w*, spans the entire width of the pillar component completely contained in the interlayer space. Both dimensions include hydrogens in the measurement.

The Ward group described an interesting feature where the material's preference for forming either monolayers or bilayers was hinged on the interlayer sterics of the synthons. Ward et. al concluded that the evolution from bilayer to single layer was related to the interlayer conformational freedom. It is almost counter intuitive in this case, but as the alkyl chain length

increases, the amount of flexibility in the interlayer space, relative to the C-S bond, increases and a monolayer forms (**Figure 1.9.5**). However, in the 1- and 2-naphthylsulfonate groups, which are both planar and rigid, Ward described a dependency on the relative width of the sulfonate. At the 1-position naphthylsulfonate, the relative width of the molecule is increased compared to the 2-position naphthylsulfonate, and is longer (4.83 Å) than the calculated distance between ion centers (4.75 Å), which determines the available space for bilayer packing; as a result, the hydrogen-bonded sheet distorts and a single layer forms. In the 2-position naphthylsulfonate, the naphthyl group is oriented more nearly along the three-fold axis of the -SO_3 moiety, and allows for a less densely packed assembly, resulting in a bilayer.[168]

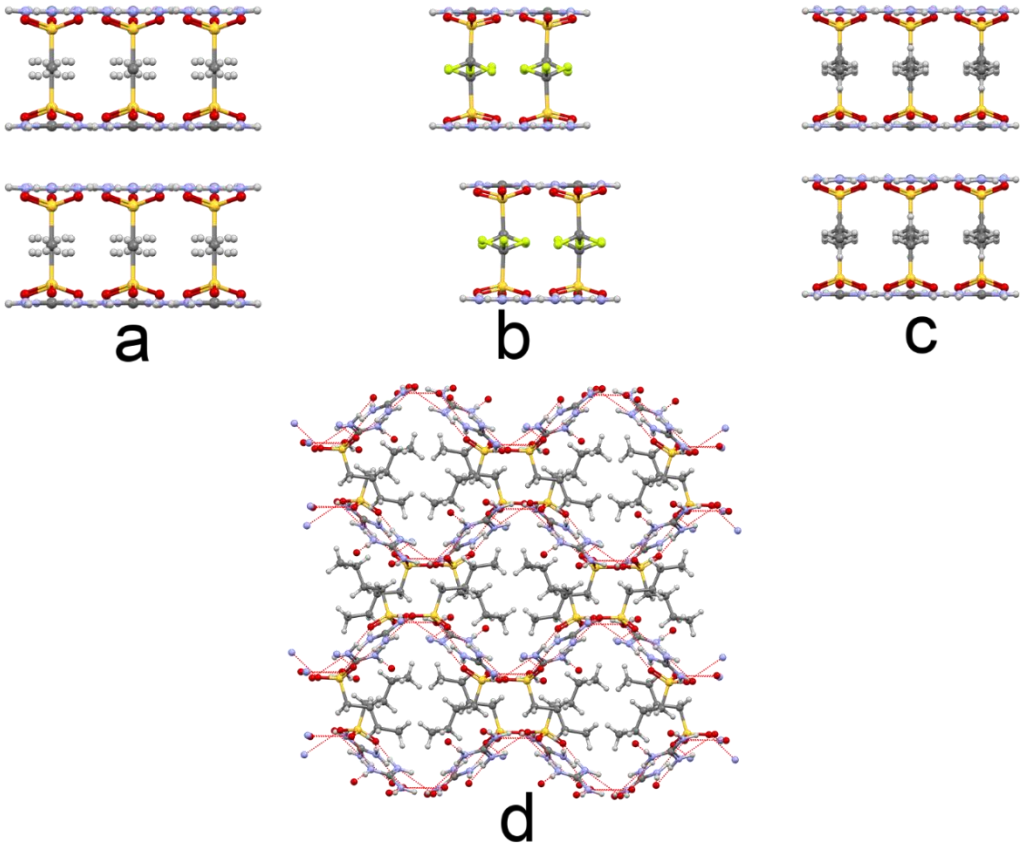

Figure 1.9.5 The transition from bilayers to monolayers in guanidinium sulfonates going from **a**, methanesulfonate (Refcode: WETNEO), to **b**, triflate (Refcode: WETNIS), **c**, ethanesulfonate (Refcode: WETNOY), and finally **d**, 1-butanesulfonate (Refcode: WETNUE).[168]

We have reviewed some examples of how sterics come into play in various venues. It is evident that sterics play a large role in a number of different chemistries, and differences of even a single carbon plays a major role in either reactivity or molecular and solid-state assembly. In examining these specific examples, where the effects of sterics are clear; the situation is unambiguous enough to safely assume that these effects will be apparent in many other chemical systems and scenarios.

1.10 Conclusions and Reassessment of Objectives

The research that follows concerns the synthesis and evaluation of two different types of materials: metal oxide clusters, and 2-D hydrogen-bonded supramolecular structures. Both types of materials will form crystalline solids whose structures will be analyzed *via* X-ray crystallographic methods, and compared to analogous structures in the database.[17, 163]

X-ray crystal data will allow us to answer the following questions:

Through utilization of a series benzoic acids featuring systematically increasing *ortho* steric influence can we:

I. **Substitute** the small peripheral acetate groups on the polynuclear manganese oxide cluster, Mn_{12}-Acetate, with this series of benzoates?
    a. If so, can we observe and evaluate any structural differences between the new complexes and the parent Mn_{12}-Acetate complexes; and if a functional difference is measured between the two, can the change be linked to the established structural differences?

II. Instead of substitutive methods, can we synthesize other manganese oxide clusters of formula $Mn_xO_y(O_2C\mathbf{R})_z(L)_w$ using the previously proposed systematic series of benzoic acids as starting materials (i.e., '**ground-up**' methods)?

a. If so, can we analyze and compare the crystal structures, and establish a connection between the shape and size of the cluster synthesized with the relative steric bulk of the *ortho*-substituted benzoic acid?

b. Additionally, if there is a measurable function associated with the newly synthesized materials, can that function also be compared between the structures, and furthermore can the change be linked to a structural difference?

III. Utilizing formic acid, and varying a complementary, typically arene based, primary amine synthons, can we predict the outcome and synthesize a large library of 2-dimensional hydrogen-bonded ammonium formates?

a. If so, can we then compare the crystal structures of these new ammonium formates with existing literature ammonium carboxylates, as well as previously synthesized and characterized ammonium 3,5-pyrazoledicarboxylates?

The following chapters seek to answer these questions. We close out, combining all the previous discussion, and move into the bulk of the research work for this dissertation.

1.11 References

1. Bragg, W. H.; Bragg, W. L., The Structure of Diamond. *Nature* **1913,** *91* (2283), 557.
2. Allen, S. J.; Lorentz, E. J., On the Comparative Absorption of γ and X Rays. *Physical Review* **1913,** *1* (1), 35-49.
3. Friedrich, W.; Knipping, P.; Laue, M., Interferenz-Erscheinungen bei Röntgenstrahlen. *München: Verl. d. Königl. Bayer. Akad. d. Wiss.* **1912**, 303-322.
4. Housecroft, C. E.; Sharpe, A. G., *Inorganic Chemistry*. Pearson: 2015.
5. Tiekink, E. R. T., *Crystal Engineering: Supramolecular Materials Chemistry*. John Wiley & Sons, Ltd.: Wiley Online Library, 2012.
6. Weber, E., *Design of Organic Solids*. Springer: 1998.
7. Debré, P., *Louis Pasteur*. Johns Hopkins University Press: Baltimore, 1994.
8. Leeson, H. B., CCVII. On Crystallography, with a Description of a New Goniometer and Crystallonome. *Mem. Proc. Chem. Soc.* **1845,** *3*, 486-560.
9. Röntgen, W. C., Ueber eine neue Art von Strahlen. Vorläufige Mitteilung. *Aus den Sitzungsberichten der Würzburger Physik.-medic. Gesellschaft Würzburg* **1895**, 137-147.
10. Michelson, A. A.; Stratton, S. W., Source of X-Rays. *Science* **1896,** *3* (71), 694-696.
11. Porter, T. C., The X-rays produced by a Wimshurst Machine. *Nature* **1896,** *55* (1411), 30-32.
12. Cattell, H. W., Application of the X-rays to Surgery. *Science* **1896,** *3* (62), 341-346.
13. Norton, C. L., The X-Rays in Medicine and Surgery. *Science* **1896,** *3* (72), 730-731.
14. Smith, J. R., Some Effects of X-rays on the Hands. *Nature* **1896,** *54* (1409), 621.
15. Bragg, W. H., X-rays and Crystals. *Nature* **1913,** *90* (2259), 572.
16. Bragg, W. H., The Reflection of X-rays by Crystals. *Nature* **1913,** *91* (2280), 477.
17. Kennard, O., From data to knowledge—Use of the Cambridge Structural Database for studying molecular interactions. *Supramolecular Chemistry*. **1992,** *1* (3), 277-295.
18. Dolomanov, O. V.; Bourhis, L. J.; Gildea, R. J.; Howard, J. A. K.; Puschmann, H., OLEX2: a complete structure solution, refinement and analysis program. *J. Appl. Cryst.* **2009,** *42*, 339-341.
19. Franklin, R. E.; Gosling, R. G., Evidence for 2-Chain Helix In Crystalline Structure of Sodium Deoxyribonucleate. *Nature* **1953,** *172*, 156-157.
20. Franklin, R. E.; Gosling, R. G., Molecular Configuration in Sodium Thymonucleate. *Nature* **1953,** *171*, 740-741.
21. Pauling, L.; Corey, R. B., A Proposed Structure for the Nucleic Acids. *Proc. Natl. Acad. Sci.* **1953**, 84-97.
22. Watson, J. D.; Crick, F. H. C., Molecular Structure of Nucleic Acids: A Structure for Deoxyribose Nucleic Acid. *Nature* **1953,** *171*, 737-738.
23. Watson, J. D.; Crick, F. H. C., Molecular Structure of Deocypentose Nucleic Acids. *Nature* **1953,** *171*, 738-741.
24. Rao, G. V. S.; Rao, C. N. R., Transition Metal Oxides. *Journal of the Indian Institute of Science* **1974,** *99*, 1-144.
25. Guntlin, C. P.; Ochsenbein, S. T.; Wörle, M.; Erni, R.; Kravchyk, K. V.; Kovalenko, M. V., Popcorn-Shaped FexO (Wüstite) Nanoparticles from a Single-Source Precursor: Colloidal Synthesis and Magnetic Properties. *Chem. Mater.* **2018**.
26. Chapman, S. K., Transition Metal Oxides: Structure, Properties, And synthesis of Ceramic Oxides. *Appl. Organometl. Chem.* **1999,** *13*, 475-480.
27. Lis, T., "Preparation, Structure, and Magnetic Properties of a Dodeeanuelear Mixed-Valence Manganese Carboxylate". *Acta Cryst.* **1980,** *B36*, 2042-2046.
28. Wahlbeck, P. G., Transition Metal Oxides. *J. Am. Chem. Soc.* **1996,** *118* (4), 931-935.
29. Ray, C.; Pal, T., Recent advances of metal–metal oxide nanocomposites and their tailored nanostructures in numerous catalytic applications. *J. Mater. Chem.* **2017,** *5* (20), 9465-9487.

30. Yu, X.; Marks, T. J.; Facchetti, A., Metal oxides for optoelectronic applications. *Nat. Mater.* **2016,** *15* (4), 383-96.
31. Xu, Z.; Shi, J.; Haroone, M. S.; Chen, W.; Zheng, S.; Lu, J., Zinc-aluminum oxide solid solution nanosheets obtained by pyrolysis of layered double hydroxide as the photoanodes for dye-sensitized solar cells. *Journal of Colloid and Interface Science* **2018,** *515*, 240-247.
32. Wang, G.; Zhang, L.; Zhang, J., A review of electrode materials for electrochemical supercapacitors. *Chem. Soc. Rev.* **2012,** *41* (2), 797-828.
33. Liu, P. P.; Yang, L. Y.; Liu, W.; Zhang, Y.; Wang, H. L.; Liu, S.; Yang, R. R.; Guo, Y. Q.; Cui, Y. P., Novel hybrid anode of MnO nanoparticles and ultrathin carbon sheets for high lithium storage performance. *Journal of Alloys and Compounds* **2018,** *740*, 375-381.
34. Özgür, U.; Alivov, Y. I.; Liu, C.; Teke, A.; Reshchikov, M. A.; Doğan, S.; Avrutin, V.; Cho, S.-J.; Morkoç, H., A comprehensive review of ZnO materials and devices. *J. Appl. Phys.* **2005,** *98*, 041301.
35. Wang, Y.; Arandiyan, H.; Scott, J.; Bagheri, A.; Dai, H.; Amal, R., Recent advances in ordered meso/macroporous metal oxides for heterogeneous catalysis: a review. *J. Mater. Chem.* **2017,** *5* (19), 8825-8846.
36. Astruc, D.; Lu, F.; Aranzaes, J. R., Nanoparticles as recyclable catalysts: the frontier between homogeneous and heterogeneous catalysis. *Angew. Chem. Int. Ed.* **2005,** *44* (48), 7852-7872.
37. Cusinato, L.; Del Rosal, I.; Poteau, R., Shape, electronic structure and steric effects of organometallic nanocatalysts: relevant tools to improve the synergy between theory and experiment. *Dalton Trans.* **2017,** *46* (2), 378-395.
38. Sarikaya, M.; Tamerler, C.; Schulten, K.; Baney, F., Molecular biomimetics: nanotechnology through biology. *Nature Matt.* **2003,** *2*, 577-586.
39. Kuehnel, M. F.; Orchard, K. L.; Dalle, K. E.; Reisner, E., Selective Photocatalytic CO2 Reduction in Water through Anchoring of a Molecular Ni Catalyst on CdS Nanocrystals. *J. Am. Chem. Soc.* **2017,** *139* (21), 7217-7223.
40. Lunghi, A.; Totti, F.; Sanvito, S.; Sessoli, R., Intra-molecular origin of the spin-phonon coupling in slow-relaxing molecular magnets. *Chem. Sci.* **2017,** *8* (9), 6051-6059.
41. Garcia-Rodriguez, R.; Wright, D. S., Steric Effects on the Structures, Reactivity, and Coordination Chemistry of Tris(2-pyridyl)aluminates. *Chemistry* **2015,** *21* (42), 14949-14957.
42. Anderson, P. W., New Approach to the Theory of Superexchange Interactions. *Phys. Rev.* **1959,** *115* (1), 2-13.
43. Lampropoulos, C.; Murugesu, M.; Harter, A. G.; Wernsdofer, W.; Hill, S.; Dalal, N. S.; Reyes, A. P.; Kuhns, P. L.; Abboud, K. A.; Christou, G., Synthesis, Structure, and Spectroscopic and Magnetic Characterization of [Mn12O12(O2CCH2But)16(MeOH)4]·MeOH, a Mn12 Single-Molecule Magnet with True Axial Symmetry. *Inorg. Chem.* **2013,** *52* (1), 258-272.
44. Gatteschi, D.; Sessoli, R.; Villain, J., *Molecular Nanomagnets*. Oxford University Press: 2006.
45. Tsai, H.-L.; Eppley, H. J.; de Vries, N.; Folting, K.; Christou, G.; Hendrickson, D. N., "Superparamagnetic-like properties of the valence-trapped $Mn^{II}Mn^{III7}Mn^{IV4}$ anion in the salt $(PPh_4)[Mn_{12}O_{12}(O_2CEt)_{16}(H_2O)_4]$". *Chem. Commun.* **1994**, 1475-1746.
46. Perenboon, J. A. A. J.; Brooks, J. S.; Hill, S.; Hathaway, T.; Dalal, N. S., Relaxation of the magnetization of Mn12 acetate. *Phys. Rev. B.* **1998,** *58* (11).
47. Hein, R. A., ac magnetic susceptibility, Meissner effect, and bulk superconductivity. *Phys. Rev. B.* **1986,** *33* (11), 7539-7549.
48. Sessoli, R.; Gatteschi, D.; Caneschi, A.; Novak, M. A., Magnetic Bistability In A Metal-Ion Cluster. *Nature* **1993,** *365*, 141-143.
49. Weighardt, K.; Pohl, K.; Jibril, I.; Huttner, G., Hydrolysis Products of the Monomeric Amine Complex (C6H15N3)FeCl3: The Structure of the Octameric Iron(III) Cation of {[(C6H15N3)6Fe8(μ3-O)2(μ2-OH)12]Br7(H2O)}Br·8H2O†. *Angew. Chem.* **1984,** *23* (1), 77-78.

50. Sasabe, H., *Hyper-Structured Molecules III*. Taylor & Francis London and New York: 2002.
51. Friedman, J. R.; Sarachik, M. P., Macroscopic Measurement of Resonant Magnetization Tunneling in High-Spin Molecules. *Phys. Rev. Lett.* **1996,** *76* (20), 3830-3833.
52. Thomas, L.; Lionti, F.; Ballou, R.; Gatteschi, D.; Sessoli, R.; Barbara, B., Magnetic Quantum Tunneling In A Single Crystal of Nanomagnets. *Nature* **1996,** *383*, 145-147.
53. Darling, S. B.; Bader, S. D., A materials chemistry perspective on nanomagnetism. *J. Mater. Chem.* **2005,** *15* (39), 4189.
54. Mannini, M., *Molecular Magnetic Materials on Solid Surfaces*. Firenze University Press: 2008.
55. Sangregorio, C.; Ohm, T.; Paulsen, C.; Sessoli, R.; Gatteschi, D., Quantum Tunneling of the Magnetization in an Iron Cluster Nanomagnet. *Phys. Rev. Lett.* **1997,** *78* (24), 4645-4649.
56. Friedman, J. R.; Sarachik, M. P., Single-Molecule Nanomagnets. *Annu. Rev. Condens. Matter Phys.* **2010,** *109* (1), 1-40.
57. Leuenberger, M. N.; Loss, D., Quantumn Computing in Molecular Magnets. *Nature* **2001,** *410*, 789-793.
58. Bogani, L.; Wernsdofer, W., Molecular spintronics using single-molecule magnets. *Nature Matt.* **2008,** *7*, 179-186.
59. Tejada, J.; Chudnovsky, E. M.; del Barco, E.; Hernandez, J. M.; Spiller, T. P., Magnetic qubits as hardware for quantum computers. *Nanotechnology* **2001,** *12* (2), 181.
60. Friedman, J. R., *Exploring the Quantum/Classical Frontier: Recent Advances in Macroscopic and Mesoscopic Quantum Phenomena,*. 2003.
61. Liu, J.; Wu, B.; Fu, L.-B.; Diener, R. B.; Niu, Q., Quantum Step Heights in Hysteresis Loops of Molecular Magnets. *Condens. Matter.* **2001,** *0105497v4*.
62. Giraud, R.; Wernsdorfer, W.; Tkachuk, A. M.; Mailly, D.; Barbara, B., Nuclear spin driven quantum relaxation in LiY0.998Ho0.002F4. *Phys. Rev. Lett.* **2001,** *87* (5), 057203.
63. Katsnelson, M. I.; Dobrovitski, V. V.; Harmon, B. N., Many-spin model and the spin Hamiltonian of Mn12 clusters. *J. Appl. Phys.* **1999,** *85* (8), 4533-4535.
64. Sessoli, R.; Gatteschi, D.; Caneschi, A.; Novak, M. A., "Magnetic bistability in a metal-ion cluster". *Nature* **1993,** *365*, 141-143.
65. Ramasesha, S.; Sahoo, S.; Raghunathan, R.; Sen, D., Computing magnetic anisotropy constants of single molecule magnets. *Chem. Sci.* **2009,** *121* (5), 823-837.
66. Sessoli, R.; Tsai, H.-L.; Schake, A. R.; Wang, S.; Vincent, J. B.; Folting, K.; Gatteschi, D.; Christou, G.; Hendrickson, D. N., "High-Spin Molecules: "$Mn_{12}O_{12}(O_2CR)_{16}(H_2O)_4$". *J. Am. Chem. Soc.* **1993,** *115*, 1804-1816.
67. Nakano, M.; Oshio, H., Magnetic anisotropies in paramagnetic polynuclear metal complexes. *Chem. Soc. Rev.* **2011,** *40* (6), 3239-3248.
68. Park, K.; Novotny, M. A.; Dalal, N. S.; Hill, S.; Rikvold, P. A.; Bhaduri, S.; Christou, G.; Hendrickson, D. N., Defects, Tunneling, and EPR Spectra of Single-Molecule Magnets. *Mat. Res. Soc. Symp. Proc.* **2003,** *746*, 1.3.1-1.3.13.
69. Kent, A. D.; Zhong, Y.; Bokacheval, L.; Ruiz, D.; Hendrickson, D. N.; Sarachik, M. P., Low-temperature magnetic hysteresis in Mn12 acetate single crystals. *Europhys. Lett.* **2000,** *49* (4), 521-527.
70. Caneschi, A.; Gatteschi, D.; Sessoli, R., "Alternating Current Susceptibility, High Field Magnetization, and Millimeter Band EPR Evidence for a Ground S = 10 State in $[Mn_{12}O_{12}(CH_3COO)_{16}(H_2O)_4)\cdot 2CH_3COOH\cdot 4H_2O$". *J. Am. Chem. Soc.* **1991,** *113*, 5873-5874.
71. Wernsdofer, W., Classical and quantum magnetization reversal studied in nanometer-sized particles and clusters. *Adv. Chem. Phys.* **2001,** *118*, 99-190.
72. Mi, Z. Y.; Zhou, Y. R.; Zhang, J.; Li, J. F.; Wang, Y. P.; Song, X. H., Comparison of magnetic relaxation between Mn12-Ac and Mn12-tBuAc single-molecule magnets. *EPL* **2017,** *117* (4), 47003.

73. Russier, V.; Petit, C.; Pileni, M. P., Hysteresis curve of magnetic nanocrystals monolayers: Influence of the structure. *J. Appl. Phys.* **2003,** *93* (12), 10001-10010.
74. Gatteschi, D.; Sessoli, R., Quantum Tunneling of Magnetization and Related Phenomena in Molecular Materials. *Angew. Chem. Int. Ed.* **2003,** *42* (3), 268-298.
75. Singh, S. K.; Rajaraman, G., Deciphering the origin of giant magnetic anisotropy and fast quantum tunnelling in Rhenium(IV) single-molecule magnets. *Nat. Commun.* **2016,** *7*, 10669-10677.
76. Jordan, S. P., Fast quantum computation at arbitrarily low energy. *Phys. Rev. A.* **2017,** *95* (3), 032325.
77. Bianchi, M.; Morales, J. F., Anomalies, RG-ows and Open / Closed String Duality. *arXiv:hep-th/0101104v1* **2001**.
78. Wernsdorfer, W.; Bhaduri, S.; Boskovic, C.; Christou, G.; Hendrickson, D. N., Spin-parity dependent tunneling of magnetization in single-molecule magnets. *Phys. Rev. B.* **2002,** *65* (18).
79. Christou, G.; Gatteschi, D.; Hendrickson, D. N.; Sessoli, R., "Single-Molecule Magnets". *MRS Bulletin* **2000,** *25* (11), 66-71.
80. Hill, S.; Datta, S.; Liu, J.; Inglis, R.; Milios, C. J.; Feng, P. L.; Henderson, J. J.; Del Barco, E.; Brechin, E. K.; Hendrickson, D. N., Magnetic quantum tunneling: Insights from simple molecule-based magnets. *Dalton. Trans.* **2010,** *39* (20), 4693-4707.
81. Mattuck, R. D.; Strandberg, M. W. P., Spin-Phonon Interaction in Paramagnetic Crystals. *Phys. Rev.* **1960,** *119* (4), 1204-1217.
82. Wernsdorfer, W.; Bhaduri, S.; Tiron, R.; Hendrickson, D. N.; Christou, G., Spin-Spin Cross Relaxation in Single-Molecule Magnets. *Phys. Rev. Lett.* **2002,** *89* (19).
83. Barbara, B.; Giraud, R.; Tkachuk, A. M., Quantum dynamics of atomic magnets. *Physica Status Solidi* **2004,** *241* (6), 1167-1173.
84. Evangelisti, M.; Luis, F.; Mettes, F. L.; Aliaga, N.; Aromí, G.; Alonso, J. J.; Christou, G.; De Jongh, L. J., Magnetic long-range order induced by quantum relaxation in single-molecule magnets. *Phys. Rev. Lett.* **2004,** *93* (11), 117202-117206.
85. Wernsdorfer, W., Quantum dynamics in molecular nanomagnets. *Comptes Rendus Chimie* **2008,** *11* (10), 1086-1109.
86. Misiorny, M.; Barnaś, J., Switching of molecular magnets. *Physica Status Solidi* **2009,** *246* (4), 695-715.
87. Mertes, K. M.; Suzuki, Y.; Sarachik, M. P.; Myasoedov, Y.; Shtrikman, H.; Zeldov, E.; Rumberger, E. M.; Hendrickson, D. N.; Christou, G., Mn12-acetate: a prototypical single molecule magnet. *Solid State Communications* **2003,** *127* (2), 131-139.
88. Aubin, S. M. J.; Sun, Z.; Rumberger, E. M.; Hendrickson, D. N.; Christou, G., Single molecule magnets: High frequency electron paramagnetic resonance study of two isomeric forms of an Mn12 molecule. *J. Appl. Phys.* **2002,** *91* (10), 7158-7161.
89. Leuenberger, M. N.; Loss, D., Spin tunneling and phonon-assisted relaxation in Mn12-acetate. *Phys. Rev. B.* **2000,** *61* (21), 1286-1303.
90. Werner, R.; Gros, C., The microscopic spin-phonon coupling constants in CuGeO3. *Condens. Matter.* **2008,** *59* (14), 356-367.
91. Callen, E.; Callen, H. B., Magnetostriction, Forced Magnetostriction, and Anomalous Thermal Expansion in Ferromagnets. *Phys. Rev. A.* **1965,** *139* (2), 455-471.
92. Chiorescu, I.; Giraud, R.; Jansen, A. G. M.; Caneschi, A.; Barbara, B., Phonon-Assisted Tunneling in the Quantum Regime of Mn12 Acetate. *Phys. Rev. Lett.* **2000,** *85* (22), 4807-4811.
93. Morello, A.; de Jongh, L. J., Dynamics and thermalization of the nuclear spin bath in the single-molecule magnetMn12−ac: Test for the theory of spin tunneling. *Phys. Rev. B.* **2007,** *76* (18), 184425-184447.
94. Shoemaker, D. P.; Donohue, J.; Schomaker, V.; Corey, R. B., The Crystal Structure of L_s-Threonine. *J. Am. Chem. Soc.* **1950,** *72* (6), 2328-2349.

95. Edelhoch, H., The Denaturation of Pepsin. II. Hydrogen Ion Equilibria of Native and Denatured Pepsin. *J. Am. Chem. Soc.* **1958,** *80* (24), 6640-6647.
96. Tobolsky, A. T.; Shen, M. C., The Effect of Hydrogen Bonds on the Viscoelastic Properties of Amorphous Polymer Networks. *J. Phys. Chem.* **1963,** *67* (9), 1886-1891.
97. Ginsberg, A. P.; Koubek, E., Hydrogen Bonding in Ferrocyanic, Ru thenocyanic, and Osmocyanic Acids. *Inorg. Chem.* **1965,** *4* (8), 1186-1194.
98. Jordan, T. H.; Mak, T. C. W., Polyhedral Clathrate Hydrates. XIII. The Structure of (CH3CH2)2NH·8⅔H2O. *The Journal of Chemical Physics* **1967,** *47* (4), 1222-1228.
99. Dickens, B.; Brown, W. E., The Crystal Structures of $CaNa_2(CO_3)_2$5 H_2O, Synthetic Gaylussite, and $CaNa_2(CO_3)_2$ $2H_2O$, Synthetic Pirrsonite. *Inorg. Chem.* **1969,** *8* (10), 2093-2104.
100. Guerra, C. F.; Bickelhaupt, F. M.; Snijders, J. G.; Baerends, E. J., Hydrogen Bonding in DNA Base Pairs: Reconciliation of Theory and Experiment. *J. Am. Chem. Soc.* **2000,** *122*, 4117-4128.
101. Snyder, P. W.; Lockett, M. R.; Moustakas, D. T.; Whitesides, G. M., Is it the shape of the cavity, or the shape of the water in the cavity? *Eur. Phys. J.* **2013,** *223* (5), 853-891.
102. Henderson, M. A., The interaction of water with solid surfaces: Fundamental aspects revisited. *Surface Science Reports* **2002,** *46* (1-8), 1-308.
103. Ludwig, R., Water: From clusters to the bulk. *Angew. Chem. Int. Ed.* **2001,** *40* (10), 1808-1827.
104. Thiel, P. A.; Madey, T. E., The interaction of water with solid surfaces: Fundamental aspects. *Surface Science Reports* **1987,** *7* (6-8), 211-385.
105. Jorgensen, W. L.; Chandrasekhar, J.; Madura, J. D., Comparison of simple potential functions for simulating liquid water. *J. Chem. Phys.* **1983,** *79* (2).
106. Chadha, R.; Rani, D.; Goyal, P., Supramolecular Cocrystals of Gliclazide: Synthesis, Characterization and Evaluation. *Pharm. Res.* **2017,** *34* (3), 552-563.
107. Janczak, J., Solid-state supramolecular structure of tetrakis(1-(diaminomethylene)thiouron-1-ium) pyromellate. *Journal of Molecular Structure* **2018,** *1155*, 443-449.
108. Rana, M.; Chowdhury, D., Perturbation of hydrogen bonding in hydrated pyrrole-2-carboxaldehyde complexes. *J. Mol. Model.* **2017,** *23* (7), 216.
109. Wolke, C. T.; Fournier, J. A.; Dzugan, L. A.; Fagiani, M. R.; Odbadrakh, T. T.; Knorke, H.; Jordan, K. D.; McCoy, A. B.; Asmis, K. R.; Johnson, M. A., Spectroscopic snapshots of the proton-transfer mechanism in water. *Science* **2016,** *354* (6316), 1131-1135.
110. Kerdpol, K.; Dawengngern, R.; Kungwan, N., Excited-state proton-transfer reactions of 7-azaindole with water, ammonia and mixed water–ammonia: microsolvated dynamics simulation. *Mol. Sim.* **2014,** *41* (14), 1177-1186.
111. Samanta, A. K., Infrared spectroscopic demonstration of cooperative and anti-cooperative effects in C-H--O hydrogen bonds. *Recent Advances In Spectroscopy* **2010,** *1*, 53-61.
112. Chakraborty, S.; Lima, B. C. d.; Silva, A. M. d.; Chaudhuri, P., Effect of hydrogen-bonded interactions on the energetics and spectral properties of the astromolecule aminoacetonitrile. *International Journal of Quantum Chemistry* **2018,** *118* (2), 25459.
113. Stanley, A. M.; Fleming, K. G., The role of a hydrogen bonding network in the transmembrane beta-barrel OMPLA. *J. Mol. Biol.* **2007,** *370* (5), 912-924.
114. Bandyopadhyay, N.; Pradhan, A. B.; Das, S.; Lu, L.; Zhu, M.; Chowdhury, S.; Naskar, J. P., Synthesis, structure, DFT calculations, electrochemistry, fluorescence, DNA binding and molecular docking aspects of a novel oxime based ligand and its palladium(II) complex. *J. Photochem. Photobiol. B.* **2016,** *160*, 336-346.
115. Krajnc, A.; Varlec, J.; Mazaj, M.; Ristić, A.; Logar, N. Z.; Mali, G., Superior Performance of Microporous Aluminophosphate with LTA Topology in Solar-Energy Storage and Heat Reallocation. *Adv. Energy Mater.* **2017,** *7* (11), 1601815.

116. Fang, H.; Kim, Y., Excited-State Tautomerization in the 7-Aza4indole-(H2O)n (n = 1 and 2) Complexes in the Gas Phase and in Solution: A Theoretical Study. *J. Chem. Theory. Comput.* **2011,** *7* (3), 642-657.
117. Arunan, E.; Desiraju, G. R.; Klein, R. A.; Sadlej, J.; Scheiner, S.; Alkorta, I.; Clary, D. C.; Crabtree, R. H.; Dannenberg, J. J.; Hobza, P.; Kjaergaard, H. G.; Legon, A. C.; Mennucci, B.; Nesbitt, D. J., Definition of the hydrogen bond (IUPAC Recommendations 2011). *Pure Appl. Chem.* **2011,** *83* (8), 1637-1641.
118. Steiner, T., The Hydrogen Bond in the Solid State. *Angew. Chem. Int. Ed.* **2002,** *41*, 48-76.
119. Mautner, M., The Ionic Hydrogen Bond. *Chem. Rev.* **2005,** *105*, 213-284.
120. Desiraju, G. R., Supramolecular Synthons in Crystal Engineering - A New Organic Synthesis. *Angew. Chem. Int. Ed.* **1995,** *34* (21), 2311-2327.
121. Karthikeyan, S.; Ramanathan, V.; Mishra, B. K., Influence of the substituents on the CH...pi interaction: benzene-methane complex. *J. Phys. Chem. A* **2013,** *117* (30), 6687-6694.
122. Mishra, B. K.; Deshmukh, M. M.; Venkatnarayan, R., C-H...pi interactions and the nature of the donor carbon atom. *J. Org. Chem.* **2014,** *79* (18), 8599-8606.
123. Mishra, B. K.; Karthikeyan, S.; Ramanathan, V., Tuning the C-H...pi Interaction by Different Substitutions in Benzene-Acetylene Complexes. *J. Chem. Theory. Comput.* **2012,** *8* (6), 1935-1942.
124. Etter, M. C., Encoding and Decoding Hydrogen-Bond Patterns of Organic Compounds. *Acc. Chem. Res.* **1990,** *23*, 120-126.
125. Gilli, G.; Gilli, P., *The Nature of the Hydrogen Bond: Outline of a Comprehensive Hydrogen Bond Theory*. Oxford University Press: 2009.
126. Subramanian, S.; Zaworotko, M. J., Exploitation of the hydrogen bond, recent developments in the context of crystal. *Coor. Chem. Rev.* **1994,** *137*, 357-401.
127. Lehn, J.-M., *Supramolecular Chemistry: Concepts and Perspectives*. VCH Verlagsgesellschaft: Weinheim, Germany, 1995.
128. Atkins; Jones; Laverman, *Chemical Principles 6th Ed.* W. H. Freeman: 2012.
129. Li, Z.-T.; Wu, L.-Z., *Hydrogen Bonded Supramolecular Structures*. Springer: 2015.
130. Nishio, M.; Hirota, M.; Umezawa, Y., *The CH/π Interaction: Evidence, Nature, and Consequences*. John Wiley & Sons: 1998.
131. Marsh, A.; Silvestri, M.; Lehn, J.-M., Self-complementary hydrogen bonding heterocycles designed for the enforced self-assembly into supramolecular macrocycles. *Chem. Commun.* **1996**, 1527.
132. Schmuck, C.; Wienand, W., Self-Complementary Quadruple Hydrogen-Bonding Motifs as a Functional Principle: From Dimeric Supramolecules to Supramolecular Polymers. *Angew. Chem. Int. Ed.* **2001,** *40* (23), 4363-4370.
133. Jaunky, W.; Hosseini, M. W.; Planeix, J. M.; De Cian, A.; Kyritsakas, N.; Fisher, J., Molecular braids: quintuple helical hydrogen bonded molecular network. *Chem. Commun.* **1999**, 2313-2314.
134. Bailey, M., The Crystal Structure of Terephthalic Acid. *Acta Cryst.* **1967,** *22*, 387-391.
135. Derissen, J. L., Isophthalic Acid. *Acta Cryst.* **1974,** *B30*, 2764-2765.
136. Vishweshwar, P.; Beauchamp, D. A.; Zaworotko, M. J., An Acetic Acid Solvate of Trimesic Acid That Exhibits Triple Inclined Interpenetration and Mixed Supramolecular Homosynthons. *Crystal Growth & Design.* **2006,** *6* (11), 2429-2431.
137. Saied, O.; Maris, T.; Wuest, J. D., Deformation of porous molecular networks induced by the exchange of guests in single crystals. *J. Am. Chem. Soc.* **2003,** *125* (49), 14956-14957.
138. Slater, A. G.; Perdigao, L. M.; Beton, P. H.; Champness, N. R., Surface-based supramolecular chemistry using hydrogen bonds. *Acc. Chem. Res.* **2014,** *47* (12), 3417-3427.
139. Ugono, O.; Rath, N. P.; Beatty, A. M., "Exceptions to the rule: new hydrogen-bonded networks from an old reliable". *CrystEngComm.* **2011,** *13* (3), 753-758.

140. Hoeben, F. J. M.; Jonkheijm, P.; Meijer, E. W.; Schenning, A. P. H., About Supramolecular Assemblies of π-Conjugated Systems. *Chem. Rev.* **2005,** *105*, 1491-1546.
141. Ballabh, A.; Trivedi, D. R.; Dastidar, P.; Suresh, E., Hydrogen bonded supramolecular network in organic salts: crystal structures of acid-base salts of dicarboxylic acids and amines. *CrystEngComm.* **2002,** *4* (24), 135-142.
142. Etter, M. C., Hydrogen Bonds as Design Elements in Organic Chemistry. *J. Phys. Chem.* **1991,** *95*, 4601-4610.
143. Aakeröy, C. B.; Beatty, A. M., Crystal Engineering of Hydrogen-Bonded Assemblies—A Progress Report. *Aust. J. Chem.* **2001,** *54*, 409-421.
144. Aakeröy, C. B.; Seddon, K. R., The Hydrogen Bond and Crystal Engineering. *Chem. Soc. Rev.* **1993,** *22* (6), 397-407.
145. Desiraju, G. R., Crystal engineering: a holistic view. *Angew. Chem. Int. Ed.* **2007,** *46* (44), 8342-8356.
146. Desiraju, G. R., Reflections on the Hydrogen Bond in Crystal Engineering. *Crystal Growth & Design* **2011,** *11* (4), 896-898.
147. Desiraju, G. R., Crystal engineering: from molecule to crystal. *J. Am. Chem. Soc.* **2013,** *135* (27), 9952-9967.
148. Félix, O.; Hosseini, M. W.; De Cian, A.; Fisher, J., Molecular Tectonics IV : Molecular Networks Based on Hydrogen Bonding and Electrostatic Interactions. *Tetrahedron Lett.* **1997,** *38* (10), 1755-1758.
149. Russell, V. A.; Ward, M. D., Molecular Crystals with Dimensionally Controlled Hydrogen-Bonded Nanostructures. *Chem. Mater.* **1996,** *8*, 1654-1666.
150. Beatty, A. M., Open-framework coordination complexes from hydrogen-bonded networks: toward host/guest complexes. *Coor. Chem. Rev.* **2003,** *246* (1-2), 131-143.
151. Yaghi, O. M.; O'Keeffe, M.; Ockwig, N. W.; Chae, H. K.; Eddaoudi, M.; Kim, J., Reticular synthesis and the design of new materials. *Nature* **2003,** *423*, 705-715.
152. Kitagawa, S.; Kitaura, R.; Noro, S., Functional porous coordination polymers. *Angew. Chem. Int. Ed.* **2004,** *43* (18), 2334-2375.
153. Wuest, J. D., Engineering Crystals By The Strategy of Molecular Tectronics. *Chem. Commun.* **2005**, 11063-11074.
154. Lee, S.; Mallik, A. B.; Xu, Z.; Lobkovsky, E. B.; Tran, L., Small Amphiphilic Organics Coordination Extended Solids and Constant Curvature Structures. *Acc. Chem. Res.* **2005,** *28*, 251-261.
155. Aakeröy, C. B.; Beatty, A. M.; Lorimer, K. R., Charge-Assisted Hydrogen Bonds and Halogen-Halogen Interactions in Organic Salts: Benzylammonium Benzoates and Pentafluorobenzoates. *Struct. Chem.* **1999,** *10* (3), 229-242.
156. Braga, D.; Maini, L.; Grepioni, F.; De Cian, A.; Fe´lix, O.; Fischer, J.; Hosseini, M. W., Charge-assisted N–H(+)···O(-) and O–H···O(-) hydrogen bonds control the supramolecular aggregation of ferrocenedicarboxylic acid and bis-amidines. *New J. Chem.* **2000,** *24* (7), 547-553.
157. Fang, Y.; Nguyen, P.; Ivasenko, O.; Aviles, M. P.; Kebede, E.; Askari, M. S.; Ottenwaelder, X.; Ziener, U.; Siri, O.; Cuccia, L. A., Charge-assisted hydrogen bond-directed self-assembly of an amphiphilic zwitterionic quinonemonoimine at the liquid-solid interface. *Chem. Commun.* **2011,** *47* (40), 11255-12257.
158. Lopes Jesus, A. J.; Redinha, J. S., Charge-assisted intramolecular hydrogen bonds in disubstituted cyclohexane derivatives. *J. Phys. Chem.* **2011,** *115* (48), 14069-14077.
159. Lie, S.; Maris, T.; Malveau, C.; Beaudoin, D.; Helzy, F.; Wuest, J. D., Molecular Networks Created by Charge-Assisted Hydrogen Bonding in Carboxylate Salts of a Bis(amidine). *Crystal Growth & Design* **2013,** *13* (5), 1872-1877.
160. Kochanek, S. E.; Clymer, T. M.; Pakkala, V. S.; Hebert, S. P.; Reeping, K.; Firestine, S. M.; Evanseck, J. D., Intramolecular charge-assisted hydrogen bond strength in pseudochair carboxyphosphate. *J. Phys. Chem.* **2015,** *119* (3), 1184-1191.

161. Lin, Z.; Hu, K.; Jin, S.; Ding, A.; Wang, Y.; Dong, L.; Gao, X.; Wang, D., Crystal and molecular structures of sixteen charge-assisted hydrogen bond-mediated diisopropylammonium salts from different carboxylic acids. *Journal of Molecular Structure* **2017,** *1146*, 577-591.
162. Sheldrick, G. M., A short history of SHELX. *Acta. Crystallogr. A* **2008,** *A64*, 112-122.
163. Groom, C. R.; Allen, F. H., The Cambridge Structural Database in retrospect and prospect. *Angew. Chem. Int. Ed. Engl.* **2014,** *53* (3), 662-671.
164. Bruice, *Organic Chemistry 7th Ed.* Pearson: 2013.
165. Moorthy, J. N., Crystal engineering with sterically-hindered molecular modules: unique supramolecular synthons and nove m olecular self assembly. *Journal of the Indian Institute of Science* **2008,** *88* (2), 131-150.
166. Bettelheim; Brown; March, *Introduction to General, Organic, and Biochemistry 6th Ed.* Holt Rinehart & Winston: 2001.
167. *Oligonucleotide synthesis : a practical approach*. Oxford: Washington, DC, 1984.
168. Russell, V. A.; Etter, M. C.; Ward, M. D., Layered Materials by Molecular Design: Structural Enforcement by Hydrogen Bonding in Guanidinium Alkane-and Arenesulfonates. *J. Am. Chem. Soc.* **1994,** *116* (5), 1941-1952.

Chapter 2

Mn_{12}-Type Substitution Compounds

2.1 Introduction

The focus of this chapter shall be on the formation of new Mn_{12}-type compounds which are derived *via* the substitution of the peripheral acetate moieties on the well-studied Mn_{12}-Acetate starting compound,[1] with *ortho*-substituted benzoates of systematically increasing size; carefully inspecting the structures for physical changes that are sterically driven.

2.1.1 The Manganese Oxide, Mn_{12}-Acetate Cluster

As discussed in Chapter 1, metal oxide clusters are found in a great number of arrangements and conformations, and research efforts rapidly shift focus as new metal oxide materials are introduced and characterized with high frequency. However, one unassuming dodecanuclear metal oxide cluster has managed to eclipse all other clusters and has fascinated researchers globally, across numerous fields in chemistry and physics, resulting in lasting and intensive study.

First proposed in 1921 *via* elemental analysis,[2] this 'deep-brown' colored polynuclear manganese cluster would have to wait until 1980 for synthetic discovery and structural characterization. Though it was not immediately apparent, the world of metal oxide clusters, chemistry, and physics, would be greatly impacted by the synthesis of the 'manganese-acetate' cluster, $Mn_{12}O_{12}(O_2CMe)_{16}(H_2O)_4$ (**Figure 2.1.1**).[3]

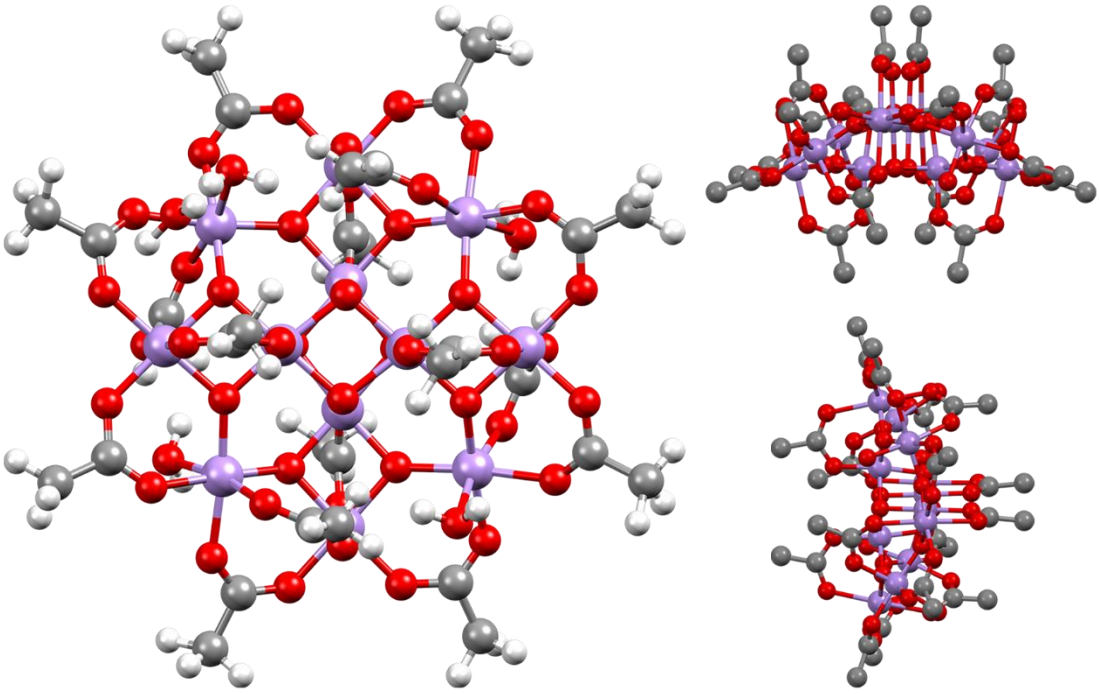

Figure 2.1.1 Introducing the Mn_{12}-Acetate metal oxide cluster. *Left*, the entire molecule viewed down the C-Axis. *Top right*, Mn_{12}-Acetate viewed down the A-axis, hydrogens removed for clarity. *Bottom right*, Mn_{12}-Acetate viewed down the B-axis, hydrogens removed for clarity. (Refcode: AQACMN).[3] *Note: in crystal structures featured in the schemes and figures to follow, dark grey spheres represent carbon atoms, light grey spheres represent hydrogen atoms, purple spheres represent manganese atoms, blue spheres represent nitrogen atoms, red spheres represent oxygen atoms, and bright green spheres represent the* ***R*** *group of a carboxylate.*

2.1.1.1 Mn_{12}-Acetate Structural Description

The Mn_{12}-Acetate cluster, also referred to as Mn_{12}-Ac, or MnOAc, or simply 'the manganese-acetate cluster', has a unique shape that is reminiscent of an 8-pointed ruzha flower. The inner core of the Mn_{12}-Acetate cluster is composed of a cubane-type tetravalent-$[Mn_4^{IV}O_4]^{8+}$ cluster, similar in structure to that of an [4Fe-4S] iron-sulfur cluster, commonly encountered in bioinorganic systems. Bound to the inner cubane Mn^{IV} ions are μ_3-oxygens, connecting the remaining eight peripheral trivalent, Jahn-Teller (JT) active, Mn^{III} ions. Finally, these peripheral

Mn^{III} ions are bridged by 16 μ_2-carboxylate moieties; 8 surrounding the equatorial periphery of the cluster, 4 pointing upwards on the face of the molecule, and 4 pointing downwards on the backside of the molecule.

In addition to the peripheral carboxylate ligands, there are four coordinated water molecules whose positions directly determine the Mn_{12}-type isomeric cluster that is encountered.[4-7] The water ligands of Mn_{12}-type clusters only coordinate axially to the four manganese (III) ions of Group III (**Section 2.1.2.2**). These Mn^{III} ions may coordinate 0-2 waters each. As a result, it is possible to identify 11 different geometric isomeric forms of Mn_{12}-type complexes based upon different coordination arrangements of the four water molecules. For example, Mn_{12}-Acetate has a single water ligand at each of the four Group III Mn^{III} ions, which can be seen below in **Figure 2.1.2**, identifying it as the 1:1:1:1 isomer. Two other commonly encountered isomers are the 2:2 isomer, where two waters are coordinated to two Mn^{III} ions at opposite positions around the Mn_{12}-type cluster (**Figure 2.1.2**); and the other common 1:2:1 isomer, where three of the Group III ions will each coordinate water, and the Mn^{III} ion in the middle of the group coordinates a second water molecule. Interestingly, the differences in water coordination does not influence the electronic structure or the superexchange interactions of the material; but is important when considering the redox chemistry of the material.[8-11]

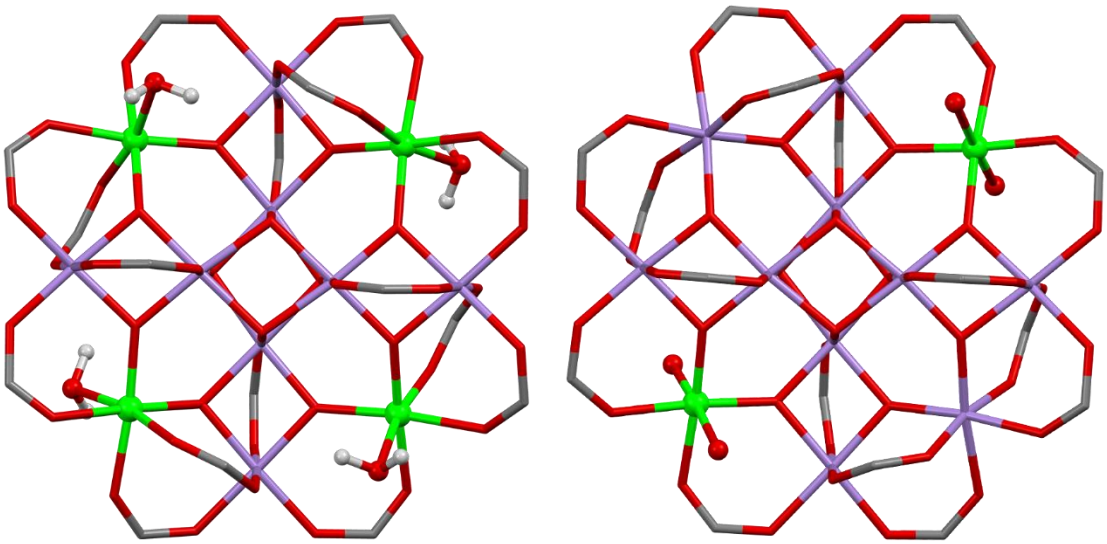

Figure 2.1.2 Common 1:1:1:1 and 2:2 water isomers of the Mn_{12}-type cluster, designated by the positions and coordination number of the waters. *Left*, Mn_{12}-Acetate 1:1:1:1 isomer, one coordinated water at each Group III Mn^{III} ion (Refcode: AQACMN).[3] *Right*, Mn_{12}-Benzoate 2:2 isomer, two waters are coordinated at spatially opposing Group III Mn^{III} ions (Refcode: KAGLEJ).[1] Group III Mn^{III} ions displayed as bright green spheres with water molecules coordinated. Other atoms displayed as sticks with hydrogens removed and carboxylate structures abridged for clarity.

2.1.2 Mn_{12}-Acetate Single-Molecule Magnetism: A Coming-of-Age Story

One of the most interesting anecdotes regarding Mn_{12}-Acetate, is its delayed ascent to popularity. While it was immediately present upon its discovery in 1980 that interesting magnetic behavior was active (**Figure 2.1.3**), it would not be until many years later when instrumental methods and clever researchers would be able to explain the unique behavior.[3] Sufficient description of this magnetic behavior was impossible at the time, and was attributed to distance-dependent, and curiously strong, Mn-O superexchange interactions. The existence of paramagnetic ions spin coupling *via* diamagnetic oxygen atoms was well known at the time,[12] but the apparent temperature dependence of the strong magnetization for the unassuming Mn_{12}-

Acetate cluster perplexed researchers. The apparent mystery strongly influenced many researchers to the field, and as a result, *many* different MnO superexchange materials were being studied at the time (and still are).[13-16] Mn_{12}-Acetate remained the standard for this type of research due to its ease of preparation, aerobic stability, and the crystal-imposed tetragonal symmetry. Later, reports of Mn_{12}-Acetates's ease of modification *via* the substitution of the peripheral acetate groups with other carboxylates would even *further* inflate its popularity.[1]

Ironically, during the discovery phase of this material, researchers Caneschi et. al comment that "...it is tempting to attribute these factors to those observed in superparamagnets, although the dimensions of the cluster are much smaller than those observed in superparamagnets."[17] They were certainly on to something. The Mn_{12}-Acetate molecule is ~1 nm in diameter, well within the size threshold of the nanoscopic, low total spin number materials which blur the lines of classical and quantum magnetism. Principally, sensitive instrumental techniques and detection were lacking, preventing a full description and classification of this phenomenon.

2.1.2.1 Mn_{12}-Acetate, A Superexchange Coupled Superparamagnet

Physically, the rise of Mn_{12}-Acetate's magnetic moment to 56.5×10^{-24} J T^{-1} around 17-31 K, from 30.9×10^{-24} J T^{-1} at around 3 K was remarkable, and the magnitude of the force was unexpected (**Figure 2.1.3**).[3] Granted, a maximum magnetic moment of 56.5×10^{-24} J T^{-1} at 20 K is not as momentous as a bulk ferromagnet, but the fact that a paramagnetic superexchange material was showing this level of response was very intriguing. In the closing remarks of his 1980 report, Professor Tadeusz Lis comments, "If exchange between all twelve Mn(1), Mn(2) and Mn(3) high-spin atoms is assumed to be *via O* atoms, such a complicated dodecameric unit should have interesting magnetic properties."[3] It is unlikely that Prof. Lis fully predicted the future legacy of his discovery!

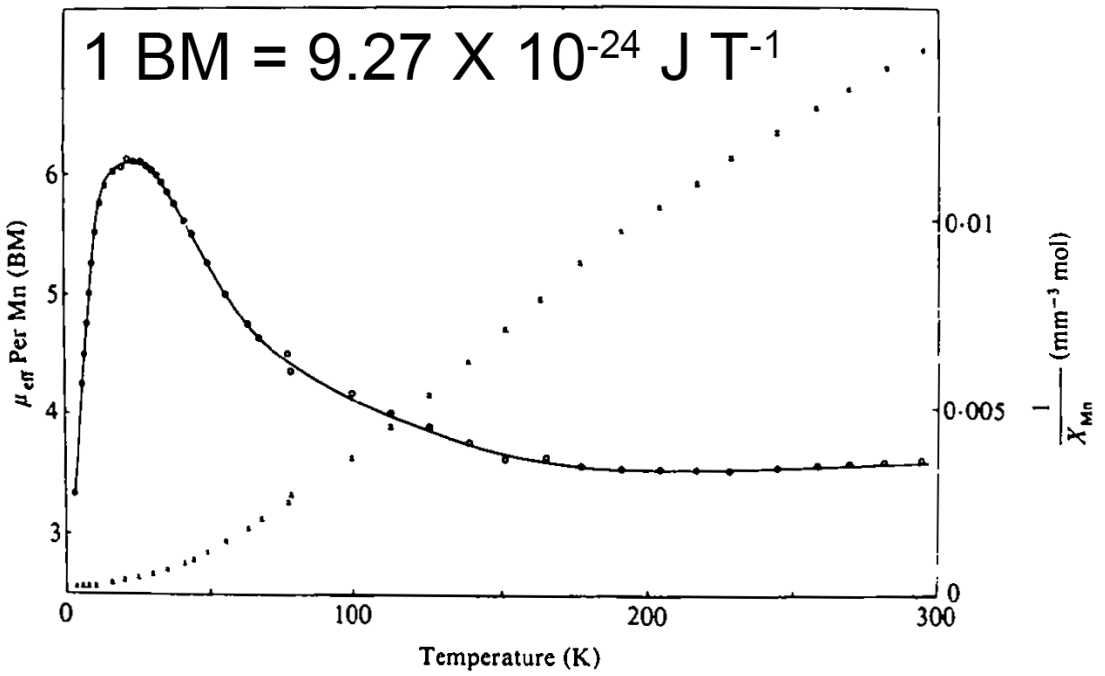

Figure 2.1.3 Measurement of the magnetic moment, and the inverse of the magnetic susceptibility (dotted curve) of Mn_{12}-Acetate. The magnetic moment increases from 30.9×10^{-24} J T^{-1} at 3.3 K to a maximum of 56.5×10^{-24} J T^{-1} in the range 17-31 K, and then decreases to 33.4×10^{-24} J T^{-1} at 280 K. Figure adapted from reference 3.

It would not be until 11 years later, spanning a time where research in this field was dominated by the study of polymetallic high-spin superexchange coupled complexes,[18-19] when the unique magnetic bistability of Mn_{12}-Acetate would finally be rationally explained, and the single-molecule magnet (SMM) class of materials would be revealed.[1, 17, 20] High-field magnetization, EPR, and AC susceptibility techniques paved the way for the measurement and calculation of Mn_{12}-Acetate's unique properties.[17]

It was discovered that Mn_{12}-Acetate demonstrates frequency-dependent out-of-phase signals, denoted χ_M'' (the imaginary part of the AC susceptibility), below a critical temperature point, known as the blocking temperature, T_B; and continues to retain its magnetization, for some time τ, after the removal of the applied magnetic field. Because the effect was attributed to a

single molecule, this discovery manifested the concept of the single magnetic domain, single-molecule magnet.

2.1.2.2 From Paramagnet to Superparamagnet

As previously alluded to, the magnetic behavior of Mn_{12}-Acetate was based upon the (correct) assumption that each peripheral Mn^{III} ion is antiferromagnetically superexchange coupled to the inner cubane Mn^{IV} ions *via* two different types of oxo-bridges. The relative spin values of each $Mn^{III/IV}$ ion differs, as well as their binary directionality, resulting in an overall ferrimagnetic material. To support this assumption, based upon the measured superexchange interactions, coordination environment, and oxidation state, the coupling of all 12 manganese ions is explained by their classification into three different groups, of overall two different spin values, (**Figure 2.1.4**), antiferromagnetically giving S = 10.

The 12 $Mn^{III/IV}$ ions for all Mn_{12}-type complexes are arranged into three groups based on their oxidation state, and superexchange interactions. Group I contains the four cubane Mn^{IV} ions, and the eight Mn^{III} ions fall into two groups of four Mn^{III} ions. Group II contains those Mn^{III} ions that are coupled to a single Mn^{IV} ion by two oxo-bridges. Group III contains those Mn^{III} ions that are coupled to two Mn^{IV} ions *via* two *independent* oxo-bridges (**Figure 2.1.4**, J_2 and J'_2). Based on the position and types of Mn^x ions present, multiple superexchange interactions have been identified within the Mn_{12}-type cluster. This spin coupling, and the symmetry of the molecule, is critical to the Mn_{12}-type superparamagnetic behavior.

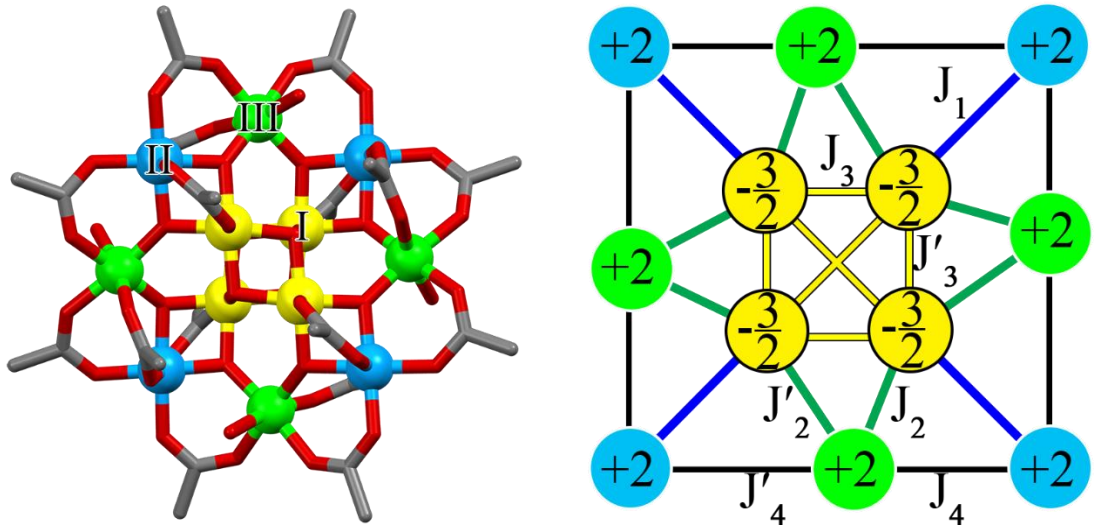

Figure 2.1.4 Grouping the manganese ions. *Left*, color coding and identifying the groups of $Mn^{III/IV}$ ions present in the Mn_{12}-type cluster. Group I, yellow, represents the Mn^{IV} ions. Group II, blue, represents the Mn^{III} ions bound to one Mn^{IV} ion by two oxo-bridges. Group III, green, represents the Mn^{III} ions bound to two Mn^{IV} ions by two oxo-bridges. *Right*, simplified illustration of the superexchange interactions present, and spin values (indicating antiferromagnetic ordering) for each $Mn^{III/IV}$ ion.

As described in Chapter 1, referencing the barrier to magnetization, U_{eff}, is often the most direct method of comparing two single-molecule magnets, *especially* those of the same family of molecules, when S and D values do not change drastically from compound to compound. Substituted and analogous Mn_{12}-type complexes have long since been compared based on their U_{eff} values compared to Mn_{12}-Acetate (U_{eff} = 62 K) parent cluster. Some trends in U_{eff} have been previously determined and established.[8, 21-23] For the Mn_{12}-type SMMs, a line has been drawn in the sand which separates out the two sub-classes of this SMM: the slow magnetic relaxers (U_{eff} = ~60-80 K) and fast magnetic relaxers (U_{eff} = ~25-45 K).[24]

2.1.2.3 Magnetic Changes from Subtle Structural Differences

It is difficult to over-emphasize the sensitivity of the magnetization of superparamagnetic SMM materials. As indicated earlier, much of a SMM's magnetic behavior is heavily influenced by spin state values and local symmetry; changes and perturbations to these parameters will cause changes in the overall magnetic behavior; even minute structural changes will influence the magnetic behavior. A SMM's magnetization can serve as a fingerprint for the specific compound.

One example of how minute physical influences alter the magnetization is demonstrated by two analogous Mn_{12}-type clusters that exhibit an equatorial orientation, as opposed to the normal axial orientation, of at least one elongated JT axis relative to Mn_{12}-Acetate. In the Mn_{12}-type complexes, $Mn_{12}O_{12}(O_2CCH_2Bu^t)_{16}(H_2O)_4$, and $Mn_{12}O_{12}(O_2CC_6H_4$-*p*-$Me)_{16}(H_2O)_4$, the barrier to magnetization was calculated as U_{eff} = 43 K, and U_{eff} = 38 K, respectively.[5] This behavior bewildered researchers for some time until the effect was simply tied to the equatorial orientation of the JT elongated Group III Mn^{III}-O bonds (**Figure 2.1.5**).[25] Further explanation of this feature attributed the cause to increased tunneling accessibility below the classical 'over the barrier' height due to reduced Mn^{III} specific site-symmetry.[22]

These effects have been associated solely with the Group III, water coordinated Mn^{III} ions, with at least one JT elongated axis laying equatorial to the axis of symmetry, rather than being axial (**Figure 2.1.5**).[8, 22, 25-26] This effect has been coined 'Jahn–Teller isomerism' and is defined simply as two or more non-equivalent distorted forms differing in the relative orientation of one (or more) JT axes.[25]

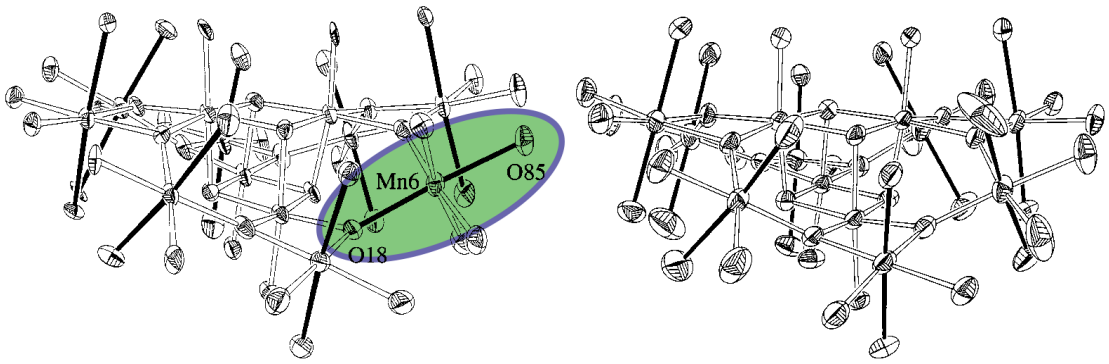

Figure 2.1.5 Two analogous Mn_{12}-type isomers with a single difference in elongated JT axis (black bars) orientation, equatorial versus axial. *Left*, $Mn_{12}O_{12}(O_2CCH_2Bu^t)_{16}(H_2O)_4$, showing equatorially oriented JT axes, Mn6-O18: 2.073(7) Å, Mn6-O85: 2.160(8) Å. *Right*, Mn_{12}-Acetate, showing normal axially oriented JT axes. Figure adapted from reference 25.

In addition, two solvates of the Mn_{12}-type compound, $Mn_{12}O_{12}(O_2CCHCl_2)_{16}(H_2O)_4$, offer another example of how the magnetic properties of Mn_{12}-type complexes are *extremely* sensitive to coordination and geometric factors. The $\cdot 4CH_2Cl_2 \cdot H_2O$ and the $\cdot 6CH_2Cl_2$ solvates of the above Mn_{12}-type compound, crystallize as plates and needles respectively and display different barriers to magnetization relaxation; U_{eff} 18.5 and 30.3 K for each respectively.[8] Because the elongated JT axes in these compounds are actually axially oriented, the differences reported are attributed directly to the reduced specific site-symmetry at each Mn^{III} JT ion *via* solvation, influencing the overall crystal symmetry.[8] This report helps to emphasize the influence of subtle changes in the coordination environment of the JT Mn^{III} ions on the overall magnetic behavior of Mn_{12}-type SMMs.

Clearly, the magnetic behavior and properties of Mn_{12}-type complexes are very dependent on the chemical environment, local symmetry, and structural description of the complex, i.e., crystallization, packing, solvation, space group (thus, crystalline symmetry). A general, and reliable, distinction is in the overall crystal symmetry, where a proportional link

between symmetry and barrier to magnetic relaxation has been demonstrated.[25, 27-28] It seems evident that almost *any* structural deviation of Mn_{12}-type clusters from the Mn_{12}-Acetate structure are accompanied by an associated change in magnetic behavior.

2.1.2.4 Amplifying Mn_{12}-Acetate's Potential via Acetate Substitution

The Mn_{12}-Acetate cluster as a parent starting material has served as a viable platform to analogous materials; especially *via* the *substitutive* procedure reported in 1993, which describes the exchange of the peripheral acetate groups by dissolution of Mn_{12}-Acetate cluster in the presence of vast amounts of benzoic acid (**Figure 2.1.6**).[1] This report has attracted an incredible number of researchers to the field who have utilized this process as a route to new Mn_{12}-**R** materials.[5-8, 19, 23, 29-51]

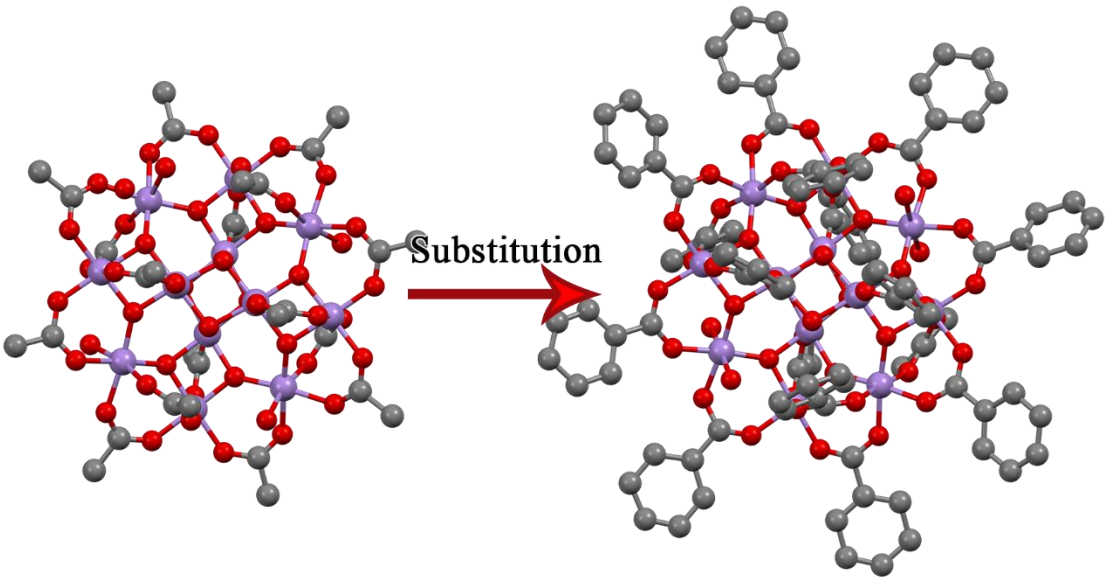

Figure 2.1.6 Showing the substitution of Mn_{12}-Acetate (Refcode: AQACMN)[3] to Mn_{12}-Benzoate (Refcode: KAGLEJ).[1] Mn_{12}-Benzoate rotated slightly to match Mn_{12}-Acetate on the C-axis. Hydrogens omitted for clarity.

Mechanistically, it has been found that the reliable and complete substitution of the acetate groups with a different carboxylate is closely linked to the acidity of the incoming carboxylic acid. In these systems the equilibrium is shifted towards the production of the weakest acid.[52-53] Additionally, the axial carboxylates, compared to their equatorial counterparts, tend to be more prone to substitution by less acidic incoming carboxylic acids.[54-56] Although there is a tendency towards axial, over equatorial, acetate appropriation, it has been shown that the generation of mixed-ligand Mn_{12}-type derivatives results in both axial and equatorial positions being substituted,[26, 57] so a fully conclusive determination of ligand substitution behavior is still being discussed. Besides ligand behavior, the solubility of the Mn_{12}-Acetate compound is an issue that is considered when substituting with various carboxylates. Intriguingly, a different 'double' substitutive strategy may be employed in instances where insolubility is a problem. Here, the *tert*-butyl Mn_{12}-type derivative compound, $Mn_{12}O_{12}(O_2C^tBu)_{16}(H_2O)_4$, is utilized as the starting material to other substituted Mn_{12}-**R** compounds, because the *tert*-butyl group strongly increases the solubility of the manganese cluster in organic solvents.[24, 58]

Apart from carboxylate substitution, other methods have been employed in order to generate new and exciting manganese oxide clusters through the direct utilization of Mn_{12}-Acetate as a starting material; such as in the generation of the convoluted, Mn_{30}-type cluster,[18-19, 59-61] and the massive Mn_{84}-type, torus-shaped (donut), cluster (**Figure 2.1.7**).[18-19, 62]

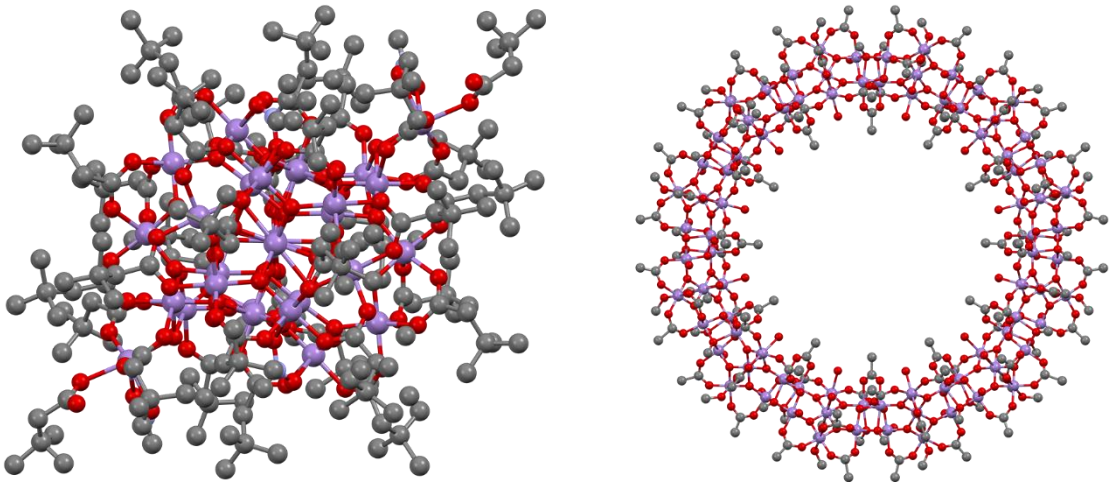

Figure 2.1.7 Generation of some different Mn_xO_y compounds from the use of Mn_{12}-Acetate as a starting material. *Left*, the Mn_{30} cluster (Refcode: ISEXIN).[61] *Right*, the Mn_{84} torus cluster (Refcode: BEQXEB).[62]

It is without question that Mn_{12}-Acetate is one of the most extensively studied SMMs; if one includes its various analogues, it is possibly one of the most studied materials in general; certainly in the same popularity echelon of metal oxide materials such as ZnO. In virtue of raw research interest, the initial report of Mn_{12}-Acetate has been referenced at least 1057 times and the report concerning the facile substitution of the acetate groups to benzoate has been referenced at least 1968 times, and new articles pop up to this day.

2.1.3 A Steric Approach to New Materials

The Mn_{12}-Acetate material has garnered the attention and support from so many different research fields and manages to stay relevant even 40 years after its initial discovery. Shockingly, considering the massive amount of effort that has gone into substituting the peripheral carboxylates of Mn_{12}-Acetate, no research group has attempted to combine the basic principles of sterics and supramolecular chemistry with the ease of ligand substitution of Mn_{12}-Acetate. A search on Scopus and SciFinder, utilizing various combinations of the terms “bulky”, “steric”,

"Mn12", and "substitution" resulted in just two publications that only have a cursory connection to sterics or supramolecular chemistry.[23, 63] It is based on this apparent gap in the research that we move into the field of Mn_{12}-**R** substituted clusters. Certainly, there are other μ_2-oxo carboxylate bound metal oxide complexes that may also deserve similar attention; but due to the readily accessible and extensive research on this type of cluster, we proceed with a focus on the substitution of Mn_{12}-Acetate.

To that end, as a group we have been very motivated by a previous discovery in the Beatty lab that a layered cadmium chloride complex will be transformed from 2-D to 0-D by systematically varying the size of the *ortho*-substituent on the dianilinium counterion (**Figure 2.1.8**).[64-65] Specifically, when the dianilinium counterion of a $[CdCl_6]^{2-}$ layer features a hydrogen substituent *ortho* to the amine functionality, a typical 2-D perovskite layer is formed. When the substituent *ortho* to the amine group is increased in size from hydrogen to methyl, a structural effect is observed as the layer morphs into an 'expanded' 2-D layer, where the average Cd-Cl distance increases by one angstrom. The expansion of the layer is attributed to the steric bulk of the methyl group pushing onto the layer. Proceeding from methyl, increasing the substituent size to ethyl results in an even more drastic change as the layer completely collapses, and a hexameric cluster is formed. This was a very exciting result indeed as cadmium-halide clusters are generally encountered very rarely, and additionally, only one other chlorocadmate structure of that type is found in the CSD.[66-67]

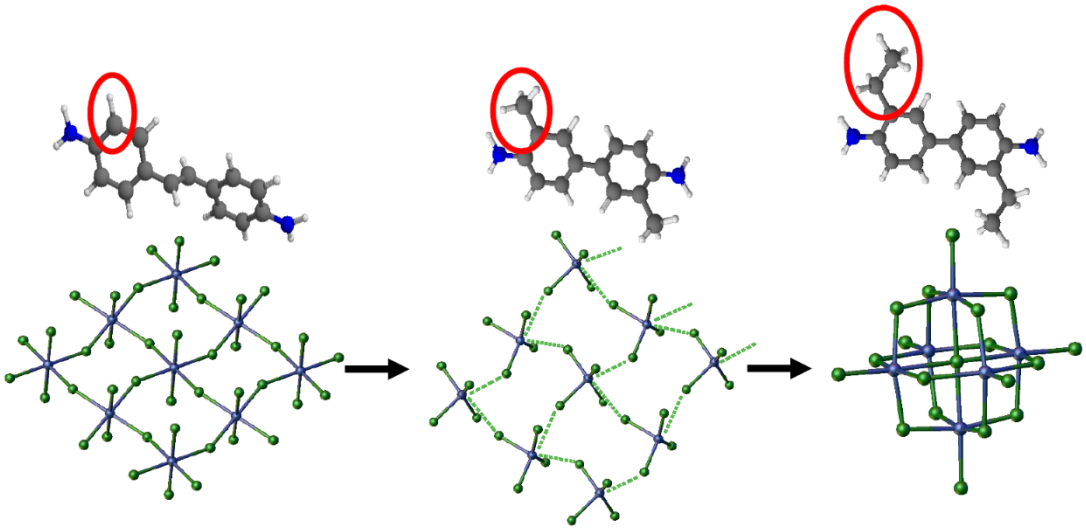

Figure 2.1.8 Influential structural ramifications *via* increasing the size of an *ortho*-substituent. Showing the expansion of a 2-D cadmium chloride perovskite layer, from *left* to *middle*, followed by the collapse of the layer, and formation of a 0-D hexameric Cd-Cl cluster, from *middle* to *right*, based on the size of the *ortho*-substituent of the dianilinium counter ion.

It is based on these results that we seek to apply the same concept to metal oxide clusters, and in particular the Mn_{12}-Acetate cluster. The Mn_{12}-Acetate cluster is surface-saturated with peripheral carboxylate groups which also serve as critical μ_2-oxo-bridges for the complex. By replacing the acetate moiety on the Mn_{12}-Acetate cluster with benzoic acid, we introduce to the system a modular and substitutable platform, allowing for thoughtful and rational structural modifications. In particular, increasing the size of the substituent at the *ortho*-position of benzoic acid will isolate the influence of steric bulk to the core of the Mn_{12}-type cluster. We hope to accomplish this investigation by systematically substituting the acetate groups on Mn_{12}-Acetate with various *ortho*-substituted benzoic acids of progressively increasing size (**Figure 2.1.9**).

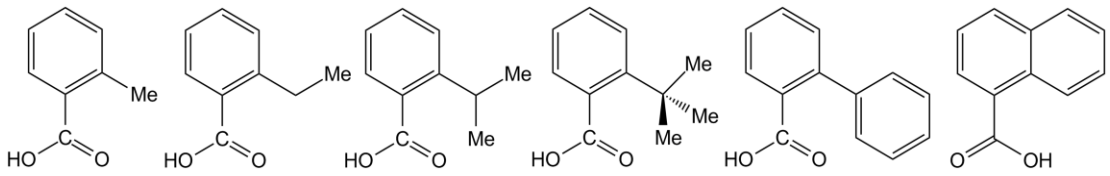

Figure 2.1.9 A series of *ortho*-substituted benzoic acids, and one naphthoic acid, of systematically increasing size.

2.1.3.1 Maximizing the Potential Steric Effect *Via Ortho*-Substituent Positioning

By focusing on the *ortho* position, the substitutable position of benzoates closest to the core of the cluster, we increase the likelihood of imparting a structural change relative to the Mn_{12}-Acetate cluster. The *meta* and *para* positions are not considered for this study due to their distance from the oxo-bridge, therefore having a low probability of affecting the size and shape of the cluster (**Figure 2.1.10**). By applying steric pressure to a critical structural zone of the Mn_{12}-type cluster, we seek to investigate the steric impact on the cluster's shape, and also the extent of such an impact, by systematically increasing the size of the *ortho*-substituent of benzoic acid. The extent of the steric physical impact on the cluster will be analyzed and charted by use of X-ray crystallography *via* comparison of the relevant bond angles and distances of the modified structure to the parent Mn_{12}-Acetate molecule.

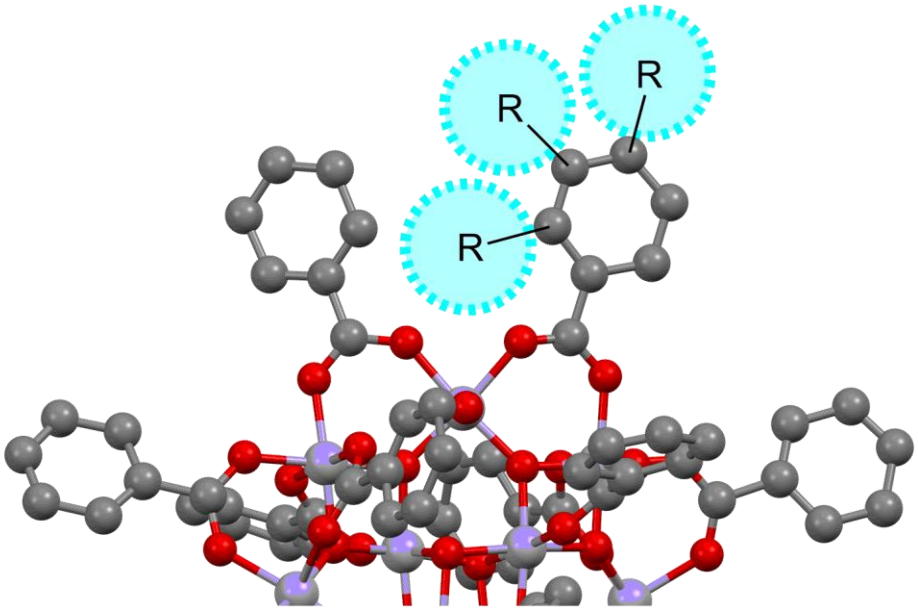

Figure 2.1.10 Demonstrating the proximity of different substitution positions relative to the Mn_{12}-type core, in this case Mn_{12}-Benzoate (Refcode: KAGLEJ).[1] Hydrogens removed for clarity.

2.1.3.2 A Role in Structure/Function Relationship

In addition to the chemical impact on the cluster, we also seek to establish a structure/function relationship between the physical changes imparted by the various substituted benzoic acids on the SMM behavior of the material. As described previously and in Chapter 1, the site-symmetry and the alignment of the Mn^{III} Jahn-Teller axis with the molecular Z-axis has a significant impact on the easy-axis type magnetic anisotropy (D value), as well as the quantum tunneling of the compound.[47, 68-72] Slight modification of those axes will result in a change in magnetic behavior as indicated by the Hamiltonian which describes the functional parameters of the Mn_{12}-type SMM. Due to the labile nature of the ligands on a JT active Mn^{III} ion, coupled with the established magnetic sensitivity of the Mn_{12}-type SMM; it is extremely likely that a notable difference in magnetic behavior will be encountered when substituting acetate with a systematic series of bulkier *ortho*-substituted benzoates.

We see above that a reduction of symmetry, and the positioning of the elongated Mn-O bond in JT influenced Mn^{III} ions, causes a lowering of the barrier to magnetization, U_{eff}, relative to the parent Mn_{12}-Acetate compound. We focus on these effects as we progressively substitute the carboxylates, the structural changes we introduce should be reflected in the U_{eff} parameter of the material.

2.1.4 The Objective

To reiterate the objectives for this part of the work: the approach is to modify the existing Mn_{12}-Acetate cluster by substituting the peripheral acetate moieties with *ortho*-substituted benzoic acids of systematically increasing size.

In doing this we hope to impact the Mn_{12}-type core structurally through sterics (i.e., bond angles and distances, coordination environment, etc.). Further, we hope to influence the formation of completely different clusters of formula Mn_xO_y *via* this method as the steric bulk increases. The magnetic behavior of the substituted compounds will also be determined, and will be compared to the parent Mn_{12}-Acetate complex. Changes in the magnetic behavior will be linked to the established structural changes.

Structurally, based upon what we have observed as a group in earlier Cd-Cl work, the **hypothesis** is that the smaller *ortho*-substituents will slightly impact the structure of the compound (e.g., methyl, ethyl), and the larger substituents (e.g., isopropyl, *tert*-butyl, phenyl) will affect the shape of the cluster, perhaps resulting in a different cluster altogether.

Magnetically, based upon what has been previously reported regarding Mn_{12}-type clusters the **hypothesis** is that the substitutive treatments of Mn_{12}-Acetate which result in new Mn_{12}-**R** *ortho*-benzoates will show canon Mn_{12}-type SMM behavior, but at a lower U_{eff} due to a reduction of symmetry in the compound, i.e., substituting acetate for an asymmetric benzoate. However, the substitutive treatments of Mn_{12}-Acetate which result in completely new MnO-type clusters will

show different magnetic behavior, which is difficult to preemptively predict due to the complex nature of superexchange coupled metal oxides.

Herein, we discuss the work on Mn_{12}-type substitution compounds!

2.2 Experimental

All chemical reagents, with the exception of 2-ethylbenzoic acid, were used as received from Sigma-Aldrich without further purification. 2-ethylbenzoic acid was purchased from Combi-Blocks and used as received. All solvents used were distilled prior to use. Water was freshly prepared from a Milli-Q® Integral Water Purification System. All crystallization was performed at room temperature in a low-vibration area. Melt point data were collected on an OptiMelt Automated Melting Point System operating in the range of 28-380 °C at a rate of 2.5 °C per minute. Additional X-ray crystallographic tables can be found in Appendix II.

2.2.1 Synthesis and Substitution of Mn_{12}-Acetate, 1

Synthesis of Mn_{12}-**R** acetate substituted materials is achieved through the initial generation of the Mn_{12}-Acetate parent compound, **1**, $Mn_{12}O_{12}(O_2CMe)_{16}(H_2O)_4$ (**Scheme 2.2.1**), followed by two passes of the substitution treatment to the slurried material in the presence of desired carboxylic acid in molar excess (**Scheme 2.2.2**). Generally, **1** is slurried in 25 mL of dichloromethane, at which point a carboxylic acid is added in 32:1 molar ratio to Mn_{12}-Acetate, resulting in a dissolved solution. The solution is left to stir for 24 hours then filtered. To the filtrate is added hexanes until a brown precipitate forms. The collected precipitate undergoes the previous treatment a second time; it is stirred 24 hours with excess added carboxylic acid, filtered, then layered with hexanes. This solution, left to sit for days, forms microcrystals which are then separated, dissolved in dichloromethane, and recrystallized in a test tube under a layer of hexane (**Figure 2.2.1**).

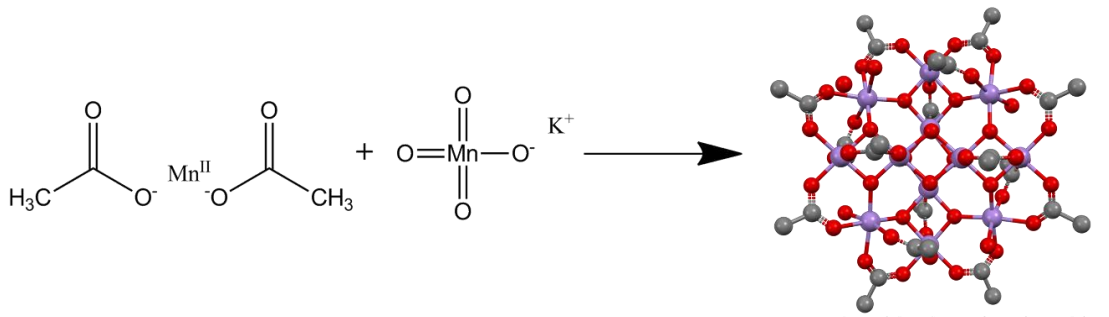

Scheme 2.2.1 Synthesis of Mn_{12}-Acetate parent compound, **1** (Refcode: AQACMN).[3] Hydrogens removed for clarity.

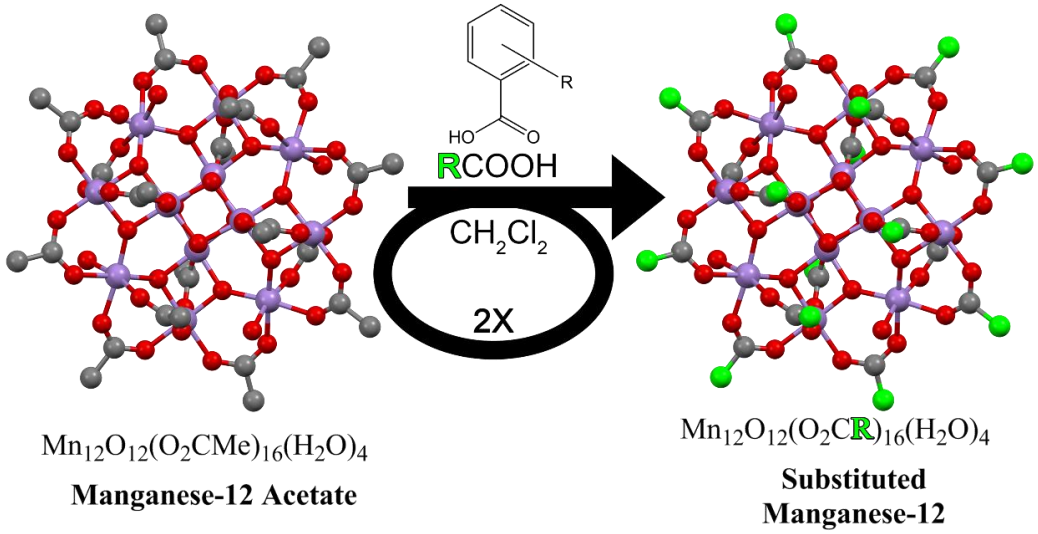

Scheme 2.2.2 Substitution of Mn_{12}-Acetate parent compound, **1** (Refcode: AQACMN),[3] with *ortho*-substituted benzoic acid (Refcode: KAGLEJ).[1] Hydrogens removed for clarity.

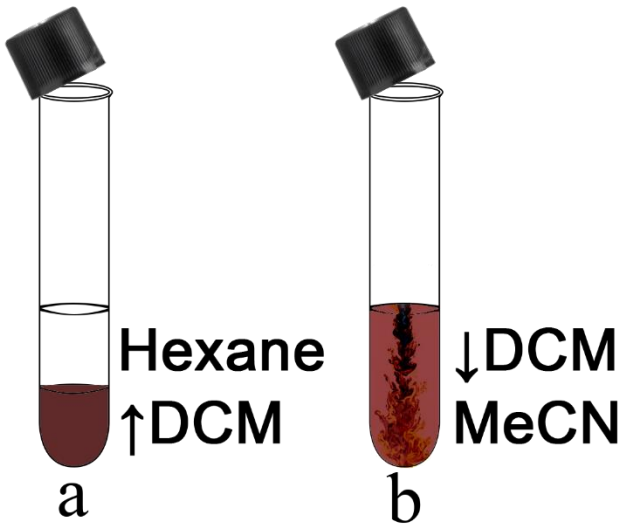

Figure 2.2.1 Layered solvent crystallization strategies for substituted Mn_{12}-type compounds. *Left*, **a**, where the dichloromethane dissolved MnO compound is slowly pipetted underneath the hexane layer (pushing the hexane layer up due to density). *Right*, **b**, where the dichloromethane dissolved MnO compound is slowly layered on top of the acetonitrile layer, and slowly diffuses through the solvent.

2.2.2 Synthesis of Mn_{12}-R Compounds 1-4

Synthesis of Mn_{12}-Acetate, **1**. Synthesis of **1** is performed as previously described,[3] with minor modifications. To 40 mL of 60% acetic acid is added 4 grams of $Mn(CH_3COO)_2 \cdot 4H_2O$. The mixture is stirred at room temperature until complete dissolution is achieved. 1 gram crystalline $KMnO_4$ is ground gently and added slowly to the stirring manganese acetate solution over 2 minutes. The solution is left to stir for an additional 1 minute, and promptly removed from stirring, and set aside for 3 days to form black rods of **1** in 57.1% yield; no additional heat is required. *Leaving reacted solution stirring for longer periods than 1 minute results in the formation of powders instead of crystals*.

Synthesis of Mn_{12}-2-Methyl, **2**. Generation of compound **2** is performed as previously described,[1] with some nuances. 250 mg (.125 mmol) of complex **1** is slurried in 20 mL of freshly distilled dichloromethane. To this suspension is added 545 mg (4 mmol) *o*-toluic acid under strong stirring. Dissolution into a dark brown solution occurs within 30 minutes of adding *o*-toluic acid, and the solution is left to stir for 24 hours; at which point the solution is filtered to remove undissolved solid. 200 mL hexanes is added to the filtrate until a brown precipitate forms. This mixture is allowed to sit refrigerated for a number of days until the supernate becomes clear. This solid is separated by filtration, washed with methanol then redissolved in 20 mL freshly distilled dichloromethane. *Failing to wash the penultimate solid with methanol will result in powder and not crystalline material*. The process is repeated by adding 545 mg (4 mmol) *o*-toluic acid and allowing to stir for an additional 24 hours. When adding hexanes to this solution, a brown precipitate will not immediately form; however, black microcrystals of **2** will form as the dark solution becomes clear over two days in 61.4% yield. To form dark brown crystal rods of **2**, 20 mg of microcrystalline **2** is dissolved in 1 mL pure dichloromethane and layered with 3 mL *n*-hexane, by slowly pipetting the solution 'under' the hexane level, in a lightly capped test tube (**Figure 2.2.1a**), forming X-ray quality crystal rods after days.

Synthesis of Mn_{12}-2-Ethyl, **3**. Synthesis of **3** is carried out generally following previously reported substitutive routes,[1] though with heavy modification. 250 mg (.125 mmol) of **1** is added to 10 mL freshly distilled dichloromethane and stirred. To this slurry is added 601 mg (4 mmol) of 2-ethylbenzoic acid and the dissolved solution is allowed to stir for 24 hours. The solution is filtered to remove undissolved solid and 100 mL hexanes is added to the filtrate. This solution is brought to dryness by rotavapor and the solid is transferred to a flask and redissolved in 10 mL fresh dichloromethane. A second treatment of 601 mg (4 mmol) 2-ethylbenzoic acid is added to the flask and is allowed to stir for an additional 24 hours. The solution is filtered, and to it is added 100 mL hexane. The solvent is again removed by rotavap, and to the dried solid is added

100 mL acetonitrile. This mixture is swirled until dissolution is achieved and then filtered. The filtrate is left to stand refrigerated for 2 days, at which point small black microcrystals of **3** shall form in 59.7% yield. To form crystals of **3**, 20 mg of microcrystalline **3** is dissolved in 1 mL distilled dichloromethane, layered on top of 3 mL freshly distilled acetonitrile, slowly diffusing through the solution, and lightly capped (**Figure 2.2.1b**). Small brown X-ray quality cubes shall form after one week.

Synthesis of Mn_{12}-2-Phenyl, **4.** Synthesis of complex **4** is performed as described previously.[1] To a slurried suspension of 250 mg (.125 mmol) compound **1** in fresh dichloromethane is added 793 mg (4 mmol) biphenyl-2-carboxylic acid under vigorous stirring. This solution is left to stir for 24 hours, at which point it is filtered to remove undissolved solid. 200 mL hexanes is added to the filtrate until a light brown precipitate is formed. This mixture is allowed to stand refrigerated for a number of days until the supernate becomes clear. The light brown solid is collected *via* filtration, redissolved in 20 mL distilled dichloromethane, and undergoes a second 24-hour treatment following addition of 793 mg biphenyl-2-carboxylic acid. Subsequent addition of 200 mL hexanes to the filtrate will not immediately form a light brown powder; however, when left to stand in refrigerated conditions, black microcrystals of **4** will form as the dark solution becomes clear in 58% yield. To form dark brown crystal rods of **4**, 20 mg of microcrystalline **4** is dissolved in 1 mL pure dichloromethane and layered with 3 mL *n*-hexane, by slowly pipetting the dissolved solution 'under' the hexane level, in a lightly capped test tube (**Figure 2.2.1a**), forming X-ray quality crystal rods after days.

2.2.3 Solvothermal Treatment of Mn_{12}-R Complexes

The procedure for the solvothermal treatment of substituted Mn_{12}-type was inspired from established literature protocols,[73] with slight modification. Generally, a sample of a crystalline manganese oxide cluster is added to a Parr Bomb in acetonitrile; additional molar amounts of

carboxylic acid may be also added. The sealed container is placed in an oven, slowly heated up to soak for hours, then slowly cooled to room temperature over hours.

2.2.3.1 Solvothermal Transformation of 4

Generation of Mn_{13}-2-Phenyl, **5**. 50 mg of freshly grown crystals of **4** are added to a 20 mL capacity Parr Bomb containing 5 mL of 1:1 isopropanol/acetonitrile. The reactor is sealed and placed in a programmable oven set to slowly ramp up to 120 °C over 4 hours, soak for 12 hours, and cool to room temperature over 12 hours (**Scheme 2.2.3**). After the solvothermal process, reddish brown cubes of **5** are isolated. This material may be recrystallized in dichloromethane/hexane to form larger X-ray quality crystals (**Figure 2.2.1a**).

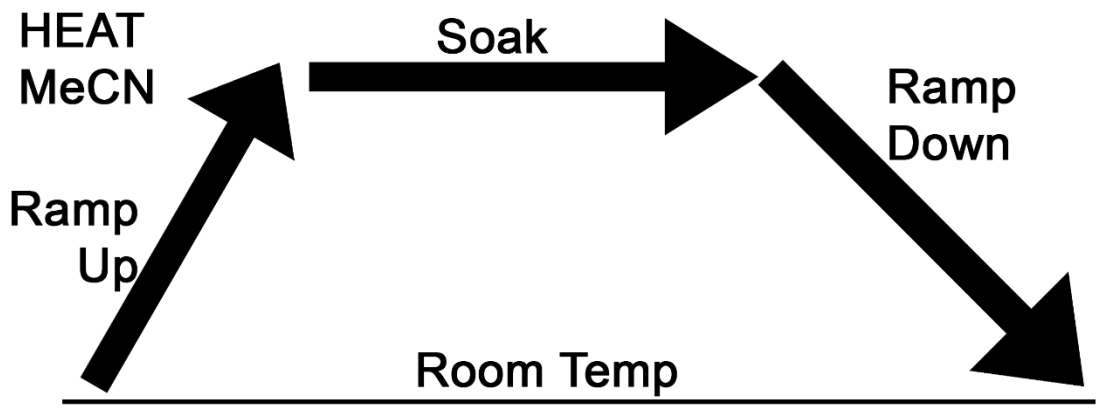

Scheme 2.2.3 General method for solvothermal treatment of Mn_{12}-**R** compounds. Solvent, ramp up rate, soak temperature and time, and ramp down rate may vary widely for different results.

2.2.4 High-Field Magnetism Measurements

Magnetization measurements were conducted on 28.4 mg of powdered **2**, and 17.1 mg of powdered **4**, using a Quantum Design Superconducting QUantum Interference Device (SQUID) magnetometer, MPMS-XL. Zero-field-cooled (ZFC) and field-cooled (FC) measurements were performed under a constant direct-current (DC) magnetic field of 100 Oe, over the temperature range of 1.8-300 K. Alternating-current (AC) magnetic susceptibility measurements were carried

out under a zero DC bias field, with the frequency of the AC field varied from 1 to 1000 Hz, at a temperature range of 1.8-20 K. Hysteresis measurements were performed at 1.8 K.

The sample holders were measured separately under identical conditions, and their magnetic response was subtracted directly from the raw data. The intrinsic diamagnetic response of the sample was calculated using Pascal's constants and subtracted from the measured susceptibilities.[74-75]

2.2.5 X-Ray Crystallography

Crystalline samples of **2-5** were suspended in Paratone oil and subsequently mounted on a MiTeGen dual-thickness microloop. All data were collected using a Bruker Kappa or SMART Apex II X-ray diffractometer. A graphite monochromated Mo Kα (λ = 0.71703 Å) radiation at 100 K was used for all samples. Crystal structures were solved utilizing the OLEX2 software package[76] which functions using SHELX protocols.[77] Structure solution was achieved by way of direct methods and refined using least squares minimization which are both part of the SHELX-97 package. Brief crystal data for each compound is tabulated in **Table 2.2.1**, full sets of crystallographic tables for each compound may be found in Appendix II.

Compound	1	2	3	4
Mol. Formula	$C_{32}H_{56}Mn_{12}O_{48}$	$C_{122}H_{108}Mn_{12}O_{50}$	$C_{144}H_{145}Mn_{12}O_{48}$	$C_{208}H_{168}Mn_{12}O_{48}$
Mol. Weight	1868.01	3036.38	3302.87	4094.70
Crystal System	Tetragonal	Monoclinic	Triclinic	Monoclinic
Space Group	I-4	C2/c	P-1	C2/c
***a* (Å)**	17.319(9)	17.3264(8)	17.7643(19)	34.202(19)
***b* (Å)**	17.319(9)	38.0559(18)	17.928(2)	21.044(10)
***c* (Å)**	12.388(7)	21.1395(10)	24.134(3)	27.235(12
α (°)	90.0	90.0	95.187(6)	90.0
β (°)	90.0	97.742(3)	95.815(6)	105.28(3)
γ (°)	90.0	90.0	92.413(7)	90.0
Volume (Å^3)	3715.75	13811.7(17)	7604.9(15)	18910(16)
Z	2	4	2	4
T (K)	295	100.1	100(2)	100.08
Ref. Measured	-	52449	89012	112944
Unique Ref.	-	5997	19724	17245
R_{int}	-	0.0597	0.0749	0.1473
R_1 [I > 2σ(I)]	0.0340	0.0738	0.1476	0.0788
wR_2 [I > 2σ(I)]	0.0340	0.2071	0.3790	0.2302

Compound	5
Mol. Formula	$C_{156}H_{108}Mn_{13}O_{38}$
Mol. Weight	3208.04
Crystal System	Monoclinic
Space Group	$P2_1/c$
***a* (Å)**	26.087(2)
***b* (Å)**	17.3638(15)
***c* (Å)**	33.476(3)
α (°)	90.0
β (°)	111.604(3)
γ (°)	90.0
Volume (Å^3)	14098(2)
Z	4
T (K)	100(2)
Ref. Measured	143201
Unique Ref.	29136
R_{int}	0.0854
R_1 [I > 2σ(I)]	0.0936
wR_2 [I > 2σ(I)]	0.2760

Table 2.2.1 Table of crystallographic data for compounds **1**-**5**

2.3 Results

The treatment of **1**, Mn_{12}-Acetate ($Mn_{12}O_{12}(O_2CMe)_{16}(H_2O)_4$), with overwhelming molar amounts of various *ortho*-substituted benzoic acids resulted in three distinct Mn_{12}-**R** substituted compounds: **2**, Mn_{12}-2-Methyl ($Mn_{12}O_{12}(O_2CPh\text{-}o\text{-}Me)_{16}(H_2O)_4$), *via* the substitution of acetate with *o*-toluic acid; **3**, Mn_{12}-2-Ethyl ($Mn_{12}O_{12}(O_2CPh\text{-}o\text{-}Et)_{16}(H_2O)_4$), *via* the substitution of acetate with 2-ethylbenzoic acid; and **4**, Mn_{12}-2-Phenyl ($Mn_{12}O_{12}(O_2CPh\text{-}o\text{-}Ph)_{16}(H_2O)_4$), *via* the substitution of acetate with biphenyl-2-carboxylic acid.

The subsequent treatment of **4** with high heat and pressure in a Parr Bomb resulted in the Mn_{13}-type solvothermal compound, **5**, Mn_{13}-2-Phenyl ($Mn_{13}O_{14}(O_2CPh\text{-}o\text{-}Ph)_{12}$).

2.3.1 Mn_{12}-2-R Substituted Compounds

The generation of compound **2** *via* the procedural substitution of **1** with *o*-toluic acid was eventually achieved. Some troubleshooting was required over the reported synthetic methods, as indicated in the synthesis section; but crystals of **2** were eventually reliably synthesized, albeit in low yields. X-ray crystallography reveals the canon Mn_{12}-type cluster featuring peripheral *ortho*-methyl substituted benzoic acids (**Figure 2.3.1**). Compound **2** crystallizes in a monoclinic space group, and is of lower symmetric order than its Mn_{12}-Acetate (tetragonal) parent. Visually, the cluster does not appear different than the Mn_{12}-Acetate parent structure, other than the 2:2 water isomeric form, where two waters molecules are coordinated to two Mn^{III} ions at the 3 and 9 o'clock positions. Slight occupancy errors are apparent in the crystal structure, but these effects are isolated to the freely rotating peripheral benzoates and do not impact the MnO core.

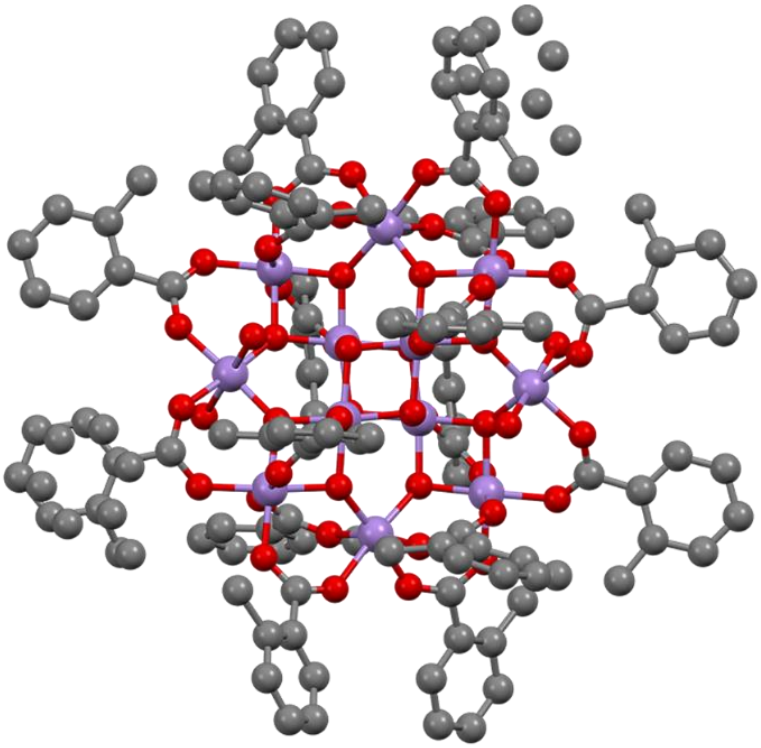

Figure 2.3.1 The substituted Mn_{12}-2-Methyl, compound **2**. Viewed down the B-axis. Hydrogens removed for clarity.

Generation of compound **3** *via* the substitution of **1** with 2-ethylbenzoic acid proved to be a challenging process. Extensive deviation from previously reported substitutive routes was required to finally generate the intended product, at low yields. X-ray diffraction data of crystals of **3** reveals the canonical Mn_{12}-type cluster, encompassed by *ortho*-ethyl substituted benzoates (**Figure 2.3.2**). Compound **3** putatively crystallizes in the triclinic space group, lower symmetry than the Mn_{12}-Acetate (tetragonal) parent. As with **2**, this compound can be identified as the 2:2 water isomer through visual inspection of the Mn^{III} ions at the 3 and 9 o'clock positions, however, due to the quality of the structure, the positions of two of the water molecules are slightly displaced above the coordinated Mn^{III} ions, but their coordination is likely.

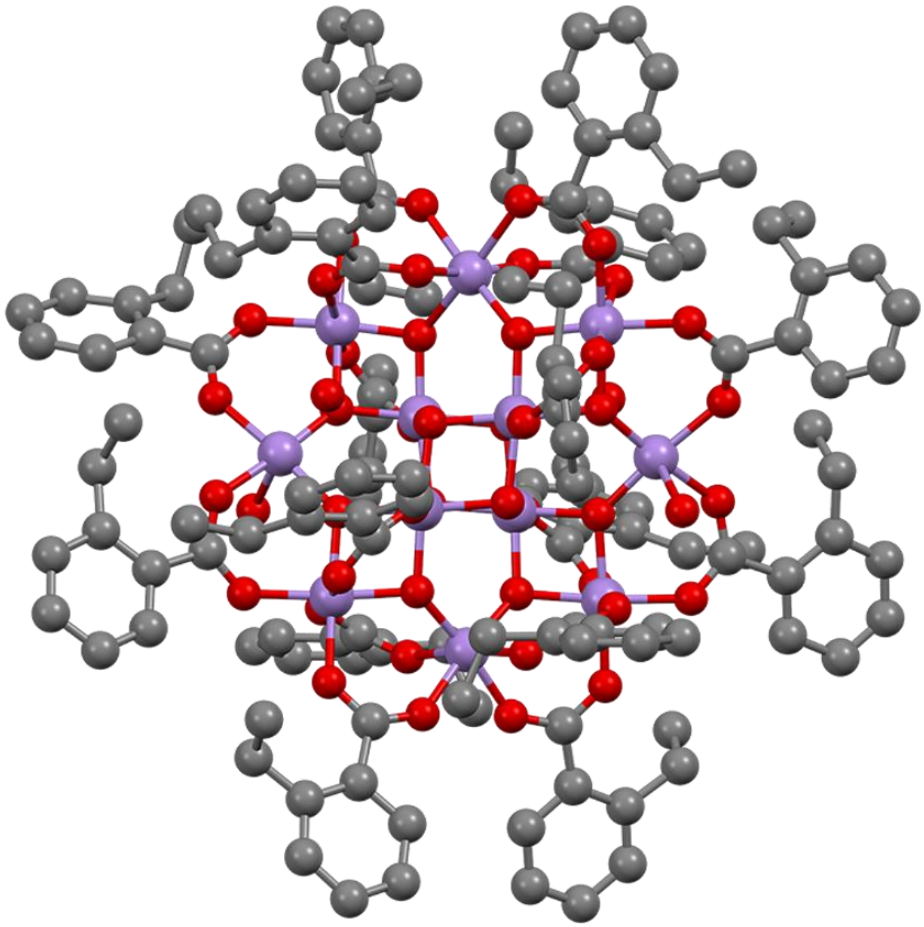

Figure 2.3.2 The substituted Mn_{12}-2-Ethyl, compound **3**. Viewed down the B-axis, rotated 45° about the X-axis, and 10° about the Y-axis. Hydrogens removed for clarity.

The generation of compound **4** *via* the substitutive treatment of **1** cleanly resulted in the desired compound, without deviation from the published procedure. X-ray crystallography reveals an Mn_{12}-type cluster with fully saturated peripheral *ortho*-phenyl substituted benzoates (**Figure 2.3.3**). Compound **4** crystallizes in a monoclinic space group, and is of lower symmetry than the Mn_{12}-Acetate (tetragonal) parent. Here, the 1:2:1 water isomer may be identified by examination of the Mn^{III} ions located at the 3, 6, and 9 o'clock positions where the 6 o'clock position contains two water ligands and the other positions have just one coordinated water.

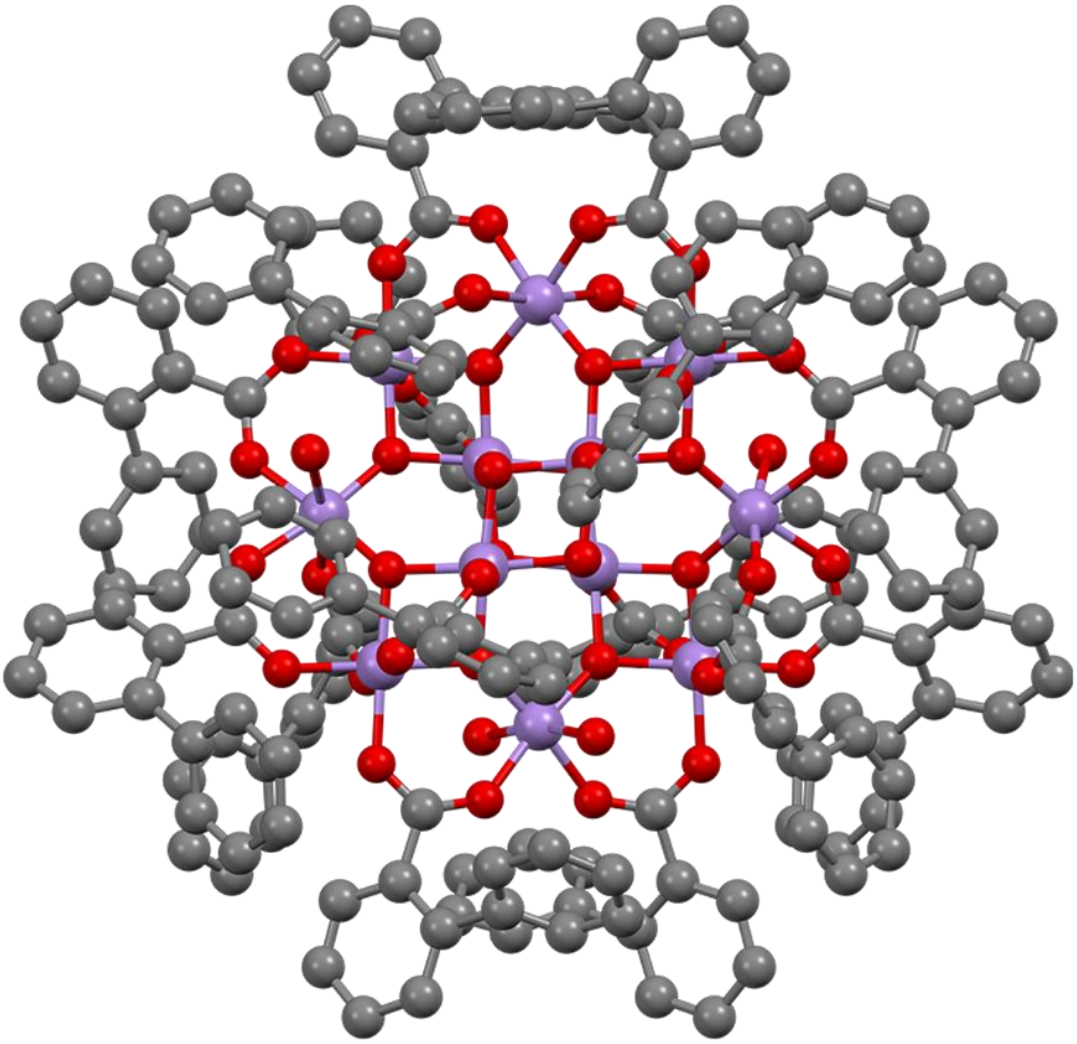

Figure 2.3.3 The substituted Mn_{12}-2-Phenyl, compound **4**. Viewed down the C-axis, rotated 18° about the Y-axis. Hydrogens removed for clarity.

2.3.2 Mn_{12}-2-R Substituted Compounds: Magnetic Susceptibility

Compounds **2** and **4** both display characteristic Mn_{12}-type SMM behavior (see **Appendix V**). Both compounds demonstrate antiferromagnetic superexchange interactions between the Mn^{III} and Mn^{IV} ions at different spin-only values, resulting in an overall ferrimagnetic ordering with S = 10. Additionally, a ligand dependence on magnetization has been identified between **2** and **4**.

Compounds **3** and **5** were only recently discovered and their high-field magnetization has not yet been analyzed by MPMS-XL.

2.3.2.1 Mn_{12}-2-Methyl SMM Behavior

The magnetic properties exhibited by **2** are greatly ligand dependent as revealed by the very different behavior exhibited versus similar Mn_{12}-type clusters. The FC and ZFC measurements performed on **2** under a magnetic field of 0.01 T exhibit no variations between FC and ZFC as seen in **Figure 2.3.4;** though this may be an aberration.

Alternating-current (AC) measurements on **2** were collected within the range of 1.8 to 20 K under an oscillating field of 5 gauss (**Figure 2.3.4**). Out-of-phase frequency dependent χ_M'' signals were found with maxima between 3.0 to 5.2 K for frequencies between 1 and 1000 Hz. The thermal relaxation time of magnetization (τ) obeys the Arrhenius law: $\tau = \tau_0 {}^{(Ueff/kT)}$, where $\tau = 1/2\pi^* \nu$ and k is the Boltzmann constant. The calculated energy barrier, U_{eff}, yielded by the Arrhenius plot is 49 K, shown in the inset.

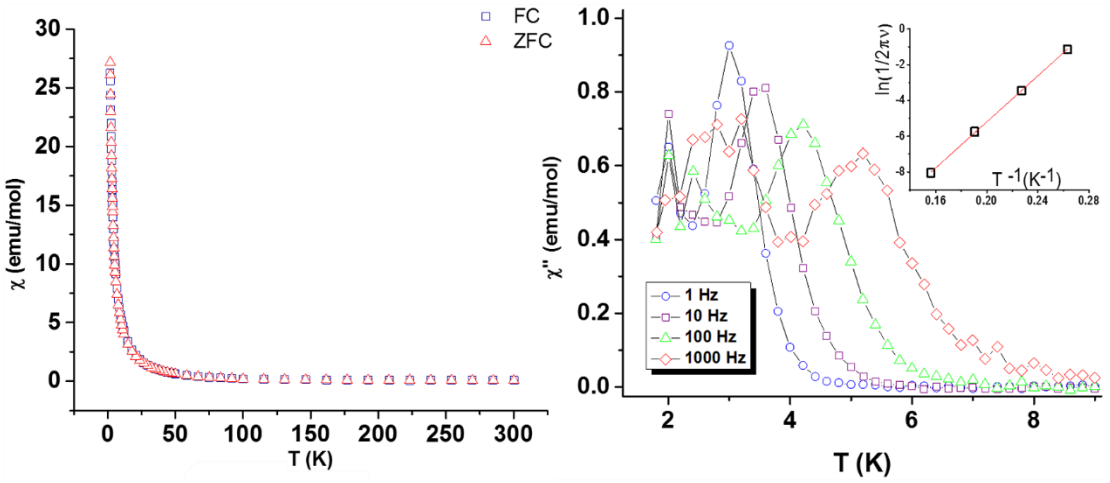

Figure 2.3.4 AC and DC magnetic susceptibility measurements for **2**. *Left*, FC and ZFC, DC susceptibility χ_M' vs. T plots. *Right*, AC susceptibility, χ_M'' vs T at variable frequencies. Inset shows the Arrhenius plot. Double χ_M'' signals in AC data due to intrinsic polymorphism.[29-30, 78]

2.3.2.2 Mn_{12}-2-Phenyl SMM Behavior

For **4** sample, we note that the direct-current temperature dependent susceptibility for the field-cooled and zero-field-cooled measurements under a field of 0.01 T and within the range of 1.8 K – 300 K shows magnetic behavior typical for Mn_{12}-based SMM complexes with a blocking temperature, T_B, around 3 K (**Figure 2.3.5**).

Alternating-current (AC) measurements **4** were collected within the range of 1.8 to 20 K under an oscillating field of 5 gauss (**Figure 2.3.5**). Out-of-phase frequency dependent χ_M'' signals were found with maxima within the range of 3.8 to 6.4 K for frequencies between 1 and 1000 Hz. Maximal χ_M'' arises at a temperature at which the spin relaxation frequency coincides with the external magnetic field frequency, ν. The thermal relaxation time of magnetization (τ) obeys the Arrhenius law: $\tau = \tau_0 {}^{(Ueff/kT)}$, where $\tau = 1/2\pi^* \nu$ and *k* is the Boltzmann constant. The calculated energy barrier, U_{eff}, yielded by the Arrhenius plot is 49 K, shown in the inset.

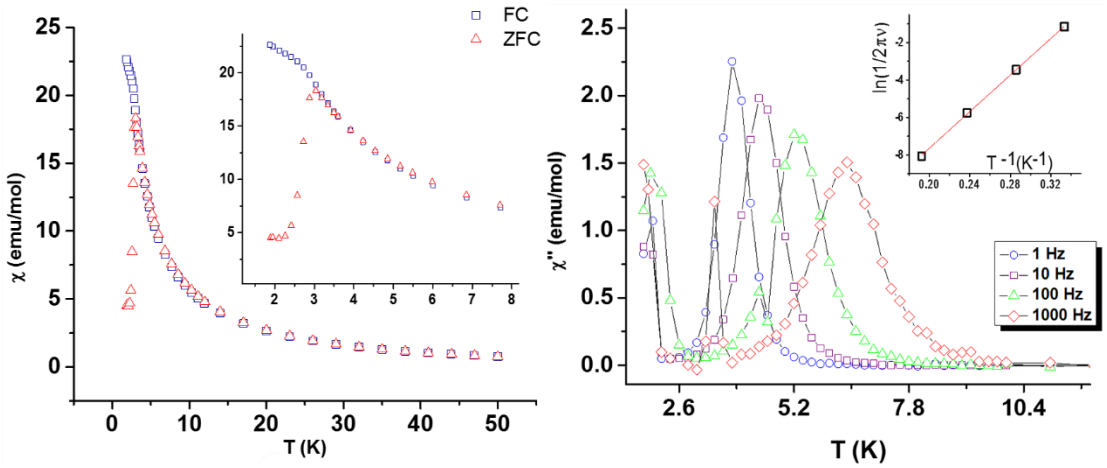

Figure 2.3.5 AC and DC magnetic susceptibility measurements for **4**. *Left*, FC and ZFC, DC susceptibility χ_M' vs. T plots. The inset focuses on the range of 1.8 K to 8 K and shows a blocking temperature around 3 K. *Right*, AC susceptibility, χ_M'' vs T at variable frequencies. Inset shows the Arrhenius plot. Double χ_M'' signals in AC data due to intrinsic polymorphism.[29-30, 78]

2.3.3 Mn_{13}-R Solvothermal Compound 5

Treatment of **4** in a Parr reactor, at high heat and pressure, resulted in the formation of a completely transformed manganese oxide cluster, $Mn_{13}O_{14}(O_2CPh\text{-}o\text{-}Ph)_{12}$ (**Figure 2.3.6**), from the Mn_{12}-2-Phenyl starting material. This MnO cluster is a tridecanuclear, multivalent MnO-type cluster with μ_3- and μ_4-oxo-bridges forming the cluster core, and archetypal peripheral μ_2-oxo-bridging carboxylates. The cluster features polyvalent $Mn^{(II/III/IV)}$ ions: the manganese ion in the center of the cluster is formally Mn^{IV}, and the outer manganese ions are formally Mn^{III} or Mn^{II}.

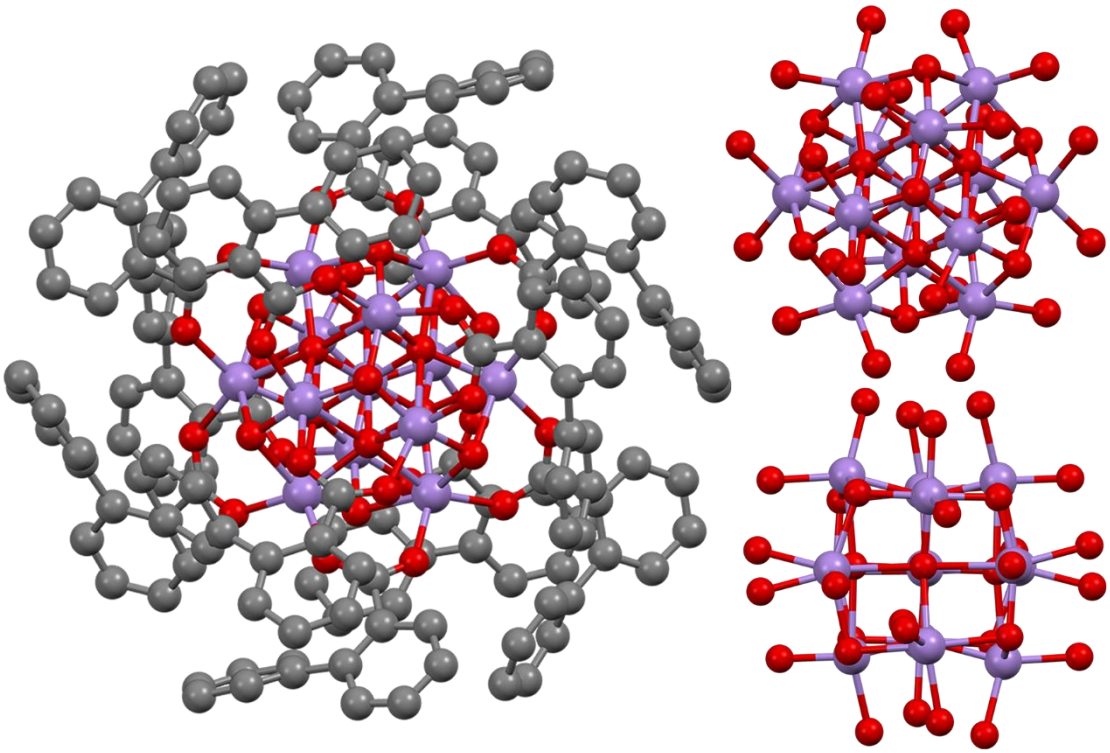

Figure 2.3.6 *Left*, the $Mn_{13}O_{14}(O_2CPh\text{-}o\text{-}Ph)_{12}$ solvothermal compound **5**, generated from solvothermal treatment of **4**. Viewed down the C-axis. *Top Right*, carbons removed for clarity. *Bottom right*, view rotated 45° along the X and Y axes to show the cube-like cluster.

As a result of the solvothermal conditions, the coordinated waters have been completely displaced, and the Mn_{12}-**R** cluster has completely reshaped; this suggests that the Mn_{12}-**R** cluster was disassembled in the reactor, and reformed as the solution cooled. The core of the cluster is remarkable, and can be described as a distorted cube with an $Mn^{II/III}$ ion at every edge, and an oxygen atom at every corner and face of the cube; with an additional Mn^{IV} ion in the center of the cube's core. Interestingly, viewing the core down one of the faces shows the cube-like nature of the core, but viewing down from corner-to-corner of the core gives the cluster a circular/spherical appearance (**Figure 2.3.6**).

This type of type of cluster has been previously reported, and has been described in the literature as a 'supercubane' type MnO cluster (**Figure 2.3.7**).[11, 79]

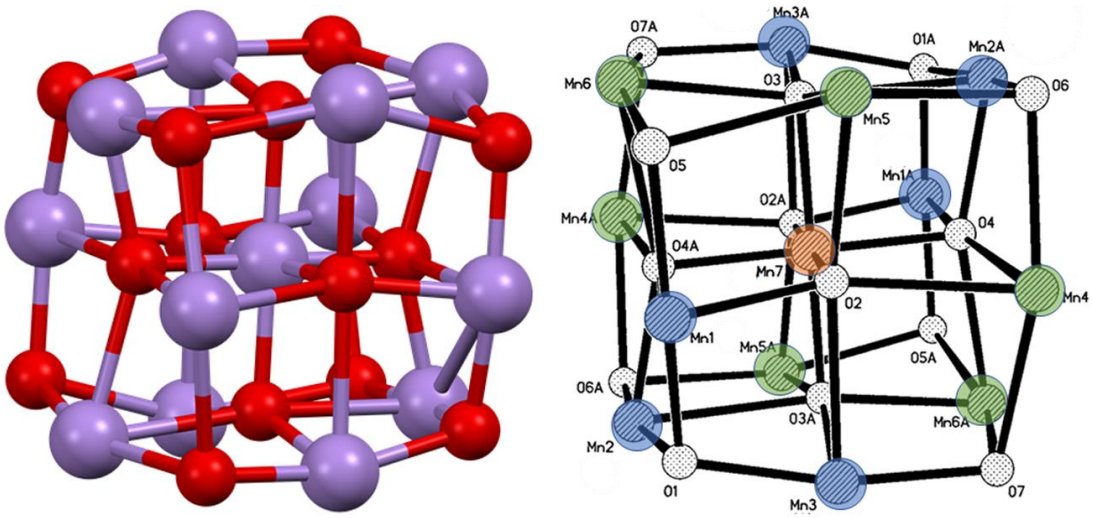

Figure 2.3.7 $Mn_{13}O$ 'supercubane' structure. *Left*, Compound **5**, $Mn_{13}O_{14}(O_2CPh\text{-}o\text{-}Ph)_{12}$. *Right*, previously reported Mn_{13}-supercubane structure.[11] Green circles highlight Mn^{II} ions, blue circles highlight Mn^{III} ions, red circle in center highlights Mn^{IV} ion. Figure adapted from reference 11.

2.4 Discussion

The results indicate that three Mn_{12}-**R** substitution compounds and one Mn_{13}-Supercubane compound, through the solvothermal treatment of one Mn_{12}-**R** compound, were generated. We proceed to discuss the implications of these results.

2.4.1 Mn_{12}-2-R Synthetic Potential *Via* Substitutive Routes

In the concluding remarks of Chapter 1, this work's intent to utilize a series of benzoic acids featuring systematically enlarging *ortho*-substituents was followed by two questions, the first simple: can we substitute the small peripheral acetate groups on the polynuclear manganese oxide cluster, Mn_{12}-Acetate, with this series of benzoic acids?

Based on the X-ray crystal structure data, we were indeed able to synthesize new Mn_{12}-**R** substituted clusters *via* the application of previously established substitutive routes. We may now confront the next proposed question.

2.4.2 Evaluation of Structural Differences from Parent Compound

The *first* part of the second question poses a simple inquiry: can we observe and evaluate any structural differences between the new complexes and the parent complexes. To begin, we shall start at the qualitative level. By viewing the molecules side by side, and overlaying the core of the Mn_{12}-Acetate parent cluster over the Mn_{12}-**R** clusters, a better evaluation of the situation is possible (**Figure 2.4.1**).

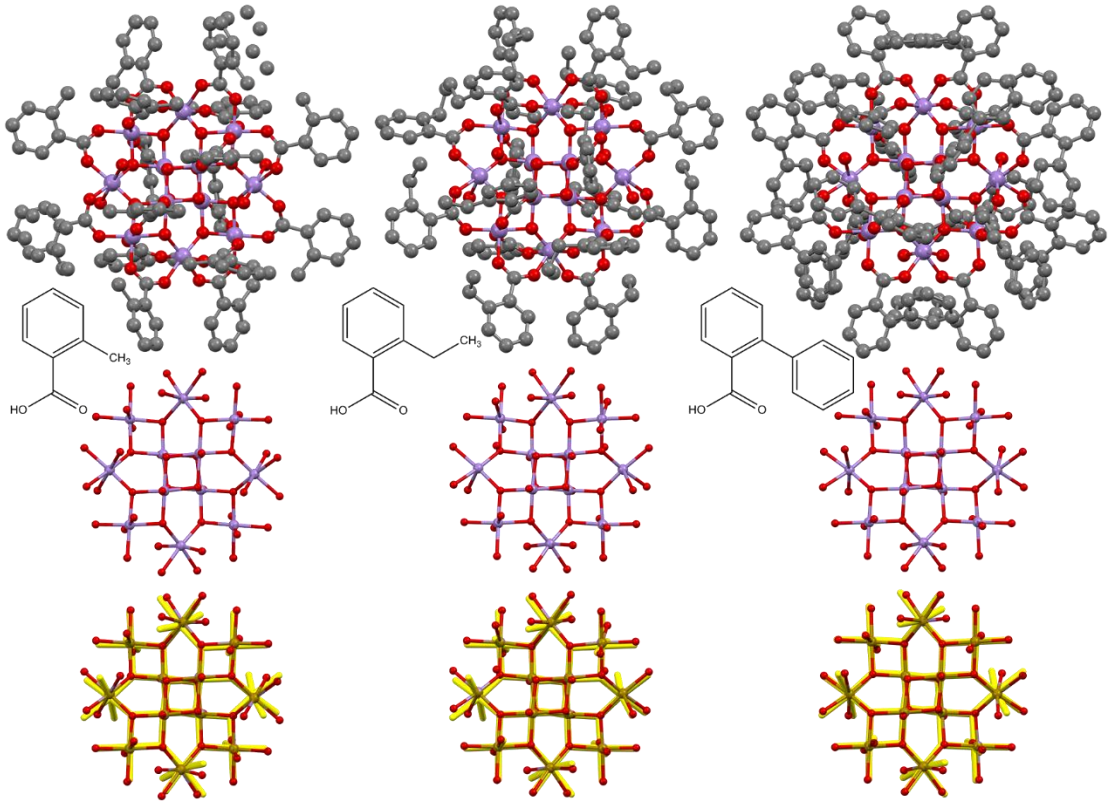

Figure 2.4.1 The Mn_{12}-**R** Substitution Bunch. *Top row*: *Left*, Mn_{12}-2-Methyl. *Middle*, Mn_{12}-2-Ethyl. *Right*, Mn_{12}-2-Phenyl. Hydrogens removed for clarity. *Middle row*: carbon component removed from each structure. *Bottom row*: Mn_{12}-Acetate cluster (yellow tubes) superimposed over middle row structures.

It is clear from **Figure 2.4.1** that no *significant* deviation from the archetypal Mn_{12}-type cluster can be seen. This is in alignment with what was hypothesized for the smaller *ortho*-substituted benzoic acids (e.g., *o*-methyl/ethyl), where the expected structural impact was predicted to be minor, relative to larger substituents.

The *ortho*-phenyl substituted benzoic acid, due to its relative size versus methyl and ethyl, was expected to demonstrate a more significant structural impact to the Mn_{12}-type cluster; and was hypothesized to completely distort the cluster, by sterically influencing a structural reorganization of the Mn_{12}-type cluster. Based upon the side-by-side comparison and the superimposition of the Mn_{12}-Acetate core, it is evident that the *ortho*-phenyl substituent negligibly impacts the Mn_{12}-Acetate core.

On the qualitative level, outside of the isomeric water forms, no significant structural impact is visually perceived; however, X-ray crystal data can be used to investigate the site-specific coordination environments. We have already noted a decrease in the crystal symmetry of the molecule from tetragonal (parent, **1**) to monoclinic (**2**, **4**) and below (**3**), which is indeed a structural impact, but more data may be gathered with respect to the bond lengths. However, instead of examining all ~490 bonds in each Mn_{12}-**R** cluster, only a few of those bonds are of particular significance to the magnetization of the Mn_{12}-family of SMM. As discussed, the positioning and length of the Group III JT elongated Mn-O bonds, J_2 and J'_2, are important in magnetization discussions, so it is those bonds which will be scrutinized.

For Mn_{12}-Acetate[3] and the closely related Mn_{12}-Benzoate,[1] the elongated Mn-O JT axes are positioned axially and range from 2.133 to 2.237 Å. Comparison of these bond lengths relative to the equatorial Mn-O bond lengths, which range from 1.871 to 1.980 Å, serves as a quick method for identifying which Mn-O bonds serve as the elongated JT axes (Mn-O $\geq$ 2.0 Å). Compounds **2** and **4** also have their elongated JT axes axially positioned, ranging from 2.189 to

2.233 Å; slightly longer than the Mn-O bonds of Mn_{12}-Acetate, and within the bond length range of Mn_{12}-Benzoate (**Table 2.4.1**).

While perhaps considered slight; through the utilization of data dense X-ray techniques, a quantitative structural difference between the parent compound and the new substitutive compounds was established. While the inner cubane core exhibits no significant deviation in physical structure, and visually the outer MnO coordination sites of these newly synthesized Mn_{12}-**R** compounds appear to be the same as the parent compound; X-ray crystallographic data has effectively revealed a structural variation in the Mn^{III} JT axial bond lengths within one angstrom. This X-ray data also has revealed an overall reduction in symmetry versus the Mn_{12}-Acetate parent. Peripheral acetate substitution with asymmetric benzoates results in reduction of symmetry from tetragonal, to lower symmetry crystal systems, monoclinic in **2** and **4**, and triclinic in **3**.

Based on these observations, one may be tempted to suggest that the steric potential of *ortho*-substituted benzoic acid may be too remote to impose a significant structural change to the Mn_{12}-type cluster. However, might other substituted benzoic acids offer enough steric brunt to force a physical, structural change on the material? Based on the crystal structure of **4**, it is evident that the phenyl moiety has the rotational freedom to orient and fit innocuously next to the cluster core. This rotational flexibility does not allow for much structural influence on the cluster, where rotation allows a minimization of steric repulsion. It is possible that a more rigid and structurally imposing substituent may offer more dramatic results. The initial targets for this type of investigation would be those *ortho*-isopropyl and *tert*-butyl substituted benzoates.

2.4.3 Mn_{12}-2-R Structure/Function Relationships: Magnetization

The second part of the second question posed in Chapter 1 asks, "[if a structural difference can be isolated] and if we establish functional differences between the two, can they be

linked to those structural differences?" A direct way of describing an Mn_{12}-type compound's function is through analysis of its magnetization. The side-by-side comparison of the AC susceptibility data offers a facile method to evaluate SMM magnetization behavior (**Figure 2.4.2**). Only the high-field magnetic characterization of compounds **2** and **4** have been obtained.

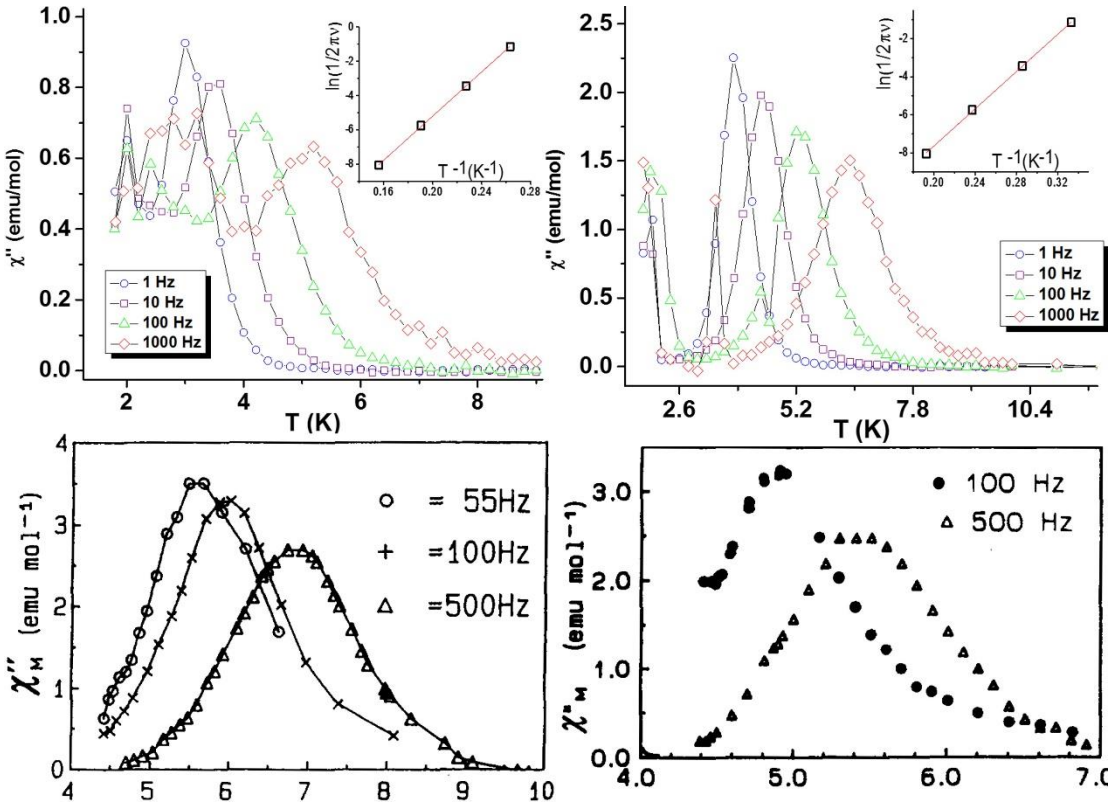

Figure 2.4.2 Comparison of AC susceptibility, χ_M'', for **2**, U_{eff} = 44 K, *top left*, **4**, U_{eff} = 49 K, *top right*, Mn_{12}-Acetate, U_{eff} = 62 K,[20] *bottom left*, and Mn_{12}-Benzoate, U_{eff} = 57.5 K,[20] *bottom right*. Insets show the Arrhenius plots.

We indeed observe changes in the magnetic behavior of the Mn_{12}-**R** compounds based on their AC susceptibility measurements. This data shows us that **2** and **4** are indeed part of the Mn_{12}-type SMM family, demonstrating the two expected out-of-phase relaxations, and that the behavior of **2** and **4** is different from their Mn_{12}-Acetate parent. Answering why is a challenging process, the question is somewhat twofold, and additionally dependent on other measurements.

As revealed above in **Section 2.3.1**, there was indeed a functional difference with respect to the magnetization of compounds **2** and **4**. Because of this measurable difference, previous literature research suggests that the difference should be relatable to a *structural* difference.

At the base level, considering the crystal system of each material reveals a large portion of the story: the high tetragonal symmetry of the Mn_{12}-Acetate cluster has been reduced to monoclinic in **2** and **4**. In general, the lower symmetry Mn_{12}-type complexes have been directly associated with a lower barrier to remagnetization, U_{eff} (fast relaxers).[25, 80-81] Based on this, we should see lower values of U_{eff} for **2** and **4** with respect to Mn_{12}-Acetate. This is indeed true as shown in **Table 2.4.1**. The benzoate substituted Mn_{12}-Type cluster shows a P-1 space group due to incomplete data (no hydrogens), but is listed to show its JT bond lengths.

Next we must examine the JT elongated Mn-O Bonds. As shown in **Table 2.4.1** the JT Mn-O bonds of **2** and **4** are axially situated, which is considered normal. Therefore, this reduction in the barrier to magnetization must be solely based off reduced crystal symmetry, because the nominal axial orientation of the Group III elongated Mn-O bonds.

Compound	**Space Group**	**U_{eff} (K)**	**JT Axis**	**Bond Length (Å)**
Acetate (AQACMN)[3]	I-4	62	Axial	2.178 / 2.133
Benzoate (KAGLEJ)[1]	P-1	55	Axial	2.232 / 2.201 & 2.183 / 2.237
2, *o*-methyl	C2/c	44	Axial	2.233 / 2.200
4, *o*-phenyl	C2/c	49	Axial	2.189 / 2.255

Table 2.4.1 Symmetry, barrier to magnetic relaxation, and JT elongated axis position and length of **2** and **4** relative to Mn_{12}-Acetate and Mn_{12}-Benzoate.

2.4.4 A New Solvothermal Hope

The treatment of **4** in very specific solvothermal reaction conditions resulted in the Mn_{13}-supercubane-type structure **5**. These reaction conditions were loosely based on previously reported literature conditions which generally agreed upon temperatures of about 100 °C and the

utilization of acetonitrile as a solvent.[73, 82-83] The generation of this new MnO-type cluster (coming from Mn_{12}-type) is thought to have been made possible not only from the reaction conditions imparted *via* solvothermal conditions (i.e., increased diffusion rates, decreased solvent viscosity, increased metal compound solubility),[24] but also from the application of a weakly coordinating solvent, acetonitrile. Ironically, initial attempts to solvothermally transform Mn_{12}-type compounds were not effective until the acetonitrile solvent was added to the solvent conditions with isopropanol. It is surmised that a weakly coordinating solvent influences the reassembly kinetics of the cluster.

This type of structure offers interesting SMM potential relative to Mn_{12}-Acetate, and other MnO-type clusters due to its access to three different oxidation states: II, III, and IV. Assuming antiferromagnetic ordering, a ground state spin value of S = 11/2 is possible from this Mn_{13}-supercubane system, lower than the Mn_{12}-Acetate S = 10 system, but the uniaxial anisotropy could potentially be higher. While the crystal symmetry is reportedly monoclinic, which could be impacted by the low crystal data quality, the overall molecular symmetry is high. This could potentially lead to a magnetic system featuring increased D values, relative to Mn_{12}-Acetate, which would result in different magnetic behavior, when coupled with a different S value for this cluster. Achieving solvent-free crystals of the cluster could potentially push it further.

The low-quality crystal data for this compound is likely due to its tendency to rapidly desolvate. In order to mount the crystals to the XRD goniometer prior to desolvation-induced lattice collapse, it was necessary to transfer the crystals from the mother liquor into grease on a glass slide resting on dry ice (followed by crystal selection and mounting quickly). Every effort was made to prevent the crystals from desolvating prior to mounting and cooling to 100 K. Apparently, the high solvent content of the material (and thus packing and ordering in the crystal

lattice), meant that the obtained crystal data was of relatively low-quality and the crystal symmetry is not known with certainty.

Further attempts to generate even more MnO-types clusters solvothermally involved supplemental additions to the reaction mixtures. A series of experiments were carried out on the Mn_{12}-**R** materials where *specific* molar amounts of additional benzoic acid were added, as per literature recommendations, to the Parr Bomb.[45, 84-86] Additional quantities of carboxylic acid were added to the reaction vessel in 1/3:1, 1:1, 3:1, and 64:1 molar ratio relative to the amount of Mn_{12}-**R** cluster in the bomb. Low-quality crystals were eventually grown, but the furthest extent of reliable structure solution reveals more Mn_{12}-type clusters (see **Appendix V).**

In future experiments, different solvent amounts and qualities, and indeed other Mn_{12}-**R** starting compounds, should be considered in subsequent experiments. Solvothermal methods were effective at generating one new cluster, but additional investigation should follow this report in order to investigate the full potential of this method.

2.5 Conclusion

Generally, the question was to see if we could synthesize different Mn_{12}-**R** materials *via* acetate substitution of the Mn_{12}-Acetate cluster, and then link any functional differences to a structural change; and both objectives were accomplished. Additionally, we forced the transformation of an Mn_{12}-**R** cluster to a Mn_{13}-supercubane type through solvothermal conditions.

Systematically increasing the size of the *ortho*-substituent of the benzoate substituted Mn_{12}-**R** cluster from methyl, to ethyl, to phenyl did not impose a significant structural change relative to the shape of the parent Mn_{12}-Acetate cluster. However, the reduction of symmetry in the Mn_{12}-**R** compounds, as well as the impact on their peripheral JT influenced Mn^{III} ions, altered

the magnetization relative to the Mn_{12}-Acetate parent, indicated by the reduction of the U_{eff} parameter. This effect could be traced back to a structural change.

A reduced U_{eff} with respect to the magnetic barrier to relaxation does not indicate a 'lower' performance material, or that the material is functioning at a depreciated rate; it simply indicates that its route to magnetic relaxation is either over a shallower energy well, or QTM is more accessible (or probably both). All molecular magnetic materials shall return to equilibrium over time. If *function* is the concern, remember that SMM molecules that relax at a faster rate, versus SMMs that relax at a slower rate, simply fit into two different categories that are individually important for study, and even for potential applications.

Certainly, it is important to consider and remember that *these* benzoates did not impart a structural change on the cluster. This is in no way to say that this cannot be accomplished with *other* bulky benzoic acids. *Ortho*-isopropyl and *ortho*-*tert*-butyl substituted benzoic acids are two immediate examples of carboxylate building blocks that may further influence the structure. Certainly, the list does not end at just *ortho*-phenyl substituted benzoic acid.

The solvothermal treatment of the Mn_{12}-**R** compounds was indeed an interesting research topic. Through exhaustive research and modulating *many* variables, the generation of a Mn_{13}-supercubane compound, **5**, has been the only new cluster derived *via* this method. For future experiments of this type, I would suggest beginning at a deeper exploration of the solvent effects first, before looking closer at other parameters, e.g., molar ratios, ramp temperatures and times, etc. Possibly considering other weakly coordinating solvents would give interesting results.

Future work in this research avenue should certainly be performed, with a focus on implementing the aforementioned substituted benzoic acids. Previously, the *ortho*-isopropyl and *tert*-butyl substituted benzoic acids were in the pipe for experimental trials; but ultimately, cost

(up to $700 per gram), coupled with synthetic uncertainty and complexity, sidelined that particular investigation.

Compounds **3** and **5**, still lack high-field magnetic characterization. While **3** may not offer significantly different magnetic behavior based upon what we see in compounds **2** and **4**, its characterization would still add nicely to the overall discussion. Additionally, the unique oxidation state, and symmetric character of **5** will result in fundamentally different S and D values, which will result in different magnetic behavior relative to Mn_{12}-type SMMs, whether they be slow or fast relaxers. As an isolated case, it would be interesting to explore this compound's magnetization.

Future work remains for this research; but for now, we proceed to investigate a different approach to generate new MnO-type clusters.

2.6 References

1. Sessoli, R.; Tsai, H.-L.; Schake, A. R.; Wang, S.; Vincent, J. B.; Folting, K.; Gatteschi, D.; Christou, G.; Hendrickson, D. N., "High-Spin Molecules: "$Mn_{12}O_{12}(O_2CR)_{16}(H_2O)_4$". *J. Am. Chem. Soc.* **1993,** *115*, 1804-1816.
2. Weinland, R. F.; Fischer, G., Über Manganiacetate und -benzoate. *Zeitschrift für anorganische Chemie* **1921,** *120* (1), 161-180.
3. Lis, T., "Preparation, Structure, and Magnetic Properties of a Dodeeanuelear Mixed-Valence Manganese Carboxylate". *Acta Cryst.* **1980,** *B36*, 2042-2046.
4. Sasabe, H., *Hyper-Structured Molecules III*. Taylor & Francis London and New York: 2002.
5. Sun, Z.; Ruiz, D.; Rumberger, E.; Incarvito, C. D.; Folting, K.; Rheingold, A. L.; Christou, G.; Hendrickson, D. N., Isomeric Forms of [Mn12O12(O2CR)16(H2O)4] Single-Molecule Magnets. *Inorg. Chem.* **1998,** *37*, 4758-4759.
6. Boukhvalov, D. W.; Dobrovitski, V. V.; Kögerler, P.; Al-Saqer, M.; Katsnelson, M. I.; Lichtenstein, A. I.; Harmon, B. N., Effect of ligand substitution on the exchange interactions in {Mn12}-type single-molecule magnets. *Inorg. Chem.* **2010,** *49*, 10902-10906.
7. Brockman, J. T.; Abboud, K. A.; Hendrickson, D. N.; Christou, G., A new family of Mn12 single-molecule magnets: replacement of carboxylate ligands with diphenylphosphinates. *Polyhedron* **2003,** *22*, 1765-1769.
8. Soler, M.; Wernsdorfer, W.; Abboud, K. A.; Huffman, J. C.; Davidson, E. R.; Hendrickson, D. N.; Christou, G., Single-Molecule Magnets: Two-Electron Reduced Version of a Mn12 Complex and Environmental Influences on the Magnetization Relaxation of (PPh4)2[Mn12O12O2CCHCl2)16(H2O)4]. *J. Am. Chem. Soc.* **2003,** *125*, 3576-3588.
9. Basler, R.; Sieber, A.; Chaboussant, G.; Güdel, H. U., Inelastic Neutron Scattering Study of Electron Reduction in Mn12 Derivatives. *Inorg. Chem.* **2005,** *44* (3), 649-653.
10. Aubin, S. M. J.; Sun, Z.; Pardi, L.; Krzystek, J.; Folting, K.; Brunel, L.-C.; Rheingold, A. L.; Christou, G.; Hendrickson, D. N., Reduced Anionic Mn12 Molecules with Half-Integer Ground States as Single-Molecule Magnets. *Inorg. Chem.* **1999,** *38*, 5329-5340.
11. Sun, Z.; Gantzel, P. K.; Hendrickson, D. N., Supercubane Mixed-Valence Tridecanuclear Manganese Complex. *Inorg. Chem.* **1996,** *35*, 6640-6641.
12. Anderson, P. W., New Approach to the Theory of Superexchange Interactions. *Phys. Rev.* **1959,** *115* (1), 2-13.
13. Baikie, A. R. E.; Howes, A. J.; Hursthouse, M. B.; Quick, M. B.; Thornton, J. M., Preparation, crystal structure, magnetic properties, and chemical reactions of a hexanuclear mixed valence manganese carboxylate. *Chem. Commun.* **1986,** *0*, 1587.
14. Baikie, A. R. E.; Hursthouse, M. B.; New, D. B.; Thornton, J. M., Preparation, crystal structure, and magnetic properties of a trinuclear mixed-valence manganese carboxylate. *Chem. Commun.* **1978,** *0*, 62-63.
15. Chan, M. K.; Armstrong, W. H., A Novel Tetranuclear Manganese Complex That Displays Multiple High-Potential Redox Processes. Synthesis, Structure, and Properties of][Mn,(TPHPN) (02CCH3) (H20)],0)(C104)4.2CH30H1. *J. Am. Chem. Soc.* **1989,** *111*, 9121-9122.
16. Mandal, S. K.; Armstrong, W. H., A novel triply bridged dinuclear manganese(III) complex containing the [MnzO(OAc)2] 2+ core: synthesis, crystal structure and properties of [Mnz(/x-O)(/x-OAc)z(bpea)2](C104)2. *Inorganica Chimica Acta* **1995,** *229*, 261-270.
17. Caneschi, A.; Gatteschi, D.; Sessoli, R., "Alternating Current Susceptibility, High Field Magnetization, and Millimeter Band EPR Evidence for a Ground S = 10 State in $[Mn_{12}O_{12}(CH_3COO)_{16}(H_2O)_4)\cdot 2CH_3COOH\cdot 4H_2O$". *J. Am. Chem. Soc.* **1991,** *113*, 5873-5874.

18. Aromí, G.; Brechin, E. K., "Synthesis of 3*d* Metallic Single-Molecule Magnets". *Struct. Bond* **2006,** *112*, 1-69.
19. Christou, G., "Single-molecule magnets: a molecular approach to nanoscale magnetic materials". *Polyhedron* **2005,** *24* (16-17), 2065-2075.
20. Sessoli, R.; Gatteschi, D.; Caneschi, A.; Novak, M. A., "Magnetic bistability in a metal-ion cluster". *Nature* **1993,** *365*, 141-143.
21. Sessoli, R.; Sorace, L.; Gatteschi, D.; Barra, A. L.; Daiguebonne, C., The origin of second-order transverse magnetic anisotropy in Mn12-acetate. *J. Am. Chem. Soc.* **2007,** *129* (35), 10754-10762.
22. Hill, S.; Murugesu, M.; Christou, G., Anisotropy barrier reduction in fast-relaxing Mn12 single-molecule magnets. *Phys. Rev. B.* **2009,** *80*, 174416-174430.
23. Lampropoulos, C.; Redler, G.; Data, S.; Abboud, K. A.; Hill, S.; Christou, G., "Binding of higher alcohols onto Mn_{12} single-molecule magnets (SMMs): access to the highest barrier Mn_{12} SMM". *Inorg. Chem.* **2010,** *49* (4), 1325-1336.
24. Gatteschi, D.; Sessoli, R.; Villain, J., *Molecular Nanomagnets*. Oxford University Press: 2006.
25. Sun, Z.; Ruiz, D.; Dilley, N. R.; Soler, M.; Ribas, J.; Folting, K.; Maple, B. M.; Christou, G.; Hendrickson, D. N., The origin of the second relaxation process in the [Mn12O12(O2CR)16(H2O)4] single-molecule magnets: 'Jahn–Teller isomerism' in the [Mn12O12] core. *Chem. Commun.* **1999**, 1973-1974.
26. Boskovic, C.; Pink, M.; Huffman, C. W.; Hendrickson, D. N.; Christou, G., Single-Molecule Magnets: Ligand-Induced Core Distortion and Multiple Jahn-Teller Isomerism in [Mn12O12(O2CMe)8(O2PPh2)8(H2O)4]. *J. Am. Chem. Soc.* **2001,** *123*, 9914-9915.
27. Aubin, S. M. J.; Sun, Z.; Eppley, H. J.; Rumberger, E.; Guzei, I. L.; Folting, K.; Gantzel, P. K.; Rheingold, A. L.; Christou, G.; Hendrickson, D. N., Single-Molecule Magnets: Jahn-Teller Isomerism and the Origin of Two Magnetization Relaxation Processes in Mn12 Complexes. *Inorg. Chem.* **2001,** *40*, 2127-2146.
28. Gatteschi, D.; Sorace, L., Hints for the Control of Magnetic Anisotropy in Molecular Materials. *J. Solid State Chem.* **2001,** *159* (2), 253-261.
29. Eppley, H. J.; Tsai, H.-L.; de Vries, N.; Folting, K.; Christou, G.; Hendrickson, D. N., "High-Spin Molecules: Unusual Magnetic Susceptibility Relaxation Effects in $[Mn_{12}O_{12}(O_2CEt)_{16}(H_2O)_4]$ (S = 9) and the One-Electron Reduction Product (PPh4)$[Mn_{12}O_{12}(O_2CEt)_{16}(H_2O)_4]$ (S = 19/2)". *J. Am. Chem. Soc.* **1995,** *117*, 301-317.
30. Aubin, S. M. J.; Sun, Z.; Guzei, I. L.; Rheingold, A. L.; Christou, G.; Hendrickson, D. N., "Single-molecule magnets: isomeric $[Mn_{12}O_{12}(O_2CC_6H_4Me\text{-}4)_{16}(H_2O)_4]$ complexes exhibiting different rates of resonant magnetization tunnelling". *Chem. Commun.* **1997**, 2239-2240.
31. Wei, Y.-G.; Zhang, S.-W.; Shai, M.-C.; Tang, Y.-Q., A mesoscopic molecular superparamagnet : preparation, crystal structure and magnetic properties of [Mn12O12(O2CMe)4(O2CEt)12(H20)4] • 2H20 4EtCO2H with an S = 9 ground state. *Polyhedron.* **1997,** *16* (9), 1471-1475.
32. An, J.; Chen, Z.-D.; Bian, J.; J-T., C.; Wang, S.-X.; Gao, S.; Xu, G.-X., "Influence of the ligands and solvents on the magnetic properties of the single molecule magnets: $[Mn_{12}O_{12}(O_2CR)_{16}(L)_4]\cdot n$S (R=3-Cl-$C_6H_4$, L=3-Cl-$C_6H_4CO_2H$ and water, n=1, S=3-Cl-$C_6H_4CO_2H$ (**1**); R=CH_2Cl, L=water, n=0 (**2**))". *Inorganica Chimica Acta.* **2000,** *299*, 28-34.
33. An, J.; Chen, Z.-D.; Zhang, X.-X.; Raubenheimer, H. G.; Esterhuysen, C.; Gao, S.; Xu, G.-X., "Synthesis, X-ray characterization and single molecule magnetic behaviour of $[Mn_{12}O_{12}(O_2CCH_2X)_{16}(H_2O)_4]\cdot m CH_2Cl_2\cdot n H_2O$ (1: X = Cl, m = 2, n = 6; 2: X = Br, m = 4, n = 0)". *Dalton Trans.* **2001,** (22), 3352.
34. Soler, M.; Artus, P.; Folting, K.; Huffman, J. C.; Hendrickson, D. N.; Christou, G., Single-Molecule Magnets: Preparation and Properties of Mixed-Carboxylate Complexes $[Mn_{12}O_{12}(O_2CR)_8(O_2CR')_8(H_2O)_4]$. *Inorg. Chem.* **2001,** *40*, 4902-4912.

35. Hachisuka, H.; Awaga, K.; Yokoyama, T.; Kubo, T.; Goto, T.; Nojiri, H., Structure and magnetic properties of the single-molecule magnet [Mn11CrO12(O2CCH3)16(H2O)4]·2CH3COOH·4H2O: Magnetization manipulation and dipolar-biased tunneling in a Mn11Cr/Mn12 mixed crystal. *Phys. Rev. B: Condens. Matter.* **2004,** *70* (10), 104427/1-104427/7.
36. Jeon, W.; Jin, M. K.; Kim, Y.; Jung, D.-Y.; Suh, B. J.; Yoon, S., Synthesis and magnetic relaxation of [Mn12O12(O2CCH2CH2CH2Cl)16(H2O)4] complex. *Bull. Korean Chem. Soc.* **2004,** *25* (7), 1036-1040.
37. Bian, G.-Q.; Kuroda-Sowa, T.; Nogami, T.; Sugimoto, K.; Maekawa, M.; Munakata, M.; Miyasaka, H.; Yamashita, M., "Syntheses, Crystal Structure, and Magnetic Properties of Mn12Single-Molecule Magnets with Naphthalenecarboxylate Bridges, $[Mn_{12}O_{12}(O_2CC_{10}H_7)_{16}(H_2O)_4]$ and Their Tetraphenylphosphonium Salts". *Bull. Chem. Soc. Jpn.* **2005,** *78* (6), 1032-1039.
38. Tasiopoulos, A. J.; Wernsdorfer, W.; Abboud, K. A.; Christou, G., "$[Mn_{12}O_{12}(OMe)_2(O_2CPh)_{16}(H_2O)_2]^{2-}$ Single-Molecule Magnets and Other Manganese Compounds from a Reductive Aggregation Procedure". *Inorg. Chem.* **2005,** *44*, 6324-6338.
39. Awaga, K.; Suzuki, Y.; Hachisuka, H.; Takeda, K., "Magneto-structural correlation in the Jahn–Teller isomers of Mn_{12}". *J. Mater. Chem.* **2006,** *16* (26), 2516-2521.
40. Chakov, N. E.; Lee, S.-C.; Harter, A. G.; Kuhns, P. L.; Reyes, A. P.; Hill, S. O.; Dalal, N. S.; Wernsdorfer, W.; Abboud, K. A.; Christou, G., The Properties of the $[Mn_{12}O_{12}(O_2CR)_{16}(H_2O)_4]$ Single-Molecule Magnets in Truly Axial Symmetry: $[Mn_{12}O_{12}(O_2CCH_2Br)_{16}(H_2O)_4]4CH_2Cl_2$. *J. Am. Chem. Soc.* **2006,** *128* (21), 6975-6989.
41. Murugesu, M.; Wernsdorfer, W.; Abboud, K. A.; Brechin, E. K.; Christou, G., "New Mn12 single-molecule magnets from edge-sharing bioctahedra". *Dalton Trans.* **2006,** (19), 2285-2287.
42. Shah, S. J.; Ramsey, C. M.; Heroux, K. J.; DiPasquale, A. G.; Dalal, N. S.; Rheingold, A. L.; del Barco, E.; Hendrickson, D. N., Molecular Wheels: New Mn12 Complexes as Single-Molecule Magnets. *Inorg. Chem.* **2008,** *47* (20), 9569-9582.
43. Bagai, R.; Christou, G., "The Drosophila of single-molecule magnetism: $[Mn_{12}O_{12}(O_2CR)_{16}(H_2O)_4]$". *Chem. Soc. Rev.* **2009,** *38* (4), 1011-26.
44. Rogez, G.; Donnio, B.; Terazzi, E.; Gallani, J.-L.; Kappler, J.-P.; Bucher, J.-P.; Drillon, M., "The Quest for Nanoscale Magnets: The example of [Mn12] Single Molecule Magnets". *Adv. Mater.* **2009,** *21* (43), 4323-33.
45. Leng, J.-D.; Dian, L.-Y.; Liu, J.-L.; Tong, M.-L., Two MnIII4MnII8 clusters from the use of tripodal ligands showing single-molecule magnet behavior. *Polyhedron* **2011,** *30* (18), 3088-3094.
46. Leng, J.-D.; Dian, L.-Y.; Liu, J.-L.; Tong, M.-L., A Series of MnIII4MnII8 Single-Molecule Magnets Mediated by Intra- and Intermolecular Interactions. *Eur. J. Inorg. Chem.* **2011,** (14), 2317-2326.
47. Kushch, L. A.; Sasnovskaya, V. D.; Dmitriev, A. I.; Yagubskii, E. B.; Koplak, O. V.; Zorina, L. V.; Boukhvalov, D. W., "New single-molecule magnet based on Mn_{12} oxocarboxylate clusters with mixed carboxylate ligands, $[Mn_{12}O_{12}(CN\text{-}o\text{-}C_6H_4CO_2)_{12}(CH_3CO_2)_4(H_2O)_4]\cdot 8CH_2Cl_2$: Synthesis, crystal and electronic structure, magnetic properties". *Dalton Trans.* **2012,** *41* (44), 13747-13754.
48. Yan, X.; Cheng, S.; Sun, L.; Chen, X.; Qin, J., π-conjugated polymers containing pendant Mn12 cluster: Synthesis and physical properties. *Polymer.* **2012,** *53* (1), 241-247.
49. Lampropoulos, C.; Murugesu, M.; Harter, A. G.; Wernsdofer, W.; Hill, S.; Dalal, N. S.; Reyes, A. P.; Kuhns, P. L.; Abboud, K. A.; Christou, G., Synthesis, Structure, and Spectroscopic and Magnetic Characterization of [Mn12O12(O2CCH2But)16(MeOH)4]·MeOH, a Mn12 Single-Molecule Magnet with True Axial Symmetry. *Inorg. Chem.* **2013,** *52* (1), 258-272.

50. Corrales, S. A.; Cain, J. M.; Uhlig, K. A.; Mowson, A. M.; Papatriantafyllopoulou, C.; Peprah, M. K.; Ozarowski, A.; Tasiopoulos, A. J.; Christou, G.; Meisel, M. W.; Lampropoulos, C., "Introducing Dimensionality to the Archetypical Mn_{12} Single-Molecule Magnet: a Family of $[Mn_{12}]n$ Chains". *Inorg. Chem.* **2016,** *55* (4), 1367-1369.
51. Fournet, A. D.; Mitchell, K. J.; Wernsdorfer, W.; Abboud, K. A.; Christou, G., Three-Dimensional (3-D) Ferromagnetic Network of Mn12 Single-Molecule Magnets: Subtle Environmental Effects and Switching to Antiferromagnetic. *Inorg. Chem.* **2017,** *56* (17), 10706-10716.
52. Soler, M.; Artus, P.; Folting, K.; Huffman, C. W.; Hendrickson, D. N.; Christou, G., Single-Molecule Magnets: Preparation and Properties of Mixed-Carboxylate Complexes [Mn12O12(O2CR)8(O2CR′)8(H2O)4]. *Inorg. Chem.* **2001,** *40*, 4902-4912.
53. Soler, M.; Wernsdorfer, W.; Abboud, K. A.; Hendrickson, D. N.; Christou, G., Single-molecule magnetism behavior of [Mn12O12(O2CR)16(H2O)4]2− salts. *Polyhedron* **2003,** *22* (14-17), 1777-1782.
54. Chakov, N. E.; Abboud, K. A.; Zakharov, L. N.; Rheingold, A. L.; Hendrickson, D. N.; Christou, G., Reaction of [Mn12O12(O2CR)16(H2O)4] single-molecule magnets with non-carboxylate ligands. *Polyhedron* **2003,** *22* (14-17), 1759-1763.
55. Chakov, N. E.; Wernsdofer, W.; Abboud, K. A.; Hendrickson, D. N.; Christou, G., Single-molecule magnets. A Mn12complex with mixedcarboxylate-sulfonate ligation: [Mn12O12(O2CMe)8(O3SPh)8(h2o)4]. *Dalton. Trans.* **2003**, 2243-2248.
56. Chakov, N. E.; Zakharov, L. N.; Rheingold, A. L.; Abboud, K. A.; Christou, G., New Polynuclear Manganese Clusters from the Use of the Hydrophobic Carboxylate Ligand 2,2-Dimethylbutyrate. *Inorg. Chem.* **2005,** *44*, 4555-4567.
57. Boskovic, C.; Brechin, E. K.; Streib, W. E.; Folting, K.; Bollinger, J. C.; Hendrickson, D. N.; Christou, G., Single-Molecule Magnets: A New Family of Mn12 Clusters of Formula [Mn12O8X4(O2CPh)8L6]. *J. Am. Chem. Soc.* **2002,** *124*, 3725-3736.
58. Gerbier, P.; Ruiz-Molina, D.; Domingo, N.; Amabilino, D. B.; Vidal-Gancedo, J.; Tejada, J.; Hendrickson, D. N.; Veciana, J., Synthesis and Characterization of a [Mn 12 O 12 (O 2 CR) 16 (H 2 O) 4] Complex Bearing Paramagnetic Carboxylate Ligands. Use of a Modified Acid Replacement Synthetic Approach. *Monatshefte für Chemie* **2003,** *134* (2), 265-276.
59. Eppley, H. J.; Tsai, H.-L.; De Vries, N.; Folting, K.; Christou, G.; Hendrickson, D. N., High-Spin Molecules: Unusual Magnetic Susceptibility Relaxation Effects in [Mn12O12(O2CEt)16(H2O)3] (S=9) and the One-Electron Reduction Product (PPh4)[Mn12O12(O2CEt)16(H2O)4] (S= 19/2). *J. Am. Chem. Soc.* **1995,** *117*, 301-317.
60. Soler, M.; Wernsdofer, W.; Folting, K.; Pink, M.; Christou, G., Single-Molecule Magnets: A Large Mn30 Molecular Nanomagnet Exhibiting Quantum Tunneling of Magnetization. *J. Am. Chem. Soc.* **2004,** *126*, 2156-2165.
61. Soler, M.; Rumberger, E.; Folting, K.; Hendrickson, D. N.; Christou, G., Synthesis, Characterization and magnetic properties of [Mn30O24(OH)8(O2CCH2C(CH3)3)32(H2O)2(CH3NO2)4]: The largest Manganese carboxylate cluster. *Polyhedron.* **2001,** *20*, 1365-1369.
62. Tasiopoulos, A. J.; Vinslava, A.; Wernsdorfer, W.; Abboud, K. A.; Christou, G., "Giant single-molecule magnets: a [Mn84] torus and its supramolecular nanotubes". *Angew. Chem. Int. Ed.* **2004,** *43* (16), 2117-21.
63. George, S. M.; Mamun, S. I.; Kim, J., One-dimensional supramolecular assembly of an Mn12 single molecule magnet by ligand interactions. *Inorg. Chem. Commun.* **2010,** *13* (3), 429-432.
64. Costin-Hogan, C. E.; Chen, C.-L.; Hughes, E.; Pickett, A.; Valencia, R.; Rath, N. P.; Beatty, A. M., “Reverse” engineering: Toward 0-D cadmium halide clusters. *CrystEngComm.* **2008,** *10* (12), 1910-1915.

65. Chen, C. L.; Beatty, A. M., "From crystal engineering to cluster engineering: How to transform cadmium chloride from 2-D to 0-D". *Chem. Commun.* **2007,** (1), 76-78.
66. Kennard, O., From data to knowledge—Use of the Cambridge Structural Database for studying molecular interactions. *Supramolecular Chemistry.* **1992,** *1* (3), 277-295.
67. Jin, Y.; Yu, C.-H.; Wang, W.-X.; Li, S.-C.; Zhang, W., Crystal structures and dielectric properties of two tert-butylammonium chlorocadmate(II) complexes. *Inorganica Chimica Acta.* **2014,** *413*, 97-101.
68. Henderson, J. J.; Koo, C.; Feng, P. L.; Ddel Barco, E.; Hill, S.; Tupitsyn, I. S.; Stamp, P. C. E.; Hendrickson, D. N., Manifestation of Spin Selection Rules on the Quantum Tunneling of Magnetization in a Single Molecule Magnet *Phys. Rev. Lett.* **2009,** *103*, 017202.
69. Hill, S.; Murugesu, M.; Christou, G., On the anisotropy barrier reduction in fast relaxing Mn12 single-molecule magnets. *Phys. Rev. B. Condens. Matter.* **2009,** *80*, 174416.
70. Parois, P.; Moggach, S. A.; Sanchez-Benitez, J.; Kamenev, K. V.; Lennie, A. R.; Warren, J. E.; Brechin, E. K.; Parsons, S.; Murrie, M., Pressure-induced Jahn-Teller switching in a Mn12 nanomagnet. *Chem. Commun.* **2010,** *46* (11), 1881-1883.
71. Nakano, M.; Oshio, H., Magnetic anisotropies in paramagnetic polynuclear metal complexes. *Chem. Soc. Rev.* **2011,** *40* (6), 3239-3248.
72. Zhu, Y.-Y.; Cui, C.; Zhang, Y.-Q.; Jia, J.-H.; Guo, X.; Gao, C.; Qian, K.; Jiang, S.-D.; Wang, B.-W.; Wang, Z.-M.; Gao, S., Zero-field slow magnetic relaxation from single Co(ii) ion: a transition metal single-molecule magnet with high anisotropy barrier. *Chem. Sci.* **2013,** *4* (4), 1802-1806.
73. Low, D. M.; Brechin, E. K.; Helliwell, M.; Mallah, T.; Rivière, E.; McInnes, E. J. L., "New routes to high nuclearity cages: dimerisation of a manganese triangle *via* solvothermal synthesis". *Chem. Commun.* **2003,** (18), 2330-2331.
74. Bain, G. A.; Berry, J. F., Diamagnetic corrections and Pascal's constants. *J. Chem. Ed.* **2008,** *85*, 532-536.
75. French, C. M., Differences in magnetic susceptibility increment in closed-ring and side-chain substitution. *Transactions of the Faraday Society* **1954,** *50*, 1320-1324.
76. Dolomanov, O. V.; Bourhis, L. J.; Gildea, R. J.; Howard, J. A. K.; Puschmann, H., OLEX2: a complete structure solution, refinement and analysis program. *J. Appl. Cryst.* **2009,** *42*, 339-341.
77. Sheldrick, G. M., A short history of SHELX. *Acta. Crystallogr. A* **2008,** *A64*, 112-122.
78. Sun, Z.; Ruiz, D.; Rumberger, E.; Incarvito, C. D.; Folting, K.; Rheingold, A. L.; Christou, G.; Hendrickson, D. N., "Isomeric Forms of $[Mn_{12}O_{12}(O_2CR)_{16}(H_2O)_4]$ Single-Molecule Magnets". *Inorg. Chem.* **1998,** *37* (4758-4759).
79. Okui, Y.; Catusanu, F. A.; Kubota, R.; Kure, B.; Nakajima, T.; Tanase, T.; Kajiwara, T.; Mikuriya, M.; Miyasaka, H.; Yamashita, M., "Systematic Expansion of Supercubane Cores in Manganese Oxo Clusters with Tricarboxylate Ligands". *Eur. J. Inorg. Chem.* **2011,** *2011* (28), 4325-4330.
80. Perenboon, J. A. A. J.; Brooks, J. S.; Hill, S.; Hathaway, T.; Dalal, N. S., Relaxation of the magnetization of Mn12 acetate. *Phys. Rev. B.* **1998,** *58* (11).
81. Leuenberger, M. N.; Loss, D., Spin tunneling and phonon-assisted relaxation in Mn12-acetate. *Phys. Rev. B.* **2000,** *61* (21), 1286-1303.
82. Yang, H.-J.; Kou, H.-Z.; Ni, Z.-H.; Cui, A.-L.; Wang, R.-J., Solvothermal synthesis of anhydrous γ-Mn(CH3COO)2: A weak ferromagnet with an ordering temperature of 40K and spin-glass behavior. *Inorg. Chem. Commun.* **2005,** *8* (9), 846-849.
83. Liu, S.; Jeppson, P.; Sandstrom, J.; Caruso, A. N.; Schulz, D. L., "Synthesis, structure and magnetic properties of $\{Mn_5(OC(O)CH_3)_6(OC(O)C_6H_5)_4\}\infty$". *Polyhedron* **2007,** *26* (9-11), 2235-2242.

84. Gutschke, S. O. H.; Price, D. J.; Powell, A. K.; Wood, P. T., "Solvothermal Synthesis of the Canted Antiferromagnet $\{K_2[CoO_3PCH_2N(CH_2CO_2)_2]\}_6 \cdot xH_2O$". *Angew. Chem. Int. Ed.* **1999,** *38* (8), 1088-1090.
85. McInnes, E. J. L.; Anson, C.; Powell, A. K.; Thomson, A. J.; Poussereau, S.; Sessoli, R., "Solvothermal synthesis of $[Cr_{10}(\mu\text{-}O_2CMe)_{10}(\mu\text{-}OR)_{20}]$ 'chromic wheels' with antiferromagnetic (R = Et) and ferromagnetic (R = Me) Cr(III)···Cr(III) interactions". *Chem. Commun.* **2001,** (1), 89-90.
86. Li, G.; Wang, W.; Zhang, S. H.; Zhang, H. Y.; Chen, F. Y., "Synthesis, Structure and Properties of Linear Trinuclear Cobalt Cluster with 5-Fluoro-2-hydroxybenzoic Acid". *J. Cluster. Sci.* **2014,** *25*, 1589-1597.

Chapter 3

$Mn_xO_y(O_2CR)_zL_w$ 'Ground-Up' Complexes

3.1 Introduction

This chapter's work is focused on altering known, published routes to different manganese oxide family clusters which feature 'ground-up' synthetic approaches. By modifying the carboxylate starting materials in these methods with systematically bulkier *ortho*-substituted benzoic acids we investigate our ability to generate new manganese oxide clusters by subverting the expected outcome.

3.1.1 The Path to New MnO Materials

Prior to the paradigm shift to their function as single-molecule magnet materials, MnO-type clusters were under intensive investigation for their potential role as biomimetic materials, i.e., synthetic complexes which emulate biological function.[1] This research focus primarily stemmed from the identification of an enzymatic active site in plants and cyanobacteria which featured an oxo-bridged MnO cluster responsible for the catalytic oxidation of water.[2-3] Since these types of MnO clusters were known to be air stable, thus able to exist reliably outside of a cloistered protein environment, and especially due to their interesting polyvalent nature; many MnO-type clusters were being actively synthesized and investigated.[4] A number of different MnO-type materials were generated from these research efforts, but some of the most encountered and characterized were the $Mn_3O(O_2C\mathbf{R})_6L_3$,[5-8] $Mn_6O_2(O_2C\mathbf{R})_{10}L_4$,[9] and the $Mn_{12}O_{12}(O_2C\mathbf{R})_{16}(H_2O)_4$ type clusters,[10] where **R** = alkyl and L = a neutral monodentate ligand.

From the 80's into the 90's, pioneering researchers who were interested in these biomimetic manganese oxide systems were seeking to gain a measure of control, to alter, the types of polynuclear MnO clusters formed in solution by adjusting the preparative Mn:O atomic ratios systematically in a variety of aqueous solvents and nonaqueous solvents, and in the presence of various oxidizing agents, e.g., permanganate or dioxygen.[11-14] Controlling the Mn:O ratio is typically accomplished for manganese by varying the amount of manganese source

starting material, i.e., $Mn(O_2CMe)_2$ or $MnCl_2$; and for oxygen by adding additional carboxylate starting material, or by introducing reagents such as iodosobenzene.[5, 7, 9, 15] Efforts to generate new compounds were aimed at the potential to explore and discover new archetypes of functional MnO-type clusters.

3.1.2 Designing a Cluster from the Ground, Up.

While the literature and reported compounds discussed in the previous chapter followed the concept of taking an existing synthetic route to a known material, then modifying it postsynthetically (and many compounds have been developed through this method); the literature compounds featured in this work, which serve as the basis for our reported compounds, are designed to proceed directly from the solution-state to the solid-state as a MnO-type cluster of basic formula, $Mn_xO_y(O_2C\mathbf{R})_zL_w$, where **R** typically is an alkyl group, and L is a neutral monodentate ligand such as H_2O, pyridine, acetonitrile, or a carboxylic acid (**Scheme 3.1.1**).[5-6, 8-9, 11, 14] The general approach of many literature reports is to generate MnO-type clusters through the control of the atomic Mn:O ratios, from the ground, up. This is accomplished by adding varying molar amounts of manganese source and carboxylic acid into a reaction vessel, then initiating the self-assembly reaction by adding equimolar amounts of an oxidizing agent.

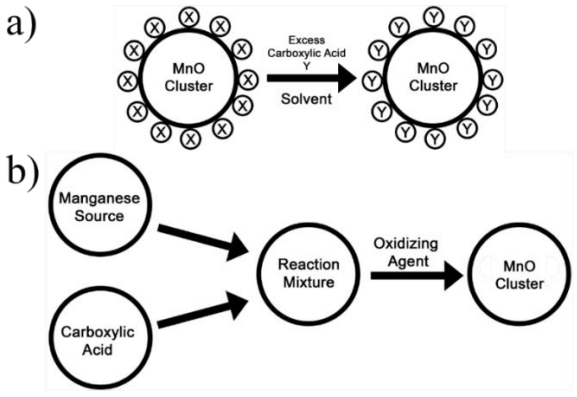

Scheme 3.1.1 Basic schematic illustrating the differences between the substitutive approach, *top*, versus the 'ground-up' approach, *bottom*, for generating new MnO-type clusters.

3.1.2.1 *Ortho*-Substituted Benzoic Acids

As introduced in Chapter 2, carboxylates, especially benzoic acids, are an effective and modular tool to use as building blocks for the structural tuning and assembly of metal oxide complexes. The vast library of arene-substituted carboxylates and their access to multiple bonding modes with metals, make substituted benzoic acids a venerable molecular design tool (**Figure 3.1.1**).[16-17] In particular, the *ortho*-position of benzoic acid offers the optimal functionalization site that would will likely influence the assemblage of the MnO-type cluster due to its proximity to the μ_2-oxygens which are critical for the architectural oxo-bridge component in any MnO-type cluster (**Scheme 3.1.2**).

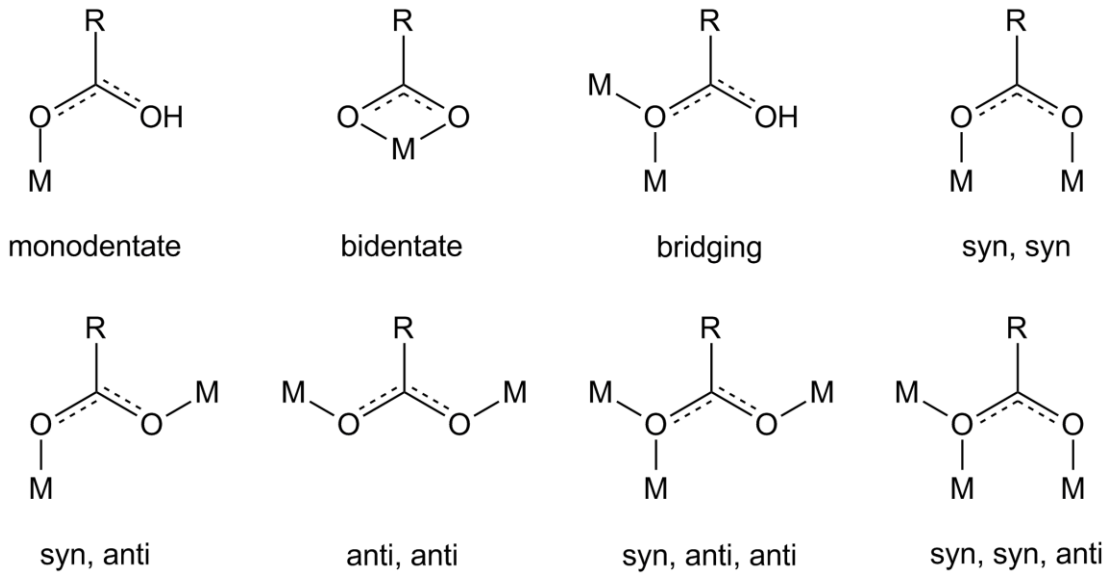

Figure 3.1.1 Various binding modes of metal carboxylates. Figure adapted from reference 17.

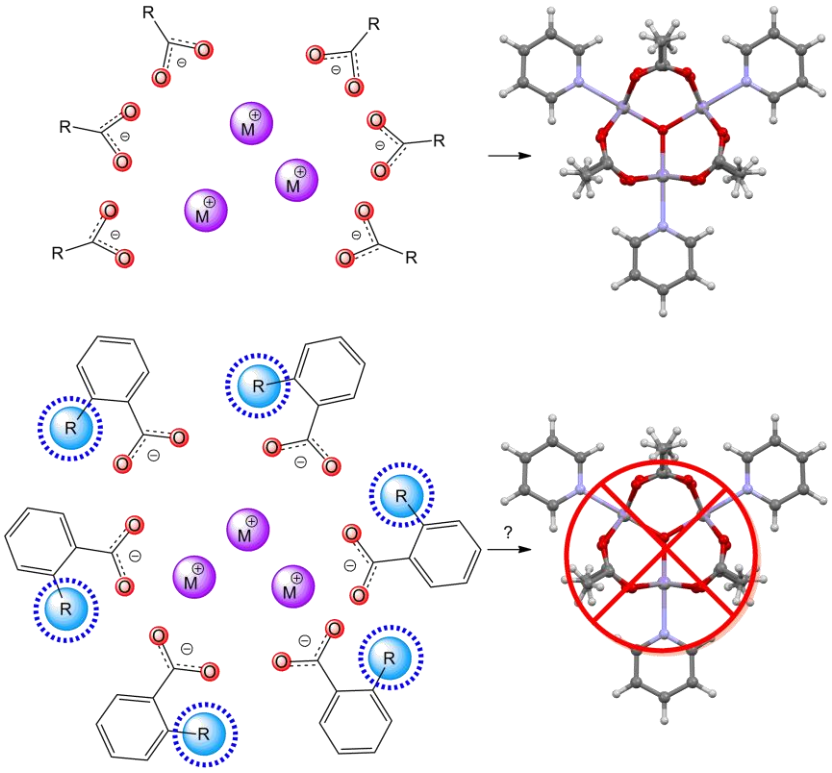

Scheme 3.1.2 Schematic of *ortho*-positioned functional group on benzoic acid interfering with assembly. *Top*, the assembly of un-obstructed carboxylates and metal ions forms the predicted Mn_3O-type cluster.[18] *Bottom*, benzoic acids with bulky *ortho*-substituents interfere with assembly and the predicted Mn_3O-type compound is not generated.

3.1.3 $Mn_xO_y(O_2CR)_zL_w$ 'Ground-Up' Complexes

As discussed above and shown in **Scheme 3.1.1** many researchers have approached the control and generation of new MnO-type clusters by varying the preparative Mn:O atomic ratios; we propose a different method of controlling the generation of new MnO-type clusters. The focus of this study is to take published and reliable procedures to MnO-type clusters and see how the methods may be altered so that the expected product is supplanted. Instead of modifying the *ratios* of Mn:O we propose to modify the size and shape of the carboxylate building blocks systematically *via ortho*-substituted benzoic acids. Specifically, we will take the existing

synthetic procedures, and exchange the carboxylic acids used in the published procedure with the following proposed *ortho*-substituted benzoic acids (**Figure 3.1.2**).

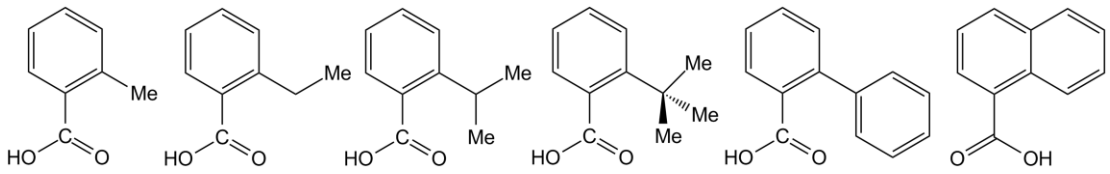

Figure 3.1.2 The proposed series of systematically enlarging *ortho*-substituted benzoic acids.

Two well studied MnO-type clusters synthesized *via* these so-called 'ground-up' methods were selected as the focus of this research; The tridecanuclear $Mn_{13}O_8$-type compound, $Mn_{13}O_8(O_2C\mathbf{R})_{12}(OEt)_6$, and the trinuclear Mn_3O-type compound, $Mn_3O(O_2C\mathbf{R})_6(Pyr)_3$. These MnO-type clusters were selected for investigation based upon their synthetic approaches, and not necessarily for their functional performance; whether it be water oxidation or magnetic behavior. One high nuclearity cluster, and one low nuclearity cluster was selected. The difference in nuclearities between the clusters opens up separate possibilities for modifying the predicted reported cluster. The high nuclearity cluster may show resistance to steric influence due to its mass, it might be more likely to modify the formation of a smaller, potentially more malleable, lower nuclearity cluster.

3.1.3.1 $Mn_{13}O_8$-Type 'Ground-Up' Cluster

One such 'ground-up' derived manganese oxide cluster of interest is the $Mn_{13}O_8$-type complex, $Mn_{13}O_8(O_2CC_6H_4OPh)_{12}(OEt)_6$.[19] Like the Mn_{12}-type compounds, this $Mn_{13}O_8$-type compound has garnered interest due to its high S_6 molecular symmetry and R-3 crystal symmetry, and also its access to an additional oxidation state, Mn^{II}. The misaligned elongated JT axis of Mn_{12}-type clusters provides a considerable rhombic component to the molecular anisotropy, which enables lower tunneling of the magnetization, and lowers the operative blocking

temperature.[20-21] Conversely, the $Mn_{13}O_8$-type cluster features increased axial anisotropy and symmetry over Mn_{12}-Acetate, potentially stabilizing the field induced magnetic states, increasing the blocking temperature, and preventing easily accessible tunneling routes. Based on these characteristics, the $Mn_{13}O_8$-type compound should feature interesting magnetic behavior when compared to Mn_{12}-type clusters.[22-26]

The $Mn_{13}O_8$-type cluster is described as a mixed valence, tridecanuclear MnO distorted-cube cluster possessing six Mn^{II} and six JT distorted Mn^{III} ions on the outer portion of the cluster, and one Mn^{IV} ion in the middle of the core (**Figure 3.1.3**).[19] The cluster core contains six μ_3-ethoxide molecules located at the corners of the distorted cube, which bridge two Mn^{II} ions and one Mn^{III} ion each. Of the eight remaining bridging oxygens: the six located on the face of the cube are μ_4-type and participate in the bridging of two Mn^{III} ions, one Mn^{II} ion, and the central Mn^{IV} atom, the last two μ_3-type oxo-groups bridge three Mn^{III} ions.

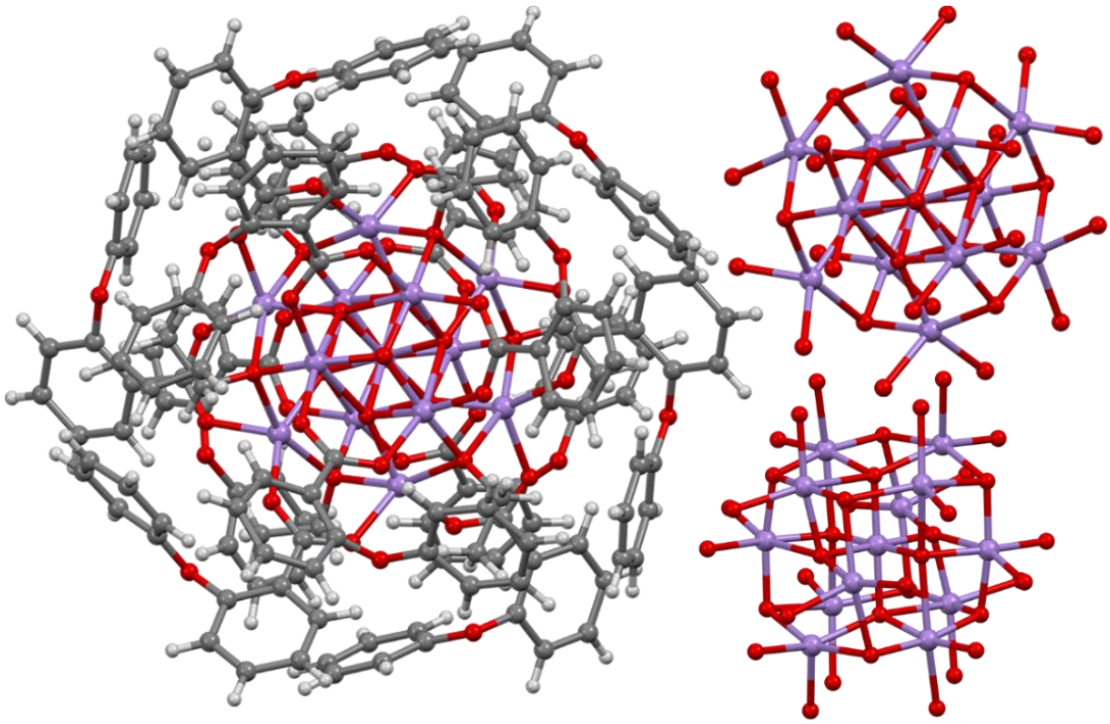

Figure 3.1.3 *Left,* the tridecanuclear $Mn_{13}O_8$-type Cluster, $Mn_{13}O_8(O_2CC_6H_4OPh)_{12}(OEt)_6$, viewed along the C-axis (Refcode: JETVOU).[19] *Top right*, Same view, carbons and hydrogens removed for clarity. *Bottom right*, core viewed along the B-axis. *Note: For all crystal structures featured in schemes and figures to follow, dark grey spheres represent carbon atoms, light grey spheres represent hydrogen atoms, purple spheres represent manganese atoms, blue spheres represent nitrogen atoms, red spheres represent oxygen atoms, and bright green spheres represent the* ***R*** *group of a carboxylate.*

3.1.3.2 Mn_3O-Type 'Ground-Up' Cluster

Another popular MnO-type 'ground-up' cluster is the trinuclear $Mn_3O(O_2C\mathbf{R})L_3$ complex. Interest in these types of trinuclear metal oxide compounds was historically focused on this cluster's potential for catalytic water oxidation,[2-3, 27] as well as its electronic and superexchange interaction comparison to analogous Fe_3O complexes;[28-31] not shocking, as this time was rife with the study of superexchange complexes. At the time, this complex represented

another example of an MnO-type cluster obtained *via* use of tetrabutylammonium permanganate in a nonaqueous solvent for inorganic synthesis, a reagent whose usefulness in MnO-type cluster generation was under investigation.[12, 15] This complex provided to researchers a variety of new and unexpected synthetic routes to explore.

This MnO-type cluster is described as a trinuclear manganese oxide cluster. Each Mn^{III} ion is bridged by equatorially bound carboxylates and a central, axially bound oxygen. Each Mn^{III} ion has an axially coordinated pyridine molecule, completing the octahedron (**Figure 3.1.4**).[18] There also exists a multivalent Mn^{II}/Mn_2^{III} version of this cluster featuring one pyridine being replaced by a water molecule.[18]

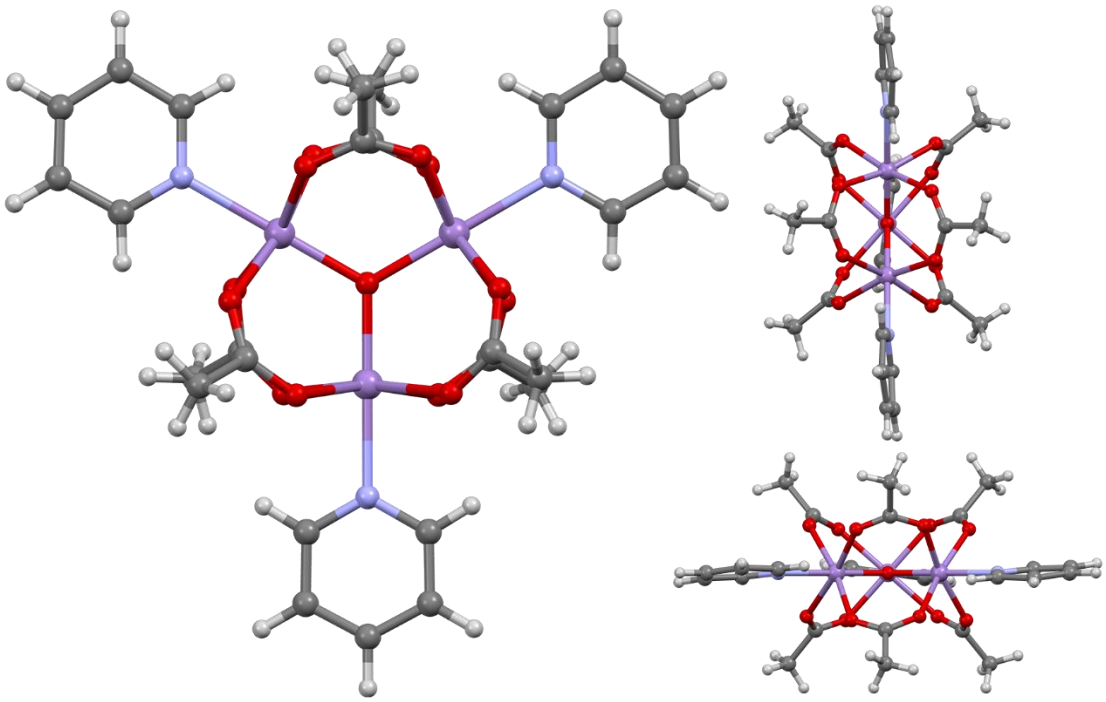

Figure 3.1.4 The Mn_3O-type complex $Mn_3O(O_2CMe)_6(Pyr)_3$ (Refcode: FOBROD).[18] *Left*, viewed along the C-axis. *Top right*, Viewed along the B-axis. *Bottom right*, viewed along the A-axis.

The Mn_3O-type cluster has also been identified as a building block for other MnO-type clusters[12] *via* postsynthetic treatment with strong oxidizing agents,[32] through solvothermal methods,[33-34] or mixed with other solvates for reaction with 2-pyridinemethanol (**Scheme 3.1.3**).[35] This extended usefulness furthered interest in the material, as additional routes to generating many different materials was introduced through this cluster.

For our purposes, this feature allows the potential for synthetic diversity. Where an initial Mn_3O-type cluster may be first synthesized *via* a bulky carboxylic acid, modifying its *initial* assembly, then a subsequent treatment route on the newly generated Mn_3-**R** compound may then be utilized as a building block for another type of material, further drifting the products from the expected materials.

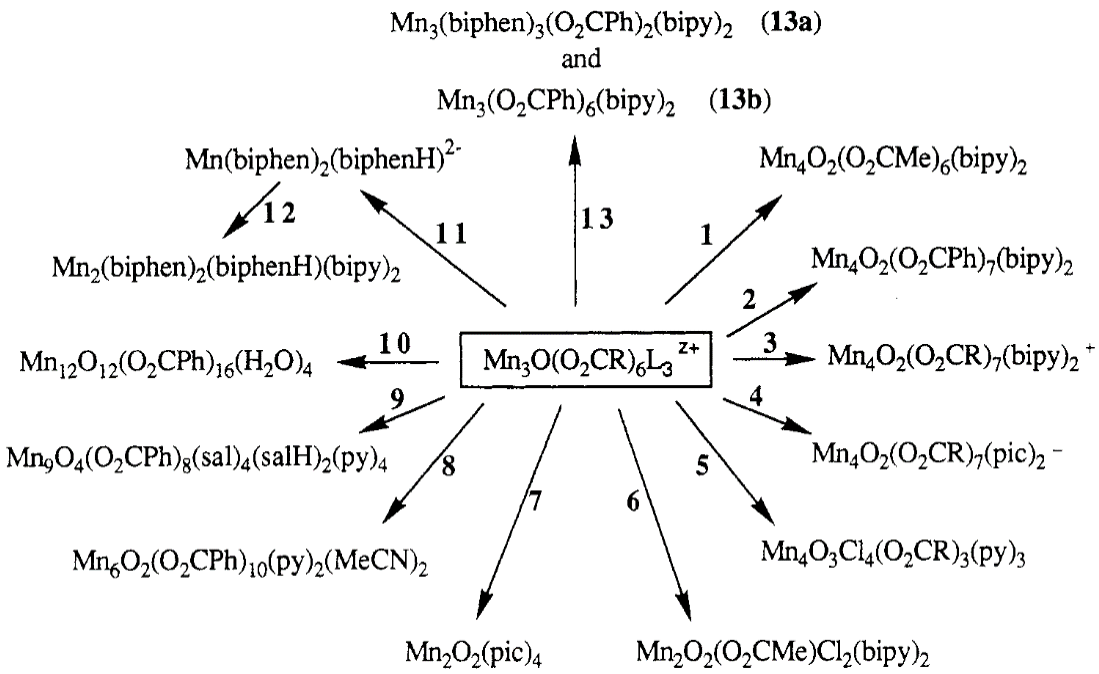

Scheme 3.1.3 Some established routes to other $Mn_xO_y(O_2C\mathbf{R})_zL_w$ clusters *via* Mn_3O-type clusters as a starting material. Scheme adapted from reference 12.

3.1.4 The Objective

To reiterate the specific goals presented in Chapter 1; we wish to investigate whether we can generate new MnO-type clusters of formula $Mn_xO_y(O_2C\mathbf{R})_zL_w$ by modifying literature published synthetic procedures which directly implement *any* carboxylic acid from the start of the synthesis.

In this chapter, rather than using the substitutive method covered in the previous chapter, we will employ flexible synthetic routes which implement the desired carboxylate from the beginning of the process, i.e., 'ground-up' synthesis. The work in this chapter is focused on synthesizing new manganese oxide clusters by deviating from the existing synthetic routes by swapping the intended carboxylic acid with various bulkier *ortho*-substituted benzoic acids. We shall generate new MnO-type clusters specifically by frustrating the physical path of the cluster's starting materials as they assemble, through rational design philosophy; achieved *via* systematic carboxylate selection.

Based on the plethora of MnO-type clusters discussed in the literature, as the synthetic building blocks change we may see a change in the structure (e.g., size, shape) of the cluster. Although it is not *explicitly* predictable, the **hypothesis** is that through these 'ground-up' methods employed in the synthesis of $Mn_{13}O_8$-type, and Mn_3O-type clusters, i.e., the desired building blocks are introduced *in situ*, the ability to impact the formation of the cluster will be much greater relative to previously the studied substitutive methods. As a result, by systematically enlarging the starting carboxylic acid from a smaller *ortho*-substituent of benzoic acid to a larger substituent, as described above in **Scheme 3.1.2**, the expected formation of the cluster will be impacted such that a different cluster will form altogether.

Moreover, we predict that as the substituent of the *ortho*-substituted benzoic acid increases in size, the type of cluster that results can be directly attributed to the size of the *ortho*-

substituent, i.e., larger substituents will result in greater product deviation. We lean on earlier results with Cd-Cl for this prediction (as described in **Section 2.1.3**).

Herein, we move to discuss a variety of compounds generated *via* 'ground-up' methods!

3.2 Experimental

All chemical reagents, with the exception of $MnCl_2$, NaOMe, and 2-ethylbenzoic acid, were used as received from Sigma-Aldrich without further purification. $MnCl_2$, as $MnCl_2 \bullet 4H_2O$, and sodium methoxide were purchased from Strem Chemicals, and used as received. 2-ethylbenzoic acid was purchased from Combi-Blocks and used as received. All solvents used, with the exception of ethanol, were distilled prior to use. Ethanol was used as 200 proof USP grade, with no further modification. Water was freshly prepared from a Milli-Q® Integral Water Purification System. All crystallization was performed at room temperature in a low-vibration area. Melt point data were collected on an OptiMelt Automated Melting Point System operating in the range of 28-380 °C, at a rate of 2.5 °C per minute. Additional X-ray crystallographic tables can be found in Appendix II.

3.2.1 Synthesis of Mn_{13}-R Complexes

Synthesis of $Mn_{13}O_8$-type complexes is performed as detailed previously.[19] Generally, synthesis of the $Mn_{13}O_8$-type cluster is achieved through the addition of two separately prepared solutions; the sodium salt of a carboxylic acid and an $MnCl_2$ solution, both in methanol. To the combined solution is added supplementary sodium methoxide which initiates the assembly process (**Scheme 3.2.1**). The solution is stirred 24 hours and filtered. The solvent is removed *in vacuo* and ethanol is added. Crystals of the Mn_{13}-**R** complex, where **R** represents the carboxylic acid utilized, are grown *via* vapor diffusion with ether (**Figure 3.2.1**).

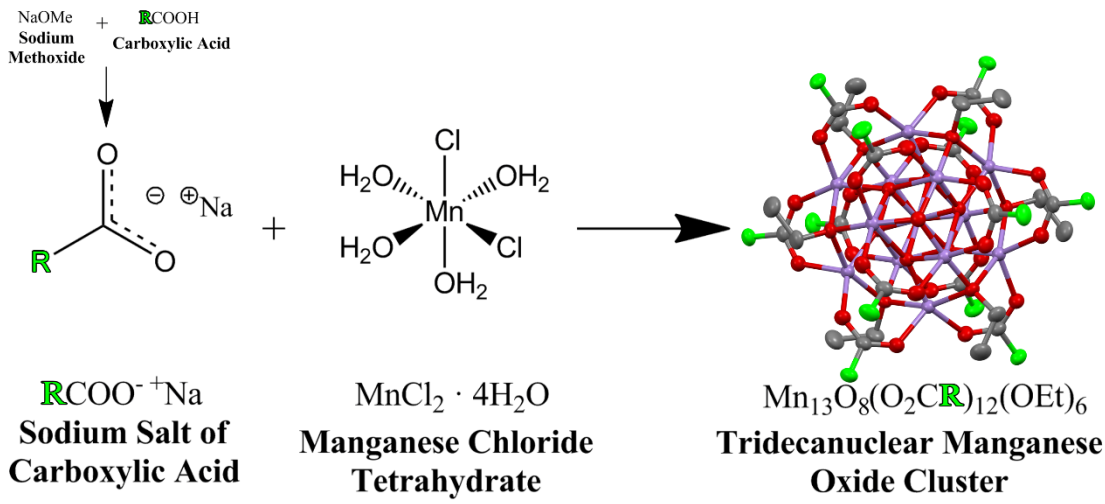

Scheme 3.2.1 General approach to synthesis of $Mn_{13}O_8$-type, Mn_{13}-**R** complexes, where bright green spheres represent the **R** group of a carboxylate. Hydrogens removed for clarity.

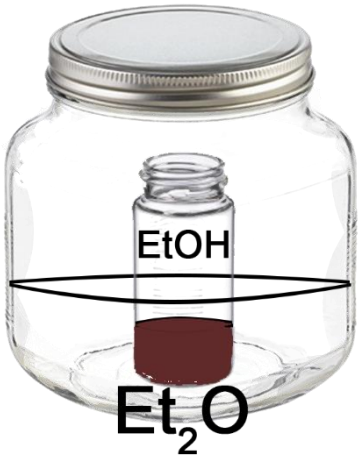

Figure 3.2.1 Vapor diffusion crystallization strategy for Mn_{13}-**R** complexes. Complex is dissolved in alcohol with ether slowly diffusing into the center vial.

3.2.1.1 Synthesis of Mn_{13}-R Compounds 1-3

Synthesis of Mn_{13}-2-Methyl, **1**, Mn_{13}-2-Ethyl, **2**, Mn_{13}-2-Phenyl, **3**. Synthesis of **1-3** is performed as reported previously.[19] To a flask containing 16.2 mmol carboxylic acid (2.211 grams *o*-toluic acid, **1**, 2.433 grams 2-ethylbenzoic acid, **2**, 3.221 grams biphenyl-2-caboxylic

acid, **3**) in 35 mL freshly distilled methanol, is added 16.2 mmol (875 mg) sodium methoxide under vigorous stirring. In a second flask, 7.75 mmol (1.533g) $MnCl_2 \cdot 4H_2O$, is dissolved in 35 mL fresh distilled methanol. After complete dissolution, these two solutions are combined, and an additional 7.75 mmol (419 mg) sodium methoxide is added to the stirring solution. This reacted solution is allowed to stir for 24-hours, then filtered through celite. A 4 mL sample of the filtrate is collected and the solvent is removed *in vacuo*. The dried solid is redissolved in 12.5 mL alcohol (methanol, **1**, ethanol, **2**-**3**), added to a scintillation vial and placed into a sealed jar containing 20 mL ether to crystallize *via* vapor diffusion. X-ray quality rods of **1**-**3** form after days in 10%, **1**, 7%, **2**, and 8%, **3**, yields.

3.2.2 Synthesis of Mn_3O-type Complexes

Generally, synthesis of Mn_3O-type compounds is performed as previously reported,[18] *method 4*. Manganese acetate tetrahydrate and carboxylic acid are dissolved in pyridine and absolute ethanol in a 1:7.5 molar ratio. Freshly synthesized N-*n*-Bu_4MnO_4 is slowly added to the stirring solution, initiating the assembly of the Mn_3O-type cluster (**Scheme 3.2.2**). The precipitate is collected after 24-hours, washed with ethanol, and dried *in vacuo*. This solid is dissolved in acetonitrile, and slowly concentrated to form crystals.

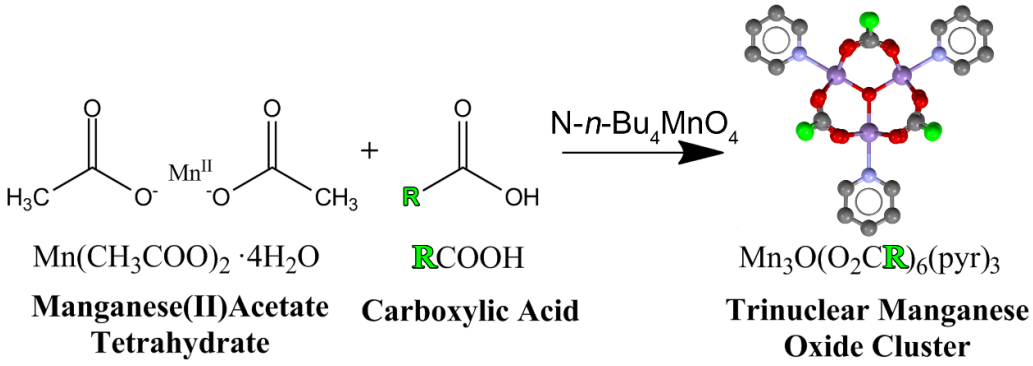

Scheme 3.2.2 Generation of Mn_3O-type complexes, *pyr* = pyridine. Hydrogens removed for clarity.

3.2.2.1 Preparation of N-*n*-Bu_4MnO_4

Generation of N-*n*-Bu_4MnO_4 is accomplished as reported previously.[36] 31 mmol (10 g) of N-*n*-Bu_4Br is dissolved in 100 mL Milli-Q® water. In a separate flask, 26.34 mmol (4.16 g) $KMnO_4$ is dissolved in 60 ml Milli-Q® water, and then added slowly to the flask containing aqueous tetrabutylammonium bromide under vigorous stirring. The immediate purple solid is collected and washed with water and ether, then dried *in vacuo* for 24 hours in 79 - 85.4% yield. ***Warning***. Extreme care must be taken in the handling of quaternary ammonium permanganate salts. These materials may detonate during drying at temperatures of 80 °C and above.

3.2.2.2 Synthesis of Mn_3-R Compounds 4-5

Synthesis of Mn_3-2-Methyl, **4**, and Mn_3-2-Ethyl, **5**. 4.075 mmol (1 g) $Mn(OAc)_2 \cdot 4H_2O$ and 30.7 mmol carboxylic acid (4.18 g *o*-toluic acid, **4**, 4.60 g 2-ethylbenzoic acid, **5**) are added to a flask containing 10 mL ethanol and 1.5 mL pyridine and stirred to dissolution. To this solution is added 1.575 mmol (570 mg) N-*n*-Bu_4MnO_4 and is allowed to stir for 24 hours. The precipitate is collected *via* filtration and washed to dryness with copious amounts of ethanol. 20 mg of solid is dissolved in 1 mL freshly distilled dichloromethane and layered in a lightly capped test tube with 3 mL fresh acetonitrile, **4**, or n-hexane, **5**. X-ray quality crystals form in days in 43% **4** as rods (**a**) and cubes (**b**), and 56.3%, **5** as rods, yields.

3.2.3 X-Ray Crystallography

Crystalline samples of **1-5** were suspended in Paratone oil and subsequently mounted on a MiTeGen dual-thickness microloop. All data were collected using a Bruker Kappa or SMART Apex II X-ray diffractometer. A graphite monochromated Mo Kα ($\lambda = 0.71703$ Å) radiation at 100 K was used for all samples. Crystal structures were solved utilizing the OLEX2 software package[37] which functions using SHELX protocols.[38] Structure solution was achieved by way of

direct methods and refined using least squares minimization which are both part of the SHELX-97 package. Brief crystal data for each compound is tabulated in **Table 3.2.1**, full sets of crystallographic tables for each compound may be found in Appendix II.

Compound	**1**	**2**	**3**
Molecular Formula	$C_{102}H_{114}Mn_{13}O_{38}$	$C_{120}H_{408}Mn_{13}O_{39}$	$C_{168}H_{138}Mn_{13}O_{38}$
Molecular Weight	2662.15	2920.53	3479.00
Crystal System	Triclinic	Triclinic	Monoclinic
Space Group	P1	P-1	C2/c
***a* (Å)**	14.6088(6)	15.0417(14)	28.1239(8)
***b* (Å)**	15.0498(9)	15.3652(14)	18.1122(6)
***c* (Å)**	15.5875(7)	16.7271(15)	30.7895(9)
α (°)	92.426(3)	107.544(5)	90.0
β (°)	111.672(2)	98.279(5)	94.279(2)
γ (°)	118.932(2)	116.328(5)	90.0
Volume (Å^3)	2682.5(2)	3124.5(5)	15640.0(8)
Z	1	1	4
T (K)	100(2)	100.02	100.02
Reflections Measured	54581	38588	55054
Unique Reflections	24370	8720	5614
R_{int}	0.0554	0.0628	0.0806
R_1 [I > 2σ(I)]	0.0512	0.0578	0.0649
wR_2 [I > 2σ(I)]	0.1155	0.1727	0.1970

Compound	**4a**	**4b**	**5**
Molecular Formula	$C_{120}H_{106}Mn_{12}O_{48}$	$C_{114}H_{96}Mn_9N_2O_{33}$	$C_{69}H_{69}Mn_3N_3O_{13}$
Molecular Weight	2580.49	2516.38	1237.99
Crystal System	Monoclinic	Monoclinic	Triclinic
Space Group	C2/c	C2/c	P-1
***a* (Å)**	17.335(4)	55.133(2)	12.0698(12)
***b* (Å)**	38.061(9)	18.8416(8)	14.3404(14)
***c* (Å)**	21.193(5)	21.8802(9)	19.1822(18)
α (°)	90.0	90.0	82.143(5)
β (°)	98.219(15)	94.757(2)	89.878(5)
γ (°)	90.0	90.0	70.928(5)
Volume (Å^3)	13839(6)	22650.6(16)	3105.3(5)
Z	4	8	2
T (K)	105(2)	100(2)	100(2)
Reflections Measured	59171	70380	52918
Unique Reflections	7707	7166	12353
R_{int}	0.1148	0.0604	0.0416
R_1 [I > 2σ(I)]	0.2260	0.0706	0.0412
wR_2 [I > 2σ(I)]	0.5847	0.2095	0.1014

Table 3.2.1 Table of crystallographic data for compounds **1**-**5**

3.3 Results

Following the reported synthetic procedures, the reactions cleanly resulted in: **1**, Mn_{13}-2-Methyl ($Mn_{13}O_8(O_2CPh\text{-}o\text{-}Me)_{12}(OEt)_6$); **2**, Mn_{13}-2-Ethyl ($Mn_{13}O_8(O_2CPh\text{-}o\text{-}Et)_{12}(OEt)_6$); **3**, Mn_{13}-2-Phenyl ($Mn_{13}O_8(O_2CPh\text{-}o\text{-}Ph)_{12}(OEt)_6$); **4a**, Mn_{12}-2-Methyl ($Mn_{12}O_{12}(O_2CPh\text{-}o\text{-}Me)_{16}(H_2O)_4$); **4b**, Mn_9-2-Methyl ($Mn_9O_7(O_2CPh\text{-}o\text{-}Me)_{13}(Pyr)_2$); and **5**, Mn_3-2-Ethyl ($Mn_3O(O_2CPh\text{-}o\text{-}Et)_6(Pyr)_3$). Following the reported procedures for the $Mn_{13}O_8$-type and the Mn_3O-type clusters utilizing various *ortho*-substituted benzoic acids resulted in crystals in the final step with negligible modification. Recrystallization of the microcrystalline powder of **4** resulted in the formation of two different materials, identifiable by their crystal shape: rods (**a**) or cubes (**b**).

In order to grow crystals of compounds **4** and **5**, a slightly modified crystallization strategy was required where instead of slowly concentrating the acetonitrile solution, the microcrystalline powder was first dissolved in dichloromethane then layered with either acetonitrile (**4**) or *n*-hexane (**5**). Following the reported crystallization procedure for these compounds resulted in an oily product, which streaked up the side of the crystallization vessel.

3.3.1 $Mn_{13}O_8$-type 'Ground-Up' Compounds 1-3

Crystals of compounds **1**, **2**, and **3**, of formula $Mn_{13}O_8(O_2CPh\text{-}o\text{-}\mathbf{R})_{12}(OEt)_6$ where **R** = methyl (**1**), ethyl (**2**), or phenyl (**3**), were generated, at expectedly low yields,[19] and solved *via* crystallographic methods. Analysis of the crystal structure reveals that three compounds of the $Mn_{13}O_8$-type cluster shape were generated regardless of the type of benzoic acid utilized (**Figure 3.3.1**).

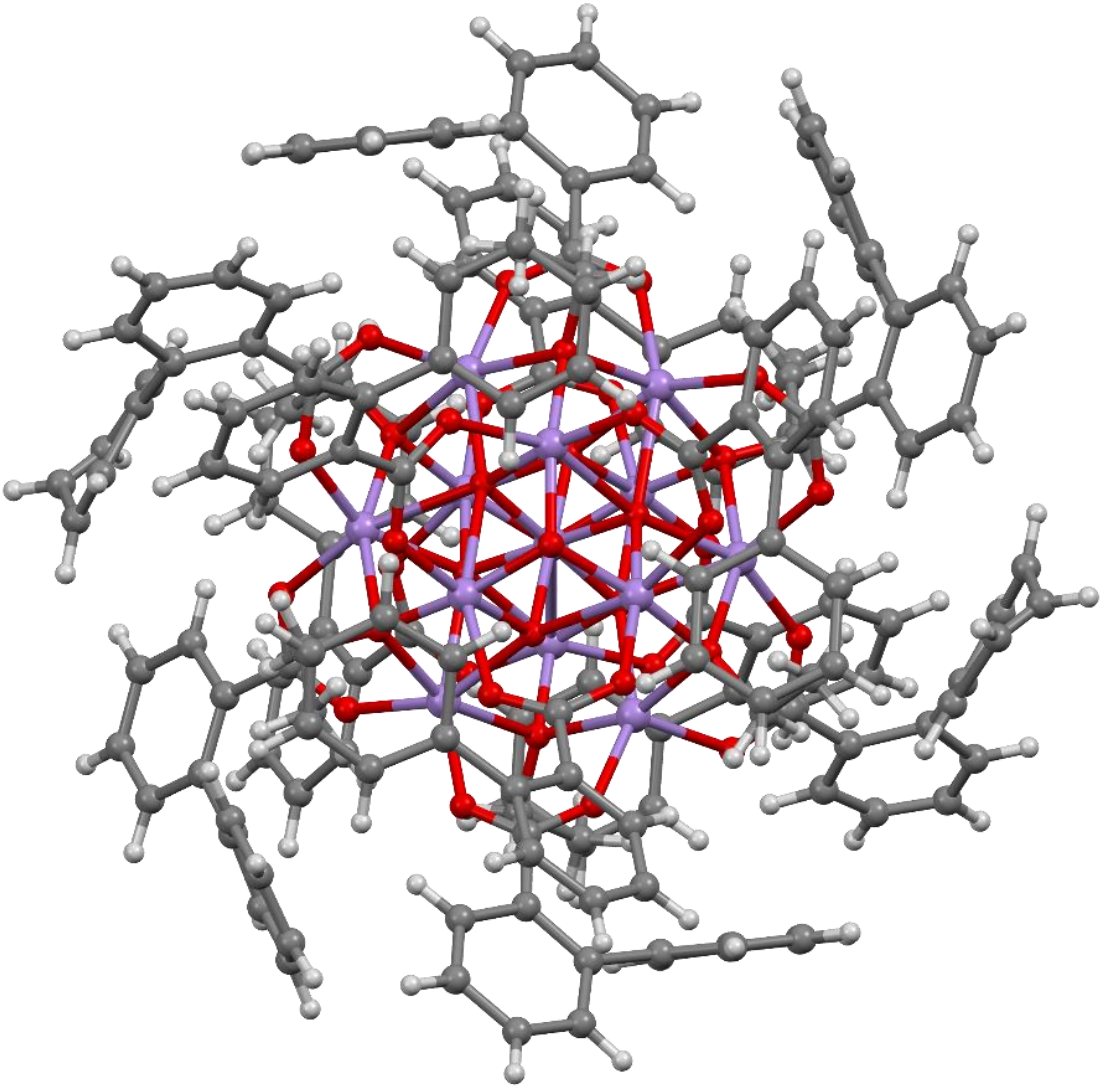

Figure 3.3.1 Mn_{13}-2-Phenyl compound **3**. Isostructural with compounds **1**-**2**.

Compounds **1** and **2** crystallize in the triclinic crystal system, and compound **3** is monoclinic; each lower symmetry than the parent $Mn_{13}O_8$-type compound (orthorhombic),[19] representing the only major structural difference from the $Mn_{13}O_8$-type parent complex outside of the starting materials utilized.

3.3.2 Mn_3O-Type 'Ground-Up' Compounds 4-5

Following the published procedure for compounds **4-5**, and layering the dissolved solutions in acetonitrile and *n*-hexane respectively, resulted in X-ray quality crystals in days.

For crystals of **4**, two types of crystals were encountered. Slightly above the solvent line were thin rods, and below the solvent line, and in high aggregates at the bottom of the vial, were small cubes. Visual inspection and unit cell determination identified different physical and unit cell parameters for each crystal, and subsequent structure solution positively revealed two different MnO-type structures: **4a,** an Mn_{12}-type compound, Mn_{12}-2-Methyl ($Mn_{12}O_{12}(O_2CPh\text{-}o\text{-}Me)_{16}(H_2O)_4$); and **4b,** an Mn_9O_7-type cluster, Mn_9-2-Methyl ($Mn_9O_7(O_2CPh\text{-}o\text{-}Me)_{13}(Pyr)_2$).

Crystals of **5** grew as the literature expected Mn_3O-type cluster, Mn_3-2-Ethyl ($Mn_3O(O_2CPh\text{-}o\text{-}Et)_6(Pyr)_3$), which exhibits no change in shape from its Mn_3O-type parent cluster.

3.3.2.1 'Mn_3O-2-Methyl' Crystalline Rods, 4a

Rods (**a**) of **4** were analyzed and found to be of different crystal dimensions from the cubes (**b**) of **4**. Data collection of the brittle crystalline rods was of overall low-quality, and a high-quality structure refinement was unobtainable, with a maximum R1 value = 22.6%. However, solving the structure to the furthest possible extent revealed a familiar face. The rods of **4** were of the Mn_{12}-type MnO cluster (**Figure 3.3.2**), and indeed even the unit cell dimensions match those of compound **2** of Chapter 2 (see **Table 2.2.1** and **Table 3.2.1**). Much of the structure is unrefined, due to the very low-quality data, but locating the positions of the core-centered oxygen and manganese atoms was possible. It is evident from visual inspection of the crystal structure that it is of Mn_{12}-type of cluster.

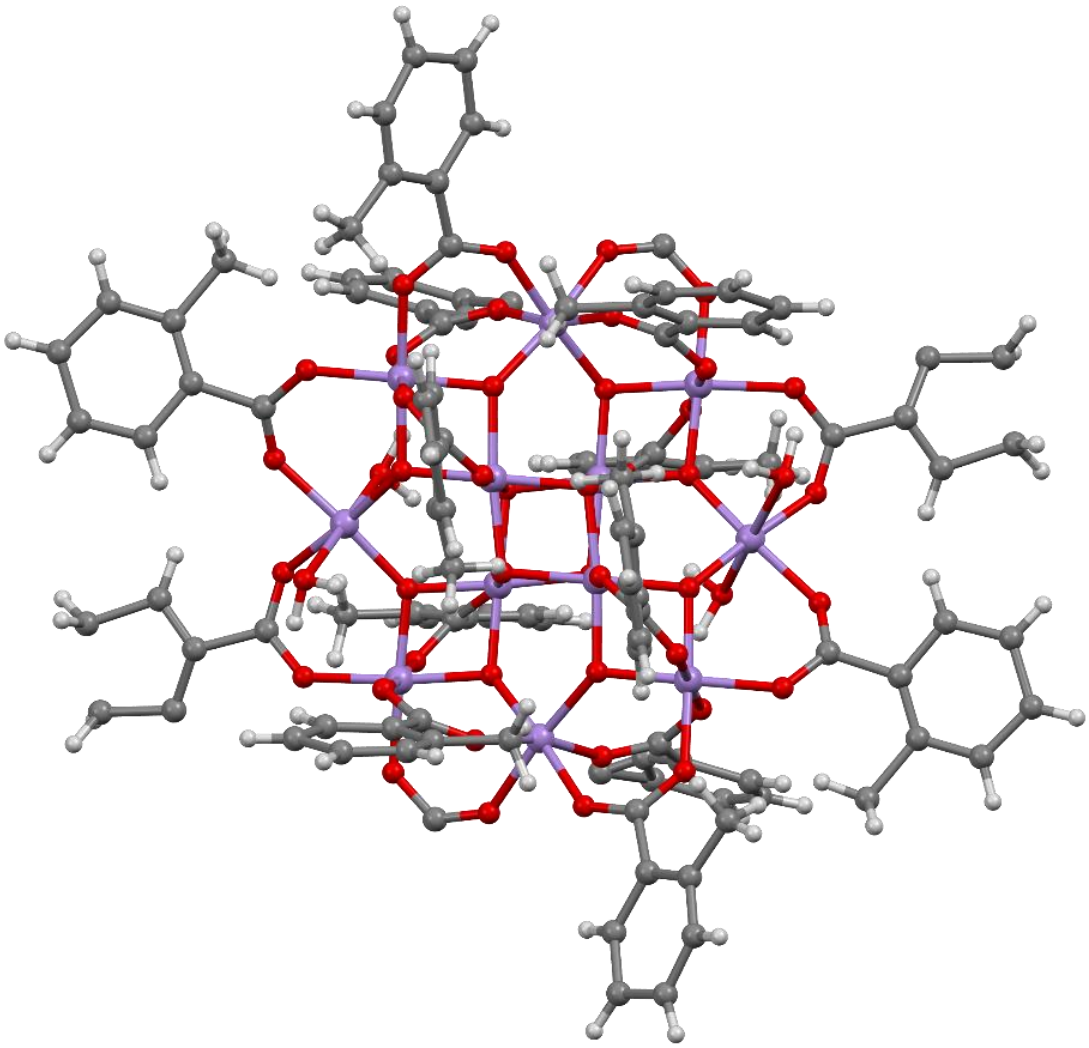

Figure 3.3.2 'Mn_3O-2-Methyl' compound **4a**, Mn_{12}-2-Methyl (likely familiar). Atoms of the Mn_{12}-type core were located, but crystal data is too poor to completely resolve the peripheral organic component.

3.3.2.2 'Mn_3O-2-Methyl' Crystalline Cubes, 4b

The second type of crystal found in the crystallization solution of **4** were cubes. X-ray crystallographic data was obtained and the subsequent structure solution revealed a compound different than the Mn_3O-type cluster! Solving the structure revealed an MnO-type cluster of formula $Mn_9O_7(O_2CPh\text{-}o\text{-}Me)_{13}(Pyr)_2$ (**Figure 3.3.3**). The constituents of the Mn_3O-type parent

compound were all accounted for (e.g., benzoic acid, pyridines), just in differing amounts, and position, indicating that the building blocks assembled in a different manner than expected. *However*, literature inspection and CSD (Cambridge Structural Database) searches[39-40] revealed two other closely related compounds, $Mn_9O_7(O_2CC_6H_5)_{13}(Pyr)_2$ and $Mn_9O_7(O_2CBut)_{13}(MeCN)_2$ (Refcodes: SIZPIA[15] and AHEQEK).[41]

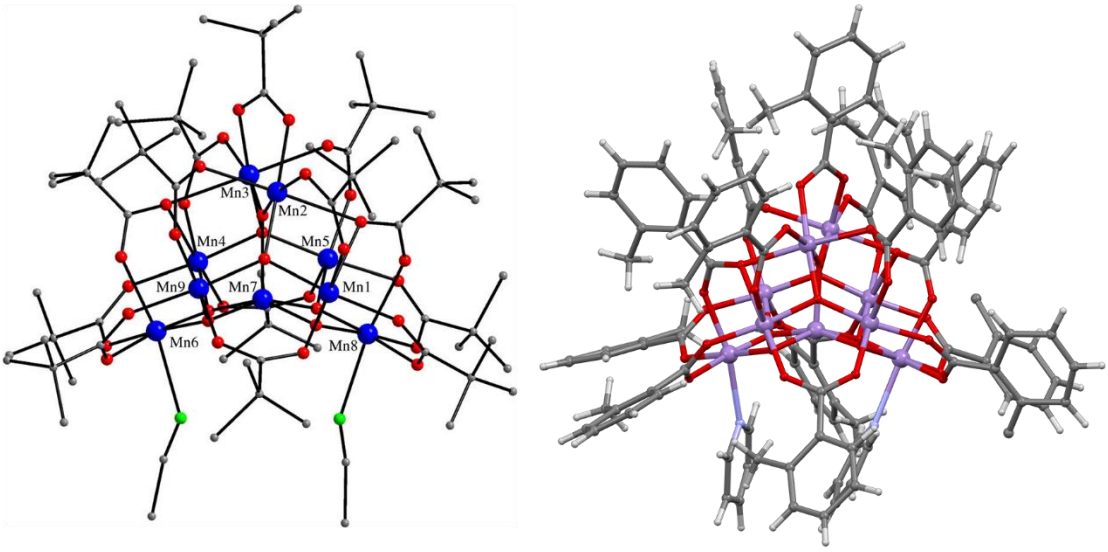

Figure 3.3.3 'Mn$_3$O-2-Methyl' compound **4b**, Mn$_9$-2-Methyl. *Left*, literature compound $Mn_9O_7(O_2CBut)_{13}(MeCN)_2$ (Refcode: AHEQEK).[41] *Right*, compound **4b**, $Mn_9O_7(O_2CPh\text{-}o\text{-}Me)_{13}(Pyr)_2$.

The Mn_9O_7-type structure is described as a nonanuclear manganese oxide cluster, or cage, composed exclusively of Mn^{III} ions (**Figure 3.3.4**) based on the Mn-O bond length data. The core of this MnO cluster is evidently derived from the dimerization of two triangular Mn$_3$O-type clusters, with an additional Mn$_3$-spine component bridging the dimers, shown below in **Figure 3.3.5**. Additionally, the Mn^{III} ions with axially bound nitrogen containing components are typically coordinated by the solvent; pyridine,[15] or acetonitrile,[41] but could theoretically be any neutral monodentate ligand.

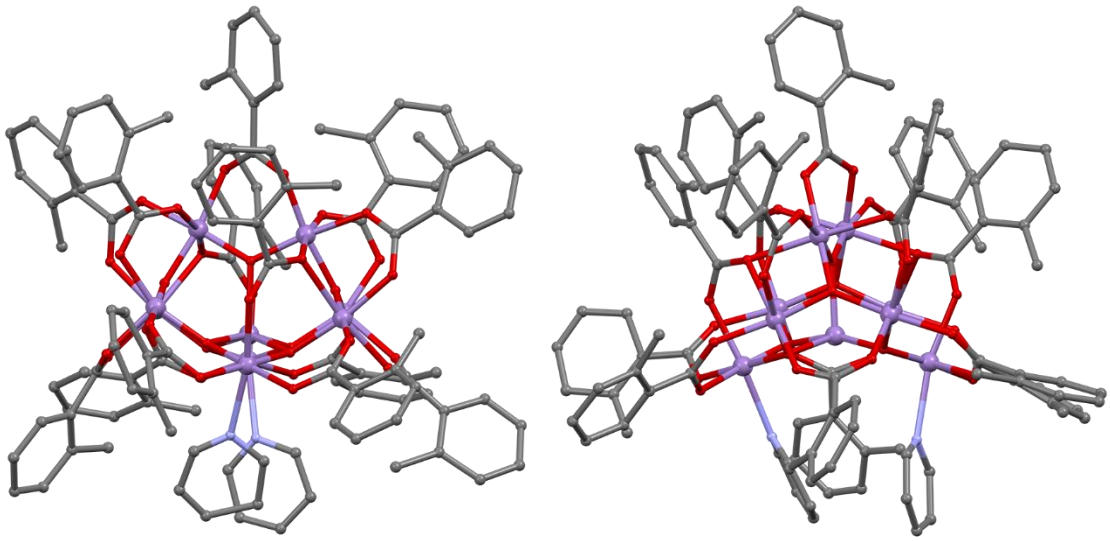

Figure 3.3.4 Mn_9O_7-type Compound **4b**, Mn_9-3-Methyl, different views with hydrogens removed for clarity. *Left* and *right* rotated by 90°.

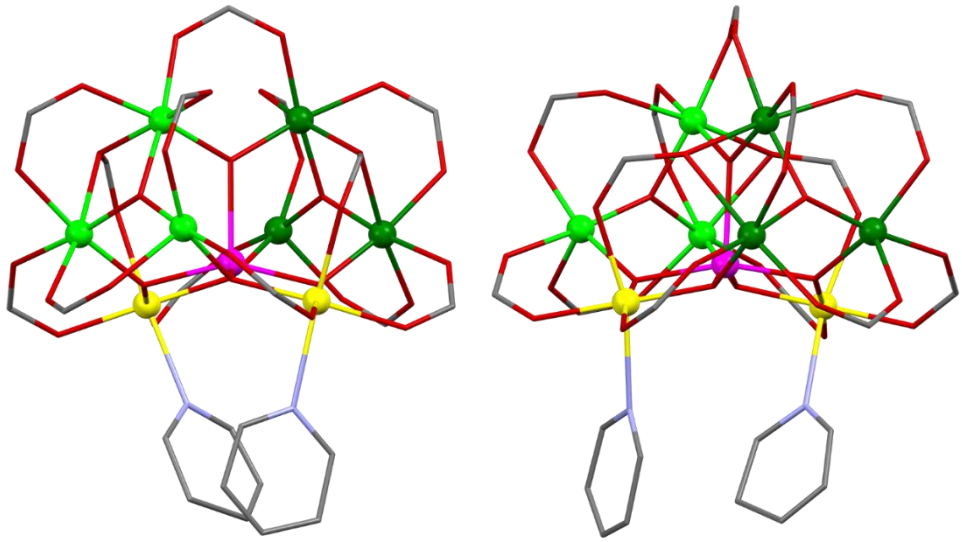

Figure 3.3.5 Compound **4b**, hydrogens and **R** groups of carboxylates removed for clarity. *Left* and *right* rotated by 90°. Metals displayed as spheres, else displayed as skinny tubes. Mn^{III} ions part of Mn_3O-type dimer shown in bright green and green, Mn^{III} ions part of the spine shown in pink and yellow. Pink Mn^{III} ion with axially open coordination site, blocked by flanking pyridine molecules bound to yellow Mn^{III} ions.

3.3.2.3 Mn_3O-2-Ethyl 'Ground-Up' Compound, 5

Following the reported literature procedure for the Mn_3O-type family of compounds utilizing *ortho*-ethyl substituted benzoic acid resulted in crystals of complex **5**. Analysis of the solved crystal structure of this compound reveals an Mn_3O-type cluster, with no visual indication of any steric influence from the *ortho*-ethyl substituted benzoate onto the cluster assembly (**Figure 3.3.6**). Physically, the crystal group has been lowered to triclinic, from the parent species' orthorhombic space group.

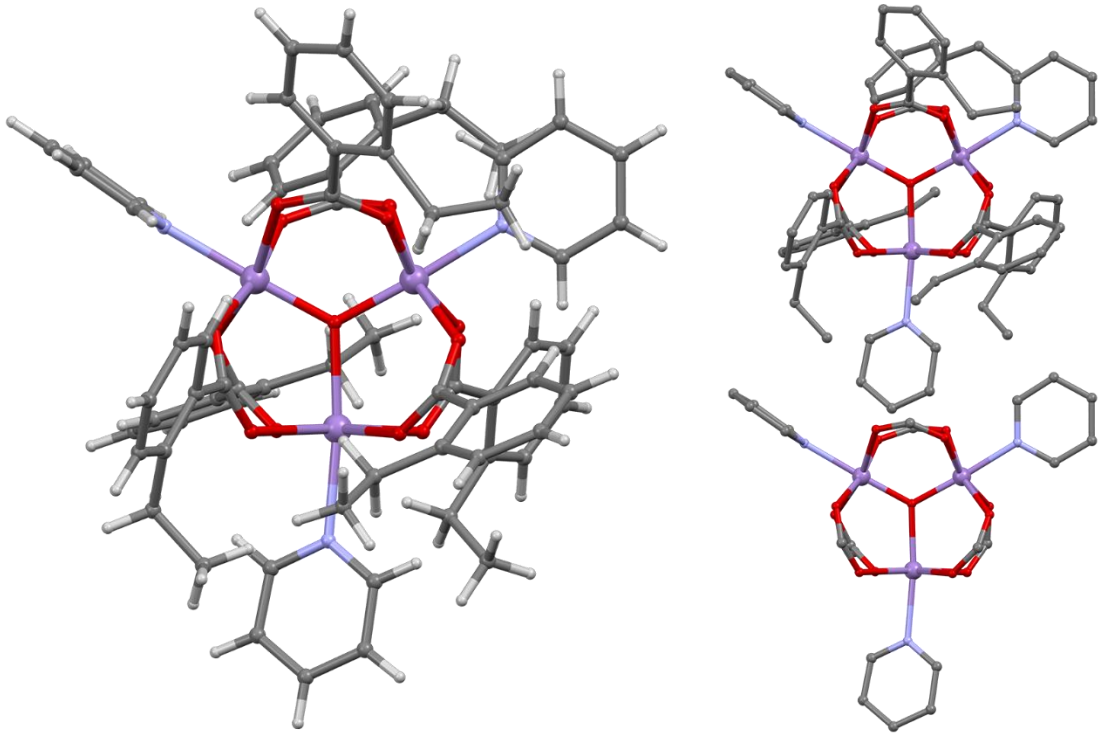

Figure 3.3.6 Mn_3O-type Compound **5**, Mn_3O-2-Ethyl ($Mn_3O(O_2CPh\text{-}o\text{-}Et)_6(Pyr)_3$), *left*. *Right*, Hydrogens removed, *top*, **R** group of carboxylates removed, *bottom*.

3.4 Discussion

In order to evaluate and discuss this work, these results should be discussed as they apply to the specific interests and research objectives proposed in Chapter 1.

The objectives presented in Chapter 1 were direct. They ask, instead of the substitutive methods, can we generate other manganese oxide clusters of formula $Mn_xO_y(O_2C\mathbf{R})_zL_w$ by altering established methods with the previously proposed series of progressively bulky *ortho*-substituted benzoic acids?

Additionally, if yes, can we analyze and compare the newly generated structures, tracing back a root/cause determination for their particular transformation, i.e., do larger substituents results in a more disrupted cluster? Finally, if there is a measurable function of the parent material, how do the new compounds compare to the parent compounds?

To evaluate the results, and provide answers to these queries, we begin with the results of the $Mn_{13}O_8$-type clusters.

3.4.1 $Mn_{13}O_8$-type 'Ground-Up' Complexes 1-3

Looking at the Mn_{13}-**R** compounds generated in this study; comparing them side by side as well as comparing them to the literature reported parent compound, clearly no new MnO-type cluster was generated in this series of experiments (**Figure 3.4.1**). Direct comparison of compounds **1-3** shows negligible change between their structures, and the overlay of the parent compound also shows a negligible change from the parent structure.

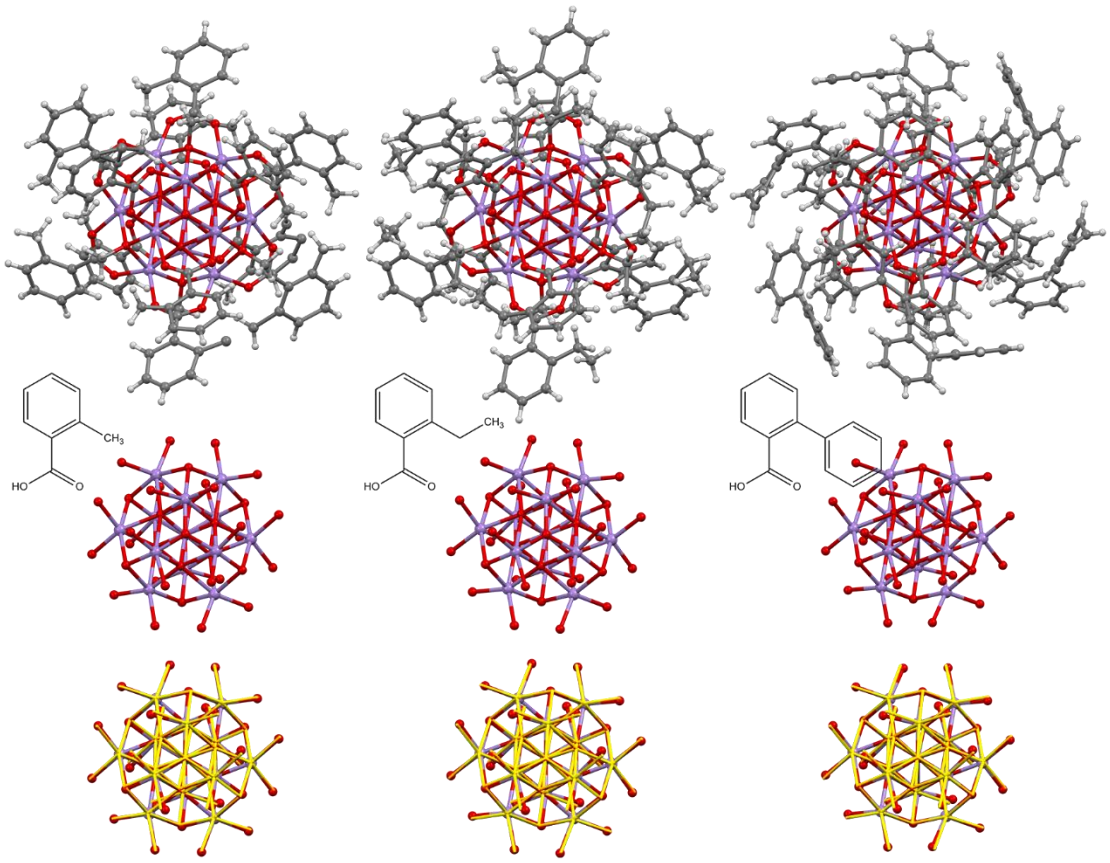

Figure 3.4.1 The Mn_{13}-2-**R** Bunch Compounds. *Top row*: *Left*, Mn_{13}-2-Methyl. *Middle*, Mn_{13}-2-Ethyl. *Right*, Mn_{13}-2-Phenyl. Hydrogens removed for clarity. *Middle row*: carbon component removed from structures. *Bottom row*: $Mn_{13}O_8$-type parent cluster (yellow tubes) superimposed over middle row structures (Refcode: JETVOU).[19]

Neither the *ortho*-phenyl, or the smaller ethyl and methyl substituents were significantly different from the original 2-phenoxybenzoate building block to elicit a change in the produced material. No new MnO-type clusters were generated.

While it may be true that this complex already begins with a 'large *ortho*-substituted benzoic acid; the benzoic acids that we utilize in this study are sterically 'bulky' and different for very specific reasons. Consider the nature of the *ortho*-phenoxy substituent, the elbow on the 2-phenoxybenzoate is in such a position that as the substituent rotates, the ability to block the

cluster's peripheral oxo-bridge is reduced relative to *ortho*-phenyl benzoate; additionally, the phenoxy elbow adds lateral distance between the phenoxy group and the oxo-bridge moiety, lowering its potential architectural impact.

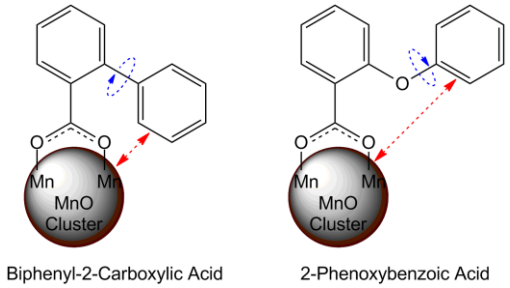

Figure 3.4.2. Potential steric effect of $Mn_{13}O_8$-type 2-phenoxybenzoic acid versus biphenyl-2-carboxylic acid. Blue ring shows rotation, red dotted line shows distance to MnO cluster core.

As for the *ortho*-methyl and ethyl substituents, while these substituents are not as bulky as phenyl or phenoxy, these substituents are important to consider as they represent a reversal of the proposed benzoate system; where we typically take small building blocks and work up systematically to larger building blocks, here we take a synthesis that starts with a relatively large 2-phenoxybenzoate complex, and we essentially work back to a smaller synthon. Additional benzoate candidates should be considered to fully investigate this system, to this end, no *ortho*-substituent influenced the formation of the expected $Mn_{13}O_8$-type cluster.

3.4.2 Mn_3O-type 'Ground-Up' Complexes 4-5

The Mn_3O-type complexes that were investigated in this work provided some interesting results. While the synthesis of **5** simply resulted in the generation of the 2-ethylbenzoic acid analogue of the reported literature compound $Mn_3O(O_2CMe)_6(Pyr)_3$ (**Figure 3.3.6**),[18] albeit at a lower symmetry due to the asymmetry of the *ortho*-substituted carboxylate, the utilization of *o*-toluic acid in the same synthetic scheme resulted in two different crystals altogether. Crystallizing from the mother liquor of **4** resulted in **4a**, an Mn_{12}-type cluster, and **4b**, an Mn_9O_7-type cluster.

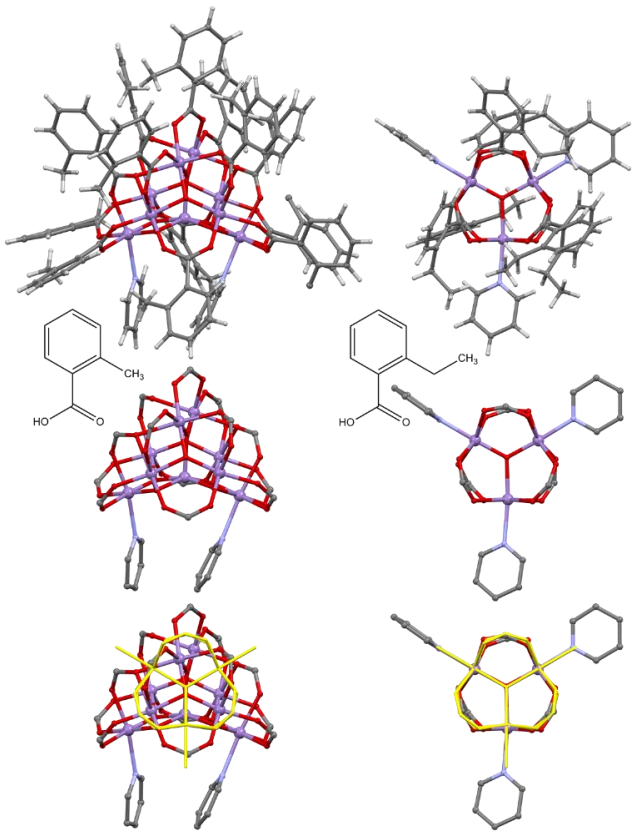

Figure 3.4.3 The Mn_3-2-**R** Bunch Compounds. *Top row*: *left*, 'Mn_3O-2-Methyl', $Mn_9O_7(O_2CPh\text{-}o\text{-}Me)_{13}(Pyr)_2$, *right*, Mn_3O-2-Ethyl, $Mn_3O(O_2CPh\text{-}o\text{-}Et)_6(Pyr)_3$. *Middle row*: **R** group removed from carboxylates. *Bottom row*: Mn_3O-type parent cluster (yellow tubes) superimposed over middle row projections (Refcode: FOBROD).[18]

The cubes of **4**, compound **4b**, were solved and revealed a new crystal structure of formula, $Mn_9O_7(O_2CPh\text{-}o\text{-}Me)_{13}(Pyr)_2$. We can see from the cascade of structures in **Figure 3.4.3** that the use of *o*-toluic acid in this synthetic route resulted in an MnO-type cluster much different from the Mn_3O-type parent complex.

Analysis of the crystal structure of **4b** reveals some interesting physical features of the Mn_9O_7-type cluster; the cluster is composed of a dimer of Mn_3O-type clusters and a 'spine' of three Mn^{III} ions in between the two Mn_3O-type triangular moieties (**Figure 3.3.5**).

The Mn_9O_7-type cluster core can also be found in two related structures in the CSD.[15, 41] While one is closely related, with acetonitrile ligands axially coordinated instead of pyridine (Refcode: AHEQEK);[41] the other is essentially the same compound, featuring benzoic acid instead of *o*-toluic acid (Refcode: SIZPIA).[15]

What is interesting regarding the flanking manganese ions with axially coordinated pyridine ligands is that the limited literature cases regarding this MnO-type cluster report the solvent coordinating, but in the case of **4b**, the crystals were grown in acetonitrile. This indicates that the pyridine is coordinating much more strongly to the Mn^{III} ions than acetonitrile.

Ironically, the unexpected generation of **4a**, by simple assembly in the crystallization media, stands as a testament to the thermodynamic sink that is the Mn_{12}-type cluster. We found in Chapter 2 with the reported compounds, as well as in unreported solvothermal compounds that also produced the same result, that the Mn_{12}-type cluster is a veritable rock, and very difficult to modify or change. Incidentally, this is likely why there are relatively few reports which discuss utilizing Mn_{12}-type clusters as a starting material for new MnO-type clusters.[42]

3.4.3 Magnetization of $Mn_xO_y(O_2CR)_zL_w$ Parent Compounds

Because each of these manganese compounds indeed feature oxo-bound $Mn^{II/III}$ atoms, these ions must be coupled through superexchange interactions. In the current age of SMM renaissance, these interactions should be investigated to probe for SMM effects.

Each MnO parent compound of this work demonstrates generally predictable in-phase magnetization as given by their DC susceptibilities measuring χ_M' versus T (**Figure 3.4.4**),[18-19, 41] and those measured values at 300 K are lower than expected calculated values, indicating classic Mn-O antiferromagnetic superexchange coupling. Unfortunately, none of the parent compounds described in this work, Mn_3O-type, $Mn_3O(O_2CMe)_6(Pyr)_3$,[18] Mn_9O_7-type,

$Mn_9O_7(O_2CBut)_{13}(MeCN)_2$,[41] and finally $Mn_{13}O_8$-type, $Mn_{13}O_8(O_2CC_6H_4OPh)_{12}(OEt)_6$,[19] demonstrate SMM behavior as reported in the literature. For Mn_3O-type and Mn_9O_7-type compounds the ground spin state is very low, S = 2 or lower. For the $Mn_{13}O_8$-type cluster, despite its high symmetry and S = 11/2 ground spin state, line fitting for the axial anisotropy parameter indicates a very low value of -0.07 cm^{-1}; which would indicate an extremely small energy barrier to reorientation of the magnetization. Indeed, no out-of-phase signals, χ_M'', are encountered down to 1.8 K for any of these compounds.

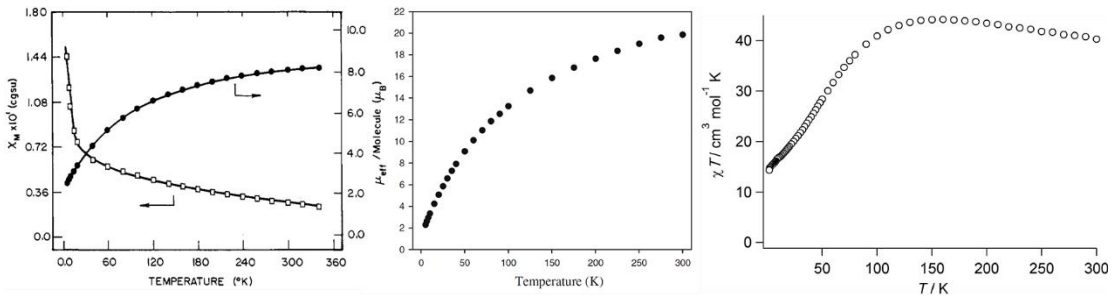

Figure 3.4.4 Variable temperature DC magnetic susceptibilities of $Mn_3O(O_2CMe)_6(Pyr)_3$,[18] *left*, $Mn_9O_7(O_2CBut)_{13}(MeCN)_2$,[41] *middle*, and $Mn_{13}O_8(O_2CC_6H_4OPh)_{12}(OEt)_6$,[19] *right*.

The magnetic susceptibilities of compounds **1-5** were not measured as the MnO clusters from Chapter 2 were, but based upon what we know from last chapter regarding how slightly the magnetization will differ from compound to compound within a SMM family, it is unlikely that any of the compounds we have generated in this study will differ significantly enough from their parent clusters. It is unlikely that our modifications have effectively 'switched-on' significant higher temperature out-of-phase transitions for these clusters.

For example, there is little that can be done to overcome the low ground state spin value of these clusters. Unless of course there was a modification that could be made to alternate the superexchange coupling mode to ferromagnetic! An S = 18 Mn_9O_7-type compound would be very desirable indeed.

The MnO clusters studied in this chapter, and last chapter, are primarily spin state driven when it comes to SMM performance. Uniaxial anisotropy is indeed an important factor for any SMM material, but even the highly symmetric Mn_{12}-Acetate demonstrates a D value of just -0.50 cm^{-1}. Even if the compounds generated in this work could approach this value for uniaxial anisotropy, they unfortunately could not match the spin only value of Mn_{12}-Acetate, S = 10. Therefore, even if the SMM out-of-phase behavior could in fact be 'switched-on', the magnetization of these synthesized clusters would likely perform within the same order of magnitude as the Mn_{12}-type clusters, and is not currently a future interest.

3.5 Conclusion

Based upon the objectives for this particular study as described in Chapter 1: this work was not *entirely* effective at accomplishing those goals. The synthetic routes for the $Mn_{13}O_8$-type and Mn_3O-type clusters proved that they are flexible in their allowance of various carboxylate building blocks; and new clusters were not generated.

The $Mn_{13}O_8$-type of clusters with systematically enlarging *ortho*-substituted benzoic acids showed no significant deviation structurally from the $Mn_{13}O_8$-type parent compound, outside the loss of symmetry. As was discussed at the end of Chapter 2; some of the future work for this study should be focused on the use of larger, or bulkier, carboxylates. The *ortho*-substituted isopropyl and *tert*-butyl benzoates may offer more steric bulk in order to impose a structural impact on the formation of these $Mn_{13}O_8$-type clusters. Outside of carboxylate selection for design control, perhaps an investigation into also modifying the ratios of Mn:O atoms would be an interesting angle to mount an additional investigation as others have done before? It might simply be that modifying the Mn:O ratio is the de facto standard to generating new MnO-type solids.

For the Mn_3O-type compounds much needs to be investigated. While a different MnO core was generated from the utilization of *ortho*-methyl substituted benzoic acid, it most certainly was not a result of the 'bulky' methyl substituent. If it were, we would have likely encountered a structural impact from the *ortho*-ethyl substituted benzoic acid as well. The only two benzoic acids which have made it from the reaction pot to X-ray quality crystals were the *ortho*-methyl and ethyl varieties; phenyl, and other large substituents still need to be investigated to form reasonable conclusions regarding the potential of a bulky *ortho* group to influence the Mn_3O-type cluster self-assembly process. The atomic Mn:O ratio should also be investigated in these compounds, as well as the published postsynthetic treatment routes discussed earlier: i.e., oxidizing agents,[32] solvothermal methods,[33-34] and others, to further probe the potential of *ortho*-substituents in these systems.

So, the book may not yet be closed on this work, and more should be done to ensure that control of molecular design *via* bulky *ortho*-substituted benzoic acids is a viable method to generate new MnO-type clusters. With that, we now leave behind the structural study of manganese oxide and move to another structural study of a vastly different type of material.

3.6 References

1. Ibers, J. A.; Holm, R. H., Modeling Coordination Sites in Metallobiomolecules. *Science* **1980,** *209* (4453), 223-235.
2. Dismuke, G. C., THE METAL CENTERS OF THE PHOTOSYNTHETIC OXYGEN-EVOLVING COMPLEX. *Photochem. Photobiol.* **1986,** *43*, 99.
3. Govindgee; Kambara, T.; Coleman, W., The electron donor side of photosystem II: the oxygen evolving complex. *Photochem. Photobiol.* **1985,** *42*, 187.
4. Yachandra, V. K.; Guiles, R. D.; McDermott, A. E.; Cole, J. L.; Britt, R. D.; Dexheimer, S. L.; Sauer, K.; Klein, M. P., Comparison of the Structure of the Manganese Complex in the S1 and S2 States of the Photosynthetic 02-Evolving Complex: An X-ray Absorption Spectroscopy Study. *Biochemistry.* **1987,** *26*, 5974-5981.
5. Lis, T.; Trzebiatowska-Jezowska, B., The Reaction between Potassium Permanganate and Formic Acid. Structural Characterization of the Polymeric Compound (K2 {Mn(H20)2[Mn30(HCOO)912})n. *Acta. Cryst.* **1977,** *B33*, 2112-2116.
6. Baikie, A. R. E.; Hursthouse, M. B.; New, D. B.; Thornton, J. M., Preparation, crystal structure, and magnetic properties of a trinuclear mixed-valence manganese carboxylate. *Chem. Commun.* **1978,** *0*, 62-63.
7. Baikie, A. R. E.; Hursthouse, M. B.; New, L.; Thornton, J. M.; White, R. G., Discrete oxidation states and X-ray crystal structure of the trinuclear manganese carboxylate [Mn3(3-ClC5H4N)3O(O2CMe)6]. *Chem. Commun.* **1980,** *0*, 687-685.
8. Mandal, S. K.; Armstrong, W. H., A novel triply bridged dinuclear manganese(III) complex containing the [MnzO(OAc)2] 2+ core: synthesis, crystal structure and properties of [Mnz(/x-O)(/x-OAc)z(bpea)2](C104)2. *Inorganica Chimica Acta* **1995,** *229*, 261-270.
9. Baikie, A. R. E.; Howes, A. J.; Hursthouse, M. B.; Quick, M. B.; Thornton, J. M., Preparation, crystal structure, magnetic properties, and chemical reactions of a hexanuclear mixed valence manganese carboxylate. *Chem. Commun.* **1986,** *0*, 1587.
10. Lis, T., "Preparation, Structure, and Magnetic Properties of a Dodeeanuelear Mixed-Valence Manganese Carboxylate". *Acta Cryst.* **1980,** *B36*, 2042-2046.
11. Chan, M. K.; Armstrong, W. H., A Novel Tetranuclear Manganese Complex That Displays Multiple High-Potential Redox Processes. Synthesis, Structure, and Properties of][Mn,(TPHPN) (02CCH3) (H20)],0)(C104)4.2CH30H1. *J. Am. Chem. Soc.* **1989,** *111*, 9121-9122.
12. Christou, G., Manganese Carboxylate Chemistry and Its Biological Relevance. *Acc. Chem. Res.* **1989,** *22*, 328-335.
13. Wieghardt, K., The Active Sites in Manganese-Containing Metalloproteins and Inorganic Model Complexes. *Angew. Chem. Int. Ed.* **1989,** *28* (9), 1153-1172.
14. Chan, M. K.; Armstrong, W. H., Tetranuclear Manganese-Oxo Complex with a 2.7A Mn...Mn Separation and Intramolecular H2O...(u-o) Hydrogen-Bonded Contacts: [Mn4o2(TPHPN)2(H2O)2(CF3SOC)2(CF3SO3)3. Possible Mode for binding of water at the active site of the Oxygen-Evolving complex in photosystem II. *J. Am. Chem. Soc.* **1990,** *1990* (112).
15. Low, D.; Eichhorn, D. M.; Draganscue, A.; Armstrong, W. H., Structure and hoperties of [Mn90,(02CC~,),,(py)2]: A Novel Nonanuclear Manganese(III)-Oxo-Carboxylate Species Synthesized by Employing an Oxygen Atom Transfer Agent. *Inorg. Chem.* **1991,** *30*, 878-880.
16. Rao, C. N. R.; Natarajan, S.; Vaidhyanathan, R., Metal Carboxylates with Open Architechtures. *Angew. Chem. Int. Ed.* **2004,** *43* (12), 1466-1496.
17. de Campos, N. R.; Ribeiro, M. A.; Oliveira, W. X.; Reis, D. O.; Stumpf, H. O.; Doriguetto, A. C.; Machado, F. C.; Pinheiro, C. B.; Lloret, F.; Julve, M.; Cano, J.; Marinho, M.

V., Magneto-structural versatility of copper(II)-3-phenylpropionate coordination polymers with N-donor coligands. *Dalton. Trans.* **2016,** *45*, 172-189.
18. Vincent, J. B.; Chang, H.-R.; Folting, K.; Huffman, J. C.; Christou, G.; Hendrickson, D. N., "Preparation and Physical Properties of Trinuclear Oxo-Centered Manganese Complexes of the General Formulation $[Mn_3O(O_2CR)_6L_3]^{0,+}$ (R = Me or Ph; L = a Neutral Donor group) and the Crystal Structures of $[Mn_3O(O_2CMe)_6(pyr)_3(pyr)$ and $[Mn_3O(O_2CPh)_6(pyr)_2(H2O)]\cdot 0.5MeCN$". *J. Am. Chem. Soc.* **1987,** *109*, 5703-5711.
19. Ferguson, A.; Thomson, K.; Parkin, A.; Cooper, P.; Milios, C. J.; Brechin, E. K.; Murrie, M., "Synthesis and characterisation of a mixed-valence Mn_{13} complex with S_6 symmetry by using 2-phenoxybenzoate". *Dalton Trans.* **2007,** (7), 728-730.
20. Aubin, S. M. J.; Sun, Z.; Eppley, H. J.; Rumberger, E.; Guzei, I. L.; Folting, K.; Gantzel, P. K.; Rheingold, A. L.; Christou, G.; Hendrickson, D. N., Single-Molecule Magnets: Jahn-Teller Isomerism and the Origin of Two Magnetization Relaxation Processes in Mn12 Complexes. *Inorg. Chem.* **2001,** *40*, 2127-2146.
21. Gatteschi, D.; Sorace, L., Hints for the Control of Magnetic Anisotropy in Molecular Materials. *J. Solid State Chem.* **2001,** *159* (2), 253-261.
22. Caneschi, A.; Gatteschi, D.; Sessoli, R., "Alternating Current Susceptibility, High Field Magnetization, and Millimeter Band EPR Evidence for a Ground S = 10 State in $[Mn_{12}O_{12}(CH_3COO)_{16}(H_2O)_4)\cdot 2CH_3COOH\cdot 4H_2O$". *J. Am. Chem. Soc.* **1991,** *113*, 5873-5874.
23. Sessoli, R.; Gatteschi, D.; Caneschi, A.; Novak, M. A., Magnetic Bistability In A Metal-Ion Cluster. *Nature* **1993,** *365*, 141-143.
24. Eppley, H. J.; Tsai, H.-L.; de Vries, N.; Folting, K.; Christou, G.; Hendrickson, D. N., "High-Spin Molecules: Unusual Magnetic Susceptibility Relaxation Effects in $[Mn_{12}O_{12}(O_2CEt)_{16}(H_2O)_4]$ (S = 9) and the One-Electron Reduction Product $(PPh4)[Mn_{12}O_{12}(O_2CEt)_{16}(H_2O)_4]$ (S = 19/2)". *J. Am. Chem. Soc.* **1995,** *117*, 301-317.
25. Sun, Z.; Ruiz, D.; Rumberger, E.; Incarvito, C. D.; Folting, K.; Rheingold, A. L.; Christou, G.; Hendrickson, D. N., Isomeric Forms of [Mn12O12(O2CR)16(H2O)4] Single-Molecule Magnets. *Inorg. Chem.* **1998,** *37*, 4758-4759.
26. Sun, Z.; Ruiz, D.; Dilley, N. R.; Soler, M.; Ribas, J.; Folting, K.; Maple, B. M.; Christou, G.; Hendrickson, D. N., The origin of the second relaxation process in the [Mn12O12(O2CR)16(H2O)4] single-molecule magnets: 'Jahn–Teller isomerism' in the [Mn12O12] core. *Chem. Commun.* **1999**, 1973-1974.
27. Amesz, J., The role of manganese in photosynthetic oxygen evolution. *Biochim. Biophys. Acta* **1983,** *726*, 1-12.
28. Oh, S. M.; Hendrickson, D. N.; Hassett, K. L.; Davis, R. E., Electron transfer in mixed-valence, oxo-centered, trinuclear iron acetate complexes: effect of statically disordered to dynamically disordered transformation in the solid state. *J. Am. Chem. Soc.* **1984,** *106*, 7984-7985.
29. Oh, S. M.; Hendrickson, D. N.; Hassett, K. L.; Davis, R. E., Valence-detrapping modes for electron transfer in the solid state of mixed-valence, oxo-centered, trinuclear iron acetate complexes: x-ray structure and physical data for [Fe3O(O2CCH3)6(4-Et-py)3](4-Et-py). *J. Am. Chem. Soc.* **1985,** *107*, 8009-8019.
30. Murch, B. P.; Bradley, F. C.; Que, L., A binuclear iron peroxide copmlex capable of olefin epoxidation. *J. Am. Chem. Soc.* **1986,** *108* (16), 5027-5028.
31. Sorai, M.; Kaji, K.; Hendrickson, D. N.; Oh, S. M., Heat capacity and phase transitions of the mixed-valence compound [Fe3O(O2CCH3)6(py)3](py). *J. Am. Chem. Soc.* **1986,** *108*, 702-708.
32. Christmas, C.; Vincent, J. B.; Chang, H.-R.; Huffman, J. C.; Christou, G.; Hendrickson, D. N., "Nonanuclear Oxide- Bridged Manganese Complex. Preparation, Structure, and Magnetic Properties of $[Mn_9O_4(O_2CPh)_8(sal)_4(salH)_2(pyr)_4]$ ($salH_2$ = Salicylic Acid; pyr = Pyridine)". *J. Am. Chem. Soc.* **1988,** *110*, 823-830.

33. Liu, S.; Jeppson, P.; Sandstrom, J.; Caruso, A. N.; Schulz, D. L., "Synthesis, structure and magnetic properties of $\{Mn_5(OC(O)CH_3)_6(OC(O)C_6H_5)_4\}\infty$". *Polyhedron* **2007,** *26* (9-11), 2235-2242.
34. Low, D. M.; Brechin, E. K.; Helliwell, M.; Mallah, T.; Rivière, E.; McInnes, E. J. L., "New routes to high nuclearity cages: dimerisation of a manganese triangle *via* solvothermal synthesis". *Chem. Commun.* **2003,** (18), 2330-2331.
35. Brechin, E. K.; Boskovic, C.; Wernsdofer, W.; Yoo, J.; Yamaguchi, A.; Sanudo, C. E.; Concolino, T. R.; Rheingold, A. L.; Ishimoto, H.; Hendrickson, D. N.; Christou, G., Quantum Tunneling of Magnetization in a New [Mn18]2+ Single-Molecule Magnet with S=13. *J. Am. Chem. Soc.* **2002,** *124*, 9710-9711.
36. Sala, T.; Sargent, M. V., Tetrabutylammonium Permanganate: an Efficient Oxidant for ·Organic Substrates. *J.C.S. Chem. Comm.* **1978**, 253-254.
37. Dolomanov, O. V.; Bourhis, L. J.; Gildea, R. J.; Howard, J. A. K.; Puschmann, H., OLEX2: a complete structure solution, refinement and analysis program. *J. Appl. Cryst.* **2009,** *42*, 339-341.
38. Sheldrick, G. M., A short history of SHELX. *Acta. Crystallogr. A* **2008,** *A64*, 112-122.
39. Kennard, O., From data to knowledge—Use of the Cambridge Structural Database for studying molecular interactions. *Supramolecular Chemistry*. **1992,** *1* (3), 277-295.
40. Groom, C. R.; Allen, F. H., The Cambridge Structural Database in retrospect and prospect. *Angew. Chem. Int. Ed. Engl.* **2014,** *53* (3), 662-671.
41. Lampropoulos, C.; Stamatatos, T. C.; Abboud, K. A.; Christou, G., A convenient MnIII starting material for the synthesis of homo- and heterometallic manganese carboxylate clusters: Mn9 and Mn10−xFex complexes. *Polyhedron* **2009,** *28* (9-10), 1958-1964.
42. Tasiopoulos, A. J.; Vinslava, A.; Wernsdorfer, W.; Abboud, K. A.; Christou, G., "Giant single-molecule magnets: a [Mn84] torus and its supramolecular nanotubes". *Angew. Chem. Int. Ed.* **2004,** *43* (16), 2117-21.

Chapter 4

2-Dimensional Hydrogen-Bonded Ammonium Formate Layered Solids

4.1 Introduction

The emphasis of this chapter, and the next, shifts focus from metal oxide complexes to organic 2-dimensional networks of hydrogen donor/acceptor complexes. This work continues the overall effort and interest in structural design, analysis, and comparison, where methodical and progressive changes to an established system may be tracked and evaluated through careful consideration of available crystallographic data.

4.1.1 Formic Acid

Formic acid is a useful and simple molecule that is capable of a wide variety of chemistry,[1-6] in an equally broad number of fields and research efforts.[7-17] Among formic acid's variety of uses and potential applications, its catalytic decomposition into syngas products H_2 and CO_2 is of heightened contemporary interest. Enthusiasm in syngas is primarily due to rising demands for environmentally friendly sources of energy, and the increasing efficacy and output of renewable energy sources as they both relate to combating observed gradual atmospheric change. Briefly, formic acid contains 4.4 weight % of atomic hydrogen which is equivalent to 53 g of hydrogen per liter of material, making it an appealing and dense hydrogen source. Reliable access to the atomic hydrogen contained within allows for realistic utilization of environmentally benign hydrogen gas as a fuel source.

Modern methods of catalysis allow for flexible fuel cycles for formic acid, where formic acid may be first catalytically degraded into immediately useful H_2, and energetic precursor, CO_2.[18-26] An alternate secondary process may convert ambient CO_2 to formic acid via reduction,[27-29] effectively closing the fuel cycle. Secondarily, the CO_2 generated from the initial dehydrogenation of formic acid can be reduced to carbon monoxide,[30-36] which may be utilized as either a fuel source or C1 source (**Figure 4.1.1**).[37-41] Clearly, formic acid is an atomically efficient, energy-dense material that deserves close attention.

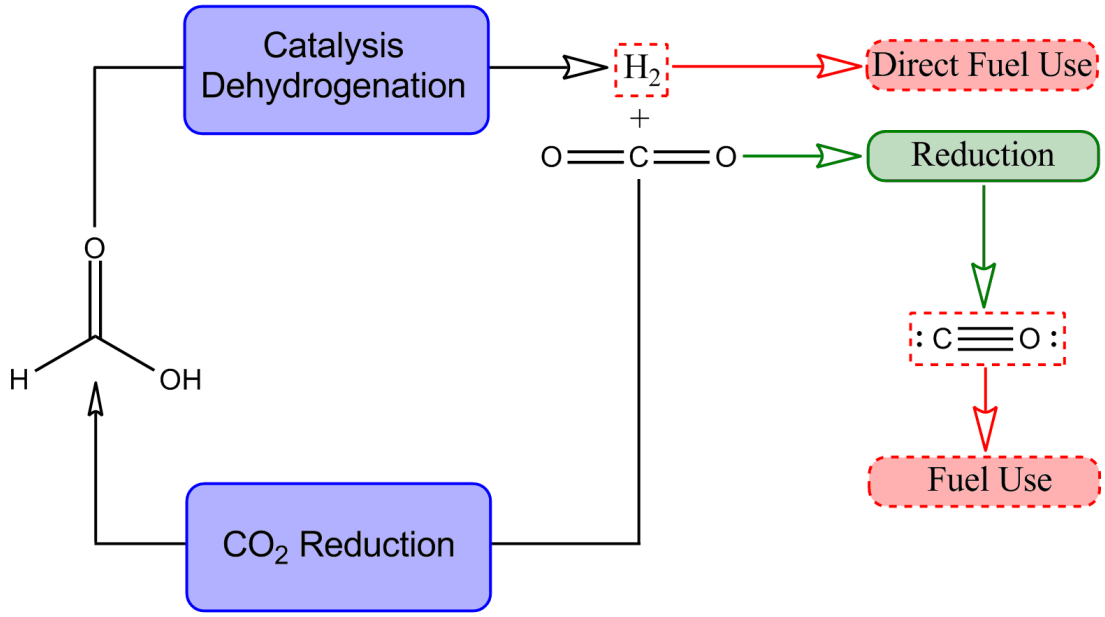

Figure 4.1.1 Basic scheme concerning formic acid and its conversion to fuel sources.

4.1.1.1 Formic Acid Storage

As formic acid's catalogue of applications expands,[42-44] its storage efficiency and safety may become of concern. One of the simplest methods to increase the theoretical storage limits of any material is to convert the material to a solid. Solids offer an additional advantage in that long-term storage and handling is generally simplified, which could in turn address potential safety concerns. Metal-formates offer a facile, reliable, and stable route to solid formates,[45-46] but the presence of metals in the solid matrix may not be ideal for all use scenarios.

One route to a completely organic solid-matrix of formic acid is to pair it with a hydrogen acceptor to generate a solid hydrogen-bonded network. By combining formic acid with a material containing an amine functionality, a proton transfer will occur and, the two components will participate in hydrogen bonds to assemble into a solid material. Formic acid is the smallest carboxylic acid, which makes it an appealing material because it is one of the simplest possible hydrogen donating compounds that may also serve as a hydrogen acceptor *via* the carbonyl moiety, enhancing its potential utility.

As will be discussed further, arene-containing primary amine analogues are appealing when considering possible hydrogen acceptors due to the ease of access and breadth of variety of functionalized ring systems. Generally, these reagents are readily commercially available, and they can serve as simple starting points from which a systematic study may be performed; gradually changing or moving substituents in sequential experiments. Additionally, various other benzylammonium based structures have been previously studied in the Beatty lab,[47-51] making their selection a natural choice.

4.1.2 Layers and Dimensional Materials

In Chapter 1 we introduced and discussed hydrogen-bonded supramolecular materials as structures that assemble in 0-dimensions to 3-dimensions, depending on the position of their hydrogen bonding substituents (**Figure 4.1.2**). In particular, 2-dimensional materials offer an attractive realm to explore based upon the simple and direct control of the layer assembly *via* stepwise synthon modifications and selection. Certainly, 2-D layered materials are not limited to those of hydrogen-bonded networks and may be composed of an extensive range of coordinated inorganic and hybrid-organic building blocks. We find examples such as the inorganic layers of metal oxides and chalcogenides for use as photocatalysts,[52] anodes,[53] cathodes,[54] dye-sensitized solar cells,[55] and magnetic materials.[56] Additionally, layered inorganic-organic hybrid materials find applications in light-harvesting[57] and sensors,[58] all the way to uranium recapture.[59] These inorganic and organic structures form wonderfully varied and useful materials; but those layered materials, which are assembled exclusively *via* multi-component hydrogen-bonded organic molecules exist in an extraordinary class of their own, and are the focus of this discussion. Herein, we elaborate and expand upon the structures of 2-dimensional hydrogen-bonded materials.

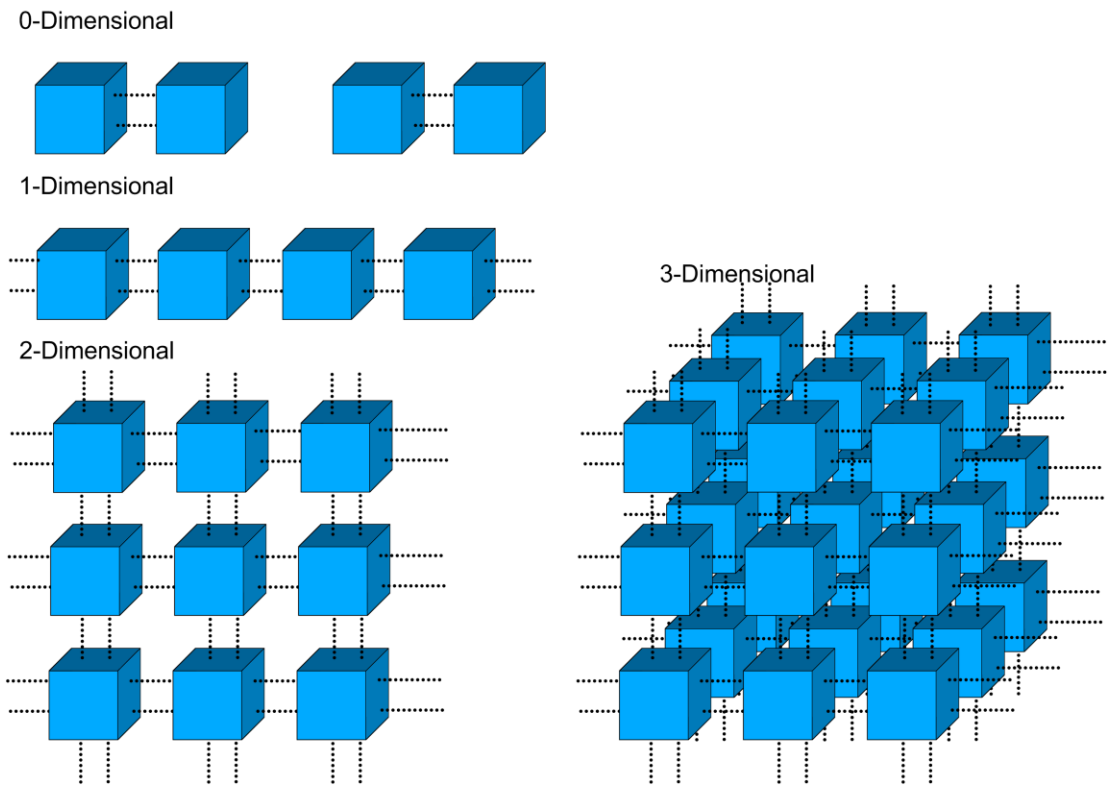

Figure 4.1.2 Basic dimensionality of supramolecular structures; 0-D, 1-D, 2-D, and 3-D.

4.1.2.1 Hydrogen-Bonded Supramolecular Networks in 2-Dimensions

In the simplest case, a single synthon which contains three equally spaced out hydrogen-bonding substituents (i.e., trimesic acid),[60] will result in an infinitely chained 2-dimensional structure. Of course, 2-dimensional hydrogen-bonded materials are not limited to the simplest case; multi-component mixtures of two different synthons or ions may also be utilized, massively expanding the potential library of 2-dimensional materials. For example, an ammonium, NH_4^+, moiety and a simple dicarboxylic acid may interact *via* hydrogen bonds and form a simple 2-dimensional sheet. But what would happen structurally if the complexity of the dicarboxylic acid increased and/or a long tether or chain was added to the ammonium containing synthon? This type of molecular design represents a simple and direct method to generate lamellar layered materials, where the 2-D sheets are separated by an organic interlayer component. When combining two complementary and systematically modifiable materials it is possible to analyze

the structural outcome from minor and systematic changes to the system. Though in addition to simple analysis, can we decide or predict '*how'* these systematically varied components will arrange and assemble as solid architectures? Controlling and predicting the self-assembly of materials *via* the mixing and matching of two component species that will hydrogen bond is crucial to crystal engineering and design.

Ammonium carboxylate layers, generated by combining essentially any carboxylic acid with any primary amine (i.e., the marriage of $\mathbf{R'}COO^{-}\ {}^{+}NH_3\mathbf{R''}$), provides an effective proving ground for the supervised combination of systematically modifiable building blocks. There are some previous examples of single-component 2-dimensional hydrogen-bonded lamellar structures, where the anion and cation moieties are contained in a single molecule,[61] but this discussion will focus on the 2-D structures of multi-component materials, i.e., discrete cation and anion synthons.

4.1.3 The Structure and Components of Hydrogen-Bonded Layers

In 2-D systems, the hydrogen bonding substituents create the layer, and the attached **R**-groups reside in the interlayer space of the lamellar material (**Figure 4.1.3**).[62] Exceptions to this ordering, where certain substitutions on the benzyl ring may slightly disrupt the typical layer motif exist,[63] and are also observable in compounds reported in this chapter. We see in some cases, that the components of the sheet may participate in additional hydrogen bonds in the 3rd dimension depending on the orientation of the sheet constituents. This sheet 'cross-linking' occurs when an appropriate 2-D structure has functionality in the axial direction resulting in *pseudo* 3-D structures, or *expanded* 2-D structures; however, for the purposes of this discussion, the sheets of hydrogen-bonded materials that are generated, expanded or not, shall be evaluated as 2-dimensional layers.

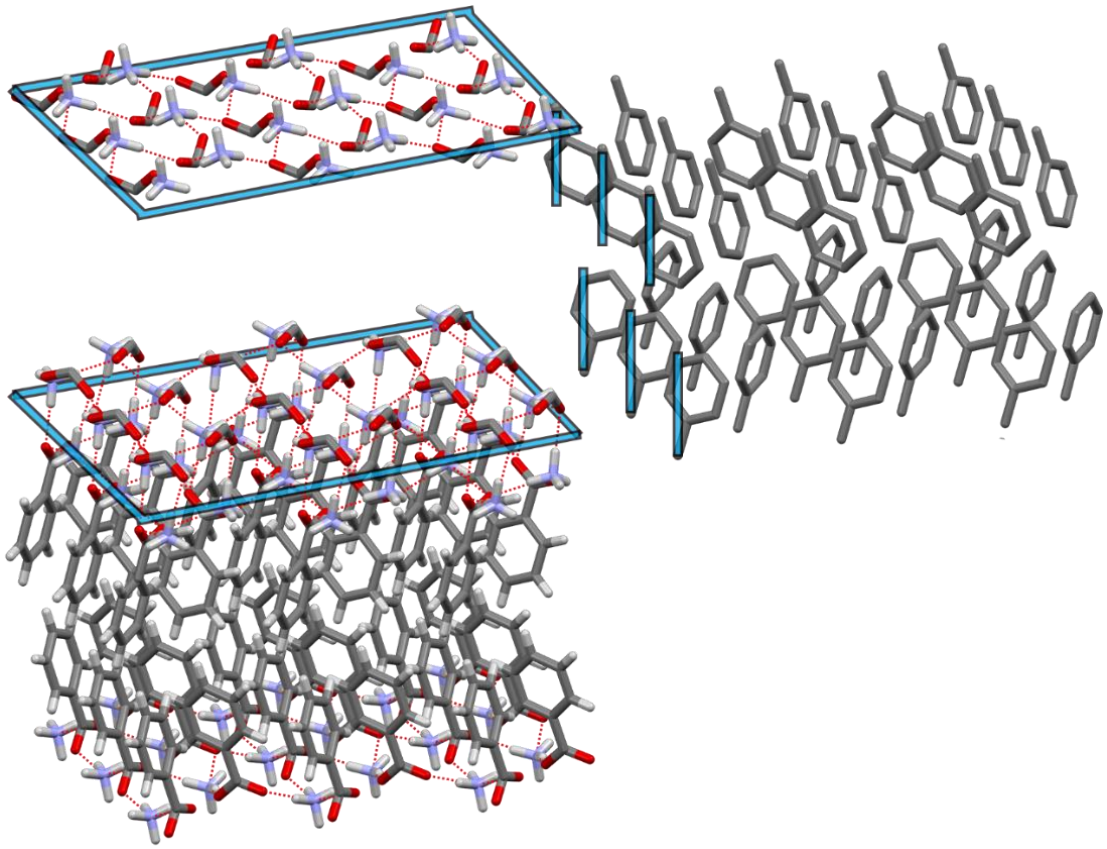

Figure 4.1.3 *Sheets and layers.* Superposition of ammonium benzoate (Refcode: YABFEO),[64] laterally sliding apart the pillars from the sheets. Blue and black boxes on *left* illustrate and isolate 'sheets', blue and black vertical lines on *right* illustrate and identify pillars. The two units combined, comprises the lamellar layer structure. Hydrogens removed on right pillars for clarity. *Note: In each figure herein, atoms are represented by either tubes or spheres. Those of dark grey represent carbon atoms, light grey represents hydrogen atoms, amber represents bromine atoms, green represents chlorine atoms, yellow-green represents fluorine atoms, purple represents iodine atoms, orange represents iron atoms, light blue represents nitrogen atoms, red represents oxygen atoms, dark purple represents potassium atoms.*

4.1.3.1 Cations and Anions in 2-Dimensional Hydrogen-Bonded Layers

The cations employed in these multi-component 2-D materials can take a variety of forms. Some of the simplest cations demonstrated in these materials are the layered compounds of potassium and sodium metal ions,[65-67] however more complicated metal phosphonates, such as those of zirconium,[68] may also be found. Many of the cations encountered in the database are those derived from protonated amines. Simple ammonium NH_4^+ moieties often serve as suitable cations that result in flat layers similar to those of the metal ion materials (**Figure 4.1.4**).[69-70] The layered solids of primary ammonium cations, $\mathbf{R}NH_3^+$ (which are almost exclusively represented by the reported structures of this chapter), are commonly reported and result in a variety of layer types.[47, 50-51, 64, 70-73] Secondary amines are also widely encounter in the database as common $\mathbf{R}_2NH_2$ moieties[74-76], or those of type $\mathbf{R}_2NH^+$ as pyridinium,[77-78] and imidazolium[79] cations, and often result in unique layered structures. Even cations of $\mathbf{R}3N^+$ type can also be found.[80] In addition to these common amines, various other nitrogen containing groups such as azides may be found in the CSD [81].

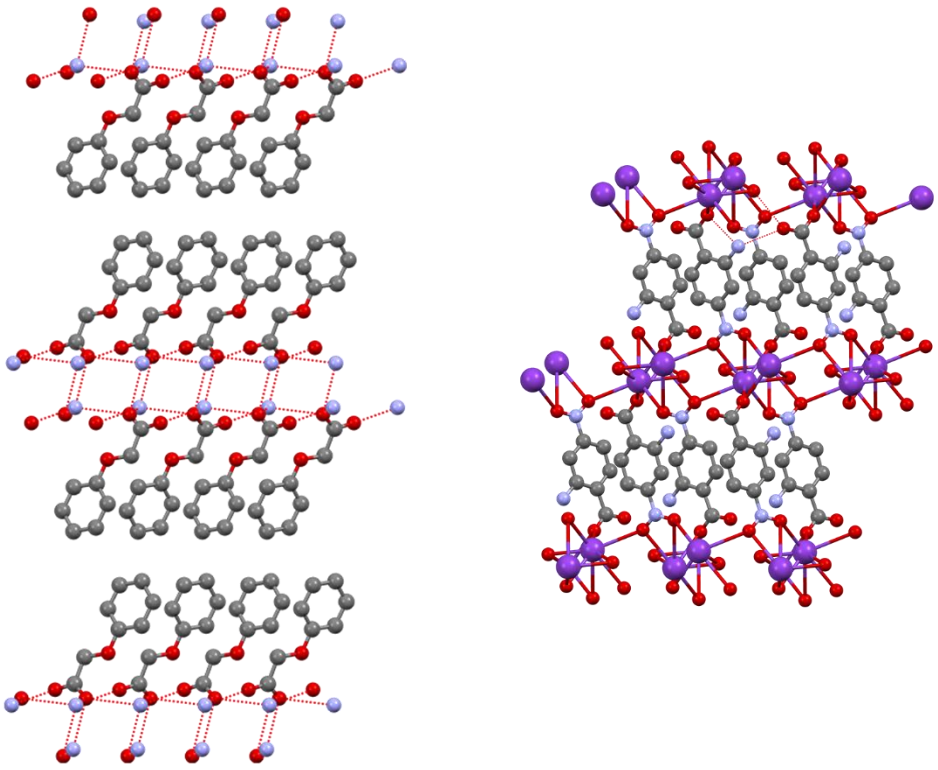

Figure 4.1.4 Some 2-D layers from small cations. *Left*, layer of an ammonium NH_4^+ cation and phenoxyacetate (Refcode: ZOWWEP).[69] *Right*, layer of a potassium cation and *para*-nitroanthranate (Refcode: DINYEG).[66] Hydrogens removed for clarity.

The types of anions present in these types of structures are overwhelmingly those of oxygen containing species such as alcohols,[76, 82-83] carboxylic acids,[63-64] phosphonates,[68] and sulfonates;[84-85] of varying chain length, ring substituents, and number of functional groups, i.e., diols, dicarboxylic acids, tricarboxylic acids, etc. Halogens are also found as anions in these sheets,[77] but for the remainder of this discussion we will focus on the sheets of hydrogen donor/acceptor complexes involving oxo-components.

4.1.4 Structural Variations in Organic 2-Dimensional Hydrogen-Bonded Compounds

Organic 2-dimensional hydrogen-bonded layers are described and identified by three primary physical parameters: the interdigitation of the organic portion of the ionic constituents

(the pillars), the shape of the hydrophilic sheet, and the binary arrangement and organization of the sheet and pillar into layers as the two components stack. These parameters are generally linked and interrelated in that one is dependent on another, and each is equally important in the overall structural motif encountered from complex to complex.

4.1.4.1 Pillar Interdigitation

Interdigitation is described as the interlocking or interlinking of molecular appendages, resembling fingers being linked together. Specifically, in ammonium carboxylate complexes, interdigitation is determined by the interlocking of the interlayer pillar subunits, forming a zipper-like pattern across the interlayer region (**Figure 4.1.5**). Whether a pillared region interdigitates or not usually influences the other physical parameters of the material (i.e., sheet shape), as described in later sections.

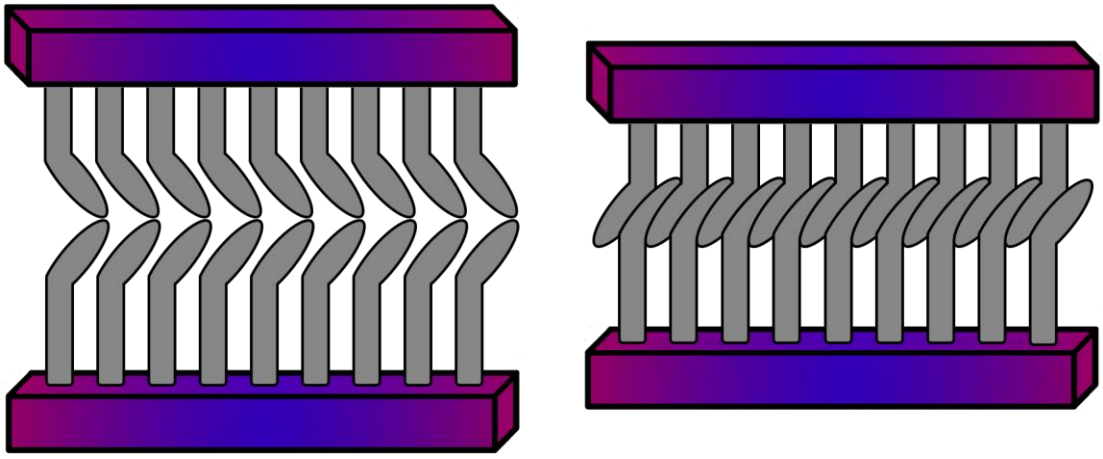

Figure 4.1.5 Illustration of non-interdigitated, *left*, versus interdigitated, *right*, pillars. The red/blue rectangular prism represents the hydrophilic substrate, and the grey, anchored, ellipses represent the organic component of the cation.

4.1.4.2 Sheet Shape

The shape of the hydrophilic sheet, when viewing the structure from the side, in lamellar materials can generally be described as either: flat, undulated, or buckled (**Figure 4.1.6**).

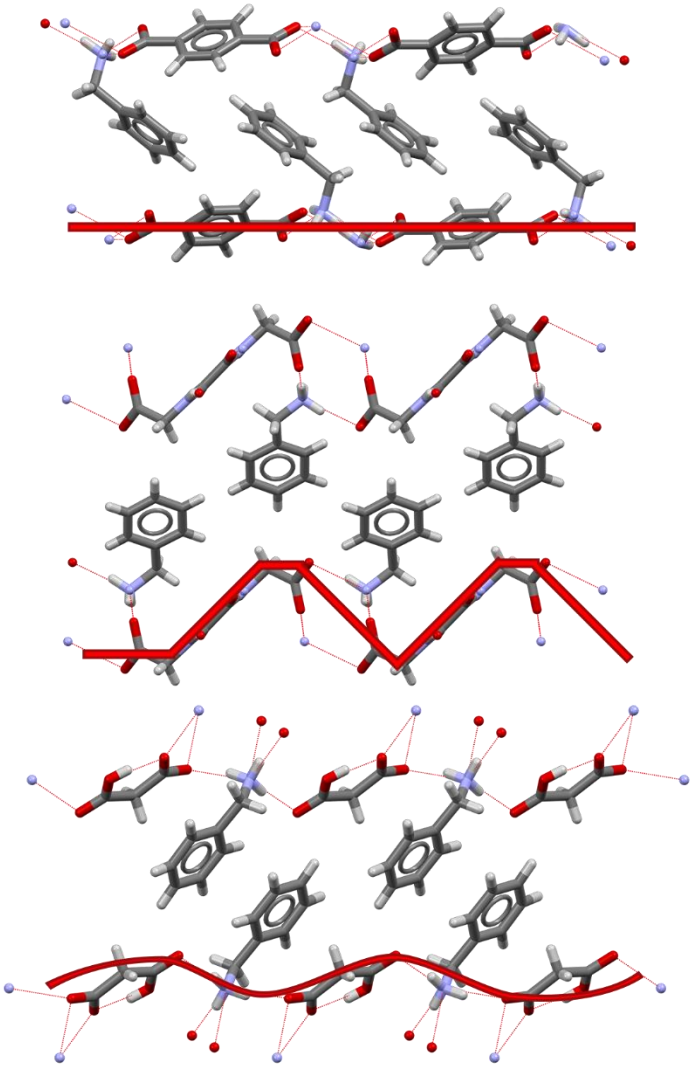

Figure 4.1.6 The three common sheet shapes, a thick red line traces the backbone. *Top*, flat hydrophilic substrate (Refcode: SOVWOQ),[63] *middle*, buckled hydrophilic substrate (Refcode: XOXQEH),[71] *bottom*, undulating hydrophilic substrate (Refcode: SEJSOP).[86]

The shape of the sheet is attributed to a number of physical conditions of the system, namely the identities of the ionic constituent, pillar interactions, or other electrostatic factors present in the overall layer. Generally, in ammonium carboxylates, non-interdigitated pillars tend to have flat sheets, interdigitated pillars with non-rigid sheet components typically result in an undulated sheet, and finally, interdigitated pillars and rigid sheet components may result in a buckled sheet (**Figure 4.1.7**).

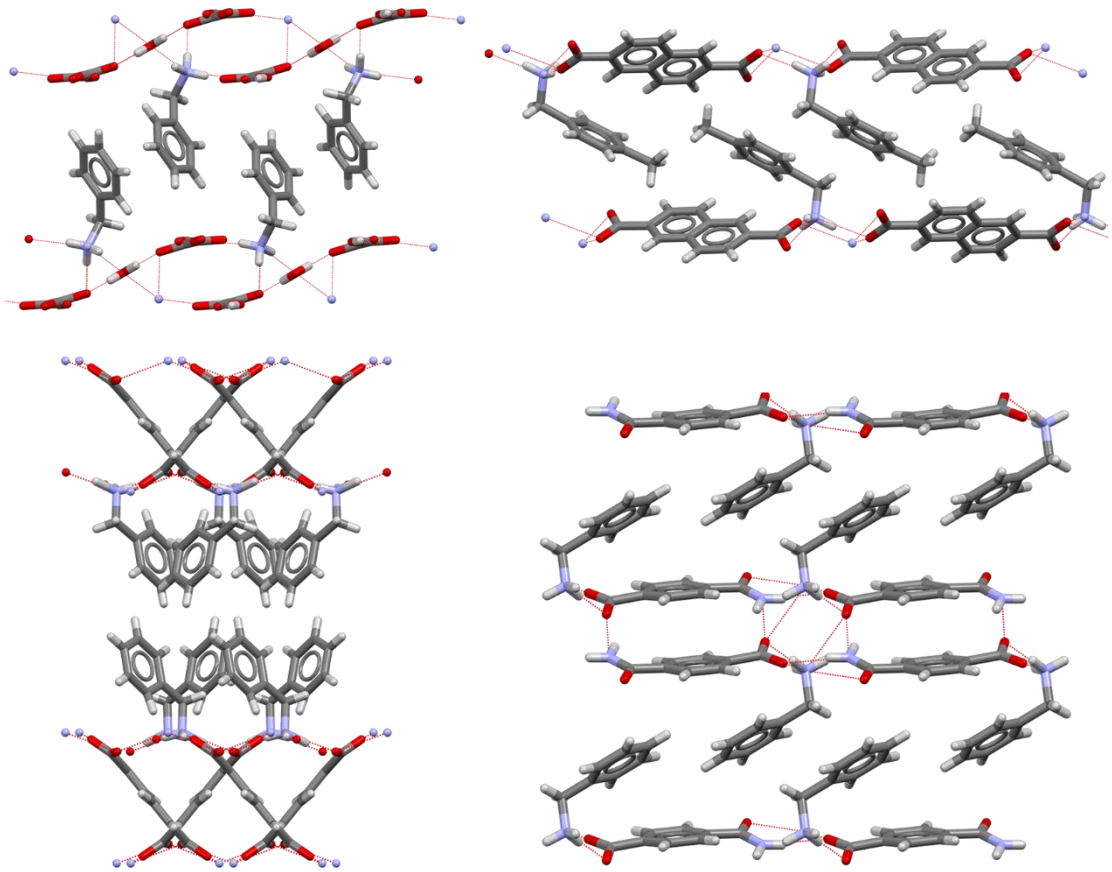

Figure 4.1.7 Demonstrating the proportionality between anion and sheet flexibility, with benzylamine pillars. *Top left*, flexible anion, ethanedioic acid, undulating sheet (Refcode: AJUMOH).[87] *Bottom left*, flexible anion, hexanedioic acid, undulating sheet (Refcode: LAYCAP).[88] *Top right*, rigid anion, 2,6-naphthalenedicarboxylic acid, buckled sheet (Refcode: SOVXEH).[63] *Bottom right*, rigid anion, 4-aminocarbonylbenzoic acid, flat sheet (Refcode: PEBDOQ).[89]

The overall assembly may be a monolayer or a bilayer (**Figure 4.1.8**).[90] In monolayers, the pillars of the sheet will point in either direction from the sheet, and in bilayers, the pillars of that sheet only orient in a single direction. The preference between the two is typically dictated by steric considerations of the interlayer pillars, as well as conductive electrostatic interactions such as van der Waals forces or arene π-interactions, which are further detailed in the next chapter. We explore below how the shape of the hydrophilic substrate is influenced by closely linked, critical physical features.

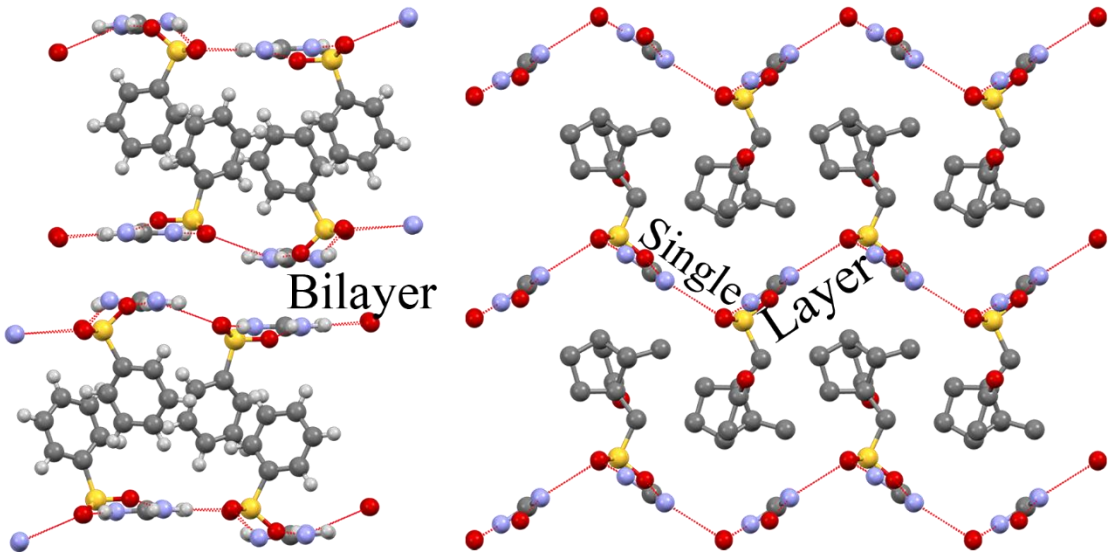

Figure 4.1.8 Bilayers versus monolayers. *Left*, bilayer example of guanidinium benzylsulfonate (Refcode: WETPIU). *Right*, (single) monolayer example of guanidinium camphorsulfonate, hydrogens removed for clarity (Refcode: WETPAM).[85]

4.1.4.3 Layer Type Binary Coding

Finally, the overall layering structural motif can be described by a simple binary code which indicates the ordering of the sheet, designated by "A", and the interlayer region, designated by "B". The two primary layer types that are common to 2-D lamellar materials are the AB and

ABA-type layers (**Figure 4.1.9**). As with the previously mentioned physical parameters, the layer type is typically a direct result of the actions of the other operative physical parameters.

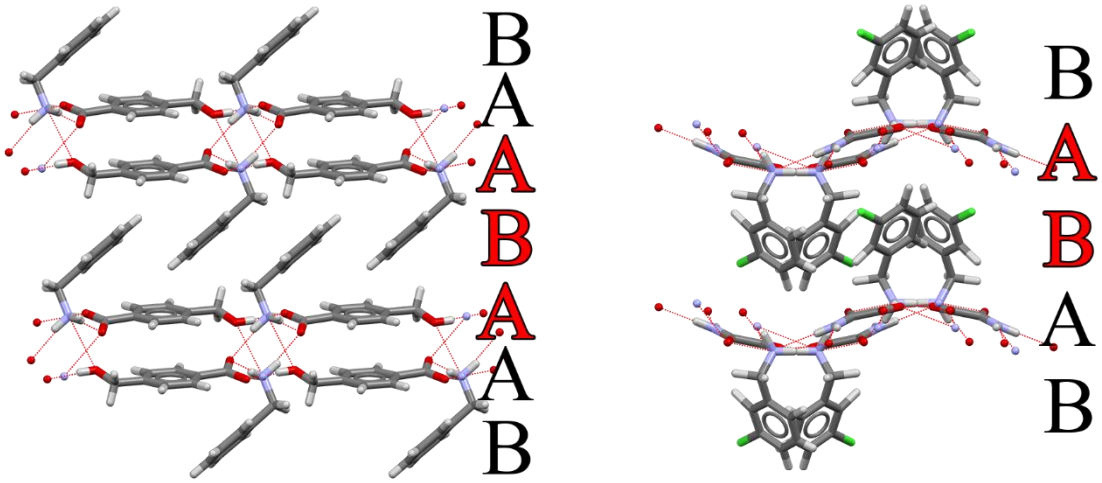

Figure 4.1.9 Binary layer order description. Brief visual depiction of the types of lamellar layers encountered, where A is hydrophilic slice and B is pillar region. *Left*, typical ABA pattern (Refcode: PEBDUW).[89] *Right*, typical AB pattern (Refcode: TOYMEZ).[91]

4.1.5 Structural Assembly Outcome Prediction of 2-Dimensional Hydrogen-Bonded Layers

Hydrogen-bonded supramolecular networks have been researched with a huge variety of synthons and dimensionalities by many researchers such as Etter,[92] Ward,[93] Desiraju,[94-95] Zaworotko,[96] Clearfield,[97] Aakeröy,[98] and Beatty.[99-100] The ultimate goal of supramolecular chemistry and crystal engineering is not only to develop useful materials, but is also to develop a set of rules and examples where chemists may reliably predict the structural assembly outcome of combining various molecular synthons. Eventually, following the development of a library of useful and predictable supramolecular synthons, the ability to preprogram assembly processes that will carry over from the solution state to the solid-state through the design of specific molecular recognition sites onto discrete molecules, will become a reality.

4.1.5.1 2-Dimensional 'Clay Mimics'

Predictive structure research has been conducted on a number of fronts, with a number of different materials. As a group, one of our aims is to generate predictable assemblies of hydrogen-bonded materials, and 2-dimensional 'clay mimic' structures offer a venerable platform to conduct this work. Clay mimics are a huge subset of hybrid supramolecular architectures which emulate the abilities of their naturally-occurring, typically metal oxide counterparts but differ in how their structures typically contain square or rectangular grids (**Figure 4.1.10**).[101-106] The grid-like arrangement of these mimetic materials imparts structural porosity which allows small molecules to intercalate into the spatial vacancies of these solids. The result is a functional material which serves as a tunable host-guest system[68, 107] for the purposes of storage,[53] separations,[46, 59] or catalysis.[57, 108] The purely organic, hydrogen-bonded, analogues of these hybrid structures offer similar possibilities.[109-111] Ionic hydrogen-bonded networks serve as reliable materials for assembling these molecular architectures due to the charge-assisted strengthening of the adhesive hydrogen bonds. This enhanced electrostatic attraction facilitates the formation and strength of the structural scaffold and assists in maintaining the lamellar structure after multiple intercalated guest cycles due to the increased strength of the charge-assisted hydrogen bonds.[112-113]

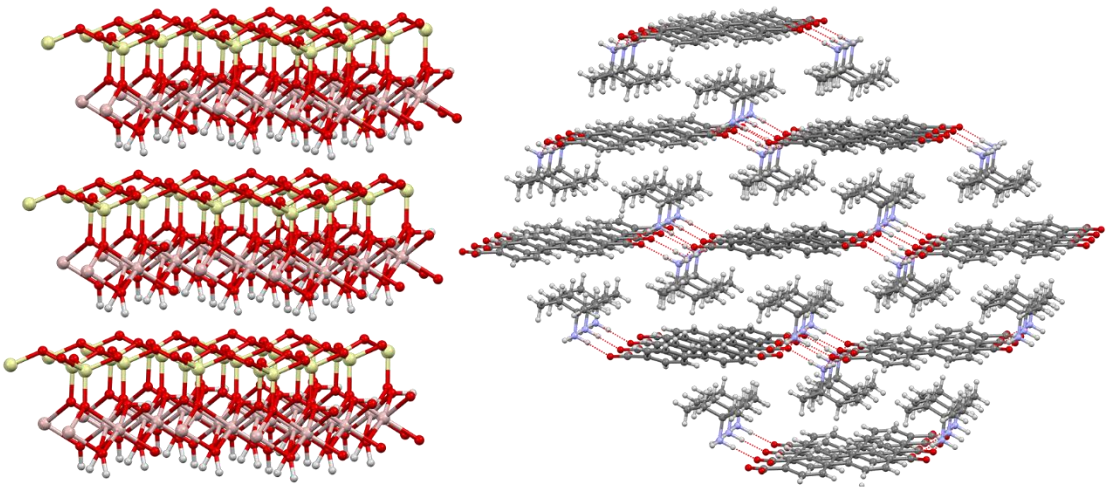

Figure 4.1.10 Natural versus mimetic clays. *Left*, crystal structure of naturally derived 2-dimensional material Kaolinite, $Al_2Si_2O_5(OH)_4$, solved *via* Rietveld refinement at 1.5 K.[114] *Right*, The organic clay mimic *tert*-amylammonium biphenyl-4,4′-dicarboxylate (Refcode: QEJVUX).[115]

2-Dimensional clay mimetic structures have also been previously studied in the Beatty lab as ammonium HPzDCA (the mono-anion of 3,5-pyrazoledicarboxylic acid) layers (**Figure 4.1.11**).[47-48, 50-51] The ammonium formate structures of this work offer a logical extension to that research by relating that anion's structures to those of formate. This work continues the efforts of many crystal engineers in that this structural data, and its predictive approach, aims to improve and strengthen the science behind forecasting the self-assembly of organic multi-component hydrogen-bonded 2-dimensional lamellar structures.

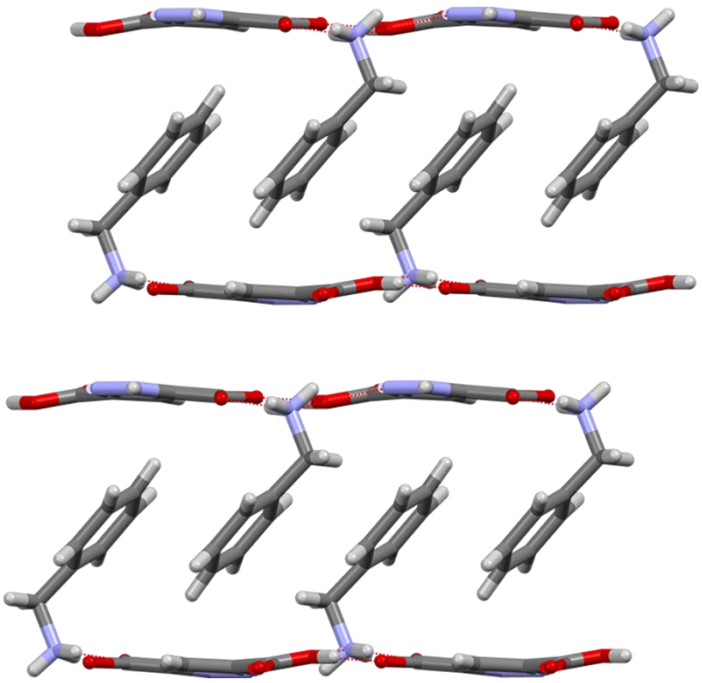

Figure 4.1.11 Benzylammonium HPzDCA, a 2-dimensional clay mimic (Refcode: XOVTIL).[47]

4.1.5.2 Prediction of Layer Assembly and Shape

Previous literature efforts have been successful in suggesting and predicting the correlation between the types of synthons present and the topology of the layer; efforts which can be applied to these proposed organic clay mimics.[64, 69, 85] Odendal et al. were able to develop a set of reliable standards and guidelines for the 'stacking and laddering' of the hydrophilic substrate, referred to as the cation and anion 'nets' (typically referred to as sheets or ribbons by Ward, Etter, us, and others), as they arrange themselves to maximize electrostatic interactions.[64, 69, 116] These rules are especially important in our case as they focus on mono-carboxylate ions with no additional competing hydrogen-bonding functionality; such as the formate anion. Odendal's rules (**Figures 4.1.12** and **4.1.13**) suggest that:

1. Ammonium ionic materials will always form sheets, whether monolayer or bilayer.
2. Formate, acetate, and propionate anions will form single monolayer sheets unless they occur with a "very bulky" cation, at which point they will form bilayers.

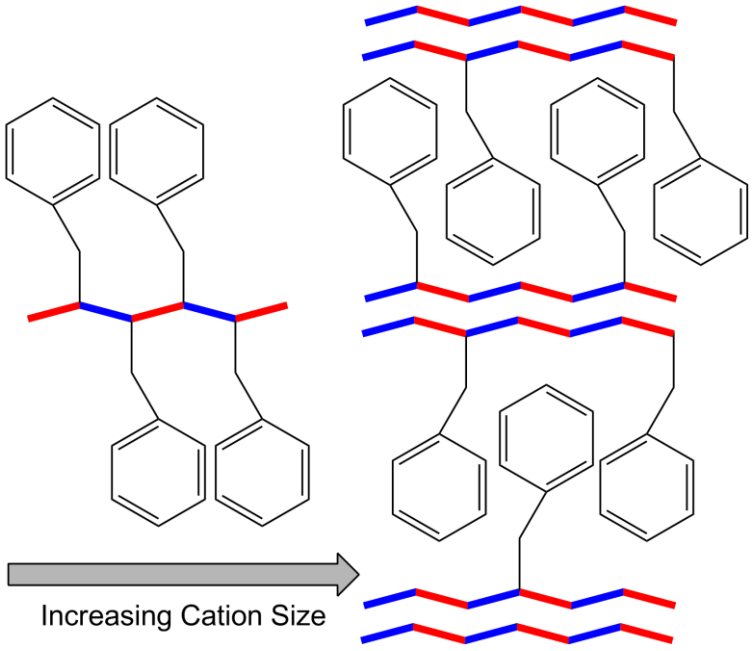

Figure 4.1.12 Illustration of Odendal's rules. As the size of the cation increases for 2-dimensional ammonium carboxylates, the net (sheet) will transition from monolayer to bilayer.

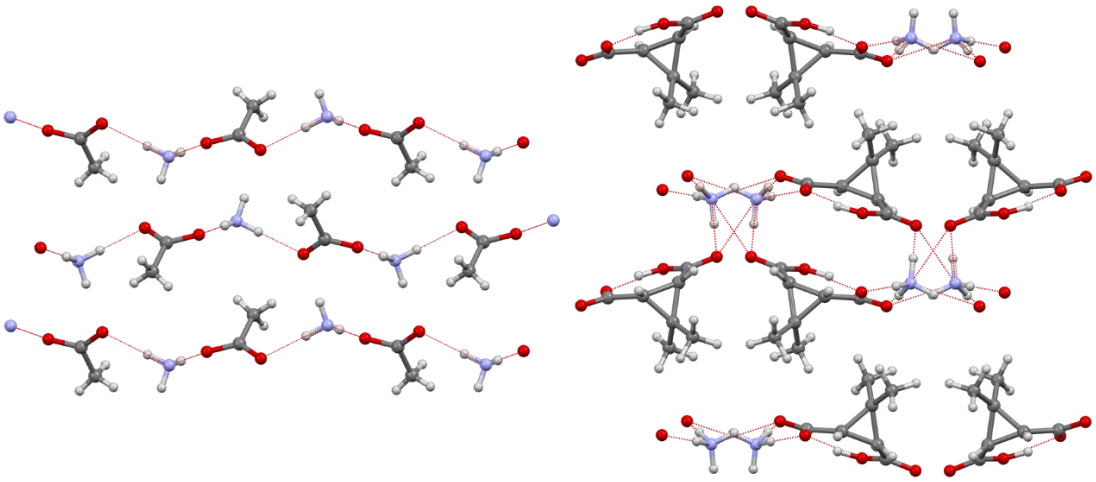

Figure 4.1.13 Going from monolayer, *left* (Refcode: AMACET),[117] to bilayer, *right* (Refcode: PATTAF),[118] as the *anion* increases size in ammonium carboxylates. The guidelines on cation size also apply to the anion in the sheet. In ammonium carboxylates, as one of the ionic constituents (anion or cation) increases in size, the layer shows a preference for monolayer or bilayer.

4.1.5.3 Prediction of Pillar Interdigitation Behavior

What remains is a description of what classifies or categorizes a 'very bulky' cation with respect to layered materials. Here, because in these layered materials the pillar moieties will approach each other from opposite sides of the layer, it is more advisable to lean towards the *steric* impact of the cations, rather than the sheer size. The discussion in Chapter 1 more closely discusses the ramifications and implications of sterics; but generally in these systems, as the two pillar moieties come into contact, interdigitation is considered. When investigating arene containing pillars, interdigitation will be perturbed by those substituents which will impede the slippage of the pillar moieties. Positionally, *meta*- and *para*-substituents of an arene are the most apt to block the interdigitation process of the pillar moieties (**Figures 4.1.14**). *Meta*- and *para*-alkyl substituents, or fused ring systems such as naphthalene, may provide a physical barrier to interdigitation. On the other hand, *meta*- and *para*-halo substituents may provide an electrostatic barrier to interdigitation (**Figure 4.1.15**). As predicted and reported by Smith, Odendal, and others,[69] these types of substituents at the *meta*- and *para*-positions of arene-based pillars prevent interdigitation. Substituent identities and their positions are important to consider when predicting the physical parameters and layering patterns of these ionic ammonium formate systems.

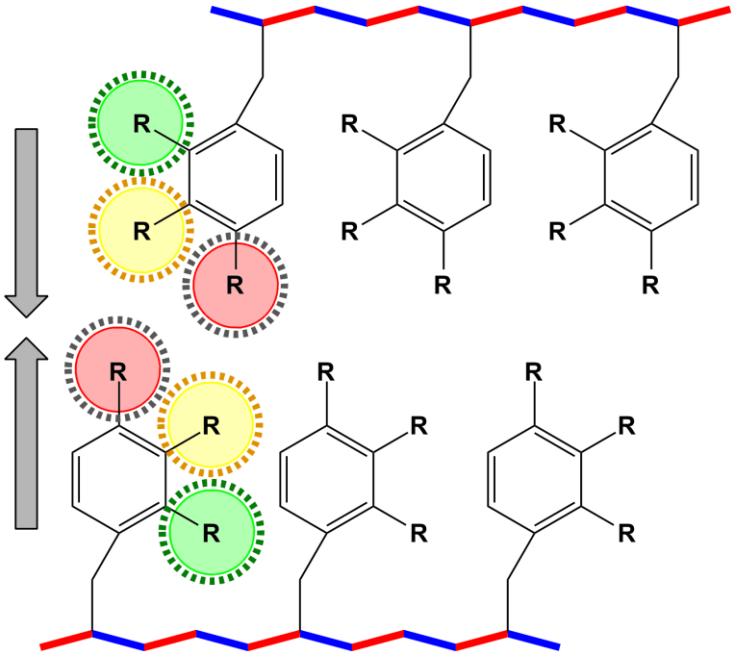

Figure 4.1.14 Steric 'risk' as pillars move to interdigitate. Red circles represent high steric risk to prevent interdigitation, yellow represents medium, and green is a light risk. Red/blue backbone represents ionic sheet. Grey arrows indicate path of travel.

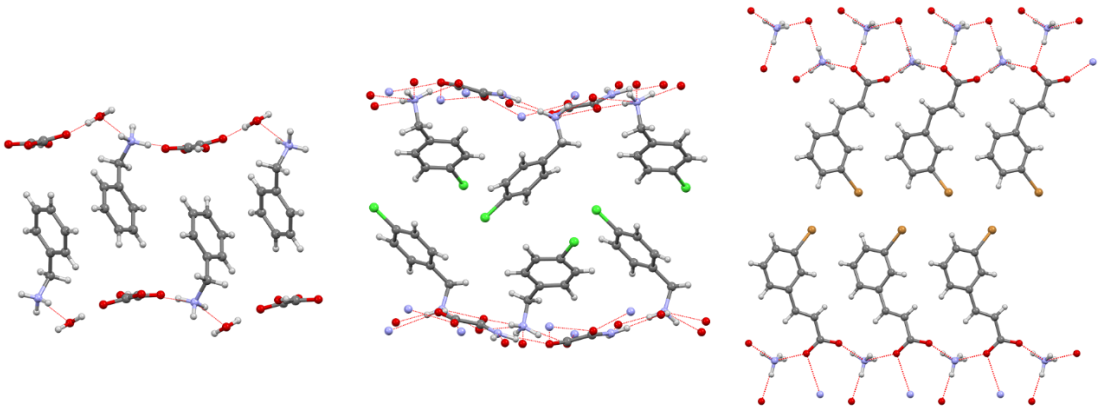

Figure 4.1.15 Literature examples of substituents effecting interdigitation. *Para*- and *meta*-substituents tend to resist interdigitation. *Left*, monolayer interdigitating benzylamine (Refcode: AJUMOH).[87] *Middle*, monolayer non-interdigitating *para*-substituted benzylamine (note bending of pillar as single sheet brings aryl moieties closer proximally) (Refcode: TOYMAV).[91] *Right*, double layer non-interdigitating *meta*-substituted arene (Refcode: ICUJIA).[119]

One exception with respect to interdigitation found by Smith is the ammonium phenoxyacetate compound (Refcode: ZOWWEP).[69] Here in this structure, which lacks any sterically demanding *meta*- or *para*-substituent, the pillars should interdigitate, especially compared to their analogous pillars with predictably non-interdigitating *para*-halo substituents. However, due to the close packing of the strong charge-assisted ionic substrate, interdigitation is not possible. Here, pillar interdigitation would require the ionic sheet to expand outward to accommodate the spatial requirements necessary to bring the pillars close, based on electrostatic repulsion. This sheet expansion would result in a separation and/or collapse of the hydrogen-bonded substrate. The resistance to sheet 'breathing' or expansion to accommodate pillar interdigitation is likely due to the strength of the connective hydrogen bonds, which in this case are enhanced by the charge-assisted ammonium carboxylates.

A pillared pyridinium phenoxyacetate structure does exist in the Cambridge Structural Database[120-121] (CSD) (Refcode: FADQUY)[122]. The difference in the pyridinium structure here versus the ammonium structure above is the cation, which does not form a hydrogen-bonded 'net', and therefore, to accommodate the interdigitating pillars, the sheet simply spreads out to adapt to the space requirements (substrate amine-amine distances increase from 4.426 Å x 7.145 Å in ZOWWEP to 6.740 Å x 7.843 Å in FADQUY). As discussed in the next chapter, the aryl components of the pillars are involved in chained CH/π interactions, which may result in dense electron density between those arenes, perturbing incoming interdigitating pillars. This observation is consistent with various similar structures and their layering preferences.[85]

4.1.6 Ammonium Formate Solids

The ammonium formate complexes described in this chapter mostly involve primary amines, and therefore should form monolayer and bilayer networks of charge-assisted hydrogen-bonded layers as demonstrated through literature examples with similar cation and anion starting materials; such as those ammonium sulfonates,[85] carboxylates,[64] and phenoxyacetates.[69] These compounds reported herein represent a unique and useful class of layered materials due to the simple nature of the sheet. By limiting the constituents of the hydrophilic sheet to **R**NH_3^+ and COO^- moieties, we encounter these materials as they form into sheets, in a pure form.

4.1.6.1 Predicting 2-Dimensional Ammonium Formate Layer Assembly

Through careful consideration of the guidelines from Odendal, Etter's Rules[123] for hydrogen bonding as discussed in Chapter 1, and previous lab interest in 2-dimensional hydrogen-bonded networks,[47, 50-51] we can move to predict the structural outcome of ammonium formate structures. For these ammonium formate materials, rule 1 will always be satisfied. When rule 2 *is* satisfied (i.e., a non-bulky cation is featured) the pillars will interdigitate, a single sheet monolayer will form, and AB-type layers will assemble; when rule 2 *is not* satisfied (i.e., a bulky cation is featured), the pillars will not interdigitate, the sheets will stack into a bilayer, and ABA-type layers shall form. X-ray analysis techniques will help us evaluate our structural assemblage predictions by investigating the crystal structures of these compounds.

4.1.7 The Objective

To reiterate the objectives for this part of the work introduced in Chapter 1: the research involves introducing formic acid and (typically arene based) primary amines in order to assemble predictable 2-dimensional hydrogen-bonded structures.

Through the generation and structural analysis of these new ammonium formate complexes, we also seek to draw a structural comparison to other previously discussed ammonium carboxylates found in the database.

Structurally, based upon what is commonly encountered regarding layered compounds of hydrogen-bonded ammonium carboxylates[64, 124] and benzylsulfonates,[85] and based on the guidelines produced in previous reports; the **hypothesis** here is that these ammonium formates shall all: 1) form sheets and pillars, and because the steric bulk of the cation will determine the occurrence of a single or stacked-sheet; 2) will form bilayers resulting in an ABA-type structure when bulky cations are utilized, and form single sheets resulting in AB-type layers when less bulky cations are utilized. Specifically, those ammonium formates with *meta*- and *para*-substituents will form the stacked sheet, ABA layers, and all other formates will form single sheet, AB layers.

Additionally, we would like to determine if there is a steric limit to the lamellar sheet-pillar-sheet format, i.e., is there a point where a lamellar material may go micellar due to perturbations introduced to the hydrophilic substrate (**Figure 4.1.16**). The **hypothesis** is that benzylamine analogues with bulky *ortho*-substituents will disrupt the canonical sheet-pillar-sheet layer motif, and this topological transition will occur.

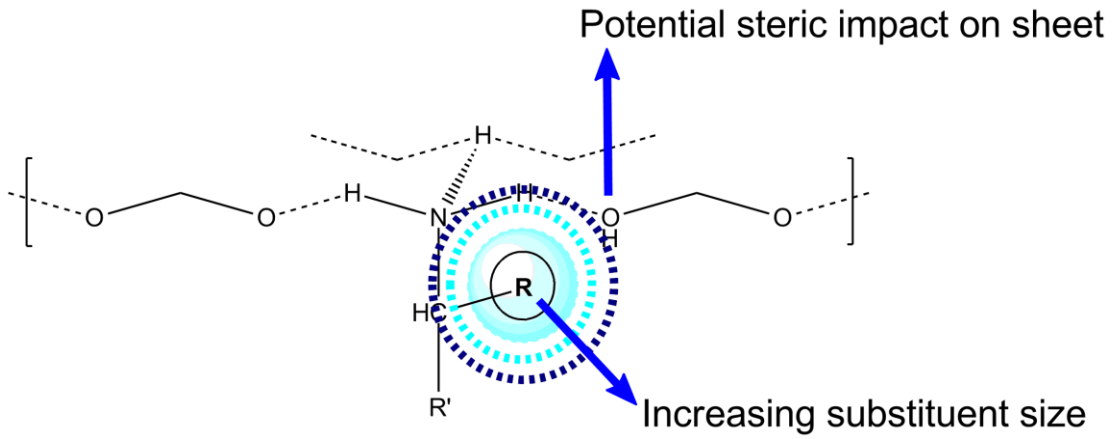

Figure 4.1.16 Illustrating possible impact on sheet linearity by substituent size in an ammonium formate structure.

Herein, we investigate, predict, and comment on the crystal structures of various ammonium formate solids!

4.2 Experimental

All chemical reagents were used as received from Sigma-Aldrich without further purification. All solvents used were distilled prior to use, except 200 proof USP-grade ethanol used as-is. Water was freshly prepared from a Milli-Q® Integral Water Purification System. All crystallization was performed at room temperature in a low-vibration area. Melt point data were collected on an OptiMelt Automated Melting Point System operating in the range of 28-300 °C, at a rate of 2.5 °C per minute. Additional X-ray crystallographic tables can be found in Appendix II.

CSD searches were carried out using the ConQuest 1.19 program which is part of the Cambridge Crystallographic Data Centre (CCDC) software suite.[121] Searches were filtered for organics which had 3-D coordinates determined. The resulting hitlist was combed to identify layered structures containing a substituted benzylamine and carboxylic acid.[120]

Safety. Extreme caution should be taken in the use of formic acid. Formic acid presents a strong danger upon skin contact as well as contact *via* the readily produced vapors. The reader is cautioned and referred to the formic acid International Chemical Safety Card which can be found on the Center for Disease Control's (CDC) website at www.cdc.gov.

4.2.1 Synthesis of Ammonium Formates

In a typical experiment, a small aliquot of formic acid is added to a small vial containing 1 mL solvent. To this vial is added an amine in 1:1, 1:2, or 2:1 ratios to formic acid, to improve chances of crystallization. The vial is loosely capped and set aside to slowly concentrate, forming X-ray quality crystals over days (**Scheme 4.2.1**). The ratios giving the best crystals were selected for analysis.

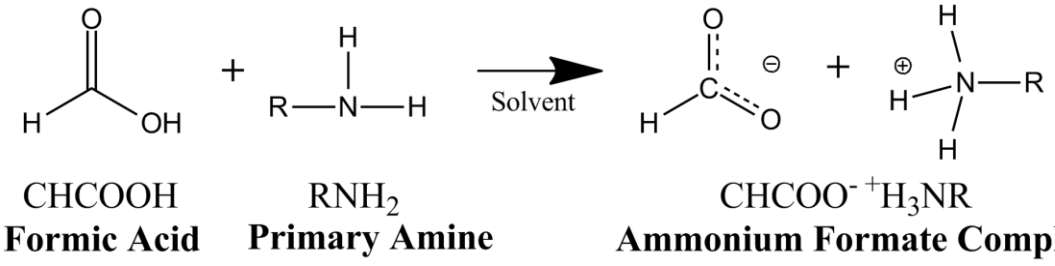

Scheme 4.2.1 The synthetic route to ammonium formate complexes.

4.2.1.1 Synthesis of benzylammonium formates 1-12

10 µL of formic acid (.265 mmol) is added to a small vial containing 1 mL solvent (ethanol (**1**-**6**, **8**, **10**), methanol (**9**, **12**), water (**7**), toluene (**11**)) and gently swirled. To this solution is added substituted benzylamine, $C_7H_6NH_2$**R**, where **R** is a substitution to the ring (**R** = H (**1**), *o*-CH_3 (**2**), *m*-CH_3 (**3**), *p*-CH_3 (**4**), *p*-CF_3 (**5**), *p*-OCH_3 (**6**), *p*-^{t}Bu (**7**), *m*-Cl (**8**), *p*-Cl (**9**), 3,5-2F (**10**), *p*-NH_2 (**12**)) or 1-(1-naphthyl)ethylamine (**11**) in a 1:1 (**3**-**6**, **10**), 1:2 (**1**, **7**-**8**) or 2:1 (**2**, **9**, **11**-**12**) molar formic acid: amine ratio (58 µL (**1**), 17 µL (**2**), 33 µL (**3**), 34 µL (**4**), 38 µL (**5**), 34 µL (**6**), 96 µL (**7**), 33 µL (**8**), 16 µL (**9**), 31 µL (**10**), 20 µL (**11**), 15 µL (**12**)). The mixed solution

is lightly capped and set aside to slowly concentrate, forming X-ray quality crystals as plates (**1**, **3**-**6**, **9**, **11**), rods (**2**, **8**, **10**, **12**), or needles (**7**) in 90% (**1**, mp 79-94 °C), 95% (**2**, mp 118-124 °C), 90% (**3**, mp 86-93 °C), 90% (**4**, mp 140-143 °C), 10% (**5**, mp 85-95 °C), 99% (**6**, mp 115-117 °C), 98% (**7**, mp 150-154 °C), 93% (**8**, mp 100-103 °C), 97% (**9**, mp 142-147 °C), 98% (**10**, mp 117-120 °C, 275-282 °C), 99%, (**11**, mp 156-160 °C) 55% (**12**, mp 139-143 °C) yield.

4.2.1.2 Synthesis of phenthylammonium formates 13-19

10 µL of formic acid (.265 mmol) is added to a small vial containing 1 mL solvent (ethanol (**13**, **15**, **17**-**19**), toluene (**14**), dichloromethane (**16**)) and gently swirled. To this solution is added substituted phenethylamine, $C_8H_8NH_2$**R**, where **R** is a substitution to the ring (**R** = H (**13**), *o*-Cl (**14**), *m*-F (**15**), *m*-Cl (**16**), *p*-Cl (**17**), *p*-Br (**18**), 2,4-2Cl (**19**)) in a 1:1 (**13**-**15**, **17**-**19**) or 2:1 (**16**) molar formic acid: amine ratio (33 µL (**13**), 37 µL (**14**), 35 µL (**15**), 19 µL (**16**), 37 µL (**17**), 41 µL (**18**), 40 µL (**19**)). The mixed solution is lightly capped and set aside to slowly concentrate, forming X-ray quality crystals as blocks (**13**, **15**, **17**), rods (**14**, **16**, **19**), or plates (**18**) in 15% (**13**, mp 119-126 °C), 89% (**14**, mp 111-115 °C), 13% (**15**, mp 102-114 °C), 67% (**16**, mp 90-130 °C), 90% (**17**, mp 112-117 °C), 90% (**18**, mp 107-125 °C), 56% (**19**, mp 140-142 °C) yield.

4.2.1.3 Synthesis of secondary ammonium formates 20-21

10 µL of formic acid (.265 mmol) is added to a small vial containing 1 mL solvent (toluene (**20**), ethanol (**21**)) and gently swirled. To this solution is added di-N-octylamine (**20**, 41 µL) or dicyclohexylamine (**21**, 26 µL) in a 2:1 molar formic acid: amine ratio. The mixed solution is lightly capped and set aside to slowly concentrate, forming X-ray quality needles (**20**) or rods (**21**) in 30% (**20**, mp 59-64 °C) or 78% (**21**, mp 161-166 °C) yield.

4.2.1.4 Synthesis of a heterocyclic ammonium formate, 22

10 µL of formic acid (.265 mmol) is added to a small vial containing 1 mL ethanol and gently swirled. To this solution is added 4-(aminomethyl)piperidine (32 µL) in a 1:2 molar formic acid: amine ratio. The mixed solution is lightly capped and set aside to slowly concentrate, forming X-ray quality rods in 78% (mp 155-162 °C) yield.

4.2.1.5 Synthesis of anilinium formates 23-32

10 µL of formic acid (.265 mmol) is added to a small vial containing 1 mL solvent (water (**23**) ethanol (**24-25, 28-29, 31**), methanol (**26-27**), or toluene (**30**,**32**)) and gently swirled. To this solution is added substituted aniline, $C_6H_4NH_2$**R**, where **R** is a substitution to the ring (**R** = 3,5-CH_3 (**23**) 2,4,6-CH_3 (**24**), $^{i}C_3H_7$ (**25**), $^{i}(C_3H_7)_2$ (**26**), C_2H_3 (**27**), *m*-Cl (**28**), *p*-I (**29**), *o*-OCH_3 (**30**), *o*-OC_2H_5 (**31**)) or 1-Amino-2-methylnaphthalene (**32**) in a 1:1 (**24**, **28**-**29**, **31**-**32**) or 1:2 (**23**, **25**-**27**, **30**) molar formic acid: amine ratio (68 µL (**23**), 32 µL (**24**), 64 µL (**25**), 62 µL (**26**), 30 mg (**27**), 34 µL (**28**), 30 mg (**29**), 58 µL (**30**), 32 µL (**31**), 29 µL (**32**)). The mixed solution is lightly capped and set aside to slowly concentrate, forming X-ray quality crystals as blocks (**24**, **26**-**27**, **31**), rods (**25**, **28**, **30**), or plates (**23**, **29**, **32**) in 50% (**23**, mp 75-78 °C), 91% (**24**, mp 180-182 °C), 90% (**25**, mp 65-68 °C), 98% (**26**, mp 156-157 °C), 70% (**27**, mp 150-154 °C), 65% (**28**, mp 52-56 °C), 60% (**29**, mp 110-115 °C), 62% (**30**, mp 84-88 °C), 96% (**31**, mp 49-53 °C), or 58% (**32**, mp 170-175 °C) yield.

4.2.2 X-Ray Crystallography

Crystalline samples of **1-32** were suspended in Paratone oil and subsequently mounted on a MiTeGen dual-thickness microloop. All data were collected using a Bruker Kappa or SMART Apex II X-ray diffractometer. A graphite monochromated Mo Kα (λ = 0.71703 Å) radiation at 100 K was used for all samples, except **2** (296 K), **4**, **7, 16** (273 K), **11** (111 K), **12** (113 K), **13** (103 K), **25** (105 K), **22** (101 K), **23** (107 K), **32** (117 K). Crystal structures were solved utilizing

the OLEX2 software package[125] which functions using SHELX protocols.[126] Structure solution was achieved by way of direct methods and refined using least squares minimization which are both part of the SHELX-97 package. Brief crystal data for each compound is tabulated in **Table 4.2.1 - Table 4.2.4**, full sets of crystallographic tables for each compound may be found in Appendix II.

Compound	1	2	3	4
Molecular Formula	$C_8H_{11}NO_2$	$C_9H_{13}NO_2$	$C_9H_{13}NO_2$	$C_9H_{13}NO_2$
Molecular Weight	153.18	167.20	167.20	167.20
Crystal System	Orthorhombic	Monoclinic	Monoclinic	Monoclinic
Space Group	Pbca	$P2_1$	$P2_1/c$	$P2_1/c$
***a* (Å)**	8.5468(5)	6.9761(6)	16.9827(8)	17.090(8)
***b* (Å)**	11.0536(7)	7.6181(6)	4.8029(2)	4.909(2)
***c* (Å)**	17.5296(10)	8.3283(7)	11.5315(6)	11.565(6)
α (°)	90.0	90.0	90.0	90.0
β (°)	90.0	94.646(4)	103.947(3)	109.75(3)
γ (°)	90.0	90.0	90.0	90.0
Volume (Å^3)	1656.07(17)	441.15(6)	912.85(8)	913.1(8)
Z	8	2	4	4
T (K)	100(2)	296(2)	100(2)	273(2)
Reflections Measured	39249	11481	16894	14322
Unique Reflections	2869	3372	2845	1882
R_{int}	0.0355	0.0283	0.0298	0.0501
R_1 [I > 2σ(I)]	0.0354	0.0651	0.0381	0.0474
wR_2 [I > 2σ(I)]	0.0975	0.2047	0.1072	0.1232

Compound	5	6	7	8
Molecular Formula	$C_9H_{10}F_3NO_2$	$C_9H_{13}NO_3$	$C_{12}H_{19}NO_2$	$C_8H_{10}ClNO_2$
Molecular Weight	221.18	183.20	246.59	187.62
Crystal System	Monoclinic	Monoclinic	Monoclinic	Monoclinic
Space Group	$P2_1/c$	Cc	$P2_1/c$	$P2_1/c$
***a* (Å)**	5.7416(4)	6.7615(3)	19.1296(13)	16.7899(10)
***b* (Å)**	21.1000(14)	18.9173(7)	6.4253(4)	4.7766(3)
***c* (Å)**	8.5319(6)	7.8044(3)	10.1620(7)	11.5500(6)
α (°)	90.0	90.0	90.0	90.0
β (°)	102.036(4)	105.9340(19)	97.440(4)	104.162(3)
γ (°)	90.0	90.0	90.0	90.0
Volume (Å^3)	1010.90(12)	959.90(7)	1238.53(14)	898.14(9)
Z	4	4	4	4
T (K)	100(2)	100(2)	273(2)	100(2)
Reflections Measured	15246	11815	20232	20733
Unique Reflections	2275	3235	2542	3009
R_{int}	0.0374	0.0230	0.0342	0.0276
R_1 [I > 2σ(I)]	0.0737	0.0273	0.0619	0.0467
wR_2 [I > 2σ(I)]	0.1858	0.0742	0.1960	0.1134

4.2.1 Table of crystallographic data for compounds **1**-**8**

Compound	9	10	11	12
Molecular Formula	$C_8H_{10}ClNO_2$	$C_8H_9F_2NO_2$	$C_{13}H_{15}NO_2$	$C_8H_{16}N_2O_2$
Molecular Weight	187.62	189.16	217.26	172.23
Crystal System	Monoclinic	Orthorhombic	Orthorhombic	Monoclinic
Space Group	$P2_1/c$	Pbca	$Pca2_1$	C2
***a* (Å)**	16.7551(13)	13.4870(14)	6.9086(3)	19.8600(11)
***b* (Å)**	4.8441(4)	7.4596(8)	17.9665(7)	5.8074(3)
***c* (Å)**	11.4478(9)	17.4603(18)	9.1840(3)	7.6922(4)
α (°)	90.0	90.0	90.0	90.0
β (°)	109.041(3)	90.0	90.0	107.785(3)
γ (°)	90.0	90.0	90.0	90.0
Volume (Å^3)	878.30(12)	1756.6(3)	1139.95(8)	844.78(8)
Z	4	8	4	4
T (K)	100(2)	100(2)	111(2)	113(2)
Reflections Measured	22278	14166	25753	11395
Unique Reflections	3502	818	3616	3237
R_{int}	0.0190	0.0453	0.0242	0.0278
R_1 [I > 2σ(I)]	0.0240	0.0255	0.0307	0.0331
wR_2 [I > 2σ(I)]	0.0709	0.0638	0.0840	0.0897

Compound	13	14	15	16
Molecular Formula	$C_9H_{13}NO_2$	$C_9H_{12}ClNO_2$	$C_9H_{12}FNO_2$	$C_9H_{12}ClNO_2$
Molecular Weight	167.20	201.65	167.78	201.65
Crystal System	Orthorhombic	Orthorhombic	Monoclinic	Monoclinic
Space Group	$Pca2_1$	Pbca	$P2_1/c$	$P2_1/c$
***a* (Å)**	19.7529(5)	19.6625(9)	11.9482(4)	6.050(4)
***b* (Å)**	11.2940(3)	8.9907(4)	19.4010(7)	20.067(13)
***c* (Å)**	8.6136(2)	22.8470(10)	12.4181(5)	9.015(7)
α (°)	90.0	90.0	90.0	90.0
β (°)	90.0	90.0	94.3991(19)	109.43(4)
γ (°)	90.0	90.0	90.0	90.0
Volume (Å^3)	1921.60(8)	4038.9(3)	2870.12(18)	1032.2(12)
Z	8	17	12	4
T (K)	103(2)	100(2)	100(2)	273(2)
Reflections Measured	21240	55203	58730	12563
Unique Reflections	2592	3331	7423	2107
R_{int}	0.0338	0.0452	0.0377	0.0513
R_1 [I > 2σ(I)]	0.0202	0.0286	0.0353	0.0453
wR_2 [I > 2σ(I)]	0.0502	0.0764	0.0886	0.1147

4.2.2 Table of crystallographic data for compounds **9**-**16**

Compound	17	18	19	20
Molecular Formula	$C_{18}H_{24}Cl_2N_2O_4$	$C_{18}H_{24}Br_2N_2O_4$	$C_9H_{11}Cl_2NO_2$	$C_{18}H_{36}NO_4$
Molecular Weight	403.29	492.21	236.09	330.49
Crystal System	Monoclinic	Monoclinic	Triclinic	Triclinic
Space Group	$P2_1/c$	$P2_1/c$	P-1	P-1
***a* (Å)**	12.170(3)	12.2325(4)	4.6609(10)	4.6682(5)
***b* (Å)**	7.5094(17)	7.5028(3)	6.9345(14)	13.5815(17)
***c* (Å)**	21.382(5)	21.5675(8)	16.340(3)	15.760(2)
α (°)	90.0	90.0	83.253(13)	79.200(6)
β (°)	97.655(12)	97.175(2)	89.558(12)	89.837(6)
γ (°)	90.0	90.0	79.517(12)	83.126(6)
Volume (Å^3)	1936.7(8)	1963.92(13)	515.67(18)	974.3(2)
Z	4	4	2	2
T (K)	100(2)	100(2)	100(2)	100.01
Reflections Measured	35013	33968	10538	10969
Unique Reflections	2107	4310	3632	3886
R_{int}	0.0449	0.0665	0.0569	0.0543
R_1 [I > 2σ(I)]	0.0389	0.0853	0.0861	0.1272
wR_2 [I > 2σ(I)]	0.1103	0.2091	0.2477	0.3464

Compound	21	22	23	24
Molecular Formula	$C_{13}H_{25}NO_4$	$C_{18}H_{22}N_2O_2$	$C_7H_{13}N_2O_2$	$C_{10}H_{15}NO_2$
Molecular Weight	227.34	298.37	157.19	181.23
Crystal System	Monoclinic	Triclinic	Triclinic	Monoclinic
Space Group	C2/c	P-1	P-1	$P2_1/n$
***a* (Å)**	19.203(4)	7.9233(2)	6.3973(4)	7.8752(11)
***b* (Å)**	8.1231(18)	8.0896(2)	7.6975(5)	16.023(2)
***c* (Å)**	16.922(4)	12.6418(3)	9.6867(6)	8.0217(11)
α (°)	90.0	78.8630(11)	74.260(2)	90.0
β (°)	94.395(11)	88.0042(11)	78.013(2)	116.558(6)
γ (°)	90.0	84.0465(10)	73.143(2)	90.0
Volume (Å^3)	2631.9(10)	790.65(3)	435.06(5)	905.4(2)
Z	8	2	2	4
T (K)	105(2)	101(2)	107(2)	100(2)
Reflections Measured	21391	21334	10998	23876
Unique Reflections	3366	6140	3333	3245
R_{int}	0.0429	0.0218	0.0276	0.0263
R_1 [I > 2σ(I)]	0.0637	0.0415	0.0462	0.0357
wR_2 [I > 2σ(I)]	0.1889	0.1260	0.1547	0.1064

4.2.3 Table of crystallographic data for compounds **17-24**

Compound	25	26	27	28
Molecular Formula	$C_{10}H_{13}NO$	$C_{13}H_{19}NO$	C_8H_9NO	C_7H_6ClNO
Molecular Weight	163.21	205.29	135.16	155.58
Crystal System	Triclinic	Monoclinic	Monoclinic	Monoclinic
Space Group	P-1	$P2_1/c$	$P2_1/n$	$P2_1/c$
***a* (Å)**	12.3625(4)	8.9276(3)	8.5664(4)	8.2862(5)
***b* (Å)**	12.6919(4)	8.7411(2)	5.1394(2)	12.1839(7)
***c* (Å)**	14.3045(5)	15.7460(5)	16.8345(7)	6.8176(4)
α (°)	67.2760(17)	90.0	90.0	90.0
β (°)	71.0574(18)	105.5263(13)	102.642(2)	92.892(4)
γ (°)	66.6694(17)	90.0	90.0	90.0
Volume (Å^3)	1861.50(11)	1183.93(6)	723.19(5)	687.42(7)
Z	8	4	4	4
T (K)	100(2)	100(2)	100(2)	100(2)
Reflections Measured	37952	30866	15479	15234
Unique Reflections	9325	4728	2235	2042
R_{int}	0.0337	0.0198	0.0245	0.0493
R_1 [I > 2σ(I)]	0.0402	0.0361	0.0375	0.0342
wR_2 [I > 2σ(I)]	0.1012	0.1011	0.1065	0.0831

Compound	29	30	31	32
Molecular Formula	C_7H_6INO	$C_8H_{11}NO_3$	$C_{18}H_{26}N_2O_4$	$C_{12}H_{11}NO$
Molecular Weight	247.03	169.18	366.41	185.22
Crystal System	Orthorhombic	Monoclinic	Monoclinic	Monoclinic
Space Group	$P2_12_12_1$	C2/c	$P2_1/c$	$P2_1/n$
***a* (Å)**	4.5281(2)	14.9152(5)	7.7260(7)	4.5837(2)
***b* (Å)**	10.3642(5)	12.8447(4)	7.5519(7)	14.0066(7)
***c* (Å)**	16.2095(8)	8.4326(3)	29.135(3)	14.4781(7)
α (°)	90.0	90.0	90.0	90.0
β (°)	90.0	111.9307(16)	91.836(5)	96.386(3)
γ (°)	90.0	90.0	90.0	90.0
Volume (Å^3)	760.71(6)	1498.62(9)	1699.0(3)	923.76(8)
Z	4	8	4	4
T (K)	100(2)	100(2)	100(2)	115(2)
Reflections Measured	19714	18714	39677	20566
Unique Reflections	3011	2247	5525	2777
R_{int}	0.0285	0.0260	0.0451	0.0306
R_1 [I > 2σ(I)]	0.0228	0.0401	0.0386	0.0454
wR_2 [I > 2σ(I)]	0.0566	0.1171	0.1007	0.1258

4.2.4 Table of crystallographic data for compounds **25-32**

4.3 Results

The hydrogen donor/acceptor interaction of an amine containing moiety and formic acid resulted in four different classes of materials: the *benzylammonium formates*, compounds **1**-**12**; *phenethylammonium formates*, compounds **13**-**19**; *secondary ammonium formates*, compounds **20**-**21**; and finally, the *reacted species* that resulted from the combination of formic acid with a heterocyclic diamine, compound **22**, and those that resulted from formic acid and various anilines, compounds **23**-**32**.

Please see Appendix I for the crystal structures for compounds that are not individually represented in this chapter.

4.3.1 Structures of Benzylammonium Formates 1-12

Compound **1**, benzylammonium formate, crystallizes in the centrosymmetric space group Pbca. The organic components of the cation interdigitate, which results in an undulating hydrophilic sheet. These conditions result in an AB-type layer viewed down the B-axis (**Figure 4.3.1**).

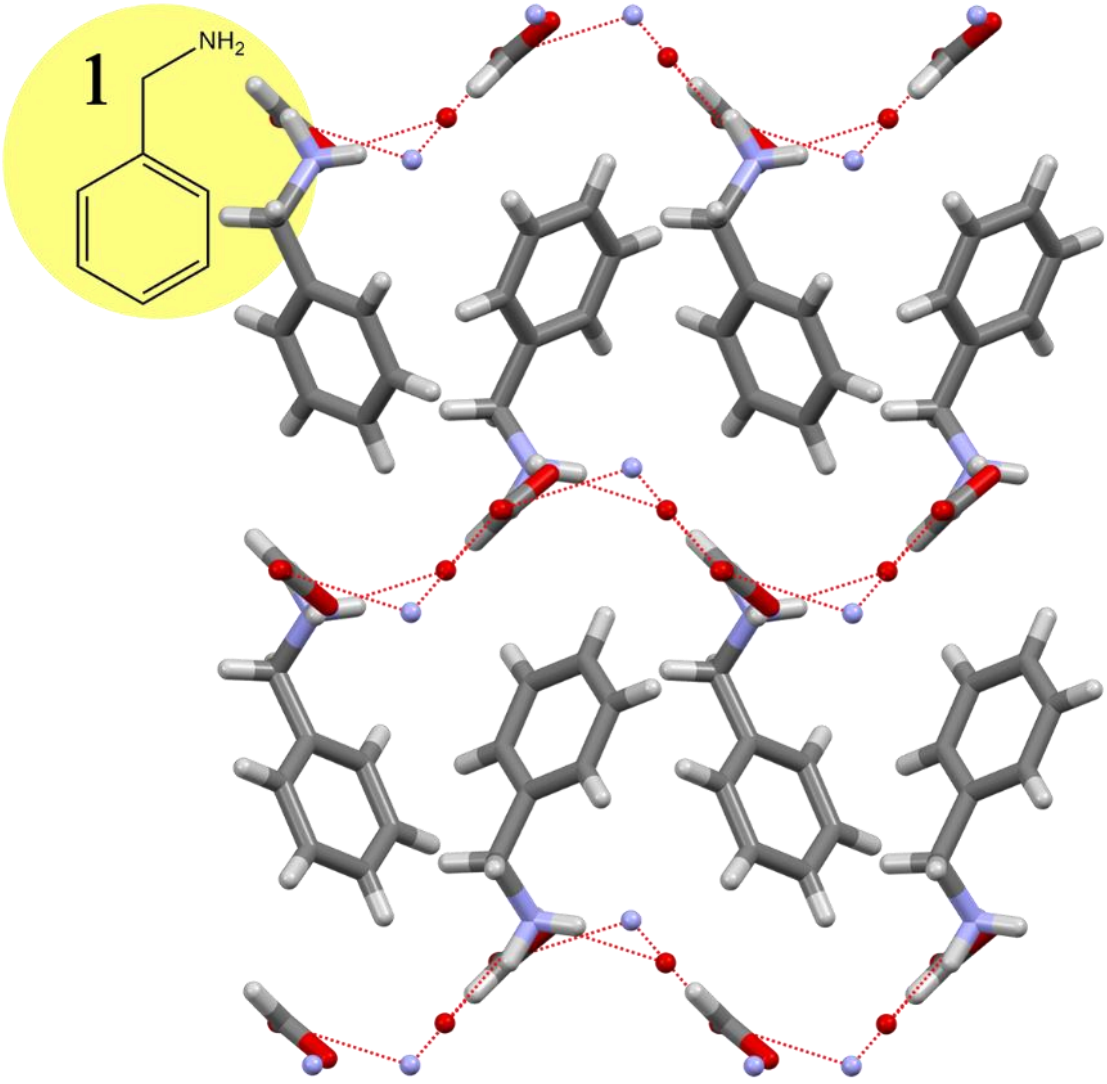

Figure 4.3.1 AB layering pattern of compound **1**. Viewed down the B-axis. *Note: in the following sections, the yellow circled inset, represents the amine starting material that was paired with formic acid for the respective compound, for convenience.*

Compound **2**, *ortho*-methylbenzylammonium formate, crystallizes in the non-centrosymmetric space group $P2_1$. The centrosymmetry of the material is broken due to the directionality of the methyl substituents within the pillared organic component. The methyl substituents of the pillar orient in the same direction. Overall, the organic components of the cations interdigitate and the hydrophilic sheet slightly undulates as the layers formulate. This assemblage results in an AB-type layer, viewed down the A-axis (**Figure 4.3.2**).

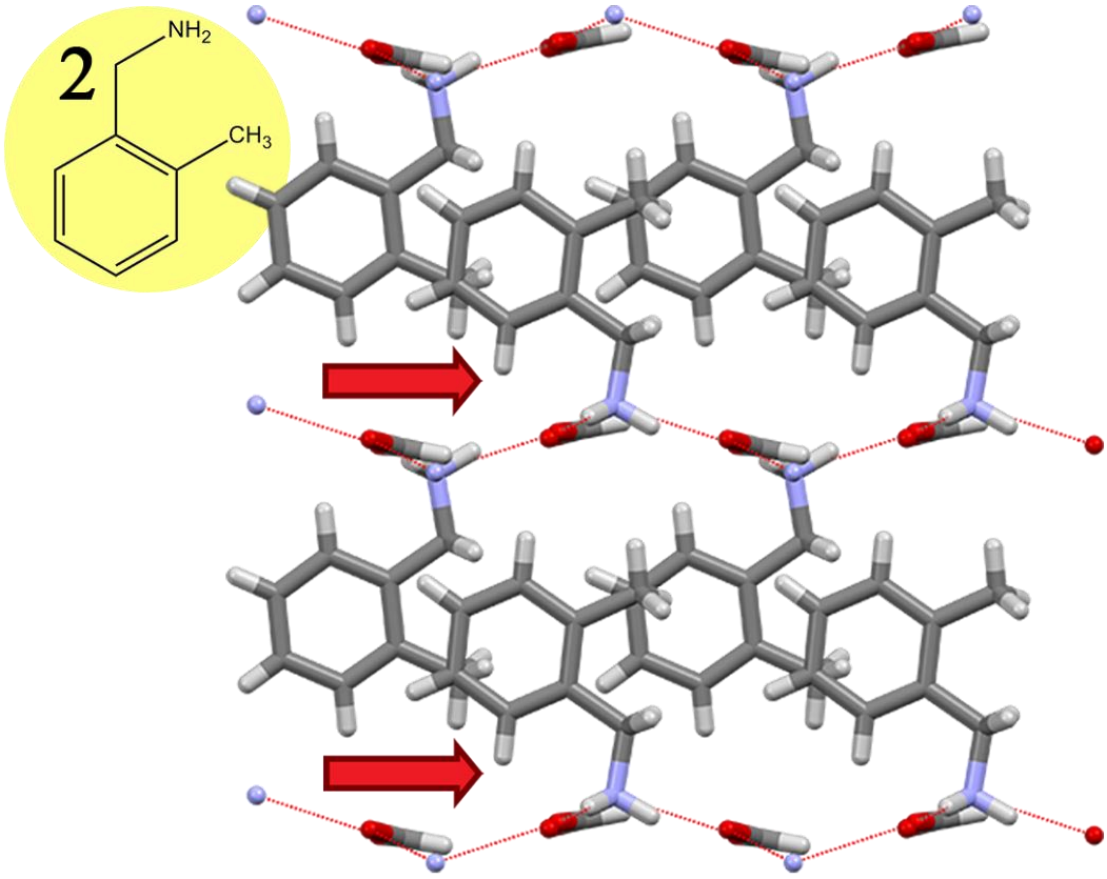

Figure 4.3.2 Layering of compound **2**. Red arrows represent directionality of centrosymmetry breaking elements. Viewed along the A-axis.

Compounds **3**, *meta*-methylbenzylammonium formate, **4**, *para*-methylbenzylammonium formate, **8**, *meta*-chlorobenzylammonium formate, and **9**, *para*-chlorobenzylammoniun formate, crystallize in the centrosymmetric space group $P2_1/c$ and are isostructural, differing only in the placement of the methyl and chloro substituents of the benzyl ring. In the absence of pillar interdigitation, the linearity of the hydrophilic substrate is not perturbed. Due to these conditions, each of these four materials organize in an ABA-type pattern viewed down the B-axis (**Figure 4.3.3**).

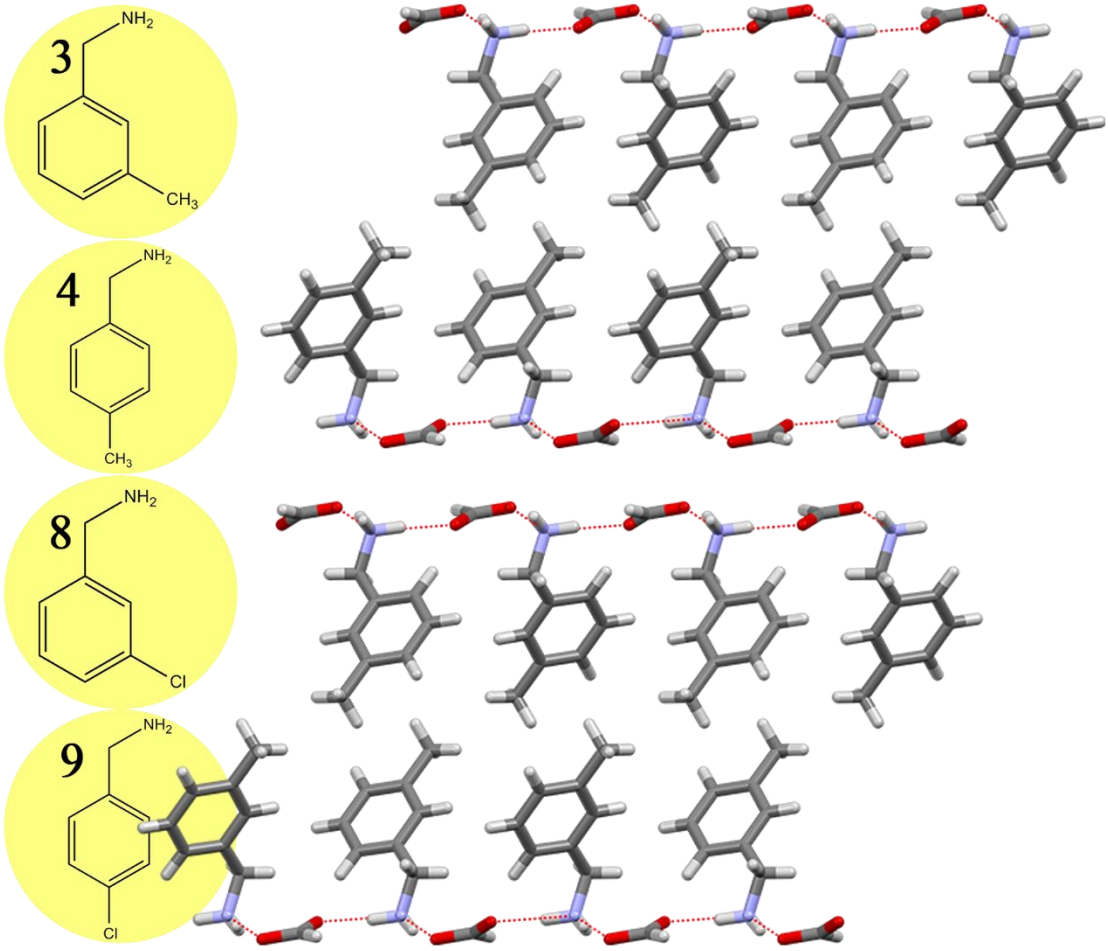

Figure 4.3.3 Layers of compound **3**. Isostructural with compounds **4**, **8**-**9**. Viewed along the B-axis.

Compound **5**, *para*-(trifluoromethyl)-benzylammonium formate crystallizes in the centrosymmetric $P2_1/c$ space group and the organic pillars do not interdigitate, however, the hydrophilic sheet is undulating this case. The components of the network organize in an AB arrangement viewed down the C-axis (**Figure 4.3.4**).

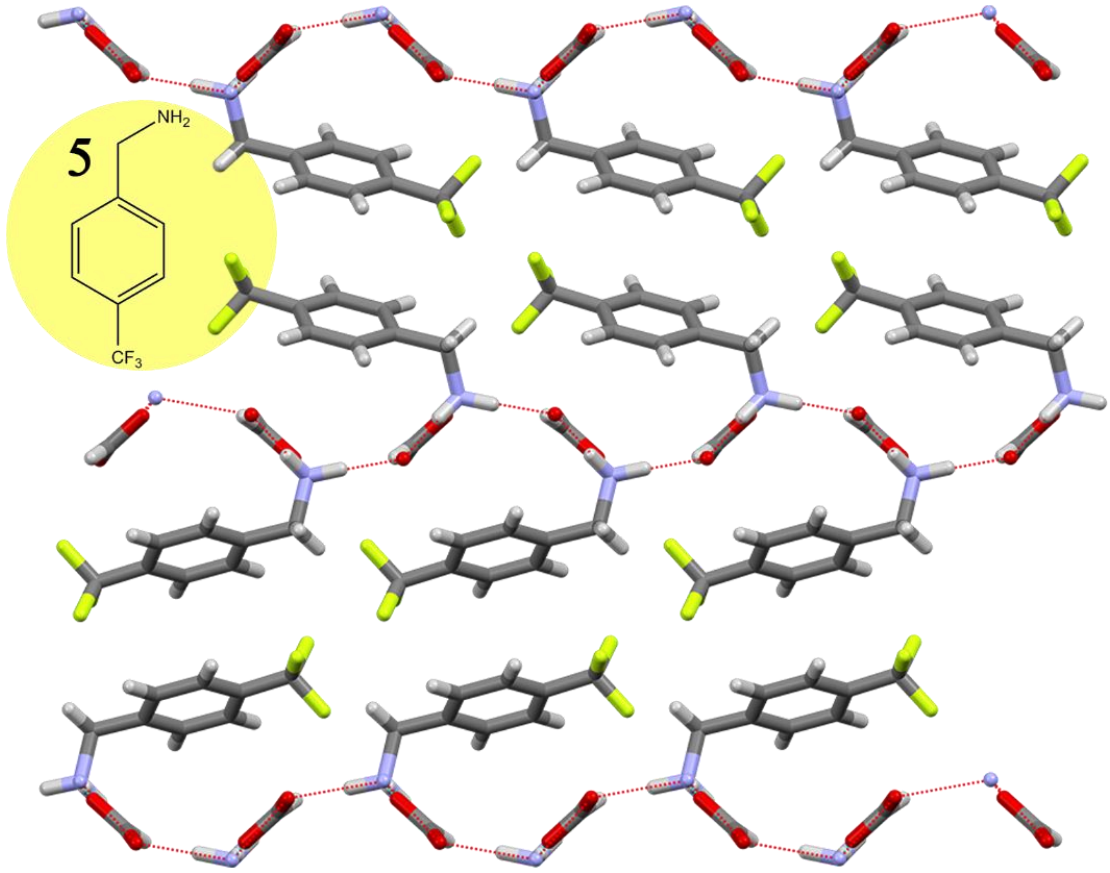

Figure 4.3.4 Layer arrangement of compound **5**. Viewed along the C-axis.

Compound **6**, *para*-methoxybenzylammonium formate, crystallizes in the non-centrosymmetric space group, Cc. Centrosymmetry is this case is broken due to the orientation of the non-interdigitating methoxy groups, which point in the same direction between each substrate. Like **5**, though the organic component does not interdigitate, the sheet's linearity is disrupted by the interlayer pillar interactions between the organic components pulling the hydrophilic sheet out of alignment. This material arranges in an AB-type patters, viewed down the A-axis (**Figure 4.3.5**).

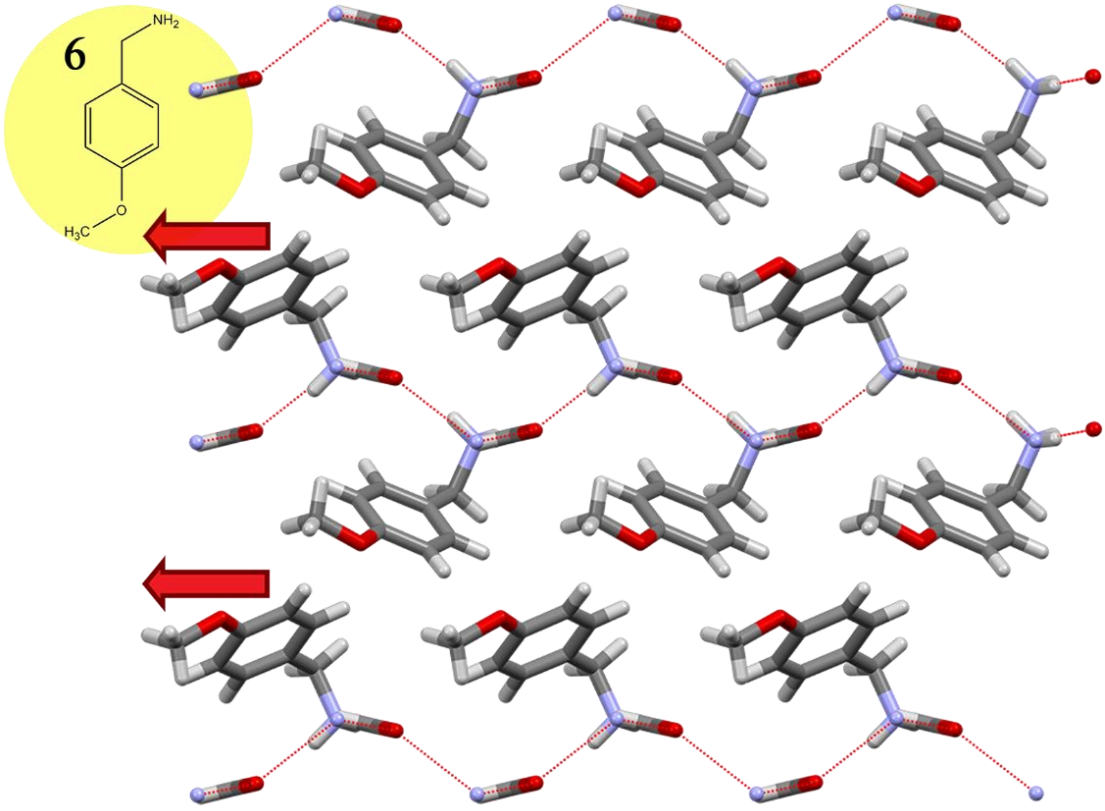

Figure 4.3.5 Compound **6** layering pattern. Red arrows represent directionality of symmetry breaking elements. Viewed down the A-axis.

Compound **7**, *para-tert*-butylbenzylammonium formate, crystallizes in the centrosymmetric $P2_1/c$, space group. The non-interdigitating *para-tert*-butylbenzylamine moieties are more vertically oriented, and the minimal pillar interactions between the hydrophilic substrate results in a flat hydrophilic sheet. The components of this material arrange in an ABA-type layer (**Figure 4.3.6**).

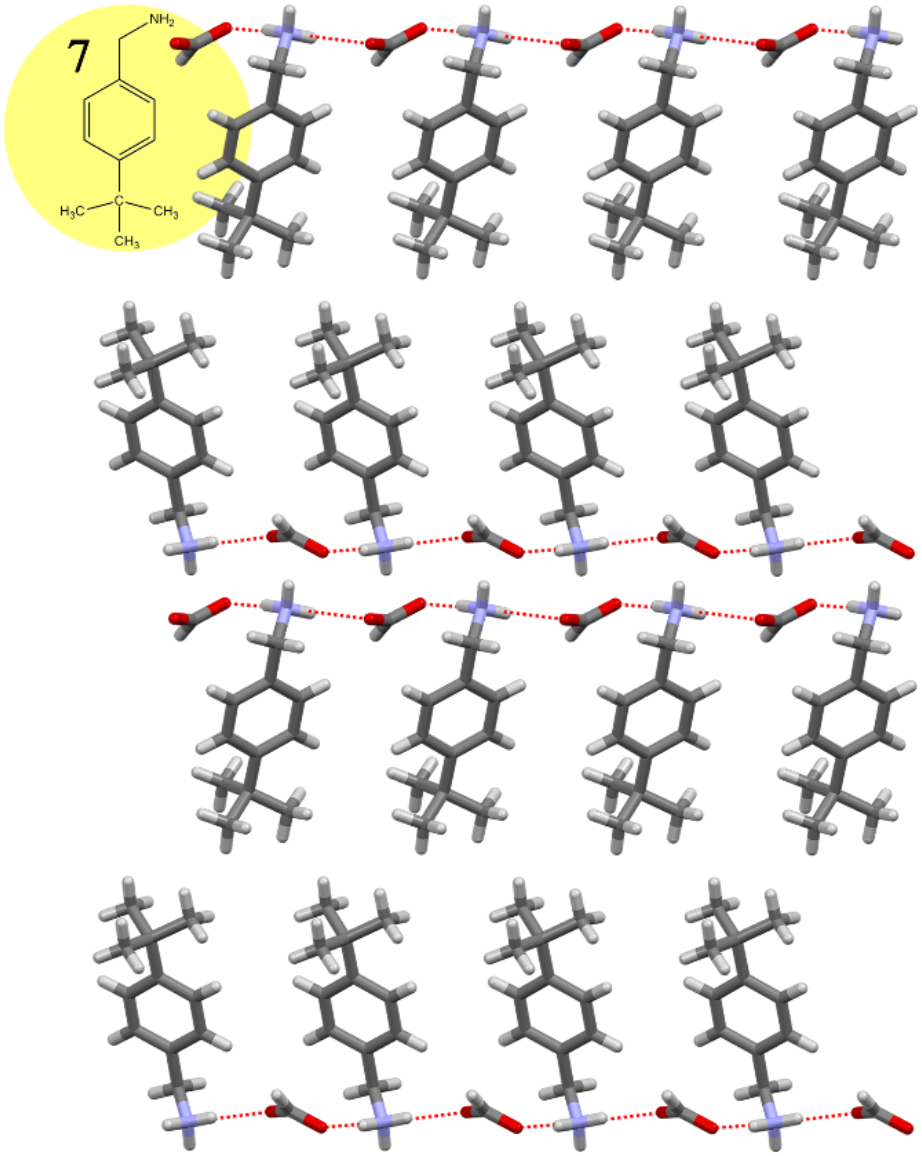

Figure 4.3.6 Layers of compound **7**. Viewed down the C-axis.

Compound **10**, 3,5-difluorobenzylammonium formate, crystallizes in the centrosymmetric space group, Pbca. The edgewise organic pillars interdigitate, pulling the sheet into an undulating wave. This results in a picturesque AB pattern viewed down the B-axis. Positioned behind the front layer, further into the B-axis, the next layer is shifted laterally which results in an overall, staggered, and interdigitated, material (**Figure 4.3.7**). The pillar arrangement is staggered down the layer similar to other di-halogen substituted benzylamines in the database such as 3,4-dichloroammonium hexanedioate (Refcode: LAYKAX).[88]

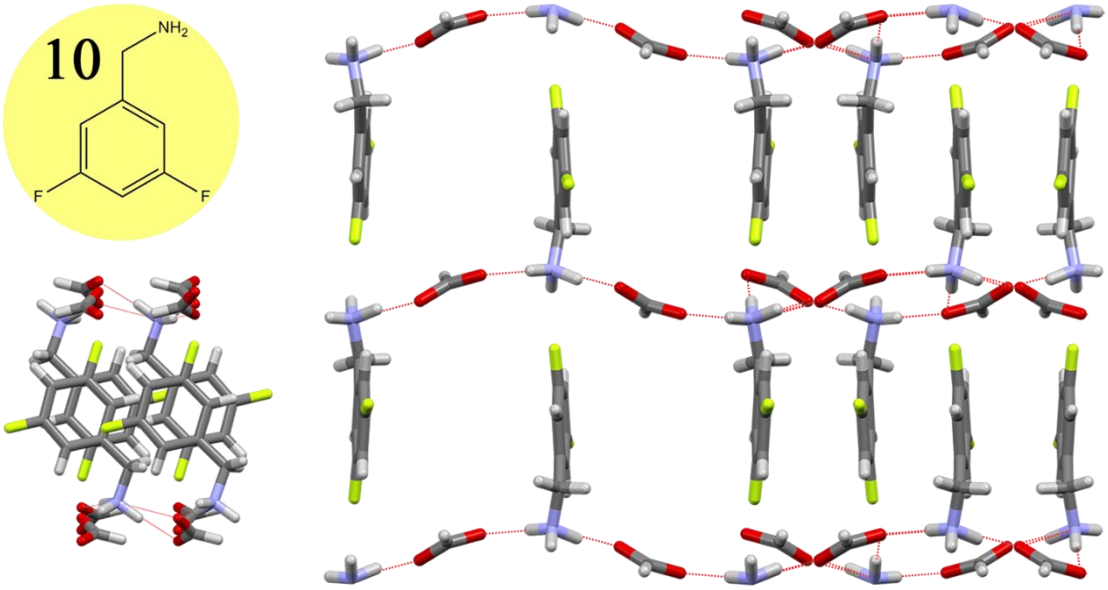

Figure 4.3.7 *Right*, layering of compound **10**, viewed down the B-axis. Progressing left to right, the layer behind is brought into view. *Bottom left*, view of staggered pillars rotated 90°, viewed down the A-axis.

Compound **11**, 1-(1-naphthyl)ethylammonium formate, crystallizes in the non-centrosymmetric space group $Pca2_1$. In this case, the arrangement of the naphthyl groups, which form crescent shaped arrangements that arc in the same direction throughout the structure, are responsible for breaking the centrosymmetry. The organic component does not interdigitate, and the hydrophilic substrate forms a jagged sheet. The layering pattern of this material is AB-type, viewed down the A-axis, but with an 'expanded' hydrophilic sheet due to the unique, vertically oriented formate anions in the substrate (**Figure 4.3.8**).

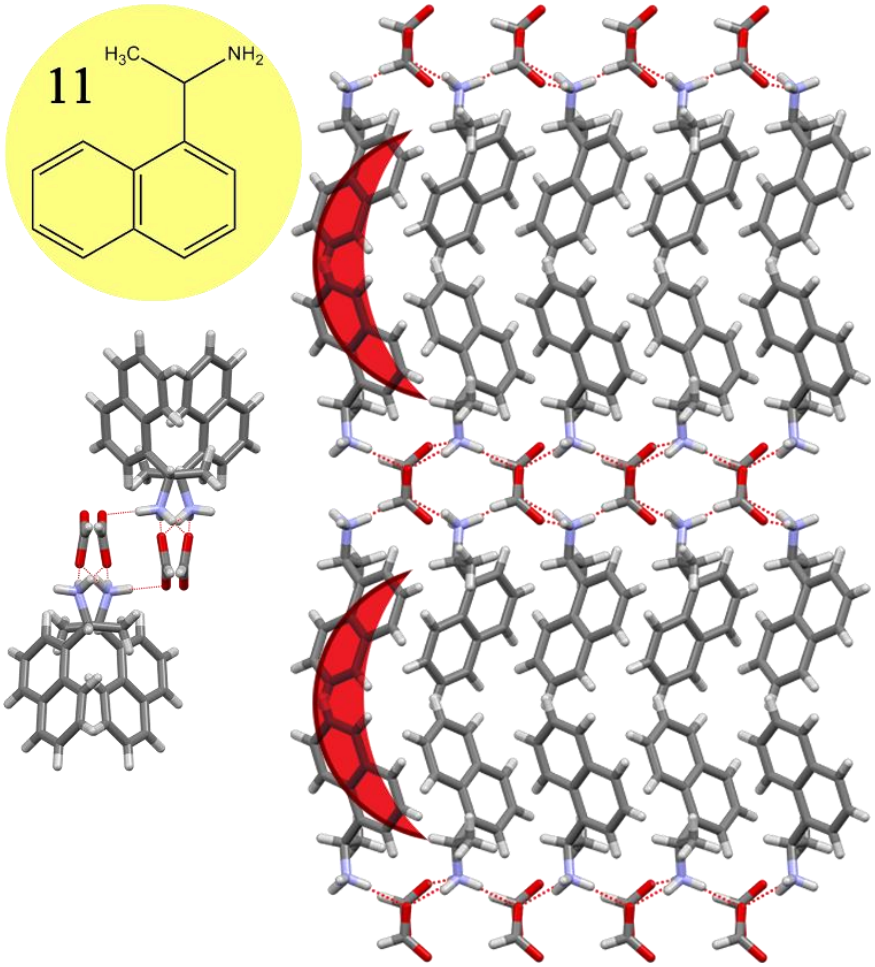

Figure 4.3.8 *Right*, compound **11** layered structure. Red crescents represent directionality of symmetry breaking elements, viewed down the A-axis. *Left*, showing the vertical formate in the sheet, view rotated 90° down the A-axis.

Compound **12**, *para*-aminobenzylammonium formate, crystallizes is the non-centrosymmetric space group, C2. The centrosymmetry of this material is broken by the directionality of the benzyl carbon 'elbow' pointing in the same direction in each pillar moiety. The benzene rings interdigitate allowing the non-polar regions to associate, and the *para*-amino groups orient to hydrogen bond with the opposite sheet. The pillar is sandwiched by two distinct, undulating, hydrophilic substrates with vertical formate ions, forming an AB-type pattern down the C-axis (**Figure 4.3.9**).

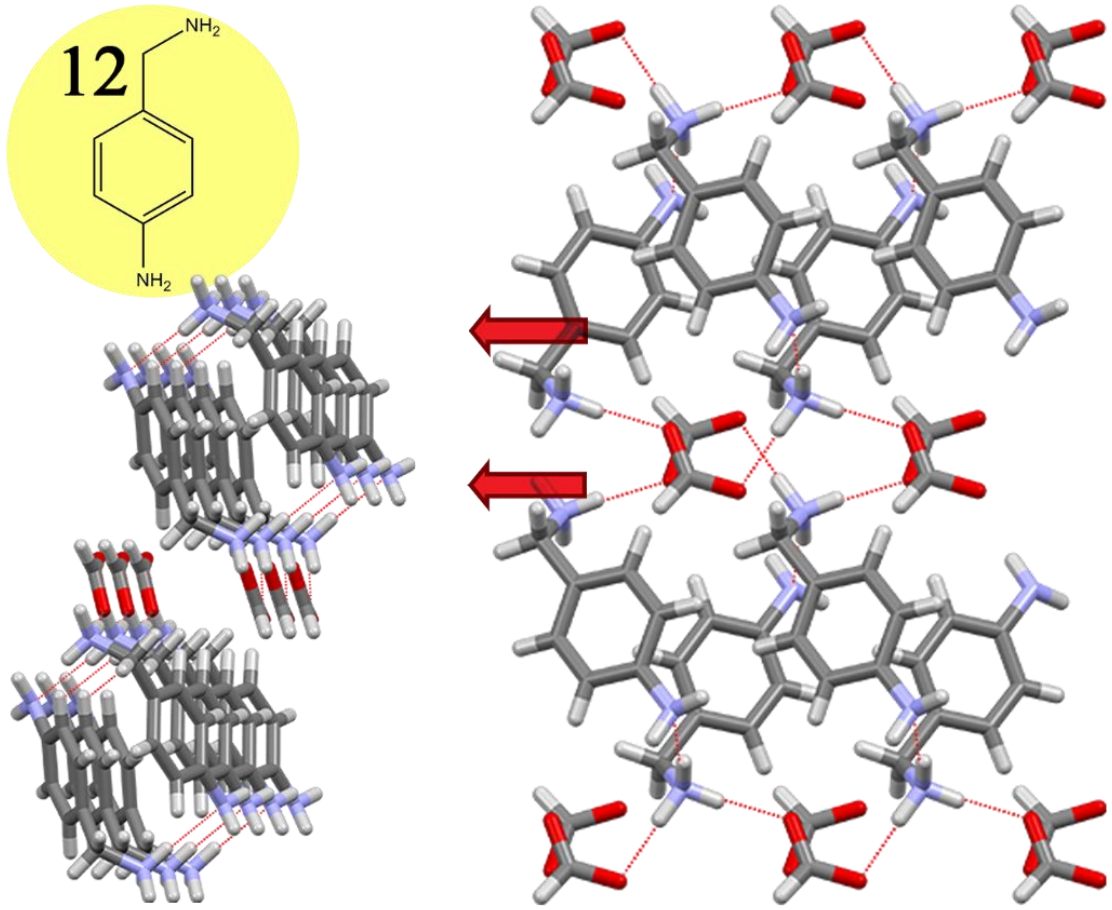

Figure 4.3.9 *Right*, layering of Compound **12**. Red arrows represent directionality of symmetry breaking elements, viewed down the C-axis. *Left*, slightly angled view down the B-axis showing the progression of the hydrophilic sheet.

4.3.2 Structures of Phenethylammonium Formates 13-19

Compound **13**, phenethylammonium formate, crystallizes in the non-centrosymmetric space group, $Pca2_1$, and features two molecules of phenethylammonium and formate ions in the asymmetric unit. Like compound **12**, the centrosymmetry of the molecule is broken by the position and directionality of the α-carbon of the phenethylamine moiety within the interlayer. The organic components of the cation interdigitate, and in doing so pushes and pulls the sheet into an undulating wave. The pillar and sheet organize in an AB-type layer viewed down the B-axis (**Figure 4.3.10**).

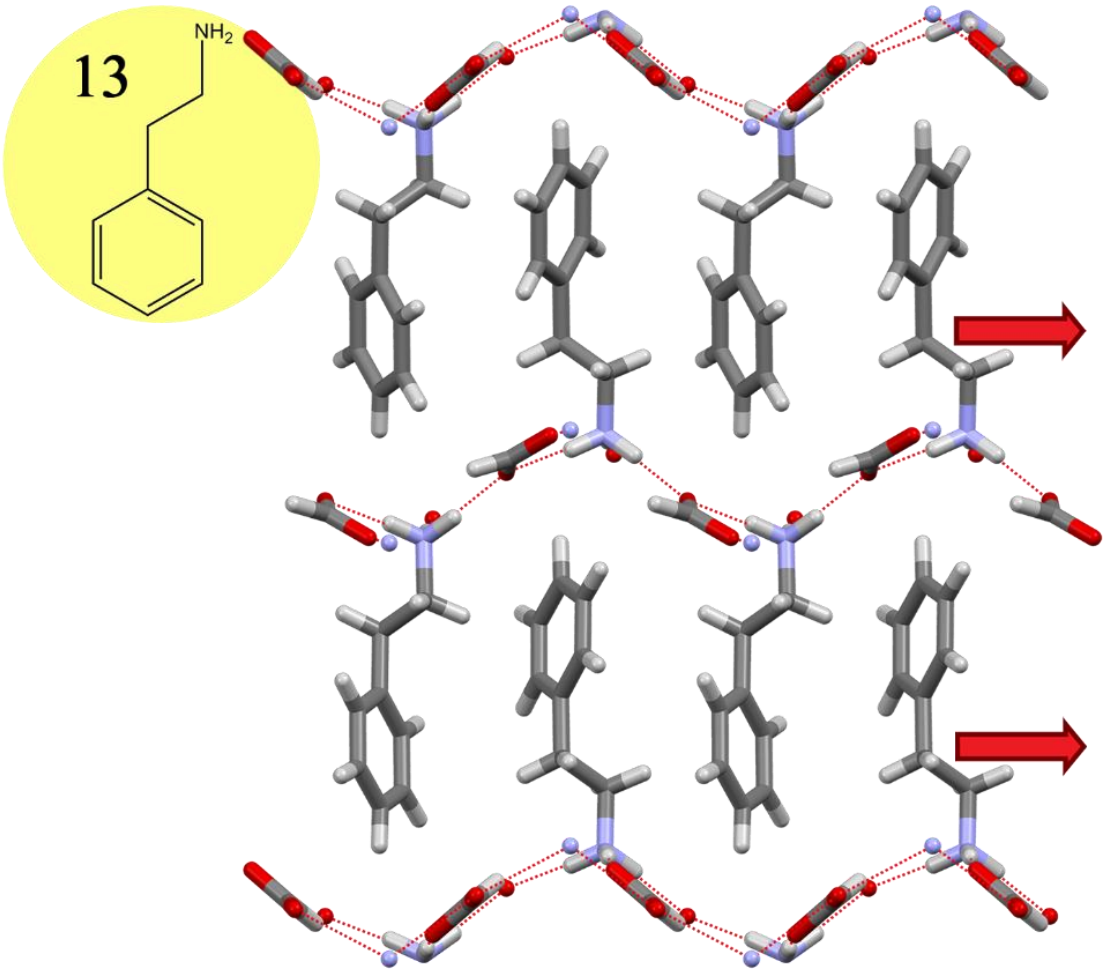

Figure 4.3.10 Layer arrangement of compound **13**. Red arrows represent directionality of symmetry breaking elements. Viewed down the B-axis.

Compound **14**, *ortho*-chlorophenthylammonium formate, crystallizes in the centrosymmetric space group Pbca, and features two 2-chlorophenethylammonium and formate molecules in the asymmetric unit. **14** also appears to have a right facing α-carbon, like **13**, but it appears that the positioning of the chloride satisfies an inversion center, placing this material into a centrosymmetric space group. Compounds **15**, *meta*-fluorophenethylammonium formate, and **16,** *meta*-chlorophenethylammonium formate are isostructural with **14**. Both crystallize in the $P2_1/c$ space group and feature three phenthylammonium and formate molecules in the asymmetric unit. In **14-16** the organic component of the pillars interdigitate, pushing and pulling the hydrophilic sheet into an undulating configuration; these materials adopt an AB arrangement viewed down the C-axis for **14** and **15**, and the A-axis for **16**. For **14-16**, within the pillars, the halide substituents point away in either direction away from the hydrocarbon component, in the direction of the hydrophilic sheet (**Figure 4.3.11**).

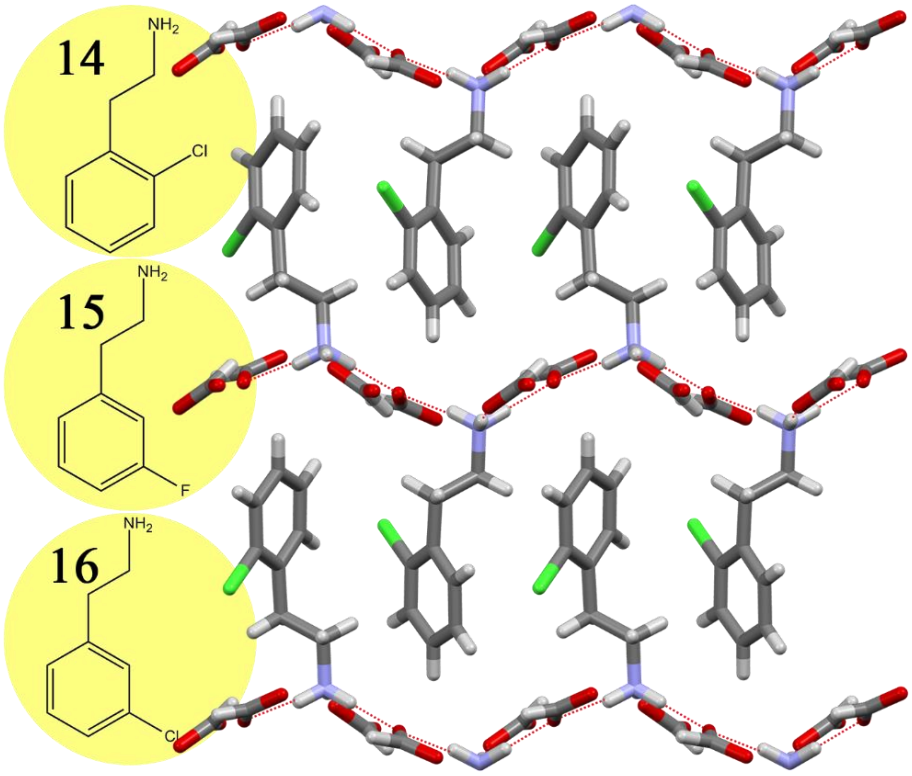

Figure 4.3.11 Compound **14** layers, viewed down the C-axis. Isostructural with **15** and **16**.

Compounds **17**, *para*-chlorophenethylammonium formate, and **18**, *para*-bromophenethylammonium formate, are isostructural and crystallize in the centrosymmetric space group, $P2_1/c$. **17** and **18** both feature two phenethylammonium molecules and two formate molecules in the asymmetric unit. The hydrophilic sheets undulate in a semi-jagged nature as the halogen-substituted aryl rings align and interdigitate. This arrangement results in an AB layering pattern for this material (**Figure 4.3.12**).

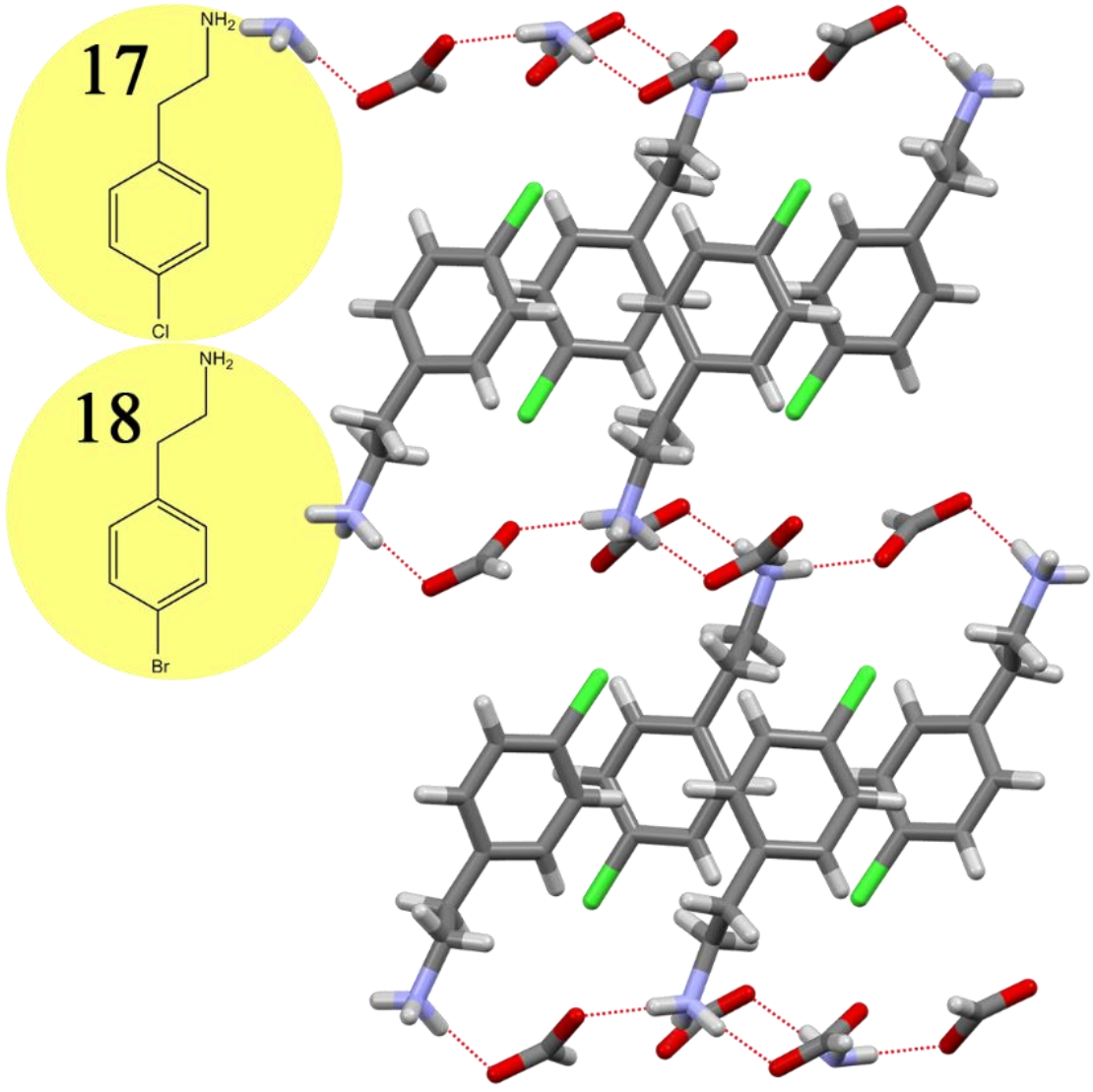

Figure 4.3.12 Compound **17** layers, viewed down the B-axis. Isostructural with **18**.

Compound **19**, 2,4-dichlorophenthylammonium formate, crystallizes in the centrosymmetric space group, P-1. An ABA layer motif is derived from the non-interdigitating pillars and flat sheets viewed down the A-axis. The ring moieties cant and angle to position the *para*-chlorine atoms towards each other, the *meta*-chlorine atoms point towards the substrate (**Figure 4.3.13**).

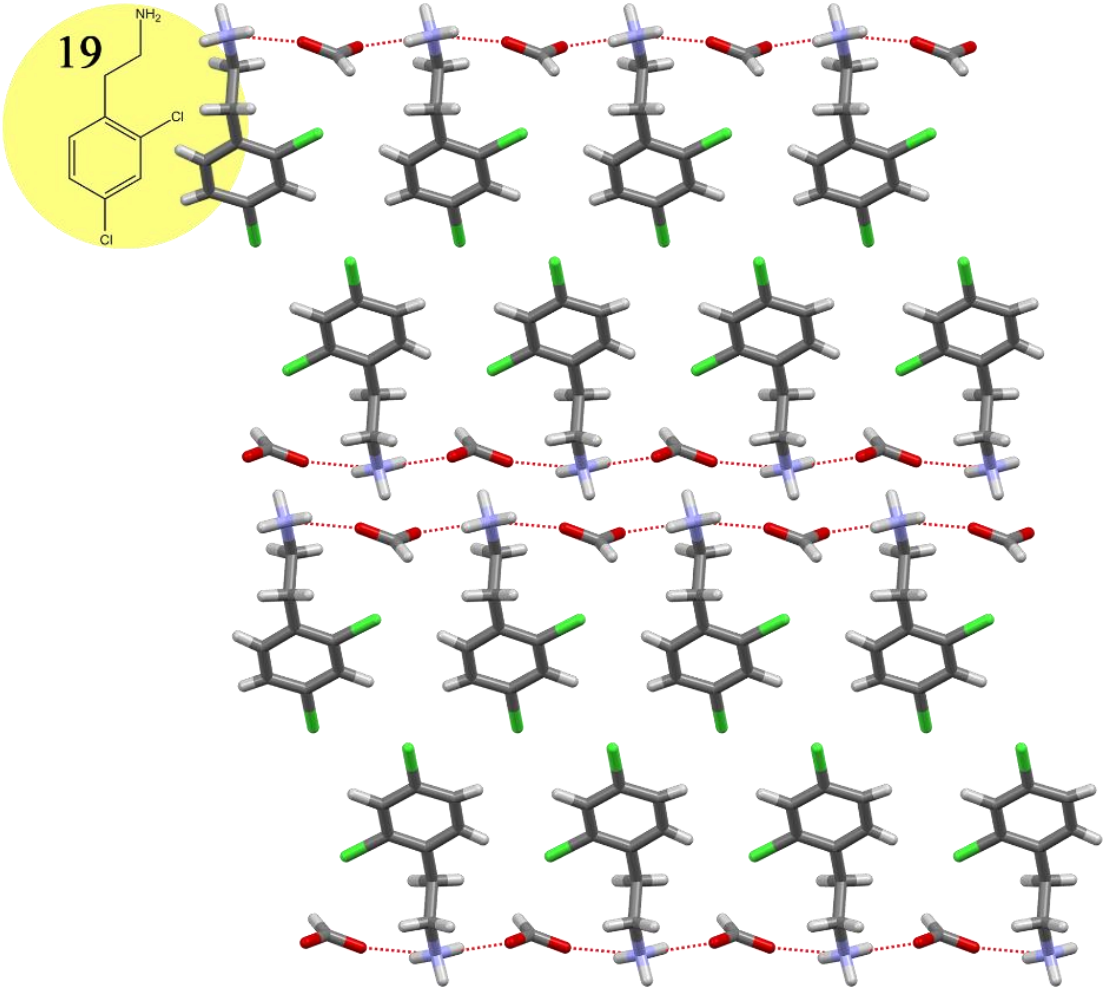

Figure 4.3.13 Layered structure of compound **19**. Viewed down the A-axis.

4.3.3 Structures of Secondary Ammonium Formates 20-21

Compound **20**, di-*N*-octylammonium formate, crystallizes in the centrosymmetric space group, P-1. The hydrophilic sheet is flat, and the octane chains orient above and below the sheet and interdigitate similar to a monolayer. The atoms pertaining to the formate ions in this structure resolve with 50% occupancy indicating that they are flipping between ammonium cations in the sheet. The pillars and sheets organize in an AB-type pattern viewed down the A-axis (**Figure 4.3.14**)

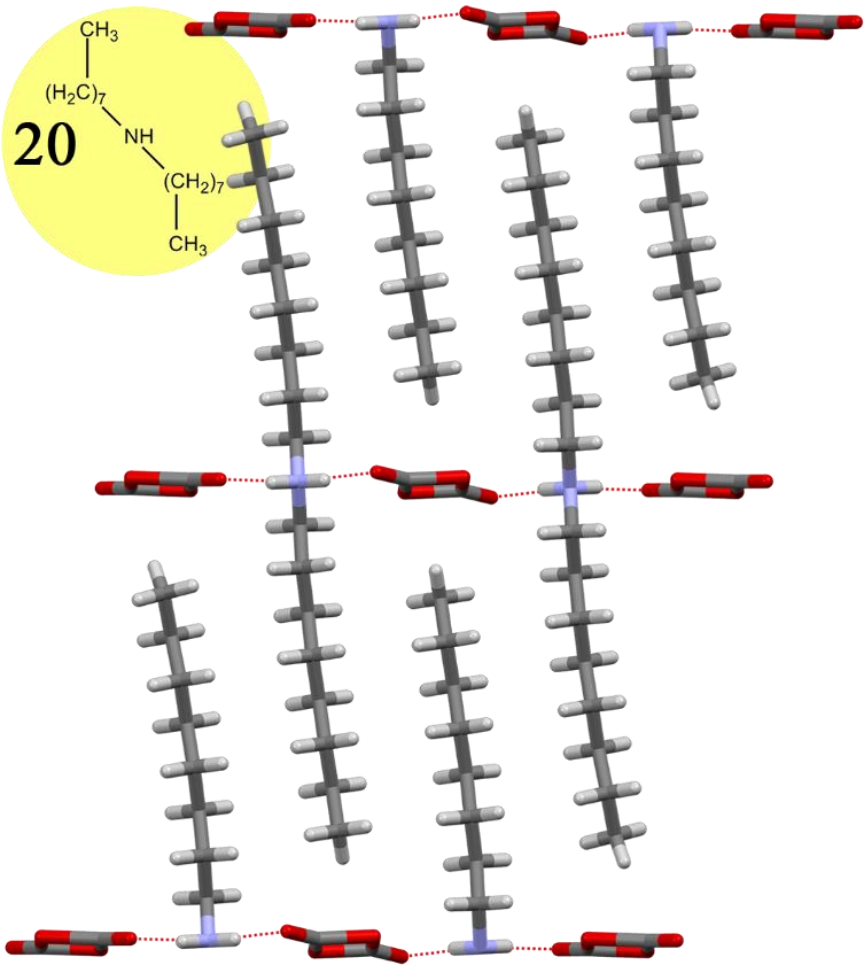

Figure 4.3.14 Layering of compound **20**. Viewed down the A-axis.

Compound **21**, dicyclohexylammonium formate, crystallizes in the centrosymmetric space group, C2/c. The hydrophilic sheet forms an irregular jagged slice that sits between the non-polar, organic component of the cation that orients above and below the ammonium moiety. The chair-conformation cyclohexane rings are quite crowded in the interlayer region and do not interdigitate. This material assembles into AB-type layer viewed down the C-axis. Interestingly this material does not form a traditional chain of hydrogen bonds; instead dimers form consisting of two pairs of formate and dicyclohexylammonium molecules, which then arrange into layers as directed by the polarity of the constituents (**Figure 4.3.15**).

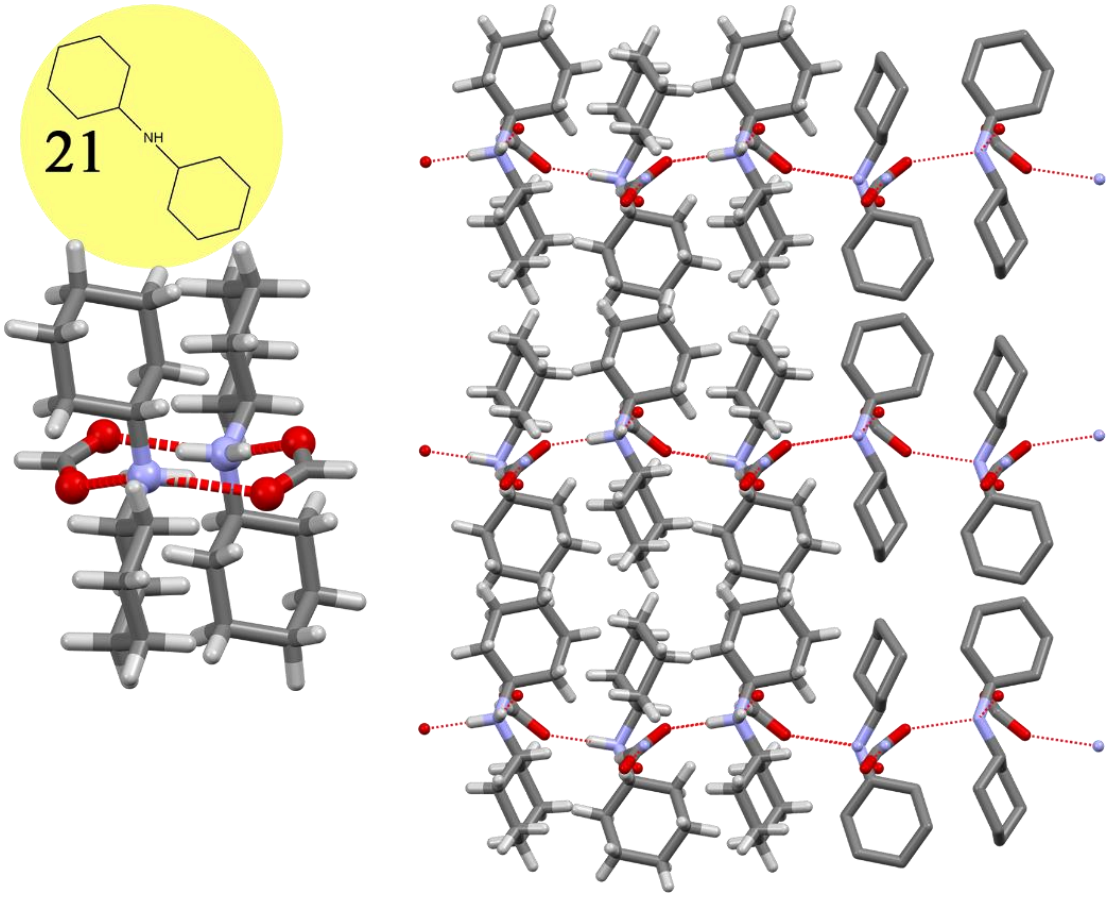

Figure 4.3.15 *Right*, layering of compound **21**, viewed down the C-axis. Hydrogens removed moving to the right for clarity. *Left*, dimer unit of layer.

4.3.4 Structures of Reacted Formic Acid/Amine Species 22-32

The combination of formic acid and a primary amine caused a reaction between the two molecules in the following compounds, **22-32**. The reactions between the starting materials have generated either a carbamate species, **22**, an aryl ketone, **27**, or various formamides, **23**-**26**, **28**-**32**. The following is a structural look at these compounds, a root/cause analysis concerning the reactions and the conditions which likely influenced these results, occurs in a later discussion **Section 4.4.5**.

4.3.4.1 Carbamate Species, 22

Compound **22**, 4-piperidinylmethylcarbamate, crystallizes in the centrosymmetric space group, P-1. Excitingly, here the formic acid reacted with the methyl amino moiety, generating a carbamate molecule. The carbamate hydrogen also bonds with interstitial water, forming the typical hydrophilic sheet. The remainder of the carbamate molecule bridges the gap between the sheets with the hydrocarbon component occupying the interlayer space. The nitrogen of the piperidine moiety faces downwards towards the lower sheet, forming a hydrogen bond, which is clearly illustrated down the B-axis. No interdigitation is possible in this structure, and the sheets slightly undulate. Viewing the structure down the A-axis reveals the familiar layering scheme in an AB pattern (**Figure 4.3.16**).

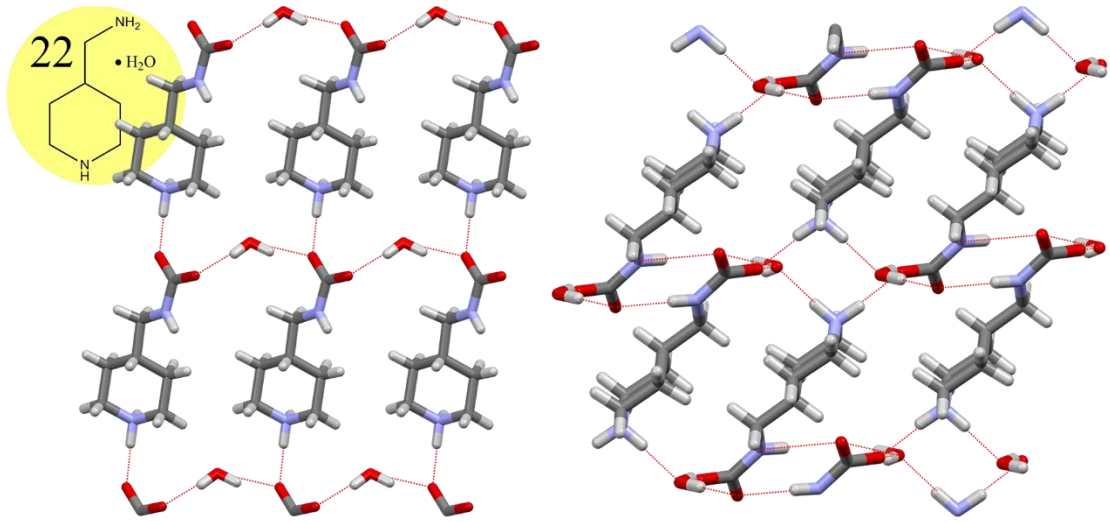

Figure 4.3.16 Compound **22** layering. *Left*, viewed down the B-axis. *Right*, viewed down the A-axis.

4.3.4.2 Formamide Species 23-26 and 28-32

Compound **23**, *N*-3,5-dimethylphenylformamide, crystallizes in the centrosymmetric space group, P-1, and features two molecules of the reacted material in the asymmetric unit. Rather than forming an ionic 2-D compound, these reagents have reacted, generating a formamide molecule. Based on the orientation of the amine hydrogen and carbonyl oxygen, the formamide molecules dimerize into discrete 0-D compliments which then organize into prototypical sheets and pillars. The flat hydrophilic sheet separates the non-interdigitating hydrocarbon portion of the molecule, resulting in an overall AB-type layering pattern viewed down the A-axis (**Figure 4.3.17**).

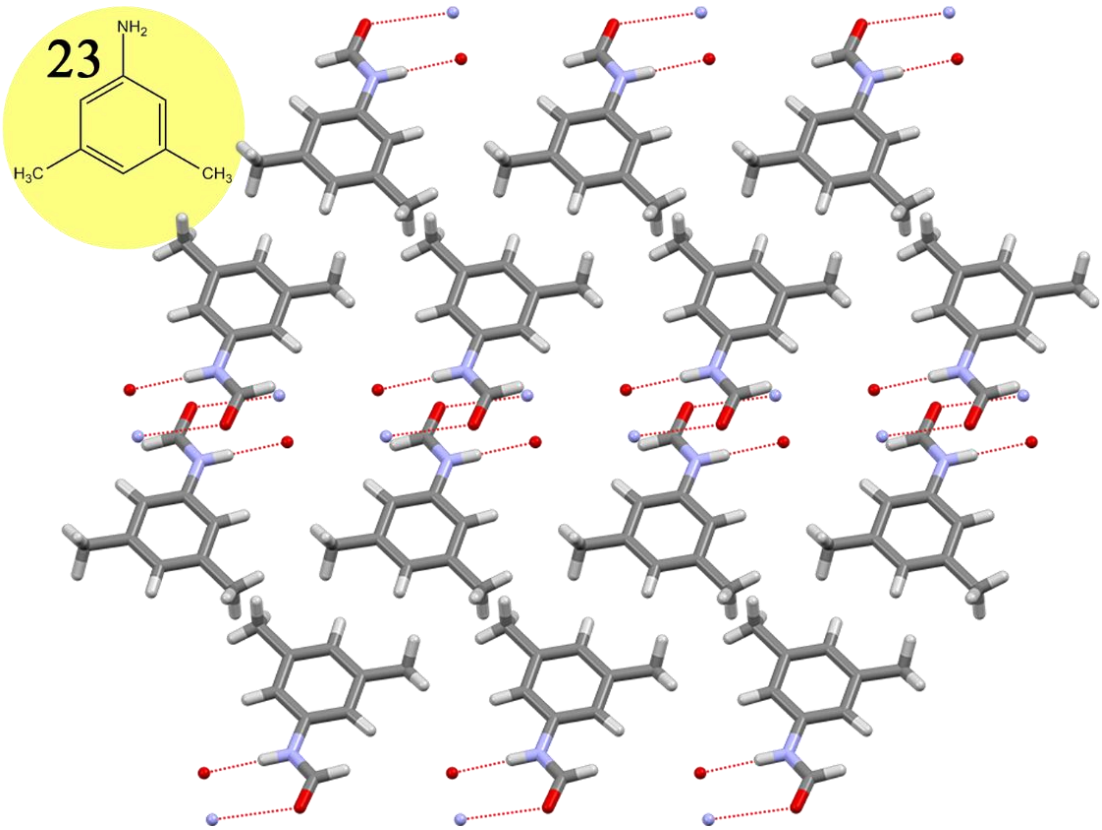

Figure 4.3.17 Compound **23** layers formed by dimers. Viewed down the A-axis.

Compound **24**, *N*-2,4,6-trimethylphenylformamide, crystallizes in the centrosymmetric space group, $P2_1/n$. The formic acid reacted with the aniline and generated a formamide molecule. The formamide molecules hydrogen bond in a chain and arrange as undulating sheets and interdigitating non-polar hydrocarbon regions in this *pseudo* AB-type network viewed down the C-axis. This is opposite of the behavior of **25** where the crosswise positions of the amine hydrogen and carbonyl oxygen leads to 1-D hydrogen-bonded chains. When the view is rotated, it is clear to see that the *ortho*-methyl substituent is directly blocking the hydrophilic substrate from forming a continuous 2-D sheet (**Figure 4.3.18**).

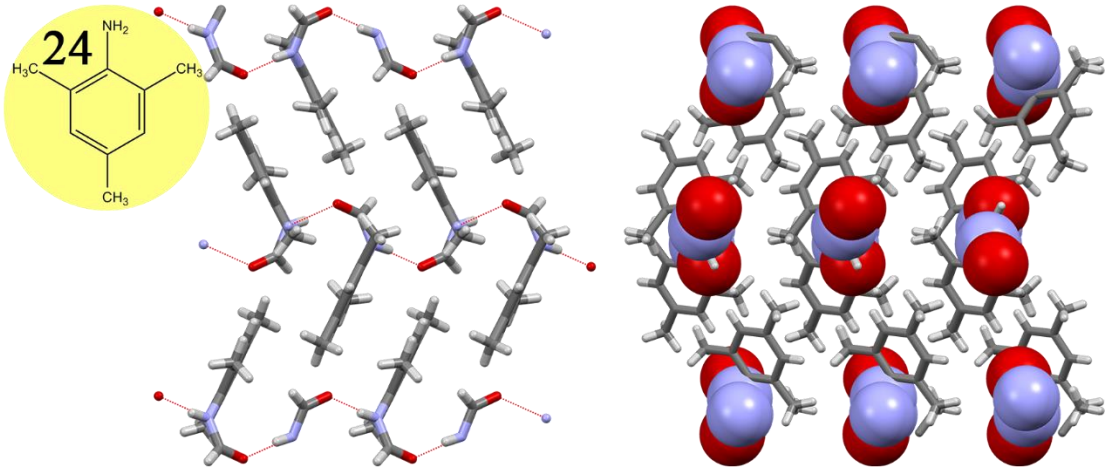

Figure 4.3.18 *Left*, layers of compound **24**, viewed down the C-axis. *Right*, view rotated 57° along the vertical axis, illustrating the disruption of the hydrophilic sheet.

Compound **25**, *N-ortho*-isopropylphenylformamide, crystallizes in the centrosymmetric space group, P-1, and features four molecules in the asymmetric unit. The formamides resulting from the reaction of formic acid with the aniline dimerize as 0-D units then arrange into typical sheets and pillars. This is opposite of the behavior for **24**; here the amine hydrogen and carbonyl oxygen of the formamide moiety are on the same side of the nitrogen-carbon(carbonyl) bond. This orientation results in the formation of discrete homomeric 0-D units. Generally, an AB-type pattern appears to have formed with flat sheets, and non-interdigitating pillars, viewed down the A-axis. However due to the sterics of the *ortho*-substituent on the formamide, as the structure is grown in three dimensions, the hydrophilic sheet's continuity is disrupted, resulting in 1-D channels of polar atoms (**Figure 4.3.19**).

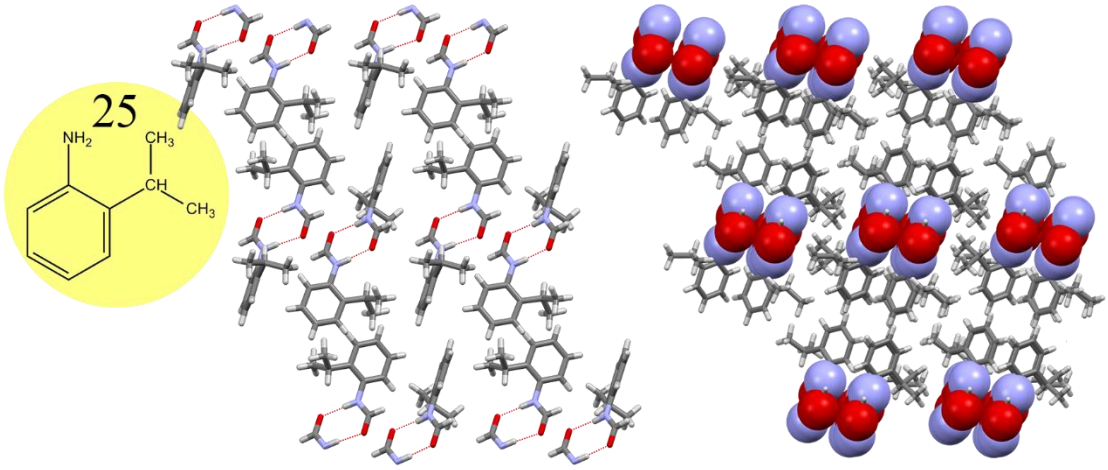

Figure 4.3.19 *Left*, 2-D layering arrangement of compound **25**, viewed down the A-axis. *Right*, layer grown in 3-dimensions, and rotated 60° along the vertical axis, illustrating 1-D channels of polar units.

Compound **26**, *N*-2,6-diisopropylphenylformamide, crystallizes in the centrosymmetric space group, $P2_1/c$. The components reacted, generating a formamide molecule, then assemble into a 1-D hydrogen-bonded network. The non-interdigitating hydrocarbon region rests between the flat hydrophilic sheet, resulting in an AB layered pattern down the A-axis. Rotating the structure 90° and viewing down the B-axis reveals that the hydrophilic sheet is perturbed by the interference of the di-*ortho*-isopropyl moieties. This disruption results in layers which appear like canon 2-D layers from a single perspective, i.e., down the A-axis, but with an obvious steric perturbation to the sheet when viewing from an alternate perspective (**Figure 4.3.20**).

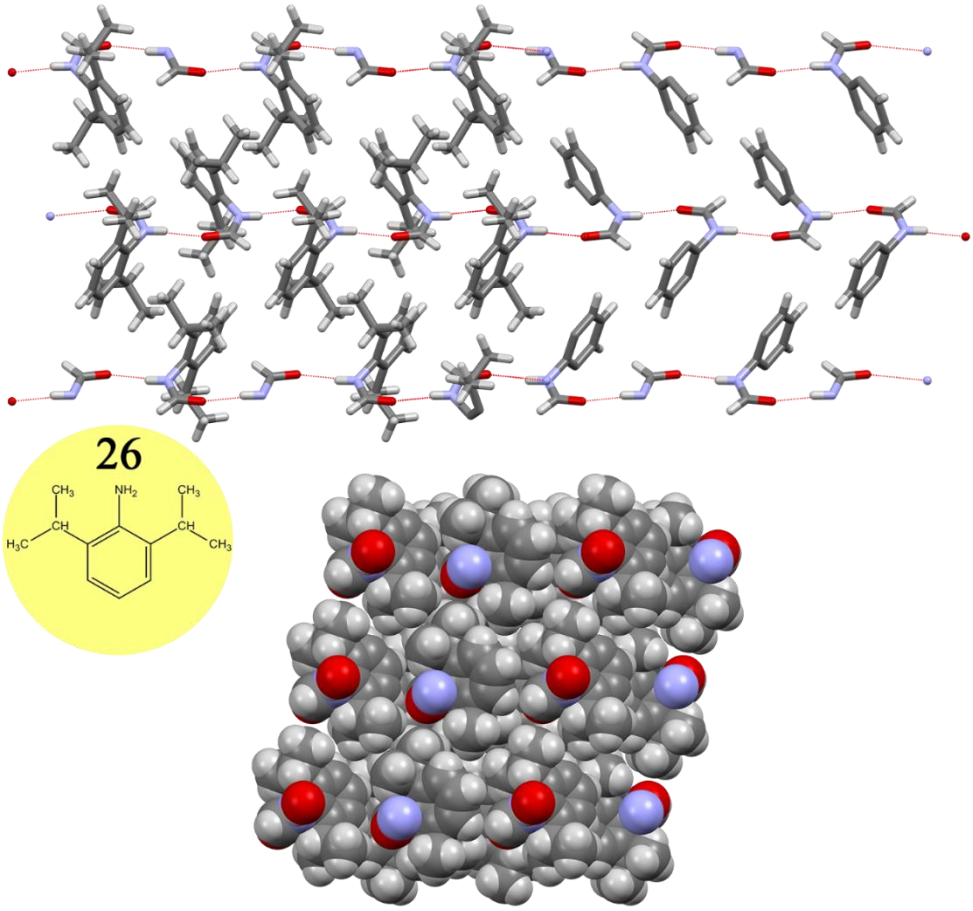

Figure 4.3.20 *Top*, layering pattern of compound **26** down the A-axis, hydrogens and isopropyl substituents removed going from right to left for clarity. *Bottom*, rotated 90°, viewing down the B-axis, showing dispensation of the sheet by the non-polar component.

Compound **28**, *N-meta*-chlorophenylformamide, crystallizes in the centrosymmetric space group, $P2_1/c$. The reacted formamide molecules dimerize as 0-D compliments then arrange into an AB-type layer featuring flat sheets and non-interdigitating pillars viewed down the C-axis. The chlorine atoms point towards a narrow band existing between the non-polar section of the layer (**Figure 4.3.21**).

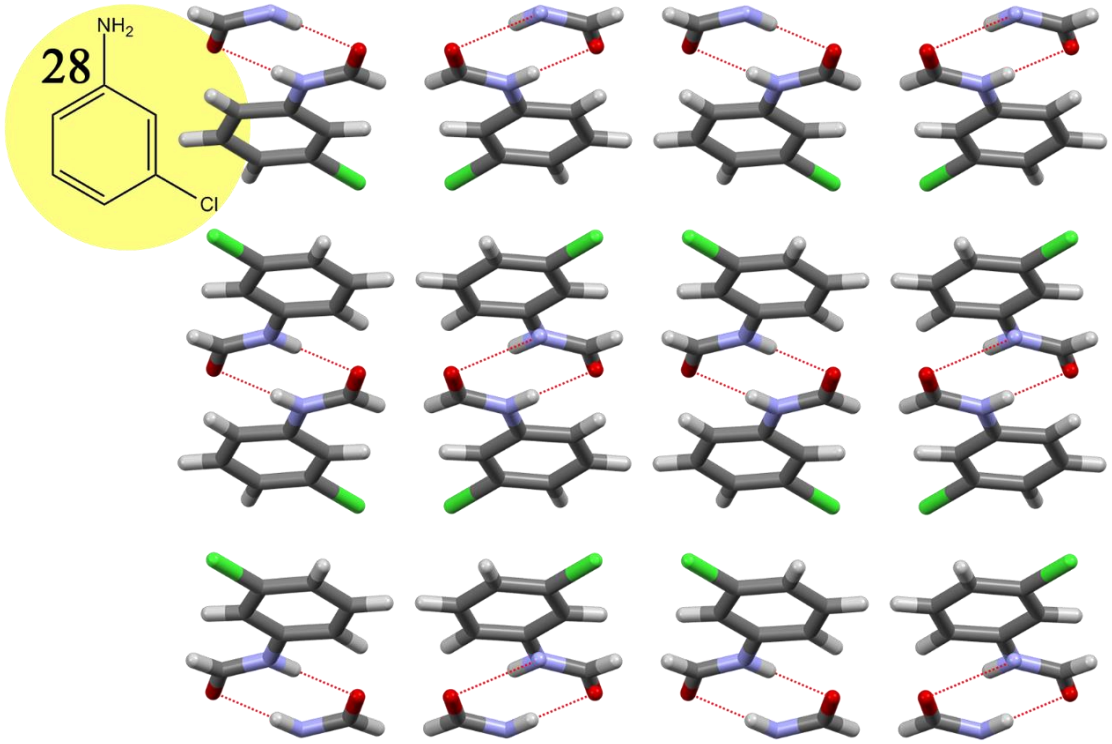

Figure 4.3.21 Layering pattern of compound **28**. Viewed down the C-axis.

Compound **29**, *N-para*-iodophenylformamide, crystallizes in the non-centrosymmetric space group, $P2_12_12_1$. The centrosymmetry is broken by the arched formation of the ring moieties in the packed structure. The crystallization conditions in this case resulted in formic acid reacting with the aniline, generating a formamide molecule. The resultant formamides hydrogen bond with an adjacent neighbor forming flat, non-interdigitating, 2-dimensional hydrogen-bonded sheets. A single slice of this network appears to follow the familiar stacking scheme, with an AB pattern; but when viewed down the A-axis, the staggered nature of the material breaks any standard sheet-pillar-sheet motif, as previously encountered (**Figure 4.3.22**).

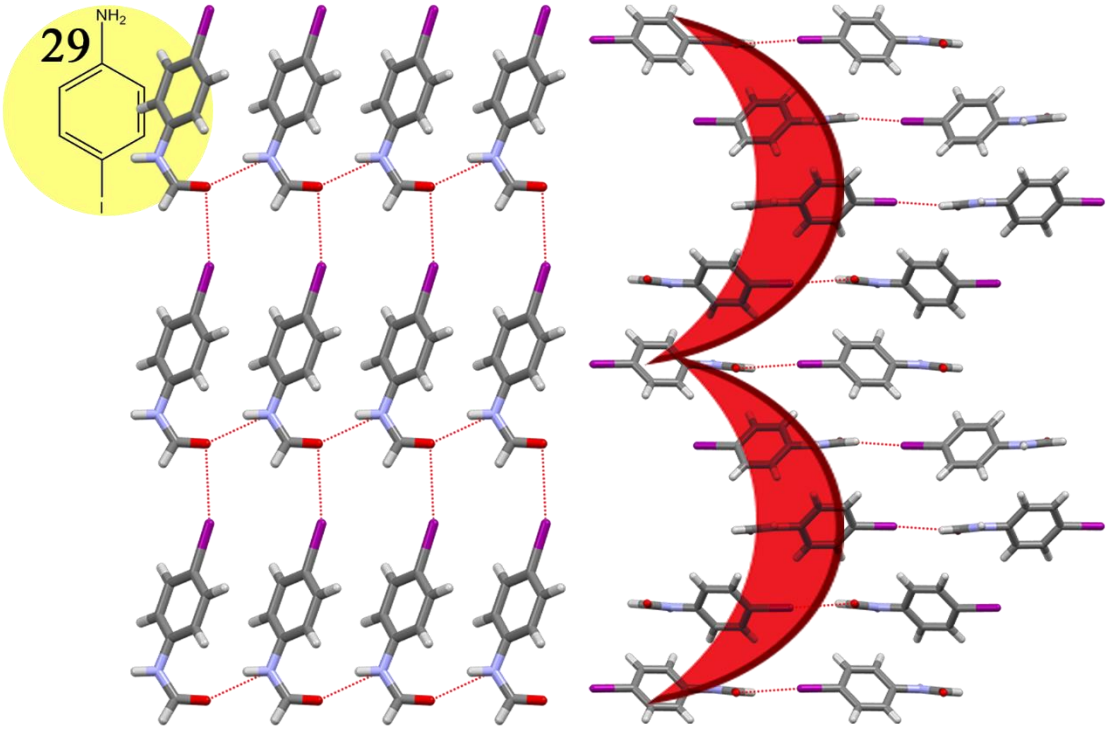

Figure 4.3.22 *Left*, compound **29** layering pattern, viewed down the C-axis. *Right*, red crescents represent directionality of symmetry breaking elements, viewed down the A-axis.

Compound **30**, *N-ortho*-methoxyphenylformamide, crystallizes in the centrosymmetric space group, C2/c. Here, a reaction has occurred between the reagents involved, generating a formamide molecule. The formamides hydrogen bond in a 1-D zig-zag network, resulting in a type of AB-type pattern with a waving hydrophilic substrate and an interdigitating pillar section viewed down the A-axis. However, these deceivingly ordered slices of 2-D networks stagger as the material packs into the 3rd dimension, breaking up the traditional sheet-pillar-sheet composition (**Figure 4.3.23**).

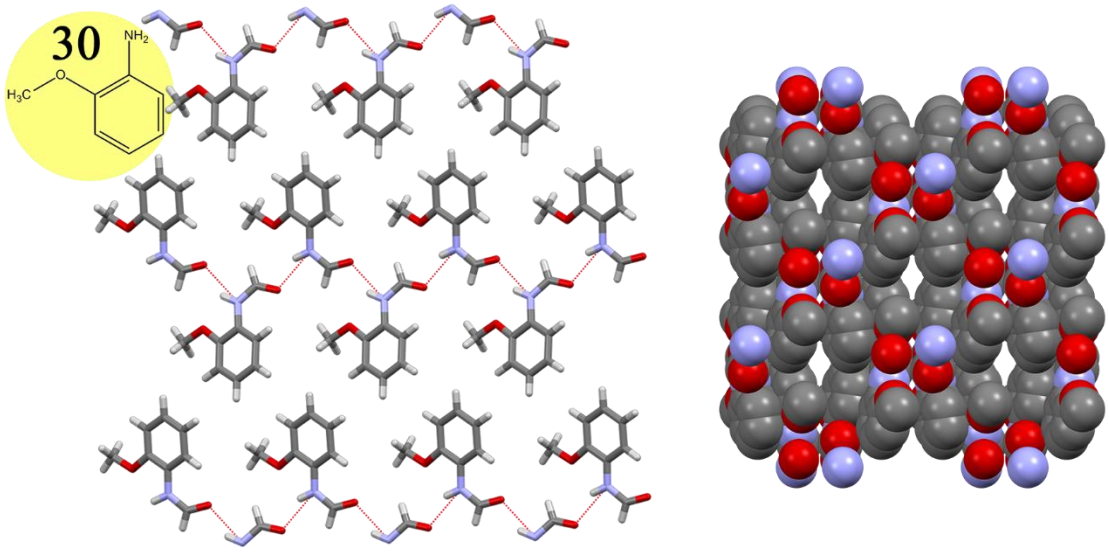

Figure 4.3.23 *Left*, layer pattern for compound **30** viewed down the A-axis. *Right*, space filling view down the C-axis showing the disruption of the polar sheet.

Compound **31**, *N-ortho*-ethoxyphenylformamide, crystallizes in the centrosymmetric space group, $P2_1/n$, and features two molecules in the asymmetric unit. Like **30**, the components of this mixture react to generate formamide molecules which hydrogen bond in a 1-D zig-zag chain, ultimately assembling into a type of AB layer type. The hydrophilic sheets undulate and the interdigitated pillar section is twisted such that the oxygen atom of the ethoxy substituent rests in close proximity to the hydrophilic sheet (**Figure 4.3.24**). Like **30**, while the facial layer may appear to follow classic layer motifs, expanding the structure into the 3rd dimension, and rotating 90° along the vertical axis reveals that the continuity of the sheet is sterically disrupted by the molecule's *ortho*-substituent.

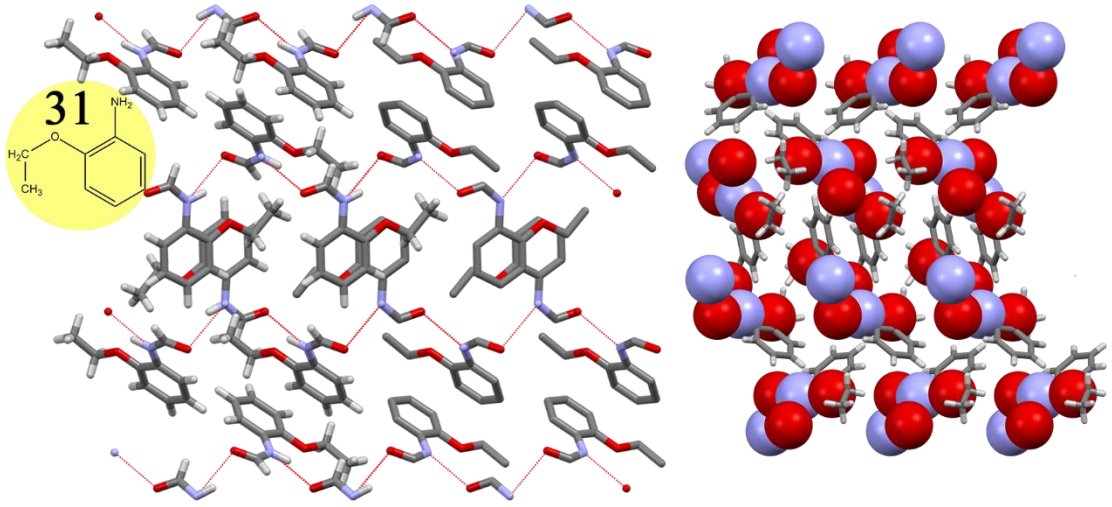

Figure 4.3.24 *Left*, layering assemblage of compound **31**, viewed down the B-axis. Hydrogens removed going from left to right for clarity. *Right*, the complex rotated 90° along the vertical axis, down the A-axis, revealing the dispensation of the hydrophilic sheet.

Compound **32**, *N*-(2-methyl-1-naphthalenyl)formamide, crystallizes in the centrosymmetric space group, $P2_1/n$. The components of this mixture reacted, generating a formamide molecule. In this compound, though the formamides coordinate into a chained 1-D hydrogen-bonded network, no prototypical layers have assembled due to perturbations of the sheet by the naphthyl constituent. The polar moieties orient inward forming columns of hydrophilic component, with the non-polar component situating as a sleeve around the channel (**Figure 4.3.25**)

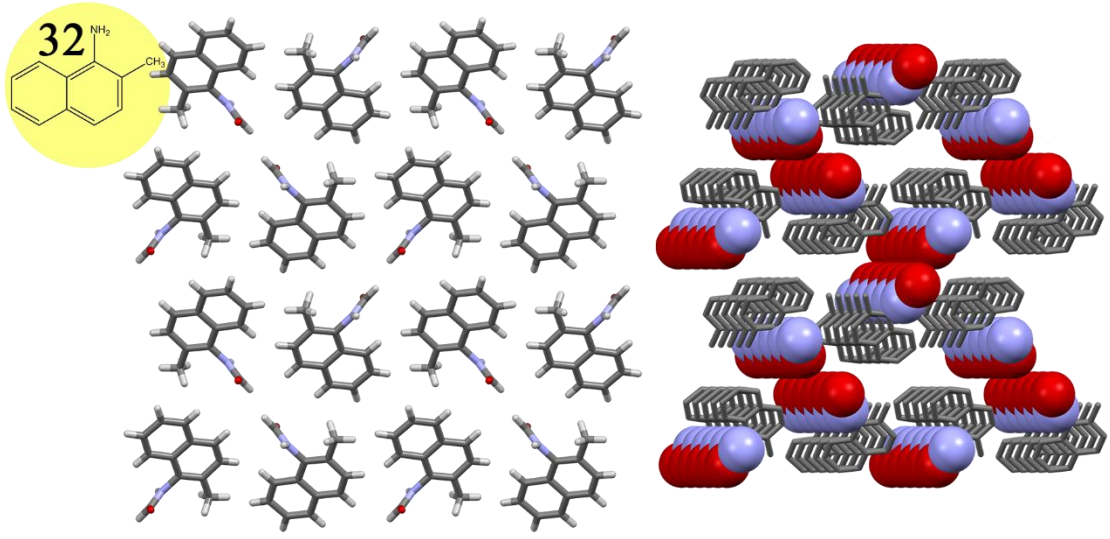

Figure 4.3.25 *Left*, packing arrangement of compound **32**, viewed down the A-axis. *Right*, perspective rotated 9° along the vertical axis, illustrating the channel-like arrangement of polar moieties (represented in space-fill style), hydrogens removed for clarity.

4.3.4.3 Ketone Species, 27

Compound **27**, 1-(4-aminophenyl)ethanone, crystallizes in the centrosymmetric space group, $P2_1/n$. The formic acid in this case reacts with the alkyne, generating a ketone. The ketone functionality hydrogen bonds with the amino group of an adjacent molecule forming a hydrogen-bonded chain. This network assembles *via* polar associations into an AB-type pattern with wavy hydrophilic sheets, and staggered, interdigitating pillars down the B-Axis. Rotating the structure 90°, viewing down the A-axis, reveals an interesting herring-bone arrangement of the hydrophobic component (**Figure 4.3.26**).

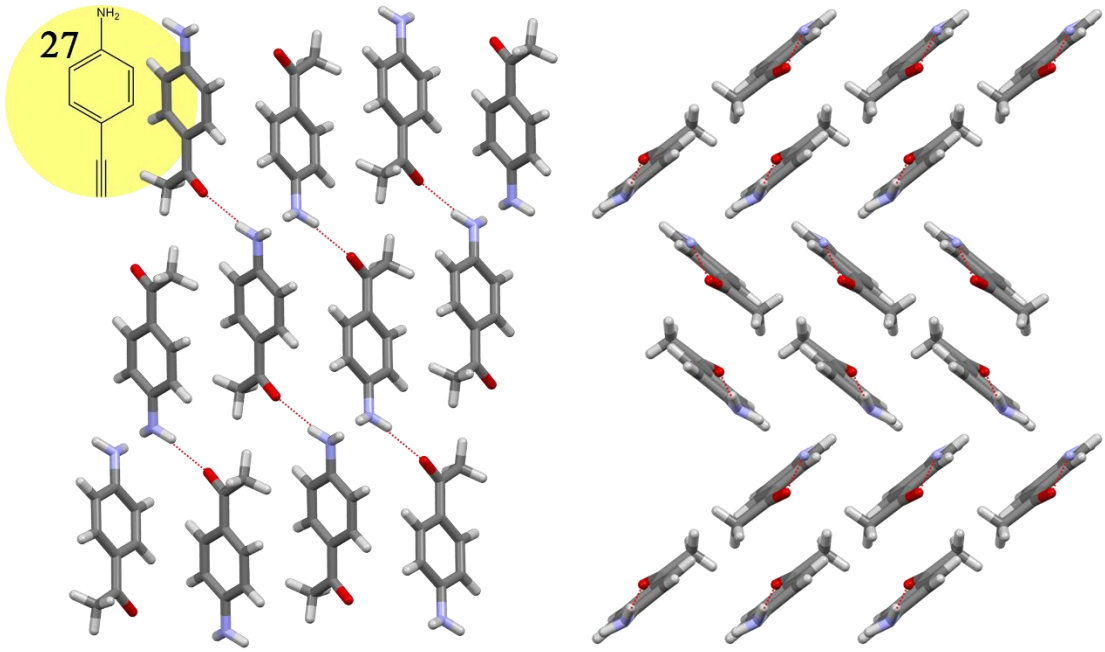

Figure 4.3.26 Compound **27** layers. Viewed down the B-axis, *left*, and A-axis, *right*.

4.4 Discussion

A diverse arrangement of organic 2-D hydrogen-bonded layers were generated in this study, exhibiting some interesting patterns and trends. Overall of this work can be discussed and evaluated based on the research objectives highlighted in Chapter 1. Ultimately, we strive to analyze these structures such that a relationship between amine and layer assembly may be made.

4.4.1 General Hydrogen-Bonded Assemblies of 1-31

It is evident from the results that two different classes of materials were obtained in this work: the *expected*, prototypical layered, 2-dimensional sheet-pillar compounds (**1**-**21**); and the *unexpected* reacted species (**22**-**32**), where the formic acid has reacted with either the amine functionality of an aniline (**23**-**26**, **28**-**32**), a functional group attached to the aryl ring of an aniline (**27**), or an isolated primary amine (**22**).

Compounds **22**-**31** reacted and assemble into *pseudo* layers, where a sheet and pillar component can be identified, but the overall ordering is not of the classic lamellar type of layer. The formamides, **23**-**26** and **28**-**31**, either form discrete 0-D homomeric compliments or 1-D hydrogen-bonded chains (as does **27**) depending on the stereochemistry of the formamide moiety. The 1-D chain in **27** is typical, due to oppositely positioned hydrogen bonding groups at either end of the molecule. These molecules organize into *pseudo* layered structures which arise from the association of neighboring polar and non-polar moieties. These complexes are visually similar to the prototypical layers facially, but violate the classic layer motif by interrupting the sheet in the 3rd dimension. **22**, with interstitial water, actually forms 2-D layers, but because this compound does not technically feature classic ‘pillars’ it cannot be evaluated in the same fashion as the other structures. The remaining compound, **32**, forms a hydrogen-bonded chain of molecules, but the nature of the organic portion disallows the formation of any type of layer.

These two classes of materials shall be handled separately. To begin, we start with the benzyl- and phenethylammonium formates **1-21** whose physical parameters are condensed in **Table 4.4.1.**

4.4.2 Layer Dynamics of Ammonium Formate Compounds 1-21

Compounds **1-21** generate typical ammonium formate complexes which participate in classic hydrogen donor/acceptor bonding pairs, where the primary amine functionality is protonated by the formic acid, followed by hydrogen bond stabilization of the formate. This interaction results in a 2-dimensional sheet, or substrate, that spans the material and the organic portion of the amine constituent sits orthogonally, above and below the substrate. The physical characteristics of the interlayer pillar constituent of the cation, i.e., its size, and shape, determines the overall layout of the material. The series of benzylamine and phenethylamines (and two diamines), covered in this work assemble in prototypical layers that also demonstrate a trend. A summation of their layer properties may be found here in **Table 4.4.1.**

#	Substituent	*l* (Å)	*w* (Å)	*s*	*i*	*μ*	Layer Code
1	H	6.045	4.083	1	✓	✓	AB
2	*ortho*-CH_3	5.770	5.284	1	✓	✓	AB
3	*meta*-CH_3	6.734	4.873	2	-	-	ABA
4	*para*-CH_3	7.002	4.071	2	-	-	ABA
5	*para*-CF_3	7.061	4.062	1	-	✓	AB
6	*para*-OCH_3	7.945	4.064	1	-	✓	AB
7	*para*-^{t}Bu	8.005	3.972	2	-	-	ABA
8	*meta*-Cl	6.045	4.739	2	-	-	ABA
9	*para*-Cl	6.800	4.084	2	-	-	ABA
10	3,5-F	6.110	4.686	1	✓	✓	AB
11	Naphthalene	7.496	5.341	2	-	✓	x-AB
12	*para*-NH_3	6.932	4.128	1	✓	✓	AB
13	H	7.415	4.068	1	✓	✓	AB
14	*ortho*-Cl	7.333	4.708	1	✓	✓	AB
15	*meta*-F	7.501	4.426	1	✓	✓	AB
16	*meta*-Cl	7.518	4.734	1	✓	✓	AB
17	*para*-Cl	8.237	4.126	1	✓	✓	AB
18	*para*-Br	8.292	4.052	1	✓	✓	AB
19	2,4-Cl	8.183	4.663	2	-	-	ABA
20	$2(CH_2)_7CH_3$	10.889	1.486	1	✓	-	AB
21	$2(C_6H_{11})$	2.941	9.75	1	-	✓	AB

Table 4.4.1 List of physical parameters for canonical layered ammonium formate materials **1**-**21**. **1**-**13** represent substituted benzylamines, **13**-**19**, substituted phenethylamines, and **20**-**21** are diamines. *l* = length of cation, *w* = width of cation (**Figure 1.9.4**), *s* = single (1) or bilayer (2), *i* = interdigitation of pillars, *μ* = undulation of the layer.

What we must accomplish now is compare how our predictions agree with this data, and then move to determine the important driving forces behind these ammonium formates, such that stronger predictions may be made in the future regarding these materials.

4.4.2.1 Predicting 2-D Outcomes of Ammonium Formates 1-21

The guidelines proposed by Odendal et al., when considering ammonium carboxylates and the steric bulk potential of the cation, held up quite well when predicting the layers of these ammonium formates. It is consistent that when the cation is not bulky, a single monolayer sheet

forms and an AB-type layer pattern emerges, and the opposite is true when the cation is bulky, a bilayer forms, and an ABA-type layer forms.

Additionally, for the benzylamines **1**-**12**, the interdigitation parameter is usually in agreement with the steric predictions concerning the appearance of either a *meta*- or *para*-substituent on the aryl group. As predicted in the introduction, bulky substituents at those two positions would likely interfere with the pillars slipping between each other and fully interdigitating.

There are certain exceptions to these guidelines, such as the *para*- (trifluoromethyl)-, and *para*-methoxybenzylamine materials (which are discussed in more detail below, **Section 4.4.3.4**), and the phenethylamine synthons, **13**-**19**. The two secondary amines **20** & **21** are special cases in which the two R groups are located on either side of the sheet, forcing the AB pattern.

However, for the phenethylamines, where one would expect the bulky *meta*- and *para*-halo substituted phenethylamines to resist interdigitation and proceed to form bilayers, resulting in ABA layers; they instead form interdigitated monolayers. Possibly, for these cations with a longer 'tether' compared to their benzylamine analogues, spatially, it may be more accessible for the phenethylamines to move and pack to use the available interlayer space. Similar behavior of pillar molecules with long chain alkyl groups resulting in monolayers over bilayers has been previously discussed.[85] Ward et al. found with their guanidinium sulfonates that their longer alky chained pillars found a preference for interdigitation. Pillars with alky lengths of methyl to propyl resulted in no interdigitation, and pillars with alky lengths of butyl and about often resulted in interdigitation in his report. To test this behavior, bulkier *para*-positioned substituents which could prevent this outcome, such as *tert*-butyl, should be investigated with the phenethylamines.

4.4.3 Driving Forces and Dynamics of Layer Shape

Based on the results above the question becomes, can a set of reliable rules or guidelines be generated in order to strengthen predictive methods for the assembly of future ammonium formates, or even other ammonium carboxylates? Specifically, can we go one step further and use what we have observed to predict whether or not undulation will occur? In order to approach this question, one must consider the observable trends from a diverse set of 2-D layered materials.

4.4.3.1 Layer Shape Trends

Based on the structural results in **Table 4.4.1**, it is clear that a single sheet is connected to the formation of AB layers and pillar interdigitation, whereas ABA-type layers are connected to the stacked, bilayer sheets, and pillars that infrequently interdigitate. Further, we see from **Table 4.4.1** that the combination of interdigitation (blue) and undulating sheet (blue) always results in an AB layered material, and the absence of interdigitation (red) and a flat sheet (red) always results in an ABA layered material. A mix of either interdigitation and flat sheet, or non-interdigitation and undulating sheet, always results in an AB-type layer, or an expanded AB-type layer. It would appear there is a strict reliance on both a small anion, and interdigitation, to encourage sheet undulation. Compounds **5**, **6**, and **11** seem to be outliers in this prediction, and their interlayer interactions will be discussed shortly.

We must now determine which conditions influence pillar interdigitation and sheet undulation; from there, more accurate predictions can be made as to how the ammonium formate materials will assemble. Like the chicken and egg conundrum; is it the interlayer pillar interactions which are influencing the sheet, or the other way around?

4.4.3.2 Anion's Role in Sheet Dynamics

In many reported benzylammonium carboxylate cases,[127-128] it seems apparent that the identity of the anion is unimportant when considering the interactions of the pillars; that the opposite is true, the dynamics of the layer are primarily governed by the pillar interactions.

In the binary modality of interdigitated or not interdigitated pillars, the identity of the anion has an impact on the possible shape of the substrate; small anions tend to allow flat or undulating sheets, and large anions tend to allow flat or buckled shapes. However, the interlayer pillar interactions pillars seem relatively unchanged by the sheet components.

Consider eight non-interdigitated examples of sterically demanding 3-, 4-, and 3,4-di, chloro-substituted benzylammonium layers[129] which feature a variety of anions, from ethanedioic acid to HPzDCA. In these examples the non-interdigitating chloro-substituents associate proximally, in the middle of the interlayer, and the arenes situate between the substrate and the chlorines. In each case, in the absence of interdigitation, regardless of the anion's identity, the sheet tends to form around the pillars accordingly. Introducing water, either directly into the substrate (Refcodes: TEWXOI, TEWWUN),[130] or adding a hydroxy group to the anion (Refcodes: NOYWOY to NOJWIS), only impacts the substrate thickness and the orientation of the anion within the substrate. In all 8 cases the identity of the oxo-anion has no effect on the interlayer pillar interactions. It would seem the influence is in the opposite direction.

4.4.3.3 Pillar's Role in Sheet Dynamics

Generally, we see that an undulating sheet is coupled with the AB-type layer. In the AB-type monolayers, the single hydrophilic sheet is a very thin and is occupied by the cation component of a pillar positioned above and below the substrate, enhancing the physical impact of the interlayer pillar interactions on the hydrophilic substrate. This is likely why a connection between AB-type layers, pillar interdigitation, and undulating sheets exists.

In ABA bilayers, the sheet is only occupied by the cation component of a pillar molecule in one direction. Additionally, there is stacked inter-sheet stabilization occurring between the two facing stacked sheets by charge-assisted hydrogen bonds which increases the rigidity of the hydrophilic sheet. In stacked sheet, ABA-type layers, the sheet rigidity is increased and undulation is less likely.

Often, an undulating substrate seems to be the direct result the pillar moieties interacting; as the components of the pillar move and orient or interact, the physical condition of the sheet seems to be at the mercy of the pillar's movements. Take for example compounds **3**-**4**, **7**-**9** and **19**; there is no interdigitation and *minimal* interaction between the pillars, whose interlayer conformation is uncrowded and completely unhindered as the pillars extend across the substrate gap. As a result, there is minimal interaction or attraction between the pillar components and the hydrophilic sheet is quite unaffected, remaining flat. Many of the pillar dynamics we encounter are a result of the interlayer interactions.

4.4.3.4 Interlayer Interaction and Sheet Dynamics

Of the 14 examples of undulating substrates (**1**-**2**, **5**-**6**, **10**-**18**, **21**), ten instances of that particular shape (**1**-**2**, **10**, **13**-**18**) appear to be the direct result of the pillars interdigitating. As the pillars shift and reorient to reduce electrostatic sheet repulsion and to maximize their interlayer polar interactions, the sheet is essentially being pushed and pulled along with the pillar (**Figure 4.4.1**). Interestingly, **20** features distinctive interdigitation that does not result in an undulating sheet. This is likely due to the unique secondary amine pillared component not requiring any additional translocation within the pillar region, thus not pulling the sheet from a linear conformation.

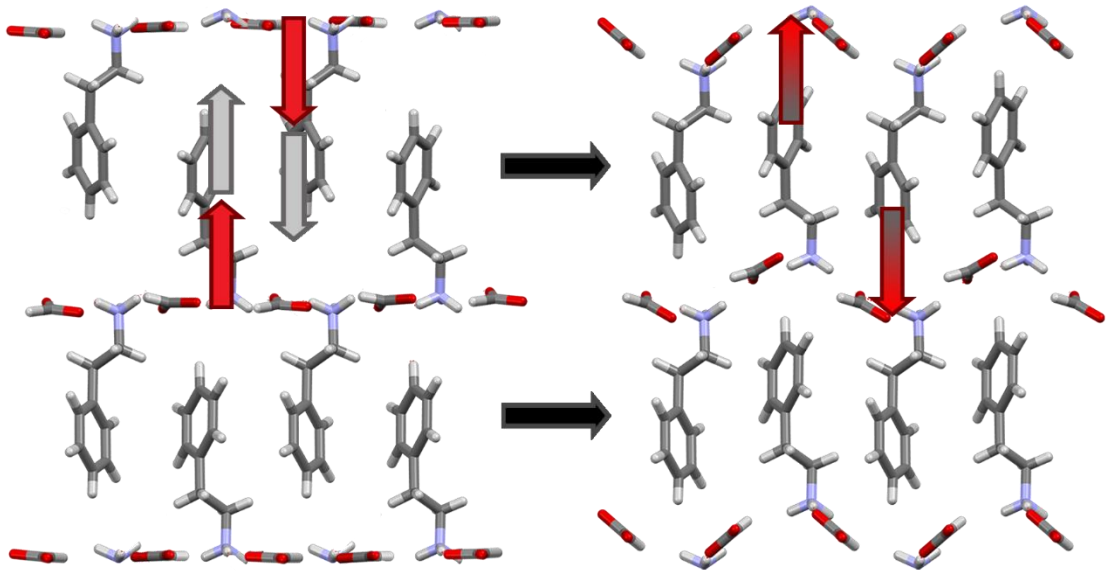

Figure 4.4.1 Illustrating how the translocation of the pillar moieties will impact the hydrophilic substrate in **13**. *Left*, grey arrows representing the direction of pillar translocation to optimize hydrophobic interactions; red arrows represent the resultant pulled sheet. *Right*, grey-red gradient arrows represent the possible repulsion cause by non-polar pillar. Hydrogen bonds removed for clarity.

As shown above in **Figure 4.4.1**, an undulating sheet is generally the result of the pillar moieties translocating to interdigitate, pushing and pulling the sheet along with the shifting pillar component; however, compounds **5** and **6** present a unique circumstance where the attraction of polar moieties within the pillar is likely the cause of the undulating sheet. In **5**, the organic component is pinched together, in effect resulting in an undulating sheet. The arene components cant and angle to face one another to maximize electrostatic interactions, and the fluorine moieties are oriented towards each other to maximize polar associations. These preferential interlayer interactions are pulling the sheet out of a linear conformation as a result. In **6**, the sheet is also pulled into an undulating shape due to the rings canting to optimize the electrostatic interactions within the interlayer; though this type of interaction is covered in greater detail in the next chapter. These two compounds give a clear exception to Odendal's guidelines, where in

these cases a single sheet was formed even though the cations are quite bulky. Clearly, the favorable spatial optimizations of the pillar constituents are causing the substrate to undulate in these compounds (**Figure 4.4.2)**.

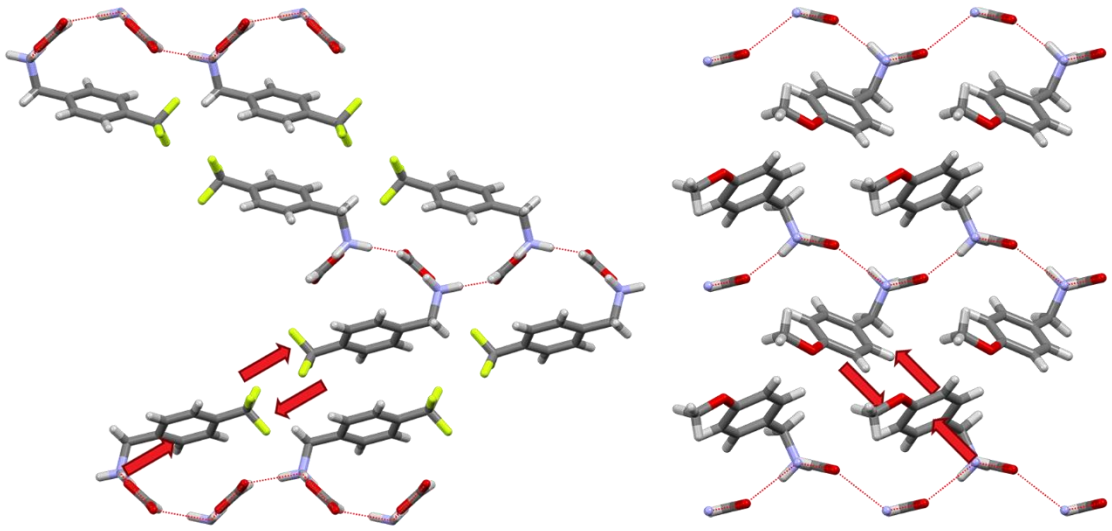

Figure 4.4.2 Illustrating how the orientation of the pillar, to promote polar or electrostatic interactions, may pull the sheet into an undulating wave in **5**, *left*, and **6**, *right*.

4.4.3.5 Pillar-Sheet Electrostatic Repulsion

Where **5** and **6** appear to cause undulation in the sheet due to interlayer pillar interactions, the undulation in **11** appears to be caused by electrostatic pillar-sheet repulsion. When considering the space-filling model of **11**, the undulating hydrophilic sheet in compound **11** is likely due to the sheer bulk of the non-polar naphthyl moieties being repelled by the polar hydrophilic sheet (**Figure 4.4.4**).

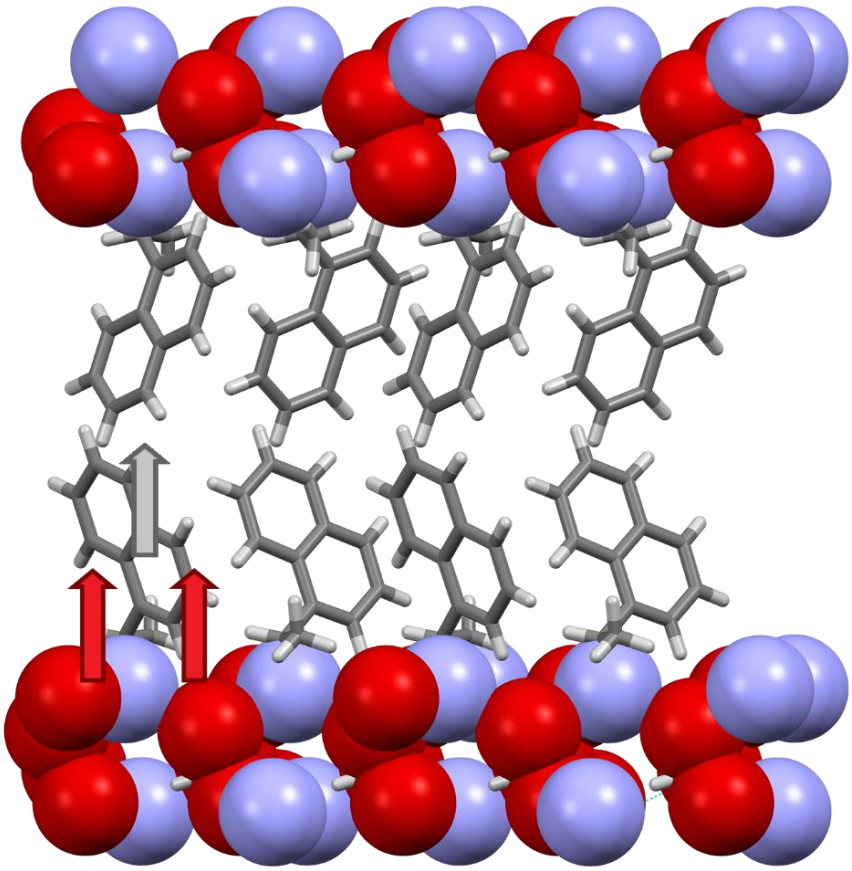

Figure 4.4.3 Electrostatic repulsion in **11**, illustrating the probable cause of undulating layer. Red arrows indicate static repulsion of the non-polar moieties, and the grey arrow represents the resultant translocation of non-polar component. Interdigitation impossible due to pillar bulk.

Incidentally, the ability of this undulating action is allowed through the size of the formate anion; as the cation displaces from the plane of the hydrophilic sheet, the formate anion simply needs to rotate to maintain its hydrogen-bonding partner (**Figure 4.3.8**). No significant reorganization is required by the small formate anion. As the size and rigidity of the anion increases (e.g., anions with aromatic rings), and its rotational flexibility within the substrate decreases, the appearance of undulating sheets disappears, though encountering significantly buckled sheets is still possible with rigid anions. The substrate dynamics (i.e., undulation, buckling, etc.), with respect to anion identity (i.e., size, flexibility, etc.), can be directly observed in analogous structures in the CSD (**Figure 4.1.7**).[131]

4.4.3.6 Predictive Methods For 2-D Ammonium Formate Architectures

It is evident from the above discussion that at least three important conditional variables exist when specifically predicting the assembly of ammonium *formates*:

1. If the pillar moieties interdigitate, the layer will be an undulating AB-type.
2. If the pillar components contain polar *para*-substituents, they will orient to associate in the interlayer space, causing sheet undulation and the layer will be of AB-type.
3. If neither of the above is true, the material will form ABA-type layers.

These guidelines allow us to make predictions on future layered ammonium formates. For example, considering an ethyl substituted benzylamine; based on the acquired data it is reasonable to suggest that the *ortho*-substitution would behave similar to the *ortho*-methyl and an interdigitated, undulated AB layer would be obtained; and the *meta*- and *para*-positions would introduce interlayer sterics and as a result, non-interdigitated flat ABA layers would form. These guidelines contribute to the ultimate goal of crystal engineering - structure prediction.

4.4.4 Layer Dynamics of Ammonium Formate Reacted Species 22-32

Remarkably, the reagents involved in compounds **22**-**32** reacted, resulting in the formation of either an *N*-formamide (**23**-**26**, **28**-**32**), a ketone (**27**), or a carbamate (**22**). Nevertheless, due to the presence of a hydrogen donor/acceptor site of the reacted compound, these compounds continue to hydrogen bond as 0-D or 1-D structures. The hydrogen-bonded constituents then consequently assemble into organized *pseudo*-layers, which masquerade as typical 2-D layers; usually *via* the association of polar and non-polar moieties in the solid-state.

Because the very nature of these reacted materials differs from the compounds previously discussed, they are handled separately, but may be discussed on loosely the same terms. The reacted compounds can be cordoned into two different sub groups, those that still *resemble* and maintain the classical lamellar, sheet-pillar, topography (**22**-**24**, **27**-**28)**, and those that also

resemble the classic lamellar layer shape from one perspective, but disrupt the uninterrupted flat sheet (**25-26**, **29-31**). Interestingly, the second group is populated by the compounds with sterically influencing *ortho*-substituents that extend and interfere with the sheet formation. Compound **32**, though forming hydrogen bonds, does not form layers in any manner due to the massive steric bulk of the hydrocarbon component of the molecule. A summation of the reacted layers can be found in **Table 4.4.2.**

Compound	Substituent	*i*	*μ*	Layer	Reaction	Formamides Only	
22	*para*-CH_3NH_2	-	✓	AB	Carbamate	**Dimer**	**Lamellar**
23	3,5-2(CH_3)	-	-	AB	Formamide	✓	✓
24	2,4,6-3(CH_3)	✓	✓	AB	Formamide	**X**	**X**
25	*ortho*-$CH(CH_3)_2$	-	-	AB	Formamide	✓	**X**
26	2,6-2$CH(CH_3)_2$	✓	-	AB	Formamide	✓	**X**
27	*para*-C_2H_2	✓	✓	AB	Ketone	-	-
28	*meta*-Cl	-	-	AB	Formamide	✓	✓
29	*para*-I	-	-	AB	Formamide	**X**	**X**
30	*ortho*-OCH_3	-	✓	AB	Formamide	**X**	**X**
31	*ortho*-OC_2H_5	-	✓	AB	Formamide	**X**	**X**
32	1-NH_2-2-CH_3	-	-	-	Formamide	**X**	**X**

Table 4.4.2 List of physical parameters for the 'reacted' ammonium formate lamellar materials **22-32**. **22** is a piperidine, **23-31** are anilines, **32** is a substituted naphthalene. *i* = interdigitation, *μ* = undulation.

Certainly, these are not classic ionic 2-D layered structures, but simple monomers that actively hydrogen bond together into layer-like assemblies. Their assembly does not follow any explicitly predictable pattern, such as the hydrogen-bonded benzyl- and phenethylammonium formates above. Nonetheless, some interesting physical behavior is encountered worth mentioning.

4.4.4.1 Chains or Dimers Based on Formamide Stereochemistry

Each reacted compound, except for **32**, assembles into a *pseudo* layer with the expected sheet-pillar-sheet motif at the facial level; even if the materials are not necessarily chained by hydrogen bonding there is the appearance of a hydrophilic sheet which is separated by a hydrophobic region, and so on. Compounds **22**, **24**, **26**-**27**, and **29**-**31** are infinitely chained by hydrogen bonds, and the remaining compounds, formamides **23**, **25**, and **28** form hydrogen-bonded dimers, that discretely cooperate as 0-D homomeric moieties, then proceed to assemble into lamellar-like materials due to their polar regions aligning and associating respectively.

The preference towards formation of dimers versus chained hydrogen-bonded chains in these compounds is dependent on the orientation of the formamide moiety **R**-NH_2-CO-H. Formamides that have the NH and O atoms on the same side proceed to form the 0-D dimers (**23**, **25**-**26**, **28**), and those that have the NH and O atoms on opposite sides proceed to form the 1-D infinite hydrogen-bonded chains (**24**, **29**-**31**) (**Figure 4.4.5**).

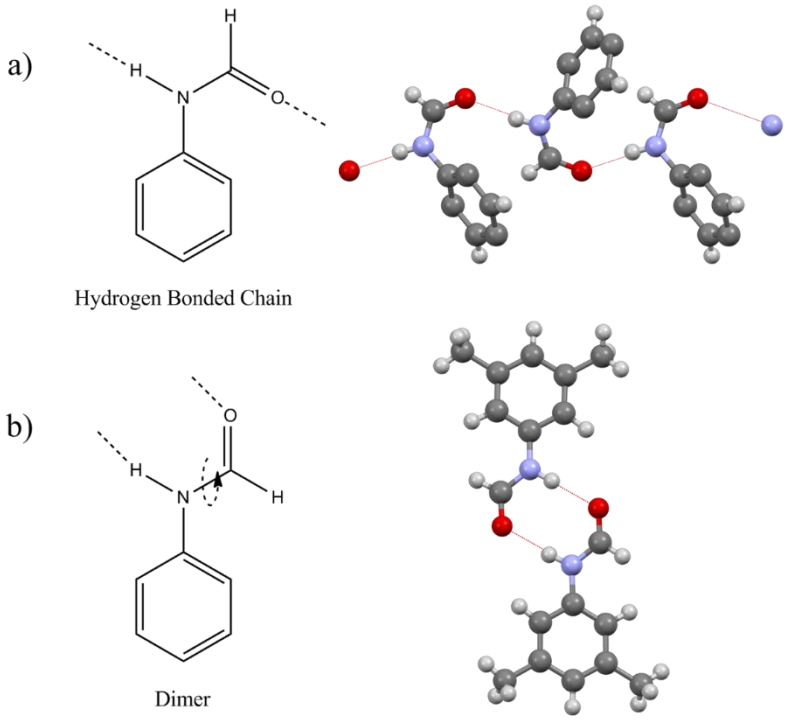

Figure 4.4.5 Rotational dependence on 0-D dimers versus 1-D chains. *Top*, **a**, the opposite positions of the formamide hydrogen and carbonyl results in hydrogen-bonded chains in **24**, substituents removed for clarity. *Bottom*, **b**, same side position of formamide hydrogen and carbonyl results in dimers in **23**.

4.4.4.2 Bulky *Ortho*-Substituents Impacting Layer

Excitingly, some of the of the *ortho*-substituted anilines have appeared to disrupt the formation and continuity of the hydrophilic sheet. Compounds **25**-**26** and **30**-**31** feature *ortho*-substituents that are of sufficient steric size that block or otherwise interfere with the hydrophilic sheet's potential to propagate infinitely. Shown in the above results, these compounds form what look appear like normal layers from one perspective, but when the view is rotated 90°, the 2-D sheet is revealed to be sterically interrupted and instead a 1-D chain has formed. This information is important to know in the event that an anilinium formate may be generated that may result in a deviation of the canon lamellar topology, i.e., may repeatedly impede the hydrophilic substrate so that it wraps upon itself as a micelle.

4.4.5 Organic Reactions of Compounds 22-32

While speculative, the following discussion aims to explain and determine the cause of the reactions that have occurred. Each assessment of the reacted compounds is limited to X-ray data and closely related published compounds, which does not reveal the mechanism. However, through close consideration of the reagents and the reaction conditions, educated mechanistic guesses can be made within reasonable doubt. Ideally, in the future, more instrumental methods, and mechanistic investigation will be conducted on these compounds as they do represent a series of unexpected, interesting, and potentially useful reactions in the field of organic chemistry, as well as hydrogen-bonded complexes for solid-state analysis.

4.4.5.1 Formylation of Primary Amines by Formic Acid, 23-26 and 28-32

The generation of an *N*-formamide molecule from a primary amine, formylation, by a carboxylic acid is a closely studied and documented reaction.[132-143] The general reaction mechanism involves the nucleophilic attack of amines on the carbonyl carbon of a carboxylic acid, in this case formic acid, which leads to the formation of an intermediate complex. Upon water loss from the intermediate, the formylated product is obtained (**Scheme 4.4.1**). Typically, these reactions call for refluxing the reagents in non-polar solvents, use of catalysts, or mechanical grinding, however, no additional influence or conditions were required for these reported compounds. Consequently, the origin of this particular reaction is elusive and curious.

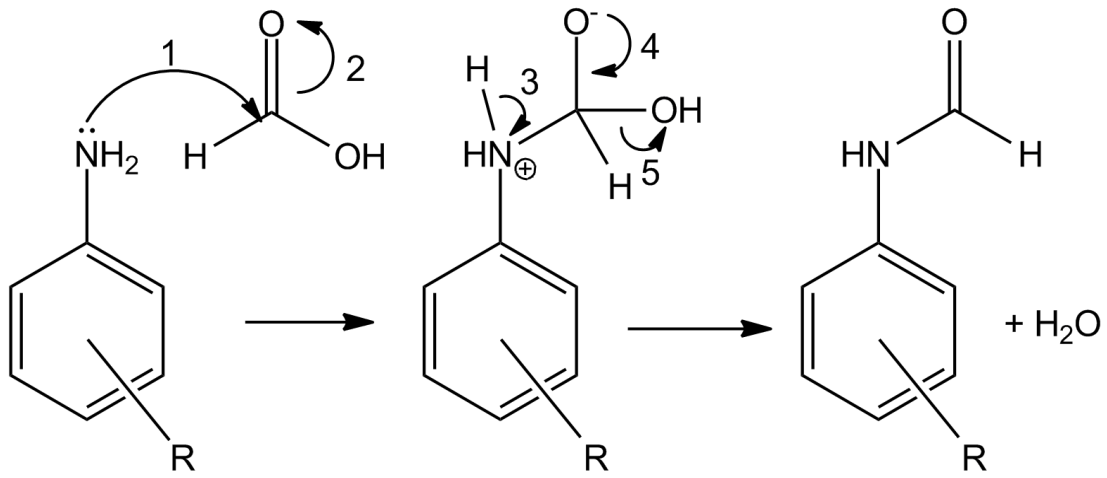

Scheme 4.4.1 Proposed mechanism for *N*-formamide generation *via* reaction of substituted benzylamine and formic acid.

The evidence for *N*-formamide generation in each case is strictly based off chemical intuition and X-ray data. Based upon computational models and experimental values from the literature and the CSD,[120-121, 144-149] an aryl *N*-formamide should demonstrate the following bond lengths: Aryl C-N, ~1.44 Å, N-C, ~1.34-1.37 Å, C=O, ~1.19-1.22 Å. The associated bond lengths of the reported compounds fall within these well documented values, supporting the assessment that an *N*-formamide has been generated. Additionally, when attempting to rearrange, or reassign atoms during the structure refinement process away from that of formamide classification; a notable increase of R1 value is observed, indicating poor atomic assignments. During structure refinement, the lowest R1 value was obtained by assuming the molecule present was a formamide and making the appropriate atomic assignments. Certainly, additional evidence could be obtained by use of NMR, IR, MS, and chromatographic techniques; however, based upon X-ray results, and related literature reports, the generation of a formamide in these compounds is likely.

4.4.5.2 Reaction of Alkyne and Formic Acid for Ketone Synthesis, 27

The formation of a ketone from the addition of formic acid to an alkyne is also a well-documented reaction.[150-153] Again, literature preparations call for elevated temperatures, and

sometimes catalyst addition; here, no additional reaction condition was required outside of simply introducing the constituents at room temperature, and allowing the solution to sit for some time. The mechanism of this type of reaction begins with the protonation of the most saturated *sp*-hybridized carbon of an alkyne *via* formic acid in a polar solvent, resulting in the formation of a carbocation. Subsequent electronic reorganization of the formate results in an oxyanion that binds the carbocation. Next, an additional molecule of formic acid forms a tetrahedral intermediate with the initial formic acid molecule, relocating charge onto the carbonyl oxygen of the first formic acid molecule. This reactive species binds a proximal hydrogen, which is in turn collected by the alkene. Finally, in a series of bond reorganization steps, a ketone is generated, and formic anhydride is released from the substrate (**Scheme 4.4.2a**). The subsequent thermal decomposition of formic anhydride results in the regeneration of a single formic acid molecule and liberation of CO gas *via* a series of bond breaking and bond making steps (**Scheme 4.4.2b**).

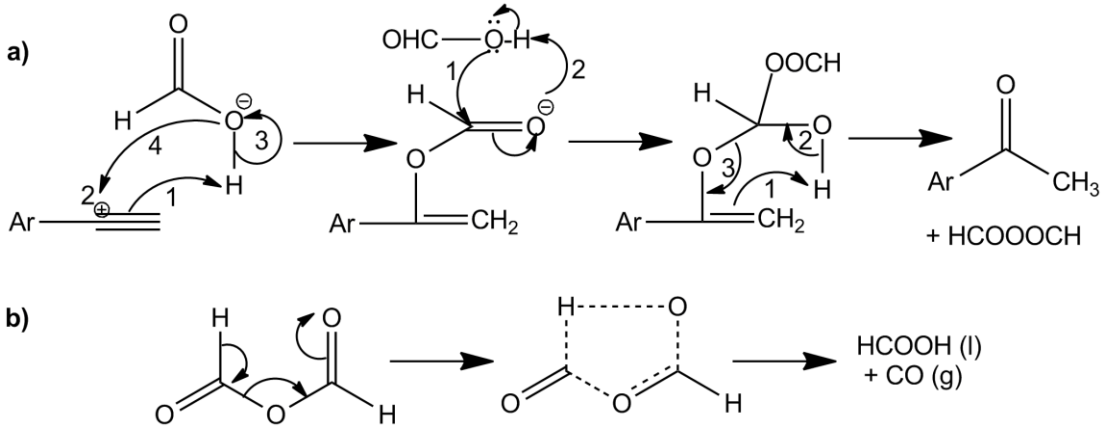

Scheme 4.4.2 *Top*, ***a*)** stepwise reaction of two molecules of formic acid hydrating an alkyne. *Bottom*, ***b*)** concerted thermal decomposition of formic anhydride to formic acid and carbon monoxide gas.

Similarly to the formation of *N*-formamides, evidence of ketone formation is based entirely on X-ray crystal structure data. Specifically, the measured bond lengths of the carbonyl carbon to oxygen, 1.23 Å, and for each flanking C-C bond, ~1.47-1.50 Å, agree nicely with

reported bond lengths for acetophenone and derivatives,[154-156] supporting the assessment. Additionally, the atomic assignments agree with the thermal probability in the structure solution, resulting in reliable thermal parameters; the reassignment of atoms during structure solution results in drastically sub-optimal R1 values. Future characterization of **27** by use of NMR, IR, MS, and chromatographic techniques would assist in verification of the putative compound as well as possible elucidation of reaction mechanism. Of all the amine compounds screened and investigated in this study, this was the only instance where an alkyne was present; certainly, applying the previously reported conditions to other alkyne containing amines would help strengthen this cursory assessment. Additionally, this reaction is unique from the previous *N*-formylations studied in that the alkyne was the target of formic acid, rather than the amine group. Subsequent experiments which increase the molar ratio of formic acid:amine to 1:1, as well as investigating non-polar solvents may help elucidate the mechanism at play.

4.4.5.3 Mysterious Carbamate Synthesis, 22

The generation of a carbamate compound is indeed a curious result, and one that does not appear to have a clearly defined origin. To achieve a better sense of the reaction, various routes to carbamate compounds have been identified previously: the reaction of alcohols with isocyanates (I),[157-159] carbonylation of amines and nitroaromatics (II),[160-168] carbon dioxide alkylation (III),[169-179] Hoffman rearrangement of amides (IV),[180-182] and Curtis rearrangement of acyl azides (V) (**Scheme 4.4.3**).[116, 183] Typically, these procedures involve the use of elevated temperatures, catalysts, or halogens; none of which were present in the reaction vessel for **22**. Some assumptions must be made in order to arrive at a likely reaction pathway.

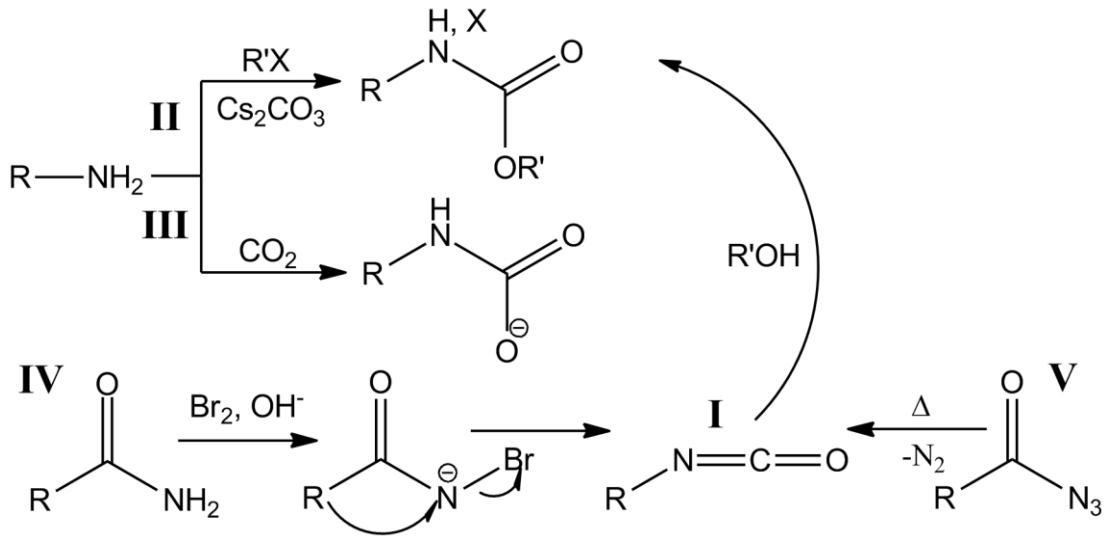

Scheme 4.4.3 Outlining the popular synthetic routes to carbamate molecules from various nitrogen containing species.

Given the components present in compound **22**: a primary amine, a nitrogen containing heterocycle, the potential presence of an *N*-formamide, formic acid, alcohol, the possibility of CO_2 diffusing into the solution, and the benefit of time as the mixture was allowed to rest until crystals formed; it is difficult to determine an absolute cause for this reaction. The simplest route to carbamate generation, when considering these reaction conditions, would be the diffusion of CO_2 into the solution. For compound **22**, 267 µmol of 4-(aminomethyl)piperidine was added to the vial; assuming that an equimolar amount of CO_2 is required to complete this reaction, 11.75 mg of CO_2 must diffuse into the solution. Based upon current atmospheric CO_2 conditions, ~407 ppm, ~15 L of ambient air would contain the requisite amount of CO_2 to react with the amine. When considering the diffusion coefficient of CO_2 into pure water,[184-187] and that reaction vessels are routinely loaded up to 1 mol CO_2,[188-190] it seems reasonable to assume that the requisite amount of CO_2 may have diffused into the crystallization solution over weeks to facilitate the putative reaction. The presence of water supports the possibility of air diffusing into the solution as well. Additionally, similar carbamate compounds have been prepared in a similar fashion.[73, 191]

Therefore, the reaction of amine with CO_2 to form a carbamate remains as the currently accepted model (**Scheme 4.4.4**). The long range protonation of the oxyanion by the adjacent ammonium in the final step is supported by observations in the Leukart Reaction.[192]

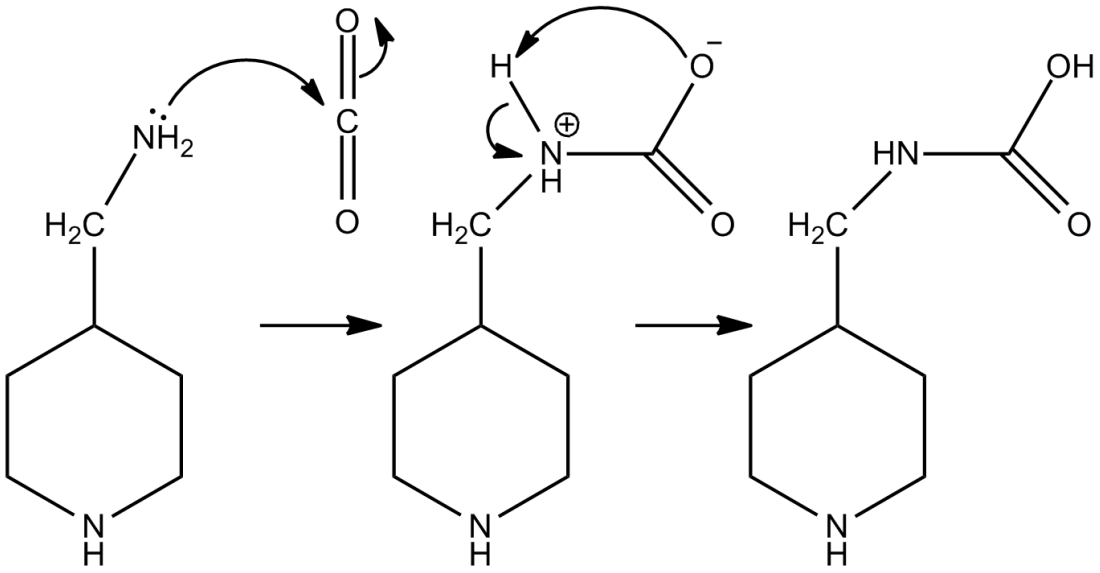

Scheme 4.4.4 The reaction of **22** with CO_2 to generate a carbamate molecule.

Verification of compound generation in this case was accomplished *via* comparison to crystal structures of closely related carbamate compounds.[73, 159, 191] Specifically, N-C (carbonyl) distance of 1.36 Å, and C=O distances of 1.26-1.27 Å are expected, which is in alignment with the crystal structure of **22**. Reassigning any of the carbamate based atoms results in a negative impact on the R1 value, suggesting that the carbamate assignment is accurate. Based on this bond length data and the agreement with the residual factor, the formation of a carbamate in this case is plausible. Instrumental methods such as NMR, IR, chromatographic methods, or MS coupled techniques would be critical for absolute determination of the alleged compound and mechanism. Future experiments could assist in rooting out the probable cause of the reaction. In this case, CO_2 derived carbamate generation seems time dependent, so closer monitoring of the crystallization, and prompt X-ray analysis when possible would reveal more information. Increasing the formic

acid: amine ratio to 1:1, as well as changing the solvent to a less polar solvent are also parameters worth investigating.

4.4.5.4 Driving Forces Behind Unexpected Reactions

What is highly interesting is determining which reaction conditions lead to one outcome or the other; the formation of a hydrogen-bonded network or the reaction of the two intended synthons. Briefly, we can clearly see that the benzyl- and phenethylamine reagents, **1**-**22**, readily form hydrogen-bonded networks, while the anilines and other heterocycles studied in this work proceeded to react with formic acid. Certainly, the conditions alone in which these reactions take place make for interesting discussion. There must be an obvious difference between the two classes of molecules that hints towards the driving force behind these reactions. Indeed, aniline, pKa 4.6, may be stabilized by resonance, and benzyl-, pKa 9.34, and phenethylamine, pKa 9.83, cannot be resonance stabilized (**Scheme 4.4.5**). This difference of pKa values has a direct influence on the interaction of the reagents.

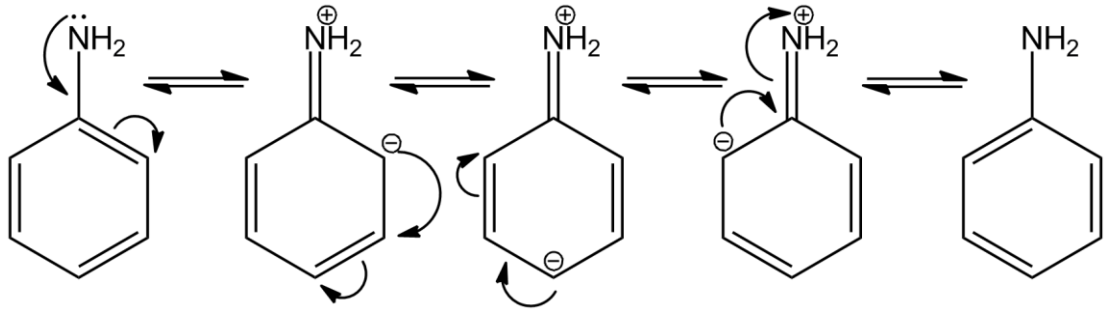

Scheme 4.4.5 Resonance stabilization of aniline.

Resonance stabilization results in a decrease in basicity,[193-197] i.e., a reduction in its pKa, bringing the value closer to that of formic acid, pKa 3.75. When considering the equilibrium constant of the reaction for formic acid and benzylamine, the difference in pKa estimates an equilibrium constant of ~$10^{5.6}$, 3.9x10^{5}, which is strongly in favor of the products side of the reaction; resulting in a typical acid-base interaction, the protonated benzylamine and formation of

a hydrogen-bonded network. When considering the reaction of formic acid and pyridine, the equilibrium constant in this case is an estimated ~$10^{0.85}$, 7.08; many orders of magnitude less than the benzylamine/formic acid equilibrium. This low equilibrium constant tells us that neither side of the equilibrium is strongly favored, and both species, protonated or not, are present in near equal amounts. In this case, the predictable acid-base reaction is less favorable, and instead the nucleophilic attack of the aniline's primary amine onto the carbonyl carbon of formic acid, the slower reaction compared to the acid-base reaction, is allowed. This delicate balance of equilibria and organic chemistry has been thoroughly discussed[198-203] and demonstrated on similar structures based on related physical guidelines.[204-205] However, this discussion begs the question of why we can find reports of the *N*-formylation of benzylamine with formic acid in the literature; which should just participate in acid-base chemistry with formic acid based upon these proposed pKa arguments. The secret here is in the reported reaction conditions: where initially the benzylammonium formate complex *is* generated, then the compound is refluxed in a non-polar solvent, usually toluene, which cannot support the charge separation, and the formylation reaction proceeds forward.[132, 134, 137-141] What we have accomplished here is satisfy the basal reaction requirements for formic acid and amine to proceed to a formamide while circumventing any special conditions; an exciting achievement considering how other groups have triumphantly reported the formylation of anilines under various special conditions.[132, 134-135, 141-143] The next step, with respect to the *N*-formylation of anilines, is to repeat the experimental conditions, closely documenting reaction time, and providing additional instrumental analysis, in order to supply a report to similar journals.

As for the preference between *N*-formamide generation versus carbamate generation; the tendency towards one or the other could simply be a matter of time; allowing enough time as atmospheric CO_2 diffuses into the solution. Alternatively, based on the high pKa of 4-(aminomethyl)piperidine (**22**), it is possible that the formylation reaction would not occur under

these reaction conditions, and would require the application of heat in a non-polar solvent as previously discussed with benzylamine. More experiments would need to be conducted to investigate the preference of formamide versus carbamate generation in solution; a host of additional anilines and amines would need to be screened and submit to X-ray analysis over various points of time to further investigate this preference.

4.5 Conclusion

Formic acid is an exciting reagent that is capable of many different types of chemistry; and our investigation of ammonium formate 2-D hydrogen-bonded networks has provided not only useful structural information, but also challenging questions.

Because so many structures were determined, we were able to establish a set of guidelines that assist in predicting the structure of benzylammonium and phenethylammonium formates, and potentially closely related structures; and the structural differences have also been compared with existing literature compounds.

However, more systematic data, featuring a wider selection of substituents of varying size and position, needs to be collected in order to make more specific predictions. For example, additional analysis of bulky-substituted benzylamines would assist in the prediction of pillar dynamics. As of this report, a *para*-*tert*-butyl substituted benzylamine represents the only substituent of considerable bulk of this series; and even so, the substituent is in a position where its effects were not surprising. Additional bulky substituents at different positions must be investigated.

A wider swath of phenthylammonium formates for analysis is also required. For this reported series, the only compound that demonstrated a departure from interdigitated pillars and undulating substrate was the di-chloro substituted phenethylamine which evidentially supplied enough repulsion within the interlayer to separate the components into an ABA layer. Further

probing into di-halo substituted rings seems to be a route worth investigating, and one that will likely enhance the reliability of a prediction method. Additionally, bulky alkyl substituted phenethylammonium formates are unrepresented in this work and should be studied.

The reaction between the aniline and formic acid reagents has impeded garnering reliable data regarding the nature of anilinium formate structures, but nonetheless some interesting results were obtained. Specifically, when considering the outcome of *ortho*-methyl (**24**) and *ortho*-isopropyl (**25**-**26**) substituted anilines, a disruption of the sheet-pillar arrangement was encountered. Had this disruption occurred in a typical hydrogen donor/acceptor scenario, with a flexible anion in the hydrophilic substrate, these materials may have generated unexpected layer types as theorized earlier (i.e., lamellar to micellar transition). Certainly, more examples of substituents that will impact the classic layering of these materials exits. If the reaction conditions can be controlled such that a hydrogen donor/acceptor pair is achieved between the reagents, rather than an organic addition-type reaction, the bulky *ortho*-substituted aniline may in fact be the basis of an interesting investigation towards the collapse of a canonical sheet-pillar-sheet layer.

If subtly increasing steric size from hydrogen to methyl *ortho*-substituents in aniline was sufficient to cause a disruption in the sheet-pillar arrangement, and moving up to isopropyl caused an even greater disruption, the same may be true with benzylamine moving up from *ortho*-methyl. Between **1**-**12**, the only *ortho*-alkyl substituent discussed was methyl. Expanding these results to ethyl and beyond must be accomplished to investigate these effects. Phenethylamines may also be worth further investigating, but based on the findings of this report, the length of alkyl tether, therefore the distance between the sheet and aryl ring, may be too great to impart any perturbation on the hydrophilic substrate. Optimally, what should follow immediately is further exploration of *ortho*-substituted benzylamines of increasing size to investigate those steric effects, alkyl-substituted phenethylamines, as well as discovering a set of conditions that promote classic

hydrogen bonding between substituted anilines and formic acid instead of supporting a reaction between the two (perhaps combining the reagents in slightly basic conditions).

What started as a side project ended up evolving into a varied set of ammonium formates and reacted species that have provided interesting data and unexpected results worthy of discussion and analysis. Future work is proposed which focuses on expanding upon this series of ammonium formates. Until then, we peer deeper into the subtle interactions between the pillars within the interlayer region.

4.6 References

1. Aloisio, S.; Hintze, P. E.; Vaida, V., The Hydration of Formic Acid. *J. Phys. Chem. A* **2002,** *106* (2), 363-370.
2. Tarkow, H.; Stamm, A. J., THE REACTION OF FORMIC ACID WITH CARBOHYDRATES. REACTION OF FORMIC ACID WITH SUGARS. *J. Phys. Chem.* **1952,** *56* (2), 262-266.
3. Wang, Z.; Lu, S.-M.; Li, J.; Wang, J.; Li, C., Unprecedentedly high formic acid dehydrogenation activity on an iridium complex with an N,N'-diimine ligand in water. *J. Phys. Chem.* **2015,** *21* (36), 12592-12595.
4. Döntgen, M.; Leonhard, K., Reactions of Chemically Activated Formic Acid Formed via HCO + OH. *J. Phys. Chem. A.* **2016,** *120* (11), 1819-1824.
5. Haas, P., Reactions of Formic Acid and its Salts. *Nature* **1951,** *167*, 325.
6. Gibson, H. W., THE CHEMISTRY OF FORMIC ACID AND ITS SIMPLE DERIVATIVES. *Chem. Rev.* **1969,** *69* (5), 673–692.
7. Tahir, M.; Shareef, A.; Bhutto, S.; Khan, N., Catalytic Reduction of Wood Kikar (Acacia Albida) by Acetosolv and Organosolv Pulping with Organic Acids. *Pak. J. Sci. Ind. Res. Ser. A Phys. Sci.* **2017,** *60* (3), 141-146.
8. Bannan, T. J.; Murray Booth, A.; Le Breton, M.; Bacak, A.; Muller, J. B. A.; Leather, K. E.; Khan, M. A. H.; Lee, D.; Dunmore, R. E.; Hopkins, J. R.; Fleming, Z. L.; Sheps, L.; Taatjes, C. A.; Shallcross, D. E.; Percival, C. J., Seasonality of Formic Acid (HCOOH) in London during the ClearfLo Campaign. *Journal of Geophysical Research: Atmospheres* **2017,** *122* (22), 12,488-12,498.
9. Wang, Q.; Guan, S.; Shen, D., Experimental and Kinetic Study on Lignin Depolymerization in Water/Formic Acid System. *Int. J. Mol. Sci.* **2017,** *18* (10).
10. Chu, L.; Yu, S.; Wang, J., Degradation of pyridine and quinoline in aqueous solution by gamma radiation. *Radiation Physics and Chemistry* **2018,** *144*, 322-328.
11. Lee, D. J.; Burrell, R. R.; Egolfopoulos, F. N., Propagation of sub-atmospheric methyl formate flames. *Combustion and Flame* **2018,** *189*, 24-32.
12. Lopez, P.; Pereboom-de Fauw, D.; Mulder, P. P. J.; Spanjer, M.; de Stoppelaar, J.; Mol, H. G. J.; de Nijs, M., Straightforward analytical method to determine opium alkaloids in poppy seeds and bakery products. *Food Chem* **2018,** *242*, 443-450.
13. Todhanakasem, T.; Yodsanga, S.; Sowatad, A.; Kanokratana, P.; Thanonkeo, P.; Champreda, V., Inhibition analysis of inhibitors derived from lignocellulose pretreatment on the metabolic activity of Zymomonas mobilis biofilm and planktonic cells and the proteomic responses. *Biotechnol. Bioeng.* **2018,** *115* (1), 70-81.
14. Wenchao, J., Enhanced reductive degradation of carbon tetrachloride by carbon dioxide radical anion-based sodium percarbonate/Fe(II)/formic acid system in aqueous solution. *Frontiers of environmental science & engineering* **2018,** *12* (2).
15. Dinnebier, R. E., X-ray Powder Diffraction in Conservation Science: Towards Routine Crystal Structure Determination of Corrosion Products on Heritage Art Objects. *Journal of visualized experiments* **2016,** *2016* (112).
16. Jelena, M., Determination of olopatadine in human tears by hydrophilic interaction liquid chromatography–MS/MS method. *Bioanalysis* **2017,** *9* (24), 1943-1954.
17. Prasad, P.; Donoghue, M., A comparative study of various decalcification techniques. *Indian J. Dent. Res.* **2013,** *24* (3), 302-308.
18. Laurenczy, G.; Dyson, P. J., Homogeneous Catalytic Dehydrogenation of Formic Acid: Progress Towards a Hydrogen-Based Economy. *Journal of the Brazilian Chemical Society.* **2014,** *25* (12), 2157-2163.
19. Czaun, M.; Kothandaraman, J.; Goeppert, A.; Yang, B.; Greenberg, S.; May, R. B.; Olah, G. A.; Prakash, G. K. S., Iridium-Catalyzed Continuous Hydrogen Generation from Formic Acid

and Its Subsequent Utilization in a Fuel Cell: Toward a Carbon Neutral Chemical Energy Storage. *ACS Catal.* **2016,** *6* (11), 7475-7484.
20. Jantke, D.; Pardatscher, L.; Drees, M.; Cokoja, M.; Herrmann, W. A.; Kuhn, F. E., Hydrogen Production and Storage on a Formic Acid/Bicarbonate Platform using Water-Soluble N-Heterocyclic Carbene Complexes of Late Transition Metals. *ChemSusChem.* **2016,** *9* (19), 2849-2854.
21. Mellmann, D.; Sponholz, P.; Junge, H.; Beller, M., Formic acid as a hydrogen storage material - development of homogeneous catalysts for selective hydrogen release. *Chem. Soc. Rev.* **2016,** *45* (14), 3954-3988.
22. Mori, K.; Masuda, S.; Tanaka, H.; Yoshizawa, K.; Che, M.; Yamashita, H., Phenylamine-functionalized mesoporous silica supported PdAg nanoparticles: a dual heterogeneous catalyst for formic acid/CO2-mediated chemical hydrogen delivery/storage. *Chem. Commun.* **2017,** *53* (34), 4677-4680.
23. Müller, K.; Brooks, K.; Autrey, T., Hydrogen Storage in Formic Acid: A Comparison of Process Options. *Energy Fuels* **2017,** *31* (11), 12603-12611.
24. Onishi, N.; Laurenczy, G.; Beller, M.; Himeda, Y., Recent progress for reversible homogeneous catalytic hydrogen storage in formic acid and in methanol. *Coor. Chem. Rev.* **2017,** *https://doi.org/10.1016/j.ccr.2017.11.021*.
25. Fink, C.; Montandon-Clerc, M.; Aurenczy, G., Hydrogen Storage in the Carbon Dioxide - Formic Acid Cycle. *Chimia* **2015,** *69* (12), 746-752.
26. Celaje, J. J. A.; Lu, Z.; Kedzi, E. A.; Terrile, N. J.; Lo, J. N.; Williams, T. J., "A prolific catalyst for dehydrogenation of neat formic acid". *Nature Communications* **2016,** *7* (11308).
27. Lyu, L.; Zeng, X.; Yun, J.; Wei, F.; Jin, F., No catalyst addition and highly efficient dissociation of H2O for the reduction of CO2 to formic acid with Mn. *Environ. Sci. Technol.* **2014,** *48* (10), 6003-6009.
28. Kortlever, R.; Peters, I.; Koper, S.; Koper, M. T. M., Electrochemical CO2 Reduction to Formic Acid at Low Overpotential and with High Faradaic Efficiency on Carbon-Supported Bimetallic Pd–Pt Nanoparticles. *ACS Catal.* **2015,** *5* (7), 3916-3923.
29. Simakov, D. S. A., *Renewable Synthetic Fuels and Chemicals from Carbon Dioxide: Fundamentals, Catalysis, Design Considerations and Technological Challenges*. Springer: 2017.
30. Benson, E. E.; Kubiak, C. P.; Sathrum, A. J.; Smieja, J. M., Electrocatalytic and homogeneous approaches to conversion of CO_2 to liquid fuels. *Chem. Soc. Rev.* **2009,** *38* (1), 89-99.
31. Finn, C.; Schnittger, S.; Yellowlees, L. J.; Love, J. B., Molecular approaches to the electrochemical reduction of carbon dioxide. *Chem. Commun.* **2012,** *48* (10), 1392-9.
32. Khadka, N.; Dean, D. R.; Smith, D.; Hoffman, B. M.; Raugei, S.; Seefeldt, L. C., CO_2 Reduction Catalyzed by Nitrogenase: Pathways to Formate, Carbon Monoxide, and Methane. *Inorg. Chem.* **2016,** *55* (17), 8321-30.
33. DuBois, D. L., *Encyclopedia of Electrochemistry* **2006,** *7a*, 202.
34. D'Alessandro, D. M.; Smit, B.; Long, J. R., Carbon dioxide capture: prospects for new materials. *Angew. Chem. Int. Ed.* **2010,** *49* (35), 6058-82.
35. Rochelle, G. T., Amine Scrubbing for CO_2 Capture. *Science* **2009,** *325* (5948), 1652-1654.
36. Seo, J.; Matsuda, R.; Sakamoto, H.; Bonneau, C.; Kitagawa, S., A Pillared-Layer Coordination Polymer with a Rotatable Pillar Acting as a Molecular Gate for Guest Molecules. *J. Am. Chem. Soc.* **2009,** *131*, 12792-12800.
37. Cipres, I.; Jenck, J.; Kalck, P., Carbon monoxide as a building block for organic synthesis. Part I. Highly regioselective alkoxycarbonylation of allylbenzene catalyzed by palladium complexes. *Journal of Molecular Catalysis* **1990,** *58* (3), 387-392.

38. Ciprés, I.; Kalck, P.; Park, D. C.; Serein-Spirau, F., Carbon monoxide as a building block for organic synthesis. Part III. Selective hydrocarbonylation of monoterpenes to give potentially biologically active aldehydes. *Journal of Molecular Catalysis* **1991,** *66* (3), 399-407.
39. Baig, T.; Molinier, J.; Kalck, P., Carbon monoxide as a building block in organic synthesis. IV. Direct preparation of amines from alkenes by aminomethylation catalysed by dinuclear rhodium complexes. *Journal of Organometallic Chemistry* **1993,** *455* (1-2), 219-224.
40. Chenal, T.; Cipres, I.; Jenck, J.; Kalck, P.; Peres, Y., Carbon monoxide as a building block in organic synthesis. Part II. One-step synthesis of esters by alkoxycarbonylation of naturally occurring allylbenzenes, propenylbenzenes and monoterpenes. *Journal of Molecular Catalysis* **1993,** *78* (3), 351-366.
41. Naigre, R.; Chenal, T.; Ciprés, I.; Kalck, P.; Daran, J. C.; Vaissermann, J., Carbon monoxide as a building block in organic synthesis. Part V. Involvement of palladium-hydride species in carbonylation reactions of monoterpenes. X-ray crystal structure of [Ph<inf>3</inf>PCH<inf>2</inf>CHCHPh]<inf>4</inf>[PdCl<inf>6</inf>][SnCl<inf>6</inf>] . *Journal of Organometallic Chemistry* **1994,** *480* (1-2), 91-102.
42. Theron, M. M.; Lues, J. F. R., *Organic Acids and Food Preservation*. CRC Press: 2010.
43. Griggs, J. P.; Jacob, J. P., Alternatives to Antibiotics for Organic Poultry Production. *Applied Poultry Research* **2005,** *14* (4), 750-756.
44. García, V.; Catalá-Gregori, P.; Hernández, F.; Megías, M. D.; Madrid, J., Effect of Formic Acid and Plant Extracts on Growth, Nutrient Digestibility, Intestine Mucosa Morphology, and Meat Yield of Broilers. *The Journal of Applied Poultry Research* **2007,** *16* (4), 555-562.
45. Nagabhushana, G. P.; Shivaramaiah, R.; Navrotsky, A., Thermochemistry of the simplest metal organic frameworks: Formates [M(HCOO) 2]·xH 2 O (M = Li, Mg, Mn, Co, Ni, and Zn). *J. Chem. Thermodynamics* **2018,** *118*, 325-330.
46. Lawler, K. V.; Hulvey, Z.; Forster, P. M., Nanoporous metal formates for krypton/xenon separation. *Chem. Commun.* **2013,** *49* (93), 10959-10961.
47. Beatty, A. M.; Granger, K. E.; Simpson, A. E., Crystal Engineering of Organic Clay Mimics from 3,5-Pyrazoledicarboxylic Acid and Amines. *Chem. Eur. J.* **2002,** *8* (14), 3254-3259.
48. Beatty, A. M.; Helfrich, B. A.; Hogan, G. A.; Reed, B.-A., Metal-Containing Dicarboxylic Acids as Building Bocks for Lamellar Inorganic-Organic Hybrid Networks. *Crystal Growth & Design* **2006,** *6* (1), 122-126.
49. Chen, C. L.; Beatty, A. M., "From crystal engineering to cluster engineering: How to transform cadmium chloride from 2-D to 0-D". *Chem. Commun.* **2007,** (1), 76-78.
50. Ugono, O.; Rath, N. P.; Beatty, A. M., Synthesis and Control of Single Layer and Polar 2-D Layered Architectures in a Series of Organic Layered Solids. *Crystal Growth & Design* **2009,** *9* (11), 4595-4598.
51. Ugono, O.; Rath, N. P.; Beatty, A. M., "Exceptions to the rule: new hydrogen-bonded networks from an old reliable". *CrystEngComm.* **2011,** *13* (3), 753-758.
52. Haque, F.; Daeneke, T.; Kalantar-zadeh, K.; Ou, J. Z., Two-Dimensional Transition Metal Oxide and Chalcogenide-Based Photocatalysts. *Nano-Micro Letters* **2017,** *10* (2), 22-49.
53. Liu, P. P.; Yang, L. Y.; Liu, W.; Zhang, Y.; Wang, H. L.; Liu, S.; Yang, R. R.; Guo, Y. Q.; Cui, Y. P., Novel hybrid anode of MnO nanoparticles and ultrathin carbon sheets for high lithium storage performance. *Journal of Alloys and Compounds* **2018,** *740*, 375-381.
54. Wang, L.; Zou, J.; Chen, S.; Zhou, G.; Bai, J.; Gao, P.; Wang, Y.; Yu, X.; Li, J.; Hu, Y. S.; Li, H., TiS2 as a high performance potassium ion battery cathode in ether-based electrolyte. *Energy Storage Materials* **2018,** *12*, 216-222.
55. Xu, Z.; Shi, J.; Haroone, M. S.; Chen, W.; Zheng, S.; Lu, J., Zinc-aluminum oxide solid solution nanosheets obtained by pyrolysis of layered double hydroxide as the photoanodes for dye-sensitized solar cells. *Journal of Colloid and Interface Science* **2018,** *515*, 240-247.

56. Yu, X.; Yang, X.; Li, G., Magnetically Separable Fe2O3C3N4 Nanocomposites with Cocoon-Like Shape: Magnetic Properties and Photocatalytic Activities. *Journal of Electronic Materials* **2018,** *47* (1), 672-676.
57. Ishida, Y.; Shimada, T.; Masui, D.; Tachibana, H.; Inoue, H.; Takagi, S., Efficient excited energy transfer reaction in clay/porphyrin complex toward an artificial light-harvesting system. *J. Am. Chem. Soc.* **2011,** *133* (36), 14280-14286.
58. Ikeda, M.; Yoshii, T.; Matsui, T.; Tanida, T.; Komatsu, H.; Hamachi, I., Montmorillonite-supramolecular hydrogel hybrid for fluorocolorimetric sensing of polyamines. *J. Am. Chem. Soc.* **2011,** *133* (6), 1670-1673.
59. Asiabi, H.; Yamini, Y.; Shamsayei, M., Highly efficient capture and recovery of uranium by reusable layered double hydroxide intercalated with 2-mercaptoethanesulfonate. *Chem. Eng.* **2018,** *337*, 609-615.
60. Vishweshwar, P.; Beauchamp, D. A.; Zaworotko, M. J., An Acetic Acid Solvate of Trimesic Acid That Exhibits Triple Inclined Interpenetration and Mixed Supramolecular Homosynthons. *Crystal Growth & Design.* **2006,** *6* (11), 2429-2431.
61. Chang, Y.-L.; West, M.-A.; Fowler, F. W.; Lauher, J. W., An Approach to the Design of Molecular Solids. Strategies for Controlling the Assembly of Molecules into Two-Dimensional Layered Structures. *J. Am. Chem. Soc.* **1993,** *115*, 5991-6000.
62. Aakeröy, C. B.; Panikkattu, S. V.; DeHaven, B.; Desper, J., Establishing Supramolecular Control over Solid-State Architectures: A Simple Mix and Match Strategy. *Crystal Growth & Design* **2012,** *12* (5), 2579-2587.
63. Yuge, T.; Sakai, T.; Kai, N.; Hisaki, I.; Miyata, M.; Tohnai, N., Topological classification and supramolecular chirality of 21-helical ladder-type hydrogen-bond networks composed of primary ammonium carboxylates: bundle control in 21-helical assemblies. *Chem. Eur. J.* **2008,** *14* (10), 2984-2993.
64. Odendal, J. A.; Bruce, J. C.; Koch, K. R.; Haynes, D. A., Packing motifs in organic ammonium carboxylate salts: extension of the ring-stacking and ring-laddering concepts. *CrystEngComm.* **2010,** *12* (8), 2398-2408.
65. Dmitricheva, E. V.; Makarova, I. P.; Grebenev, V. V., The structure of (K0.43(NH4)0.57)3H(SO4)2 single crystals. *Crystallography Reports* **2015,** *60* (6), 814-820.
66. Smith, G., Coordination polymeric structures in the sodium salt of 4-chloro-3-nitrobenzoic acid and the sodium and potassium salts of 4-nitroanthranilic acid. *Acta Cryst. C.* **2013,** *69* (12), 1472-1477.
67. Smith, G., Crystal structures of the potassium and rubidium salts of (3,5-di-chloro-phen-oxy)acetic acid: two isotypic coordination polymers. *Acta Cryst.* **2015,** *E71* (10), 1177-1180.
68. Clearfield, A., *Metal Phosphonate Chemistry: From Synthesis to Applications*. The Royal Society of Chemistry: 2011.
69. Smith, G., Two-dimensional hydrogen-bonded polymers in the crystal structures of the ammonium salts of phen-oxy-acetic acid, (4-fluoro-phen-oxy)acetic acid and (4-chloro-2-methyl-phen-oxy)acetic acid. *Acta Cryst.* **2014,** *E70* (12), 528-532.
70. Baudron, S. A., Dipyrrin based homo- and hetero-metallic infinite architectures. *CrystEngComm.* **2010,** *12* (8), 2288-2408.
71. Li, Z.; Fowler, F. W.; Lauher, J. W., Weak Interactions Dominating the Supramolecular Self-Assembly in a Salt: A Designed Single-Crystal-to-Single-Crystal Topochemical Polymerization of a Terminal Aryldiacetylene. *J. Am. Chem. Soc.* **2009,** *131* (2), 634-643.
72. Aakeröy, C. B.; Bahra, G. S.; Hitchcock, P. B.; Patell, Y.; Seddon, K. R., Crystal engineering: hydrogen-bonded salts of hydroxybenzoic acids for second harmonic generation. *Chem. Commun.* **1993,** (2), 152-156.
73. Aakeröy, C. B.; Nieuwenhuyzen, M., 4-Methylbenzylammonium 4-Methylbenzyl-carbamate. *Acta Cryst.* **1996,** *C52*, 957-930.

74. Sow, Y.; Diop, L., R2NH2C2O4SnC2O4SnBu3, (R2NH2)4(C2O4)3(SnR'3)2(R = Cy, i-Bu; R' = Me, Bu) AND SOME MIXEDORGANO- AND HALOTIN (IV) OXALATO NEW MOETIESCONTAINING COMPLEXES: SYNTHESIS, INFRARED, MOSSBAUER AND NMR STUDIES. *St. Cerc. St. CICBIA* **2015,** *16* (2), 123-132.
75. Li, Q.; Mak, T. C. W., Hydrogen-Bonded Urea-Anion Host Lattices. Part 4. Comparative Study of Inclusion Compounds of Urea with Tetraethylammonium and Tetraethylphosphonium Chlorides. *Journal of Inclusion Phenomena and Molecular Recognition in Chemistry* **1997,** *28*, 151-161.
76. Aakeröy, C. B.; Hitchcock, P. B.; Seddon, K. R., Organic salts of L-tartaric acid: materials for second harmonic generation with a crystal structure governed by an anionic hydrogen-bonded network. *Chem. Commun.* **1992,** *0*, 553-555.
77. Shaviv, R.; Lowe, C. B.; Zora, J. A.; Aakeröy, C. B.; Hitchcock, P. B.; Seddon, K. R.; Carlin, R. L., Magnetochemistry of the tetrahaloferrate(III) ions. 6. Crystal structure and magnetic ordering in [(pyH)3Cl][FeCl4]2. *Inorganica Chimica Acta.* **1992,** *198*, 613-621.
78. Sharma, C. V. K.; Zaworotko, M. J., X-Ray crystal structure of C6H3(CO2H)3-1,3,5·1.5(4,4′-bipy): a 'super trimesic acid' chicken-wire grid. *Chem. Commun.* **1996,** *0*, 2655-2656.
79. Aakeröy, C. B.; Hitchcock, P. B., Hydrogen-bonded layers of hydrogentartrate anions: two-dimensional building blocks for crystal engineering. *J. Mater. Chem.* **1993,** *11*, 1129-1135.
80. Erel-Unan, I.; Sukhishvili, S. A., Hydrogen-Bonded Multilayers of a Neutral Polymer and a Polyphenol. *Macromolecules* **2008,** *41*, 3962-3970.
81. Evers, J.; Gobel, M.; Krumm, B.; Martin, F.; Medvedyev, S.; Oehlinger, G.; Steemann, F. X.; Troyan, I.; Klapotke, T. M.; Eremets, M. I., Molecular structure of hydrazoic acid with hydrogen-bonded tetramers in nearly planar layers. *J. Am. Chem. Soc.* **2011,** *133* (31), 12100-12105.
82. Aakeröy, C. B.; Nieuwenhuyzen, M., Hydrogen bonding in crystal engineering: two-dimensional layers of hydrogen l-malate anions. *Journal of Molecular Structure* **1996,** *374* (1), 223-239.
83. Aakeröy, C. B.; Cooke, T. I.; Nieuwenhuyzen, M., The crystal structure of the molecular cocrystal L-malic acid L-tartaric acid (1/1). *Supramolecular Chemistry.* **1996,** *7* (2), 153-156.
84. Ashiq, M. I.; Hussain, I.; Dixon, S.; Light, M. E.; Kilburn, J. D., Dimeric supramolecular motifs of two carboxylate-guanidinium compounds. *Acta. Cryst.* **2010,** *A66* (9), 455-458.
85. Russell, V. A.; Etter, M. C.; Ward, M. D., Layered Materials by Molecular Design: Structural Enforcement by Hydrogen Bonding in Guanidinium Alkane-and Arenesulfonates. *J. Am. Chem. Soc.* **1994,** *116* (5), 1941-1952.
86. Djinovic, K.; Golic, L.; Leban, I., Structures of benzylammonium hydrogen malonate (I) and 4-picolinium hydrogen malonate (II). *Acta Cryst.* **1990,** *C46* (2), 281-286.
87. Barnes, J., Benzylammonium hydrogen oxalate hemihydrate. *Acta Cryst.* **2003,** *E59* (7), 931-933.
88. Matsumoto, A.; Odani, T.; Chikada, M.; Sada, K.; Miyata, M., Crystal-Lattice Controlled Photopolymerization of Di(benzylammonium) (Z,Z)-Muconates. *J. Am. Chem. Soc.* **1999,** *121* (48), 11122-11129.
89. Parshad, H.; Frydenvang, K.; Liljefors, T.; Sorensen, H. O.; Larsen, C., Aqueous solubility study of salts of benzylamine derivatives and p-substituted benzoic acid derivatives using X-ray crystallographic analysis. *International Journal of Pharmaceutics* **2004,** *269* (1), 157-168.
90. Liu, Y.; Ward, M. D., Molecular Capsules in Modular Frameworks. *Crystal Growth & Design* **2009,** *9* (9), 3859-3861.
91. Aakeröy, C. B.; Hughes, D. P.; Nieuwenhuyzen, M., The Oxamate Anion: A Flexible Building Block of Hydrogen-Bonded Architectures for Crystal Engineering. *J. Am. Chem. Soc.* **1996,** *118* (42), 10134-10140.

92. Etter, M. C., Hydrogen Bonds as Design Elements in Organic Chemistry. *J. Phys. Chem.* **1991,** *95*, 4601-4610.
93. Ward, M. D., Bulk Crystals to Surfaces: Combining X-ray Diffraction and Atomic Force Microscopy to Probe the Structure and Formation of Crystal Interfaces. *Chem. Rev.* **2001,** *101*, 1697-1725.
94. Desiraju, G. R., Reflections on the Hydrogen Bond in Crystal Engineering. *Crystal Growth & Design* **2011,** *11* (4), 896-898.
95. Desiraju, G. R., Supramolecular Synthons in Crystal Engineering - A New Organic Synthesis. *Angew. Chem. Int. Ed.* **1995,** *34* (21), 2311-2327.
96. Moulton, B.; Zaworotko, M. J., From Molecules to Crystal Engineering: Supramolecular Isomerism and Polymorphism in Network Solids. *Chem. Rev.* **2001,** *101* (6), 1629-1658.
97. Clearfield, A., Role of Ion Exchange in Solid-State Chemistry. *Chem. Rev.* **1988,** *88*, 125-148.
98. Aakeröy, C. B.; Seddon, K. R., The Hydrogen Bond and Crystal Engineering. *Chem. Soc. Rev.* **1993,** *22* (6), 397-407.
99. Aakeröy, C. B.; Beatty, A. M., Crystal Engineering of Hydrogen-Bonded Assemblies—A Progress Report. *Aust. J. Chem.* **2001,** *54*, 409-421.
100. Beatty, A. M., Open-framework coordination complexes from hydrogen-bonded networks: toward host/guest complexes. *Coor. Chem. Rev.* **2003,** *246* (1-2), 131-143.
101. Triantafillidis, C. S.; LeBaron, P. C.; Pinnavaia, T. J., Homostructured Mixed Inorganic-Organic Ion Clays: A New Approach to Epoxy Polymer-Exfoliated Clay Nanocomposites with a Reduced Organic Modifier Content. *Chem. Mater.* **2002,** *14*, 4088-4095.
102. Chesnut, D. J.; Hagrman, D.; Zapf, P. J.; Hammond, R. P.; LaDuca, R. J.; Haushalter, R. C.; Zubieta, J., Organic/inorganic composite materials: the roles of organoamine ligands in the design of inorganic solids. *Coor. Chem. Rev.* **1999,** *190-192*, 737-769.
103. Kumaraswamy, G.; Deshmukh, Y.; Agrawal, V. V.; Rajmohana, P., Layered Inorganic-Organic Clay-like Nanocomposites Rearrange To Form Silsesquioxanes on Acid Treatment. *J. Phys. Chem.* **2005,** *B109*, 16034-16039.
104. Cattaneo, A. S.; Bracco, S.; Comotti, A.; Galimberti, M.; Sozzani, P.; Eckert, H., Structural Characterization of Pristine and Modified Fluoromica Using Multinuclear Solid-State NMR. *J. Phys. Chem.* **2011,** *C115* (25), 12517-12529.
105. Finocchio, E.; Baccini, I.; Cristiani, C.; Dotelli, G.; Gallo Stampino, P.; Zampori, L., Hybrid organo-inorganic clay with nonionic interlayers. mid- and near-IR spectroscopic studies. *J. Phys. Chem.* **2011,** *A115* (26), 7484-7493.
106. Zeng, Z.; Matuschek, D.; Studer, A.; Schwickert, C.; Pottgen, R.; Eckert, H., Synthesis and characterization of inorganic-organic hybrid materials based on the intercalation of stable organic radicals into a fluoromica clay. *Dalton. Trans.* **2013,** *42* (24), 8585-8596.
107. Saied, O.; Maris, T.; Wuest, J. D., Deformation of porous molecular networks induced by the exchange of guests in single crystals. *J. Am. Chem. Soc.* **2003,** *125* (49), 14956-14957.
108. Ariga, K.; Yamauchi, Y.; Rydzek, G.; Ji, Q.; Yonamine, Y.; Wu, K. C. W.; Hill, J. P., Layer-by-layer Nanoarchitectonics: Invention, Innovation, and Evolution. *Chem. Lett.* **2014,** *43* (1), 36-68.
109. Zaworotko, M. J., Superstructural diversity in two dimensions: crystal engineering of laminated solids. *Chem. Commun.* **2001**, 1-9.
110. Biradha, K.; Dennis, D.; MacKinnon, V. A.; Sharma, C. V. K.; Zaworotko, M. J., Supramolecular Synthesis of Organic Laminates with Affinity for Aromatic Guests: A New Class of Clay Mimics. *J. Am. Chem. Soc.* **1998,** *120*, 11894-11903.
111. Holman, K. T.; Pivovar, A. M.; Swift, J. A.; Ward, M. D., Metric Engineering of Soft Molecular Host Frameworks. *Acc. Chem. Res.* **2001,** *34* (2), 107-118.

112. Aakeröy, C. B.; Beatty, A. M.; Lorimer, K. R., Charge-Assisted Hydrogen Bonds and Halogen-Halogen Interactions in Organic Salts: Benzylammonium Benzoates and Pentafluorobenzoates. *Struct. Chem.* **1999,** *10* (3), 229-242.
113. Braga, D.; Maini, L.; Grepioni, F.; De Cian, A.; Fe´lix, O.; Fischer, J.; Hosseini, M. W., Charge-assisted N–H(+)···O(-) and O–H···O(-) hydrogen bonds control the supramolecular aggregation of ferrocenedicarboxylic acid and bis-amidines. *New J. Chem.* **2000,** *24* (7), 547-553.
114. Bish, D. L., RIETVELD REFINEMENT OF THE KAOLINITE STRUCTURE AT 1.5 K. *Clay and Clay Minerals* **1993,** *41* (6), 738-744.
115. Yuge, T.; Miyata, M.; Tohnai, N., Novel Design of Tunable Organic Clay Mimic Structures Based on the Connection of One-Dimensional Supramolecular Synthons. *Crystal Growth & Design* **2006,** *6* (6), 1271-1273.
116. El-Hiti, G. A.; Smith, K.; Alshammari, M. B.; Ajarim, M. D.; Kariuki, B. M., Crystal structure of tert-butyl 2-phenylethylcarbamate, C13H19NO2. *Zeitschrift für Kristallographie - New Crystal Structures* **2016,** *231* (4).
117. Nahringbaurer, I., Hydrogen bond studies. XIV. The crystal structure of ammonium acetate. *Acta Cryst.* **1967,** *23*, 956-965.
118. Kuppers, H.; Jessen, S. M., Ammonium hydrogen carobnate. *Zeitschrift fur Kristallographie* **1993,** *203*, 167.
119. Chowdhury, M.; Kariuki, B. M., Supramolecular Assembly in Cinnamate Structures: The Influence of the Ammonium Ion and Halogen Interactions. *Crystal Growth & Design* **2014,** *6*, 774.
120. Groom, C. R.; Allen, F. H., The Cambridge Structural Database in retrospect and prospect. *Angew. Chem. Int. Ed. Engl.* **2014,** *53* (3), 662-671.
121. Kennard, O., From data to knowledge—Use of the Cambridge Structural Database for studying molecular interactions. *Supramolecular Chemistry*. **1992,** *1* (3), 277-295.
122. Lin, Z.; Hu, K.; Jin, S.; Ding, A.; Wang, Y.; Dong, L.; Gao, X.; Wang, D., Crystal and molecular structures of sixteen charge-assisted hydrogen bond-mediated diisopropylammonium salts from different carboxylic acids. *Journal of Molecular Structure* **2017,** *1146*, 577-591.
123. Etter, M. C., Encoding and Decoding Hydrogen-Bond Patterns of Organic Compounds. *Acc. Chem. Res.* **1990,** *23*, 120-126.
124. Schneller, T.; Griesche, D., *Chemical Solution Deposition of Functional Oxide Thin Films*. Springer-Verlag Wien: 2013; p 29-49.
125. Dolomanov, O. V.; Bourhis, L. J.; Gildea, R. J.; Howard, J. A. K.; Puschmann, H., OLEX2: a complete structure solution, refinement and analysis program. *J. Appl. Cryst.* **2009,** *42*, 339-341.
126. Sheldrick, G. M., A short history of SHELX. *Acta. Crystallogr. A* **2008,** *A64*, 112-122.
127. Refcodes: PEBDOQ, P., SOVWOQ, LAYGAT, SOVXAD, SOVXEH, SOVXOR, SOVXUX.
128. REFCODES: YABFEO, Y., YABGOZ, WETPIU, WETPOA, AJUMOH, SEJSOP, PEBDUW, TOHXOE,TEWXIC, XINSAO, LAYCAP, LAYJUC, LAYGAT, NOJWIS, NOJWOY, NOJWEO, SOVWOQ, SOVWUW, SOVXAD, SOVXEH, SOVXOR, XOVXUX.
129. Chloro Containing Benzylamines: NOJWOY, T., TEWWUN, NOJWIS, LAYKAX, DUVCUT, XOVVEJ, XOVVIN.
130. Aakeröy, C. B.; Nieuwenhuyzen, M., Hydrogen Bonding and Structural Motifs in Organic l-Malate(2−) Salts. *Chem. Mater.* **1996,** *8* (6), 1229-1235.
131. Refcodes: AJUMOH (1), L., PEBCIJ (1), PEBDOQ (1), PEBDUW (1), SEJSOP (1), SOVWOQ (1), SOVWUW (1), TOHXOE (1), XINSAO (1), SINSIW (1), XOXQEH (1), YABGEP (1), YABGIT (1), LAYGAT (3), TEWXIC (3), NOJWEO (4), SOVXAD (4), SOVXEH (4), LAYJUQ (5), SOVXOR(5), SOVXUX (5), DUVCUT (6), NOJWOY (6), TEWXOI (6), TOYMEZ (6), NOJWIS (7), TEWWUN (7), TOYMAV(7).

132. Jung, S. H.; Ahn, J. H.; Park, S. K.; Choi, J.-K., A Practical and Convenient Procedure for the N-Formylation of Amines Using Formic Acid. *Bull. Korean Chem. Soc.* **2002,** *23* (1), 149-150.
133. Min, L.; Lei, M.; Lihong, H., A convenient one-pot synthesis of formamide derivatives using thiamine hydrochloride as a novel catalyst. *Tetrahedron Lett.* **2010,** *51* (32), 4186-4188.
134. Bandgar, P. D.; Kinkar, S. N.; Chobe, S. S.; Mandawad, G. G.; Yemul, O. S.; Dawane, B. S., Clean and Green Approach for N-formylation of Amines using Formic acid under neat reaction condition. *Arch. Appl. Sci. Res.* **2011,** *3* (3), 246-251.
135. Dhake, K. P.; Tambade, P. J.; Singhal, R. S.; Bhanage, B. M., An efficient, catalyst- and solvent-freeN-formylation of aromatic and aliphatic amines. *Green Chemistry Letters and Reviews* **2011,** *4* (2), 151-157.
136. Dhorajiya, B. D.; Ibrahim, A. S.; Badria, F. A.; Dholakiya, B. Z., Design and synthesis of novel nucleobase-based barbiturate derivatives as potential anticancer agents. *Med. Chem. Res.* **2013,** *23* (2), 839-847.
137. Ojeda-Porras, A.; Hernández-Santana, A.; Gamba-Sánchez, D., Direct amidation of carboxylic acids with amines under microwave irradiation using silica gel as a solid support. *Green Chem.* **2015,** *17*, 3157-3163.
138. Fieser, L. F.; Jones, J. E., N-Methylformanilide. *Organic Synth.* **1955,** *20* (3), 590, 66.
139. Gerack, C. J.; McElwee-White, L., Formylation of Amines. *Molecules* **2014,** *19* (6), 7689-7713.
140. Huffman, C. W., Formylation of Amines. *J. Org. Chem.* **1958,** *23* (5), 727-729.
141. Aleiwi, B. A.; Mitachi, K.; Kurosu, M., Mild and convenient N-formylation protocol in water-containing solvents. *Tetrahedron Lett.* **2013,** *54* (16), 2077-2081.
142. Habibi, D.; Rahmani, P.; Askbaripanah, Z., N-Formylation of Anilines with Silica Sulfuric Acid under Solvent-Free Conditions. *Journal of Chemistry* **2013,** *1*, 1-6.
143. Bhat, S. U.; Naikoo, R. A.; Tomar, R.; Bhat, R. A.; Malla, M. A.; Garnie, J. A.; Kumar, N.; Tiwari, K. R., Synthesis of N-Formylation of Amines using Various Ion Exchanged Forms of Zeolite-A as Catalysts. *Pharm. Pharmacol. Int. J.* **2017,** *5* (4), 130-137.
144. Schultz, G.; Hargittai, I., Molecular Structure of N,N-Dimethylformamide from Gas-Phase Electron Diffraction. *J. Phys. Chem.* **1993,** *97*, 4966-4969.
145. Zhou, X.; Krauser, J. A.; Tate, D. R.; VanBuren, A. S.; Clark, J. A.; Moody, P. R.; Liu, R., Theoretical Study of the Structure and Vibrational Spectrum of N,N-Dimethylformamide. *J. Phys. Chem.* **1996,** *100*, 16822-16827.
146. Lei, Y.; Li, H.; Pan, H.; Han, S., Structures and Hydrogen Bonding Analysis of N,N-Dimethylformamide and N,N-Dimethylformamide-Water Mixtures by Molecular Dynamics Simulations. *J. Phys. Chem.* **2003,** *2003* (107), 1574-1583.
147. Steele, D.; Quatermain, A., The vibrational spectra of amides-II. The force field and isotopic shifts of N,N-dimethyl formamide. *Spectrochimica Acta.* **1987,** *43A* (6), 781-789.
148. Stålhandske, C. M. V.; Mink, J.; Sandström, M.; Pápai, I.; Johannson, P., Vibrational spectroscopic and force field studies of N, N-dimethylthioformamide, N, N-dimethylformamide, their deuterated analogues and bis(N, N-dimethylthioformamide) mercury(II) perchlorate. *Vibrational Spectroscopy* **1997,** *14*, 207-227.
149. Renugopalakrishnan, V.; Madrid, G.; Cuevas, G.; Hagler, A. T., Density functional studies of molecular structures of N-methylformamide, N,N-dimethyl formamide, and N,N-dimethylacetamide. *Chem. Sci.* **2000,** *112* (1), 35-42.
150. Menashe, N.; Reshef, D.; Shvo, Y., The Reaction of Alkynes and Formic Acid. *J. Org. Chem.* **1991,** *56*, 2912-2914.
151. Menashe, N.; Shvo, Y., Hydration of Alkynes in Anhydrous Medium with Formic Acid as Water Donor. *J. Org. Chem.* **1993,** *58*, 7434-7439.
152. Wan, Z.; Jones, C. D.; Mitchell, D.; Pu, J. Y.; Zhang, T. Y., Practical Method for Transforming Alkynes into alpha-Diketones. *J. Org. Chem.* **2006,** *71*, 826-828.

153. Wu, G.; Shlykov, S.; Alsenoy, C. V.; Geise, H. J.; Sluyts, E.; Van der Veken, B. J., Formic Anhydride in the Gas Phase, Studied by Electron Diffraction and Microwave and Infrared Spectroscopy, Supplemented with ab-Initio Calculations of Geometries and Force Fields. *J. Phys. Chem.* **1995,** *99*, 8589-8598.
154. Ferraz, K. S. O.; Silva, N. F.; Da Silva, J. G.; Speziali, N. L.; Mendes, I. C.; Beraldo, H., Structural studies on acetophenone- and benzophenone-derived thiosemicarbazones and their zinc(II) complexes. *Journal of Molecular Structure* **2012,** *1008*, 102-107.
155. Lizarraga, E.; Romano, E.; Rudyk, R. A.; Catalan, C. A.; Brandan, S. A., Structural study, coordinated normal analysis and vibrational spectra of 4-hydroxy-3-(3-methyl-2-butenyl)acetophenone. *Spectrochimica Acta.* **2012,** *97*, 202-208.
156. Aitipamula, S.; Chow, P. S.; Tan, R. B. H., Solvates and polymorphic phase transformations of 2-chloro-4-nitrobenzoic acid. *CrystEngComm.* **2011,** *13* (3), 1037-1045.
157. Ulrich, H.; Tucker, B.; Sayigh, A. A. R., Base-Catalyzed Reactions of Isocyanates. The Synthesis of 2,4-Dialkylallophanates. *J. Org. Chem.* **1967,** *32*, 3938-3941.
158. Walkman, T. E.; Mcghee, W. D., Isocyanates from primary amines and carbon-dioxide← dehydration of carbamate anions. *Chem. Commun.* **1994**, 957-958.
159. Ikeshima, M.; Mamada, M.; Katagiri, H.; Minami, T.; Okada, S.; Tokito, S., Synthesis and Solid-State Polymerization of Diacetylene Derivatives with an N-Carbazolylphenyl Group. *Bull. Chem. Soc. Jpn.* **2015,** *88* (6), 843-849.
160. Cenini, S.; Crotti, C.; Pizzotti, M.; Porta, F., Ruthenium Carbonyl Catalyzed Reductive Carbonylation of Aromatic Nitro Compounds. A Selective Route to Carbamates. *J. Org. Chem.* **1988,** *52*, 1243-1250.
161. Dodd, R. H.; Hyaric, M. L., The oxidation of aromatic alhedydes to carboxylic acids using hydrogen peroxide in formic acid. *Synthesis* **1993,** *1*, 295-297.
162. Burk, M. J.; Allen, J. G., A Mild Amide to Carbamate Transformation. *J. Org. Chem.* **1997,** *62*, 7054-7057.
163. Salvatore, R. N.; A., L. J.; Jung, K. W., An efficient one-pot synthesis of N-alkyl carbamates from primary amines using Cs2CO3. *Tetrahedron Lett.* **2001,** *42*, 6023-6025.
164. Salvatore, R. N.; Chu, F.; Nagle, A. S.; Kapxhiu, E. A.; Cross, R. M.; Jung, K. W., Efficient Cs_2CO_3-promoted solution and solid phase synthesis of carbonates and carbamates in the presence of TBAI. *Tetrahedron* **2002,** *58*, 3329-3347.
165. Salvatore, R. N.; Yoon, C. H.; Jung, K. W., Synthesis of secondary amines. *Tetrahedron* **2011,** *57*, 7785-7811.
166. Lundberg, H.; Tinnis, F.; Selander, N.; Adolfsson, H., Catalytic amide formation from non-activated carboxylic acids and amines. *Chem. Soc. Rev.* **2014,** *43* (8), 2714-42.
167. Yalfani, M. S.; Lolli, G.; Muller, T. E.; Wolf, A.; Mleczko, L., Methyl N-phenyl carbamate synthesis from aniline and methyl formate: carbon recycling to chemical products. *ChemSusChem.* **2015,** *8* (3), 443-7.
168. Lim, V. T.; Tsukanov, S. V.; Stephens, A. B.; Johnston, J. N., Enantioselective Synthesis of alpha-Bromonitroalkanes for Umpolung Amide Synthesis: Preparation of tert-Butyl ((1R)-1-(4-(benzyloxy)phenyl)-2-bromo-2-nitroethyl)carbamate. *Organic Synth.* **2016,** *93*, 88-99.
169. McCann, N.; Phan, D.; Wang, X.; Conway, W.; Burns, R.; Attalla, M.; Puxty, G.; Maeder, M., Kinetics and Mechanism of Carbamate Formation from CO2(aq), Carbonate Species, and Monoethanolamine in Aqueous Solution. *J. Phys. Chem. A* **2009,** *113*, 5022-5029.
170. Darensbourg, D. J.; Niezgoda, S. A.; Draper, J. D.; Reibenspies, J. H., Mechanistic Aspects of the Copolymerization of CO2 and Epoxides by Soluble Zinc Bis(phenoxide) Catalysts as Revealed by Their Cadmium Analogues. *J. Am. Chem. Soc.* **1998,** *120*, 4690-4698.
171. Sakakura, T.; Saito, Y.; Okano, M.; Choi, J.-C.; Sako, T., Selective Conversion of Carbon Dioxide to Dimethyl Carbonate by Molecular Catalysis. *J. Org. Chem.* **1998,** *63*, 7095-7096.

172. Bavbek, O.; Alper, E., Reaction Mechanism and Kinetics of Aqueous Solutions of Primary and Secondary Alkanolamines and Carbon Dioxide. *Turk J. Chem.* **1999,** *23*, 293-300.
173. Yoshida, M.; Hara, N.; Okuyama, S., Catalytic production of urethanes from amines and alkyl halides in supercritical carbon dioxide. *Chem. Commun.* **2000**, 151-152.
174. Selva, M.; Tundo, P.; Perosa, A.; Dall'Acqua, F., Synthesis of Methyl Carbamates from Primary Aliphatic Amines and Dimethyl Carbonate in Supercritical CO2: Effects of Pressure and Cosolvents and Chemoselectivity. *J. Org. Chem.* **2005,** *70*, 2771-2777.
175. Peterson, S. L.; Stucka, S. M.; J., D. C., Parallel Synthesis of Ureas and Carbamates from Amines and CO2 under Mild Conditions. *Org. Lett.* **2010,** *12* (6), 1340-1343.
176. Ciftja, A. F.; Hartono, A.; Svendsen, H. F., Carbamate Formation in Aqueous - diamine - CO2 Systems. *Energy Procedia* **2013,** *37*, 1605-1612.
177. Budisa, N.; Schulze-Makuch, D., Supercritical carbon dioxide and its potential as a life-sustaining solvent in a planetary environment. *Life (Basel)* **2014,** *4* (3), 331-40.
178. Inagaki, F.; Matsumoto, C.; Iwata, T.; Mukai, C., CO2-Selective Absorbents in Air: Reverse Lipid Bilayer Structure Forming Neutral Carbamic Acid in Water without Hydration. *J. Am. Chem. Soc.* **2017,** *139* (13), 4639-4642.
179. Polleta, P.; Liotta, C. L., Sustainable Chemistry: Reversible reaction of CO2 with amines. *French-Ukrainian Journal of Chemistry* **2016,** *4* (1), 14-22.
180. Matsumura, Y.; Maki, T.; Y., S., Electrochemically Induced Hofmann Rearrangement. *Tetrahedron Lett.* **1997,** *38* (51), 8879-8882.
181. Gogoi, P.; Konwar, D., An efficient modification of the Hofmann rearrangement: synthesis of methyl carbamates. *Tetrahedron Lett.* **2007,** *48* (4), 531-533.
182. Ghosh, A. K.; Brindisi, M., Organic carbamates in drug design and medicinal chemistry. *J. Med. Chem.* **2015,** *58* (7), 2895-940.
183. Scriven, E. F. V.; Turnbull, K., Azides: Their Preparation and Synthetic Uses. *Chem. Rev.* **1988,** *88*, 297-368.
184. Belgodere, C.; Dubessy, J.; Sterpenich, J.; Pironon1, J.; Vautrin, D.; Caumon, M. C.; Robert, P.; Randi, A.; Birat, J. P., Experimental determination of CO2 diffusion coefficient in aqueous solutions under pressure via Raman spectroscopy at room temperature: impact of salinity (NaCl) on dissolved CO2 diffusivity. *11th GeoRaman International Conference* **2014,** *Abstract*, 1-2.
185. Tamimi, A.; Rinker, E. B.; Sandall, O. C., Diffusion Coefficients for Hydrogen Sulfide, Carbon Dioxide, and Nitrous Oxide in Water over the Temperature Range 293-368 K. *J. Chem. Eng. Data* **1994,** *39*, 330-332.
186. Cadogan, S. P.; Maitland, G. C.; Trusler, J. P. M., Diffusion Coefficients of CO2 and N2 in Water at Temperatures between 298.15 K and 423.15 K at Pressures up to 45 MPa. *J. Chem. Eng. Data* **2014,** *59* (2), 519-525.
187. Zarghami, S.; Boukadi, F.; Al-Wahaibi, Y., Diffusion of carbon dioxide in formation water as a result of CO2 enhanced oil recovery and CO2 sequestration. *J. Petrol. Explor. Prod. Technol.* **2016,** *7* (1), 161-168.
188. Dimitrijevic, N. M.; Vijayan, B. K.; Poluektov, O. G.; Rajh, T.; Gray, K. A.; He, H.; Zapol, P., Role of water and carbonates in photocatalytic transformation of CO2 to CH4 on titania. *J. Am. Chem. Soc.* **2011,** *133* (11), 3964-3971.
189. Sahara, G.; Kumagai, H.; Maeda, K.; Kaeffer, N.; Artero, V.; Higashi, M.; Abe, R.; Ishitani, O., Photoelectrochemical Reduction of CO2 Coupled to Water Oxidation Using a Photocathode With a Ru(II)-Re(I) Complex Photocatalyst and a CoOx/TaON Photoanode. *J. Am. Chem. Soc.* **2016,** *138*, 14152-14158.
190. Kuehnel, M. F.; Orchard, K. L.; Dalle, K. E.; Reisner, E., Selective Photocatalytic CO2 Reduction in Water through Anchoring of a Molecular Ni Catalyst on CdS Nanocrystals. *J. Am. Chem. Soc.* **2017,** *139* (21), 7217-7223.

191. Tiritiris, I.; Kantlehner, W., Orthoamides and Iminium Salts, LXX [1]. Capturing of Carbon Dioxide with Organic Bases (Part 1) - Reactions of Diamines with Carbon Dioxide. *Z. Naturforsch. 2011, 66b, 164 – 176* **2011,** *66*, 164-168.
192. Alexander, E. R.; Wildman, R. B., Studies on the Mechanism of the Leuckart Reaction. *J. Am. Chem. Soc.* **1947,** *70* (3), 1187-1189.
193. Witt, M.; Grützmacher, H.-F., Proton Bound Homodimers and Heterodimers of Amides and Amines in the Gas Phase. Equilibrium Studies by Fourier Transform Ion Cyclotron Resonance Spectrometry. *J. Am. Soc. Mass. Spectrom.* **2002,** *13* (11), 1273-1281.
194. Crugeiras, J.; Rios, A.; Riveiros, E.; Richard, J. P., Substituent Effects on the Thermodynamic Stability of Imines Formed from Glycine and Aromatic Aldehydes: Implications for the Catalytic Activity of Pyridoxal-5′-phosphate. *J. Am. Chem. Soc.* **2009,** *131*, 15815-15824.
195. Bandar, J. S.; Lambert, T. H., Enantioselective Bronsted base catalysis with chiral cyclopropenimines. *J. Am. Chem. Soc.* **2012,** *134* (12), 5552-5555.
196. Vianello, R.; Maskill, H.; Maksić, Z. B., Basicity of Amines in the Gas Phase – Analysis of the Base-Strengthening Effect of anN-Trityl Group by Use of a Triadic Formula. *Eur. J. Org. Chem.* **2006,** *2006* (11), 2581-2589.
197. Hansch, C.; Leo, A.; Taft, R. W., A Survey of Hammett Substituent Constants and Resonance and Field Parameters. *Chem. Rev.* **1991,** *91*, 165-195.
198. Kallen, R. G.; Jencks, W. P., Equilibria For the Reaction of Amines with Formaldehyde and Protons in Aqueous Solution: A Re-Exampination of the Formol Titration. *J. Biol. Chem.* **1966,** *241* (24), 5864-5878.
199. Bettelheim; Brown; March, *Introduction to General, Organic, and Biochemistry 6th Ed.* Holt Rinehart & Winston: 2001.
200. Atkins; Jones; Laverman, *Chemical Principles 6th Ed.* W. H. Freeman: 2012.
201. Bruice, *Organic Chemistry 7th Ed.* Pearson: 2013.
202. Shokri, A.; Abedin, A.; Fattahi, A.; Kass, S. R., Effect of hydrogen bonds on pKa values: importance of networking. *J. Am. Chem. Soc.* **2012,** *134* (25), 10646-10650.
203. Gilli, P.; Pretto, L.; Bertolasi, V.; Gilli, G., Predicting Hydrogen-Bond Strengths from Acid-Base Molecular Properties. The pKa Slide Rule: Toward the Solution of a Long-Lasting Problem. *Acc. Chem. Res.* **2009,** *42* (1), 33-44.
204. Bhogala, B. R.; Basavoju, S.; Nangia, A., Tape and layer structures in cocrystals of some di- and tricarboxylic acids with 4,4′-bipyridines and isonicotinamide. From binary to ternary cocrystals. *CrystEngComm* **2005,** *7* (90), 551-562.
205. Lemmerer, A., Six two- and three-component ammonium carboxylate salt structures with a ladder-type hydrogen-bonding motif, three incorporating neutral carboxylic acid molecules. *Acta. Cryst.* **2011,** *A67* (3), 92-99.

Chapter 5

π-Choreography in Aromatic Ammonium Formate Solids

5.1 Introduction

Where the previous chapter focused on discussing and evaluating the physical layering behavior of each ammonium formate compound, this chapter shall focus specifically on the interlayer aryl ring π-π interactions[1] for a selection of ammonium formates that have analogous ammonium HPzDCA (the mono-anion of 3,5-pyrazoledicarboxylic acid) layered materials.[2-3] Additionally, each compound's interlayer π-interactions shall be compared to related 2-D layered structures in the Cambridge Structural Database (CSD).[4]

5.1.1 Arene "π-π Interactions"

The study of intermolecular interactions of aryl ring systems in the solid-state, and beyond, has been a developing field of research for many years.[1, 5] These interactions have been measured and described experimentally and theoretically due to their importance in solid and solution-state chemistry, and their influence in biological sciences. Examples of π-interactions are widespread, and their presence in various chemical systems is often the driving force responsible for achieving tremendous functionalities.[6-8] Biologically, π-interactions are responsible for phenomena such as the stabilization of DNA base pairs,[9] directing the tertiary structure of proteins,[7] even mediating electron transport *via* flavin molecules.[10] Medically, π-interactions are exploited in drug delivery and design.[11-12] In addition, π-interactions may also be encountered in: molecular electronics, such as transistors;[13-14] graphene applications,[15] solar arrays,[16] and photovoltaics.[17] This list is in no way exhaustive, and will likely continue to expand for as long as discovery is possible.

π-π interactions generally involves the electrostatically-driven assembly and organization of aryl rings.[1, 5, 18-21] This interaction is still being understood, and efforts are continuously underway to achieve a comprehensive definition, but it is generally accepted that the nature of the force originates from the attraction between the π-system of one ring with the σ-framework of a

neighboring ring, in turn overcoming the π-π repulsion present between the pair (**Figure 5.1.1**).[22-25]

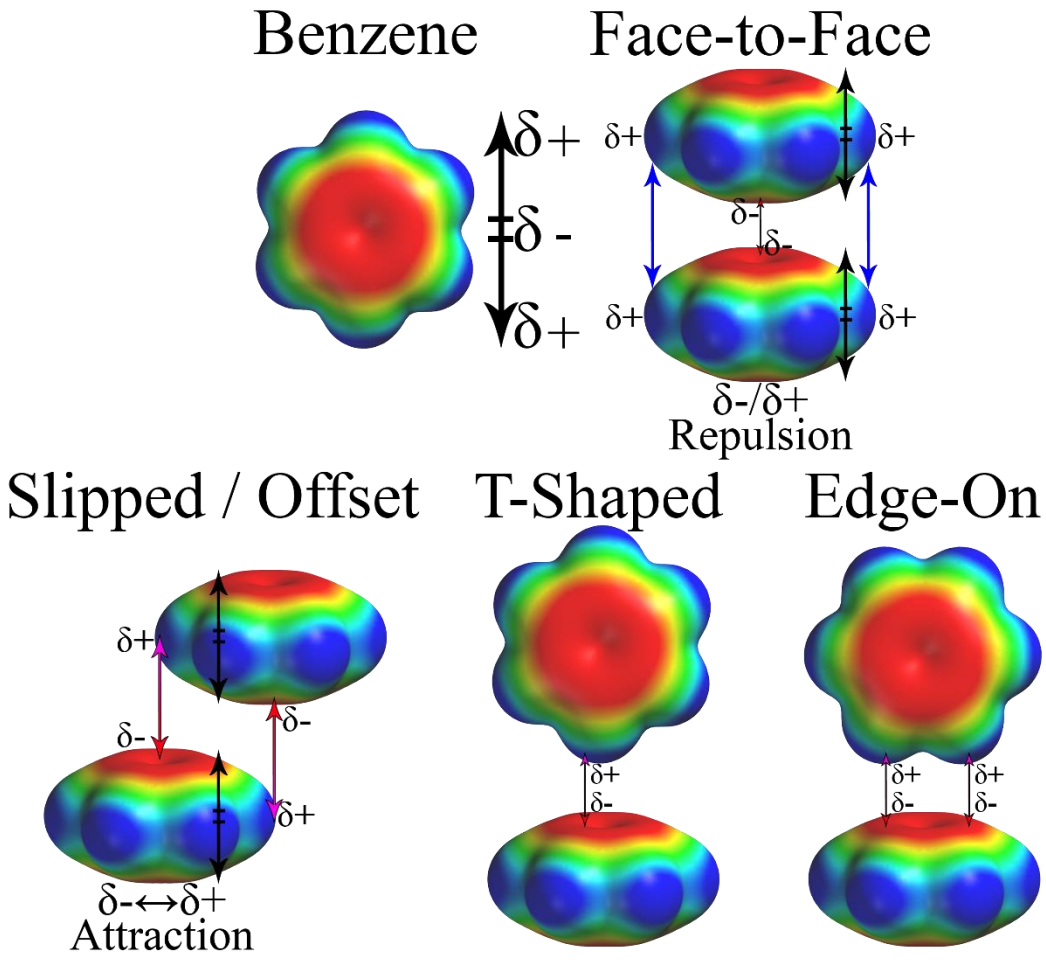

Figure 5.1.1 δ+ and δ- attract. Prevailing model of π-stacking compatibility in benzene based on Electrostatic Potential (ESP).

5.1.2 Arene π-Interaction Guidelines

In 1990, Hunter and Sanders developed a set of rules and standards, based on experimental and calculated data to assist in uniting researchers towards the productive and consistent assignment of π-interactions in various materials.[1] These rules read as follows:

1. "π-π repulsion dominates in a face-to-face π-stacked geometry."
2. "π-σ attraction dominates in an edge-on or T-shaped geometry."
3. "π-σ attraction dominates in an offset π-stacked geometry."

These effects typically chain to the next ring in a series, forming a connected column of π-interactions, hence the term "π-π stacking', or simply "π-stacking". Though it could be argued that the use of the word "stacking" in this manner is a misnomer as the direct, eclipsed, ring-over-ring arrangements are infrequently encountered. For the purposes of this discussion these effects shall be generalized as "π-interactions," because "stacking" is not always guaranteed.

5.1.2.1 Spatial Domains of π-Interactions

Arene π-interactions will normally be encountered in one of the following canonical forms: a direct overlap of aryl rings, a slipped/offset stack, or an edge-on T-shaped orientation (**Figure 5.1.2**).[5]

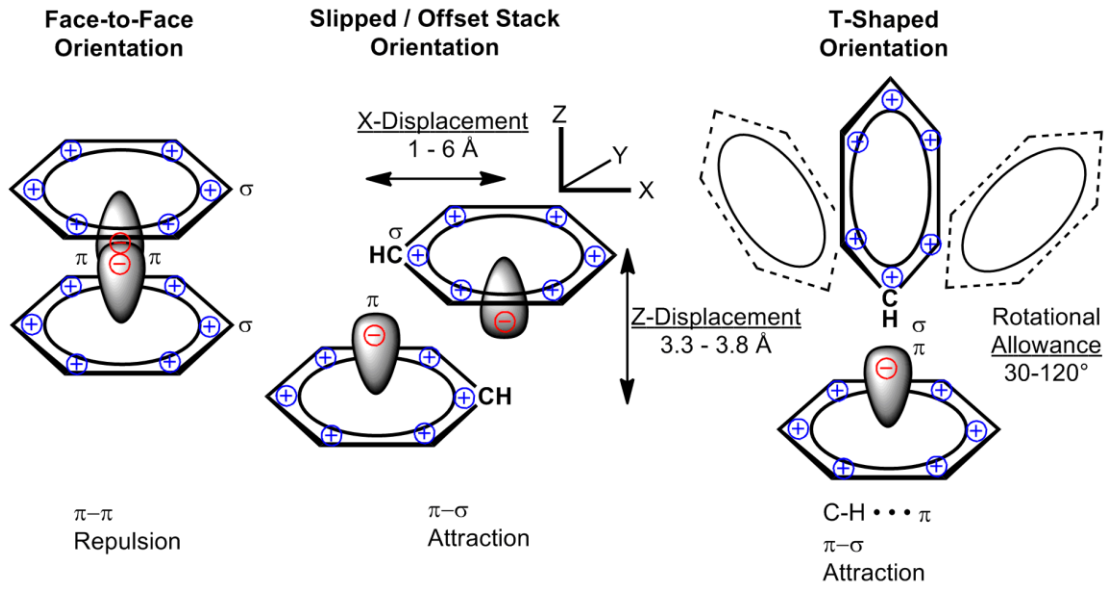

Figure 5.1.2 Typical arrangement and distance thresholds for ring-to-ring π-interactions. Figure adapted from reference 1.

The lateral displacement encountered between rings is closely tied to the angle of the π-interaction. When the angle between the ring planes is less than 30°, essentially parallel to one

another, the displacement between centroids will be between 1 - 4.4 Å, and when the angle between the planes is between 60° and 120°, such as in the interactions of proteins (i.e., alanine-alanine),[6] the maximum distance threshold between centroids increases to upwards of 5.5 Å.[1]

5.1.2.2 Face-to-Face π-π Considerations and Realities

The Hunter-Sanders rules, backed by calculated energetic considerations, helped to clarify the thresholds of vertical separation between rings of ~3.3-3.8 Å, as well as the acceptable rotational, and face-to-face lateral displacement, shown above in **Figure 5.1.2**. Direct face-to-face "π-stacking" is almost never encountered, except in situations where π to π* electron transfer is occurring,[1, 5, 10, 13-15, 17-18] though reports concerned with optimizing conditions which may coax direct face-to-face interactions exist.[26-27] Three additional rules exist for face-to-face systems:

4. "For interaction between highly charged atoms, charge-charge interaction dominates."
5. "A favorable face-to-face interaction with a neutral or weakly polarized site requires as a π polarization, a π-deficient atom in the aromatic ring."
6. "A favorable face-to-face interaction with a neutral or weakly polarized site requires as a σ polarization, a positively charged atom in the aromatic ring."

5.1.3 Modern Thought on Hunter-Sanders Rules

The above rules are very helpful in establishing a base set of standards with which aryl rings may interact with their neighbors; especially as they relate to solid-state interactions. As a model, these standards have served as a valuable platform, allowing for the consistent discussion of their causes and effects. However, it is without great surprise that these rules and guidelines have come under question after nearly 30 years.[14, 18-19, 27-33]

Generally, Hunter and Sanders' description of the effects of π-polarized aryl rings has both provided an important basis for predicting T-Shaped and offset geometries, and also *correctly* predicts the face-to-face stacking in aromatic 'donor/acceptor' scenarios.[8, 34] However, the concept of complementary interacting π clouds (i.e., electron rich pairing with electron poor) being favored in associated aromatic molecules was brought under scrutiny due to the noticeable lack of face-centered stacking in synthetic and biological systems.[35-36]

5.1.3.1 Reassessing the Subtle Influence on π-π Interactions

Certain observed inconsistencies, such as strong stacking interactions from electron deficient naphthalene diimides, dismantled the idea of complementary association of aryl π clouds.[30, 37-39] It became clear that the classic description of substituent effects on arene π-π interactions was flawed. Exhaustive research conducted by Rashkin, Waters, Wheeler, Houk, and others, has implicated substituent-arene interactions, over arene-arene centroid π-interactions, as being the major contributor to the putative weak forces.[29, 33-34, 36, 40-45] Additionally, electrostatics, and dispersion forces between rings, have become a major discussion point on the topic based on theoretical calculations by Sherrill and others.[8, 35, 46]

The role of substituents actively influencing the overall polarization of the aryl ring, which then pairs with a compatible polarized ring, has not held up in a number of directed studies; especially so with modern computational methods, including DFT-D and CCSD(T) interaction energies.[30, 44-45] The original school of thought has been attributed to a broad misinterpretation by researchers of the connection between the electronic effects of substituents on the arene's centroid-localized π-density and arene ESP maps.[44-45] Modern thought has simplified the system to consider only the local, direct interactions of the substituent on the ring centroid, and the closest end of the other ring (**Figure 5.1.3**). Clearly, the origin of these

interactions is still an evolving debate and we seek to provide additional case studies to the matter.

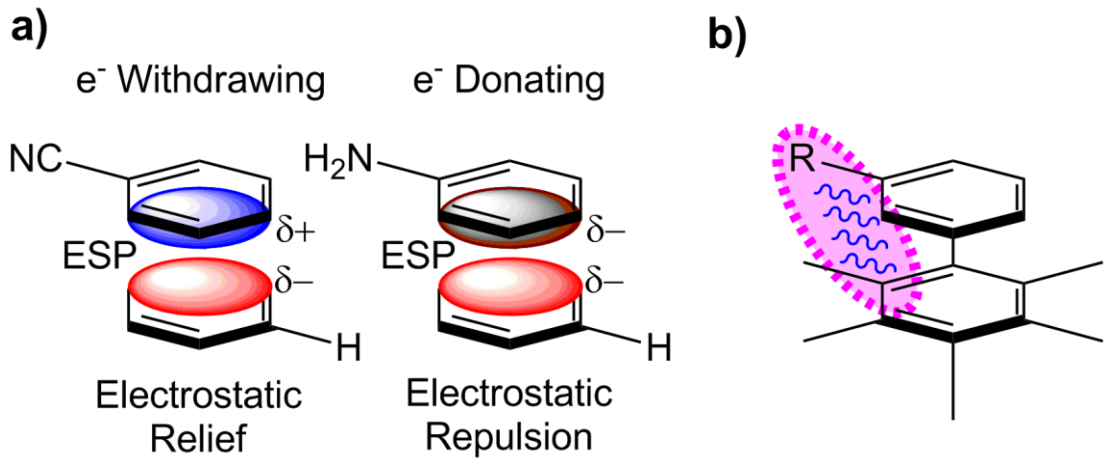

Figure 5.1.3 How substituents influence π-stacking; old model vs new model. **a)** *Left*, prevailing view of substituent effects where an electron withdrawing group will relieve electrostatic repulsion, and electron donating group increases repulsion. **b)** *Right*, Modern consensus where only the substituent and closest end of other ring are considered when comparing substituent effects in stacking interactions; changes to the other parts of the two rings can be ignored.

5.1.4 CH/π Interactions

In addition to direct arene π-π interactions (e.g., T-Shape, slipped stack, etc), another prevalent π-interaction mode involving arenes is the CH/π interaction, which has been thoroughly described and modeled theoretically, as well as experimentally, by Nishio and others.[47-60] As the name would suggest, evidence began to accumulate concerning an attractive force, not a bond, between C-H groups, and sites of π-electron density.[61-62] An early series of conformational studies on aryl compounds bearing an aliphatic group showed that the alkyl group preferred synclinal orientations with respect to the arene. Since these initial discoveries the CH/π interaction has been studied *via* X-ray, NMR, IR, dipole moment measurements, and circular dichroism, and has been

encountered in a number of different physical modes and orientations (**Figure 5.1.4**).[63-64] These interactions have been shown to stabilize interacting ring systems and substituents, such as sugars, proteins, intermediates, and others.[51, 54, 56, 60] Extensive work concerning the cartography of CH/π interactions has detected the interaction occurring at many points around arenes, and also at a variety of distances from the accumulated π-density, ranging from 2.1 Å to upwards of 3.6 Å.[57-59] The distance dependence is primarily based on both the electronics of the ring and the acidity of the interacting hydrogen, similar to hydrogen bonding polarization. When describing and investigating systems which involve numerous arenes, such as proteins, not only are potential arene π-π interactions important to consider, but the diverse possibility and participation of CH/π interactions (and even RX/π interactions[27, 44, 50, 64]) must also be considered.

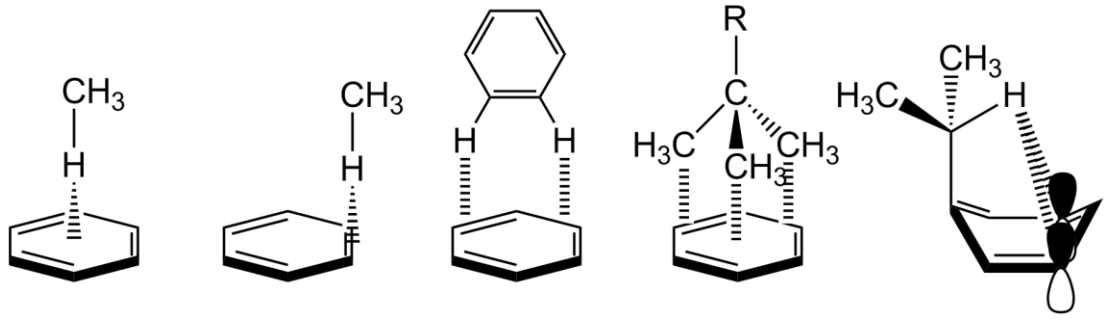

Figure 5.1.4 Various modes and sources of CH/π interactions on an aryl ring. Multiple H atoms can interact simultaneously with multiple sp^2 atoms, and single hydrogen atoms may position themselves to optimize π-interaction on all surfaces.

5.1.5 π-Interactions in Ammonium Carboxylate Solids

Apart from the constituents of proteins and others, another system exists which contains an isolated and broad array of potentially interacting aryl rings by way of π-π interactions (i.e., T-Shape, slipped/offset) and CH/π interactions; even so, one that has been fairly recently discussed...

In Chapter 4 we introduced and discussed a vast collection of systematically substituted (and essentially tethered to a substrate) benzylamines and phenethylamines that are fundamentally granted full freedom of movement to interact with their surroundings, within the interlayer space. This original system will serve as an interesting host of materials to study in virtue of the varied π-interactions that have been introduced. These ammonium formate structures are unique and interesting materials to analyze in this regard because their resulting π-interactions are specifically isolated to the interlayer space, so as to compartmentalize their behavior.

Having recently investigated the physical crystal structures of ammonium formates featuring aromatic substituents, it became clear that there were some similarities between these structures and those of ammonium HPzDCA.[2-3, 65] We seek to report an analysis of the crystal structures of a series of benzylammonium formates, and compare them to analogous benzylammonium HPzDCA compounds, especially so the π-interactions between the constituents of each material. The subsequent comparison of the π-interactions in each series will allow us to evaluate which types of π-interactions are most favorable.

5.1.5.1 Classification of π-Interactions in this Work

This work is a purely empirical case study of how substituents organize and arrange when given the opportunity to interact and self-assemble. By isolating the aryl groups to the interlayer space between the hydrophilic substrates, they are free to interact with each other to their best advantage. Do the arene groups adopt the same π-interactions between each structure? For the purpose of this chapter's discussion the different modes of π-interaction will be described as five separate *types* (**Figure 5.1.5**), sometimes denoted by π^x, where *x* indicates the designated type number:

Type 1: The direct, face-to-face π-interaction of two proximal aryl rings.

Type 2: The edge-on-to-face T-shaped π-interaction between two proximal aryl rings.

Type 3: The slipped, offset ring-to-ring π-interaction as a C-H···π interaction.

Type 4: The interaction of a benzyl carbon to a proximal aryl ring's centroid.

Type 5: The C-H···π interaction of a *substituent* carbon to a proximal aryl ring's centroid.

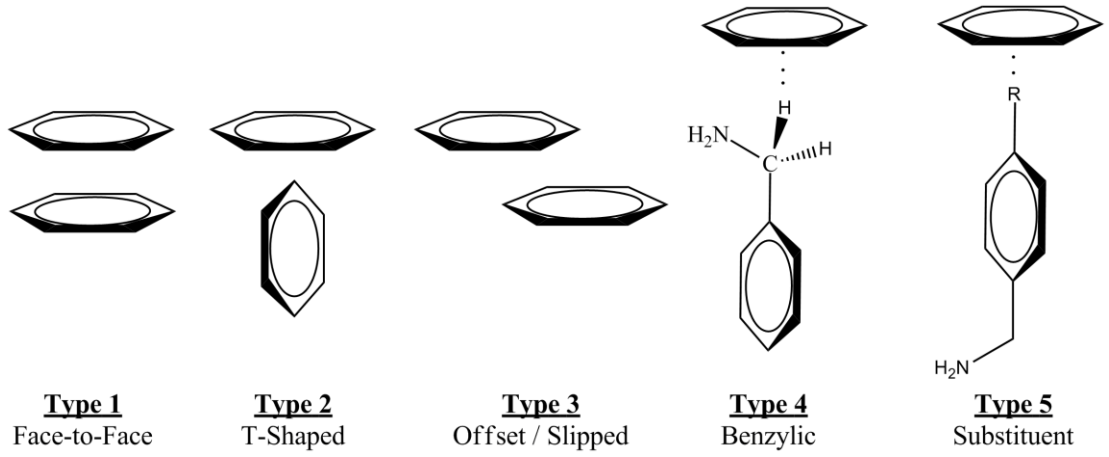

Figure 5.1.5 The various classifications of π-interactions, as *types*, discussed in this report.

5.1.6 Structural Differences in 2-Dimensional Structures Ammonium Formate

As with each ammonium formate discussed in Chapter 4, the ammonium HPzDCA complexes, generated and discussed previously by the Beatty group, abide the general layering protocol previously examined; each synthon pair forms a lamellar, layered solid, that is effectively described by its interdigitation, substrate shape, and layering pattern.[2-3, 65-67] This leaves the only difference between the ammonium complexes in this chapter down a single synthon, the identity of the anion; formic acid versus 3,5-pyrazoledicarboxylic acid (**Figure 5.1.6**).

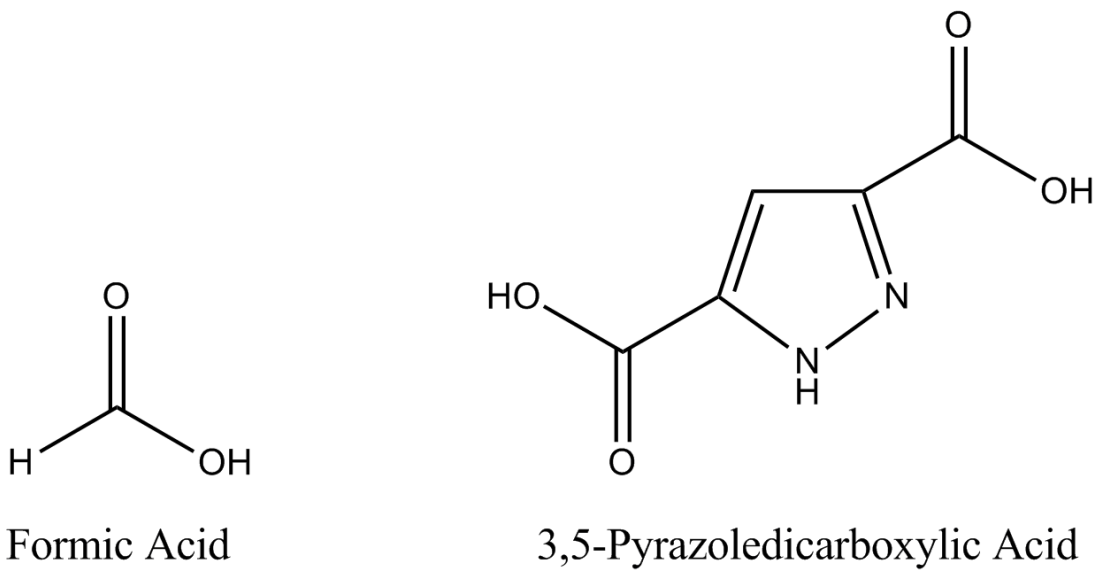

Figure 5.1.6 Side-by-side visual identification of the two anions featured in this study.

5.1.6.1 The Anion's Role in Layer Formation

The differences between these two synthons is the overall size of the molecule, the number of carboxylate sites, and the presence of a heterocyclic ring in HPzDCA. Structurally, based on Etter's rules[68] and observations made in Odendal's report on ammonium carboxylates[69] (discussed here and Chapter 4), the following 2-D layers would be expected from the larger-anion, ammonium HPzDCA compounds:

1. The cation will be protonated and form a hydrogen-bonded sheet as per Etter's rules
2. A 'stack of nets', i.e., bilayer sheet will assemble due to the large anion

As an exercise; if the guidelines are reliable, each ammonium HPzDCA compound discussed in this chapter should assemble as an ABA-type, based upon our previous ammonium carboxylate predictive methods. As shown below, with the exception of the naphthalene containing material **8***, this is the case for these ammonium HPzDCA structures, but an additional impact of the anion should be discussed. As discussed in the previous chapter, the anion's size,

linked to its flexibility within the substrate, will impact the assembly and shape of the hydrophilic substrate. The rigid ring in HPzDCA, for example, will result in a reduction of the rotational tolerance in the substrate and as a result, flatter sheets will be observed compared to those of ammonium formates.

5.1.6.2 The Anion's Impact on Pillar Organization

The size of the anion within the sheet has an impact on the spatial density of the pillars. Generally, each pillar's cationic ammonium moiety sits in the middle of four anionic constituents (**Figure 5.1.7a**). Based on the size of the anion, the distance from cation to cation, and as a result the pillar-to-pillar distance, is increased going from formate to HPzDCA. For example, between benzylammonium formate, **1**, and benzylammonium HPzDCA, **1***, the anion size increases and in turn the distance from cation to cation increases by up to 4 angstroms (**Figure 5.1.7b**). As a result, the pillar-to-pillar distance also increases, and we encounter different physical layer behavior between **1** and **1***. This gives rise to observable differences in the interlayer space between **1** and **1***, which invariably leads to changes in each pillar's physical environment, and thus the extent of their potential interactions with other pillars. For this study, we shall evaluate the impact of the additional separation between pillars on the total, and type of, intermolecular π-interactions present between pillars within the interlayer region of these solids.

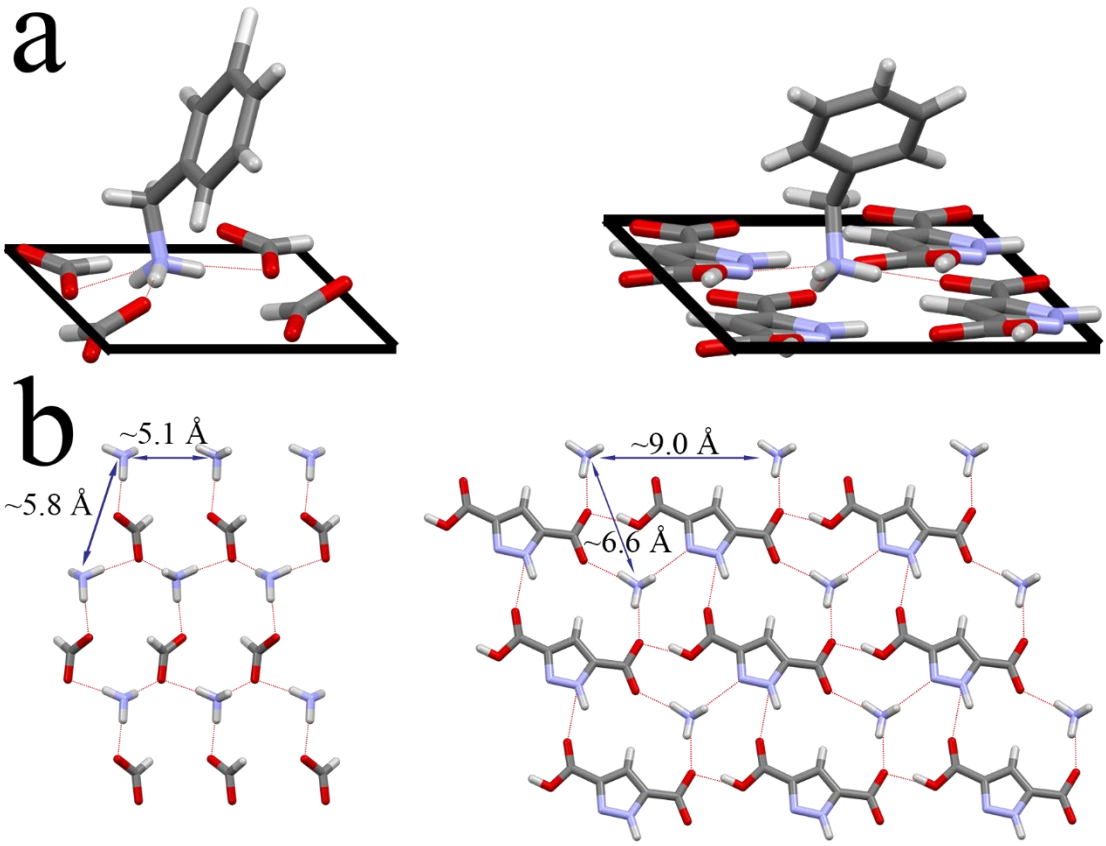

Figure 5.1.7 Ionic environment for ammonium formates and ammonium HPzDCA. **a**) *Left*, cation-anion domain for **1**, benzylammonium formate. *Right*, cation-anion domain for **1***, benzylammonium HPzDCA. **b**) *Left*, top-view of hydrophilic sheet for **1**. *Right*, top-view of hydrophilic sheet for **1***. *Note: In each figure, dark grey tubes represent carbon atoms, light grey tubes represent hydrogen atoms, amber tubes represent bromine atoms, green tubes represent chlorine atoms, yellow-green tubes represent fluorine atoms, purple tubes represent iodine atoms, light blue tubes represent nitrogen atoms, and red tubes represent oxygen atoms*.

5.1.7 Trends in 2-D Ammonium Carboxylate Interlayer π-Interactions

In order to assess and predict how arenes might interact in these ammonium carboxylate solids, a series of *similar* hydrogen-bonded layers of ammonium carboxylates[69-78], and guanidinium sulfonates,[79] from the CSD were analyzed. In these reported literature compounds,[80] some consistent trends in arene π-interactions were identified and observed. Individually, the observed types of π-interactions between pillars within the interlayer region of these literature compounds could be described using the classification system explained above. However, it also became clear that the interlayer pillars were systematizing *via* one or more types simultaneously, which has further implications.

5.1.7.1 Partnered and Chained Interlayer π-Interactions

Through this systemization, two basic types of interlayer pillar cooperativity were detected: a chained-type of cooperation, where one or more π-interaction type handshakes from pillar to pillar infinitely, and a partnered-type of cooperation, where two pillars share reciprocated, or paired, π-interactions. The type of interlayer pillar π-cooperation is dependent on the distance between pillars within a layer, distance A (sometimes referred to as intra-sheet distance), and between layers, distance B (sometimes referred to as inter-sheet distance) (**Figure 5.1.8**). Of the chained-type of cooperation, four distinct modes were observed: a diagonal zig-zag shape (**Figure 5.1.8**), a sawtooth pattern (**Figure 5.1.10**), a direct columnar shape (**Figure 5.1.9b**), and finally an omnidirectional mode, where the π-interaction chains through the entire pillar region (**Figure 5.1.9a**).

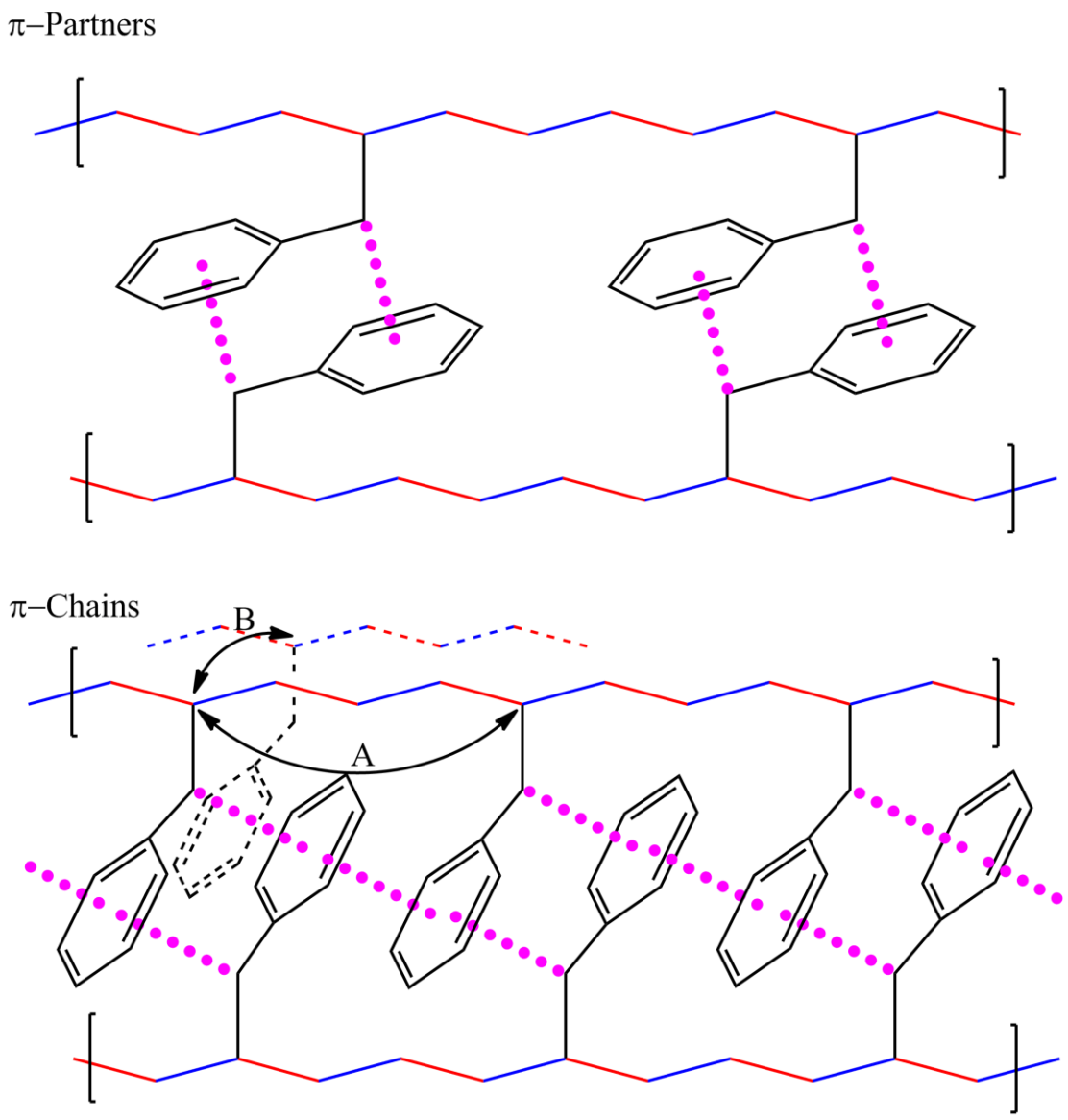

Figure 5.1.8 π-Partners and π-chains. A representation of the paired vs. chained interlayer pillar π-interactions. *Top*, generalization of paired "π-partner" interactions in the pillared region, in this case by reciprocated type 4 interactions. *Bottom*, generalization of the infinite "π-chain" interactions in the pillar region, here induced by type 3 and 4 interactions (diagonal zig-zag). Also describing the 'A' distance between pillars in a chained series, and 'B' distance. Purple balls indicate arene π-interactions (i.e., σ-π and C-H···π).

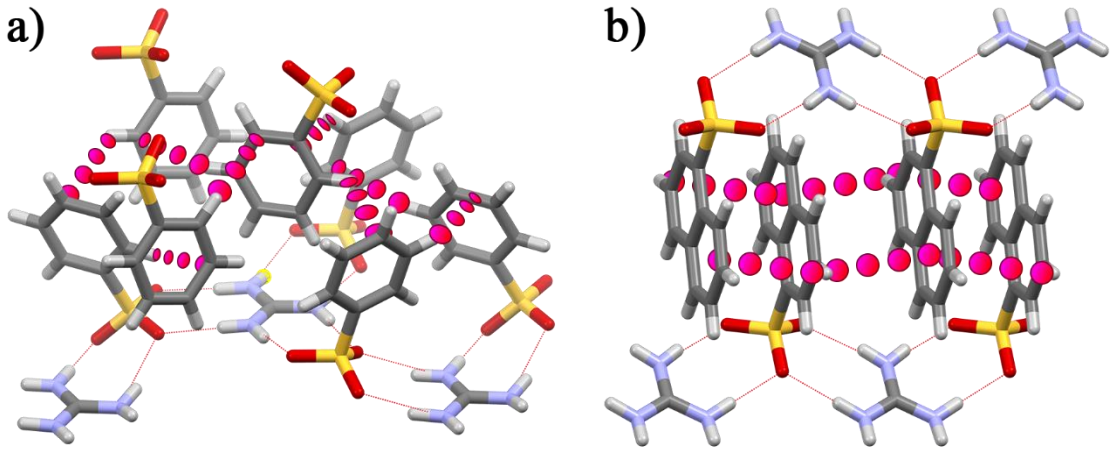

Figure 5.1.9 Omnidirectional and columnar π-chains. *Left*, **a**, overhead view along the A-axis showing the omnidirectional π-chain present in guanidinium benzylsulfonate *via* type 2 π-interactions (Refcode: WETPIU). *Right*, **b**, the columnar π-chain present in guanidinium 1-naphthylsulfohate *via* type 3 π-interactions, viewed down the B-axis, and rotated 75° along the Y-axis (Refcode: WETPOA).[79] *Note: The visualization of arene π-interactions is assisted via drawn-in pink/red balls, representing intermolecular π-interactions, placed between molecules connecting sites of π-interaction.*

5.1.7.2 Specificity of π-Chaining

The specific mode of π-chain is typically conditional on the π-interaction types present; such as the chain of type 3 π-interactions which generally results in columnar chains, chained T-Shape type 2 π-interactions generally result in omnidirectional π-chains. Moreover, different combinations of π-interaction types will result in the other types of chains, i.e., the combination of type 3 and 4 π-interactions generally results in diagonal zig-zags, and the combination of type 2 and 4 π-interactions generally results in sawtooth chains. However, for the purpose of this discussion, these materials will typically be designated as pillars that chain, and those that do not; the individual π-chain mode will be stated in instances which necessitate the specificity.

5.1.7.3 Spatial Allowance of π-Chains

The incidence of π-chaining appears linked primarily to: the separation between pillar moieties, pillar interdigitation, and the pillar's ability to span an appreciable distance to interact with an adjacent pillar (usually accomplished *via* arenes with long substituents, e.g., methoxy, ethoxy, etc.). To a lesser extent, the angle of the arene with respect to the sheet, from orthogonal-90° to parallel-0°, has an impact on the chaining outcome but with much less frequency.

Based upon what is normally encountered in the CSD, the size of the ions in the sheet has a direct impact on the pillar spacing, and therefore affects the incidence of π-chaining. The generic assignment 'ion' is used in this case because the base of the pillar moiety, as it associates with the sheet, may be anionic or cationic, and the orthogonal complementary synthon in the sheet will be the opposite ion. The effect is not isolated to only the anion, or only the cation. For example, in ammonium carboxylates the base of the pillar is the cationic ammonium moiety, and the complementary sheet synthon is the carboxylate anion.

We see from the data in **Table 5.1.1** that as the distance increases from one pillar to its two adjacent neighbors, one in each direction in two dimensions (A and B distances), the incidence of π-chaining decreases. Generally, when the distance between both adjacent pillars is within ~8.20 angstroms, π-chains appear much more favored. Alternatively, as the distance between a pillar and one of its neighbors approaches 9 angstroms and beyond, the ability to π-chain from pillar to pillar diminishes, and the formation of π-partners is favored.

There are some physical variables which may assist the π-chaining incidence, especially interdigitation and substituent assistance, which aid in chaining together pillars that are at extensive distances. The results of the data accumulated from CSD sources and searches is condensed in **Table 5.1.1**.

REFCODE	ANION	CATION	Axis & Pillar Distance A/ B	*i*
π-Chains				
YABFEO	Benzoate	NH_4^+	A 7.05 / 4.77	-
YABGIT	Acetate	Benzylammonium	B 5.42 / 8.00	✓
YABGOZ	Propionate	Benzylammonium	B 8.13 / 5.89	✓
WETPIU	Benzylsulfonate	Guanidinium	A 6.90 / 7.50	✓
WETPOA	1-Naphthylsulfonate	Guanidinium	B 7.10 / 7.39	✓
WETPUG	2-Naphthylsulfonate	Guanidinium	A 6.79 / 7.50	✓
LAYCAP	Hexanedioate	Benzylammonium	B 5.53 / 4.86	-
LAYJUQ	Hexanedioate	4-Methoxybenzylammonium	C 10.86 / 5.60	✓
LAYGAT	Hexanedioate	3-Methylbenzylammonium	B 5.73 / 5.73	✓
TEWXIC	Malate	3-Methylbenzylammonium	C 8.38 / 8.21	✓
XINSAO	Malate	Benzylammonium	B 6.79 / 7.97	✓
TOHXOE	3-Iodobenzoate	Benzylammonium	B 4.51 / 10.54	✓
AJUMOH	Ethandioate	Benzylammonium	C 8.26 / 5.64	✓
NOJWOY	Malate	3-ChloroBenzylammonium	C 6.34 / 7.50	-
SOVXAD	Terephthalate	4-Methylbenzylammonium	B 10.56 / 6.39	✓
SOVXOR	Terephthalate	4-Methoxybenzylammonium	B 10.70 / 6.04	✓
π-Partners				
NOJWEO	Malate	4-Methylbenzylammonium	A 7.52 / 6.22	-
NOJWIS	Malate	4-Chlorobenzylammonium	A 7.51 / 6.24	-
SOVWOQ	Terephthalate	Benzylammonium	B 10.48 / 6.32	✓
SOVXUX	2,6-naphthalenedicaroxylate	4-Methoxybenzylammonium	B 12.28 / 6.37	✓
SOVXEH	2,6-naphthalenedicaroxylate	4-Methylbenzylammonium	B 12.44 / 6.47	✓
SOVWUW	4,4'-(1,2-hydrazine)bis-benzoate	Benzylammonium	B 16.31 / 6.45	✓
PEBDUW	4-hydroxymethylbenzoate	Benzylammonium	A 9.85 / 6.65	✓
SEJSOP	Malonate	Benzylammonium	A 8.79 / 5.46	✓

Table 5.1.1 Collation of the π-interaction and pertinent physical layer parameters from CSD data. Pillar distance measures the distance between the two nearest pillars. *i* = interdigitation.

5.1.7.4 Special Case π-Chains

There are a few outliers in this data. In NOJWIS and NOJWEO, which form π-partners, and NOJWOY, which forms π-chains in the interlayer space, one might notice that the pillar separation is near identical between the three complexes. Neither of the structures interdigitate, so why is there a difference between their cooperative π-interaction mode? In NOJWIS and NOJWEO, the substituent in the *para* position is actively preventing interdigitation, and in lieu of

interdigitating, the arene components of the ABA-type layer align and stack like a sandwich, isolating their π-interactions to those of pairs. However, in NOJWOY, the *para*-position of the arene is occupied by a hydrogen which participates in a T-Shape C-H···π interaction with the ring opposite its position; and the interaction forms a chained sawtooth shape, i.e., a π-chain down the length of the layer in an alternating fashion (**Figure 5.1.10**). As a result, the arenes π-chain and align in an anti-parallel fashion.

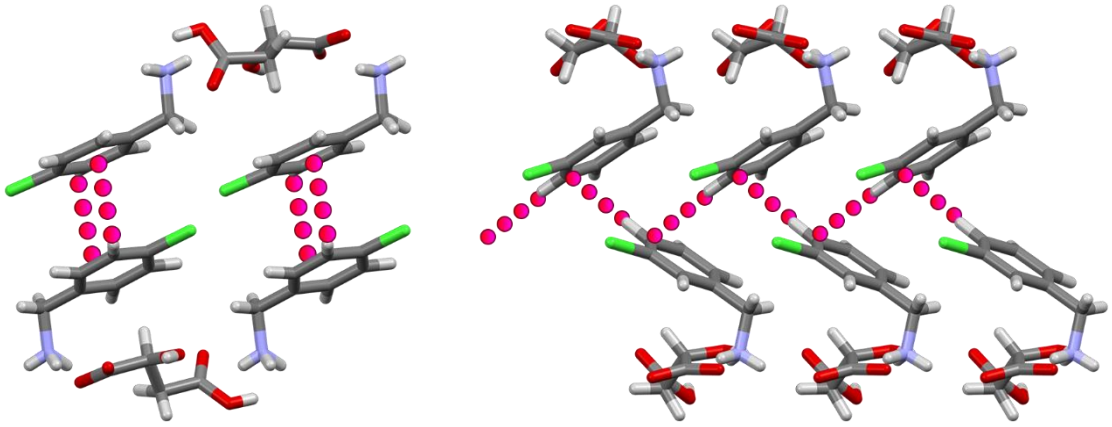

Figure 5.1.10 Substituent position effects. 4-Chloro π-partners vs 3-chloro π-chains. Demonstrating how the accessibility of T-Shape C-H···π interaction may provide support for chaining π-interactions in NOJWOY, *right*, and prevent chaining in NOJWIS, *left*.[78]

The four more extreme distance cases, LAYJUQ, TOHXOE, SOVXOR, and SOVXAD, where the pillar separation in one direction is over 10 angstroms, the π-chain is dependent on a specific situational parameter. In LAYJUQ, the chain is at the extent of π-interaction by a type 4 interaction with the B pillar, 5.60 angstroms away; the two units are very contorted to allow this chain. In TOHXOE, the 10.54 angstrom distance between the 'pillars' is made irrelevant due to the anion in this case also containing an arene moiety that participates as a pillar in the interlayer region, supplementing the π-chain. Finally, for SOVXOR and SOVXAD, a sawtooth chain *via* type 4 interactions allows π-chains in the later (similar to NOJWOY), and the length of the

substituent in the former allows the π-chain to continue by spanning the distance between pillars. In instances where the A and B distance between pillars seems too great to allow it, π-chaining is usually possible by some special molecular action.

5.1.8 Prediction of Interlayer Arene π-Interactions

Between this broad array of ionic layered 2-D materials, the ability to designate a *strict* set of rules that apply to all ammonium carboxylates is unlikely. Perhaps more feasibly, these materials are best compared on a *per specific* anion/cation basis. Nevertheless, based upon the above literature examples, interdigitation seems to have a role which is critical for π-chains, effectively serving as a bridge between distant pillars of the same sheet (A pillars), except when the range between pillars increases past 10 angstroms. Additionally, *meta*- and *para*-substituted arenes that are not interdigitating, are likely sandwiched and form π-partners, as well as in those pillars that are separated by 9 angstroms and above.

By applying these basic principles to the ammonium carboxylates reported in this chapter; it is likely that the ammonium *formates* will feature more instances of π-chaining than will be encountered in the ammonium *HPzDCA* structures based upon the close pillar to pillar distance in the ammonium formates versus the analogous ammonium HPzDCA compounds. Additionally, based on the established lack of interdigitation encountered in the ammonium HPzDCA compounds, π-partner interactions will be even more favored in these complexes.

5.1.9 The Objective

The objectives of this work serve as an extension to the third specific objective posed in Chapter 1 which asks if we can compare the crystal structures of these ammonium formates to other ammonium carboxylates. Here we continue to compare the crystal structures reported in the previous chapter, but we change focus and compare some of the weak forces which are present

between pillars within the interlayer space of these 2-dimensional architectures, and other ammonium carboxylates.

Additionally, through the analysis and comparison of the weak forces present in these structures, we hope to make some conclusions regarding the broad origin and preference of π-interactions in arene containing structures.

Based upon what has been established through literature reports and similar structures studied *via* the CSD, the **hypothesis** for this work is that the interlayer arene components of each ammonium carboxylate material will orient and arrange such that type 2-5 interactions will be favored, and face-to-face type 1 interactions will not be encountered. Additionally, we predict that the π-interactions demonstrated in the ammonium formate complexes will differ from their analogous ammonium HPzDCA complexes due to the shorter pillar to pillar distances, as implied by the cation separation in the sheet.

Specifically, as per the literature examples, we **hypothesize** that the ammonium formates will all form π-chain type layers due to the short A and B distance between pillars, whereas the ammonium HPzDCA solids, with the much larger linking anion (relative to formate), will find their potential for forming π-chained interlayer pillars reduced, instead forming π-partners. We predict that interdigitation will play an important role in ammonium HPzDCA structures with respect to encountering π-chains or partners. It is likely that only the benzyl- (**1***), and 2-methylbenzylammonium (**2***) HPzDCA structures will feature interdigitated pillars and proceed to form interlayer π-chains; compared to the ammonium formates, which should all π-chain.

Herein, we head into the final sections of this manuscript to discuss the subtle π-interactions that are present between the arene containing pillars within the interlayer space of previously described ammonium carboxylates!

5.2 Experimental

All chemical reagents were used as received from Sigma-Aldrich without further purification. All solvents used, except ethanol, were distilled prior to use. 200 proof USP-specification ethanol was used as-is. All crystallization was performed at room temperature in a low-vibration area. Melt point data were collected on an OptiMelt Automated Melting Point System operating in the range of 28-300 °C, heating at a rate of 2.5 °C per minute. Additional X-ray crystallographic tables can be found in Appendix II.

CSD searches were carried out using the ConQuest 1.19 program which is part of the Cambridge Crystallographic Data Centre (CCDC) software suite.[4] Searches were filtered for organics which had 3-D coordinates determined. The resulting hitlist was combed to identify layered structures containing a substituted benzylamine and carboxylic acid. Manual inspection for ring stacking and interaction occurring in each structure was performed using the crystal visualization program, Mercury, which is part of the CCDC software suite. Surveying interlayer arenes and their adjacent neighbors within the van der Waals radius, i.e., short contacts, of their constituents are suspect of participating in ring-to-ring π-interactions. Visual inspection of a reliable crystal structure, while maintaining focus on established π-π, σ-π, and CH/π interaction thresholds, i.e., within appropriate atomic distance for interacting π clouds, is a powerful tool in confirming the presence of different forms of π-interaction.

Safety. Extreme caution should be taken in the use of formic acid. Formic acid presents a strong danger upon skin contact as well as contact *via* the readily produced vapors. The reader is cautioned and referred to the formic acid International Chemical Safety Card which can be found on the Center for Disease Control's (CDC) website at www.cdc.gov.

5.2.1 Synthesis

Synthesis for all materials is as discussed in Chapter 4 for the following amines: benzyl (**1**), 2-methylbenzyl (**2**), 3-methylbenzyl (**3**), 4-methylbenzyl (**4**), 4-methoxybenzyl (**5**), 3-chlorobenzyl (**6**), 4-chlorobenzyl (**7**), and 1-naphthylamine (**8**). The synthesis for each compound will be reiterated below for convenience and to accommodate a different numbering scheme. The synthesis for the analogous ammonium HPzDCA compounds, designated by a *****, was completed previously as discussed in older publications by the Beatty group (**1***-**7***,[2] **8***[3]) and whose structures can be found on the CSD *via* the following Refcodes: **1***, benzylammonium HPzDCA (XOVTIL), **2***, 2-methylbenzylammonium HPzDCA (XOVTUX), **3***, 3-methylbenzylammonium HPzDCA (XOVVOT), **4***, 4-methylbenzylammonium HPzDCA (XOVVUZ), **5***, 4-methoxybenzylammonium HPzDCA (XOVVAF), **6***, 3-chlorobenzylammonium HPzDCA (XOVVIN), **7***, 4-chlorobenzylammonium HPzDCA (XOVVEJ), **8***, 1-naphthylethylammonium HPzDCA (QUCSIR).

Generally, synthesis of all materials involves combining stoichiometric amounts of formic acid and target primary amine acceptor in 1 mL of solvent in a 7 mL scintillation vial at room temperature. The solutions are lightly swirled, loosely capped, and left undisturbed to crystallize *via* solvent evaporation. Double, and half, stoichiometric amounts of acid and base were also investigated, and the ratio which gave the best crystals is noted below, along with the specific synthesis of each material.

Specifically, for each compound**:** 10 µL of formic acid (.265 mmol) is added to a small vial containing 1 mL solvent (ethanol (**1**-**6**), methanol (**7**), toluene (**8**)) and gently swirled. To this solution is added substituted benzylamine, $C_7H_6NH_2$**R**, where **R** is a substitution to the ring (**R** = H (**1**), *o*-CH_3 (**2**), *m*-CH_3 (**3**), *p*-CH_3 (**4**), *p*-OCH_3 (**5**), *m*-Cl (**6**), *p*-Cl (**7**)) or 1-(1-naphthyl)ethylamine (**8**) in a 1:1 (**3**-**5**), 1:2 (**1**, **6**) or 2:1 (**2**, **8**) molar formic acid: amine ratio (58 µL (**1**), 17 µL (**2**), 33 µL (**3**), 34 µL (**4**), 34 µL (**5**), 33 µL (**6**), 16 µL (**7**), 20 µL (**8**)). The mixed

solution is lightly capped and set aside to slowly concentrate, forming X-ray quality crystals as plates (**1**, **3**-**5**, **7**-**8**), or rods (**2**, **6**), in 90% (**1**, mp 79-94 °C), 95% (**2**, mp 118-124 °C), 90% (**3**, mp 86-93 °C), 90% (**4**, mp 140-143 °C), 99% (**5**, mp 115-117 °C), 93% (**6**, mp 100-103 °C), 97% (**7**, mp 142-147 °C), 99%, (**8**, mp 156-160 °C) yield.

5.2.2 X-Ray Crystallography

Crystalline samples of **1**-**8** were suspended in Paratone oil and subsequently mounted on a MiTeGen dual-thickness microloop. All data were collected using a Bruker Kappa or SMART Apex II X-ray diffractometer. A graphite monochromated Mo Kα (λ = 0.71703 Å) radiation at 100 K was used for all samples, except data for **2** and **4** which were collected at 298 and 273 K, respectively. Crystal structures were solved utilizing the OLEX2 software package[81] which functions using SHELX protocols.[82] Structure solution was achieved by way of direct methods and refined using least squares minimization which are both part of the SHELX-97 package. Brief crystal data for each compound is tabulated in **Table 5.2.1**, full sets of crystallographic tables for each compound may be found in Appendix II.

Compound	1	2	3	4
Molecular Formula	$C_8H_{11}NO_2$	$C_9H_{13}NO_2$	$C_9H_{13}NO_2$	$C_9H_{13}NO_2$
Molecular Weight	153.18	167.20	167.20	167.20
Crystal System	Orthorhombic	Monoclinic	Monoclinic	Monoclinic
Space Group	Pbca	$P2_1$	$P2_1/c$	$P2_1/c$
***a* (Å)**	8.5468(5)	6.9761(6)	16.9827(8)	17.090(8)
***b* (Å)**	11.0536(7)	7.6181(6)	4.8029(2)	4.909(2)
***c* (Å)**	17.5296(10)	8.3283(7)	11.5315(6)	11.565(6)
α (°)	90.0	90.0	90.0	90.0
β (°)	90.0	94.646(4)	103.947(3)	109.75(3)
γ (°)	90.0	90.0	90.0	90.0
Volume (Å^3)	1656.07(17)	441.15(6)	912.85(8)	913.10(8)
Z	8	2	4	4
T (K)	100(2)	296(2)	100(2)	273(2)
Reflections Measured	42345	11507	18011	15777
Unique Reflections	39249	11481	16747	14322
R_{int}	0.0355	0.0283	0.0298	0.0501
R_1 [I > 2σ(I)]	0.0354	0.0709	0.0365	0.0483
wR_2 [I > 2σ(I)]	0.0975	0.2021	0.0982	0.1261

Compound	5	6	7	8
Molecular Formula	$C_9H_{11}NO_3$	$C_8H_{10}ClNO_2$	$C_8H_{10}ClNO_2$	$C_{13}H_{14}NO_2$
Molecular Weight	181.19	187.62	187.62	216.25
Crystal System	Monoclinic	Monoclinic	Monoclinic	Orthorhombic
Space Group	Cc	$P2_1/c$	$P2_1/c$	$Pca2_1$
***a* (Å)**	6.7615(3)	16.7899(10)	16.7551(13)	6.9086(3)
***b* (Å)**	18.9173(7)	4.7766(3)	4.8441(4)	17.9665(7)
***c* (Å)**	7.8044(3)	11.5500(6)	11.4478(9)	9.1840(3)
α (°)	90.0	90.0	90.0	90.0
β (°)	105.9340(19)	104.162(3)	109.041(3)	90.0
γ (°)	90.0	90.0	90.0	90.0
Volume (Å^3)	959.90(7)	898.14(9)	878.30(12)	1139.95(8)
Z	4	4	4	4
T (K)	100(2)	100(2)	100(2)	111(2)
Reflections Measured	11996	22058	23525	27251
Unique Reflections	11804	20616	22168	25693
R_{int}	0.0230	0.0276	0.0190	0.0242
R_1 [I > 2σ(I)]	0.0272	0.0446	0.0231	0.0299
wR_2 [I > 2σ(I)]	0.0738	0.1072	0.0648	0.0793

Table 5.2.1 Table of crystallographic data for compounds **1-8**

5.3 Results

Each combination of formic acid and substituted benzylamine resulted in the ammonium formates **1**-**8**; and the previously published combination of HPzDCA and benzylamines resulted in the ammonium HPzDCA compounds **1***-**8***. For a more detailed discussion of the physical description of the ammonium formate layers please refer to **Section 4.3.1** of this dissertation. Please see Appendix I for the crystal structures of compounds that are not individually represented in this chapter.

5.3.1 Benzylammonium Formate Layering Patterns

Briefly, for compounds **1**-**8**, the following layer parameters were observed: AB-type layers with interdigitating pillars and undulating hydrophilic substrates were observed for compounds **1**-**2**, AB-type layers with non-interdigitating pillars and undulating hydrophilic sheets were observed for compounds **5** and **8**, and ABA-type layers with non-interdigitating pillars and flat sheets were observed for the remaining compounds **3**-**4**, and **6**-**7**.

5.3.2 Benzylammonium HPzDCA Layering Patterns

Each of the previously discussed ammonium formates have analogous ammonium HPzDCA structures which have been previously reported.[2-3, 83] The structures of these compounds are summarized here for convenience.

Compounds **1*** and **4*-5*** feature flat hydrophilic sheets, and interdigitating pillars (**Figure 5.3.1**), compounds **2*-3***, and **6*-7*** also show flat sheets, however the pillars are non-interdigitating (**Figure 5.3.2**), and compound 8* forms a unique structure with flat sheets, but with its pillared constituents only extending in a single direction (**Figure 5.3.3**). Each of these compounds forms a typical lamellar structure featuring an ABA pattern except **8***, which forms AB-type layers.

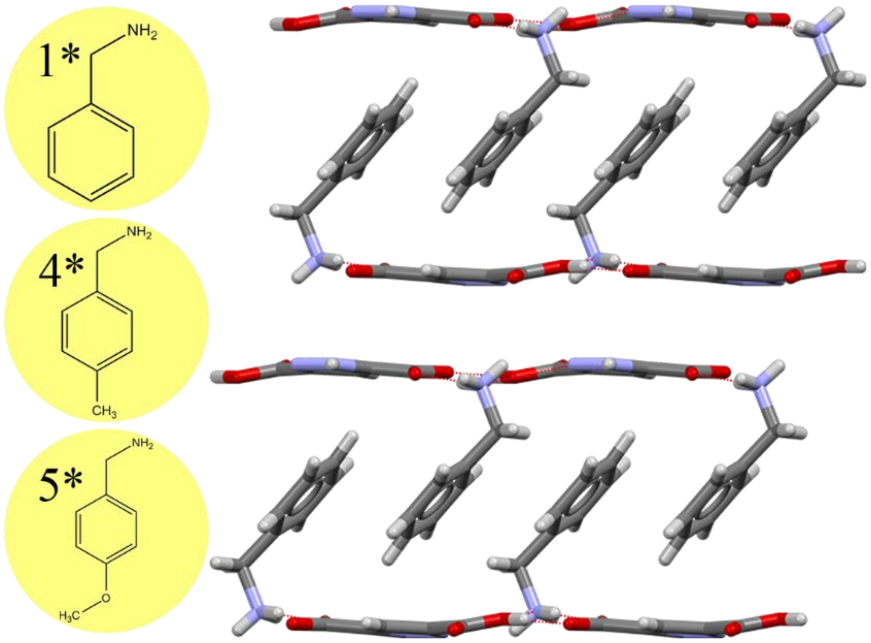

Figure 5.3.1 Layering pattern for compound **1*** (isostructural with compounds **4*-5***). Viewed down the A-axis.

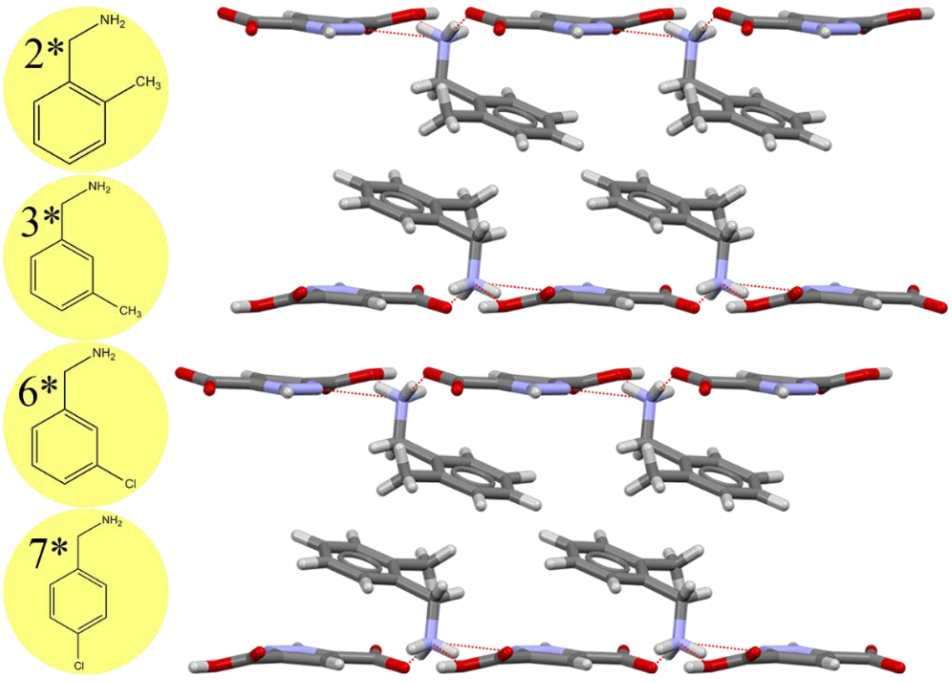

Figure 5.3.2 Layering pattern for compound **2* (**isostructural with compounds **3***, **6*-7*)**. Viewed down the A-axis.

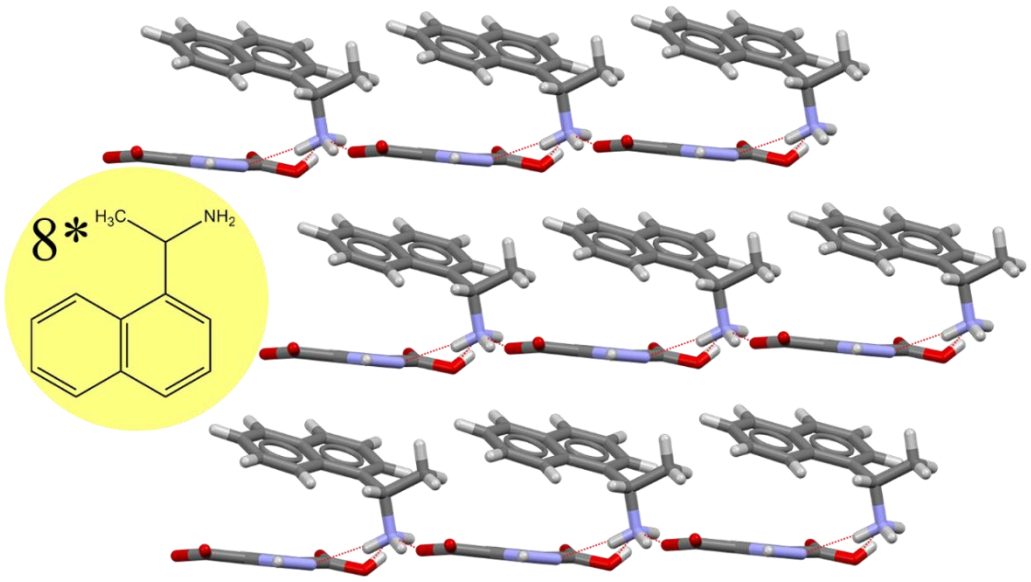

Figure 5.3.3 Layering pattern for compound **8***. Viewed down the A-axis, and rotated about the Z-axis 45°.

5.3.3 Benzylammonium Formate π-Interactions

The pillared components of each benzylammonium formate studied in this section participate in a chain of π-interactions, from a variety of types, from type 2 to 5. Anecdotally, the chained continuum of π-interactions has been lovingly termed 'conga-line π-interaction' and may be referred to as such henceforth. Generally, each pillar moiety participates in an overall total of four π-interactions *via* type 2, 3, 4, or 5 interactions, with the exception of compound **5**, which only participates in two total. These interactions are comprised of two π-interactions being 'received' by the ring face of the molecule, and two π-interactions 'contributed' by that molecule. The summation of all π-interaction types for compounds **1**-**8** are condensed in **Table 5.4.1**.

5.3.3.1 Compound 1 π-Interactions

For benzylammonium formate, **1**, Type 2 (T-shaped) and type 4 π-interactions (from the hydrogen of a benzylic carbon to the B pillar) can be observed π-chaining omnidirectionally

between the organic constituents of the pillar (**Figure 5.3.4**). The type 2 interactions form a 'conga-line' chain from molecule to molecule in the π-chained layer, and type 4 interactions are reciprocated by pillars behind it (transparent benzylamine in **Figure 5.3.4**). In an individual sense, each benzylammonium is contributing one type 2 & 4 π-interaction and also receiving one type 2 & 4 π-interaction from two separate benzylammonium molecules. Additionally, the undulating sheet in this compound appears to be the result of the pillars spatially optimizing to permit the chained continuum of π-interactions. In a flat sheet, the required alignment of pillars would not be satisfactory to allow for π-chains. So here we see the benzyl π-interactions are directing the shape of the hydrophilic sheet; as though the pillars associate, and pull the sheet into a wave.

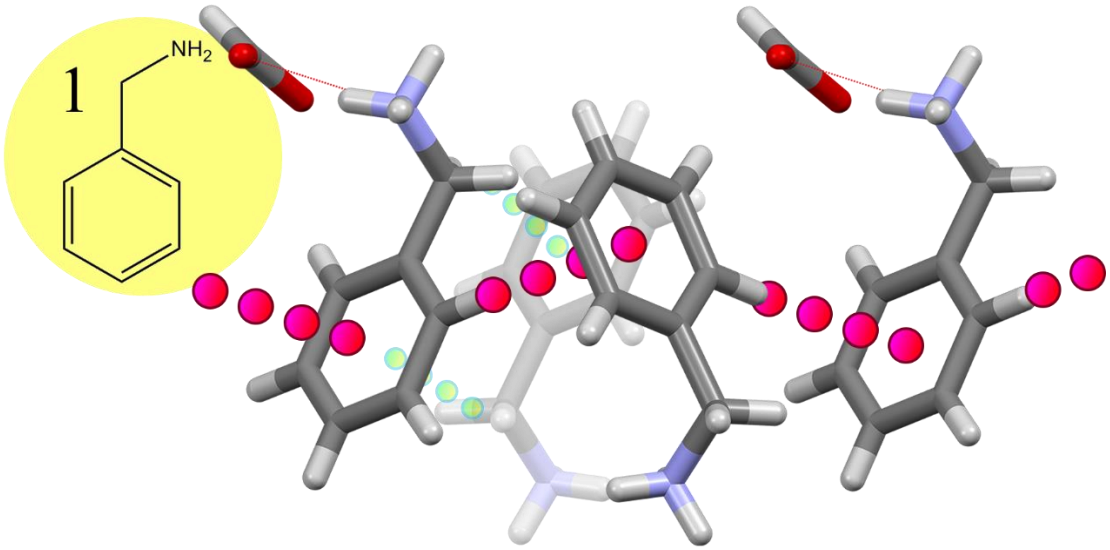

Figure 5.3.4 'Conga-line' type 2 π-interactions forming a chain in **1**. The type 4 π-interactions are reciprocated, represented by the transparent benzylamine and the smaller green balls. Viewed down the B-axis.

5.3.3.2 Compound 2 π-Interactions

In compound **2**, only type 5 π-interactions, between the *ortho*-methyl CH moieties and the proximal rings are observed in the interlayer region. Each methyl substituent of the methylbenzylammonium pillars sits between two adjacent ring centroids, within the distance threshold for CH/π interactions, contributing two π-interactions to two separate molecules, while itself being sandwiched between two CH/π interactions from two other methylbenzylammonium molecules (transparent molecules and green balls in **Figure 5.3.5**). This results in a columnar chain *via* a donor/acceptor continuum of π-interactions that persists throughout the structure.

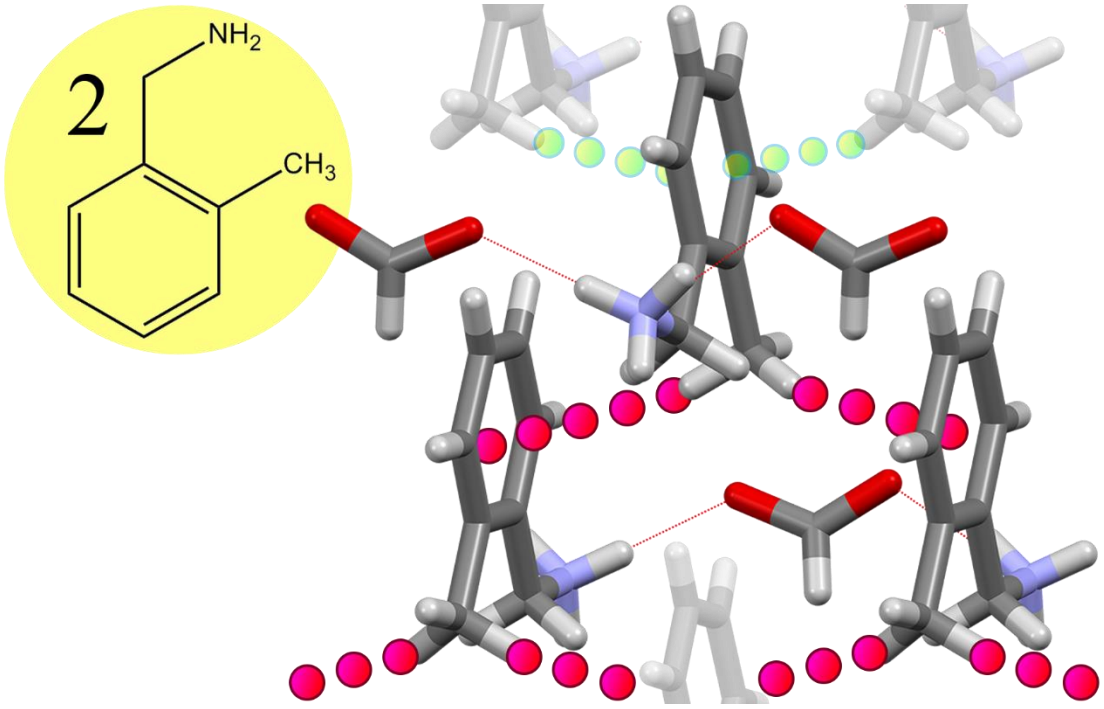

Figure 5.3.5 'Conga-line' type 5 π-interactions in **2**. Transparent and green balls represent further grown structure. Viewed down the C-axis, rotated 12° about the Y-axis.

5.3.3.3 Isostructural Compounds 3-4 and 6-7 π-Interactions

Compounds **3-4** and **6-7**, all participate in 'conga-line' π-interactions of a similar sort, where the continuum of π-interactions is propagated *via* two types of π-interaction in a diagonal, zig-zag fashion. In each case, the benzylic, type 4 interaction chains infinitely, connecting each benzylic carbon to the next closest ring; and in addition, whichever moiety occupies the *para*-position of the ring participates in a chained π-interaction with the adjacent ring. For compounds **3** and **6**, the *para*-position is occupied by a hydrogen, making the interaction a type 3, slipped stack π-interaction (**Figure 5.3.6**); and in compounds **4** and **7**, the *para*-position is occupied by the benzylamine's **R**-group, making the interaction a type 5 substituent C-H···π interaction (**Figure 5.3.7**). On an individual level, each molecule in **3-4** and **6-7** participates in four total π-interactions; where a pillar molecule both contributes and receives a type 4 interaction, and similarly, a type 2 (**3**, **6**) or a type 5 (**4**, **7**) π-interaction. Technically, the type 5 interaction in **7** is that of a CH/anion interaction,[84-85] but based on the conditions and environment, the nature of this interaction behaves similar to a CH/π interaction.

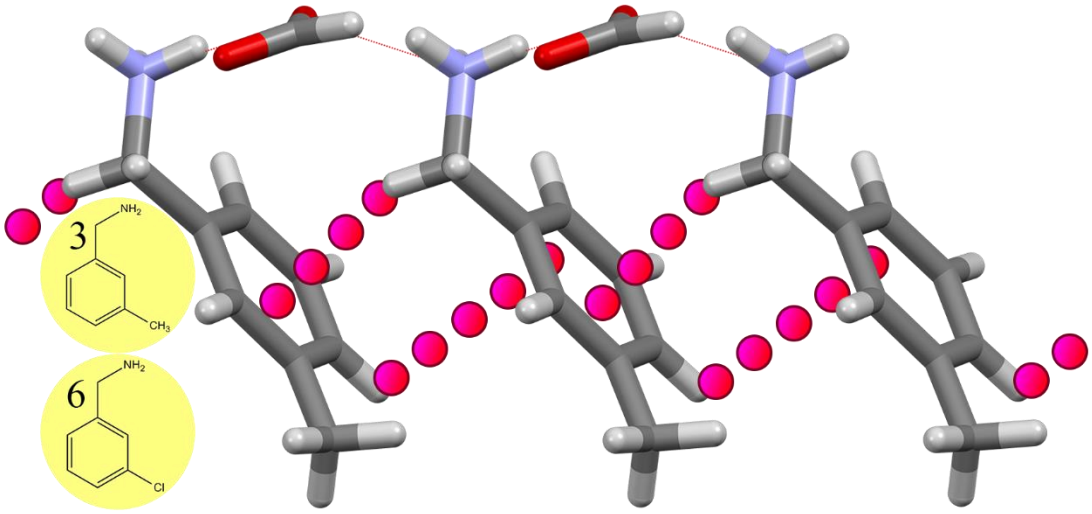

Figure 5.3.6 'Conga-line' type 3 & 4 π-interactions in **3** (isostructural with **6**). Viewed down the C-axis.

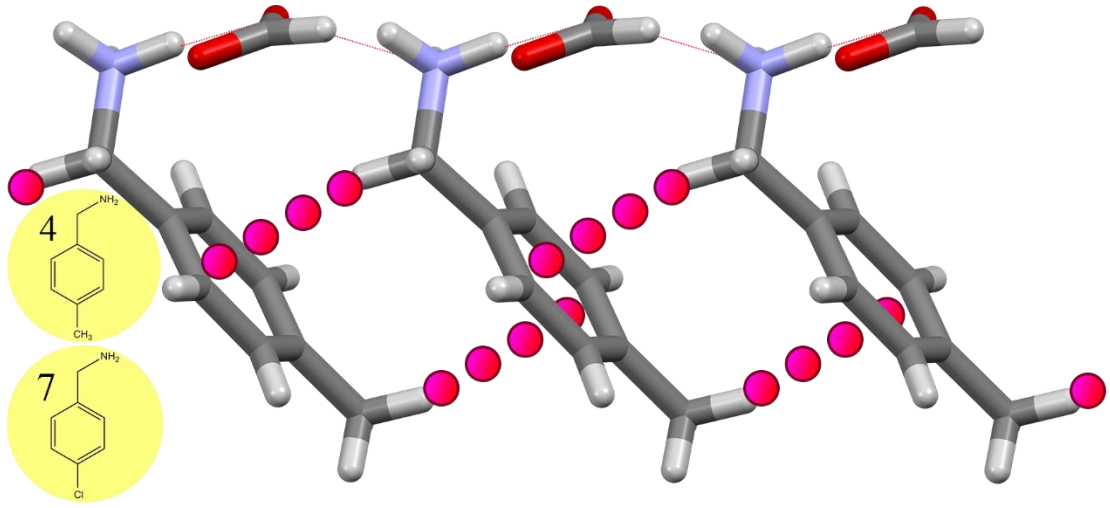

Figure 5.3.7 'Conga-line' type 4 & 5 π-interactions in **4** (isostructural with **7**). Viewed down the C-axis.

5.3.3.4 Compounds 5 and 8 π-Interactions

Like compound **2**, compounds **5** and **8** participate in the π-chained type 2, T-shape π-interaction that processes down the pillar region of the layer (**Figures 5.3.8** and **5.3.9)**. In **8**, the remaining two of the four expected π-interactions are satisfied by two additional type 2 interactions with the layers behind the pillar resulting in an omnidirectional π-chain. Compound **5** is unique in that it only displays two type 2 interactions per molecule, π-chained in a sawtooth mode, but no additional interactions between the constituents of the interlayer region are observed. However, there appears to be contribution from the substrate, as the C-H of the formate in the sheet points directly to the centroid of the benzyl ring of the pillar. However, investigating the pillar-to-substrate π-interactions is not a facet of this investigation. As in compound **1**, the undulating substrate of **5** and **8** seems to be a direct result of the pillar moieties coming into contact to optimize their π-interactions. It appears that the pillar moieties will orient and arrange in order to achieve ideal π-interaction conditions, locking into position and forcing the substrate to move with those pillar interactions.

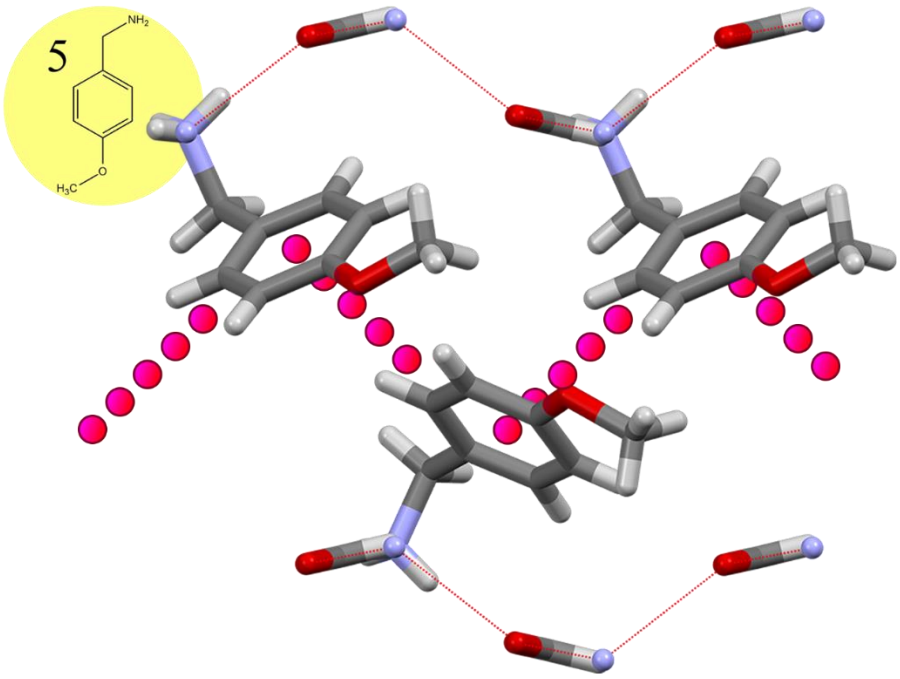

Figure 5.3.8 'Conga-line' type 2 π-interactions in **5**. Viewed down the A-axis.

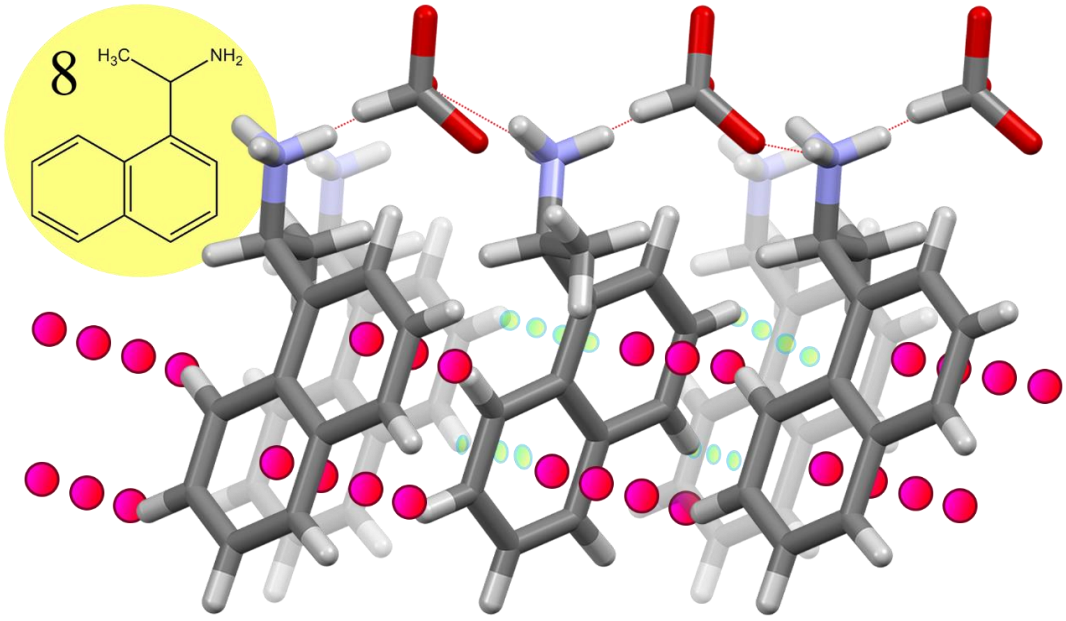

Figure 5.3.9 'Conga-line' type 2 π-interactions in **8**. The type 2 π-interactions are chained with transparent B pillar molecules, and are represented by the smaller green balls. Viewed down the A-axis.

5.3.4 Benzylammonium HPzDCA π-Interactions

The same types of π-interactions are encountered in the analogous ammonium HPzDCA compounds, but in a much more limited abundance. Where the ammonium formate pillar moieties generally participate in four separate instances of π-interaction, the analogous ammonium HPzDCA compounds commonly participate in just two. With the exception of **1***, each ammonium HPzDCA compound forms π-interacting 'partners', instead of a continuous chain, where two pillar components originating from opposite hydrophilic sheets associate and reciprocate a single type of π-interaction. Instead of a broad connected network of π-interactions, the ammonium HPzDCA compounds tend towards isolated and discrete π-interactions. This preference relative to ammonium formates is directly linked to the anion, which increases the distances between pillars. The summation of all π-interaction types for compounds **1***-**8*** are condensed in **Table 5.4.1**.

5.3.4.1 Unique Chaining π-Interactions of 1*

As alluded to earlier, compound **1*** is the unique example of the ammonium HPzDCA series of structures. Instead of forming π-partners, the interdigitating benzylamine moieties form a distinctive 'conga-line' type chain where type 3 & 4 interactions are reciprocated between pillar constituents in a diagonal zig-zag (**Figure 5.3.10**). This results in a π-chained environment similar to the ammonium formates, in that a single pillar constituent will encounter four instances of π-interaction. Each pillar constituent contributes two different types of π-interaction to two adjacent molecules, and is reciprocated the same type of π-interaction from the adjacent molecules.

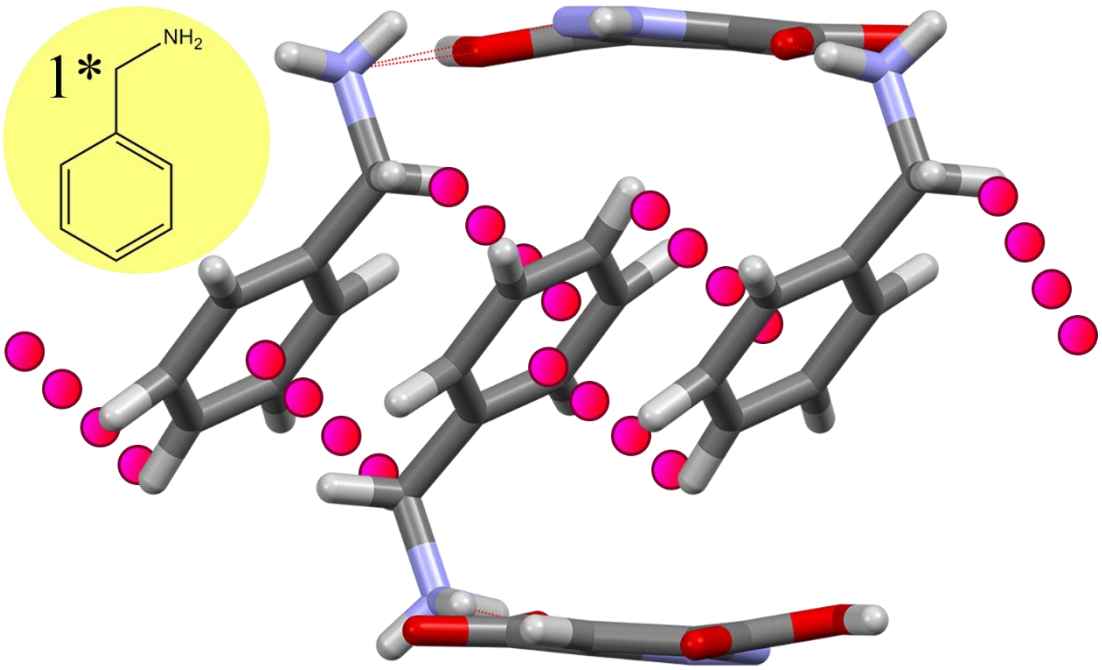

Figure 5.3.10 'Conga-line' type 3 & 4 π-interactions in **1***. Viewed down the A-axis, rotated 15° about the Y-axis.

5.3.4.2 Partnered π-Interactions of 2*-7*

Compounds **2*-7*** follow similar π-partnering trends, but the interactions originate from different sources. In each case, the two pillar components from each sheet couple and reciprocate a single type of π-interaction between the two, in the middle of the interlayer space. The interaction cannot chain because distance between the π-partners, and the adjacent pillar moieties is too great to facilitate what would be a continuous chain of π-interactions. The following compounds each form isostructural π-interacting partners but the interaction derives from the substituents in compound **2*** (**Figure 5.3.11**), the slipped stack, π-interaction, of non-interdigitating pillars in compounds **3***, **6*-7*** (**Figure 5.3.12**), or the slipped stack, π-interaction, of interdigitating moieties in compounds **4*-5*** (**Figure 5.3.13**).

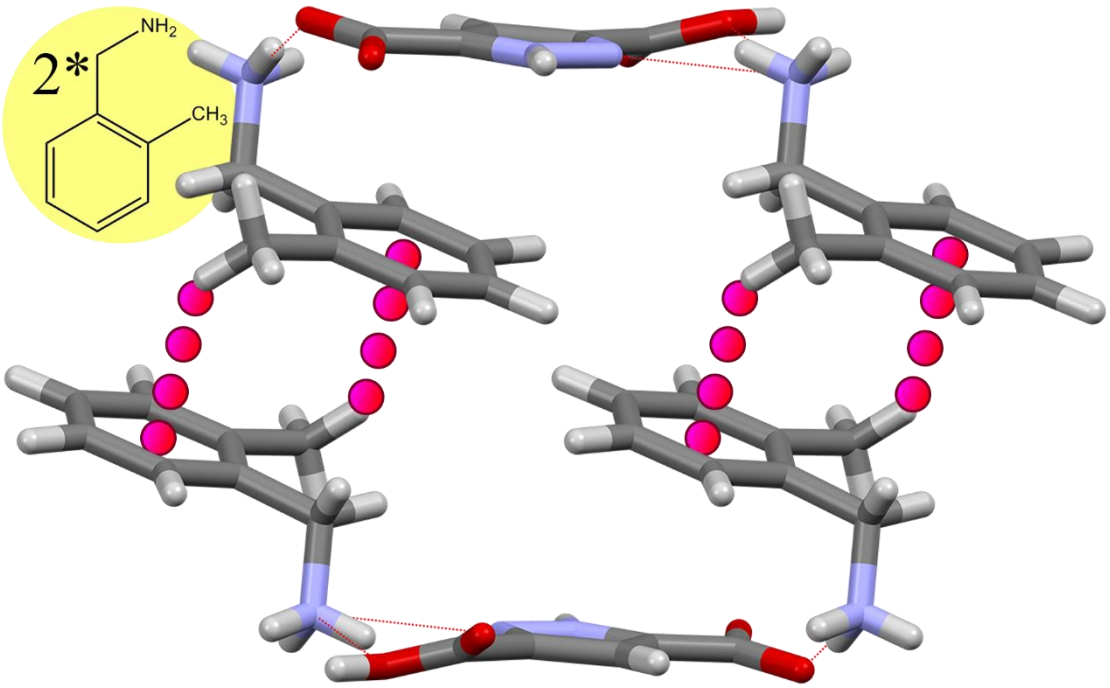

Figure 5.3.11 Partnered type 5 π-interactions in **2***. Viewed down the A-axis.

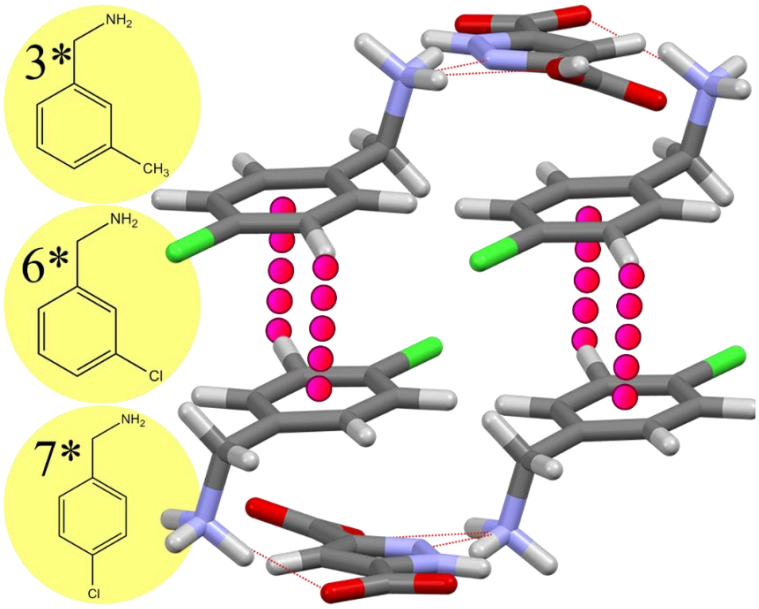

Figure 5.3.12 Partnered type 3, non-interdigitated, π-interactions in **7*** (isostructural with **3***, **6***). Viewed down the A-axis, rotated 60° about the Y-axis, 15° about the X-axis, and 12° about the Z-axis.

Compound **5*** may feature an additional type 5 interaction between the *ortho*-methoxy carbon of one pillar constituent and an adjacent ring. The CH_3 moiety points towards the neighboring ring, and hovers above by 3.4 angstroms, *just* within the typical distance threshold of a C-H···π interaction. However, the lateral displacement positions the hydrogen *just* in line with the spine of the ring's carbon framework (**Figure 5.3.13**). Here a substituent C-H···π interaction may be too remote to be realistic; but this side-on CH/π orientation has been defended in previous reports.[47-49, 51, 54-60] Therefore, it may be appropriate to consider this actually a *chained*-type of interaction, but a decisive conclusion would require computational calculations to model the ESP map to fully describe this remote type 5 interaction; visual inspection is insufficient in this case.

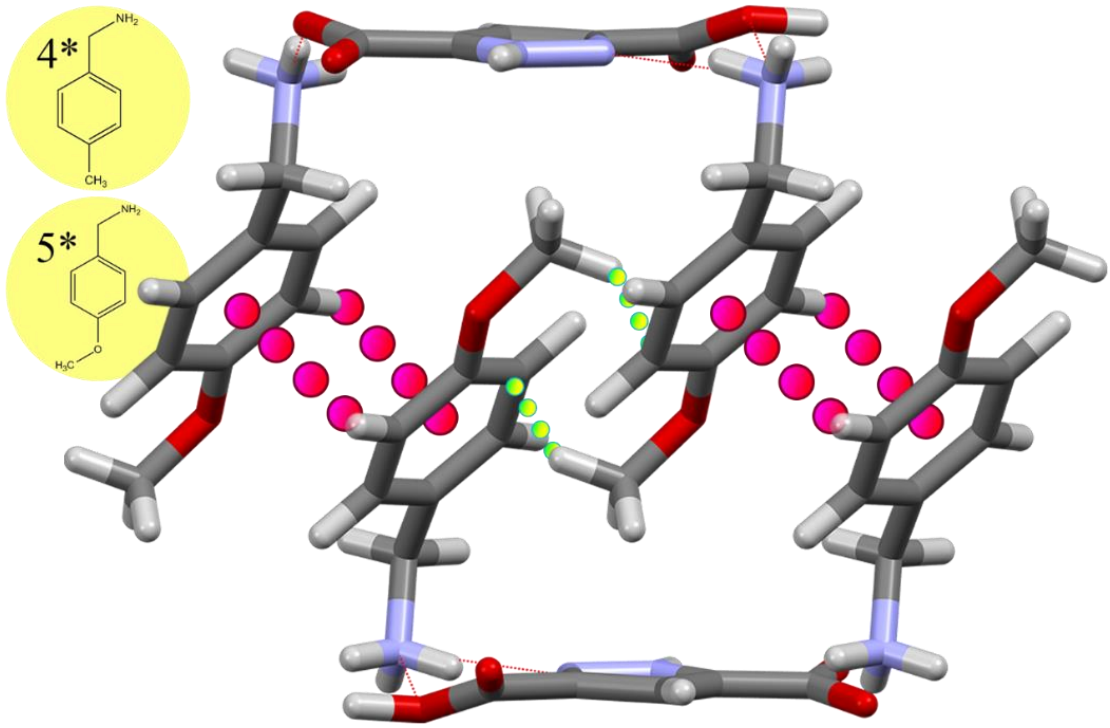

Figure 5.3.13 Partnered type 3, interdigitated, π-interactions in **5* (**isostructural with **4*)**. Small green balls represent the proposed type 5 interaction only present in compound **5***. Viewed down the A-axis, rotated 15° about the Y-axis.

5.3.4.3 Absence of Interlayer π-Interactions in 8*

Compound **8*** results in a unique and unexpected layer pattern, and continues to subvert all structural expectations with its decided approach to layering and π-interaction. Though the naphthyl moiety should feature an abundance of centralized π-density, no stacking, no chaining, nor partnering is observed in this compound. Here, a much stronger driving force must be directing the self-assembled layer. The only apparent type of π-interaction that seems active in this compound is a C-H···π interaction to the naphthyl ring from the apical pyrazole hydrogen of the HPzDCA anion (**Figure 5.3.14**). This result is an outlier considering the extended potential for π-interaction that a naphthyl moiety possesses; and still none of the expected π-interaction types are encountered.

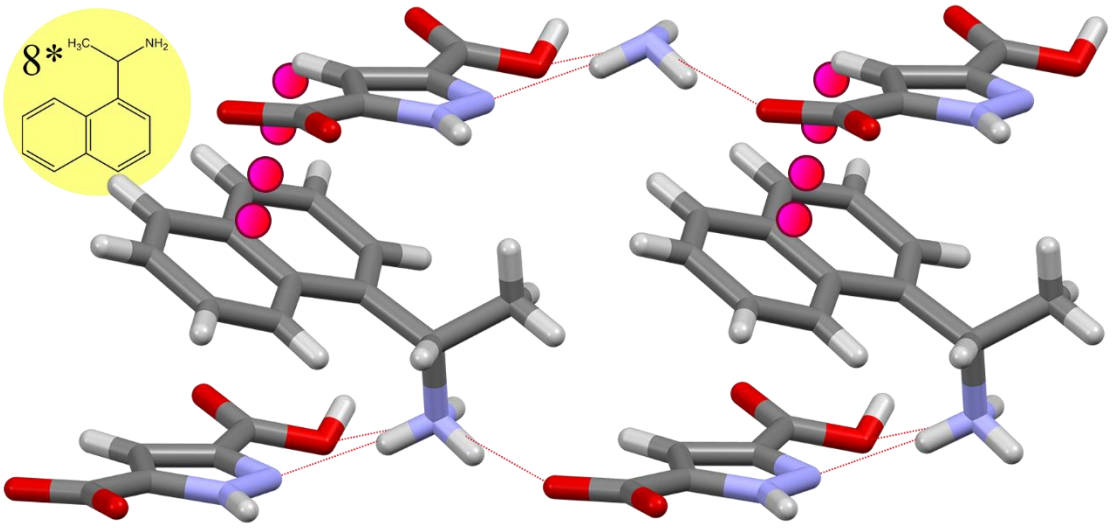

Figure 5.3.14 Hydrophilic substrate π-interactions in **8***. Viewed down the A-axis, rotated 15° about the X-axis, and 60° about the Z-axis.

5.4 Discussion

Each ammonium formate compound and analogous ammonium HPzDCA compound, except **8***, displays weak interlayer π-interactions as identified through visual inspection of the

orientation of the rings and substituents within close contact distance, as well as careful consideration of the measured atomic distances in the crystal data.

5.4.1 General Benzylammonium Formate π-Interaction Trends

In general, the ammonium formate solids in this study show a definitive preference for side/edge-on σ-π and CH/π interactions; zero face-to-face type 1 π-π interactions were observed (**Table 5.4.1**). Of these interactions, five instances of the type 4 interaction are encountered, three type 2 interactions, and two of types 3 & 5. The formate π-chaining interactions range generally between 2.567 and 2.914 angstroms, which is in alignment for these π-interactions in a variety of orientations.[57-59] Specifically, the type 2, 4 & 5 interactions seem more involved with the actual 'chaining' interaction based on the distance from the C-H to the arene centroid (**Table 5.4.2**).

Cmpd	Substituent (Benzylamine)	Formates						HPzDCA					
		i	***u***	**π^2**	**π^3**	**π^4**	**π^5**	***i***	***u***	**π^2**	**π^3**	**π^4**	**π^5**
1	H	✓	✓	✓	-	✓	-	✓	-	-	✓	✓	-
2	*ortho*-Methyl	✓	✓	-	-	-	✓	-	-	-	-	○	✓
3	*meta*-Methyl	-	-	-	✓	✓	-	-	-	-	✓	-	-
4	*para*-Methyl	-	-	-	-	✓	✓	✓	-	-	✓	-	-
5	*para*-Methoxy	-	✓	✓	-	-	-	✓	-	-	✓	-	✓
6	*meta*-Chloro	-	-	-	✓	✓	-	-	-	-	✓	-	-
7	*para*-Chloro	-	-	-	-	✓	✓	-	-	-	✓	-	-
8	1-Naphthylethylamine	-	✓	✓	-	-	-	-	-	-	-	-	-

Table 5.4.1 Summary of layer parameters and π-interactions for compounds **1(*)-8(*)**. *i*: interdigitation, *u*: undulating, π^2: type 2 π-interaction, π^3: type 3 π-interaction, π^4: type 4 π-interaction, π^5: type 5 π-interaction. ○ indicates questionable presence. *Note:* π^1 *not included due to zero occurrence in these compounds.*

5.4.2 General Benzylammonium HPzDCA π-Interaction Trends

The major source of π-interactions in the analogous ammonium HPzDCA compounds is in the form of six type 3, offset ring interactions; two type 5 interactions and one type 4

interaction is also encountered. The type 2, 4 & 5 interactions are similar with respect to **1**-**8**; and the C-H···π bond distances do not seem to be affected by the anion in this case, ranging between 2.780 and 2.940 angstroms. However, the type 3 interactions of **3*** and **6*** appear to deviate from the formates. These ammonium HPzDCA type 3 interactions appear to be derived from a σ-π interaction, rather than a C-H···π interaction. As seen in **Table 5.4.2**, the π^3 interactions are exceeding the threshold for side-on C-H···π interaction (~3.6 Å); but the centroid to centroid distance is well within 4.4 Å, very indicative of a common σ-π interaction (σ^3). Those same centroid distances for the analogous formate compounds are much further than 4.4 Å, and must be C-H···π derived in those cases.

#	CH/π Distances (Å)			
	Formic Acid		**HPzDCA**	
1	$\boldsymbol{\pi^4}$: 2.854	$\boldsymbol{\pi^2}$: 2.892	$\boldsymbol{\pi^4}$: 2.939	$\boldsymbol{\pi^3}$: 3.372
2	$\boldsymbol{\pi^5}$: 2.733	$\boldsymbol{\pi^5}$: 2.914	$\boldsymbol{\pi^5}$: 2.779	
3	$\boldsymbol{\pi^4}$: 2.567	$\boldsymbol{\pi^3}$: 3.555	$\boldsymbol{\pi^3}$: 3.813	$\boldsymbol{\sigma^3}$: 3.940
4	$\boldsymbol{\pi^4}$: 2.665	$\boldsymbol{\pi^5}$: 2.731	$\boldsymbol{\pi^3}$: 3.302	$\boldsymbol{\sigma^3}$: 3.944
5	$\boldsymbol{\pi^2}$: 3.281		$\boldsymbol{\sigma^3}$: 3.677	$\boldsymbol{\pi^5}$: 3.412
6	$\boldsymbol{\pi^4}$: 2.537	$\boldsymbol{\pi^3}$: 3.585	$\boldsymbol{\pi^3}$: 3.623	$\boldsymbol{\sigma^3}$: 3.980
7	$\boldsymbol{\pi^4}$: 2.653	$\boldsymbol{\pi^3}$: 3.582	$\boldsymbol{\pi^3}$: 3.280	$\boldsymbol{\sigma^3}$: 3.822
8	$\boldsymbol{\pi^2}$: 2.876		-	

Table 5.4.2 Distances of π-interactions in the analogous ammonium formates. σ^3 refers to a type 3 interaction that is derived from σ-π interaction, rather than a C-H···π interaction.

5.4.3 Typical Sources and Major Contributors of Interlayer π-Interactions

Always coupled with another type of π-interaction, the benzylic type 4 interaction appears to be the strongest chaining interaction, ranging between 2.567 and 2.892 angstroms. Especially relative to **3**, **6**, and **7**; where the coupled type 3 C-H···π interaction sits ~3.5 angstroms above the spine of the adjacent arene. The summation of all π-interaction types and relevant distances for compounds **1**-**8** (and *****) can be found above in **Tables 5.4.1** and **5.4.2**.

In general, we see a distinctive difference in the interlayer π-interactions between the ammonium formates and their analogous ammonium HPzDCA compounds. Where the ammonium HPzDCA solid layers typically participate in two combined π-interactions from a pair of pillar partners (except **1***, four π-interactions per π-chained pillar molecule), the ammonium formates routinely participate in four π-interactions per pillar moiety, in a chain (except **5,** two π-interactions per π-chained molecule). Clearly, the interlayer pillar region of the ammonium formates shows an increased abundance and variety of π-interaction over the ammonium HPzDCA layers due to the spatial pillar density.

5.4.4 Anion Size Impacts in Ammonium Carboxylates 1-8 and 1*-8*

Fundamentally, the difference between the two ammonium layers is the nature of the anion. Formate is the smallest possible carboxylate anion and is much smaller and flexible than the aromatic ring containing HPzDCA anion. As such, the latter provides a much larger and more rigid scaffold for the hydrophilic layers (**Figure 5.1.7**). While the HPzDCA anion could potentially allow for kinks every 8 angstroms, the formate anion allows for much enhanced flexibility every few angstroms. As seen in Chapter 4, the added flexibility of the hydrophilic substrate in the formates generally results in undulating sheets, especially when pillar interdigitation is present. The increased flexibility of the sheet allows the pillar moieties increased freedom of movement within the interlayer space, and increases the availability of potential π-interaction. This seems very true of **5** (compared to **5***), where the observed chained type 2 π-interaction seems to be a directly permitted by the hydrophilic substrate which has a wider tolerance for undulation.

5.4.4.1 Cation to Cation Distance: Ammonium HPzDCA Pillar Impacts

The most notable consequence of the larger anion in the ammonium HPzDCA structures appears to be a greater separation between the cations (**Table 5.4.3**) within the sheet (A pillar distance), and to a lesser extent, across sheets (B pillar distance).

#	Substituent Identity	Pillar Distance (A)		Pillar Distance (B)	
		Formic Acid (Å)	HPzDCA (Å)	Formic Acid (Å)	HPzDCA (Å)
1	Hydrogen	5.84	9.00	5.84	6.57
2	*ortho*-CH_3	4.82	8.90	6.98	6.66
3	*meta*-CH_3	4.83	8.88	5.85	6.71
4	*para*-CH_3	4.91	8.98	5.89	6.61
5	*para*-OCH_3	4.85	8.96	6.76	6.60
6	*meta*-Cl	4.78	8.84	5.87	6.68
7	*para*-Cl	4.84	8.90	5.82	6.64
8	Naphthyl	4.77	9.00	6.91	6.63

Table 5.4.3 Displaying the side to side pillar distances in the layer (*pillar distance* **A**), and between pillar moieties in front and behind the pillar (*pillar distance* **B**).

While there is a negligible difference in cation-cation distance between layers (B pillar distance), ultimately within one angstrom; there is a significant difference between the A distances within the layer, roughly 3-4 angstroms between the two series of anions. This separation generally precludes the formation of the benzylic, type 4 π-interactions between neighboring benzylamine moieties, the particular π-interactions which tend to assist 'conga-line' formation in ammonium carboxylate layers. In instances where the anion is large, if type 4 interactions are present, they always participate in π-partners instead of π-chains, this can be seen in a number of literature cases.[86] However, in the case of **1***, chained type 4 interactions are managed through the orientation and interdigitation of the benzylamines. The benzyl moieties in **1*** are able to deeply interdigitate, to a position where the face of the ring is well within range of an adjacent benzyl carbon. The absence of any *meta*- or *para*-substituent is likely allowing this

deeper interdigitation; incidentally, this is likely what is *preventing* **4*** from achieving a definite chain of π-interactions.

Likewise, in **5***, the interdigitation of pillar moieties, and stretching of the *para* substituent to interact with the adjacent ring, is likely allowing the formation of a π-chain; but definitive classification of this π-interaction is outside the ability of visual inspection, and would require calculation and modeling.

In ammonium HPzDCA hydrogen-bonded solids, the 'conga-line' π-interaction appears limited to those structures that are interdigitated; where the longer pillar to pillar distance is bridged by an interdigitating pillar moiety that facilitates a chain of π-interactions. When interdigitation is not present, the lateral distance from pillar to pillar is too great to allow for any continuous chain of π-interaction.

5.4.4.2 Cation to Cation Distance: Ammonium Formate Pillar Impacts

Compared to ammonium HPzDCA complexes, regardless of interdigitation, the ammonium formate pillar moieties are in close enough proximity to chain together *via* π-interactions. Of the ammonium HPzDCA compounds**,** while the type 4 interaction is effectively shut off, the pillar arrangement generates ideal conditions for type 3 and 5 partner-based π-interactions. Generally, the major consequence of the larger anion in this work, seems to be the larger separation between cations, leading to π-partners, unless interdigitated auxiliary support is present. Likewise, in the ammonium formates, the pillar to pillar distance is minimized due to the size of the anion, and thus more instances of the π-chain 'conga-line' are encountered.

5.4.4.3 Cation to Cation Distance: Literature Ammonium Carboxylate Pillar Impacts

The observations made concerning the ammonium formate and ammonium HPzDCA structures are consistent with similar ammonium carboxylate compounds in the database.[87] In

situations where a smaller anion (i.e., oxalic acid, malic acid) is featured, usually more than one π-interaction is present, including the nearest neighbor benzylic carbon, type 4 π-interaction. Likewise, for the larger anions (i.e., terephthalic acid, 2,6-naphthalenedicarboxylic acid) fewer overall types of π-interactions are observed from within the pillar region. In the literature examples featuring larger, more-rigid, anions, the π-interactions almost exclusively result in π-partners and not the π-'conga-lines.'[80, 86-87]

5.4.5 π-Interactions in Other Ammonium Formates

Generally, concerning the remaining ammonium formates that were described in Chapter 4, the same observations apply. Each pillar moiety experiences four π-interactions where typically two are contributed by either the substituent (type 5), benzylic carbon (type 4), or sometimes an angled T-shape interaction (type 2), and two are received by the aryl ring.

Phenethylamines **13** and **15** are interesting in that the chain of π-interactions is provided by the typical type 4 interaction, the benzyl carbon, but also the α-carbon of the phenethylamine. Here each carbon of the alkyl chain linking the amino functional group to the benzene ring in these pillars is participating in chained π-interactions. Ironically, the only exception to the trend of chained π-interactions in the ammonium formate series is found in compound **5** of Chapter 4. The trifluoromethyl substituents orient and move towards each other in order to associate in the middle of the interlayer region, resulting in the bending and angling of the aryl rings to the point where a π-chain is not possible (**Figure 5.4.1**). This is an interesting result where the distance between the pillar moieties is short, due to the smaller formate, and the hydrophilic substrate undulates, which brings the pillar moieties even closer together; but the orientation of the aryl rings simply precludes a chain of π-interactions from occurring. Ironically, the distance between coextending ammonium cations within the hydrophilic substrate is about 8.5 angstroms, generally on the same order as the ammonium HPzDCA solids.

Nonetheless, with the exception of compound **5** from Chapter 4, each ammonium formate forms a 'conga-line' of π-interactions that continues infinitely down the layer, and in some cases, participates in specific π-interactions that will connect adjacent layers. This is likely an effect of the spatial density of the pillar moieties permitted by the diminutive size of the formate anion; an effect that is only disrupted by very specific interlayer reorganization required by some pillar moieties (i.e., Chapter 4, compound **5**).

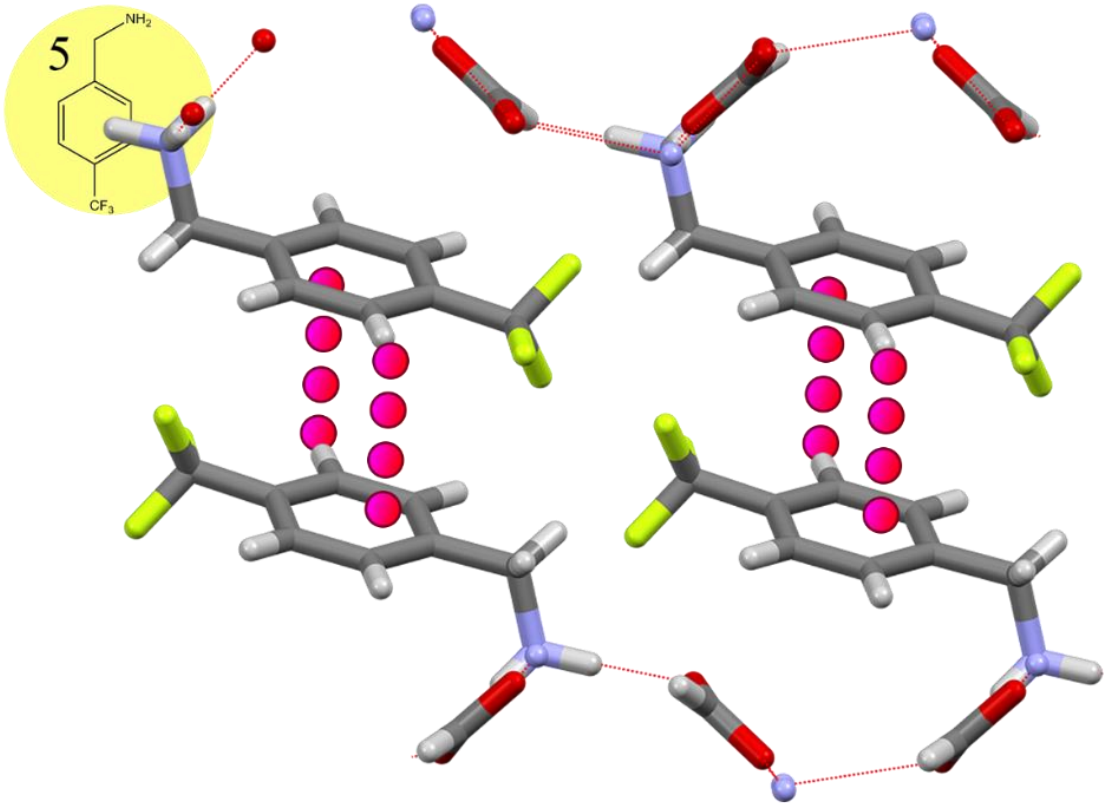

Figure 5.4.1 The singular ammonium formate π-sandwich. The pillars in p*ara*-(trifluoromethyl)-benzylammonium formate (Chapter 4, compound **5**), orient and angle as such, forming π-partners. Viewed down the A-axis.

5.5 Conclusion

The analysis of the interlayer arene π-interactions in various ammonium formates, as well as the subsequent comparison to analogous structures and comparable structures from the literature presented interesting results.

In this work, we have described eight new ammonium formate structures which feature interesting behavior when compared to their analogous ammonium HPzDCA compounds. The general arrangements of the layers, hydrophilic sheets and hydrophobic pillars, share similarities despite the anion present. What differs greatly are the types, and amounts of π-interaction present in the interlayer space of these lamellar structures. It is likely that due to the close proximity of the cations, a result of the diminutive size of the formate anion, an additional dimension of interaction between the pillars is allowed. Where the ammonium HPzDCA compounds may only interact with the pillar moieties from the opposite hydrophilic sheet, resulting in π-interacting partners, the formate structures can interact with the neighboring pillars within the sheet, pillars on the opposite sheet, as well as the pillars in front and behind its own sheet, resulting in a high abundance of π-chained 'conga-line' π-interactions.

It is evident from our findings that the ammonium carboxylates studied in this work favor σ-π, CH/π, or substituent-π interactions. Moreover, based upon the types of π-interaction encountered and the variety of substituents covered, it seems obvious that the π-interactions present in these materials are substituent-derived, favoring more modern schools of thought regarding the origin of π-interaction. In each case, where two reagents were introduced and allowed to self-assemble, a ring-to-ring σ-π motif, or a carbon (substituent, benzylic, or α-) C-H···π motif, was favored and observed in these crystal structures. The distance between the interacting species and the amount of displacement from one ring centroid to its partner were all within expected thresholds, and are in agreement with the literature as described by Hunter,

Sanders, and others.[1, 22, 28, 30, 32] In the ammonium formate and analogous ammonium HPzDCA compounds, as well as in literature cases[87] that featured the same ammonium cations, there was no evidence of direct face-to-face π-interactions, while a plethora of CH/π interactions were encountered. This is a trend we have noticed, but there are some reported accounts of lamellar materials where there is clear evidence of interlayer π-chaining *via* CH/π interactions, but is not considered by the author.[88]

While fairly well represented as is; the series of ammonium carboxylate layers studied in this chapter suffers from some missing entrants; mainly those featuring bulky *ortho*- and *meta*-alkyl substituents. The inclusion of these substituents would help to investigate the outcome of a sizeable steric effect between pillar moieties. For example, would *ortho-tert*-butylbenzylammonium HPzDCA impact the pillars in such a way that the steric bulk located on one side of the ring pushes the pillar components within range to form π-chains? There was a specific case (Chapter 4, compound **5**) where an ammonium formate resulted in the classically ammonium HPzDCA style π-partner interactions, could there be an ammonium HPzDCA compound that causes similar reorganization in the interlayer pillar region such that they may chain together *via* π-interactions, other than **1***? Alternatively, is there an *ortho* steric effect that could influence an ammonium formate structure to assemble as π-partners?

For the purposes of crystal engineering, these are important questions that could result in interesting results. Future work in this area should focus on the investigation of layer formation, and π-interaction, with respect to bulky ammonium formate and ammonium HPzDCA layers. In order to supplement the analysis and qualitative work already accomplished, additional calculations and modeling would be of major importance to the field. Due to the uniquely solvent-free conditions of each material, critical chemical data can be extracted from these structures, allowing this report to not only contribute to those concerned with supramolecular

chemistry and crystal engineering, but to those seeking to explain, describe, and model the physical nature of these π-interactions.

In this chapter we have observed the interplay of π-interactions between various arene molecules in nearly their purest form, isolated and crystallized solvent-free. When given freedom to self-direct, we have witnessed these aryl molecules participating in a combination of diverse modes of interaction that may chain, or partner, *via* σ-π interactions and CH/π interactions. Clearly there is a wide range of interactions available for arenes to associate and cooperate. Therefore, we ask, is the nature and notoriety of these interactions best denoted by terminology that generalizes and narrows the perceived repertoire of their activity? Because "π-stacking" seems to imply that a face-to-face orientation is either preferred or perhaps the only outcome, we have used the term "π-interactions" throughout so as to be more inclusive. In our minds, these interactions are all part of π-choreography, the delicate arrangement and directing of aryl ring-containing compounds − molecular dancers on an electrostatic stage.

5.6 References

1. Hunter, C. A.; Sanders, J. K. M., The Nature of π-π Interactions. *J. Am. Chem. Soc.* **1990,** *112* (14), 5525-5534.
2. Beatty, A. M.; Granger, K. E.; Simpson, A. E., Crystal Engineering of Organic Clay Mimics from 3,5-Pyrazoledicarboxylic Acid and Amines. *Chem. Eur. J.* **2002,** *8* (14), 3254-3259.
3. Ugono, O.; Rath, N. P.; Beatty, A. M., Synthesis and Control of Single Layer and Polar 2-D Layered Architectures in a Series of Organic Layered Solids. *Crystal Growth & Design* **2009,** *9* (11), 4595-4598.
4. Kennard, O., From data to knowledge—Use of the Cambridge Structural Database for studying molecular interactions. *Supramolecular Chemistry.* **1992,** *1* (3), 277-295.
5. Janiak, C., A critical account on π–π stacking in metal complexes with aromatic nitrogen-containing ligands*J. Chem. Soc., Dalton Trans.* **2000,** *0* (21), 3885-3896.
6. Hunter, C. A.; Singh, J.; Thornton, J. M., π-π interactions: the geometry and energetics of phenylalanine-phenylalanine interactions in proteins. *J. Mol. Biol.* **1991,** *218* (4), 837-846.
7. McGuaghey, G. B.; Gagné, M.; Rappé, A. K., p-Stacking Interactions ALIVE AND WELL IN PROTEINS. *J. Biol. Chem.* **1998,** *273* (35), 15458-15463.
8. Sinnokrot, M. O.; Sherrill, C. D., High-Accuracy Quantum Mechanical Studies of π-π Interactions in Benzene Dimers. *J. Phys. Chem. A* **2006,** *110*, 10656-10668.
9. Yakovchuk, P.; Protozanova, E.; Frank-Kamenetskii, M. D., Base-stacking and base-pairing contributions into thermal stability of the DNA double helix. *Nucleic Acids Res.* **2006,** *34* (2), 564-574.
10. Pellett, J. D.; Becker, D. F.; Saenger, A. K.; Fuchs, J. A.; Stankovich, M. T., Role of Aromatic Stacking Interactions in the Modulation of the Two-Electron Reduction Potentials of Flavin and Substrate/Product in Megasphaera elsdenii Short-Chain Acyl-Coenzyme A Dehydrogenase. *Biochemistry.* **2001,** *40* (25), 7720-7728.
11. Shi, Y.; van Steenbergen, M. J.; Teunissen, E. A.; Novo, L.; Gradmann, S.; Baldus, M.; van Nostrum, C. F.; Hennink, W. E., Pi-pi stacking increases the stability and loading capacity of thermosensitive polymeric micelles for chemotherapeutic drugs. *Biomacromolecules.* **2013,** *14* (6), 1826-1837.
12. Kohli, A. G.; Kierstead, P. H.; Venditto, V. J.; Walsh, C. L.; Szoka, F. C., Designer lipids for drug delivery: from heads to tails. *J. Control Release.* **2014,** (0), 274-287.
13. Bittle, E. G.; Brill, J. W.; Anthony, J. E., Electro-optic measurement of carrier mobility in an organic thin-film transistor. *Appl. Phys. Lett.* **2010,** *97* (1), 013302.
14. Kraft, U.; Anthony, J. E.; Ripaud, E.; Loth, M. A.; Weber, E.; Klauk, H., Low-Voltage Organic Transistors Based on Tetraceno[2,3-b]thiophene: Contact Resistance and Air Stability. *Chem. Mater.* **2015,** *27* (3), 998-1004.
15. Deka, M. J.; Chowdhury, D., Tuning Electrical Properties of Graphene with Different π-Stacking Organic Molecules. *J. Phys. Chem. C.* **2016,** *120* (7), 4121-4129.
16. Yum, J. H.; Holcombe, T. W.; Kim, Y.; Rakstys, K.; Moehl, T.; Teuscher, J.; Delcamp, J. H.; Nazeeruddin, M. K.; Gratzel, M., Blue-coloured highly efficient dye-sensitized solar cells by implementing the diketopyrrolopyrrole chromophore. *Sci. Rep.* **2013,** *3*, 2446.
17. Ghosh, T.; Panicker, J. S.; Nair, V. C., Self-Assembled Organic Materials for Photovoltaic Application. *Polymers* **2017,** *9* (3), 112-142.
18. Sengupta, S.; Goswami, A.; Ganguly, S.; Bala, S.; Bhunia, M. K.; Mondal, R., Influence of chloro···chloro interaction and π-π Stacking in 3D supramolecular framework construction. *CrystEngComm.* **2011,** *13* (20), 6136-6149.
19. Zhang, F.; Duan, L.; Qiao, J.; Dong, G.; Wang, L.; Qiu, Y., The intramolecular π-π Stacking interaction does not always work for improving the stabilities of light-emitting

electrochemical cells. *Organic Electronics: physics, materials, applications* **2012,** *13* (11), 2442-2449.
20. Zhao, R.; Zhang, R. Q., A new insight into π-π Stacking involving remarkable orbital interactions. *Phys. Chem. Chem. Phys.* **2016,** *18* (36), 25452-25457.
21. Yao, Z. F.; Wang, J. Y.; Pei, J., Control of π-π Stacking via Crystal Engineering in Organic Conjugated Small Molecule Crystals. *Crystal Growth & Design* **2018,** *18* (1), 7-15.
22. Piovesan, D.; Minervini, G.; Tosatto, S. C., The RING 2.0 web server for high quality residue interaction networks. *Nucleic Acids Res.* **2016,** *44* (1), 367-374.
23. Carter, P. W.; DiMagno, S. G.; Porter, J. D.; Streitwieser, A., π-Stacking and Aggregation of Pyridinium-Substituted Indolizines. *J. Phys. Chem.* **1993,** *97* (5), 1085-1096.
24. Hoeben, F. J. M.; Jonkheijm, P.; Meijer, E. W.; Schenning, A. P. H., About Supramolecular Assemblies of π-Conjugated Systems. *Chem. Rev.* **2005,** *105* (4), 1491-1546.
25. Sanyal, N.; Lahti, P. M., Hydrogen-Bond-Assisted, Crossed Dipole π-Stacking in 1,4-Bis(phenylethynyl)benzene. *Crystal Growth & Design* **2006,** *6* (6), 1253-1255.
26. Chang, Y.-C.; Chen, Y.-D.; Chen, C.-H.; Wen, Y.-S.; Lin, J. T.; Chen, H.-Y.; Kuo, M.-Y.; Chao, I., Crystal Engineering for π-π Stacking via Interaction between Electron-Rich and Electron-Deficient Heteroaromatics. *J. Org. Chem.* **2008,** *73* (12), 4608-4614.
27. Zhao, R.; Zhang, R. Q., A new insight into pi-pi stacking involving remarkable orbital interactions. *Phys. Chem. Chem. Phys.* **2016,** *18* (36), 25452-25457.
28. Grimme, S., Do special noncovalent pi-pi stacking interactions really exist? *Angew. Chem. Int. Ed.* **2008,** *47* (18), 3430-3434.
29. Wheeler, S. E.; Houk, K. N., Through-Space Effects of Substituents Dominate Molecular Electrostatic Potentials of Substituted Arenes. *J. Chem. Theory Comput.* **2009,** *5*, 2301-2312.
30. Martinez, C. R.; Iverson, B. L., Rethinking the term "pi-stacking". *Chem. Sci.* **2012,** *3* (7), 2191-2201.
31. Alvarez, S., A cartography of the van der Waals territories. *Dalton Trans.* **2013,** *42*, 8617-8636.
32. Avasthi, K.; Shukla, L.; Kant, R.; Ravikumar, K., Folded conformations due to arene interactions in dissymmetric and symmetric butylidene-linker models based on pyrazolo[3,4-d]pyrimidine, purine and 7-deazapurine. *Acta Cryst. C.* **2014,** *C70*, 555-561.
33. Hwang, J.; Li, P.; Carroll, W. R.; Smith, M. D.; Pellechia, P. J.; Shimizu, K. D., Additivity of substituent effects in aromatic stacking interactions. *J. Am. Chem. Soc.* **2014,** *136* (40), 14060-14067.
34. Wheeler, S. E.; Houk, K. N., Substituent Effects in the Benzene Dimer are Due to Direct Interactions of the Substituents with the Unsubstituted Benzene. *J. Am. Chem. Soc.* **2008,** *130*, 10854-10855.
35. Sinnokrot, M. O.; Sherrill, C. D., Unexpected Substituent Effects in Face-to-Face π-Stacking Interactions. *J. Phys. Chem. A* **2003,** *107* (41), 8377-8379.
36. Sinnokrot, M. O.; Valeev, E. F.; Sherrill, C. D., Estimates of the Ab Initio Limit for π-π Interactions: The Benzene Dimer. *J. Am. Chem. Soc.* **2002,** *124* (9), 10887-10893.
37. Nakano, M.; Hashizume, D.; Takimiya, K., N,N′-Bis(2-cyclohexylethyl)naphtho[2,3-b:6,7-b′]dithiophene Diimides: Effects of Substituents. *Molecules* **2016,** *21* (8), 921.
38. Li, C.; Lin, Z.; Li, Y.; Wang, Z., Synthesis and Applications of p-Extended Naphthalene Diimides. *Chem. Rec.* **2016,** *16*, 873-885.
39. Kobaisi, M. A.; Bhosale, S. V.; Latham, K.; Raynor, A. M.; Bhosale, S. V., Functional Naphthalene Diimides: Synthesis, Properties, and Applications. *Chem. Rev.* **2016,** *116* (19), 11685-11796.
40. Gung, B. W.; Emenike, B. U.; Alverez, C. N.; Rakovan, J.; Kirschbaum, K.; Jain, N., Relative substituent position on the strength of pi-pi stacking interactions. *Tetrahedron Lett.* **2010,** *51* (13), 1648-1650.

41. Huber, R. G.; Margreiter, M. A.; Fuchs, J. E.; von Grafenstein, S.; Tautermann, C. S.; Liedl, K. R.; Fox, T., Heteroaromatic pi-stacking energy landscapes. *J. Chem. Inf. Model.* **2014,** *54* (5), 1371-1379.
42. Rashkin, M. J.; Waters, M. L., Unexpected Substituent Effects in Offset π-π Stacked Interactions in Water. *J. Am. Chem. Soc.* **2002,** *124* (9), 1860-1861.
43. Ringer, A. L.; Sinnokrot, M. O.; Lively, R. P.; Sherrill, C. D., The effect of multiple substituents on sandwich and T-shaped pi-pi interactions. *Chem. Eur. J.* **2006,** *12* (14), 3821-3828.
44. Wheeler, S. E., Local nature of substituent effects in stacking interactions. *J. Am. Chem. Soc.* **2011,** *133* (26), 10262-10274.
45. Wheeler, S. E.; Bloom, J. W., Toward a more complete understanding of noncovalent interactions involving aromatic rings. *J. Phys. Chem. A* **2014,** *118* (32), 6133-6147.
46. Neel, A. J.; Hilton, M. J.; Sigman, M. S.; Toste, F. D., Exploiting non-covalent pi interactions for catalyst design. *Nature* **2017,** *543* (7647), 637-646.
47. Nishio, M.; Umezawa, Y.; Hirota, M.; Takeuchi, Y., The CH/pi Interaction: Significance in Molecular Recognition. *Tetrahedron* **1995,** *51* (32), 8665-8701.
48. Ma, J. C.; Dougherty, D. A., The Cation−π Interaction. *Chem. Rev.* **1997,** *97*, 1303-1324.
49. Nishio, M.; Hirota, M.; Umezawa, Y., *The CH/π Interaction: Evidence, Nature, and Consequences*. John Wiley & Sons: 1998.
50. Tsuzuki, S.; Honda, K.; Uchimaru, T.; Mikami, M.; Tanabe, K., The Magnitude of the CH/π Interaction between Benzene and Some Model Hydrocarbons. *J. Am. Chem. Soc.* **2000,** *122*, 3746-3753.
51. Brandl, M.; Weiss, M. S.; Jabs, A.; Sühnel, J.; Hilgenfeld, R., CH ✓ ✓ pi Interactions in Proteins. *J. Mol. Biol.* **2001,** *307*, 357-377.
52. Tsuzuki, S.; Honda, K.; Uchimaru, T.; Mikami, M.; Fujii, A., Magnitude and Directionality of the Interaction Energy of the Aliphatic CH/π Interaction: Significant Difference from Hydrogen Bond. *J. Phys. Chem. A* **2006,** *110*, 10163-10168.
53. Tsuzuki, S.; Fujii, A., Nature and physical origin of CH/p interaction: significant difference from conventional hydrogen bonds. *Phys. Chem. Chem. Phys.* **2008,** *10* (19), 2584-2594.
54. Nishio, M., The CH/pi hydrogen bond in chemistry. Conformation, supramolecules, optical resolution and interactions involving carbohydrates. *Phys. Chem. Chem. Phys.* **2011,** *13* (31), 13873-13900.
55. Mishra, B. K.; Karthikeyan, S.; Ramanathan, V., Tuning the C-H...pi Interaction by Different Substitutions in Benzene-Acetylene Complexes. *J. Chem. Theory. Comput.* **2012,** *8* (6), 1935-1942.
56. Nishio, M., The CH/π hydrogen bond: Implication in chemistry. *Journal of Molecular Structure* **2012,** *1018*, 2-7.
57. Karthikeyan, S.; Ramanathan, V.; Mishra, B. K., Influence of the substituents on the CH...pi interaction: benzene-methane complex. *J. Phys. Chem. A* **2013,** *117* (30), 6687-6694.
58. Brunner, H.; Tsuno, T.; Balazs, G.; Bodensteiner, M., Methyl/phenyl attraction by CH/pi interaction in 1,2-substitution patterns. *J. Org. Chem.* **2014,** *79* (23), 11454-11462.
59. Mishra, B. K.; Deshmukh, M. M.; Venkatnarayan, R., C-H...pi interactions and the nature of the donor carbon atom. *J. Org. Chem.* **2014,** *79* (18), 8599-8606.
60. Jimenez-Moreno, E.; Jimenez-Oses, G.; Gomez, A. M.; Santana, A. G.; Corzana, F.; Bastida, A.; Jimenez-Barbero, J.; Asensio, J. L., A thorough experimental study of CH/pi interactions in water: quantitative structure-stability relationships for carbohydrate/aromatic complexes. *Chem. Sci.* **2015,** *6* (11), 6076-6085.
61. Nishio, M.; Hirota, M., CH/π interaction: Implications in organic chemistry. *Tetrahedron* **1989,** *45* (23), 7201-7245.
62. Hirota, M.; Nishio, M., *Kagaku (Kyoto)* **1991,** *46*, 592.

63. Nishio, M., CH/© Hydrogen Bond in Crystals. *CrystEngComm.* **2004,** *6*, 130-158.
64. Nishio, M.; Umezawa, Y.; Honda, K.; Tsuboyama, S.; Suezawa, H., CH/π hydrogen bonds in organic and organometallic chemistry. *CrystEngComm.* **2009,** *11* (9), 1757-1788.
65. Ugono, O.; Rath, N. P.; Beatty, A. M., "Exceptions to the rule: new hydrogen-bonded networks from an old reliable". *CrystEngComm.* **2011,** *13* (3), 753-758.
66. Beatty, A. M.; Helfrich, B. A.; Hogan, G. A.; Reed, B.-A., Metal-Containing Dicarboxylic Acids as Building Bocks for Lamellar Inorganic-Organic Hybrid Networks. *Crystal Growth & Design* **2006,** *6* (1), 122-126.
67. Chen, C. L.; Beatty, A. M., "From crystal engineering to cluster engineering: How to transform cadmium chloride from 2-D to 0-D". *Chem. Commun.* **2007,** (1), 76-78.
68. Etter, M. C., Encoding and Decoding Hydrogen-Bond Patterns of Organic Compounds. *Acc. Chem. Res.* **1990,** *23*, 120-126.
69. Odendal, J. A.; Bruce, J. C.; Koch, K. R.; Haynes, D. A., Packing motifs in organic ammonium carboxylate salts: extension of the ring-stacking and ring-laddering concepts. *CrystEngComm.* **2010,** *12* (8), 2398-2408.
70. Barnes, J., Benzylammonium hydrogen oxalate hemihydrate. *Acta Cryst.* **2003,** *E59* (7), 931-933.
71. Djinovic, K.; Golic, L.; Leban, I., Structures of benzylammonium hydrogen malonate (I) and 4-picolinium hydrogen malonate (II). *Acta Cryst.* **1990,** *C46* (2), 281-286.
72. Yuge, T.; Sakai, T.; Kai, N.; Hisaki, I.; Miyata, M.; Tohnai, N., Topological Classification and Supramolecular Chirality of 21-Helical Ladder-Type Hydrogen-Bond Networks Composed of Primary Ammonium Carboxylates: Bundle Control in 21-Helical Assemblies. *Chem. Eur. J.* **2008,** *14* (10), 2984-2993.
73. Aakeröy, C. B.; Nieuwenhuyzen, M., Hydrogen Bonding and Structural Motifs in Organic l-Malate(2−) Salts. *Chem. Mater.* **1996,** *8* (6), 1229-1235.
74. Ballabh, A.; Trivedi, D. R.; Dastidar, P.; Suresh, E., Hydrogen bonded supramolecular network in organic salts: crystal structures of acid-base salts of dicarboxylic acids and amines. *CrystEngComm.* **2002,** *4* (24), 135-142.
75. Lemmerer, A.; Bourne, S. A.; Fernandes, M. A., Disruption of a robust supramolecular heterosynthon in achiral benzylammonium and (pyridylmethyl)ammonium m-iodobenzoate salts. *CrystEngComm.* **2008,** *10* (12), 1750-1757.
76. Parshad, H.; Frydenvang, K.; Liljefors, T.; Sorensen, H. O.; Larsen, C., Aqueous solubility study of salts of benzylamine derivatives and p-substituted benzoic acid derivatives using X-ray crystallographic analysis. *International Journal of Pharmaceutics* **2004,** *269* (1), 157-168.
77. Matsumoto, A.; Odani, T.; Chikada, M.; Sada, K.; Miyata, M., Crystal-Lattice Controlled Photopolymerization of Di(benzylammonium) (Z,Z)-Muconates. *J. Am. Chem. Soc.* **1999,** *121* (48), 11122-11129.
78. Aakeröy, C. B.; Nieuwenhuyzen, M., Hydrogen bonding in crystal engineering: two-dimensional layers of hydrogen l-malate anions. *Journal of Molecular Structure* **1996,** *374* (1), 223-239.
79. Russell, V. A.; Etter, M. C.; Ward, M. D., Layered Materials by Molecular Design: Structural Enforcement by Hydrogen Bonding in Guanidinium Alkane-and Arenesulfonates. *J. Am. Chem. Soc.* **1994,** *116* (5), 1941-1952.
80. REFCODES: YABFEO, Y., YABGOZ, WETPIU, WETPOA, AJUMOH, SEJSOP, PEBDUW, TOHXOE,TEWXIC, XINSAO, LAYCAP, LAYJUC, LAYGAT, NOJWIS, NOJWOY, NOJWEO, SOVWOQ, SOVWUW, SOVXAD, SOVXEH, SOVXOR, XOVXUX.
81. Dolomanov, O. V.; Bourhis, L. J.; Gildea, R. J.; Howard, J. A. K.; Puschmann, H., OLEX2: a complete structure solution, refinement and analysis program. *J. Appl. Cryst.* **2009,** *42*, 339-341.
82. Sheldrick, G. M., A short history of SHELX. *Acta. Crystallogr. A* **2008,** *A64*, 112-122.

83. Refcodes: XOVTIL (1*), X., XOVVOT (3*), XOVVUZ (4*), XOVVAF (5*), XOVVIN (6*), XOVVEJ (7*), QUCSIR (8*).
84. Frontera, A.; Gamez, P.; Mascal, M.; Mooibroek, T. J.; Reedijk, J., Putting anion-pi interactions into perspective. *Angew. Chem. Int. Ed.* **2011,** *50* (41), 9564-9583.
85. Schottel, B. L.; Chifotides, H. T.; Dunbar, K. R., Anion-pi interactions. *Chem. Soc. Rev.* **2008,** *37* (1), 68-83.
86. Refcodes: PEBDOQ, P., SOVWOQ, LAYGAT, SOVXAD, SOVXEH, SOVXOR, SOVXUX.
87. Refcodes: AJUMOH (1), L., PEBCIJ (1), PEBDOQ (1), PEBDUW (1), SEJSOP (1), SOVWOQ (1), SOVWUW (1), TOHXOE (1), XINSAO (1), SINSIW (1), XOXQEH (1), YABGEP (1), YABGIT (1), LAYGAT (3), TEWXIC (3), NOJWEO (4), SOVXAD (4), SOVXEH (4), LAYJUQ (5), SOVXOR(5), SOVXUX (5), DUVCUT (6), NOJWOY (6), TEWXOI (6), TOYMEZ (6), NOJWIS (7), TEWWUN (7), TOYMAV(7).
88. Smith, G., Two-dimensional hydrogen-bonded polymers in the crystal structures of the ammonium salts of phen-oxy-acetic acid, (4-fluoro-phen-oxy)acetic acid and (4-chloro-2-methyl-phen-oxy)acetic acid. *Acta Cryst.* **2014,** *E70* (12), 528-532.

Chapter 6

Conclusion

6.1 Concluding Remarks

The development of supramolecular chemistry has assisted in opening many new gates of scientific inquiry, revealing many paths to novel research opportunities and permitting the influx of unique research efforts, ideas, and objectives. Considering the results of our work and others', there is a definite link between the utilization of different molecular building blocks and the subsequent formation of new materials demonstrating *observable* structural changes and *measurable* functional changes. Moreover, we show that the control of the structure/function relationship spans a wide range of scientific fields, and its scope is not just limited to *only* crystal engineering. Even magnetochemistry may be influenced through the application of supramolecular principles.

In summary of this work, we have fruitfully synthesized, and reported herein: 3 novel substituted Mn_{12}-type complexes; 1 Mn_{13}-supercubane structure *via* solvothermal transformation of the Mn_{12}-2-Phenyl compound; 3 $Mn_{13}O_8$-type compounds; 1 Mn_3O-2-Ethyl compound; an unexpected Mn_9O_7-type cluster; and 32 novel organic 2-D (usually) hydrogen-bonded networks. Each of these 41 compounds has been prepared using systematically and rationally substituted arenes, either benzoic acids or benzylamine analogues.

The ultimate question: have the objectives of this project been sufficiently achieved? To form a proper response to this question, we must re-examine the principle inquiries proposed in Chapter 1. Question **I** asks if we can substitute the peripheral acetate groups of Mn_{12}-Acetate, and impose structure/function changes. Question **II** asks if we can modify the synthetic routes to known MnO-type clusters by altering the carboxylate starting materials, to obtain new MnO-type clusters. Finally, question **III** asks if we can design, predict, and compare new 2-D hydrogen-bonded materials with literature and database entrants. The caveat? We must accomplish each objective through systematically bulky, modular, building blocks.

In Chapter 2 we focused our attention on the *ortho*-position of benzoic acids as a potential steric influencer of the structural shape of the Mn_{12}-type cluster, $Mn_{12}O_{12}(O_2C\mathbf{R})_{16}(H_2O)_4$. Through our efforts, the cluster core was not drastically changed, but important ancillary structural features *were* affected. As a result, we observed and commented on the functional change of the material's magnetic signature, relative to the Mn_{12}-Acetate parent, based up on the minor physical variations. This work satisfies the research goals given in question I. Though minor, a structural change *was* observed in the Mn_{12}-Acetate parent cluster, and a measured functional change *was* encountered as a direct result of substituting acetate with asymmetric benzoates. Eventually, a drastic structural change on the Mn_{12}-type cluster was forced solvothermally when an ideal set of reaction conditions was eventually discovered which could facilitate the transformation of Mn_{12}-2-Phenyl to a supercubane-type $Mn_{13}O_{14}(O_2CPh\text{-}o\text{-}Ph)_{12}$ cluster; adding to the fanfare.

In Chapter 3 we investigated carboxylates as design pieces in the synthesis of various MnO-type clusters. We hoped to obtain new MnO-type clusters by utilizing systematically bulkier *ortho*-substituted benzoic acids instead of the carboxylates used in the published synthetic procedures. Ultimately, the *ortho*-substituted benzoates we studied imposed no structural change relative to their MnO-parent clusters, and no undiscovered MnO-type clusters were generated. Exchanging the carboxylate reagents in the preparation of the $Mn_{13}O_8$-type materials and of the Mn_3O-type clusters, resulted in just one unexpected outcome. In altering the route to Mn_3O-type clusters, the utilization of *ortho*-methyl benzoate resulted in two *different* unexpected clusters: one Mn_{12}-type and one Mn_9O_7-type. The Mn_{12}-type cluster has been encountered previously, and a pour through the CSD revealed two similar Mn_9O_7-type clusters. Therefore, while an *unexpected* cluster was certainly synthesized, a *new* MnO cluster core was not discovered. Because the ineffectual *ortho*-ethyl substituted benzoic acid would offer more steric bulk relative to the *ortho*-methyl variety, this result likely stems more from reaction or crystallization

conditions, and not steric effect on the published procedure. The results of this work just scratches the surface of question II.

In Chapter 4 we investigated the physical shapes of 2-D ammonium formate architectures featuring substituted benzylamines, close siblings of benzoic acid, as building blocks for these hydrogen-bonded structures. In Chapter 5, we narrowed the lens, and evaluated the interlayer π-interactions present in those 2-D architectures as well as analogous ammonium HPzDCA structures and similar layered materials in the database. Remarkably, a plethora of newly generated compounds assembled predictably, and displayed physical properties and preferences that could be traced back to structural features of the synthons. Additionally, each ammonium formate structure could be compared to analogous ammonium HPzDCA structures of the Beatty Lab, as well as other literature sources. Through these comparisons, structural observations could be made which help to enable reliable predictive efforts in connecting synthon identity to the type of layer assembled. This work resolutely addresses question III.

To conclude, the work towards new MnO-type clusters in question II showed some promising results, and was slightly satisfied by the generation of the unexpected Mn_9O_7-type compound. Unfortunately, that cluster type has been previously described. Certainly, the principles of the research explained in Chapter 3 must be able to be implemented to a more impactful degree in *some* established route to MnO-type clusters. When considering the results and extent of the work described in Chapters 2, 4 and 5, and their role in fully satisfying questions I and III; surely these efforts were productive, and the objectives of this work have both been accomplished and have introduced future research curiosities. In all, we have added data to two huge fields of chemistry, manganese oxide clusters and 2-dimensional hydrogen-bonded lamellar materials. This data will serve to add to the wealth of knowledge that already exists in these fields, and will provide observations and research conclusions which may guide current and new researchers in those fields. We have performed unique work, with a unique twist, and in the end,

have obtained some interesting results. To those who may directly follow this work, we offer examples of positive results, where the research has gone, and where it may go in the future.

6.2 Epilogue

To close, the ups and downs of graduate school and dissertation research were truly formative and critical to becoming a well-rounded scientist! Here at the end of the process, I now understand that the journey, and the learning process, is based on the rational response to *success* and *failure*. In research, both states are just perceived, and data will be data. The important part is to set scientific expectations aside, rely on the methods, and interpret the results. Separately, outside the laboratory component, physically composing a dissertation has been another formative process. It certainly is a personal journey of mind, body, and spirit as any scientist makes their way from undergraduate to doctorate. While no two experiences could ever be the same, the end result will be the same in that there emerges a forged scientist who has persevered through challenges and struggles, and one who will look back at their work and say that they have grown positively from the experience.

Appendix I

Supplemental Crystal Structures

I.1 Supplemental Crystal Structures for Chapter 3

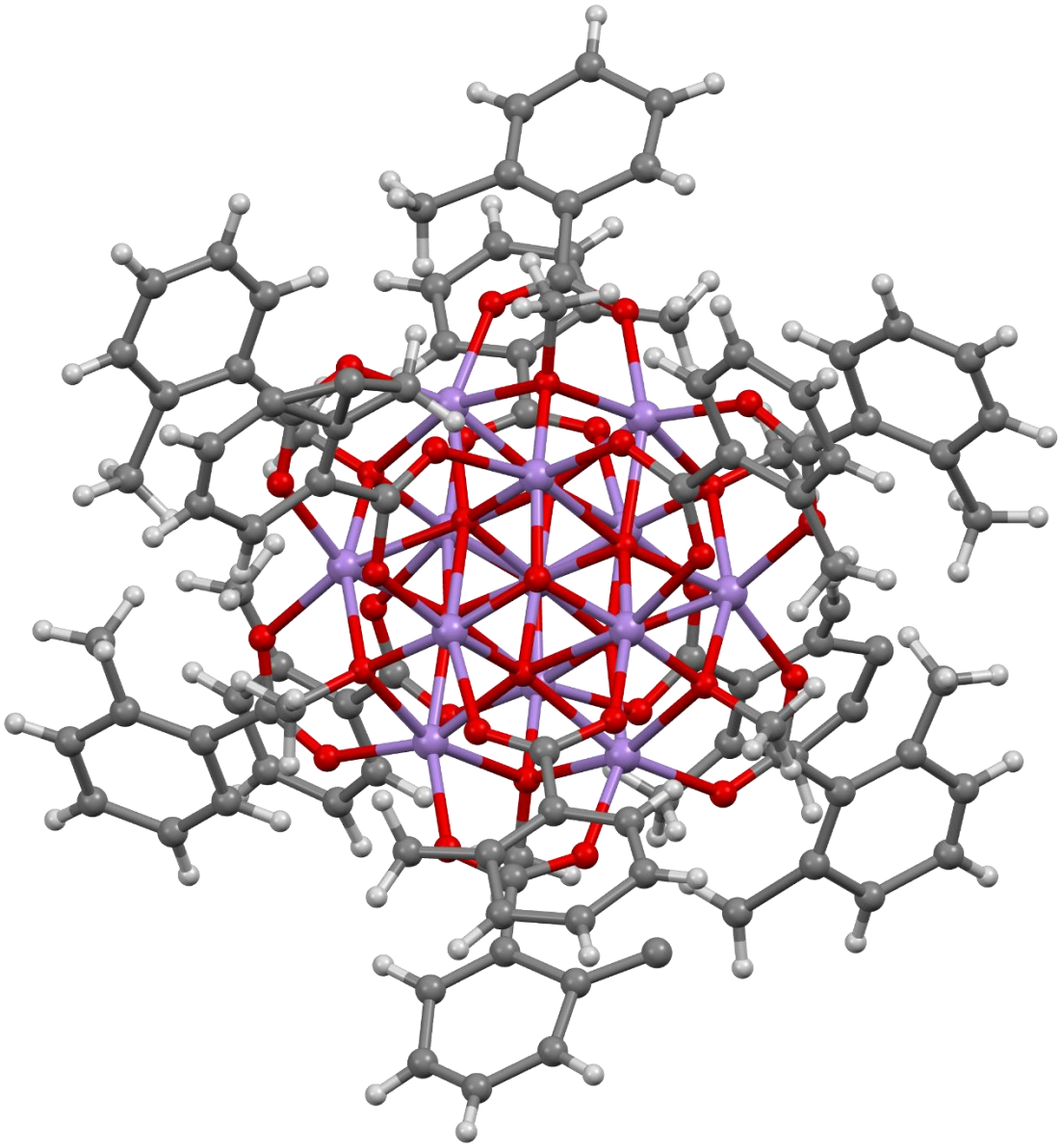

Figure I.1.1 Mn_{13}-2-Methyl, $Mn_{13}O_8(O_2CPh\text{-}o\text{-}Me)_{12}(OEt)6$, compound **1**

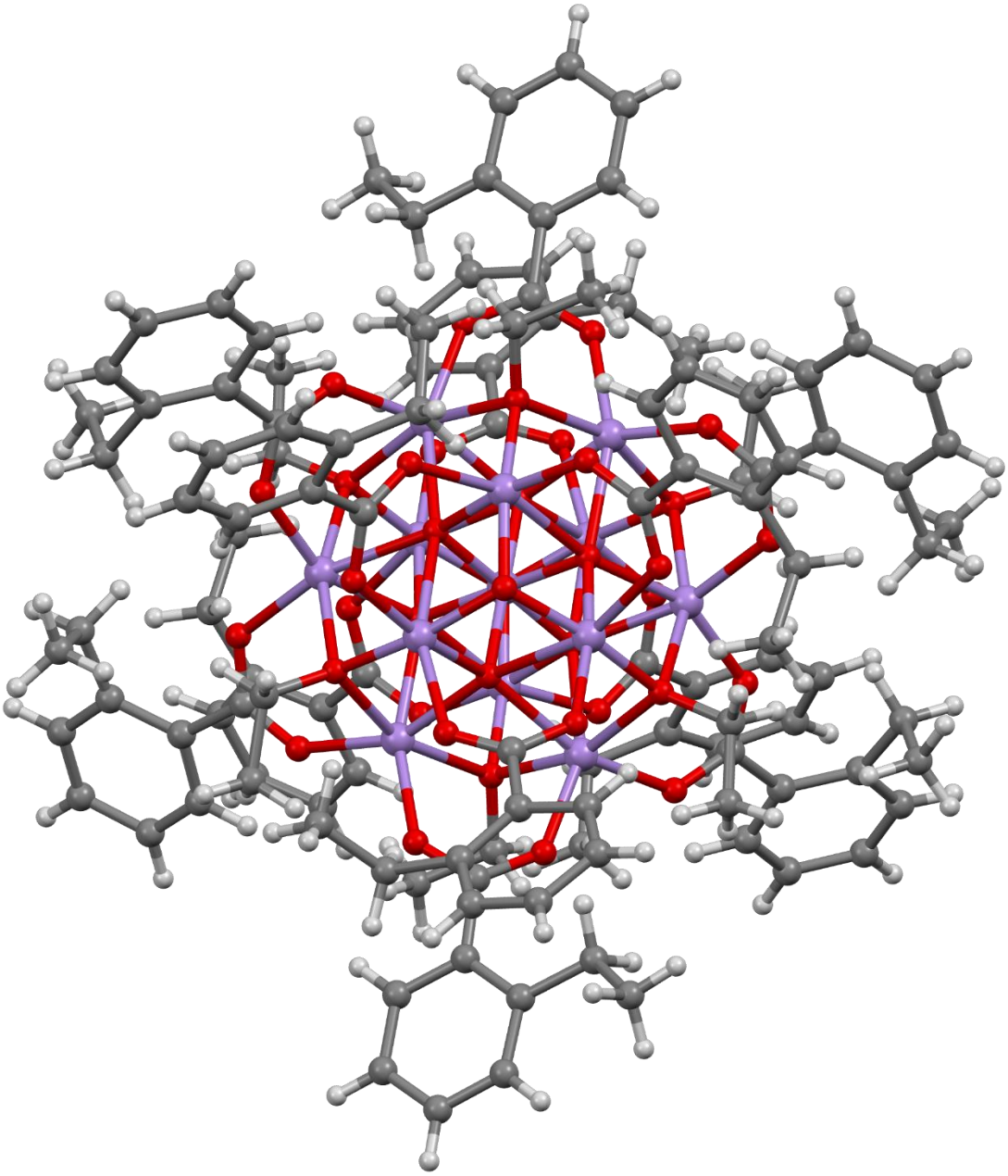

Figure I.1.2 Mn_{13}-2-Ethyl, $Mn_{13}O_8(O_2CPh\text{-}o\text{-}Et)_{12}(OEt)6$, compound **2**

I.2 Supplemental Crystal Structures for Chapter 4

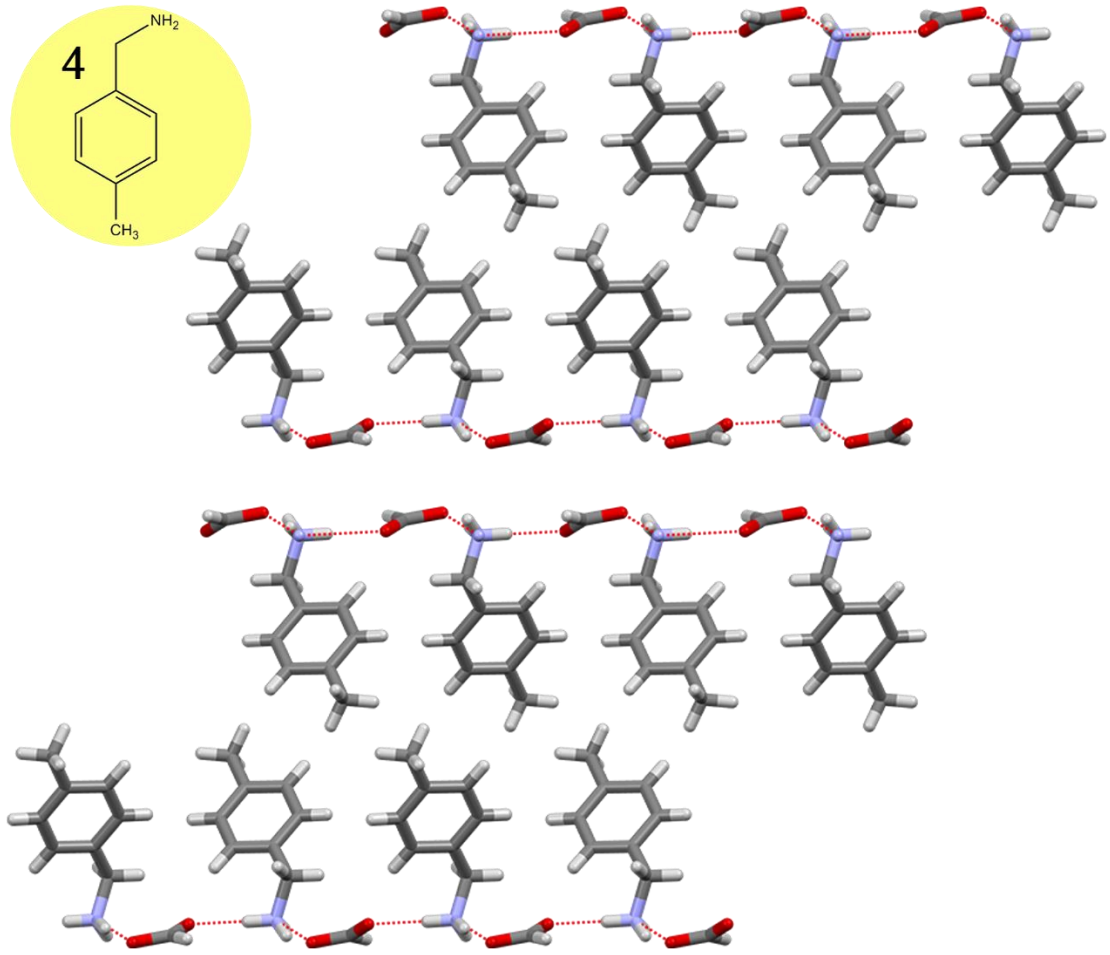

Figure I.2.1 Layer pattern of compound **4**. Viewed along the B-axis.

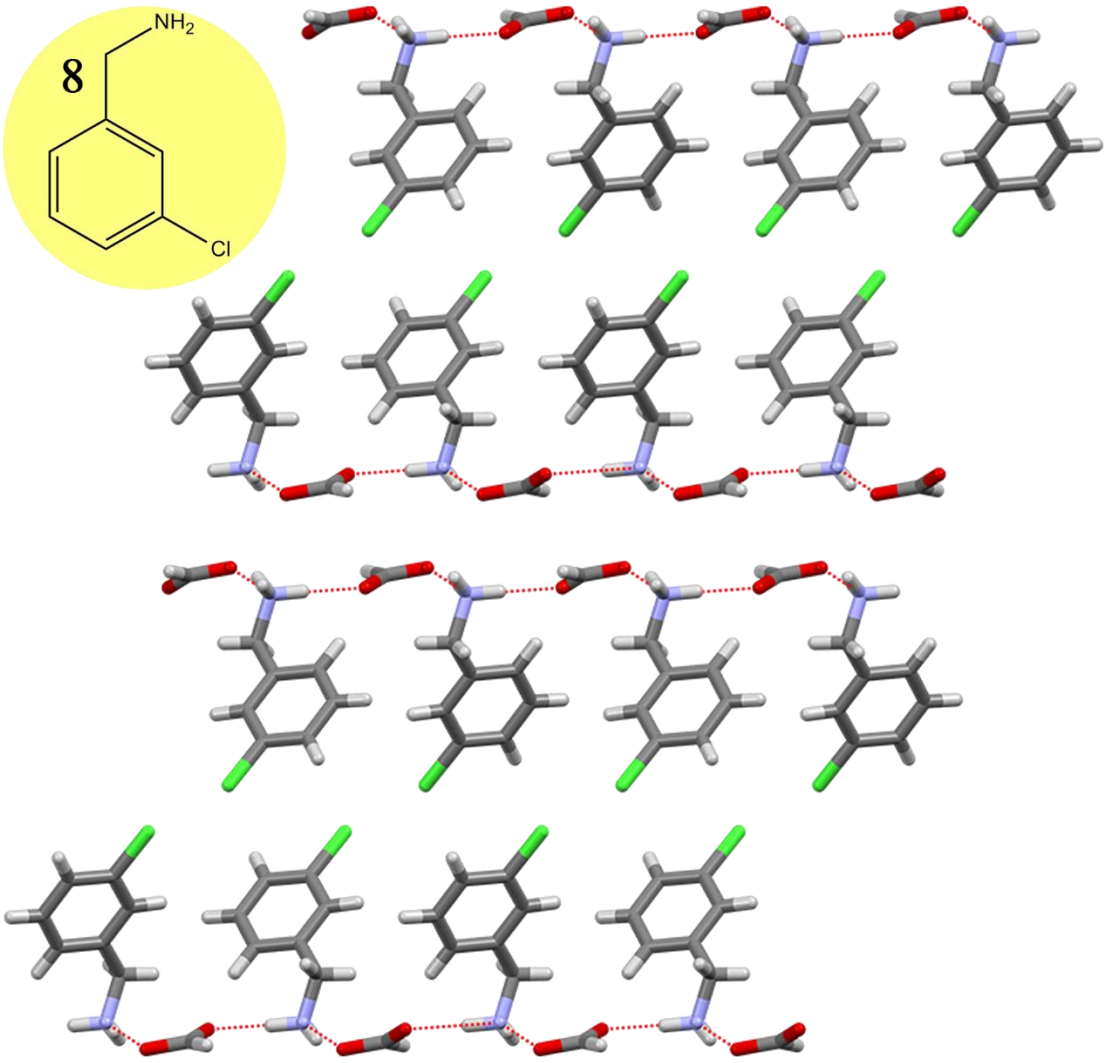

Figure I.2.2 Compound **8** layers. Viewed along the B-axis.

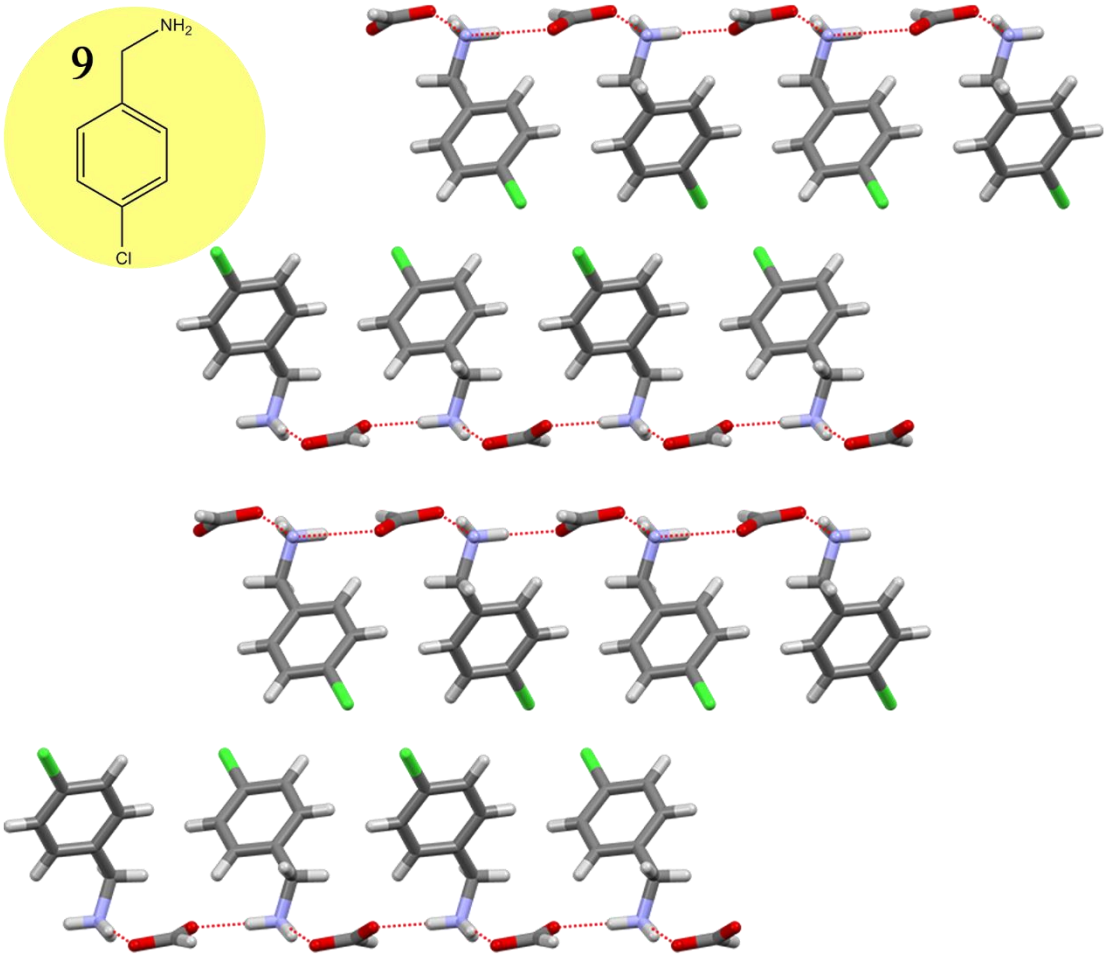

Figure I.2.3 Layered compound **9**. Viewed along the B-axis.

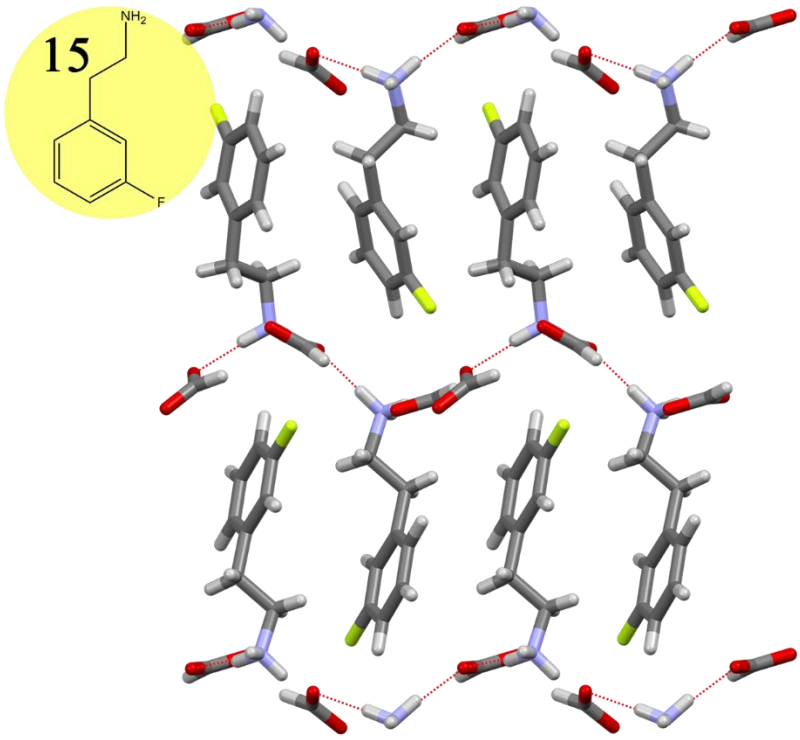

Figure I.2.4 Compound **15** layering pattern. Viewed down the C-axis.

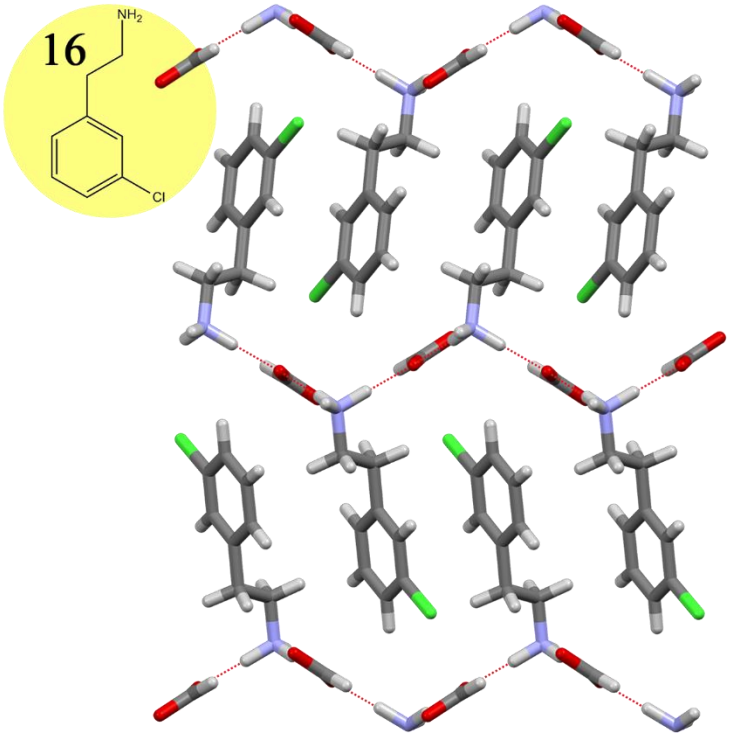

Figure I.2.5 Layering pattern of compound **16**. Viewed down the A-axis.

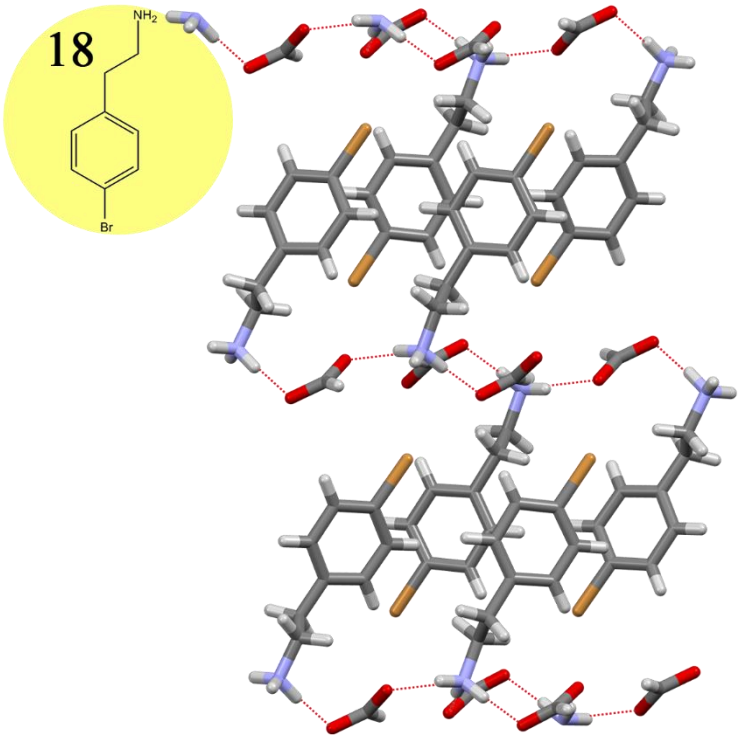

Figure I.2.6 Layering arrangement of compound **18**. Viewed down the B-axis.

I.3 Supplemental Crystal Structures for Chapter 5

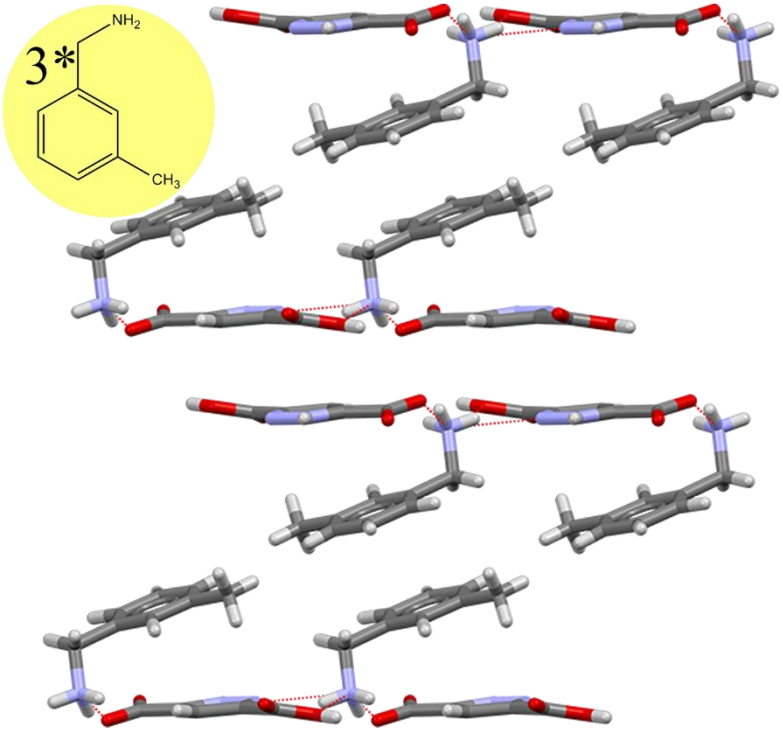

Figure I.3.1 Layering pattern for compound **3***

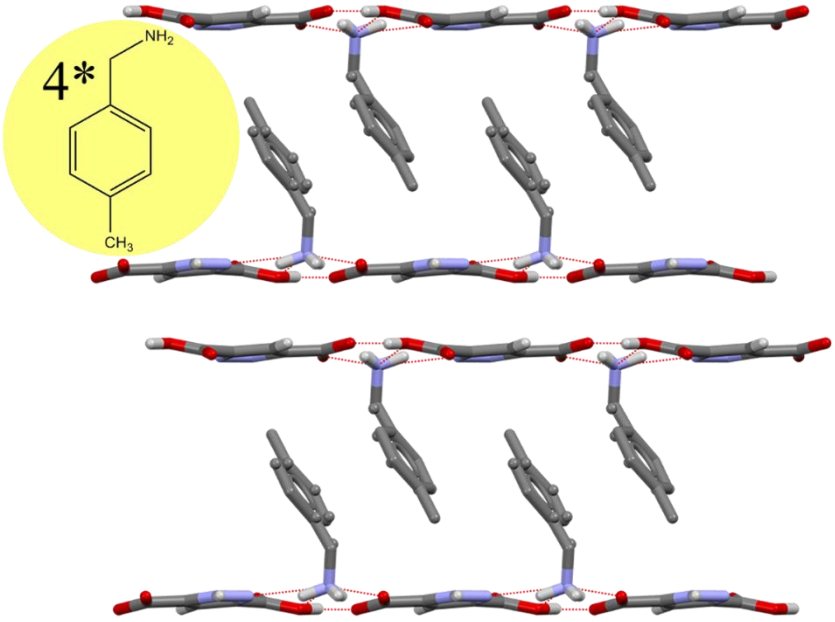

Figure I.3.2 Layering pattern for compound **4***

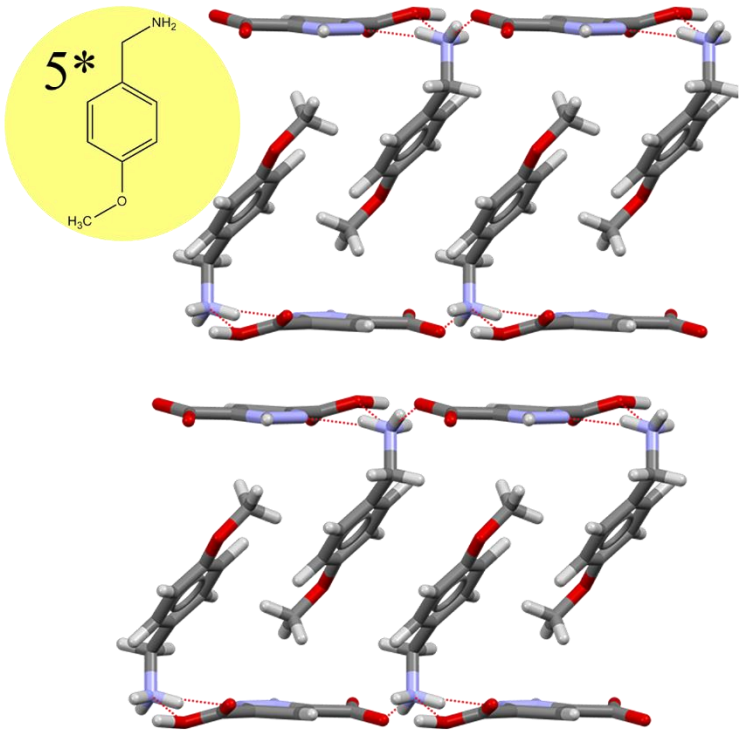

Figure I.3.3 Layering pattern for compound **5***

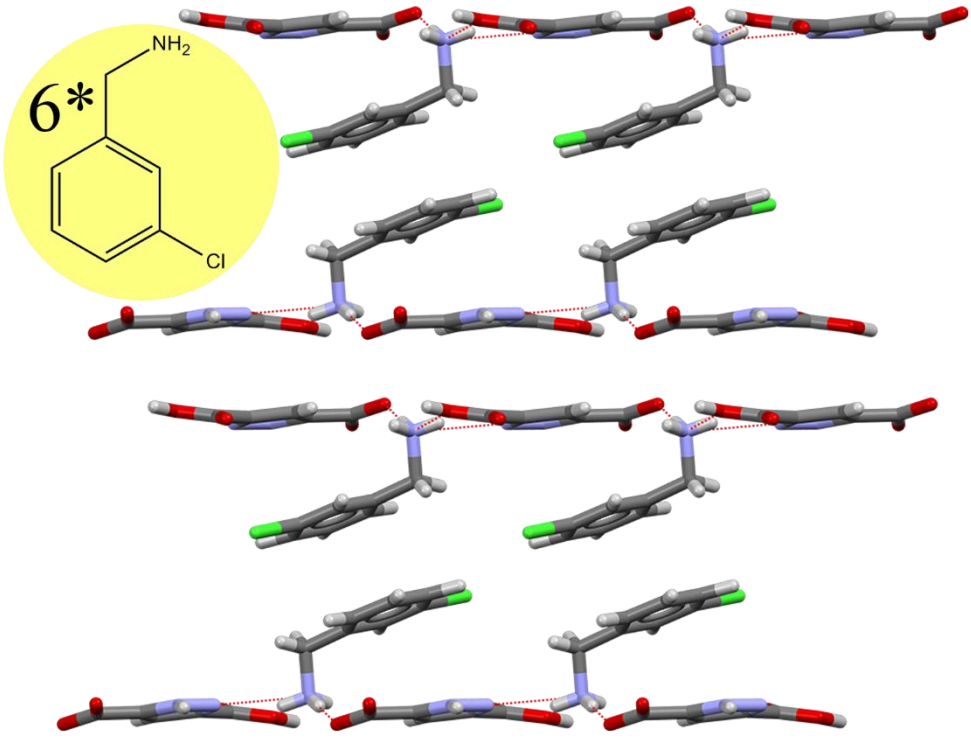

Figure I.3.4 Layering pattern for compound **6***

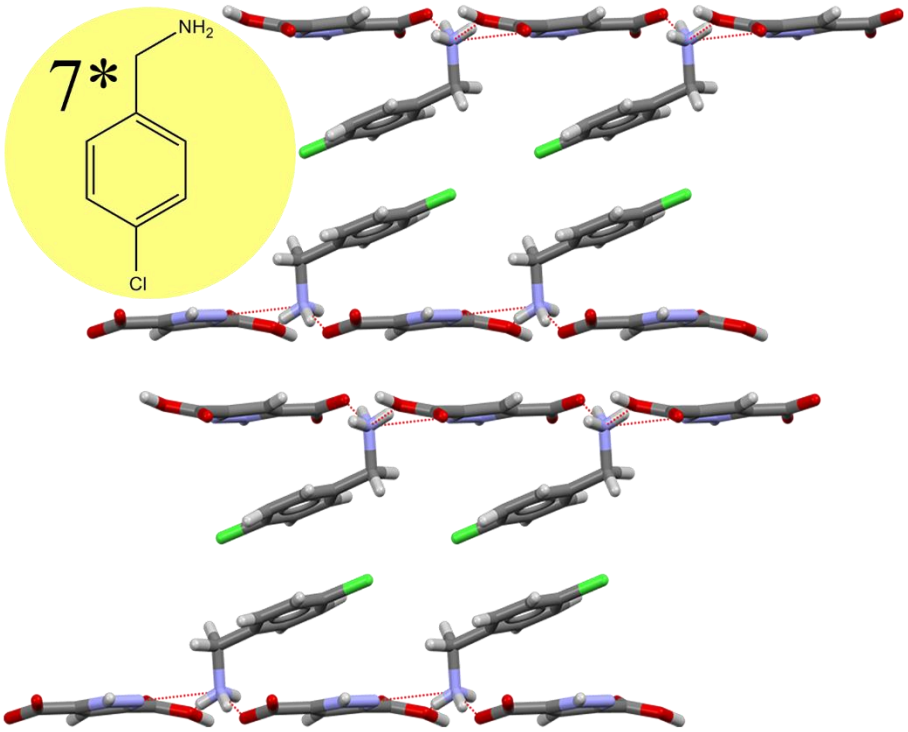

Figure I.3.5 Layering pattern for compound **7***

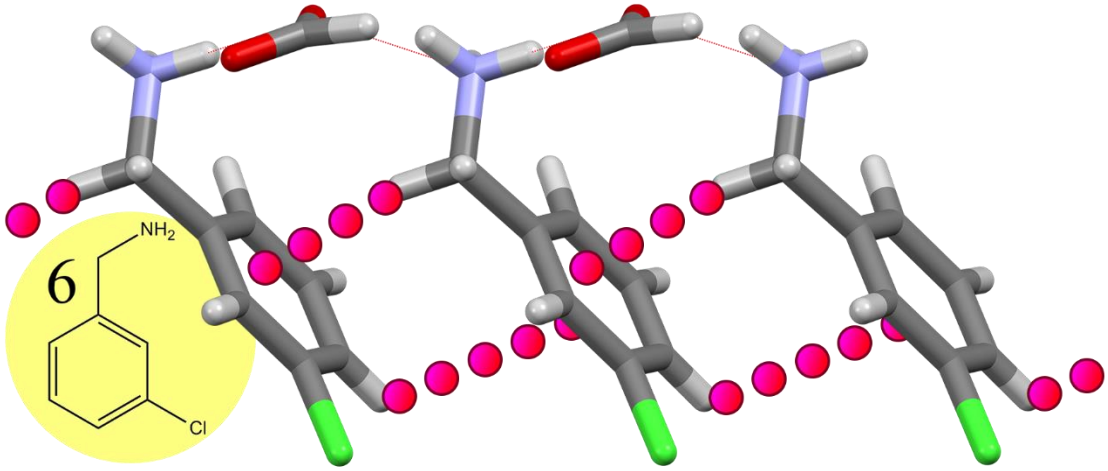

Figure I.3.6 Conga-line type-3 & 4 π-interactions in **6**. Viewed down the C-axis.

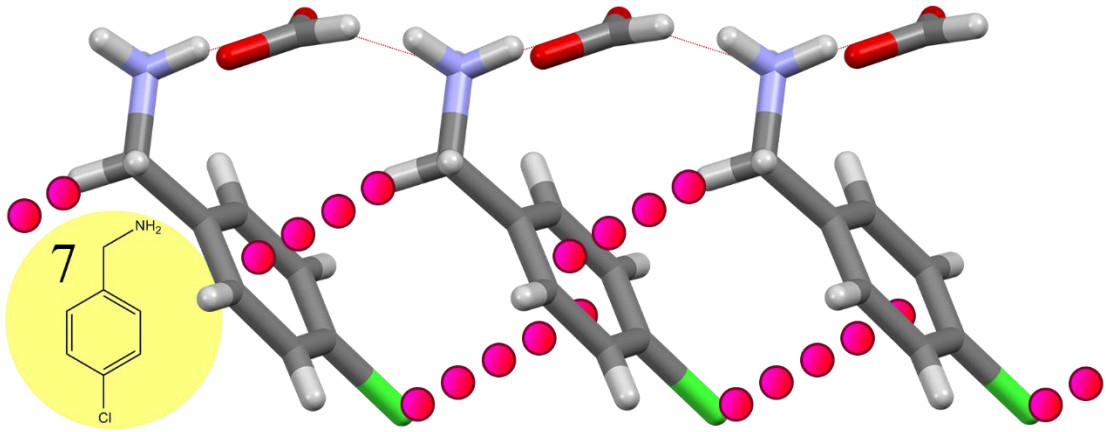

Figure I.3.7 Conga-line type-4 & 5 π-interactions in **7**. Viewed down the C-axis.

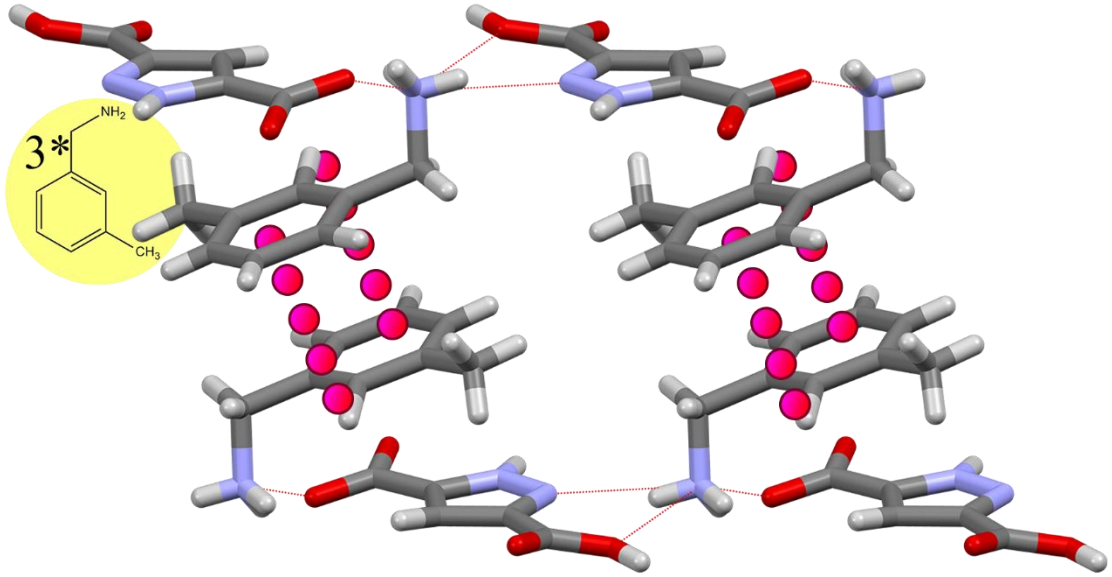

Figure I.3.8 Partner type-3 π-interactions for compound **3***. Viewed down the A-axis, rotated 20° about the X-axis, and 20° about the Y-axis.

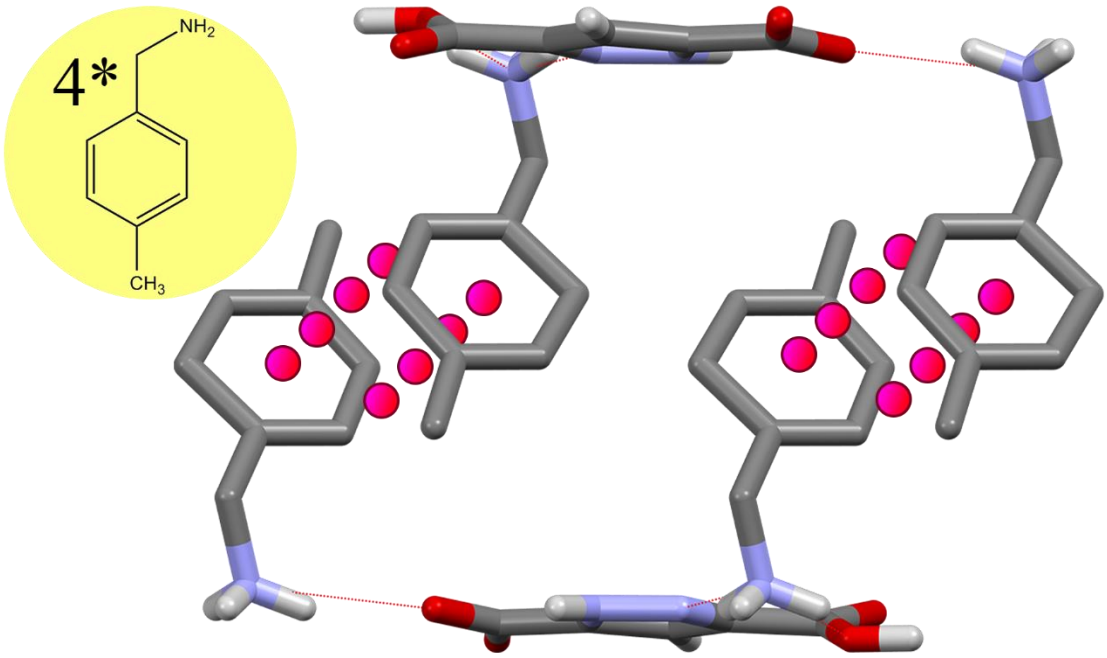

Figure I.3.9 Partner type-3 π-interactions for compound **4***. Viewed down the A-axis, rotated 20° about the Y-axis.

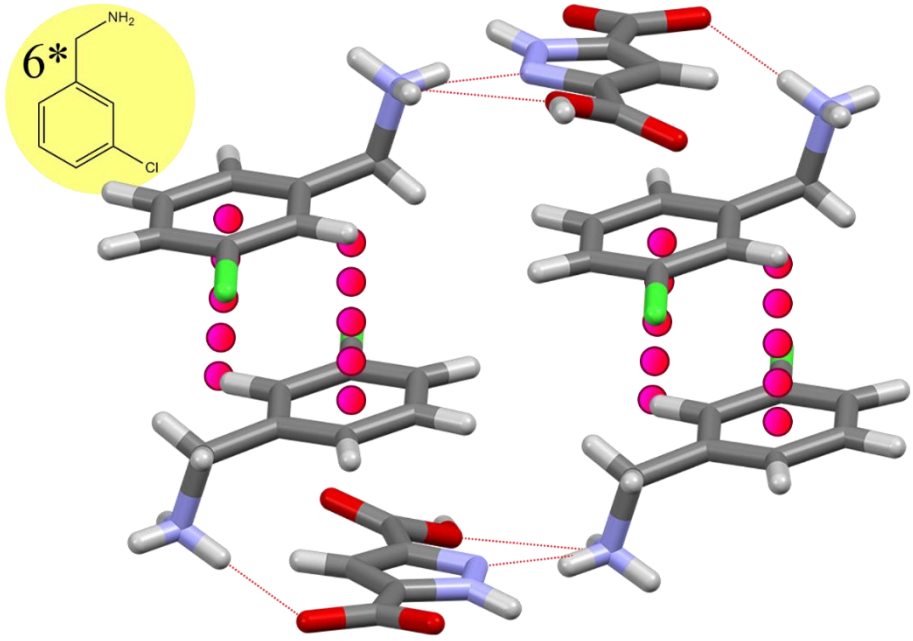

Figure I.3.10 Partner type-3 π-interactions for compound **6***. Viewed down the A-axis, rotated 20° about the X-axis, 45° about the Y-axis, and 20° about the Z-axis.

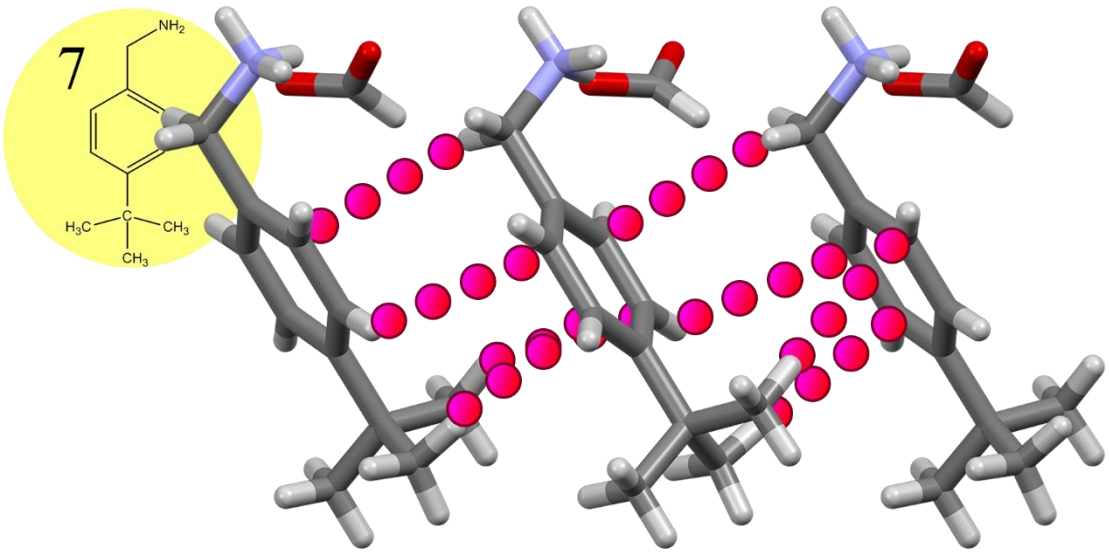

Figure I.3.11 Diverse CH/π type 4, 5, and angled type 2 chained π-interactions in compound **7** (Chapter 4). Viewed down the B-axis.

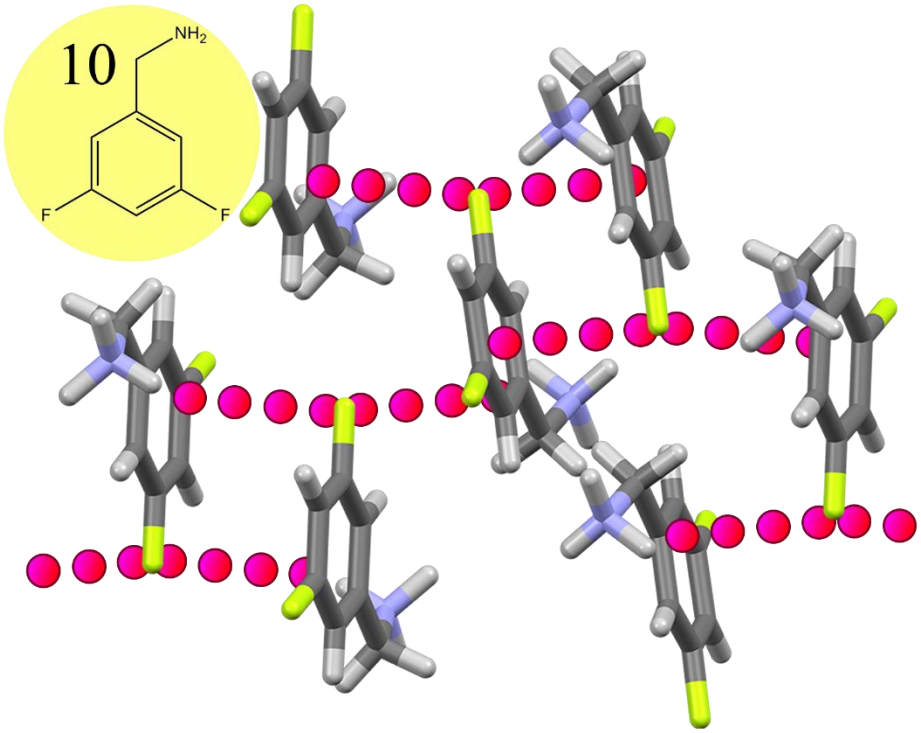

Figure I.3.12 Very staggered type 5 chained π-interactions for compound **10** (Chapter 4). Viewed down the B-axis, rotated 15° about the X-axis.

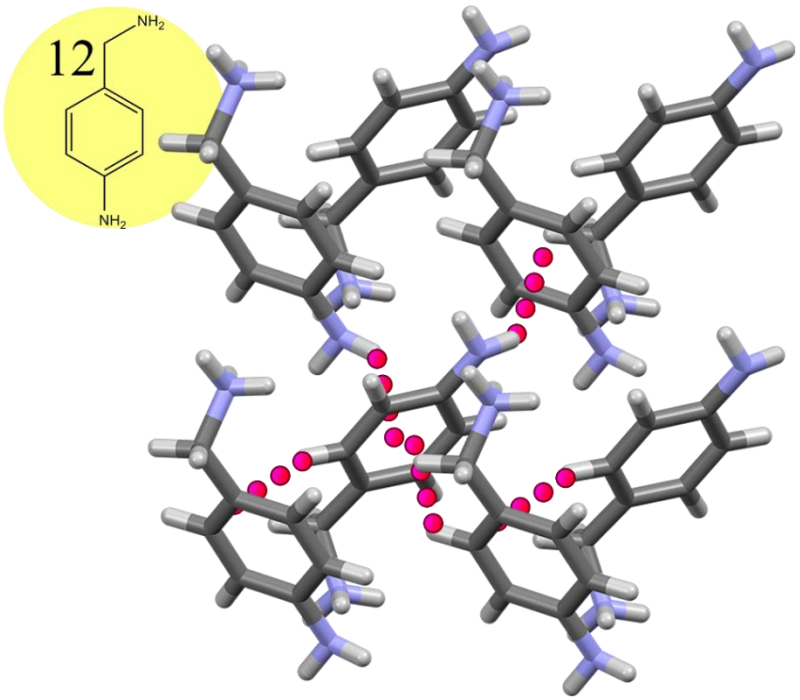

Figure I.3.13 Angled type 2 chained π-interactions in compound **12** (Chapter 4**).** Type 5 interactions connect the stratum. Viewed down the A-axis.

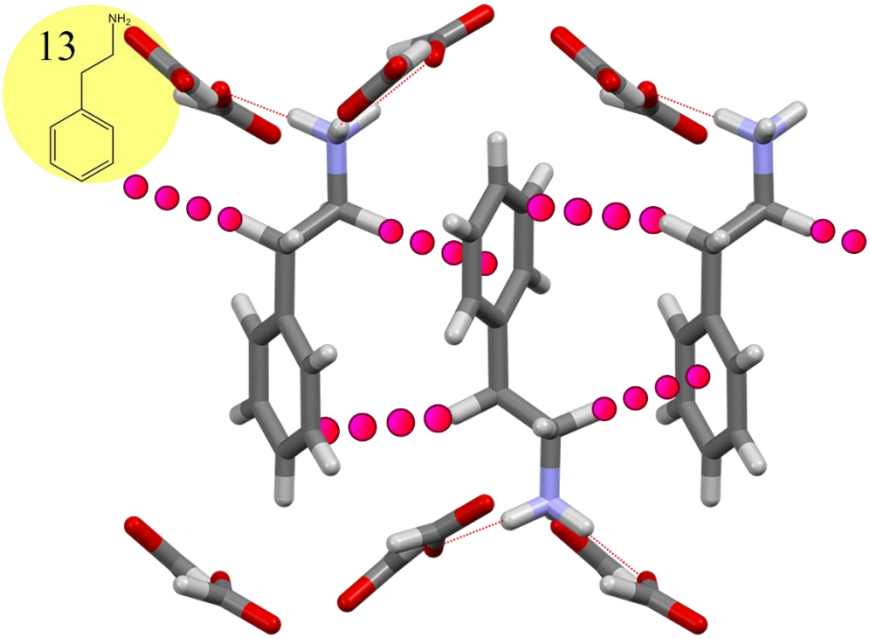

Figure I.3.14 Type 4 (α-carbon) and type 4 (benzylic carbon) chained π-interactions in compound **13** (Chapter 4). Viewed down the B-axis.

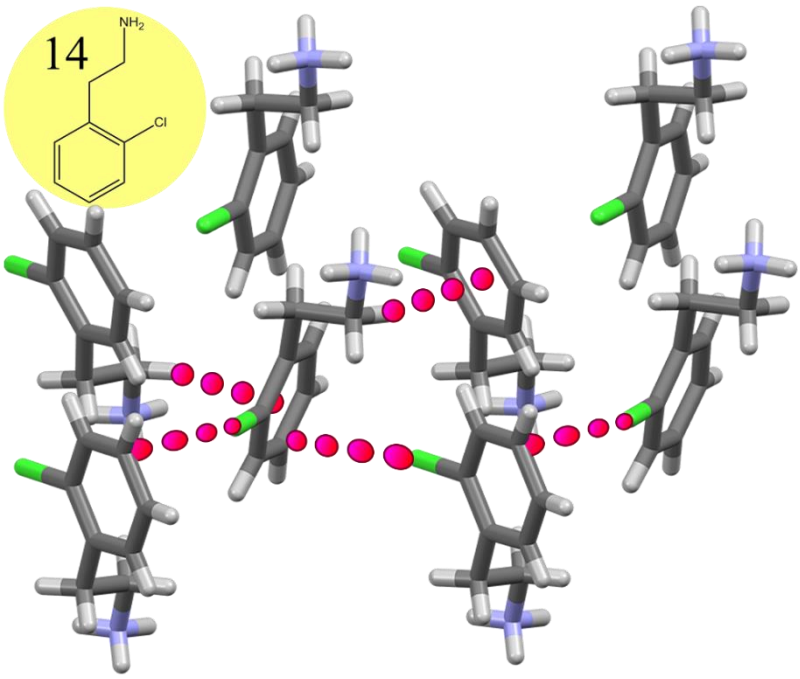

Figure I.3.15 Type 5 chained π-interactions in compound **14** (Chapter 4). Type 4 (α-carbon) π-interactions connect the different stratum. Viewed down the A-axis, rotated 15° about the X and Y-axis.

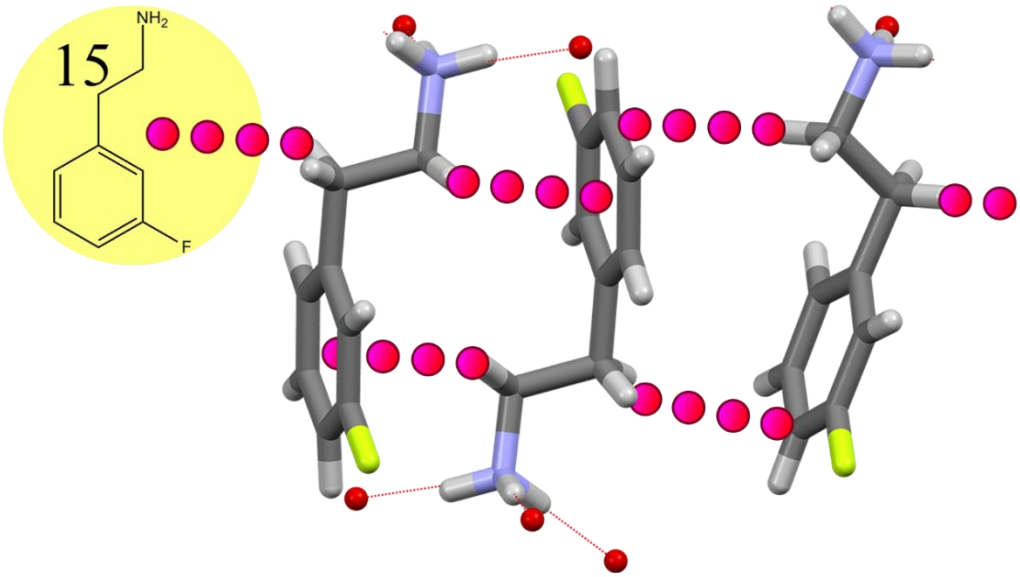

Figure I.3.16 Type (α-carbon) and type 4 (benzylic carbon) chained π-interactions in compound **15** (Chapter 4). Viewed down the A-axis.

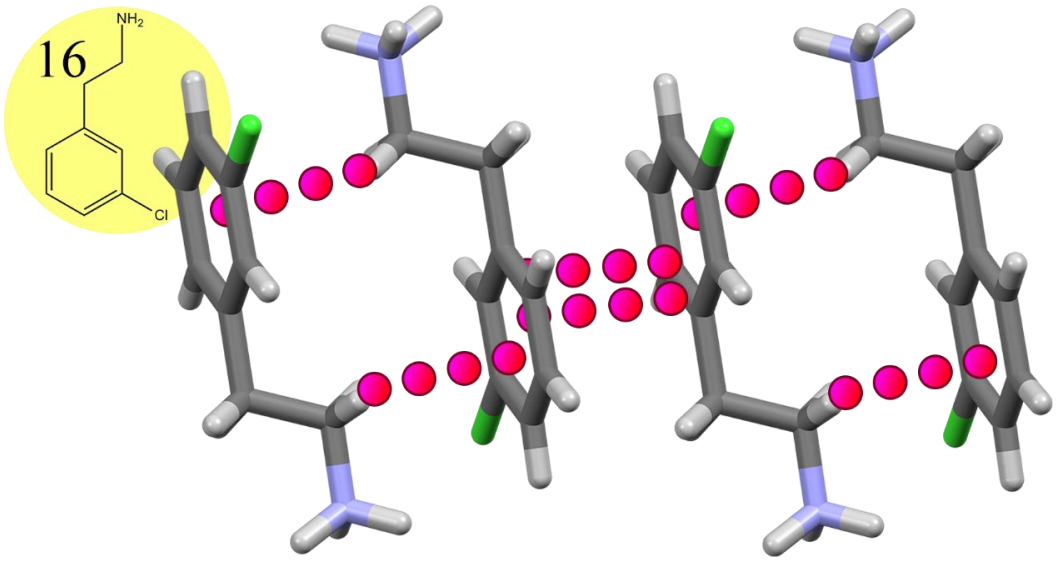

Figure I.3.17 Reciprocated type 4 π-interactions and reciprocated type 3 π-interactions, that when combined form an overall chained structure in compound **16** (Chapter 4). Viewed down the C-axis, rotated 30° about the Y-axis.

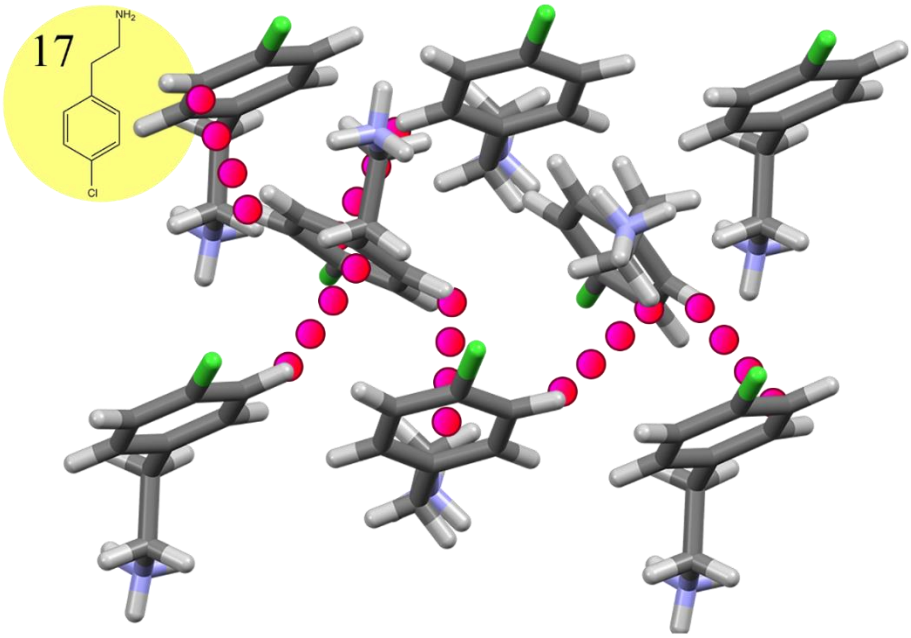

Figure I.3.18 Angled type 2 chained π-interactions in compound **17** (Chapter 4). Additional angled type 2 π-interactions connect the strata. Viewed down the B-axis, rotated 45° about the X-axis.

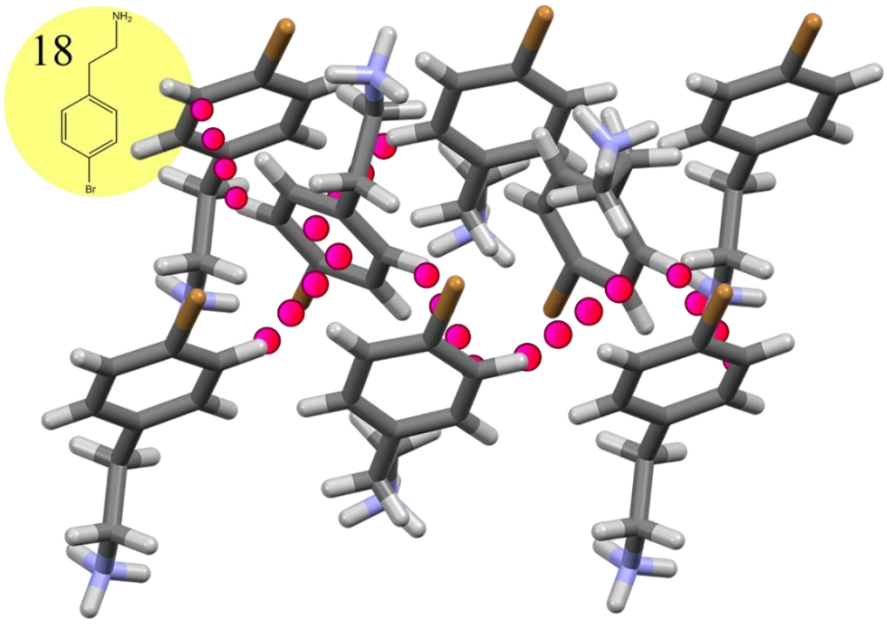

Figure I.3.19 Angled type 2 chained π-interactions in compound **18** (Chapter 4). Additional angled type 2 π-interactions connect the strata. Viewed down the B-axis, rotated 45° about the X-axis.

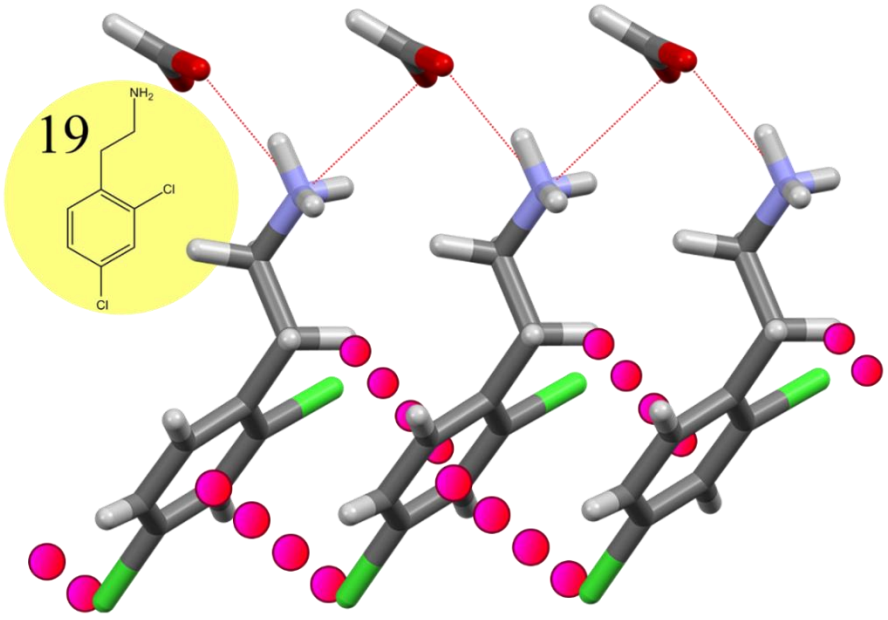

Figure I.3.20 Type 4 and 5 chained π-interactions in compound **19** (Chapter 4). Viewed down the B-axis.

Appendix II

Crystal Structure Information and Tables

II.1 Crystal Structure Information and Tables for Chapter 2 Compounds

II.1.1 Compound 2, Mn_{12}-2-Me, $Mn_{12}O_{12}(O_2CPh\text{-}o\text{-}Me)_{16}(H_2O)_4$, ab10613

Table II.1.1.1 Crystal data and structure refinement for ab10613

Identification code	ab10613
Empirical formula	$C_{128}H_{120}Mn_{12}O_{48}$
Formula weight	3085.52
Temperature/K	100(2)
Crystal system	N/A
Space group	C2/c
a/Å	17.3264(8)
b/Å	38.0559(18)
c/Å	21.1395(10)
α/°	90.00
β/°	97.742(3)
γ/°	90.00
Volume/Å^3	13811.7(11)
Z	4
ρ_{calc}g/cm^3	1.484
μ/mm^{-1}	1.140
F(000)	6288.0
Crystal size/mm^3	? × ? × ?
Radiation	MoKα (λ = 0.71073)
2Θ range for data collection/°	2.14 to 39
Index ranges	-16 ≤ h ≤ 16, -35 ≤ k ≤ 35, -19 ≤ l ≤ 19
Reflections collected	52449
Independent reflections	5997 [R_{int} = 0.0597, R_{sigma} = N/A]
Data/restraints/parameters	5997/0/491
Goodness-of-fit on F^2	1.098
Final R indexes [I>=2σ (I)]	R_1 = 0.0846, wR_2 = 0.2305
Final R indexes [all data]	R_1 = 0.1080, wR_2 = 0.2616
Largest diff. peak/hole / e Å^{-3}	2.20/-0.66

Table II.1.1.2 Fractional Atomic Coordinates (×10^4) and Equivalent Isotropic Displacement Parameters (Å^2×10^3) for ab10613. U_{eq} is defined as 1/3 of of the trace of the orthogonalised U_{IJ} tensor.

Atom	*x*	*y*	*z*	U(eq)
Mn1	5553.3(10)	3444.4(5)	-7971.9(8)	26.9(6)
Mn2	4337.9(9)	3945.9(5)	-8022.1(8)	25.7(6)
Mn3	6547.1(10)	3437.5(5)	-8906.9(9)	32.2(6)
Mn4	3039.2(10)	3951.7(5)	-8940.6(9)	29.9(6)
Mn5	2562.5(10)	3714.4(5)	-7500.9(9)	31.4(6)
Mn6	4647.1(10)	3603.8(5)	-9475.2(9)	30.0(6)

O1	4436(4)	3450.3(19)	-7936(3)	22.6(19)
O2	5467(4)	3936.7(19)	-7893(3)	24.1(19)
O3	4140(4)	3886.4(19)	-8908(4)	25.0(19)
O4	3263(4)	3935(2)	-8054(4)	28(2)
O5	2825(4)	3980(2)	-9870(4)	33(2)
O6	5473(4)	3492(2)	-8843(4)	28(2)
O7	6394(4)	3388(2)	-9833(4)	40(2)
O8	6626(4)	3464(2)	-8002(4)	30(2)
O9	6673(5)	3997(2)	-9031(4)	38(2)
O10	2712(5)	3397(2)	-9032(4)	39(2)
O11	5281(5)	4056(2)	-9799(4)	45(2)
O12	5549(4)	2939(2)	-8025(4)	36(2)
O13	4337(4)	4451(2)	-8095(3)	30(2)
O14	1951(5)	4087(2)	-8942(4)	39(2)
O15	7629(5)	3355(3)	-8953(4)	58(3)
O17	5105(4)	3319(2)	-10097(4)	40(2)
O18	3812(5)	3668(2)	-10175(4)	40(2)
O19	1754(5)	3502(2)	-6992(4)	49(2)
O20	1670(5)	3970(2)	-7960(4)	40(2)
O21	6319(5)	2873(2)	-8795(4)	39(2)
O22	4086(5)	3110(2)	-9194(4)	40(2)
O23	2296(5)	3297(2)	-8084(4)	42(2)
O24	7366(5)	4133(2)	-8107(4)	42(2)
O25	3343(5)	4519(2)	-8878(4)	34(2)
C1	1523(7)	4103(3)	-8507(6)	33(3)
C2	4750(8)	5170(4)	-8391(7)	51(4)
C3	-574(9)	4347(4)	-8413(7)	61(4)
C4	5450(10)	4963(5)	-8338(8)	79(5)
C5	3345(9)	5238(4)	-8557(7)	55(4)
C6	5712(10)	2162(5)	-8880(8)	75(5)
C7	5648(12)	1778(6)	-8777(10)	99(6)
C8	3888(7)	4635(3)	-8488(6)	32(3)
C9	3317(9)	3862(4)	-11429(7)	51(4)
C10	168(8)	4194(4)	-8299(7)	50(4)
C11	768(8)	4289(4)	-8646(7)	47(4)
C12	-102(10)	4723(5)	-9182(8)	76(5)
C13	-679(11)	4607(5)	-8839(8)	78(5)
C14	655(9)	4563(4)	-9068(7)	63(4)
C15	7057(7)	4207(3)	-8657(6)	30(3)
C16	2826(7)	3849(3)	-10971(6)	35(3)
C17	2409(8)	3209(3)	-8633(6)	39(3)
C18	7180(7)	4570(3)	-8873(6)	34(3)
C19	7088(8)	4627(4)	-9526(6)	46(4)
C20	3161(8)	3837(3)	-10281(6)	36(3)
C21	4017(7)	5021(3)	-8472(6)	34(3)

C22	2184(8)	2847(4)	-8832(7)	48(4)
C23	2251(11)	2578(5)	-8386(9)	78(5)
C24	2020(8)	3866(3)	-11149(6)	45(4)
C25	1788(6)	3379(3)	-6486(5)	62(4)
C26	1091(6)	3129(3)	-6447(5)	40(7)
C27	386(6)	3253(3)	-6759(5)	43(7)
C28	-287(6)	3054(3)	-6761(5)	66(9)
C29	-256(6)	2731(3)	-6451(5)	65(9)
C30	449(6)	2607(3)	-6139(5)	62(9)
C31	1122(6)	2806(3)	-6137(5)	54(8)
C32	1890(7)	2643(3)	-5718(6)	75(10)
C33	962(7)	3458(3)	-6122(6)	50(8)
C34	348(7)	3282(3)	-6478(6)	62(9)
C35	-386(7)	3284(3)	-6282(6)	58(8)
C36	-506(7)	3462(3)	-5730(6)	63(9)
C37	107(7)	3639(3)	-5374(6)	48(7)
C38	841(7)	3637(3)	-5570(6)	55(8)
C39	1470(20)	3871(9)	-5173(16)	69(9)
C40	5807(9)	2374(4)	-8354(7)	59(4)
C41	1752(10)	3889(4)	-11809(8)	69(5)
C42	2255(11)	3906(5)	-12255(9)	79(5)
C43	4784(11)	5541(5)	-8412(8)	78(5)
C44	3037(11)	3894(5)	-12069(9)	84(6)
C45	5899(12)	2222(6)	-7744(11)	105(7)
C46	5750(14)	1661(7)	-8163(12)	122(8)
C47	7403(7)	4852(3)	-8456(6)	38(3)
C48	7457(8)	5226(4)	-9369(7)	52(4)
C49	7523(8)	5181(4)	-8726(7)	51(4)
C50	7517(9)	4815(4)	-7732(7)	58(4)
C51	7228(8)	4956(4)	-9771(7)	55(4)
C52	5901(8)	2757(4)	-8418(6)	42(4)
C53	3409(10)	5599(4)	-8573(7)	68(5)
C54	1887(10)	2783(5)	-9459(8)	74(5)
C55	2035(12)	2228(6)	-8597(10)	101(7)
C56	1716(12)	2182(6)	-9202(10)	94(6)
C57	4124(10)	5747(5)	-8506(8)	77(5)
C58	1634(13)	2427(6)	-9624(11)	108(7)
C59	1423(12)	3834(5)	-10724(10)	99(6)
C60	1256(12)	4706(5)	-9463(10)	102(7)
C61	5602(15)	2303(7)	-9535(12)	42(7)
C62	2270(30)	2632(12)	-7690(20)	122(16)
C63	1610(20)	3010(11)	-9900(19)	97(12)
C64	5893(15)	1861(7)	-7623(14)	47(7)
C65	5788(6)	3301(3)	-10226(5)	51(4)
C66	5871(6)	3305(3)	-10908(5)	27(6)

C67	5191(6)	3290(3)	-11339(5)	54(8)
C68	5231(6)	3238(3)	-11985(5)	81(11)
C69	5951(6)	3201(3)	-12199(5)	107(14)
C70	6631(6)	3216(3)	-11768(5)	99(13)
C71	6590(6)	3268(3)	-11122(5)	43(7)
C72	7315(9)	3458(4)	-10836(7)	115(19)
C73	5964(9)	3030(4)	-10760(7)	43(7)
C74	5323(9)	2873(4)	-11119(7)	60(8)
C75	5407(9)	2707(4)	-11690(7)	72(10)
C76	6132(9)	2696(4)	-11903(7)	114(15)
C77	6772(9)	2852(4)	-11545(7)	170(20)
C78	6688(9)	3019(4)	-10973(7)	170(20)
C79	7360(20)	3299(12)	-10709(18)	79(11)
O16	4495(8)	4686(4)	-9995(6)	105(4)

Table II.1.1.3 Anisotropic Displacement Parameters ($Å^2×10^3$) for ab10613. The Anisotropic displacement factor exponent takes the form: $-2\pi^2[h^2a^{*2}U_{11}+2hka^*b^*U_{12}+\ldots]$.

Atom	U_{11}	U_{22}	U_{33}	U_{23}	U_{13}	U_{12}
Mn1	17.0(11)	31.0(12)	32.5(12)	0.7(8)	3.0(9)	2.1(8)
Mn2	13.1(11)	30.6(12)	32.5(12)	-0.9(9)	-0.2(8)	1.9(8)
Mn3	17.6(11)	42.8(13)	36.3(13)	-4.1(9)	4.0(9)	4.1(9)
Mn4	14.5(11)	42.0(13)	31.9(12)	0.7(9)	-1.4(8)	0.7(9)
Mn5	16.4(11)	43.6(13)	33.4(12)	-2.2(9)	0.4(9)	1.1(9)
Mn6	18.3(11)	39.8(12)	31.5(12)	-2.0(9)	1.5(9)	0.7(9)
O1	9(4)	28(5)	30(5)	0(4)	2(3)	-1(3)
O2	7(4)	30(5)	35(5)	3(4)	-1(3)	-4(3)
O3	8(4)	34(5)	33(5)	3(4)	4(3)	-1(3)
O4	11(4)	36(5)	36(5)	3(4)	4(4)	5(4)
O5	18(5)	45(5)	35(5)	1(4)	-2(4)	3(4)
O6	14(4)	34(5)	37(5)	4(4)	4(4)	3(4)
O7	19(5)	62(6)	40(6)	0(4)	4(4)	1(4)
O8	13(4)	36(5)	38(5)	2(4)	-1(4)	4(4)
O9	30(5)	45(6)	39(5)	-2(4)	1(4)	-1(4)
O10	29(5)	47(6)	40(5)	3(4)	1(4)	-10(4)
O11	24(5)	58(6)	50(6)	16(5)	-4(4)	0(4)
O12	31(5)	37(5)	41(5)	-7(4)	7(4)	0(4)
O13	21(5)	38(5)	30(5)	0(4)	-1(4)	5(4)
O14	13(5)	69(7)	36(5)	2(5)	1(4)	10(4)
O15	20(5)	109(8)	43(6)	-30(6)	-5(4)	17(5)
O17	12(5)	73(6)	38(5)	-8(5)	9(4)	3(4)
O18	34(5)	48(6)	36(5)	-7(4)	1(4)	1(4)
C1	9(7)	53(9)	34(8)	4(7)	-6(7)	3(6)

Table II.1.1.4 Bond Lengths for ab10613.

Atom	Atom	Length/Å	Atom	Atom	Length/Å
Mn1	Mn1[1]	2.947(3)	C8	C21	1.485(17)
Mn1	Mn2[1]	2.826(3)	C9	C16	1.373(18)
Mn1	Mn2	2.834(2)	C9	C44	1.38(2)
Mn1	Mn3	2.791(3)	C10	C11	1.398(19)
Mn1	O1[1]	1.916(7)	C11	C14	1.37(2)
Mn1	O1	1.948(7)	C12	C13	1.38(2)
Mn1	O2	1.889(7)	C12	C14	1.44(2)
Mn1	O6	1.837(8)	C14	C60	1.52(2)
Mn1	O8	1.870(7)	C15	O24	1.244(14)
Mn1	O12	1.926(8)	C15	C18	1.480(17)
Mn2	Mn1[1]	2.826(3)	C16	C20	1.495(18)
Mn2	Mn2[1]	2.962(3)	C16	C24	1.399(18)
Mn2	Mn4	2.767(2)	C17	O23	1.249(14)
Mn2	O1	1.901(7)	C17	C22	1.477(19)
Mn2	O2	1.939(7)	C18	C19	1.386(17)
Mn2	O2[1]	1.918(7)	C18	C47	1.408(17)
Mn2	O3	1.872(8)	C19	C51	1.386(19)
Mn2	O4	1.855(7)	C22	C23	1.39(2)
Mn2	O13	1.927(8)	C22	C54	1.38(2)
Mn3	O6	1.895(7)	C23	C55	1.44(3)
Mn3	O7	1.949(8)	C23	C62	1.48(4)
Mn3	O8	1.902(8)	C24	C41	1.41(2)
Mn3	O9	2.159(8)	C24	C59	1.46(2)
Mn3	O15	1.915(8)	C25	O15[1]	1.280(13)
Mn3	O21	2.204(8)	C25	C26	1.5480
Mn4	O3	1.915(7)	C25	C33	1.741(15)
Mn4	O4	1.863(8)	C26	C27	1.3900
Mn4	O5	1.953(8)	C26	C31	1.3900
Mn4	O10	2.187(8)	C27	C28	1.3900
Mn4	O14	1.954(8)	C28	C29	1.3900
Mn4	O25	2.221(8)	C29	C30	1.3900
Mn5	O4	1.981(7)	C30	C31	1.3900
Mn5	O8[1]	1.901(8)	C31	C32	1.618(16)
Mn5	O19	2.045(9)	C33	C34	1.3900
Mn5	O20	1.968(9)	C33	C38	1.3900
Mn5	O23	2.026(9)	C34	C35	1.3900
Mn5	O24[1]	2.041(9)	C35	C36	1.3900
Mn6	O3	1.910(7)	C36	C37	1.3900
Mn6	O6	1.871(7)	C37	C38	1.3900
Mn6	O11	2.200(9)	C38	C39	1.56(4)
Mn6	O17	1.952(8)	C40	C45	1.40(2)
Mn6	O18	1.940(8)	C40	C52	1.47(2)
Mn6	O22	2.234(8)	C41	C42	1.37(2)

O1	Mn1[1]	1.916(7)	C42	C44	1.36(2)
O2	Mn2[1]	1.918(7)	C43	C57	1.38(2)
O5	C20	1.235(15)	C45	C64	1.40(3)
O7	C65	1.291(12)	C46	C64	1.37(3)
O8	Mn5[1]	1.901(8)	C47	C49	1.402(18)
O9	C15	1.253(14)	C47	C50	1.525(18)
O10	C17	1.273(15)	C48	C49	1.359(19)
O12	C52	1.296(15)	C48	C51	1.358(19)
O13	C8	1.271(14)	C53	C57	1.35(2)
O14	C1	1.259(14)	C54	C58	1.45(3)
O15	C25[1]	1.280(13)	C54	C63	1.31(4)
O17	C65	1.250(12)	C55	C56	1.34(3)
O18	C20	1.293(15)	C56	C58	1.29(3)
O19	C25	1.161(12)	C65	C66	1.4676
O21	C52	1.230(14)	C65	C73	1.590(19)
O24	Mn5[1]	2.041(9)	C66	C67	1.3900
C1	O20	1.256(14)	C66	C71	1.3900
C1	C11	1.482(18)	C67	C68	1.3900
C2	C4	1.44(2)	C68	C69	1.3900
C2	C21	1.381(18)	C69	C70	1.3900
C2	C43	1.41(2)	C70	C71	1.3900
C3	C10	1.40(2)	C71	C72	1.503(19)
C3	C13	1.33(2)	C73	C74	1.3900
C5	C21	1.417(19)	C73	C78	1.3900
C5	C53	1.38(2)	C74	C75	1.3900
C6	C7	1.49(3)	C75	C76	1.3900
C6	C40	1.37(2)	C76	C77	1.3900
C6	C61	1.47(3)	C77	C78	1.3900
C7	C46	1.36(3)	C78	C79	1.62(4)
C8	O25	1.249(14)			

[1]1-X,+Y,-3/2-Z

Table II.1.1.5 Bond Angles for ab10613.

Atom	Atom	Atom	Angle/°	Atom	Atom	Atom	Angle/°
Mn2	Mn1	Mn1[1]	58.49(6)	Mn2	O1	Mn1[1]	95.5(3)
Mn2[1]	Mn1	Mn1[1]	58.74(6)	Mn1	O2	Mn2[1]	95.9(3)
Mn2[1]	Mn1	Mn2	63.11(7)	Mn1	O2	Mn2	95.5(3)
Mn3	Mn1	Mn1[1]	177.49(11)	Mn2[1]	O2	Mn2	100.3(3)
Mn3	Mn1	Mn2[1]	123.17(8)	Mn2	O3	Mn4	93.9(3)
Mn3	Mn1	Mn2	120.40(8)	Mn2	O3	Mn6	131.2(4)
O1[1]	Mn1	Mn1[1]	40.7(2)	Mn6	O3	Mn4	126.2(4)
O1	Mn1	Mn1[1]	39.9(2)	Mn2	O4	Mn4	96.2(3)
O1[1]	Mn1	Mn2	86.4(2)	Mn2	O4	Mn5	132.9(4)
O1	Mn1	Mn2	41.9(2)	Mn4	O4	Mn5	123.2(4)

O1[1]	Mn1	Mn2[1]	42.0(2)	C20	O5	Mn4	129.9(8)
O1	Mn1	Mn2[1]	86.0(2)	Mn1	O6	Mn3	96.8(3)
O1	Mn1	Mn3	137.7(2)	Mn1	O6	Mn6	133.3(4)
O1[1]	Mn1	Mn3	141.7(2)	Mn6	O6	Mn3	129.6(4)
O1[1]	Mn1	O1	80.6(3)	C65	O7	Mn3	131.3(7)
O1[1]	Mn1	O12	94.0(3)	Mn1	O8	Mn3	95.4(3)
O2	Mn1	Mn1[1]	82.7(2)	Mn1	O8	Mn5[1]	131.6(4)
O2	Mn1	Mn2[1]	42.5(2)	Mn5[1]	O8	Mn3	122.4(4)
O2	Mn1	Mn2	42.9(2)	C15	O9	Mn3	127.4(8)
O2	Mn1	Mn3	97.8(2)	C17	O10	Mn4	127.7(8)
O2	Mn1	O1	83.9(3)	C52	O12	Mn1	125.1(8)
O2	Mn1	O1[1]	83.7(3)	C8	O13	Mn2	126.7(7)
O2	Mn1	O12	174.7(3)	C1	O14	Mn4	132.5(8)
O6	Mn1	Mn1[1]	135.3(2)	C25[1]	O15	Mn3	129.3(7)
O6	Mn1	Mn2	86.6(2)	C65	O17	Mn6	131.3(7)
O6	Mn1	Mn2[1]	131.8(2)	C20	O18	Mn6	137.7(8)
O6	Mn1	Mn3	42.4(2)	C25	O19	Mn5	133.7(8)
O6	Mn1	O1[1]	172.6(3)	C1	O20	Mn5	134.6(8)
O6	Mn1	O1	95.6(3)	C52	O21	Mn3	123.3(8)
O6	Mn1	O2	89.7(3)	C17	O23	Mn5	136.5(8)
O6	Mn1	O8	84.5(3)	C15	O24	Mn5[1]	138.3(8)
O6	Mn1	O12	92.3(3)	C8	O25	Mn4	122.4(8)
O8	Mn1	Mn1[1]	139.8(3)	O14	C1	C11	118.0(11)
O8	Mn1	Mn2[1]	91.8(2)	O20	C1	O14	125.9(11)
O8	Mn1	Mn2	135.2(2)	O20	C1	C11	116.1(12)
O8	Mn1	Mn3	42.7(2)	C21	C2	C4	122.4(14)
O8	Mn1	O1[1]	99.1(3)	C21	C2	C43	116.6(14)
O8	Mn1	O1	177.1(3)	C43	C2	C4	120.8(15)
O8	Mn1	O2	93.2(3)	C13	C3	C10	117.5(16)
O8	Mn1	O12	91.9(3)	C53	C5	C21	121.1(14)
O12	Mn1	Mn1[1]	92.4(2)	C40	C6	C7	117.6(16)
O12	Mn1	Mn2[1]	135.8(2)	C40	C6	C61	122.6(18)
O12	Mn1	Mn2	132.3(2)	C61	C6	C7	119.5(18)
O12	Mn1	Mn3	87.0(2)	C46	C7	C6	117(2)
O12	Mn1	O1	91.0(3)	O13	C8	C21	117.1(11)
Mn1[1]	Mn2	Mn1	62.77(8)	O25	C8	O13	125.3(11)
Mn1	Mn2	Mn2[1]	58.32(6)	O25	C8	C21	117.6(11)
Mn1[1]	Mn2	Mn2[1]	58.56(6)	C16	C9	C44	121.6(15)
Mn4	Mn2	Mn1[1]	119.58(8)	C11	C10	C3	122.1(14)
Mn4	Mn2	Mn1	124.17(8)	C10	C11	C1	118.0(13)
Mn4	Mn2	Mn2[1]	176.42(11)	C14	C11	C1	122.6(13)
O1	Mn2	Mn1	43.3(2)	C14	C11	C10	119.3(14)
O1	Mn2	Mn1[1]	42.4(2)	C13	C12	C14	119.0(17)
O1	Mn2	Mn2[1]	83.0(2)	C3	C13	C12	123.2(18)
O1	Mn2	Mn4	97.4(2)	C11	C14	C12	118.6(15)

O1	Mn2	O2[1]	83.3(3)	C11	C14	C60	125.6(15)
O1	Mn2	O2	83.9(3)	C12	C14	C60	115.7(15)
O1	Mn2	O13	175.0(3)	O9	C15	C18	119.2(11)
O2	Mn2	Mn1	41.6(2)	O24	C15	O9	124.8(11)
O2	Mn2	Mn1[1]	85.3(2)	O24	C15	C18	116.0(11)
O2[1]	Mn2	Mn1[1]	41.7(2)	C9	C16	C20	119.5(12)
O2[1]	Mn2	Mn1	85.5(2)	C9	C16	C24	120.0(12)
O2	Mn2	Mn2[1]	39.6(2)	C24	C16	C20	120.4(12)
O2[1]	Mn2	Mn2[1]	40.1(2)	O10	C17	C22	117.0(12)
O2	Mn2	Mn4	144.0(2)	O23	C17	O10	126.4(12)
O2[1]	Mn2	Mn4	136.4(2)	O23	C17	C22	116.6(12)
O2[1]	Mn2	O2	79.6(3)	C19	C18	C15	116.9(11)
O2[1]	Mn2	O13	95.6(3)	C19	C18	C47	119.3(12)
O3	Mn2	Mn1	89.5(2)	C47	C18	C15	123.8(11)
O3	Mn2	Mn1[1]	130.3(2)	C18	C19	C51	120.7(13)
O3	Mn2	Mn2[1]	139.9(2)	O5	C20	O18	125.4(12)
O3	Mn2	Mn4	43.7(2)	O5	C20	C16	121.1(12)
O3	Mn2	O1	88.7(3)	O18	C20	C16	113.6(11)
O3	Mn2	O2[1]	172.0(3)	C2	C21	C5	120.1(12)
O3	Mn2	O2	100.6(3)	C2	C21	C8	122.9(12)
O3	Mn2	O13	92.4(3)	C5	C21	C8	117.0(12)
O4	Mn2	Mn1[1]	88.7(2)	C23	C22	C17	120.0(14)
O4	Mn2	Mn1	136.3(2)	C54	C22	C17	119.3(13)
O4	Mn2	Mn2[1]	134.4(3)	C54	C22	C23	120.7(15)
O4	Mn2	Mn4	42.0(2)	C22	C23	C55	118.5(17)
O4	Mn2	O1	93.2(3)	C22	C23	C62	124(2)
O4	Mn2	O2[1]	94.4(3)	C55	C23	C62	114(2)
O4	Mn2	O2	173.6(3)	C16	C24	C41	116.9(13)
O4	Mn2	O3	85.0(3)	C16	C24	C59	126.4(14)
O4	Mn2	O13	91.7(3)	C41	C24	C59	116.5(14)
O13	Mn2	Mn1[1]	137.1(2)	O15[1]	C25	C26	117.6(6)
O13	Mn2	Mn1	131.8(2)	O15[1]	C25	C33	107.9(8)
O13	Mn2	Mn2[1]	93.0(2)	O19	C25	O15[1]	129.3(10)
O13	Mn2	Mn4	86.8(2)	O19	C25	C26	110.7(7)
O13	Mn2	O2	91.1(3)	O19	C25	C33	113.2(9)
O6	Mn3	Mn1	40.8(2)	C26	C25	C33	52.4(5)
O6	Mn3	O7	94.6(3)	C27	C26	C25	114.1
O6	Mn3	O8	82.0(3)	C27	C26	C31	120.0
O6	Mn3	O9	91.0(3)	C31	C26	C25	125.9
O6	Mn3	O15	176.6(4)	C28	C27	C26	120.0
O6	Mn3	O21	84.7(3)	C29	C28	C27	120.0
O7	Mn3	Mn1	134.3(2)	C28	C29	C30	120.0
O7	Mn3	O9	88.6(3)	C29	C30	C31	120.0
O7	Mn3	O21	90.6(3)	C26	C31	C32	125.0(6)
O8	Mn3	Mn1	41.8(2)	C30	C31	C26	120.0

O8	Mn3	O7	175.5(3)	C30	C31	C32	114.9(6)
O8	Mn3	O9	94.4(3)	C34	C33	C25	106.9(5)
O8	Mn3	O15	97.0(3)	C34	C33	C38	120.0
O8	Mn3	O21	86.1(3)	C38	C33	C25	133.0(5)
O9	Mn3	Mn1	99.1(2)	C35	C34	C33	120.0
O9	Mn3	O21	175.5(3)	C36	C35	C34	120.0
O15	Mn3	Mn1	137.6(3)	C35	C36	C37	120.0
O15	Mn3	O7	86.3(4)	C38	C37	C36	120.0
O15	Mn3	O9	92.3(4)	C33	C38	C39	124.0(13)
O15	Mn3	O21	92.0(4)	C37	C38	C33	120.0
O21	Mn3	Mn1	78.3(2)	C37	C38	C39	115.7(13)
O3	Mn4	Mn2	42.5(2)	C6	C40	C45	119.6(17)
O3	Mn4	O5	95.5(3)	C6	C40	C52	120.7(14)
O3	Mn4	O10	97.1(3)	C45	C40	C52	119.4(15)
O3	Mn4	O14	171.9(4)	C42	C41	C24	121.8(17)
O3	Mn4	O25	84.1(3)	C44	C42	C41	120.1(18)
O4	Mn4	Mn2	41.8(2)	C57	C43	C2	122.4(17)
O4	Mn4	O3	83.6(3)	C42	C44	C9	119.5(18)
O4	Mn4	O5	178.4(3)	C64	C45	C40	125(2)
O4	Mn4	O10	94.1(3)	C7	C46	C64	127(3)
O4	Mn4	O14	94.6(3)	C18	C47	C50	123.1(12)
O4	Mn4	O25	87.6(3)	C49	C47	C18	117.9(12)
O5	Mn4	Mn2	137.1(2)	C49	C47	C50	119.0(12)
O5	Mn4	O10	87.3(3)	C51	C48	C49	120.7(14)
O5	Mn4	O14	86.1(3)	C48	C49	C47	121.4(14)
O5	Mn4	O25	91.0(3)	C48	C51	C19	119.9(14)
O10	Mn4	Mn2	103.4(2)	O12	C52	C40	113.8(12)
O10	Mn4	O25	178.0(3)	O21	C52	O12	126.3(12)
O14	Mn4	Mn2	134.1(3)	O21	C52	C40	119.8(13)
O14	Mn4	O10	90.9(3)	C57	C53	C5	119.2(17)
O14	Mn4	O25	87.9(3)	C22	C54	C58	117.2(17)
O25	Mn4	Mn2	78.6(2)	C63	C54	C22	128(2)
O4	Mn5	O19	174.6(3)	C63	C54	C58	112(2)
O4	Mn5	O23	94.6(3)	C56	C55	C23	119(2)
O4	Mn5	O24[1]	92.9(3)	C58	C56	C55	124(2)
O8[1]	Mn5	O4	94.4(3)	C53	C57	C43	120.7(18)
O8[1]	Mn5	O19	90.8(4)	C56	C58	C54	121(2)
O8[1]	Mn5	O20	175.1(4)	C46	C64	C45	114(3)
O8[1]	Mn5	O23	92.1(3)	O7	C65	C66	116.8(6)
O8[1]	Mn5	O24[1]	93.6(3)	O7	C65	C73	114.0(10)
O20	Mn5	O4	90.2(3)	O17	C65	O7	123.8(9)
O20	Mn5	O19	84.6(4)	O17	C65	C66	115.7(6)
O20	Mn5	O23	89.3(3)	O17	C65	C73	118.0(10)
O20	Mn5	O24[1]	84.4(3)	C66	C65	C73	41.9(6)
O23	Mn5	O19	83.9(4)	C67	C66	C65	117.2

O23	Mn5	O24[1]	170.2(4)	C67	C66	C71	120.0
O24[1]	Mn5	O19	88.1(4)	C71	C66	C65	122.0
O3	Mn6	O11	92.6(3)	C66	C67	C68	120.0
O3	Mn6	O17	176.2(3)	C69	C68	C67	120.0
O3	Mn6	O18	92.8(3)	C68	C69	C70	120.0
O3	Mn6	O22	93.1(3)	C69	C70	C71	120.0
O6	Mn6	O3	93.0(3)	C66	C71	C72	123.9(7)
O6	Mn6	O11	91.9(3)	C70	C71	C66	120.0
O6	Mn6	O17	90.8(3)	C70	C71	C72	108.3(7)
O6	Mn6	O18	173.4(4)	C74	C73	C65	116.7(7)
O6	Mn6	O22	86.4(3)	C74	C73	C78	120.0
O11	Mn6	O22	174.1(3)	C78	C73	C65	121.2(7)
O17	Mn6	O11	87.6(4)	C73	C74	C75	120.0
O17	Mn6	O22	86.8(3)	C76	C75	C74	120.0
O18	Mn6	O11	90.9(3)	C77	C76	C75	120.0
O18	Mn6	O17	83.5(3)	C78	C77	C76	120.0
O18	Mn6	O22	90.2(3)	C73	C78	C79	120.5(15)
Mn1[1]	O1	Mn1	99.4(3)	C77	C78	C73	120.0
Mn2	O1	Mn1	94.8(3)	C77	C78	C79	116.4(15)

[1]1-X,+Y,-3/2-Z

Table II.1.1.6 Hydrogen Atom Coordinates (Å×10^4) and Isotropic Displacement Parameters (Å^2×10^3) for ab10613

Atom	*x*	*y*	*z*	U(eq)
H10A	5734	4062	-9592	95
H10B	5101	4195	-10096	76
H1B	4312	2896	-9163	48
H18A	3625	3154	-9122	60
H1MA	-997	4263	-8204	73
H1OA	5330	4717	-8330	118
H1OB	5711	5013	-8700	118
H1OC	5782	5026	-7953	118
H1PA	2841	5129	-8603	66
H2RA	5558	1616	-9129	118
H23A	3869	3853	-11295	61
H1A	271	4018	-7973	61
H2A	-205	4912	-9482	92
H31A	-1177	4721	-8909	93
H9A	6939	4434	-9809	55
H25A	1200	3898	-11940	83
H14B	2051	3925	-12699	95
H30A	5288	5650	-8356	94
H32A	3389	3903	-12382	101
H36A	6009	2379	-7387	126
H40A	5721	1413	-8094	147

H18B	7581	5449	-9539	62
H19A	7645	5380	-8451	61
H1AA	7419	4576	-7618	87
H1AB	8043	4877	-7567	87
H1AC	7164	4968	-7553	87
H1BA	7156	4992	-10225	66
H1DA	2950	5743	-8626	82
H1GA	2127	2033	-8310	122
H1HA	1542	1949	-9326	113
H1IA	4172	5998	-8530	93
H1JA	1388	2373	-10047	129
H1KA	1662	3817	-10289	149
H1KB	1091	4037	-10774	149
H1KC	1120	3627	-10837	149
H1LA	1737	4580	-9356	154
H1LB	1072	4675	-9908	154
H1LC	1341	4951	-9374	154
H1QA	5654	2554	-9520	63
H1QB	5982	2205	-9776	63
H1QC	5089	2241	-9734	63
H71A	2408	2870	-7577	182
H71B	1773	2578	-7558	182
H71C	2657	2475	-7485	182
H71D	1797	3242	-9780	146
H71E	1763	2950	-10307	146
H71F	1055	3005	-9928	146
H1TA	5954	1768	-7197	56

Table II.1.1.7 Atomic Occupancy for ab10613

Atom	***Occupancy***	**Atom**	***Occupancy***	**Atom**	***Occupancy***
C26	0.50	C27	0.50	C28	0.50
C29	0.50	C30	0.50	C31	0.50
C32	0.50	C33	0.50	C34	0.50
C35	0.50	C36	0.50	C37	0.50
C38	0.50	C39	0.50	C61	0.50
H1QA	0.50	H1QB	0.50	H1QC	0.50
C62	0.50	H71A	0.50	H71B	0.50
H71C	0.50	C63	0.50	H71D	0.50
H71E	0.50	H71F	0.50	C64	0.50
H1TA	0.50	C66	0.50	C67	0.50
C68	0.50	C69	0.50	C70	0.50
C71	0.50	C72	0.50	C73	0.50
C74	0.50	C75	0.50	C76	0.50

C77 0.50 C78 0.50 C79 0.50

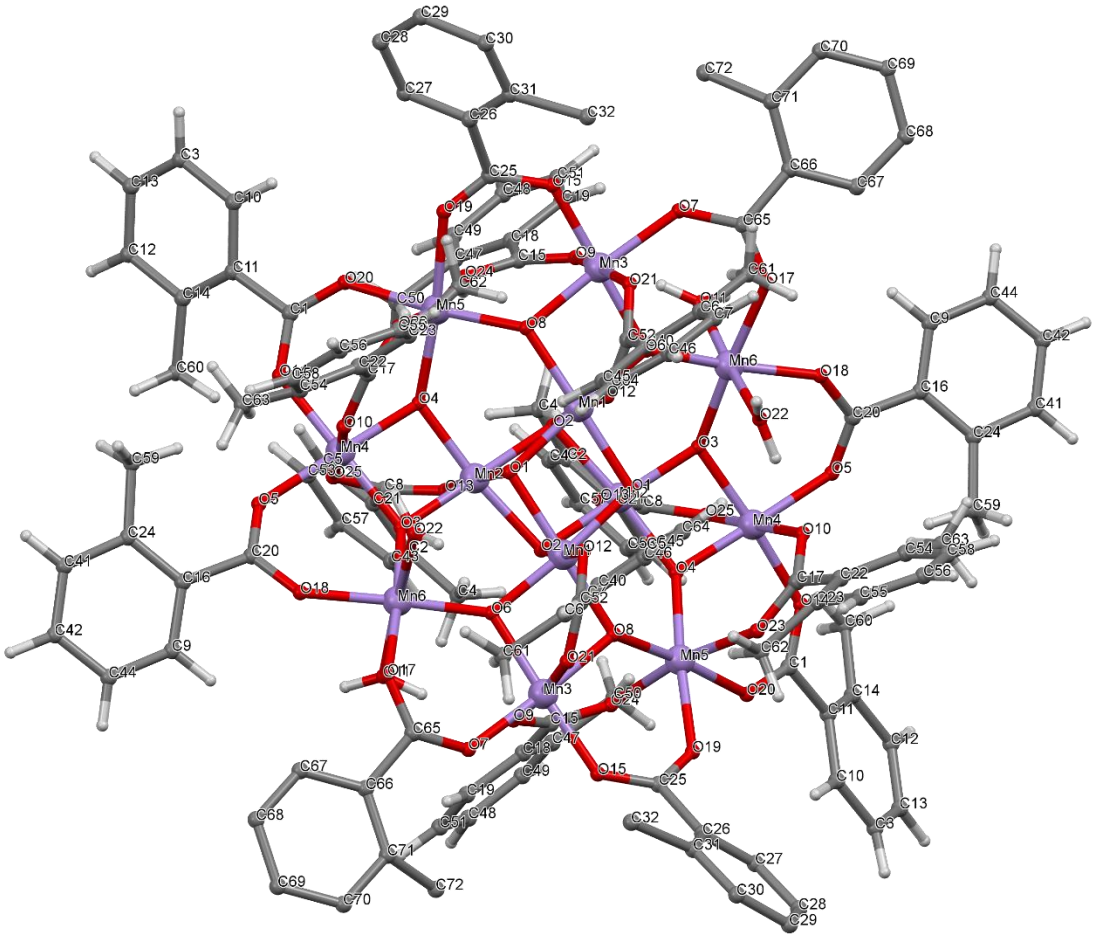

Figure II.1.1 Crystal Structure with atomic labels for compound **2, Mn_{12}-2-Me, $Mn_{12}O_{12}(O_2CPh\text{-}o\text{-}Me)_{16}(H_2O)_4$, ab10613**

II.1.2 Compound 3, Mn_{12}-2-Et, $Mn_{12}O_{12}(O_2CPh\text{-}o\text{-}Et)_{16}(H_2O)_4$, ab50416

Table II.1.2.1 Crystal data and structure refinement for ab50416.

Identification code	ab50416
Empirical formula	$C_{144}H_{145}O_{48}Mn_{12}$
Formula weight	3302.87
Temperature/K	100(2)
Crystal system	Triclinic
Space group	P-1
a/Å	17.7643(19)
b/Å	17.928(2)
c/Å	24.134(3)
α/°	95.187(6)
β/°	95.815(6)
γ/°	92.413(7)
Volume/Å^3	7604.9(15)
Z	2
ρ_{calc}g/cm^3	1.442
μ/mm^{-1}	1.040
F(000)	3386
Crystal size/mm^3	0.20 × 0.13 × 0.09
Radiation	Mo Kα (λ = 0.71073)
2Θ range for data collection/°	2.10 to 40
Index ranges	$-16 \le h \le 16$, $-35 \le k \le 35$, $-19 \le l \le 19$
Reflections collected	890012
Independent reflections	19724 [R_{int} = 0.0749, R_{sigma} = 0.0308]
Data/restraints/parameters	19724 /0/489
Goodness-of-fit on F^2	1.103
Final R indexes [I>=2σ (I)]	R_1 = 0.1476, wR_2 = 0.3790
Final R indexes [all data]	R_1 = 0.1635, wR_2 = 0.3895
Largest diff. peak/hole / e Å^{-3}	4.7/-1.6

Table II.1.2.2 Fractional Atomic Coordinates (×10^4) and Equivalent Isotropic Displacement Parameters (Å^2×10^3) for ab50416. U_{eq} is defined as 1/3 of of the trace of the orthogonalised U_{IJ} tensor.

Atom	Atom	X	Y	Z	U(eq)
Mn1	Mn	0.91720(13)	0.61966(12)	0.38100(9)	0.0150(5)
Mn2	Mn	0.94373(13)	0.55574(12)	0.24965(9)	0.0149(5)
Mn3	Mn	0.87967(13)	0.58006(13)	0.11783(9)	0.0158(5)
Mn4	Mn	0.75837(13)	0.70563(14)	0.41753(10)	0.0202(6)
Mn5	Mn	0.85381(13)	0.70793(13)	0.30113(9)	0.0157(5)
Mn6	Mn	0.78859(14)	0.73516(13)	0.07751(10)	0.0197(6)
Mn7	Mn	0.78843(13)	0.64067(13)	0.19530(9)	0.0154(5)
Mn8	Mn	0.69479(13)	0.70633(14)	0.27837(10)	0.0216(6)

Mn9	Mn	0.78383(14)	0.79807(13)	0.21554(10)	0.0208(6)
Mn10	Mn	0.72134(16)	0.89428(15)	0.14263(11)	0.0295(7)
Mn11	Mn	0.59226(16)	0.76145(17)	0.34946(11)	0.0334(7)
Mn12	Mn	0.60538(17)	0.86627(17)	0.24367(12)	0.0384(8)
O1	O	0.7125(6)	0.5629(6)	0.1646(4)	0.018(2)
O2	O	0.7726(6)	0.6364(6)	0.2725(4)	0.020(2)
O3	O	0.6507(9)	0.9295(8)	0.3083(6)	0.049(4)
O4	O	0.6235(8)	0.8738(8)	0.3829(5)	0.043(4)
O5	O	0.8829(6)	0.5860(6)	0.0378(4)	0.017(2)
O6	O	0.6224(6)	0.6199(7)	0.2620(4)	0.025(3)
O7	O	0.6183(6)	0.7727(6)	0.2775(4)	0.024(3)
O8	O	0.7134(6)	0.7141(6)	0.2023(4)	0.021(2)
O9	O	0.5815(9)	0.9600(8)	0.2079(6)	0.049(4)
O10	O	0.8287(6)	0.7026(6)	0.4851(4)	0.019(2)
O11	O	0.8111(6)	0.6575(6)	0.1236(4)	0.016(2)
O12	O	0.7328(7)	0.5838(6)	0.4216(5)	0.029(3)
O13	O	0.7771(6)	0.7804(6)	0.2925(4)	0.025(3)
O14	O	0.6725(9)	0.9897(8)	0.1523(6)	0.053(4)
O15	O	0.9210(5)	0.6326(6)	0.3029(4)	0.016(2)
O16	O	1.0246(6)	0.6282(6)	0.2167(4)	0.022(2)
O17	O	0.7675(7)	0.8099(7)	0.0245(4)	0.028(3)
O18	O	0.8578(5)	0.7224(5)	0.2244(4)	0.014(2)
O19	O	0.4980(8)	0.8805(8)	0.2772(6)	0.049(4)
O20	O	0.9291(6)	0.7864(6)	0.3323(4)	0.018(2)
O21	O	0.9391(6)	0.4902(6)	0.1122(4)	0.019(2)
O22	O	0.9091(6)	0.7621(6)	0.0744(4)	0.026(3)
O23	O	0.7793(6)	0.8066(6)	0.1385(4)	0.020(2)
O24	O	0.5522(7)	0.8124(8)	0.1796(5)	0.042(3)
O25	O	0.6855(6)	0.7123(7)	0.3562(4)	0.026(3)
O26	O	0.7952(6)	0.6650(6)	0.0098(4)	0.022(3)
O27	O	0.8672(6)	0.8725(6)	0.2327(4)	0.023(3)
O28	O	0.5696(7)	0.7438(7)	0.4249(5)	0.036(3)
O29	O	0.9116(6)	0.6172(5)	0.4610(4)	0.018(2)
O30	O	0.9725(6)	0.4710(6)	0.2013(4)	0.020(2)
O31	O	0.7388(7)	0.9192(6)	0.0681(5)	0.030(3)
O32	O	0.5378(6)	0.6525(8)	0.3226(5)	0.035(3)
O33	O	0.9890(6)	0.7224(6)	0.3989(4)	0.021(2)
O34	O	0.8653(6)	0.5753(6)	0.1940(4)	0.018(2)
O35	O	0.6086(8)	0.8534(8)	0.1081(5)	0.041(3)
O36	O	0.4902(8)	0.7964(10)	0.3366(6)	0.056(4)
O37	O	0.8726(6)	0.4747(6)	0.2825(4)	0.022(3)
O38	O	1.0283(6)	0.5288(6)	0.2997(4)	0.020(2)
O39	O	0.7103(6)	0.8655(7)	0.2129(5)	0.029(3)

O40	O	0.8359(6)	0.6845(6)	0.3730(4)	0.017(2)
O41	O	0.8413(6)	0.5235(6)	0.3666(4)	0.019(2)
O42	O	1.0085(6)	0.5636(6)	0.3888(4)	0.018(2)
O43	O	0.8279(7)	0.9580(7)	0.1726(5)	0.033(3)
O44	O	0.6844(6)	0.7273(7)	0.4717(4)	0.029(3)
O45	O	0.9745(6)	0.6593(6)	0.1342(4)	0.019(2)
O46	O	0.7784(6)	0.5069(6)	0.0991(4)	0.018(2)
C1	C	1.0499(9)	0.5353(8)	0.3522(7)	0.024(4)
C2	C	0.7564(9)	0.8788(10)	0.0272(6)	0.023(4)
C3	C	0.9673(8)	0.4510(9)	0.1495(7)	0.020(4)
C4	C	1.2290(11)	0.4815(11)	0.4324(8)	0.038(5)
C5	C	0.3610(14)	0.7686(14)	0.3893(12)	0.066(7)
C6	C	0.5184(10)	0.5326(10)	0.2696(7)	0.030(4)
C7	C	0.8825(9)	0.6622(9)	0.4962(6)	0.021(4)
C8	C	0.6778(11)	0.9954(12)	0.3967(8)	0.043(5)
C9	C	0.9534(9)	0.3704(10)	0.0276(7)	0.028(4)
C10	C	0.8336(9)	0.5755(9)	-0.0572(6)	0.020(4)
C11	C	0.4824(10)	0.7961(10)	0.0901(7)	0.032(4)
C12	C	0.9241(12)	0.7047(10)	0.6549(7)	0.034(5)
C13	C	0.6473(8)	0.4730(9)	0.0964(7)	0.019(4)
C14	C	0.9766(9)	0.7818(9)	0.3767(7)	0.021(4)
C15	C	0.5963(9)	0.4537(9)	0.1353(7)	0.026(4)
C16	C	0.9865(10)	0.6331(9)	0.5642(7)	0.025(4)
C17	C	0.6295(9)	0.4555(9)	0.0387(6)	0.020(4)
C18	C	0.7193(10)	0.5171(9)	0.1215(6)	0.023(4)
C19	C	0.8329(10)	0.4935(11)	-0.1617(8)	0.034(4)
C20	C	0.8679(9)	0.5059(10)	-0.0637(6)	0.023(4)
C21	C	0.9922(11)	0.6722(10)	0.6612(7)	0.033(5)
C22	C	1.1939(11)	0.8073(11)	0.2204(8)	0.039(5)
C23	C	1.1462(11)	0.6329(10)	0.4815(8)	0.036(4)
C24	C	0.5588(10)	0.4182(10)	0.0202(7)	0.031(4)
C25	C	0.7670(10)	0.9186(11)	-0.0244(7)	0.033(4)
C26	C	0.7555(10)	0.3922(10)	0.3764(7)	0.027(4)
C27	C	0.5739(10)	0.7269(11)	0.5193(8)	0.037(5)
C28	C	1.1632(11)	0.6844(12)	0.3071(8)	0.044(5)
C29	C	1.0678(10)	0.9784(10)	0.3842(8)	0.032(4)
C30	C	1.1139(12)	0.7459(11)	0.2838(8)	0.040(5)
C31	C	1.1599(9)	0.4708(9)	0.3247(7)	0.026(4)
C32	C	1.0355(10)	0.8692(9)	0.4589(7)	0.025(4)
C33	C	0.526(3)	1.218(2)	0.1558(11)	0.14(2)
C34	C	1.0877(11)	0.9817(13)	0.2337(8)	0.044(5)
C35	C	0.5277(11)	0.4172(11)	0.1154(8)	0.038(5)
C36	C	0.5435(15)	0.9014(14)	-0.0080(11)	0.066(7)

C37	C	0.5089(11)	0.3985(11)	0.0568(9)	0.041(5)
C38	C	0.4647(12)	0.8478(14)	0.3114(9)	0.050(6)
C39	C	1.2117(11)	0.8252(11)	0.1662(8)	0.036(5)
C40	C	0.5610(10)	0.6085(12)	0.2864(8)	0.036(5)
C41	C	0.8696(10)	0.3492(11)	0.0220(8)	0.036(4)
C42	C	0.6126(10)	0.7345(10)	0.4679(7)	0.029(4)
C43	C	0.5559(11)	0.4701(10)	0.2748(7)	0.033(4)
C44	C	1.0647(11)	0.2388(10)	0.1154(9)	0.040(5)
C45	C	0.5159(14)	0.7720(14)	0.5323(10)	0.058(6)
C46	C	0.7430(10)	0.3686(9)	0.2754(7)	0.026(4)
C47	C	1.0693(11)	0.2752(10)	0.1695(9)	0.038(5)
C48	C	0.6770(10)	0.6691(12)	-0.0940(8)	0.040(5)
C49	C	0.8749(11)	0.9331(10)	0.2072(8)	0.032(4)
C50	C	1.0159(12)	0.9405(12)	0.2212(8)	0.042(5)
C51	C	1.2313(11)	0.4425(12)	0.3360(8)	0.040(5)
C52	C	0.6934(11)	0.3057(10)	0.2810(8)	0.039(5)
C53	C	1.0703(10)	0.9407(10)	0.4779(7)	0.030(4)
C54	C	0.4203(10)	0.7732(11)	0.1175(8)	0.037(5)
C55	C	0.6521(10)	0.4638(11)	-0.0644(7)	0.033(4)
C56	C	1.1663(10)	0.7938(11)	0.1185(7)	0.035(5)
C57	C	1.0869(11)	0.9952(10)	0.4422(7)	0.033(4)
C58	C	0.7089(11)	0.3319(11)	0.3821(8)	0.039(5)
C59	C	1.0230(9)	0.6675(10)	0.1765(7)	0.024(4)
C60	C	0.3627(12)	0.9366(13)	0.2996(10)	0.058(7)
C61	C	0.312(2)	0.744(2)	0.4319(14)	0.101(11)
C62	C	0.6252(18)	1.1332(13)	0.1576(9)	0.069(8)
C63	C	1.2662(11)	0.4487(13)	0.3896(8)	0.042(5)
C64	C	0.5531(11)	0.8228(12)	0.1286(8)	0.041(5)
C65	C	0.2538(15)	0.9378(15)	0.3466(10)	0.062(7)
C66	C	0.6099(13)	1.0014(13)	0.1773(9)	0.049(6)
C67	C	0.5168(17)	0.3991(14)	0.2631(9)	0.064(7)
C68	C	0.7610(10)	0.6778(10)	-0.1046(7)	0.030(4)
C69	C	0.4083(12)	0.7677(14)	0.0015(10)	0.057(6)
C70	C	0.5470(15)	0.6479(16)	0.5913(10)	0.068(7)
C71	C	0.3410(12)	0.8415(14)	0.3593(9)	0.054(6)
C72	C	0.7515(14)	0.8700(13)	-0.0789(10)	0.057(6)
C73	C	0.7310(14)	1.1245(14)	0.4136(11)	0.064(7)
C74	C	0.6967(15)	0.9864(17)	0.4545(10)	0.066(7)
C75	C	0.4410(16)	0.3965(17)	0.2466(11)	0.068(7)
C76	C	0.3500(13)	0.7495(14)	0.0855(9)	0.058(6)
C77	C	0.5887(12)	0.6651(13)	0.5471(10)	0.053(6)
C78	C	0.8061(11)	0.7362(11)	0.5969(7)	0.035(4)
C79	C	0.4889(15)	0.6902(16)	0.6019(11)	0.068(7)

C80	C	0.6938(14)	1.0661(12)	0.3762(9)	0.053(6)
C81	C	0.798(3)	1.0191(19)	-0.0773(13)	0.140(19)
C82	C	0.7482(17)	1.1107(19)	0.4710(13)	0.086(10)
C83	C	0.2966(14)	0.9717(17)	0.3138(12)	0.074(8)
C84	C	0.4012(15)	0.630(2)	0.2194(12)	0.090(10)
C85	C	0.784(2)	0.9747(19)	-0.1271(14)	0.100(12)
C86	C	0.2728(13)	0.8740(14)	0.3704(10)	0.061(7)
C87	C	0.7990(8)	0.6052(9)	-0.1049(6)	0.021(4)
C88	C	0.5760(16)	1.0903(16)	0.3106(10)	0.072(8)
C89	C	0.473(3)	1.159(2)	0.1667(13)	0.124(18)
C90	C	0.4044(15)	0.462(2)	0.2433(14)	0.098(13)
C91	C	0.380(3)	0.604(3)	0.2631(15)	0.19(3)
C92	C	0.867(3)	1.121(3)	0.2220(17)	0.16(2)
C93	C	0.738(2)	1.0877(19)	0.0390(16)	0.113(13)
C94	C	0.603(2)	1.2088(15)	0.1513(11)	0.096(12)
C95	C	0.8154(14)	0.8207(11)	0.5877(8)	0.047(5)
C96	C	0.811(2)	1.0412(18)	0.0275(17)	0.105(11)
C97	C	0.7754(9)	0.4100(10)	0.3237(7)	0.028(4)
C98	C	1.0352(10)	0.3423(9)	0.1787(7)	0.024(4)
C99	C	0.8336(9)	0.4745(9)	0.3230(7)	0.021(4)
C100	C	1.0270(10)	0.2734(9)	0.0716(7)	0.026(4)
C101	C	0.9986(8)	0.3765(8)	0.1331(7)	0.020(4)
C102	C	1.1235(10)	0.5065(9)	0.3688(7)	0.025(4)
C103	C	0.9163(9)	0.6647(8)	0.5564(6)	0.018(3)
C104	C	1.0880(9)	0.7271(8)	0.1765(6)	0.020(4)
C105	C	1.1601(10)	0.5110(9)	0.4232(7)	0.027(4)
C106	C	0.8013(10)	0.5644(11)	-0.1565(7)	0.032(4)
C107	C	0.8832(10)	0.7009(10)	0.6012(7)	0.030(4)
C108	C	1.0161(9)	0.8541(10)	0.4025(7)	0.025(4)
C109	C	0.8373(9)	0.6127(9)	0.0008(6)	0.018(4)
C110	C	0.9489(11)	0.9794(10)	0.2245(8)	0.034(4)
C111	C	0.9945(9)	0.3407(9)	0.0775(6)	0.019(4)
C112	C	1.0177(10)	0.8152(10)	0.5010(7)	0.030(4)
C113	C	1.1274(10)	0.5492(9)	0.4748(7)	0.028(4)
C114	C	1.0250(10)	0.6364(10)	0.6195(8)	0.032(4)
C115	C	1.1055(9)	0.7458(10)	0.1240(8)	0.030(4)
C116	C	1.1315(9)	0.7582(9)	0.2250(7)	0.023(4)
C117	C	1.0412(12)	0.8423(11)	0.5636(7)	0.041(5)
C118	C	0.8675(10)	0.4643(10)	-0.1146(7)	0.033(4)
C119	C	0.3852(10)	0.8752(11)	0.3260(8)	0.036(5)
C120	C	1.0303(10)	0.9084(9)	0.3635(7)	0.027(4)
C121	C	0.7567(11)	0.3822(10)	0.2164(7)	0.035(5)
C122	C	0.5411(12)	0.8145(12)	-0.0024(9)	0.047(5)

C123	C	0.6755(12)	0.2874(12)	0.3332(9)	0.047(5)
C124	C	0.6834(9)	0.4785(10)	-0.0038(7)	0.026(4)
C125	C	0.6477(11)	0.9283(11)	0.3605(7)	0.035(5)
C126	C	1.0894(14)	1.0576(14)	0.2490(10)	0.059(6)
C127	C	0.9521(13)	1.0551(12)	0.2389(13)	0.072(9)
C128	C	0.4401(12)	0.5313(16)	0.2518(15)	0.087(11)
C129	C	0.8189(12)	0.3344(12)	0.1943(8)	0.048(6)
C130	C	0.665(2)	1.0847(14)	0.3190(12)	0.084(10)
C131	C	0.4769(13)	0.7922(11)	0.0313(9)	0.047(6)
C132	C	0.7630(17)	0.9028(16)	-0.1282(10)	0.070(8)
C133	C	1.0230(17)	1.0942(13)	0.2533(15)	0.084(9)
C134	C	0.7330(15)	1.0423(18)	0.4894(11)	0.069(7)
C135	C	0.553(2)	0.915(2)	0.5464(14)	0.111(12)
C136	C	0.779(4)	0.9884(17)	-0.0265(12)	0.18(3)
C137	C	0.3451(14)	0.7453(15)	0.0272(11)	0.064(7)
C138	C	0.5767(15)	1.0750(13)	0.1685(8)	0.053(6)
C139	C	0.4987(17)	0.8447(16)	0.5042(13)	0.080(8)
C140	C	0.4745(16)	0.7547(18)	0.5764(11)	0.079(9)
C141	C	0.499(2)	1.086(2)	0.1711(12)	0.104(14)
C142	C	0.433(2)	1.020(2)	0.1775(15)	0.106(13)
C143	C	0.4144(19)	0.9745(16)	0.1239(17)	0.099(12)
C144	C	0.866(3)	1.102(3)	0.273(2)	0.16(2)
O47	O	0.8135(15)	0.867(3)	0.4029(16)	0.38(4)
O48	O	0.625(3)	0.6684(17)	0.0896(15)	0.40(4)

Table II.1.2.3 Anisotropic Displacement Parameters ($Å^2×10^3$) for ab50416. The Anisotropic displacement factor exponent takes the form: $-2\pi^2[h^2a^{*2}U_{11}+2hka^*b^*U_{12}+\ldots]$.

Atom	U_{11}	U_{22}	U_{33}	U_{12}	U_{13}	U_{23}
Mn1	0.0176(12)	0.0184(12)	0.0079(12)	0.0021(9)	-0.0013(9)	-0.0085(10)
Mn2	0.0165(12)	0.0187(12)	0.0081(11)	0.0008(9)	-0.0018(9)	-0.0079(10)
Mn3	0.0162(12)	0.0214(13)	0.0090(12)	0.0019(9)	-0.0003(9)	-0.0068(10)
Mn4	0.0212(13)	0.0279(14)	0.0122(12)	0.0054(10)	0.0047(10)	-0.0044(10)
Mn5	0.0175(12)	0.0201(13)	0.0094(12)	0.0038(9)	0.0020(9)	-0.0066(10)
Mn6	0.0241(13)	0.0218(13)	0.0137(12)	0.0054(10)	0.0040(10)	-0.0031(10)
Mn7	0.0161(12)	0.0202(13)	0.0086(12)	0.0021(9)	-0.0009(9)	-0.0088(10)
Mn8	0.0200(13)	0.0299(14)	0.0168(13)	0.0083(10)	0.0057(10)	0.0015(11)
Mn9	0.0273(14)	0.0216(13)	0.0146(13)	0.0051(10)	0.0047(10)	-0.0006(11)
Mn10	0.0437(17)	0.0289(15)	0.0190(14)	0.0106(11)	0.0076(12)	0.0098(12)
Mn11	0.0311(16)	0.0500(18)	0.0240(15)	0.0138(13)	0.0127(12)	0.0152(13)
Mn12	0.0461(18)	0.0485(18)	0.0261(15)	0.0139(13)	0.0126(13)	0.0238(15)
O1	0.017(6)	0.018(6)	0.017(6)	0.001(5)	-0.002(4)	-0.015(4)
O2	0.016(6)	0.032(6)	0.011(5)	0.006(5)	0.000(4)	0.000(5)

O3	0.077(11)	0.040(8)	0.032(8)	0.006(6)	0.006(7)	0.020(7)
O4	0.065(9)	0.051(9)	0.019(7)	0.008(6)	0.017(6)	0.024(7)
O5	0.019(6)	0.024(6)	0.006(5)	-0.001(4)	-0.002(4)	-0.006(5)
O6	0.020(6)	0.042(7)	0.015(6)	0.010(5)	0.005(5)	-0.005(5)
O7	0.024(6)	0.032(6)	0.018(6)	0.011(5)	0.004(5)	-0.004(5)
O8	0.015(6)	0.036(7)	0.011(5)	0.008(5)	-0.004(4)	-0.005(5)
O9	0.064(10)	0.051(9)	0.041(8)	0.020(7)	0.021(7)	0.027(8)
O10	0.017(6)	0.024(6)	0.013(6)	-0.002(5)	-0.003(4)	-0.011(5)
O11	0.018(6)	0.028(6)	0.004(5)	0.006(4)	0.002(4)	-0.009(5)
O12	0.033(7)	0.032(7)	0.023(6)	0.013(5)	0.004(5)	-0.011(5)
O13	0.024(6)	0.034(7)	0.020(6)	0.010(5)	0.004(5)	0.002(5)
O14	0.079(11)	0.048(9)	0.040(8)	0.018(7)	0.012(8)	0.039(8)
O15	0.015(5)	0.022(6)	0.010(5)	0.000(4)	0.002(4)	-0.014(4)
O16	0.019(6)	0.031(6)	0.014(6)	0.005(5)	0.004(5)	-0.015(5)
O17	0.045(8)	0.030(7)	0.011(6)	0.007(5)	0.001(5)	0.006(6)
O18	0.014(5)	0.023(6)	0.003(5)	-0.005(4)	-0.001(4)	-0.015(4)
O19	0.046(9)	0.052(9)	0.052(9)	0.004(7)	0.006(7)	0.009(7)
O20	0.016(6)	0.024(6)	0.011(5)	-0.001(4)	-0.005(5)	-0.010(5)
O21	0.019(6)	0.027(6)	0.011(6)	-0.001(5)	0.002(4)	-0.004(5)
O22	0.020(6)	0.033(7)	0.023(6)	0.001(5)	-0.001(5)	-0.010(5)
O23	0.024(6)	0.024(6)	0.012(6)	0.002(4)	0.006(4)	-0.012(5)
O24	0.045(8)	0.063(9)	0.021(7)	0.017(6)	0.008(6)	0.020(7)
O25	0.020(6)	0.042(7)	0.019(6)	0.011(5)	0.007(5)	0.004(5)
O26	0.027(6)	0.029(6)	0.013(6)	0.012(5)	0.008(5)	-0.003(5)
O27	0.030(6)	0.020(6)	0.020(6)	0.005(5)	0.005(5)	-0.010(5)
O28	0.032(7)	0.056(8)	0.023(7)	0.012(6)	0.015(6)	0.011(6)
O29	0.027(6)	0.016(5)	0.010(5)	0.000(4)	0.004(5)	-0.007(5)
O30	0.024(6)	0.026(6)	0.007(6)	-0.003(5)	-0.006(4)	-0.004(5)
O31	0.042(7)	0.022(6)	0.028(7)	0.012(5)	0.008(6)	-0.001(5)
O32	0.018(6)	0.057(9)	0.032(7)	0.007(7)	0.003(5)	-0.004(6)
O33	0.025(6)	0.024(6)	0.013(6)	0.002(5)	-0.002(5)	-0.004(5)
O34	0.027(6)	0.018(6)	0.009(5)	0.005(4)	0.002(4)	-0.010(5)
O35	0.046(8)	0.050(8)	0.033(7)	0.013(6)	0.011(6)	0.022(7)
O36	0.040(8)	0.098(12)	0.041(8)	0.037(9)	0.019(7)	0.038(8)
O37	0.025(6)	0.028(6)	0.012(6)	0.002(5)	0.000(5)	-0.014(5)
O38	0.018(6)	0.031(6)	0.008(6)	0.003(5)	-0.010(4)	-0.010(5)
O39	0.030(7)	0.035(7)	0.024(6)	0.014(5)	0.002(5)	0.005(5)
O40	0.023(6)	0.029(6)	0.000(5)	0.002(4)	0.004(4)	-0.003(5)
O41	0.022(6)	0.024(6)	0.011(6)	0.002(5)	0.003(4)	-0.015(5)
O42	0.023(6)	0.019(6)	0.010(5)	0.000(4)	-0.003(5)	-0.014(5)
O43	0.039(7)	0.032(7)	0.025(7)	0.002(5)	-0.011(6)	-0.004(6)
O44	0.027(7)	0.046(8)	0.017(6)	0.008(5)	0.009(5)	0.002(6)
O45	0.021(6)	0.025(6)	0.007(5)	-0.003(4)	-0.007(5)	-0.018(5)

O46	0.012(6)	0.031(6)	0.007(5)	-0.004(4)	-0.006(4)	-0.012(5)
C1	0.031(10)	0.008(8)	0.033(11)	0.009(7)	0.008(8)	-0.008(7)
C2	0.028(9)	0.039(11)	0.004(8)	0.007(8)	0.006(7)	-0.006(8)
C3	0.010(8)	0.021(9)	0.025(10)	0.002(7)	-0.002(7)	-0.015(7)
C4	0.031(11)	0.049(12)	0.041(12)	0.028(10)	0.008(9)	0.009(9)
C5	0.061(16)	0.059(15)	0.081(19)	0.018(14)	0.020(14)	-0.004(12)
C6	0.026(10)	0.035(11)	0.026(10)	-0.014(8)	0.007(8)	-0.019(8)
C7	0.029(10)	0.018(8)	0.013(8)	-0.002(7)	-0.006(7)	-0.014(8)
C8	0.031(11)	0.063(14)	0.033(11)	-0.004(10)	0.000(9)	0.009(10)
C9	0.019(9)	0.031(10)	0.031(10)	-0.011(8)	0.002(7)	-0.011(7)
C10	0.017(8)	0.034(10)	0.011(8)	0.012(7)	0.004(6)	-0.007(7)
C11	0.030(10)	0.040(11)	0.023(10)	0.002(8)	-0.008(8)	-0.003(8)
C12	0.059(14)	0.026(10)	0.016(9)	0.000(7)	0.005(9)	-0.014(9)
C13	0.013(8)	0.021(8)	0.023(9)	0.006(7)	0.002(7)	-0.016(7)
C14	0.015(8)	0.017(9)	0.030(10)	-0.004(7)	0.005(7)	-0.016(7)
C15	0.019(9)	0.024(9)	0.033(10)	0.008(8)	0.001(7)	-0.014(7)
C16	0.031(10)	0.018(9)	0.026(10)	0.008(7)	-0.004(8)	-0.012(7)
C17	0.023(9)	0.028(9)	0.007(8)	0.001(7)	0.001(6)	-0.018(7)
C18	0.031(10)	0.033(10)	0.007(8)	0.007(7)	0.002(7)	0.000(8)
C19	0.032(10)	0.041(11)	0.028(10)	-0.004(8)	0.008(8)	-0.013(9)
C20	0.031(10)	0.039(10)	0.000(7)	0.001(7)	0.004(7)	-0.007(8)
C21	0.043(12)	0.041(11)	0.011(9)	0.010(8)	-0.005(8)	-0.034(10)
C22	0.036(11)	0.038(11)	0.043(12)	0.005(9)	0.006(9)	-0.011(9)
C23	0.047(12)	0.032(10)	0.029(10)	0.002(8)	0.008(9)	-0.008(9)
C24	0.025(10)	0.036(11)	0.030(10)	0.002(8)	-0.004(8)	-0.009(8)
C25	0.037(11)	0.041(12)	0.023(10)	0.017(8)	0.009(8)	-0.006(9)
C26	0.031(10)	0.035(10)	0.013(9)	0.002(7)	-0.005(7)	-0.013(8)
C27	0.032(11)	0.055(13)	0.029(10)	0.020(9)	0.016(8)	0.008(9)
C28	0.037(11)	0.060(14)	0.031(11)	0.017(10)	-0.014(9)	-0.025(10)
C29	0.034(10)	0.025(10)	0.034(11)	-0.002(8)	0.004(8)	-0.011(8)
C30	0.055(13)	0.042(12)	0.023(10)	-0.007(8)	0.014(9)	-0.021(10)
C31	0.022(9)	0.028(9)	0.031(10)	0.011(8)	0.010(8)	0.002(7)
C32	0.034(10)	0.021(9)	0.017(9)	-0.003(7)	0.001(7)	-0.008(7)
C33	0.30(6)	0.11(3)	0.023(14)	-0.001(16)	-0.01(2)	0.15(4)
C34	0.037(12)	0.070(16)	0.027(11)	0.022(10)	0.008(9)	-0.015(10)
C35	0.033(11)	0.048(12)	0.035(11)	0.016(9)	0.012(9)	-0.011(9)
C36	0.069(17)	0.053(15)	0.078(18)	0.030(13)	-0.004(14)	0.003(12)
C37	0.027(10)	0.046(12)	0.049(13)	0.005(10)	0.002(9)	-0.013(9)
C38	0.042(13)	0.073(16)	0.041(13)	0.019(12)	0.014(11)	0.025(12)
C39	0.035(11)	0.039(11)	0.032(11)	0.009(9)	0.004(9)	-0.014(9)
C40	0.028(11)	0.057(13)	0.023(10)	0.014(9)	-0.002(8)	0.001(9)
C41	0.031(10)	0.046(12)	0.028(10)	-0.001(9)	0.001(8)	-0.011(9)
C42	0.036(12)	0.031(10)	0.022(10)	0.009(8)	0.004(8)	-0.002(8)

C43	0.042(11)	0.035(11)	0.017(9)	-0.003(8)	-0.014(8)	-0.014(9)
C44	0.038(11)	0.023(10)	0.063(14)	0.011(10)	0.033(10)	-0.010(8)
C45	0.062(15)	0.065(16)	0.051(14)	0.008(12)	0.017(12)	0.023(13)
C46	0.030(10)	0.026(9)	0.021(9)	0.005(7)	-0.005(7)	-0.008(8)
C47	0.038(11)	0.027(10)	0.053(13)	0.011(9)	0.024(10)	-0.007(8)
C48	0.015(9)	0.062(14)	0.047(12)	0.015(10)	0.010(8)	0.004(9)
C49	0.044(12)	0.023(10)	0.028(10)	-0.001(8)	0.017(9)	-0.006(8)
C50	0.056(14)	0.049(12)	0.027(11)	0.021(9)	0.012(9)	0.003(11)
C51	0.039(12)	0.053(13)	0.035(12)	0.025(10)	0.015(9)	0.011(10)
C52	0.039(11)	0.028(10)	0.048(13)	0.004(9)	0.002(9)	-0.023(9)
C53	0.035(10)	0.027(10)	0.022(9)	-0.006(8)	-0.006(8)	-0.023(8)
C54	0.027(10)	0.043(11)	0.041(11)	0.010(9)	0.003(9)	0.005(9)
C55	0.027(10)	0.050(12)	0.018(9)	0.003(8)	-0.003(7)	-0.028(9)
C56	0.034(11)	0.042(11)	0.024(10)	-0.003(8)	-0.004(8)	-0.022(9)
C57	0.040(11)	0.033(10)	0.025(10)	0.004(8)	0.001(8)	-0.011(9)
C58	0.047(12)	0.037(11)	0.028(10)	-0.002(8)	0.006(9)	-0.027(9)
C59	0.017(9)	0.035(10)	0.020(10)	-0.003(8)	0.005(8)	0.003(7)
C60	0.040(13)	0.063(15)	0.065(16)	-0.019(12)	-0.016(11)	0.024(11)
C61	0.12(3)	0.11(3)	0.09(2)	0.03(2)	0.04(2)	0.01(2)
C62	0.12(2)	0.046(14)	0.027(12)	-0.017(10)	-0.032(13)	0.016(15)
C63	0.031(11)	0.071(15)	0.029(11)	0.021(10)	0.002(9)	0.009(10)
C64	0.044(12)	0.052(13)	0.034(12)	0.029(10)	0.015(9)	0.014(10)
C65	0.070(17)	0.066(17)	0.044(14)	-0.020(12)	0.007(13)	-0.003(14)
C66	0.065(15)	0.055(14)	0.033(12)	0.002(11)	0.018(11)	0.024(12)
C67	0.11(2)	0.062(16)	0.023(11)	0.012(10)	0.007(12)	-0.008(15)
C68	0.026(10)	0.036(10)	0.033(10)	0.013(8)	0.016(8)	-0.009(8)
C69	0.034(13)	0.068(16)	0.063(16)	-0.004(12)	-0.012(11)	0.012(11)
C70	0.070(17)	0.09(2)	0.047(15)	0.021(14)	0.013(13)	0.022(15)
C71	0.030(12)	0.081(17)	0.040(13)	-0.030(12)	-0.008(10)	0.002(11)
C72	0.069(16)	0.060(15)	0.051(14)	0.019(12)	0.025(12)	0.023(12)
C73	0.058(15)	0.062(16)	0.062(16)	-0.019(13)	-0.020(12)	0.014(12)
C74	0.061(16)	0.10(2)	0.045(15)	0.017(14)	0.017(12)	0.016(15)
C75	0.061(18)	0.09(2)	0.054(16)	-0.011(14)	0.025(14)	-0.030(15)
C76	0.053(14)	0.081(17)	0.043(14)	0.010(12)	0.000(11)	0.032(13)
C77	0.037(12)	0.063(15)	0.066(15)	0.030(12)	0.016(11)	-0.003(11)
C78	0.036(11)	0.044(11)	0.025(10)	-0.005(8)	0.011(8)	0.006(9)
C79	0.059(16)	0.09(2)	0.060(16)	0.022(15)	0.030(13)	0.014(15)
C80	0.075(16)	0.050(14)	0.033(12)	0.004(10)	-0.005(11)	0.017(12)
C81	0.31(6)	0.07(2)	0.042(18)	0.023(16)	0.02(3)	-0.03(3)
C82	0.070(19)	0.09(2)	0.08(2)	-0.035(18)	-0.021(16)	0.024(17)
C83	0.045(15)	0.10(2)	0.075(19)	-0.002(16)	-0.010(14)	0.024(15)
C84	0.059(17)	0.14(3)	0.061(18)	0.016(17)	-0.003(14)	-0.065(18)
C85	0.15(3)	0.09(2)	0.09(2)	0.06(2)	0.07(2)	0.04(2)

C86	0.046(14)	0.069(17)	0.060(15)	-0.022(13)	-0.015(11)	0.020(12)
C87	0.006(8)	0.040(10)	0.015(9)	0.001(7)	-0.003(6)	-0.016(7)
C88	0.080(19)	0.09(2)	0.039(14)	-0.003(13)	-0.009(13)	0.033(16)
C89	0.22(5)	0.11(3)	0.08(2)	0.07(2)	0.09(3)	0.12(3)
C90	0.036(15)	0.14(3)	0.10(2)	-0.07(2)	0.022(15)	-0.055(18)
C91	0.21(5)	0.28(6)	0.05(2)	-0.05(3)	0.03(3)	-0.18(5)
C92	0.21(5)	0.17(4)	0.09(3)	-0.02(3)	0.04(3)	-0.14(4)
C93	0.17(4)	0.08(2)	0.11(3)	0.04(2)	0.05(3)	0.04(2)
C94	0.16(3)	0.057(17)	0.052(17)	-0.028(13)	-0.067(19)	0.04(2)
C95	0.082(16)	0.028(11)	0.033(11)	0.001(9)	0.012(11)	0.004(10)
C96	0.11(3)	0.06(2)	0.14(3)	0.01(2)	0.00(2)	-0.013(18)
C97	0.024(9)	0.031(10)	0.028(10)	0.008(8)	0.003(8)	-0.010(8)
C98	0.037(10)	0.013(8)	0.023(9)	0.003(7)	0.006(8)	-0.002(7)
C99	0.015(8)	0.030(10)	0.017(9)	0.013(8)	-0.014(7)	-0.012(7)
C100	0.032(10)	0.027(10)	0.018(9)	-0.007(7)	0.010(7)	-0.003(8)
C101	0.014(8)	0.017(8)	0.030(10)	0.002(7)	0.006(7)	-0.015(7)
C102	0.033(10)	0.017(9)	0.025(10)	0.008(7)	0.007(8)	-0.002(7)
C103	0.029(9)	0.011(8)	0.010(8)	0.003(6)	-0.005(7)	-0.015(7)
C104	0.030(9)	0.018(8)	0.013(8)	0.004(7)	0.008(7)	-0.003(7)
C105	0.030(10)	0.029(10)	0.023(10)	0.015(7)	0.003(8)	-0.012(8)
C106	0.023(9)	0.051(12)	0.025(10)	0.008(9)	0.010(8)	-0.009(9)
C107	0.038(11)	0.028(10)	0.023(10)	0.006(8)	0.006(8)	-0.014(8)
C108	0.022(9)	0.032(10)	0.022(9)	0.008(8)	0.000(7)	0.004(7)
C109	0.015(8)	0.025(9)	0.014(8)	0.005(7)	0.009(7)	-0.011(7)
C110	0.038(11)	0.025(10)	0.042(11)	0.014(8)	0.013(9)	-0.005(8)
C111	0.018(8)	0.028(9)	0.010(8)	0.003(7)	0.001(6)	-0.011(7)
C112	0.043(11)	0.033(10)	0.011(9)	0.005(7)	0.001(8)	-0.022(8)
C113	0.035(10)	0.027(9)	0.021(9)	0.007(7)	0.000(8)	-0.009(8)
C114	0.028(10)	0.035(10)	0.031(11)	0.011(8)	-0.002(8)	-0.024(8)
C115	0.018(9)	0.031(10)	0.042(11)	0.013(8)	0.010(8)	-0.011(8)
C116	0.025(9)	0.025(9)	0.016(9)	-0.009(7)	0.002(7)	-0.014(7)
C117	0.060(13)	0.046(12)	0.012(9)	-0.001(8)	-0.006(9)	-0.011(10)
C118	0.032(10)	0.038(11)	0.028(10)	-0.003(8)	0.004(8)	-0.014(8)
C119	0.026(10)	0.044(12)	0.034(11)	-0.009(9)	-0.013(9)	0.000(9)
C120	0.032(10)	0.025(9)	0.022(9)	-0.002(7)	0.003(8)	-0.012(8)
C121	0.058(13)	0.034(10)	0.007(8)	0.000(7)	-0.016(8)	-0.031(9)
C122	0.050(13)	0.045(12)	0.047(13)	0.014(10)	0.008(10)	-0.004(10)
C123	0.045(13)	0.046(12)	0.052(14)	0.005(10)	0.017(10)	-0.015(10)
C124	0.022(9)	0.033(10)	0.024(9)	0.013(8)	0.006(7)	-0.019(8)
C125	0.051(12)	0.038(11)	0.022(11)	0.012(9)	0.023(9)	0.013(9)
C126	0.070(17)	0.057(16)	0.052(14)	0.032(12)	0.004(12)	-0.017(13)
C127	0.038(13)	0.032(13)	0.13(3)	-0.011(14)	-0.030(14)	-0.007(10)
C128	0.015(11)	0.072(18)	0.16(3)	-0.049(19)	-0.005(14)	-0.009(12)

C129	0.048(13)	0.059(14)	0.032(11)	-0.015(10)	0.005(10)	-0.025(11)
C130	0.15(3)	0.042(15)	0.069(19)	0.000(13)	0.038(19)	0.009(16)
C131	0.057(14)	0.040(12)	0.054(14)	0.027(10)	0.026(11)	0.018(10)
C132	0.09(2)	0.08(2)	0.040(14)	0.021(13)	0.020(13)	0.022(16)
C133	0.08(2)	0.030(13)	0.14(3)	0.002(15)	-0.013(18)	-0.009(13)
C134	0.055(16)	0.09(2)	0.065(18)	0.000(16)	0.004(13)	0.015(15)
C135	0.12(3)	0.12(3)	0.08(2)	-0.04(2)	-0.03(2)	0.00(2)
C136	0.47(9)	0.049(19)	0.034(17)	0.023(14)	0.05(3)	0.06(3)
C137	0.046(14)	0.075(17)	0.073(18)	0.013(14)	-0.005(13)	0.020(13)
C138	0.087(18)	0.049(14)	0.026(11)	0.005(10)	0.005(11)	0.034(14)
C139	0.08(2)	0.067(18)	0.10(2)	0.020(16)	0.025(17)	0.021(15)
C140	0.083(19)	0.12(2)	0.056(16)	0.049(16)	0.041(15)	0.054(18)
C141	0.13(3)	0.14(3)	0.059(18)	0.042(18)	0.028(18)	0.11(3)
C142	0.13(3)	0.13(3)	0.09(2)	0.07(2)	0.06(2)	0.05(2)
C143	0.10(2)	0.056(17)	0.15(3)	0.003(19)	0.07(2)	-0.029(16)
C144	0.15(4)	0.16(4)	0.18(5)	0.12(4)	0.00(3)	0.00(3)
O47	0.12(2)	0.62(8)	0.30(4)	-0.40(5)	-0.18(3)	0.28(4)
O48	0.59(7)	0.19(3)	0.29(4)	-0.23(3)	-0.40(5)	0.33(4)

Table II.1.2.4 Bond Lengths for ab50416.

Atom 1	**Atom 2**	**Length (A)**
Mn1	O40	1.897(10)
Mn1	O15	1.926(10)
Mn1	O29	1.947(10)
Mn1	O42	1.946(11)
Mn1	O41	2.124(10)
Mn1	O33	2.180(11)
Mn2	O15	1.883(10)
Mn2	O34	1.901(10)
Mn2	O38	1.936(10)
Mn2	O30	1.948(10)
Mn2	O37	2.143(10)
Mn2	O16	2.155(10)
Mn3	O11	1.891(11)
Mn3	O34	1.890(10)
Mn3	O5	1.950(10)
Mn3	O21	1.964(11)
Mn3	O45	2.140(10)
Mn3	O46	2.165(10)
Mn4	O40	1.861(10)
Mn4	O25	1.880(11)
Mn4	O10	1.957(10)

Mn4	O44	1.972(11)
Mn4	O12	2.225(11)
Mn5	O15	1.841(11)
Mn5	O40	1.877(9)
Mn5	O18	1.902(9)
Mn5	O2	1.920(11)
Mn5	O13	1.931(11)
Mn5	O20	1.944(10)
Mn6	O23	1.888(10)
Mn6	O11	1.890(10)
Mn6	O17	1.957(11)
Mn6	O26	1.986(11)
Mn6	O22	2.185(11)
Mn7	O34	1.838(11)
Mn7	O11	1.863(9)
Mn7	O18	1.910(9)
Mn7	O2	1.919(10)
Mn7	O8	1.922(11)
Mn7	O1	1.941(10)
Mn8	O7	1.844(11)
Mn8	O25	1.897(11)
Mn8	O2	1.913(10)
Mn8	O8	1.914(10)
Mn8	O13	1.916(11)
Mn8	O6	1.957(11)
Mn9	O39	1.816(11)
Mn9	O23	1.872(10)
Mn9	O8	1.899(11)
Mn9	O13	1.928(11)
Mn9	O18	1.938(10)
Mn9	O27	1.937(11)
Mn10	O39	1.843(11)
Mn10	O23	1.915(11)
Mn10	O31	1.943(11)
Mn10	O14	1.957(13)
Mn10	O35	2.161(15)
Mn10	O43	2.192(12)
Mn11	O7	1.868(10)
Mn11	O25	1.909(11)
Mn11	O36	1.947(13)
Mn11	O28	1.955(11)
Mn11	O4	2.131(15)
Mn11	O32	2.157(13)

Mn12	O24	1.891(14)
Mn12	O3	1.927(15)
Mn12	O7	1.942(11)
Mn12	O9	2.000(13)
Mn12	O39	2.076(12)
Mn12	O19	2.162(15)
O1	C18	1.284(19)
O3	C125	1.27(2)
O4	C125	1.24(2)
O5	C109	1.283(19)
O6	C40	1.31(2)
O9	C66	1.22(3)
O10	C7	1.25(2)
O14	C66	1.33(3)
O16	C59	1.25(2)
O17	C2	1.26(2)
O19	C38	1.24(3)
O20	C14	1.307(19)
O21	C3	1.268(19)
O24	C64	1.26(2)
O26	C109	1.242(19)
O27	C49	1.31(2)
O28	C42	1.25(2)
O29	C7	1.281(19)
O30	C3	1.264(19)
O31	C2	1.25(2)
O32	C40	1.24(2)
O33	C14	1.252(19)
O35	C64	1.27(2)
O36	C38	1.23(2)
O37	C99	1.255(19)
O38	C1	1.28(2)
O41	C99	1.30(2)
O42	C1	1.29(2)
O43	C49	1.24(2)
O44	C42	1.28(2)
O45	C59	1.261(19)
O46	C18	1.243(19)
C1	C102	1.46(2)
C2	C25	1.51(2)
C3	C101	1.51(2)
C4	C105	1.36(3)
C4	C63	1.38(3)

C5	C61	1.50(4)
C5	C71	1.59(4)
C6	C43	1.34(3)
C6	C128	1.41(3)
C6	C40	1.53(3)
C7	C103	1.51(2)
C8	C74	1.43(3)
C8	C80	1.43(3)
C8	C125	1.47(3)
C9	C111	1.50(2)
C9	C41	1.51(2)
C10	C87	1.41(2)
C10	C20	1.41(2)
C10	C109	1.49(2)
C11	C54	1.41(3)
C11	C131	1.41(3)
C11	C64	1.52(3)
C12	C21	1.36(3)
C12	C107	1.41(3)
C13	C17	1.40(2)
C13	C15	1.42(2)
C13	C18	1.52(2)
C14	C108	1.50(2)
C15	C35	1.38(3)
C16	C103	1.39(2)
C16	C114	1.43(2)
C17	C24	1.41(2)
C17	C124	1.54(2)
C19	C118	1.39(3)
C19	C106	1.41(3)
C20	C118	1.38(2)
C21	C114	1.34(3)
C22	C116	1.40(2)
C22	C39	1.44(3)
C23	C113	1.51(2)
C24	C37	1.37(3)
C25	C136	1.27(4)
C25	C72	1.50(3)
C26	C58	1.36(2)
C26	C97	1.41(2)
C27	C77	1.37(3)
C27	C45	1.38(3)
C27	C42	1.49(2)

C28	C30	1.55(3)
C29	C57	1.41(3)
C29	C120	1.42(2)
C30	C116	1.52(2)
C31	C51	1.40(3)
C31	C102	1.42(2)
C32	C108	1.37(2)
C32	C53	1.42(2)
C32	C112	1.51(2)
C33	C94	1.41(6)
C33	C89	1.44(7)
C34	C126	1.37(3)
C34	C50	1.44(3)
C35	C37	1.43(3)
C36	C122	1.57(3)
C38	C119	1.58(3)
C39	C56	1.40(3)
C43	C67	1.41(3)
C44	C100	1.40(3)
C44	C47	1.40(3)
C45	C140	1.40(3)
C45	C139	1.55(4)
C46	C97	1.38(2)
C46	C52	1.43(2)
C46	C121	1.51(2)
C47	C98	1.38(2)
C48	C68	1.54(2)
C49	C110	1.53(3)
C50	C110	1.41(3)
C51	C63	1.37(3)
C52	C123	1.39(3)
C53	C57	1.40(3)
C54	C76	1.43(3)
C55	C124	1.51(2)
C56	C115	1.38(2)
C58	C123	1.43(3)
C59	C104	1.54(2)
C60	C119	1.37(3)
C60	C83	1.41(3)
C62	C138	1.39(4)
C62	C94	1.44(4)
C65	C83	1.32(4)
C65	C86	1.37(4)

C66	C138	1.49(3)
C67	C75	1.36(4)
C68	C87	1.49(2)
C69	C137	1.40(3)
C69	C131	1.38(3)
C70	C79	1.34(3)
C70	C77	1.41(3)
C71	C119	1.34(3)
C71	C86	1.41(3)
C72	C132	1.40(3)
C73	C80	1.41(3)
C73	C82	1.44(4)
C74	C134	1.35(4)
C75	C90	1.36(4)
C76	C137	1.40(3)
C78	C107	1.53(3)
C78	C95	1.56(3)
C79	C140	1.38(4)
C80	C130	1.49(4)
C81	C85	1.38(5)
C81	C136	1.45(4)
C82	C134	1.37(4)
C84	C91	1.28(5)
C85	C132	1.32(4)
C87	C106	1.39(2)
C88	C130	1.58(4)
C89	C141	1.42(4)
C90	C128	1.37(4)
C91	C128	1.74(7)
C92	C144	1.30(6)
C92	C127	1.99(7)
C93	C96	1.60(5)
C96	C136	1.58(5)
C97	C99	1.52(2)
C98	C101	1.42(2)
C100	C111	1.36(2)
C101	C111	1.43(2)
C102	C105	1.40(2)
C103	C107	1.40(2)
C104	C115	1.40(2)
C104	C116	1.39(2)
C105	C113	1.54(2)
C108	C120	1.45(2)

C110	C127	1.37(3)
C112	C117	1.55(2)
C121	C129	1.54(3)
C122	C131	1.53(3)
C126	C133	1.38(4)
C127	C133	1.41(3)
C127	C144	1.98(6)
C135	C139	1.74(4)
C138	C141	1.40(4)
C141	C142	1.66(5)
C142	C143	1.47(5)

Table II.1.2.5 Bond Angles for ab50416

Atom 1	Atom 2	Atom 3	Angle (Deg)
O40	Mn1	O15	82.6(4)
O40	Mn1	O29	93.1(4)
O15	Mn1	O29	174.3(4)
O40	Mn1	O42	173.2(4)
O15	Mn1	O42	95.5(4)
O29	Mn1	O42	88.4(4)
O40	Mn1	O41	91.4(4)
O15	Mn1	O41	95.0(4)
O29	Mn1	O41	88.8(4)
O42	Mn1	O41	95.3(4)
O40	Mn1	O33	85.3(4)
O15	Mn1	O33	86.9(4)
O29	Mn1	O33	89.1(4)
O42	Mn1	O33	88.2(4)
O41	Mn1	O33	175.9(4)
O15	Mn2	O34	95.5(4)
O15	Mn2	O38	90.9(4)
O34	Mn2	O38	173.5(5)
O15	Mn2	O30	173.7(4)
O34	Mn2	O30	90.3(4)
O38	Mn2	O30	83.4(4)
O15	Mn2	O37	92.2(4)
O34	Mn2	O37	92.0(4)
O38	Mn2	O37	89.3(4)
O30	Mn2	O37	85.1(4)
O15	Mn2	O16	92.1(4)
O34	Mn2	O16	92.2(4)
O38	Mn2	O16	86.1(4)

O30	Mn2	O16	90.1(4)
O37	Mn2	O16	173.7(4)
O11	Mn3	O34	82.6(4)
O11	Mn3	O5	92.9(4)
O34	Mn3	O5	173.9(5)
O11	Mn3	O21	172.3(4)
O34	Mn3	O21	95.1(4)
O5	Mn3	O21	88.8(4)
O11	Mn3	O45	91.3(4)
O34	Mn3	O45	94.8(4)
O5	Mn3	O45	89.3(4)
O21	Mn3	O45	96.2(4)
O11	Mn3	O46	84.5(4)
O34	Mn3	O46	86.4(4)
O5	Mn3	O46	89.1(4)
O21	Mn3	O46	88.0(4)
O45	Mn3	O46	175.5(4)
O40	Mn4	O25	93.9(4)
O40	Mn4	O10	90.4(4)
O25	Mn4	O10	175.5(5)
O40	Mn4	O44	173.8(5)
O25	Mn4	O44	92.3(5)
O10	Mn4	O44	83.3(5)
O40	Mn4	O12	90.8(4)
O25	Mn4	O12	93.9(5)
O10	Mn4	O12	87.3(4)
O44	Mn4	O12	88.8(5)
O15	Mn5	O40	85.5(4)
O15	Mn5	O18	95.9(4)
O40	Mn5	O18	171.0(4)
O15	Mn5	O2	90.4(4)
O40	Mn5	O2	87.4(4)
O18	Mn5	O2	83.7(4)
O15	Mn5	O13	173.8(5)
O40	Mn5	O13	97.2(5)
O18	Mn5	O13	80.5(4)
O2	Mn5	O13	84.1(5)
O15	Mn5	O20	94.4(4)
O40	Mn5	O20	91.1(4)
O18	Mn5	O20	97.6(4)
O2	Mn5	O20	174.8(5)
O13	Mn5	O20	91.1(5)
O23	Mn6	O11	93.6(4)

O23	Mn6	O17	91.1(5)
O11	Mn6	O17	175.2(5)
O23	Mn6	O26	176.0(5)
O11	Mn6	O26	90.3(4)
O17	Mn6	O26	85.0(4)
O23	Mn6	O22	94.7(4)
O11	Mn6	O22	91.1(4)
O17	Mn6	O22	87.8(5)
O26	Mn6	O22	86.1(4)
O34	Mn7	O11	84.8(4)
O34	Mn7	O18	91.5(4)
O11	Mn7	O18	88.7(4)
O34	Mn7	O2	96.9(4)
O11	Mn7	O2	172.0(5)
O18	Mn7	O2	83.5(4)
O34	Mn7	O8	174.8(5)
O11	Mn7	O8	97.6(4)
O18	Mn7	O8	83.9(4)
O2	Mn7	O8	80.1(4)
O34	Mn7	O1	92.5(4)
O11	Mn7	O1	90.7(4)
O18	Mn7	O1	175.9(5)
O2	Mn7	O1	97.0(4)
O8	Mn7	O1	92.1(4)
O7	Mn8	O25	83.7(5)
O7	Mn8	O2	175.1(5)
O25	Mn8	O2	101.0(4)
O7	Mn8	O8	95.0(5)
O25	Mn8	O8	171.3(5)
O2	Mn8	O8	80.5(4)
O7	Mn8	O13	96.4(5)
O25	Mn8	O13	89.3(5)
O2	Mn8	O13	84.7(5)
O8	Mn8	O13	82.3(5)
O7	Mn8	O6	92.1(5)
O25	Mn8	O6	93.0(5)
O2	Mn8	O6	86.7(5)
O8	Mn8	O6	95.6(4)
O13	Mn8	O6	171.4(5)
O39	Mn9	O23	83.6(5)
O39	Mn9	O8	93.5(5)
O23	Mn9	O8	90.3(4)
O39	Mn9	O13	95.2(5)

O23	Mn9	O13	172.5(5)
O8	Mn9	O13	82.4(5)
O39	Mn9	O18	174.5(5)
O23	Mn9	O18	101.2(4)
O8	Mn9	O18	83.8(4)
O13	Mn9	O18	79.7(4)
O39	Mn9	O27	95.3(5)
O23	Mn9	O27	93.0(4)
O8	Mn9	O27	171.0(5)
O13	Mn9	O27	94.4(5)
O18	Mn9	O27	87.3(4)
O39	Mn10	O23	81.7(5)
O39	Mn10	O31	175.7(5)
O23	Mn10	O31	94.1(5)
O39	Mn10	O14	96.7(5)
O23	Mn10	O14	173.3(6)
O31	Mn10	O14	87.4(5)
O39	Mn10	O35	94.2(5)
O23	Mn10	O35	103.8(5)
O31	Mn10	O35	87.7(5)
O14	Mn10	O35	82.8(6)
O39	Mn10	O43	91.9(5)
O23	Mn10	O43	87.1(5)
O31	Mn10	O43	87.0(5)
O14	Mn10	O43	86.4(6)
O35	Mn10	O43	168.2(5)
O7	Mn11	O25	82.8(5)
O7	Mn11	O36	95.8(5)
O25	Mn11	O36	170.9(7)
O7	Mn11	O28	176.0(5)
O25	Mn11	O28	93.6(5)
O36	Mn11	O28	87.6(5)
O7	Mn11	O4	96.1(5)
O25	Mn11	O4	103.6(5)
O36	Mn11	O4	85.5(7)
O28	Mn11	O4	86.2(5)
O7	Mn11	O32	91.5(5)
O25	Mn11	O32	87.0(5)
O36	Mn11	O32	84.0(6)
O28	Mn11	O32	86.8(5)
O4	Mn11	O32	167.7(5)
O24	Mn12	O3	173.4(6)
O24	Mn12	O7	89.5(5)

O3	Mn12	O7	95.3(5)
O24	Mn12	O9	87.4(6)
O3	Mn12	O9	87.5(6)
O7	Mn12	O9	174.6(6)
O24	Mn12	O39	95.4(5)
O3	Mn12	O39	88.8(6)
O7	Mn12	O39	93.9(4)
O9	Mn12	O39	90.8(5)
O24	Mn12	O19	88.3(6)
O3	Mn12	O19	87.1(6)
O7	Mn12	O19	91.3(5)
O9	Mn12	O19	84.1(6)
O39	Mn12	O19	173.6(5)
C18	O1	Mn7	124.0(10)
Mn8	O2	Mn7	99.7(5)
Mn8	O2	Mn5	94.8(5)
Mn7	O2	Mn5	95.3(5)
C125	O3	Mn12	133.4(14)
C125	O4	Mn11	130.9(12)
C109	O5	Mn3	132.0(10)
C40	O6	Mn8	126.3(12)
Mn8	O7	Mn11	96.9(5)
Mn8	O7	Mn12	132.3(6)
Mn11	O7	Mn12	121.5(6)
Mn9	O8	Mn8	97.5(5)
Mn9	O8	Mn7	95.4(5)
Mn8	O8	Mn7	99.6(5)
C66	O9	Mn12	138.5(14)
C7	O10	Mn4	131.8(10)
Mn7	O11	Mn3	95.3(4)
Mn7	O11	Mn6	132.8(6)
Mn3	O11	Mn6	131.1(5)
Mn8	O13	Mn9	96.5(5)
Mn8	O13	Mn5	94.3(5)
Mn9	O13	Mn5	99.5(5)
C66	O14	Mn10	126.0(14)
Mn5	O15	Mn2	133.4(6)
Mn5	O15	Mn1	95.3(4)
Mn2	O15	Mn1	123.7(5)
C59	O16	Mn2	135.2(10)
C2	O17	Mn6	136.7(10)
Mn5	O18	Mn7	96.2(4)
Mn5	O18	Mn9	100.2(4)

Mn7	O18	Mn9	94.5(4)
C38	O19	Mn12	133.4(13)
C14	O20	Mn5	124.3(9)
C3	O21	Mn3	131.0(10)
Mn9	O23	Mn6	131.6(6)
Mn9	O23	Mn10	93.6(5)
Mn6	O23	Mn10	130.1(6)
C64	O24	Mn12	129.5(14)
Mn4	O25	Mn8	130.8(6)
Mn4	O25	Mn11	131.9(6)
Mn8	O25	Mn11	93.8(5)
C109	O26	Mn6	131.4(10)
C49	O27	Mn9	124.7(11)
C42	O28	Mn11	130.8(11)
C7	O29	Mn1	130.8(10)
C3	O30	Mn2	137.1(10)
C2	O31	Mn10	130.2(11)
C40	O32	Mn11	123.0(12)
C14	O33	Mn1	124.3(10)
Mn7	O34	Mn3	96.2(5)
Mn7	O34	Mn2	131.6(6)
Mn3	O34	Mn2	123.6(6)
C64	O35	Mn10	133.6(12)
C38	O36	Mn11	132.2(15)
C99	O37	Mn2	135.6(10)
C1	O38	Mn2	138.4(11)
Mn9	O39	Mn10	97.9(5)
Mn9	O39	Mn12	131.6(6)
Mn10	O39	Mn12	120.5(6)
Mn4	O40	Mn5	133.0(6)
Mn4	O40	Mn1	131.5(5)
Mn5	O40	Mn1	95.1(4)
C99	O41	Mn1	127.1(9)
C1	O42	Mn1	131.5(10)
C49	O43	Mn10	120.7(11)
C42	O44	Mn4	134.7(11)
C59	O45	Mn3	127.8(10)
C18	O46	Mn3	123.5(10)
O42	C1	O38	122.5(15)
O42	C1	C102	121.4(15)
O38	C1	C102	116.1(15)
O31	C2	O17	127.4(14)
O31	C2	C25	115.4(16)

O17	C2	C25	117.2(15)
O30	C3	O21	124.0(14)
O30	C3	C101	115.8(14)
O21	C3	C101	120.2(14)
C105	C4	C63	122.6(18)
C61	C5	C71	119(2)
C43	C6	C128	122.5(18)
C43	C6	C40	118.7(16)
C128	C6	C40	118.7(19)
O10	C7	O29	125.8(14)
O10	C7	C103	118.0(14)
O29	C7	C103	116.2(15)
C74	C8	C80	120(2)
C74	C8	C125	117(2)
C80	C8	C125	123.4(18)
C111	C9	C41	111.9(14)
C87	C10	C20	119.0(14)
C87	C10	C109	124.3(15)
C20	C10	C109	116.6(13)
C54	C11	C131	120.6(17)
C54	C11	C64	114.8(16)
C131	C11	C64	124.6(17)
C21	C12	C107	119.5(17)
C17	C13	C15	121.6(14)
C17	C13	C18	122.9(13)
C15	C13	C18	115.5(14)
O33	C14	O20	124.4(13)
O33	C14	C108	119.6(14)
O20	C14	C108	116.0(14)
C35	C15	C13	119.0(16)
C103	C16	C114	119.1(16)
C13	C17	C24	117.5(14)
C13	C17	C124	121.8(13)
C24	C17	C124	120.6(14)
O46	C18	O1	125.9(15)
O46	C18	C13	118.6(14)
O1	C18	C13	115.5(14)
C118	C19	C106	119.9(16)
C118	C20	C10	123.1(15)
C114	C21	C12	124.7(16)
C116	C22	C39	120.0(17)
C37	C24	C17	122.0(16)
C136	C25	C72	118(2)

C136	C25	C2	127(2)
C72	C25	C2	114.9(16)
C58	C26	C97	122.3(16)
C77	C27	C45	121.0(18)
C77	C27	C42	116.7(18)
C45	C27	C42	121.2(17)
C57	C29	C120	119.8(16)
C116	C30	C28	110.1(16)
C51	C31	C102	120.0(16)
C108	C32	C53	117.3(15)
C108	C32	C112	123.1(15)
C53	C32	C112	119.5(14)
C94	C33	C89	124(3)
C126	C34	C50	119(2)
C15	C35	C37	120.1(16)
C24	C37	C35	119.7(17)
O36	C38	O19	124.6(19)
O36	C38	C119	116.7(19)
O19	C38	C119	118.7(18)
C56	C39	C22	119.3(16)
O32	C40	O6	125.0(18)
O32	C40	C6	119.4(16)
O6	C40	C6	115.5(17)
O28	C42	O44	127.5(16)
O28	C42	C27	115.1(16)
O44	C42	C27	117.4(15)
C6	C43	C67	119.9(19)
C100	C44	C47	118.2(17)
C27	C45	C140	118(2)
C27	C45	C139	123(2)
C140	C45	C139	118(2)
C97	C46	C52	118.0(16)
C97	C46	C121	126.0(15)
C52	C46	C121	115.9(15)
C98	C47	C44	119.9(18)
O43	C49	O27	127.4(17)
O43	C49	C110	117.6(15)
O27	C49	C110	114.9(16)
C110	C50	C34	118.8(19)
C63	C51	C31	120.1(18)
C123	C52	C46	121.7(18)
C57	C53	C32	123.5(15)
C76	C54	C11	119.7(18)

C115	C56	C39	119.8(17)
C53	C57	C29	118.6(16)
C26	C58	C123	118.9(17)
O16	C59	O45	125.0(15)
O16	C59	C104	117.8(14)
O45	C59	C104	117.1(14)
C119	C60	C83	119(3)
C138	C62	C94	125(3)
C51	C63	C4	119.2(18)
O35	C64	O24	125(2)
O35	C64	C11	119.1(16)
O24	C64	C11	116.3(17)
C83	C65	C86	123(3)
O9	C66	O14	126.2(19)
O9	C66	C138	119.4(19)
O14	C66	C138	114(2)
C43	C67	C75	118(2)
C87	C68	C48	112.3(14)
C137	C69	C131	123(2)
C79	C70	C77	118(2)
C119	C71	C86	118(2)
C119	C71	C5	125.1(19)
C86	C71	C5	117(2)
C132	C72	C25	118(2)
C80	C73	C82	118(3)
C134	C74	C8	121(3)
C90	C75	C67	120(2)
C137	C76	C54	119(2)
C27	C77	C70	121(2)
C107	C78	C95	110.7(16)
C70	C79	C140	123(2)
C73	C80	C8	119(2)
C73	C80	C130	118(2)
C8	C80	C130	123(2)
C85	C81	C136	119(3)
C134	C82	C73	122(3)
C65	C83	C60	118(3)
C132	C85	C81	121(2)
C65	C86	C71	119(3)
C106	C87	C10	117.7(16)
C106	C87	C68	117.3(15)
C10	C87	C68	125.1(15)
C141	C89	C33	119(4)

C75	C90	C128	124(3)
C84	C91	C128	87(4)
C144	C92	C127	70(4)
C33	C94	C62	113(4)
C136	C96	C93	101(3)
C46	C97	C26	119.9(15)
C46	C97	C99	122.6(15)
C26	C97	C99	117.5(15)
C47	C98	C101	120.4(16)
O37	C99	O41	125.2(14)
O37	C99	C97	118.4(15)
O41	C99	C97	116.3(14)
C111	C100	C44	124.7(15)
C111	C101	C98	120.5(14)
C111	C101	C3	125.5(14)
C98	C101	C3	114.0(14)
C31	C102	C105	118.5(16)
C31	C102	C1	115.4(15)
C105	C102	C1	126.1(16)
C16	C103	C107	121.6(15)
C16	C103	C7	115.0(14)
C107	C103	C7	123.3(15)
C115	C104	C116	120.3(15)
C115	C104	C59	116.3(14)
C116	C104	C59	123.3(14)
C4	C105	C102	119.5(17)
C4	C105	C113	116.7(16)
C102	C105	C113	123.8(15)
C19	C106	C87	122.3(16)
C12	C107	C103	117.4(17)
C12	C107	C78	117.2(16)
C103	C107	C78	125.3(15)
C32	C108	C120	121.9(16)
C32	C108	C14	123.1(15)
C120	C108	C14	115.0(14)
O26	C109	O5	125.4(14)
O26	C109	C10	118.2(14)
O5	C109	C10	116.4(14)
C127	C110	C50	120.7(19)
C127	C110	C49	123.2(18)
C50	C110	C49	116.0(16)
C100	C111	C101	116.3(14)
C100	C111	C9	119.6(14)

C101	C111	C9	124.1(15)
C32	C112	C117	116.6(14)
C23	C113	C105	111.4(14)
C21	C114	C16	117.7(17)
C56	C115	C104	121.5(17)
C22	C116	C104	119.1(15)
C22	C116	C30	116.6(15)
C104	C116	C30	124.2(14)
C20	C118	C19	117.8(17)
C60	C119	C71	122(2)
C60	C119	C38	113.7(19)
C71	C119	C38	124.6(19)
C29	C120	C108	118.9(15)
C129	C121	C46	112.7(16)
C131	C122	C36	110.6(18)
C52	C123	C58	119.0(17)
C55	C124	C17	115.3(13)
O4	C125	O3	124.7(19)
O4	C125	C8	118.1(16)
O3	C125	C8	117.2(17)
C34	C126	C133	121(2)
C110	C127	C133	120(2)
C110	C127	C92	124.3(19)
C133	C127	C92	114(2)
C110	C127	C144	120(2)
C133	C127	C144	115(2)
C92	C127	C144	38.3(15)
C90	C128	C6	115(3)
C90	C128	C91	114(2)
C6	C128	C91	126(2)
C80	C130	C88	113(2)
C69	C131	C11	118.2(19)
C69	C131	C122	117(2)
C11	C131	C122	125(2)
C85	C132	C72	121(3)
C126	C133	C127	120(2)
C74	C134	C82	121(3)
C25	C136	C81	122(3)
C25	C136	C96	121(3)
C81	C136	C96	112(4)
C76	C137	C69	119(2)
C62	C138	C141	120(2)
C62	C138	C66	117(2)

C141	C138	C66	122(3)
C45	C139	C135	104(2)
C79	C140	C45	119(2)
C89	C141	C138	119(4)
C89	C141	C142	116(3)
C138	C141	C142	125(2)
C143	C142	C141	110(2)
C92	C144	C127	71(4)

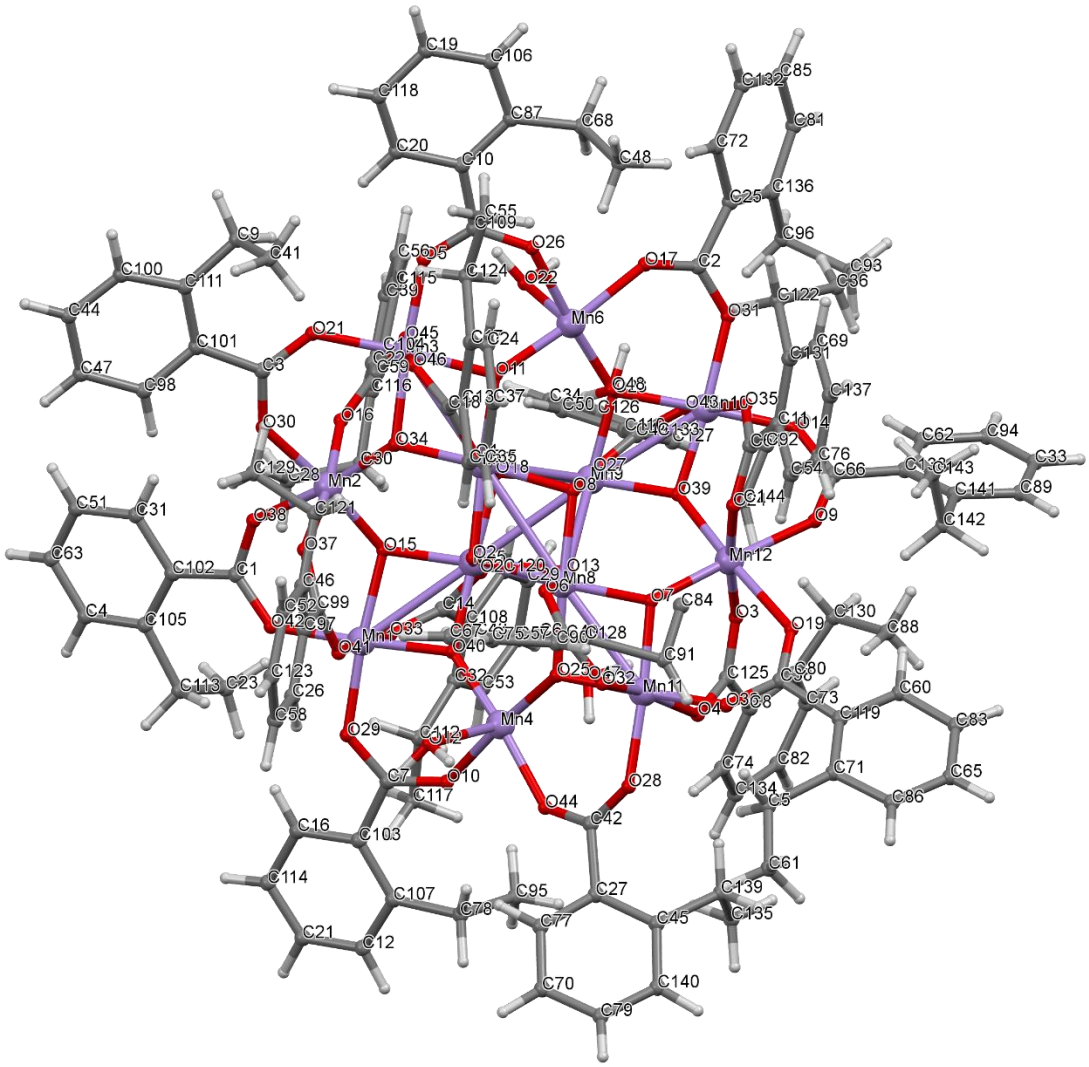

Figure II.1.2 Crystal Structure with atomic labels for compound **3**, Mn_{12}-2-Et, $Mn_{12}O_{12}(O_2CPh\text{-}o\text{-}Et)_{16}(H_2O)_4$, ab50416

II.1.3 Compound 4, Mn_{12}-2-Ph, $Mn_{12}O_{12}(O_2CPh\text{-}o\text{-}Ph)_{16}(H_2O)_4$, ab8213

Table II.1.3.1 Crystal data and structure refinement for ab8213.

Identification code	ab8213
Empirical formula	$C_{208}H_{168}Mn_{12}O_{48}$
Formula weight	4094.70
Temperature/K	100.08
Crystal system	monoclinic
Space group	C2/c
a/Å	34.202(19)
b/Å	21.044(10)
c/Å	27.235(12)
α/°	90.00
β/°	105.28(3)
γ/°	90.00
Volume/Å^3	18910(16)
Z	4
ρ_{calc}g/cm^3	1.438
μ/mm^{-1}	0.852
F(000)	8400.0
Crystal size/mm^3	0.185 × 0.097 × 0.096
Radiation	MoKα (λ = 0.71073)
2Θ range for data collection/°	2.3 to 51.26
Index ranges	$-30 \le h \le 41$, $-24 \le k \le 25$, $-32 \le l \le 32$
Reflections collected	112944
Independent reflections	17245 [R_{int} = 0.1473, R_{sigma} = 0.1202]
Data/restraints/parameters	17245/0/1210
Goodness-of-fit on F^2	1.022
Final R indexes [I>=2σ (I)]	R_1 = 0.0788, wR_2 = 0.2302
Final R indexes [all data]	R_1 = 0.1655, wR_2 = 0.2938
Largest diff. peak/hole / e Å^{-3}	1.84/-0.72

Table II.1.3.2 Fractional Atomic Coordinates (×10^4) and Equivalent Isotropic Displacement Parameters (Å^2×10^3) for ab8213. U_{eq} is defined as 1/3 of of the trace of the orthogonalised U_{IJ} tensor.

Atom	*x*	*y*	*z*	U(eq)
Mn1	0	5032.6(7)	2500	32.0(4)
Mn2	-954.7(4)	5598.2(5)	2210.6(4)	34.0(3)
Mn3	-384.2(3)	6545.8(5)	2591.5(4)	28.0(3)
Mn4	-1236.1(4)	7034.5(5)	1652.0(4)	33.4(3)
Mn5	-225.9(3)	7536.7(5)	1974.4(4)	27.4(3)
Mn6	0	9018.3(7)	2500	32.2(4)
Mn7	-820.5(4)	8456.5(5)	1578.0(4)	31.5(3)
O1	174.3(14)	6629(2)	2980.0(16)	27.0(11)

O2	-336.0(14)	7454(2)	2614.8(16)	25.7(11)
O3	-280.2(14)	8416(2)	2023.7(17)	27.1(11)
O4	-787.0(15)	7562(2)	1620.4(17)	30.3(12)
O5	-914.6(15)	6492(2)	2151.4(17)	30.0(12)
O6	-833.0(16)	9379(2)	1521(2)	40.6(13)
O7	-1361.3(17)	8488(2)	1097.1(19)	39.7(13)
O8	-535.2(17)	8371(2)	955.0(18)	38.8(13)
O9	-66.6(16)	7633(2)	1350.6(17)	33.6(12)
O10	-993.4(17)	4692(2)	2312(2)	48.9(15)
O11	-561.4(16)	6540(2)	3194.3(17)	33.4(12)
O12	-1529.3(17)	5545(2)	1889(2)	44.9(14)
O13	-1062.3(17)	5816(3)	2934(2)	43.5(14)
O14	497.9(17)	9123(3)	2140(2)	46.3(14)
O15	-1734.2(16)	6528(2)	1601(2)	41.2(13)
O16	-1411.3(17)	7621(3)	2180(2)	48.2(15)
O17	-1605.1(17)	7503(2)	1096(2)	49.7(15)
O18	-1139.9(19)	6465(3)	1005.4(19)	48.2(15)
O19	238.4(18)	9713(2)	2963(2)	43.2(14)
O20	-1095.0(17)	8561(2)	2198.4(18)	38.6(13)
O21	-859.6(18)	5434(3)	1478(2)	46.6(15)
O22	-393.4(15)	5662(2)	2543.3(17)	31.4(12)
O23	-221.1(18)	4966(2)	1701(2)	45.9(15)
O24	-366.2(18)	4320(2)	2571(2)	43.2(14)
C1	-1637(3)	8072(4)	949(3)	37.2(19)
C2	-574(3)	9807(4)	1714(3)	35.5(19)
C3	-1790(3)	5952(4)	1688(3)	41(2)
C4	25(3)	8167(4)	627(3)	41(2)
C5	-1478(3)	8361(4)	2789(3)	40(2)
C6	-147(3)	8083(4)	85(3)	46(2)
C7	-1527(3)	8080(5)	3623(4)	71(3)
C8	-1830(3)	9349(4)	2337(3)	48(2)
C9	-1315(3)	8171(4)	2354(3)	42(2)
C10	-2569(3)	6052(4)	1507(3)	46(2)
C11	-1299(3)	3494(4)	2168(3)	56(3)
C12	-736(3)	4255(4)	2469(3)	36.8(19)
C13	-1137(3)	7726(6)	-866(4)	67(3)
C14	408(3)	8425(4)	825(3)	48(2)
C15	-1394(3)	7950(4)	3202(3)	52(2)
C16	634(3)	8629(4)	505(4)	60(3)
C17	-910(3)	3621(4)	2508(3)	43(2)
C18	-2226(2)	5705(4)	1497(3)	40(2)
C19	-2369(3)	7927(4)	588(3)	46(2)
C20	-752(3)	6802(4)	4062(3)	51(2)
C21	-1707(3)	9174(4)	192(3)	46(2)
C22	-858(3)	6194(4)	3256(3)	36.7(19)

C23	-1035(3)	6972(5)	-174(4)	68(3)
C24	-1252(3)	5954(4)	3876(3)	51(2)
C25	-220(3)	8052(4)	1003(3)	37.3(19)
C26	-953(2)	6306(4)	3747(3)	38.4(19)
C27	-1704(3)	8912(4)	2779(3)	45(2)
C28	-2750(3)	8078(4)	268(3)	47(2)
C29	-1491(3)	2918(5)	2175(4)	69(3)
C30	-1357(3)	6140(5)	4317(4)	61(3)
C31	-1075(4)	9961(5)	104(3)	67(3)
C32	-545(3)	7785(4)	-157(3)	47(2)
C33	-1824(3)	10007(5)	2413(4)	67(3)
C34	-2062(3)	8767(4)	230(3)	45(2)
C35	-2022(2)	8265(4)	575(3)	36.6(19)
C36	-1449(3)	5361(5)	3587(4)	57(3)
C37	-2995(3)	5230(5)	1013(3)	56(2)
C38	-1972(3)	10413(5)	1995(5)	74(3)
C39	-2951(3)	5797(5)	1265(3)	54(2)
C40	-2651(3)	4883(4)	1021(3)	53(2)
C41	100(3)	8282(4)	-214(3)	53(2)
C42	-1712(3)	9839(4)	283(3)	60(3)
C43	-785(3)	8003(5)	-617(3)	57(3)
C44	-1751(4)	8616(6)	3615(4)	85(4)
C45	-1845(3)	9038(5)	3200(3)	59(3)
C46	-1374(3)	8912(4)	63(3)	55(2)
C47	-1401(3)	10216(5)	244(3)	59(3)
C48	-2125(3)	10183(5)	1511(4)	73(3)
C49	-2264(3)	5110(4)	1264(3)	45(2)
C50	-685(3)	7271(5)	60(3)	56(2)
C51	-1159(3)	6633(5)	4621(4)	63(3)
C52	-1996(3)	9121(4)	1840(3)	54(2)
C53	-1062(3)	9311(5)	28(3)	61(3)
C54	-2303(4)	7222(7)	2604(5)	96(4)
C55	-2538(3)	6647(4)	1805(4)	59(3)
C56	-725(3)	3151(4)	2870(3)	52(2)
C57	-2787(3)	8563(4)	-87(3)	55(2)
C58	-687(3)	10481(4)	1573(3)	45(2)
C59	-387(3)	10919(4)	1535(3)	57(3)
C60	-934(4)	2587(4)	2874(4)	68(3)
C61	468(3)	8561(5)	-23(4)	64(3)
C62	-331(3)	3241(4)	3275(4)	54(2)
C63	-865(3)	6956(4)	4497(3)	58(3)
C64	-2449(3)	8894(4)	-93(3)	54(2)
C65	-1087(3)	10661(4)	1530(4)	59(3)
C66	-2753(3)	7184(5)	1580(5)	76(3)
C67	-2135(3)	9530(5)	1436(4)	68(3)

C68	-1309(4)	2468(5)	2527(5)	78(3)
C69	-1273(3)	7188(6)	-648(4)	81(4)
C70	-2317(3)	6652(5)	2316(4)	70(3)
C71	-512(4)	11561(4)	1479(4)	75(3)
C72	-2519(5)	7755(7)	2377(7)	104(5)
C73	-1186(4)	11282(5)	1472(5)	81(3)
C74	-2742(4)	7738(6)	1870(7)	104(5)
C75	-537(4)	5226(5)	1386(4)	63(3)
C76	87(3)	10352(4)	1159(4)	59(3)
C77	35(3)	10737(4)	1536(4)	52(2)
C78	-835(3)	5191(4)	402(4)	62(3)
C79	472(4)	10184(5)	1132(4)	69(3)
C80	804(4)	10418(5)	1496(5)	76(3)
C81	-1226(4)	4352(6)	723(5)	85(4)
C82	759(4)	10803(5)	1886(5)	76(3)
C83	-1226(4)	4873(5)	409(4)	70(3)
C84	-503(3)	5316(5)	847(4)	66(3)
C85	369(4)	10954(5)	1898(5)	73(3)
C86	-142(4)	5605(6)	803(4)	99(4)
C87	52(4)	3230(5)	3199(5)	75(3)
C88	-769(4)	5282(6)	-64(4)	83(4)
C89	-396(5)	5555(6)	-92(5)	102(5)
C90	409(3)	3271(5)	3598(5)	73(3)
C91	-329(4)	3228(6)	3808(5)	93(4)
C92	-905(4)	11751(5)	1455(5)	90(4)
C93	45(5)	3276(7)	4186(5)	108(5)
C94	387(4)	3293(7)	4083(5)	100(5)
C95	-86(4)	5737(6)	348(4)	86(4)
C96	-1916(6)	4247(11)	352(8)	58(7)
C97	-1588(6)	4045(7)	685(6)	41(5)
C98	-1945(5)	4713(10)	58(8)	49(5)
C99	-1586(5)	5068(7)	84(5)	109(5)
C100	-1239(4)	4818(6)	3572(4)	88(4)
C101	-1853(4)	5356(6)	3327(5)	95(4)
C102	-1460(8)	4302(7)	3289(6)	57(7)
C103	-1837(8)	4357(9)	3031(9)	66(8)
C104	-2015(6)	4813(11)	3058(8)	74(8)

Table II.1.3.3 Anisotropic Displacement Parameters ($Å^2×10^3$) for ab8213. The Anisotropic displacement factor exponent takes the form: $-2\pi^2[h^2a^{*2}U_{11}+2hka^*b^*U_{12}+\ldots]$.

Atom	U_{11}	U_{22}	U_{33}	U_{23}	U_{13}	U_{12}
Mn1	36.6(10)	20.9(8)	36.1(9)	0	5.3(8)	0
Mn2	36.4(7)	23.7(6)	38.3(7)	1.2(5)	3.8(6)	-2.4(5)
Mn3	34.2(7)	21.8(6)	26.8(6)	0.7(4)	5.6(5)	-1.0(5)

Mn4	35.5(7)	24.2(6)	36.3(7)	1.9(5)	1.8(5)	-0.8(5)
Mn5	35.8(7)	21.2(6)	24.4(6)	0.7(4)	6.5(5)	1.0(5)
Mn6	41.4(11)	19.6(8)	32.8(9)	0	4.8(8)	0
Mn7	36.4(7)	22.9(6)	32.5(6)	1.9(5)	4.3(5)	1.6(5)
O1	32(3)	22(3)	26(3)	1(2)	6(2)	1(2)
O2	31(3)	24(3)	22(2)	2(2)	7(2)	-1(2)
O3	31(3)	13(2)	35(3)	1(2)	7(2)	-3(2)
O4	36(3)	22(3)	32(3)	2(2)	8(2)	4(2)
O5	33(3)	20(3)	36(3)	1(2)	7(2)	-1(2)
O6	39(3)	27(3)	51(3)	5(3)	4(3)	9(3)
O7	44(4)	30(3)	41(3)	6(2)	3(3)	7(3)
O8	41(4)	41(3)	33(3)	10(2)	7(3)	8(3)
O9	45(3)	29(3)	28(3)	5(2)	12(2)	3(2)
O10	41(4)	24(3)	78(4)	3(3)	8(3)	-4(3)
O11	42(3)	33(3)	26(3)	2(2)	9(2)	-4(3)
O12	41(4)	28(3)	58(4)	2(3)	1(3)	2(3)
O13	46(4)	43(3)	41(3)	2(3)	11(3)	-13(3)
O14	55(4)	36(3)	48(3)	3(3)	14(3)	-4(3)
O15	37(3)	27(3)	59(4)	3(3)	12(3)	-1(2)
O16	46(4)	37(3)	68(4)	-6(3)	27(3)	-4(3)
O17	48(4)	31(3)	57(4)	13(3)	-12(3)	-2(3)
O18	62(4)	48(4)	33(3)	-6(3)	10(3)	-1(3)
O19	54(4)	24(3)	46(3)	-5(2)	3(3)	0(3)
O20	48(4)	30(3)	37(3)	-1(2)	8(3)	-4(3)
O21	49(4)	42(4)	48(3)	-12(3)	12(3)	5(3)
O22	35(3)	24(3)	33(3)	-3(2)	5(2)	-5(2)
O23	61(4)	37(3)	35(3)	-4(3)	3(3)	4(3)
O24	44(4)	28(3)	56(4)	6(3)	10(3)	-2(3)
C1	38(5)	30(5)	40(5)	-1(4)	4(4)	-5(4)
C2	49(6)	24(4)	32(4)	2(3)	7(4)	5(4)
C3	42(6)	41(5)	40(5)	-10(4)	12(4)	-6(4)
C4	54(6)	34(5)	36(5)	5(4)	16(4)	4(4)
C5	42(5)	37(5)	43(5)	-3(4)	14(4)	2(4)
C6	57(6)	43(5)	40(5)	6(4)	17(4)	5(4)
C7	75(8)	84(8)	59(6)	16(6)	28(6)	33(6)
C8	42(6)	48(6)	55(6)	-3(4)	15(4)	13(4)
C9	47(6)	28(5)	47(5)	3(4)	7(4)	6(4)
C10	45(6)	42(5)	46(5)	8(4)	2(4)	-5(4)
C11	75(7)	38(5)	56(6)	-1(4)	18(5)	-17(5)
C12	41(6)	25(4)	43(5)	-4(4)	9(4)	-4(4)
C13	72(8)	93(8)	41(6)	12(5)	23(6)	20(7)
C14	61(7)	45(5)	38(5)	-2(4)	10(5)	-14(5)
C15	51(6)	53(6)	53(6)	1(5)	18(5)	6(5)
C16	60(7)	51(6)	68(7)	12(5)	13(5)	-16(5)
C17	55(6)	28(5)	46(5)	-5(4)	16(4)	-7(4)

C18	35(5)	41(5)	41(5)	6(4)	5(4)	-2(4)
C19	52(6)	34(5)	48(5)	1(4)	7(5)	0(4)
C20	49(6)	55(6)	51(5)	3(5)	17(5)	-6(5)
C21	48(6)	49(5)	32(4)	14(4)	-2(4)	1(4)
C22	47(5)	25(4)	39(5)	14(4)	11(4)	5(4)
C23	83(8)	75(8)	42(6)	-9(5)	12(6)	-18(6)
C24	52(6)	47(6)	60(6)	20(5)	22(5)	11(5)
C25	41(5)	38(5)	28(4)	-2(4)	0(4)	-6(4)
C26	40(5)	36(5)	42(5)	12(4)	15(4)	1(4)
C27	39(5)	50(5)	47(5)	-5(4)	11(4)	4(4)
C28	35(5)	51(6)	51(5)	-4(4)	5(4)	-8(4)
C29	76(8)	62(7)	66(7)	-8(6)	12(6)	-25(6)
C30	67(7)	56(6)	71(7)	11(5)	39(6)	3(5)
C31	80(8)	62(7)	49(6)	11(5)	-2(6)	-30(6)
C32	56(6)	53(6)	33(5)	3(4)	13(4)	-1(5)
C33	73(8)	48(6)	76(7)	-2(5)	14(6)	16(5)
C34	49(6)	37(5)	39(5)	4(4)	-4(4)	1(4)
C35	36(5)	33(5)	36(4)	-5(4)	1(4)	1(4)
C36	67(7)	50(6)	67(6)	-1(5)	41(6)	-14(5)
C37	49(6)	60(7)	54(6)	2(5)	4(5)	-15(5)
C38	83(9)	35(6)	106(9)	-4(6)	27(7)	11(5)
C39	41(6)	57(6)	61(6)	10(5)	10(5)	-6(5)
C40	58(7)	49(6)	46(5)	-1(4)	3(5)	-17(5)
C41	70(7)	52(6)	38(5)	17(4)	16(5)	3(5)
C42	77(8)	46(6)	60(6)	4(5)	21(6)	-4(5)
C43	56(7)	71(7)	41(5)	1(5)	11(5)	-3(5)
C44	104(10)	104(10)	59(7)	8(6)	42(7)	25(8)
C45	61(7)	65(7)	54(6)	-2(5)	20(5)	17(5)
C46	69(7)	44(5)	55(6)	14(4)	19(5)	5(5)
C47	79(8)	44(6)	54(6)	-4(4)	18(6)	-8(6)
C48	83(9)	68(8)	79(8)	15(6)	39(7)	26(6)
C49	51(6)	38(5)	45(5)	1(4)	9(4)	-6(4)
C50	66(7)	61(6)	38(5)	-3(5)	8(5)	-7(5)
C51	81(8)	69(7)	49(6)	4(5)	32(6)	14(6)
C52	58(6)	51(6)	51(6)	3(5)	13(5)	16(5)
C53	56(7)	69(7)	58(6)	19(5)	15(5)	0(5)
C54	74(9)	122(12)	103(10)	-17(9)	41(8)	10(9)
C55	51(6)	48(6)	79(7)	0(5)	19(6)	2(5)
C56	74(7)	27(5)	56(6)	-3(4)	22(5)	-8(4)
C57	49(6)	61(6)	44(5)	13(5)	-9(4)	5(5)
C58	63(6)	21(4)	44(5)	10(4)	0(4)	2(4)
C59	80(8)	35(5)	54(6)	10(4)	17(5)	-5(5)
C60	93(9)	34(6)	80(7)	5(5)	27(7)	-7(5)
C61	80(8)	60(7)	58(6)	21(5)	28(6)	-10(6)
C62	70(8)	34(5)	55(6)	11(4)	12(5)	0(5)

C63	90(8)	48(6)	45(5)	-8(4)	35(6)	-7(5)
C64	52(6)	50(6)	53(6)	15(4)	4(5)	-2(5)
C65	65(7)	29(5)	79(7)	11(5)	12(6)	14(5)
C66	68(8)	63(8)	97(9)	4(6)	21(7)	1(6)
C67	76(8)	73(8)	51(6)	-4(5)	11(5)	33(6)
C68	91(10)	46(7)	97(9)	3(6)	21(8)	-23(6)
C69	62(8)	123(11)	56(7)	-25(7)	13(6)	-14(7)
C70	72(8)	70(8)	72(7)	-22(6)	24(6)	-5(6)
C71	108(10)	25(5)	100(8)	16(5)	41(8)	8(6)
C72	82(11)	96(11)	154(14)	-49(11)	63(11)	-8(9)
C73	66(8)	45(7)	127(10)	17(6)	20(7)	19(6)
C74	78(10)	58(8)	182(16)	-5(9)	44(11)	14(7)
C75	89(9)	43(6)	52(6)	-7(5)	10(6)	-13(6)
C76	77(8)	52(6)	49(6)	16(5)	15(5)	4(5)
C77	69(7)	21(4)	66(6)	11(4)	18(6)	-1(4)
C78	88(8)	47(6)	52(6)	-18(5)	22(6)	-7(5)
C79	94(10)	52(6)	67(7)	16(5)	35(7)	5(6)
C80	79(9)	52(7)	105(9)	30(7)	36(8)	14(6)
C81	112(11)	65(8)	85(8)	-38(7)	38(8)	-11(7)
C82	63(8)	47(6)	114(10)	-10(6)	16(7)	-10(6)
C83	81(9)	60(7)	68(7)	-28(6)	14(7)	-1(6)
C84	80(8)	66(7)	52(6)	-14(5)	16(6)	-8(6)
C85	77(9)	41(6)	103(9)	-8(6)	27(7)	-4(6)
C86	124(12)	122(11)	59(7)	-22(7)	40(8)	-51(9)
C87	69(9)	73(8)	85(8)	0(6)	24(7)	3(6)
C88	108(10)	89(9)	46(6)	-6(6)	8(6)	-24(8)
C89	169(15)	82(9)	69(8)	0(7)	56(9)	-24(9)
C90	60(8)	56(7)	101(9)	23(6)	15(7)	8(5)
C91	94(11)	101(10)	89(9)	9(8)	35(8)	-6(8)
C92	94(10)	40(6)	152(12)	27(7)	60(9)	21(6)
C93	119(13)	131(12)	57(8)	7(8)	-5(9)	-13(10)
C94	58(9)	148(13)	89(10)	49(9)	9(8)	-14(8)
C95	102(10)	92(9)	66(8)	-21(7)	24(7)	-33(7)
C96	43(13)	79(15)	73(14)	-91(13)	52(12)	-52(12)
C97	65(13)	35(9)	41(10)	-43(8)	44(10)	-39(10)
C98	18(10)	67(14)	70(13)	-59(12)	25(9)	-11(10)
C99	150(15)	102(11)	65(8)	-42(7)	10(9)	47(11)
C100	132(11)	73(8)	80(8)	38(7)	67(8)	40(8)
C101	76(10)	97(10)	129(11)	-12(8)	53(9)	-1(8)
C102	150(20)	0(7)	42(10)	-8(7)	67(13)	-6(11)
C103	100(19)	39(12)	92(17)	-59(12)	82(16)	-65(13)
C104	48(13)	99(17)	97(15)	-80(14)	61(12)	-81(13)

Table II.1.3.4 Bond Lengths for ab8213.

Atom	Atom	Length/Å	Atom	Atom	Length/Å
Mn1	O22[1]	1.914(5)	C20	C63	1.378(11)
Mn1	O23[1]	2.113(5)	C21	C34	1.510(12)
Mn1	O24[1]	1.995(5)	C21	C42	1.422(12)
Mn3	O1[1]	1.886(4)	C21	C46	1.393(12)
Mn5	O1[1]	1.920(5)	C22	O11	1.297(9)
Mn5	O2[1]	1.960(5)	C22	O13	1.251(9)
Mn6	O3[1]	1.885(5)	C22	C26	1.474(10)
Mn6	O14[1]	2.188(5)	C23	C50	1.355(13)
Mn6	O19[1]	1.962(5)	C23	C69	1.409(14)
O1	Mn3[1]	1.886(4)	C24	C26	1.381(11)
O1	Mn3	1.932(5)	C24	C30	1.398(12)
O1	Mn5[1]	1.920(5)	C24	C36	1.533(13)
O2	Mn3	1.918(5)	C25	O8	1.246(9)
O2	Mn5[1]	1.960(5)	C25	O9	1.299(9)
O2	Mn5	1.887(4)	C27	C45	1.379(11)
O3	Mn5	1.868(4)	C28	C57	1.388(12)
O3	Mn6	1.885(5)	C29	C68	1.374(14)
O3	Mn7	1.927(5)	C30	C51	1.389(14)
O4	Mn4	1.915(5)	C31	C47	1.378(14)
O4	Mn5	1.908(5)	C31	C53	1.386(13)
O4	Mn7	1.888(5)	C32	C43	1.383(12)
O5	Mn2	1.897(5)	C32	C50	1.378(12)
O5	Mn3	1.896(5)	C33	C38	1.406(14)
O5	Mn4	1.890(5)	C34	C35	1.398(11)
O6	Mn7	1.947(5)	C34	C64	1.408(12)
O7	Mn7	1.966(6)	C36	C100	1.356(13)
O8	Mn7	2.176(5)	C36	C101	1.377(15)
O9	Mn5	1.927(5)	C37	C39	1.364(13)
O10	Mn2	1.936(5)	C37	C40	1.382(13)
O11	Mn3	1.894(5)	C38	C48	1.372(15)
O12	Mn2	1.933(6)	C40	C49	1.397(12)
O13	Mn2	2.148(5)	C41	C61	1.363(13)
O14	Mn6	2.188(5)	C42	C47	1.354(13)
O15	Mn4	1.983(5)	C44	C45	1.408(14)
O16	Mn4	2.098(5)	C46	C53	1.378(13)
O17	Mn4	1.962(5)	C48	C67	1.388(14)
O18	Mn4	2.225(5)	C51	C63	1.329(13)
O19	Mn6	1.962(5)	C52	C67	1.378(12)
O19	C2[1]	1.265(9)	C54	C70	1.427(16)
O20	Mn7	2.149(5)	C54	C72	1.394(19)
O21	Mn2	2.132(6)	C55	C66	1.398(14)
O22	Mn1	1.914(5)	C55	C70	1.398(14)
O22	Mn2	1.899(5)	C56	C60	1.389(12)

O22	Mn3	1.863(5)	C56	C62	1.513(13)
O23	Mn1	2.113(5)	C57	C64	1.352(12)
O24	Mn1	1.995(5)	C58	C59	1.404(12)
C1	O7	1.271(9)	C58	C65	1.396(13)
C1	O17	1.258(9)	C59	C71	1.413(12)
C1	C35	1.493(11)	C59	C77	1.491(13)
C2	O6	1.275(9)	C60	C68	1.401(14)
C2	O19[1]	1.265(9)	C62	C87	1.379(14)
C2	C58	1.492(10)	C62	C91	1.451(14)
C3	O12	1.254(10)	C65	C73	1.350(12)
C3	O15	1.258(9)	C66	C74	1.403(17)
C3	C18	1.534(11)	C71	C92	1.386(15)
C4	C6	1.448(11)	C72	C74	1.393(19)
C4	C14	1.390(12)	C73	C92	1.387(15)
C4	C25	1.505(11)	C75	O21	1.272(12)
C5	C9	1.493(11)	C75	O23	1.309(12)
C5	C15	1.387(11)	C75	C84	1.515(13)
C5	C27	1.389(11)	C76	C77	1.356(12)
C6	C32	1.485(12)	C76	C79	1.384(14)
C6	C41	1.384(11)	C77	C85	1.375(14)
C7	C15	1.367(12)	C78	C83	1.501(15)
C7	C44	1.362(14)	C78	C84	1.450(14)
C8	C27	1.487(12)	C78	C88	1.360(13)
C8	C33	1.400(12)	C79	C80	1.387(15)
C8	C52	1.408(12)	C80	C82	1.376(15)
C9	O16	1.260(9)	C81	C83	1.389(15)
C9	O20	1.261(9)	C81	C97	1.375(18)
C10	C18	1.390(12)	C82	C85	1.381(14)
C10	C39	1.404(12)	C83	C99	1.377(16)
C10	C55	1.480(13)	C84	C86	1.409(15)
C11	C17	1.431(12)	C86	C95	1.331(14)
C11	C29	1.379(12)	C87	C90	1.408(15)
C12	O10	1.266(9)	C88	C89	1.420(17)
C12	O24	1.231(9)	C89	C95	1.427(17)
C12	C17	1.475(11)	C90	C94	1.343(16)
C13	C43	1.348(13)	C91	C93	1.416(17)
C13	C69	1.413(15)	C93	C94	1.276(17)
C14	C16	1.376(12)	C96	C97	1.31(3)
C16	C61	1.408(13)	C96	C98	1.25(3)
C17	C56	1.422(12)	C98	C99	1.42(2)
C18	C49	1.393(11)	C100	C102	1.43(2)
C19	C28	1.401(11)	C101	C104	1.39(2)
C19	C35	1.392(11)	C102	C103	1.30(3)
C20	C26	1.410(12)	C103	C104	1.15(3)

[1]-X,+Y,1/2-Z

Table II.1.3.5 Bond Angles for ab8213.

Atom	Atom	Atom	Angle/°	Atom	Atom	Atom	Angle/°
O22	Mn1	O22[1]	92.4(3)	C4	C6	C32	125.7(7)
O22	Mn1	O23[1]	92.8(2)	C41	C6	C4	114.6(8)
O22[1]	Mn1	O23	92.8(2)	C41	C6	C32	119.7(8)
O22	Mn1	O23	92.5(2)	C44	C7	C15	117.6(9)
O22[1]	Mn1	O23[1]	92.5(2)	C33	C8	C27	120.1(8)
O22[1]	Mn1	O24[1]	92.6(2)	C33	C8	C52	117.8(9)
O22[1]	Mn1	O24	174.6(2)	C52	C8	C27	121.8(8)
O22	Mn1	O24[1]	174.6(2)	O16	C9	O20	126.2(8)
O22	Mn1	O24	92.6(2)	O16	C9	C5	115.5(7)
O23[1]	Mn1	O23	172.4(3)	O20	C9	C5	118.2(7)
O24[1]	Mn1	O23	85.1(2)	C18	C10	C39	118.4(8)
O24	Mn1	O23	89.2(2)	C18	C10	C55	121.1(8)
O24[1]	Mn1	O23[1]	89.2(2)	C39	C10	C55	120.4(9)
O24	Mn1	O23[1]	85.1(2)	C29	C11	C17	121.3(9)
O24	Mn1	O24[1]	82.6(3)	O10	C12	C17	115.1(8)
O5	Mn2	O10	176.7(2)	O24	C12	O10	125.2(7)
O5	Mn2	O12	96.1(2)	O24	C12	C17	119.6(7)
O5	Mn2	O13	84.3(2)	C43	C13	C69	118.8(9)
O5	Mn2	O21	92.8(2)	C16	C14	C4	120.3(8)
O5	Mn2	O22	83.3(2)	C7	C15	C5	120.8(9)
O10	Mn2	O13	92.5(2)	C14	C16	C61	118.4(9)
O10	Mn2	O21	90.4(2)	C11	C17	C12	116.5(7)
O12	Mn2	O10	84.7(2)	C56	C17	C11	119.1(8)
O12	Mn2	O13	91.7(2)	C56	C17	C12	124.4(8)
O12	Mn2	O21	87.3(2)	C10	C18	C3	124.4(8)
O21	Mn2	O13	176.8(2)	C10	C18	C49	120.2(8)
O22	Mn2	O10	95.8(2)	C49	C18	C3	115.2(7)
O22	Mn2	O12	178.4(2)	C35	C19	C28	121.8(8)
O22	Mn2	O13	86.7(2)	C63	C20	C26	119.7(8)
O22	Mn2	O21	94.2(2)	C42	C21	C34	120.0(8)
O1[1]	Mn3	O1	84.7(2)	C46	C21	C34	121.2(8)
O1[1]	Mn3	O2	83.50(18)	C46	C21	C42	118.7(9)
O1[1]	Mn3	O5	89.6(2)	O11	C22	C26	113.2(7)
O1[1]	Mn3	O11	173.8(2)	O13	C22	O11	125.3(7)
O2	Mn3	O1	80.09(19)	O13	C22	C26	121.4(7)
O5	Mn3	O1	174.11(19)	C50	C23	C69	120.4(10)
O5	Mn3	O2	98.0(2)	C26	C24	C30	116.3(9)
O11	Mn3	O1	91.2(2)	C26	C24	C36	124.1(8)
O11	Mn3	O2	91.25(19)	C30	C24	C36	119.4(8)
O11	Mn3	O5	94.4(2)	O8	C25	O9	128.0(7)
O22	Mn3	O1	97.2(2)	O8	C25	C4	117.6(7)

O22	Mn3	O1[1]	92.1(2)	O9	C25	C4	114.4(7)
O22	Mn3	O2	175.0(2)	C20	C26	C22	118.8(7)
O22	Mn3	O5	84.3(2)	C24	C26	C20	121.2(8)
O22	Mn3	O11	93.0(2)	C24	C26	C22	119.9(8)
O4	Mn4	O15	173.0(2)	C5	C27	C8	124.9(7)
O4	Mn4	O16	93.9(2)	C45	C27	C5	117.3(8)
O4	Mn4	O17	92.0(2)	C45	C27	C8	117.7(8)
O4	Mn4	O18	89.4(2)	C57	C28	C19	120.0(8)
O5	Mn4	O4	93.5(2)	C68	C29	C11	119.0(10)
O5	Mn4	O15	93.0(2)	C51	C30	C24	121.7(9)
O5	Mn4	O16	94.5(2)	C47	C31	C53	119.0(9)
O5	Mn4	O17	173.0(2)	C43	C32	C6	121.3(8)
O5	Mn4	O18	93.7(2)	C50	C32	C6	121.5(8)
O15	Mn4	O16	88.2(2)	C50	C32	C43	117.3(9)
O15	Mn4	O18	87.6(2)	C8	C33	C38	119.6(10)
O16	Mn4	O18	170.9(2)	C35	C34	C21	122.4(7)
O17	Mn4	O15	81.4(2)	C35	C34	C64	118.2(8)
O17	Mn4	O16	89.5(2)	C64	C34	C21	119.4(7)
O17	Mn4	O18	81.9(2)	C19	C35	C1	116.6(7)
O1[1]	Mn5	O2[1]	79.33(19)	C19	C35	C34	118.1(8)
O1[1]	Mn5	O9	96.8(2)	C34	C35	C1	125.2(7)
O2	Mn5	O1[1]	83.43(19)	C100	C36	C24	122.5(11)
O2	Mn5	O2[1]	82.4(2)	C100	C36	C101	116.6(11)
O2	Mn5	O4	92.9(2)	C101	C36	C24	121.0(10)
O2	Mn5	O9	175.2(2)	C39	C37	C40	118.2(9)
O3	Mn5	O1[1]	172.04(19)	C48	C38	C33	121.8(10)
O3	Mn5	O2	88.70(19)	C37	C39	C10	122.5(9)
O3	Mn5	O2[1]	98.5(2)	C37	C40	C49	121.5(9)
O3	Mn5	O4	84.5(2)	C61	C41	C6	123.5(9)
O3	Mn5	O9	90.9(2)	C47	C42	C21	121.2(10)
O4	Mn5	O1[1]	97.1(2)	C13	C43	C32	123.5(10)
O4	Mn5	O2[1]	174.39(19)	C7	C44	C45	122.9(9)
O4	Mn5	O9	91.8(2)	C27	C45	C44	119.4(9)
O9	Mn5	O2[1]	92.9(2)	C53	C46	C21	118.4(9)
O3	Mn6	O3[1]	95.5(3)	C42	C47	C31	120.2(9)
O3	Mn6	O14	94.2(2)	C38	C48	C67	118.6(10)
O3[1]	Mn6	O14	93.5(2)	C18	C49	C40	119.1(9)
O3	Mn6	O14[1]	93.5(2)	C23	C50	C32	121.8(9)
O3[1]	Mn6	O14[1]	94.2(2)	C63	C51	C30	120.9(9)
O3[1]	Mn6	O19[1]	173.3(2)	C67	C52	C8	121.4(9)
O3	Mn6	O19	173.3(2)	C46	C53	C31	122.4(10)
O3[1]	Mn6	O19	90.5(2)	C72	C54	C70	119.7(14)
O3	Mn6	O19[1]	90.5(2)	C66	C55	C10	119.3(10)
O14	Mn6	O14[1]	168.5(3)	C70	C55	C10	119.6(9)
O19[1]	Mn6	O14[1]	88.4(2)	C70	C55	C66	120.9(10)

O19	Mn6	O14[1]	83.0(2)	C17	C56	C62	124.6(7)
O19	Mn6	O14	88.4(2)	C60	C56	C17	117.7(9)
O19[1]	Mn6	O14	83.0(2)	C60	C56	C62	117.5(8)
O19	Mn6	O19[1]	83.7(3)	C64	C57	C28	117.8(9)
O3	Mn7	O6	95.3(2)	C59	C58	C2	119.9(8)
O3	Mn7	O7	177.4(2)	C65	C58	C2	117.4(8)
O3	Mn7	O8	86.3(2)	C65	C58	C59	122.4(8)
O3	Mn7	O20	93.1(2)	C58	C59	C71	115.4(10)
O4	Mn7	O3	83.4(2)	C58	C59	C77	123.8(8)
O4	Mn7	O6	177.3(2)	C71	C59	C77	120.8(9)
O4	Mn7	O7	96.0(2)	C56	C60	C68	121.8(10)
O4	Mn7	O8	86.1(2)	C41	C61	C16	121.0(9)
O4	Mn7	O20	94.9(2)	C87	C62	C56	126.0(9)
O6	Mn7	O7	85.2(2)	C87	C62	C91	113.3(10)
O6	Mn7	O8	91.5(2)	C91	C62	C56	119.7(10)
O6	Mn7	O20	87.5(2)	C51	C63	C20	120.1(9)
O7	Mn7	O8	91.1(2)	C57	C64	C34	124.1(8)
O7	Mn7	O20	89.5(2)	C73	C65	C58	118.9(10)
O20	Mn7	O8	178.7(2)	C55	C66	C74	119.5(12)
Mn3[1]	O1	Mn3	94.4(2)	C52	C67	C48	120.8(10)
Mn3[1]	O1	Mn5[1]	95.6(2)	C29	C68	C60	120.9(10)
Mn5[1]	O1	Mn3	100.7(2)	C23	C69	C13	118.1(10)
Mn3	O2	Mn5[1]	99.8(2)	C55	C70	C54	119.0(11)
Mn5	O2	Mn3	95.62(19)	C92	C71	C59	122.9(10)
Mn5	O2	Mn5[1]	96.6(2)	C74	C72	C54	120.5(13)
Mn5	O3	Mn6	132.3(3)	C65	C73	C92	122.5(11)
Mn5	O3	Mn7	95.5(2)	C72	C74	C66	120.4(13)
Mn6	O3	Mn7	129.3(2)	O21	C75	O23	128.7(9)
Mn5	O4	Mn4	132.3(2)	O21	C75	C84	116.1(9)
Mn7	O4	Mn4	123.0(3)	O23	C75	C84	115.1(10)
Mn7	O4	Mn5	95.5(2)	C77	C76	C79	120.6(11)
Mn3	O5	Mn2	94.8(2)	C76	C77	C59	118.1(9)
Mn4	O5	Mn2	128.2(3)	C76	C77	C85	119.4(10)
Mn4	O5	Mn3	134.2(3)	C85	C77	C59	122.5(9)
C2	O6	Mn7	132.3(5)	C84	C78	C83	125.1(9)
C1	O7	Mn7	132.6(5)	C88	C78	C83	116.2(10)
C25	O8	Mn7	121.0(5)	C88	C78	C84	118.0(10)
C25	O9	Mn5	124.0(5)	C76	C79	C80	118.9(11)
C12	O10	Mn2	134.1(5)	C82	C80	C79	121.5(11)
C22	O11	Mn3	123.8(5)	C97	C81	C83	118.0(15)
C3	O12	Mn2	132.8(5)	C80	C82	C85	117.4(11)
C22	O13	Mn2	125.4(5)	C81	C83	C78	120.3(11)
C3	O15	Mn4	132.4(5)	C99	C83	C78	120.5(13)
C9	O16	Mn4	134.8(5)	C99	C83	C81	119.1(13)
C1	O17	Mn4	135.1(5)	C78	C84	C75	122.9(10)

C2[1]	O19	Mn6	135.4(5)	C86	C84	C75	115.5(9)
C9	O20	Mn7	128.4(5)	C86	C84	C78	121.1(10)
C75	O21	Mn2	126.4(6)	C77	C85	C82	122.1(11)
Mn2	O22	Mn1	124.0(2)	C95	C86	C84	121.0(12)
Mn3	O22	Mn1	134.1(3)	C62	C87	C90	123.3(11)
Mn3	O22	Mn2	95.8(2)	C78	C88	C89	118.6(11)
C75	O23	Mn1	131.0(6)	C88	C89	C95	122.9(11)
C12	O24	Mn1	134.2(5)	C94	C90	C87	119.9(11)
O7	C1	C35	118.4(7)	C93	C91	C62	119.5(12)
O17	C1	O7	124.1(7)	C71	C92	C73	117.8(10)
O17	C1	C35	117.5(7)	C94	C93	C91	123.1(13)
O6	C2	C58	117.4(7)	C93	C94	C90	120.6(13)
O19[1]	C2	O6	125.5(7)	C86	C95	C89	117.9(12)
O19[1]	C2	C58	117.0(7)	C98	C96	C97	127.2(18)
O12	C3	O15	127.9(8)	C96	C97	C81	119.3(17)
O12	C3	C18	115.6(7)	C96	C98	C99	117.1(19)
O15	C3	C18	116.5(8)	C83	C99	C98	119.2(16)
C6	C4	C25	121.6(8)	C36	C100	C102	116.5(15)
C14	C4	C6	122.1(7)	C36	C101	C104	118.9(15)
C14	C4	C25	115.9(7)	C103	C102	C100	122.3(16)
C15	C5	C9	115.8(7)	C104	C103	C102	120.4(19)
C15	C5	C27	122.1(8)	C103	C104	C101	125(2)
C27	C5	C9	122.1(7)				

[1]-X,+Y,1/2-Z

Table II.1.3.6 Hydrogen Atom Coordinates (Å×10^4) and Isotropic Displacement Parameters (Å^2×10^3) for ab8213.

Atom	*x*	*y*	*z*	U(eq)
H14A	523	9527	2061	70
H14B	451	8894	1857	70
H18A	-947	6645	869	72
H18B	-1372	6428	742	72
H7	-1465	7806	3910	85
H11	-1427	3812	1933	67
H13	-1291	7891	-1183	80
H14	515	8461	1183	58
H15	-1243	7574	3192	62
H16	895	8810	637	72
H19	-2346	7584	821	55
H20	-540	7029	3974	61
H23	-1121	6614	-17	81
H28	-2983	7849	294	56
H29	-1745	2835	1940	83
H30	-1570	5923	4411	73
H31	-862	10226	62	81

H33	-1721	10178	2745	80
H37	-3256	5078	837	67
H38	-1966	10859	2050	89
H39	-3187	6027	1278	64
H40	-2677	4481	857	64
H41	8	8219	-571	64
H42	-1937	10022	373	72
H43	-698	8366	-765	68
H44	-1848	8710	3904	102
H45	-2004	9406	3208	71
H46	-1361	8469	0	67
H47	-1408	10658	312	70
H48	-2222	10465	1233	88
H49	-2031	4862	1271	54
H50	-531	7122	383	67
H51	-1235	6742	4922	76
H52	-2014	8675	1781	64
H53	-831	9134	-51	73
H54	-2147	7238	2949	116
H57	-3040	8659	-318	66
H60	-820	2272	3120	82
H61	615	8713	-250	76
H63	-732	7292	4708	69
H64	-2475	9234	-329	65
H65	-1287	10351	1540	71
H66	-2906	7173	1234	91
H67	-2238	9364	1103	81
H68	-1439	2071	2534	94
H69	-1517	6978	-817	97
H70	-2178	6282	2469	84
H71	-319	11876	1457	90
H72	-2513	8132	2570	125
H73	-1459	11403	1442	97
H74	-2887	8104	1718	125
H76	-143	10195	912	71
H79	508	9914	868	82
H80	1069	10310	1476	92
H81	-983	4213	958	102
H82	987	10959	2137	91
H85	330	11215	2166	87
H86	64	5706	1101	118
H87	76	3192	2861	90
H88	-969	5166	-365	100
H89	-350	5619	-418	123
H90	666	3284	3524	88

H91	-576	3189	3903	112
H92	-978	12187	1429	108
H93	40	3295	4533	129
H94	629	3321	4351	120
H95	153	5947	317	104
H96	-2157	4014	332	70
H97	-1600	3691	897	49
H98	-2196	4824	-172	59
H99	-1595	5436	-120	131
H100	-959	4782	3742	105
H101	-2018	5718	3331	115
H102	-1328	3905	3290	68
H103	-1965	4018	2818	80
H104	-2295	4819	2883	88

Table II.1.3.7 Atomic Occupancy for ab8213.

Atom	***Occupancy***	**Atom**	***Occupancy***	**Atom**	***Occupancy***
C96	0.50	C97	0.50	C98	0.50
C102	0.50	C103	0.50	C104	0.50

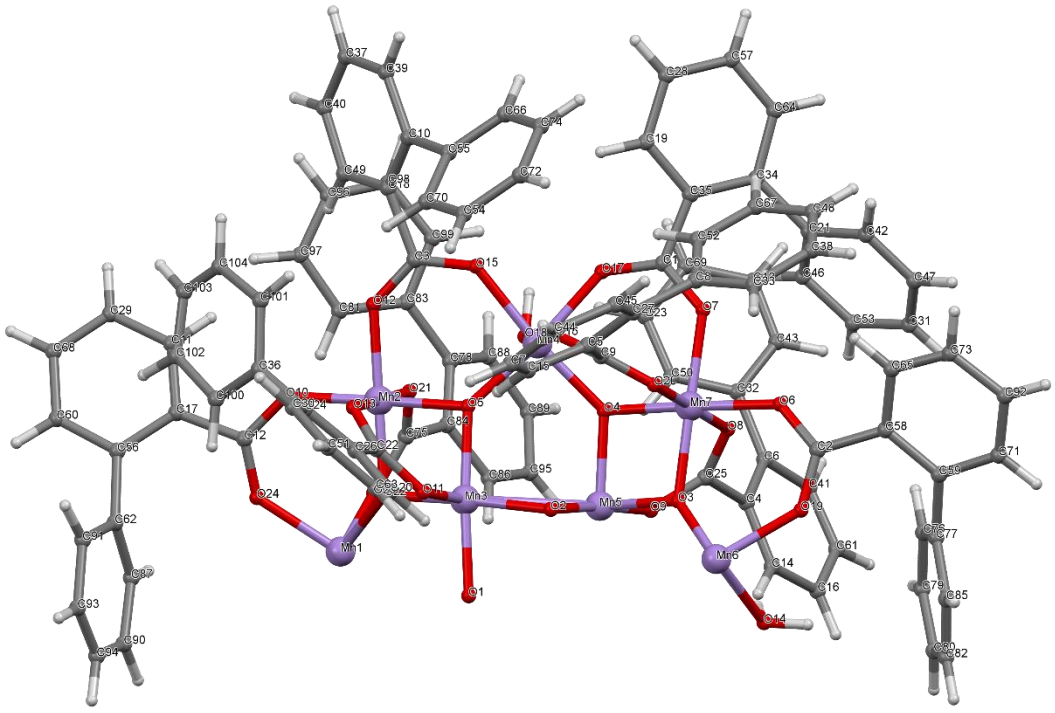

Figure II.1.3 Crystal Structure with atomic labels for compound **4**, Mn_{12}-2-Ph, $Mn_{12}O_{12}(O_2CPh\text{-}o\text{-}Ph)_{16}(H_2O)_4$, ab8213

II.1.4 Compound 5, Mn_{13}-2-Ph, $Mn_{13}O_{14}(O_2CPh_2)_{12}$, ab22515

Table II.1.5.1 Crystal data and structure refinement for ab22515.

Identification code	ab22515
Empirical formula	$C_{157}H_{0.25}Mn_{13}O_{38}$
Formula weight	3208.04
Temperature/K	100.01
Crystal system	monoclinic
Space group	$P2_1/c$
a/Å	26.087(2)
b/Å	17.3638(15)
c/Å	33.476(3)
α/°	90
β/°	111.604(3)
γ/°	90
Volume/Å^3	14098(2)
Z	4
ρ_{calc}g/cm^3	1.511
μ/mm^{-1}	1.200
F(000)	6285.0
Crystal size/mm^3	0.399 × 0.307 × 0.122
Radiation	MoKα (λ = 0.71073)
2Θ range for data collection/°	2.536 to 53.028
Index ranges	$-29 \le h \le 32$, $-21 \le k \le 21$, $-41 \le l \le 41$
Reflections collected	143201
Independent reflections	29136 [R_{int} = 0.0854, R_{sigma} = 0.0939]
Data/restraints/parameters	29136/0/1867
Goodness-of-fit on F^2	1.050
Final R indexes [I>=2σ (I)]	R_1 = 0.0936, wR_2 = 0.2760
Final R indexes [all data]	R_1 = 0.1534, wR_2 = 0.3254
Largest diff. peak/hole / e Å^{-3}	6.79/-0.99

Table II.1.5.2 Fractional Atomic Coordinates (×10^4) and Equivalent Isotropic Displacement Parameters (Å^2×10^3) for ab22515. U_{eq} is defined as 1/3 of of the trace of the orthogonalised U_{IJ} tensor.

Atom	*x*	*y*	*z*	U(eq)
Mn1	173.0(4)	6728.5(7)	4958.0(3)	26.5(3)
Mn2	0	5000	5000	22.8(3)
Mn3	643.0(4)	5677.8(7)	4493.3(3)	26.2(3)
Mn4	-715.0(4)	6149.7(7)	5352.3(3)	28.1(3)
Mn5	-980.7(4)	6007.2(7)	4329.2(3)	27.5(3)
Mn6	408.3(4)	5345.7(7)	6016.7(3)	27.3(3)
Mn7	1123.3(4)	5754.1(7)	5436.5(3)	27.9(3)
O1	-91.0(18)	5607(3)	4506.0(14)	24.2(11)

O2	614(2)	7445(3)	5486.1(17)	35.0(13)
O3	-1567(2)	6248(4)	5088.9(17)	36.1(13)
O4	-405(2)	6927(3)	5859.0(17)	33.1(12)
O5	-1719(2)	6296(4)	4386.7(17)	38.0(14)
O6	-597(2)	6865(3)	4853.8(15)	28.6(12)
O7	1824(2)	5556(4)	5270.1(17)	35.5(13)
O8	478(2)	4763(3)	4143.5(15)	27.6(11)
O9	1400(2)	5586(3)	4557.3(16)	31.1(12)
O10	170.9(19)	5905(3)	5344.6(14)	25.2(11)
O11	103(2)	7400(3)	4483.4(16)	29.6(12)
O12	845.6(19)	6385(3)	4947.9(15)	27.4(11)
O13	756.6(19)	4863(3)	5093.8(15)	26.1(11)
O14	412(2)	6441(3)	6261.9(16)	32.7(12)
O15	402(2)	6620(3)	4072.7(15)	29.5(12)
O16	-1216(2)	4854(3)	4064.5(15)	30.2(12)
O17	1343(2)	6667(3)	5787.3(16)	30.9(12)
O18	-976(2)	6440(3)	3749.6(15)	29.8(12)
O19	672(2)	4560(3)	6519.1(15)	31.1(12)
C1	-246(3)	8483(5)	3789(2)	36.1(19)
C2	1900(6)	9158(10)	6574(5)	102(5)
C3	-1871(3)	6320(5)	4699(3)	35.7(19)
C4	1444(6)	9269(8)	6238(5)	89(4)
C5	-1004(3)	8241(5)	4075(3)	39(2)
C6	-1282(4)	8431(6)	4340(3)	45(2)
C7	-526(3)	8646(5)	4102(3)	33.5(18)
C8	87(3)	7859(5)	3813(2)	29.8(17)
C9	1084(3)	7290(5)	5755(2)	35.1(19)
C10	342(4)	7763(5)	3513(3)	37.1(19)
C11	-49(5)	8321(6)	6279(3)	54(3)
C12	2354(3)	5378(6)	4835(3)	47(2)
C13	1159(4)	6747(7)	7419(3)	60(3)
C14	2828(4)	5507(7)	5172(3)	56(3)
C15	-1106(5)	7313(6)	2294(3)	58(3)
C16	465(4)	7605(5)	6903(3)	40(2)
C17	1373(3)	7920(6)	6061(3)	46(2)
C18	1805(4)	6477(7)	6717(3)	56(3)
C19	577(4)	8284(6)	7130(3)	52(2)
C20	-1102(4)	9007(7)	4637(3)	56(3)
C21	207(3)	7247(5)	4142(2)	25.5(16)
C22	67(6)	9005(7)	6503(4)	77(4)
C23	-2151(4)	6487(8)	3123(3)	57(3)
C24	-1880(4)	7124(7)	3045(3)	53(3)
C25	2043(4)	5765(8)	6877(3)	63(3)
C26	251(5)	8295(6)	3185(3)	52(3)
C27	-2689(3)	6921(6)	4844(3)	49(2)

C28	-98(4)	8897(6)	3155(3)	50(2)
C29	3355(5)	5130(8)	4766(4)	75(4)
C30	1638(4)	4203(6)	3970(4)	56(3)
C31	255(4)	6270(5)	7092(3)	46(2)
C32	2847(4)	6100(8)	6740(4)	66(3)
C33	-2436(6)	7380(8)	5595(5)	84(4)
C34	-1911(4)	7844(6)	5190(4)	58(3)
C35	43(3)	6946(5)	6171(2)	31.5(18)
C36	405(5)	5590(6)	7308(3)	57(3)
C37	-1675(6)	8247(8)	5911(5)	91(5)
C38	1235(5)	4048(7)	3594(3)	63(3)
C39	2109(5)	8430(8)	6673(4)	77(4)
C40	-2554(4)	6567(9)	3289(3)	67(3)
C41	-624(4)	9414(7)	4662(4)	64(3)
C42	-3602(4)	6583(8)	4371(5)	73(4)
C43	1172(4)	8650(7)	5965(4)	62(3)
C44	3337(4)	5384(8)	5142(4)	71(4)
C45	2619(4)	6818(8)	6588(3)	68(3)
C46	-2831(3)	6093(7)	4237(3)	56(3)
C47	-3403(4)	6149(8)	4114(4)	75(4)
C48	1683(5)	5470(9)	3742(4)	80(4)
C49	1261(7)	5321(10)	3361(4)	109(6)
C50	1822(3)	5516(5)	4899(3)	35.9(19)
C51	-3259(5)	6951(8)	4718(4)	71(4)
C52	-1588(6)	8260(8)	5530(6)	86(4)
C53	924(5)	5484(7)	7578(3)	59(3)
C54	-2670(5)	7275(10)	3399(4)	76(4)
C55	-2482(3)	6459(6)	4593(3)	40(2)
C56	-869(3)	6107(5)	3458(2)	29.2(17)
C57	-974(3)	6528(5)	3037(2)	32.8(18)
C58	639(4)	6856(6)	7140(2)	41(2)
C59	1881(4)	4927(6)	4047(3)	50(2)
C60	2370(4)	5091(6)	4448(3)	49(2)
C61	147(3)	7630(5)	6462(3)	37.8(19)
C62	-608(4)	6425(6)	2840(3)	44(2)
C63	2099(4)	7011(7)	6573(3)	57(3)
C64	-340(4)	9004(5)	3458(3)	46(2)
C65	-1434(4)	7040(5)	2858(3)	42(2)
C66	-2343(5)	7375(6)	5208(4)	63(3)
C67	1856(4)	7794(7)	6425(3)	56(3)
C68	1309(5)	6034(7)	7642(3)	63(3)
C69	-1486(5)	7410(6)	2485(3)	57(3)
C70	-2019(5)	7833(7)	3136(3)	66(3)
C71	-674(5)	6834(6)	2461(3)	56(3)
C72	2563(4)	5593(8)	6881(3)	66(3)

C73	-347(4)	9240(7)	4407(4)	59(3)
C74	2876(4)	4945(7)	4423(4)	63(3)
C75	1039(6)	4580(9)	3272(4)	89(5)
C76	-2423(5)	7910(9)	3321(3)	72(4)
C77	383(5)	8970(7)	6934(4)	70(3)
C78	-2086(7)	7819(8)	5945(5)	97(5)
Mn8	3869.1(5)	10651.0(9)	4466.8(4)	38.3(3)
Mn9	5000	10000	5000	36.7(4)
Mn10	4096.6(5)	10232.7(9)	5369.1(4)	39.6(3)
Mn11	4628.3(5)	11580.5(9)	5157.3(4)	39.6(3)
Mn12	4063.6(5)	8836.9(9)	4403.0(4)	39.7(3)
Mn13	5364.7(5)	11467.5(9)	4572.4(4)	39.4(3)
Mn14	5330.3(5)	9939.2(9)	6023.0(4)	40.8(4)
O20	3248(2)	9896(4)	5054.9(18)	42.1(15)
O21	4465(2)	9475(4)	5790.3(18)	41.2(15)
O22	3137(2)	10321(4)	4389.1(17)	39.7(14)
O23	4532(2)	11970(4)	5724.7(19)	46.6(16)
O24	6148(2)	11933(4)	4761.3(19)	46.6(16)
O25	4115(2)	10898(4)	5839.9(18)	44.9(16)
O26	3704(2)	11773(4)	4187.8(19)	44.5(15)
O27	4028(3)	8353(4)	3827.5(19)	49.6(17)
O28	3404(2)	8396(4)	4549.9(18)	42.5(15)
O29	5475(2)	10895(4)	6430.7(18)	45.4(16)
O30	4295(2)	9623(4)	4959.3(17)	38.1(14)
O31	4649(2)	10771(4)	4589.8(17)	40.3(14)
O32	3943(2)	11076(4)	4996.9(17)	38.9(14)
O33	5007(2)	10676(4)	5449.8(17)	39.4(14)
O34	3863(2)	9937(4)	4029.3(18)	40.7(15)
O35	4846(2)	12048(4)	4029.2(18)	43.1(15)
O36	4271(2)	12403(4)	4768.7(18)	41.8(15)
O37	5334(2)	11948(4)	5180.7(18)	40.7(14)
O38	5546(2)	8961(4)	6395.9(19)	47.0(16)
C79	5989(8)	13870(20)	3773(5)	168(14)
C80	6163(13)	13299(13)	7086(8)	220(16)
C81	4316(3)	11581(7)	5932(3)	48(3)
C82	2281(3)	9828(6)	3698(3)	41(2)
C83	5912(6)	13129(16)	3662(5)	131(9)
C84	2441(3)	7574(6)	4625(3)	44(2)
C85	5771(4)	11469(6)	6445(3)	43(2)
C86	2895(3)	7876(6)	4959(3)	41(2)
C87	2057(3)	9732(5)	4053(3)	40(2)
C88	1964(4)	7415(6)	4712(3)	53(3)
C89	4179(4)	12289(6)	3332(3)	47(2)
C90	4288(4)	11935(7)	6333(3)	58(3)
C91	4526(3)	11756(6)	3683(3)	42(2)

C92	3978(6)	11685(10)	6551(4)	102(6)
C93	2844(4)	6972(7)	4131(3)	58(3)
C94	5975(7)	12390(11)	7529(5)	109(6)
C95	3301(4)	13170(7)	3793(3)	55(3)
C96	2783(4)	9345(6)	3277(3)	45(2)
C97	2130(4)	10459(6)	3422(3)	47(2)
C98	1492(4)	9563(6)	3923(3)	46(2)
C99	5134(4)	13635(7)	4644(4)	58(3)
C100	3154(4)	13846(7)	3554(3)	57(3)
C101	2867(4)	8001(7)	5360(3)	52(3)
C102	4642(4)	13795(6)	4676(3)	54(3)
C103	1572(4)	9439(6)	4656(3)	49(2)
C104	1944(4)	7554(7)	5109(4)	62(3)
C105	4348(4)	12987(7)	3242(3)	55(3)
C106	6104(10)	13132(13)	7454(7)	162(11)
C107	4925(4)	13304(9)	3443(3)	68(4)
C108	4337(6)	12593(10)	7096(4)	87(5)
C109	5762(5)	11026(8)	7334(3)	65(3)
C110	2645(4)	9984(7)	3011(3)	51(3)
C111	5368(4)	12805(12)	3484(4)	102(6)
C112	5625(4)	13631(7)	5019(4)	60(3)
C113	1974(4)	7592(6)	3835(3)	51(2)
C114	3962(5)	13443(8)	2932(3)	65(3)
C115	3980(5)	14434(7)	4048(4)	62(3)
C116	4631(5)	12566(7)	6504(4)	72(3)
C117	2391(4)	7863(7)	5437(3)	63(3)
C118	2357(7)	7039(9)	3361(4)	85(4)
C119	3924(3)	12369(6)	4378(3)	38(2)
C120	3492(6)	11215(11)	6351(5)	99(5)
C121	4617(5)	13950(7)	5087(3)	63(3)
C122	6071(7)	10400(11)	7297(4)	101(6)
C123	4672(8)	12890(9)	6885(4)	104(5)
C124	4018(6)	11994(13)	6937(4)	117(7)
C125	5914(6)	12003(8)	6826(4)	72(4)
C126	1942(5)	7431(7)	3426(4)	67(3)
C127	5025(6)	14057(10)	3566(4)	92(5)
C128	2815(6)	6794(9)	3713(4)	83(4)
C129	3432(6)	10520(13)	6562(8)	171(12)
C130	5949(13)	9702(13)	7415(6)	192(14)
C131	6048(10)	12745(10)	6760(7)	159(10)
C132	5363(9)	10922(10)	7507(6)	135(8)
C133	2607(3)	9255(6)	3618(3)	39(2)
C134	3087(6)	11278(10)	5932(5)	89(4)
C135	2590(7)	10162(11)	6031(6)	112(6)
C136	2658(5)	10764(10)	5776(5)	88(4)

C137	5560(20)	9610(14)	7606(11)	310(30)
C138	3096(14)	9850(30)	6399(8)	450(40)
C139	5320(20)	10211(15)	7669(12)	330(30)
C140	5535(7)	14386(13)	3720(5)	123(8)
C141	3421(3)	8133(6)	4905(3)	40(2)
C142	2370(3)	9773(6)	4483(3)	41(2)
C143	2967(3)	10017(6)	4666(3)	41(2)
C144	3777(4)	13119(6)	4158(3)	43(2)
C145	2316(4)	10533(7)	3080(3)	56(3)
C146	4118(4)	13783(6)	4293(3)	51(2)
C147	3442(4)	13205(8)	2718(3)	57(3)
C148	2119(4)	9614(6)	4782(3)	44(2)
C149	2428(4)	7385(6)	4186(3)	45(2)
C150	1255(4)	9431(6)	4219(3)	51(2)
C151	5081(5)	13931(8)	5440(4)	71(4)
C152	3487(5)	14472(8)	3675(4)	71(3)
C153	3277(4)	12513(7)	2792(3)	55(3)
C154	3637(4)	12052(7)	3100(3)	52(3)
C155	5870(5)	11821(8)	7217(3)	68(3)
C156	5605(4)	13755(7)	5419(4)	65(3)

Table II.1.5.3 Anisotropic Displacement Parameters ($Å^2×10^3$) for ab22515. The Anisotropic displacement factor exponent takes the form: $-2\pi^2[h^2a^{*2}U_{11}+2hka^*b^*U_{12}+\ldots]$.

Atom	U_{11}	U_{22}	U_{33}	U_{23}	U_{13}	U_{12}
Mn1	23.6(5)	37.6(7)	19.3(5)	2.6(5)	9.3(4)	4.0(5)
Mn2	17.5(7)	37.0(10)	14.4(7)	3.6(7)	6.4(6)	4.8(6)
Mn3	22.8(5)	38.0(7)	19.8(5)	2.9(5)	10.3(4)	3.0(5)
Mn4	25.3(6)	40.8(7)	19.8(5)	3.1(5)	10.3(4)	7.6(5)
Mn5	21.7(5)	42.4(8)	18.0(5)	3.9(5)	6.7(4)	8.4(5)
Mn6	24.1(5)	40.0(7)	18.0(5)	2.1(5)	8.2(4)	6.6(5)
Mn7	20.5(5)	42.8(8)	19.8(5)	3.1(5)	6.7(4)	1.3(5)
O1	19(2)	38(3)	16(2)	3(2)	5.5(19)	2(2)
O2	32(3)	46(4)	28(3)	-4(3)	11(2)	-5(3)
O3	34(3)	50(4)	29(3)	10(3)	17(2)	15(3)
O4	31(3)	39(3)	28(3)	1(2)	9(2)	5(2)
O5	26(3)	62(4)	29(3)	9(3)	12(2)	17(3)
O6	26(3)	40(3)	22(2)	3(2)	11(2)	4(2)
O7	23(3)	52(4)	31(3)	8(3)	9(2)	6(2)
O8	24(3)	37(3)	21(2)	-1(2)	8(2)	2(2)
O9	29(3)	44(3)	24(3)	3(2)	14(2)	5(2)
O10	25(2)	36(3)	15(2)	1(2)	7(2)	2(2)
O11	33(3)	34(3)	24(3)	-1(2)	12(2)	1(2)
O12	22(2)	37(3)	24(3)	3(2)	10(2)	4(2)
O13	19(2)	37(3)	21(2)	5(2)	7(2)	6(2)

O14	31(3)	44(4)	23(3)	-1(2)	9(2)	4(3)
O15	29(3)	40(3)	20(2)	4(2)	10(2)	4(2)
O16	26(3)	45(4)	21(3)	3(2)	10(2)	1(2)
O17	24(3)	43(4)	25(3)	2(2)	8(2)	-2(2)
O18	33(3)	39(3)	16(2)	0(2)	7(2)	4(2)
O19	34(3)	38(3)	18(3)	2(2)	7(2)	3(2)
C1	40(4)	42(5)	24(4)	3(4)	9(3)	-7(4)
C2	68(9)	110(13)	110(12)	-64(11)	12(8)	-30(9)
C3	29(4)	42(5)	39(5)	11(4)	16(4)	12(4)
C4	76(9)	56(8)	111(11)	-28(8)	6(8)	0(7)
C5	40(5)	34(5)	35(4)	-2(4)	6(4)	2(4)
C6	32(4)	51(6)	48(5)	3(5)	11(4)	-1(4)
C7	36(4)	34(5)	29(4)	0(4)	11(3)	-1(4)
C8	32(4)	32(5)	24(4)	-1(3)	9(3)	-3(3)
C9	30(4)	51(6)	28(4)	2(4)	15(3)	-7(4)
C10	55(5)	33(5)	29(4)	-1(4)	24(4)	3(4)
C11	71(7)	37(6)	46(5)	8(5)	14(5)	6(5)
C12	30(4)	72(7)	39(5)	22(5)	13(4)	11(4)
C13	52(6)	79(8)	47(6)	-8(6)	16(5)	11(6)
C14	34(5)	88(8)	48(6)	18(6)	18(4)	5(5)
C15	89(8)	50(7)	35(5)	13(5)	22(5)	-11(6)
C16	41(5)	45(6)	38(5)	-10(4)	19(4)	0(4)
C17	32(4)	66(7)	41(5)	-12(5)	13(4)	-6(4)
C18	41(5)	90(9)	34(5)	-3(5)	10(4)	-6(5)
C19	49(5)	55(7)	46(5)	-5(5)	10(4)	5(5)
C20	52(6)	71(8)	53(6)	-16(5)	28(5)	5(5)
C21	21(3)	39(5)	15(3)	-1(3)	6(3)	-7(3)
C22	104(10)	40(7)	74(8)	0(6)	18(8)	11(6)
C23	37(5)	88(9)	37(5)	19(5)	5(4)	3(5)
C24	51(6)	63(7)	27(4)	-5(5)	-5(4)	20(5)
C25	39(5)	114(11)	30(5)	0(6)	5(4)	-14(6)
C26	84(7)	45(6)	46(5)	5(5)	46(5)	1(5)
C27	28(4)	62(7)	65(6)	17(5)	27(4)	10(4)
C28	79(7)	39(6)	39(5)	12(4)	28(5)	6(5)
C29	53(7)	119(11)	66(7)	18(7)	38(6)	23(7)
C30	64(7)	54(7)	60(7)	-11(5)	36(6)	0(5)
C31	73(6)	36(5)	35(5)	-2(4)	27(5)	2(5)
C32	40(5)	94(9)	66(7)	18(7)	20(5)	2(6)
C33	103(10)	77(9)	103(10)	-22(8)	75(9)	-8(8)
C34	49(6)	50(7)	84(8)	2(6)	36(6)	6(5)
C35	37(4)	37(5)	25(4)	0(3)	16(3)	-2(4)
C36	87(8)	54(7)	38(5)	-6(5)	31(6)	0(6)
C37	97(10)	72(9)	128(13)	-32(9)	71(10)	-10(8)
C38	79(8)	76(8)	44(6)	-6(6)	36(6)	-7(6)
C39	52(7)	83(10)	69(8)	-31(7)	-8(6)	-3(6)

C40	48(6)	105(11)	45(6)	4(6)	12(5)	5(6)
C41	48(6)	81(8)	65(7)	-39(6)	24(5)	-17(6)
C42	22(5)	93(10)	104(10)	31(8)	22(6)	11(5)
C43	49(6)	65(8)	70(7)	-20(6)	17(5)	-11(5)
C44	27(5)	120(11)	63(7)	29(7)	15(5)	-1(6)
C45	34(5)	109(10)	53(6)	23(7)	8(5)	3(6)
C46	24(4)	88(8)	49(6)	20(6)	6(4)	11(5)
C47	27(5)	104(10)	88(9)	34(8)	13(5)	3(6)
C48	75(8)	92(10)	57(7)	17(7)	5(6)	-27(7)
C49	130(13)	116(13)	54(8)	15(8)	2(8)	-65(11)
C50	32(4)	43(5)	36(5)	15(4)	17(4)	4(4)
C51	47(6)	85(9)	105(10)	26(8)	54(7)	22(6)
C52	73(8)	58(8)	145(14)	13(9)	61(10)	15(7)
C53	76(8)	56(7)	46(6)	-6(5)	21(6)	0(6)
C54	67(8)	109(12)	52(7)	7(7)	20(6)	1(8)
C55	25(4)	59(6)	38(5)	24(4)	13(4)	15(4)
C56	27(4)	35(5)	21(4)	-1(3)	5(3)	-5(3)
C57	41(4)	37(5)	18(4)	-7(3)	7(3)	-6(4)
C58	50(5)	56(6)	19(4)	-6(4)	13(4)	12(4)
C59	41(5)	64(7)	53(6)	-2(5)	28(5)	1(5)
C60	38(5)	51(6)	65(6)	2(5)	30(5)	-4(4)
C61	38(4)	38(5)	40(5)	-2(4)	18(4)	-2(4)
C62	60(6)	44(6)	32(4)	-6(4)	24(4)	-13(4)
C63	45(5)	88(9)	30(5)	-13(5)	4(4)	-12(5)
C64	69(6)	35(5)	35(5)	3(4)	18(4)	4(4)
C65	56(5)	37(5)	23(4)	3(4)	3(4)	-11(4)
C66	64(7)	54(7)	97(9)	18(6)	61(7)	19(5)
C67	42(5)	74(8)	45(6)	-11(5)	9(4)	-2(5)
C68	76(8)	81(9)	25(5)	5(5)	11(5)	26(7)
C69	80(7)	46(6)	38(5)	11(5)	14(5)	-2(5)
C70	72(7)	73(8)	36(5)	0(5)	-2(5)	21(6)
C71	76(7)	61(7)	39(5)	-5(5)	32(5)	-16(6)
C72	51(6)	105(10)	39(5)	4(6)	14(5)	-5(6)
C73	46(6)	71(8)	68(7)	-24(6)	29(5)	-7(5)
C74	53(6)	72(8)	77(8)	7(6)	39(6)	10(6)
C75	93(10)	121(12)	46(7)	-6(7)	18(6)	-48(9)
C76	63(7)	101(11)	42(6)	-6(6)	7(5)	36(7)
C77	88(9)	37(6)	80(8)	-18(6)	27(7)	-16(6)
C78	138(13)	77(10)	122(12)	-29(9)	103(12)	3(9)
Mn8	26.9(6)	60.6(9)	29.2(6)	-8.3(6)	12.3(5)	-6.8(6)
Mn9	25.5(8)	60.4(13)	26.4(9)	-8.4(8)	12.0(7)	-6.1(8)
Mn10	29.2(6)	62.9(10)	29.9(7)	-6.8(6)	14.7(5)	-4.9(6)
Mn11	29.1(6)	60.2(9)	31.1(7)	-9.2(6)	13.0(5)	-5.4(6)
Mn12	30.2(6)	62.2(10)	27.7(6)	-7.2(6)	12.0(5)	-9.7(6)
Mn13	27.7(6)	63.2(10)	28.0(6)	-7.3(6)	11.1(5)	-7.7(6)

Mn14	29.8(6)	65.5(10)	28.0(6)	-8.0(6)	11.7(5)	-8.7(6)
O20	26(3)	72(5)	30(3)	-7(3)	12(2)	-7(3)
O21	31(3)	63(4)	32(3)	-8(3)	16(2)	-5(3)
O22	28(3)	62(4)	31(3)	-4(3)	13(2)	-4(3)
O23	39(3)	70(5)	35(3)	-13(3)	18(3)	-1(3)
O24	31(3)	70(5)	37(3)	-4(3)	11(3)	-13(3)
O25	42(3)	65(5)	33(3)	-12(3)	20(3)	-3(3)
O26	35(3)	62(4)	39(3)	-6(3)	16(3)	-4(3)
O27	43(3)	71(5)	36(3)	-12(3)	15(3)	-10(3)
O28	34(3)	64(4)	31(3)	0(3)	14(3)	-9(3)
O29	41(3)	65(5)	32(3)	-6(3)	15(3)	-2(3)
O30	31(3)	61(4)	26(3)	-7(3)	14(2)	-7(3)
O31	28(3)	65(4)	30(3)	-6(3)	13(2)	-7(3)
O32	28(3)	60(4)	31(3)	-4(3)	14(2)	-6(3)
O33	30(3)	64(4)	25(3)	-11(3)	12(2)	-5(3)
O34	28(3)	64(4)	31(3)	-16(3)	12(2)	-7(3)
O35	32(3)	67(4)	29(3)	-5(3)	10(2)	0(3)
O36	33(3)	64(4)	30(3)	-7(3)	14(2)	-6(3)
O37	27(3)	62(4)	33(3)	-10(3)	11(2)	-7(3)
O38	40(3)	68(5)	32(3)	-1(3)	12(3)	-2(3)
C79	78(12)	370(40)	43(8)	-7(14)	12(8)	-130(20)
C80	400(40)	150(20)	230(30)	-132(19)	250(30)	-160(20)
C81	26(4)	82(8)	33(5)	-19(5)	9(4)	-2(5)
C82	30(4)	56(6)	33(4)	-4(4)	5(3)	-4(4)
C83	41(7)	290(30)	51(8)	48(13)	10(6)	-34(12)
C84	35(4)	48(6)	49(5)	7(4)	14(4)	-9(4)
C85	44(5)	54(6)	33(5)	-7(4)	18(4)	-4(4)
C86	29(4)	52(6)	41(5)	4(4)	10(4)	0(4)
C87	35(4)	45(6)	38(5)	-7(4)	13(4)	-3(4)
C88	31(5)	61(7)	59(6)	12(5)	8(4)	-11(4)
C89	36(5)	75(7)	26(4)	-6(5)	9(4)	0(5)
C90	35(5)	93(9)	46(6)	-22(6)	15(4)	4(5)
C91	34(4)	62(7)	35(5)	2(5)	18(4)	0(4)
C92	93(9)	175(16)	58(7)	-62(9)	51(7)	-81(10)
C93	41(5)	78(8)	51(6)	-10(6)	10(5)	-12(5)
C94	136(14)	140(15)	82(10)	-62(10)	77(10)	-50(12)
C95	46(5)	82(8)	40(5)	-8(5)	21(4)	1(5)
C96	34(4)	61(7)	39(5)	-12(5)	11(4)	-11(4)
C97	42(5)	51(6)	47(5)	-2(5)	18(4)	1(4)
C98	38(5)	57(6)	45(5)	-6(5)	16(4)	-5(4)
C99	48(6)	69(8)	66(7)	-4(6)	31(5)	-14(5)
C100	55(6)	63(7)	51(6)	5(6)	17(5)	3(5)
C101	35(5)	82(8)	43(5)	-5(5)	18(4)	-7(5)
C102	45(5)	64(7)	50(6)	-13(5)	14(5)	-17(5)
C103	42(5)	61(7)	49(6)	-8(5)	22(4)	-6(5)

C104	45(6)	84(9)	62(7)	20(6)	26(5)	-12(5)
C105	48(5)	81(8)	31(5)	1(5)	10(4)	-3(5)
C106	250(30)	146(18)	170(19)	-111(16)	160(20)	-102(18)
C107	49(6)	116(11)	36(5)	11(6)	11(5)	-32(7)
C108	92(10)	129(13)	51(7)	-15(8)	39(7)	34(9)
C109	77(7)	92(9)	29(5)	-5(5)	23(5)	21(7)
C110	43(5)	81(8)	32(5)	-6(5)	15(4)	-4(5)
C111	36(6)	226(19)	43(6)	34(9)	13(5)	-9(8)
C112	48(6)	63(7)	66(7)	-4(6)	19(5)	-7(5)
C113	47(5)	53(6)	45(5)	4(5)	6(4)	-15(5)
C114	67(7)	75(8)	50(6)	5(6)	17(6)	-8(6)
C115	61(7)	64(8)	66(7)	-3(6)	29(6)	-11(6)
C116	95(9)	71(8)	56(7)	-12(6)	36(7)	7(7)
C117	55(6)	100(9)	45(6)	7(6)	30(5)	-16(6)
C118	113(12)	88(10)	45(7)	-9(7)	18(7)	-41(9)
C119	31(4)	54(6)	34(4)	-9(4)	17(4)	-5(4)
C120	80(9)	160(16)	70(9)	30(10)	43(8)	51(10)
C121	56(6)	84(9)	56(6)	-17(6)	29(5)	-11(6)
C122	121(12)	131(14)	45(7)	5(8)	25(7)	69(11)
C123	174(17)	85(11)	63(8)	-16(8)	55(10)	8(11)
C124	71(9)	240(20)	52(8)	-50(11)	36(7)	-41(12)
C125	102(9)	77(9)	54(7)	-29(6)	48(7)	-26(7)
C126	77(8)	52(7)	54(7)	6(6)	4(6)	-18(6)
C127	86(9)	137(14)	52(7)	-11(8)	25(7)	-60(10)
C128	84(9)	97(11)	57(7)	-22(7)	15(7)	-22(8)
C129	59(9)	200(20)	210(20)	150(20)	2(11)	-12(11)
C130	400(40)	125(18)	90(13)	42(12)	140(20)	120(20)
C131	290(30)	98(13)	175(19)	-77(13)	190(20)	-84(16)
C132	230(20)	81(11)	182(18)	5(12)	181(18)	14(12)
C133	34(4)	50(6)	32(4)	-9(4)	10(4)	-6(4)
C134	67(8)	125(13)	82(9)	3(9)	36(7)	5(8)
C135	101(12)	141(16)	113(13)	13(12)	62(11)	-17(11)
C136	59(8)	119(13)	89(10)	-10(9)	31(7)	-4(8)
C137	740(80)	94(17)	320(40)	40(20)	450(50)	40(30)
C138	350(40)	660(70)	140(20)	240(30)	-150(20)	-400(50)
C139	740(80)	100(18)	400(50)	0(20)	520(60)	0(30)
C140	95(12)	200(20)	64(9)	-7(11)	22(8)	-93(14)
C141	31(4)	58(6)	31(4)	-4(4)	12(4)	-11(4)
C142	22(4)	61(6)	39(5)	-1(4)	10(3)	1(4)
C143	27(4)	59(6)	39(5)	-9(4)	17(4)	-6(4)
C144	44(5)	50(6)	40(5)	-7(4)	22(4)	-1(4)
C145	59(6)	61(7)	46(6)	4(5)	17(5)	5(5)
C146	46(5)	60(7)	51(6)	8(5)	25(5)	3(5)
C147	46(6)	84(9)	37(5)	-1(5)	9(4)	12(6)
C148	38(5)	57(6)	40(5)	-3(4)	18(4)	-5(4)

C149	37(5)	45(6)	50(5)	-4(5)	12(4)	-15(4)
C150	33(5)	60(7)	60(6)	-2(5)	18(4)	-10(4)
C151	54(6)	109(11)	52(6)	-24(7)	21(5)	-15(6)
C152	81(8)	72(9)	63(7)	1(6)	32(7)	0(7)
C153	41(5)	79(8)	42(5)	-11(5)	10(4)	11(5)
C154	43(5)	80(8)	33(5)	-5(5)	12(4)	5(5)
C155	64(7)	101(10)	47(6)	-25(6)	29(5)	-12(6)
C156	45(6)	76(8)	70(7)	-17(6)	17(5)	-4(5)

Table II.1.5.4 Bond Lengths for ab22515.

Atom	Atom	Length/Å	Atom	Atom	Length/Å
Mn1	O1	2.406(5)	Mn8	O26	2.134(7)
Mn1	O2	2.121(6)	Mn8	O30	2.405(6)
Mn1	O6	1.924(5)	Mn8	O31	1.932(5)
Mn1	O10	1.930(5)	Mn8	O32	1.865(6)
Mn1	O11	1.925(5)	Mn8	O34	1.915(6)
Mn1	O12	1.865(5)	Mn9	O30	1.909(5)
Mn2	O1	1.901(5)	Mn9	$O30^{2}$	1.909(5)
Mn2	$O1^{1}$	1.901(5)	Mn9	O31	1.895(6)
Mn2	O10	1.903(5)	Mn9	$O31^{2}$	1.895(6)
Mn2	$O10^{1}$	1.903(5)	Mn9	$O33^{2}$	1.904(5)
Mn2	O13	1.896(5)	Mn9	O33	1.904(5)
Mn2	$O13^{1}$	1.896(5)	Mn10	O20	2.153(5)
Mn3	O1	1.935(5)	Mn10	O21	1.909(6)
Mn3	O8	1.925(5)	Mn10	O25	1.940(6)
Mn3	O9	1.912(5)	Mn10	O30	1.947(6)
Mn3	O12	1.874(5)	Mn10	O32	1.868(6)
Mn3	O13	2.386(5)	Mn10	O33	2.416(6)
Mn3	O15	2.098(5)	Mn11	O23	2.116(6)
Mn4	O3	2.074(5)	Mn11	O31	2.380(6)
Mn4	O4	2.084(6)	Mn11	O32	1.882(6)
Mn4	O6	2.191(5)	Mn11	O33	1.921(7)
Mn4	$O8^{1}$	2.231(5)	Mn11	O36	1.925(7)
Mn4	O10	2.359(5)	Mn11	O37	1.923(5)
Mn4	$O13^{1}$	2.283(5)	Mn12	O27	2.073(6)
Mn5	O1	2.282(5)	Mn12	O28	2.101(6)
Mn5	O5	2.067(5)	Mn12	O30	2.207(6)
Mn5	O6	2.238(5)	Mn12	$O33^{2}$	2.440(6)
Mn5	$O13^{1}$	2.350(5)	Mn12	O34	2.237(7)
Mn5	O16	2.185(6)	Mn12	$O37^{2}$	2.158(6)
Mn5	O18	2.085(5)	Mn13	$O21^{2}$	2.179(6)
Mn6	$O1^{1}$	2.328(5)	Mn13	O24	2.067(6)
Mn6	$O8^{1}$	2.181(5)	Mn13	$O30^{2}$	2.410(6)

Mn6	O10	2.316(5)	Mn13	O31	2.244(6)
Mn6	O14	2.069(6)	Mn13	O35	2.084(6)
Mn6	O16[1]	2.247(5)	Mn13	O37	2.229(6)
Mn6	O19	2.077(5)	Mn14	O21	2.248(6)
Mn7	O7	2.125(5)	Mn14	O29	2.092(7)
Mn7	O10	2.403(5)	Mn14	O31[2]	2.411(6)
Mn7	O12	1.878(5)	Mn14	O33	2.200(6)
Mn7	O13	1.954(5)	Mn14	O34[2]	2.185(5)
Mn7	O16[1]	1.915(5)	Mn14	O38	2.060(7)
Mn7	O17	1.930(6)	O20	C143	1.254(10)
O1	Mn6[1]	2.328(5)	O21	Mn13[2]	2.179(6)
O2	C9	1.253(10)	O22	C143	1.281(10)
O3	C3	1.259(10)	O23	C81	1.243(12)
O4	C35	1.250(9)	O24	C141[2]	1.267(10)
O5	C3	1.249(9)	O25	C81	1.287(12)
O7	C50	1.243(9)	O26	C119	1.242(11)
O8	Mn4[1]	2.231(5)	O27	C85[2]	1.248(10)
O8	Mn6[1]	2.181(5)	O28	C141	1.257(10)
O9	C50	1.269(10)	O29	C85	1.251(11)
O11	C21	1.295(8)	O30	Mn13[2]	2.410(6)
O13	Mn4[1]	2.283(5)	O31	Mn14[2]	2.411(6)
O13	Mn5[1]	2.350(5)	O33	Mn12[2]	2.440(6)
O14	C35	1.255(10)	O34	Mn14[2]	2.185(5)
O15	C21	1.259(9)	O35	C91	1.258(11)
O16	Mn6[1]	2.247(5)	O36	C119	1.288(10)
O16	Mn7[1]	1.915(5)	O37	Mn12[2]	2.158(6)
O17	C9	1.259(10)	O38	C91[2]	1.271(12)
O18	C56	1.251(9)	C79	C83	1.34(4)
O19	C56[1]	1.257(10)	C79	C140	1.44(3)
C1	C7	1.509(11)	C80	C106	1.33(3)
C1	C8	1.373(12)	C80	C131	1.40(2)
C1	C64	1.381(12)	C81	C90	1.503(13)
C2	C4	1.317(19)	C82	C87	1.510(12)
C2	C39	1.37(2)	C82	C97	1.394(13)
C3	C55	1.519(10)	C82	C133	1.398(13)
C4	C43	1.421(16)	C83	C111	1.44(2)
C5	C6	1.376(12)	C84	C86	1.398(12)
C5	C7	1.404(12)	C84	C88	1.408(12)
C6	C20	1.366(14)	C84	C149	1.493(13)
C7	C73	1.406(13)	C85	O27[2]	1.248(10)
C8	C10	1.404(10)	C85	C125	1.507(14)
C8	C21	1.479(11)	C86	C101	1.389(12)
C9	C17	1.500(13)	C86	C141	1.514(11)
C10	C26	1.386(12)	C87	C98	1.406(12)
C11	C22	1.378(15)	C87	C142	1.371(12)

C11	C61	1.359(13)	C88	C104	1.371(15)
C12	C14	1.350(13)	C89	C91	1.509(13)
C12	C50	1.499(11)	C89	C105	1.362(15)
C12	C60	1.403(13)	C89	C154	1.400(13)
C13	C58	1.347(13)	C90	C92	1.346(15)
C13	C68	1.424(16)	C90	C116	1.396(17)
C14	C44	1.386(13)	C91	O38[2]	1.271(12)
C15	C69	1.375(15)	C92	C120	1.45(2)
C15	C71	1.345(16)	C92	C124	1.368(17)
C16	C19	1.374(13)	C93	C128	1.406(16)
C16	C58	1.505(13)	C93	C149	1.369(14)
C16	C61	1.404(12)	C94	C106	1.38(2)
C17	C43	1.364(15)	C94	C155	1.388(17)
C17	C67	1.411(13)	C95	C100	1.393(15)
C18	C25	1.399(17)	C95	C144	1.387(13)
C18	C63	1.397(15)	C96	C110	1.385(14)
C19	C77	1.365(16)	C96	C133	1.388(12)
C20	C41	1.409(15)	C97	C145	1.407(13)
C22	C77	1.372(17)	C98	C150	1.367(13)
C23	C24	1.388(16)	C99	C102	1.357(14)
C23	C40	1.367(14)	C99	C112	1.428(15)
C24	C65	1.519(14)	C100	C152	1.356(16)
C24	C70	1.348(15)	C101	C117	1.380(12)
C25	C72	1.385(15)	C102	C121	1.427(14)
C26	C28	1.364(14)	C102	C146	1.491(14)
C27	C51	1.390(13)	C103	C148	1.365(12)
C27	C55	1.406(13)	C103	C150	1.388(13)
C27	C66	1.451(16)	C104	C117	1.383(15)
C28	C64	1.390(13)	C105	C107	1.508(14)
C29	C44	1.351(16)	C105	C114	1.396(15)
C29	C74	1.388(17)	C107	C111	1.41(2)
C30	C38	1.334(15)	C107	C127	1.37(2)
C30	C59	1.388(15)	C108	C123	1.41(2)
C31	C36	1.363(14)	C108	C124	1.32(2)
C31	C58	1.395(14)	C109	C122	1.386(17)
C32	C45	1.393(17)	C109	C132	1.377(18)
C32	C72	1.342(16)	C109	C155	1.490(18)
C33	C66	1.405(16)	C110	C145	1.358(14)
C33	C78	1.41(2)	C112	C156	1.377(15)
C34	C52	1.350(18)	C113	C126	1.372(15)
C34	C66	1.410(15)	C113	C149	1.374(13)
C35	C61	1.495(12)	C114	C147	1.345(15)
C36	C53	1.334(16)	C115	C146	1.365(15)
C37	C52	1.38(2)	C115	C152	1.428(16)
C37	C78	1.343(19)	C116	C123	1.360(16)

C38	C75	1.368(18)	C118	C126	1.361(19)
C39	C67	1.395(16)	C118	C128	1.400(19)
C40	C54	1.348(19)	C119	C144	1.475(13)
C41	C73	1.340(14)	C120	C129	1.43(2)
C42	C47	1.380(19)	C120	C134	1.416(19)
C42	C51	1.340(18)	C121	C151	1.344(15)
C45	C63	1.381(14)	C122	C130	1.35(3)
C46	C47	1.397(13)	C125	C131	1.37(2)
C46	C55	1.361(14)	C125	C155	1.393(15)
C48	C49	1.367(17)	C127	C140	1.362(18)
C48	C59	1.346(16)	C129	C138	1.44(4)
C49	C75	1.40(2)	C130	C137	1.40(4)
C53	C68	1.344(16)	C132	C139	1.37(3)
C54	C76	1.351(19)	C134	C136	1.38(2)
C56	O19[1]	1.257(10)	C135	C136	1.40(2)
C56	C57	1.522(11)	C135	C138	1.53(3)
C57	C62	1.355(12)	C137	C139	1.27(3)
C57	C65	1.435(13)	C141	O24[2]	1.267(10)
C59	C60	1.501(14)	C142	C143	1.509(11)
C60	C74	1.376(13)	C142	C148	1.413(12)
C62	C71	1.407(13)	C144	C146	1.425(14)
C63	C67	1.504(16)	C147	C153	1.331(16)
C65	C69	1.367(12)	C151	C156	1.426(15)
C70	C76	1.412(17)	C153	C154	1.368(14)
Mn8	O22	1.917(5)			

[1]-X,1-Y,1-Z; [2]1-X,2-Y,1-Z

Table II.1.5.5 Bond Angles for ab22515.

Atom	Atom	Atom	Angle/°	Atom	Atom	Atom	Angle/°
O2	Mn1	O1	160.2(2)	O22	Mn8	O26	100.5(3)
O6	Mn1	O1	87.0(2)	O22	Mn8	O30	93.3(2)
O6	Mn1	O2	106.8(2)	O22	Mn8	O31	168.2(3)
O6	Mn1	O10	87.3(2)	O26	Mn8	O30	160.9(2)
O6	Mn1	O11	90.0(2)	O31	Mn8	O26	91.3(3)
O10	Mn1	O1	75.60(19)	O31	Mn8	O30	75.5(2)
O10	Mn1	O2	90.6(2)	O32	Mn8	O22	89.8(2)
O11	Mn1	O1	93.04(19)	O32	Mn8	O26	89.3(3)
O11	Mn1	O2	100.9(2)	O32	Mn8	O30	77.4(2)
O11	Mn1	O10	168.4(2)	O32	Mn8	O31	91.3(2)
O12	Mn1	O1	77.5(2)	O32	Mn8	O34	162.4(3)
O12	Mn1	O2	88.7(2)	O34	Mn8	O22	88.6(2)
O12	Mn1	O6	164.4(2)	O34	Mn8	O26	108.2(3)
O12	Mn1	O10	90.6(2)	O34	Mn8	O30	85.2(2)
O12	Mn1	O11	89.0(2)	O34	Mn8	O31	86.8(2)

O1	Mn2	O1[1]	180.0	O30	Mn9	O30[2]	180.0
O1[1]	Mn2	O10	90.3(2)	O31	Mn9	O30	89.6(2)
O1[1]	Mn2	O10[1]	89.7(2)	O31	Mn9	O30[2]	90.4(2)
O1	Mn2	O10[1]	90.3(2)	O31[2]	Mn9	O30	90.4(2)
O1	Mn2	O10	89.7(2)	O31[2]	Mn9	O30[2]	89.6(2)
O10	Mn2	O10[1]	180.0	O31	Mn9	O31[2]	180.0
O13	Mn2	O1	90.2(2)	O31[2]	Mn9	O33	90.1(3)
O13[1]	Mn2	O1	89.8(2)	O31	Mn9	O33	89.9(3)
O13[1]	Mn2	O1[1]	90.2(2)	O31	Mn9	O33[2]	90.1(3)
O13	Mn2	O1[1]	89.8(2)	O31[2]	Mn9	O33[2]	90.0(3)
O13[1]	Mn2	O10	89.6(2)	O33	Mn9	O30[2]	90.2(2)
O13	Mn2	O10	90.4(2)	O33[2]	Mn9	O30[2]	89.8(2)
O13	Mn2	O10[1]	89.6(2)	O33[2]	Mn9	O30	90.2(2)
O13[1]	Mn2	O10[1]	90.4(2)	O33	Mn9	O30	89.8(2)
O13	Mn2	O13[1]	180.0	O33	Mn9	O33[2]	180.0
O1	Mn3	O13	76.17(18)	O20	Mn10	O33	158.9(2)
O1	Mn3	O15	90.6(2)	O21	Mn10	O20	108.7(3)
O8	Mn3	O1	87.7(2)	O21	Mn10	O25	87.4(3)
O8	Mn3	O13	87.3(2)	O21	Mn10	O30	87.4(3)
O8	Mn3	O15	106.9(2)	O21	Mn10	O33	86.0(2)
O9	Mn3	O1	169.0(2)	O25	Mn10	O20	105.8(2)
O9	Mn3	O8	89.4(2)	O25	Mn10	O30	164.2(2)
O9	Mn3	O13	93.07(19)	O25	Mn10	O33	89.4(2)
O9	Mn3	O15	100.5(2)	O30	Mn10	O20	90.0(2)
O12	Mn3	O1	90.5(2)	O30	Mn10	O33	75.3(2)
O12	Mn3	O8	165.4(2)	O32	Mn10	O20	87.6(2)
O12	Mn3	O9	89.6(2)	O32	Mn10	O21	163.5(2)
O12	Mn3	O13	78.1(2)	O32	Mn10	O25	90.6(3)
O12	Mn3	O15	87.7(2)	O32	Mn10	O30	90.2(3)
O15	Mn3	O13	160.32(19)	O32	Mn10	O33	77.6(2)
O3	Mn4	O4	109.1(2)	O23	Mn11	O31	161.8(3)
O3	Mn4	O6	93.3(2)	O32	Mn11	O23	89.5(2)
O3	Mn4	O8[1]	109.6(2)	O32	Mn11	O31	78.2(2)
O3	Mn4	O10	155.60(19)	O32	Mn11	O33	91.2(3)
O3	Mn4	O13[1]	90.0(2)	O32	Mn11	O36	88.8(3)
O4	Mn4	O6	97.5(2)	O32	Mn11	O37	163.8(2)
O4	Mn4	O8[1]	85.9(2)	O33	Mn11	O23	90.7(2)
O4	Mn4	O10	92.16(19)	O33	Mn11	O31	76.4(2)
O4	Mn4	O13[1]	160.38(19)	O33	Mn11	O36	168.8(2)
O6	Mn4	O8[1]	154.40(19)	O33	Mn11	O37	86.9(3)
O6	Mn4	O10	71.42(18)	O36	Mn11	O23	100.5(3)
O6	Mn4	O13[1]	85.69(19)	O36	Mn11	O31	92.7(2)
O8[1]	Mn4	O10	83.14(17)	O37	Mn11	O23	106.6(2)
O8[1]	Mn4	O13[1]	83.16(18)	O37	Mn11	O31	85.8(2)
O13[1]	Mn4	O10	70.44(17)	O37	Mn11	O36	90.0(3)

O1	Mn5	O13[1]	70.72(16)	O27	Mn12	O28	108.0(2)
O5	Mn5	O1	160.62(19)	O27	Mn12	O30	160.1(2)
O5	Mn5	O6	85.9(2)	O27	Mn12	O33[2]	91.7(2)
O5	Mn5	O13[1]	92.15(19)	O27	Mn12	O34	84.6(2)
O5	Mn5	O16	97.4(2)	O27	Mn12	O37[2]	96.7(2)
O5	Mn5	O18	108.9(2)	O28	Mn12	O30	91.2(2)
O6	Mn5	O1	83.18(18)	O28	Mn12	O33[2]	156.6(2)
O6	Mn5	O13[1]	83.03(18)	O28	Mn12	O34	113.6(2)
O16	Mn5	O1	86.15(19)	O28	Mn12	O37[2]	94.8(2)
O16	Mn5	O6	154.96(19)	O30	Mn12	O33[2]	70.88(19)
O16	Mn5	O13[1]	72.06(18)	O30	Mn12	O34	83.0(2)
O18	Mn5	O1	89.86(18)	O34	Mn12	O33[2]	80.0(2)
O18	Mn5	O6	109.7(2)	O37[2]	Mn12	O30	86.4(2)
O18	Mn5	O13[1]	155.76(19)	O37[2]	Mn12	O33[2]	69.8(2)
O18	Mn5	O16	92.9(2)	O37[2]	Mn12	O34	149.9(2)
O8[1]	Mn6	O1[1]	72.66(17)	O21[2]	Mn13	O30[2]	70.7(2)
O8[1]	Mn6	O10	85.26(18)	O21[2]	Mn13	O31	87.2(2)
O8[1]	Mn6	O16[1]	155.88(19)	O21[2]	Mn13	O37	150.8(2)
O10	Mn6	O1[1]	70.97(18)	O24	Mn13	O21[2]	94.8(2)
O14	Mn6	O1[1]	154.12(19)	O24	Mn13	O30[2]	91.3(2)
O14	Mn6	O8[1]	91.6(2)	O24	Mn13	O31	160.2(2)
O14	Mn6	O10	87.7(2)	O24	Mn13	O35	109.2(3)
O14	Mn6	O16[1]	108.7(2)	O24	Mn13	O37	86.4(2)
O14	Mn6	O19	109.3(2)	O31	Mn13	O30[2]	70.8(2)
O16[1]	Mn6	O1[1]	83.64(18)	O35	Mn13	O21[2]	94.4(2)
O16[1]	Mn6	O10	82.78(17)	O35	Mn13	O30[2]	156.0(2)
O19	Mn6	O1[1]	93.5(2)	O35	Mn13	O31	90.2(2)
O19	Mn6	O8[1]	98.5(2)	O35	Mn13	O37	112.7(2)
O19	Mn6	O10	162.3(2)	O37	Mn13	O30[2]	80.1(2)
O19	Mn6	O16[1]	87.2(2)	O37	Mn13	O31	82.4(2)
O7	Mn7	O10	158.81(19)	O21	Mn14	O31[2]	81.75(19)
O12	Mn7	O7	87.7(2)	O29	Mn14	O21	115.3(2)
O12	Mn7	O10	77.04(18)	O29	Mn14	O31[2]	154.8(2)
O12	Mn7	O13	90.1(2)	O29	Mn14	O33	91.6(2)
O12	Mn7	O16[1]	164.9(2)	O29	Mn14	O34[2]	91.5(2)
O12	Mn7	O17	89.1(2)	O33	Mn14	O21	83.8(2)
O13	Mn7	O7	90.0(2)	O33	Mn14	O31[2]	71.1(2)
O13	Mn7	O10	75.63(18)	O34[2]	Mn14	O21	151.7(2)
O16[1]	Mn7	O7	107.2(2)	O34[2]	Mn14	O31[2]	69.98(19)
O16[1]	Mn7	O10	87.92(19)	O34[2]	Mn14	O33	86.8(2)
O16[1]	Mn7	O13	87.3(2)	O38	Mn14	O21	86.0(2)
O16[1]	Mn7	O17	90.5(2)	O38	Mn14	O29	108.4(3)
O17	Mn7	O7	101.6(2)	O38	Mn14	O31[2]	90.4(2)
O17	Mn7	O10	92.87(19)	O38	Mn14	O33	160.0(2)
O17	Mn7	O13	168.3(2)	O38	Mn14	O34[2]	94.2(2)

Mn2	O1	Mn1	89.23(18)	C143	O20	Mn10	124.4(5)
Mn2	O1	Mn3	104.3(2)	Mn10	O21	Mn13[2]	104.9(2)
Mn2	O1	Mn5	100.59(19)	Mn10	O21	Mn14	100.2(3)
Mn2	O1	Mn6[1]	99.0(2)	Mn13[2]	O21	Mn14	94.5(2)
Mn3	O1	Mn1	84.61(18)	C143	O22	Mn8	128.2(5)
Mn3	O1	Mn5	153.5(3)	C81	O23	Mn11	123.7(6)
Mn3	O1	Mn6[1]	96.28(19)	C141[2]	O24	Mn13	133.8(6)
Mn5	O1	Mn1	86.86(17)	C81	O25	Mn10	129.0(6)
Mn5	O1	Mn6[1]	88.57(16)	C119	O26	Mn8	123.8(6)
Mn6[1]	O1	Mn1	171.2(2)	C85[2]	O27	Mn12	133.9(6)
C9	O2	Mn1	123.9(6)	C141	O28	Mn12	127.4(5)
C3	O3	Mn4	128.1(5)	C85	O29	Mn14	128.3(5)
C35	O4	Mn4	131.4(5)	Mn8	O30	Mn13[2]	174.4(3)
C3	O5	Mn5	132.9(5)	Mn9	O30	Mn8	89.1(2)
Mn1	O6	Mn4	102.8(2)	Mn9	O30	Mn10	105.2(3)
Mn1	O6	Mn5	101.3(2)	Mn9	O30	Mn12	103.2(2)
Mn4	O6	Mn5	94.2(2)	Mn9	O30	Mn13[2]	96.2(2)
C50	O7	Mn7	125.8(5)	Mn10	O30	Mn8	84.5(2)
Mn3	O8	Mn4[1]	100.9(2)	Mn10	O30	Mn12	150.4(3)
Mn3	O8	Mn6[1]	101.6(2)	Mn10	O30	Mn13[2]	95.7(2)
Mn6[1]	O8	Mn4[1]	95.6(2)	Mn12	O30	Mn8	88.11(19)
C50	O9	Mn3	128.9(5)	Mn12	O30	Mn13[2]	89.0(2)
Mn1	O10	Mn4	96.8(2)	Mn8	O31	Mn11	84.4(2)
Mn1	O10	Mn6	153.7(3)	Mn8	O31	Mn13	150.9(4)
Mn1	O10	Mn7	84.76(17)	Mn8	O31	Mn14[2]	96.6(2)
Mn2	O10	Mn1	105.3(2)	Mn9	O31	Mn8	105.6(3)
Mn2	O10	Mn4	98.2(2)	Mn9	O31	Mn11	89.2(2)
Mn2	O10	Mn6	99.3(2)	Mn9	O31	Mn13	102.4(2)
Mn2	O10	Mn7	89.31(18)	Mn9	O31	Mn14[2]	95.7(3)
Mn4	O10	Mn7	171.5(2)	Mn11	O31	Mn14[2]	174.5(3)
Mn6	O10	Mn4	88.71(16)	Mn13	O31	Mn11	88.0(2)
Mn6	O10	Mn7	86.32(16)	Mn13	O31	Mn14[2]	88.49(18)
C21	O11	Mn1	128.1(5)	Mn8	O32	Mn10	104.3(3)
Mn1	O12	Mn3	103.8(2)	Mn8	O32	Mn11	102.2(2)
Mn1	O12	Mn7	103.6(2)	Mn10	O32	Mn11	103.1(3)
Mn3	O12	Mn7	103.2(3)	Mn9	O33	Mn10	89.6(2)
Mn2	O13	Mn3	89.26(18)	Mn9	O33	Mn11	104.3(3)
Mn2	O13	Mn4[1]	101.1(2)	Mn9	O33	Mn12[2]	95.3(2)
Mn2	O13	Mn5[1]	98.4(2)	Mn9	O33	Mn14	102.7(3)
Mn2	O13	Mn7	104.6(2)	Mn10	O33	Mn12[2]	174.8(2)
Mn4[1]	O13	Mn3	86.82(16)	Mn11	O33	Mn10	84.5(2)
Mn4[1]	O13	Mn5[1]	88.88(19)	Mn11	O33	Mn12[2]	96.1(3)
Mn5[1]	O13	Mn3	171.8(2)	Mn11	O33	Mn14	151.7(3)
Mn7	O13	Mn3	84.64(19)	Mn14	O33	Mn10	87.6(2)
Mn7	O13	Mn4[1]	152.7(2)	Mn14	O33	Mn12[2]	89.6(2)

Mn7	O13	Mn5[1]	96.13(19)	Mn8	O34	Mn12	101.0(2)
C35	O14	Mn6	131.0(5)	Mn8	O34	Mn14[2]	105.1(3)
C21	O15	Mn3	126.3(4)	Mn14[2]	O34	Mn12	95.5(2)
Mn5	O16	Mn6[1]	93.2(2)	C91	O35	Mn13	127.3(7)
Mn7[1]	O16	Mn5	103.0(2)	C119	O36	Mn11	129.5(6)
Mn7[1]	O16	Mn6[1]	101.4(2)	Mn11	O37	Mn12[2]	106.0(3)
C9	O17	Mn7	128.5(5)	Mn11	O37	Mn13	101.2(2)
C56	O18	Mn5	129.7(5)	Mn12[2]	O37	Mn13	95.2(2)
C56[1]	O19	Mn6	131.3(5)	C91[2]	O38	Mn14	134.0(6)
C8	C1	C7	124.5(7)	C83	C79	C140	121.8(15)
C8	C1	C64	119.0(8)	C106	C80	C131	120.5(19)
C64	C1	C7	116.5(8)	O23	C81	O25	126.5(8)
C4	C2	C39	119.8(13)	O23	C81	C90	117.2(10)
O3	C3	C55	117.8(7)	O25	C81	C90	116.3(9)
O5	C3	O3	126.2(7)	C97	C82	C87	120.7(8)
O5	C3	C55	116.0(7)	C97	C82	C133	118.3(8)
C2	C4	C43	121.3(14)	C133	C82	C87	120.7(8)
C6	C5	C7	120.3(8)	C79	C83	C111	121(2)
C20	C6	C5	121.5(9)	C86	C84	C88	117.4(9)
C5	C7	C1	120.5(7)	C86	C84	C149	125.2(8)
C5	C7	C73	117.7(8)	C88	C84	C149	117.4(8)
C73	C7	C1	121.6(8)	O27[2]	C85	O29	126.0(8)
C1	C8	C10	120.6(7)	O27[2]	C85	C125	115.2(9)
C1	C8	C21	124.5(7)	O29	C85	C125	118.8(8)
C10	C8	C21	114.9(7)	C84	C86	C141	123.5(8)
O2	C9	O17	126.9(8)	C101	C86	C84	120.1(8)
O2	C9	C17	116.5(8)	C101	C86	C141	116.3(8)
O17	C9	C17	116.6(7)	C98	C87	C82	116.5(8)
C26	C10	C8	119.9(8)	C142	C87	C82	124.5(8)
C61	C11	C22	123.0(10)	C142	C87	C98	119.0(8)
C14	C12	C50	117.7(9)	C104	C88	C84	121.4(9)
C14	C12	C60	120.1(8)	C105	C89	C91	124.6(8)
C60	C12	C50	122.1(8)	C105	C89	C154	118.8(9)
C58	C13	C68	119.8(11)	C154	C89	C91	116.5(9)
C12	C14	C44	121.3(10)	C92	C90	C81	126.1(11)
C71	C15	C69	121.3(9)	C92	C90	C116	116.9(10)
C19	C16	C58	119.3(8)	C116	C90	C81	117.0(10)
C19	C16	C61	118.6(9)	O35	C91	O38[2]	125.7(9)
C61	C16	C58	121.9(8)	O35	C91	C89	118.3(9)
C43	C17	C9	117.6(9)	O38[2]	C91	C89	115.9(8)
C43	C17	C67	119.5(10)	C90	C92	C120	122.0(10)
C67	C17	C9	122.8(10)	C90	C92	C124	122.3(13)
C63	C18	C25	119.8(10)	C124	C92	C120	114.0(12)
C77	C19	C16	121.1(10)	C149	C93	C128	119.6(11)
C6	C20	C41	118.1(9)	C106	C94	C155	121.5(14)

O11	C21	C8	117.0(7)	C144	C95	C100	121.8(11)
O15	C21	O11	124.8(7)	C110	C96	C133	122.2(9)
O15	C21	C8	118.2(6)	C82	C97	C145	121.0(9)
C77	C22	C11	117.4(11)	C150	C98	C87	121.0(9)
C40	C23	C24	121.1(12)	C102	C99	C112	120.0(10)
C23	C24	C65	121.3(9)	C152	C100	C95	119.6(11)
C70	C24	C23	119.2(11)	C117	C101	C86	121.8(9)
C70	C24	C65	119.4(11)	C99	C102	C121	119.8(10)
C72	C25	C18	119.3(11)	C99	C102	C146	121.5(9)
C28	C26	C10	119.0(8)	C121	C102	C146	118.7(9)
C51	C27	C55	116.3(10)	C148	C103	C150	118.6(9)
C51	C27	C66	120.0(10)	C88	C104	C117	121.0(9)
C55	C27	C66	123.7(8)	C89	C105	C107	125.4(10)
C26	C28	C64	121.2(9)	C89	C105	C114	117.7(10)
C44	C29	C74	121.2(10)	C114	C105	C107	116.9(11)
C38	C30	C59	120.4(11)	C80	C106	C94	119.4(15)
C36	C31	C58	121.0(10)	C111	C107	C105	117.8(13)
C72	C32	C45	119.9(11)	C127	C107	C105	122.2(13)
C66	C33	C78	119.4(12)	C127	C107	C111	120.0(12)
C52	C34	C66	122.4(12)	C124	C108	C123	120.2(12)
O4	C35	O14	125.6(8)	C122	C109	C155	122.0(13)
O4	C35	C61	117.0(7)	C132	C109	C122	119.3(15)
O14	C35	C61	117.4(7)	C132	C109	C155	118.6(11)
C53	C36	C31	120.1(11)	C145	C110	C96	119.0(9)
C78	C37	C52	120.0(15)	C107	C111	C83	116.7(19)
C30	C38	C75	122.9(12)	C156	C112	C99	120.8(10)
C2	C39	C67	121.9(11)	C126	C113	C149	121.0(11)
C54	C40	C23	119.2(13)	C147	C114	C105	122.1(12)
C73	C41	C20	121.5(10)	C146	C115	C152	121.1(11)
C51	C42	C47	121.3(10)	C123	C116	C90	121.8(13)
C17	C43	C4	119.6(11)	C101	C117	C104	118.2(9)
C29	C44	C14	118.8(10)	C126	C118	C128	120.0(12)
C63	C45	C32	120.8(11)	O26	C119	O36	125.4(9)
C55	C46	C47	121.5(11)	O26	C119	C144	119.6(8)
C42	C47	C46	117.3(12)	O36	C119	C144	115.0(8)
C59	C48	C49	121.8(13)	C129	C120	C92	118.8(14)
C48	C49	C75	120.1(14)	C134	C120	C92	128.4(16)
O7	C50	O9	125.2(7)	C134	C120	C129	112.1(17)
O7	C50	C12	119.3(7)	C151	C121	C102	119.7(10)
O9	C50	C12	115.5(7)	C130	C122	C109	118.1(18)
C42	C51	C27	122.8(11)	C116	C123	C108	118.0(16)
C34	C52	C37	120.4(13)	C108	C124	C92	120.6(14)
C36	C53	C68	121.4(12)	C131	C125	C85	116.0(11)
C40	C54	C76	121.3(13)	C131	C125	C155	118.6(12)
C27	C55	C3	123.4(8)	C155	C125	C85	125.1(11)

C46	C55	C3	115.9(8)	C118	C126	C113	120.2(11)
C46	C55	C27	120.7(8)	C140	C127	C107	124.6(18)
O18	C56	O19[1]	125.6(7)	C118	C128	C93	119.2(14)
O18	C56	C57	119.1(7)	C138	C129	C120	130.9(19)
O19[1]	C56	C57	115.4(7)	C122	C130	C137	121.8(19)
C62	C57	C56	118.0(8)	C125	C131	C80	120.8(17)
C62	C57	C65	120.6(8)	C139	C132	C109	117.8(19)
C65	C57	C56	121.4(7)	C96	C133	C82	119.2(9)
C13	C58	C16	121.2(10)	C136	C134	C120	122.1(16)
C13	C58	C31	118.4(10)	C136	C135	C138	119.1(15)
C31	C58	C16	120.3(8)	C134	C136	C135	121.4(15)
C30	C59	C60	121.3(10)	C139	C137	C130	118(2)
C48	C59	C30	118.1(11)	C129	C138	C135	104(3)
C48	C59	C60	120.5(10)	C137	C139	C132	124(2)
C12	C60	C59	126.0(8)	C127	C140	C79	116(2)
C74	C60	C12	118.6(10)	O24[2]	C141	C86	114.7(7)
C74	C60	C59	115.4(9)	O28	C141	O24[2]	125.2(7)
C11	C61	C16	118.7(9)	O28	C141	C86	120.1(7)
C11	C61	C35	117.4(8)	C87	C142	C143	124.6(8)
C16	C61	C35	123.7(8)	C87	C142	C148	118.9(8)
C57	C62	C71	119.8(10)	C148	C142	C143	116.4(8)
C18	C63	C67	119.7(10)	O20	C143	O22	126.5(7)
C45	C63	C18	118.8(12)	O20	C143	C142	119.8(7)
C45	C63	C67	121.4(10)	O22	C143	C142	113.7(7)
C1	C64	C28	120.3(9)	C95	C144	C119	118.7(9)
C57	C65	C24	122.6(7)	C95	C144	C146	118.6(10)
C69	C65	C24	119.8(9)	C146	C144	C119	122.6(8)
C69	C65	C57	117.3(9)	C110	C145	C97	120.3(10)
C33	C66	C27	120.8(10)	C115	C146	C102	117.3(10)
C33	C66	C34	116.5(13)	C115	C146	C144	119.0(10)
C34	C66	C27	122.7(10)	C144	C146	C102	123.5(9)
C17	C67	C63	124.0(10)	C153	C147	C114	120.8(11)
C39	C67	C17	117.9(11)	C103	C148	C142	121.9(9)
C39	C67	C63	118.1(9)	C93	C149	C84	121.0(9)
C53	C68	C13	119.3(11)	C93	C149	C113	120.0(10)
C65	C69	C15	121.4(10)	C113	C149	C84	118.9(9)
C24	C70	C76	119.4(13)	C98	C150	C103	120.5(9)
C15	C71	C62	119.5(10)	C121	C151	C156	122.2(10)
C32	C72	C25	121.3(13)	C100	C152	C115	119.7(12)
C41	C73	C7	121.0(10)	C147	C153	C154	119.2(10)
C60	C74	C29	119.8(11)	C153	C154	C89	121.3(11)
C38	C75	C49	116.6(12)	C94	C155	C109	117.8(12)
C54	C76	C70	119.7(13)	C94	C155	C125	118.9(14)
C19	C77	C22	121.2(11)	C125	C155	C109	123.1(10)
C37	C78	C33	121.2(13)	C112	C156	C151	117.5(11)

[1]-X,1-Y,1-Z; [2]1-X,2-Y,1-Z

Table II.1.5.6 Hydrogen Atom Coordinates (Å×10⁴) and Isotropic Displacement Parameters (Å²×10³) for ab22515.

Atom	*x*	*y*	*z*	U(eq)
H0AA	2084	9582	6747	123
H1AA	1294	9774	6177	107
H1C	-1136	7834	3873	46
H1E	-1607	8155	4316	54
H1K	577	7334	3534	44
H1P	-276	8334	5982	64
H1R	1425	7144	7466	72
H1S	2812	5687	5436	67
H1T	-1149	7589	2038	70
H1X	1445	6597	6707	67
H1Y	792	8275	7429	63
H1Z	-1293	9129	4821	67
H2AA	-67	9482	6366	92
H2C	-2055	5987	3059	68
H2H	1849	5403	6981	76
H2I	428	8242	2985	62
H2S	-176	9250	2923	61
H2T	3701	5078	4735	90
H2U	1759	3816	4184	67
H2V	-117	6345	6906	55
H2W	3202	5970	6743	80
H2X	-2731	7091	5622	101
H2Z	-1844	7867	4930	69
H3A	141	5192	7266	69
H3AA	-1446	8539	6149	109
H3B	1078	3547	3549	75
H3C	2435	8356	6919	92
H3G	-2750	6130	3328	81
H3I	-495	9821	4864	77
H3N	-3988	6622	4299	88
H3T	851	8743	5717	75
H3V	3668	5477	5381	85
H3W	2825	7180	6495	81
H4D	-2682	5792	4069	67
H4J	-3646	5898	3863	90
H4L	1841	5970	3792	96
H4Y	1119	5722	3157	131
H5C	-3413	7245	4886	86
H5J	-1298	8565	5507	103
H5P	1023	5010	7728	71
H5Z	-2931	7328	3534	92

H15	-309	6077	2957	52
H20	-571	9437	3438	55
H27	1676	5949	7835	75
H30	-1793	7741	2354	69
H32	-1847	8276	3075	80
H34	-415	6773	2325	67
H41	2723	5107	6985	79
H44	-24	9522	4433	71
H46	2897	4718	4171	75
H47	766	4451	3001	106
H48	-2520	8406	3390	87
H49	468	9431	7098	84
H60	-2143	7811	6210	117
H0BA	6355	14071	3889	201
H0CA	6284	13798	7044	264
H1BA	6222	12809	3703	157
H1M	1649	7208	4491	63
H2B	3150	6806	4373	70
H2BA	5959	12264	7800	131
H2E	3068	12732	3704	66
H2F	3006	8955	3224	54
H2G	1898	10846	3466	56
H2J	1272	9541	3626	55
H2K	5151	13525	4371	70
H2L	2823	13869	3308	68
H2N	3183	8187	5587	63
H2P	1411	9326	4861	59
H2R	1617	7435	5160	74
H3BA	6150	13522	7664	195
H3F	4342	12826	7355	105
H3J	2779	10038	2784	61
H3K	5309	12281	3399	122
H3L	5971	13541	4993	71
H3M	1677	7851	3877	62
H3P	4070	13938	2870	79
H3Q	4217	14870	4128	74
H3R	4841	12774	6351	86
H3X	2371	7977	5709	76
H3Z	2336	6932	3077	102
H4B	4274	14065	5112	75
H4BA	6360	10462	7191	121
H4G	4919	13304	7004	125
H4K	3813	11775	7092	140
H4R	1630	7593	3187	80
H4V	4718	14372	3542	110

H4W	3102	6511	3670	99
H5AA	3652	10499	6860	205
H5BA	6135	9260	7368	231
H5E	6063	12884	6490	190
H5F	5124	11330	7514	161
H6	2707	8809	3794	47
H6AA	3112	11690	5753	107
H6BA	2235	9949	5976	134
H7AA	2403	10817	5489	105
H7BA	5472	9115	7686	376
H8AA	3170	9335	6497	542
H8BA	5102	10165	7839	391
H9AA	5587	14919	3789	147
H21	2211	10969	2896	67
H25	3190	13534	2512	69
H28	2337	9629	5081	52
H31	871	9332	4126	61
H33	5060	14038	5711	85
H35	3393	14933	3511	85
H36	2912	12341	2634	66
H37	3518	11561	3157	63
H40	5927	13726	5672	78

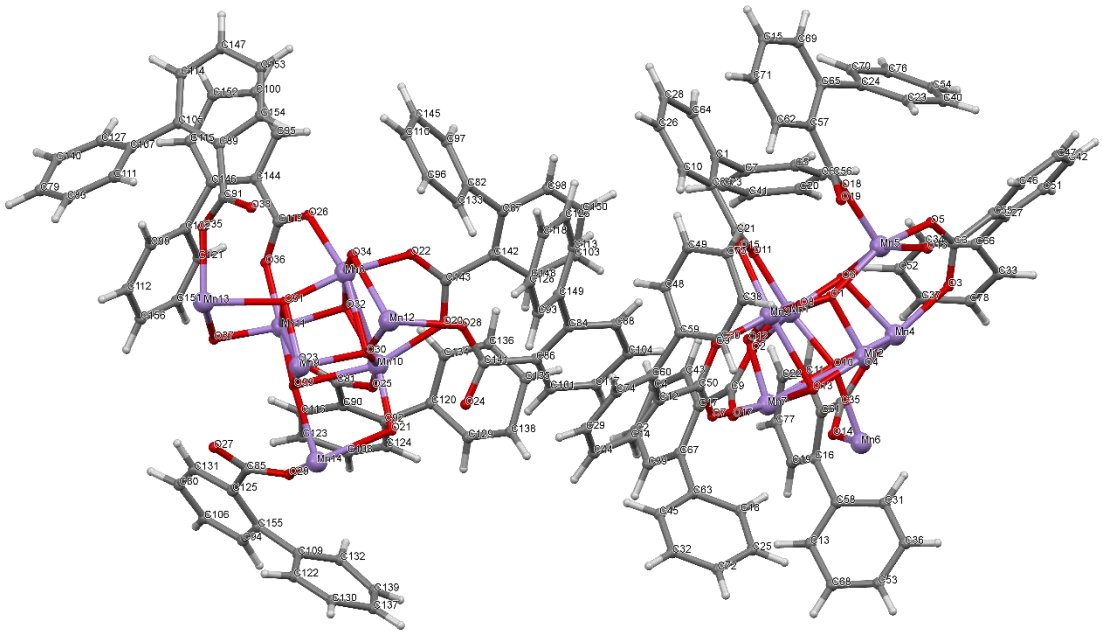

Figure II.1.4 Crystal Structure with atomic labels for compound **5**, Mn_{13}-2-Ph, $Mn_{13}O_{14}(O_2CPh_2)_{12}$, ab22515

II.2 Crystal Structure Information and Tables for Chapter 3 Compounds

II.2.1 Compound 1, Mn_{13}-2-Methyl, $Mn_{13}O_8(O_2CPh\text{-}o\text{-}Me)_{12}(OEt)_6$, ab52414a

Table II.2.1.1 Crystal data and structure refinement for ab52414a.

Identification code	ab52414a
Empirical formula	$C_{102}H_{114}Mn_{13}O_{38}$
Formula weight	2662.15
Temperature/K	100.0
Crystal system	triclinic
Space group	P1
a/Å	14.6088(6)
b/Å	15.0498(9)
c/Å	15.5875(7)
α/°	92.426(3)
β/°	111.672(2)
γ/°	118.932(2)
Volume/Å^3	2682.5(2)
Z	1
ρ_{calc}g/cm^3	1.648
μ/mm^{-1}	1.556
F(000)	1355.0
Crystal size/mm^3	0.01 × 0.01 × 0.01
Radiation	MoKα (λ = 0.71073)
2Θ range for data collection/°	3.212 to 57.332
Index ranges	$-19 \le h \le 19$, $-20 \le k \le 20$, $-21 \le l \le 21$
Reflections collected	54581
Independent reflections	24370 [R_{int} = 0.0554, R_{sigma} = 0.0797]
Data/restraints/parameters	24370/3/1421
Goodness-of-fit on F^2	1.011
Final R indexes [I>=2σ (I)]	R_1 = 0.0512, wR_2 = 0.1155
Final R indexes [all data]	R_1 = 0.0999, wR_2 = 0.1434
Largest diff. peak/hole / e Å^{-3}	0.82/-0.61
Flack parameter	0.43(3)

Table II.2.1.2 Fractional Atomic Coordinates (×10^4) and Equivalent Isotropic Displacement Parameters (Å^2×10^3) for ab52414a. U_{eq} is defined as 1/3 of of the trace of the orthogonalised U_{IJ} tensor.

Atom	*x*	*y*	*z*	U(eq)
Mn1	8610(2)	4709(2)	1566(2)	25.3(7)
Mn2	8663(2)	4143(2)	3548(2)	25.1(7)
Mn3	11020(3)	5294(3)	3307(3)	17.79(17)
Mn4	9843(2)	2952(2)	3200.2(19)	21.4(6)
Mn5	10005(2)	3609(2)	1489.0(19)	22.9(7)
Mn6	12108(2)	4040(2)	3151.5(19)	23.5(7)

Mn7	11050(2)	4589(2)	5244(2)	26.6(7)
Mn8	10986(2)	5992(2)	1375(2)	26.9(7)
Mn9	9928(2)	6540(2)	3474.9(19)	23.3(7)
Mn10	12030(2)	6972(2)	5135.3(19)	23.2(7)
Mn11	12186(2)	7625(2)	3422(2)	21.6(7)
Mn12	13423(2)	5869(2)	5054(2)	23.7(7)
Mn13	13366(2)	6436(2)	3069(2)	24.3(7)
O1	9541(10)	3999(9)	2667(8)	23(3)
O2	12511(11)	6567(10)	3963(10)	21(3)
O3	10411(12)	6031(10)	2602(9)	23(3)
O4	11583(12)	8440(10)	2755(10)	26(3)
O5	10437(11)	2161(10)	3872(10)	27(3)
O6	10547(11)	2987(10)	2394(9)	22(3)
O7	9363(10)	3166(10)	4126(9)	22(3)
O8	11407(11)	5037(10)	2339(9)	23(3)
O9	11643(11)	4541(9)	4018(9)	22(3)
O10	8418(11)	5323(11)	2776(10)	25(3)
O11	11507(11)	7602(10)	4232(9)	26(3)
O12	13625(12)	5316(11)	3840(10)	28(3)
O13	12649(12)	7401(10)	2477(10)	25(3)
O14	12634(11)	6228(9)	5888(9)	26(3)
O15	10623(11)	5591(10)	4293(9)	21(3)
O16	8260(11)	1720(10)	2102(9)	29(3)
O17	9424(11)	4350(10)	756(9)	24(3)
O18	8537(12)	2253(10)	820(9)	24(3)
O19	13535(12)	8352(10)	5803(10)	35(3)
O20	13786(11)	8859(10)	4552(10)	30(3)
O21	12513(12)	3720(11)	2163(9)	31(3)
O22	7006(12)	2927(11)	2508(11)	33(3)
O23	14989(11)	7257(10)	5485(10)	32(3)
O24	9549(12)	6862(11)	4465(11)	33(4)
O25	15017(12)	7606(12)	4094(11)	34(3)
O26	7023(11)	3298(11)	1144(9)	35(3)
O27	12028(11)	4017(10)	6034(9)	32(3)
O28	12234(11)	2974(10)	3930(9)	26(3)
O29	11086(13)	7155(11)	5802(10)	39(4)
O30	9805(11)	7611(11)	2704(10)	31(3)
O31	9969(12)	6543(11)	580(10)	37(3)
O32	10958(12)	3419(10)	832(9)	31(3)
O33	13502(12)	6156(12)	1845(10)	36(4)
O34	8535(12)	4451(11)	4800(11)	37(4)
O35	13750(12)	4971(11)	5947(10)	33(4)
O36	8306(12)	5635(10)	680(10)	34(3)
O37	10164(13)	4674(12)	5991(10)	38(4)
O38	11899(11)	5923(11)	650(10)	35(3)

C1	10656(16)	8354(11)	2609(11)	24(4)
C2	7976(17)	1539(14)	1222(14)	35(5)
C3	14016(13)	9027(12)	5418(11)	22(4)
C4	11450(15)	2236(15)	4057(13)	27(4)
C5	11850(20)	3404(16)	1231(16)	35(5)
C6	10135(19)	7157(16)	5351(17)	36(5)
C7	10482(16)	9193(15)	2254(14)	29(4)
C8	14957(17)	10086(14)	6044(14)	28(4)
C9	6997(18)	431(16)	542(16)	36(5)
C10	11565(19)	1363(14)	4406(13)	28(5)
C11	9230(20)	4656(17)	5690(16)	35(5)
C12	12825(18)	5915(15)	966(15)	32(4)
C13	15440(13)	7831(13)	4998(13)	29(4)
C14	6554(17)	2698(16)	1598(15)	36(5)
C15	8050(40)	6690(40)	5000(40)	360(30)
C16	8953(16)	6330(13)	399(13)	29(4)
C17	13055(17)	4253(16)	6182(13)	34(5)
C18	11470(20)	2157(16)	6599(15)	62(7)
C19	6306(17)	-329(15)	883(16)	38(5)
C20	16720(20)	12111(19)	7349(17)	59(7)
C21	15673(19)	10913(17)	5751(15)	44(6)
C22	13588(16)	3427(11)	1210(13)	51(5)
C23	14680(30)	4000(30)	7100(20)	102(11)
C24	17430(20)	9394(19)	5229(16)	53(5)
C25	12700(30)	630(20)	5130(20)	78(8)
C26	16623(18)	8895(15)	5578(16)	41(6)
C27	3670(20)	120(20)	740(20)	106(14)
C28	8755(16)	3890(14)	-275(12)	35(5)
C29	14684(15)	5288(15)	4042(13)	41(5)
C30	5475(16)	1714(15)	1046(16)	41(5)
C31	6016(16)	-736(15)	-1016(14)	50(6)
C32	13335(17)	6654(15)	6913(12)	34(5)
C33	7417(14)	5360(15)	2601(14)	35(5)
C34	13106(15)	5614(14)	230(13)	48(5)
C35	16830(20)	9287(17)	6478(17)	44(6)
C36	8855(17)	4936(12)	6397(12)	40(5)
C37	5213(17)	1293(16)	88(17)	48(6)
C38	5490(20)	-1302(17)	212(18)	55(7)
C39	16550(20)	11928(18)	6402(17)	56(7)
C40	13319(18)	8280(16)	2160(15)	42(6)
C41	12230(30)	5060(20)	-734(17)	107(11)
C42	9394(19)	9110(17)	1892(15)	47(6)
C43	12590(20)	1407(16)	4731(16)	47(6)
C44	8694(17)	2280(13)	4430(14)	34(4)
C45	12418(17)	3096(13)	733(14)	68(7)

C46	13420(20)	4939(18)	-1238(15)	74(7)
C47	6841(19)	237(16)	-406(15)	39(5)
C48	14530(20)	2660(30)	7810(20)	162(16)
C49	15120(20)	10323(16)	6971(15)	44(6)
C50	8530(20)	6957(18)	-160(15)	48(6)
C51	13508(18)	3657(17)	6746(16)	45(5)
C52	11480(20)	10099(16)	2303(15)	48(6)
C53	10594(16)	487(14)	4399(15)	39(5)
C54	8590(30)	7300(20)	5580(20)	128(12)
C55	8313(15)	8249(17)	1920(20)	69(8)
C56	8750(40)	8440(30)	-800(30)	112(12)
C57	11654(18)	-274(13)	5064(15)	56(6)
C58	10360(20)	10823(17)	1612(12)	62(7)
C59	11379(19)	10924(14)	1953(11)	51(6)
C60	10603(17)	-306(15)	4706(16)	62(6)
C61	18442(19)	10289(17)	5763(16)	57(5)
C62	17840(20)	10210(20)	7037(18)	73(8)
C63	9182(19)	7869(18)	-311(17)	47(5)
C64	13350(30)	2500(20)	-195(18)	87(8)
C65	12700(20)	2661(16)	6909(15)	56(7)
C66	14180(20)	5779(19)	384(18)	64(7)
C67	5380(20)	-1511(19)	-676(19)	76(9)
C68	12410(20)	4820(20)	-1399(18)	97(8)
C69	13330(20)	2230(20)	7440(20)	86(9)
C70	6403(19)	-195(19)	1846(17)	62(7)
C71	7991(11)	7451(14)	5908(12)	59(5)
C72	8820(30)	8260(30)	6790(20)	104(11)
C73	7746(19)	4710(18)	6086(17)	48(5)
C74	15970(20)	11331(19)	7606(17)	73(8)
C75	10504(18)	8379(14)	22(15)	60(7)
C76	4208(18)	309(15)	-470(19)	66(7)
C77	15611(19)	10786(17)	4744(13)	51(6)
C78	7280(20)	6420(30)	-570(20)	86(8)
C79	14310(20)	5400(20)	-360(20)	83(8)
C80	9456(19)	10019(16)	1618(16)	46(5)
C81	11739(15)	2545(18)	-70(20)	110(10)
C82	3490(20)	-210(20)	-118(18)	93(9)
C83	4682(18)	1133(19)	1424(19)	75(9)
C84	18674(19)	10776(18)	6690(20)	88(10)
C85	4820(20)	1680(20)	2429(16)	78(7)
C86	17210(20)	9130(20)	4278(19)	106(12)
C87	6817(14)	4288(16)	5191(12)	66(5)
C88	9930(20)	8810(30)	7380(20)	152(15)
C89	10590(20)	1913(16)	-546(16)	94(8)
C90	6800(20)	6990(30)	-1030(30)	200(20)

C91	15160(30)	3540(30)	7720(20)	184(18)
C92	7430(30)	5010(30)	6740(30)	135(14)
C93	7560(40)	7970(40)	-1250(30)	200(20)
C94	13690(20)	2300(20)	4820(20)	88(9)
C95	8130(40)	5480(30)	7620(30)	163(18)
C96	9728(17)	5427(19)	7334(16)	64(7)
C97	11640(20)	8470(30)	7376(16)	210(20)
C98	12270(20)	2200(20)	-644(15)	98(9)
C99	11090(30)	1360(20)	-972(18)	178(12)
C100	9380(30)	5810(20)	8000(20)	137(17)
C101	10470(20)	8281(19)	6856(9)	85(8)
C102	15250(30)	6350(30)	1430(30)	220(20)
C103	9789(18)	7593(15)	5959(11)	49(5)
C104	13940(40)	3010(30)	620(30)	209(19)
C105	11130(60)	6430(40)	8050(60)	740(80)

Table II.2.1.3 Anisotropic Displacement Parameters ($Å^2×10^3$) for ab52414a. The Anisotropic displacement factor exponent takes the form: $-2\pi^2[h^2a^{*2}U_{11}+2hka^*b^*U_{12}+\ldots]$.

Atom	U_{11}	U_{22}	U_{33}	U_{23}	U_{13}	U_{12}
Mn1	18.9(15)	26.9(17)	25.9(17)	8.9(14)	6.9(14)	11.6(13)
Mn2	21.8(16)	31.1(18)	24.9(17)	12.3(14)	9.5(14)	16.3(14)
Mn3	17.4(4)	16.0(4)	19.8(4)	6.8(3)	6.7(3)	9.8(3)
Mn4	19.7(15)	17.2(15)	24.6(15)	6.7(12)	7.6(13)	9.6(13)
Mn5	26.0(16)	20.1(16)	22.0(16)	8.1(12)	7.9(14)	13.7(13)
Mn6	23.4(16)	21.4(16)	28.8(17)	9.1(13)	10.0(14)	15.1(14)
Mn7	22.6(16)	27.2(17)	24.0(17)	9.1(14)	6.9(14)	11.8(14)
Mn8	24.7(17)	27.7(17)	26.8(17)	11.8(14)	10.4(14)	13.5(14)
Mn9	23.4(16)	23.7(16)	26.6(17)	9.6(13)	10.7(14)	15.4(13)
Mn10	27.0(16)	20.8(16)	21.0(16)	5.4(13)	8.2(14)	14.1(14)
Mn11	22.8(16)	18.1(15)	22.9(16)	9.0(12)	7.6(13)	11.8(13)
Mn12	20.4(16)	25.2(16)	24.7(16)	11.4(13)	8.6(14)	12.5(13)
Mn13	21.2(16)	25.9(16)	25.9(17)	10.5(13)	10.3(14)	12.5(13)
O1	22(7)	21(6)	20(6)	6(5)	7(6)	9(5)
O2	18(7)	13(6)	32(8)	9(6)	10(6)	9(5)
O3	30(7)	25(7)	20(7)	7(5)	9(6)	18(6)
O4	30(8)	22(7)	30(7)	11(6)	13(6)	18(6)
O5	27(7)	24(7)	30(8)	14(6)	11(6)	14(6)
O6	25(7)	19(7)	25(7)	9(6)	12(6)	13(6)
O7	19(7)	18(6)	27(7)	12(5)	11(6)	7(5)
O8	18(6)	25(7)	24(7)	7(5)	7(5)	12(5)
O9	15(6)	16(6)	29(7)	10(5)	6(6)	8(5)
O10	16(6)	27(7)	28(7)	7(6)	4(6)	13(5)
O11	30(7)	21(6)	24(7)	8(5)	7(6)	15(6)
O12	21(7)	29(7)	37(8)	14(6)	13(6)	16(6)

O13	30(7)	25(7)	26(7)	11(6)	17(6)	15(6)
O14	31(7)	19(6)	18(6)	8(5)	3(6)	11(6)
O15	27(7)	17(6)	21(7)	6(5)	13(6)	11(5)
O16	25(7)	28(7)	21(7)	4(5)	5(6)	10(6)
O17	24(7)	33(7)	17(7)	6(6)	7(6)	19(6)
O18	31(7)	19(7)	20(7)	5(6)	5(6)	16(6)
O19	35(8)	25(7)	31(8)	7(6)	7(7)	11(6)
O20	28(8)	16(7)	41(8)	7(6)	10(7)	11(6)
O21	36(8)	33(8)	37(7)	13(6)	24(7)	21(7)
O22	23(7)	30(7)	36(8)	13(6)	10(6)	9(6)
O23	18(6)	23(7)	43(8)	11(6)	13(6)	4(5)
O24	35(8)	43(8)	38(9)	19(7)	19(7)	30(7)
O25	23(7)	38(8)	34(8)	13(6)	10(6)	15(6)
O26	28(7)	39(8)	24(7)	12(6)	1(6)	16(6)
O27	30(7)	35(8)	25(7)	15(6)	5(6)	19(6)
O28	22(7)	23(7)	36(8)	11(6)	10(6)	15(6)
O29	57(10)	47(9)	39(8)	26(7)	25(8)	42(8)
O30	35(8)	32(8)	30(8)	12(7)	9(7)	24(7)
O31	40(8)	34(8)	44(8)	13(6)	23(7)	20(7)
O32	44(8)	31(7)	27(7)	4(5)	22(7)	22(6)
O33	40(9)	44(9)	30(8)	13(7)	20(7)	23(7)
O34	26(8)	40(8)	42(9)	14(7)	17(7)	16(7)
O35	36(8)	38(8)	31(8)	23(7)	14(7)	23(7)
O36	28(7)	30(8)	41(8)	10(6)	10(7)	17(6)
O37	45(9)	48(9)	29(7)	18(7)	12(7)	34(8)
O38	30(7)	43(8)	33(8)	17(6)	20(7)	15(6)
C1	38(10)	7(6)	17(7)	5(5)	2(7)	13(7)
C2	43(11)	30(10)	42(11)	21(8)	13(9)	31(9)
C3	12(7)	18(8)	20(8)	-9(6)	-3(6)	5(6)
C4	23(9)	40(10)	26(9)	6(8)	11(7)	23(8)
C5	57(13)	30(11)	56(14)	27(10)	46(12)	34(10)
C6	44(11)	34(11)	43(13)	17(9)	25(10)	26(9)
C7	34(10)	28(10)	29(10)	9(8)	12(8)	20(9)
C8	31(8)	17(7)	30(9)	8(6)	5(7)	17(7)
C9	29(9)	23(9)	36(10)	1(7)	-7(7)	15(7)
C10	54(12)	24(9)	17(9)	9(7)	13(9)	30(9)
C11	47(14)	24(11)	33(12)	15(9)	25(11)	13(10)
C12	40(11)	33(11)	31(11)	13(9)	23(10)	19(9)
C13	8(6)	16(7)	33(10)	2(6)	-9(6)	1(6)
C14	36(10)	42(11)	47(11)	27(9)	26(9)	27(9)
C15	220(50)	430(80)	330(70)	40(60)	90(50)	140(50)
C16	35(10)	22(8)	28(9)	9(7)	18(7)	12(7)
C17	39(10)	42(11)	20(8)	2(8)	-3(7)	33(9)
C18	74(15)	49(12)	45(12)	-2(9)	21(11)	27(11)
C19	22(9)	18(9)	44(12)	5(8)	-1(9)	2(7)

C20	71(16)	30(13)	42(13)	-4(10)	-1(12)	23(12)
C21	47(11)	42(12)	29(11)	12(9)	-2(9)	27(10)
C22	64(10)	32(6)	68(9)	-1(6)	39(8)	28(6)
C23	67(16)	126(18)	170(30)	121(19)	65(17)	75(15)
C24	32(11)	47(11)	50(11)	30(9)	3(9)	11(9)
C25	100(19)	108(19)	77(16)	32(13)	35(14)	93(17)
C26	29(11)	25(10)	44(11)	12(8)	-7(9)	14(9)
C27	34(11)	68(16)	130(30)	75(17)	-2(13)	-8(10)
C28	44(10)	33(9)	19(8)	12(7)	2(7)	23(8)
C29	32(10)	47(11)	46(12)	12(9)	6(9)	31(9)
C30	22(9)	39(11)	54(13)	32(9)	13(9)	12(8)
C31	47(10)	29(10)	30(9)	-3(8)	-12(8)	13(8)
C32	36(11)	33(9)	25(9)	0(7)	6(8)	18(9)
C33	13(8)	36(9)	58(13)	11(9)	14(8)	15(7)
C34	28(8)	53(10)	59(11)	44(8)	19(7)	17(7)
C35	41(12)	38(11)	52(13)	25(10)	12(10)	25(10)
C36	72(12)	25(7)	48(10)	8(6)	50(9)	27(8)
C37	21(10)	33(10)	55(12)	-9(8)	-10(8)	10(8)
C38	47(13)	21(10)	62(16)	22(10)	6(12)	6(9)
C39	52(15)	31(11)	40(14)	1(10)	-11(11)	15(10)
C40	35(11)	32(11)	49(12)	24(10)	23(10)	7(9)
C41	170(30)	110(20)	40(13)	38(13)	66(16)	61(19)
C42	64(13)	65(12)	64(13)	51(10)	39(11)	59(11)
C43	55(12)	31(8)	53(12)	6(8)	18(10)	27(8)
C44	45(11)	27(9)	37(10)	13(7)	23(9)	20(8)
C45	59(10)	32(7)	47(10)	12(7)	5(8)	-6(7)
C46	130(18)	80(15)	53(9)	17(9)	39(11)	85(15)
C47	47(11)	37(11)	32(10)	10(8)	9(9)	28(9)
C48	135(19)	260(30)	290(30)	270(30)	160(20)	180(20)
C49	53(12)	23(10)	34(10)	-4(8)	1(9)	21(9)
C50	75(15)	57(13)	43(11)	35(10)	25(10)	56(12)
C51	56(12)	58(12)	57(13)	29(10)	47(11)	38(10)
C52	85(15)	42(11)	39(10)	19(9)	23(10)	51(11)
C53	36(9)	25(9)	49(12)	20(8)	18(9)	13(7)
C54	220(30)	230(30)	210(20)	200(20)	210(20)	220(20)
C55	31(8)	54(12)	140(20)	55(13)	41(11)	32(8)
C56	230(30)	140(20)	140(30)	120(20)	150(30)	170(30)
C57	71(13)	26(8)	93(15)	39(9)	47(12)	32(9)
C58	130(20)	74(14)	28(8)	25(8)	34(11)	84(15)
C59	107(15)	39(9)	31(7)	26(7)	26(8)	58(10)
C60	51(11)	41(11)	101(16)	25(10)	43(11)	22(9)
C61	33(9)	50(9)	53(10)	24(8)	4(8)	9(7)
C62	69(16)	67(16)	58(13)	16(12)	-5(12)	43(14)
C63	58(10)	56(12)	66(13)	34(10)	46(10)	43(9)
C64	112(19)	120(20)	69(15)	2(13)	45(15)	91(16)

C65	120(19)	43(11)	46(11)	27(9)	55(12)	57(12)
C66	81(14)	56(10)	62(11)	21(8)	23(10)	48(10)
C67	80(17)	26(11)	36(14)	-7(10)	-24(12)	7(11)
C68	129(18)	150(20)	70(14)	43(13)	60(13)	99(17)
C69	108(17)	97(16)	160(30)	107(17)	109(18)	85(14)
C70	32(11)	43(14)	80(17)	17(12)	14(11)	7(10)
C71	32(6)	71(10)	57(9)	9(8)	3(6)	30(7)
C72	120(20)	102(17)	79(17)	14(13)	-10(14)	90(17)
C73	63(12)	68(12)	58(11)	36(9)	50(10)	47(10)
C74	120(20)	47(14)	44(13)	1(11)	29(13)	49(14)
C75	59(13)	36(10)	71(14)	41(10)	37(11)	8(9)
C76	32(11)	21(8)	84(16)	-21(9)	-8(10)	1(8)
C77	54(13)	27(11)	30(9)	11(8)	7(9)	2(10)
C78	89(16)	160(20)	113(18)	105(17)	79(15)	106(17)
C79	116(16)	150(20)	107(17)	96(18)	94(15)	117(17)
C80	54(10)	47(10)	59(10)	32(8)	23(8)	42(9)
C81	27(7)	87(13)	190(30)	8(15)	18(12)	34(8)
C82	69(16)	47(14)	70(14)	19(11)	-27(11)	10(12)
C83	27(9)	68(13)	79(15)	61(12)	4(9)	2(9)
C84	27(9)	34(11)	120(20)	27(13)	-5(11)	-16(8)
C85	34(10)	116(16)	40(10)	36(10)	14(8)	10(10)
C86	41(12)	130(20)	89(18)	77(16)	33(12)	-2(11)
C87	36(8)	83(12)	79(11)	8(9)	23(8)	35(8)
C88	54(12)	250(40)	100(20)	70(20)	27(13)	47(18)
C89	130(20)	85(12)	86(17)	8(12)	64(17)	61(15)
C90	118(18)	260(30)	420(50)	300(40)	200(30)	160(20)
C91	200(30)	370(50)	230(30)	260(30)	160(30)	250(30)
C92	240(40)	130(20)	170(30)	71(19)	180(30)	130(20)
C93	290(40)	310(50)	310(50)	240(40)	270(40)	270(40)
C94	90(18)	100(20)	100(20)	63(17)	32(16)	76(17)
C95	310(50)	120(20)	210(40)	90(30)	240(40)	130(30)
C96	55(10)	60(12)	41(12)	-2(9)	25(9)	3(9)
C97	138(19)	380(50)	55(11)	-112(19)	-70(12)	200(30)
C98	86(15)	190(20)	26(7)	-15(10)	15(9)	90(17)
C99	360(40)	180(30)	123(19)	77(19)	120(30)	220(30)
C100	210(40)	61(13)	71(18)	-19(12)	100(20)	0(19)
C101	170(20)	130(18)	8(5)	12(7)	30(9)	128(18)
C102	260(40)	270(40)	440(60)	280(40)	310(40)	220(30)
C103	117(15)	88(12)	44(9)	53(8)	66(10)	101(12)
C104	420(50)	250(40)	260(40)	170(30)	300(40)	280(40)
C105	980(130)	600(90)	1800(200)	870(130)	1200(160)	720(100)

Table II.2.1.4 Bond Lengths for ab52414a.

Atom	Atom	Length/Å	Atom	Atom	Length/Å
Mn1	O1	2.403(13)	O36	C16	1.25(2)
Mn1	O3	2.238(14)	O37	C11	1.26(3)
Mn1	O10	2.233(14)	O38	C12	1.26(2)
Mn1	O17	2.230(12)	C1	C7	1.49(2)
Mn1	O26	2.076(14)	C2	C9	1.54(3)
Mn1	O36	2.087(14)	C3	C8	1.46(2)
Mn2	O1	2.263(13)	C4	C10	1.50(2)
Mn2	O7	2.214(13)	C5	C45	1.53(3)
Mn2	O10	2.283(14)	C6	C103	1.49(2)
Mn2	O15	2.364(13)	C7	C42	1.41(3)
Mn2	O22	2.098(14)	C7	C52	1.41(3)
Mn2	O34	2.083(15)	C8	C21	1.41(3)
Mn3	O1	1.905(12)	C8	C49	1.38(3)
Mn3	O2	1.900(13)	C9	C19	1.39(3)
Mn3	O3	1.888(13)	C9	C47	1.40(3)
Mn3	O8	1.881(13)	C10	C43	1.36(3)
Mn3	O9	1.923(13)	C10	C53	1.39(3)
Mn3	O15	1.935(12)	C11	C36	1.52(3)
Mn4	O1	1.970(13)	C12	C34	1.47(3)
Mn4	O5	1.923(13)	C13	C26	1.55(2)
Mn4	O6	1.884(13)	C14	C30	1.43(3)
Mn4	O7	1.898(13)	C15	C54	1.00(7)
Mn4	O9	2.333(13)	C15	C71	1.85(5)
Mn4	O16	2.091(13)	C16	C50	1.51(2)
Mn5	O1	2.321(13)	C17	C51	1.49(3)
Mn5	O6	1.870(13)	C18	C65	1.43(3)
Mn5	O8	2.016(13)	C19	C38	1.39(3)
Mn5	O17	1.892(13)	C19	C70	1.45(3)
Mn5	O18	1.945(13)	C20	C39	1.39(3)
Mn5	O32	2.118(13)	C20	C74	1.36(4)
Mn6	O6	1.860(13)	C21	C39	1.42(3)
Mn6	O8	2.365(13)	C21	C77	1.54(3)
Mn6	O9	1.985(13)	C22	C45	1.39(3)
Mn6	O12	1.924(14)	C22	C104	1.46(3)
Mn6	O21	1.960(13)	C23	C51	1.39(3)
Mn6	O28	2.090(13)	C23	C91	1.38(3)
Mn7	O7	2.258(13)	C24	C26	1.38(3)
Mn7	O9	2.383(13)	C24	C61	1.33(3)
Mn7	O14	2.236(13)	C24	C86	1.39(3)
Mn7	O15	2.298(13)	C25	C43	1.40(3)
Mn7	O27	2.068(13)	C25	C57	1.44(3)
Mn7	O37	2.075(15)	C26	C35	1.36(3)
Mn8	O3	2.365(14)	C27	C82	1.28(4)
Mn8	O8	2.249(13)	C27	C83	1.47(4)

Mn8	O13	2.231(14)	C30	C37	1.43(3)
Mn8	O17	2.227(13)	C30	C83	1.42(3)
Mn8	O31	2.086(15)	C31	C47	1.35(3)
Mn8	O38	2.074(14)	C31	C67	1.37(3)
Mn9	O3	2.020(13)	C34	C41	1.42(3)
Mn9	O10	1.886(13)	C34	C66	1.38(3)
Mn9	O11	1.878(13)	C35	C62	1.35(3)
Mn9	O15	2.301(13)	C36	C73	1.36(3)
Mn9	O24	1.936(14)	C36	C96	1.39(3)
Mn9	O30	2.088(14)	C37	C76	1.40(2)
Mn10	O2	2.341(14)	C38	C67	1.34(4)
Mn10	O11	1.867(13)	C41	C68	1.24(3)
Mn10	O14	1.926(12)	C42	C55	1.50(3)
Mn10	O15	1.977(13)	C42	C80	1.42(2)
Mn10	O19	1.985(14)	C43	C94	1.46(3)
Mn10	O29	2.112(14)	C45	C81	1.20(3)
Mn11	O2	2.005(13)	C46	C68	1.32(4)
Mn11	O3	2.321(14)	C46	C79	1.34(4)
Mn11	O4	1.960(13)	C48	C69	1.40(3)
Mn11	O11	1.866(13)	C48	C91	1.25(4)
Mn11	O13	1.911(14)	C49	C74	1.40(3)
Mn11	O20	2.121(13)	C50	C63	1.33(3)
Mn12	O2	2.366(13)	C50	C78	1.43(3)
Mn12	O9	2.227(13)	C51	C65	1.50(3)
Mn12	O12	2.208(14)	C52	C59	1.43(2)
Mn12	O14	2.228(13)	C53	C60	1.31(3)
Mn12	O23	2.043(12)	C54	C71	1.26(2)
Mn12	O35	2.071(13)	C54	C103	1.44(3)
Mn13	O2	2.245(14)	C56	C63	1.40(3)
Mn13	O8	2.341(13)	C56	C93	1.37(5)
Mn13	O12	2.208(13)	C57	C60	1.40(3)
Mn13	O13	2.221(14)	C58	C59	1.31(3)
Mn13	O25	2.068(15)	C58	C80	1.29(3)
Mn13	O33	2.036(14)	C61	C84	1.43(4)
O4	C1	1.23(2)	C62	C84	1.43(4)
O5	C4	1.34(2)	C63	C75	1.54(3)
O7	C44	1.45(2)	C64	C98	1.28(3)
O10	C33	1.41(2)	C64	C104	1.19(5)
O12	C29	1.48(2)	C65	C69	1.42(3)
O13	C40	1.45(2)	C66	C79	1.38(3)
O14	C32	1.44(2)	C66	C102	1.59(5)
O16	C2	1.25(2)	C71	C72	1.43(3)
O17	C28	1.45(2)	C72	C88	1.30(4)
O18	C2	1.34(2)	C73	C87	1.37(3)
O19	C3	1.25(2)	C73	C92	1.40(3)

O20	C3	1.25(2)	C76	C82	1.29(4)
O21	C5	1.32(2)	C78	C90	1.41(3)
O22	C14	1.27(2)	C81	C89	1.33(3)
O23	C13	1.28(2)	C81	C98	1.60(3)
O24	C6	1.24(2)	C81	C99	1.80(3)
O25	C13	1.26(2)	C83	C85	1.64(4)
O26	C14	1.26(2)	C88	C101	1.72(3)
O27	C17	1.29(2)	C89	C99	1.60(3)
O28	C4	1.24(2)	C90	C93	1.51(4)
O29	C6	1.31(2)	C92	C95	1.26(5)
O30	C1	1.27(2)	C95	C100	1.48(5)
O31	C16	1.27(2)	C96	C100	1.52(4)
O32	C5	1.23(2)	C96	C105	1.70(8)
O33	C12	1.26(2)	C97	C101	1.46(3)
O34	C11	1.29(3)	C98	C99	1.43(4)
O35	C17	1.26(2)	C101	C103	1.37(2)

Table II.2.1.5 Bond Angles for ab52414a.

Atom	Atom	Atom	Angle/°	Atom	Atom	Atom	Angle/°
O3	Mn1	O1	71.3(4)	Mn3	O9	Mn6	102.5(6)
O10	Mn1	O1	86.1(5)	Mn3	O9	Mn7	96.8(5)
O10	Mn1	O3	74.3(5)	Mn3	O9	Mn12	101.0(5)
O17	Mn1	O1	80.8(5)	Mn4	O9	Mn7	85.8(4)
O17	Mn1	O3	87.5(5)	Mn6	O9	Mn4	85.1(5)
O17	Mn1	O10	160.3(5)	Mn6	O9	Mn7	158.8(6)
O26	Mn1	O1	88.7(5)	Mn6	O9	Mn12	97.4(5)
O26	Mn1	O3	155.5(5)	Mn12	O9	Mn4	167.0(6)
O26	Mn1	O10	90.8(5)	Mn12	O9	Mn7	87.4(5)
O26	Mn1	O17	103.5(5)	Mn1	O10	Mn2	91.1(5)
O26	Mn1	O36	107.3(5)	Mn9	O10	Mn1	100.6(6)
O36	Mn1	O1	163.1(5)	Mn9	O10	Mn2	99.5(6)
O36	Mn1	O3	94.2(5)	C33	O10	Mn1	120.5(11)
O36	Mn1	O10	98.6(5)	C33	O10	Mn2	118.8(11)
O36	Mn1	O17	90.1(5)	C33	O10	Mn9	120.6(11)
O1	Mn2	O10	88.4(5)	Mn10	O11	Mn9	103.1(6)
O1	Mn2	O15	72.7(4)	Mn11	O11	Mn9	102.8(6)
O7	Mn2	O1	73.5(5)	Mn11	O11	Mn10	103.7(6)
O7	Mn2	O10	160.5(5)	Mn6	O12	Mn12	99.9(6)
O7	Mn2	O15	86.4(4)	Mn6	O12	Mn13	101.0(6)
O10	Mn2	O15	81.3(5)	Mn12	O12	Mn13	93.9(5)
O22	Mn2	O1	92.2(5)	C29	O12	Mn6	119.3(11)
O22	Mn2	O7	98.4(5)	C29	O12	Mn12	118.9(11)
O22	Mn2	O10	89.2(5)	C29	O12	Mn13	119.1(11)

O22	Mn2	O15	162.2(5)	Mn11	O13	Mn8	101.5(6)
O34	Mn2	O1	155.9(5)	Mn11	O13	Mn13	100.1(6)
O34	Mn2	O7	90.6(5)	Mn13	O13	Mn8	92.4(5)
O34	Mn2	O10	104.2(5)	C40	O13	Mn8	118.5(12)
O34	Mn2	O15	88.7(5)	C40	O13	Mn11	120.3(12)
O34	Mn2	O22	108.2(6)	C40	O13	Mn13	118.9(12)
O1	Mn3	O9	88.8(6)	Mn10	O14	Mn7	100.0(5)
O1	Mn3	O15	91.1(5)	Mn10	O14	Mn12	101.3(5)
O2	Mn3	O1	178.5(8)	Mn12	O14	Mn7	91.1(5)
O2	Mn3	O9	89.7(6)	C32	O14	Mn7	121.3(11)
O2	Mn3	O15	88.9(6)	C32	O14	Mn10	120.7(11)
O3	Mn3	O1	91.1(6)	C32	O14	Mn12	116.8(11)
O3	Mn3	O2	90.3(6)	Mn3	O15	Mn2	95.6(5)
O3	Mn3	O9	179.6(8)	Mn3	O15	Mn7	99.3(5)
O3	Mn3	O15	89.3(6)	Mn3	O15	Mn9	91.6(5)
O8	Mn3	O1	89.5(6)	Mn3	O15	Mn10	102.8(6)
O8	Mn3	O2	90.4(6)	Mn7	O15	Mn2	87.4(4)
O8	Mn3	O3	89.3(6)	Mn7	O15	Mn9	167.9(6)
O8	Mn3	O9	90.3(6)	Mn9	O15	Mn2	86.3(4)
O8	Mn3	O15	178.4(8)	Mn10	O15	Mn2	160.2(6)
O9	Mn3	O15	91.1(6)	Mn10	O15	Mn7	96.4(5)
O1	Mn4	O9	76.5(5)	Mn10	O15	Mn9	86.2(5)
O1	Mn4	O16	90.7(5)	C2	O16	Mn4	127.0(13)
O5	Mn4	O1	168.9(6)	Mn5	O17	Mn1	102.2(5)
O5	Mn4	O9	92.4(5)	Mn5	O17	Mn8	101.5(5)
O5	Mn4	O16	100.2(5)	Mn8	O17	Mn1	91.5(5)
O6	Mn4	O1	88.5(5)	C28	O17	Mn1	118.9(10)
O6	Mn4	O5	89.6(6)	C28	O17	Mn5	117.3(10)
O6	Mn4	O7	169.8(6)	C28	O17	Mn8	120.9(11)
O6	Mn4	O9	79.1(5)	C2	O18	Mn5	126.7(12)
O6	Mn4	O16	88.0(5)	C3	O19	Mn10	126.4(12)
O7	Mn4	O1	87.6(5)	C3	O20	Mn11	125.5(12)
O7	Mn4	O5	92.4(6)	C5	O21	Mn6	125.7(12)
O7	Mn4	O9	90.8(5)	C14	O22	Mn2	130.9(13)
O7	Mn4	O16	101.5(5)	C13	O23	Mn12	130.7(11)
O16	Mn4	O9	161.9(5)	C6	O24	Mn9	129.4(13)
O6	Mn5	O1	79.0(5)	C13	O25	Mn13	129.7(12)
O6	Mn5	O8	89.2(6)	C14	O26	Mn1	133.4(13)
O6	Mn5	O17	169.3(6)	C17	O27	Mn7	129.4(12)
O6	Mn5	O18	89.2(6)	C4	O28	Mn6	127.9(12)
O6	Mn5	O32	86.9(5)	C6	O29	Mn10	124.3(13)
O8	Mn5	O1	75.5(5)	C1	O30	Mn9	124.1(11)
O8	Mn5	O32	91.1(5)	C16	O31	Mn8	133.3(12)
O17	Mn5	O1	90.4(5)	C5	O32	Mn5	126.6(13)
O17	Mn5	O8	86.4(5)	C12	O33	Mn13	133.0(13)

O17	Mn5	O18	93.5(5)	C11	O34	Mn2	131.4(14)
O17	Mn5	O32	103.0(5)	C17	O35	Mn12	128.3(12)
O18	Mn5	O1	94.4(5)	C16	O36	Mn1	131.4(13)
O18	Mn5	O8	169.9(6)	C11	O37	Mn7	129.4(14)
O18	Mn5	O32	98.8(5)	C12	O38	Mn8	129.0(13)
O32	Mn5	O1	160.5(5)	O4	C1	O30	127.2(14)
O6	Mn6	O8	79.5(5)	O4	C1	C7	116.9(15)
O6	Mn6	O9	89.4(5)	O30	C1	C7	115.9(16)
O6	Mn6	O12	168.5(6)	O16	C2	O18	123.4(17)
O6	Mn6	O21	90.2(6)	O16	C2	C9	120.6(18)
O6	Mn6	O28	87.6(5)	O18	C2	C9	115.9(17)
O9	Mn6	O8	76.1(5)	O19	C3	C8	117.1(16)
O9	Mn6	O28	90.3(5)	O20	C3	O19	125.2(15)
O12	Mn6	O8	89.1(5)	O20	C3	C8	117.6(17)
O12	Mn6	O9	86.5(6)	O5	C4	C10	116.1(16)
O12	Mn6	O21	91.9(6)	O28	C4	O5	121.7(16)
O12	Mn6	O28	103.1(5)	O28	C4	C10	122.2(17)
O21	Mn6	O8	93.5(5)	O21	C5	C45	108.4(17)
O21	Mn6	O9	169.4(6)	O32	C5	O21	125.4(17)
O21	Mn6	O28	100.2(6)	O32	C5	C45	126.0(19)
O28	Mn6	O8	161.2(5)	O24	C6	O29	124.4(19)
O7	Mn7	O9	81.4(4)	O24	C6	C103	119.4(18)
O7	Mn7	O15	87.0(5)	O29	C6	C103	116.1(19)
O14	Mn7	O7	159.2(5)	C42	C7	C1	123.4(18)
O14	Mn7	O9	84.9(4)	C52	C7	C1	115.8(17)
O14	Mn7	O15	73.8(5)	C52	C7	C42	120.8(18)
O15	Mn7	O9	72.1(4)	C21	C8	C3	124.7(18)
O27	Mn7	O7	105.9(5)	C49	C8	C3	118.2(19)
O27	Mn7	O9	91.1(5)	C49	C8	C21	117.0(18)
O27	Mn7	O14	89.9(5)	C19	C9	C2	119.4(19)
O27	Mn7	O15	157.3(5)	C19	C9	C47	122.9(19)
O27	Mn7	O37	105.4(6)	C47	C9	C2	117.7(19)
O37	Mn7	O7	89.5(5)	C43	C10	C4	122.0(19)
O37	Mn7	O9	162.9(5)	C43	C10	C53	119.1(18)
O37	Mn7	O14	99.3(5)	C53	C10	C4	118.9(18)
O37	Mn7	O15	93.0(5)	O34	C11	C36	114(2)
O8	Mn8	O3	70.0(5)	O37	C11	O34	125(2)
O13	Mn8	O3	81.2(5)	O37	C11	C36	120(2)
O13	Mn8	O8	86.4(5)	O33	C12	O38	124.5(18)
O17	Mn8	O3	84.5(4)	O33	C12	C34	120.0(18)
O17	Mn8	O8	73.4(5)	O38	C12	C34	115.4(18)
O17	Mn8	O13	158.3(5)	O23	C13	C26	116.6(17)
O31	Mn8	O3	91.0(5)	O25	C13	O23	125.9(15)
O31	Mn8	O8	155.5(5)	O25	C13	C26	117.5(18)
O31	Mn8	O13	106.5(5)	O22	C14	C30	119.6(18)

O31	Mn8	O17	89.9(5)	O26	C14	O22	122.9(18)
O38	Mn8	O3	161.4(5)	O26	C14	C30	117.5(18)
O38	Mn8	O8	93.9(5)	C54	C15	C71	40(2)
O38	Mn8	O13	88.6(5)	O31	C16	C50	118.3(16)
O38	Mn8	O17	100.2(5)	O36	C16	O31	122.4(17)
O38	Mn8	O31	106.9(6)	O36	C16	C50	119.2(18)
O3	Mn9	O15	76.6(5)	O27	C17	C51	116.9(18)
O3	Mn9	O30	90.9(5)	O35	C17	O27	127.1(17)
O10	Mn9	O3	87.4(6)	O35	C17	C51	115.9(17)
O10	Mn9	O15	92.1(5)	C9	C19	C70	126.5(19)
O10	Mn9	O24	92.2(6)	C38	C19	C9	114(2)
O10	Mn9	O30	101.1(6)	C38	C19	C70	120(2)
O11	Mn9	O3	88.7(6)	C74	C20	C39	119(2)
O11	Mn9	O10	170.8(6)	C8	C21	C39	121(2)
O11	Mn9	O15	78.9(5)	C8	C21	C77	123.8(18)
O11	Mn9	O24	89.9(6)	C39	C21	C77	115(2)
O11	Mn9	O30	87.3(5)	C45	C22	C104	112(2)
O24	Mn9	O3	168.6(6)	C91	C23	C51	121(3)
O24	Mn9	O15	92.0(5)	C26	C24	C86	125(2)
O24	Mn9	O30	100.3(6)	C61	C24	C26	121(2)
O30	Mn9	O15	161.5(5)	C61	C24	C86	114(2)
O11	Mn10	O2	79.5(5)	C43	C25	C57	117(2)
O11	Mn10	O14	169.0(6)	C24	C26	C13	123(2)
O11	Mn10	O15	88.2(6)	C35	C26	C13	115(2)
O11	Mn10	O19	88.4(6)	C35	C26	C24	122(2)
O11	Mn10	O29	88.0(5)	C82	C27	C83	125(2)
O14	Mn10	O2	89.6(5)	C37	C30	C14	118.1(18)
O14	Mn10	O15	88.4(5)	C83	C30	C14	123(2)
O14	Mn10	O19	93.1(6)	C83	C30	C37	119(2)
O14	Mn10	O29	102.4(5)	C47	C31	C67	119(2)
O15	Mn10	O2	76.5(5)	C41	C34	C12	121(2)
O15	Mn10	O19	169.8(6)	C66	C34	C12	125.7(19)
O15	Mn10	O29	89.9(6)	C66	C34	C41	113(2)
O19	Mn10	O2	93.4(5)	C62	C35	C26	120(2)
O19	Mn10	O29	99.7(6)	C73	C36	C11	119.9(18)
O29	Mn10	O2	161.7(5)	C73	C36	C96	125.6(17)
O2	Mn11	O3	76.4(5)	C96	C36	C11	114.5(19)
O2	Mn11	O20	89.6(5)	C76	C37	C30	121(2)
O4	Mn11	O2	169.7(6)	C67	C38	C19	124(2)
O4	Mn11	O3	93.3(5)	C20	C39	C21	120(2)
O4	Mn11	O20	100.3(5)	C68	C41	C34	124(3)
O11	Mn11	O2	89.0(6)	C7	C42	C55	125.2(17)
O11	Mn11	O3	80.5(5)	C7	C42	C80	113(2)
O11	Mn11	O4	89.1(6)	C80	C42	C55	121.4(18)
O11	Mn11	O13	169.9(6)	C10	C43	C25	121(2)

O11	Mn11	O20	86.6(6)	C10	C43	C94	125(2)
O13	Mn11	O2	87.4(6)	C25	C43	C94	114(2)
O13	Mn11	O3	89.5(5)	C22	C45	C5	120.9(17)
O13	Mn11	O4	92.8(6)	C81	C45	C5	112(2)
O13	Mn11	O20	102.8(6)	C81	C45	C22	127(2)
O20	Mn11	O3	161.1(5)	C68	C46	C79	120(2)
O9	Mn12	O2	71.8(4)	C31	C47	C9	119(2)
O9	Mn12	O14	89.0(5)	C91	C48	C69	118.8(18)
O12	Mn12	O2	84.0(5)	C8	C49	C74	122(2)
O12	Mn12	O9	74.3(5)	C63	C50	C16	126(2)
O12	Mn12	O14	161.0(5)	C63	C50	C78	122(2)
O14	Mn12	O2	82.2(5)	C78	C50	C16	111(2)
O23	Mn12	O2	89.1(5)	C17	C51	C65	120.6(19)
O23	Mn12	O9	156.1(5)	C23	C51	C17	120.1(19)
O23	Mn12	O12	89.9(5)	C23	C51	C65	119(2)
O23	Mn12	O14	102.8(5)	C7	C52	C59	119(2)
O23	Mn12	O35	106.0(6)	C60	C53	C10	124.0(19)
O35	Mn12	O2	164.1(5)	C15	C54	C71	109(4)
O35	Mn12	O9	94.7(5)	C15	C54	C103	114(3)
O35	Mn12	O12	100.8(5)	C71	C54	C103	135(3)
O35	Mn12	O14	89.3(5)	C93	C56	C63	117(3)
O2	Mn13	O8	71.6(5)	C60	C57	C25	120.5(18)
O12	Mn13	O2	86.9(5)	C80	C58	C59	121.8(19)
O12	Mn13	O8	83.3(5)	C58	C59	C52	119(2)
O12	Mn13	O13	160.3(5)	C53	C60	C57	118.3(18)
O13	Mn13	O2	74.6(5)	C24	C61	C84	120(2)
O13	Mn13	O8	84.4(5)	C35	C62	C84	121(3)
O25	Mn13	O2	92.8(5)	C50	C63	C56	124(2)
O25	Mn13	O8	162.0(6)	C50	C63	C75	122(2)
O25	Mn13	O12	87.0(5)	C56	C63	C75	113(2)
O25	Mn13	O13	100.5(5)	C104	C64	C98	122(2)
O33	Mn13	O2	156.8(5)	C18	C65	C51	129(2)
O33	Mn13	O8	90.2(5)	C69	C65	C18	122(2)
O33	Mn13	O12	105.6(6)	C69	C65	C51	110(2)
O33	Mn13	O13	89.8(5)	C34	C66	C79	120(2)
O33	Mn13	O25	107.1(6)	C34	C66	C102	120(2)
Mn2	O1	Mn1	87.3(4)	C79	C66	C102	119(2)
Mn2	O1	Mn5	166.8(6)	C38	C67	C31	121(2)
Mn3	O1	Mn1	95.4(5)	C41	C68	C46	122(3)
Mn3	O1	Mn2	99.9(5)	C48	C69	C65	127(2)
Mn3	O1	Mn4	103.7(6)	C54	C71	C15	31(2)
Mn3	O1	Mn5	91.9(5)	C54	C71	C72	105(2)
Mn4	O1	Mn1	159.3(6)	C72	C71	C15	136(2)
Mn4	O1	Mn2	96.9(5)	C88	C72	C71	142(3)
Mn4	O1	Mn5	85.9(5)	C36	C73	C87	132.4(17)

Mn5	O1	Mn1	85.7(4)	C36	C73	C92	119(3)
Mn3	O2	Mn10	91.7(5)	C87	C73	C92	108(2)
Mn3	O2	Mn11	101.7(6)	C20	C74	C49	121(2)
Mn3	O2	Mn12	96.9(5)	C82	C76	C37	119(3)
Mn3	O2	Mn13	100.0(6)	C90	C78	C50	116(2)
Mn10	O2	Mn12	86.3(5)	C46	C79	C66	120(2)
Mn11	O2	Mn10	84.6(5)	C58	C80	C42	126(2)
Mn11	O2	Mn12	159.5(7)	C45	C81	C89	136(3)
Mn11	O2	Mn13	96.5(6)	C45	C81	C98	115.2(19)
Mn13	O2	Mn10	167.8(6)	C45	C81	C99	149(2)
Mn13	O2	Mn12	88.8(5)	C89	C81	C98	107(2)
Mn1	O3	Mn8	87.8(5)	C89	C81	C99	59.4(17)
Mn1	O3	Mn11	166.4(6)	C98	C81	C99	49.3(15)
Mn3	O3	Mn1	101.6(6)	C27	C82	C76	124(2)
Mn3	O3	Mn8	97.9(5)	C27	C83	C85	126(2)
Mn3	O3	Mn9	102.4(6)	C30	C83	C27	112(3)
Mn3	O3	Mn11	91.5(5)	C30	C83	C85	121(2)
Mn9	O3	Mn1	96.4(5)	C61	C84	C62	117(2)
Mn9	O3	Mn8	157.9(7)	C72	C88	C101	102(2)
Mn9	O3	Mn11	84.4(5)	C81	C89	C99	75(2)
Mn11	O3	Mn8	86.6(5)	C78	C90	C93	119(2)
C1	O4	Mn11	126.6(11)	C48	C91	C23	122(3)
C4	O5	Mn4	128.3(11)	C95	C92	C73	123(3)
Mn5	O6	Mn4	102.8(6)	C56	C93	C90	119(3)
Mn6	O6	Mn4	103.0(6)	C92	C95	C100	121(2)
Mn6	O6	Mn5	103.8(6)	C36	C96	C100	113(2)
Mn2	O7	Mn7	92.1(5)	C36	C96	C105	145(3)
Mn4	O7	Mn2	100.7(5)	C100	C96	C105	88(2)
Mn4	O7	Mn7	100.8(5)	C64	C98	C81	117.5(18)
C44	O7	Mn2	119.5(10)	C64	C98	C99	146(3)
C44	O7	Mn4	119.6(10)	C99	C98	C81	72.8(15)
C44	O7	Mn7	119.0(11)	C89	C99	C81	45.4(11)
Mn3	O8	Mn5	103.0(6)	C98	C99	C81	57.9(15)
Mn3	O8	Mn6	91.0(5)	C98	C99	C89	101(2)
Mn3	O8	Mn8	102.2(6)	C95	C100	C96	117(2)
Mn3	O8	Mn13	97.3(5)	C97	C101	C88	121.8(16)
Mn5	O8	Mn6	83.8(5)	C103	C101	C88	121(2)
Mn5	O8	Mn8	96.9(5)	C103	C101	C97	117.0(16)
Mn5	O8	Mn13	157.1(7)	C54	C103	C6	118.5(19)
Mn8	O8	Mn6	166.1(6)	C101	C103	C6	128.6(18)
Mn8	O8	Mn13	88.9(5)	C101	C103	C54	112.9(16)
Mn13	O8	Mn6	85.5(4)	C64	C104	C22	126(3)
Mn3	O9	Mn4	90.9(5)				

Table II.2.1.6 Hydrogen Atom Coordinates (Å×10^4) and Isotropic Displacement Parameters (Å^2×10^3) for ab52414a.

Atom	*x*	*y*	*z*	U(eq)
H0AA	9927	6234	8640	165
H1B	14097	3873	1846	61
H1C	15173	4565	6913	122
H1E	13436	694	5427	94
H1G	3109	-326	941	127
H1HA	7929	3406	-436	52
H1HB	9044	3501	-489	52
H1HC	8840	4451	-596	52
H1IA	14455	4600	3694	61
H1IB	15106	5400	4732	61
H1IC	15191	5846	3832	61
H1K	5878	-876	-1666	60
H1LA	12834	6581	7220	52
H1LB	13931	7402	7061	52
H1LC	13714	6269	7155	52
H1MA	7462	5937	2311	53
H1MB	7381	5480	3207	53
H1MC	6714	4690	2162	53
H1O	16276	8916	6711	53
H1Q	5729	1688	-173	58
H1R	4968	-1851	391	66
H1S	17011	12482	6192	67
H1TA	13541	8038	1722	64
H1TB	14024	8837	2717	64
H1TC	12843	8557	1826	64
H1U	11455	4864	-877	129
H1XA	8798	2534	5068	50
H1XB	8966	1796	4453	50
H1XC	7865	1908	3973	50
H1Z	13521	4694	-1751	89
H2A	11673	-854	5266	67
H2B	10279	11356	1353	75
H2C	12039	11537	1968	61
H2D	9915	-888	4687	75
H2E	19011	10604	5530	68
H2F	17992	10478	7670	88
H2H	13683	2297	-523	105
H2K	4861	-2214	-1077	92
H2LA	4060	1303	2449	117
H2LB	5072	2418	2470	117
H2LC	5394	1635	2972	117
H2M	11813	4547	-2038	116

H2N	12888	1583	7564	103
H2OA	7170	-39	2304	93
H2OB	5789	-846	1883	93
H2OC	6317	389	2002	93
H2S	16021	11475	8227	87
H2TA	10889	8452	709	89
H2TB	10835	9076	-96	89
H2TC	10629	7931	-336	89
H2U	4054	21	-1098	79
H2VA	15655	10177	4579	77
H2VB	16266	11424	4734	77
H2VC	14872	10677	4276	77
H2W	6804	5724	-543	103
H2X	15033	5473	-237	100
H2Y	8769	10036	1420	55
H2ZA	17085	8427	4117	160
H2ZB	17889	9648	4193	160
H2ZC	16519	9120	3856	160
H3A	6659	4862	6515	163
H3AA	12068	9015	7985	312
H3AB	12068	8715	6987	312
H3AC	11580	7819	7504	312
H3B	7213	8262	-1693	237
H3CA	13651	2318	4182	132
H3CB	14333	2221	5210	132
H3CC	13813	2954	5130	132
H3D	7862	5631	8037	195
H7AA	14719	3164	911	251
H8AA	15566	7108	1573	328
H8AB	15856	6226	1452	328
H8AC	14980	6063	1902	328
H9AA	11585	6887	7770	890
H9AB	11453	6522	8720	890
H14	7799	6165	4454	431
H19	17350	12764	7807	71
H20	7312	784	-618	47
H21	14861	2286	8121	194
H22	14639	9787	7187	53
H25	12218	10161	2564	58
H26	9880	462	4156	46
H28A	8065	7571	1532	103
H28B	7690	8389	1653	103
H28C	8478	8223	2581	103
H29	9256	9130	-826	134
H31	2792	-859	-514	111

H33	19356	11451	7054	106
H34A	7016	4760	4786	100
H34B	6134	4205	5246	100
H34C	6637	3598	4901	100
H35A	10069	8709	8033	182
H35B	10275	9567	7422	182
H37A	10182	2198	-989	113
H37B	10179	1538	-170	113
H38	6009	6750	-1193	241
H39	15979	3908	8086	221

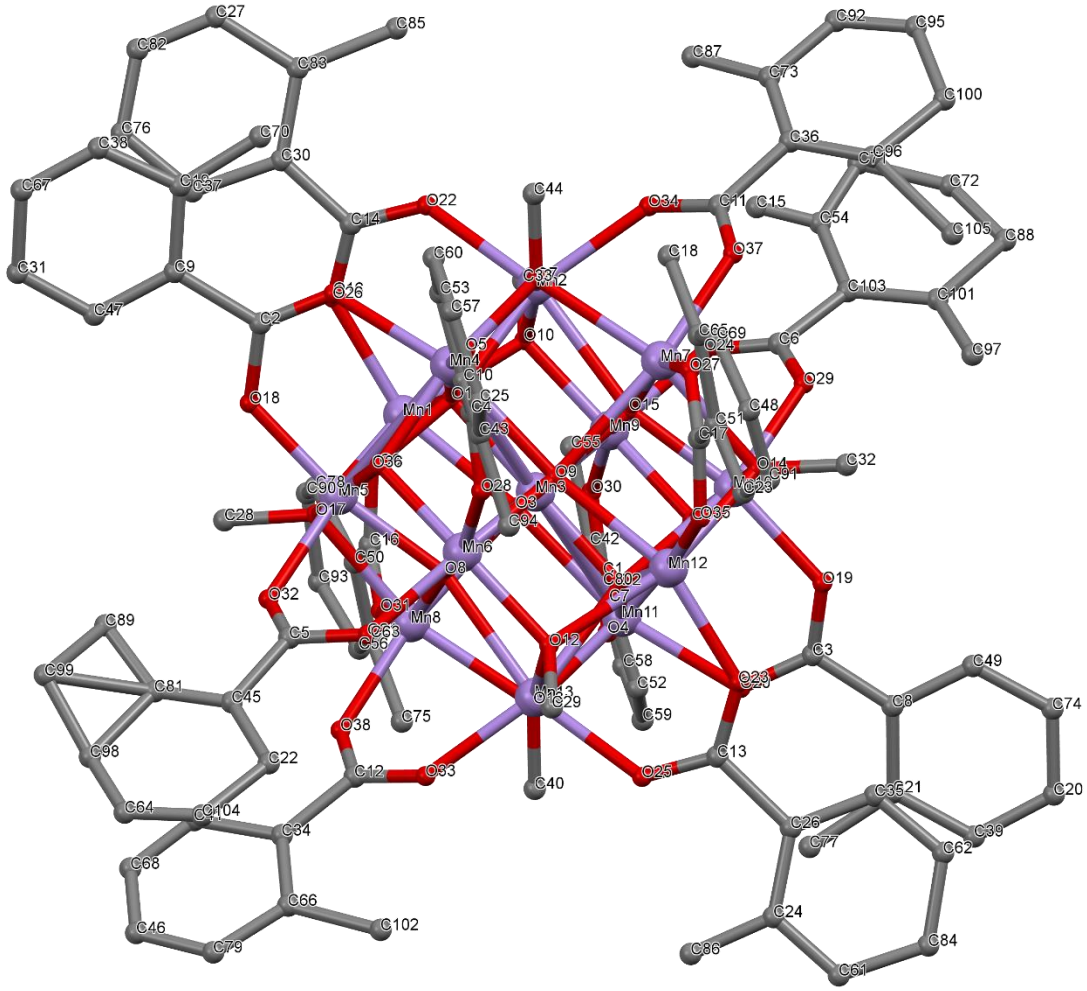

Figure II.2.1 Crystal Structure with atomic labels for compound **1**, Mn_{13}-2-Methyl, $Mn_{13}O_8(O_2CPh\text{-}o\text{-}Me)_{12}(OEt)_6$, ab52414a

II.2.2 Compound 2, Mn_{13}-2-Ethyl, $Mn_{13}O_8(O_2CPh\text{-}o\text{-}Et)_{12}(OEt)_6$, ab54113_0m

Table II.2.2.1 Crystal data and structure refinement for ab54113_0m.

Identification code	ab54113_0m
Empirical formula	$C_{120}H_{140}Mn_{13}O_{39}$
Formula weight	2920.53
Temperature/K	100.01
Crystal system	triclinic
Space group	P-1
a/Å	15.0417(14)
b/Å	15.3652(14)
c/Å	16.7271(15)
α/°	107.544(5)
β/°	98.279(5)
γ/°	116.328(5)
Volume/Å^3	3124.5(5)
Z	1
ρ_{calc}g/cm^3	1.552
μ/mm^{-1}	1.344
F(000)	1497.0
Crystal size/mm^3	0.1 × 0.1 × 0.1
Radiation	MoKα (λ = 0.71073)
2Θ range for data collection/°	2.7 to 46.154
Index ranges	-16 ≤ h ≤ 16, -16 ≤ k ≤ 16, -17 ≤ l ≤ 18
Reflections collected	38588
Independent reflections	8720 [R_{int} = 0.0628, R_{sigma} = 0.0511]
Data/restraints/parameters	8720/0/791
Goodness-of-fit on F^2	1.050
Final R indexes [I>=2σ (I)]	R_1 = 0.0578, wR_2 = 0.1727
Final R indexes [all data]	R_1 = 0.0701, wR_2 = 0.1858
Largest diff. peak/hole / e Å^{-3}	5.51/-0.73

Table II.2.2.2 Fractional Atomic Coordinates (×10^4) and Equivalent Isotropic Displacement Parameters (Å^2×10^3) for ab54113_0m. U_{eq} is defined as 1/3 of of the trace of the orthogonalised U_{IJ} tensor.

Atom	*x*	*y*	*z*	U(eq)
Mn1	10000	0	0	9.4(3)
Mn2	11075.7(7)	-1272.4(7)	70.3(5)	10.7(2)
Mn3	11925.0(7)	1870.2(7)	1737.9(6)	13.1(2)
Mn4	9539.4(7)	1024.7(7)	1735.5(6)	11.8(2)
Mn5	7632.6(7)	-954.3(7)	55.4(6)	11.6(2)
Mn6	10473.1(7)	-474.9(7)	1603.0(6)	11.1(2)
Mn7	11143.3(7)	2231.8(7)	54.1(6)	11.5(2)
O1	11272(3)	174(3)	631(3)	11.8(9)

O2	10444(3)	1427(3)	733(2)	12.3(9)
O3	9358(3)	-470(3)	810(2)	12.4(9)
O4	9378(3)	-1439(3)	2082(3)	15.9(9)
O5	11763(3)	2760(3)	-769(3)	15.9(9)
O6	11084(3)	3574(3)	807(3)	15.5(9)
O7	8222(3)	795(3)	712(3)	14.3(9)
O8	7567(3)	-2466(3)	-715(3)	13.4(9)
O9	10646(3)	-2750(3)	-609(3)	14.8(9)
O10	9817(3)	1735(3)	-710(2)	11.7(9)
O11	11730(3)	-355(3)	2261(3)	14.1(9)
O12	12317(3)	-883(3)	1156(3)	14.8(9)
O13	10892(3)	939(3)	2376(2)	13.9(9)
O14	8476(3)	276(3)	2331(3)	18.1(9)
O15	11999(3)	3243(3)	2558(3)	19.4(10)
O16	10333(3)	2631(3)	2528(3)	16.8(9)
O17	7219(3)	-1160(3)	1140(3)	16.8(9)
O18	6291(3)	-1476(3)	-943(3)	16.7(9)
O19	13396(3)	2082(3)	2204(3)	15.6(9)
C1	12342(4)	-629(4)	1949(4)	13.2(13)
C2	13986(4)	1933(4)	1778(4)	14.4(13)
C3	10316(5)	6518(5)	1873(4)	26.3(16)
C4	5976(6)	-2168(6)	3465(5)	30.4(17)
C5	8068(5)	-3070(5)	2046(4)	18.2(14)
C6	7043(5)	-4556(6)	2722(5)	31.5(17)
C7	7379(5)	-4154(5)	1481(4)	23.6(15)
C8	12259(5)	5272(5)	3018(4)	20.8(14)
C9	16870(5)	2997(5)	2220(5)	27.3(16)
C10	6626(5)	-3516(5)	-1060(4)	24.0(15)
C11	16537(5)	3007(5)	3575(5)	27.1(16)
C12	11515(5)	4493(5)	3208(4)	16.3(13)
C13	7053(5)	-1092(5)	2535(4)	17.6(14)
C14	11240(5)	5818(5)	4135(4)	22.6(15)
C15	8223(5)	-2717(5)	2966(4)	19.3(14)
C16	14727(5)	2316(5)	3721(4)	25.1(15)
C17	10232(5)	3990(5)	4084(4)	24.1(15)
C18	6273(5)	-2169(5)	2113(4)	22.3(15)
C19	10962(5)	5490(5)	1002(4)	16.6(13)
C20	14402(5)	-478(5)	1684(4)	19.7(14)
C21	12793(5)	5899(5)	1033(4)	25.5(15)
C22	14028(5)	-634(5)	2452(4)	16.9(13)
C23	6724(5)	-1107(6)	3888(4)	25.0(16)
C24	14063(5)	-1520(5)	917(4)	25.7(15)
C25	5736(6)	-2706(6)	2564(5)	30.7(17)
C26	12475(5)	6309(5)	3356(4)	23.5(15)
C27	10996(5)	4762(5)	3787(4)	16.7(13)

C28	6867(5)	-4896(6)	1817(5)	29.4(16)
C29	7276(5)	-532(5)	3447(4)	18.5(14)
C30	11074(7)	1201(7)	3332(5)	51(2)
C31	8937(5)	-1588(5)	3637(4)	25.2(15)
C32	12156(7)	1804(8)	3852(6)	61(3)
C33	7614(6)	1326(5)	3734(4)	30.0(16)
C34	8604(5)	-2362(5)	1618(4)	15.5(13)
C35	11264(5)	3376(5)	2738(4)	14.9(13)
C36	9687(5)	4730(5)	1710(4)	17.4(13)
C37	7628(5)	-616(5)	1966(4)	13.7(13)
C38	13536(5)	-818(5)	3975(4)	19.5(14)
C39	11957(5)	6574(5)	3914(4)	26.0(16)
C40	15465(5)	2568(5)	3189(4)	19.2(14)
C41	10315(5)	4632(5)	1189(4)	16.4(13)
C42	10266(5)	3585(5)	839(4)	15.6(13)
C43	15804(5)	2545(5)	1808(4)	19.3(14)
C44	14636(5)	-754(5)	3065(4)	18.6(14)
C45	15104(5)	2352(4)	2280(4)	14.4(13)
C46	7621(5)	1239(5)	1073(4)	19.4(14)
C47	14404(5)	-850(5)	3812(4)	21.5(15)
C48	9693(5)	5669(5)	2057(4)	23.9(15)
C49	13122(4)	-653(4)	2596(4)	13.1(13)
C50	7697(5)	-3491(6)	3271(5)	27.2(16)
C51	12903(5)	-723(5)	3367(4)	17.2(13)
C52	8023(5)	648(5)	3966(4)	22.6(15)
C53	10930(5)	6420(5)	1345(4)	22.7(15)
C54	11671(5)	5466(5)	459(4)	22.7(15)
C55	17223(5)	3222(6)	3115(5)	30.6(17)
C56	6457(5)	443(5)	695(5)	27.8(16)
C57	10053(6)	-1338(6)	4020(5)	41(2)
C58	15132(6)	2156(7)	4528(5)	39.9(19)
C59	5945(6)	-3632(6)	-482(5)	34.8(18)
C60	10781(6)	3736(6)	4742(5)	34.1(18)
O20	15000	5000	5000	45.0(19)

Table II.2.2.3 Anisotropic Displacement Parameters ($Å^2×10^3$) for ab54113_0m. The Anisotropic displacement factor exponent takes the form: $-2\pi^2[h^2a^{*2}U_{11}+2hka^*b^*U_{12}+\ldots]$.

Atom	U_{11}	U_{22}	U_{33}	U_{23}	U_{13}	U_{12}
Mn1	10.6(6)	9.3(6)	9.0(6)	3.1(5)	2.5(5)	6.3(5)
Mn2	11.7(5)	10.5(5)	11.8(5)	4.3(4)	4.0(4)	7.3(4)
Mn3	11.0(5)	13.7(5)	12.4(5)	1.8(4)	2.4(4)	7.2(4)
Mn4	12.1(5)	11.7(5)	11.3(5)	2.8(4)	3.7(4)	7.2(4)
Mn5	12.2(5)	11.5(5)	11.1(5)	3.6(4)	3.6(4)	6.8(4)
Mn6	13.4(5)	12.0(5)	10.2(5)	3.9(4)	3.2(4)	8.9(4)

Mn7	11.5(5)	11.2(5)	12.7(5)	4.6(4)	2.8(4)	7.1(4)
O1	11(2)	10(2)	13(2)	3.0(17)	2.5(17)	6.0(17)
O2	14(2)	10(2)	13(2)	2.1(17)	3.5(17)	7.5(18)
O3	13(2)	15(2)	12(2)	6.4(18)	3.9(17)	9.1(18)
O4	18(2)	17(2)	18(2)	9.1(19)	8.0(19)	11(2)
O5	13(2)	17(2)	19(2)	7.0(19)	4.0(18)	9.3(19)
O6	16(2)	13(2)	18(2)	3.1(18)	4.4(18)	10.5(18)
O7	15(2)	16(2)	16(2)	5.7(18)	7.4(18)	11.3(18)
O8	11(2)	14(2)	16(2)	5.5(18)	4.7(17)	7.6(18)
O9	14(2)	13(2)	18(2)	4.9(18)	6.1(18)	8.2(19)
O10	12(2)	13(2)	12(2)	5.2(17)	4.7(17)	8.7(18)
O11	14(2)	16(2)	16(2)	7.2(18)	3.6(18)	10.3(18)
O12	16(2)	17(2)	14(2)	6.6(18)	3.6(17)	10.1(19)
O13	19(2)	16(2)	6(2)	2.1(17)	1.2(17)	10.8(19)
O14	19(2)	20(2)	19(2)	8.7(19)	8.6(19)	11(2)
O15	19(2)	21(2)	13(2)	1.1(18)	3.3(18)	11(2)
O16	15(2)	15(2)	15(2)	1.2(18)	3.3(18)	7(2)
O17	18(2)	18(2)	13(2)	6.5(19)	5.1(18)	7.5(19)
O18	17(2)	19(2)	16(2)	6.0(19)	4.8(18)	11.2(19)
O19	11(2)	20(2)	16(2)	7.4(18)	3.9(18)	8.9(19)
C1	13(3)	9(3)	16(3)	7(3)	3(3)	4(3)
C2	13(3)	12(3)	21(4)	9(3)	5(3)	8(3)
C3	24(4)	16(3)	29(4)	-1(3)	0(3)	12(3)
C4	40(4)	35(4)	44(5)	31(4)	29(4)	28(4)
C5	15(3)	22(3)	26(4)	15(3)	7(3)	13(3)
C6	26(4)	28(4)	49(5)	26(4)	19(4)	12(3)
C7	24(4)	19(4)	24(4)	10(3)	5(3)	8(3)
C8	21(3)	22(4)	16(3)	4(3)	5(3)	11(3)
C9	13(3)	21(4)	48(5)	12(3)	15(3)	9(3)
C10	20(3)	11(3)	31(4)	5(3)	1(3)	4(3)
C11	26(4)	25(4)	27(4)	8(3)	0(3)	15(3)
C12	17(3)	16(3)	16(3)	6(3)	0(3)	10(3)
C13	18(3)	24(4)	19(3)	11(3)	5(3)	17(3)
C14	32(4)	20(3)	21(4)	9(3)	15(3)	15(3)
C15	16(3)	22(3)	27(4)	13(3)	9(3)	13(3)
C16	26(4)	29(4)	18(3)	10(3)	3(3)	13(3)
C17	35(4)	23(4)	20(3)	6(3)	16(3)	19(3)
C18	27(4)	27(4)	26(4)	15(3)	14(3)	20(3)
C19	20(3)	14(3)	14(3)	3(3)	0(3)	10(3)
C20	15(3)	21(3)	29(4)	14(3)	8(3)	10(3)
C21	20(4)	22(4)	31(4)	12(3)	7(3)	9(3)
C22	16(3)	13(3)	19(3)	6(3)	2(3)	6(3)
C23	36(4)	41(4)	22(4)	21(3)	17(3)	31(4)
C24	31(4)	27(4)	29(4)	17(3)	16(3)	19(3)
C25	39(4)	25(4)	41(4)	21(3)	25(4)	18(3)

C26	24(4)	14(3)	20(3)	4(3)	4(3)	3(3)
C27	21(3)	15(3)	15(3)	5(3)	4(3)	11(3)
C28	25(4)	24(4)	40(4)	18(3)	8(3)	12(3)
C29	19(3)	35(4)	18(3)	16(3)	10(3)	23(3)
C30	72(6)	39(5)	33(5)	-3(4)	-8(4)	40(5)
C31	33(4)	32(4)	20(4)	16(3)	11(3)	20(3)
C32	55(6)	63(6)	51(6)	15(5)	15(5)	25(5)
C33	33(4)	26(4)	23(4)	0(3)	9(3)	15(3)
C34	16(3)	18(4)	21(4)	8(3)	7(3)	15(3)
C35	21(4)	16(3)	9(3)	5(3)	4(3)	11(3)
C36	12(3)	18(3)	18(3)	5(3)	4(3)	7(3)
C37	15(3)	15(3)	20(4)	9(3)	8(3)	13(3)
C38	23(3)	16(3)	17(3)	8(3)	2(3)	8(3)
C39	34(4)	18(3)	23(4)	1(3)	7(3)	16(3)
C40	22(4)	17(3)	19(3)	8(3)	2(3)	11(3)
C41	16(3)	16(3)	16(3)	5(3)	-4(3)	10(3)
C42	20(4)	17(3)	11(3)	6(3)	3(3)	12(3)
C43	19(3)	16(3)	23(3)	6(3)	5(3)	11(3)
C44	13(3)	19(3)	22(3)	7(3)	3(3)	9(3)
C45	15(3)	7(3)	18(3)	4(3)	2(3)	5(3)
C46	22(3)	18(3)	25(4)	8(3)	12(3)	16(3)
C47	20(3)	22(3)	20(4)	8(3)	-1(3)	12(3)
C48	24(4)	18(3)	21(4)	-3(3)	1(3)	13(3)
C49	13(3)	13(3)	14(3)	5(3)	1(2)	7(3)
C50	34(4)	36(4)	28(4)	24(3)	19(3)	21(4)
C51	14(3)	14(3)	18(3)	3(3)	3(3)	5(3)
C52	18(3)	31(4)	16(3)	7(3)	7(3)	11(3)
C53	26(4)	12(3)	25(4)	5(3)	0(3)	10(3)
C54	28(4)	21(3)	22(4)	13(3)	8(3)	13(3)
C55	16(4)	31(4)	35(4)	7(3)	-4(3)	13(3)
C56	30(4)	30(4)	39(4)	19(3)	20(3)	22(3)
C57	34(4)	33(4)	41(5)	10(4)	-9(4)	14(4)
C58	43(5)	48(5)	24(4)	17(4)	7(3)	18(4)
C59	25(4)	31(4)	45(5)	14(4)	7(3)	13(3)
C60	49(5)	31(4)	31(4)	14(3)	22(4)	25(4)
O20	51(5)	50(5)	32(4)	14(4)	6(4)	28(4)

Table II.2.2.4 Bond Lengths for ab54113_0m.

Atom	Atom	Length/Å	Atom	Atom	Length/Å
Mn1	$O1^{1}$	1.909(4)	C5	C15	1.413(9)
Mn1	$O2^{1}$	1.898(4)	C5	C34	1.484(9)
Mn1	$O3^{1}$	1.907(4)	C6	C28	1.386(10)
Mn2	$O2^{1}$	2.351(4)	C6	C50	1.377(10)

Mn2	O7[1]	1.911(4)	C7	C28	1.393(9)
Mn2	O10[1]	1.865(4)	C8	C12	1.389(9)
Mn3	O8[1]	2.247(4)	C8	C26	1.382(9)
Mn5	O1[1]	2.256(4)	C9	C43	1.391(9)
Mn6	O10[1]	1.868(4)	C9	C55	1.391(10)
Mn7	O3[1]	2.346(4)	C10	O8	1.455(7)
Mn7	O8[1]	1.907(4)	C10	C59	1.499(10)
O1	Mn1	1.909(4)	C11	C40	1.395(9)
O1	Mn2	1.996(4)	C11	C55	1.359(10)
O1	Mn3	2.342(4)	C12	C27	1.407(9)
O1	Mn5[1]	2.256(4)	C12	C35	1.494(8)
O2	Mn1	1.898(4)	C13	C18	1.395(9)
O2	Mn2[1]	2.351(4)	C13	C29	1.409(9)
O2	Mn3	2.267(4)	C13	C37	1.512(8)
O2	Mn7	1.990(4)	C14	C27	1.396(9)
O3	Mn1	1.907(4)	C14	C39	1.382(9)
O3	Mn4	2.219(4)	C15	C31	1.500(9)
O3	Mn6	1.987(4)	C15	C50	1.396(9)
O3	Mn7[1]	2.346(4)	C16	C40	1.512(9)
O4	Mn6	2.117(4)	C16	C58	1.533(9)
O5	Mn7	1.948(4)	C17	C27	1.513(9)
O5	C34[1]	1.284(7)	C17	C60	1.525(10)
O6	Mn7	2.116(4)	C18	C25	1.366(9)
O7	Mn2[1]	1.911(4)	C19	C41	1.407(9)
O7	Mn4	2.240(4)	C19	C53	1.396(9)
O7	Mn5	2.245(4)	C19	C54	1.501(9)
O8	Mn3[1]	2.247(4)	C20	C22	1.515(9)
O8	Mn5	2.241(4)	C20	C24	1.522(9)
O8	Mn7[1]	1.907(4)	C21	C54	1.538(9)
O9	Mn2	1.948(4)	C22	C44	1.385(9)
O9	C42[1]	1.291(7)	C22	C49	1.408(8)
O10	Mn2[1]	1.865(4)	C23	C29	1.391(9)
O10	Mn6[1]	1.868(4)	C26	C39	1.381(9)
O10	Mn7	1.878(4)	C29	C52	1.506(9)
O11	Mn6	1.947(4)	C30	O13	1.478(9)
O12	Mn2	2.126(4)	C30	C32	1.425(12)
O13	Mn3	2.242(4)	C31	C57	1.533(10)
O13	Mn4	2.236(4)	C33	C52	1.536(10)
O13	Mn6	1.909(4)	C34	O4	1.257(7)
O14	Mn4	2.095(4)	C34	O5[1]	1.284(7)
O15	Mn3	2.085(4)	C35	O15	1.271(7)
O16	Mn4	2.057(4)	C35	O16	1.260(7)
O17	Mn5	2.068(4)	C36	C41	1.399(9)
O18	Mn5	2.072(4)	C36	C48	1.378(9)
O18	C2[1]	1.264(7)	C37	O14	1.265(7)

O19	Mn3	2.079(4)	C37	O17	1.260(7)
C1	O11	1.282(7)	C38	C47	1.390(9)
C1	O12	1.255(7)	C38	C51	1.377(9)
C1	C49	1.500(8)	C40	C45	1.419(8)
C2	O18[1]	1.264(7)	C41	C42	1.500(8)
C2	O19	1.269(7)	C42	O6	1.247(7)
C2	C45	1.502(8)	C42	O9[1]	1.291(7)
C3	C48	1.383(10)	C43	C45	1.388(9)
C3	C53	1.391(10)	C44	C47	1.377(9)
C4	C23	1.368(10)	C46	O7	1.451(7)
C4	C25	1.383(10)	C46	C56	1.510(9)
C5	C7	1.408(9)	C49	C51	1.398(8)

[1]2-X,-Y,-Z

Table II.2.2.5 Bond Angles for ab54113_0m.

Atom	Atom	Atom	Angle/°	Atom	Atom	Atom	Angle/°
O1[1]	Mn1	O1	180.0	Mn6	O3	Mn7[1]	84.82(14)
O2[1]	Mn1	O1	89.69(16)	C34	O4	Mn6	125.4(4)
O2	Mn1	O1	90.31(16)	C34[1]	O5	Mn7	128.9(4)
O2	Mn1	O1[1]	89.70(16)	C42	O6	Mn7	125.3(4)
O2[1]	Mn1	O1[1]	90.31(16)	Mn2[1]	O7	Mn4	101.13(17)
O2	Mn1	O2[1]	180.00(16)	Mn2[1]	O7	Mn5	99.97(16)
O2[1]	Mn1	O3[1]	90.05(16)	Mn4	O7	Mn5	90.57(14)
O2	Mn1	O3	90.05(16)	C46	O7	Mn2[1]	120.2(3)
O2[1]	Mn1	O3	89.95(16)	C46	O7	Mn4	114.3(3)
O2	Mn1	O3[1]	89.95(16)	C46	O7	Mn5	124.7(3)
O3[1]	Mn1	O1	90.18(16)	Mn5	O8	Mn3[1]	91.19(14)
O3	Mn1	O1	89.82(16)	Mn7[1]	O8	Mn3[1]	100.12(16)
O3[1]	Mn1	O1[1]	89.82(16)	Mn7[1]	O8	Mn5	101.47(17)
O3	Mn1	O1[1]	90.18(16)	C10	O8	Mn3[1]	115.5(3)
O3	Mn1	O3[1]	180.0	C10	O8	Mn5	123.5(3)
O1	Mn2	O2[1]	75.79(15)	C10	O8	Mn7[1]	119.4(4)
O1	Mn2	O12	90.65(15)	C42[1]	O9	Mn2	127.3(4)
O7[1]	Mn2	O1	87.58(16)	Mn2[1]	O10	Mn6[1]	104.04(18)
O7[1]	Mn2	O2[1]	89.98(15)	Mn2[1]	O10	Mn7	103.24(18)
O7[1]	Mn2	O9	92.81(17)	Mn6[1]	O10	Mn7	103.14(18)
O7[1]	Mn2	O12	103.43(16)	C1	O11	Mn6	127.8(4)
O9	Mn2	O1	169.88(16)	C1	O12	Mn2	125.8(4)
O9	Mn2	O2[1]	94.10(15)	Mn4	O13	Mn3	92.26(14)
O9	Mn2	O12	99.08(16)	Mn6	O13	Mn3	100.23(16)
O10[1]	Mn2	O1	89.02(16)	Mn6	O13	Mn4	99.01(16)
O10[1]	Mn2	O2[1]	79.23(15)	C30	O13	Mn3	127.9(4)
O10[1]	Mn2	O7[1]	169.19(17)	C30	O13	Mn4	113.0(4)
O10[1]	Mn2	O9	88.76(16)	C30	O13	Mn6	118.3(4)

O10[1]	Mn2	O12	86.87(16)	C37	O14	Mn4	127.9(4)
O12	Mn2	O2[1]	160.61(15)	C35	O15	Mn3	129.4(4)
O2	Mn3	O1	71.67(13)	C35	O16	Mn4	133.3(4)
O8[1]	Mn3	O1	85.19(14)	C37	O17	Mn5	134.1(4)
O8[1]	Mn3	O2	73.63(14)	C2[1]	O18	Mn5	132.3(4)
O13	Mn3	O1	83.03(14)	C2	O19	Mn3	129.6(4)
O13	Mn3	O2	87.55(14)	O11	C1	C49	115.9(5)
O13	Mn3	O8[1]	160.20(14)	O12	C1	O11	124.8(5)
O15	Mn3	O1	161.22(15)	O12	C1	C49	119.3(5)
O15	Mn3	O2	90.70(15)	O18[1]	C2	O19	124.5(5)
O15	Mn3	O8[1]	96.20(15)	O18[1]	C2	C45	116.5(5)
O15	Mn3	O13	89.99(15)	O19	C2	C45	119.0(5)
O19	Mn3	O1	93.18(14)	C48	C3	C53	120.0(6)
O19	Mn3	O2	157.73(15)	C23	C4	C25	120.1(6)
O19	Mn3	O8[1]	89.27(15)	C7	C5	C15	119.8(6)
O19	Mn3	O13	107.20(15)	C7	C5	C34	116.2(6)
O19	Mn3	O15	105.55(16)	C15	C5	C34	124.0(6)
O3	Mn4	O2	71.88(14)	C50	C6	C28	119.7(6)
O3	Mn4	O7	89.06(14)	C28	C7	C5	121.0(6)
O3	Mn4	O13	74.53(14)	C26	C8	C12	121.5(6)
O7	Mn4	O2	82.26(14)	C43	C9	C55	118.8(6)
O13	Mn4	O2	85.36(14)	O8	C10	C59	114.0(5)
O13	Mn4	O7	161.91(14)	C55	C11	C40	122.5(6)
O14	Mn4	O2	164.62(15)	C8	C12	C27	120.0(5)
O14	Mn4	O3	94.91(15)	C8	C12	C35	117.2(5)
O14	Mn4	O7	89.85(15)	C27	C12	C35	122.7(5)
O14	Mn4	O13	98.94(15)	C18	C13	C29	119.4(6)
O16	Mn4	O2	88.33(15)	C18	C13	C37	116.1(5)
O16	Mn4	O3	155.16(16)	C29	C13	C37	124.4(6)
O16	Mn4	O7	103.35(15)	C39	C14	C27	121.5(6)
O16	Mn4	O13	89.38(15)	C5	C15	C31	125.0(6)
O16	Mn4	O14	106.39(16)	C50	C15	C5	117.0(6)
O1[1]	Mn5	O3	71.25(14)	C50	C15	C31	117.9(6)
O7	Mn5	O1[1]	73.86(14)	C40	C16	C58	114.6(6)
O7	Mn5	O3	85.04(14)	C27	C17	C60	112.2(6)
O8	Mn5	O1[1]	87.36(14)	C25	C18	C13	121.8(6)
O8	Mn5	O3	81.72(13)	C41	C19	C54	124.6(5)
O8	Mn5	O7	159.75(15)	C53	C19	C41	117.0(6)
O17	Mn5	O1[1]	154.84(15)	C53	C19	C54	118.4(6)
O17	Mn5	O3	88.14(14)	C22	C20	C24	113.4(5)
O17	Mn5	O7	90.54(15)	C44	C22	C20	117.1(5)
O17	Mn5	O8	104.23(15)	C44	C22	C49	117.5(6)
O17	Mn5	O18	108.64(16)	C49	C22	C20	125.4(5)
O18	Mn5	O1[1]	93.94(15)	C4	C23	C29	122.5(6)
O18	Mn5	O3	161.83(15)	C18	C25	C4	119.0(7)

O18	Mn5	O7	101.25(15)	C39	C26	C8	118.7(6)
O18	Mn5	O8	87.27(15)	C12	C27	C17	124.0(5)
O3	Mn6	O1	76.11(15)	C14	C27	C12	117.6(6)
O3	Mn6	O4	91.66(16)	C14	C27	C17	118.3(5)
O4	Mn6	O1	161.47(15)	C6	C28	C7	119.2(6)
O10[1]	Mn6	O1	78.79(15)	C13	C29	C52	125.0(6)
O10[1]	Mn6	O3	89.32(16)	C23	C29	C13	117.2(6)
O10[1]	Mn6	O4	87.33(16)	C23	C29	C52	117.7(6)
O10[1]	Mn6	O11	89.43(16)	C32	C30	O13	113.6(8)
O10[1]	Mn6	O13	168.99(17)	C15	C31	C57	112.5(6)
O11	Mn6	O1	93.18(15)	O4	C34	O5[1]	123.8(5)
O11	Mn6	O3	169.26(17)	O4	C34	C5	120.2(5)
O11	Mn6	O4	98.94(16)	O5[1]	C34	C5	115.9(5)
O13	Mn6	O1	90.20(15)	O15	C35	C12	117.7(5)
O13	Mn6	O3	87.64(16)	O16	C35	O15	124.3(5)
O13	Mn6	O4	103.34(16)	O16	C35	C12	118.0(5)
O13	Mn6	O11	91.59(16)	C48	C36	C41	120.9(6)
O2	Mn7	O3[1]	76.19(15)	O14	C37	C13	119.6(5)
O2	Mn7	O6	91.95(15)	O17	C37	O14	124.1(5)
O5	Mn7	O2	169.26(16)	O17	C37	C13	116.3(5)
O5	Mn7	O3[1]	93.08(15)	C51	C38	C47	119.0(6)
O5	Mn7	O6	98.41(16)	C26	C39	C14	120.6(6)
O6	Mn7	O3[1]	161.56(15)	C11	C40	C16	120.7(6)
O8[1]	Mn7	O2	87.88(16)	C11	C40	C45	117.1(6)
O8[1]	Mn7	O3[1]	90.07(15)	C45	C40	C16	122.2(5)
O8[1]	Mn7	O5	92.37(17)	C19	C41	C42	121.8(5)
O8[1]	Mn7	O6	103.75(16)	C36	C41	C19	120.6(5)
O10	Mn7	O2	89.09(16)	C36	C41	C42	117.6(5)
O10	Mn7	O3[1]	79.01(15)	O6	C42	O9[1]	124.9(5)
O10	Mn7	O5	88.67(16)	O6	C42	C41	119.5(5)
O10	Mn7	O6	86.85(16)	O9[1]	C42	C41	115.6(5)
O10	Mn7	O8[1]	169.07(17)	C45	C43	C9	121.0(6)
Mn1	O1	Mn2	103.01(17)	C47	C44	C22	122.4(6)
Mn1	O1	Mn3	97.23(15)	C40	C45	C2	123.8(5)
Mn1	O1	Mn5[1]	101.05(16)	C43	C45	C2	116.1(5)
Mn2	O1	Mn3	157.6(2)	C43	C45	C40	120.0(5)
Mn2	O1	Mn5[1]	97.03(15)	O7	C46	C56	112.3(5)
Mn5[1]	O1	Mn3	88.41(13)	C44	C47	C38	119.9(6)
Mn1	O2	Mn2[1]	91.39(15)	C36	C48	C3	119.4(6)
Mn1	O2	Mn3	100.10(16)	C22	C49	C1	123.3(5)
Mn1	O2	Mn7	103.01(18)	C51	C49	C1	116.9(5)
Mn3	O2	Mn2[1]	167.69(19)	C51	C49	C22	119.8(5)
Mn7	O2	Mn2[1]	84.62(14)	C6	C50	C15	123.2(6)
Mn7	O2	Mn3	96.96(16)	C38	C51	C49	121.3(6)
Mn1	O3	Mn4	101.00(17)	C29	C52	C33	113.3(5)

Mn1	O3	Mn6	103.23(18)	C3	C53	C19	122.1(6)
Mn1	O3	Mn7[1]	90.78(15)	C19	C54	C21	112.5(5)
Mn4	O3	Mn7[1]	167.2(2)	C11	C55	C9	120.4(6)
Mn6	O3	Mn4	97.24(16)				

[1]2-X,-Y,-Z

Table II.2.2.6 Hydrogen Atom Coordinates (Å×10^4) and Isotropic Displacement Parameters (Å^2×10^3) for ab54113_0m.

Atom	*x*	*y*	*z*	U(eq)
H1	14250(40)	4860(40)	4240(30)	-1(12)
H10A	7767	1867	942	23
H10B	7849	1483	1725	23
H11A	8700	844	3853	27
H11B	8157	817	4607	27
H11C	11693	5896	117	27
H11D	11377	4723	31	27
H11E	6230	188	49	42
H11F	6081	784	939	42
H11G	6304	-161	854	42
H11H	10359	-1426	3544	61
H11I	10032	-1825	4293	61
H11J	10482	-602	4469	61
H11K	15277	1578	4334	60
H11L	14600	1973	4823	60
H11M	15778	2815	4943	60
H11N	5344	-4363	-742	52
H11O	5693	-3135	-435	52
H11P	6351	-3473	110	52
H12A	11180	3443	4473	51
H12B	10256	3213	4898	51
H12C	11260	4390	5278	51
H63	10323	7167	2107	32
H64	5620	-2534	3791	36
H66	6714	-5056	2962	38
H67	7261	-4384	861	28
H68	12627	5088	2648	25
H69	17349	3149	1898	33
H70A	6835	-4055	-1136	29
H70B	6211	-3668	-1653	29
H71	16798	3163	4184	33
H74	10907	6022	4532	27
H76A	14052	1661	3327	30
H76B	14588	2904	3927	30
H77A	9718	3321	3560	29
H77B	9842	4299	4364	29

H78	6110	-2538	1494	27
H80A	15177	-35	1901	24
H80B	14126	-86	1466	24
H81A	13243	5943	659	38
H81B	12788	5421	1311	38
H81C	13065	6611	1493	38
H83	6873	-751	4506	30
H84A	14305	-1368	435	39
H84B	13297	-1969	704	39
H84C	14370	-1892	1119	39
H85	5206	-3439	2264	37
H86	12971	6830	3207	28
H88	6403	-5627	1430	35
H90A	10738	1608	3553	61
H90B	10732	530	3413	61
H91A	8647	-1457	4125	30
H91B	8961	-1100	3354	30
H92A	12509	1434	3609	92
H92B	12222	1885	4465	92
H92C	12481	2510	3839	92
H93A	7462	1150	3097	45
H93B	8147	2083	4069	45
H93C	6972	1177	3887	45
H96	9250	4141	1826	21
H98	13382	-861	4498	23
H99	12093	7283	4148	31
H103	15552	2367	1193	23
H104	15236	-771	2967	22
H107	14836	-938	4215	26
H108	9275	5733	2419	29
H110	7794	-3272	3888	33
H111	12307	-704	3473	21
H113	11341	7004	1214	27
H115	17948	3527	3405	37

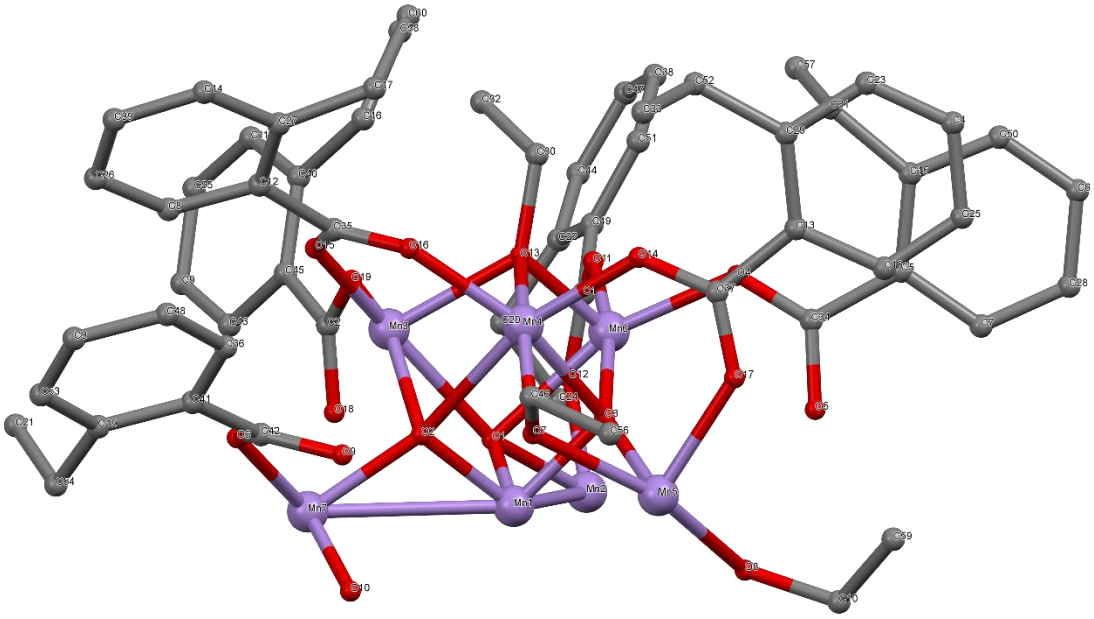

Figure II.2.2 Crystal Structure with atomic labels for compound **2**, Mn_{13}-2-Ethyl, $Mn_{13}O_8(O_2CPh\text{-}o\text{-}Et)_{12}(OEt)_6$, ab54113_0m

II.2.3 Compound 3, Mn_{13}-2-Phenyl, $Mn_{13}O_8(O_2CPh\text{-}o\text{-}Ph)_{12}(OEt)_6$, ab10813_0m

Table II.2.3.1 Crystal data and structure refinement for ab10813_0m.

Identification code	ab10813_0m
Empirical formula	$C_{168}H_{138}Mn_{13}O_{38}$
Formula weight	3479.00
Temperature/K	100.02
Crystal system	monoclinic
Space group	C2/c
a/Å	28.1239(8)
b/Å	18.1122(6)
c/Å	30.7895(9)
α/°	90.00
β/°	94.279(2)
γ/°	90.00
Volume/Å^3	15640.0(8)
Z	4
ρ_{calc}g/cm^3	1.477
μ/mm^{-1}	1.087
F(000)	7100.0
Crystal size/mm^3	0.69 × 0.24 × 0.1
Radiation	MoKα (λ = 0.71073)
2Θ range for data collection/°	2.66 to 36.58
Index ranges	-24 ≤ h ≤ 24, -15 ≤ k ≤ 15, -27 ≤ l ≤ 27
Reflections collected	55054
Independent reflections	5614 [R_{int} = 0.0806, R_{sigma} = 0.0359]
Data/restraints/parameters	5614/0/991
Goodness-of-fit on F^2	1.058
Final R indexes [I>=2σ (I)]	R_1 = 0.0649, wR_2 = 0.1970
Final R indexes [all data]	R_1 = 0.0805, wR_2 = 0.2129
Largest diff. peak/hole / e Å^{-3}	4.27/-0.41

Table II.2.3.2 Fractional Atomic Coordinates (×10^4) and Equivalent Isotropic Displacement Parameters (Å^2×10^3) for ab10813_0m. U_{eq} is defined as 1/3 of of the trace of the orthogonalised U_{IJ} tensor.

Atom	*x*	*y*	*z*	U(eq)
Mn1	2500	2500	0	13.9(7)
Mn2	3405.5(6)	3502.2(10)	332.0(6)	18.0(6)
Mn3	2862.7(6)	2489.3(9)	956.3(6)	16.2(6)
Mn4	1991.9(6)	1657.1(10)	686.1(6)	16.7(6)
Mn5	2350.2(6)	3987.3(9)	561.7(6)	16.1(6)
Mn6	2926.7(6)	1122.5(9)	442.9(6)	15.8(6)
Mn7	1433.9(6)	2984.0(9)	228.6(6)	16.7(6)
O1	2396(2)	1462(4)	45(2)	14.3(19)
O2	3071(2)	2398(4)	366(2)	13.5(19)

O3	2691(3)	5010(4)	502(2)	22(2)
O4	3502(3)	973(4)	818(3)	18(2)
O5	2154(3)	2653(4)	502(2)	14.8(19)
O6	1228(3)	3425(4)	815(3)	18(2)
O7	2628(3)	1520(4)	909(2)	15.1(19)
O8	1866(3)	626(5)	774(2)	21(2)
O9	1738(3)	4085(4)	66(2)	16(2)
O10	1845(3)	2049(4)	1320(3)	22(2)
O11	2998(3)	3519(4)	914(2)	18(2)
O12	3403(3)	4636(5)	302(3)	29(2)
O13	4077(3)	3168(5)	572(2)	22(2)
O14	2553(3)	2620(4)	1487(2)	19(2)
O15	3530(3)	2031(5)	1209(2)	19(2)
O16	1900(3)	3998(4)	1061(2)	19(2)
O17	1401(3)	1781(4)	342(2)	18(2)
O18	2539(3)	118(4)	559(2)	20(2)
O19	4133(3)	2058(5)	241(3)	22(2)
C1	3675(5)	1393(9)	1122(4)	21(3)
C2	4109(5)	1097(7)	1378(4)	22(3)
C3	4839(5)	397(7)	1367(5)	33(4)
C4	3116(6)	-1612(8)	959(4)	28(3)
C5	1296(5)	-1453(8)	958(4)	31(4)
C6	1477(5)	-788(8)	834(4)	29(4)
C7	3101(6)	5134(8)	386(4)	26(4)
C8	3602(6)	-1561(8)	1053(4)	37(4)
C9	5128(4)	1775(9)	144(5)	32(4)
C10	5526(5)	2012(8)	1335(5)	34(4)
C11	4780(5)	2621(7)	1207(5)	31(4)
C12	1197(5)	4700(8)	2172(4)	27(4)
C13	4437(5)	698(7)	1150(4)	27(3)
C14	4077(5)	2185(9)	2370(5)	44(4)
C15	4188(5)	1203(7)	1831(4)	23(3)
C16	2180(4)	3178(8)	2222(5)	26(3)
C17	3077(14)	7079(17)	-29(7)	21(7)
C18	1697(5)	5582(8)	1266(5)	34(4)
C19	5233(6)	856(12)	-408(8)	76(6)
C20	1811(5)	2906(9)	2871(5)	34(4)
C21	1404(5)	4615(7)	1772(4)	23(3)
C22	5040(4)	2283(9)	-190(6)	41(4)
C23	1969(6)	-648(7)	877(4)	26(4)
C24	3127(5)	1855(10)	2422(5)	41(4)
C25	4593(5)	871(8)	2036(4)	33(4)
C26	5512(5)	1818(7)	895(5)	36(4)
C27	2458(6)	6166(8)	1430(7)	51(4)
C28	3021(6)	-542(7)	1402(4)	32(4)

C29	2074(5)	3367(8)	2636(5)	36(4)
C30	5121(5)	2014(7)	613(4)	26(4)
C31	3247(6)	5925(8)	313(5)	35(4)
C32	3391(5)	1471(8)	2133(4)	30(4)
C33	2177(6)	5269(8)	1915(5)	37(4)
C34	3876(5)	1635(7)	2104(4)	25(3)
C35	1476(5)	3798(7)	1092(4)	14(3)
C36	3504(6)	-512(8)	1492(4)	34(4)
C37	2816(5)	-1108(8)	1134(4)	25(4)
C38	2526(6)	5760(9)	1810(6)	48(4)
C39	1762(5)	5157(7)	1642(5)	28(4)
C40	1264(5)	4001(8)	1509(4)	23(3)
C41	2288(5)	-1197(8)	1060(4)	25(4)
C42	4913(5)	477(8)	1817(5)	38(4)
C43	4750(5)	2406(7)	770(4)	19(3)
C44	2023(4)	2525(8)	2031(4)	21(3)
C45	948(12)	391(18)	2005(7)	30(9)
C46	3335(7)	2401(10)	2681(5)	56(5)
C47	5239(5)	1050(10)	26(6)	59(5)
C48	1602(6)	-1997(8)	1139(4)	33(4)
C49	5168(6)	2418(8)	1482(5)	34(4)
C50	2930(6)	6411(10)	91(4)	44(4)
C51	2054(7)	6075(8)	1158(5)	45(4)
C52	3796(9)	6936(13)	252(9)	113(11)
C53	1581(6)	1282(9)	2114(4)	43(4)
C54	3793(5)	-1006(9)	1322(5)	36(4)
C55	4285(4)	2563(9)	502(4)	19(3)
C56	1697(12)	27(10)	1900(5)	110(11)
C57	877(5)	4211(9)	2308(4)	32(4)
C58	3806(7)	2564(10)	2662(5)	64(5)
C59	3101(5)	3993(11)	1320(6)	76(6)
C60	1893(6)	728(10)	1999(5)	52(5)
C61	2088(6)	-1852(8)	1192(4)	31(4)
C62	1098(7)	1080(13)	2107(5)	78(6)
C63	1752(5)	2042(8)	2268(5)	30(4)
C64	1650(5)	2246(9)	2694(5)	32(4)
C65	5042(5)	2067(12)	-623(6)	50(4)
C66	5122(6)	1365(15)	-734(7)	74(6)
C67	3483(17)	7353(18)	54(9)	32(11)
C68	1212(13)	-137(18)	1901(8)	31(10)
C69	3729(7)	6155(10)	426(7)	77(6)
C70	982(5)	1368(8)	443(5)	46(4)
C71	2141(6)	2372(7)	1579(4)	20(3)
C72	734(5)	3613(8)	2052(5)	37(4)
C73	1551(5)	5421(7)	-41(5)	40(4)

C74	920(5)	3523(8)	1656(4)	28(4)
C75	1364(5)	4656(7)	69(4)	39(4)
C76	2146(6)	79(8)	724(4)	21(3)
C77	861(5)	1470(9)	917(5)	60(5)
C78	3512(6)	3659(10)	1631(6)	80(6)
C79	4010(20)	5410(30)	1068(17)	190(50)
C80	4090(11)	5655(12)	725(19)	200(20)
C81	4489(19)	4952(19)	1200(20)	390(50)
C82	4810(30)	5060(30)	1080(50)	350(80)
C83	4490(20)	5560(20)	460(20)	160(30)
C84	4800(30)	5150(40)	610(30)	180(50)

Table II.2.3.3 Anisotropic Displacement Parameters ($Å^2×10^3$) for ab10813_0m. The Anisotropic displacement factor exponent takes the form: $-2\pi^2[h^2a^{*2}U_{11}+2hka^*b^*U_{12}+\ldots]$.

Atom	U_{11}	U_{22}	U_{33}	U_{23}	U_{13}	U_{12}
Mn1	15.6(16)	12.6(16)	13.5(16)	-0.5(12)	0.7(12)	-1.4(12)
Mn2	18.8(12)	13.8(12)	21.1(12)	-3.5(9)	0.3(9)	-2.4(9)
Mn3	20.0(12)	14.6(12)	13.5(12)	-0.5(9)	-2.2(9)	0.8(9)
Mn4	19.9(12)	14.3(12)	15.9(12)	0.9(9)	0.9(9)	-0.8(9)
Mn5	18.3(12)	14.0(12)	15.4(12)	-2.2(9)	-1.8(9)	-0.3(9)
Mn6	19.3(12)	13.9(12)	13.7(12)	-0.1(9)	-1.6(9)	1.4(9)
Mn7	16.7(12)	16.0(12)	17.1(12)	-2.7(9)	-1.3(9)	-0.4(9)
O1	14(5)	11(4)	17(5)	-3(4)	-3(4)	1(4)
O2	14(5)	10(5)	16(5)	1(4)	-3(4)	0(4)
O3	26(6)	16(5)	24(5)	-3(4)	0(5)	-1(5)
O4	21(5)	20(5)	12(5)	-9(5)	-7(4)	6(4)
O5	21(5)	11(5)	13(5)	-3(4)	-3(4)	-2(4)
O6	18(5)	20(5)	17(5)	-7(4)	1(4)	-3(4)
O7	23(5)	12(5)	10(5)	0(4)	-1(4)	-3(4)
O8	28(5)	11(5)	25(5)	3(4)	3(4)	4(5)
O9	18(5)	13(5)	16(5)	-3(4)	1(4)	1(4)
O10	29(6)	24(5)	11(5)	-4(4)	1(5)	1(5)
O11	22(5)	18(5)	13(5)	-13(4)	-8(4)	-4(4)
O12	26(6)	19(6)	43(6)	-4(4)	5(5)	-8(5)
O13	22(5)	16(6)	27(6)	-10(4)	-3(4)	2(5)
O14	22(6)	16(5)	20(5)	0(4)	6(4)	1(4)
O15	23(5)	22(6)	10(5)	-4(4)	0(4)	4(5)
O16	16(6)	21(5)	18(5)	-3(4)	1(4)	2(4)
O17	8(5)	17(5)	28(5)	0(4)	-1(4)	-11(4)
O18	29(6)	14(5)	15(5)	1(4)	-1(5)	0(5)
O19	18(5)	26(6)	21(5)	-6(5)	-3(4)	-2(4)
C1	26(10)	31(11)	7(9)	0(9)	8(8)	6(9)
C2	28(10)	16(8)	20(10)	10(7)	-9(9)	-6(7)
C3	19(9)	48(10)	32(11)	-5(8)	-7(8)	16(8)

C4	33(11)	36(10)	17(8)	5(7)	12(8)	12(9)
C5	36(9)	25(10)	33(9)	5(8)	12(8)	-22(10)
C6	19(10)	34(11)	35(9)	-2(8)	5(7)	-6(8)
C7	24(11)	29(12)	26(9)	-10(7)	-1(7)	1(10)
C8	53(14)	32(11)	25(9)	8(8)	6(8)	11(9)
C9	9(8)	56(12)	31(12)	-7(11)	-4(7)	11(7)
C10	17(10)	58(11)	28(12)	14(8)	-3(8)	-5(9)
C11	18(10)	40(9)	33(11)	4(8)	-7(8)	2(7)
C12	28(9)	48(10)	4(9)	-8(7)	0(7)	12(9)
C13	29(9)	25(8)	28(9)	-11(7)	11(9)	11(8)
C14	32(9)	71(12)	27(9)	-16(10)	-2(9)	14(10)
C15	25(9)	27(9)	17(11)	-2(8)	-3(8)	8(8)
C16	36(9)	22(10)	20(11)	1(8)	3(7)	2(8)
C17	70(30)	0(20)	0(15)	13(13)	18(16)	-8(17)
C18	53(11)	7(8)	43(11)	3(8)	7(8)	6(9)
C19	72(14)	99(17)	56(15)	-45(15)	-3(11)	43(12)
C20	48(10)	32(10)	21(9)	-8(10)	-6(8)	16(8)
C21	30(9)	12(9)	25(10)	-5(8)	-11(8)	10(8)
C22	22(9)	60(11)	40(12)	-16(12)	5(8)	-5(8)
C23	57(13)	4(9)	18(8)	0(7)	6(8)	0(9)
C24	31(10)	64(12)	30(10)	27(10)	12(10)	29(10)
C25	34(10)	39(9)	24(9)	2(8)	-1(9)	13(8)
C26	17(10)	41(9)	48(13)	-4(8)	3(9)	4(7)
C27	57(13)	38(11)	58(13)	-22(11)	12(11)	-9(9)
C28	58(14)	9(9)	32(9)	8(8)	9(8)	3(8)
C29	58(11)	23(9)	26(11)	-2(9)	-2(8)	-3(8)
C30	13(9)	34(9)	29(11)	3(8)	-4(9)	0(8)
C31	57(13)	12(10)	39(10)	-24(8)	25(9)	-22(10)
C32	31(11)	41(9)	18(9)	15(8)	-1(8)	11(9)
C33	45(11)	28(10)	40(10)	-3(8)	15(10)	-11(9)
C34	34(12)	29(9)	10(9)	3(8)	-10(8)	5(8)
C35	16(10)	10(8)	18(10)	8(7)	6(9)	8(7)
C36	25(11)	46(11)	30(9)	15(8)	-5(8)	-10(10)
C37	32(11)	26(10)	16(8)	20(8)	5(8)	-10(9)
C38	57(13)	49(11)	37(12)	-14(10)	-5(9)	5(11)
C39	39(11)	15(9)	32(10)	-14(9)	7(9)	3(8)
C40	20(9)	25(9)	22(10)	11(9)	1(8)	3(8)
C41	49(12)	12(10)	15(8)	4(7)	15(8)	-11(10)
C42	39(10)	41(10)	31(11)	3(8)	-8(8)	22(8)
C43	10(9)	27(8)	21(10)	-7(7)	1(8)	-2(7)
C44	17(8)	27(10)	19(10)	5(9)	7(7)	0(7)
C45	80(20)	0(16)	10(16)	-34(13)	15(15)	-90(20)
C46	57(15)	85(14)	22(10)	-19(10)	-12(9)	36(11)
C47	44(11)	65(14)	68(16)	-22(11)	-6(9)	33(9)
C48	52(13)	21(10)	29(9)	7(8)	19(8)	-12(10)

C49	24(10)	52(10)	25(9)	-5(8)	-7(10)	-5(8)
C50	68(12)	47(13)	16(9)	-8(9)	4(9)	23(12)
C51	89(14)	9(9)	39(11)	1(8)	15(12)	7(10)
C52	120(20)	60(18)	180(20)	-98(17)	120(20)	-103(17)
C53	59(14)	61(14)	11(8)	8(9)	17(8)	-6(12)
C54	27(9)	40(10)	41(10)	18(9)	10(9)	15(10)
C55	14(10)	31(11)	13(9)	8(8)	3(7)	-14(9)
C56	310(40)	5(12)	22(11)	-14(8)	49(15)	-1(16)
C57	21(9)	56(11)	22(9)	12(10)	22(8)	9(8)
C58	51(14)	99(15)	35(11)	-29(10)	-34(10)	22(12)
C59	28(10)	125(17)	74(14)	56(14)	-12(9)	8(10)
C60	70(12)	50(14)	40(10)	-4(9)	25(9)	5(11)
C61	42(12)	24(11)	28(9)	5(7)	9(8)	5(8)
C62	50(15)	120(20)	65(13)	5(13)	26(10)	13(13)
C63	29(9)	33(11)	27(11)	-15(9)	-16(8)	17(8)
C64	35(9)	41(11)	21(10)	3(8)	15(7)	11(8)
C65	31(10)	88(16)	33(14)	-13(10)	12(8)	-11(10)
C66	41(12)	120(20)	59(15)	-49(17)	11(10)	10(12)
C67	100(40)	0(20)	7(17)	-1(15)	57(19)	10(30)
C68	90(30)	10(20)	0(15)	-19(14)	31(16)	-90(20)
C69	52(14)	49(14)	135(18)	-37(12)	30(12)	-34(13)
C70	48(11)	45(10)	44(11)	0(8)	2(8)	6(9)
C71	40(11)	10(8)	11(10)	5(7)	3(9)	16(8)
C72	32(9)	30(10)	46(12)	-14(9)	-15(9)	0(7)
C73	51(10)	11(9)	59(10)	-6(7)	13(8)	6(7)
C74	32(9)	46(10)	6(9)	-17(7)	3(7)	10(9)
C75	39(9)	40(11)	37(9)	-9(7)	-8(7)	14(9)
C76	26(10)	28(12)	10(8)	0(7)	-1(7)	-3(10)
C77	50(11)	73(12)	57(12)	-7(9)	12(9)	-10(9)
C78	73(13)	70(13)	97(15)	-16(11)	-2(12)	7(11)
C79	220(70)	110(50)	200(50)	180(40)	-200(50)	-190(50)
C80	50(20)	22(14)	520(70)	0(30)	-150(30)	-34(15)
C81	310(60)	130(30)	650(100)	190(40)	-390(70)	-220(40)
C82	100(50)	50(40)	800(200)	70(70)	-360(100)	-110(40)
C83	0(30)	30(30)	430(100)	-50(40)	-50(40)	10(20)
C84	50(50)	160(80)	340(100)	-190(80)	60(60)	-100(50)

Table II.2.3.4 Bond Lengths for ab10813_0m.

Atom	Atom	Length/Å	Atom	Atom	Length/Å
Mn1	$O1^{1}$	1.910(7)	C16	C29	1.375(17)
Mn1	$O2^{1}$	1.902(7)	C16	C44	1.378(17)
Mn1	$O5^{1}$	1.906(7)	C17	C50	1.34(3)
Mn2	$O1^{1}$	2.459(7)	C17	C67	1.25(4)

Mn2	O17[1]	2.243(8)	C18	C39	1.392(18)
Mn5	O1[1]	2.204(7)	C18	C51	1.404(19)
Mn6	O9[1]	1.926(7)	C19	C47	1.38(2)
Mn7	O2[1]	2.480(7)	C19	C66	1.38(3)
Mn7	O19[1]	2.073(9)	C20	C29	1.359(18)
O1	Mn1	1.910(7)	C20	C64	1.376(18)
O1	Mn4	2.377(7)	C21	C39	1.481(18)
O1	Mn5[1]	2.204(7)	C21	C40	1.413(17)
O1	Mn6	1.957(7)	C22	C65	1.39(2)
O2	Mn1	1.902(7)	C23	C41	1.426(18)
O2	Mn2	2.216(7)	C23	C76	1.496(18)
O2	Mn3	1.957(7)	C24	C32	1.388(18)
O2	Mn6	2.360(7)	C24	C46	1.38(2)
O3	Mn5	2.100(9)	C25	C42	1.367(17)
O4	Mn6	1.935(8)	C26	C30	1.395(17)
O5	Mn1	1.906(7)	C27	C38	1.38(2)
O5	Mn3	2.366(7)	C27	C51	1.37(2)
O5	Mn4	1.955(7)	C28	C36	1.365(18)
O5	Mn7	2.218(7)	C28	C37	1.414(18)
O6	Mn7	2.095(8)	C30	C43	1.381(17)
O7	Mn3	1.877(7)	C31	C50	1.396(19)
O7	Mn4	1.883(7)	C31	C69	1.44(2)
O7	Mn6	1.863(7)	C32	C34	1.407(18)
O8	Mn4	1.924(8)	C33	C38	1.382(19)
O9	Mn5	2.220(7)	C33	C39	1.401(18)
O9	Mn6[1]	1.926(7)	C35	O6	1.258(14)
O9	Mn7	2.241(7)	C35	O16	1.256(14)
O10	Mn4	2.145(8)	C35	C40	1.501(17)
O11	Mn2	2.199(7)	C36	C54	1.340(18)
O11	Mn3	1.910(7)	C37	C41	1.494(18)
O11	Mn5	2.218(7)	C40	C74	1.399(17)
O12	Mn2	2.056(9)	C41	C61	1.388(18)
O13	Mn2	2.066(9)	C43	C55	1.520(18)
O14	Mn3	1.923(8)	C44	C63	1.399(18)
O15	Mn3	2.145(8)	C44	C71	1.483(17)
O16	Mn5	2.065(9)	C45	C62	1.35(3)
O17	Mn2[1]	2.243(7)	C45	C68	1.27(4)
O17	Mn4	1.915(7)	C46	C58	1.36(2)
O17	Mn7	2.210(7)	C48	C61	1.391(18)
O18	Mn6	2.163(8)	C52	C67	1.28(3)
O19	Mn7[1]	2.073(9)	C52	C69	1.53(3)
C1	O4	1.275(15)	C53	C60	1.39(2)
C1	O15	1.260(15)	C53	C62	1.41(2)
C1	C2	1.501(18)	C53	C63	1.52(2)
C2	C13	1.402(17)	C55	O13	1.270(15)

C2	C15	1.407(17)	C55	O19	1.268(15)
C3	C13	1.382(17)	C56	C60	1.41(2)
C3	C42	1.391(18)	C56	C68	1.40(3)
C4	C8	1.379(18)	C57	C72	1.379(18)
C4	C37	1.381(17)	C59	O11	1.52(2)
C5	C6	1.374(17)	C59	C78	1.57(2)
C5	C48	1.395(18)	C63	C64	1.413(18)
C6	C23	1.404(17)	C65	C66	1.34(2)
C7	O3	1.253(15)	C69	C80	1.60(3)
C7	O12	1.277(15)	C70	O17	1.449(16)
C7	C31	1.513(19)	C70	C77	1.535(19)
C8	C54	1.386(19)	C71	O10	1.254(15)
C9	C22	1.387(19)	C71	O14	1.293(15)
C9	C30	1.508(19)	C72	C74	1.373(18)
C9	C47	1.40(2)	C73	C75	1.530(18)
C10	C26	1.399(18)	C75	O9	1.476(14)
C10	C49	1.351(18)	C76	O8	1.283(15)
C11	C43	1.395(17)	C76	O18	1.254(14)
C11	C49	1.382(17)	C79	C80	1.18(7)
C12	C21	1.410(17)	C79	C81	1.61(7)
C12	C57	1.351(17)	C80	C83	1.44(7)
C14	C34	1.383(18)	C81	C82	1.01(13)
C14	C58	1.40(2)	C82	C84	1.46(14)
C15	C25	1.396(17)	C83	C84	1.21(10)
C15	C34	1.482(18)			

[1]1/2-X,1/2-Y,-Z

Table II.2.3.5 Bond Angles for ab10813_0m.

Atom	Atom	Atom	Angle/°	Atom	Atom	Atom	Angle/°
O1[1]	Mn1	O1	180.0	C7	O12	Mn2	134.0(8)
O2	Mn1	O1	89.3(3)	C55	O13	Mn2	127.7(8)
O2[1]	Mn1	O1	90.7(3)	C71	O14	Mn3	127.8(8)
O2	Mn1	O1[1]	90.7(3)	C1	O15	Mn3	124.5(8)
O2[1]	Mn1	O1[1]	89.3(3)	C35	O16	Mn5	133.8(8)
O2	Mn1	O2[1]	180.0(6)	Mn4	O17	Mn2[1]	103.0(3)
O2[1]	Mn1	O5[1]	89.6(3)	Mn4	O17	Mn7	99.1(3)
O2	Mn1	O5[1]	90.4(3)	Mn7	O17	Mn2[1]	93.6(3)
O2	Mn1	O5	89.6(3)	C70	O17	Mn2[1]	109.8(7)
O2[1]	Mn1	O5	90.4(3)	C70	O17	Mn4	120.5(7)
O5[1]	Mn1	O1[1]	89.7(3)	C70	O17	Mn7	125.9(7)
O5[1]	Mn1	O1	90.3(3)	C76	O18	Mn6	125.9(8)
O5	Mn1	O1[1]	90.3(3)	C55	O19	Mn7[1]	132.3(8)
O5	Mn1	O1	89.7(3)	O4	C1	C2	115.1(13)
O5	Mn1	O5[1]	180.0(6)	O15	C1	O4	126.2(12)

O2	Mn2	O1[1]	70.7(2)	O15	C1	C2	118.6(13)
O2	Mn2	O17[1]	88.3(3)	C13	C2	C1	117.5(12)
O11	Mn2	O1[1]	82.5(3)	C13	C2	C15	120.3(11)
O11	Mn2	O2	74.0(3)	C15	C2	C1	122.2(13)
O11	Mn2	O17[1]	159.1(3)	C13	C3	C42	119.8(12)
O12	Mn2	O1[1]	87.3(3)	C8	C4	C37	120.0(13)
O12	Mn2	O2	154.7(3)	C6	C5	C48	120.0(12)
O12	Mn2	O11	91.3(3)	C5	C6	C23	121.0(13)
O12	Mn2	O13	107.9(3)	O3	C7	O12	124.9(12)
O12	Mn2	O17[1]	100.8(3)	O3	C7	C31	118.5(13)
O13	Mn2	O1[1]	163.4(3)	O12	C7	C31	116.5(13)
O13	Mn2	O2	95.6(3)	C4	C8	C54	120.5(13)
O13	Mn2	O11	103.3(3)	C22	C9	C30	120.3(14)
O13	Mn2	O17[1]	89.2(3)	C22	C9	C47	117.4(14)
O17[1]	Mn2	O1[1]	81.2(2)	C47	C9	C30	122.2(15)
O2	Mn3	O5	76.1(3)	C49	C10	C26	119.6(12)
O2	Mn3	O15	89.4(3)	C49	C11	C43	120.4(12)
O7	Mn3	O2	88.7(3)	C57	C12	C21	121.8(12)
O7	Mn3	O5	78.2(3)	C3	C13	C2	120.4(12)
O7	Mn3	O11	168.1(3)	C34	C14	C58	121.1(14)
O7	Mn3	O14	90.1(3)	C2	C15	C34	125.2(12)
O7	Mn3	O15	87.7(3)	C25	C15	C2	116.9(12)
O11	Mn3	O2	86.8(3)	C25	C15	C34	117.9(12)
O11	Mn3	O5	90.0(3)	C29	C16	C44	121.5(12)
O11	Mn3	O14	92.4(3)	C67	C17	C50	127(3)
O11	Mn3	O15	103.3(3)	C39	C18	C51	119.9(14)
O14	Mn3	O2	170.2(3)	C66	C19	C47	121.4(17)
O14	Mn3	O5	94.2(3)	C29	C20	C64	119.9(13)
O14	Mn3	O15	100.3(3)	C12	C21	C39	119.7(12)
O15	Mn3	O5	159.8(3)	C12	C21	C40	118.1(12)
O5	Mn4	O1	76.1(3)	C40	C21	C39	122.2(12)
O5	Mn4	O10	91.4(3)	C9	C22	C65	120.7(15)
O7	Mn4	O1	77.5(3)	C6	C23	C41	120.0(12)
O7	Mn4	O5	89.5(3)	C6	C23	C76	118.6(13)
O7	Mn4	O8	90.1(3)	C41	C23	C76	121.5(13)
O7	Mn4	O10	87.3(3)	C46	C24	C32	120.6(14)
O7	Mn4	O17	167.9(3)	C42	C25	C15	123.2(12)
O8	Mn4	O1	94.4(3)	C30	C26	C10	120.2(12)
O8	Mn4	O5	170.4(3)	C51	C27	C38	120.6(15)
O8	Mn4	O10	98.2(3)	C36	C28	C37	120.2(13)
O10	Mn4	O1	160.2(3)	C20	C29	C16	120.4(13)
O17	Mn4	O1	90.4(3)	C26	C30	C9	117.2(13)
O17	Mn4	O5	86.7(3)	C43	C30	C9	123.3(13)
O17	Mn4	O8	91.7(3)	C43	C30	C26	119.6(12)
O17	Mn4	O10	104.3(3)	C50	C31	C7	119.9(15)

O1[1]	Mn5	O5	70.2(3)	C50	C31	C69	119.6(14)
O1[1]	Mn5	O9	74.4(3)	C69	C31	C7	120.1(16)
O1[1]	Mn5	O11	88.2(3)	C24	C32	C34	120.2(14)
O3	Mn5	O1[1]	94.1(3)	C38	C33	C39	122.0(14)
O3	Mn5	O5	162.2(3)	C14	C34	C15	119.0(13)
O3	Mn5	O9	101.8(3)	C14	C34	C32	118.0(13)
O3	Mn5	O11	91.0(3)	C32	C34	C15	122.8(13)
O9	Mn5	O5	82.5(2)	O6	C35	C40	118.4(12)
O11	Mn5	O5	80.4(3)	O16	C35	O6	125.8(11)
O11	Mn5	O9	158.9(3)	O16	C35	C40	115.7(13)
O16	Mn5	O1[1]	152.9(3)	C54	C36	C28	121.2(14)
O16	Mn5	O3	111.5(3)	C4	C37	C28	118.2(13)
O16	Mn5	O5	85.4(3)	C4	C37	C41	120.0(13)
O16	Mn5	O9	91.4(3)	C28	C37	C41	121.7(14)
O16	Mn5	O11	99.5(3)	C27	C38	C33	119.0(14)
O1	Mn6	O2	76.1(3)	C18	C39	C21	122.7(14)
O1	Mn6	O18	89.9(3)	C18	C39	C33	118.0(13)
O4	Mn6	O1	169.0(3)	C33	C39	C21	119.3(13)
O4	Mn6	O2	93.1(3)	C21	C40	C35	124.8(13)
O4	Mn6	O18	101.1(3)	C74	C40	C21	118.2(12)
O7	Mn6	O1	89.7(3)	C74	C40	C35	117.0(13)
O7	Mn6	O2	77.8(3)	C23	C41	C37	125.0(12)
O7	Mn6	O4	90.0(3)	C61	C41	C23	117.1(13)
O7	Mn6	O9[1]	168.5(3)	C61	C41	C37	117.9(13)
O7	Mn6	O18	86.3(3)	C25	C42	C3	119.3(12)
O9[1]	Mn6	O1	87.0(3)	C11	C43	C55	117.4(12)
O9[1]	Mn6	O2	90.7(3)	C30	C43	C11	119.2(12)
O9[1]	Mn6	O4	91.2(3)	C30	C43	C55	123.1(13)
O9[1]	Mn6	O18	104.7(3)	C16	C44	C63	119.0(12)
O18	Mn6	O2	158.7(3)	C16	C44	C71	118.2(13)
O5	Mn7	O2[1]	70.0(2)	C63	C44	C71	122.7(13)
O5	Mn7	O9	88.4(3)	C68	C45	C62	125(3)
O6	Mn7	O2[1]	161.7(3)	C58	C46	C24	120.3(14)
O6	Mn7	O5	94.6(3)	C19	C47	C9	120.0(16)
O6	Mn7	O9	89.3(3)	C61	C48	C5	119.1(12)
O6	Mn7	O17	102.9(3)	C10	C49	C11	120.9(13)
O9	Mn7	O2[1]	80.7(2)	C17	C50	C31	120.3(19)
O17	Mn7	O2[1]	82.8(3)	C27	C51	C18	120.4(14)
O17	Mn7	O5	73.8(3)	C67	C52	C69	128(3)
O17	Mn7	O9	159.0(3)	C60	C53	C62	115.8(16)
O19[1]	Mn7	O2[1]	85.3(3)	C60	C53	C63	122.6(15)
O19[1]	Mn7	O5	152.6(3)	C62	C53	C63	121.5(16)
O19[1]	Mn7	O6	111.6(3)	C36	C54	C8	119.8(14)
O19[1]	Mn7	O9	99.5(3)	O13	C55	C43	117.1(13)
O19[1]	Mn7	O17	92.0(3)	O19	C55	O13	126.4(11)

Mn1	O1	Mn4	89.9(3)	O19	C55	C43	116.4(13)
Mn1	O1	Mn5[1]	104.0(3)	C68	C56	C60	124(2)
Mn1	O1	Mn6	104.0(3)	C12	C57	C72	120.7(12)
Mn5[1]	O1	Mn4	164.5(4)	C46	C58	C14	119.8(15)
Mn6	O1	Mn4	85.2(3)	O11	C59	C78	111.7(14)
Mn6	O1	Mn5[1]	97.8(3)	C53	C60	C56	117.4(18)
Mn1	O2	Mn2	103.1(3)	C41	C61	C48	122.8(13)
Mn1	O2	Mn3	104.1(3)	C45	C62	C53	122(2)
Mn1	O2	Mn6	90.6(3)	C44	C63	C53	125.1(13)
Mn2	O2	Mn6	164.8(4)	C44	C63	C64	118.4(12)
Mn3	O2	Mn2	97.2(3)	C64	C63	C53	116.4(14)
Mn3	O2	Mn6	85.7(3)	C20	C64	C63	120.8(13)
C7	O3	Mn5	128.2(8)	C66	C65	C22	121.7(17)
C1	O4	Mn6	127.7(8)	C65	C66	C19	118.7(17)
Mn1	O5	Mn3	90.2(3)	C17	C67	C52	117(3)
Mn1	O5	Mn4	104.2(3)	C45	C68	C56	116(2)
Mn1	O5	Mn7	103.8(3)	C31	C69	C52	108.8(18)
Mn4	O5	Mn3	85.3(3)	C31	C69	C80	121.4(18)
Mn4	O5	Mn7	97.6(3)	C52	C69	C80	129.5(19)
Mn7	O5	Mn3	164.4(4)	O17	C70	C77	112.6(11)
C35	O6	Mn7	127.9(8)	O10	C71	O14	125.9(11)
Mn3	O7	Mn4	103.0(3)	O10	C71	C44	120.0(13)
Mn6	O7	Mn3	104.2(3)	O14	C71	C44	114.0(13)
Mn6	O7	Mn4	103.9(3)	C74	C72	C57	119.1(13)
C76	O8	Mn4	127.7(8)	C72	C74	C40	122.1(12)
Mn5	O9	Mn7	93.7(3)	O9	C75	C73	112.1(10)
Mn6[1]	O9	Mn5	98.2(3)	O8	C76	C23	114.8(13)
Mn6[1]	O9	Mn7	103.0(3)	O18	C76	O8	125.0(12)
C75	O9	Mn5	124.7(7)	O18	C76	C23	120.2(13)
C75	O9	Mn6[1]	122.3(7)	C80	C79	C81	101(6)
C75	O9	Mn7	109.7(7)	C79	C80	C69	125(5)
C71	O10	Mn4	124.7(8)	C79	C80	C83	132(5)
Mn2	O11	Mn5	93.7(3)	C83	C80	C69	103(4)
Mn3	O11	Mn2	99.2(3)	C82	C81	C79	124(6)
Mn3	O11	Mn5	104.3(3)	C81	C82	C84	116(6)
C59	O11	Mn2	126.6(7)	C84	C83	C80	116(7)
C59	O11	Mn3	121.4(8)	C83	C84	C82	113(7)
C59	O11	Mn5	106.5(7)				

[1]1/2-X,1/2-Y,-Z

Table II.2.3.6 Hydrogen Atom Coordinates (Å×10^4) and Isotropic Displacement Parameters (Å^2×10^3) for ab10813_0m.

Atom	*x*	*y*	*z*	U(eq)
H14A	2808	4033	1478	92
H14B	3191	4496	1231	92

H15A	1036	837	388	55
H15B	707	1531	247	55
H15C	1659	5416	-336	60
H15D	1818	5552	167	60
H15E	1296	5786	-25	60
H15F	1238	4671	361	47
H15G	1098	4522	-145	47
H16A	541	1277	953	89
H16B	872	1996	992	89
H16C	1094	1201	1111	89
H16D	3802	3617	1475	121
H16E	3418	3169	1729	121
H16F	3573	3983	1884	121
H87	5065	138	1210	40
H88	2988	-1993	773	34
H89	963	-1544	921	37
H90	1265	-417	717	35
H92	3808	-1909	933	44
H94	5786	1860	1530	41
H95	4532	2909	1315	37
H96	1285	5112	2351	32
H97	4383	633	844	32
H98	4404	2307	2355	52
H100	2366	3506	2063	31
H101	2851	7376	-194	26
H102	1411	5537	1082	41
H103	5307	363	-484	91
H104	1738	3040	3157	41
H106	4978	2784	-122	49
H108	2799	1740	2440	49
H109	4648	922	2342	39
H110	5770	1553	787	43
H111	2694	6512	1358	61
H112	2823	-181	1521	39
H113	2185	3821	2759	43
H116	3243	1096	1954	36
H117	2219	5000	2180	44
H120	3637	-135	1678	41
H122	2809	5818	1996	58
H126	5184	259	1970	45
H129	617	293	2012	36
H130	3150	2667	2874	67
H131	5317	692	246	71
H132	1479	-2459	1224	40
H133	5184	2565	1779	41

H134	2607	6267	26	52
H135	2016	6348	894	54
H136	4108	7136	297	135
H138	4128	-975	1387	43
H140	1908	-357	1827	132
H141	749	4279	2582	38
H142	3951	2934	2847	76
H144	2225	820	1989	62
H145	2293	-2218	1326	37
H146	871	1441	2177	94
H148	1469	1924	2860	38
H149	4984	2426	-846	60
H150	5104	1220	-1032	88
H151	3555	7844	-27	39
H152	1089	-613	1829	37
H156	510	3269	2150	44
H158	811	3122	1476	34
H163	3731	5471	1225	227
H165	4471	4553	1397	463
H166	5091	5106	1268	414
H167	4503	5797	190	187
H168	5025	4915	436	216

Table II.2.3.7 Atomic Occupancy for ab10813_0m.

Atom	***Occupancy***	**Atom**	***Occupancy***	**Atom**	***Occupancy***
C17	0.50	C45	0.50	C67	0.50
C68	0.50	C79	0.50	C82	0.50
C83	0.50	C84	0.50	H129	0.50
H151	0.50	H152	0.50	H163	0.50
H166	0.50	H167	0.50	H168	0.50

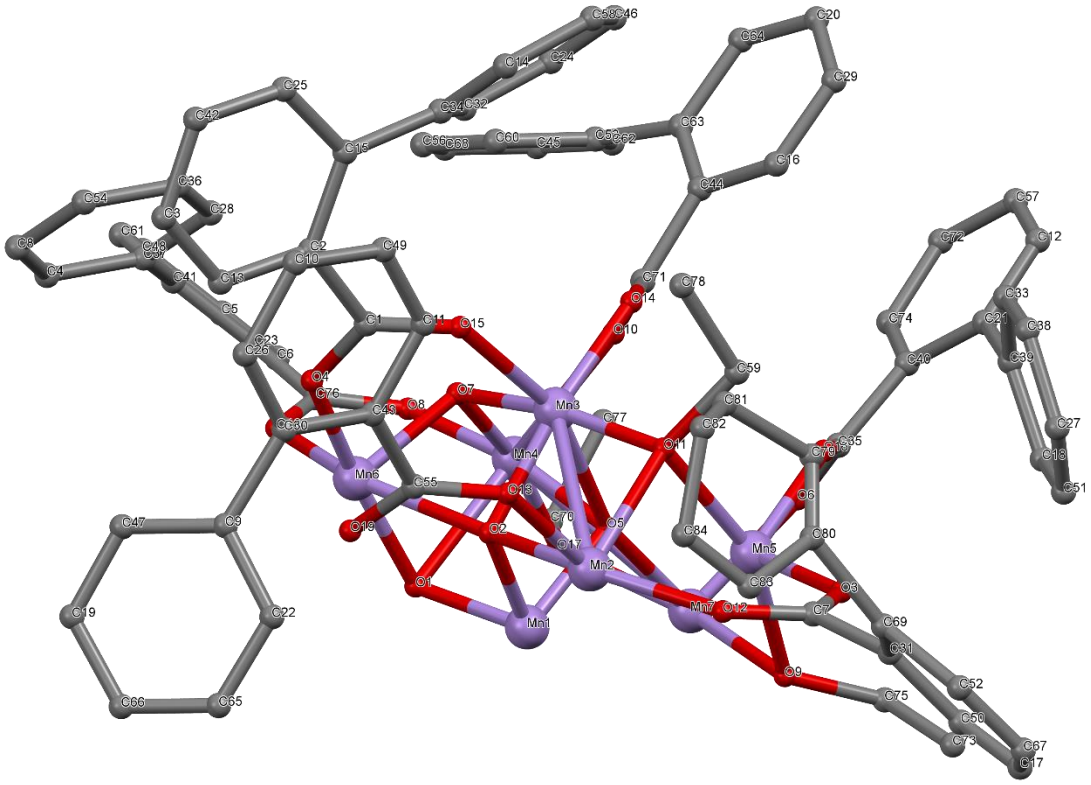

Figure II.2.3 Crystal Structure with atomic labels for compound **3**, Mn_{13}-2-Phenyl, $Mn_{13}O_8(O_2CPh\text{-}o\text{-}Ph)_{12}(OEt)_6$, ab10813_0m

II.2.4 Compound 4a, "Mn_3O-2-Methyl" (rod), $Mn_{12}O_{12}(O_2CPh\text{-}o\text{-}Me)_{16}(H_2O)_4$, ab56516

Table II.2.4.1 Crystal data and structure refinement for ab56516.

Identification code	ab56516
Empirical formula	$C_{57}H_{54}Mn_6O_{24}$
Formula weight	1452.64
Temperature/K	105(2)
Crystal system	Monoclinic
Space group	C2/c
a/Å	17.335(4)
b/Å	38.061(9)
c/Å	21.193(5)
α/°	90
β/°	98.219(15)
γ/°	90
Volume/Å^3	13839(6)
Z	8
ρ_{calc}g/cm^3	1.394
μ/mm^{-1}	1.132
F(000)	5904
Crystal size/mm^3	0.34 × 0.15 × 0.11
Radiation	MoKα (λ = 0.71073)
2Θ range for data collection/°	2.14 to 42.984
Index ranges	$-17 \le h \le 17$, $-38 \le k \le 39$, $-21 \le l \le 21$
Reflections collected	59171
Independent reflections	7707 [R_{int} = 0.0644, R_{sigma} = 0.1148]
Data/restraints/parameters	7707/0/794
Goodness-of-fit on F^2	2.850
Final R indexes [I>=2σ (I)]	R_1 = 0.2248, wR_2 = 0.5855
Final R indexes [all data]	R_1 = 0.2586, wR_2 = 0.6077
Largest diff. peak/hole / e Å^{-3}	2.9/-1.50

Table II.2.4.2 Fractional Atomic Coordinates (×10^4) and Equivalent Isotropic Displacement Parameters (Å^2×10^3) for ab56516. U_{eq} is defined as 1/3 of of the trace of the orthogonalised U_{IJ} tensor.

Atom	Atom	X	Y	Z	U(eq)
Mn1	Mn	0.0552(2)	0.34541(10)	0.20259(18)	0.0300(12)
Mn2	Mn	0.2441(2)	0.37183(10)	0.2501(2)	0.0331(12)
Mn3	Mn	-0.1969(2)	0.39537(10)	0.10625(19)	0.0328(13)
Mn4	Mn	0.1544(2)	0.34471(10)	0.1094(2)	0.0338(13)
Mn5	Mn	-0.0669(2)	0.39528(10)	0.19802(19)	0.0301(13)
Mn6	Mn	-0.0358(2)	0.36057(12)	0.0530(2)	0.0407(13)
O1	O	-0.0555(9)	0.3452(4)	0.2074(7)	0.027(4)
O2	O	0.0446(8)	0.3948(4)	0.2099(8)	0.022(4)

O3	O	-0.2183(11)	0.3982(5)	0.0139(9)	0.040(5)
O4	O	0.1383(11)	0.3400(5)	0.0169(9)	0.043(5)
O5	O	0.0492(9)	0.3504(4)	0.1159(8)	0.033(4)
O6	O	0.1606(9)	0.3480(4)	0.1991(8)	0.029(4)
O7	O	-0.2278(11)	0.3407(4)	0.0980(10)	0.046(5)
O8	O	-0.0894(9)	0.3894(4)	0.1091(9)	0.035(5)
O9	O	0.2404(10)	0.4141(4)	0.1910(9)	0.033(4)
O10	O	0.1746(10)	0.3937(4)	0.3047(9)	0.035(4)
O11	O	-0.3050(10)	0.4079(5)	0.1067(11)	0.042(6)
O12	O	0.2600(11)	0.3358(6)	0.1051(10)	0.056(6)
O13	O	0.3310(11)	0.3965(6)	0.2964(11)	0.053(6)
O14	O	0.1288(11)	0.2888(5)	0.1215(9)	0.043(5)
O15	O	-0.0934(10)	0.3109(5)	0.0822(10)	0.052(6)
O16	O	-0.1683(12)	0.4523(5)	0.1131(9)	0.049(5)
O17	O	0.0558(11)	0.2946(5)	0.1963(9)	0.042(5)
O18	O	-0.0680(10)	0.4451(4)	0.1909(9)	0.036(5)
O19	O	0.0122(12)	0.3323(5)	-0.0094(11)	0.059(6)
O20	O	-0.1207(10)	0.3658(5)	-0.0158(9)	0.045(5)
O21	O	0.2694(11)	0.3294(6)	0.3080(11)	0.059(6)
O22	O	0.1674(12)	0.3991(5)	0.0983(9)	0.045(5)
O23	O	0.3246(13)	0.3516(6)	0.2006(14)	0.075(8)
O24	O	0.0289(12)	0.4064(5)	0.0205(11)	0.057(6)
C1	C	-0.2612(16)	0.3210(8)	0.1355(18)	0.051(9)
C2	C	-0.2181(15)	0.3846(6)	-0.0979(13)	0.032(7)
C3	C	0.2097(15)	0.4205(7)	0.1361(19)	0.048(9)
C4	C	0.4859(13)	0.4188(8)	0.3316(14)	0.041(7)
C5	C	0.2527(14)	0.5178(7)	0.1323(17)	0.044(8)
C6	C	-0.2984(19)	0.3845(8)	-0.1161(16)	0.058(9)
C7	C	0.4577(15)	0.3256(9)	0.165(2)	0.093(16)
C8	C	-0.0993(15)	0.5038(6)	0.1513(13)	0.033(6)
C9	C	-0.2806(15)	0.2841(8)	0.1182(16)	0.046(8)
C10	C	0.2458(16)	0.5234(8)	0.062(2)	0.063(11)
C11	C	0.433(2)	0.4594(8)	0.4073(17)	0.066(11)
C12	C	-0.1616(16)	0.3870(8)	-0.1398(15)	0.045(8)
C13	C	-0.274(2)	0.2586(7)	0.1574(16)	0.055(9)
C14	C	-0.030(2)	0.5174(8)	0.1576(16)	0.057(9)
C15	C	0.2173(16)	0.4575(9)	0.1138(15)	0.051(8)
C16	C	0.2422(14)	0.4860(7)	0.1554(14)	0.040(7)
C17	C	-0.298(5)	0.2206(15)	0.137(6)	0.25(6)
C18	C	0.0795(18)	0.2398(8)	0.166(2)	0.060(10)
C19	C	0.252(2)	0.4815(7)	0.2271(16)	0.056(9)
C20	C	0.0865(15)	0.2736(7)	0.1587(15)	0.043(8)
C21	C	-0.0227(19)	0.5538(9)	0.1604(17)	0.062(10)

C22	C	0.3203(16)	0.3389(9)	0.1495(18)	0.051(8)
C23	C	0.4236(17)	0.4295(8)	0.3629(15)	0.051(8)
C24	C	0.2223(16)	0.4959(8)	0.0186(18)	0.057(10)
C25	C	-0.276(3)	0.3917(11)	-0.227(2)	0.105(18)
C26	C	0.065(2)	0.1778(10)	0.128(3)	0.090(14)
C27	C	-0.326(3)	0.2171(12)	0.077(3)	0.11(2)
C28	C	-0.1654(18)	0.5227(7)	0.1452(15)	0.047(8)
C29	C	-0.160(2)	0.5616(9)	0.1434(16)	0.063(9)
C30	C	0.081(3)	0.1686(13)	0.192(3)	0.11(2)
C31	C	0.091(2)	0.3261(16)	-0.086(2)	0.13(2)
C32	C	-0.091(2)	0.5766(9)	0.1513(17)	0.066(10)
C33	C	0.045(2)	0.4974(9)	0.1683(18)	0.065(10)
C34	C	0.3717(19)	0.4684(9)	0.4456(19)	0.078(13)
C35	C	-0.1123(15)	0.4641(8)	0.1506(16)	0.047(8)
C36	C	-0.325(3)	0.3889(9)	-0.180(2)	0.079(12)
C37	C	-0.304(3)	0.2756(14)	0.054(2)	0.107(16)
C38	C	0.0666(19)	0.2177(8)	0.110(2)	0.074(12)
C39	C	-0.189(3)	0.3892(9)	-0.206(3)	0.104(16)
C40	C	0.3480(19)	0.4116(8)	0.3490(15)	0.049(8)
C41	C	-0.1825(17)	0.3828(6)	-0.0270(14)	0.036(7)
C42	C	-0.357(2)	0.3829(13)	-0.071(2)	0.095(14)
C43	C	0.057(2)	0.2311(11)	0.045(2)	0.080(12)
C44	C	0.085(2)	0.3289(10)	-0.0211(18)	0.069(11)
C45	C	0.2080(19)	0.4637(8)	0.0466(17)	0.062(10)
C46	C	0.092(2)	0.2245(9)	0.224(2)	0.081(12)
C47	C	0.5677(16)	0.4621(8)	0.3857(17)	0.055(9)
C48	C	0.556(2)	0.4356(9)	0.337(2)	0.081(12)
C49	C	0.5088(19)	0.4722(9)	0.4116(19)	0.067(10)
C50	C	0.082(5)	0.1891(14)	0.238(3)	0.17(4)
C51	C	0.021(4)	0.3263(16)	-0.150(5)	0.26(6)
C53	C	0.390(3)	0.302(4)	0.122(6)	0.42(10)
C54	C	-0.315(14)	0.416(6)	0.088(12)	1.8(4)
C56	C	-0.327(3)	0.2435(14)	0.033(3)	0.12(2)
C57	C	-0.340(3)	0.3037(19)	0.003(3)	0.16(3)
C52	C	-0.0521(19)	0.4680(8)	0.0006(13)	0.050(8)
C55	C	0.451(6)	0.3640(15)	0.057(4)	0.29(6)

Table II.2.4.3 Anisotropic Displacement Parameters ($Å^2×10^3$) for ab56516. The Anisotropic displacement factor exponent takes the form: $-2\pi^2[h^2a^{*2}U_{11}+2hka^*b^*U_{12}+\ldots]$.

Atom	U_{11}	U_{22}	U_{33}	U_{12}	U_{13}	U_{23}
Mn1	0.021(2)	0.026(2)	0.043(3)	-0.0010(18)	0.0050(18)	0.0008(16)
Mn2	0.022(2)	0.032(2)	0.045(3)	0.0031(19)	0.0018(18)	-0.0036(17)

Mn3	0.023(2)	0.032(2)	0.041(3)	0.0026(19)	-0.0008(18)	0.0016(17)
Mn4	0.027(2)	0.029(2)	0.046(3)	0.0009(19)	0.0094(19)	0.0009(17)
Mn5	0.020(2)	0.023(2)	0.046(3)	0.0009(18)	0.0023(19)	0.0037(15)
Mn6	0.028(2)	0.047(3)	0.046(3)	0.002(2)	0.004(2)	-0.0013(19)
O1	0.020(9)	0.031(10)	0.029(10)	-0.003(8)	0.003(7)	0.019(7)
O2	0.010(8)	0.014(9)	0.041(11)	0.015(7)	-0.003(7)	0.004(6)
O3	0.043(11)	0.033(11)	0.038(12)	-0.011(9)	-0.013(9)	0.001(9)
O4	0.033(11)	0.055(13)	0.043(12)	-0.004(10)	0.013(10)	-0.005(10)
O5	0.019(9)	0.035(10)	0.048(11)	-0.011(9)	0.017(8)	-0.010(7)
O6	0.013(9)	0.028(9)	0.040(11)	0.009(8)	-0.014(7)	-0.002(7)
O7	0.057(13)	0.009(9)	0.075(15)	0.002(9)	0.026(11)	-0.002(9)
O8	0.021(10)	0.028(10)	0.064(13)	0.001(9)	0.028(9)	0.001(7)
O9	0.034(11)	0.026(10)	0.040(12)	0.013(9)	0.004(9)	-0.013(8)
O10	0.026(10)	0.028(10)	0.051(12)	0.007(9)	0.006(8)	0.004(8)
O11	0.012(10)	0.041(12)	0.068(16)	0.005(10)	-0.011(10)	-0.013(8)
O12	0.025(12)	0.086(17)	0.059(14)	-0.001(12)	0.012(11)	0.016(10)
O13	0.029(11)	0.064(14)	0.064(16)	-0.010(12)	-0.001(10)	-0.024(10)
O14	0.042(12)	0.037(11)	0.051(13)	-0.011(9)	0.008(10)	-0.006(9)
O15	0.015(9)	0.064(14)	0.079(15)	-0.007(11)	0.009(9)	0.001(9)
O16	0.052(14)	0.044(12)	0.050(13)	0.004(10)	0.001(11)	0.009(10)
O17	0.054(13)	0.027(11)	0.044(12)	0.001(9)	0.003(10)	-0.005(9)
O18	0.033(11)	0.019(10)	0.054(12)	0.005(9)	-0.003(9)	-0.005(8)
O19	0.040(13)	0.047(13)	0.087(17)	-0.008(11)	-0.001(12)	0.006(10)
O20	0.030(11)	0.053(13)	0.054(13)	0.000(10)	0.012(9)	-0.005(10)
O21	0.027(11)	0.084(17)	0.063(16)	0.025(13)	-0.002(10)	0.021(10)
O22	0.058(13)	0.025(10)	0.042(12)	-0.010(9)	-0.025(10)	0.001(10)
O23	0.052(15)	0.069(17)	0.10(2)	-0.034(15)	-0.023(14)	0.018(12)
O24	0.058(14)	0.025(10)	0.085(17)	0.017(10)	-0.007(12)	-0.003(9)
C1	0.028(16)	0.04(2)	0.08(3)	0.013(19)	0.003(16)	-0.033(14)
C2	0.033(16)	0.025(15)	0.041(18)	0.002(12)	0.015(14)	0.006(11)
C3	0.018(15)	0.031(17)	0.10(3)	0.024(19)	0.020(17)	-0.005(13)
C4	0.000(13)	0.07(2)	0.057(19)	-0.008(16)	0.006(12)	-0.004(13)
C5	0.015(14)	0.022(16)	0.10(3)	0.011(16)	0.019(15)	0.012(11)
C6	0.06(2)	0.05(2)	0.06(2)	0.010(16)	-0.019(18)	0.003(16)
C7	0.000(15)	0.05(2)	0.23(5)	-0.02(3)	0.00(2)	-0.006(13)
C8	0.024(16)	0.022(14)	0.050(18)	-0.011(12)	-0.003(12)	-0.003(13)
C9	0.027(15)	0.04(2)	0.07(2)	-0.026(17)	-0.016(14)	0.016(13)
C10	0.013(15)	0.05(2)	0.14(4)	0.01(2)	0.033(18)	-0.005(13)
C11	0.07(2)	0.042(19)	0.08(3)	-0.017(17)	-0.027(19)	0.016(17)
C12	0.031(17)	0.048(19)	0.06(2)	0.003(15)	0.003(15)	0.008(13)
C13	0.08(2)	0.018(16)	0.07(2)	0.003(16)	0.023(19)	-0.005(15)
C14	0.06(3)	0.04(2)	0.07(2)	-0.003(16)	0.004(18)	0.007(17)
C15	0.034(17)	0.06(2)	0.06(2)	-0.014(18)	0.006(15)	-0.011(15)

C16	0.015(14)	0.041(19)	0.06(2)	-0.006(15)	-0.007(13)	-0.009(12)
C17	0.24(9)	0.07(4)	0.51(16)	-0.14(8)	0.31(11)	-0.09(5)
C18	0.044(19)	0.03(2)	0.12(3)	0.01(2)	0.05(2)	-0.007(15)
C19	0.07(2)	0.030(17)	0.07(2)	-0.010(15)	0.027(18)	-0.016(15)
C20	0.025(15)	0.033(19)	0.07(2)	0.005(17)	0.023(15)	0.002(13)
C21	0.05(2)	0.06(2)	0.08(3)	0.009(19)	0.014(18)	-0.026(17)
C22	0.015(17)	0.06(2)	0.08(3)	-0.001(19)	0.012(17)	0.009(14)
C23	0.034(18)	0.06(2)	0.06(2)	0.005(17)	0.005(15)	-0.021(15)
C24	0.018(15)	0.040(19)	0.12(3)	0.01(2)	0.028(17)	0.011(13)
C25	0.16(5)	0.06(3)	0.09(3)	0.00(2)	0.00(3)	0.08(3)
C26	0.05(2)	0.05(2)	0.17(5)	-0.02(3)	0.01(3)	0.021(18)
C27	0.13(4)	0.02(3)	0.18(6)	-0.04(3)	0.01(4)	-0.02(2)
C28	0.048(19)	0.031(17)	0.06(2)	0.012(14)	0.006(15)	0.010(14)
C29	0.08(3)	0.05(2)	0.05(2)	-0.007(17)	0.003(18)	-0.004(19)
C30	0.07(3)	0.09(4)	0.19(6)	0.10(4)	0.04(3)	0.00(3)
C31	0.021(19)	0.25(6)	0.13(4)	-0.10(4)	0.04(2)	-0.07(3)
C32	0.07(3)	0.06(2)	0.07(3)	0.016(18)	0.001(19)	0.00(2)
C33	0.07(3)	0.05(2)	0.08(3)	-0.002(18)	0.03(2)	-0.026(18)
C34	0.05(2)	0.07(2)	0.12(3)	-0.07(2)	0.02(2)	-0.008(17)
C35	0.012(14)	0.046(19)	0.08(2)	-0.003(18)	-0.007(15)	0.006(14)
C36	0.12(4)	0.04(2)	0.09(3)	-0.02(2)	0.03(3)	0.00(2)
C37	0.12(4)	0.10(4)	0.10(4)	0.01(3)	0.00(3)	0.02(3)
C38	0.038(19)	0.03(2)	0.14(4)	-0.02(2)	-0.01(2)	-0.019(15)
C39	0.10(3)	0.03(2)	0.18(5)	0.00(2)	0.00(3)	0.04(2)
C40	0.05(2)	0.07(2)	0.028(18)	-0.022(16)	-0.011(17)	0.019(16)
C41	0.049(19)	0.006(13)	0.05(2)	-0.005(13)	0.011(16)	0.000(13)
C42	0.07(3)	0.13(4)	0.09(3)	0.03(3)	0.00(2)	-0.03(3)
C43	0.07(3)	0.08(3)	0.09(3)	-0.02(2)	0.03(2)	0.00(2)
C44	0.06(3)	0.09(3)	0.06(3)	-0.02(2)	0.04(2)	-0.03(2)
C45	0.06(2)	0.05(2)	0.08(3)	0.028(19)	0.032(18)	0.001(16)
C46	0.10(3)	0.03(2)	0.11(3)	0.02(2)	0.03(3)	0.00(2)
C47	0.021(16)	0.05(2)	0.10(3)	0.014(19)	0.022(17)	-0.025(14)
C48	0.10(3)	0.04(2)	0.11(3)	0.02(2)	0.02(2)	-0.03(2)
C49	0.03(2)	0.06(2)	0.11(3)	-0.01(2)	0.02(2)	-0.010(16)
C50	0.25(8)	0.05(3)	0.16(6)	-0.01(3)	-0.10(6)	0.03(4)
C51	0.10(5)	0.10(5)	0.59(18)	0.15(8)	0.08(8)	0.05(4)
C53	0.02(3)	0.8(3)	0.44(16)	0.28(17)	0.04(6)	0.12(9)
C54	2.0(4)	2.0(4)	2.0(4)	2.0(4)	2.0(4)	2.0(4)
C56	0.11(4)	0.06(3)	0.19(6)	-0.08(4)	0.00(4)	-0.02(3)
C57	0.10(4)	0.19(7)	0.17(6)	-0.08(5)	-0.03(4)	-0.04(4)
C52	0.08(2)	0.047(18)	0.022(15)	0.008(13)	-0.009(14)	0.029(16)
C55	0.41(12)	0.10(4)	0.28(8)	-0.17(5)	-0.24(9)	0.12(6)

Table II.2.4.4 Bond Lengths for ab56516

Atom 1	Atom 2	Length (A)
Mn1	O5	1.835(18)
Mn1	O6	1.842(16)
Mn1	O2	1.898(15)
Mn1	O1	1.906(16)
Mn1	O1	1.938(15)
Mn1	O17	1.940(18)
Mn2	O6	1.907(15)
Mn2	O13	1.922(18)
Mn2	O10	1.970(17)
Mn2	O23	2.01(3)
Mn2	O21	2.04(2)
Mn2	O9	2.035(17)
Mn3	O8	1.869(15)
Mn3	O10	1.872(18)
Mn3	O11	1.934(19)
Mn3	O3	1.942(18)
Mn3	O7	2.149(17)
Mn3	C54	2.17(16)
Mn4	O5	1.860(16)
Mn4	O12	1.877(18)
Mn4	O6	1.892(17)
Mn4	O4	1.95(2)
Mn4	O22	2.100(18)
Mn4	O14	2.196(19)
Mn5	O10	1.861(17)
Mn5	O8	1.882(19)
Mn5	O18	1.904(16)
Mn5	O2	1.913(14)
Mn5	O1	1.922(16)
Mn5	O2	1.934(16)
Mn6	O5	1.881(18)
Mn6	O20	1.929(19)
Mn6	O8	1.948(16)
Mn6	O19	1.98(2)
Mn6	O24	2.24(2)
Mn6	O15	2.26(2)
O1	Mn1	1.906(16)
O2	Mn5	1.934(16)
O3	C41	1.28(3)
O4	C44	1.22(4)
O7	C1	1.29(3)

O9	C3	1.23(4)
O10	Mn5	1.861(16)
O10	Mn3	1.872(18)
O11	C40	1.29(4)
O12	C22	1.31(4)
O13	C40	1.25(3)
O14	C20	1.29(3)
O16	C35	1.25(3)
O17	C20	1.29(3)
O18	C35	1.28(3)
O19	C44	1.32(4)
O20	C41	1.24(3)
O21	C1	1.27(4)
O22	C3	1.29(4)
O23	C22	1.18(4)
C1	O21	1.27(4)
C1	C9	1.48(4)
C2	C6	1.39(4)
C2	C12	1.42(4)
C2	C41	1.54(4)
C3	C15	1.50(4)
C4	C48	1.37(4)
C4	C23	1.41(4)
C5	C16	1.33(4)
C5	C10	1.50(5)
C6	C36	1.38(5)
C6	C42	1.49(5)
C7	C53	1.64(14)
C8	C14	1.29(4)
C8	C28	1.34(4)
C8	C35	1.53(4)
C9	C13	1.27(4)
C9	C37	1.40(6)
C10	C24	1.41(5)
C11	C49	1.39(5)
C11	C34	1.47(5)
C11	C23	1.47(4)
C12	C39	1.41(6)
C13	C17	1.55(6)
C14	C21	1.39(4)
C14	C33	1.50(5)
C15	C16	1.43(4)
C15	C45	1.43(4)

C16	C19	1.51(4)
C17	C27	1.30(13)
C18	C20	1.31(4)
C18	C46	1.36(5)
C18	C38	1.44(5)
C21	C32	1.45(5)
C22	C53	1.99(13)
C23	C40	1.47(4)
C24	C45	1.40(4)
C25	C36	1.39(6)
C25	C39	1.51(6)
C26	C30	1.41(7)
C26	C38	1.56(5)
C27	C56	1.37(8)
C28	C29	1.49(4)
C29	C32	1.32(5)
C30	C50	1.23(8)
C31	C44	1.40(5)
C31	C51	1.68(10)
C37	C56	1.34(6)
C37	C57	1.58(8)
C38	C43	1.46(6)
C40	O11	1.29(4)
C40	C54	1.53(11)
C46	C50	1.39(6)
C47	C49	1.28(5)
C47	C48	1.43(5)
C54	C40	1.53(10)

Table II.2.4.5 Bond Angles for ab56516

Atom 1	Atom 2	Atom 3	Angle (deg)
O5	Mn1	O6	82.5(7)
O5	Mn1	O2	89.3(7)
O6	Mn1	O2	93.3(7)
O5	Mn1	O1	173.5(8)
O6	Mn1	O1	100.3(7)
O2	Mn1	O1	84.7(7)
O5	Mn1	O1	98.0(7)
O6	Mn1	O1	177.0(7)
O2	Mn1	O1	83.7(7)
O1	Mn1	O1	78.9(7)
O5	Mn1	O17	92.0(8)

O6	Mn1	O17	92.1(8)
O2	Mn1	O17	174.6(7)
O1	Mn1	O17	93.8(7)
O1	Mn1	O17	90.9(7)
O6	Mn2	O13	176.3(9)
O6	Mn2	O10	93.1(8)
O13	Mn2	O10	89.6(8)
O6	Mn2	O23	92.9(9)
O13	Mn2	O23	84.4(9)
O10	Mn2	O23	173.9(9)
O6	Mn2	O21	92.6(8)
O13	Mn2	O21	89.7(9)
O10	Mn2	O21	94.4(8)
O23	Mn2	O21	84.6(10)
O6	Mn2	O9	94.1(7)
O13	Mn2	O9	83.2(8)
O10	Mn2	O9	93.4(7)
O23	Mn2	O9	86.8(10)
O21	Mn2	O9	169.3(8)
O8	Mn3	O10	84.4(8)
O8	Mn3	O11	172.4(8)
O10	Mn3	O11	93.7(9)
O8	Mn3	O3	94.9(8)
O10	Mn3	O3	178.6(8)
O11	Mn3	O3	86.9(9)
O8	Mn3	O7	96.9(7)
O10	Mn3	O7	93.5(7)
O11	Mn3	O7	90.5(7)
O3	Mn3	O7	87.8(8)
O8	Mn3	C54	164(4)
O10	Mn3	C54	104(6)
O11	Mn3	C54	12.3(18)
O3	Mn3	C54	76(6)
O7	Mn3	C54	96(8)
O5	Mn4	O12	176.0(9)
O5	Mn4	O6	80.4(7)
O12	Mn4	O6	98.3(8)
O5	Mn4	O4	94.9(8)
O12	Mn4	O4	86.2(9)
O6	Mn4	O4	174.9(8)
O5	Mn4	O22	90.9(8)
O12	Mn4	O22	92.9(9)
O6	Mn4	O22	93.2(7)

O4	Mn4	O22	88.8(8)
O5	Mn4	O14	83.5(7)
O12	Mn4	O14	92.7(9)
O6	Mn4	O14	86.1(7)
O4	Mn4	O14	91.5(8)
O22	Mn4	O14	174.4(8)
O10	Mn5	O8	84.3(7)
O10	Mn5	O18	91.8(7)
O8	Mn5	O18	92.4(7)
O10	Mn5	O2	173.8(7)
O8	Mn5	O2	101.1(7)
O18	Mn5	O2	91.0(7)
O10	Mn5	O1	93.3(7)
O8	Mn5	O1	89.4(7)
O18	Mn5	O1	174.7(7)
O2	Mn5	O1	83.7(6)
O10	Mn5	O2	94.9(7)
O8	Mn5	O2	172.6(7)
O18	Mn5	O2	95.0(7)
O2	Mn5	O2	79.3(7)
O1	Mn5	O2	83.3(6)
O5	Mn6	O20	173.3(8)
O5	Mn6	O8	94.5(8)
O20	Mn6	O8	91.4(8)
O5	Mn6	O19	90.0(8)
O20	Mn6	O19	84.2(8)
O8	Mn6	O19	175.6(9)
O5	Mn6	O24	90.1(7)
O20	Mn6	O24	92.7(8)
O8	Mn6	O24	93.1(8)
O19	Mn6	O24	86.6(9)
O5	Mn6	O15	88.0(7)
O20	Mn6	O15	88.6(8)
O8	Mn6	O15	92.1(7)
O19	Mn6	O15	88.4(8)
O24	Mn6	O15	174.7(8)
Mn1	O1	Mn5	94.9(7)
Mn1	O1	Mn1	101.1(7)
Mn5	O1	Mn1	94.5(8)
Mn1	O2	Mn5	96.1(7)
Mn1	O2	Mn5	94.8(6)
Mn5	O2	Mn5	100.7(7)
C41	O3	Mn3	128.1(18)

C44	O4	Mn4	133(2)
Mn1	O5	Mn4	98.4(8)
Mn1	O5	Mn6	131.1(9)
Mn4	O5	Mn6	130.4(10)
Mn1	O6	Mn4	97.0(7)
Mn1	O6	Mn2	132.9(10)
Mn4	O6	Mn2	122.1(9)
C1	O7	Mn3	130(2)
Mn3	O8	Mn5	94.7(7)
Mn3	O8	Mn6	127.5(10)
Mn5	O8	Mn6	129.0(9)
C3	O9	Mn2	135.1(17)
Mn5	O10	Mn3	95.3(8)
Mn5	O10	Mn2	133.7(10)
Mn3	O10	Mn2	123.5(9)
C40	O11	Mn3	133.8(19)
C22	O12	Mn4	129.4(19)
C40	O13	Mn2	138(2)
C20	O14	Mn4	130.4(18)
C35	O16	Mn3	122.6(18)
C20	O17	Mn1	131.5(18)
C35	O18	Mn5	127.6(17)
C44	O19	Mn6	133(2)
C41	O20	Mn6	137.8(19)
C1	O21	Mn2	137(2)
C3	O22	Mn4	127.6(18)
C22	O23	Mn2	133(2)
O7	C1	O21	124(3)
O7	C1	C9	120(3)
O21	C1	C9	115(3)
C6	C2	C12	126(3)
C6	C2	C41	121(3)
C12	C2	C41	113(2)
O9	C3	O22	126(2)
O9	C3	C15	116(3)
O22	C3	C15	118(3)
C48	C4	C23	124(3)
C16	C5	C10	120(3)
C36	C6	C2	117(3)
C36	C6	C42	118(3)
C2	C6	C42	125(3)
C14	C8	C28	124(3)
C14	C8	C35	122(2)

C28	C8	C35	114(2)
C13	C9	C37	116(3)
C13	C9	C1	125(3)
C37	C9	C1	119(4)
C24	C10	C5	121(3)
C49	C11	C34	129(3)
C49	C11	C23	110(3)
C34	C11	C23	120(3)
C39	C12	C2	117(3)
C9	C13	C17	122(6)
C8	C14	C21	119(3)
C8	C14	C33	126(3)
C21	C14	C33	115(3)
C16	C15	C45	118(3)
C16	C15	C3	124(3)
C45	C15	C3	118(3)
C5	C16	C15	121(3)
C5	C16	C19	118(3)
C15	C16	C19	121(3)
C27	C17	C13	114(8)
C20	C18	C46	122(4)
C20	C18	C38	119(4)
C46	C18	C38	119(3)
O17	C20	O14	115(2)
O17	C20	C18	119(3)
O14	C20	C18	126(3)
C14	C21	C32	121(3)
O23	C22	O12	129(3)
O23	C22	C53	127(4)
O12	C22	C53	101(4)
C4	C23	C11	120(3)
C4	C23	C40	119(3)
C11	C23	C40	120(3)
C45	C24	C10	115(3)
C36	C25	C39	117(4)
C30	C26	C38	117(4)
C17	C27	C56	124(5)
C8	C28	C29	119(3)
C32	C29	C28	119(3)
C50	C30	C26	125(5)
C44	C31	C51	130(4)
C29	C32	C21	118(3)
O16	C35	O18	124(3)

O16	C35	C8	118(2)
O18	C35	C8	118(2)
C25	C36	C6	124(4)
C56	C37	C9	124(5)
C56	C37	C57	109(5)
C9	C37	C57	123(4)
C43	C38	C18	124(3)
C43	C38	C26	124(4)
C18	C38	C26	113(4)
C12	C39	C25	119(4)
O13	C40	O11	121(3)
O13	C40	C23	119(3)
O11	C40	C23	120(3)
O13	C40	C54	139(5)
O11	C40	C54	18(3)
C23	C40	C54	102(6)
O20	C41	O3	127(3)
O20	C41	C2	115(2)
O3	C41	C2	118(2)
O4	C44	O19	120(3)
O4	C44	C31	121(3)
O19	C44	C31	114(3)
C24	C45	C15	124(3)
C18	C46	C50	126(4)
C49	C47	C48	119(3)
C4	C48	C47	115(3)
C47	C49	C11	132(3)
C30	C50	C46	117(7)
C7	C53	C22	83(7)
C40	C54	Mn3	106(10)
C37	C56	C27	118(5)

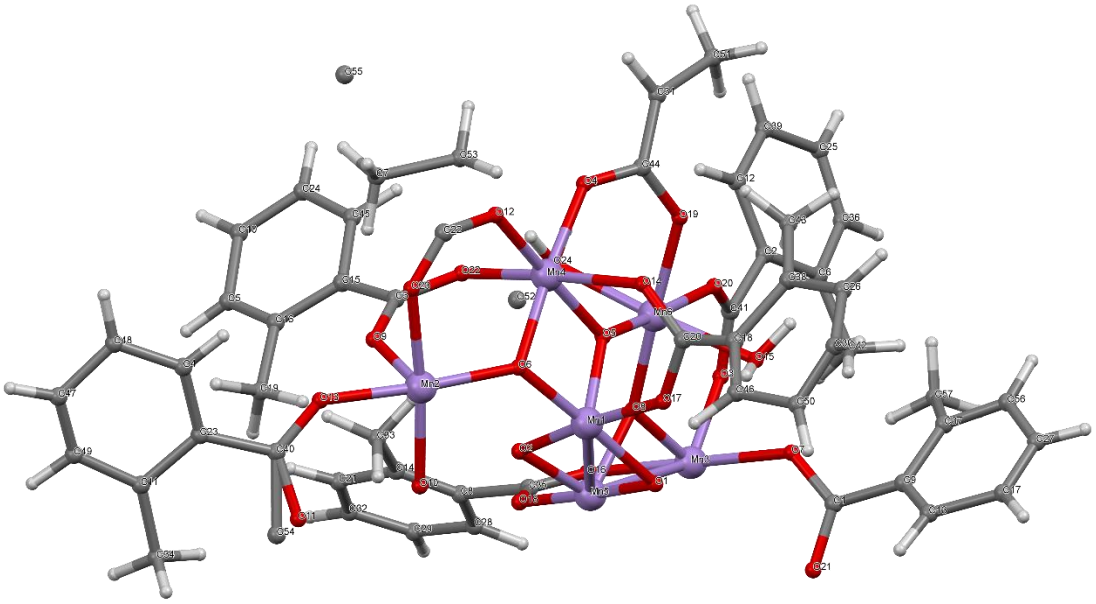

Figure II.2.4 Crystal Structure with atomic labels for compound **4a**, "Mn_3O-2-Methyl" (rod), $Mn_{12}O_{12}(O_2CPh\text{-}o\text{-}Me)_{16}(H_2O)_4$, ab56516

II.2.5 Compound 4b, "Mn_{13}-2-Methyl" (cube), $Mn_9O_7(O_2CPh\text{-}o\text{-}Me)_{13}(Pyr)_2$, ab58027

Table II.2.5.1 Crystal data and structure refinement for ab58027.

Identification code	ab58027
Empirical formula	$C_{114}H_{96}Mn_9N_2O_{33}$
Formula weight	2516.38
Temperature/K	100.0
Crystal system	monoclinic
Space group	C2/c
a/Å	55.133(2)
b/Å	18.8416(8)
c/Å	21.8802(9)
α/°	90
β/°	94.757(2)
γ/°	90
Volume/Å^3	22650.6(16)
Z	8
ρ_{calc}g/cm^3	1.476
μ/mm^{-1}	1.048
F(000)	10264.0
Crystal size/mm^3	0.197 × 0.166 × 0.079
Radiation	MoKα (λ = 0.71073)
2Θ range for data collection/°	1.482 to 34.982
Index ranges	$-46 \le h \le 46$, $-15 \le k \le 15$, $-18 \le l \le 18$
Reflections collected	70380
Independent reflections	7166 [R_{int} = 0.0604, R_{sigma} = 0.0285]
Data/restraints/parameters	7166/0/1434
Goodness-of-fit on F^2	1.035
Final R indexes [I>=2σ (I)]	R_1 = 0.0706, wR_2 = 0.2095
Final R indexes [all data]	R_1 = 0.0814, wR_2 = 0.2272
Largest diff. peak/hole / e Å^{-3}	2.55/-0.52

Table II.2.5.2 Fractional Atomic Coordinates (×10^4) and Equivalent Isotropic Displacement Parameters (Å^2×10^3) for ab58027. U_{eq} is defined as 1/3 of of the trace of the orthogonalised U_{IJ} tensor.

Atom	*x*	*y*	*z*	U(eq)
Mn1	928.9(3)	5883.6(10)	2104.8(9)	35.1(7)
Mn2	1123.9(3)	8312.3(10)	1754.7(9)	31.2(7)
Mn3	1477.4(3)	8073.1(10)	3036.3(9)	30.3(7)
Mn4	1792.2(3)	6393.4(10)	1178.8(8)	29.0(7)
Mn5	1213.4(3)	5874.9(10)	805.8(9)	32.9(7)
Mn6	1865.5(3)	6811.7(10)	2648.3(9)	31.0(7)
Mn7	1369.4(3)	6690.5(10)	2132.4(9)	29.6(6)
Mn8	903.6(3)	7465.9(11)	2721.4(9)	34.3(7)

Mn9	1427.3(3)	7497.2(10)	734.7(9)	29.8(7)
O1	2176.7(15)	6382(4)	2472(5)	35(2)
O2	1799.4(17)	5282(5)	1062(4)	36(2)
O3	1077.5(13)	6636(4)	2551(3)	30(2)
O4	1180.2(13)	7992(4)	2574(3)	29(2)
O5	1201.4(13)	5967(4)	1653(3)	31(2)
O6	1468.6(13)	6508(4)	851(3)	27(2)
O7	1691.0(13)	6365(4)	1983(3)	28(2)
O8	596.3(16)	6978(6)	2807(4)	40(3)
O9	1890.0(14)	6574(5)	340(4)	30(2)
O10	1297.2(14)	7549(4)	1486(3)	29(2)
O11	1620.9(18)	7423(5)	8(4)	29(2)
O12	729.8(15)	8384(6)	2788(4)	39(2)
O13	657.0(17)	5827(6)	2639(4)	39(2)
O14	1433.9(15)	9021(5)	1948(5)	40(3)
O15	1469.5(14)	9120(5)	2964(5)	36(2)
O16	914.1(18)	5317(5)	709(4)	38(2)
O17	1556.5(13)	7145(4)	2802(3)	27(2)
O18	1802.0(16)	7593(5)	1203(4)	29(2)
O19	1379.6(18)	8480(5)	488(4)	32(2)
O20	1106.0(15)	7233(6)	140(5)	39(2)
O21	973.5(19)	7409(5)	3672(5)	41(2)
O22	2136.4(17)	6357(4)	1449(5)	31(2)
O23	2040.6(15)	7291(6)	3351(4)	33(2)
O24	787.8(14)	5088(4)	1620(6)	37(2)
O25	1791.8(19)	8219(5)	3484(4)	34(2)
O26	1045.1(17)	8750(5)	958(5)	40(2)
O27	784.6(15)	7651(5)	1710(4)	34(2)
O28	1333.4(19)	7941(5)	3881(4)	41(2)
O29	707.2(15)	6515(6)	1443(4)	38(3)
O30	1949.0(15)	7769(5)	2172(5)	42(3)
O31	1140.1(17)	6076(6)	-66(4)	46(3)
O32	1408.8(19)	4948(5)	793(4)	41(3)
O33	911.1(17)	9037(4)	2094(4)	34(2)
N1	1847(2)	5916(7)	3371(5)	37(3)
N2	1154(3)	5039(9)	2657(8)	54(4)
C1	1145(4)	7651(8)	4035(8)	42(4)
C2	1950(3)	7135(7)	-583(7)	30(3)
C3	2060(2)	8580(8)	1427(8)	28(4)
C4	2313(3)	7086(7)	-1111(10)	46(4)
C5	996(3)	6282(10)	4605(8)	69(5)
C6	534(2)	6940(9)	281(9)	43(4)
C7	1263(4)	4546(16)	2467(13)	101(8)
C8	2254(3)	6242(7)	1947(9)	27(4)
C9	424(3)	8059(11)	715(8)	49(5)

C10	1112(3)	9386(9)	72(8)	56(5)
C11	409(3)	7112(11)	-277(8)	57(5)
C12	404(3)	8588(9)	1228(7)	65(5)
C13	691(2)	7158(12)	1343(7)	35(4)
C14	2665(2)	6364(8)	2979(7)	52(4)
C15	2230(3)	8955(8)	1823(7)	30(4)
C16	2945(4)	5266(10)	1762(11)	76(5)
C17	1269(3)	9663(9)	-335(8)	52(4)
C18	1186(3)	8831(9)	529(7)	37(4)
C19	285(3)	7746(12)	-335(9)	63(5)
C20	1626(4)	4828(8)	965(6)	38(4)
C21	575(3)	4604(8)	748(10)	48(5)
C22	2325(3)	9699(8)	964(10)	45(4)
C23	2152(3)	8128(7)	4129(7)	32(4)
C24	2686(3)	5971(7)	2399(8)	41(4)
C25	1983(3)	7851(10)	3608(6)	30(4)
C26	1200(4)	5118(13)	3261(17)	119(8)
C27	2153(3)	9346(9)	580(7)	44(4)
C28	2758(4)	5221(9)	1316(8)	72(5)
C29	2539(3)	5525(9)	1388(8)	52(4)
C30	2256(4)	8689(7)	5084(7)	46(4)
C31	293(3)	8205(9)	160(11)	65(5)
C32	1808(3)	7047(8)	-46(7)	27(4)
C33	2500(3)	5913(8)	1917(8)	35(4)
C34	978(3)	7017(15)	5605(11)	112(9)
C35	1923(2)	7949(8)	1621(9)	27(4)
C36	503(3)	4818(13)	91(12)	113(10)
C37	1026(3)	6958(12)	4964(9)	67(5)
C38	2011(3)	4356(11)	1961(9)	99(7)
C39	1896(3)	3835(11)	1524(8)	54(5)
C40	1942(4)	7542(9)	-1635(9)	68(5)
C41	1834(3)	7428(7)	-1110(10)	46(4)
C42	1135(3)	8211(12)	5071(10)	73(6)
C43	515(3)	3862(11)	1602(11)	95(6)
C44	1404(7)	4040(20)	2722(13)	125(13)
C45	1103(3)	7596(12)	4716(8)	52(4)
C46	546(3)	7398(10)	772(8)	37(4)
C47	2025(2)	8794(8)	822(8)	40(4)
C48	448(4)	4074(12)	1041(11)	77(6)
C49	2405(4)	8014(9)	4082(7)	62(5)
C50	1950(3)	3110(11)	1561(9)	56(5)
C51	2577(3)	8275(10)	4526(10)	74(5)
C52	2499(4)	8591(9)	5030(8)	60(5)
C53	770(3)	5031(8)	1044(9)	31(4)
C54	2913(3)	5640(10)	2302(9)	64(5)

C55	2082(3)	8480(8)	4633(9)	40(4)
C56	1709(3)	4078(9)	1096(7)	41(4)
C57	2201(3)	6969(7)	-587(7)	37(4)
C58	1354(5)	4660(20)	3653(16)	183(18)
C59	1588(4)	3567(13)	776(11)	116(9)
C60	2361(2)	9511(8)	1567(9)	40(4)
C61	2183(5)	7371(9)	-1635(8)	68(6)
C62	192(5)	4005(14)	77(11)	121(9)
C63	1835(4)	2643(10)	1221(12)	93(8)
C64	1643(5)	2873(14)	813(13)	160(13)
C65	532(3)	6344(11)	2836(6)	40(4)
C66	298(3)	6156(13)	3091(7)	54(5)
C67	1496(2)	10548(10)	1853(8)	41(4)
C68	626(3)	10242(12)	2401(7)	56(4)
C69	1450(2)	10191(9)	2381(8)	38(4)
C70	764(3)	8950(9)	2497(8)	35(4)
C71	225(4)	5458(12)	3123(8)	80(6)
C72	1453(2)	9392(10)	2423(9)	41(4)
C73	605(3)	9567(10)	2634(7)	43(4)
C74	879(3)	6253(11)	-1193(10)	65(5)
C75	966(3)	6827(11)	-855(8)	50(4)
C76	1379(4)	10552(11)	2888(8)	89(7)
C77	1082(2)	6721(11)	-219(8)	40(4)
C78	1530(3)	9472(7)	-348(6)	50(4)
C79	2281(3)	8797(8)	2480(7)	54(4)
C80	1476(3)	11276(12)	1865(9)	58(5)
C81	457(4)	10783(9)	2577(9)	71(5)
C82	1811(3)	8640(9)	4728(7)	70(5)
C83	1575(4)	10197(9)	1285(8)	88(6)
C84	1180(4)	10184(10)	-763(8)	74(5)
C85	-60(5)	6511(17)	3505(10)	91(7)
C86	-136(4)	5830(20)	3535(9)	102(9)
C87	1402(4)	11630(9)	2369(13)	103(8)
C88	2348(3)	6667(9)	-34(8)	70(5)
C89	150(4)	6706(12)	3279(9)	79(6)
C90	239(3)	3711(10)	667(12)	93(7)
C91	1001(5)	7640(20)	5920(10)	148(13)
C92	927(5)	7484(13)	-1125(12)	108(9)
C93	12(5)	5292(14)	3350(11)	110(8)
C94	1981(3)	5345(11)	3422(8)	54(5)
C95	2002(3)	4901(8)	3962(11)	63(5)
C96	938(5)	10353(13)	-797(9)	121(9)
C97	441(5)	9475(12)	3070(12)	123(8)
C98	1351(5)	11265(14)	2872(9)	134(11)
C99	300(5)	10635(14)	2974(14)	127(9)

C100	790(4)	10435(10)	1940(14)	155(11)
C101	778(4)	6332(17)	-1783(13)	110(8)
C102	280(7)	9990(20)	3246(17)	230(20)
C103	755(6)	6970(30)	-2005(12)	175(16)
C104	829(7)	7572(17)	-1694(17)	169(15)
C105	783(4)	10090(15)	-430(12)	141(11)
C106	1874(5)	5085(18)	4416(11)	148(12)
C107	1742(4)	6063(11)	3859(13)	114(8)
C108	959(5)	8131(16)	-827(12)	154(11)
C109	1464(5)	4060(20)	3260(30)	230(30)
C110	1750(6)	5687(16)	4396(13)	172(14)
C111	861(4)	9620(12)	32(9)	99(7)
C112	1085(4)	8230(14)	5652(12)	115(9)
C113	297(5)	4519(16)	-185(12)	136(10)
C114	201(6)	7454(14)	3250(20)	250(20)

Table II.2.5.3 Anisotropic Displacement Parameters ($Å^2×10^3$) for ab58027. The Anisotropic displacement factor exponent takes the form: $-2\pi^2[h^2a^{*2}U_{11}+2hka^*b^*U_{12}+\ldots]$.

Atom	U_{11}	U_{22}	U_{33}	U_{23}	U_{13}	U_{12}
Mn1	21.3(13)	42.7(15)	41.6(14)	9.1(11)	5.2(11)	-4.6(10)
Mn2	22.5(13)	37.7(14)	34.1(14)	4.8(10)	6.5(10)	0.7(10)
Mn3	21.6(13)	36.7(14)	33.1(13)	3.2(10)	5.3(10)	-1.3(10)
Mn4	21.8(13)	34.5(14)	31.2(14)	0.0(10)	4.6(10)	-2.2(10)
Mn5	25.6(14)	36.3(14)	36.4(14)	1.2(10)	-0.2(10)	-6.7(10)
Mn6	21.1(13)	40.3(14)	31.8(14)	0.2(10)	3.4(10)	-0.8(10)
Mn7	19.2(13)	36.7(14)	33.1(13)	3.6(10)	4.1(10)	-1.7(10)
Mn8	19.8(13)	46.0(15)	38.1(15)	5.9(10)	9.0(11)	-1.5(10)
Mn9	23.4(13)	33.7(14)	32.7(14)	2.5(10)	4.2(11)	-2.8(10)
O1	24(6)	53(6)	30(7)	-4(5)	4(5)	2(5)
O2	34(6)	32(6)	41(6)	-1(5)	5(5)	-3(6)
O3	19(5)	40(5)	32(5)	3(4)	7(4)	2(4)
O4	19(5)	38(5)	31(5)	6(4)	6(4)	-1(4)
O5	18(5)	40(5)	35(5)	3(4)	4(4)	-5(4)
O6	16(5)	32(5)	34(5)	2(4)	5(4)	-1(4)
O7	19(5)	36(5)	28(5)	-4(4)	4(4)	-4(4)
O8	32(6)	40(7)	49(7)	3(5)	9(5)	-7(6)
O9	20(6)	37(6)	32(6)	-3(6)	4(5)	0(5)
O10	25(5)	33(5)	30(5)	3(4)	6(4)	2(4)
O11	19(6)	36(6)	33(6)	5(4)	6(5)	5(5)
O12	26(6)	48(7)	44(6)	5(6)	9(5)	-1(5)
O13	24(6)	49(7)	44(6)	19(5)	6(5)	-14(6)
O14	33(6)	55(7)	34(7)	-4(6)	15(5)	-10(5)
O15	25(6)	35(6)	47(7)	-4(6)	2(5)	2(4)
O16	26(6)	37(6)	50(7)	4(5)	-3(5)	-12(5)

O17	19(5)	30(5)	33(5)	0(4)	1(4)	0(4)
O18	20(6)	33(6)	33(6)	-2(5)	5(5)	-4(5)
O19	22(6)	35(6)	41(6)	8(5)	14(5)	11(5)
O20	30(6)	51(7)	34(6)	-4(6)	-2(5)	1(5)
O21	25(6)	49(6)	49(7)	7(5)	2(6)	-7(5)
O22	27(6)	39(6)	27(6)	4(5)	6(5)	3(4)
O23	28(6)	39(6)	33(6)	-4(5)	4(5)	2(5)
O24	17(6)	36(6)	57(8)	8(5)	-6(5)	-10(4)
O25	20(6)	43(6)	39(6)	2(5)	3(5)	-1(5)
O26	31(6)	44(6)	45(7)	11(5)	7(6)	11(5)
O27	16(6)	46(7)	41(6)	8(6)	5(5)	1(5)
O28	26(6)	63(7)	33(6)	-6(5)	7(5)	-14(6)
O29	28(6)	37(7)	49(7)	11(6)	4(5)	9(5)
O30	40(7)	47(7)	37(7)	9(6)	-1(5)	-15(5)
O31	51(7)	41(7)	44(7)	8(6)	-6(5)	-13(6)
O32	11(6)	53(7)	58(7)	1(5)	-7(5)	-1(5)
O33	24(6)	39(6)	40(6)	6(5)	13(6)	3(5)
N1	28(7)	56(10)	30(9)	0(7)	12(7)	18(8)
N2	38(10)	74(12)	50(11)	13(9)	6(8)	-13(9)
C1	27(13)	46(10)	52(16)	8(9)	10(11)	-5(9)
C2	30(13)	33(9)	28(12)	5(8)	7(11)	-1(8)
C3	17(9)	34(11)	32(12)	-9(10)	-4(9)	8(9)
C4	43(11)	39(10)	63(13)	-5(9)	39(13)	-2(8)
C5	51(11)	93(15)	63(12)	29(12)	12(9)	-14(10)
C6	25(9)	71(13)	32(11)	6(12)	-3(9)	-9(8)
C7	40(14)	88(18)	180(20)	30(20)	23(16)	29(13)
C8	13(12)	35(9)	33(13)	0(9)	-3(10)	-12(8)
C9	25(9)	84(17)	35(13)	15(12)	-14(9)	-5(11)
C10	53(15)	76(13)	43(11)	30(11)	24(11)	11(12)
C11	48(11)	79(16)	44(15)	-13(10)	6(10)	-13(11)
C12	52(11)	78(13)	62(12)	-14(11)	-11(9)	22(9)
C13	1(9)	74(16)	28(12)	11(12)	-2(8)	5(10)
C14	30(10)	48(10)	77(13)	15(10)	-7(9)	-3(8)
C15	20(9)	34(10)	39(12)	1(10)	11(10)	0(9)
C16	59(15)	116(16)	54(13)	13(13)	17(14)	26(11)
C17	63(15)	40(11)	52(12)	8(10)	1(12)	16(11)
C18	34(12)	50(12)	27(11)	9(10)	7(11)	-10(10)
C19	44(11)	63(13)	81(17)	28(14)	-4(10)	13(11)
C20	69(16)	13(13)	34(9)	-5(8)	20(10)	-17(13)
C21	20(11)	36(10)	94(17)	2(11)	25(13)	-9(9)
C22	36(11)	38(10)	63(14)	22(11)	15(10)	1(9)
C23	33(13)	31(9)	33(12)	5(9)	10(11)	3(8)
C24	36(13)	42(10)	47(13)	6(9)	7(12)	-1(9)
C25	15(11)	56(12)	20(11)	7(10)	2(9)	-2(11)
C26	75(18)	120(20)	160(30)	30(20)	42(18)	-37(16)

C27	40(10)	47(11)	46(10)	9(11)	3(11)	3(9)
C28	74(15)	91(14)	51(13)	14(10)	12(14)	40(13)
C29	40(13)	74(12)	44(13)	4(10)	13(9)	36(10)
C30	47(13)	53(11)	39(12)	-22(8)	4(12)	-10(9)
C31	70(13)	55(12)	69(15)	-13(13)	3(13)	22(10)
C32	34(12)	23(10)	26(12)	1(9)	1(11)	-16(10)
C33	16(12)	55(10)	36(11)	2(9)	3(11)	7(8)
C34	76(15)	210(30)	48(17)	58(17)	-14(12)	-83(16)
C35	16(9)	16(11)	51(14)	5(11)	7(10)	1(8)
C36	21(12)	160(20)	150(30)	-120(20)	-47(12)	14(12)
C37	42(11)	108(18)	50(16)	23(15)	1(9)	-39(11)
C38	78(14)	109(17)	104(16)	24(15)	-24(13)	33(13)
C39	26(11)	79(19)	54(12)	-14(12)	-8(10)	-24(12)
C40	36(14)	103(15)	68(17)	29(10)	26(11)	10(10)
C41	35(10)	49(10)	56(13)	8(9)	18(13)	7(8)
C42	58(12)	140(20)	25(12)	-20(13)	30(9)	-26(11)
C43	74(15)	112(17)	96(17)	-12(14)	-13(13)	-12(12)
C44	110(30)	140(30)	130(20)	20(20)	-9(18)	0(20)
C45	33(10)	92(16)	30(14)	-2(14)	4(9)	-9(10)
C46	21(10)	57(13)	33(14)	4(12)	-1(9)	-1(10)
C47	32(10)	44(11)	43(14)	1(9)	2(9)	-14(9)
C48	55(16)	101(18)	78(17)	-20(15)	14(14)	43(16)
C49	45(14)	102(14)	38(11)	-21(10)	6(11)	16(11)
C50	42(11)	20(12)	106(15)	28(12)	8(11)	15(11)
C51	34(12)	125(16)	61(13)	-42(12)	-7(13)	2(11)
C52	55(17)	83(13)	40(13)	-20(10)	-5(10)	-21(10)
C53	13(11)	30(10)	50(14)	0(10)	-2(11)	-6(9)
C54	25(13)	95(13)	70(16)	19(12)	-8(10)	20(10)
C55	36(13)	37(9)	46(12)	-2(9)	9(12)	-3(9)
C56	38(11)	33(14)	52(11)	-9(10)	-4(10)	-23(11)
C57	34(14)	38(9)	39(13)	4(8)	8(11)	-7(8)
C58	63(18)	240(40)	240(40)	200(40)	-50(20)	-20(20)
C59	121(18)	18(13)	190(20)	33(15)	-86(18)	10(14)
C60	34(10)	28(10)	57(14)	-6(9)	-5(9)	-3(9)
C61	120(20)	51(11)	37(14)	13(10)	34(13)	-21(11)
C62	190(30)	120(20)	49(16)	-15(14)	6(16)	-40(20)
C63	97(18)	22(12)	160(20)	-22(14)	-8(16)	-24(13)
C64	170(30)	70(20)	210(30)	8(17)	-140(20)	-19(17)
C65	29(14)	51(14)	39(10)	-9(10)	-1(9)	21(13)
C66	10(12)	110(20)	41(10)	19(11)	16(8)	-15(16)
C67	34(9)	40(15)	46(14)	13(12)	-3(8)	-5(8)
C68	47(13)	63(16)	60(11)	-4(12)	22(9)	-5(12)
C69	42(10)	26(13)	44(13)	7(13)	-2(8)	-4(8)
C70	30(11)	36(13)	39(11)	-5(10)	1(9)	2(11)
C71	48(16)	83(18)	112(16)	37(12)	26(12)	-40(12)

C72	23(9)	74(18)	25(13)	14(13)	-2(8)	-1(8)
C73	22(10)	55(16)	53(11)	3(11)	7(9)	2(11)
C74	40(10)	102(19)	51(15)	-17(14)	-12(10)	24(11)
C75	66(12)	45(14)	38(14)	-8(14)	6(10)	-7(10)
C76	210(20)	18(14)	44(14)	5(11)	12(13)	24(12)
C77	20(9)	56(16)	43(15)	4(13)	2(9)	-15(9)
C78	55(13)	39(10)	56(11)	6(8)	6(8)	3(9)
C79	49(11)	65(11)	46(13)	-3(9)	-10(8)	-31(9)
C80	70(12)	36(15)	65(15)	34(12)	-6(10)	6(9)
C81	88(15)	53(13)	72(13)	-10(11)	14(12)	12(14)
C82	64(14)	96(14)	52(11)	-34(10)	9(9)	-2(10)
C83	144(18)	54(12)	72(14)	2(11)	54(13)	-21(12)
C84	87(18)	74(13)	66(14)	22(12)	36(11)	25(12)
C85	44(19)	130(20)	101(17)	-11(15)	42(12)	15(15)
C86	29(14)	210(30)	65(14)	45(18)	14(11)	0(20)
C87	190(20)	22(12)	97(19)	-17(17)	-13(16)	21(13)
C88	48(11)	95(14)	70(13)	-24(11)	29(11)	-5(10)
C89	17(13)	110(20)	117(16)	-4(13)	46(12)	-9(14)
C90	45(13)	103(16)	140(20)	-40(16)	50(14)	-57(12)
C91	120(20)	270(40)	46(16)	-100(20)	8(14)	-110(20)
C92	240(30)	44(18)	48(18)	-7(15)	29(16)	8(16)
C93	55(16)	140(20)	140(20)	58(17)	32(14)	-44(19)
C94	23(10)	63(13)	79(15)	2(12)	18(9)	13(10)
C95	36(11)	32(10)	117(17)	40(13)	-13(12)	10(8)
C96	120(20)	190(20)	59(14)	78(15)	50(15)	100(20)
C97	124(19)	85(17)	170(20)	12(16)	90(20)	34(16)
C98	310(40)	54(19)	43(14)	13(13)	47(16)	28(17)
C99	130(20)	100(20)	170(20)	23(17)	80(20)	68(16)
C100	120(20)	66(15)	290(30)	16(18)	130(20)	20(14)
C101	88(16)	150(30)	90(20)	-43(17)	-38(15)	47(16)
C102	280(40)	160(30)	280(40)	80(30)	200(40)	150(30)
C103	230(30)	230(40)	70(20)	-20(30)	-38(19)	170(30)
C104	330(40)	110(30)	70(20)	32(19)	40(20)	110(30)
C105	87(17)	230(30)	106(18)	120(20)	31(17)	104(18)
C106	150(20)	220(40)	85(18)	83(19)	69(17)	80(20)
C107	160(20)	81(15)	107(18)	83(16)	57(18)	70(15)
C108	160(30)	150(30)	140(20)	50(20)	-37(19)	-40(20)
C109	23(16)	140(30)	530(100)	200(50)	10(40)	21(18)
C110	220(30)	150(20)	170(30)	70(20)	110(20)	140(20)
C111	61(17)	150(20)	85(16)	57(15)	29(11)	54(14)
C112	95(17)	160(20)	90(20)	-38(17)	48(14)	-91(16)
C113	140(30)	160(20)	120(20)	20(20)	80(20)	-20(20)
C114	170(30)	80(20)	530(70)	-60(30)	240(40)	-27(18)

Table II.2.5.4 Bond Lengths for ab58027.

Atom	Atom	Length/Å	Atom	Atom	Length/Å
Mn1	O3	1.871(8)	C10	C17	1.40(2)
Mn1	O5	1.872(8)	C10	C18	1.48(2)
Mn1	O13	1.978(10)	C10	C111	1.45(2)
Mn1	O24	1.959(10)	C11	C19	1.38(2)
Mn1	O29	2.171(11)	C13	C46	1.50(2)
Mn1	N2	2.297(16)	C14	C24	1.482(19)
Mn2	O4	1.893(8)	C15	C60	1.413(18)
Mn2	O10	1.849(8)	C15	C79	1.473(18)
Mn2	O14	2.182(9)	C16	C28	1.36(2)
Mn2	O26	1.945(10)	C16	C54	1.40(2)
Mn2	O27	2.244(10)	C17	C78	1.48(2)
Mn2	O33	1.985(10)	C17	C84	1.42(2)
Mn3	O4	1.859(8)	C19	C31	1.38(2)
Mn3	O15	1.979(9)	C20	O32	1.245(18)
Mn3	O17	1.883(8)	C20	C56	1.51(2)
Mn3	O25	1.939(10)	C21	C36	1.51(3)
Mn3	O28	2.087(10)	C21	C48	1.40(2)
Mn4	O2	2.111(10)	C21	C53	1.45(2)
Mn4	O6	1.879(8)	C22	C27	1.383(18)
Mn4	O7	1.890(8)	C22	C60	1.363(18)
Mn4	O9	1.985(10)	C23	C25	1.504(19)
Mn4	O18	2.262(9)	C23	C49	1.423(19)
Mn4	O22	1.941(10)	C23	C55	1.370(18)
Mn5	O5	1.868(8)	C24	C33	1.413(18)
Mn5	O6	1.841(8)	C24	C54	1.43(2)
Mn5	O16	1.953(11)	C26	C58	1.44(3)
Mn5	O31	1.954(10)	C27	C47	1.387(18)
Mn5	O32	2.054(10)	C28	C29	1.36(2)
Mn6	O1	1.964(10)	C29	C33	1.400(19)
Mn6	O7	1.877(8)	C30	C52	1.37(2)
Mn6	O17	1.873(8)	C30	C55	1.374(19)
Mn6	O23	1.967(10)	C34	C37	1.45(3)
Mn6	O30	2.151(11)	C34	C91	1.37(3)
Mn6	N1	2.322(12)	C36	C113	1.36(3)
Mn7	O3	1.919(8)	C37	C45	1.40(2)
Mn7	O5	1.912(8)	C38	C39	1.48(2)
Mn7	O7	1.929(8)	C39	C50	1.40(2)
Mn7	O10	2.164(7)	C39	C56	1.41(2)
Mn7	O17	1.922(8)	C40	C41	1.36(2)
Mn8	O3	1.887(8)	C40	C61	1.37(2)
Mn8	O4	1.869(8)	C42	C45	1.40(2)
Mn8	O8	1.950(10)	C42	C112	1.32(2)
Mn8	O12	1.988(11)	C43	C48	1.32(2)

Mn8	O21	2.087(10)	C44	C109	1.21(6)
Mn8	O27	2.283(10)	C48	C90	1.52(3)
Mn9	O6	1.892(8)	C49	C51	1.39(2)
Mn9	O10	1.850(8)	C50	C63	1.29(2)
Mn9	O11	1.992(10)	C51	C52	1.36(2)
Mn9	O18	2.236(10)	C55	C82	1.55(2)
Mn9	O19	1.940(9)	C56	C59	1.34(2)
Mn9	O20	2.167(10)	C57	C88	1.51(2)
O1	C8	1.285(16)	C58	C109	1.57(6)
O2	C20	1.287(17)	C59	C64	1.34(3)
O8	C65	1.249(17)	C62	C90	1.41(3)
O9	C32	1.285(15)	C62	C113	1.29(3)
O11	C32	1.265(16)	C63	C64	1.40(3)
O12	C70	1.265(17)	C65	C66	1.49(2)
O13	C65	1.287(16)	C66	C71	1.38(2)
O14	C72	1.249(17)	C66	C89	1.40(2)
O15	C72	1.286(16)	C67	C69	1.379(18)
O16	C53	1.247(16)	C67	C80	1.38(2)
O18	C35	1.277(16)	C67	C83	1.50(2)
O19	C18	1.268(17)	C68	C73	1.38(2)
O20	C77	1.244(17)	C68	C81	1.45(2)
O21	C1	1.269(17)	C68	C100	1.45(2)
O22	C8	1.240(15)	C69	C72	1.51(2)
O23	C25	1.248(17)	C69	C76	1.38(2)
O24	C53	1.261(16)	C70	C73	1.50(2)
O25	C25	1.274(16)	C71	C93	1.35(3)
O26	C18	1.275(16)	C73	C97	1.38(2)
O27	C13	1.306(18)	C74	C75	1.37(2)
O29	C13	1.234(18)	C74	C101	1.37(3)
O30	C35	1.249(16)	C75	C77	1.50(2)
O31	C77	1.293(17)	C75	C92	1.38(3)
O33	C70	1.258(17)	C76	C98	1.35(2)
N1	C94	1.306(18)	C80	C87	1.38(2)
N1	C107	1.28(2)	C81	C99	1.31(3)
N2	C26	1.33(3)	C84	C96	1.37(2)
C1	O28	1.244(17)	C85	C86	1.35(3)
C1	C45	1.53(2)	C85	C89	1.34(3)
C2	C32	1.473(19)	C86	C93	1.38(3)
C2	C41	1.386(18)	C87	C98	1.35(3)
C2	C57	1.417(18)	C89	C114	1.44(3)
C3	C15	1.412(17)	C91	C112	1.35(3)
C3	C35	1.489(19)	C92	C104	1.33(3)
C3	C47	1.381(18)	C92	C108	1.39(3)
C4	C57	1.367(19)	C94	C95	1.44(2)
C4	C61	1.41(2)	C95	C106	1.31(3)

C5	C37	1.50(2)	C96	C105	1.32(3)
C6	C11	1.39(2)	C97	C102	1.39(3)
C6	C46	1.374(19)	C99	C102	1.37(3)
C7	N2	1.20(2)	C101	C103	1.31(4)
C7	C44	1.33(4)	C103	C104	1.36(4)
C8	C33	1.500(19)	C105	C111	1.39(2)
C9	C12	1.51(2)	C106	C110	1.33(3)
C9	C31	1.39(2)	C107	C110	1.37(3)
C9	C46	1.42(2)			

Table II.2.5.5 Bond Angles for ab58027.

Atom	Atom	Atom	Angle/°	Atom	Atom	Atom	Angle/°
O3	Mn1	O5	82.9(3)	C26	N2	Mn1	119.5(17)
O3	Mn1	O13	93.1(4)	O21	C1	C45	114.8(15)
O3	Mn1	O24	177.3(4)	O28	C1	O21	125.7(14)
O3	Mn1	O29	97.5(4)	O28	C1	C45	119.4(16)
O3	Mn1	N2	93.3(5)	C41	C2	C32	117.9(16)
O5	Mn1	O13	175.5(4)	C41	C2	C57	117.9(13)
O5	Mn1	O24	94.5(4)	C57	C2	C32	124.2(16)
O5	Mn1	O29	91.9(3)	C15	C3	C35	123.4(16)
O5	Mn1	N2	85.1(5)	C47	C3	C15	118.2(13)
O13	Mn1	O29	90.6(4)	C47	C3	C35	118.3(15)
O13	Mn1	N2	93.1(5)	C57	C4	C61	120.7(14)
O24	Mn1	O13	89.5(4)	C46	C6	C11	121.8(15)
O24	Mn1	O29	83.2(4)	N2	C7	C44	135(3)
O24	Mn1	N2	85.8(5)	O1	C8	C33	119.5(15)
O29	Mn1	N2	168.4(5)	O22	C8	O1	124.2(13)
O4	Mn2	O14	87.0(4)	O22	C8	C33	116.3(14)
O4	Mn2	O26	172.4(4)	C31	C9	C12	117.1(18)
O4	Mn2	O27	86.3(3)	C31	C9	C46	117.4(15)
O4	Mn2	O33	85.5(4)	C46	C9	C12	125.2(16)
O10	Mn2	O4	90.3(3)	C17	C10	C18	123.1(16)
O10	Mn2	O14	96.9(4)	C17	C10	C111	119.3(15)
O10	Mn2	O26	97.3(4)	C111	C10	C18	117.6(17)
O10	Mn2	O27	90.3(3)	C19	C11	C6	119.4(15)
O10	Mn2	O33	172.4(4)	O27	C13	C46	117.1(17)
O14	Mn2	O27	170.1(4)	O29	C13	O27	124.7(13)
O26	Mn2	O14	91.6(4)	O29	C13	C46	118.2(16)
O26	Mn2	O27	94.2(4)	C3	C15	C60	117.5(13)
O26	Mn2	O33	87.0(4)	C3	C15	C79	124.1(14)
O33	Mn2	O14	89.1(4)	C60	C15	C79	118.3(15)
O33	Mn2	O27	83.2(4)	C28	C16	C54	119.9(16)
O4	Mn3	O15	91.5(4)	C10	C17	C78	125.1(15)

O4	Mn3	O17	89.4(3)	C10	C17	C84	118.7(15)
O4	Mn3	O25	175.8(4)	C84	C17	C78	116.1(18)
O4	Mn3	O28	95.1(4)	O19	C18	O26	123.8(14)
O15	Mn3	O28	100.5(4)	O19	C18	C10	120.5(15)
O17	Mn3	O15	155.2(4)	O26	C18	C10	115.7(16)
O17	Mn3	O25	93.0(4)	C11	C19	C31	119.0(15)
O17	Mn3	O28	104.1(3)	O2	C20	C56	112.4(16)
O25	Mn3	O15	84.9(4)	O32	C20	O2	127.7(14)
O25	Mn3	O28	87.6(4)	O32	C20	C56	119.9(15)
O2	Mn4	O18	173.7(3)	C48	C21	C36	121.4(18)
O6	Mn4	O2	95.4(4)	C48	C21	C53	124.8(18)
O6	Mn4	O7	90.8(3)	C53	C21	C36	113.7(16)
O6	Mn4	O9	87.1(3)	C60	C22	C27	120.0(13)
O6	Mn4	O18	85.1(3)	C49	C23	C25	116.2(16)
O6	Mn4	O22	173.3(4)	C55	C23	C25	125.4(15)
O7	Mn4	O2	95.4(3)	C55	C23	C49	118.4(14)
O7	Mn4	O9	171.7(4)	C33	C24	C14	125.0(15)
O7	Mn4	O18	90.8(3)	C33	C24	C54	116.4(14)
O7	Mn4	O22	94.2(4)	C54	C24	C14	118.5(16)
O9	Mn4	O2	92.8(3)	O23	C25	O25	126.9(13)
O9	Mn4	O18	81.0(3)	O23	C25	C23	118.1(14)
O22	Mn4	O2	88.5(4)	O25	C25	C23	115.0(15)
O22	Mn4	O9	87.3(4)	N2	C26	C58	125(3)
O22	Mn4	O18	90.4(3)	C22	C27	C47	118.1(13)
O5	Mn5	O16	93.4(4)	C29	C28	C16	121.2(16)
O5	Mn5	O31	158.3(4)	C28	C29	C33	120.8(15)
O5	Mn5	O32	98.9(4)	C52	C30	C55	122.0(14)
O6	Mn5	O5	88.7(3)	C19	C31	C9	122.8(15)
O6	Mn5	O16	171.7(4)	O9	C32	C2	114.9(15)
O6	Mn5	O31	91.2(4)	O11	C32	O9	124.9(13)
O6	Mn5	O32	98.8(4)	O11	C32	C2	120.2(14)
O16	Mn5	O31	83.9(4)	C24	C33	C8	122.6(15)
O16	Mn5	O32	88.9(4)	C29	C33	C8	116.8(15)
O31	Mn5	O32	102.6(4)	C29	C33	C24	120.6(13)
O1	Mn6	O23	87.9(4)	C91	C34	C37	122(2)
O1	Mn6	O30	91.4(4)	O18	C35	C3	117.5(15)
O1	Mn6	N1	85.6(5)	O30	C35	O18	124.0(13)
O7	Mn6	O1	93.6(4)	O30	C35	C3	118.2(15)
O7	Mn6	O23	178.5(4)	C113	C36	C21	117(2)
O7	Mn6	O30	96.7(4)	C34	C37	C5	123(2)
O7	Mn6	N1	98.8(4)	C45	C37	C5	123.4(17)
O17	Mn6	O1	175.0(4)	C45	C37	C34	113.3(18)
O17	Mn6	O7	82.8(3)	C50	C39	C38	122.2(19)
O17	Mn6	O23	95.8(4)	C50	C39	C56	119.8(14)
O17	Mn6	O30	92.3(3)	C56	C39	C38	117.7(18)

O17	Mn6	N1	91.6(4)	C41	C40	C61	117.2(15)
O23	Mn6	O30	83.2(4)	C40	C41	C2	124.3(14)
O23	Mn6	N1	81.3(4)	C112	C42	C45	122.0(18)
O30	Mn6	N1	164.3(4)	C109	C44	C7	119(5)
O3	Mn7	Mn1	40.4(2)	C37	C45	C1	120.8(18)
O3	Mn7	O7	152.0(3)	C42	C45	C1	117.6(18)
O3	Mn7	O10	103.6(3)	C42	C45	C37	121.6(16)
O3	Mn7	O17	94.5(3)	C6	C46	C9	119.5(14)
O5	Mn7	Mn1	40.4(2)	C6	C46	C13	116.7(17)
O5	Mn7	O3	80.6(3)	C9	C46	C13	123.8(17)
O5	Mn7	O7	95.2(3)	C3	C47	C27	123.5(13)
O5	Mn7	O10	96.9(3)	C21	C48	C90	117.3(19)
O5	Mn7	O17	160.2(3)	C43	C48	C21	122(2)
O7	Mn7	Mn1	128.1(2)	C43	C48	C90	121(2)
O7	Mn7	O10	104.4(3)	C51	C49	C23	120.7(14)
O10	Mn7	Mn1	105.9(2)	C63	C50	C39	122.8(16)
O17	Mn7	Mn1	130.8(2)	C52	C51	C49	118.7(15)
O17	Mn7	O7	80.1(3)	C51	C52	C30	120.6(14)
O17	Mn7	O10	102.9(3)	O16	C53	O24	123.5(14)
O3	Mn8	O8	95.0(4)	O16	C53	C21	117.4(16)
O3	Mn8	O12	172.2(4)	O24	C53	C21	119.0(16)
O3	Mn8	O21	95.7(3)	C16	C54	C24	121.1(15)
O3	Mn8	O27	92.6(3)	C23	C55	C30	119.4(13)
O4	Mn8	O3	88.3(3)	C23	C55	C82	122.7(15)
O4	Mn8	O8	173.9(4)	C30	C55	C82	118.0(17)
O4	Mn8	O12	87.5(4)	C39	C56	C20	128.7(17)
O4	Mn8	O21	96.5(4)	C59	C56	C20	116.4(17)
O4	Mn8	O27	85.7(3)	C59	C56	C39	114.9(15)
O8	Mn8	O12	88.6(4)	C2	C57	C88	122.7(15)
O8	Mn8	O21	88.3(4)	C4	C57	C2	118.6(14)
O8	Mn8	O27	89.0(3)	C4	C57	C88	118.7(16)
O12	Mn8	O21	91.2(4)	C26	C58	C109	110(3)
O12	Mn8	O27	80.6(4)	C56	C59	C64	124.7(18)
O21	Mn8	O27	171.5(3)	C22	C60	C15	122.5(13)
O6	Mn9	O11	88.4(4)	C40	C61	C4	121.2(14)
O6	Mn9	O18	85.5(3)	C113	C62	C90	130(2)
O6	Mn9	O19	171.6(3)	C50	C63	C64	118.1(18)
O6	Mn9	O20	86.4(4)	C59	C64	C63	119.7(18)
O10	Mn9	O6	89.1(3)	O8	C65	O13	123.0(15)
O10	Mn9	O11	170.4(4)	O8	C65	C66	120.2(16)
O10	Mn9	O18	90.0(3)	O13	C65	C66	116.8(18)
O10	Mn9	O19	98.2(4)	C71	C66	C65	121(2)
O10	Mn9	O20	100.8(3)	C71	C66	C89	120.5(15)
O11	Mn9	O18	80.6(3)	C89	C66	C65	119(2)
O11	Mn9	O20	88.3(4)	C69	C67	C83	124.4(17)

O19	Mn9	O11	85.1(4)	C80	C67	C69	116.6(14)
O19	Mn9	O18	98.6(4)	C80	C67	C83	118.9(17)
O19	Mn9	O20	88.1(4)	C73	C68	C81	118.2(15)
O20	Mn9	O18	166.4(4)	C73	C68	C100	124.2(18)
C8	O1	Mn6	128.3(9)	C81	C68	C100	117(2)
C20	O2	Mn4	131.1(9)	C67	C69	C72	122.3(17)
Mn1	O3	Mn7	98.0(4)	C67	C69	C76	121.1(14)
Mn1	O3	Mn8	121.5(4)	C76	C69	C72	116.4(17)
Mn8	O3	Mn7	120.7(4)	O12	C70	C73	116.2(16)
Mn3	O4	Mn2	123.8(4)	O33	C70	O12	126.5(14)
Mn3	O4	Mn8	130.2(4)	O33	C70	C73	117.3(16)
Mn8	O4	Mn2	105.1(4)	C93	C71	C66	120(2)
Mn1	O5	Mn7	98.2(4)	O14	C72	O15	122.5(16)
Mn5	O5	Mn1	127.7(4)	O14	C72	C69	120.5(15)
Mn5	O5	Mn7	123.7(4)	O15	C72	C69	116.9(16)
Mn4	O6	Mn9	105.3(4)	C68	C73	C70	125.0(17)
Mn5	O6	Mn4	130.0(4)	C68	C73	C97	116.9(16)
Mn5	O6	Mn9	123.2(4)	C97	C73	C70	117.8(18)
Mn4	O7	Mn7	119.7(4)	C101	C74	C75	121(2)
Mn6	O7	Mn4	122.5(4)	C74	C75	C77	119.9(18)
Mn6	O7	Mn7	98.3(3)	C74	C75	C92	116.1(18)
C65	O8	Mn8	135.1(10)	C92	C75	C77	124(2)
C32	O9	Mn4	128.3(9)	C98	C76	C69	120.5(16)
Mn2	O10	Mn7	116.4(4)	O20	C77	O31	123.6(15)
Mn2	O10	Mn9	124.9(4)	O20	C77	C75	120.0(16)
Mn9	O10	Mn7	118.5(4)	O31	C77	C75	116.3(17)
C32	O11	Mn9	127.5(9)	C67	C80	C87	121.8(15)
C70	O12	Mn8	127.2(9)	C99	C81	C68	120.1(17)
C65	O13	Mn1	127.6(10)	C96	C84	C17	118.7(16)
C72	O14	Mn2	121.0(8)	C89	C85	C86	124(2)
C72	O15	Mn3	118.0(10)	C85	C86	C93	119(2)
C53	O16	Mn5	137.8(10)	C98	C87	C80	120.1(16)
Mn3	O17	Mn7	120.0(4)	C66	C89	C114	126(2)
Mn6	O17	Mn3	126.5(4)	C85	C89	C66	116.5(19)
Mn6	O17	Mn7	98.8(4)	C85	C89	C114	117(3)
Mn9	O18	Mn4	83.6(4)	C62	C90	C48	113.1(18)
C35	O18	Mn4	123.5(8)	C112	C91	C34	121(2)
C35	O18	Mn9	141.2(7)	C75	C92	C108	125(3)
C18	O19	Mn9	125.1(9)	C104	C92	C75	123(2)
C77	O20	Mn9	126.7(9)	C104	C92	C108	111(3)
C1	O21	Mn8	132.3(9)	C71	C93	C86	119(2)
C8	O22	Mn4	134.4(9)	N1	C94	C95	123.6(14)
C25	O23	Mn6	127.9(9)	C106	C95	C94	117.1(16)
C53	O24	Mn1	126.9(9)	C105	C96	C84	123.9(17)
C25	O25	Mn3	136.1(9)	C73	C97	C102	125(2)

C18	O26	Mn2	127.4(9)	C87	C98	C76	119.8(18)
Mn2	O27	Mn8	82.6(4)	C81	C99	C102	124(2)
C13	O27	Mn2	135.1(8)	C103	C101	C74	118(2)
C13	O27	Mn8	123.7(9)	C99	C102	C97	115(2)
C1	O28	Mn3	132.8(10)	C101	C103	C104	124(3)
C13	O29	Mn1	133.3(9)	C92	C104	C103	117(2)
C35	O30	Mn6	133.1(9)	C96	C105	C111	120.5(18)
C77	O31	Mn5	117.5(10)	C95	C106	C110	121(2)
C20	O32	Mn5	129.9(9)	N1	C107	C110	128.1(18)
C70	O33	Mn2	127.5(9)	C44	C109	C58	118(4)
C94	N1	Mn6	126.8(12)	C106	C110	C107	117(2)
C107	N1	Mn6	117.2(12)	C105	C111	C10	118.5(17)
C107	N1	C94	113.4(13)	C42	C112	C91	120(2)
C7	N2	Mn1	128.2(18)	C62	C113	C36	120(3)
C7	N2	C26	112(2)				

Table II.2.5.6 Hydrogen Atom Coordinates (Å×10^4) and Isotropic Displacement Parameters (Å^2×10^3) for ab58027.

Atom	*x*	*y*	*z*	U(eq)
H0BA	1514	11541	1516	69
H0CA	164	9894	3534	279
H0DA	753	9455	316	119
H1	2070	5216	3086	65
H1BA	1388	12133	2362	124
H1CA	193	11001	3080	152
H1DA	231	4691	-572	163
H1I	1431	8142	4215	49
H1M	2480	6973	-1122	56
H1PA	1006	5877	4886	103
H1PB	1124	6246	4323	103
H1PC	837	6281	4370	103
H1Q	614	6494	325	51
H1R	1244	4511	2032	121
H1X	409	6794	-614	69
H1YA	558	8847	1299	97
H1YB	370	8336	1603	97
H1YC	272	8923	1114	97
H2AA	890	5793	-1015	78
H2BA	1648	6486	3846	137
H2CA	959	10409	2119	232
H2CB	754	10919	1797	232
H2CC	768	10106	1593	232
H2E	1124	5506	3448	143
H2F	2124	9478	161	53

H2G	2782	4974	947	86
H2H	2410	5474	1075	62
H2J	2206	8908	5443	55
H2K	206	8639	117	78
H2O	928	6605	5812	134
H2R	597	5146	-119	136
H2TA	2084	4107	2324	148
H2TB	1887	4689	2084	148
H2TC	2137	4618	1766	148
H2Y	1853	7732	-1990	81
H2Z	1667	7558	-1102	55
H3A	2457	7756	3743	74
H3BA	1669	5850	4737	206
H3C	2077	2957	1850	67
H3CA	725	5931	-2022	132
H3D	2746	8232	4477	89
H3F	2614	8747	5349	72
H3J	3045	5674	2609	77
H3X	1385	4722	4084	220
H4AA	-36	4810	3383	132
H5	1879	2156	1246	112
H5A	1871	4783	4763	178
H4CA	682	7028	-2411	211
H4N	1552	2540	562	192
H5	461	11245	2404	85
H5AA	1286	10412	-1022	89
H5BA	2104	4494	3986	75
H5CA	812	8029	-1875	202
H6AA	1611	9513	67	75
H6AB	1607	9794	-624	75
H6AC	1543	8983	-493	75
H6BA	1295	11507	3214	161
H6CA	1575	3724	3451	278
H7AA	2321	6951	329	104
H7AB	2522	6680	-104	104
H7AC	2299	6175	31	104
H7BA	616	10224	-482	169
H7CA	1107	8657	5880	138
H8A	1696	9829	1401	131
H8AA	2132	8859	2689	81
H8AB	2406	9121	2658	81
H8AC	2338	8306	2530	81
H8B	1647	10552	1027	131
H8BA	877	10680	-1104	146
H8C	1434	9980	1055	131

H9	325	5092	2984	96
H9AA	1752	9022	4449	105
H9AB	1798	8789	5153	105
H9AC	1714	8212	4641	105
H9BA	438	9025	3265	148
H10	-160	6872	3652	109
H11	-289	5722	3682	123
H15	150	3324	815	112
H16	958	7663	6332	178
H18A	838	8470	-1004	232
H18B	1123	8311	-878	232
H18C	938	8069	-390	232
H19	1351	10298	3250	107
H20A	2594	6833	2887	79
H20B	2827	6419	3195	79
H20C	2560	6099	3238	79
H22	3096	5043	1707	91
H25	195	7866	-710	76
H28	2418	10072	809	54
H30	1195	8627	4891	87
H32	1457	3658	2480	151
H37	1908	8550	558	48
H40	1453	3704	504	139
H42	2478	9763	1825	48
H43	2265	7448	-1995	82
H45	61	3791	-166	145

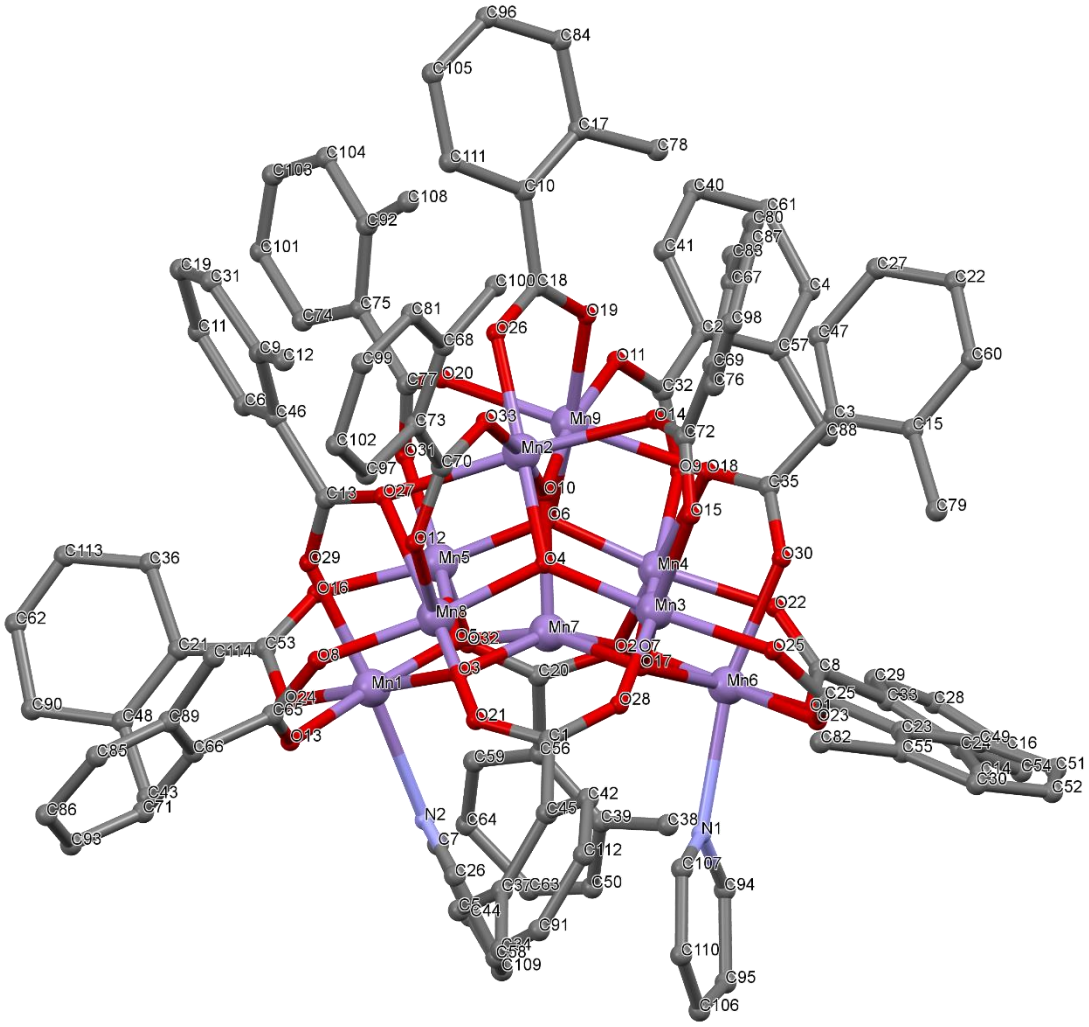

Figure II.2.5 Crystal Structure with atomic labels for compound **4b**, "Mn_{13}-2-Methyl" (cube), $Mn_9O_7(O_2CPh\text{-}o\text{-}Me)_{13}(Pyr)_2$, ab58027

II.2.6 Compound 5, Mn_3O-2-Ethyl, $Mn_3O(O_2CPh\text{-}o\text{-}Et)_6(Pyr)_3$, ab58029

Table II.2.6.1 Crystal data and structure refinement for ab58029.

Identification code	ab58029
Empirical formula	$C_{64}H_{66}Mn_3NO_{14}$
Formula weight	1237.99
Temperature/K	100.0
Crystal system	triclinic
Space group	P-1
a/Å	12.0698(12)
b/Å	14.3404(14)
c/Å	19.1822(18)
α/°	82.143(5)
β/°	89.878(5)
γ/°	70.928(5)
Volume/Å^3	3105.3(5)
Z	2
ρ_{calc}g/cm^3	1.324
μ/mm^{-1}	0.664
F(000)	1288.0
Crystal size/mm^3	0.29 × 0.121 × 0.09
Radiation	MoKα (λ = 0.71073)
2Θ range for data collection/°	2.146 to 52.31
Index ranges	$-14 \le h \le 14$, $-17 \le k \le 17$, $-23 \le l \le 23$
Reflections collected	52918
Independent reflections	12353 [R_{int} = 0.0416, R_{sigma} = 0.0328]
Data/restraints/parameters	12353/0/799
Goodness-of-fit on F^2	1.048
Final R indexes [I>=2σ (I)]	R_1 = 0.0412, wR_2 = 0.1014
Final R indexes [all data]	R_1 = 0.0504, wR_2 = 0.1102
Largest diff. peak/hole / e Å^{-3}	1.12/-1.09

Table II.2.6.2 Fractional Atomic Coordinates (×10^4) and Equivalent Isotropic Displacement Parameters (Å^2×10^3) for ab58029. U_{eq} is defined as 1/3 of of the trace of the orthogonalised U_{IJ} tensor.

Atom	*x*	*y*	*z*	U(eq)
Mn1	1575.6(3)	6807.6(2)	1528.4(2)	14.13(9)
Mn2	4023.9(3)	6678.6(2)	2269.1(2)	13.79(8)
Mn3	1845.9(3)	6506.1(2)	3333.1(2)	16.44(9)
O1	2512.3(13)	6674.7(11)	2309.8(8)	15.4(3)
O2	166.8(14)	7656.2(12)	2956.9(9)	23.6(4)
O3	2383.4(15)	7672.3(13)	3658.7(9)	26.1(4)
O4	870.3(16)	5629.2(13)	1919.9(9)	28.7(4)
O5	3460.1(15)	5392.0(14)	3765.9(9)	30.8(4)

O6	2099.3(16)	7971.1(13)	916.2(9)	27.6(4)
O7	4477.0(15)	5711.8(14)	1463.7(11)	31.5(4)
O8	3684.4(15)	7873.8(13)	1551.5(10)	28.7(4)
O9	1295.4(17)	5287.0(13)	3078.5(9)	27.9(4)
O10	2715.4(15)	5762.4(13)	1102.1(9)	26.2(4)
O11	4729.4(15)	5441.1(13)	2931.5(10)	30.7(4)
O12	277.8(15)	7914.9(13)	1786.2(9)	25.7(4)
O13	3965.1(15)	7607.5(13)	3042.5(10)	29.7(4)
N1	529.0(17)	6988.6(15)	606.7(10)	19.9(4)
N2	5762.6(16)	6652.1(14)	2164.2(10)	18.4(4)
N3	930.1(17)	6417.2(15)	4360.5(10)	21.1(4)
C1	5781(2)	3113.0(18)	409.7(14)	26.9(5)
C2	5748(2)	2399(2)	4500.0(14)	28.9(6)
C3	4404(2)	8989.4(19)	3762.4(13)	25.9(5)
C4	3231(2)	3355(2)	2729.6(15)	29.7(6)
C5	550(3)	6195(2)	294.9(15)	34.3(6)
C6	3815(2)	3621(2)	4711.1(14)	29.8(6)
C7	7341(2)	6772.4(19)	1444.7(17)	33.8(6)
C8	2976(2)	9217.7(17)	634.3(14)	24.0(5)
C9	2324(2)	9626.9(18)	3972.3(12)	24.5(5)
C10	-893(2)	9249.6(17)	2320.7(12)	21.6(5)
C11	-2587(2)	10546(2)	2611.1(15)	31.5(6)
C12	3509(2)	3882.7(19)	811.5(14)	26.5(5)
C13	8059(2)	6633(2)	2035.5(19)	39.7(7)
C14	-609(2)	9964(2)	1850.6(15)	31.5(6)
C15	6808(2)	2087.2(19)	4182.4(14)	30.0(6)
C16	2539(3)	10420(2)	4234.0(14)	32.6(6)
C17	-90.6(19)	8185.4(17)	2378.5(12)	19.7(5)
C18	-77(2)	7894.1(19)	276.0(13)	25.9(5)
C19	3652(3)	10488(2)	4273.4(14)	34.7(6)
C20	-689(2)	7235(2)	-669.2(14)	33.6(6)
C21	901(3)	2117(2)	2561.9(14)	31.0(6)
C22	7087(2)	2715.9(19)	3656.4(14)	27.3(5)
C23	-2261(2)	8827(2)	3239.5(15)	30.1(6)
C24	-693(2)	8044(2)	-360.9(14)	30.9(6)
C25	-112(2)	2930(2)	2444.3(14)	30.4(6)
C26	1084(2)	9591(2)	3936.5(16)	34.1(6)
C27	6470(2)	6498.5(18)	2740.2(15)	27.4(6)
C28	4387(2)	5021.6(17)	3481.9(12)	19.6(5)
C29	-2291(3)	11240(2)	2150.3(16)	38.3(7)
C30	3525(3)	9831(2)	899.5(19)	45.7(8)
C31	-1296(3)	10957(2)	1769.9(16)	39.0(7)
C32	7049(3)	4164(2)	1462.3(17)	41.6(7)
C33	-757(3)	6217(3)	4932.7(17)	47.0(8)
C34	4323(2)	2470(2)	2646.8(18)	39.5(7)

C35	-398(3)	6443(3)	5551.0(16)	45.4(8)
C36	3348(3)	10745(2)	-272(2)	52.8(10)
C37	-36(3)	6292(2)	-343.6(16)	40.6(7)
C38	111(3)	10534(2)	4070.9(19)	45.1(8)
C39	634(3)	6636(3)	5563.8(16)	53.6(9)
C40	3702(3)	10585(2)	421(2)	56.6(10)
C41	3788(5)	9810(3)	1703(2)	97(2)
C42	4985(5)	9575(5)	1920(2)	103(2)
C43	4301(2)	4389.1(17)	895.7(12)	19.4(5)
C44	1030(2)	4023.3(17)	2503.4(12)	19.5(5)
C45	5215(2)	4000.7(17)	3774.4(12)	18.6(5)
C46	1978(2)	2248.0(19)	2647.9(13)	28.2(6)
C47	2553(2)	9416.3(18)	-62.8(14)	27.3(5)
C48	3821.7(19)	5357.6(16)	1182.3(12)	17.5(5)
C49	1069.9(19)	5066.9(17)	2499.3(12)	19.3(5)
C50	-43(2)	3884.5(19)	2410.0(13)	24.9(5)
C51	2065(2)	3199.6(18)	2622.0(12)	22.6(5)
C52	-1891(2)	9536.6(19)	2718.5(13)	24.6(5)
C53	5466(2)	3999.9(17)	694.9(13)	21.6(5)
C54	2888(2)	8289.1(16)	1067.9(12)	18.1(5)
C55	6292(2)	3666.9(18)	3456.5(12)	21.7(5)
C56	6391(2)	4487.7(19)	762.0(14)	26.5(5)
C57	4931(2)	3351.3(19)	4311.8(12)	22.4(5)
C58	3190(2)	7993.4(17)	3454.9(12)	19.0(5)
C59	6199(2)	6779.7(18)	1527.3(14)	24.9(5)
C60	3291(2)	8897.9(17)	3735.3(12)	20.5(5)
C61	4598(3)	9773(2)	4038.2(14)	32.3(6)
C62	4992(2)	2615(2)	325.3(16)	33.3(6)
C63	2746(3)	10180(2)	-524.9(16)	40.3(7)
C64	7619(2)	6487(2)	2683.8(18)	38.7(7)
C65	-1898(3)	8846(2)	4000.5(15)	42.3(7)
C66	3848(3)	3003(2)	530.9(16)	35.7(7)
C67	1270(3)	6622(2)	4961.9(15)	38.7(7)
C68	-73(2)	6216(2)	4356.8(15)	37.3(7)
C69	3894(3)	4204(2)	5304.4(14)	38.7(7)

Table II.2.6.3 Anisotropic Displacement Parameters ($Å^2×10^3$) for ab58029. The Anisotropic displacement factor exponent takes the form: $-2\pi^2[h^2a^{*2}U_{11}+2hka^*b^*U_{12}+\ldots]$.

Atom	U_{11}	U_{22}	U_{33}	U_{23}	U_{13}	U_{12}
Mn1	12.17(16)	15.10(17)	14.87(17)	-2.17(13)	0.97(12)	-4.16(13)
Mn2	12.01(16)	13.77(16)	15.37(17)	-2.09(13)	0.64(12)	-3.97(13)
Mn3	14.77(17)	18.04(17)	15.40(17)	-2.69(13)	2.13(13)	-3.80(13)
O1	14.2(7)	16.6(7)	16.1(8)	-3.0(6)	1.8(6)	-5.6(6)
O2	19.4(8)	24.4(9)	20.6(9)	0.6(7)	4.2(7)	-0.1(7)

O3	27.9(9)	32.2(10)	26.0(9)	-11.4(8)	8.2(7)	-17.6(8)
O4	29.7(10)	29.1(9)	29.6(10)	10.5(8)	-12.5(8)	-18.5(8)
O5	25.5(9)	34.8(10)	19.2(9)	-1.5(8)	1.4(7)	6.6(8)
O6	33.8(10)	31.6(10)	22.7(9)	5.8(7)	-6.7(7)	-21.8(8)
O7	19.2(9)	32.9(10)	50.3(12)	-26.1(9)	7.4(8)	-11.2(8)
O8	18.4(8)	25.1(9)	39.4(11)	11.6(8)	-4.7(7)	-9.2(7)
O9	42.6(11)	23.9(9)	23.1(9)	-6.8(7)	10.0(8)	-17.5(8)
O10	20.3(9)	26.9(9)	28.0(9)	-14.4(7)	-3.4(7)	1.0(7)
O11	19.7(9)	23.7(9)	43.8(11)	10.2(8)	-2.0(8)	-6.6(7)
O12	22.6(9)	26.1(9)	19.7(9)	-6.1(7)	-0.5(7)	4.8(7)
O13	26.2(9)	30.9(10)	40.3(11)	-20.0(8)	13.5(8)	-14.9(8)
N1	17.4(9)	23.6(10)	18.7(10)	-1.1(8)	1.1(8)	-7.7(8)
N2	13.5(9)	14.6(9)	27.4(11)	-5.0(8)	-0.7(8)	-4.2(7)
N3	20.2(10)	24.6(10)	18.1(10)	-0.9(8)	1.1(8)	-7.8(8)
C1	22.9(13)	21.9(12)	36.4(15)	-11.5(11)	9.5(11)	-5.0(10)
C2	31.7(14)	28.6(13)	25.1(13)	5.1(11)	-3.0(11)	-11.7(11)
C3	29.3(13)	29.0(13)	22.3(13)	-6.1(10)	5.7(10)	-12.7(11)
C4	23.5(13)	27.9(13)	36.4(15)	-9.9(11)	-4.1(11)	-4.7(11)
C5	39.7(16)	27.8(14)	35.9(15)	-0.3(12)	-13.8(12)	-13.7(12)
C6	25.7(13)	37.9(15)	27.2(14)	-1.7(11)	4.5(10)	-13.6(12)
C7	23.0(13)	23.1(13)	57.4(19)	-8.1(12)	16.5(13)	-9.4(11)
C8	18.1(12)	18.2(11)	32.8(14)	2.7(10)	1.7(10)	-4.7(9)
C9	32.2(14)	23.4(12)	16.4(12)	-2.8(9)	3.0(10)	-7.2(11)
C10	21.1(12)	20.7(12)	20.3(12)	-3.3(9)	-0.8(9)	-3.0(10)
C11	25.7(13)	28.6(14)	36.4(15)	-10.5(12)	5.5(11)	-1.6(11)
C12	22.5(12)	27.6(13)	35.8(14)	-13.7(11)	11.9(10)	-13.1(10)
C13	16.0(12)	23.4(13)	80(2)	-3.6(14)	1.9(14)	-8.8(11)
C14	32.6(14)	26.8(13)	33.5(15)	-4.3(11)	7.3(11)	-7.8(11)
C15	27.6(13)	21.0(12)	33.5(15)	1.2(11)	-7.4(11)	0.7(10)
C16	46.1(17)	26.3(13)	24.4(14)	-10.3(11)	6.7(12)	-8.0(12)
C17	14.6(11)	22.1(12)	22.5(12)	-4.8(10)	1.9(9)	-5.5(9)
C18	23.6(12)	24.1(12)	25.7(13)	-0.9(10)	-1.0(10)	-3.3(10)
C19	53.1(18)	31.5(14)	27.8(14)	-11.8(12)	3.5(12)	-22.0(13)
C20	30.7(14)	48.8(17)	21.7(13)	0.1(12)	-6.8(11)	-15.5(13)
C21	46.3(16)	25.3(13)	26.9(14)	-3.8(11)	3.0(12)	-19.1(12)
C22	18.0(12)	28.9(13)	31.2(14)	-8.1(11)	2.6(10)	-1.1(10)
C23	23.5(13)	28.5(13)	38.5(15)	-9.6(12)	10.5(11)	-6.9(11)
C24	28.0(14)	33.1(14)	25.2(13)	5.4(11)	-4.2(11)	-5.2(11)
C25	33.5(14)	38.7(15)	29.2(14)	-8.0(12)	4.2(11)	-24.5(13)
C26	28.5(14)	35.4(15)	36.3(16)	-11.8(12)	8.3(12)	-5.2(12)
C27	22.2(13)	22.6(12)	37.8(15)	-2.5(11)	-6.4(11)	-8.7(10)
C28	18.0(11)	21.4(11)	19.6(12)	-6.0(9)	-5.1(9)	-5.7(9)
C29	42.6(17)	22.2(13)	42.7(17)	-5.1(12)	1.3(13)	-0.4(12)
C30	39.2(17)	30.2(15)	68(2)	18.3(15)	-21.0(15)	-21.8(13)
C31	51.2(18)	22.0(13)	41.6(17)	-1.8(12)	7.7(14)	-9.9(13)

C32	41.1(17)	37.9(16)	44.9(18)	0.8(14)	-9.8(14)	-14.5(14)
C33	33.9(16)	76(2)	36.0(17)	-3.8(16)	9.6(13)	-27.0(16)
C34	26.0(14)	35.7(16)	53.7(19)	-15.9(14)	-1.8(13)	-2.2(12)
C35	45.5(18)	60(2)	30.4(16)	-5.7(15)	19.6(14)	-18.0(16)
C36	41.7(18)	30.6(16)	79(3)	22.6(16)	12.5(17)	-14.9(14)
C37	46.9(18)	41.6(17)	37.4(17)	-8.7(13)	-12.3(13)	-18.7(14)
C38	35.1(16)	34.7(16)	58(2)	-4.1(14)	15.5(14)	-1.6(13)
C39	69(2)	87(3)	24.5(16)	-24.9(17)	14.1(15)	-47(2)
C40	45.8(19)	39.1(18)	84(3)	30.2(18)	-21.2(18)	-28.7(16)
C41	150(5)	70(3)	93(3)	54(2)	-92(3)	-90(3)
C42	94(4)	194(6)	57(3)	-35(3)	11(3)	-91(4)
C43	19.8(11)	19.1(11)	20.6(12)	-4.1(9)	4.0(9)	-7.3(9)
C44	23.6(12)	23.4(12)	13.2(11)	-1.5(9)	2.1(9)	-10.3(10)
C45	18.5(11)	20.8(11)	15.7(11)	-3.4(9)	-3.0(9)	-5.1(9)
C46	36.6(15)	21.9(12)	24.6(13)	-1.7(10)	-4.3(11)	-8.4(11)
C47	28.7(13)	18.9(12)	28.2(14)	0.7(10)	7.5(11)	-1.5(10)
C48	17.8(11)	17.4(11)	17.7(11)	-2.4(9)	3.8(9)	-6.4(9)
C49	12.1(10)	20.6(11)	24.5(12)	0.1(10)	2.0(9)	-5.9(9)
C50	22.9(12)	28.8(13)	25.1(13)	-4.9(10)	1.6(10)	-11.1(10)
C51	26.7(13)	24.4(12)	17.1(12)	-3.1(9)	-1.2(9)	-9.0(10)
C52	21.0(12)	27.3(13)	23.1(13)	-6.2(10)	1.0(10)	-3.8(10)
C53	19.9(12)	19.7(11)	26.0(13)	-4.7(10)	3.6(9)	-7.0(9)
C54	17.4(11)	14.7(10)	21.1(12)	-3.3(9)	5.8(9)	-3.7(9)
C55	23.9(12)	21.7(12)	19.5(12)	-1.6(9)	-0.6(9)	-7.8(10)
C56	18.0(12)	23.8(12)	39.0(15)	-8.4(11)	4.3(10)	-7.1(10)
C57	20.2(12)	29.3(13)	17.7(12)	-3.8(10)	-1.1(9)	-8.0(10)
C58	18.1(11)	18.2(11)	19.5(11)	-1.6(9)	0.6(9)	-4.7(9)
C59	19.9(12)	21.3(12)	35.7(14)	-7.4(10)	7.4(10)	-8.6(10)
C60	28.4(13)	19.8(11)	14.2(11)	-0.8(9)	1.0(9)	-9.7(10)
C61	40.0(16)	39.8(15)	26.9(14)	-7.5(12)	3.4(11)	-25.4(13)
C62	36.3(15)	23.6(13)	46.1(17)	-18.4(12)	14.8(13)	-12.8(12)
C63	41.5(17)	29.7(15)	34.7(16)	10.3(12)	10.9(13)	2.5(13)
C64	23.1(14)	33.3(15)	59(2)	-1.9(14)	-16.3(13)	-9.9(12)
C65	55(2)	37.4(16)	31.2(16)	-3.7(13)	10.3(14)	-11.4(15)
C66	34.4(15)	33.6(15)	51.5(18)	-20.9(13)	14.9(13)	-22.0(13)
C67	39.4(16)	61(2)	28.3(15)	-14.2(14)	6.9(12)	-30.9(15)
C68	31.1(15)	63(2)	23.5(14)	-3.6(13)	1.8(11)	-25.0(14)
C69	34.3(15)	59(2)	22.7(14)	-9.0(13)	5.0(11)	-14.4(14)

Table II.2.6.4 Bond Lengths for ab58029.

Atom	Atom	Length/Å	Atom	Atom	Length/Å
O1	Mn1	1.8302(15)	C18	N1	1.334(3)
O1	Mn2	1.8278(15)	C18	C24	1.385(4)

O1	Mn3	2.1329(15)	C19	C61	1.385(4)
O2	Mn3	2.2011(16)	C20	C24	1.372(4)
O3	Mn3	2.1456(17)	C20	C37	1.384(4)
O4	Mn1	2.1760(17)	C21	C25	1.380(4)
O5	Mn3	2.1559(17)	C21	C46	1.386(4)
O6	Mn1	2.1709(17)	C22	C55	1.390(3)
O7	Mn2	2.1667(18)	C23	C52	1.500(4)
O8	Mn2	1.9745(17)	C23	C65	1.531(4)
O9	Mn3	2.1749(17)	C25	C50	1.391(4)
O10	Mn1	1.9470(17)	C26	C38	1.527(4)
O11	Mn2	1.9721(17)	C27	N2	1.347(3)
O12	Mn1	1.9508(16)	C27	C64	1.386(4)
O13	Mn2	2.1115(17)	C28	O5	1.232(3)
N1	Mn1	2.111(2)	C28	O11	1.279(3)
N2	Mn2	2.0963(19)	C28	C45	1.510(3)
N3	Mn3	2.266(2)	C29	C31	1.377(4)
C1	C53	1.391(3)	C30	C40	1.392(4)
C1	C62	1.385(4)	C30	C41	1.568(5)
C2	C15	1.380(4)	C32	C56	1.498(4)
C2	C57	1.398(4)	C33	C35	1.378(5)
C3	C60	1.393(3)	C33	C68	1.378(4)
C3	C61	1.391(4)	C35	C39	1.361(5)
C4	C34	1.528(4)	C36	C40	1.364(5)
C4	C51	1.513(3)	C36	C63	1.384(5)
C5	N1	1.349(3)	C39	C67	1.384(4)
C5	C37	1.383(4)	C41	C42	1.422(6)
C6	C57	1.512(3)	C43	C48	1.499(3)
C6	C69	1.522(4)	C43	C53	1.407(3)
C7	C13	1.380(4)	C44	C49	1.512(3)
C7	C59	1.384(3)	C44	C50	1.389(3)
C8	C30	1.405(4)	C44	C51	1.404(3)
C8	C47	1.391(4)	C45	C55	1.400(3)
C8	C54	1.505(3)	C45	C57	1.411(3)
C9	C16	1.401(4)	C46	C51	1.397(3)
C9	C26	1.517(4)	C47	C63	1.392(4)
C9	C60	1.411(3)	C48	O7	1.230(3)
C10	C14	1.399(4)	C48	O10	1.270(3)
C10	C17	1.506(3)	C49	O4	1.254(3)
C10	C52	1.400(3)	C49	O9	1.250(3)
C11	C29	1.376(4)	C53	C56	1.513(3)
C11	C52	1.402(4)	C54	O6	1.233(3)
C12	C43	1.398(3)	C54	O8	1.272(3)
C12	C66	1.377(4)	C58	O3	1.247(3)
C13	C64	1.368(5)	C58	O13	1.259(3)
C14	C31	1.382(4)	C58	C60	1.511(3)

C15	C22	1.376(4)	C59	N2	1.343(3)
C16	C19	1.381(4)	C62	C66	1.389(4)
C17	O2	1.233(3)	C67	N3	1.327(3)
C17	O12	1.283(3)	C68	N3	1.333(3)

Table II.2.6.5 Bond Angles for ab58029.

Atom	Atom	Atom	Angle/°	Atom	Atom	Atom	Angle/°
O1	Mn1	O4	96.53(6)	C52	C10	C17	122.4(2)
O1	Mn1	O6	95.99(6)	C29	C11	C52	121.8(3)
O1	Mn1	O10	94.95(7)	C66	C12	C43	121.0(2)
O1	Mn1	O12	95.45(7)	C64	C13	C7	118.5(2)
O1	Mn1	N1	178.01(7)	C31	C14	C10	121.2(3)
O6	Mn1	O4	167.23(7)	C22	C15	C2	120.2(2)
O10	Mn1	O4	83.99(8)	C19	C16	C9	122.0(3)
O10	Mn1	O6	92.45(8)	O2	C17	O12	125.5(2)
O10	Mn1	O12	169.39(7)	O2	C17	C10	120.6(2)
O10	Mn1	N1	84.64(7)	O12	C17	C10	113.9(2)
O12	Mn1	O4	96.90(8)	N1	C18	C24	122.7(2)
O12	Mn1	O6	84.37(8)	C16	C19	C61	120.4(2)
O12	Mn1	N1	84.89(7)	C24	C20	C37	118.7(2)
N1	Mn1	O4	85.38(7)	C25	C21	C46	120.4(2)
N1	Mn1	O6	82.08(7)	C15	C22	C55	119.0(2)
O1	Mn2	O7	94.24(7)	C52	C23	C65	112.7(2)
O1	Mn2	O8	95.82(7)	C20	C24	C18	119.3(2)
O1	Mn2	O11	96.58(7)	C21	C25	C50	119.4(2)
O1	Mn2	O13	98.17(7)	C9	C26	C38	116.0(2)
O1	Mn2	N2	176.58(7)	N2	C27	C64	121.2(3)
O8	Mn2	O7	91.12(8)	O5	C28	O11	124.6(2)
O8	Mn2	O13	87.96(8)	O5	C28	C45	120.7(2)
O8	Mn2	N2	83.25(7)	O11	C28	C45	114.7(2)
O11	Mn2	O7	84.73(8)	C11	C29	C31	120.4(3)
O11	Mn2	O8	167.18(7)	C8	C30	C41	124.2(3)
O11	Mn2	O13	93.49(8)	C40	C30	C8	117.0(3)
O11	Mn2	N2	84.18(7)	C40	C30	C41	118.3(3)
O13	Mn2	O7	167.58(7)	C29	C31	C14	119.1(3)
N2	Mn2	O7	82.50(7)	C68	C33	C35	118.8(3)
N2	Mn2	O13	85.09(7)	C39	C35	C33	117.9(3)
O1	Mn3	O2	90.00(6)	C40	C36	C63	120.7(3)
O1	Mn3	O3	92.99(6)	C5	C37	C20	119.0(3)
O1	Mn3	O5	93.31(6)	C35	C39	C67	119.9(3)
O1	Mn3	O9	90.69(6)	C36	C40	C30	122.4(3)
O1	Mn3	N3	173.42(7)	C42	C41	C30	116.5(5)
O2	Mn3	N3	83.71(7)	C12	C43	C48	116.2(2)

O3	Mn3	O2	87.49(7)	C12	C43	C53	120.1(2)
O3	Mn3	O5	91.32(7)	C53	C43	C48	123.7(2)
O3	Mn3	O9	176.10(7)	C50	C44	C49	119.4(2)
O3	Mn3	N3	88.70(7)	C50	C44	C51	120.3(2)
O5	Mn3	O2	176.54(6)	C51	C44	C49	120.3(2)
O5	Mn3	O9	87.16(8)	C55	C45	C28	117.2(2)
O5	Mn3	N3	93.01(7)	C55	C45	C57	119.0(2)
O9	Mn3	O2	93.82(7)	C57	C45	C28	123.7(2)
O9	Mn3	N3	87.79(7)	C21	C46	C51	121.1(2)
Mn1	O1	Mn3	119.82(7)	C8	C47	C63	120.5(3)
Mn2	O1	Mn1	123.41(8)	O7	C48	O10	124.5(2)
Mn2	O1	Mn3	116.77(7)	O7	C48	C43	120.9(2)
C17	O2	Mn3	128.57(15)	O10	C48	C43	114.6(2)
C58	O3	Mn3	130.51(16)	O4	C49	C44	117.3(2)
C49	O4	Mn1	129.68(15)	O9	C49	O4	126.2(2)
C28	O5	Mn3	130.13(16)	O9	C49	C44	116.5(2)
C54	O6	Mn1	127.38(15)	C44	C50	C25	120.7(2)
C48	O7	Mn2	126.46(15)	C44	C51	C4	120.1(2)
C54	O8	Mn2	134.09(15)	C46	C51	C4	121.8(2)
C49	O9	Mn3	131.14(15)	C46	C51	C44	118.1(2)
C48	O10	Mn1	133.35(15)	C10	C52	C11	117.5(2)
C28	O11	Mn2	134.57(16)	C10	C52	C23	123.8(2)
C17	O12	Mn1	133.23(15)	C11	C52	C23	118.7(2)
C58	O13	Mn2	132.90(15)	C1	C53	C43	117.6(2)
C5	N1	Mn1	120.78(17)	C1	C53	C56	118.0(2)
C18	N1	Mn1	121.05(17)	C43	C53	C56	124.3(2)
C18	N1	C5	117.8(2)	O6	C54	O8	125.4(2)
C27	N2	Mn2	120.24(17)	O6	C54	C8	118.9(2)
C59	N2	Mn2	121.23(16)	O8	C54	C8	115.7(2)
C59	N2	C27	118.5(2)	C22	C55	C45	121.8(2)
C67	N3	Mn3	124.82(17)	C32	C56	C53	112.6(2)
C67	N3	C68	116.7(2)	C2	C57	C6	117.5(2)
C68	N3	Mn3	118.31(17)	C2	C57	C45	117.9(2)
C62	C1	C53	122.1(2)	C45	C57	C6	124.6(2)
C15	C2	C57	122.2(2)	O3	C58	O13	125.3(2)
C61	C3	C60	121.5(2)	O3	C58	C60	118.6(2)
C51	C4	C34	115.9(2)	O13	C58	C60	116.0(2)
N1	C5	C37	122.5(3)	N2	C59	C7	122.3(3)
C57	C6	C69	111.8(2)	C3	C60	C9	119.9(2)
C13	C7	C59	119.1(3)	C3	C60	C58	117.1(2)
C30	C8	C54	122.2(2)	C9	C60	C58	123.0(2)
C47	C8	C30	120.7(2)	C19	C61	C3	118.7(3)
C47	C8	C54	117.0(2)	C1	C62	C66	119.7(2)
C16	C9	C26	119.9(2)	C36	C63	C47	118.6(3)
C16	C9	C60	117.4(2)	C13	C64	C27	120.3(3)

C60	C9	C26	122.7(2)	C12	C66	C62	119.5(2)
C14	C10	C17	117.6(2)	N3	C67	C39	122.9(3)
C14	C10	C52	120.0(2)	N3	C68	C33	123.8(3)

Table II.2.6.6 Hydrogen Atom Coordinates (Å×10^4) and Isotropic Displacement Parameters (Å^2×10^3) for ab58029.

Atom	*x*	*y*	*z*	U(eq)
H1	6562	2840	268	32
H1A	5567	1951	4858	35
H1B	5044	8505	3588	31
H1CA	3271	3530	3208	36
H1CB	3252	3933	2389	36
H1D	982	5546	523	41
H1EA	3660	3003	4910	36
H1EB	3149	4026	4381	36
H1F	7627	6862	987	41
H1J	-3282	10755	2864	38
H1K	2725	4150	950	32
H1L	8842	6638	1993	48
H1M	69	9763	1582	38
H1N	7345	1437	4327	36
H1O	1900	10927	4389	39
H1Q	-86	8459	486	31
H1R	3769	11029	4463	42
H1S	-1127	7320	-1098	40
H1T	860	1463	2584	37
H1U	7813	2503	3433	33
H1VA	-1907	8143	3124	36
H1VB	-3125	9001	3198	36
H1W	-1113	8701	-582	37
H1X	-850	2839	2387	36
H1YA	1040	9029	4285	41
H1YB	929	9443	3464	41
H1Z	6176	6396	3194	33
H2A	-2775	11920	2094	46
H2C	-1086	11438	1456	47
H2DA	7647	4488	1476	62
H2DB	7428	3438	1532	62
H2DC	6502	4353	1837	62
H2E	-1463	6064	4904	56
H2FA	4281	2266	2183	59
H2FB	4364	1913	3015	59
H2FC	5024	2664	2689	59
H2G	-855	6463	5956	55

H2H	3518	11249	-585	63
H2I	10	5720	-555	49
H2JA	168	11105	3746	68
H2JB	196	10647	4558	68
H2JC	-654	10455	3995	68
H2K	915	6779	5985	64
H2L	4083	11004	584	68
H2MA	3345	10473	1831	117
H2MB	3479	9318	1974	117
H2NA	5294	10080	1678	154
H2NB	5438	8919	1800	154
H2NC	5048	9566	2430	154
H6	2668	1681	2726	34
H7	2130	9028	-225	33
H10	-737	4447	2322	30
H15	6485	4103	3094	26
H16A	6953	4321	385	32
H16B	6010	5221	695	32
H19	5707	6878	1119	30
H21	5364	9818	4065	39
H22	5233	2012	128	40
H23	2469	10310	-1003	48
H24	8103	6376	3097	46
H25A	-1040	8636	4052	63
H25B	-2184	8390	4320	63
H25C	-2237	9524	4116	63
H26	3303	2663	478	43
H27	1983	6767	4980	46
H28	-330	6062	3932	45
H29A	4001	4835	5106	58
H29B	4563	3811	5626	58
H29C	3170	4342	5562	58

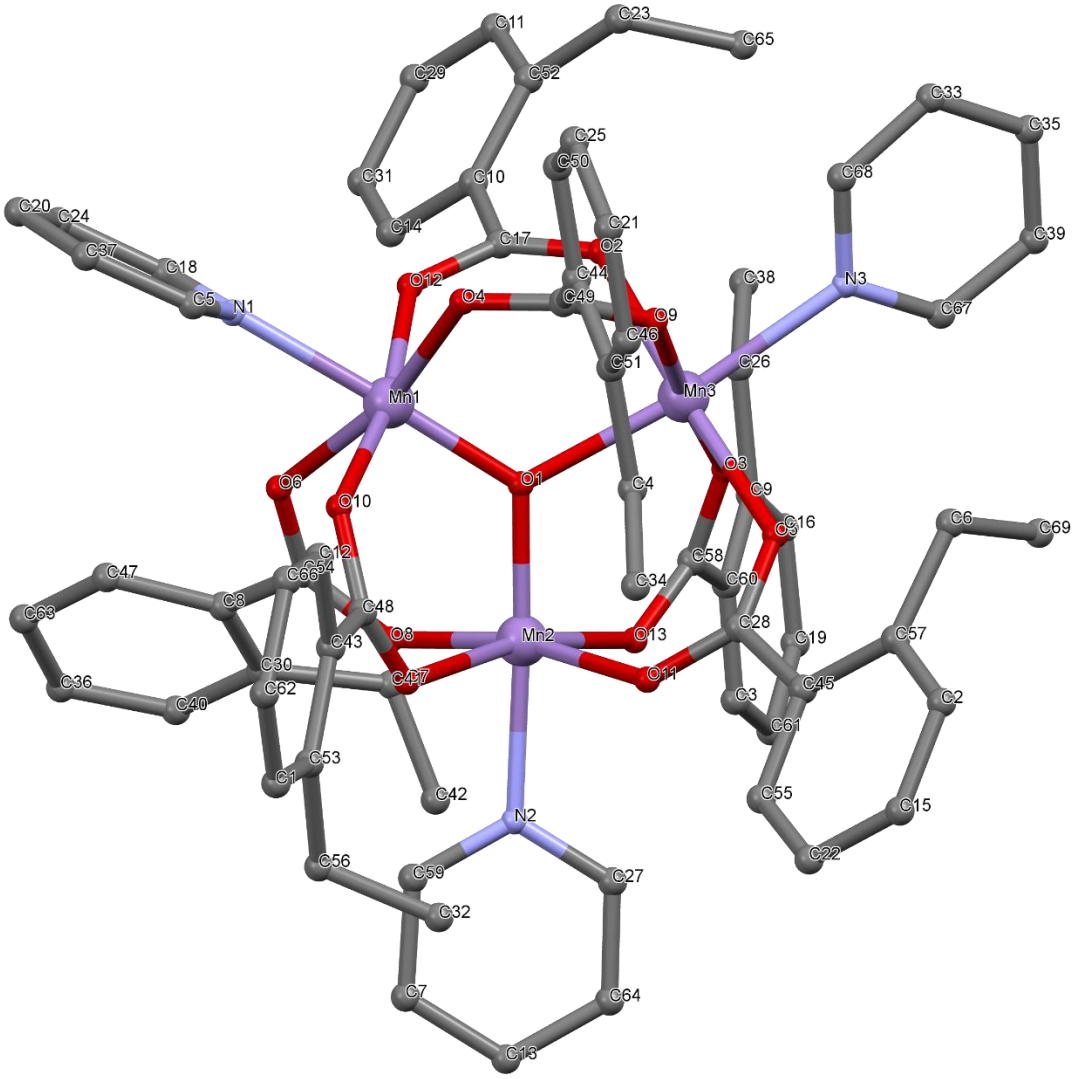

Figure II.2.6 Crystal Structure with atomic labels for compound **5**, Mn_3O-2-Ethyl, $Mn_3O(O_2CPh\text{-}o\text{-}Et)_6(Pyr)_3$, ab58029

II.3 Crystal Structure Information and Tables for Chapter 4 (& 5) Compounds

II.3.1 Compound 1, Benzylammonium Formate, ab54016

Table II.3.1.1 Crystal data and structure refinement for ab54016.

Identification code	ab54016
Empirical formula	$C_8H_{11}NO_2$
Formula weight	153.18
Temperature/K	99.99
Crystal system	orthorhombic
Space group	Pbca
a/Å	8.5468(5)
b/Å	11.0536(7)
c/Å	17.5296(10)
α/°	90
β/°	90
γ/°	90
Volume/Å^3	1656.07(17)
Z	8
ρ_{calc}g/cm^3	1.229
μ/mm^{-1}	0.089
F(000)	656.0
Crystal size/mm^3	0.467 × 0.363 × 0.152
Radiation	MoKα (λ = 0.71073)
2Θ range for data collection/°	4.648 to 63.932
Index ranges	$-12 \le h \le 12$, $-16 \le k \le 15$, $-26 \le l \le 26$
Reflections collected	39249
Independent reflections	2869 [R_{int} = 0.0355, R_{sigma} = 0.0133]
Data/restraints/parameters	2869/0/144
Goodness-of-fit on F^2	1.048
Final R indexes [I>=2σ (I)]	R_1 = 0.0354, wR_2 = 0.0973
Final R indexes [all data]	R_1 = 0.0397, wR_2 = 0.1024
Largest diff. peak/hole / e Å^{-3}	0.40/-0.19

Table II.3.1.2 Fractional Atomic Coordinates (×10^4) and Equivalent Isotropic Displacement Parameters (Å^2×10^3) for ab54016. U_{eq} is defined as 1/3 of of the trace of the orthogonalised U_{IJ} tensor.

Atom	*x*	*y*	*z*	U(eq)
O1	1727.1(7)	8952.5(5)	1770.6(3)	22.46(13)
O2	606.7(6)	10667.8(5)	2164.4(3)	20.19(12)
C1	766.1(8)	9531.3(6)	2162.1(4)	17.84(14)
N1	-1396.4(7)	13537.9(5)	-1698.8(3)	16.26(12)
C2	-1283.1(8)	13847.8(6)	-282.0(4)	16.41(13)
C3	-537.4(8)	14094.3(7)	-1044.3(4)	18.64(14)

C4	-3170.8(8)	14368.6(7)	691.3(4)	20.48(14)
C5	-1317.4(10)	12763.7(7)	918.6(4)	23.24(15)
C6	-683.3(9)	12950.7(7)	195.2(4)	21.56(15)
C7	-2532.3(8)	14556.4(6)	-30.1(4)	17.90(14)
C8	-2561.4(9)	13473.4(7)	1165.7(4)	21.35(15)

Table II.3.1.3 Anisotropic Displacement Parameters ($Å^2×10^3$) for ab54016. The Anisotropic displacement factor exponent takes the form: $-2\pi^2[h^2a^{*2}U_{11}+2hka^*b^*U_{12}+\ldots]$.

Atom	U_{11}	U_{22}	U_{33}	U_{23}	U_{13}	U_{12}
O1	26.7(3)	16.9(2)	23.8(3)	-1.69(18)	2.6(2)	-0.03(19)
O2	22.3(3)	18.4(2)	19.9(2)	0.01(17)	2.02(18)	1.31(18)
C1	19.4(3)	18.9(3)	15.2(3)	1.7(2)	-1.8(2)	-2.9(2)
N1	17.7(3)	15.3(2)	15.8(2)	-0.72(19)	0.46(19)	-0.53(19)
C2	17.9(3)	16.1(3)	15.2(3)	-1.9(2)	-0.3(2)	-2.2(2)
C3	18.5(3)	21.2(3)	16.2(3)	-2.4(2)	1.0(2)	-4.5(2)
C4	18.8(3)	23.1(3)	19.5(3)	-2.3(2)	1.7(2)	-1.0(2)
C5	30.6(4)	19.4(3)	19.7(3)	2.5(2)	-2.1(3)	1.0(3)
C6	25.8(3)	18.2(3)	20.7(3)	-0.8(2)	0.4(3)	3.8(3)
C7	17.3(3)	18.5(3)	17.9(3)	0.5(2)	-0.5(2)	-0.3(2)
C8	24.8(3)	23.2(3)	16.1(3)	-0.4(2)	0.4(2)	-4.7(3)

Table II.3.1.4 Bond Lengths for ab54016.

Atom	Atom	Length/Å	Atom	Atom	Length/Å
O1	C1	1.2469(9)	C2	C7	1.3958(10)
O2	C1	1.2635(9)	C4	C7	1.3928(10)
N1	C3	1.4946(9)	C4	C8	1.3936(11)
C2	C3	1.5053(10)	C5	C6	1.3945(11)
C2	C6	1.3950(10)	C5	C8	1.3905(11)

Table II.3.1.5 Bond Angles for ab54016.

Atom	Atom	Atom	Angle/°	Atom	Atom	Atom	Angle/°
O1	C1	O2	125.65(7)	C7	C4	C8	120.08(7)
C6	C2	C3	120.36(6)	C8	C5	C6	119.79(7)
C6	C2	C7	119.36(6)	C5	C6	C2	120.52(7)
C7	C2	C3	120.21(6)	C4	C7	C2	120.22(7)
N1	C3	C2	113.51(6)	C5	C8	C4	120.03(7)

Table II.3.1.6 Hydrogen Atom Coordinates (Å×10^4) and Isotropic Displacement Parameters (Å^2×10^3) for ab54016.

Atom	*x*	*y*	*z*	U(eq)
H7	58(14)	9058(10)	2508(7)	28(3)
H2A	-843(14)	13742(11)	-2156(6)	26(3)
H2B	-2354(15)	13866(11)	-1762(7)	29(3)
H2C	-1445(14)	12673(11)	-1664(7)	29(3)
H4A	538(16)	13803(12)	-1067(7)	32(3)
H4B	-505(14)	14954(10)	-1139(7)	25(3)
H5	-4046(15)	14885(11)	862(7)	28(3)
H6	-856(14)	12150(11)	1249(7)	31(3)
H8	179(15)	12474(11)	22(7)	30(3)
H9	-2914(14)	15176(11)	-347(7)	29(3)
H10	-2998(14)	13350(11)	1658(7)	28(3)

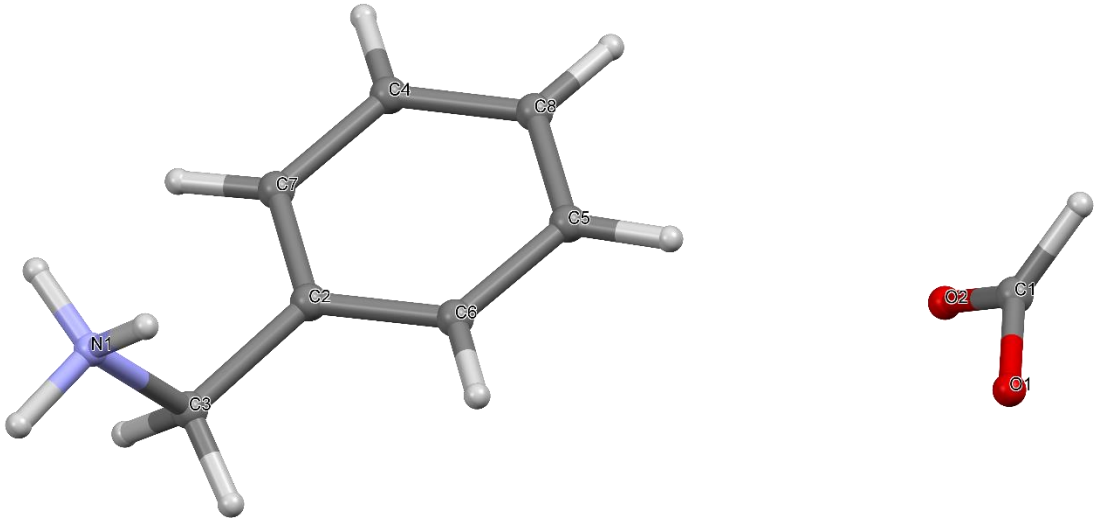

Figure II.3.1 Crystal Structure with atomic labels for compound **1**, Benzylammonium Formate, ab54016

II.3.2 Compound 2, 2-Methylbenzylammonium Formate, ab50716

Table II.3.2.1 Crystal data and structure refinement for ab50716.

Identification code	ab50716
Empirical formula	$C_9H_{13}NO_2$
Formula weight	167.20
Temperature/K	296.15
Crystal system	monoclinic
Space group	$P2_1$
a/Å	6.9761(6)
b/Å	7.6181(6)
c/Å	8.3283(7)
α/°	90
β/°	94.646(4)
γ/°	90
Volume/Å^3	441.15(6)
Z	2
ρ_{calc}g/cm^3	1.259
μ/mm^{-1}	0.089
F(000)	180.0
Crystal size/mm^3	0.92 × 0.21 × 0.192
Radiation	MoKα (λ = 0.71073)
2Θ range for data collection/°	4.908 to 68.414
Index ranges	-11 ≤ h ≤ 10, -11 ≤ k ≤ 12, -12 ≤ l ≤ 13
Reflections collected	11481
Independent reflections	3372 [R_{int} = 0.0283, R_{sigma} = 0.0252]
Data/restraints/parameters	3372/1/111
Goodness-of-fit on F^2	1.127
Final R indexes [I>=2σ (I)]	R_1 = 0.0651, wR_2 = 0.2046
Final R indexes [all data]	R_1 = 0.0659, wR_2 = 0.2050
Largest diff. peak/hole / e Å^{-3}	0.84/-0.36
Flack parameter	-0.1(3)

Table II.3.2.2 Fractional Atomic Coordinates (×10^4) and Equivalent Isotropic Displacement Parameters (Å^2×10^3) for ab50716. U_{eq} is defined as 1/3 of of the trace of the orthogonalised U_{IJ} tensor.

Atom	*x*	*y*	*z*	U(eq)
O1	159(3)	7242(3)	5014(3)	18.9(5)
O2	3363(3)	7484(3)	5165(3)	18.7(5)
C1	1678(4)	8098(4)	5218(3)	15.1(5)
N1	3063(4)	4071(4)	4135(3)	15.4(5)
C2	2682(4)	2775(4)	1361(4)	13.7(5)
C3	2372(4)	2976(4)	-322(4)	17.0(6)
C4	2901(4)	1095(4)	2024(4)	15.1(5)

C5	2549(5)	-206(5)	-624(4)	19.6(6)
C6	2772(4)	4403(4)	2391(4)	15.5(5)
C7	2296(5)	1480(5)	-1282(4)	19.9(6)
C8	2820(5)	-389(4)	1018(4)	18.2(6)
C9	2138(5)	4775(5)	-1074(4)	21.1(6)

Table II.3.2.3 Anisotropic Displacement Parameters ($Å^2×10^3$) for ab50716. The Anisotropic displacement factor exponent takes the form: $-2\pi^2[h^2a^{*2}U_{11}+2hka^*b^*U_{12}+\ldots]$.

Atom	U_{11}	U_{22}	U_{33}	U_{23}	U_{13}	U_{12}
O1	13.4(9)	17.8(10)	25.4(11)	-2.4(8)	1.3(8)	-0.6(8)
O2	12.7(9)	17.1(10)	25.9(11)	-3.2(9)	-0.6(8)	-0.2(8)
C1	16.0(12)	13.2(12)	15.8(12)	-1.2(10)	-0.4(9)	0.2(9)
N1	11.5(10)	13.2(10)	21.6(12)	-4.2(9)	1.9(8)	-0.7(8)
C2	12.8(11)	11.3(11)	17.1(12)	-0.1(9)	1.9(9)	-0.1(9)
C3	13.8(12)	16.0(13)	21.7(14)	0.3(10)	4.6(10)	-0.4(9)
C4	15.8(12)	13.3(12)	15.9(12)	-0.2(9)	-1.2(9)	0.1(9)
C5	21.0(14)	17.0(13)	20.5(13)	-6.5(11)	-0.5(11)	-2.0(11)
C6	15.9(12)	13.0(13)	17.5(12)	-0.4(9)	1.3(10)	-0.5(9)
C7	19.5(13)	21.5(16)	18.8(13)	-0.4(11)	1.4(11)	-0.9(11)
C8	18.9(13)	11.8(12)	23.7(14)	-1.6(11)	0.2(11)	0.2(10)
C9	19.0(14)	20.5(15)	24.0(15)	7.3(13)	1.9(11)	2.0(11)

Table II.3.2.4 Bond Lengths for ab50716.

Atom	Atom	Length/Å	Atom	Atom	Length/Å
O1	C1	1.244(4)	C3	C7	1.391(5)
O2	C1	1.270(4)	C3	C9	1.510(5)
N1	C6	1.472(4)	C4	C8	1.405(4)
C2	C3	1.410(4)	C5	C7	1.402(5)
C2	C4	1.397(4)	C5	C8	1.372(5)
C2	C6	1.506(4)			

Table II.3.2.5 Bond Angles for ab50716.

Atom	Atom	Atom	Angle/°	Atom	Atom	Atom	Angle/°
O1	C1	O2	125.6(3)	C7	C3	C9	120.5(3)
C3	C2	C6	118.2(3)	C2	C4	C8	120.2(3)
C4	C2	C3	119.7(3)	C8	C5	C7	119.0(3)
C4	C2	C6	122.1(3)	N1	C6	C2	114.6(2)
C2	C3	C9	120.9(3)	C3	C7	C5	121.9(3)
C7	C3	C2	118.6(3)	C5	C8	C4	120.5(3)

Table II.3.2.6 Hydrogen Atom Coordinates (Å×10⁴) and Isotropic Displacement Parameters (Å²×10³) for ab50716.

Atom	*x*	*y*	*z*	U(eq)
H5	1569	9292	5428	18
H7A	4213	3586	4365	18
H7B	2154	3345	4429	18
H7C	2996	5080	4666	18
H6	3100	958	3134	18
H8	2533	-1186	-1290	24
H9A	3814	5138	2077	19
H9B	1584	5054	2174	19
H10	2071	1601	-2393	24
H11	2952	-1503	1469	22
H12A	1138	5400	-589	32
H12B	1804	4658	-2210	32
H12C	3325	5412	-900	32

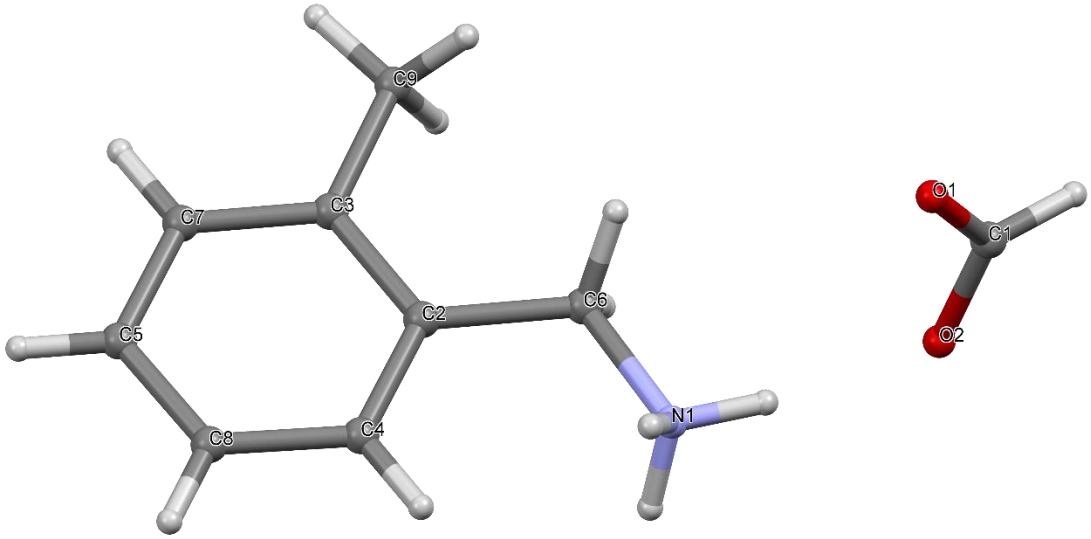

Figure II.3.2 Crystal Structure with atomic labels for compound **2**, 2-Methylbenzylammonium Formate, ab50716

II.3.3 Compound 3, 3-Methylbenzylammonium Formate, ab50617

Table II.3.3.1 Crystal data and structure refinement for ab50617a.

Identification code	ab50617a
Empirical formula	$C_9H_{13}NO_2$
Formula weight	167.20
Temperature/K	100.0
Crystal system	monoclinic
Space group	$P2_1/c$
a/Å	16.9827(8)
b/Å	4.8029(2)
c/Å	11.5315(6)
α/°	90
β/°	103.947(3)
γ/°	90
Volume/Å^3	912.85(8)
Z	4
ρ_{calc}g/cm^3	1.217
μ/mm^{-1}	0.086
F(000)	360.0
Crystal size/mm^3	0.758 × 0.612 × 0.043
Radiation	MoKα (λ = 0.71073)
2Θ range for data collection/°	2.47 to 61.604
Index ranges	$-24 \le h \le 24$, $-6 \le k \le 6$, $-16 \le l \le 16$
Reflections collected	16894
Independent reflections	2845 [R_{int} = 0.0298, R_{sigma} = 0.0186]
Data/restraints/parameters	2845/0/161
Goodness-of-fit on F^2	1.103
Final R indexes [I>=2σ (I)]	R_1 = 0.0381, wR_2 = 0.1070
Final R indexes [all data]	R_1 = 0.0466, wR_2 = 0.1213
Largest diff. peak/hole / e Å^{-3}	0.46/-0.27

Table II.3.3.2 Fractional Atomic Coordinates (×10^4) and Equivalent Isotropic Displacement Parameters (Å^2×10^3) for ab50617a. U_{eq} is defined as 1/3 of of the trace of the orthogonalised U_{IJ} tensor.

Atom	*x*	*y*	*z*	U(eq)
O1	4344.0(4)	3493.8(14)	2972.9(6)	15.28(16)
O2	3996.1(4)	5928.8(17)	4427.1(6)	19.89(17)
C1	4213.7(5)	3749(2)	4003.2(8)	14.28(18)
N1	3869.2(5)	6455.8(17)	6789.2(7)	12.68(16)
C2	3011.1(5)	6169.4(19)	6859.1(8)	13.65(18)
C3	2455.0(5)	8374.6(19)	6171.0(8)	12.87(18)
C4	1791.9(5)	9255(2)	6600.7(8)	14.85(18)
C5	1240.3(6)	11222(2)	5984.9(9)	17.6(2)

C6	2019.0(6)	11467(2)	4483.8(9)	21.5(2)
C7	2564.3(6)	9487(2)	5102.5(8)	17.4(2)
C8	535.0(6)	12182(3)	6465.9(11)	26.0(2)
C9	1364.0(6)	12324(2)	4921.7(9)	20.6(2)

Table II.3.3.3 Anisotropic Displacement Parameters ($Å^2×10^3$) for ab50617a. The Anisotropic displacement factor exponent takes the form: $-2\pi^2[h^2a^{*2}U_{11}+2hka^*b^*U_{12}+\ldots]$.

Atom	U_{11}	U_{22}	U_{33}	U_{23}	U_{13}	U_{12}
O1	17.1(3)	16.1(3)	13.2(3)	-2.7(2)	4.9(2)	-0.9(2)
O2	22.7(4)	24.9(4)	13.0(3)	-0.9(3)	6.1(3)	7.2(3)
C1	13.1(4)	17.1(4)	12.9(4)	1.4(3)	3.6(3)	-0.3(3)
N1	13.0(3)	14.5(4)	10.7(3)	0.9(3)	3.2(3)	1.5(3)
C2	12.4(4)	16.1(4)	12.8(4)	2.0(3)	3.6(3)	0.1(3)
C3	12.3(4)	14.8(4)	11.2(4)	-1.3(3)	2.0(3)	-0.2(3)
C4	12.3(4)	18.1(4)	14.5(4)	-2.5(3)	3.9(3)	-1.5(3)
C5	12.2(4)	22.5(5)	17.2(4)	-4.8(3)	1.7(3)	1.5(3)
C6	23.6(5)	27.3(5)	13.8(4)	4.9(4)	4.7(3)	9.4(4)
C7	18.3(4)	21.5(5)	13.4(4)	2.8(3)	5.7(3)	6.4(3)
C8	14.6(4)	36.3(6)	27.8(5)	-5.1(5)	6.2(4)	5.4(4)
C9	18.2(4)	24.3(5)	17.2(4)	0.2(4)	0.2(3)	7.7(4)

Table II.3.3.4 Bond Lengths for ab50617a.

Atom	Atom	Length/Å	Atom	Atom	Length/Å
O1	C1	1.2658(11)	C4	C5	1.3977(13)
O2	C1	1.2485(12)	C5	C8	1.5085(14)
N1	C2	1.4850(12)	C5	C9	1.3969(14)
C2	C3	1.5106(12)	C6	C7	1.3976(13)
C3	C4	1.4006(12)	C6	C9	1.3900(14)
C3	C7	1.3958(12)			

Table II.3.3.5 Bond Angles for ab50617a.

Atom	Atom	Atom	Angle/°	Atom	Atom	Atom	Angle/°
O2	C1	O1	125.72(9)	C4	C5	C8	120.95(9)
N1	C2	C3	113.83(7)	C9	C5	C4	118.54(8)
C4	C3	C2	118.69(8)	C9	C5	C8	120.50(9)
C7	C3	C2	122.18(8)	C9	C6	C7	120.38(9)
C7	C3	C4	119.08(8)	C3	C7	C6	119.89(9)
C5	C4	C3	121.46(8)	C6	C9	C5	120.63(9)

Table II.3.3.6 Hydrogen Atom Coordinates (Å×10^4) and Isotropic Displacement Parameters (Å^2×10^3) for ab50617a.

Atom	*x*	*y*	*z*	U(eq)
H1	4291(8)	2060(30)	4503(12)	21(3)
HA	4150(9)	5070(30)	7221(13)	23(3)
HB	3946(9)	6290(30)	5999(15)	29(4)
HC	4079(9)	8090(30)	7131(13)	22(3)
H2A	3000(9)	6270(30)	7704(13)	22(3)
H2B	2842(8)	4340(30)	6567(12)	17(3)
H4	1698(9)	8480(30)	7364(13)	21(3)
H6	2096(9)	12310(40)	3728(14)	29(4)
H7	3021(10)	8970(30)	4759(14)	28(4)
H8A	521(16)	11200(50)	7190(20)	85(8)
H8B	33(12)	11970(40)	5850(17)	50(5)
H8C	581(17)	14240(60)	6630(20)	85(8)
H9	984(10)	13750(30)	4482(15)	35(4)

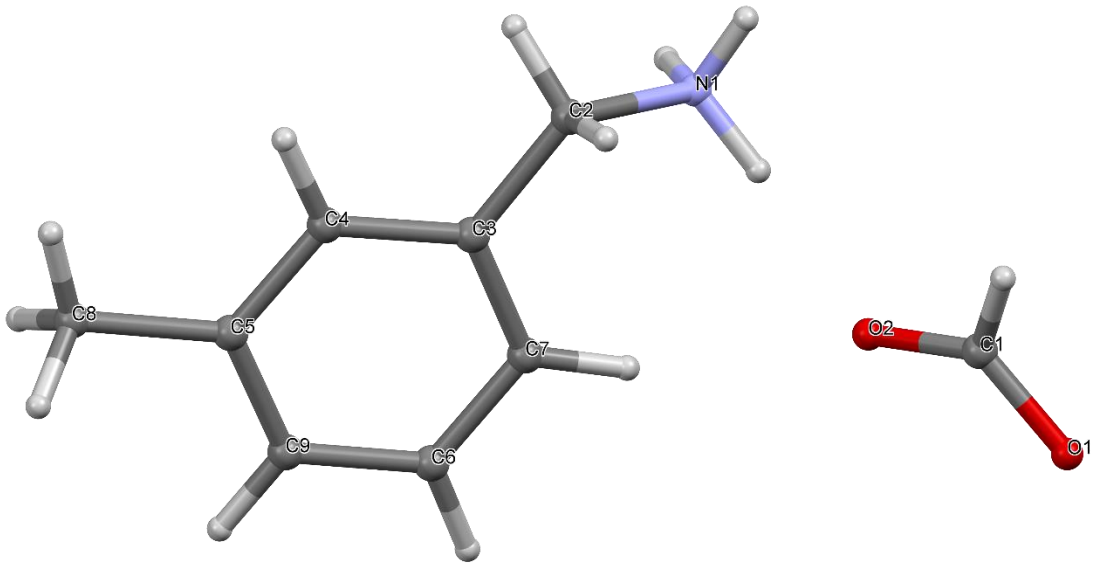

Figure II.3.3 Crystal Structure with atomic labels for compound **3**, 3-Methylbenzylammonium Formate, ab50617

II.3.4 Compound 4, 4-Methylbenzylammonium Formate, ab18715

Table II.3.4.1 Crystal data and structure refinement for ab18715a.

Identification code	ab18715a
Empirical formula	$C_9H_{13}NO_2$
Formula weight	167.20
Temperature/K	273.15
Crystal system	monoclinic
Space group	$P2_1/c$
a/Å	17.090(8)
b/Å	4.909(2)
c/Å	11.565(6)
α/°	90
β/°	109.75(3)
γ/°	90
Volume/Å^3	913.1(8)
Z	4
ρ_{calc}g/cm^3	1.216
μ/mm^{-1}	0.086
F(000)	360.0
Crystal size/mm^3	0.259 × 0.152 × 0.068
Radiation	MoKα (λ = 0.71073)
2Θ range for data collection/°	5.066 to 52.972
Index ranges	$-21 \le h \le 21$, $-4 \le k \le 6$, $-14 \le l \le 14$
Reflections collected	14322
Independent reflections	1882 [R_{int} = 0.0501, R_{sigma} = 0.0329]
Data/restraints/parameters	1882/0/161
Goodness-of-fit on F^2	1.035
Final R indexes [I>=2σ (I)]	R_1 = 0.0474, wR_2 = 0.1232
Final R indexes [all data]	R_1 = 0.0705, wR_2 = 0.1382
Largest diff. peak/hole / e Å^{-3}	0.19/-0.17

Table II.3.4.2 Fractional Atomic Coordinates (×10^4) and Equivalent Isotropic Displacement Parameters (Å^2×10^3) for ab18715a. U_{eq} is defined as 1/3 of of the trace of the orthogonalised U_{IJ} tensor.

Atom	*x*	*y*	*z*	U(eq)
O1	4299.4(7)	6399(2)	7835.6(11)	43.3(4)
O2	3931.0(9)	4075(3)	9214.7(12)	59.2(5)
C1	4159.4(11)	6169(4)	8823.9(18)	43.0(5)
N1	3844.5(9)	3623(3)	11584.9(14)	36.7(4)
C2	2376.6(10)	1887(3)	10790.8(14)	33.6(4)
C3	1176.9(11)	-952(4)	10544.5(17)	43.6(5)
C4	1190.6(10)	-1966(3)	9435.0(16)	39.0(4)
C5	2969.8(10)	4049(4)	11505.9(17)	37.6(4)
C6	1810.2(12)	-1022(4)	9018.7(17)	46.4(5)

C7	568.6(14)	-4047(5)	8721(2)	50.2(5)
C8	1760.2(11)	932(4)	11212.6(17)	42.1(5)
C9	2394.4(12)	880(4)	9680.8(16)	44.2(5)

Table II.3.4.3 Anisotropic Displacement Parameters ($Å^2×10^3$) for ab18715a. The Anisotropic displacement factor exponent takes the form: $-2\pi^2[h^2a^{*2}U_{11}+2hka^*b^*U_{12}+\ldots]$.

Atom	U_{11}	U_{22}	U_{33}	U_{23}	U_{13}	U_{12}
O1	49.5(8)	40.4(7)	43.0(7)	6.2(5)	19.8(6)	2.3(5)
O2	70.4(10)	67.4(10)	45.2(8)	0.5(7)	26.7(7)	-21.6(7)
C1	43.1(10)	44.6(11)	43.3(10)	-4.7(9)	17.2(8)	-0.1(8)
N1	36.9(8)	38.1(9)	35.8(8)	-3.5(7)	13.3(6)	-3.8(7)
C2	33.9(9)	31.3(9)	34.2(9)	1.1(7)	9.5(7)	1.0(7)
C3	38.3(10)	49.7(12)	46.3(11)	0.4(8)	18.8(9)	-7.2(8)
C4	38.9(9)	32.7(9)	41.0(10)	4.7(7)	7.9(8)	-0.1(7)
C5	35.8(9)	36.2(10)	40.2(10)	-3.1(8)	12.2(8)	0.5(7)
C6	54.7(12)	50.2(11)	36.5(10)	-7.4(8)	18.3(9)	-12.0(9)
C7	46.1(12)	45.1(13)	51.9(13)	-1.8(9)	6.5(10)	-10.5(9)
C8	45.8(11)	45.9(11)	37.8(10)	-4.6(8)	18.4(8)	-4.4(8)
C9	45.7(10)	52.3(12)	38.8(10)	-6.9(8)	19.8(8)	-13.6(9)

Table II.3.4.4 Bond Lengths for ab18715a.

Atom	Atom	Length/Å	Atom	Atom	Length/Å
O1	C1	1.250(2)	C3	C4	1.384(3)
O2	C1	1.238(2)	C3	C8	1.388(3)
N1	C5	1.481(2)	C4	C6	1.383(3)
C2	C5	1.507(2)	C4	C7	1.504(3)
C2	C8	1.384(2)	C6	C9	1.392(3)
C2	C9	1.386(2)			

Table II.3.4.5 Bond Angles for ab18715a.

Atom	Atom	Atom	Angle/°	Atom	Atom	Atom	Angle/°
O2	C1	O1	126.19(18)	C6	C4	C3	117.20(17)
C8	C2	C5	119.75(15)	C6	C4	C7	121.27(18)
C8	C2	C9	117.61(16)	N1	C5	C2	114.34(14)
C9	C2	C5	122.58(15)	C4	C6	C9	121.64(17)
C4	C3	C8	121.46(17)	C2	C8	C3	121.25(17)
C3	C4	C7	121.52(18)	C2	C9	C6	120.84(17)

Table II.3.4.6 Hydrogen Atom Coordinates (Å×10^4) and Isotropic Displacement Parameters (Å^2×10^3) for ab18715a.

Atom	*x*	*y*	*z*	U(eq)
H4	4194(13)	7860(50)	9290(20)	68(6)
H2A	3912(12)	3730(40)	10780(20)	55(6)
H2B	4141(13)	5080(50)	12072(19)	60(6)
H2C	4048(13)	1830(50)	12000(20)	68(6)
H6	756(13)	-1480(40)	10865(19)	57(6)
H8A	2809(12)	5880(40)	11152(17)	51(5)
H8B	2960(12)	4180(40)	12340(19)	53(5)
H9	1854(12)	-1740(40)	8240(20)	52(5)
H10A	50(20)	-3730(50)	8680(30)	103(10)
H10B	490(20)	-4040(50)	7880(30)	111(10)
H10C	704(19)	-5910(60)	8990(30)	108(10)
H11	1747(12)	1700(40)	11981(19)	49(5)
H12	2836(13)	1450(40)	9353(18)	57(6)

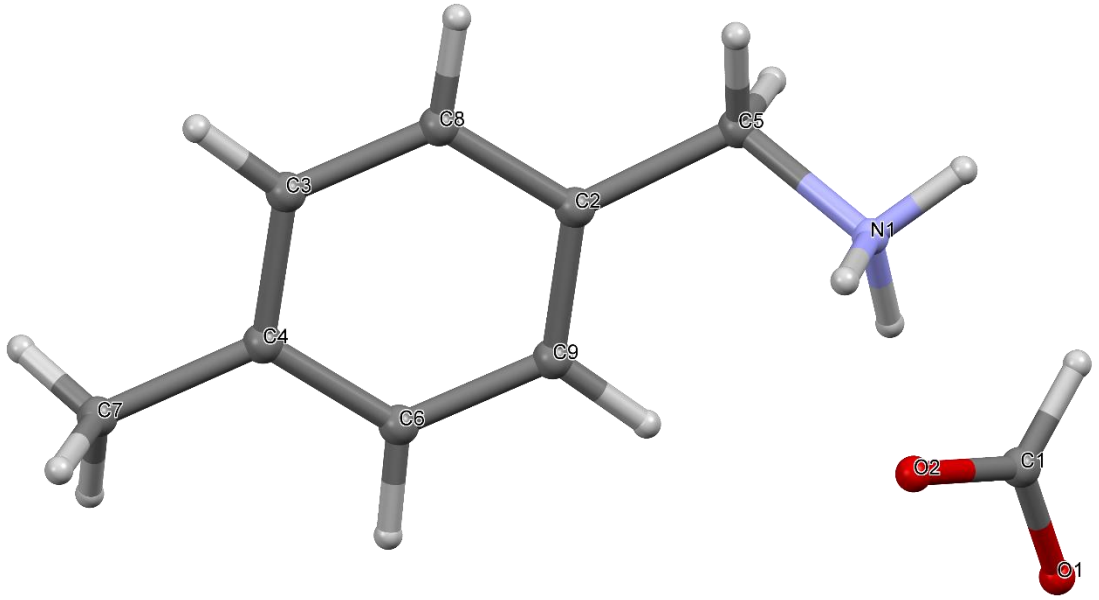

Figure II.3.4 Crystal Structure with atomic labels for compound **4**, 4-Methylbenzylammonium Formate, ab18715

II.3.5 Compound 5, 4-(Trifluoro)Methylbenzylammonium Formate, ab58116

Table II.3.5.1 Crystal data and structure refinement for ab58116.

Identification code	ab58116
Empirical formula	$C_9H_{10}F_3NO_2$
Formula weight	221.18
Temperature/K	100.0
Crystal system	monoclinic
Space group	$P2_1/c$
a/Å	5.7416(4)
b/Å	21.1000(14)
c/Å	8.5319(6)
α/°	90
β/°	102.036(4)
γ/°	90
Volume/Å^3	1010.90(12)
Z	4
ρ_{calc}g/cm^3	1.453
μ/mm^{-1}	0.138
F(000)	456.0
Crystal size/mm^3	0.599 × 0.503 × 0.054
Radiation	MoKα (λ = 0.71073)
2Θ range for data collection/°	3.86 to 54.822
Index ranges	$-7 \le h \le 7$, $-26 \le k \le 27$, $-10 \le l \le 11$
Reflections collected	15246
Independent reflections	2275 [R_{int} = 0.0374, R_{sigma} = 0.0239]
Data/restraints/parameters	2275/0/176
Goodness-of-fit on F^2	1.093
Final R indexes [I>=2σ (I)]	R_1 = 0.0737, wR_2 = 0.1858
Final R indexes [all data]	R_1 = 0.0807, wR_2 = 0.1911
Largest diff. peak/hole / e Å^{-3}	0.78/-0.81

Table II.3.5.2 Fractional Atomic Coordinates (×10^4) and Equivalent Isotropic Displacement Parameters (Å^2×10^3) for ab58116. U_{eq} is defined as 1/3 of of the trace of the orthogonalised U_{IJ} tensor.

Atom	*x*	*y*	*z*	U(eq)
F1	-1334(6)	4810.2(12)	6269(3)	87.4(12)
F2	-4854(7)	4626(2)	6599(3)	137(2)
F3	-2856(4)	3927.2(10)	5729(2)	52.8(6)
N1	921(4)	3013.5(11)	13756(3)	19.9(5)
C1	280(5)	3844.7(12)	11632(3)	21.4(5)
C2	-1724(5)	4182.0(13)	8484(3)	27.1(6)
C3	1416(5)	3679.1(13)	13347(3)	23.2(5)
C4	1450(5)	3705.1(14)	10397(3)	27.0(6)

C5	-2925(5)	4314.7(15)	9696(3)	31.4(6)
C6	-1909(5)	4145.6(14)	11271(3)	28.7(6)
C7	-2741(6)	4389.4(15)	6796(3)	36.5(7)
C8	451(5)	3873.2(14)	8820(3)	29.6(6)
O1	3139(3)	2789.1(9)	6916(2)	23.7(4)
O2	6133(3)	2221.1(10)	8321(2)	29.3(5)
C9	5282(5)	2605.4(12)	7255(3)	22.2(5)

Table II.3.5.3 Anisotropic Displacement Parameters ($Å^2×10^3$) for ab58116. The Anisotropic displacement factor exponent takes the form: $-2\pi^2[h^2a^{*2}U_{11}+2hka^*b^*U_{12}+\ldots]$.

Atom	U_{11}	U_{22}	U_{33}	U_{23}	U_{13}	U_{12}
F1	148(3)	61.2(15)	33.6(12)	22.7(11)	-26.3(14)	-54.5(17)
F2	125(3)	259(5)	26.6(12)	37.7(19)	12.1(14)	142(3)
F3	83.6(17)	47.6(12)	19.8(9)	-0.4(8)	-6.2(9)	-10.6(11)
N1	17.0(10)	29.1(11)	13.2(9)	-0.2(8)	2.6(8)	-0.2(8)
C1	24.2(12)	24.3(12)	14.4(11)	0.9(9)	1.3(9)	-1.0(9)
C2	35.2(15)	27.4(13)	16.5(12)	1.6(9)	0.6(10)	3.7(11)
C3	23.9(13)	28.1(13)	15.8(12)	0.1(10)	-0.2(9)	-0.8(10)
C4	26.9(14)	32.4(14)	22.2(13)	5.1(10)	6.2(10)	7.6(11)
C5	28.6(14)	40.6(16)	22.2(13)	0.5(11)	-1.1(11)	10.7(12)
C6	27.3(14)	39.9(15)	19.0(12)	-1.7(11)	5.1(10)	7.6(11)
C7	52.1(19)	34.7(15)	18.7(13)	4.0(11)	-1.7(12)	6.2(14)
C8	36.2(16)	37.0(15)	17.5(12)	3.7(10)	9.9(11)	8.1(12)
O1	24.3(9)	30.0(10)	16.4(8)	2.7(7)	3.1(7)	2.7(7)
O2	20.2(9)	42.5(12)	25.1(10)	11.3(8)	5.1(7)	3.4(8)
C9	22.3(12)	27.6(12)	17.8(11)	0.3(9)	7.0(9)	-1.8(10)

Table II.3.5.4 Bond Lengths for ab58116.

Atom	Atom	Length/Å	Atom	Atom	Length/Å
F1	C7	1.340(4)	C2	C5	1.386(4)
F2	C7	1.290(4)	C2	C7	1.501(4)
F3	C7	1.326(4)	C2	C8	1.385(4)
N1	C3	1.489(3)	C4	C8	1.394(4)
C1	C3	1.513(3)	C5	C6	1.395(4)
C1	C4	1.394(4)	O1	C9	1.264(3)
C1	C6	1.385(4)	O2	C9	1.240(3)

Table II.3.5.5 Bond Angles for ab58116.

Atom	Atom	Atom	Angle/°	Atom	Atom	Atom	Angle/°
C4	C1	C3	120.2(2)	C1	C6	C5	120.6(3)

C6	C1	C3	120.6(2)	F1	C7	C2	112.0(3)
C6	C1	C4	119.2(2)	F2	C7	F1	108.5(4)
C5	C2	C7	120.2(3)	F2	C7	F3	106.5(3)
C8	C2	C5	120.5(2)	F2	C7	C2	113.9(3)
C8	C2	C7	119.3(3)	F3	C7	F1	101.8(3)
N1	C3	C1	112.3(2)	F3	C7	C2	113.4(2)
C8	C4	C1	120.6(3)	C2	C8	C4	119.5(3)
C2	C5	C6	119.6(3)	O2	C9	O1	125.7(2)

Table II.3.5.6 Hydrogen Atom Coordinates (Å×10^4) and Isotropic Displacement Parameters (Å^2×10^3) for ab58116.

Atom	***x***	***y***	***z***	**U(eq)**
H2A	-690(70)	2940(16)	13580(40)	34(9)
H2B	1480(60)	2746(16)	13090(40)	26(8)
H2C	1620(70)	2923(16)	14850(50)	36(9)
H7A	3150(60)	3722(15)	13480(40)	22(7)
H7B	820(50)	3953(14)	14100(40)	19(7)
H8	2980(60)	3503(15)	10630(40)	25(8)
H9	-4380(70)	4513(19)	9430(50)	46(10)
H10	-2780(70)	4246(17)	12110(50)	41(10)
H12	1340(70)	3781(18)	8020(50)	41(10)
H4	6340(60)	2770(16)	6650(40)	31(9)

Figure II.3.5 Crystal Structure with atomic labels for compound **5**, 4-

(Trifluoro)Methylbenzylammonium Formate, ab58116

I.3.6 Compound 6, 4-Methoxybenzylammonium Formate, ab51517

Table II.3.6.1 Crystal data and structure refinement for ab51517.

Identification code	ab51517
Empirical formula	$C_9H_{13}NO_3$
Formula weight	183.20
Temperature/K	99.98
Crystal system	monoclinic
Space group	Cc
a/Å	6.7615(3)
b/Å	18.9173(7)
c/Å	7.8044(3)
α/°	90
β/°	105.9340(19)
γ/°	90
Volume/Å^3	959.90(7)
Z	4
ρ_{calc}g/cm^3	1.268
μ/mm^{-1}	0.095
F(000)	392.0
Crystal size/mm^3	0.725 × 0.206 × 0.128
Radiation	MoKα (λ = 0.71073)
2Θ range for data collection/°	4.306 to 63.404
Index ranges	$-9 \le h \le 9$, $-27 \le k \le 26$, $-11 \le l \le 11$
Reflections collected	11815
Independent reflections	3235 [R_{int} = 0.0230, R_{sigma} = 0.0188]
Data/restraints/parameters	3235/2/170
Goodness-of-fit on F^2	1.055
Final R indexes [I>=2σ (I)]	R_1 = 0.0273, wR_2 = 0.0741
Final R indexes [all data]	R_1 = 0.0282, wR_2 = 0.0750
Largest diff. peak/hole / e Å^{-3}	0.32/-0.18
Flack parameter	-0.2(2)

Table II.3.6.2 Fractional Atomic Coordinates (×10^4) and Equivalent Isotropic Displacement Parameters (Å^2×10^3) for ab51517. U_{eq} is defined as 1/3 of of the trace of the orthogonalised U_{IJ} tensor.

Atom	*x*	*y*	*z*	U(eq)
O1	14791.9(13)	2875.6(5)	15913.5(11)	17.38(17)
O2	18115.9(14)	2870.7(6)	15962.5(13)	23.04(19)
O3	2337.4(13)	4475.5(5)	9709.1(11)	18.85(17)
N1	10798.9(15)	3034.3(5)	13853.7(13)	15.85(18)
C1	5320(2)	4566.4(6)	12095.8(15)	19.1(2)
C2	4351.9(17)	4279.9(6)	10424.7(14)	14.68(19)
C3	7489.8(18)	3681.7(6)	10430.2(15)	16.8(2)
C4	10667.4(17)	3753.6(7)	13028.5(16)	19.7(2)

C5	8480.5(17)	3955.1(6)	12106.0(14)	16.4(2)
C6	7366.6(19)	4404.2(6)	12922.8(15)	19.2(2)
C7	16254.8(18)	2937.4(6)	15197.9(15)	16.0(2)
C8	5436.1(17)	3836.2(6)	9582.6(14)	15.75(19)
C9	1232.1(19)	4121.5(7)	8113.1(18)	22.5(2)

Table II.3.6.3 Anisotropic Displacement Parameters ($Å^2×10^3$) for ab51517. The Anisotropic displacement factor exponent takes the form: $-2\pi^2[h^2a^{*2}U_{11}+2hka^*b^*U_{12}+\ldots]$.

Atom	U_{11}	U_{22}	U_{33}	U_{23}	U_{13}	U_{12}
O1	12.3(3)	24.8(4)	15.1(4)	0.4(3)	3.8(3)	-1.4(3)
O2	13.8(4)	35.3(5)	21.1(4)	3.7(3)	6.6(3)	0.8(3)
O3	17.6(4)	20.2(4)	17.2(4)	-0.8(3)	2.2(3)	4.2(3)
N1	11.8(4)	22.1(4)	13.4(4)	1.0(3)	3.0(3)	-0.5(3)
C1	23.0(5)	17.5(4)	16.6(5)	-4.0(4)	4.8(4)	1.4(4)
C2	17.0(5)	12.9(4)	13.8(4)	1.4(3)	3.6(3)	1.0(3)
C3	17.5(5)	17.5(4)	15.5(4)	0.7(4)	4.6(4)	1.5(4)
C4	14.8(5)	23.6(5)	19.0(5)	3.9(4)	1.7(4)	-4.1(4)
C5	16.1(5)	16.7(5)	15.7(5)	3.0(3)	3.1(4)	-2.3(4)
C6	22.4(5)	19.0(5)	14.5(4)	-2.9(4)	2.1(4)	-3.1(4)
C7	15.8(5)	18.2(5)	14.0(4)	0.5(3)	4.2(4)	-2.0(3)
C8	18.3(5)	15.6(4)	12.6(4)	-0.9(3)	3.0(4)	1.6(4)
C9	17.0(5)	28.1(6)	20.2(5)	-2.8(4)	1.1(4)	-0.8(4)

Table II.3.6.4 Bond Lengths for ab51517.

Atom	Atom	Length/Å	Atom	Atom	Length/Å
O1	C7	1.2678(14)	C1	C6	1.3912(17)
O2	C7	1.2423(15)	C2	C8	1.3923(15)
O3	C2	1.3735(13)	C3	C5	1.3949(15)
O3	C9	1.4309(15)	C3	C8	1.3953(16)
N1	C4	1.4976(16)	C4	C5	1.5052(16)
C1	C2	1.3980(15)	C5	C6	1.3997(17)

Table II.3.6.5 Bond Angles for ab51517.

Atom	Atom	Atom	Angle/°	Atom	Atom	Atom	Angle/°
C2	O3	C9	116.78(9)	C3	C5	C4	120.69(10)
C6	C1	C2	119.91(10)	C3	C5	C6	118.17(10)
O3	C2	C1	115.66(10)	C6	C5	C4	121.11(10)
O3	C2	C8	124.22(9)	C1	C6	C5	120.91(10)
C8	C2	C1	120.12(10)	O2	C7	O1	126.08(10)
C5	C3	C8	121.74(10)	C2	C8	C3	119.14(10)

N1	C4	C5	111.74(9)

Table II.3.6.6 Hydrogen Atom Coordinates (Å×10^4) and Isotropic Displacement Parameters (Å^2×10^3) for ab51517.

Atom	*x*	*y*	*z*	U(eq)
H1A	12150(30)	2957(9)	14480(30)	19(4)
H1B	10010(30)	3007(11)	14550(30)	22(5)
H1C	10530(30)	2715(11)	13060(30)	21(4)
H1	4580(30)	4859(11)	12680(30)	29(5)
H3	8280(30)	3369(10)	9890(30)	21(4)
H4A	11500(30)	3746(10)	12240(30)	19(4)
H4B	11300(30)	4080(11)	13980(30)	22(4)
H6	7910(30)	4605(11)	14070(30)	28(5)
H7	15860(30)	3057(10)	13960(30)	19(4)
H8	4840(30)	3646(10)	8470(30)	18(4)
H9A	-160(40)	4268(14)	7880(40)	46(7)
H9B	1800(30)	4232(12)	7110(30)	28(5)
H9C	1280(40)	3621(12)	8300(30)	31(5)

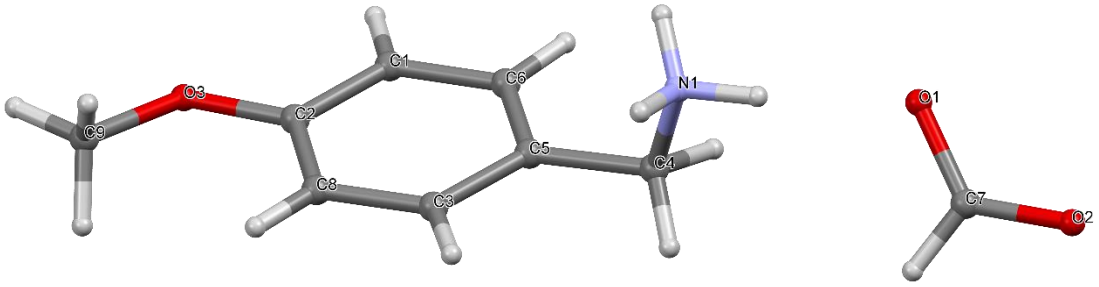

Figure II.3.6 Crystal Structure with atomic labels for compound **6**, 4-Methoxybenzylammonium Formate, ab51517

II.3.7 Compound 7, 4-*Tert*-Butylbenzylammonium Formate, ab18115a

Table II.3.7.1 Crystal data and structure refinement for ab18115a.

Identification code	ab18115a
Empirical formula	$C_{12}H_{19}NO_2$
Formula weight	246.59
Temperature/K	273.15
Crystal system	monoclinic
Space group	$P2_1/c$
a/Å	19.1296(13)
b/Å	6.4253(4)
c/Å	10.1620(7)
α/°	90
β/°	97.440(4)
γ/°	90
Volume/Å^3	1238.53(14)
Z	4
ρ_{calc}g/cm^3	1.322
μ/mm^{-1}	0.090
F(000)	540.0
Crystal size/mm^3	0.588 × 0.112 × 0.081
Radiation	MoKα (λ = 0.71073)
2Θ range for data collection/°	2.146 to 52.904
Index ranges	$-23 \leq h \leq 23$, $-6 \leq k \leq 8$, $-12 \leq l \leq 12$
Reflections collected	20232
Independent reflections	2542 [R_{int} = 0.0342, R_{sigma} = 0.0256]
Data/restraints/parameters	2542/0/144
Goodness-of-fit on F^2	1.026
Final R indexes [I>=2σ (I)]	R_1 = 0.0619, wR_2 = 0.1960
Final R indexes [all data]	R_1 = 0.1035, wR_2 = 0.2408
Largest diff. peak/hole / e Å^{-3}	0.51/-0.24

Table II.3.7.2 Fractional Atomic Coordinates (×10^4) and Equivalent Isotropic Displacement Parameters (Å^2×10^3) for ab18115a. U_{eq} is defined as 1/3 of of the trace of the orthogonalised U_{IJ} tensor.

Atom	*x*	*y*	*z*	U(eq)
O1	716.8(9)	6936(3)	6136.2(18)	59.4(5)
O2	446.1(11)	9513(3)	7422.7(19)	73.5(6)
C12	738.4(14)	7888(4)	7213(3)	57.1(7)
N1	533.2(10)	2659(3)	5572(2)	55.0(6)
C1	1800.6(12)	1818(4)	5786(2)	51.5(6)
C2	2700.0(14)	3013(4)	7490(3)	62.7(7)
C3	3053.4(12)	1142(4)	7516(2)	51.8(6)
C4	1135.4(13)	2168(4)	4857(2)	62.2(7)
C5	2147.4(14)	-58(4)	5821(3)	60.6(7)

C6	2754.5(14)	-380(4)	6658(3)	62.6(7)
C7	3729.2(13)	736(5)	8456(2)	63.5(7)
C8	2086.6(14)	3350(4)	6643(3)	64.7(7)
C9	4275.1(19)	-261(9)	7741(4)	134(2)
C10	4052(2)	2769(8)	9038(6)	141.3(19)
C11	3563(2)	-555(10)	9584(4)	145(2)

Table II.3.7.3 Anisotropic Displacement Parameters ($Å^2×10^3$) for ab18115a. The Anisotropic displacement factor exponent takes the form: $-2\pi^2[h^2a^{*2}U_{11}+2hka^*b^*U_{12}+\ldots]$.

Atom	U_{11}	U_{22}	U_{33}	U_{23}	U_{13}	U_{12}
O1	50.8(10)	52.3(10)	72.6(12)	-6.1(9)	-2.0(8)	1.0(8)
O2	92.2(15)	54.4(11)	75.7(13)	-1.8(9)	18.2(11)	10.5(10)
C12	60.0(16)	50.8(14)	57.3(15)	6.7(12)	-4.6(12)	2.9(12)
N1	47.0(11)	47.2(11)	66.0(12)	-2.5(9)	-10.5(9)	5.1(8)
C1	44.2(13)	57.9(14)	51.5(13)	2.0(11)	3.4(10)	1.3(10)
C2	56.1(15)	64.6(16)	64.1(16)	-13.4(13)	-4.9(12)	6.4(12)
C3	43.3(13)	64.4(15)	48.7(13)	3.4(11)	9.7(10)	7.7(11)
C4	55.0(15)	73.4(17)	54.9(14)	2.8(13)	-5.3(11)	4.6(13)
C5	56.4(15)	56.0(14)	67.7(16)	-10.8(12)	0.9(12)	2.7(12)
C6	56.4(16)	54.1(14)	75.3(17)	-0.6(13)	1.1(13)	15.2(12)
C7	48.7(14)	86.8(19)	53.2(14)	5.2(13)	0.1(11)	13.1(13)
C8	54.5(15)	56.2(15)	78.7(18)	-6.5(13)	-8.4(13)	15.1(12)
C9	67(2)	242(6)	89(3)	-17(3)	-6.4(18)	67(3)
C10	87(3)	138(4)	177(4)	-19(3)	-65(3)	8(3)
C11	94(3)	241(6)	96(3)	87(3)	-3(2)	10(3)

Table II.3.7.4 Bond Lengths for ab18115a.

Atom	Atom	Length/Å	Atom	Atom	Length/Å
C12	O1	1.250(3)	C3	C6	1.383(4)
C12	O2	1.216(3)	C3	C7	1.527(3)
C1	C4	1.501(3)	C4	N1	1.474(3)
C1	C5	1.374(4)	C5	C6	1.363(4)
C1	C8	1.380(4)	C7	C9	1.492(4)
C2	C3	1.377(4)	C7	C10	1.531(5)
C2	C8	1.379(3)	C7	C11	1.483(5)

Table II.3.7.5 Bond Angles for ab18115a.

Atom	Atom	Atom	Angle/°	Atom	Atom	Atom	Angle/°
O2	C12	O1	127.6(2)	C6	C5	C1	121.2(2)
C5	C1	C4	121.0(2)	C5	C6	C3	122.3(2)

C5	C1	C8	117.3(2)	C3	C7	C10	111.2(2)
C8	C1	C4	121.7(2)	C9	C7	C3	111.0(2)
C3	C2	C8	121.7(2)	C9	C7	C10	106.4(4)
C2	C3	C6	116.3(2)	C11	C7	C3	109.3(3)
C2	C3	C7	122.3(2)	C11	C7	C9	111.7(4)
C6	C3	C7	121.4(2)	C11	C7	C10	107.1(4)
N1	C4	C1	112.02(19)	C2	C8	C1	121.1(2)

Table II.3.7.6 Hydrogen Atom Coordinates (Å×10^4) and Isotropic Displacement Parameters (Å^2×10^3) for ab18115a.

Atom	***x***	***y***	***z***	**U(eq)**
H8	1003(16)	7230(50)	7970(30)	81(9)
H2A	143	2766	4994	66
H2B	613	3859	6003	66
H2C	480	1650	6150	66
H5	2880	4075	8057	75
H7A	1207	3306	4261	75
H7B	1028	928	4324	75
H9	1965	-1128	5263	73
H10	2975	-1668	6653	75
H12	1862	4633	6650	78
H13A	4705	-406	8334	201
H13B	4357	591	7000	201
H13C	4114	-1610	7428	201
H14A	4110	3719	8331	212
H14B	4503	2487	9538	212
H14C	3745	3375	9610	212
H15A	3210	130	10019	218
H15B	3982	-743	10204	218
H15C	3390	-1887	9262	218

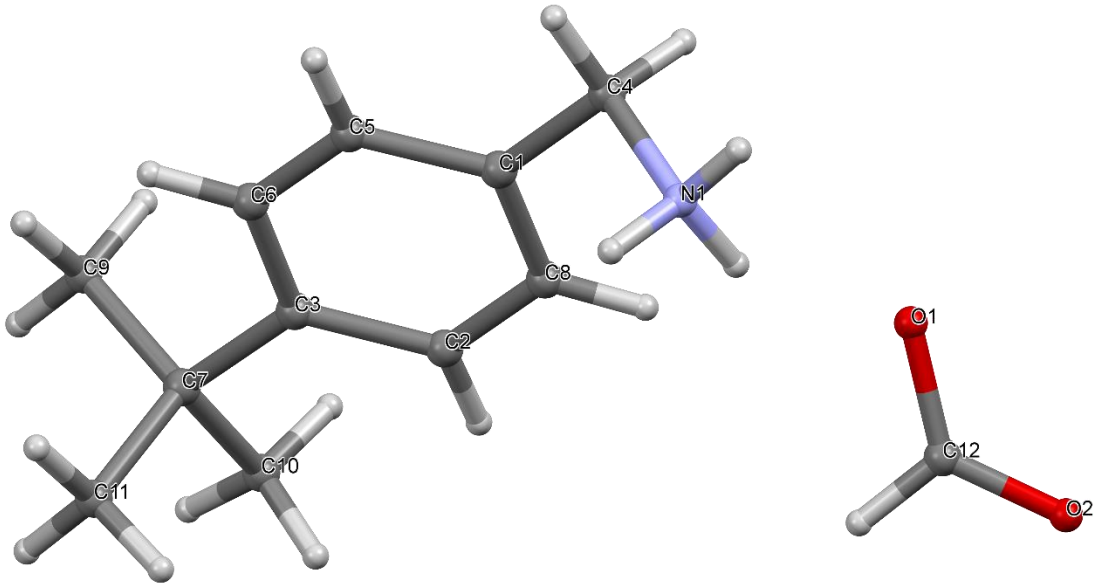

Figure II.3.7 Crystal Structure with atomic labels for compound **7**, 4-*Tert*-Butylbenzylammonium Formate, ab18115a

II.3.8 Compound 8, 3-Chloronenzylammonium Formate, ab57316a

Table II.3.8.1 Crystal data and structure refinement for ab57316a.

Identification code	ab57316a
Empirical formula	$C_8H_{10}ClNO_2$
Formula weight	187.62
Temperature/K	100.0
Crystal system	monoclinic
Space group	$P2_1/c$
a/Å	16.7899(10)
b/Å	4.7766(3)
c/Å	11.5500(6)
α/°	90
β/°	104.162(3)
γ/°	90
Volume/Å^3	898.14(9)
Z	4
ρ_{calc}g/cm^3	1.388
μ/mm^{-1}	0.383
F(000)	392.0
Crystal size/mm^3	0.488 × 0.187 × 0.09
Radiation	MoKα (λ = 0.71073)
2Θ range for data collection/°	2.502 to 63.3
Index ranges	$-24 \le h \le 22$, $-7 \le k \le 7$, $-17 \le l \le 17$
Reflections collected	20733
Independent reflections	3009 [R_{int} = 0.0276, R_{sigma} = 0.0168]
Data/restraints/parameters	3009/0/149
Goodness-of-fit on F^2	1.202
Final R indexes [I>=2σ (I)]	R_1 = 0.0467, wR_2 = 0.1136
Final R indexes [all data]	R_1 = 0.0494, wR_2 = 0.1148
Largest diff. peak/hole / e Å^{-3}	0.62/-0.27

Table II.3.8.2 Fractional Atomic Coordinates (×10^4) and Equivalent Isotropic Displacement Parameters (Å^2×10^3) for ab57316a. U_{eq} is defined as 1/3 of of the trace of the orthogonalised U_{IJ} tensor.

Atom	*x*	*y*	*z*	U(eq)
Cl1	420.3(2)	2740.5(10)	1627.9(4)	24.54(12)
N1	3857.0(8)	8588(3)	1778.9(11)	13.2(2)
C1	1215.0(9)	3873(3)	1017.6(14)	16.8(3)
C2	2415.8(9)	6741(3)	1172.8(13)	13.2(3)
C3	2991.9(9)	8945(3)	1842.5(13)	14.5(3)
C4	1769.1(9)	5838(3)	1641.4(13)	14.7(3)
C5	1282.3(10)	2774(4)	-65.2(14)	19.0(3)
C6	2491.3(10)	5656(4)	83.7(14)	18.4(3)

C7	1928.9(11)	3691(4)	-524.6(15)	21.5(3)
O1	4338.8(7)	11461(2)	-2026.4(10)	15.5(2)
O2	3978.9(8)	9034(3)	-582.0(10)	20.4(2)
C8	4201.1(9)	11214(3)	-1002.9(13)	15.1(3)

Table II.3.8.3 Anisotropic Displacement Parameters ($Å^2×10^3$) for ab57316a. The Anisotropic displacement factor exponent takes the form: $-2\pi^2[h^2a^{*2}U_{11}+2hka^*b^*U_{12}+\ldots]$.

Atom	U_{11}	U_{22}	U_{33}	U_{23}	U_{13}	U_{12}
Cl1	16.15(17)	33.0(2)	25.8(2)	-0.19(16)	7.80(14)	-7.20(15)
N1	14.2(5)	12.9(5)	12.8(5)	-0.4(4)	3.8(4)	-1.3(4)
C1	12.7(6)	19.3(7)	18.2(7)	4.1(5)	3.1(5)	-0.9(5)
C2	13.7(6)	12.3(6)	12.9(6)	1.1(5)	2.0(5)	-0.4(5)
C3	14.4(6)	14.5(6)	14.7(6)	-2.5(5)	3.8(5)	-0.5(5)
C4	13.2(6)	16.4(6)	14.6(6)	0.6(5)	3.8(5)	1.0(5)
C5	18.0(7)	21.0(7)	16.2(7)	-0.4(6)	0.5(5)	-5.7(6)
C6	20.7(7)	20.6(7)	14.6(6)	-2.2(5)	5.8(5)	-5.3(6)
C7	24.9(8)	24.8(8)	15.0(7)	-4.9(6)	5.1(6)	-8.8(6)
O1	19.2(5)	13.9(5)	14.3(5)	2.3(4)	5.8(4)	1.0(4)
O2	24.8(6)	22.9(6)	14.9(5)	0.8(4)	7.5(4)	-7.1(5)
C8	15.3(6)	16.1(7)	14.0(6)	-1.5(5)	3.5(5)	0.2(5)

Table II.3.8.4 Bond Lengths for ab57316a.

Atom	Atom	Length/Å	Atom	Atom	Length/Å
Cl1	C1	1.7407(16)	C2	C6	1.394(2)
N1	C3	1.4821(19)	C5	C7	1.391(2)
C1	C4	1.392(2)	C6	C7	1.394(2)
C1	C5	1.386(2)	O1	C8	1.2644(18)
C2	C3	1.509(2)	O2	C8	1.2444(19)
C2	C4	1.395(2)			

Table II.3.8.5 Bond Angles for ab57316a.

Atom	Atom	Atom	Angle/°	Atom	Atom	Atom	Angle/°
C4	C1	Cl1	118.78(12)	N1	C3	C2	114.04(12)
C5	C1	Cl1	119.16(12)	C1	C4	C2	119.53(14)
C5	C1	C4	122.05(14)	C1	C5	C7	117.94(15)
C4	C2	C3	118.63(13)	C7	C6	C2	120.34(15)
C6	C2	C3	122.23(13)	C5	C7	C6	121.04(15)
C6	C2	C4	119.10(14)	O2	C8	O1	125.75(15)

Table II.3.8.6 Hydrogen Atom Coordinates (Å×10^4) and Isotropic Displacement Parameters (Å^2×10^3) for ab57316a.

Atom	*x*	*y*	*z*	U(eq)
H1A	4013(15)	6820(60)	2030(20)	26(6)
H1B	4153(15)	9970(60)	2210(20)	27(6)
H1C	3930(16)	8650(60)	1010(20)	33(7)
H3A	2985(13)	8900(50)	2660(19)	14(5)
H3B	2813(14)	10830(50)	1490(20)	26(6)
H4	1691(14)	6580(50)	2380(20)	21(6)
H5	905(16)	1480(60)	-470(20)	36(7)
H6	2977(14)	6220(50)	-240(20)	22(6)
H7	1965(15)	2930(50)	-1300(20)	27(6)
H8	4261(16)	13090(60)	-530(20)	34(7)

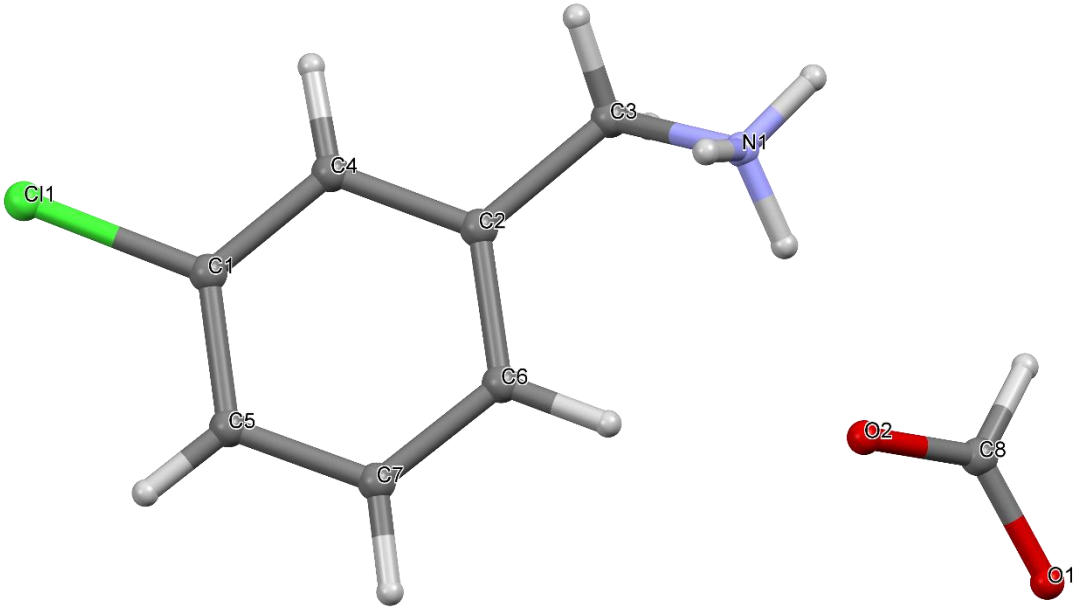

Figure II.3.8 Crystal Structure with atomic labels for compound **8**, 3-Chloronenzylammonium Formate, ab57316a

II.3.9 Compound 9, 4-Chlorobenzylammonium Formate, ab50516a

Table II.3.8.1 Crystal data and structure refinement for ab57316a.

Identification code	ab57316a
Empirical formula	$C_8H_{10}ClNO_2$
Formula weight	187.62
Temperature/K	100.0
Crystal system	monoclinic
Space group	$P2_1/c$
a/Å	16.7899(10)
b/Å	4.7766(3)
c/Å	11.5500(6)
α/°	90
β/°	104.162(3)
γ/°	90
Volume/Å^3	898.14(9)
Z	4
ρ_{calc}g/cm^3	1.388
μ/mm^{-1}	0.383
F(000)	392.0
Crystal size/mm^3	0.488 × 0.187 × 0.09
Radiation	MoKα (λ = 0.71073)
2Θ range for data collection/°	2.502 to 63.3
Index ranges	$-24 \le h \le 22$, $-7 \le k \le 7$, $-17 \le l \le 17$
Reflections collected	20733
Independent reflections	3009 [R_{int} = 0.0276, R_{sigma} = 0.0168]
Data/restraints/parameters	3009/0/149
Goodness-of-fit on F^2	1.202
Final R indexes [I>=2σ (I)]	R_1 = 0.0467, wR_2 = 0.1136
Final R indexes [all data]	R_1 = 0.0494, wR_2 = 0.1148
Largest diff. peak/hole / e Å^{-3}	0.62/-0.27

Table II.3.8.2 Fractional Atomic Coordinates (×10^4) and Equivalent Isotropic Displacement Parameters (Å^2×10^3) for ab57316a. U_{eq} is defined as 1/3 of of the trace of the orthogonalised U_{IJ} tensor.

Atom	*x*	*y*	*z*	U(eq)
Cl1	420.3(2)	2740.5(10)	1627.9(4)	24.54(12)
N1	3857.0(8)	8588(3)	1778.9(11)	13.2(2)
C1	1215.0(9)	3873(3)	1017.6(14)	16.8(3)
C2	2415.8(9)	6741(3)	1172.8(13)	13.2(3)
C3	2991.9(9)	8945(3)	1842.5(13)	14.5(3)
C4	1769.1(9)	5838(3)	1641.4(13)	14.7(3)
C5	1282.3(10)	2774(4)	-65.2(14)	19.0(3)
C6	2491.3(10)	5656(4)	83.7(14)	18.4(3)

C7	1928.9(11)	3691(4)	-524.6(15)	21.5(3)
O1	4338.8(7)	11461(2)	-2026.4(10)	15.5(2)
O2	3978.9(8)	9034(3)	-582.0(10)	20.4(2)
C8	4201.1(9)	11214(3)	-1002.9(13)	15.1(3)

Table II.3.8.3 Anisotropic Displacement Parameters ($Å^2×10^3$) for ab57316a. The Anisotropic displacement factor exponent takes the form: $-2\pi^2[h^2a^{*2}U_{11}+2hka^*b^*U_{12}+\ldots]$.

Atom	U_{11}	U_{22}	U_{33}	U_{23}	U_{13}	U_{12}
Cl1	16.15(17)	33.0(2)	25.8(2)	-0.19(16)	7.80(14)	-7.20(15)
N1	14.2(5)	12.9(5)	12.8(5)	-0.4(4)	3.8(4)	-1.3(4)
C1	12.7(6)	19.3(7)	18.2(7)	4.1(5)	3.1(5)	-0.9(5)
C2	13.7(6)	12.3(6)	12.9(6)	1.1(5)	2.0(5)	-0.4(5)
C3	14.4(6)	14.5(6)	14.7(6)	-2.5(5)	3.8(5)	-0.5(5)
C4	13.2(6)	16.4(6)	14.6(6)	0.6(5)	3.8(5)	1.0(5)
C5	18.0(7)	21.0(7)	16.2(7)	-0.4(6)	0.5(5)	-5.7(6)
C6	20.7(7)	20.6(7)	14.6(6)	-2.2(5)	5.8(5)	-5.3(6)
C7	24.9(8)	24.8(8)	15.0(7)	-4.9(6)	5.1(6)	-8.8(6)
O1	19.2(5)	13.9(5)	14.3(5)	2.3(4)	5.8(4)	1.0(4)
O2	24.8(6)	22.9(6)	14.9(5)	0.8(4)	7.5(4)	-7.1(5)
C8	15.3(6)	16.1(7)	14.0(6)	-1.5(5)	3.5(5)	0.2(5)

Table II.3.8.4 Bond Lengths for ab57316a.

Atom	Atom	Length/Å	Atom	Atom	Length/Å
Cl1	C1	1.7407(16)	C2	C6	1.394(2)
N1	C3	1.4821(19)	C5	C7	1.391(2)
C1	C4	1.392(2)	C6	C7	1.394(2)
C1	C5	1.386(2)	O1	C8	1.2644(18)
C2	C3	1.509(2)	O2	C8	1.2444(19)
C2	C4	1.395(2)			

Table II.3.8.5 Bond Angles for ab57316a.

Atom	Atom	Atom	Angle/°	Atom	Atom	Atom	Angle/°
C4	C1	Cl1	118.78(12)	N1	C3	C2	114.04(12)
C5	C1	Cl1	119.16(12)	C1	C4	C2	119.53(14)
C5	C1	C4	122.05(14)	C1	C5	C7	117.94(15)
C4	C2	C3	118.63(13)	C7	C6	C2	120.34(15)
C6	C2	C3	122.23(13)	C5	C7	C6	121.04(15)
C6	C2	C4	119.10(14)	O2	C8	O1	125.75(15)

Table II.3.8.6 Hydrogen Atom Coordinates (Å×10^4) and Isotropic Displacement Parameters (Å^2×10^3) for ab57316a.

Atom	*x*	*y*	*z*	U(eq)
H1A	4013(15)	6820(60)	2030(20)	26(6)
H1B	4153(15)	9970(60)	2210(20)	27(6)
H1C	3930(16)	8650(60)	1010(20)	33(7)
H3A	2985(13)	8900(50)	2660(19)	14(5)
H3B	2813(14)	10830(50)	1490(20)	26(6)
H4	1691(14)	6580(50)	2380(20)	21(6)
H5	905(16)	1480(60)	-470(20)	36(7)
H6	2977(14)	6220(50)	-240(20)	22(6)
H7	1965(15)	2930(50)	-1300(20)	27(6)
H8	4261(16)	13090(60)	-530(20)	34(7)

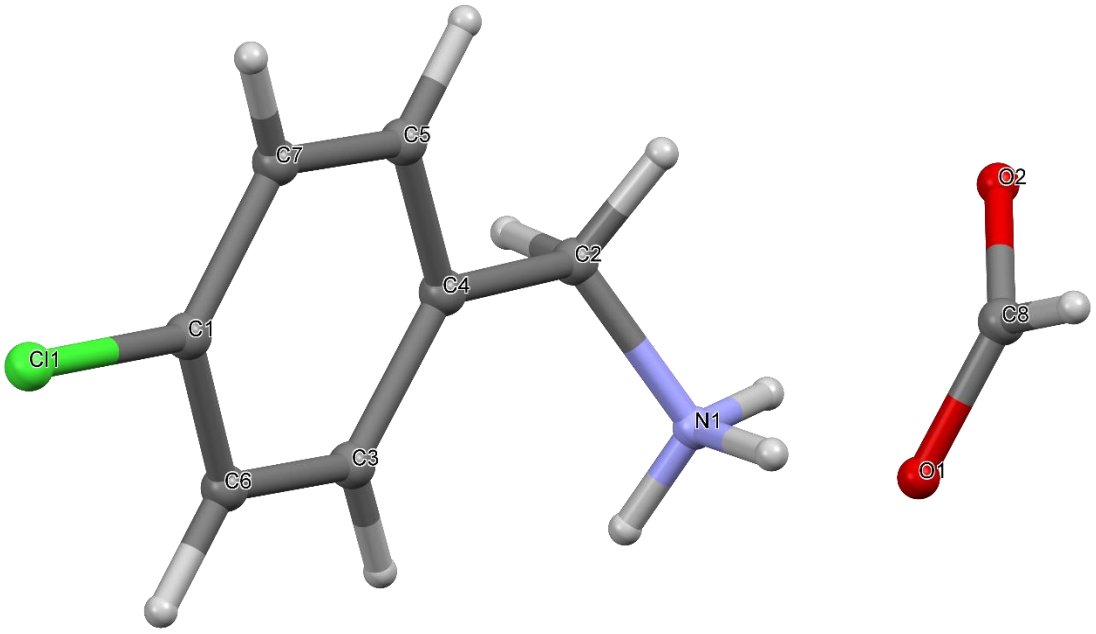

Figure II.3.9 Crystal Structure with atomic labels for compound **9**, 4-Chlorobenzylammonium Formate, ab50516a

II.3.10 Compound 10, 3,5-Difluorobenzylammonium Formate, ab57516a

Table II.3.10.1 Crystal data and structure refinement for ab57516a.

Identification code	ab57516a
Empirical formula	$C_8H_9NO_2F_2$
Formula weight	189.16
Temperature/K	100.0
Crystal system	orthorhombic
Space group	Pbca
a/Å	13.4870(14)
b/Å	7.4596(8)
c/Å	17.4603(18)
α/°	90
β/°	90
γ/°	90
Volume/Å^3	1756.6(3)
Z	8
ρ_{calc}g/cm^3	1.431
μ/mm^{-1}	0.130
F(000)	784.0
Crystal size/mm^3	0.644 × 0.085 × 0.031
Radiation	MoKα (λ = 0.71073)
2Θ range for data collection/°	4.666 to 39.952
Index ranges	$-12 \le h \le 12$, $-7 \le k \le 7$, $-16 \le l \le 16$
Reflections collected	14166
Independent reflections	818 [R_{int} = 0.0453, R_{sigma} = 0.0160]
Data/restraints/parameters	818/0/154
Goodness-of-fit on F^2	1.135
Final R indexes [I>=2σ (I)]	R_1 = 0.0254, wR_2 = 0.0636
Final R indexes [all data]	R_1 = 0.0299, wR_2 = 0.0689
Largest diff. peak/hole / e Å^{-3}	0.10/-0.15

Table II.3.10.2 Fractional Atomic Coordinates (×10^4) and Equivalent Isotropic Displacement Parameters (Å^2×10^3) for ab57516a. U_{eq} is defined as 1/3 of of the trace of the orthogonalised U_{IJ} tensor.

Atom	*x*	*y*	*z*	U(eq)
F1	8974.6(9)	2106.8(16)	6441.2(6)	39.2(4)
F2	8634.5(9)	6687.7(15)	4623.5(6)	34.3(4)
N1	9031.9(14)	1096(3)	2984.5(9)	19.6(5)
C1	8837.2(13)	1886(3)	4373.8(11)	18.5(6)
C2	8745.7(14)	3698(3)	4203.7(13)	21.5(6)
C3	8894.6(14)	1357(3)	5140.4(12)	22.0(6)
C4	8780.0(14)	4451(3)	5556.5(13)	24.4(6)
C5	8717.4(14)	4909(3)	4800.3(13)	23.2(6)

C6	8875.8(14)	2643(3)	5698.7(12)	24.6(6)
C7	8849.6(17)	444(3)	3773.8(11)	21.9(6)
O1	10826.8(10)	2069.4(17)	7870.1(7)	23.2(4)
O2	12344.5(10)	2065.6(17)	7366.8(8)	25.9(4)
C8	11642.4(17)	2809(3)	7698.8(12)	22.7(6)

Table II.3.10.3 Anisotropic Displacement Parameters ($Å^2×10^3$) for ab57516a. The Anisotropic displacement factor exponent takes the form: $-2\pi^2[h^2a^{*2}U_{11}+2hka^*b^*U_{12}+\ldots]$.

Atom	U_{11}	U_{22}	U_{33}	U_{23}	U_{13}	U_{12}
F1	58.7(9)	40.0(8)	19.0(8)	-0.1(6)	3.0(6)	5.7(6)
F2	44.6(9)	19.5(8)	38.8(8)	-2.1(6)	-0.9(6)	0.3(6)
N1	20.3(12)	17.3(11)	21.2(11)	-0.5(9)	0.6(8)	-3.8(10)
C1	12.9(11)	18.9(14)	23.6(14)	-0.6(11)	-0.3(8)	-0.7(9)
C2	22.3(13)	25.9(15)	16.4(15)	-1.6(12)	-2.9(9)	-0.1(10)
C3	23.0(13)	21.1(14)	21.9(15)	3.4(12)	1.9(9)	0.6(10)
C4	22.6(13)	26.3(17)	24.4(16)	-9.1(12)	1.2(9)	0.0(10)
C5	20.7(12)	15.4(13)	33.6(17)	2.3(12)	-0.3(10)	-0.8(9)
C6	26.4(13)	32.9(17)	14.6(14)	0.7(12)	1.5(9)	2.7(10)
C7	24.8(14)	21.0(13)	20.0(14)	2.5(11)	-1.7(10)	-0.4(12)
O1	20.0(9)	21.4(9)	28.3(9)	1.4(6)	3.3(6)	-0.9(7)
O2	22.1(9)	24.6(9)	31.1(9)	-5.7(7)	5.0(7)	-1.7(7)
C8	27.6(15)	17.3(15)	23.0(12)	0.3(11)	-0.4(11)	-2.7(13)

Table II.3.10.4 Bond Lengths for ab57516a.

Atom	Atom	Length/Å	Atom	Atom	Length/Å
F1	C6	1.363(2)	C2	C5	1.379(3)
F2	C5	1.367(2)	C3	C6	1.368(3)
N1	C7	1.482(3)	C4	C5	1.366(3)
C1	C2	1.389(3)	C4	C6	1.377(3)
C1	C3	1.398(3)	O1	C8	1.267(2)
C1	C7	1.502(3)	O2	C8	1.241(2)

Table II.3.10.5 Bond Angles for ab57516a.

Atom	Atom	Atom	Angle/°	Atom	Atom	Atom	Angle/°
C2	C1	C3	119.0(2)	C4	C5	F2	117.78(18)
C2	C1	C7	123.29(19)	C4	C5	C2	124.3(2)
C3	C1	C7	117.73(19)	F1	C6	C3	118.05(19)
C5	C2	C1	118.6(2)	F1	C6	C4	117.90(19)
C6	C3	C1	118.9(2)	C3	C6	C4	124.0(2)
C5	C4	C6	115.1(2)	N1	C7	C1	114.54(18)

F2	C5	C2	117.87(19)	O2	C8	O1	125.3(2)

Table II.3.10.6 Hydrogen Atom Coordinates (Å×10^4) and Isotropic Displacement Parameters (Å^2×10^3) for ab57516a.

Atom	*x*	*y*	*z*	U(eq)
H1A	9576(17)	1780(30)	2956(11)	28(6)
H1B	8425(18)	1890(30)	2796(13)	51(7)
H1C	9058(15)	0(30)	2643(13)	43(7)
H2	8691(11)	4090(20)	3688(11)	6(5)
H3	8955(14)	120(30)	5271(11)	27(6)
H4	8777(13)	5360(30)	5966(12)	25(5)
H7A	8210(15)	-210(30)	3758(11)	28(6)
H7B	9354(15)	-400(30)	3889(10)	22(6)
H8	11725(14)	4130(30)	7840(11)	32(6)

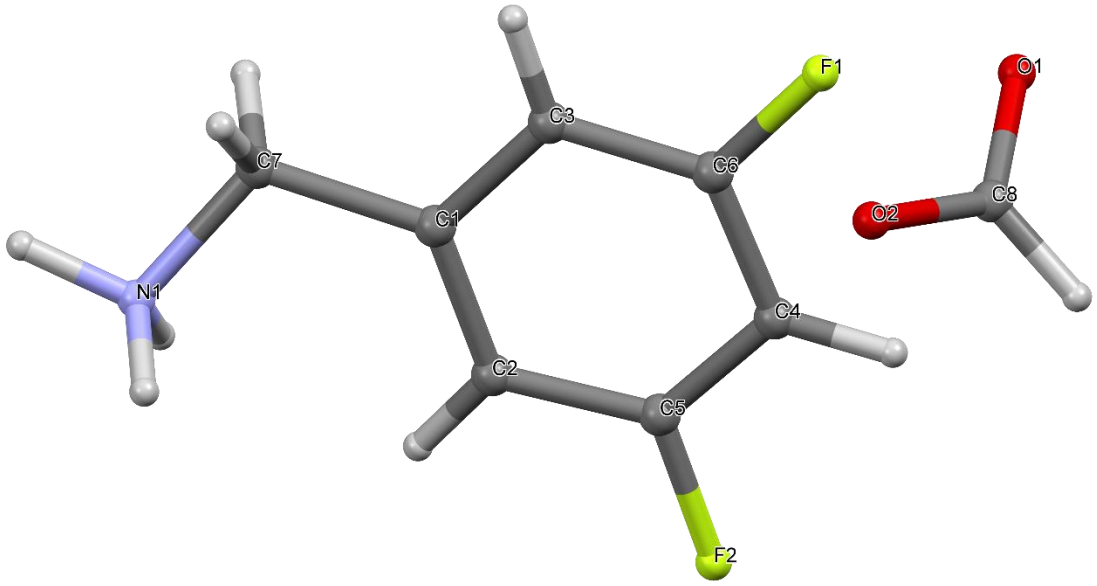

Figure II.3.10 Crystal Structure with atomic labels for compound **10**, 3,5-

Difluorobenzylammonium Formate, ab57516a

II.3.11 Compound 11, 1-(1-Naphthyl)-Benzylammonium Formate, ab53716a

Table II.3.11.1 Crystal data and structure refinement for ab53716a.

Identification code	ab53716a
Empirical formula	$C_{13}H_{15}NO_2$
Formula weight	217.26
Temperature/K	110.96
Crystal system	orthorhombic
Space group	$Pca2_1$
a/Å	6.9086(3)
b/Å	17.9665(7)
c/Å	9.1840(3)
α/°	90
β/°	90
γ/°	90
Volume/Å^3	1139.95(8)
Z	4
ρ_{calc}g/cm^3	1.266
μ/mm^{-1}	0.085
F(000)	464.0
Crystal size/mm^3	0.471 × 0.34 × 0.148
Radiation	MoKα (λ = 0.71073)
2Θ range for data collection/°	2.266 to 62.13
Index ranges	$-10 \le h \le 10$, $-26 \le k \le 26$, $-13 \le l \le 12$
Reflections collected	25753
Independent reflections	3616 [R_{int} = 0.0242, R_{sigma} = 0.0149]
Data/restraints/parameters	3616/1/205
Goodness-of-fit on F^2	1.104
Final R indexes [I>=2σ (I)]	R_1 = 0.0307, wR_2 = 0.0840
Final R indexes [all data]	R_1 = 0.0330, wR_2 = 0.0920
Largest diff. peak/hole / e Å^{-3}	0.38/-0.17
Flack parameter	0.6(2)

Table II.3.11.2 Fractional Atomic Coordinates (×10^4) and Equivalent Isotropic Displacement Parameters (Å^2×10^3) for ab53716a. U_{eq} is defined as 1/3 of of the trace of the orthogonalised U_{IJ} tensor.

Atom	*x*	*y*	*z*	U(eq)
O1	6666.7(14)	4685.6(5)	2357.0(11)	19.3(2)
O2	6958.2(15)	5834.9(6)	3277.7(13)	23.2(2)
C1	6965.5(18)	5378.2(7)	2257.3(16)	17.0(2)
N1	6554.3(17)	4024.3(6)	9668.4(13)	16.0(2)
C2	5694.5(16)	1946.4(7)	9799.3(14)	14.8(2)
C3	3209(2)	1712.3(8)	11672.2(17)	20.0(3)
C4	5786.0(17)	2705.9(7)	10281.8(13)	13.7(2)

C5	4387.9(18)	1448.7(7)	10510.6(15)	17.5(2)
C6	7208.0(17)	3233.2(6)	9566.4(14)	14.0(2)
C7	6827.2(18)	1665.3(7)	8624.1(16)	17.9(2)
C8	4608.5(18)	2936.1(7)	11406.0(14)	16.0(2)
C9	4285(2)	695.2(7)	10037.7(18)	21.4(3)
C10	6671(2)	933.6(8)	8186.0(19)	22.4(3)
C11	3316.7(18)	2440.1(8)	12107.5(15)	19.0(2)
C12	9248.2(18)	3169.7(8)	10204.6(16)	18.3(2)
C13	5395(2)	442.9(8)	8907.0(19)	24.1(3)

Table II.3.11.3 Anisotropic Displacement Parameters ($Å^2×10^3$) for ab53716a. The Anisotropic displacement factor exponent takes the form: $-2\pi^2[h^2a^{*2}U_{11}+2hka^*b^*U_{12}+\ldots]$.

Atom	U_{11}	U_{22}	U_{33}	U_{23}	U_{13}	U_{12}
O1	24.2(4)	17.4(4)	16.4(4)	1.6(3)	-2.8(4)	-3.1(3)
O2	22.4(5)	22.2(4)	25.0(5)	-7.1(4)	4.4(4)	-1.4(4)
C1	16.1(5)	18.4(5)	16.6(5)	0.6(4)	1.0(4)	2.0(4)
N1	19.6(5)	14.1(4)	14.2(5)	1.6(4)	-1.3(4)	-1.8(3)
C2	12.9(5)	15.0(5)	16.4(6)	2.2(4)	-1.9(4)	-1.1(4)
C3	16.4(5)	22.2(6)	21.5(6)	5.5(5)	0.0(5)	-4.4(4)
C4	12.6(5)	14.2(5)	14.2(5)	2.1(4)	-1.4(4)	-0.9(3)
C5	14.6(5)	17.3(5)	20.6(6)	4.2(4)	-3.6(4)	-2.8(4)
C6	15.1(5)	13.2(4)	13.7(5)	1.3(4)	0.3(4)	-1.4(4)
C7	15.9(5)	16.6(5)	21.4(6)	-1.3(4)	0.3(4)	-0.3(4)
C8	15.0(5)	17.0(5)	16.0(6)	1.8(4)	0.0(4)	-0.2(4)
C9	20.1(6)	16.2(5)	28.0(7)	3.9(5)	-5.0(5)	-4.3(4)
C10	20.7(6)	18.1(5)	28.3(7)	-4.3(5)	-1.7(5)	1.8(4)
C11	14.8(5)	23.8(6)	18.4(6)	3.1(5)	2.6(4)	-1.2(4)
C12	14.7(5)	22.5(6)	17.6(6)	1.4(5)	-0.8(4)	-2.3(4)
C13	23.3(6)	15.2(5)	33.6(8)	-1.3(5)	-6.7(6)	-0.4(5)

Table II.3.11.4 Bond Lengths for ab53716a.

Atom	Atom	Length/Å	Atom	Atom	Length/Å
O1	C1	1.2645(16)	C4	C6	1.5147(16)
O2	C1	1.2456(18)	C4	C8	1.3780(17)
N1	C6	1.4943(15)	C5	C9	1.4235(18)
C2	C4	1.4361(16)	C6	C12	1.5308(18)
C2	C5	1.4287(16)	C7	C10	1.3790(18)
C2	C7	1.4256(19)	C8	C11	1.4161(17)
C3	C5	1.423(2)	C9	C13	1.368(2)
C3	C11	1.370(2)	C10	C13	1.412(2)

Table II.3.11.5 Bond Angles for ab53716a.

Atom	Atom	Atom	Angle/°	Atom	Atom	Atom	Angle/°
O2	C1	O1	126.38(14)	C9	C5	C2	119.16(13)
C5	C2	C4	118.78(11)	N1	C6	C4	111.82(10)
C7	C2	C4	123.09(11)	N1	C6	C12	108.98(10)
C7	C2	C5	118.12(11)	C4	C6	C12	112.61(10)
C11	C3	C5	120.37(12)	C10	C7	C2	121.05(13)
C2	C4	C6	119.28(11)	C4	C8	C11	121.61(12)
C8	C4	C2	119.36(11)	C13	C9	C5	121.24(13)
C8	C4	C6	121.35(11)	C7	C10	C13	120.48(15)
C3	C5	C2	119.74(12)	C3	C11	C8	120.15(13)
C3	C5	C9	121.10(12)	C9	C13	C10	119.94(13)

Table II.3.11.6 Hydrogen Atom Coordinates (Å×10^4) and Isotropic Displacement Parameters (Å^2×10^3) for ab53716a.

Atom	*x*	*y*	*z*	U(eq)
H1	7200(30)	5550(11)	1250(20)	21(5)
H1A	5340(40)	4099(13)	9370(30)	32(6)
H1B	6630(30)	4206(12)	10550(30)	21(5)
H1C	7330(40)	4296(13)	9070(30)	31(6)
H3	2300(40)	1390(13)	12100(30)	33(6)
H6	7210(30)	3113(9)	8540(20)	10(4)
H7	7770(30)	1987(12)	8160(30)	23(5)
H8	4650(30)	3467(12)	11730(30)	21(5)
H9	3390(30)	358(13)	10590(30)	29(6)
H10	7450(40)	752(11)	7370(30)	31(5)
H11	2560(40)	2599(11)	12850(20)	23(5)
H12A	10130(40)	3477(14)	9700(30)	32(6)
H12B	9220(40)	3327(13)	11210(30)	32(6)
H12C	9690(30)	2639(13)	10150(30)	29(5)
H13	5320(30)	-82(12)	8560(30)	26(5)

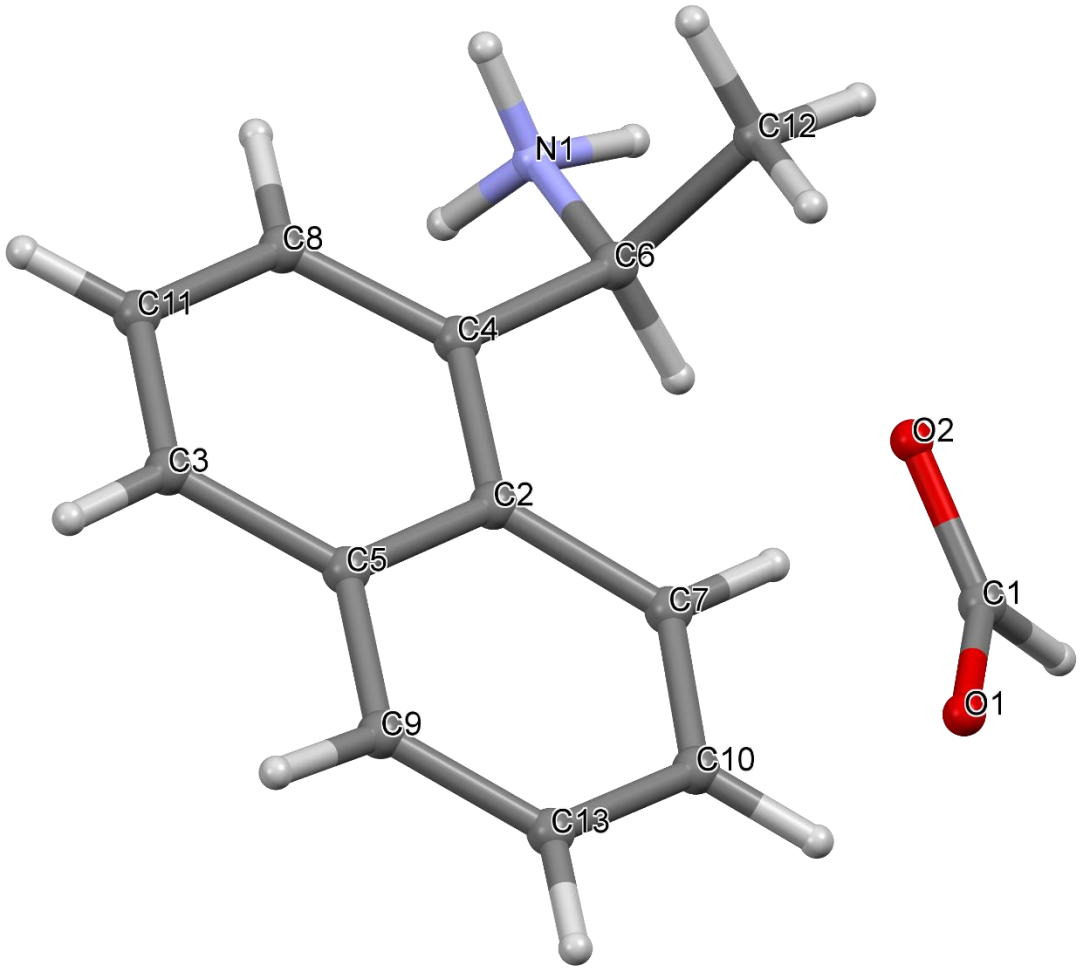

Figure II.3.11 Crystal Structure with atomic labels for compound **11**, 1-(1-Naphthyl)-Benzylammonium Formate, ab53716a

II.3.12 Compound 12, 4-Aminobenzylammonium Formate, ab53616

Table II.3.12.1 Crystal data and structure refinement for ab53616.

Identification code	ab53616
Empirical formula	$C_8H_{16}N_2O_2$
Formula weight	172.23
Temperature/K	113.19
Crystal system	monoclinic
Space group	C2
a/Å	19.8600(11)
b/Å	5.8074(3)
c/Å	7.6922(4)
α/°	90
β/°	107.785(3)
γ/°	90
Volume/Å^3	844.78(8)
Z	4
ρ_{calc}g/cm^3	1.354
μ/mm^{-1}	0.098
F(000)	376.0
Crystal size/mm^3	0.802 × 0.172 × 0.105
Radiation	MoKα (λ = 0.71073)
2Θ range for data collection/°	4.308 to 68.518
Index ranges	$-30 \le h \le 31$, $-9 \le k \le 8$, $-12 \le l \le 11$
Reflections collected	11395
Independent reflections	3237 [R_{int} = 0.0278, R_{sigma} = 0.0252]
Data/restraints/parameters	3237/1/157
Goodness-of-fit on F^2	1.061
Final R indexes [I>=2σ (I)]	R_1 = 0.0331, wR_2 = 0.0897
Final R indexes [all data]	R_1 = 0.0351, wR_2 = 0.0916
Largest diff. peak/hole / e Å^{-3}	0.34/-0.20
Flack parameter	-0.1(3)

Table II.3.12.2 Fractional Atomic Coordinates (×10^4) and Equivalent Isotropic Displacement Parameters (Å^2×10^3) for ab53616. U_{eq} is defined as 1/3 of of the trace of the orthogonalised U_{IJ} tensor.

Atom	*x*	*y*	*z*	U(eq)
O1	320.1(5)	2324.8(18)	2600.0(14)	24.3(2)
O2	-463.4(5)	5136.4(18)	1530.6(13)	21.4(2)
C8	-274.3(6)	3056(2)	1710.5(15)	17.2(2)
N1	3272.1(5)	2402.7(19)	9406.2(14)	16.25(19)
N2	737.9(5)	-2188.4(19)	2858.1(13)	15.57(18)
C1	2029.9(6)	1869.0(19)	7660.7(14)	13.89(19)
C2	2346.5(6)	-2420(2)	6490.0(14)	14.2(2)

C3	2882.2(6)	-1111(2)	7666.3(15)	14.3(2)
C4	1648.8(6)	-1626.3(18)	5898.5(14)	13.5(2)
C5	1502.9(5)	543.8(19)	6486.4(14)	14.3(2)
C6	2729.5(6)	1045.4(19)	8277.0(14)	13.10(19)
C7	1061.9(6)	-3112(2)	4746.6(15)	16.4(2)

Table II.3.12.3 Anisotropic Displacement Parameters ($Å^2×10^3$) for ab53616. The Anisotropic displacement factor exponent takes the form: $-2\pi^2[h^2a^{*2}U_{11}+2hka^*b^*U_{12}+\ldots]$.

Atom	U_{11}	U_{22}	U_{33}	U_{23}	U_{13}	U_{12}
O1	22.4(4)	17.4(4)	27.4(5)	0.0(4)	-0.8(3)	3.1(3)
O2	16.2(4)	19.1(4)	25.5(4)	-1.2(4)	1.3(3)	1.7(3)
C8	16.9(5)	18.4(5)	16.5(4)	-1.4(4)	5.3(4)	-3.4(4)
N1	14.4(4)	17.1(4)	14.9(4)	-2.7(3)	1.0(3)	-1.5(3)
N2	14.8(4)	15.0(4)	15.4(4)	-0.6(3)	2.4(3)	-0.1(3)
C1	14.7(4)	13.2(5)	13.5(4)	-0.5(3)	4.0(3)	1.6(4)
C2	16.0(4)	12.2(5)	14.1(4)	-0.2(3)	4.1(3)	0.7(4)
C3	13.6(4)	14.2(5)	14.5(4)	0.1(4)	3.2(3)	0.9(4)
C4	14.2(4)	13.6(5)	12.1(4)	-0.3(3)	3.1(3)	-1.6(3)
C5	12.9(4)	15.7(5)	13.5(4)	0.5(4)	3.1(3)	0.8(4)
C6	14.2(4)	13.1(4)	11.6(4)	0.0(3)	3.3(3)	-0.6(3)
C7	17.3(5)	16.2(5)	14.6(4)	0.0(4)	2.9(4)	-3.4(4)

Table II.3.12.4 Bond Lengths for ab53616.

Atom	Atom	Length/Å	Atom	Atom	Length/Å
O1	C8	1.2444(15)	C2	C3	1.3930(15)
O2	C8	1.2601(16)	C2	C4	1.3981(15)
N1	C6	1.4020(14)	C3	C6	1.4030(16)
N2	C7	1.4970(15)	C4	C5	1.3988(15)
C1	C5	1.3878(15)	C4	C7	1.5025(15)
C1	C6	1.4077(15)			

Table II.3.12.5 Bond Angles for ab53616.

Atom	Atom	Atom	Angle/°	Atom	Atom	Atom	Angle/°
O1	C8	O2	126.05(12)	C5	C4	C7	120.54(9)
C5	C1	C6	120.09(10)	C1	C5	C4	121.37(10)
C3	C2	C4	121.06(10)	N1	C6	C1	120.70(10)
C2	C3	C6	120.28(10)	N1	C6	C3	120.36(10)
C2	C4	C5	118.32(10)	C3	C6	C1	118.86(10)
C2	C4	C7	121.05(10)	N2	C7	C4	113.11(9)

Table II.3.12.6 Hydrogen Atom Coordinates (Å×10⁴) and Isotropic Displacement Parameters (Å²×10³) for ab53616.

Atom	*x*	*y*	*z*	U(eq)
H8	-652(12)	1900(50)	1020(30)	37(6)
H1A	3112(10)	3580(40)	9950(20)	20(4)
H1B	3634(12)	1590(40)	10170(30)	33(6)
H2A	570(11)	-780(40)	2850(30)	30(5)
H2B	1059(9)	-2150(40)	2250(30)	22(4)
H2C	335(11)	-3160(40)	2230(30)	27(5)
H1	1915(8)	3380(30)	8040(20)	14(4)
H2	2470(10)	-3940(40)	6100(30)	19(4)
H3	3368(10)	-1650(40)	8130(30)	24(5)
H5	1005(9)	1190(40)	6100(30)	18(4)
H7A	1234(10)	-4710(50)	4660(30)	25(5)
H7B	696(10)	-3240(40)	5320(30)	24(5)

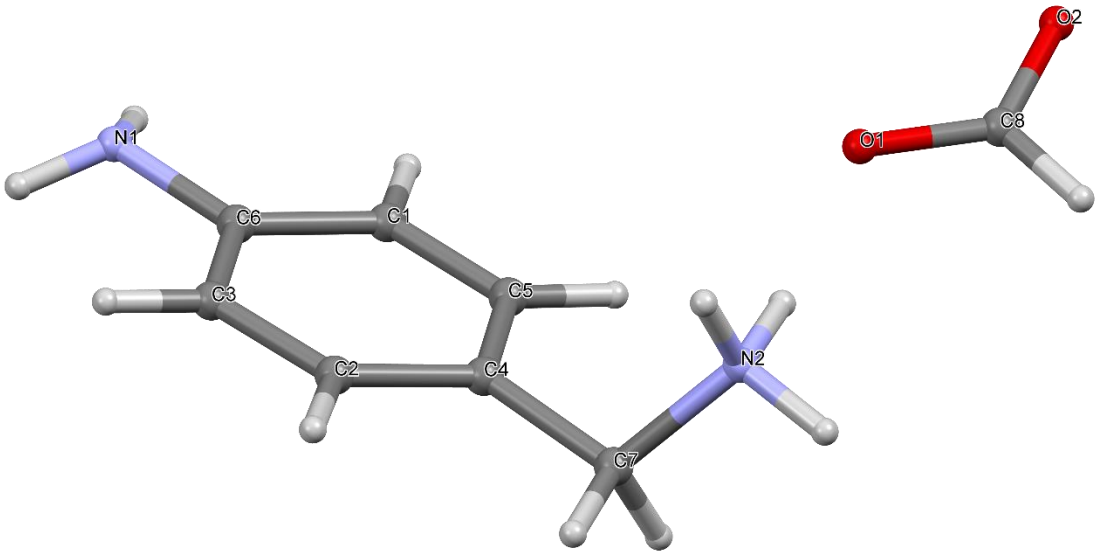

Figure II.3.12 Crystal Structure with atomic labels for compound **12**, 4-Aminobenzylammonium Formate, ab53616

II.3.13 Compound 13, Phenethylammonium Formate, ab50917

Table II.3.13.1 Crystal data and structure refinement for ab50917a.

Identification code	ab50917a
Empirical formula	$C_9H_{13}NO_2$
Formula weight	167.20
Temperature/K	103.63
Crystal system	orthorhombic
Space group	$Pca2_1$
a/Å	19.7529(5)
b/Å	11.2940(3)
c/Å	8.6136(2)
α/°	90
β/°	90
γ/°	90
Volume/Å^3	1921.60(8)
Z	8
ρ_{calc}g/cm^3	1.156
μ/mm^{-1}	0.082
F(000)	720.0
Crystal size/mm^3	0.38 × 0.278 × 0.151
Radiation	MoKα (λ = 0.71073)
2Θ range for data collection/°	3.606 to 45.426
Index ranges	$-21 \leq h \leq 21$, $-12 \leq k \leq 12$, $-9 \leq l \leq 9$
Reflections collected	21240
Independent reflections	2592 [R_{int} = 0.0338, R_{sigma} = 0.0177]
Data/restraints/parameters	2592/1/321
Goodness-of-fit on F^2	1.083
Final R indexes [I>=2σ (I)]	R_1 = 0.0202, wR_2 = 0.0503
Final R indexes [all data]	R_1 = 0.0213, wR_2 = 0.0511
Largest diff. peak/hole / e Å^{-3}	0.07/-0.12
Flack parameter	0.1(3)

Table II.3.13.2 Fractional Atomic Coordinates (×10^4) and Equivalent Isotropic Displacement Parameters (Å^2×10^3) for ab50917a. U_{eq} is defined as 1/3 of of the trace of the orthogonalised U_{IJ} tensor.

Atom	*x*	*y*	*z*	U(eq)
O1	3113.6(7)	-2147.2(11)	3971.9(18)	28.6(4)
O2	2668.3(6)	-3711.8(11)	2773.6(16)	23.5(3)
N1	3128.4(8)	-4749.9(16)	5495(2)	18.7(4)
N2	3179.2(8)	290.7(15)	4544(2)	17.9(4)
C1	3909.0(10)	602.0(18)	4720(2)	19.6(5)
C2	6115.1(10)	-176.0(18)	4193(3)	24.7(5)
C3	4985.8(9)	-4829.5(17)	4276(2)	21.7(4)

C4	4246.6(9)	-5173.8(18)	4302(3)	24.2(5)
C5	5424.5(10)	-307.9(18)	4009(2)	23.9(5)
C6	5031.3(9)	583.6(17)	3355(2)	21.3(5)
C7	3867.0(10)	-4468.2(18)	5530(2)	18.4(5)
C8	4275.3(10)	423(2)	3189(3)	26.5(5)
C9	5188.2(11)	-3737.0(18)	3674(3)	26.5(5)
C10	6045.5(11)	1751.6(19)	3071(3)	32.8(6)
C11	6427.4(10)	857.0(18)	3729(3)	27.1(5)
C12	2831.8(10)	-2638.0(17)	2857(3)	22.1(5)
C13	5351.6(11)	1620.5(19)	2887(3)	28.2(5)
C14	6157.8(11)	-5240(2)	4899(3)	32.9(6)
C15	5864.7(11)	-3413(2)	3679(3)	31.2(5)
C16	5479.3(11)	-5574(2)	4882(3)	27.6(5)
C17	6349.8(11)	-4161(2)	4299(3)	32.1(5)
O3	2585.0(7)	1286.5(11)	1937.3(16)	23.5(3)
O4	2110.8(7)	2837.0(11)	747.1(17)	24.0(3)
C18	2487.2(10)	2378.5(16)	1742(3)	21.0(4)

Table II.3.13.3 Anisotropic Displacement Parameters ($Å^2×10^3$) for ab50917a. The Anisotropic displacement factor exponent takes the form: $-2\pi^2[h^2a^{*2}U_{11}+2hka^*b^*U_{12}+\ldots]$.

Atom	U_{11}	U_{22}	U_{33}	U_{23}	U_{13}	U_{12}
O1	32.7(8)	19.2(7)	34.0(9)	-2.8(7)	-10.6(7)	0.8(6)
O2	25.5(7)	20.1(8)	24.8(8)	-0.8(6)	-4.3(6)	-1.1(6)
N1	17.8(9)	18.6(10)	19.7(10)	0.8(8)	2.9(8)	0.9(7)
N2	16.2(9)	17.2(10)	20.1(11)	0.4(8)	0.1(8)	0.7(7)
C1	16.3(10)	21.9(11)	20.6(12)	0.0(9)	-0.9(8)	0.9(8)
C2	23.7(11)	25.2(11)	25.1(11)	4.4(10)	-1.1(10)	4.9(9)
C3	21.5(10)	26.3(10)	17.4(9)	-7.5(9)	3.3(9)	0.1(8)
C4	21.9(10)	26.7(12)	23.9(11)	-5.1(10)	2.2(10)	-0.9(9)
C5	23.6(11)	23.5(10)	24.6(13)	1.4(10)	3.4(9)	-2.3(9)
C6	20.1(10)	27.6(10)	16.2(11)	-3.2(8)	2.2(8)	2.0(9)
C7	17.6(11)	18.6(11)	19.1(12)	0.8(8)	-1.1(8)	0.7(8)
C8	20.5(11)	37.1(13)	22.0(12)	-2.6(10)	0.2(9)	1.4(10)
C9	23.0(11)	27.8(11)	28.6(12)	-5.9(10)	2.2(9)	2.8(9)
C10	27.1(12)	24.6(12)	46.8(15)	7.2(11)	2.1(11)	-3.2(10)
C11	18.2(11)	31.0(11)	32.0(12)	0.5(10)	0.3(9)	-1.6(9)
C12	20.8(10)	22.7(11)	22.7(12)	2.0(11)	1.5(9)	4.7(9)
C13	26.2(11)	26.1(11)	32.4(12)	5.4(11)	-0.2(10)	5.9(9)
C14	24.8(12)	52.3(15)	21.5(11)	0.6(11)	-2.1(9)	8.9(12)
C15	28.0(12)	27.8(11)	37.8(13)	-10.2(11)	7.9(10)	-4.9(10)
C16	28.2(13)	33.8(14)	20.7(11)	1.3(10)	4.1(10)	2.8(10)
C17	19.5(11)	47.6(14)	29.3(12)	-15.4(11)	0.9(10)	-3.4(10)
O3	25.4(7)	20.1(7)	24.8(8)	0.5(6)	-5.9(6)	3.0(6)
O4	25.3(7)	19.7(7)	27.1(8)	1.5(7)	-2.7(7)	2.3(6)

C18	20.0(9)	22.5(11)	20.5(10)	-1.6(10)	1.1(9)	-1.0(9)

Table II.3.13.4 Bond Lengths for ab50917a.

Atom	Atom	Length/Å	Atom	Atom	Length/Å
O1	C12	1.241(3)	C5	C6	1.391(3)
O2	C12	1.257(2)	C6	C8	1.511(3)
N1	C7	1.494(2)	C6	C13	1.391(3)
N2	C1	1.492(2)	C9	C15	1.386(3)
C1	C8	1.518(3)	C10	C11	1.382(3)
C2	C5	1.381(3)	C10	C13	1.388(3)
C2	C11	1.379(3)	C14	C16	1.392(3)
C3	C4	1.511(3)	C14	C17	1.377(3)
C3	C9	1.397(3)	C15	C17	1.385(3)
C3	C16	1.389(3)	O3	C18	1.260(2)
C4	C7	1.522(3)	O4	C18	1.247(2)

Table II.3.13.5 Bond Angles for ab50917a.

Atom	Atom	Atom	Angle/°	Atom	Atom	Atom	Angle/°
N2	C1	C8	109.92(17)	C6	C8	C1	111.92(17)
C11	C2	C5	119.99(19)	C15	C9	C3	120.5(2)
C9	C3	C4	120.61(18)	C11	C10	C13	120.5(2)
C16	C3	C4	121.12(18)	C2	C11	C10	119.54(19)
C16	C3	C9	118.25(18)	O1	C12	O2	126.2(2)
C3	C4	C7	110.58(17)	C10	C13	C6	120.40(19)
C2	C5	C6	121.31(19)	C17	C14	C16	120.1(2)
C5	C6	C8	120.20(18)	C17	C15	C9	120.5(2)
C13	C6	C5	118.23(18)	C3	C16	C14	121.0(2)
C13	C6	C8	121.57(18)	C14	C17	C15	119.6(2)
N1	C7	C4	110.85(16)	O4	C18	O3	126.14(19)

Table II.3.13.6 Hydrogen Atom Coordinates (Å×10^4) and Isotropic Displacement Parameters (Å^2×10^3) for ab50917a.

Atom	*x*	*y*	*z*	U(eq)
H1A	2947(11)	-4460(20)	4570(30)	36(7)
H1B	3046(10)	-5570(20)	5580(30)	28(6)
H1C	2876(11)	-4360(20)	6310(30)	34(6)
H2A	3126(10)	-510(20)	4390(30)	27(6)
H2B	2982(12)	690(20)	3720(30)	36(6)
H2C	2917(13)	520(20)	5420(30)	37(7)
H1D	4111(10)	80(19)	5480(30)	18(5)

H1E	3929(10)	1470(20)	5040(30)	27(6)
H2	6376(11)	-774(18)	4670(30)	21(5)
H4A	4027(10)	-5009(17)	3290(30)	20(5)
H4B	4183(11)	-6030(20)	4500(30)	36(6)
H5	5212(11)	-1010(19)	4340(30)	29(6)
H7A	3899(9)	-3609(17)	5320(20)	15(5)
H7B	4054(9)	-4665(15)	6550(30)	14(5)
H8A	4161(11)	-390(20)	2740(30)	30(6)
H8B	4080(12)	1000(20)	2410(30)	42(6)
H9	4837(11)	-3214(17)	3260(30)	26(5)
H10	6271(12)	2480(20)	2720(30)	44(7)
H11	6914(12)	958(18)	3870(30)	34(6)
H12	2711(10)	-2127(19)	1900(30)	33(6)
H13	5091(11)	2260(19)	2390(30)	31(6)
H14	6498(12)	-5765(19)	5360(30)	37(7)
H15	5976(11)	-2680(20)	3220(30)	37(7)
H16	5356(12)	-6330(20)	5290(30)	34(6)
H17	6816(13)	-3950(19)	4270(30)	37(6)
H18	2751(11)	2960(20)	2500(30)	39(7)

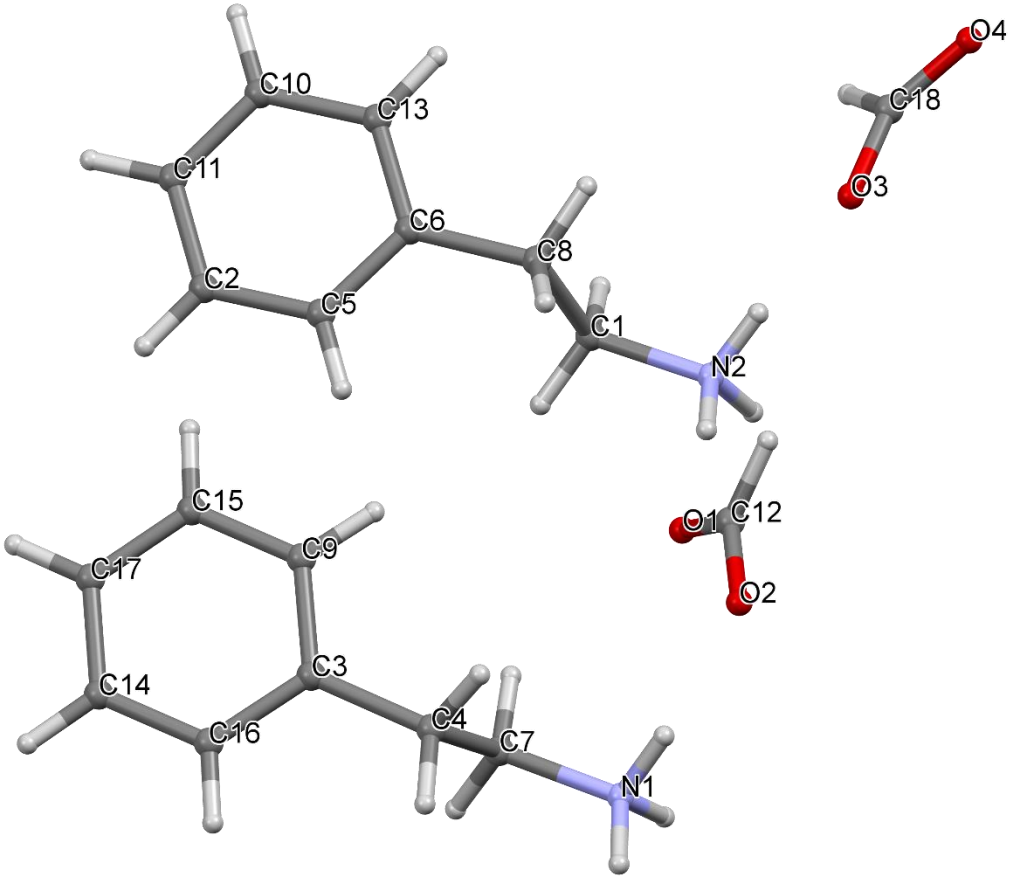

Figure II.3.13 Crystal Structure with atomic labels for compound **13**, Phenethylammonium Formate, ab50917

II.3.14 Compound 14, 2-Chlorophenethylammonium Formate, ab54716a

Table II.3.14.1 Crystal data and structure refinement for ab54716a.

Identification code	ab54716a
Empirical formula	$C_9H_{12}NO_2Cl$
Formula weight	201.65
Temperature/K	100.01
Crystal system	orthorhombic
Space group	Pbca
a/Å	19.6625(9)
b/Å	8.9907(4)
c/Å	22.8470(10)
α/°	90
β/°	90
γ/°	90
Volume/Å^3	4038.9(3)
Z	17
ρ_{calc}g/cm^3	1.409
μ/mm^{-1}	0.368
F(000)	1802.0
Crystal size/mm^3	0.289 × 0.158 × 0.135
Radiation	MoKα (λ = 0.71073)
2Θ range for data collection/°	3.566 to 48.804
Index ranges	$-22 \le h \le 22$, $-10 \le k \le 10$, $-26 \le l \le 26$
Reflections collected	55203
Independent reflections	3331 [R_{int} = 0.0452, R_{sigma} = 0.0155]
Data/restraints/parameters	3331/0/331
Goodness-of-fit on F^2	1.066
Final R indexes [I>=2σ (I)]	R_1 = 0.0286, wR_2 = 0.0764
Final R indexes [all data]	R_1 = 0.0337, wR_2 = 0.0810
Largest diff. peak/hole / e Å^{-3}	0.24/-0.22

Table II.3.14.2 Fractional Atomic Coordinates (×10^4) and Equivalent Isotropic Displacement Parameters (Å^2×10^3) for ab54716a. U_{eq} is defined as 1/3 of of the trace of the orthogonalised U_{IJ} tensor.

Atom	*x*	*y*	*z*	U(eq)
Cl1	276.4(2)	9806.6(4)	3738.9(2)	25.38(13)
N1	1922.3(6)	7311.8(16)	4798.5(6)	17.5(3)
C1	1192.6(8)	7169.6(17)	4635.3(7)	18.9(3)
C2	-233.9(8)	8743.2(16)	4206.3(6)	18.7(3)
C3	-1078.8(8)	7156.6(19)	4938.9(8)	26.7(4)
C4	768.2(8)	8411.4(18)	4904.0(7)	19.2(3)
C5	31.8(8)	8221.4(16)	4733.3(6)	18.5(3)
C6	-408.7(8)	7426.7(18)	5094.2(7)	22.9(4)

C7	-1321.1(8)	7666.2(19)	4409.1(8)	26.5(4)
C8	-901.4(8)	8474.7(18)	4041.4(7)	23.4(4)
Cl2	-461.8(2)	14555.4(4)	3717.7(2)	24.99(13)
N2	-1940.5(7)	11482.4(16)	2696.1(6)	18.3(3)
C9	-124.0(8)	12980.2(16)	2738.2(7)	19.4(3)
C10	362.3(8)	12289.2(18)	2388.1(7)	23.2(4)
C11	-1203.4(7)	11537.2(17)	2849.3(7)	18.0(3)
C12	1265.5(8)	12979.9(18)	3038.4(7)	25.0(4)
C13	114.7(8)	13680.2(16)	3244.2(6)	19.5(3)
C14	799.3(8)	13709.2(18)	3392.8(7)	22.2(3)
C15	1047.7(9)	12266.2(18)	2534.9(8)	25.8(4)
C16	-866.7(8)	12895.3(18)	2574.1(7)	21.9(3)
O1	2207.7(6)	6168.8(13)	3506.2(5)	24.6(3)
O2	2544.0(6)	4888.3(12)	4291.0(4)	24.5(3)
C17	2536.1(8)	5158.8(18)	3749.5(6)	21.0(4)
O3	2417.1(6)	9093.0(13)	1799.8(4)	25.6(3)
O4	2034.1(5)	7888.2(13)	1014.3(5)	24.1(3)
C18	2260.2(8)	9003.3(19)	1266.0(7)	21.6(4)

Table II.3.14.3 Anisotropic Displacement Parameters ($Å^2×10^3$) for ab54716a. The Anisotropic displacement factor exponent takes the form: $-2\pi^2[h^2a^{*2}U_{11}+2hka^*b^*U_{12}+\ldots]$.

Atom	U_{11}	U_{22}	U_{33}	U_{23}	U_{13}	U_{12}
Cl1	30.3(2)	25.0(2)	20.8(2)	3.82(15)	3.02(15)	-1.48(17)
N1	17.4(7)	18.0(7)	17.0(7)	0.5(6)	-0.8(5)	1.1(6)
C1	17.0(8)	17.5(8)	22.1(9)	-1.2(6)	-1.3(6)	0.6(6)
C2	21.5(8)	14.3(7)	20.3(8)	-1.0(6)	3.3(6)	2.6(6)
C3	22.4(9)	22.7(9)	35.1(10)	6.8(7)	5.8(7)	0.5(7)
C4	19.8(8)	18.6(8)	19.0(8)	-2.2(6)	-0.9(6)	1.4(7)
C5	20.8(8)	15.1(8)	19.7(8)	-2.5(6)	1.0(6)	3.9(6)
C6	22.8(8)	22.1(8)	23.8(9)	4.0(7)	0.2(7)	4.6(7)
C7	16.9(9)	23.3(9)	39.4(10)	-3.4(7)	-3.8(7)	2.3(7)
C8	26.6(9)	21.0(8)	22.6(8)	-1.7(7)	-4.4(7)	5.5(7)
Cl2	27.6(2)	25.9(2)	21.5(2)	1.98(15)	5.79(15)	3.60(16)
N2	20.1(7)	19.2(7)	15.5(7)	-0.2(6)	-0.7(5)	-1.9(6)
C9	20.9(8)	15.5(7)	21.7(8)	5.7(6)	0.8(6)	-2.5(6)
C10	26.9(9)	17.2(8)	25.6(9)	-0.2(7)	2.7(7)	-3.4(7)
C11	17.1(8)	18.1(8)	18.6(8)	0.1(6)	-0.5(6)	0.2(6)
C12	18.7(9)	23.6(9)	32.8(9)	6.3(7)	-1.5(7)	-1.7(7)
C13	23.5(8)	15.6(7)	19.3(8)	4.2(6)	4.5(6)	0.3(6)
C14	24.3(9)	19.4(8)	23.1(8)	2.8(7)	-2.1(7)	-4.3(7)
C15	24.2(9)	20.7(8)	32.6(10)	1.0(7)	7.9(7)	1.0(7)
C16	21.8(8)	22.2(8)	21.7(9)	3.8(7)	-1.1(7)	-2.0(7)
O1	27.7(6)	26.9(6)	19.4(6)	1.3(5)	-2.7(5)	1.0(5)
O2	29.5(6)	23.1(6)	20.8(6)	0.2(5)	-0.2(5)	6.5(5)

C17	20.8(8)	22.0(8)	20.1(9)	-3.6(7)	1.7(7)	-0.9(7)
O3	29.4(6)	25.5(6)	21.9(6)	-1.3(5)	-2.8(5)	-8.1(5)
O4	22.4(6)	30.8(7)	19.1(6)	-2.6(5)	0.9(4)	-3.5(5)
C18	18.7(8)	23.3(9)	22.7(9)	2.7(7)	3.2(6)	0.1(7)

Table II.3.14.4 Bond Lengths for ab54716a.

Atom	Atom	Length/Å	Atom	Atom	Length/Å
Cl1	C2	1.7496(15)	C9	C10	1.393(2)
N1	C1	1.4878(19)	C9	C13	1.397(2)
C1	C4	1.523(2)	C9	C16	1.510(2)
C2	C5	1.394(2)	C10	C15	1.389(2)
C2	C8	1.387(2)	C11	C16	1.525(2)
C3	C6	1.386(2)	C12	C14	1.388(2)
C3	C7	1.379(2)	C12	C15	1.385(2)
C4	C5	1.509(2)	C13	C14	1.389(2)
C5	C6	1.393(2)	O1	C17	1.245(2)
C7	C8	1.384(2)	O2	C17	1.2609(18)
Cl2	C13	1.7534(15)	O3	C18	1.2604(19)
N2	C11	1.4919(19)	O4	C18	1.238(2)

Table II.3.14.5 Bond Angles for ab54716a.

Atom	Atom	Atom	Angle/°	Atom	Atom	Atom	Angle/°
N1	C1	C4	111.36(12)	C10	C9	C16	119.92(14)
C5	C2	Cl1	119.74(12)	C13	C9	C16	123.59(14)
C8	C2	Cl1	118.17(12)	C15	C10	C9	122.29(16)
C8	C2	C5	122.07(14)	N2	C11	C16	110.58(13)
C7	C3	C6	119.66(16)	C15	C12	C14	119.95(15)
C5	C4	C1	109.78(12)	C9	C13	Cl2	119.69(12)
C2	C5	C4	123.01(14)	C14	C13	Cl2	117.87(12)
C6	C5	C2	116.80(14)	C14	C13	C9	122.44(14)
C6	C5	C4	120.10(14)	C12	C14	C13	119.26(15)
C3	C6	C5	121.97(16)	C12	C15	C10	119.57(16)
C3	C7	C8	120.09(15)	C9	C16	C11	110.98(13)
C7	C8	C2	119.40(15)	O1	C17	O2	125.81(15)
C10	C9	C13	116.44(14)	O4	C18	O3	126.08(15)

Table II.3.14.6 Hydrogen Atom Coordinates (Å×10^4) and Isotropic Displacement Parameters (Å^2×10^3) for ab54716a.

Atom	*x*	*y*	*z*	U(eq)
H1A	1976(9)	7280(20)	5180(9)	25(5)

H1B	2088(9)	8180(20)	4652(8)	31(5)
H1C	2172(9)	6470(20)	4638(8)	29(5)
H1D	1159(8)	7169(19)	4197(8)	24(4)
H1E	1017(9)	6210(20)	4786(7)	26(5)
H3	-1353(10)	6660(20)	5192(8)	33(5)
H4A	948(9)	9370(20)	4779(7)	23(4)
H4B	803(8)	8367(18)	5319(8)	21(4)
H6	-233(9)	7069(19)	5440(8)	22(4)
H7	-1760(10)	7460(20)	4293(8)	30(5)
H8	-1065(9)	8842(19)	3677(7)	22(4)
H2A	-2011(8)	11405(19)	2326(9)	20(4)
H2B	-2139(9)	12320(20)	2818(8)	26(5)
H2C	-2151(10)	10680(20)	2888(9)	36(5)
H10	207(9)	11850(20)	2029(8)	31(5)
H11A	-1183(8)	11576(18)	3278(7)	18(4)
H11B	-988(8)	10620(19)	2704(7)	18(4)
H12	1734(9)	12978(19)	3145(7)	24(4)
H14	958(9)	14260(20)	3741(7)	23(4)
H15	1358(9)	11800(20)	2290(8)	26(5)
H16A	-909(9)	12820(20)	2159(8)	29(5)
H16B	-1110(10)	13790(20)	2698(8)	33(5)
H17	2834(9)	4480(20)	3505(8)	32(5)
H18	2332(9)	9950(20)	1052(8)	28(5)

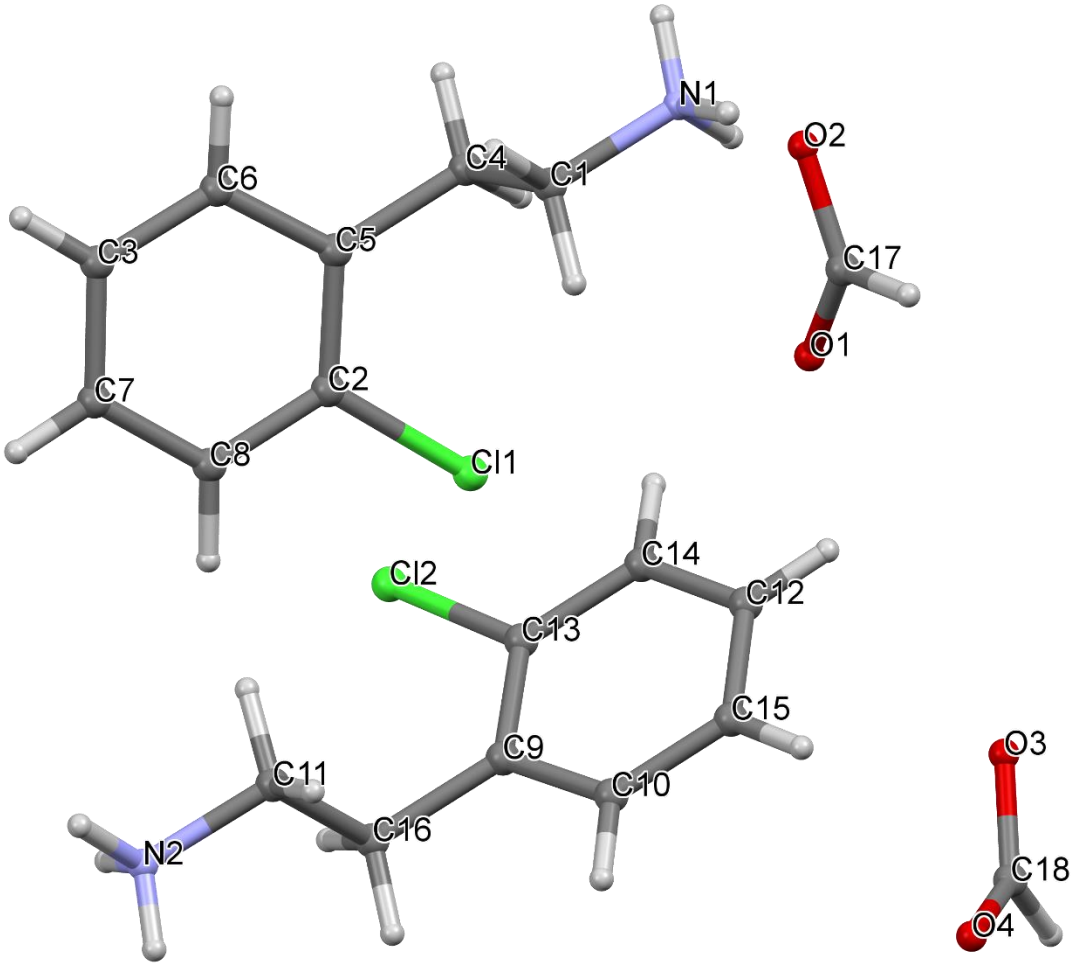

Figure II.3.14 Crystal Structure with atomic labels for compound **14**, 2-Chlorophenethylammonium Formate, ab54716a

II.3.15 Compound 15, 3-Fluorophenethylammonium Formate, ab52117

Table II.3.15.1 Crystal data and structure refinement for ab52117.

Identification code	ab52117
Empirical formula	$C_9H_{12}NO_2F_{0.08}$
Formula weight	167.78
Temperature/K	100.02
Crystal system	monoclinic
Space group	$P2_1/c$
a/Å	11.9482(4)
b/Å	19.4010(7)
c/Å	12.4181(5)
α/°	90
β/°	94.3991(19)
γ/°	90
Volume/Å^3	2870.12(18)
Z	12
ρ_{calc}g/cm^3	1.165
μ/mm^{-1}	0.084
F(000)	1077.0
Crystal size/mm^3	0.47 × 0.256 × 0.19
Radiation	MoKα (λ = 0.71073)
2Θ range for data collection/°	3.418 to 57.436
Index ranges	$-16 \leq h \leq 16$, $-26 \leq k \leq 26$, $-16 \leq l \leq 16$
Reflections collected	58730
Independent reflections	7423 [R_{int} = 0.0377, R_{sigma} = 0.0199]
Data/restraints/parameters	7423/0/496
Goodness-of-fit on F^2	1.032
Final R indexes [I>=2σ (I)]	R_1 = 0.0353, wR_2 = 0.0887
Final R indexes [all data]	R_1 = 0.0436, wR_2 = 0.0940
Largest diff. peak/hole / e Å^{-3}	0.28/-0.21

Table II.3.15.2 Fractional Atomic Coordinates (×10^4) and Equivalent Isotropic Displacement Parameters (Å^2×10^3) for ab52117. U_{eq} is defined as 1/3 of of the trace of the orthogonalised U_{IJ} tensor.

Atom	*x*	*y*	*z*	U(eq)
F1	-442.5(7)	-6471.5(4)	6444.9(9)	53.1(2)
N1	158.5(7)	-2945.0(4)	7216.8(7)	17.46(17)
C1	365.8(10)	-5974.3(6)	6492.3(11)	30.5(3)
C2	947.9(9)	-4840.2(5)	7040.3(8)	19.5(2)
C3	725.2(10)	-4153.8(5)	7551.0(8)	22.2(2)

C4	1964.4(9)	-4966.4(6)	6593.8(8)	21.7(2)
C5	292.2(8)	-3628.7(5)	6706.6(8)	17.37(19)
C6	134.8(9)	-5357.0(6)	6984.4(10)	25.7(2)
C7	1364.9(10)	-6111.8(6)	6055.6(10)	28.5(2)
C8	2173.1(9)	-5595.9(6)	6113.9(9)	25.0(2)
F2	2525.8(6)	1631.6(3)	8635.5(6)	31.39(16)
N2	3585.7(7)	-1762.8(4)	9543.6(7)	16.61(16)
C9	3478.6(9)	-797.0(5)	8215.6(8)	17.66(19)
C10	5078.1(9)	866.1(5)	7816.4(9)	21.5(2)
C11	2968.2(9)	463.2(5)	8381.8(8)	20.1(2)
C12	3280.1(9)	1149.1(5)	8365.1(9)	20.2(2)
C13	3740.0(8)	-39.3(5)	8116.5(8)	16.31(18)
C14	4791.1(8)	171.1(5)	7827.5(8)	19.5(2)
C15	4319.2(9)	1366.6(5)	8097.5(8)	20.1(2)
C16	3535.5(10)	-1001.4(5)	9405.2(8)	20.4(2)
F3	6015.4(6)	1670.1(4)	5090.5(7)	38.31(19)
N3	6759.8(7)	-1881.6(4)	5497.2(7)	16.72(16)
C17	8571.8(10)	854.6(6)	4383.5(9)	25.5(2)
C18	6817.0(9)	1182.6(5)	4981.4(9)	23.2(2)
C19	7463.2(8)	27.6(5)	5302.7(8)	18.57(19)
C20	7326.6(10)	-679.9(5)	5781.0(9)	23.0(2)
C21	7767.5(10)	1361.6(6)	4489.2(9)	24.8(2)
C22	8417.9(9)	193.0(6)	4779.9(9)	22.6(2)
C23	6742.5(8)	-1185.5(5)	4991.4(8)	16.61(18)
C24	6642.0(9)	530.9(5)	5390.3(9)	21.0(2)
O1	5721.1(6)	-3217.8(4)	2422.5(6)	23.06(16)
O2	5753.8(6)	-2864.4(4)	4138.0(6)	22.05(16)
C25	6161.0(8)	-2923.0(5)	3234.7(8)	17.67(19)
O3	2763.7(6)	-3048.2(4)	6528.3(6)	21.75(16)
O4	2307.0(6)	-2496.0(4)	8007.4(6)	20.19(15)
C26	2990.3(8)	-2695.4(5)	7352.1(8)	19.23(19)
O5	-917.2(6)	-2881.6(4)	10691.8(6)	23.40(16)
O6	-1152.8(7)	-3080.6(4)	8921.4(6)	27.36(18)
C27	-588.9(8)	-2904.2(5)	9754.7(9)	18.94(19)

Table II.3.15.3 Anisotropic Displacement Parameters ($Å^2×10^3$) for ab52117. The Anisotropic displacement factor exponent takes the form: $-2\pi^2[h^2a^{*2}U_{11}+2hka^*b^*U_{12}+\ldots]$.

Atom	U_{11}	U_{22}	U_{33}	U_{23}	U_{13}	U_{12}
F1	39.7(5)	28.6(4)	91.6(7)	-6.9(4)	8.4(4)	-16.4(3)

N1	15.6(4)	19.4(4)	17.6(4)	2.6(3)	2.6(3)	1.3(3)
C1	27.9(6)	20.1(5)	43.1(7)	2.5(5)	-0.6(5)	-7.6(4)
C2	23.3(5)	18.6(5)	16.3(4)	5.1(4)	-1.0(4)	0.5(4)
C3	29.6(5)	19.4(5)	17.5(5)	3.3(4)	0.7(4)	1.9(4)
C4	22.1(5)	22.7(5)	20.2(5)	3.9(4)	0.6(4)	-3.5(4)
C5	16.9(4)	18.9(5)	16.2(4)	1.2(4)	0.6(3)	-0.1(3)
C6	21.5(5)	23.1(5)	32.7(6)	4.9(4)	4.0(4)	-0.5(4)
C7	33.1(6)	20.9(5)	30.9(6)	-2.3(4)	-1.8(5)	2.7(4)
C8	24.6(5)	28.1(5)	22.2(5)	1.4(4)	1.7(4)	3.2(4)
F2	25.2(3)	17.6(3)	52.2(4)	-4.0(3)	8.6(3)	6.1(2)
N2	20.3(4)	13.7(4)	16.1(4)	0.0(3)	3.3(3)	-0.6(3)
C9	22.3(5)	14.3(4)	16.4(4)	-1.9(3)	1.9(4)	-0.3(4)
C10	18.9(5)	21.0(5)	25.1(5)	2.6(4)	4.2(4)	-1.3(4)
C11	17.6(4)	17.9(5)	25.0(5)	-0.6(4)	3.7(4)	0.2(4)
C12	19.9(5)	16.1(4)	24.8(5)	-0.8(4)	1.7(4)	4.6(4)
C13	19.6(4)	15.2(4)	14.0(4)	0.1(3)	0.7(3)	0.5(3)
C14	19.4(5)	18.7(5)	20.7(5)	0.2(4)	4.0(4)	3.0(4)
C15	22.6(5)	15.3(4)	22.0(5)	2.1(4)	-0.8(4)	-0.9(4)
C16	32.0(6)	12.9(4)	16.7(5)	-1.3(3)	3.8(4)	0.0(4)
F3	28.9(4)	20.8(3)	64.4(5)	-1.9(3)	-1.4(3)	7.9(3)
N3	17.2(4)	15.8(4)	17.4(4)	-1.1(3)	3.1(3)	-1.7(3)
C17	26.2(5)	28.7(6)	22.0(5)	-3.4(4)	4.7(4)	-7.1(4)
C18	22.3(5)	16.8(5)	29.6(5)	-2.0(4)	-3.6(4)	2.9(4)
C19	22.7(5)	15.6(4)	16.8(4)	-2.6(3)	-2.6(4)	-1.5(4)
C20	32.7(6)	15.6(5)	19.7(5)	-0.8(4)	-5.0(4)	-1.5(4)
C21	30.4(6)	19.2(5)	23.9(5)	3.5(4)	-3.5(4)	-5.7(4)
C22	21.6(5)	21.2(5)	24.8(5)	-6.0(4)	1.4(4)	1.4(4)
C23	17.1(4)	15.7(4)	17.0(4)	0.1(3)	0.7(3)	-0.5(3)
C24	20.0(5)	19.5(5)	23.5(5)	-2.0(4)	2.6(4)	-1.5(4)
O1	25.1(4)	25.5(4)	19.3(4)	-2.6(3)	5.7(3)	-3.3(3)
O2	23.7(4)	23.1(4)	19.8(4)	-3.5(3)	4.2(3)	-4.5(3)
C25	15.6(4)	15.4(4)	22.2(5)	3.2(4)	3.0(4)	1.3(3)
O3	23.1(4)	22.1(4)	20.7(4)	-4.0(3)	5.8(3)	-1.3(3)
O4	17.7(3)	21.7(4)	21.6(4)	-4.5(3)	3.7(3)	0.3(3)
C26	16.6(4)	17.4(4)	24.0(5)	-1.5(4)	2.9(4)	0.2(3)
O5	22.5(4)	25.8(4)	22.1(4)	-5.9(3)	3.4(3)	-5.0(3)
O6	23.6(4)	38.5(5)	20.6(4)	-3.1(3)	6.0(3)	-6.6(3)
C27	16.3(4)	14.9(4)	26.0(5)	1.4(4)	3.8(4)	0.4(3)

Table II.3.15.4 Bond Lengths for ab52117.

Atom	Atom	Length/Å	Atom	Atom	Length/Å
F1	C1	1.3630(13)	C12	C15	1.3759(14)
N1	C5	1.4839(13)	C13	C14	1.3934(14)
C1	C6	1.3819(17)	F3	C18	1.3602(12)
C1	C7	1.3746(17)	N3	C23	1.4889(12)
C2	C3	1.5073(14)	C17	C21	1.3882(16)
C2	C4	1.3949(15)	C17	C22	1.3920(16)
C2	C6	1.3942(15)	C18	C21	1.3750(16)
C3	C5	1.5237(14)	C18	C24	1.3842(15)
C4	C8	1.3899(16)	C19	C20	1.5095(14)
C7	C8	1.3888(16)	C19	C22	1.3925(15)
F2	C12	1.3594(11)	C19	C24	1.3944(14)
N2	C16	1.4880(12)	C20	C23	1.5184(14)
C9	C13	1.5099(13)	O1	C25	1.2407(13)
C9	C16	1.5260(14)	O2	C25	1.2616(12)
C10	C14	1.3916(14)	O3	C26	1.2433(13)
C10	C15	1.3912(14)	O4	C26	1.2572(12)
C11	C12	1.3825(14)	O5	C27	1.2569(13)
C11	C13	1.3985(14)	O6	C27	1.2389(13)

Table II.3.15.5 Bond Angles for ab52117.

Atom	Atom	Atom	Angle/°	Atom	Atom	Atom	Angle/°
F1	C1	C6	117.87(11)	C14	C13	C11	118.69(9)
F1	C1	C7	118.66(11)	C10	C14	C13	120.93(9)
C7	C1	C6	123.47(10)	C12	C15	C10	117.65(9)
C4	C2	C3	120.63(9)	N2	C16	C9	111.60(8)
C6	C2	C3	120.77(10)	C21	C17	C22	120.58(10)
C6	C2	C4	118.59(10)	F3	C18	C21	118.73(10)
C2	C3	C5	111.27(8)	F3	C18	C24	118.11(10)
C8	C4	C2	121.00(10)	C21	C18	C24	123.15(10)
N1	C5	C3	110.24(8)	C22	C19	C20	120.68(9)
C1	C6	C2	118.90(10)	C22	C19	C24	118.78(9)
C1	C7	C8	117.46(11)	C24	C19	C20	120.54(10)
C7	C8	C4	120.57(10)	C19	C20	C23	113.06(8)
C13	C9	C16	109.74(8)	C18	C21	C17	117.67(10)
C15	C10	C14	120.53(9)	C17	C22	C19	120.83(10)
C12	C11	C13	118.95(9)	N3	C23	C20	108.83(8)
F2	C12	C11	118.34(9)	C18	C24	C19	118.95(10)
F2	C12	C15	118.43(9)	O1	C25	O2	126.59(9)
C15	C12	C11	123.23(9)	O3	C26	O4	126.22(9)

C11	C13	C9	121.01(9)	O6	C27	O5	126.49(10)
C14	C13	C9	120.15(9)				

Table II.3.15.6 Hydrogen Atom Coordinates (Å×10^4) and Isotropic Displacement Parameters (Å^2×10^3) for ab52117.

Atom	*x*	*y*	*z*	U(eq)
H1A	-312(12)	-2975(7)	7787(12)	28(3)
H1B	-140(11)	-2641(7)	6707(11)	27(3)
H1C	826(13)	-2788(7)	7477(11)	29(4)
H3A	1423(12)	-3967(7)	7920(11)	32(4)
H3B	185(12)	-4207(7)	8087(12)	34(4)
H4	2521(11)	-4599(7)	6638(10)	24(3)
H5A	811(10)	-3575(6)	6155(10)	18(3)
H5B	-415(11)	-3759(7)	6372(10)	22(3)
H6	-586(12)	-5279(7)	7291(11)	27(3)
H7	1486(12)	-6544(7)	5737(12)	31(4)
H8	2934(11)	-5679(6)	5800(10)	20(3)
H2A	4293(12)	-1911(7)	9395(11)	25(3)
H2B	3423(12)	-1881(7)	10243(12)	30(4)
H2C	3084(12)	-1993(7)	9046(11)	26(3)
H9A	4016(11)	-1067(7)	7863(11)	24(3)
H9B	2739(11)	-897(7)	7880(11)	26(3)
H10	5824(11)	1002(7)	7634(10)	23(3)
H11	2223(12)	335(7)	8575(11)	28(3)
H14	5333(11)	-182(7)	7652(11)	26(3)
H15	4511(11)	1845(7)	8130(11)	26(3)
H16A	4207(12)	-806(7)	9804(11)	30(4)
H16B	2890(12)	-835(7)	9758(11)	30(4)
H3C	7467(12)	-2002(7)	5618(11)	24(3)
H3D	6438(12)	-1873(7)	6147(12)	31(4)
H3E	6423(12)	-2210(8)	5044(12)	33(4)
H17	9281(11)	974(6)	4025(10)	20(3)
H20A	8061(13)	-871(8)	6006(12)	38(4)
H20B	6922(12)	-648(7)	6433(12)	33(4)
H21	7859(12)	1824(8)	4217(12)	35(4)
H22	8984(12)	-169(7)	4707(11)	30(4)
H23A	7136(10)	-1216(7)	4324(10)	21(3)
H23B	5962(12)	-1055(7)	4806(11)	27(3)
H24	5958(12)	426(7)	5727(11)	32(4)
H25	6908(11)	-2700(7)	3167(10)	25(3)

H26	3791(12)	-2546(7)	7534(11)	34(4)
H27	192(12)	-2757(7)	9674(11)	29(3)

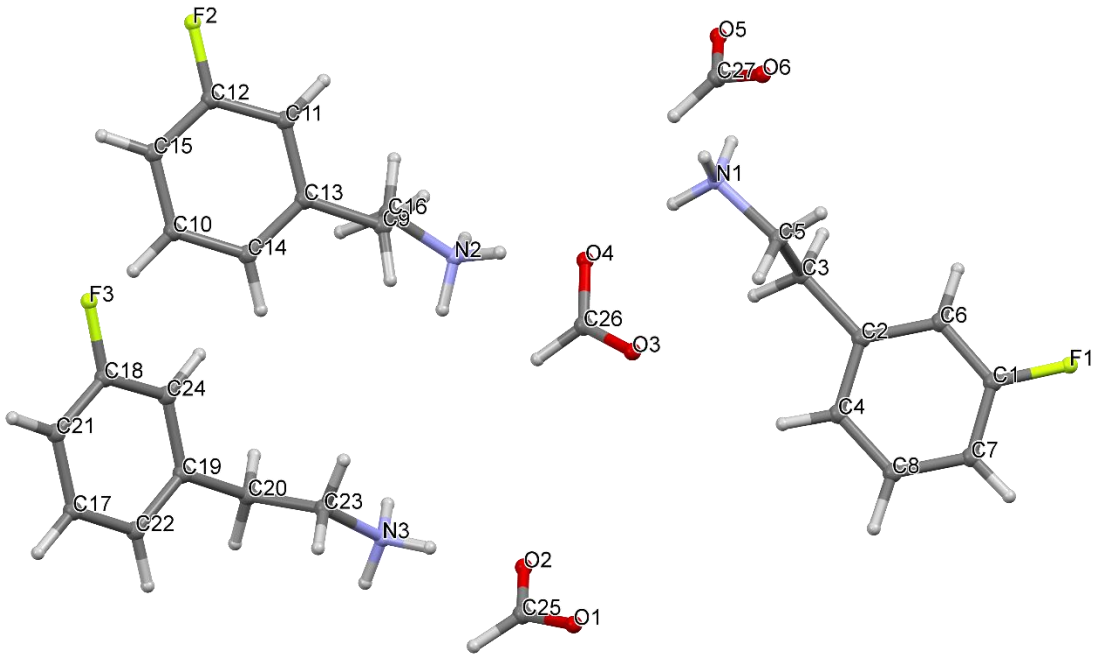

Figure II.3.15 Crystal Structure with atomic labels for compound **15**, 3-Fluorophenethylammonium Formate, ab52117

II.3.16 Compound 16, 3-Chlorophenethylammonium Formate, ab57915

Table II.3.16.1 Crystal data and structure refinement for ab57915.

Identification code	ab57915
Empirical formula	$C_9H_{12}NO_2Cl$
Formula weight	201.65
Temperature/K	273.15
Crystal system	monoclinic
Space group	$P2_1/c$
a/Å	6.050(4)
b/Å	20.067(13)
c/Å	9.015(7)
α/°	90
β/°	109.43(4)
γ/°	90
Volume/Å^3	1032.2(12)
Z	4
ρ_{calc}g/cm^3	1.298
μ/mm^{-1}	0.339
F(000)	424.0
Crystal size/mm^3	0.5 × 0.3 × 0.13
Radiation	MoKα (λ = 0.71073)
2Θ range for data collection/°	4.06 to 53.1
Index ranges	$-7 \le h \le 7$, $-25 \le k \le 23$, $-11 \le l \le 11$
Reflections collected	12563
Independent reflections	2107 [R_{int} = 0.0513, R_{sigma} = 0.0358]
Data/restraints/parameters	2107/0/166
Goodness-of-fit on F^2	1.058
Final R indexes [I>=2σ (I)]	R_1 = 0.0453, wR_2 = 0.1146
Final R indexes [all data]	R_1 = 0.0715, wR_2 = 0.1312
Largest diff. peak/hole / e Å^{-3}	0.16/-0.23

Table II.3.16.2 Fractional Atomic Coordinates (×10^4) and Equivalent Isotropic Displacement Parameters (Å^2×10^3) for ab57915. U_{eq} is defined as 1/3 of of the trace of the orthogonalised U_{IJ} tensor.

Atom	*x*	*y*	*z*	U(eq)
Cl1	3782.9(12)	6366.9(3)	335.4(8)	76.0(3)
N1	5480(3)	3141.2(9)	3844(2)	49.3(5)
C2	3051(4)	5176.0(11)	1526(3)	52.4(6)
C3	2001(3)	4749.6(10)	2324(2)	47.7(5)
C4	883(4)	6117.9(12)	1984(3)	57.3(6)
C5	409(4)	5025.9(12)	2953(3)	56.4(6)
C6	2477(4)	5847.0(11)	1369(2)	50.6(5)
C7	4956(4)	3871.2(11)	3666(3)	57.3(6)

C8	2573(4)	4009.5(11)	2484(3)	53.6(6)
C9	-138(4)	5700.0(13)	2786(3)	63.4(7)
O1	3593(3)	2551.6(8)	5994.5(18)	61.5(5)
O2	195(3)	2991.4(9)	4565(2)	72.5(5)
C1	1478(4)	2676.2(11)	5695(3)	53.3(6)

Table II.3.16.3 Anisotropic Displacement Parameters ($Å^2×10^3$) for ab57915. The Anisotropic displacement factor exponent takes the form: $-2\pi^2[h^2a^{*2}U_{11}+2hka^*b^*U_{12}+\ldots]$.

Atom	U_{11}	U_{22}	U_{33}	U_{23}	U_{13}	U_{12}
Cl1	92.7(6)	57.9(4)	90.7(6)	17.5(3)	48.2(4)	2.1(3)
N1	44.0(10)	48.5(10)	55.5(12)	5.4(9)	16.7(9)	1.8(8)
C2	52.4(12)	50.0(13)	58.4(14)	3.3(10)	23.4(11)	5.8(9)
C3	42.9(11)	48.7(12)	48.6(12)	1.1(9)	11.4(9)	0.4(8)
C4	65.8(15)	48.3(13)	58.4(14)	0.6(11)	21.5(12)	9.5(11)
C5	57.1(13)	59.4(15)	57.9(14)	2.8(11)	26.0(11)	-5.4(11)
C6	54.6(12)	49.0(12)	48.9(12)	4.6(9)	18.2(10)	1.7(9)
C7	53.0(13)	46.7(13)	65.4(16)	2.7(11)	10.5(12)	-2.1(10)
C8	47.9(12)	46.8(13)	62.2(15)	5.0(10)	13.1(11)	-2.2(9)
C9	59.9(15)	69.0(17)	68.1(16)	-4.6(12)	30.2(12)	7.8(11)
O1	51.1(9)	69.2(10)	68.1(11)	12.8(8)	24.9(8)	9.4(7)
O2	51.4(9)	80.6(12)	87.2(13)	26.5(10)	25.4(9)	10.6(8)
C1	56.9(14)	45.4(13)	65.9(15)	2.3(11)	31.6(12)	3.8(10)

Table II.3.16.4 Bond Lengths for ab57915.

Atom	Atom	Length/Å	Atom	Atom	Length/Å
Cl1	C6	1.753(2)	C4	C6	1.374(3)
N1	C7	1.496(3)	C4	C9	1.380(3)
C2	C3	1.399(3)	C5	C9	1.389(4)
C2	C6	1.386(3)	C7	C8	1.507(3)
C3	C5	1.386(3)	O1	C1	1.242(3)
C3	C8	1.521(3)	O2	C1	1.231(3)

Table II.3.16.5 Bond Angles for ab57915.

Atom	Atom	Atom	Angle/°	Atom	Atom	Atom	Angle/°
C6	C2	C3	120.3(2)	C4	C6	Cl1	118.68(18)
C2	C3	C8	121.2(2)	C4	C6	C2	122.0(2)
C5	C3	C2	117.5(2)	N1	C7	C8	112.03(19)
C5	C3	C8	121.3(2)	C7	C8	C3	112.40(18)
C6	C4	C9	117.8(2)	C4	C9	C5	121.1(2)
C3	C5	C9	121.2(2)	O2	C1	O1	127.1(2)

C2	C6	Cl1	119.35(17)

Table II.3.16.6 Hydrogen Atom Coordinates (Å×10^4) and Isotropic Displacement Parameters (Å^2×10^3) for ab57915.

Atom	*x*	*y*	*z*	U(eq)
H1A	4800(40)	2950(11)	4500(30)	58(7)
H1B	4770(50)	2874(14)	2780(40)	93(9)
H1C	7210(50)	3062(13)	4260(30)	87(8)
H2	4220(40)	4994(11)	1100(30)	60(6)
H4	550(40)	6594(12)	1880(20)	64(7)
H5	-280(40)	4732(10)	3500(20)	46(5)
H7A	6120(50)	4066(13)	3350(30)	79(8)
H7B	5180(50)	4083(14)	4750(30)	95(9)
H8A	1480(40)	3736(13)	2810(30)	78(8)
H8B	2360(40)	3811(13)	1370(30)	80(8)
H9	-1270(50)	5865(14)	3220(30)	96(9)
H1	830(40)	2479(12)	6510(30)	74(7)

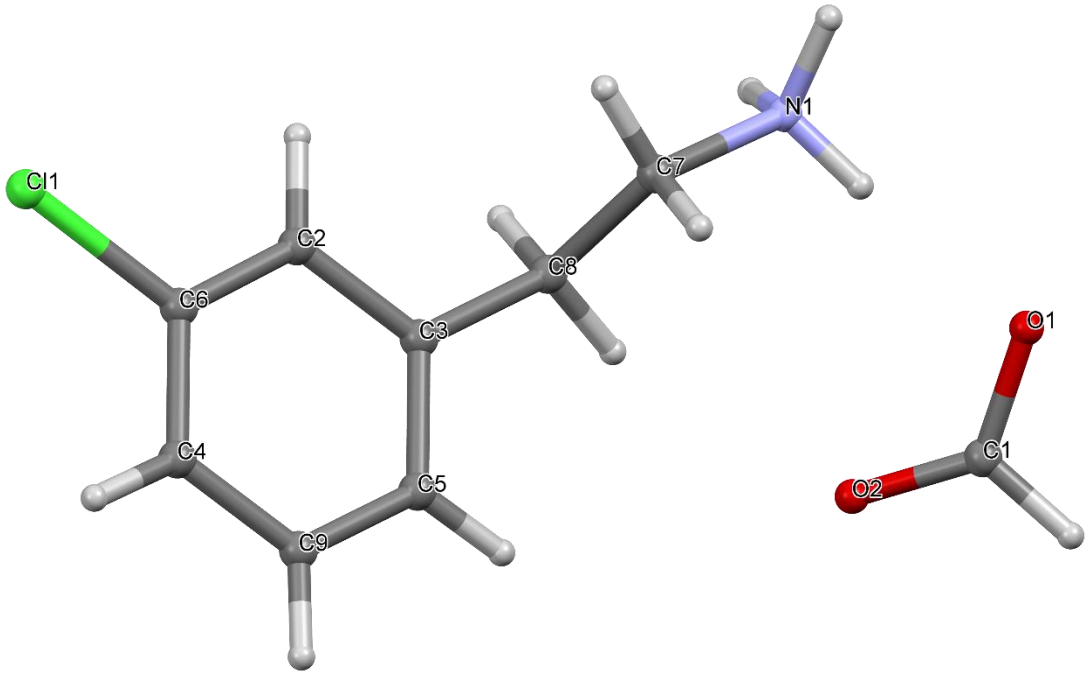

Figure II.3.16 Crystal Structure with atomic labels for compound **16**, 3-Chlorophenethylammonium Formate, ab57915

II.3.17 Compound 17, 4-Chlorophenethylammonium Formate, ab53416

Table II.3.17.1 Crystal data and structure refinement for ab53416.

Identification code	ab53416
Empirical formula	$C_{18}H_{24}Cl_2N_2O_4$
Formula weight	403.29
Temperature/K	100.0
Crystal system	monoclinic
Space group	$P2_1/c$
a/Å	12.170(3)
b/Å	7.5094(17)
c/Å	21.382(5)
α/°	90
β/°	97.655(12)
γ/°	90
Volume/Å^3	1936.7(8)
Z	4
ρ_{calc}g/cm^3	1.383
μ/mm^{-1}	0.361
F(000)	848.0
Crystal size/mm^3	0.36 × 0.34 × 0.116
Radiation	MoKα (λ = 0.71073)
2Θ range for data collection/°	3.376 to 58.63
Index ranges	$-16 \le h \le 16$, $-10 \le k \le 10$, $-27 \le l \le 29$
Reflections collected	35013
Independent reflections	5231 [R_{int} = 0.0449, R_{sigma} = 0.0283]
Data/restraints/parameters	5231/0/331
Goodness-of-fit on F^2	1.078
Final R indexes [I>=2σ (I)]	R_1 = 0.0389, wR_2 = 0.1102
Final R indexes [all data]	R_1 = 0.0490, wR_2 = 0.1219
Largest diff. peak/hole / e Å^{-3}	0.49/-0.32

Table II.3.17.2 Fractional Atomic Coordinates (×10^4) and Equivalent Isotropic Displacement Parameters (Å^2×10^3) for ab53416. U_{eq} is defined as 1/3 of of the trace of the orthogonalised U_{IJ} tensor.

Atom	*x*	*y*	*z*	U(eq)
Cl1	2931.2(3)	3252.4(5)	3632.8(2)	24.44(11)
N1	-1133.4(10)	1190.9(15)	314.8(6)	15.3(2)
C1	1971.6(11)	3164.4(17)	2947.5(7)	17.3(3)
C2	1476.4(11)	3882.6(17)	1850.8(7)	17.0(3)
C3	-361.7(11)	2976.8(17)	1247.3(7)	16.2(3)
C4	2241.4(11)	3955.3(17)	2398.5(7)	17.4(3)
C5	454.0(11)	3031.9(16)	1848.0(6)	15.1(3)
C6	209.3(11)	2249.4(17)	2406.8(7)	17.1(3)

C7	957.6(11)	2315.4(17)	2961.3(7)	17.1(3)
C8	-457.9(11)	1125.7(17)	953.7(7)	16.4(3)
Cl2	2259.2(3)	8758.8(6)	1338.1(2)	28.13(12)
N2	6241.7(10)	8788.9(15)	4718.6(6)	16.1(2)
C9	3502.8(12)	8214.1(18)	3155.9(7)	18.2(3)
C10	3168.8(11)	8361.3(17)	2026.0(6)	16.6(3)
C11	4582.7(11)	7596.0(17)	3128.4(6)	15.8(3)
C12	4238.1(11)	7784.2(17)	1981.9(6)	15.9(3)
C13	4935.9(11)	7389.6(17)	2537.2(7)	15.8(3)
C14	2794.2(11)	8594.5(18)	2607.7(7)	18.4(3)
C15	5346.9(12)	7252.4(18)	3736.6(7)	17.2(3)
C16	5669.2(12)	9028.5(17)	4062.6(7)	17.1(3)
O1	6787.2(8)	2218.5(13)	5199.6(5)	18.4(2)
O2	5193.8(8)	3042.9(14)	4619.5(5)	20.6(2)
C17	6143.5(11)	3337.5(17)	4890.9(7)	16.9(3)
O3	-1693.9(8)	-2234.1(13)	-147.4(5)	18.4(2)
O4	-122.3(8)	-3113.2(14)	442.6(5)	20.9(2)
C18	-1095.6(12)	-3336.8(17)	191.8(7)	17.6(3)

Table II.3.17.3 Anisotropic Displacement Parameters ($Å^2×10^3$) for ab53416. The Anisotropic displacement factor exponent takes the form: $-2\pi^2[h^2a^{*2}U_{11}+2hka^*b^*U_{12}+\ldots]$.

Atom	U_{11}	U_{22}	U_{33}	U_{23}	U_{13}	U_{12}
Cl1	22.50(19)	29.5(2)	18.85(19)	-0.90(13)	-6.35(14)	-0.18(13)
N1	15.1(5)	13.9(5)	16.0(6)	-0.7(4)	-1.8(4)	-0.1(4)
C1	16.6(6)	16.6(6)	17.3(6)	-2.2(5)	-3.3(5)	2.3(5)
C2	17.9(6)	16.2(6)	16.4(6)	0.9(5)	0.8(5)	-0.2(5)
C3	16.8(6)	14.6(5)	16.0(6)	0.0(5)	-1.7(5)	1.4(4)
C4	14.3(6)	17.3(6)	20.3(7)	-1.3(5)	0.9(5)	-1.1(4)
C5	14.9(6)	12.9(5)	16.9(6)	-1.7(4)	-0.5(5)	1.5(4)
C6	16.1(6)	15.2(6)	19.3(7)	-0.7(5)	-0.4(5)	-0.8(4)
C7	19.4(6)	15.7(6)	15.9(6)	0.4(5)	1.8(5)	1.1(5)
C8	17.5(6)	13.7(6)	16.4(6)	0.4(5)	-3.2(5)	1.1(4)
Cl2	22.34(19)	38.5(2)	20.8(2)	2.17(14)	-7.27(14)	3.79(14)
N2	15.7(6)	14.2(5)	17.0(6)	-1.0(4)	-2.6(4)	-0.3(4)
C9	17.5(6)	19.7(6)	17.5(7)	-1.8(5)	2.1(5)	0.0(5)
C10	16.4(6)	15.2(6)	16.6(6)	1.0(5)	-3.5(5)	-0.9(4)
C11	16.3(6)	13.2(5)	17.2(6)	0.6(5)	-0.9(5)	-0.8(4)
C12	17.5(6)	14.7(5)	15.1(6)	-1.2(5)	1.0(5)	-1.5(4)
C13	14.3(6)	13.9(5)	18.5(6)	-1.6(5)	-0.6(5)	0.2(4)
C14	14.1(6)	19.3(6)	21.1(7)	-2.0(5)	0.6(5)	1.1(5)
C15	19.8(6)	15.1(6)	15.6(6)	-0.8(5)	-2.2(5)	1.8(5)
C16	18.4(6)	14.6(6)	17.2(6)	1.4(5)	-2.0(5)	0.7(5)
O1	18.0(5)	16.3(4)	19.7(5)	0.6(4)	-1.7(4)	-1.1(3)
O2	16.4(5)	23.8(5)	20.5(5)	-0.1(4)	-1.4(4)	-1.8(4)

C17	17.3(6)	15.4(6)	17.8(6)	-1.0(5)	1.8(5)	-1.1(5)
O3	19.1(5)	15.1(4)	19.8(5)	1.5(4)	-1.8(4)	-1.0(3)
O4	17.8(5)	22.0(5)	21.7(5)	2.7(4)	-1.9(4)	-2.1(4)
C18	17.7(6)	15.7(6)	19.3(7)	1.2(5)	1.9(5)	-1.8(5)

Table II.3.17.4 Bond Lengths for ab53416.

Atom	Atom	Length/Å	Atom	Atom	Length/Å
Cl1	C1	1.7492(14)	C9	C11	1.4024(19)
N1	C8	1.4985(17)	C9	C14	1.3893(19)
C1	C4	1.393(2)	C10	C12	1.3866(19)
C1	C7	1.3928(19)	C10	C14	1.392(2)
C2	C4	1.3969(19)	C11	C13	1.397(2)
C2	C5	1.3980(19)	C11	C15	1.5168(18)
C3	C5	1.5157(18)	C12	C13	1.3966(18)
C3	C8	1.5232(18)	C15	C16	1.5316(18)
C5	C6	1.3987(19)	O1	C17	1.2719(16)
C6	C7	1.3963(18)	O2	C17	1.2421(16)
Cl2	C10	1.7447(14)	O3	C18	1.2654(16)
N2	C16	1.4917(17)	O4	C18	1.2448(17)

Table II.3.17.5 Bond Angles for ab53416.

Atom	Atom	Atom	Angle/°	Atom	Atom	Atom	Angle/°
C4	C1	Cl1	118.92(11)	C12	C10	Cl2	119.47(11)
C7	C1	Cl1	119.62(11)	C12	C10	C14	121.48(12)
C7	C1	C4	121.46(12)	C14	C10	Cl2	119.03(11)
C4	C2	C5	120.99(13)	C9	C11	C15	119.42(12)
C5	C3	C8	112.32(10)	C13	C11	C9	118.54(12)
C1	C4	C2	118.96(13)	C13	C11	C15	121.98(12)
C2	C5	C3	119.88(12)	C10	C12	C13	118.58(13)
C2	C5	C6	118.62(12)	C12	C13	C11	121.35(12)
C6	C5	C3	121.50(12)	C9	C14	C10	119.20(13)
C7	C6	C5	121.43(12)	C11	C15	C16	109.43(11)
C1	C7	C6	118.54(13)	N2	C16	C15	112.47(11)
N1	C8	C3	110.40(10)	O2	C17	O1	126.52(13)
C14	C9	C11	120.83(13)	O4	C18	O3	126.91(13)

Table II.3.17.6 Hydrogen Atom Coordinates (Å×10^4) and Isotropic Displacement Parameters (Å^2×10^3) for ab53416.

Atom	*x*	*y*	*z*	U(eq)
H1A	-1296(15)	120(30)	153(9)	26(5)

H1B	-1802(18)	1720(30)	311(10)	35(6)
H1C	-783(15)	1810(30)	40(9)	22(4)
H2	1646(15)	4510(30)	1478(9)	27(5)
H3A	-1099(15)	3380(20)	1335(9)	22(4)
H3B	-126(15)	3850(20)	948(9)	23(5)
H4	2942(16)	4560(30)	2387(9)	29(5)
H6	-513(16)	1640(30)	2430(9)	26(5)
H7	779(15)	1810(30)	3356(9)	27(5)
H8A	246(14)	680(20)	903(8)	16(4)
H8B	-840(15)	300(30)	1222(8)	24(4)
H2A	6866(17)	8180(30)	4755(9)	30(5)
H2B	6391(15)	9830(30)	4894(9)	24(5)
H2C	5809(16)	8210(30)	4968(10)	31(5)
H9	3252(15)	8350(20)	3550(9)	24(5)
H12	4479(14)	7760(20)	1583(8)	18(4)
H13	5682(15)	6920(20)	2510(8)	20(4)
H14	2027(15)	8980(20)	2646(9)	23(5)
H15A	4978(14)	6500(20)	4015(8)	18(4)
H15B	6009(15)	6620(20)	3668(8)	21(4)
H16A	5018(14)	9770(20)	4090(8)	17(4)
H16B	6150(14)	9660(20)	3832(8)	16(4)
H17	6442(15)	4550(30)	4872(8)	24(5)
H18	-1455(16)	-4490(30)	266(9)	34(5)

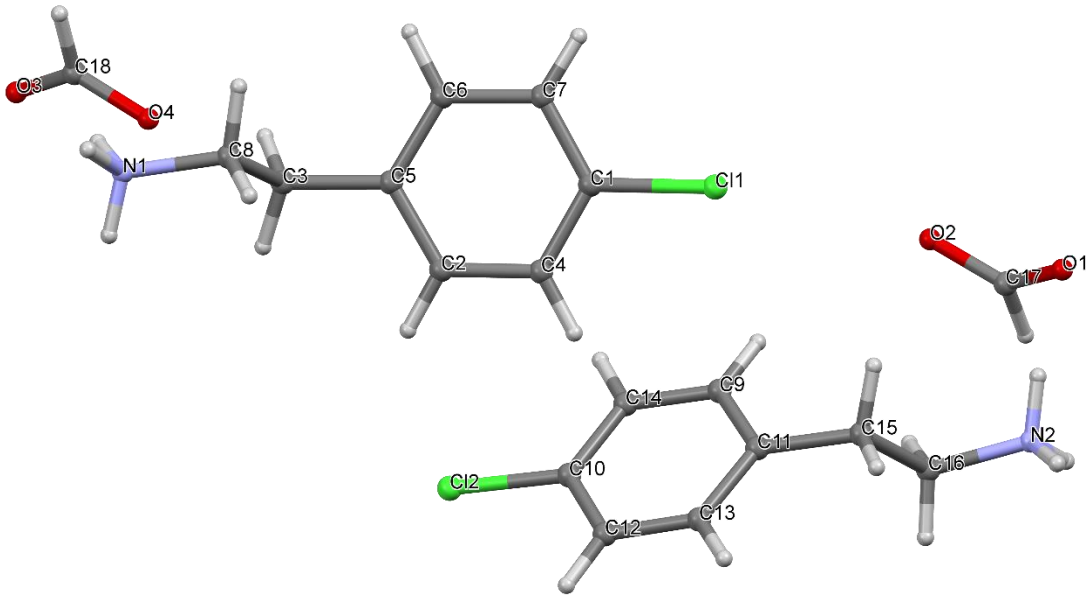

Figure II.3.17 Crystal Structure with atomic labels for compound **17**, 4-

Chlorophenethylammonium Formate, ab53416

II.3.18 Compound 18, 4-Bromophenethylammonium Formate, ab58416

Table II.3.18.1 Crystal data and structure refinement for ab58416.

Identification code	ab58416
Empirical formula	$C_{18}H_{24}Br_2N_2O_4$
Formula weight	492.21
Temperature/K	100.0
Crystal system	monoclinic
Space group	$P2_1/c$
a/Å	12.2325(4)
b/Å	7.5028(3)
c/Å	21.5675(8)
α/°	90
β/°	97.175(2)
γ/°	90
Volume/Å^3	1963.92(13)
Z	4
ρ_{calc}g/cm^3	1.665
μ/mm^{-1}	4.153
F(000)	992.0
Crystal size/mm^3	0.365 × 0.209 × 0.042
Radiation	MoKα (λ = 0.71073)
2Θ range for data collection/°	3.356 to 54.024
Index ranges	$-15 \le h \le 15$, $-9 \le k \le 9$, $-27 \le l \le 27$
Reflections collected	33968
Independent reflections	4310 [R_{int} = 0.0665, R_{sigma} = 0.0363]
Data/restraints/parameters	4310/0/237
Goodness-of-fit on F^2	1.056
Final R indexes [I>=2σ (I)]	R_1 = 0.0853, wR_2 = 0.2091
Final R indexes [all data]	R_1 = 0.0937, wR_2 = 0.2160
Largest diff. peak/hole / e Å^{-3}	8.39/-1.11

Table II.3.18.2 Fractional Atomic Coordinates (×10^4) and Equivalent Isotropic Displacement Parameters (Å^2×10^3) for ab58416. U_{eq} is defined as 1/3 of of the trace of the orthogonalised U_{IJ} tensor.

Atom	*x*	*y*	*z*	U(eq)
Br1	7019.3(5)	8212.9(9)	1355.9(3)	18.5(2)
N1	11164(4)	6193(6)	4680(2)	12.3(10)
C1	10413(5)	7951(8)	3743(3)	13.2(11)
C2	8572(5)	8806(8)	3166(3)	14.9(12)
C3	9599(5)	7980(8)	3160(3)	13.2(11)
C4	9849(5)	7251(8)	2603(3)	13.9(11)
C5	7806(5)	8887(8)	2633(3)	14.2(11)
C6	8071(5)	8126(8)	2084(3)	13.9(11)

C7	9091(5)	7301(8)	2050(3)	12.8(11)
C8	10491(5)	6110(7)	4050(3)	12.5(11)
Br2	2172.3(5)	8585.4(10)	1349.9(3)	22.9(2)
N2	6269(4)	8802(6)	4716(2)	11.5(9)
C9	3565(5)	8194(8)	3192(3)	16.3(12)
C10	5407(5)	7235(8)	3745(3)	12.0(11)
C11	3198(5)	8268(8)	2082(3)	14.3(11)
C12	4637(5)	7564(8)	3154(3)	12.8(11)
C13	4256(5)	7699(8)	2017(3)	13.6(11)
C14	4975(5)	7352(8)	2575(3)	13.9(11)
C15	2843(5)	8534(8)	2658(3)	15.4(12)
C16	5715(5)	9033(8)	4066(3)	12.1(11)
O1	5171(3)	13023(6)	4622(2)	16.2(9)
O2	6751(3)	12226(6)	5191(2)	14.6(8)
C17	6115(5)	13317(8)	4887(3)	13.5(11)
O3	1666(3)	2233(6)	147.6(19)	13.9(8)
O4	106(4)	3100(6)	-425(2)	17.3(9)
C18	1076(5)	3325(8)	-176(3)	14.2(11)

Table II.3.18.3 Anisotropic Displacement Parameters ($Å^2×10^3$) for ab58416. The Anisotropic displacement factor exponent takes the form: $-2\pi^2[h^2a^{*2}U_{11}+2hka^*b^*U_{12}+\ldots]$.

Atom	U_{11}	U_{22}	U_{33}	U_{23}	U_{13}	U_{12}
Br1	16.5(3)	23.9(4)	14.0(3)	0.7(2)	-2.7(2)	0.1(2)
N1	13(2)	9(2)	13(2)	1.0(18)	-2.2(18)	-0.9(18)
C1	16(3)	14(3)	8(2)	1(2)	-6(2)	-3(2)
C2	16(3)	17(3)	13(3)	-1(2)	4(2)	-1(2)
C3	9(3)	16(3)	14(3)	2(2)	-2(2)	-4(2)
C4	11(3)	15(3)	15(3)	2(2)	0(2)	1(2)
C5	13(3)	15(3)	15(3)	1(2)	2(2)	-1(2)
C6	15(3)	14(3)	13(3)	6(2)	0(2)	-1(2)
C7	14(3)	9(2)	15(3)	-3(2)	0(2)	-1(2)
C8	20(3)	9(2)	7(3)	0(2)	-4(2)	-2(2)
Br2	18.2(3)	33.4(4)	15.3(4)	2.1(2)	-4.8(2)	3.5(2)
N2	11(2)	11(2)	12(2)	-0.6(18)	-2.0(18)	0.8(18)
C9	17(3)	19(3)	14(3)	-1(2)	4(2)	1(2)
C10	13(3)	13(3)	8(2)	-1(2)	-4(2)	2(2)
C11	13(3)	15(3)	14(3)	4(2)	-1(2)	-1(2)
C12	9(3)	13(3)	16(3)	-4(2)	-2(2)	-1(2)
C13	18(3)	11(3)	12(3)	0(2)	2(2)	0(2)
C14	13(3)	13(3)	16(3)	0(2)	0(2)	-1(2)
C15	10(3)	18(3)	18(3)	-1(2)	2(2)	0(2)
C16	17(3)	11(3)	8(3)	0(2)	-1(2)	4(2)
O1	14(2)	19(2)	16(2)	-0.3(17)	0.1(16)	-0.3(17)
O2	15(2)	11.9(19)	16(2)	0.0(16)	0.0(16)	-1.0(16)

C17	13(3)	11(3)	17(3)	-1(2)	4(2)	-2(2)
O3	16(2)	11.8(19)	13(2)	0.1(16)	-1.7(16)	-1.6(16)
O4	16(2)	16(2)	20(2)	0.6(17)	0.2(17)	-2.2(16)
C18	14(3)	10(3)	19(3)	-2(2)	3(2)	-2(2)

Table II.3.18.4 Bond Lengths for ab58416.

Atom	Atom	Length/Å	Atom	Atom	Length/Å
Br1	C6	1.903(6)	C9	C12	1.405(8)
N1	C8	1.498(7)	C9	C15	1.386(9)
C1	C3	1.503(8)	C10	C12	1.507(8)
C1	C8	1.530(8)	C10	C16	1.541(8)
C2	C3	1.402(8)	C11	C13	1.386(8)
C2	C5	1.390(8)	C11	C15	1.380(9)
C3	C4	1.388(8)	C12	C14	1.375(8)
C4	C7	1.416(8)	C13	C14	1.422(8)
C5	C6	1.388(9)	O1	C17	1.242(7)
C6	C7	1.403(8)	O2	C17	1.256(7)
Br2	C11	1.906(6)	O3	C18	1.246(7)
N2	C16	1.488(7)	O4	C18	1.251(7)

Table II.3.18.5 Bond Angles for ab58416.

Atom	Atom	Atom	Angle/°	Atom	Atom	Atom	Angle/°
C3	C1	C8	112.0(5)	C12	C10	C16	109.2(5)
C5	C2	C3	121.6(5)	C13	C11	Br2	118.7(5)
C2	C3	C1	120.0(5)	C15	C11	Br2	118.6(4)
C4	C3	C1	121.6(5)	C15	C11	C13	122.6(6)
C4	C3	C2	118.4(5)	C9	C12	C10	119.7(5)
C3	C4	C7	121.7(5)	C14	C12	C9	118.7(5)
C6	C5	C2	118.8(6)	C14	C12	C10	121.6(5)
C5	C6	Br1	119.0(4)	C11	C13	C14	117.2(5)
C5	C6	C7	122.0(6)	C12	C14	C13	121.6(5)
C7	C6	Br1	119.1(5)	C11	C15	C9	118.8(5)
C6	C7	C4	117.4(5)	N2	C16	C10	112.2(4)
N1	C8	C1	110.7(4)	O1	C17	O2	127.1(6)
C15	C9	C12	121.1(6)	O3	C18	O4	127.1(6)

Table II.3.18.6 Hydrogen Atom Coordinates (Å×10^4) and Isotropic Displacement Parameters (Å^2×10^3) for ab58416.

Atom	*x*	*y*	*z*	U(eq)
H1A	11785	6841	4653	15

H1B	11353	5069	4811	15
H1C	10763	6718	4957	15
H1D	10189	8836	4043	16
H1E	11148	8299	3637	16
H2	8395	9322	3543	18
H4	10547	6705	2592	17
H5	7114	9453	2644	17
H7	9267	6796	1671	15
H8A	9742	5673	4096	15
H8B	10833	5261	3781	15
H2A	6872	8095	4711	14
H2B	5793	8283	4954	14
H2C	6479	9885	4879	14
H9	3332	8389	3591	20
H10A	6080	6626	3645	14
H10B	5044	6459	4030	14
H13	4490	7546	1617	16
H14	5706	6965	2545	17
H15	2116	8943	2687	18
H16A	6210	9694	3819	15
H16B	5038	9753	4075	15
H17	6386	14496	4855	16
H18	1398	4451	-241	17

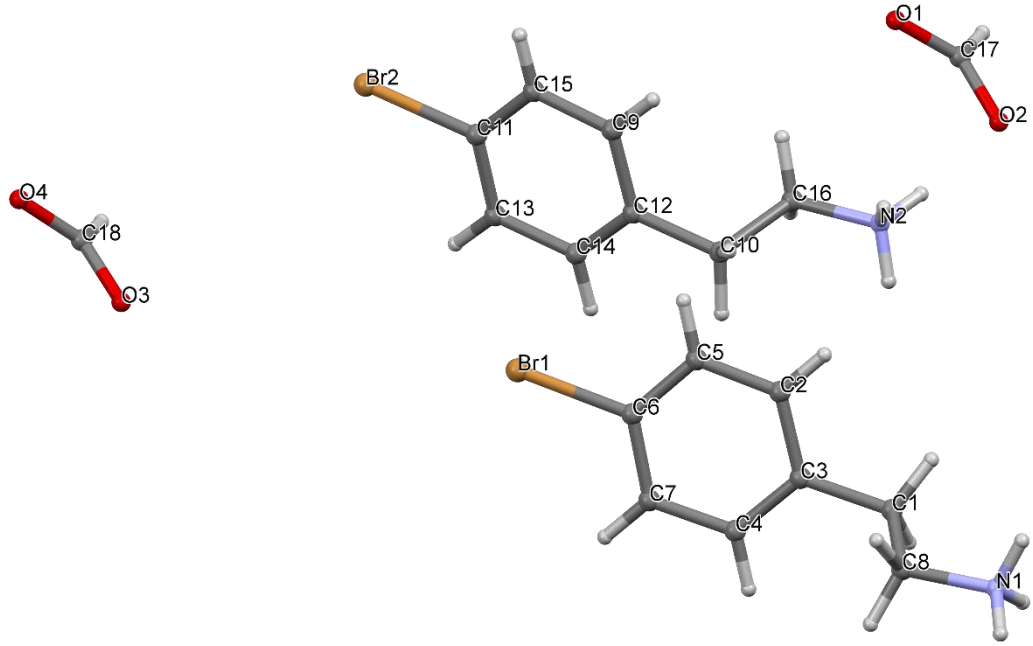

Figure II.3.18 Crystal Structure with atomic labels for compound **18**, 4-Bromophenethylammonium Formate, ab58416

II.3.19 Compound 19, 2,4-Dichlorophenethylammonium Formate, ab53516

Table II.3.19.1 Crystal data and structure refinement for ab53516.

Identification code	ab53516
Empirical formula	$C_9H_{11}Cl_2NO_2$
Formula weight	236.09
Temperature/K	100.01
Crystal system	triclinic
Space group	P-1
a/Å	4.6609(10)
b/Å	6.9345(14)
c/Å	16.340(3)
α/°	83.253(13)
β/°	89.558(12)
γ/°	79.517(12)
Volume/Å^3	515.67(18)
Z	2
ρ_{calc}g/cm^3	1.520
μ/mm^{-1}	0.602
F(000)	244.0
Crystal size/mm^3	0.502 × 0.232 × 0.094
Radiation	MoKα (λ = 0.71073)
2Θ range for data collection/°	2.51 to 68.504
Index ranges	$-7 \leq h \leq 6$, $-10 \leq k \leq 10$, $-24 \leq l \leq 25$
Reflections collected	10538
Independent reflections	3632 [R_{int} = 0.0569, R_{sigma} = 0.0622]
Data/restraints/parameters	3632/0/171
Goodness-of-fit on F^2	1.157
Final R indexes [I>=2σ (I)]	R_1 = 0.0861, wR_2 = 0.2477
Final R indexes [all data]	R_1 = 0.1164, wR_2 = 0.3122
Largest diff. peak/hole / e Å^{-3}	0.85/-1.22

Table II.3.19.2 Fractional Atomic Coordinates (×10^4) and Equivalent Isotropic Displacement Parameters (Å^2×10^3) for ab53516. U_{eq} is defined as 1/3 of of the trace of the orthogonalised U_{IJ} tensor.

Atom	*x*	*y*	*z*	U(eq)
Cl1	6633.1(15)	7263.4(13)	218.0(4)	30.1(3)
Cl2	14793.8(15)	3598.2(10)	2434.2(5)	27.7(3)
N1	15798(5)	7424(3)	4453.2(14)	18.9(4)
C1	13722(5)	7295(4)	3786.9(16)	18.7(5)
C2	15079(5)	7681(4)	2943.4(17)	19.4(5)
C3	10700(6)	5671(4)	1378.3(17)	23.2(6)
C4	13016(5)	7572(4)	2257.7(16)	19.6(5)
C5	11289(6)	9279(4)	1861.6(18)	21.9(5)

C6	9042(6)	7409(5)	1003.4(17)	22.9(6)
C7	9312(6)	9212(5)	1236.3(18)	24.7(6)
C8	12676(6)	5789(4)	1995.3(17)	20.4(5)
O1	17444(5)	11125(3)	4214.4(13)	25.0(5)
O2	19380(5)	13791(3)	4313.5(14)	27.7(5)
C9	19302(6)	12203(4)	4051.1(17)	22.2(5)

Table II.3.19.3 Anisotropic Displacement Parameters ($Å^2×10^3$) for ab53516. The Anisotropic displacement factor exponent takes the form: $-2\pi^2[h^2a^{*2}U_{11}+2hka^*b^*U_{12}+\ldots]$.

Atom	U_{11}	U_{22}	U_{33}	U_{23}	U_{13}	U_{12}
Cl1	22.8(4)	41.8(5)	25.5(4)	-5.6(3)	-1.5(3)	-4.3(3)
Cl2	26.5(4)	17.5(4)	36.6(5)	0.8(3)	-1.1(3)	-0.1(2)
N1	15.7(9)	17.9(10)	21.5(10)	-0.3(7)	1.6(7)	-0.2(7)
C1	14.2(9)	17.5(11)	22.8(11)	-0.3(8)	1.9(8)	0.0(8)
C2	15.7(10)	18.9(11)	23.7(12)	-0.9(9)	2.4(8)	-4.2(8)
C3	20.5(11)	23.6(13)	25.5(13)	-3.1(10)	5.2(10)	-4.2(9)
C4	13.9(10)	21.4(12)	22.7(12)	1.0(9)	3.7(8)	-3.7(8)
C5	22.0(11)	17.2(11)	26.3(12)	-2.7(9)	1.2(9)	-2.9(9)
C6	16.1(10)	28.6(14)	22.2(12)	-0.4(10)	3.4(9)	-1.3(9)
C7	20.3(11)	24.9(13)	26.0(13)	1.9(10)	0.4(9)	0.6(9)
C8	17.5(10)	19.5(11)	22.7(12)	0.1(9)	2.3(9)	-1.5(8)
O1	25.1(9)	19.3(10)	29.7(10)	0.5(7)	1.8(8)	-3.6(7)
O2	23.9(9)	16.4(9)	41.5(12)	-4.8(8)	-1.8(9)	0.8(7)
C9	19.9(11)	19.4(12)	25.4(12)	-2.5(9)	5.6(9)	1.4(8)

Table II.3.19.4 Bond Lengths for ab53516.

Atom	Atom	Length/Å	Atom	Atom	Length/Å
Cl1	C6	1.735(3)	C4	C5	1.396(4)
Cl2	C8	1.734(3)	C4	C8	1.391(4)
N1	C1	1.483(4)	C5	C7	1.391(4)
C1	C2	1.527(4)	C6	C7	1.376(5)
C2	C4	1.499(4)	O1	C9	1.251(4)
C3	C6	1.386(4)	O2	C9	1.234(4)
C3	C8	1.390(4)			

Table II.3.19.5 Bond Angles for ab53516.

Atom	Atom	Atom	Angle/°	Atom	Atom	Atom	Angle/°
N1	C1	C2	110.5(2)	C7	C6	Cl1	120.5(2)
C4	C2	C1	111.6(2)	C7	C6	C3	121.2(3)
C6	C3	C8	118.4(3)	C6	C7	C5	119.1(3)

C5	C4	C2	120.9(3)	C3	C8	Cl2	117.4(2)
C8	C4	C2	122.3(2)	C3	C8	C4	122.6(2)
C8	C4	C5	116.7(3)	C4	C8	Cl2	120.0(2)
C7	C5	C4	122.0(3)	O2	C9	O1	126.8(2)
C3	C6	Cl1	118.3(3)				

Table II.3.19.6 Hydrogen Atom Coordinates (Å×10^4) and Isotropic Displacement Parameters (Å^2×10^3) for ab53516.

Atom	***x***	***y***	***z***	**U(eq)**
H1C	16770(80)	8570(60)	4330(20)	14(8)
H1D	15080(100)	7600(70)	4990(30)	29(10)
H1E	16990(80)	6370(60)	4530(20)	17(8)
H1A	13200(70)	6030(50)	3876(19)	11(7)
H1B	11790(110)	8240(80)	3890(30)	41(12)
H2A	16920(110)	6740(80)	2940(30)	42(13)
H2B	15660(100)	8950(70)	2920(20)	30(10)
H3	10380(120)	4310(90)	1160(30)	46(13)
H5	11400(140)	10400(90)	2090(30)	55(15)
H7	8410(120)	10410(90)	1070(30)	52(15)
H9	21070(90)	11660(60)	3730(20)	23(9)

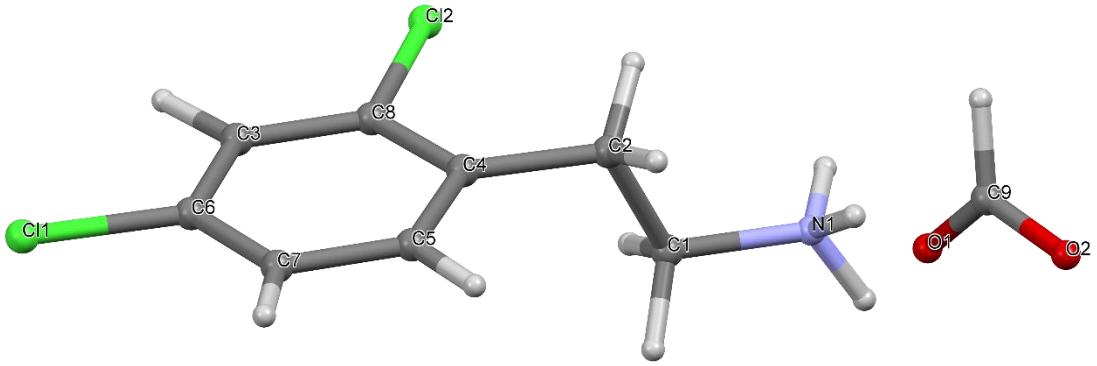

Figure II.3.19 Crystal Structure with atomic labels for compound **19**, 2,4-

Dichlorophenethylammonium Formate, ab53516

II.3.20 Compound 20, Di-N-Octylammonium Formate, ab22115

Table II.3.20.1 Crystal data and structure refinement for ab22115.

Identification code	ab22115
Empirical formula	$C_{18}H_{36}NO_4$
Formula weight	330.48
Temperature/K	100.01
Crystal system	triclinic
Space group	P-1
a/Å	4.6682(5)
b/Å	13.5815(17)
c/Å	15.760(2)
α/°	79.200(6)
β/°	89.837(6)
γ/°	83.126(6)
Volume/Å^3	974.3(2)
Z	2
ρ_{calc}g/cm^3	1.127
μ/mm^{-1}	0.078
F(000)	366.0
Crystal size/mm^3	0.64 × 0.094 × 0.067
Radiation	MoKα (λ = 0.71073)
2Θ range for data collection/°	2.632 to 52.788
Index ranges	$-4 \le h \le 5$, $-16 \le k \le 16$, $-19 \le l \le 19$
Reflections collected	10969
Independent reflections	3886 [R_{int} = 0.0543, R_{sigma} = 0.0934]
Data/restraints/parameters	3886/0/210
Goodness-of-fit on F^2	1.188
Final R indexes [I>=2σ (I)]	R_1 = 0.1272, wR_2 = 0.3463
Final R indexes [all data]	R_1 = 0.2120, wR_2 = 0.3983
Largest diff. peak/hole / e Å^{-3}	0.78/-0.94

Table II.3.20.2 Fractional Atomic Coordinates (×10^4) and Equivalent Isotropic Displacement Parameters (Å^2×10^3) for ab22115. U_{eq} is defined as 1/3 of of the trace of the orthogonalised U_{IJ} tensor.

Atom	*x*	*y*	*z*	U(eq)
C1	3172(9)	8840(3)	1611(3)	19.5(10)
C2	7217(10)	2217(3)	3145(3)	21.7(11)
C3	5685(9)	1284(3)	3379(3)	20.6(11)
C4	6194(9)	6002(3)	2311(3)	20.9(11)
C5	5365(9)	7897(3)	1863(3)	18.6(10)
C6	4548(10)	9796(3)	1325(3)	20.8(11)
C7	7712(10)	307(3)	3665(3)	21.0(11)

C8	6181(10)	-633(3)	3929(3)	21.0(11)
C9	2373(10)	10731(3)	1054(3)	20.2(11)
C10	6824(10)	4116(3)	2692(3)	24.2(11)
C11	3961(9)	6921(3)	2106(3)	20.0(11)
C12	5204(9)	3193(3)	2883(3)	21.7(11)
C13	8261(11)	-1593(3)	4216(3)	25.5(12)
C14	3741(11)	11690(3)	735(3)	26.1(12)
C15	6724(11)	-2532(3)	4482(3)	29.7(12)
C16	1519(12)	12619(4)	438(3)	33.0(13)
N1	4744(8)	5062(2)	2500(2)	17.1(9)
C17	3220(20)	5115(7)	4483(7)	87(3)
O1	6049(14)	4829(5)	4487(4)	96(2)
O2	1515(7)	5271(3)	3906(2)	28.3(9)
C18	3110(20)	5096(6)	529(7)	85(3)
O3	5994(14)	4864(5)	570(4)	110(2)
O4	1565(7)	5101(3)	1064(2)	27.3(10)

Table II.3.20.3 Anisotropic Displacement Parameters ($Å^2×10^3$) for ab22115. The Anisotropic displacement factor exponent takes the form: $-2\pi^2[h^2a^{*2}U_{11}+2hka^*b^*U_{12}+\ldots]$.

Atom	U_{11}	U_{22}	U_{33}	U_{23}	U_{13}	U_{12}
C1	20(2)	17(2)	21(2)	-0.7(19)	0.8(19)	-2.1(19)
C2	20(2)	17(2)	27(3)	-1.8(19)	-1.4(19)	-0.9(19)
C3	20(2)	19(2)	20(2)	0.1(19)	-1.0(19)	-1(2)
C4	15(2)	16(2)	30(3)	0.9(19)	-3.4(19)	-6.2(19)
C5	17(2)	14(2)	22(2)	1.1(19)	0.1(18)	-0.5(19)
C6	24(2)	16(2)	21(2)	-1.6(19)	-1.8(19)	0(2)
C7	24(3)	19(2)	19(2)	-2.5(19)	-2.6(19)	-2(2)
C8	25(3)	17(2)	21(2)	-1.9(19)	0.5(19)	-6(2)
C9	23(3)	16(2)	21(2)	-1.6(19)	0.6(19)	0(2)
C10	17(2)	16(2)	37(3)	-1(2)	-2(2)	3(2)
C11	19(2)	13(2)	27(3)	-1.4(19)	-2.3(19)	-3.1(19)
C12	18(2)	17(2)	29(3)	-1(2)	1.0(19)	-2(2)
C13	32(3)	17(2)	26(3)	-1(2)	-5(2)	1(2)
C14	36(3)	19(3)	23(3)	-2(2)	-1(2)	-6(2)
C15	40(3)	16(3)	32(3)	-3(2)	1(2)	-2(2)
C16	43(3)	18(3)	38(3)	-2(2)	1(2)	-6(2)
N1	14.7(19)	13(2)	23(2)	0.0(15)	-1.6(15)	-2.0(15)
C17	77(7)	92(7)	104(8)	-35(6)	38(6)	-38(5)
O1	86(4)	129(6)	82(4)	-33(4)	19(3)	-30(4)
O2	21.0(19)	46(2)	17.0(18)	-2.9(15)	-8.2(14)	-4.1(16)
C18	90(7)	70(6)	93(8)	-7(5)	-52(6)	-21(5)
O3	81(5)	150(6)	98(5)	-7(4)	-9(4)	-30(4)
O4	16.8(18)	44(2)	21.0(19)	-6.0(16)	9.6(15)	-5.3(16)

Table II.3.20.4 Bond Lengths for ab22115.

Atom	Atom	Length/Å	Atom	Atom	Length/Å
C1	C5	1.530(6)	C10	C12	1.522(6)
C1	C6	1.510(6)	C10	N1	1.497(5)
C2	C3	1.514(6)	C13	C15	1.528(7)
C2	C12	1.520(6)	C14	C16	1.534(6)
C3	C7	1.528(6)	C17	$O1^{1}$	1.678(12)
C4	C11	1.512(6)	C17	O1	1.331(10)
C4	N1	1.498(5)	C17	O2	1.181(10)
C5	C11	1.534(6)	O1	$C17^{1}$	1.678(12)
C6	C9	1.522(6)	C18	$O3^{2}$	1.773(13)
C7	C8	1.527(6)	C18	O3	1.346(11)
C8	C13	1.525(6)	C18	O4	1.108(12)
C9	C14	1.520(6)	O3	$C18^{2}$	1.773(13)

Table II.3.20.5 Bond Angles for ab22115.

Atom	Atom	Atom	Angle/°	Atom	Atom	Atom	Angle/°
C6	C1	C5	113.4(4)	C8	C13	C15	113.0(4)
C3	C2	C12	114.2(4)	C9	C14	C16	113.2(4)
C2	C3	C7	114.0(4)	C10	N1	C4	113.3(3)
N1	C4	C11	110.1(3)	O1	C17	$O1^{1}$	81.8(7)
C1	C5	C11	113.3(4)	O2	C17	$O1^{1}$	148.1(8)
C1	C6	C9	113.6(4)	O2	C17	O1	129.8(8)
C8	C7	C3	114.3(4)	C17	O1	$C17^{1}$	98.2(7)
C13	C8	C7	113.1(4)	O3	C18	$O3^{2}$	77.3(8)
C14	C9	C6	113.9(4)	O4	C18	O3	128.9(8)
N1	C10	C12	110.4(3)	O4	C18	$O3^{2}$	153.4(8)
C4	C11	C5	111.7(3)	C18	O3	$C18^{2}$	102.7(8)
C2	C12	C10	112.4(3)				

Table II.3.20.6 Hydrogen Atom Coordinates (Å×10^{4}) and Isotropic Displacement Parameters (Å^{2}×10^{3}) for ab22115.

Atom	*x*	*y*	*z*	U(eq)
H1A	1911	8743	1137	23
H1B	1940	8918	2112	23
H2A	8528	2132	2662	26
H2B	8418	2273	3646	26
H3A	4527	1216	2872	25
H3B	4334	1376	3851	25
H4A	7485	5977	1814	25

H4B	7383	6049	2818	25
H5A	6556	7977	2358	22
H5B	6665	7839	1373	22
H6A	5819	9711	833	25
H6B	5771	9901	1805	25
H7A	9022	205	3185	25
H7B	8916	384	4159	25
H8A	4866	-534	4408	25
H8B	4992	-717	3434	25
H9A	1104	10615	589	24
H9B	1147	10829	1552	24
H10A	8062	4134	3197	29
H10B	8084	4071	2191	29
H11A	2735	6960	2615	24
H11B	2705	6851	1621	24
H12A	3836	3269	3354	26
H12B	4069	3156	2363	26
H13A	9453	-1508	4710	31
H13B	9573	-1693	3737	31
H14A	5013	11587	248	31
H14B	4958	11821	1206	31
H15A	5574	-2630	3992	45
H15B	5455	-2445	4965	45
H15C	8159	-3124	4659	45
H16A	198	12474	7	50
H16B	2519	13194	181	50
H16C	420	12780	935	50
H1C	3576	5090	2960	21
H1D	3612	5036	2037	21

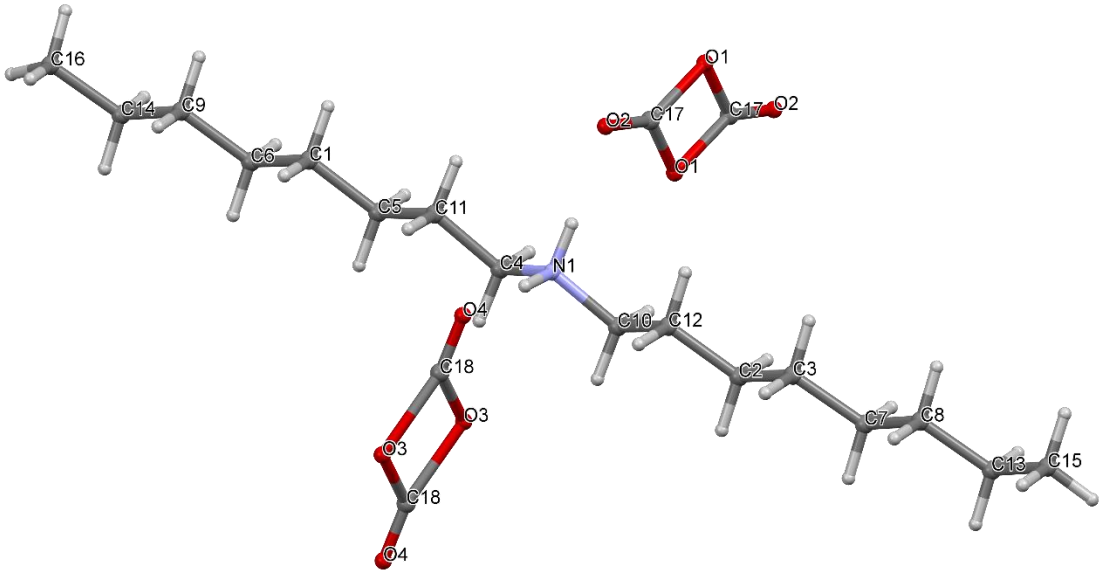

Figure II.3.20 Crystal Structure with atomic labels for compound **20**, Di-N-Octylammonium Formate, ab22115

II.3.21 Compound 21, Dicyclohexylammonium Formate, ab53316

Table II.3.21.1 Crystal data and structure refinement for ab53316.

Identification code	ab53316
Empirical formula	$C_{13}H_{25}NO_2$
Formula weight	227.34
Temperature/K	105.51
Crystal system	monoclinic
Space group	C2/c
a/Å	19.203(4)
b/Å	8.1231(18)
c/Å	16.922(4)
α/°	90
β/°	94.395(11)
γ/°	90
Volume/Å^3	2631.9(10)
Z	8
ρ_{calc}g/cm^3	1.147
μ/mm^{-1}	0.076
F(000)	1008.0
Crystal size/mm^3	0.744 × 0.212 × 0.125
Radiation	MoKα (λ = 0.71073)
2Θ range for data collection/°	4.254 to 57.954
Index ranges	-25 ≤ h ≤ 25, -11 ≤ k ≤ 10, -22 ≤ l ≤ 22
Reflections collected	21391
Independent reflections	3366 [R_{int} = 0.0429, R_{sigma} = 0.0313]
Data/restraints/parameters	3366/0/245
Goodness-of-fit on F^2	1.070
Final R indexes [I>=2σ (I)]	R_1 = 0.0637, wR_2 = 0.1890
Final R indexes [all data]	R_1 = 0.0730, wR_2 = 0.2123
Largest diff. peak/hole / e Å^{-3}	0.49/-0.41

Table II.3.21.2 Fractional Atomic Coordinates (×10^4) and Equivalent Isotropic Displacement Parameters (Å^2×10^3) for ab53316. U_{eq} is defined as 1/3 of of the trace of the orthogonalised U_{IJ} tensor.

Atom	*x*	*y*	*z*	U(eq)
O1	3140.3(6)	10262.4(13)	744.0(6)	27.5(3)
O2	2452.5(6)	8607.0(13)	1399.4(6)	29.8(3)
C1	2854.0(7)	9791.9(16)	1340.5(8)	22.3(3)
N1	2259.4(5)	5545.5(12)	778.5(6)	15.4(3)
C2	2935.4(6)	4653.4(14)	967.9(7)	16.1(3)
C3	4404.4(6)	4659.0(16)	1609.1(8)	21.8(3)
C4	3495.2(6)	5534.5(16)	531.9(8)	19.2(3)
C5	1639.5(6)	5010.4(15)	1197.2(7)	16.1(3)

C6	4210.0(7)	4742.4(17)	715.4(8)	22.1(3)
C7	3129.6(6)	4596.9(16)	1861.3(8)	20.0(3)
C8	1489.6(6)	3184.0(16)	1071.0(8)	21.7(3)
C9	1017.2(6)	6067.6(16)	895.3(8)	20.4(3)
C10	207.7(7)	3738.8(18)	1161.4(10)	30.0(4)
C11	360.9(7)	5562.5(18)	1288.1(9)	26.2(3)
C12	3840.7(6)	3772.7(17)	2029.0(8)	23.3(3)
C13	831.8(7)	2692.1(18)	1463.1(10)	29.6(4)

Table II.3.21.3 Anisotropic Displacement Parameters ($Å^2×10^3$) for ab53316. The Anisotropic displacement factor exponent takes the form: $-2\pi^2[h^2a^{*2}U_{11}+2hka^*b^*U_{12}+\ldots]$.

Atom	U_{11}	U_{22}	U_{33}	U_{23}	U_{13}	U_{12}
O1	34.7(6)	30.3(6)	18.2(5)	-0.2(4)	5.9(4)	-7.7(4)
O2	40.6(6)	20.6(5)	29.8(6)	-6.2(4)	13.4(4)	-9.1(4)
C1	30.4(7)	18.7(6)	18.1(6)	-3.0(4)	3.6(5)	-3.1(5)
N1	14.3(5)	15.2(5)	17.1(5)	0.3(4)	3.6(4)	-1.6(3)
C2	14.3(6)	16.2(6)	18.3(6)	0.3(4)	3.5(4)	-1.4(4)
C3	16.9(6)	21.2(7)	27.3(7)	-1.8(5)	1.4(5)	-2.7(4)
C4	18.2(6)	20.1(6)	20.0(6)	0.2(4)	6.7(4)	-1.8(4)
C5	14.7(6)	17.9(6)	16.1(6)	1.0(4)	4.7(4)	-2.3(4)
C6	17.3(6)	25.5(7)	24.2(7)	-3.3(5)	6.4(5)	-0.9(4)
C7	17.1(6)	24.5(7)	18.5(6)	3.6(4)	2.8(4)	-2.6(4)
C8	17.0(6)	16.3(6)	31.9(7)	2.6(5)	3.3(5)	-1.4(4)
C9	18.0(6)	17.0(6)	26.7(7)	1.5(4)	5.3(5)	0.9(4)
C10	16.7(6)	24.0(7)	49.8(9)	5.9(6)	6.5(6)	-1.7(5)
C11	18.6(6)	24.3(7)	36.9(8)	1.2(5)	10.5(5)	0.7(5)
C12	19.4(6)	23.9(7)	26.1(7)	4.8(5)	-0.8(5)	-3.8(4)
C13	19.9(6)	22.0(7)	47.6(9)	11.7(6)	6.2(6)	-2.4(5)

Table II.3.21.4 Bond Lengths for ab53316.

Atom	Atom	Length/Å	Atom	Atom	Length/Å
O1	C1	1.2460(16)	C4	C6	1.5262(18)
O2	C1	1.2420(17)	C5	C8	1.5231(18)
N1	C2	1.4997(15)	C5	C9	1.5274(17)
N1	C5	1.4959(15)	C7	C12	1.5278(18)
C2	C4	1.5277(16)	C8	C13	1.5244(18)
C2	C7	1.5298(17)	C9	C11	1.5254(17)
C3	C6	1.5312(19)	C10	C11	1.522(2)
C3	C12	1.5208(18)	C10	C13	1.5252(19)

Table II.3.21.5 Bond Angles for ab53316.

Atom	Atom	Atom	Angle/°	Atom	Atom	Atom	Angle/°
O2	C1	O1	128.16(13)	C8	C5	C9	111.48(10)
C5	N1	C2	117.74(9)	C4	C6	C3	111.54(10)
N1	C2	C4	107.45(9)	C12	C7	C2	110.08(10)
N1	C2	C7	111.54(10)	C5	C8	C13	110.38(11)
C4	C2	C7	111.36(10)	C11	C9	C5	110.75(10)
C12	C3	C6	110.73(10)	C11	C10	C13	110.91(12)
C6	C4	C2	111.06(11)	C10	C11	C9	110.95(11)
N1	C5	C8	111.43(10)	C3	C12	C7	111.34(11)
N1	C5	C9	107.99(9)	C8	C13	C10	111.36(11)

Table II.3.21.6 Hydrogen Atom Coordinates (Å×10^4) and Isotropic Displacement Parameters (Å^2×10^3) for ab53316.

Atom	*x*	*y*	*z*	U(eq)
H1	2962(10)	10450(20)	1825(12)	32(5)
H1A	2335(9)	6640(20)	897(10)	21(4)
H1B	2178(10)	5410(20)	240(13)	26(4)
H2	2879(8)	3540(20)	750(9)	17(4)
H3A	4465(9)	5740(20)	1828(10)	21(4)
H3B	4865(10)	4090(30)	1699(13)	34(5)
H4A	3496(9)	6650(20)	681(10)	24(4)
H4B	3356(10)	5520(20)	-37(12)	25(4)
H5	1756(9)	5260(20)	1769(11)	21(4)
H6A	4210(9)	3640(20)	485(10)	22(4)
H6B	4567(11)	5340(30)	452(13)	37(5)
H7A	3165(8)	5700(20)	2083(10)	15(3)
H7B	2767(9)	4000(20)	2138(10)	22(4)
H8A	1421(9)	2940(20)	510(11)	26(4)
H8B	1885(10)	2530(20)	1287(11)	29(4)
H9A	1127(10)	7260(20)	984(11)	28(4)
H9B	978(10)	5930(20)	337(12)	30(4)
H10A	109(10)	3520(20)	581(12)	31(5)
H10B	-222(11)	3430(30)	1395(12)	41(5)
H11A	-38(10)	6210(20)	1071(11)	26(4)
H11B	444(10)	5860(30)	1882(12)	31(4)
H12A	3810(9)	2650(30)	1871(11)	29(5)
H12B	3971(11)	3740(30)	2629(12)	38(5)
H13A	745(10)	1490(30)	1384(12)	38(5)
H13B	913(11)	2860(30)	2028(13)	38(5)

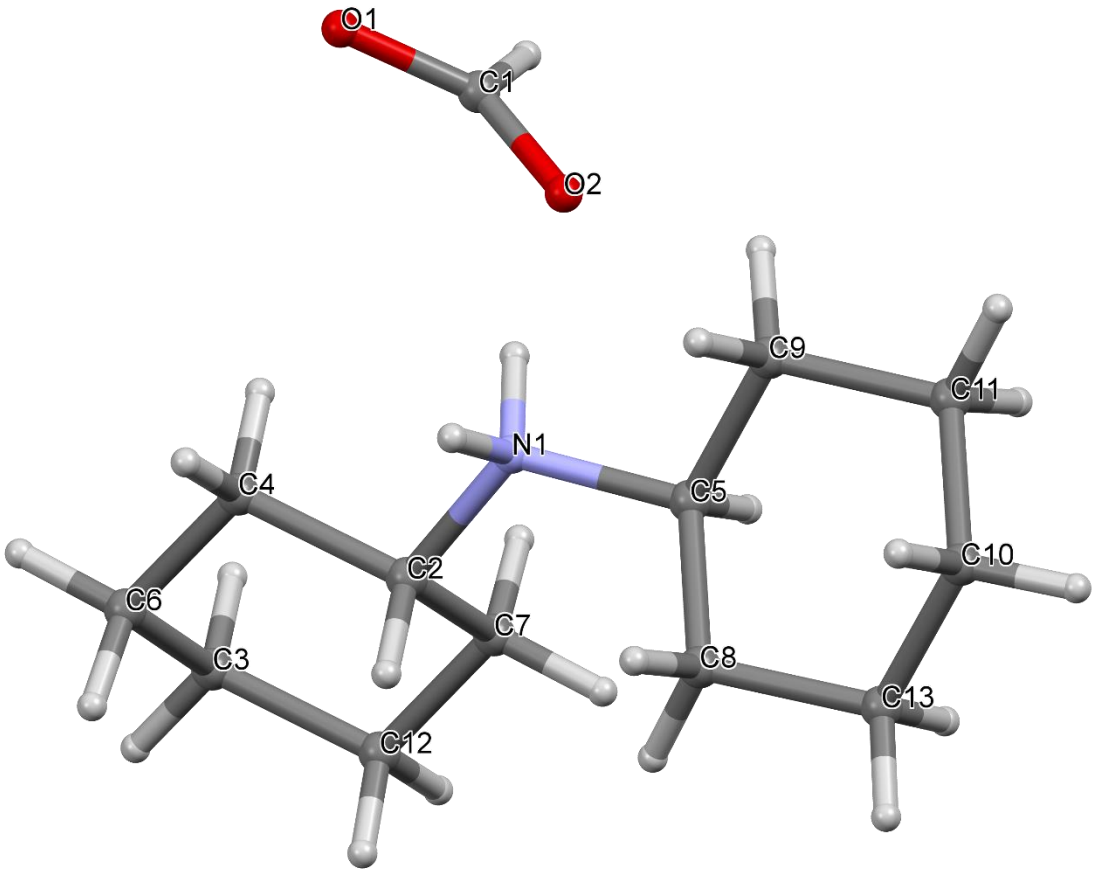

Figure II.3.21 Crystal Structure with atomic labels for compound **21**, Dicyclohexylammonium Formate, ab53316

II.3.22 Compound 22, 4-Aminomethylpiperidine Carbamate, ab57216

Table II.3.22.1 Crystal data and structure refinement for ab57216.

Identification code	ab57216
Empirical formula	$C_7H_{16}N_2O_3$
Formula weight	176.22
Temperature/K	106.9
Crystal system	triclinic
Space group	P-1
a/Å	6.3973(4)
b/Å	7.6975(5)
c/Å	9.6867(6)
α/°	74.260(2)
β/°	78.013(2)
γ/°	73.143(2)
Volume/Å^3	435.06(5)
Z	2
ρ_{calc}g/cm^3	1.345
μ/mm^{-1}	0.104
F(000)	192.0
Crystal size/mm^3	0.734 × 0.492 × 0.438
Radiation	MoKα (λ = 0.71073)
2Θ range for data collection/°	4.412 to 68.46
Index ranges	-9 ≤ h ≤ 10, -11 ≤ k ≤ 12, -14 ≤ l ≤ 14
Reflections collected	10998
Independent reflections	3333 [R_{int} = 0.0276, R_{sigma} = 0.0252]
Data/restraints/parameters	3333/0/173
Goodness-of-fit on F^2	1.252
Final R indexes [I>=2σ (I)]	R_1 = 0.0462, wR_2 = 0.1548
Final R indexes [all data]	R_1 = 0.0474, wR_2 = 0.1553
Largest diff. peak/hole / e Å^{-3}	0.53/-0.35

Table II.3.22.2 Fractional Atomic Coordinates (×10^4) and Equivalent Isotropic Displacement Parameters (Å^2×10^3) for ab57216. U_{eq} is defined as 1/3 of of the trace of the orthogonalised U_{IJ} tensor.

Atom	*x*	*y*	*z*	U(eq)
O1	242.0(17)	860.0(14)	7933.5(11)	14.96(19)
O2	2744.9(17)	2597.0(15)	7098.1(10)	15.4(2)
N1	2906.8(19)	3141.3(16)	14218.6(12)	13.4(2)
N2	1841.1(19)	1575.6(16)	9508.7(11)	13.8(2)
C1	5094(2)	2762.9(18)	11844.3(13)	12.5(2)
C2	3301.8(19)	2070.1(16)	11482.0(12)	9.9(2)
C3	1063(2)	2983(2)	12242.2(14)	15.5(2)
C4	3354(2)	2444.6(18)	9849.3(13)	12.6(2)

C5	5116(2)	2302(2)	13474.0(14)	15.0(2)
C6	1592(2)	1679.3(17)	8122.0(13)	10.9(2)
C7	1075(2)	2560(2)	13868.7(15)	18.9(3)
O3	3063.4(17)	6834.7(15)	3528.7(12)	17.7(2)

Table II.3.22.3 Anisotropic Displacement Parameters ($Å^2×10^3$) for ab57216. The Anisotropic displacement factor exponent takes the form: $-2\pi^2[h^2a^{*2}U_{11}+2hka^*b^*U_{12}+\ldots]$.

Atom	U_{11}	U_{22}	U_{33}	U_{23}	U_{13}	U_{12}
O1	17.2(4)	17.8(4)	13.3(4)	-2.3(3)	-5.0(3)	-8.6(3)
O2	18.4(4)	22.4(5)	7.5(4)	-1.5(3)	-0.4(3)	-11.1(4)
N1	16.2(5)	17.3(5)	8.1(4)	-4.1(3)	0.0(3)	-6.5(4)
N2	19.0(5)	19.6(5)	6.9(4)	-2.1(3)	-0.5(3)	-12.7(4)
C1	11.9(5)	18.3(5)	9.1(5)	-4.4(4)	0.3(4)	-6.4(4)
C2	11.1(4)	11.8(4)	7.8(4)	-2.5(3)	0.0(3)	-5.0(4)
C3	10.8(5)	25.5(6)	12.5(5)	-9.3(4)	0.0(4)	-4.5(4)
C4	15.7(5)	17.1(5)	7.5(4)	-2.7(4)	-0.2(4)	-9.0(4)
C5	13.7(5)	21.9(6)	9.7(5)	-4.6(4)	-2.6(4)	-3.5(4)
C6	11.8(5)	12.6(5)	8.7(4)	-2.8(4)	-1.7(4)	-3.0(4)
C7	16.6(6)	33.1(7)	11.8(5)	-10.1(5)	4.2(4)	-13.1(5)
O3	14.8(4)	19.0(4)	16.2(4)	1.1(3)	-0.1(3)	-5.5(3)

Table II.3.22.4 Bond Lengths for ab57216.

Atom	Atom	Length/Å	Atom	Atom	Length/Å
O1	C6	1.2732(15)	C1	C2	1.5313(17)
O2	C6	1.2825(15)	C1	C5	1.5235(17)
N1	C5	1.4952(17)	C2	C3	1.5318(18)
N1	C7	1.4967(18)	C2	C4	1.5238(17)
N2	C4	1.4562(16)	C3	C7	1.5210(19)
N2	C6	1.3636(15)			

Table II.3.22.5 Bond Angles for ab57216.

Atom	Atom	Atom	Angle/°	Atom	Atom	Atom	Angle/°
C5	N1	C7	112.70(10)	N2	C4	C2	110.76(9)
C6	N2	C4	122.60(10)	N1	C5	C1	110.10(10)
C5	C1	C2	111.02(10)	O1	C6	O2	124.66(11)
C1	C2	C3	108.70(10)	O1	C6	N2	117.98(11)
C4	C2	C1	111.04(9)	O2	C6	N2	117.36(11)
C4	C2	C3	112.44(10)	N1	C7	C3	111.45(11)
C7	C3	C2	110.73(11)				

Table II.3.22.6 Hydrogen Atom Coordinates (Å×10⁴) and Isotropic Displacement Parameters (Å²×10³) for ab57216.

Atom	*x*	*y*	*z*	U(eq)
H1C	2710(40)	4380(30)	13940(30)	22(5)
H1D	2890(40)	2870(40)	15210(30)	29(6)
H2A	1110(40)	860(30)	10230(30)	23(5)
H1A	4770(40)	4090(30)	11490(20)	19(5)
H1B	6560(40)	2180(30)	11380(20)	19(5)
H2	3650(40)	730(30)	11860(20)	19(5)
H3A	800(40)	4360(40)	11760(30)	29(6)
H3B	-100(40)	2560(30)	12080(30)	24(6)
H4A	2960(40)	3780(30)	9480(30)	21(5)
H4B	4950(40)	1940(30)	9420(30)	25(6)
H5A	5510(40)	960(30)	13830(30)	25(6)
H5B	6220(40)	2730(30)	13710(30)	23(5)
H7A	1330(40)	1210(30)	14310(30)	23(5)
H7B	-310(40)	3260(40)	14370(30)	33(6)
H3C	4400(50)	7060(40)	3120(30)	37(7)
H3D	2130(50)	7620(40)	3020(30)	44(8)

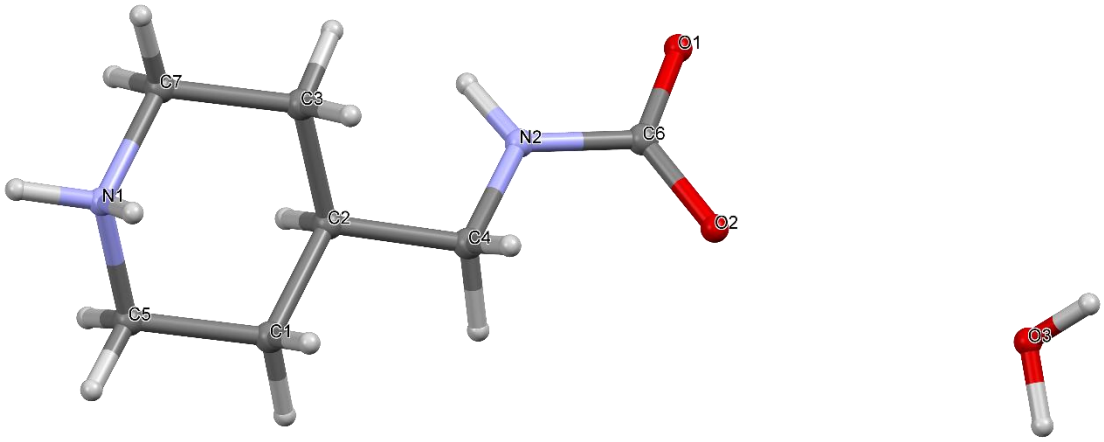

Figure II.3.22 Crystal Structure with atomic labels for compound **22**, 4-Aminomethylpiperidine Carbamate, ab57216

II.3.23 Compound 23, 3,5-Dimethylaniline-N-Formamide, ab20517

Table II.3.23.1 Crystal data and structure refinement for ab50217.

Identification code	ab50217
Empirical formula	$C_{18}H_{22}N_2O_2$
Formula weight	298.37
Temperature/K	101.24
Crystal system	triclinic
Space group	P-1
a/Å	7.9233(2)
b/Å	8.0896(2)
c/Å	12.6418(3)
α/°	78.8630(11)
β/°	88.0042(11)
γ/°	84.0465(10)
Volume/Å^3	790.65(3)
Z	2
ρ_{calc}g/cm^3	1.253
μ/mm^{-1}	0.082
F(000)	320.0
Crystal size/mm^3	? × ? × ?
Radiation	MoKα (λ = 0.71073)
2Θ range for data collection/°	3.284 to 68.354
Index ranges	-12 ≤ h ≤ 12, -12 ≤ k ≤ 12, -19 ≤ l ≤ 18
Reflections collected	21334
Independent reflections	6140 [R_{int} = 0.0218, R_{sigma} = 0.0189]
Data/restraints/parameters	6140/0/287
Goodness-of-fit on F^2	1.070
Final R indexes [I>=2σ (I)]	R_1 = 0.0415, wR_2 = 0.1259
Final R indexes [all data]	R_1 = 0.0473, wR_2 = 0.1329
Largest diff. peak/hole / e Å^{-3}	0.51/-0.24

Table II.3.23.2 Fractional Atomic Coordinates (×10^4) and Equivalent Isotropic Displacement Parameters (Å^2×10^3) for ab50217. U_{eq} is defined as 1/3 of of the trace of the orthogonalised U_{IJ} tensor.

Atom	*x*	*y*	*z*	U(eq)
O1	9131.1(7)	12029.6(7)	-5680.1(5)	23.10(13)
N1	6927.5(7)	11996.6(7)	-4466.4(5)	16.25(12)
C1	3750.5(10)	12036.6(10)	-1045.5(6)	21.14(14)
C2	8201.4(9)	11256.8(9)	-4990.1(6)	18.83(13)
C3	4676.0(8)	8598.1(8)	-2735.8(5)	15.95(12)
C4	4338.7(11)	6785.0(9)	-2688.9(6)	22.10(14)
C5	5596.7(8)	9445.9(8)	-3603.9(5)	15.58(12)
C6	4089.6(8)	9456.8(9)	-1914.0(5)	17.03(13)
C7	5956.6(8)	11110.1(8)	-3622.1(5)	14.20(12)

C8	5357.4(8)	11948.3(8)	-2795.5(5)	15.39(12)
C9	4410.1(8)	11134.2(9)	-1936.2(5)	15.90(12)
O2	-3008.2(7)	5622.7(7)	5217.5(5)	23.53(12)
N2	-1096.3(8)	5693.6(7)	3821.4(5)	16.86(12)
C10	2213.7(10)	5367.1(10)	472.8(6)	23.07(15)
C11	545.6(8)	5601.1(8)	2187.9(5)	16.27(13)
C12	780.7(10)	10989.7(9)	1621.5(6)	21.20(14)
C13	-243.0(8)	6557.8(8)	2913.3(5)	14.48(12)
C14	-2234.8(9)	6415.2(9)	4451.6(6)	18.11(13)
C15	651.5(8)	9113.3(8)	1798.5(5)	15.86(12)
C16	1399.1(9)	8147.8(9)	1069.6(5)	17.31(13)
C17	1370.6(9)	6391.0(9)	1261.0(5)	16.84(13)
C18	-170.1(8)	8310.2(8)	2721.9(5)	15.40(12)

Table II.3.23.3 Anisotropic Displacement Parameters ($Å^2×10^3$) for ab50217. The Anisotropic displacement factor exponent takes the form: $-2\pi^2[h^2a^{*2}U_{11}+2hka^*b^*U_{12}+\ldots]$.

Atom	U_{11}	U_{22}	U_{33}	U_{23}	U_{13}	U_{12}
O1	22.8(2)	19.3(2)	24.9(3)	-1.07(19)	9.8(2)	-0.88(19)
N1	18.6(2)	14.0(2)	15.5(2)	-2.21(19)	3.81(19)	-1.45(18)
C1	25.0(3)	22.2(3)	17.6(3)	-8.0(2)	4.5(2)	-2.3(2)
C2	18.6(3)	15.9(3)	20.5(3)	-1.6(2)	4.5(2)	-0.2(2)
C3	17.7(3)	14.5(3)	15.7(3)	-2.7(2)	0.5(2)	-2.2(2)
C4	29.8(4)	15.3(3)	21.6(3)	-3.2(2)	3.0(3)	-5.7(2)
C5	17.9(3)	14.5(3)	14.4(3)	-3.4(2)	1.6(2)	-1.7(2)
C6	18.6(3)	17.2(3)	15.3(3)	-2.9(2)	2.9(2)	-3.4(2)
C7	14.8(2)	14.3(3)	13.1(2)	-1.9(2)	1.11(19)	-1.11(19)
C8	16.7(3)	14.8(3)	15.1(3)	-4.1(2)	1.1(2)	-1.6(2)
C9	16.6(3)	17.0(3)	14.6(3)	-4.5(2)	1.6(2)	-1.3(2)
O2	25.8(3)	21.0(2)	23.1(3)	-4.1(2)	10.1(2)	-3.28(19)
N2	20.4(3)	13.6(2)	15.6(2)	-1.76(19)	4.55(19)	-0.91(19)
C10	27.5(4)	21.9(3)	21.6(3)	-8.9(3)	8.1(3)	-4.5(3)
C11	18.8(3)	13.8(3)	16.5(3)	-4.0(2)	2.5(2)	-1.9(2)
C12	26.9(3)	14.6(3)	22.6(3)	-2.8(2)	0.9(3)	-5.8(2)
C13	15.8(3)	13.8(3)	13.5(2)	-1.9(2)	0.71(19)	-1.69(19)
C14	18.9(3)	16.8(3)	18.7(3)	-4.2(2)	3.3(2)	-1.9(2)
C15	17.7(3)	14.3(3)	15.8(3)	-2.4(2)	-0.6(2)	-3.6(2)
C16	19.8(3)	17.3(3)	15.3(3)	-3.1(2)	1.9(2)	-5.1(2)
C17	18.0(3)	17.5(3)	15.8(3)	-4.9(2)	2.5(2)	-3.3(2)
C18	17.5(3)	14.1(3)	14.8(3)	-3.2(2)	0.6(2)	-1.9(2)

Table II.3.23.4 Bond Lengths for ab50217.

Atom	Atom	Length/Å	Atom	Atom	Length/Å

O1	C2	1.2387(8)	O2	C14	1.2347(8)
N1	C2	1.3404(9)	N2	C13	1.4134(8)
N1	C7	1.4166(8)	N2	C14	1.3452(9)
C1	C9	1.5071(10)	C10	C17	1.5109(10)
C3	C4	1.5076(10)	C11	C13	1.4015(9)
C3	C5	1.4015(9)	C11	C17	1.3974(9)
C3	C6	1.3985(9)	C12	C15	1.5047(9)
C5	C7	1.4005(9)	C13	C18	1.3983(9)
C6	C9	1.4010(9)	C15	C16	1.3978(9)
C7	C8	1.3963(9)	C15	C18	1.3965(9)
C8	C9	1.3951(9)	C16	C17	1.3973(9)

Table II.3.23.5 Bond Angles for ab50217.

Atom	Atom	Atom	Angle/°	Atom	Atom	Atom	Angle/°
C2	N1	C7	123.85(6)	C14	N2	C13	125.64(6)
O1	C2	N1	124.47(6)	C17	C11	C13	120.47(6)
C5	C3	C4	120.28(6)	C11	C13	N2	117.88(6)
C6	C3	C4	120.78(6)	C18	C13	N2	122.32(6)
C6	C3	C5	118.94(6)	C18	C13	C11	119.80(6)
C7	C5	C3	119.92(6)	O2	C14	N2	124.30(6)
C3	C6	C9	121.60(6)	C16	C15	C12	120.84(6)
C5	C7	N1	121.82(6)	C18	C15	C12	119.78(6)
C8	C7	N1	117.88(6)	C18	C15	C16	119.34(6)
C8	C7	C5	120.30(6)	C17	C16	C15	121.16(6)
C9	C8	C7	120.50(6)	C11	C17	C10	120.69(6)
C6	C9	C1	120.56(6)	C16	C17	C10	120.32(6)
C8	C9	C1	120.72(6)	C16	C17	C11	118.99(6)
C8	C9	C6	118.72(6)	C15	C18	C13	120.22(6)

Table II.3.23.6 Hydrogen Atom Coordinates (Å×10^4) and Isotropic Displacement Parameters (Å^2×10^3) for ab50217.

Atom	*x*	*y*	*z*	U(eq)
H1	6822(18)	13147(19)	-4566(12)	44(4)
H1A	4150(20)	11432(19)	-375(13)	55(4)
H1B	2530(20)	12260(20)	-1067(13)	63(5)
H1C	4110(30)	13080(30)	-1146(16)	86(6)
H2	8351(15)	10010(15)	-4738(9)	30(3)
H4A	4540(20)	6380(20)	-3358(14)	65(5)
H4B	3120(20)	6680(20)	-2652(14)	72(5)
H4C	4960(20)	6100(20)	-2185(15)	72(5)
H5	5953(16)	8839(16)	-4212(10)	35(3)
H6	3393(16)	8916(15)	-1339(10)	32(3)

H8	5687(15)	13075(16)	-2858(10)	32(3)
H2A	-979(18)	4540(19)	3975(11)	42(3)
H10A	2440(20)	4250(20)	804(13)	61(4)
H10B	1580(20)	5470(20)	-151(13)	57(4)
H10C	3330(20)	5690(20)	239(14)	71(5)
H11	473(15)	4351(15)	2403(10)	28(3)
H12A	444(18)	11523(18)	863(11)	46(4)
H12B	1830(20)	11241(18)	1818(12)	50(4)
H12C	-10(20)	11550(20)	2024(14)	70(5)
H14	-2455(15)	7690(15)	4245(9)	30(3)
H16	1973(17)	8680(16)	406(10)	38(3)
H18	-682(15)	9059(15)	3203(9)	30(3)

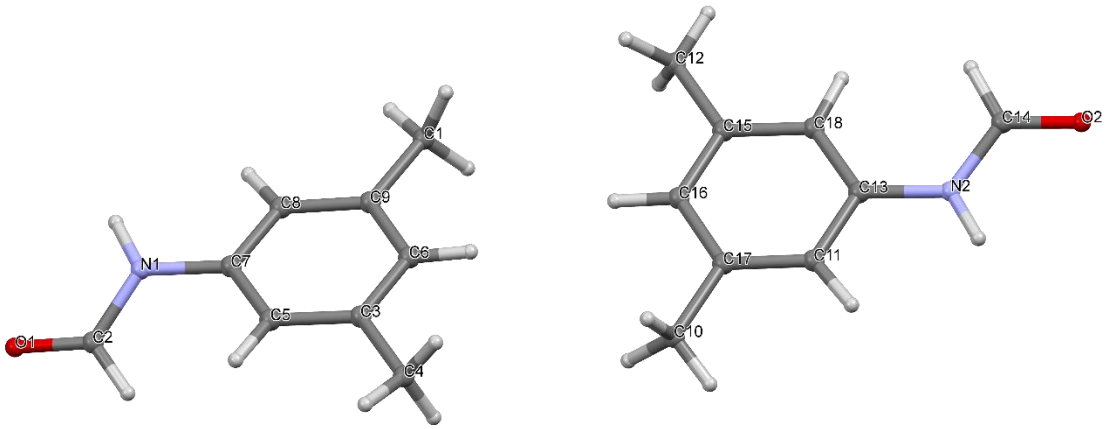

Figure II.3.23 Crystal Structure with atomic labels for compound **23**, 3,5-Dimethylaniline-N-Formamide, ab20517

II.3.24 Compound 24, 2,4,6-Trimethylaniline-N-Formamide, ab50717

Table II.3.24.1 Crystal data and structure refinement for ab50717.

Identification code	ab50717
Empirical formula	$C_{10}H_{13}NO$
Formula weight	163.21
Temperature/K	100.01
Crystal system	monoclinic
Space group	$P2_1/n$
a/Å	7.8752(11)
b/Å	16.023(2)
c/Å	8.0217(11)
α/°	90
β/°	116.558(6)
γ/°	90
Volume/Å^3	905.4(2)
Z	4
ρ_{calc}g/cm^3	1.197
μ/mm^{-1}	0.077
F(000)	352.0
Crystal size/mm^3	0.45 × 0.273 × 0.249
Radiation	MoKα (λ = 0.71073)
2Θ range for data collection/°	5.084 to 68.404
Index ranges	$-12 \le h \le 12$, $-25 \le k \le 23$, $-12 \le l \le 12$
Reflections collected	23876
Independent reflections	3614 [R_{int} = 0.0263, R_{sigma} = 0.0146]
Data/restraints/parameters	3614/0/161
Goodness-of-fit on F^2	1.066
Final R indexes [I>=2σ (I)]	R_1 = 0.0357, wR_2 = 0.1065
Final R indexes [all data]	R_1 = 0.0392, wR_2 = 0.1099
Largest diff. peak/hole / e Å^{-3}	0.53/-0.21

Table II.3.24.2 Fractional Atomic Coordinates (×10^4) and Equivalent Isotropic Displacement Parameters (Å^2×10^3) for ab50717. U_{eq} is defined as 1/3 of of the trace of the orthogonalised U_{IJ} tensor.

Atom	*x*	*y*	*z*	U(eq)
O1	2790.5(7)	3317.5(3)	6997.4(7)	22.01(12)
N1	4867.0(7)	2261.3(3)	8532.7(7)	13.57(11)
C1	4178.6(8)	1727.1(4)	5417.7(8)	13.02(11)
C2	3358.2(8)	906.7(3)	7523.8(8)	11.51(11)
C3	4097.6(8)	1633.1(3)	7120.2(8)	11.40(11)
C4	3446.9(8)	1086.7(4)	4106.6(8)	14.06(11)
C5	2672.9(8)	362.4(4)	4450.6(8)	13.46(11)
C6	2656.4(8)	278.5(3)	6176.0(8)	13.16(11)
C7	1894.3(10)	-310.2(4)	2989.2(9)	19.16(13)
C8	3313.2(9)	804.7(4)	9371.1(8)	15.75(12)
C9	4169.6(8)	3034.7(4)	8365.0(8)	15.73(12)

C10	5072.5(10)	2478.7(4)	5005.5(10)	20.07(13)

Table II.3.24.3 Anisotropic Displacement Parameters ($Å^2×10^3$) for ab50717. The Anisotropic displacement factor exponent takes the form: $-2\pi^2[h^2a^{*2}U_{11}+2hka^*b^*U_{12}+\ldots]$.

Atom	U_{11}	U_{22}	U_{33}	U_{23}	U_{13}	U_{12}
O1	20.4(2)	16.3(2)	18.2(2)	-3.10(16)	-1.38(18)	4.73(16)
N1	13.6(2)	12.4(2)	10.3(2)	-1.35(15)	1.37(16)	0.58(15)
C1	13.8(2)	13.4(2)	11.5(2)	1.16(17)	5.29(18)	-0.21(17)
C2	11.8(2)	11.9(2)	10.2(2)	0.69(16)	4.40(17)	1.22(16)
C3	11.8(2)	11.0(2)	9.6(2)	-0.36(16)	3.14(17)	0.52(16)
C4	15.8(2)	15.8(2)	10.7(2)	-0.20(17)	6.07(19)	0.77(18)
C5	13.5(2)	13.7(2)	11.8(2)	-2.26(17)	4.39(18)	0.93(17)
C6	14.2(2)	11.5(2)	13.1(2)	-0.23(17)	5.51(19)	-0.02(17)
C7	20.6(3)	18.4(3)	16.2(3)	-6.6(2)	6.2(2)	-1.5(2)
C8	18.0(2)	18.6(3)	11.9(2)	1.21(19)	7.7(2)	0.79(19)
C9	15.1(2)	13.5(2)	13.9(2)	-3.11(18)	2.30(19)	0.01(18)
C10	24.8(3)	18.5(3)	18.5(3)	1.3(2)	11.0(2)	-5.6(2)

Table II.3.24.4 Bond Lengths for ab50717.

Atom	Atom	Length/Å	Atom	Atom	Length/Å
O1	C9	1.2342(7)	C2	C3	1.4026(8)
N1	C3	1.4318(7)	C2	C6	1.3976(8)
N1	C9	1.3377(8)	C2	C8	1.5069(8)
C1	C3	1.4035(8)	C4	C5	1.3946(8)
C1	C4	1.3961(8)	C5	C6	1.3964(8)
C1	C10	1.5045(9)	C5	C7	1.5063(8)

Table II.3.24.5 Bond Angles for ab50717.

Atom	Atom	Atom	Angle/°	Atom	Atom	Atom	Angle/°
C9	N1	C3	124.21(5)	C2	C3	N1	118.24(5)
C3	C1	C10	121.94(5)	C2	C3	C1	121.19(5)
C4	C1	C3	118.11(5)	C5	C4	C1	122.16(5)
C4	C1	C10	119.92(5)	C4	C5	C6	118.35(5)
C3	C2	C8	120.78(5)	C4	C5	C7	120.21(5)
C6	C2	C3	118.72(5)	C6	C5	C7	121.43(5)
C6	C2	C8	120.51(5)	C5	C6	C2	121.45(5)
C1	C3	N1	120.49(5)	O1	C9	N1	126.03(5)

Table II.3.24.6 Hydrogen Atom Coordinates (Å×10^4) and Isotropic Displacement Parameters (Å^2×10^3) for ab50717.

Atom	*x*	*y*	*z*	U(eq)
H1	5802(16)	2128(8)	9603(16)	27(3)
H4	3509(16)	1151(7)	2924(16)	25(3)
H6	2154(16)	-229(7)	6457(15)	22(2)
H7A	2833(19)	-500(9)	2585(18)	38(3)
H7B	850(20)	-96(9)	1896(19)	40(3)
H7C	1490(20)	-800(9)	3410(20)	47(4)
H8A	4586(17)	869(7)	10429(16)	25(3)
H8B	2814(17)	239(8)	9469(17)	30(3)
H8C	2468(17)	1217(8)	9506(16)	31(3)
H9	4842(15)	3381(7)	9459(14)	20(2)
H10A	5377(19)	2369(9)	3970(20)	42(4)
H10B	6260(20)	2619(9)	6080(20)	42(3)
H10C	4243(19)	2963(9)	4679(19)	39(3)

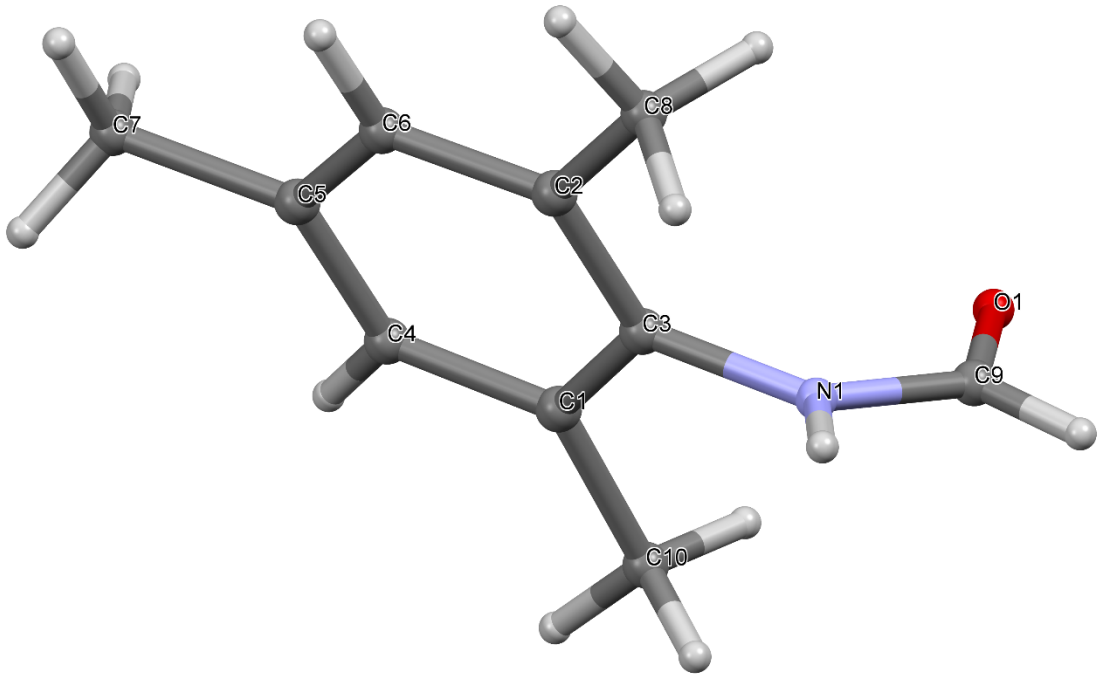

Figure II.3.24 Crystal Structure with atomic labels for compound **24**, 2,4,6-Trimethylaniline-N-Formamide, ab50717

II.3.25 Compound 25, 2-Isopropylaniline-N-Formamide, ab51317

Table II.3.25.1 Crystal data and structure refinement for ab51317.

Identification code	ab51317
Empirical formula	$C_{10}H_{13}NO$
Formula weight	163.21
Temperature/K	100.01
Crystal system	triclinic
Space group	P-1
a/Å	12.3625(4)
b/Å	12.6919(4)
c/Å	14.3045(5)
α/°	67.2760(17)
β/°	71.0574(18)
γ/°	66.6694(17)
Volume/Å^3	1861.50(11)
Z	8
ρ_{calc}g/cm^3	1.165
μ/mm^{-1}	0.075
F(000)	704.0
Crystal size/mm^3	0.259 × 0.176 × 0.123
Radiation	MoKα (λ = 0.71073)
2Θ range for data collection/°	3.152 to 56.79
Index ranges	-16 ≤ h ≤ 16, -16 ≤ k ≤ 16, -19 ≤ l ≤ 19
Reflections collected	37952
Independent reflections	9325 [R_{int} = 0.0337, R_{sigma} = 0.0296]
Data/restraints/parameters	9325/0/641
Goodness-of-fit on F^2	1.036
Final R indexes [I>=2σ (I)]	R_1 = 0.0402, wR_2 = 0.1010
Final R indexes [all data]	R_1 = 0.0567, wR_2 = 0.1116
Largest diff. peak/hole / e Å^{-3}	0.30/-0.25

Table II.3.25.2 Fractional Atomic Coordinates (×10^4) and Equivalent Isotropic Displacement Parameters (Å^2×10^3) for ab51317. U_{eq} is defined as 1/3 of of the trace of the orthogonalised U_{IJ} tensor.

Atom	*x*	*y*	*z*	U(eq)
O1	1793.4(6)	1792.2(6)	5051.5(5)	18.96(16)
N1	3026.8(8)	1981.3(8)	3461.6(6)	15.39(18)
C1	2067.7(9)	2397.3(9)	4151.1(8)	16.3(2)
C2	3320.7(9)	2686.5(9)	2420.5(8)	14.9(2)
C3	3630.8(9)	2198.6(9)	1606.2(8)	16.4(2)
C4	3304.3(9)	3857.8(9)	2227.6(9)	19.3(2)
C5	3562.9(10)	4573.1(10)	1219.7(9)	22.7(2)
C6	3666.7(10)	924.1(10)	1786.2(8)	20.5(2)
C7	3913.4(10)	2934.6(10)	604.1(8)	21.1(2)
C8	2930.4(13)	901.3(13)	1120.5(11)	31.6(3)
C9	4963.0(12)	103.8(12)	1600.1(12)	33.9(3)

C10	3874.0(10)	4107.9(10)	403.3(9)	23.1(2)
O2	6589.5(6)	6576.4(7)	5032.7(6)	19.72(16)
N2	7913.6(8)	6819.7(8)	3488.9(7)	15.67(18)
C11	6886.8(9)	7188.7(9)	4139.6(8)	16.9(2)
C12	8096.4(10)	8755.2(9)	2308.0(9)	19.9(2)
C13	8251.4(9)	7551.3(9)	2468.8(8)	15.0(2)
C14	8745.9(9)	7054.2(9)	1644.8(8)	15.9(2)
C15	8409.8(10)	9489.5(10)	1321.5(9)	23.6(2)
C16	8942.2(10)	5743.6(9)	1789.8(8)	18.7(2)
C17	9074.9(10)	7809.9(10)	666.6(8)	20.7(2)
C18	8443.5(13)	5616.4(12)	1003.7(10)	29.6(3)
C19	10273.8(11)	5017.2(11)	1738.0(10)	26.6(3)
C20	8904.3(10)	9015.4(10)	495.5(9)	23.2(2)
O3	4543.8(7)	9612.5(7)	4244.1(6)	22.45(17)
N3	3144.1(8)	9344.6(8)	5737.4(7)	16.79(18)
C21	4213.8(9)	8992.1(10)	5123.4(8)	18.9(2)
C22	2786.6(9)	8630.5(9)	6761.3(8)	15.7(2)
C23	1623.8(9)	8525.1(9)	7093.7(8)	16.3(2)
C24	3599.5(10)	8057.9(10)	7425.0(9)	21.2(2)
C25	716.2(10)	9142.3(10)	6390.2(8)	20.4(2)
C26	1318.2(10)	7837.2(10)	8114.8(8)	20.9(2)
C27	3277.9(11)	7361.2(10)	8427.0(9)	23.5(2)
C28	-228.6(11)	10247.9(12)	6677.9(11)	30.4(3)
C29	119.4(13)	8285.4(13)	6400.1(11)	33.7(3)
C30	2129.8(11)	7255.8(10)	8773.7(9)	22.6(2)
O4	489.5(7)	5477.7(7)	5660.8(6)	25.33(18)
N4	1878.4(8)	5778.7(8)	4167.3(7)	17.64(19)
C31	2236.6(9)	6483.6(9)	3141.8(8)	16.1(2)
C32	3391.2(9)	6613.7(9)	2828.5(8)	17.5(2)
C33	789.0(10)	6093.5(10)	4773.0(9)	20.5(2)
C34	1452.2(10)	7018.5(10)	2456.6(9)	21.0(2)
C35	3708.1(11)	7295.9(10)	1812.6(9)	22.7(2)
C36	4219.7(10)	6090.9(11)	3593.8(9)	22.8(2)
C37	1788.8(11)	7709.1(10)	1455.9(9)	24.6(2)
C38	2921.2(11)	7845.6(10)	1130.0(9)	25.0(2)
C39	3863.4(13)	6937.4(14)	4246.4(11)	34.0(3)
C40	5556.5(11)	5829.9(15)	3085.3(12)	36.5(3)

Table II.3.25.3 Anisotropic Displacement Parameters ($Å^2×10^3$) for ab51317. The Anisotropic displacement factor exponent takes the form: $-2\pi^2[h^2a^{*2}U_{11}+2hka^*b^*U_{12}+\ldots]$.

Atom	U_{11}	U_{22}	U_{33}	U_{23}	U_{13}	U_{12}
O1	17.5(4)	19.1(4)	16.0(4)	-5.3(3)	-0.5(3)	-3.6(3)
N1	15.3(4)	13.8(4)	14.6(4)	-4.7(3)	-2.4(3)	-2.0(3)
C1	14.1(5)	16.4(5)	18.3(5)	-7.4(4)	-3.6(4)	-2.2(4)

C2	11.2(4)	14.9(5)	16.4(5)	-4.3(4)	-3.0(4)	-2.2(4)
C3	13.9(5)	17.4(5)	17.0(5)	-5.5(4)	-2.1(4)	-4.5(4)
C4	17.0(5)	17.3(5)	23.9(5)	-9.4(4)	-2.4(4)	-3.9(4)
C5	18.4(5)	14.8(5)	29.8(6)	-3.4(4)	-3.3(4)	-4.5(4)
C6	25.8(6)	20.1(5)	17.8(5)	-8.0(4)	-1.0(4)	-9.9(4)
C7	20.4(5)	25.4(6)	16.8(5)	-6.0(4)	-1.9(4)	-8.1(4)
C8	37.3(7)	33.0(7)	35.6(7)	-15.1(6)	-8.2(6)	-16.4(6)
C9	32.3(7)	20.3(6)	46.7(8)	-13.6(6)	-6.3(6)	-3.5(5)
C10	19.9(5)	23.2(6)	19.5(5)	1.0(4)	-2.9(4)	-8.0(4)
O2	17.2(4)	18.9(4)	17.7(4)	-5.4(3)	-0.4(3)	-2.8(3)
N2	15.1(4)	14.6(4)	15.4(4)	-5.9(3)	-2.6(3)	-1.7(3)
C11	15.5(5)	16.6(5)	17.6(5)	-6.7(4)	-3.2(4)	-2.8(4)
C12	20.0(5)	17.8(5)	23.3(5)	-9.8(4)	-3.7(4)	-4.1(4)
C13	12.1(4)	16.6(5)	16.0(5)	-5.1(4)	-3.9(4)	-3.2(4)
C14	14.1(5)	17.6(5)	17.6(5)	-6.9(4)	-3.1(4)	-5.0(4)
C15	23.8(6)	15.6(5)	30.3(6)	-5.0(5)	-6.5(5)	-5.9(4)
C16	22.9(5)	17.9(5)	16.2(5)	-7.5(4)	0.7(4)	-8.6(4)
C17	20.8(5)	24.1(5)	17.1(5)	-7.5(4)	-1.0(4)	-7.9(4)
C18	39.6(7)	28.6(7)	30.2(7)	-14.1(5)	-8.0(6)	-14.0(6)
C19	27.3(6)	19.0(6)	29.3(6)	-9.0(5)	-3.2(5)	-3.3(5)
C20	23.3(6)	21.6(5)	21.3(6)	-0.9(4)	-3.9(4)	-9.4(5)
O3	19.0(4)	19.7(4)	19.9(4)	-4.9(3)	0.8(3)	-1.9(3)
N3	13.4(4)	13.7(4)	18.3(4)	-2.9(3)	-1.9(3)	-2.0(3)
C21	16.9(5)	16.1(5)	20.3(5)	-6.2(4)	-2.1(4)	-2.1(4)
C22	16.9(5)	12.2(4)	16.2(5)	-4.2(4)	-2.5(4)	-3.5(4)
C23	17.2(5)	15.6(5)	16.5(5)	-5.1(4)	-3.4(4)	-5.1(4)
C24	17.1(5)	20.3(5)	25.1(6)	-6.2(4)	-6.4(4)	-3.7(4)
C25	18.2(5)	25.9(6)	16.8(5)	-1.8(4)	-4.2(4)	-10.3(4)
C26	23.1(6)	22.5(5)	18.2(5)	-4.0(4)	-2.8(4)	-11.1(4)
C27	26.0(6)	19.9(5)	23.0(6)	-3.3(4)	-12.0(5)	-3.0(5)
C28	22.7(6)	28.5(6)	33.3(7)	-3.2(5)	-9.2(5)	-4.3(5)
C29	38.8(7)	38.2(7)	34.0(7)	-5.3(6)	-16.8(6)	-19.4(6)
C30	31.5(6)	18.5(5)	17.2(5)	-1.9(4)	-6.2(5)	-9.5(5)
O4	18.3(4)	23.5(4)	22.9(4)	-5.3(3)	1.0(3)	-0.9(3)
N4	13.6(4)	15.7(4)	20.3(5)	-4.8(4)	-2.3(3)	-2.5(3)
C31	16.8(5)	12.6(5)	18.2(5)	-6.7(4)	-2.7(4)	-2.6(4)
C32	18.4(5)	16.3(5)	18.9(5)	-6.7(4)	-3.1(4)	-5.6(4)
C33	16.3(5)	17.7(5)	22.8(5)	-6.5(4)	-2.5(4)	-1.2(4)
C34	18.2(5)	19.1(5)	27.1(6)	-9.5(4)	-7.9(4)	-2.0(4)
C35	27.2(6)	22.5(5)	20.6(5)	-6.4(4)	-1.6(4)	-12.5(5)
C36	18.2(5)	27.0(6)	23.5(6)	-3.0(5)	-6.1(4)	-10.0(5)
C37	32.0(6)	19.2(5)	24.6(6)	-6.7(5)	-15.4(5)	-2.0(5)
C38	37.7(7)	18.8(5)	18.2(5)	-3.6(4)	-6.2(5)	-10.0(5)
C39	36.5(7)	43.8(8)	31.0(7)	-11.7(6)	-13.9(6)	-15.5(6)
C40	19.7(6)	46.8(8)	39.7(8)	-7.2(7)	-6.5(6)	-12.0(6)

Table II.3.25.4 Bond Lengths for ab51317.

Atom	Atom	Length/Å	Atom	Atom	Length/Å
O1	C1	1.2337(12)	O3	C21	1.2348(13)
N1	C1	1.3433(13)	N3	C21	1.3421(13)
N1	C2	1.4239(12)	N3	C22	1.4260(13)
C2	C3	1.4024(14)	C22	C23	1.4035(14)
C2	C4	1.3963(14)	C22	C24	1.3955(14)
C3	C6	1.5210(14)	C23	C25	1.5209(14)
C3	C7	1.3958(14)	C23	C26	1.3986(14)
C4	C5	1.3872(15)	C24	C27	1.3870(16)
C5	C10	1.3862(17)	C25	C28	1.5292(17)
C6	C8	1.5301(16)	C25	C29	1.5312(16)
C6	C9	1.5293(17)	C26	C30	1.3893(16)
C7	C10	1.3869(16)	C27	C30	1.3858(17)
O2	C11	1.2351(12)	O4	C33	1.2320(13)
N2	C11	1.3400(13)	N4	C31	1.4236(13)
N2	C13	1.4249(13)	N4	C33	1.3445(13)
C12	C13	1.3962(14)	C31	C32	1.4070(14)
C12	C15	1.3874(15)	C31	C34	1.3941(15)
C13	C14	1.4008(14)	C32	C35	1.3936(15)
C14	C16	1.5215(14)	C32	C36	1.5219(15)
C14	C17	1.3950(14)	C34	C37	1.3869(16)
C15	C20	1.3859(17)	C35	C38	1.3925(16)
C16	C18	1.5297(16)	C36	C39	1.5338(18)
C16	C19	1.5286(16)	C36	C40	1.5304(17)
C17	C20	1.3907(16)	C37	C38	1.3832(17)

Table II.3.25.5 Bond Angles for ab51317.

Atom	Atom	Atom	Angle/°	Atom	Atom	Atom	Angle/°
C1	N1	C2	123.10(9)	C21	N3	C22	123.37(9)
O1	C1	N1	123.82(10)	O3	C21	N3	123.97(10)
C3	C2	N1	119.97(9)	C23	C22	N3	119.93(9)
C4	C2	N1	119.11(9)	C24	C22	N3	119.16(9)
C4	C2	C3	120.92(9)	C24	C22	C23	120.91(9)
C2	C3	C6	122.43(9)	C22	C23	C25	122.13(9)
C7	C3	C2	117.15(9)	C26	C23	C22	117.15(9)
C7	C3	C6	120.42(9)	C26	C23	C25	120.71(9)
C5	C4	C2	120.32(10)	C27	C24	C22	120.58(10)
C10	C5	C4	119.68(10)	C23	C25	C28	110.66(9)
C3	C6	C8	111.32(9)	C23	C25	C29	112.17(9)
C3	C6	C9	111.03(9)	C28	C25	C29	110.88(10)
C9	C6	C8	111.27(10)	C30	C26	C23	122.06(10)

C10	C7	C3	122.35(10)	C30	C27	C24	119.41(10)
C5	C10	C7	119.54(10)	C27	C30	C26	119.88(10)
C11	N2	C13	123.20(9)	C33	N4	C31	124.28(9)
O2	C11	N2	124.13(10)	C32	C31	N4	119.27(9)
C15	C12	C13	120.43(10)	C34	C31	N4	119.88(9)
C12	C13	N2	119.26(9)	C34	C31	C32	120.84(10)
C12	C13	C14	120.89(9)	C31	C32	C36	120.81(9)
C14	C13	N2	119.84(9)	C35	C32	C31	117.17(10)
C13	C14	C16	122.50(9)	C35	C32	C36	121.92(9)
C17	C14	C13	117.24(9)	O4	C33	N4	123.74(10)
C17	C14	C16	120.26(9)	C37	C34	C31	120.48(10)
C20	C15	C12	119.63(10)	C38	C35	C32	122.17(11)
C14	C16	C18	111.57(9)	C32	C36	C39	109.48(10)
C14	C16	C19	110.74(9)	C32	C36	C40	113.78(10)
C19	C16	C18	111.15(10)	C40	C36	C39	110.40(11)
C20	C17	C14	122.29(10)	C38	C37	C34	119.65(10)
C15	C20	C17	119.49(10)	C37	C38	C35	119.66(11)

Table II.3.25.6 Hydrogen Atom Coordinates (Å×10^4) and Isotropic Displacement Parameters (Å^2×10^3) for ab51317.

Atom	*x*	*y*	*z*	U(eq)
H1	3506(13)	1197(13)	3708(10)	31(4)
H1A	1545(11)	3225(11)	3888(9)	17(3)
H4	3119(11)	4177(11)	2807(10)	23(3)
H5	3524(12)	5369(13)	1099(10)	32(4)
H6	3288(11)	621(11)	2515(10)	22(3)
H7	4129(12)	2608(12)	33(10)	27(3)
H8A	2907(13)	102(13)	1282(11)	37(4)
H8B	3315(13)	1148(13)	352(12)	42(4)
H8C	2080(15)	1450(14)	1233(12)	52(5)
H9A	4976(13)	-708(14)	1718(11)	40(4)
H9B	5340(13)	390(13)	880(12)	36(4)
H9C	5430(15)	127(14)	2033(12)	48(4)
H10	4055(12)	4594(12)	-298(10)	28(3)
H2	8420(13)	6057(13)	3748(11)	37(4)
H11	6348(11)	8006(11)	3847(9)	20(3)
H12	7776(11)	9055(11)	2897(10)	26(3)
H15	8275(12)	10325(12)	1230(10)	31(4)
H16	8503(10)	5423(10)	2466(9)	14(3)
H17	9414(12)	7489(12)	77(10)	29(3)
H18A	8869(13)	5910(13)	289(12)	36(4)
H18B	8507(13)	4776(13)	1152(11)	38(4)
H18C	7603(15)	6093(14)	1032(12)	44(4)
H19A	10745(13)	5321(12)	1058(11)	35(4)

H19B	10571(13)	5083(13)	2278(11)	37(4)
H19C	10386(13)	4184(13)	1828(11)	37(4)
H20	9123(12)	9511(12)	-196(11)	31(4)
H3	2666(13)	10098(13)	5492(11)	32(4)
H21	4735(11)	8180(11)	5422(9)	23(3)
H24	4387(12)	8185(11)	7170(10)	26(3)
H25	1164(10)	9409(10)	5668(9)	18(3)
H26	494(12)	7756(11)	8351(10)	27(3)
H27	3849(12)	6970(12)	8875(10)	29(3)
H28A	-815(14)	10644(13)	6217(12)	45(4)
H28B	-667(14)	10002(13)	7380(12)	40(4)
H28C	161(13)	10826(13)	6637(11)	42(4)
H29A	-418(13)	8058(13)	7089(12)	37(4)
H29B	723(15)	7538(15)	6266(12)	50(5)
H29C	-374(14)	8672(14)	5867(12)	48(4)
H30	1878(12)	6783(12)	9483(10)	29(3)
H4A	2396(13)	5059(13)	4451(11)	34(4)
H33	237(12)	6870(12)	4451(10)	28(3)
H34	673(12)	6889(12)	2704(10)	27(3)
H35	4514(13)	7421(12)	1581(10)	33(4)
H36	4098(12)	5314(12)	4060(10)	28(3)
H37	1234(13)	8073(13)	1003(11)	35(4)
H38	3189(12)	8299(12)	426(11)	31(4)
H39A	4382(14)	6599(13)	4763(12)	43(4)
H39B	3971(14)	7737(14)	3771(12)	45(4)
H39C	2984(15)	7065(14)	4628(12)	50(4)
H40A	5764(14)	5313(14)	2664(12)	40(4)
H40B	6057(14)	5395(14)	3627(12)	48(4)
H40C	5762(14)	6587(15)	2684(12)	49(5)

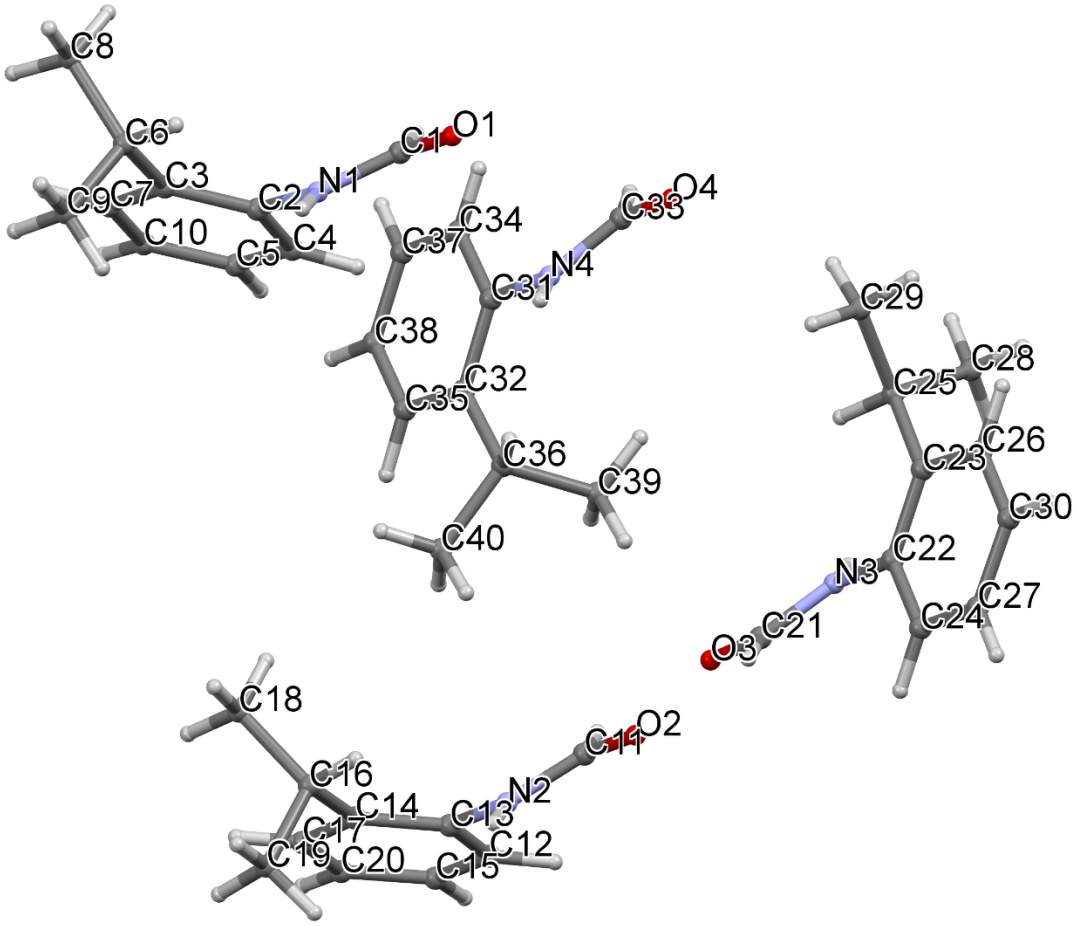

Figure II.3.25 Crystal Structure with atomic labels for compound **25**, 2-Isopropylaniline-N-Formamide, ab51317

II.3.26 Compound 26, 2,6-Isopropylaniline-N-Formamide, ab51117

Table II.3.26.1 Crystal data and structure refinement for ab51117.

Identification code	ab51117
Empirical formula	$C_{13}H_{19}NO$
Formula weight	205.29
Temperature/K	100.01
Crystal system	monoclinic
Space group	$P2_1/c$
a/Å	8.9276(3)
b/Å	8.7411(2)
c/Å	15.7460(5)
α/°	90
β/°	105.5263(13)
γ/°	90
Volume/Å^3	1183.93(6)
Z	4
ρ_{calc}g/cm^3	1.152
μ/mm^{-1}	0.072
F(000)	448.0
Crystal size/mm^3	0.737 × 0.571 × 0.234
Radiation	MoKα (λ = 0.71073)
2Θ range for data collection/°	5.37 to 68.658
Index ranges	$-13 \leq h \leq 14$, $-13 \leq k \leq 13$, $-24 \leq l \leq 24$
Reflections collected	30866
Independent reflections	4728 [R_{int} = 0.0198, R_{sigma} = 0.0123]
Data/restraints/parameters	4728/0/212
Goodness-of-fit on F^2	1.038
Final R indexes [I>=2σ (I)]	R_1 = 0.0361, wR_2 = 0.1008
Final R indexes [all data]	R_1 = 0.0400, wR_2 = 0.1043
Largest diff. peak/hole / e Å^{-3}	0.48/-0.26

Table II.3.26.2 Fractional Atomic Coordinates (×10^4) and Equivalent Isotropic Displacement Parameters (Å^2×10^3) for ab51117. U_{eq} is defined as 1/3 of of the trace of the orthogonalised U_{IJ} tensor.

Atom	*x*	*y*	*z*	U(eq)
O1	4015.9(6)	7401.2(5)	2909.0(3)	18.33(10)
N1	5227.0(6)	5585.0(5)	2278.4(3)	12.23(9)
C1	5673.2(6)	6581.9(6)	1660.5(3)	10.76(10)
C2	7240.8(6)	7035.9(6)	1837.0(4)	11.95(10)
C3	7668.4(7)	7966.2(6)	1218.2(4)	14.19(10)
C4	4553.8(6)	7030.2(6)	890.7(3)	11.94(10)
C5	5041.8(7)	7947.6(7)	285.0(4)	14.76(11)
C6	2863.6(6)	6539.6(7)	687.3(4)	14.61(11)
C7	6578.9(7)	8411.1(7)	446.9(4)	15.51(11)

C8	8415.9(7)	6534.7(7)	2680.1(4)	15.97(11)
C9	4422.3(7)	6072.5(7)	2835.0(4)	14.29(11)
C10	1791.0(8)	7917.9(8)	654.1(5)	22.29(13)
C11	8267.9(8)	7523.0(9)	3460.4(4)	22.80(13)
C12	10099.3(8)	6556.5(9)	2617.6(5)	23.87(14)
C13	2382.3(8)	5632.8(9)	-174.9(5)	24.23(14)

Table II.3.26.3 Anisotropic Displacement Parameters ($Å^2×10^3$) for ab51117. The Anisotropic displacement factor exponent takes the form: $-2\pi^2[h^2a^{*2}U_{11}+2hka^*b^*U_{12}+\ldots]$.

Atom	U_{11}	U_{22}	U_{33}	U_{23}	U_{13}	U_{12}
O1	23.1(2)	14.6(2)	20.6(2)	-2.09(15)	11.59(17)	-1.57(15)
N1	15.5(2)	9.24(19)	12.75(19)	1.59(14)	5.16(15)	-0.63(15)
C1	13.1(2)	8.8(2)	11.3(2)	0.51(15)	4.87(16)	-0.04(15)
C2	12.9(2)	9.7(2)	14.0(2)	-0.36(16)	4.93(17)	0.19(16)
C3	15.4(2)	11.5(2)	18.2(2)	-0.21(18)	8.98(18)	-0.68(17)
C4	14.1(2)	10.9(2)	11.3(2)	0.15(16)	4.24(16)	0.14(16)
C5	18.7(2)	14.2(2)	12.4(2)	2.46(17)	5.84(18)	1.37(18)
C6	13.9(2)	15.2(2)	14.0(2)	0.37(18)	2.42(17)	-1.03(17)
C7	20.4(2)	13.0(2)	16.2(2)	2.08(18)	10.30(19)	0.42(18)
C8	13.3(2)	15.0(2)	18.4(2)	2.51(18)	2.16(18)	0.49(18)
C9	16.6(2)	14.2(2)	13.1(2)	0.83(17)	5.77(17)	-3.25(18)
C10	16.2(2)	23.6(3)	27.2(3)	-8.2(2)	5.9(2)	2.3(2)
C11	19.0(3)	32.0(3)	15.7(3)	-2.8(2)	1.8(2)	-2.1(2)
C12	14.0(2)	25.5(3)	31.4(3)	2.4(3)	4.7(2)	3.9(2)
C13	20.7(3)	22.8(3)	26.8(3)	-11.7(2)	2.2(2)	-0.8(2)

Table II.3.26.4 Bond Lengths for ab51117.

Atom	Atom	Length/Å	Atom	Atom	Length/Å
O1	C9	1.2316(7)	C4	C5	1.4018(8)
N1	C1	1.4395(7)	C4	C6	1.5181(8)
N1	C9	1.3427(7)	C5	C7	1.3874(8)
C1	C2	1.4089(7)	C6	C10	1.5310(9)
C1	C4	1.4046(7)	C6	C13	1.5309(9)
C2	C3	1.3984(8)	C8	C11	1.5364(9)
C2	C8	1.5197(8)	C8	C12	1.5323(9)
C3	C7	1.3928(8)			

Table II.3.26.5 Bond Angles for ab51117.

Atom	Atom	Atom	Angle/°	Atom	Atom	Atom	Angle/°
C9	N1	C1	122.84(5)	C5	C4	C6	119.37(5)

C2	C1	N1	118.50(5)	C7	C5	C4	120.95(5)
C4	C1	N1	119.37(5)	C4	C6	C10	111.23(5)
C4	C1	C2	122.10(5)	C4	C6	C13	111.13(5)
C1	C2	C8	120.54(5)	C13	C6	C10	110.65(5)
C3	C2	C1	117.92(5)	C5	C7	C3	120.28(5)
C3	C2	C8	121.53(5)	C2	C8	C11	110.46(5)
C7	C3	C2	120.85(5)	C2	C8	C12	113.57(5)
C1	C4	C6	122.73(5)	C12	C8	C11	109.88(5)
C5	C4	C1	117.89(5)	O1	C9	N1	125.72(5)

Table II.3.26.6 Hydrogen Atom Coordinates (Å×10^4) and Isotropic Displacement Parameters (Å^2×10^3) for ab51117.

Atom	*x*	*y*	*z*	U(eq)
H1	5431(12)	4610(13)	2272(7)	23(2)
H3	8740(13)	8308(13)	1315(7)	26(3)
H5	4286(13)	8243(13)	-273(7)	27(3)
H6	2747(12)	5858(13)	1181(7)	26(3)
H7	6927(12)	9054(13)	21(7)	26(3)
H8	8163(11)	5462(12)	2787(6)	20(2)
H9	4162(11)	5234(12)	3196(6)	20(2)
H10A	1785(14)	8608(14)	150(8)	35(3)
H10B	2090(15)	8501(14)	1211(9)	37(3)
H10C	688(14)	7559(14)	561(8)	34(3)
H11A	8610(14)	8611(15)	3379(8)	36(3)
H11B	7209(14)	7535(13)	3512(8)	29(3)
H11C	8952(15)	7106(15)	4018(9)	39(3)
H12A	10224(13)	5985(14)	2105(8)	32(3)
H12B	10479(14)	7618(14)	2566(8)	32(3)
H12C	10812(14)	6092(15)	3162(8)	36(3)
H13A	3046(14)	4761(15)	-166(8)	39(3)
H13B	1281(13)	5257(14)	-274(7)	33(3)
H13C	2455(14)	6269(14)	-680(8)	32(3)

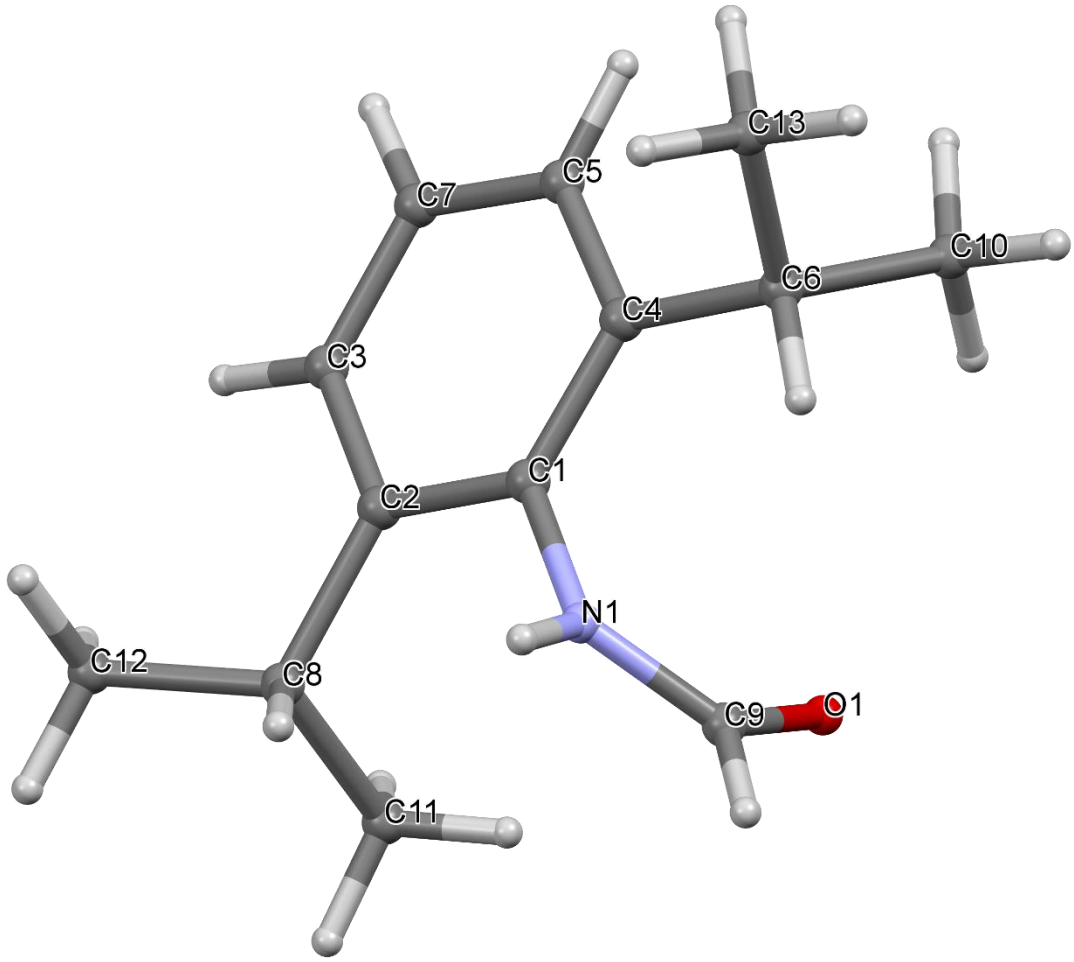

Figure II.3.26 Crystal Structure with atomic labels for compound **26**, 2,6-Isopropylaniline-N-Formamide, ab51117

II.3.27 Compound 27, 1-(4-Aminophenyl)-Ethanone, ab5201

Table II.3.27.1 Crystal data and structure refinement for ab52017.

Identification code	ab52017
Empirical formula	C_8H_9NO
Formula weight	135.16
Temperature/K	99.99
Crystal system	monoclinic
Space group	$P2_1/n$
a/Å	8.5664(4)
b/Å	5.1394(2)
c/Å	16.8345(7)
α/°	90
β/°	102.642(2)
γ/°	90
Volume/Å^3	723.19(5)
Z	4
ρ_{calc}g/cm^3	1.241
μ/mm^{-1}	0.083
F(000)	288.0
Crystal size/mm^3	0.614 × 0.244 × 0.09
Radiation	MoKα (λ = 0.71073)
2Θ range for data collection/°	4.96 to 61.23
Index ranges	$-12 \le h \le 12$, $-7 \le k \le 7$, $-24 \le l \le 24$
Reflections collected	15479
Independent reflections	2235 [R_{int} = 0.0245, R_{sigma} = 0.0152]
Data/restraints/parameters	2235/0/127
Goodness-of-fit on F^2	1.054
Final R indexes [I>=2σ (I)]	R_1 = 0.0374, wR_2 = 0.1063
Final R indexes [all data]	R_1 = 0.0434, wR_2 = 0.1131
Largest diff. peak/hole / e Å^{-3}	0.41/-0.17

Table II.3.27.2 Fractional Atomic Coordinates (×10^4) and Equivalent Isotropic Displacement Parameters (Å^2×10^3) for ab52017. U_{eq} is defined as 1/3 of of the trace of the orthogonalised U_{IJ} tensor.

Atom	*x*	*y*	*z*	U(eq)
O1	9327.9(7)	5363.4(15)	1077.8(4)	27.99(18)
N1	2523.4(9)	6772.7(15)	1959.7(5)	21.34(17)
C1	6662.5(9)	4613.2(15)	1163.3(5)	15.87(17)
C2	5333.6(10)	7394.5(16)	1980.3(5)	17.25(17)
C3	5222.0(10)	3250.4(16)	905.6(5)	19.10(18)
C4	8125.8(10)	4003.9(17)	872.3(5)	18.58(17)
C5	3880.4(9)	6063.2(16)	1698.4(5)	16.35(17)

C6	3854.1(10)	3945.4(17)	1165.3(5)	20.18(18)
C7	6687.5(9)	6684.9(16)	1712.8(5)	17.13(17)
C8	8163.5(12)	1694.2(18)	324.5(6)	26.2(2)

Table II.3.27.3 Anisotropic Displacement Parameters ($Å^2×10^3$) for ab52017. The Anisotropic displacement factor exponent takes the form: $-2\pi^2[h^2a^{*2}U_{11}+2hka^*b^*U_{12}+\ldots]$.

Atom	U_{11}	U_{22}	U_{33}	U_{23}	U_{13}	U_{12}
O1	17.5(3)	35.7(4)	31.8(4)	-3.4(3)	7.6(3)	-2.7(3)
N1	16.1(3)	22.8(4)	26.3(4)	-3.0(3)	7.3(3)	-0.2(3)
C1	15.2(3)	15.8(3)	16.7(3)	1.4(3)	3.6(3)	0.9(3)
C2	18.2(3)	16.3(3)	17.2(3)	-1.8(3)	3.8(3)	-1.0(3)
C3	19.5(4)	16.4(3)	21.9(4)	-3.9(3)	5.6(3)	-1.8(3)
C4	17.6(3)	19.6(4)	18.8(3)	3.4(3)	4.6(3)	3.4(3)
C5	15.8(3)	16.1(3)	17.6(3)	1.6(3)	4.7(3)	0.4(3)
C6	16.7(3)	19.2(4)	24.8(4)	-4.4(3)	4.9(3)	-4.0(3)
C7	15.3(3)	18.1(4)	17.2(3)	-0.8(3)	2.1(3)	-1.9(3)
C8	28.9(4)	21.7(4)	31.6(5)	-1.3(3)	14.2(4)	4.8(3)

Table II.3.27.4 Bond Lengths for ab52017.

Atom	Atom	Length/Å	Atom	Atom	Length/Å
O1	C4	1.2298(11)	C2	C5	1.4087(11)
N1	C5	1.3790(10)	C2	C7	1.3819(11)
C1	C3	1.4026(11)	C3	C6	1.3842(11)
C1	C4	1.4759(11)	C4	C8	1.5079(12)
C1	C7	1.4075(11)	C5	C6	1.4077(11)

Table II.3.27.5 Bond Angles for ab52017.

Atom	Atom	Atom	Angle/°	Atom	Atom	Atom	Angle/°
C3	C1	C4	123.03(7)	C1	C4	C8	120.23(7)
C3	C1	C7	117.83(7)	N1	C5	C2	120.57(7)
C7	C1	C4	119.13(7)	N1	C5	C6	120.72(7)
C7	C2	C5	120.32(7)	C6	C5	C2	118.69(7)
C6	C3	C1	121.45(7)	C3	C6	C5	120.28(7)
O1	C4	C1	120.39(8)	C2	C7	C1	121.38(7)
O1	C4	C8	119.38(8)				

Table II.3.27.6 Hydrogen Atom Coordinates ($Å×10^4$) and Isotropic Displacement Parameters ($Å^2×10^3$) for ab52017.

Atom	*x*	*y*	*z*	U(eq)
H1A	2552(16)	8350(30)	2199(8)	31(3)
H1B	1620(17)	6330(30)	1639(9)	35(3)
H2	5364(14)	8820(20)	2349(7)	22(3)
H3	5138(16)	1790(30)	520(8)	33(3)
H6	2823(18)	3010(30)	952(9)	41(4)
H7	7687(16)	7650(30)	1914(8)	31(3)
H8A	7174(17)	1540(30)	-109(8)	37(3)
H8B	9090(20)	1880(30)	54(10)	54(4)
H8C	8327(19)	180(30)	651(10)	52(4)

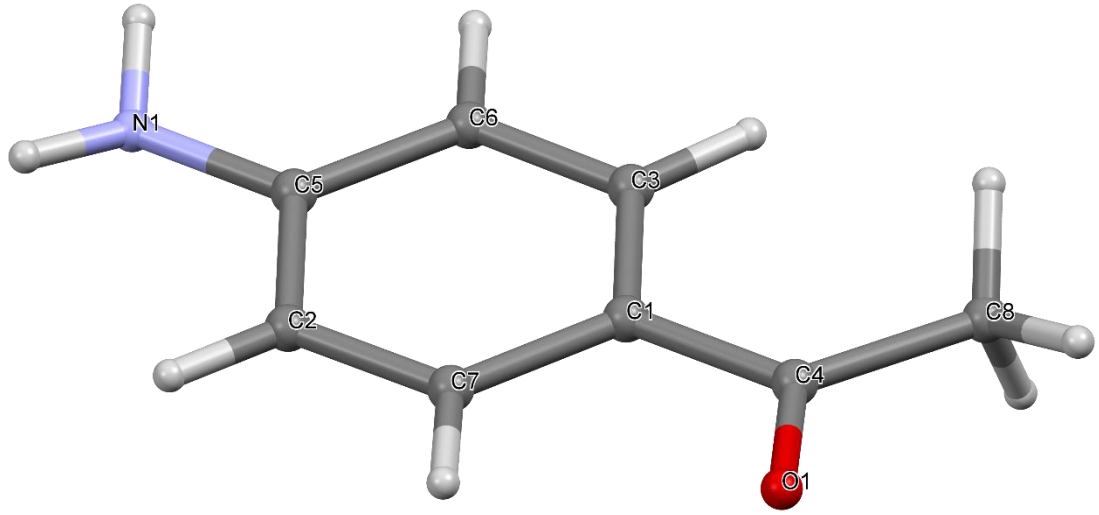

Figure II.3.27 Crystal Structure with atomic labels for compound **27**, 1-(4-Aminophenyl)-Ethanone, ab52017

II.3.28 Compound 28, 3-Chloroaniline-N-Formamide, ab50817a

Table II.3.28.1 Crystal data and structure refinement for ab50817a.

Identification code	ab50817a
Empirical formula	C_7H_6ClNO
Formula weight	155.58
Temperature/K	100.02
Crystal system	monoclinic
Space group	$P2_1/c$
a/Å	8.2862(5)
b/Å	12.1839(7)
c/Å	6.8176(4)
α/°	90
β/°	92.892(4)
γ/°	90
Volume/Å^3	687.42(7)
Z	4
ρ_{calc}g/cm^3	1.503
μ/mm^{-1}	0.474
F(000)	320.0
Crystal size/mm^3	0.255 × 0.082 × 0.076
Radiation	MoKα (λ = 0.71073)
2Θ range for data collection/°	4.922 to 60.442
Index ranges	-11 ≤ h ≤ 11, -17 ≤ k ≤ 17, -9 ≤ l ≤ 9
Reflections collected	15234
Independent reflections	2042 [R_{int} = 0.0493, R_{sigma} = 0.0296]
Data/restraints/parameters	2042/0/115
Goodness-of-fit on F^2	1.027
Final R indexes [I>=2σ (I)]	R_1 = 0.0342, wR_2 = 0.0831
Final R indexes [all data]	R_1 = 0.0466, wR_2 = 0.0892
Largest diff. peak/hole / e Å^{-3}	0.36/-0.27

Table II.3.28.2 Fractional Atomic Coordinates (×10^4) and Equivalent Isotropic Displacement Parameters (Å^2×10^3) for ab50817a. U_{eq} is defined as 1/3 of of the trace of the orthogonalised U_{IJ} tensor.

Atom	*x*	*y*	*z*	U(eq)
Cl1	9157.8(4)	1508.1(3)	1773.4(5)	26.78(12)
O1	5065.8(13)	1519.5(7)	10026.7(15)	22.2(2)
N1	6096.8(14)	339.7(9)	7839.4(16)	18.3(2)
C1	7758.5(17)	-1353.0(12)	3957(2)	23.1(3)
C2	6873.1(14)	72.5(10)	6102.7(18)	16.1(2)
C3	6972.8(16)	-1037.6(11)	5613(2)	19.0(3)
C4	8307.3(15)	513.2(11)	3249.5(19)	19.3(3)
C5	8442.0(17)	-582.8(12)	2750(2)	22.9(3)

C6	7536.9(15)	861.2(11)	4905.1(19)	18.7(3)
C7	5741.5(17)	1346.1(11)	8487(2)	19.2(3)

Table II.3.28.3 Anisotropic Displacement Parameters ($Å^2×10^3$) for ab50817a. The Anisotropic displacement factor exponent takes the form: $-2\pi^2[h^2a^{*2}U_{11}+2hka^*b^*U_{12}+\ldots]$.

Atom	U_{11}	U_{22}	U_{33}	U_{23}	U_{13}	U_{12}
Cl1	25.04(19)	31.8(2)	24.26(19)	6.88(14)	9.08(13)	-0.14(14)
O1	31.9(5)	17.3(5)	17.8(5)	-0.9(4)	6.3(4)	1.3(4)
N1	26.3(6)	14.2(5)	14.9(5)	1.6(4)	5.5(4)	0.2(4)
C1	25.7(7)	19.1(7)	24.4(7)	-4.2(5)	1.3(5)	4.1(5)
C2	16.5(6)	16.9(6)	14.7(6)	-0.3(4)	0.3(4)	1.8(5)
C3	21.4(6)	15.6(6)	19.9(6)	0.1(5)	0.4(5)	1.4(5)
C4	16.7(6)	23.9(6)	17.3(6)	2.9(5)	2.4(5)	0.2(5)
C5	21.1(6)	28.3(7)	19.6(6)	-4.4(6)	4.0(5)	4.1(5)
C6	21.6(6)	16.0(6)	18.6(6)	-0.9(5)	2.6(5)	0.8(5)
C7	24.9(6)	16.2(6)	16.9(6)	0.3(5)	3.2(5)	0.0(5)

Table II.3.28.4 Bond Lengths for ab50817a.

Atom	Atom	Length/Å	Atom	Atom	Length/Å
Cl1	C4	1.7465(13)	C1	C5	1.388(2)
O1	C7	1.2329(16)	C2	C3	1.3966(18)
N1	C2	1.4138(16)	C2	C6	1.3921(18)
N1	C7	1.3408(17)	C4	C5	1.384(2)
C1	C3	1.385(2)	C4	C6	1.3907(18)

Table II.3.28.5 Bond Angles for ab50817a.

Atom	Atom	Atom	Angle/°	Atom	Atom	Atom	Angle/°
C7	N1	C2	127.08(12)	C5	C4	Cl1	119.21(10)
C3	C1	C5	121.21(13)	C5	C4	C6	122.67(13)
C3	C2	N1	117.28(12)	C6	C4	Cl1	118.11(10)
C6	C2	N1	122.83(12)	C4	C5	C1	117.79(13)
C6	C2	C3	119.89(12)	C4	C6	C2	118.47(12)
C1	C3	C2	119.96(13)	O1	C7	N1	123.62(13)

Table II.3.28.6 Hydrogen Atom Coordinates ($Å×10^4$) and Isotropic Displacement Parameters ($Å^2×10^3$) for ab50817a.

Atom	*x*	*y*	*z*	U(eq)
H1	5780(20)	-168(16)	8470(30)	27(5)

H1A	7840(20)	-2111(17)	3680(30)	35(5)
H3	6500(20)	-1574(13)	6380(30)	22(4)
H5	8963(19)	-781(15)	1670(30)	26(4)
H6	7490(20)	1617(15)	5190(30)	27(5)
H7	6045(19)	1932(15)	7630(30)	24(4)

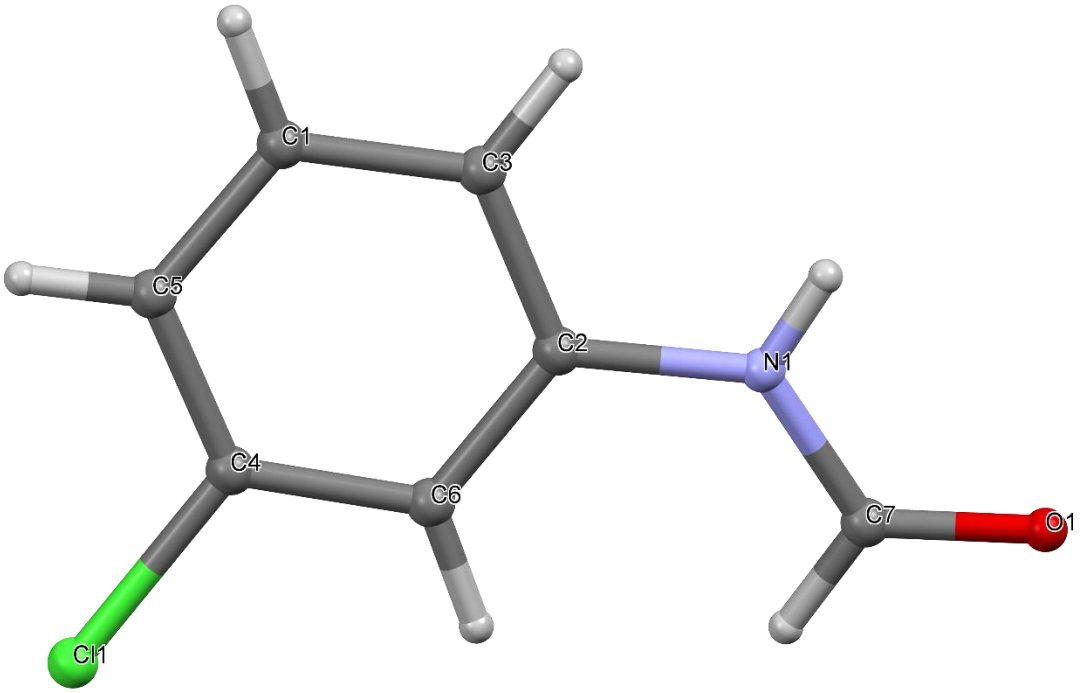

Figure II.3.28 Crystal Structure with atomic labels for compound **28**, 3-Chloroaniline-N-Formamide, ab50817a

II.3.29 Compound 29, 4-Iodoaniline-N-Formamide, ab52217

Table II.3.29.1 Crystal data and structure refinement for b52217.

Identification code	b52217
Empirical formula	C_7H_6INO
Formula weight	247.03
Temperature/K	99.99
Crystal system	orthorhombic
Space group	$P2_12_12_1$
a/Å	4.5281(2)
b/Å	10.3642(5)
c/Å	16.2095(8)
α/°	90
β/°	90
γ/°	90
Volume/Å^3	760.71(6)
Z	4
ρ_{calc}g/cm^3	2.157
μ/mm^{-1}	4.136
F(000)	464.0
Crystal size/mm^3	0.42 × 0.215 × 0.129
Radiation	MoKα (λ = 0.71073)
2Θ range for data collection/°	4.664 to 68.494
Index ranges	$-7 \le h \le 7$, $-15 \le k \le 15$, $-24 \le l \le 25$
Reflections collected	19714
Independent reflections	3011 [R_{int} = 0.0285, R_{sigma} = 0.0186]
Data/restraints/parameters	3011/0/115
Goodness-of-fit on F^2	1.391
Final R indexes [I>=2σ (I)]	R_1 = 0.0228, wR_2 = 0.0565
Final R indexes [all data]	R_1 = 0.0230, wR_2 = 0.0566
Largest diff. peak/hole / e Å^{-3}	1.51/-1.70
Flack parameter	0.042(13)

Table II.3.29.2 Fractional Atomic Coordinates (×10^4) and Equivalent Isotropic Displacement Parameters (Å^2×10^3) for b52217. U_{eq} is defined as 1/3 of of the trace of the orthogonalised U_{IJ} tensor.

Atom	*x*	*y*	*z*	U(eq)
I1	1849.7(5)	7767.4(2)	1243.9(2)	15.90(6)
O1	2159(6)	14652(3)	1377.9(18)	15.3(5)
N1	6458(6)	13502(3)	1263(3)	13.6(5)
C1	3239(8)	9697(3)	1232(2)	13.0(5)
C2	5276(7)	12234(3)	1245(2)	11.9(5)
C3	3140(9)	11835(3)	1818(2)	14.0(6)
C4	2117(9)	10571(4)	1809(2)	13.4(6)
C5	5348(9)	10084(4)	656(2)	14.2(6)

C6	6352(9)	11356(3)	663(2)	13.9(7)
C7	4871(8)	14587(3)	1334(3)	12.2(6)

Table II.3.29.3 Anisotropic Displacement Parameters ($Å^2×10^3$) for b52217. The Anisotropic displacement factor exponent takes the form: $-2\pi^2[h^2a^{*2}U_{11}+2hka^*b^*U_{12}+\ldots]$.

Atom	U_{11}	U_{22}	U_{33}	U_{23}	U_{13}	U_{12}
I1	17.10(9)	11.14(8)	19.46(9)	0.61(9)	1.76(10)	-2.83(8)
O1	8.1(11)	12.8(10)	25.1(15)	-1.8(10)	-0.7(11)	-1.6(8)
N1	11.0(11)	10.3(11)	19.4(12)	-0.2(12)	-0.6(14)	-1.5(9)
C1	13.2(12)	12.1(12)	13.8(12)	1.5(13)	-1.1(19)	-1.6(11)
C2	10.7(11)	10.8(11)	14.3(12)	2.7(16)	-0.9(13)	0.8(11)
C3	13.4(14)	13.7(13)	14.9(13)	-0.7(11)	1.3(14)	0.8(13)
C4	13.7(15)	12.6(13)	13.8(13)	1.1(11)	2.6(13)	-0.1(13)
C5	18.5(16)	9.2(14)	14.9(15)	-0.5(11)	3.1(12)	-0.2(13)
C6	16.9(17)	9.8(14)	15.1(15)	-0.2(11)	4.2(12)	0.3(11)
C7	10.2(13)	9.4(12)	17.1(16)	0.9(12)	-1.7(13)	-2.1(10)

Table II.3.29.4 Bond Lengths for b52217.

Atom	Atom	Length/Å	Atom	Atom	Length/Å
I1	C1	2.096(3)	C1	C5	1.394(5)
O1	C7	1.232(4)	C2	C3	1.404(5)
N1	C2	1.419(4)	C2	C6	1.398(5)
N1	C7	1.340(4)	C3	C4	1.390(5)
C1	C4	1.398(5)	C5	C6	1.394(5)

Table II.3.29.5 Bond Angles for b52217.

Atom	Atom	Atom	Angle/°	Atom	Atom	Atom	Angle/°
C7	N1	C2	125.2(3)	C6	C2	C3	119.7(3)
C4	C1	I1	120.2(3)	C4	C3	C2	120.0(3)
C5	C1	I1	119.1(3)	C3	C4	C1	119.8(3)
C5	C1	C4	120.7(3)	C1	C5	C6	119.4(3)
C3	C2	N1	121.2(3)	C5	C6	C2	120.5(3)
C6	C2	N1	119.0(3)	O1	C7	N1	125.9(3)

Table II.3.29.6 Hydrogen Atom Coordinates ($Å×10^4$) and Isotropic Displacement Parameters ($Å^2×10^3$) for b52217.

Atom	*x*	*y*	*z*	U(eq)
H1	8430(110)	13530(40)	1230(40)	8(10)

H3	2340(120)	12420(50)	2210(30)	12(12)
H4	540(140)	10290(60)	2200(30)	20(14)
H5	6120(130)	9490(60)	280(30)	17(14)
H6	7930(150)	11610(60)	280(40)	26(15)
H7	5960(100)	15400(40)	1370(30)	-1(9)

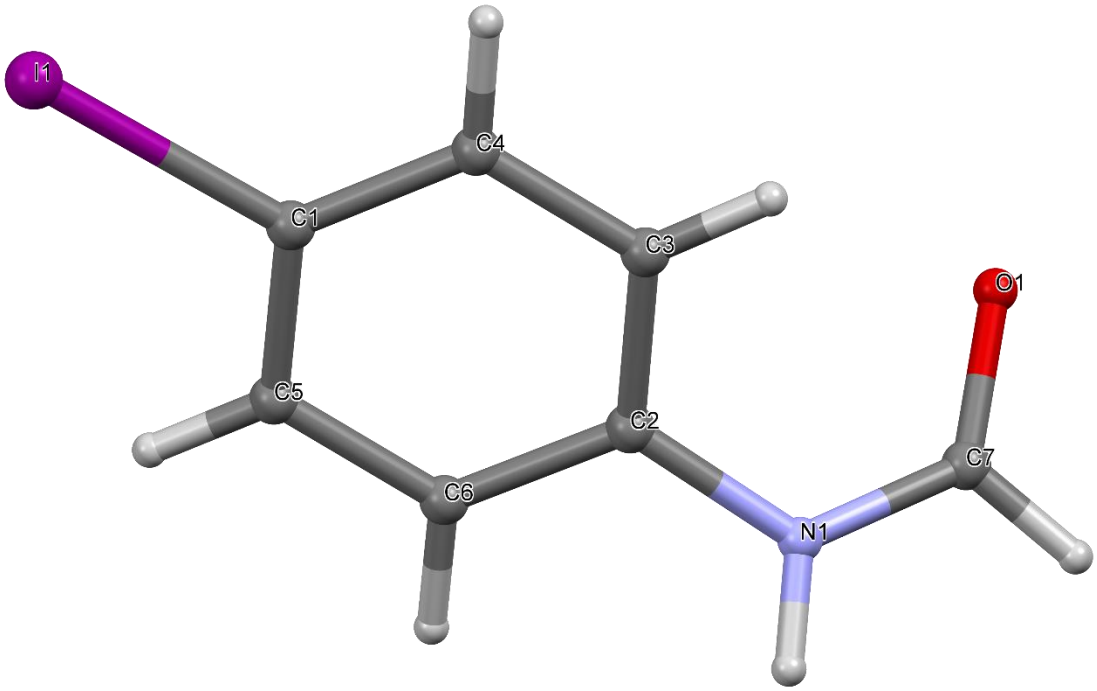

Figure II.3.29 Crystal Structure with atomic labels for compound **29**, 4-Iodoaniline-N-Formamide, ab52217

II.3.30 Compound 30, *o*-Anisidine-N-Formamide, ab54816

Table II.3.30.1 Crystal data and structure refinement for ab54816.

Identification code	ab54816
Empirical formula	$C_8H_9NO_2$
Formula weight	151.16
Temperature/K	100.0
Crystal system	monoclinic
Space group	C2/c
a/Å	14.9152(5)
b/Å	12.8447(4)
c/Å	8.4326(3)
α/°	90
β/°	111.9307(16)
γ/°	90
Volume/Å^3	1498.62(9)
Z	8
ρ_{calc}g/cm^3	1.340
μ/mm^{-1}	0.097
F(000)	640.0
Crystal size/mm^3	0.77 × 0.126 × 0.102
Radiation	MoKα (λ = 0.71073)
2Θ range for data collection/°	4.326 to 64.476
Index ranges	-22 ≤ h ≤ 22, -19 ≤ k ≤ 18, -12 ≤ l ≤ 12
Reflections collected	18714
Independent reflections	2660 [R_{int} = 0.0260, R_{sigma} = 0.0151]
Data/restraints/parameters	2660/0/136
Goodness-of-fit on F^2	1.069
Final R indexes [I>=2σ (I)]	R_1 = 0.0401, wR_2 = 0.1171
Final R indexes [all data]	R_1 = 0.0478, wR_2 = 0.1277
Largest diff. peak/hole / e Å^{-3}	0.44/-0.24

Table II.3.30.2 Fractional Atomic Coordinates (×10^4) and Equivalent Isotropic Displacement Parameters (Å^2×10^3) for ab54816. U_{eq} is defined as 1/3 of of the trace of the orthogonalised U_{IJ} tensor.

Atom	*x*	*y*	*z*	U(eq)
O1	4033.5(5)	2115.0(5)	110.8(7)	23.18(15)
O2	3877.5(6)	555.1(5)	5222.8(8)	28.86(17)
N1	3752.3(5)	1026.0(5)	2513.9(8)	20.33(16)
C1	3765.5(5)	2687.1(6)	1225.6(9)	18.53(16)
C2	3881.7(6)	350.0(6)	3798.5(10)	22.54(17)
C3	3611.8(6)	2108.8(6)	2521.0(9)	18.11(16)
C4	3643.7(6)	3761.4(6)	1152.8(10)	23.44(18)
C5	4194.4(7)	2663.3(7)	-1234.4(12)	26.87(19)
C6	3318.0(6)	2618.9(6)	3703.5(10)	22.64(17)

C7	3179.9(7)	3696.6(7)	3604.6(11)	27.05(19)
C8	3349.1(7)	4260.8(6)	2346.6(11)	26.80(19)

Table II.3.30.3 Anisotropic Displacement Parameters ($Å^2×10^3$) for ab54816. The Anisotropic displacement factor exponent takes the form: $-2\pi^2[h^2a^{*2}U_{11}+2hka^*b^*U_{12}+\ldots]$.

Atom	U_{11}	U_{22}	U_{33}	U_{23}	U_{13}	U_{12}
O1	35.5(3)	19.9(3)	20.5(3)	1.78(19)	17.9(2)	0.9(2)
O2	49.9(4)	23.2(3)	18.3(3)	2.1(2)	18.4(3)	1.2(3)
N1	32.8(4)	16.0(3)	15.2(3)	-0.5(2)	12.4(3)	-0.5(2)
C1	22.5(3)	18.0(3)	16.0(3)	-0.1(2)	8.3(3)	-0.4(2)
C2	34.0(4)	17.7(3)	18.8(3)	1.1(2)	13.3(3)	-0.9(3)
C3	23.2(3)	16.3(3)	15.1(3)	-0.7(2)	7.5(2)	-0.8(2)
C4	31.5(4)	17.8(3)	21.3(4)	2.0(3)	10.3(3)	-0.2(3)
C5	36.8(5)	26.3(4)	24.9(4)	5.2(3)	20.2(4)	0.7(3)
C6	32.4(4)	20.2(3)	18.1(3)	-1.5(3)	12.6(3)	0.8(3)
C7	39.5(5)	20.8(4)	22.8(4)	-3.1(3)	14.0(3)	3.5(3)
C8	38.6(5)	17.2(3)	24.7(4)	-0.5(3)	11.8(3)	2.4(3)

Table II.3.30.4 Bond Lengths for ab54816.

Atom	Atom	Length/Å	Atom	Atom	Length/Å
O1	C1	1.3653(9)	C1	C4	1.3901(11)
O1	C5	1.4295(9)	C3	C6	1.3935(10)
O2	C2	1.2319(10)	C4	C8	1.3959(12)
N1	C2	1.3448(10)	C6	C7	1.3974(11)
N1	C3	1.4069(10)	C7	C8	1.3835(12)
C1	C3	1.4088(10)			

Table II.3.30.5 Bond Angles for ab54816.

Atom	Atom	Atom	Angle/°	Atom	Atom	Atom	Angle/°
C1	O1	C5	117.41(6)	C6	C3	N1	123.71(7)
C2	N1	C3	127.71(6)	C6	C3	C1	119.52(7)
O1	C1	C3	115.11(7)	C1	C4	C8	119.70(7)
O1	C1	C4	124.81(7)	C3	C6	C7	120.12(7)
C4	C1	C3	120.07(7)	C8	C7	C6	119.98(7)
O2	C2	N1	126.57(8)	C7	C8	C4	120.59(8)
N1	C3	C1	116.76(6)				

Table II.3.30.6 Hydrogen Atom Coordinates (Å×10^4) and Isotropic Displacement Parameters (Å^2×10^3) for ab54816.

Atom	*x*	*y*	*z*	U(eq)
H1	3800(10)	766(11)	1550(18)	38(4)
H2	3995(9)	-365(10)	3460(17)	29(3)
H4	3778(9)	4159(10)	213(16)	30(3)
H5A	3603(9)	2991(10)	-1953(16)	27(3)
H5B	4738(9)	3149(11)	-778(17)	32(3)
H5C	4391(11)	2124(12)	-1870(20)	43(4)
H6	3218(10)	2205(11)	4585(17)	34(3)
H7	2961(10)	4048(11)	4467(17)	38(3)
H8	3252(10)	5031(12)	2289(19)	45(4)

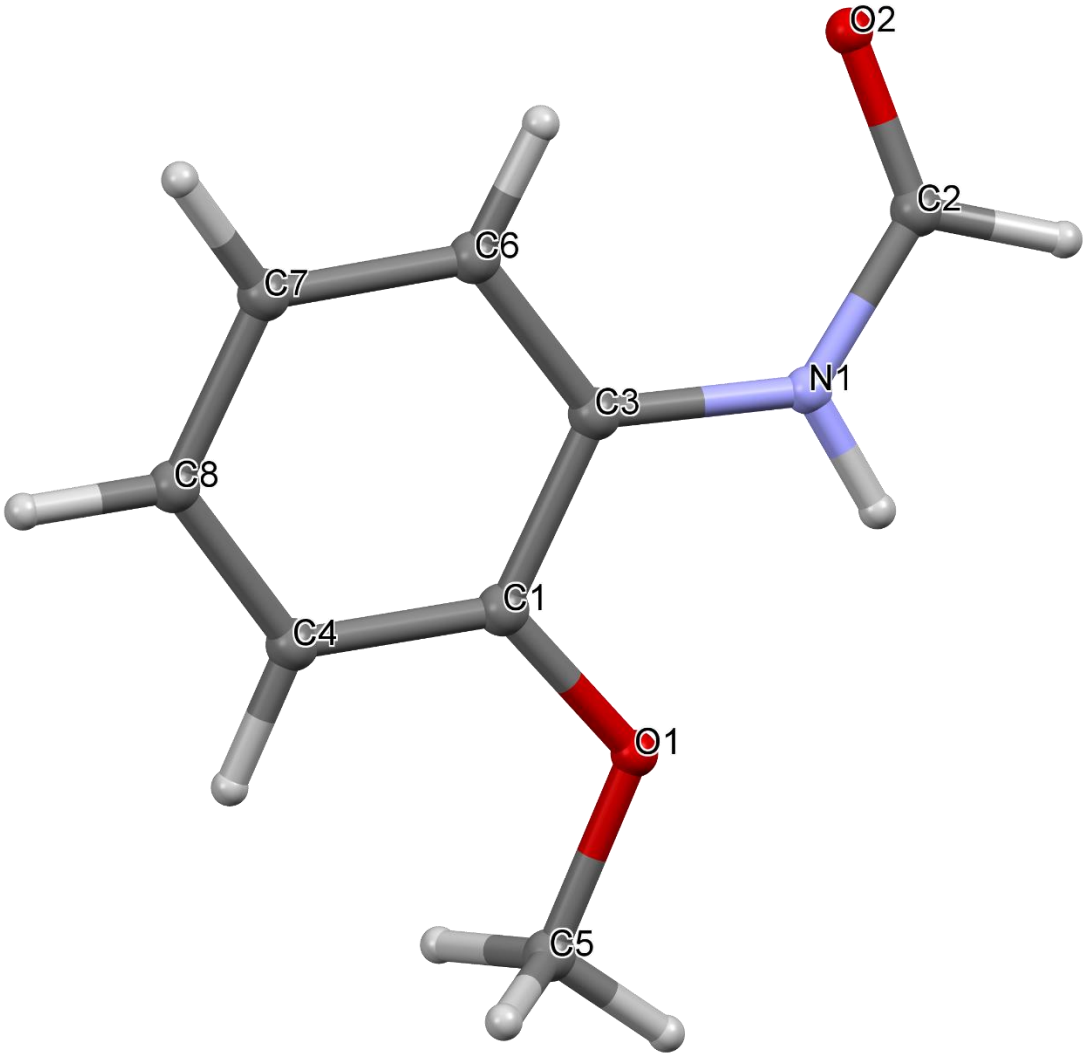

Figure II.3.30 Crystal Structure with atomic labels for compound **30**, *o*-Anisidine-N-Formamide, ab54816

II.3.31 Compound 31, *o*-Phenetidine-N-Formamide, ab58316

Table II.3.31.1 Crystal data and structure refinement for ab58316.

Identification code	ab58316
Empirical formula	$C_{18}H_{22}N_2O_4$
Formula weight	330.37
Temperature/K	100.0
Crystal system	monoclinic
Space group	$P2_1/c$
a/Å	7.7260(7)
b/Å	7.5519(7)
c/Å	29.135(3)
α/°	90
β/°	91.836(5)
γ/°	90
Volume/Å^3	1699.0(3)
Z	4
ρ_{calc}g/cm^3	1.292
μ/mm^{-1}	0.092
F(000)	704.0
Crystal size/mm^3	0.325 × 0.302 × 0.169
Radiation	MoKα (λ = 0.71073)
2Θ range for data collection/°	5.276 to 62.556
Index ranges	$-11 \le h \le 11$, $-11 \le k \le 10$, $-42 \le l \le 40$
Reflections collected	39677
Independent reflections	5525 [R_{int} = 0.0451, R_{sigma} = 0.0242]
Data/restraints/parameters	5525/0/305
Goodness-of-fit on F^2	1.038
Final R indexes [I>=2σ (I)]	R_1 = 0.0386, wR_2 = 0.1007
Final R indexes [all data]	R_1 = 0.0467, wR_2 = 0.1071
Largest diff. peak/hole / e Å^{-3}	0.40/-0.21

Table II.3.31.2 Fractional Atomic Coordinates (×10^4) and Equivalent Isotropic Displacement Parameters (Å^2×10^3) for ab58316. U_{eq} is defined as 1/3 of of the trace of the orthogonalised U_{IJ} tensor.

Atom	*x*	*y*	*z*	U(eq)
O1	6550.7(8)	7793.2(9)	500.0(2)	18.58(13)
O2	1385.6(9)	4702.4(11)	1003.7(3)	29.00(16)
N1	3895.5(9)	6226.5(10)	871.9(2)	17.57(14)
C1	5197.8(10)	7406.9(11)	201.1(3)	15.65(15)
C2	3753.5(10)	6603.8(11)	398.0(3)	15.44(15)
C3	5180.3(11)	7741.4(12)	-268.4(3)	18.35(16)
C4	8040.7(11)	8625.9(12)	309.1(3)	18.84(16)
C5	2300.9(11)	6194.1(11)	121.2(3)	17.92(16)

C6	3729.3(11)	7305.5(12)	-542.3(3)	19.60(16)
C7	2290.4(11)	6547.2(12)	-348.3(3)	19.40(16)
C8	2797.5(11)	5304.0(12)	1129.6(3)	20.77(17)
C9	9290.3(12)	9070.0(14)	700.5(4)	24.69(19)
O3	891.8(8)	1088.1(9)	1680.3(2)	20.97(14)
O4	-3612.1(9)	5623.7(10)	1641.6(2)	26.31(15)
N2	-1265.7(9)	3742.7(10)	1611.8(3)	19.14(15)
C10	2251.6(12)	-193.8(13)	1745.5(3)	24.04(18)
C11	3673.3(13)	293.4(14)	1427.9(4)	26.76(19)
C12	-835.0(13)	-462.3(13)	2243.2(3)	25.09(19)
C13	-2313.8(14)	-441.4(14)	2507.9(3)	27.9(2)
C14	-2185.3(11)	5213.1(13)	1504.7(3)	21.60(17)
C15	-1700.7(11)	2359.8(11)	1911.2(3)	17.05(15)
C16	-3167.9(11)	2357.3(12)	2177.9(3)	20.28(17)
C17	-525.2(11)	940.0(12)	1948.0(3)	18.80(16)
C18	-3460.1(12)	957.1(14)	2477.7(3)	24.64(19)

Table II.3.31.3 Anisotropic Displacement Parameters ($Å^2×10^3$) for ab58316. The Anisotropic displacement factor exponent takes the form: $-2\pi^2[h^2a^{*2}U_{11}+2hka^*b^*U_{12}+\ldots]$.

Atom	U_{11}	U_{22}	U_{33}	U_{23}	U_{13}	U_{12}
O1	15.0(3)	21.8(3)	19.0(3)	1.5(2)	1.0(2)	-3.4(2)
O2	19.1(3)	39.0(4)	29.0(4)	10.7(3)	3.7(3)	-5.7(3)
N1	16.1(3)	19.4(3)	17.3(3)	1.1(2)	2.4(2)	-0.3(3)
C1	14.8(3)	14.0(3)	18.2(3)	-0.4(3)	1.4(3)	0.8(3)
C2	16.1(3)	14.0(3)	16.4(3)	0.2(3)	2.9(3)	1.4(3)
C3	18.2(4)	18.4(4)	18.6(4)	1.2(3)	3.7(3)	0.3(3)
C4	15.6(3)	18.2(4)	22.9(4)	2.1(3)	2.5(3)	-2.0(3)
C5	15.7(3)	17.1(4)	21.0(4)	0.3(3)	1.4(3)	0.0(3)
C6	22.0(4)	19.4(4)	17.4(4)	0.9(3)	1.3(3)	1.6(3)
C7	18.8(4)	18.6(4)	20.7(4)	-1.0(3)	-1.2(3)	0.3(3)
C8	18.6(4)	24.0(4)	19.9(4)	4.8(3)	4.5(3)	2.7(3)
C9	19.6(4)	25.4(4)	28.8(4)	4.5(4)	-3.3(3)	-4.5(3)
O3	19.3(3)	23.7(3)	20.1(3)	4.7(2)	3.6(2)	3.4(2)
O4	22.6(3)	30.8(4)	25.7(3)	3.6(3)	3.3(3)	5.5(3)
N2	16.5(3)	22.3(4)	18.8(3)	4.4(3)	2.4(2)	-0.1(3)
C10	23.7(4)	24.1(4)	24.3(4)	3.1(3)	1.3(3)	4.9(3)
C11	22.7(4)	29.5(5)	28.3(5)	-1.4(4)	3.5(3)	2.4(4)
C12	28.5(4)	24.0(4)	22.8(4)	5.9(3)	1.3(3)	0.1(4)
C13	32.7(5)	28.4(5)	23.0(4)	8.2(4)	4.5(4)	-5.0(4)
C14	20.3(4)	23.5(4)	21.0(4)	4.5(3)	0.7(3)	0.1(3)
C15	17.2(3)	19.8(4)	14.1(3)	0.9(3)	-0.3(3)	-3.2(3)
C16	18.6(4)	24.7(4)	17.7(4)	-0.2(3)	2.2(3)	-3.0(3)
C17	19.7(4)	21.7(4)	15.1(3)	1.5(3)	0.7(3)	-1.6(3)
C18	23.9(4)	30.8(5)	19.5(4)	2.5(3)	5.1(3)	-6.4(4)

Table II.3.31.4 Bond Lengths for ab58316.

Atom	Atom	Length/Å	Atom	Atom	Length/Å
O1	C1	1.3704(10)	O3	C10	1.4367(11)
O1	C4	1.4391(10)	O3	C17	1.3688(10)
O2	C8	1.2268(11)	O4	C14	1.2242(11)
N1	C2	1.4106(11)	N2	C14	1.3494(12)
N1	C8	1.3453(11)	N2	C15	1.4083(11)
C1	C2	1.4082(11)	C10	C11	1.5044(14)
C1	C3	1.3904(12)	C12	C13	1.3987(14)
C2	C5	1.3955(11)	C12	C17	1.3900(13)
C3	C6	1.3945(12)	C13	C18	1.3793(15)
C4	C9	1.5080(13)	C15	C16	1.3948(11)
C5	C7	1.3934(12)	C15	C17	1.4070(12)
C6	C7	1.3869(12)	C16	C18	1.3944(13)

Table II.3.31.5 Bond Angles for ab58316.

Atom	Atom	Atom	Angle/°	Atom	Atom	Atom	Angle/°
C1	O1	C4	116.79(7)	C17	O3	C10	117.67(7)
C8	N1	C2	128.34(8)	C14	N2	C15	128.25(7)
O1	C1	C2	115.53(7)	O3	C10	C11	107.40(8)
O1	C1	C3	124.73(7)	C17	C12	C13	119.50(9)
C3	C1	C2	119.74(7)	C18	C13	C12	120.50(9)
C1	C2	N1	116.61(7)	O4	C14	N2	127.30(9)
C5	C2	N1	123.83(7)	C16	C15	N2	124.09(8)
C5	C2	C1	119.55(7)	C16	C15	C17	119.38(8)
C1	C3	C6	120.16(8)	C17	C15	N2	116.49(7)
O1	C4	C9	107.80(7)	C18	C16	C15	120.05(9)
C7	C5	C2	120.27(8)	O3	C17	C12	124.86(8)
C7	C6	C3	120.29(8)	O3	C17	C15	114.86(7)
C6	C7	C5	119.97(8)	C12	C17	C15	120.28(8)
O2	C8	N1	126.54(9)	C13	C18	C16	120.27(8)

Table II.3.31.6 Hydrogen Atom Coordinates (Å×10^4) and Isotropic Displacement Parameters (Å^2×10^3) for ab58316.

Atom	*x*	*y*	*z*	U(eq)
H1	4908(16)	6534(17)	1007(4)	24(3)
H3	6169(16)	8282(17)	-405(4)	24(3)
H4A	7676(14)	9704(16)	148(4)	17(3)
H4B	8575(15)	7786(16)	89(4)	22(3)
H5	1317(16)	5638(16)	264(4)	22(3)

H6	3737(16)	7542(17)	-878(4)	27(3)
H7	1257(16)	6261(17)	-530(4)	25(3)
H8	3250(16)	5180(17)	1442(5)	27(3)
H9A	9810(18)	8000(20)	851(5)	38(4)
H9B	8712(18)	9760(20)	946(5)	37(4)
H9C	10281(18)	9771(19)	589(5)	38(4)
H2	-228(18)	3637(18)	1476(5)	31(3)
H10A	1788(17)	-1406(19)	1681(4)	31(3)
H10B	2647(17)	-143(18)	2070(5)	31(3)
H11A	4048(18)	1540(20)	1480(5)	36(4)
H11B	4683(19)	-488(19)	1478(5)	38(4)
H11C	3250(19)	140(20)	1100(5)	40(4)
H12	-11(17)	-1444(18)	2270(4)	29(3)
H13	-2521(18)	-1440(20)	2711(5)	40(4)
H14	-1567(17)	5960(17)	1291(4)	26(3)
H16	-3954(16)	3326(17)	2154(4)	23(3)
H18	-4469(18)	987(19)	2663(5)	33(3)

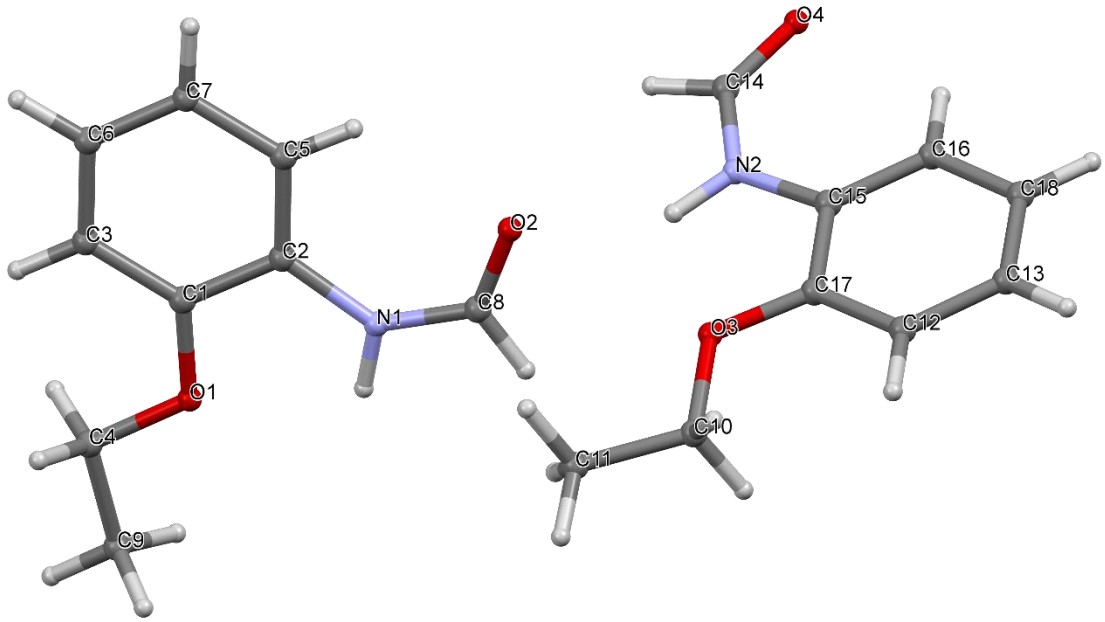

Figure II.3.21 Crystal Structure with atomic labels for compound **32**, 1-Amino-2-Methylnaphthyene-N-Formamide, ab50517

II.3.32 Compound 32, 1-Amino-2-Methylnaphthyene-N-Formamide, ab50517

Table II.3.32.1 Crystal data and structure refinement for ab50517.

Identification code	ab50517
Empirical formula	$C_{12}H_{11}NO$
Formula weight	185.22
Temperature/K	115.21
Crystal system	monoclinic
Space group	$P2_1/n$
a/Å	4.5837(2)
b/Å	14.0066(7)
c/Å	14.4781(7)
α/°	90
β/°	96.386(3)
γ/°	90
Volume/Å^3	923.76(8)
Z	4
ρ_{calc}g/cm^3	1.332
μ/mm^{-1}	0.085
F(000)	392.0
Crystal size/mm^3	0.253 × 0.205 × 0.074
Radiation	MoKα (λ = 0.71073)
2Θ range for data collection/°	4.058 to 60.722
Index ranges	$-6 \le h \le 6$, $-19 \le k \le 19$, $-19 \le l \le 20$
Reflections collected	20566
Independent reflections	2777 [R_{int} = 0.0306, R_{sigma} = 0.0185]
Data/restraints/parameters	2777/0/128
Goodness-of-fit on F^2	1.078
Final R indexes [I>=2σ (I)]	R_1 = 0.0454, wR_2 = 0.1257
Final R indexes [all data]	R_1 = 0.0527, wR_2 = 0.1314
Largest diff. peak/hole / e Å^{-3}	0.45/-0.33

Table II.3.32.2 Fractional Atomic Coordinates (×10^4) and Equivalent Isotropic Displacement Parameters (Å^2×10^3) for ab50517. U_{eq} is defined as 1/3 of of the trace of the orthogonalised U_{IJ} tensor.

Atom	*x*	*y*	*z*	U(eq)
O1	6751.5(17)	5764.7(6)	5886.5(6)	18.8(2)
N1	2685(2)	6191.0(6)	6588.9(6)	13.86(19)
C1	6251(2)	6632.0(7)	7933.5(7)	12.5(2)
C2	7509(2)	7352.2(8)	8551.8(7)	14.3(2)
C3	2931(2)	7821.5(8)	7139.7(7)	14.2(2)
C4	3990(2)	6896.3(7)	7222.3(7)	12.2(2)
C5	9495(3)	5464.1(9)	8752.8(8)	18.0(2)
C6	4166(2)	8517.6(8)	7780.5(8)	16.8(2)

C7	7295(2)	5679.2(8)	8060.8(8)	15.0(2)
C8	564(2)	8098.4(8)	6382.1(8)	17.7(2)
C9	9819(2)	7109.1(9)	9248.7(7)	17.5(2)
C10	6399(3)	8299.3(8)	8458.5(8)	17.1(2)
C11	4110(2)	5713.0(8)	5969.1(7)	14.7(2)
C12	10803(3)	6186.7(9)	9343.7(8)	19.7(2)

Table II.3.32.3 Anisotropic Displacement Parameters ($Å^2×10^3$) for ab50517. The Anisotropic displacement factor exponent takes the form: $-2\pi^2[h^2a^{*2}U_{11}+2hka^*b^*U_{12}+\ldots]$.

Atom	U_{11}	U_{22}	U_{33}	U_{23}	U_{13}	U_{12}
O1	13.6(4)	25.0(4)	17.9(4)	-5.4(3)	1.8(3)	-0.7(3)
N1	10.7(4)	14.6(4)	15.9(4)	-1.9(3)	-0.1(3)	-2.1(3)
C1	12.2(4)	13.7(5)	11.9(4)	-0.4(3)	1.7(3)	-1.8(3)
C2	14.2(5)	16.5(5)	12.4(5)	-2.1(4)	2.6(4)	-3.3(4)
C3	13.0(4)	14.5(5)	15.3(5)	0.5(4)	3.3(4)	0.1(4)
C4	10.8(4)	13.5(5)	12.5(4)	-0.9(3)	1.6(3)	-1.9(3)
C5	19.0(5)	19.2(5)	15.4(5)	2.3(4)	0.3(4)	1.5(4)
C6	18.9(5)	13.3(5)	18.5(5)	-1.5(4)	4.2(4)	-0.4(4)
C7	15.5(5)	14.9(5)	14.6(5)	0.5(3)	1.4(4)	-0.7(4)
C8	16.0(5)	17.8(5)	19.3(5)	2.0(4)	1.3(4)	2.8(4)
C9	16.4(5)	23.5(6)	12.3(5)	-2.3(4)	-0.2(4)	-3.6(4)
C10	20.5(5)	15.0(5)	16.2(5)	-3.4(4)	2.9(4)	-2.9(4)
C11	15.2(5)	15.0(5)	13.3(5)	-0.9(3)	-0.6(4)	-1.1(4)
C12	18.5(5)	26.1(6)	13.6(5)	1.2(4)	-1.5(4)	-1.0(4)

Table II.3.32.4 Bond Lengths for ab50517.

Atom	Atom	Length/Å	Atom	Atom	Length/Å
O1	C11	1.2320(14)	C3	C4	1.3843(15)
N1	C4	1.4326(13)	C3	C6	1.4196(15)
N1	C11	1.3454(14)	C3	C8	1.5052(15)
C1	C2	1.4271(14)	C5	C7	1.3736(15)
C1	C4	1.4263(14)	C5	C12	1.4147(16)
C1	C7	1.4228(15)	C6	C10	1.3714(16)
C2	C9	1.4205(15)	C9	C12	1.3704(17)
C2	C10	1.4217(15)			

Table II.3.32.5 Bond Angles for ab50517.

Atom	Atom	Atom	Angle/°	Atom	Atom	Atom	Angle/°
C11	N1	C4	124.83(9)	C1	C4	N1	120.08(9)
C4	C1	C2	118.67(10)	C3	C4	N1	118.22(9)

C7	C1	C2	118.37(9)	C3	C4	C1	121.67(9)
C7	C1	C4	122.95(9)	C7	C5	C12	120.76(11)
C9	C2	C1	119.56(10)	C10	C6	C3	121.76(10)
C9	C2	C10	121.45(10)	C5	C7	C1	120.62(10)
C10	C2	C1	118.99(10)	C12	C9	C2	120.56(10)
C4	C3	C6	118.42(10)	C6	C10	C2	120.44(10)
C4	C3	C8	121.43(10)	O1	C11	N1	126.20(10)
C6	C3	C8	120.14(10)	C9	C12	C5	120.08(10)

Table II.3.32.6 Hydrogen Atom Coordinates (Å×10^4) and Isotropic Displacement Parameters (Å^2×10^3) for ab50517.

Atom	***x***	***y***	***z***	**U(eq)**
H1	814	6061	6606	17
H5	10146	4823	8836	22
H6	3427	9152	7739	20
H7	6463	5187	7663	18
H8A	1143	7903	5778	27
H8B	284	8792	6388	27
H8C	-1275	7780	6486	27
H9	10689	7590	9652	21
H10	7209	8784	8869	21
H11	2970	5296	5556	18
H12	12366	6032	9807	24

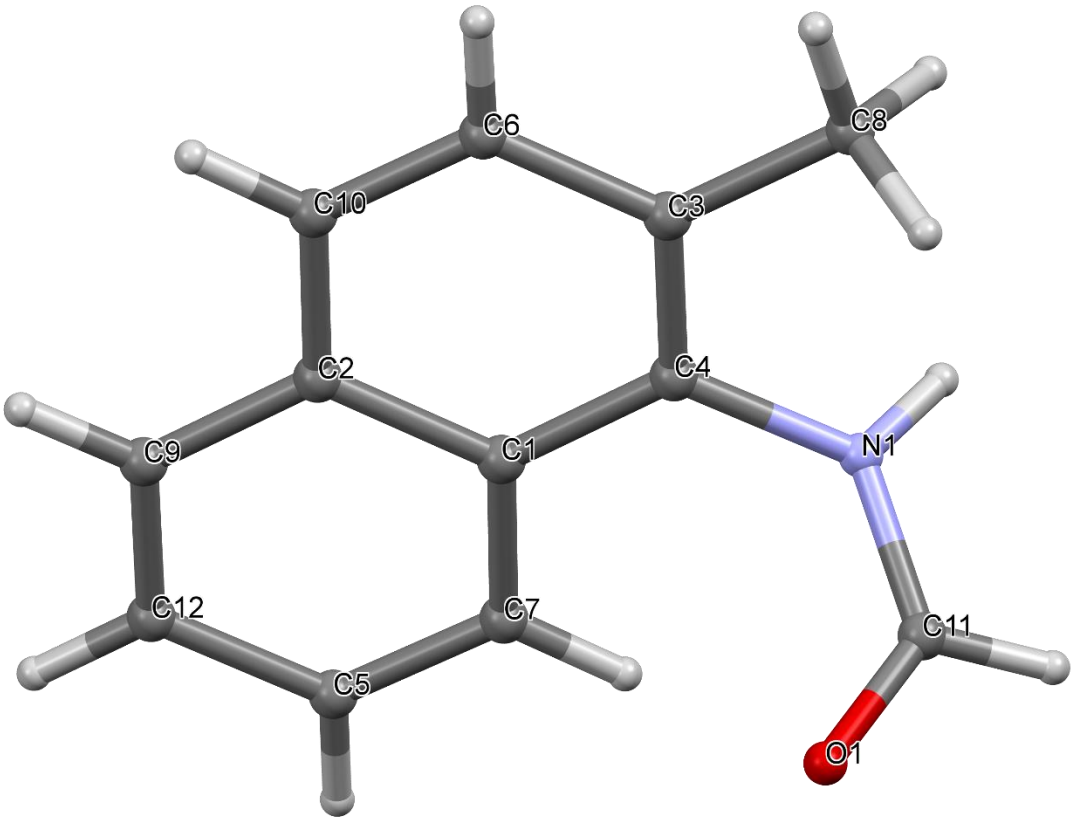

Figure II.3.32 Crystal Structure with atomic labels for compound **32**, 1-Amino-2-Methylnaphthyene-N-Formamide, ab50517

Appendix III

Powder Pattern Data

All PXRD patterns were collected on a Rigaku Ultima IV, In-Plane, X-ray diffractometer containing a CuKα source (λ = 1.54051Å), and the data was viewed using either MDI Jade 9 software, or the raw files were interpreted by Microsoft Excel. For all PXRD experiments, crystals of the material were isolated and washed, dried, then ground in a marble mortar. The powder was placed on a quartz, zero background, sample holder for data collection. Each pattern was collected at 2Θ (5 - 60°) at 0.02° per step, at a rate of 0.5 degree per minute. For each experiment, a continuous scan mode was used with variable DivSlit and SctSlit parameters, and DivH.L.Slit and RecSlit set at 5mm and 0.3mm respectively.

III.1 Powder Pattern Data for Chapter 2 Compounds

III.1.1 Powder Pattern for Compound 2, Mn_{12}-2-Me, $Mn_{12}O_{12}(O_2CPh\text{-}o\text{-}Me)_{16}(H_2O)_4$

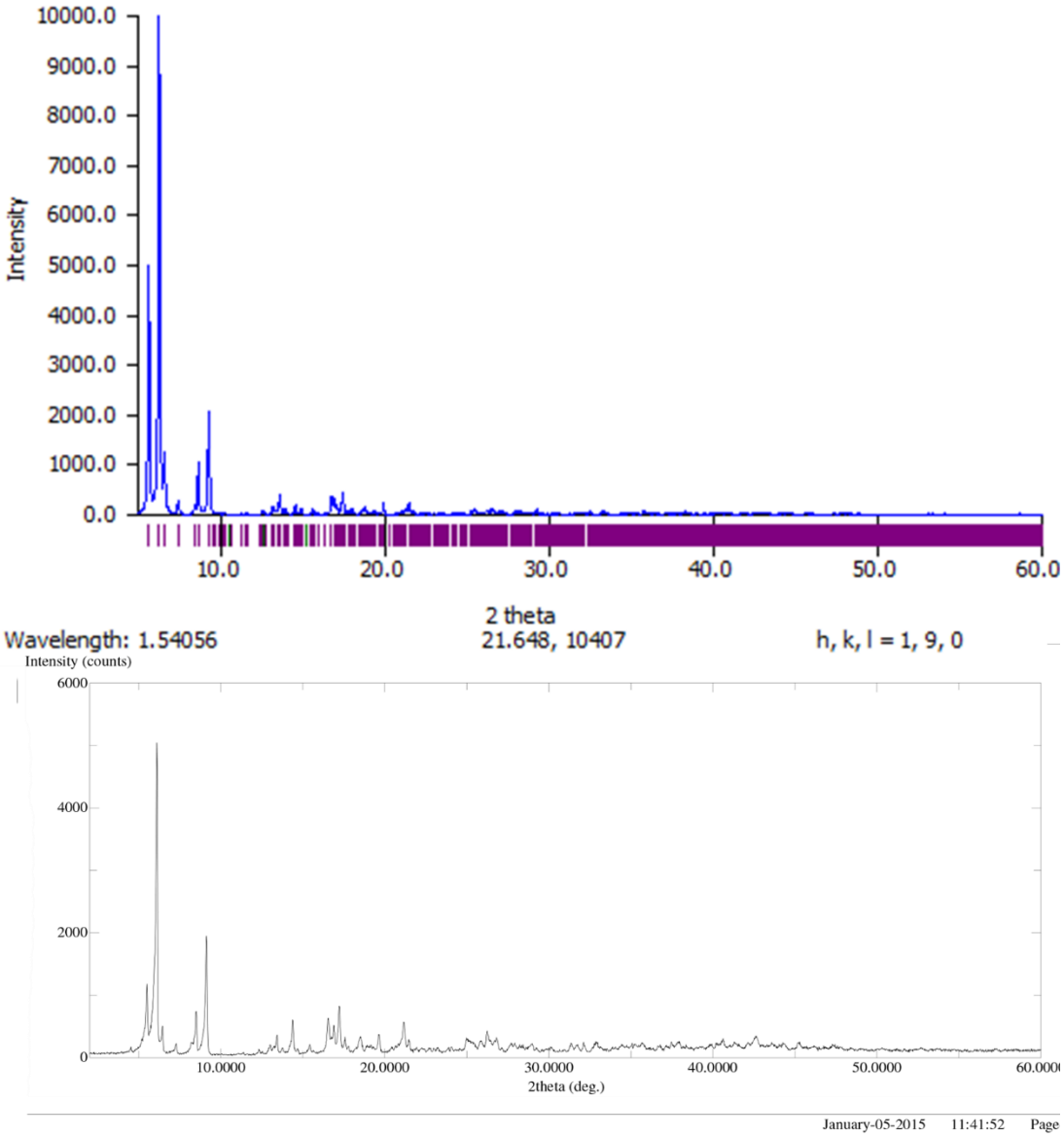

Figure III.1.1 PXRD Pattern (*top*, calculated; *bottom*, experimental) for compound **2**, Mn_{12}-2-Me, $Mn_{12}O_{12}(O_2CPh\text{-}o\text{-}Me)_{16}(H_2O)_4$

III.1.2 Powder Pattern for Compound 3, Mn_{12}-2-Et, $Mn_{12}O_{12}(O_2CPh\text{-}o\text{-}Et)_{16}(H_2O)_4$

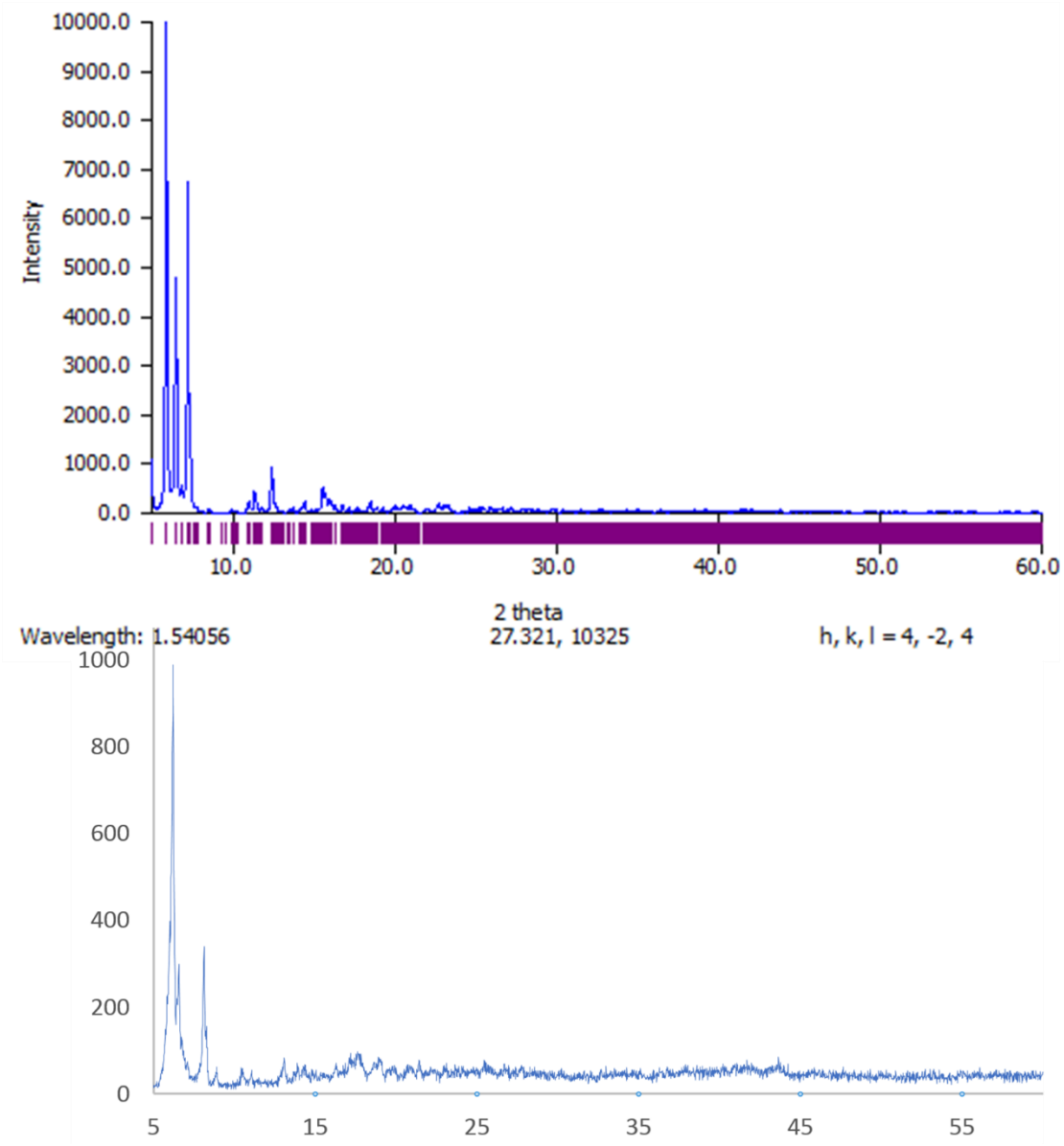

Figure III.1.2 PXRD Pattern (*top*, calculated; *bottom*, experimental) for compound **3**, Mn_{12}-2-Et, $Mn_{12}O_{12}(O_2CPh\text{-}o\text{-}Et)_{16}(H_2O)_4$

III.1.3 Powder Pattern for Compound 4, Mn_{12}-2-Ph, $Mn_{12}O_{12}(O_2CPh\text{-}o\text{-}Ph)_{16}(H_2O)_4$

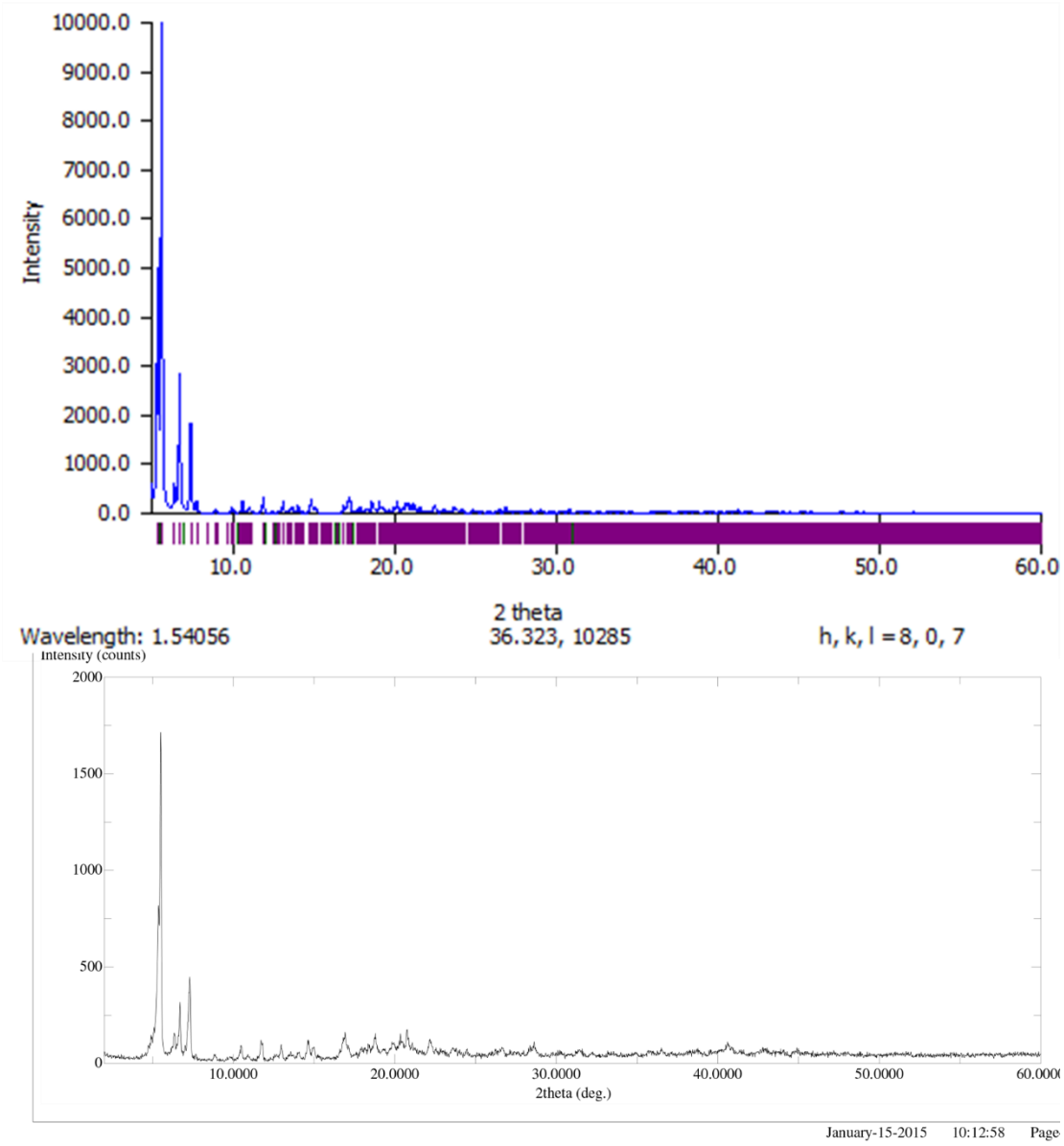

Figure III.1.3 PXRD Pattern (*top*, calculated; *bottom*, experimental) for compound **4**, Mn_{12}-2-Ph, $Mn_{12}O_{12}(O_2CPh\text{-}o\text{-}Ph)_{16}(H_2O)_4$

III.1.4 Powder Pattern for Compound 5, Mn_{13}-2-Ph, $Mn_{13}O_{14}(O_2CPh_2)_{12}$

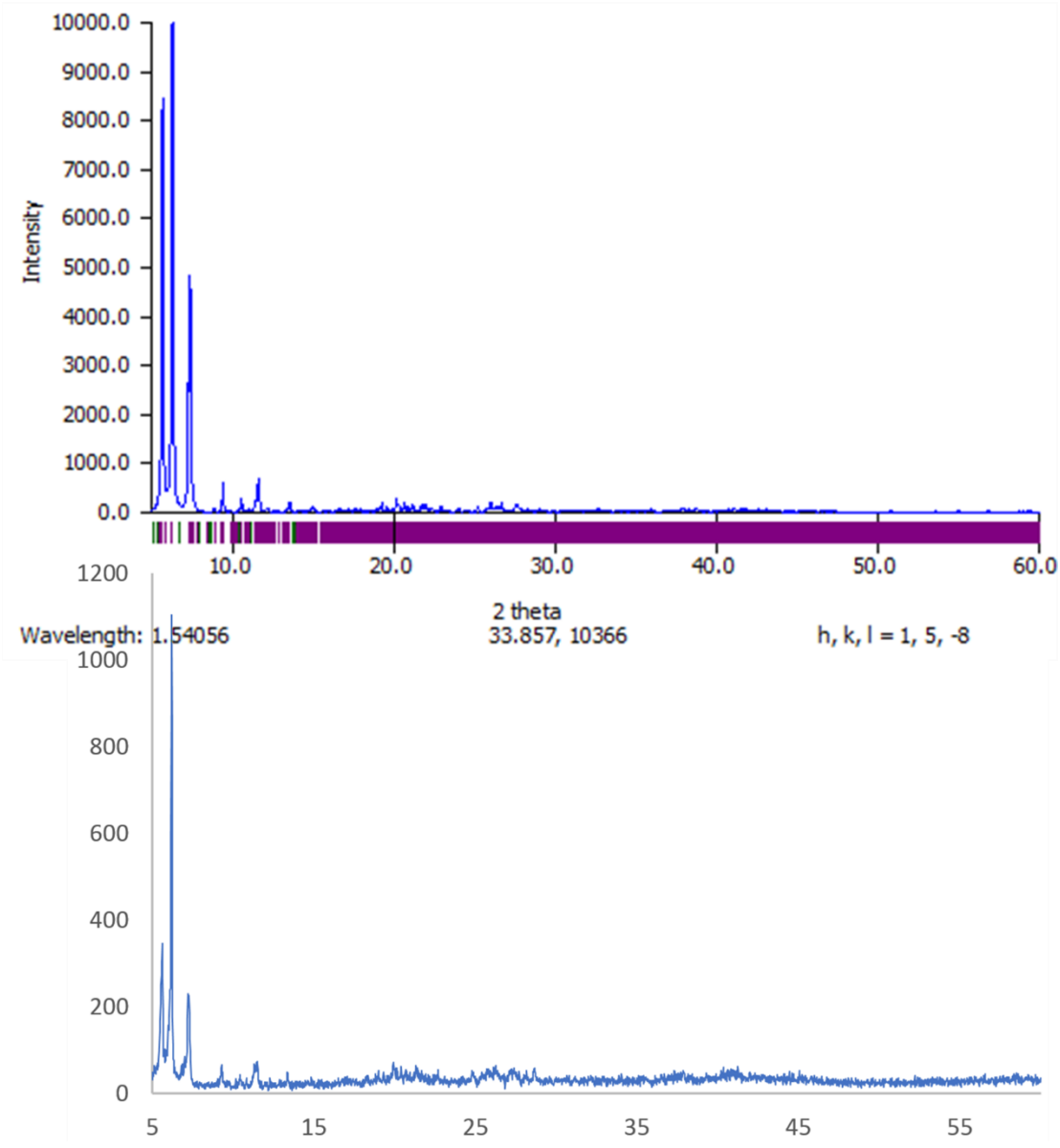

Figure III.1.4 PXRD Pattern (*top*, calculated; *bottom*, experimental) for compound **5**, Mn_{13}-2-Ph, $Mn_{13}O_{14}(O_2CPh_2)_{12}$

III.2 Powder Pattern Data for Chapter 3 Compounds

III.2.1 Powder Pattern for Compound 1, Mn_{13}-2-Methyl, $Mn_{13}O_8(O_2CPh\text{-}o\text{-}Me)_{12}(OEt)_6$

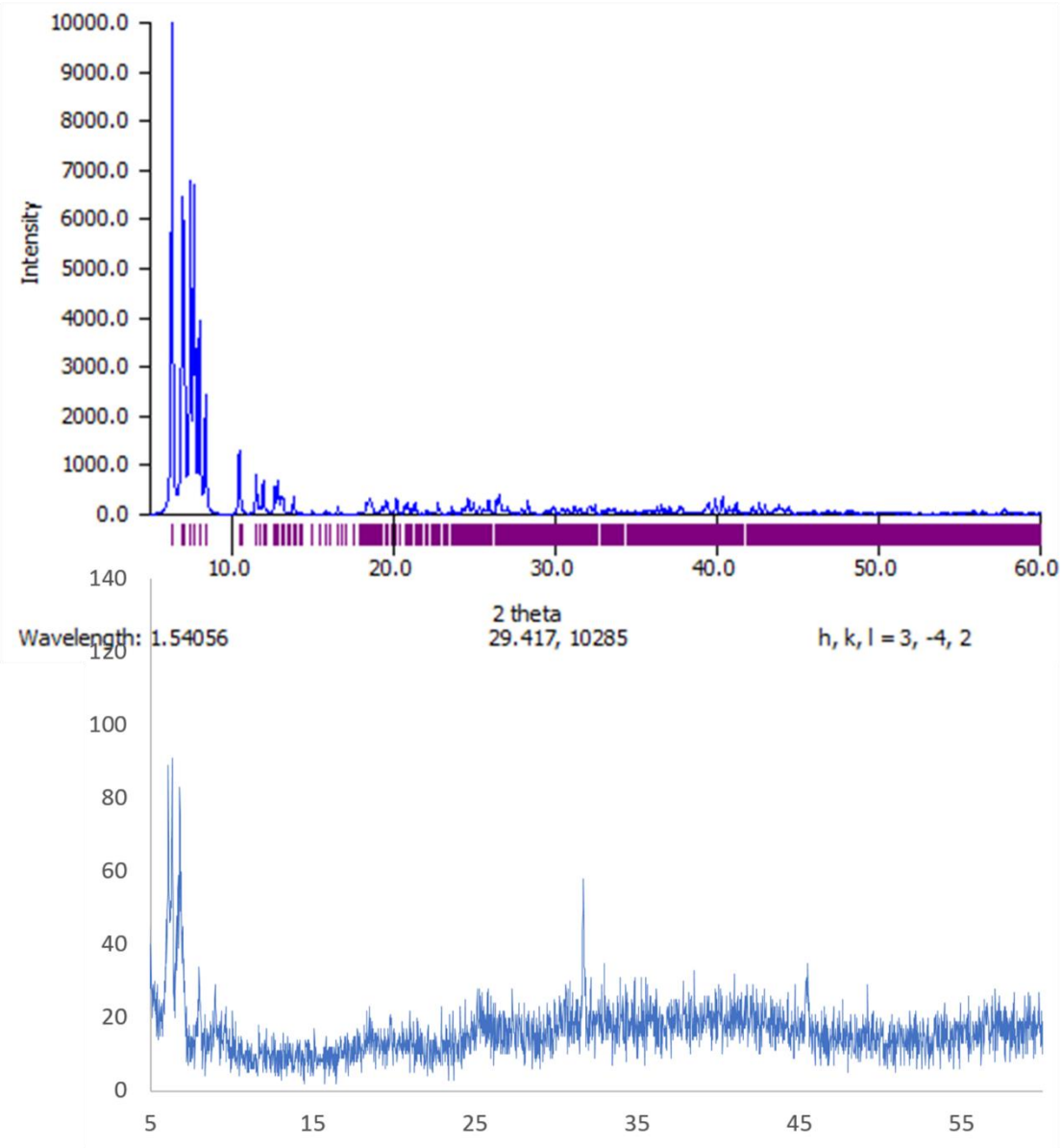

Figure III.2.1 PXRD Pattern (*top*, calculated; *bottom*, experimental) for compound **1**, Mn_{13}-2-Methyl, $Mn_{13}O_8(O_2CPh\text{-}o\text{-}Me)_{12}(OEt)_6$

III.2.2 Powder Pattern for Compound 3, Mn_{13}-2-Phenyl, $Mn_{13}O_8(O_2CPh\text{-}o\text{-}Ph)_{12}(OEt)_6$

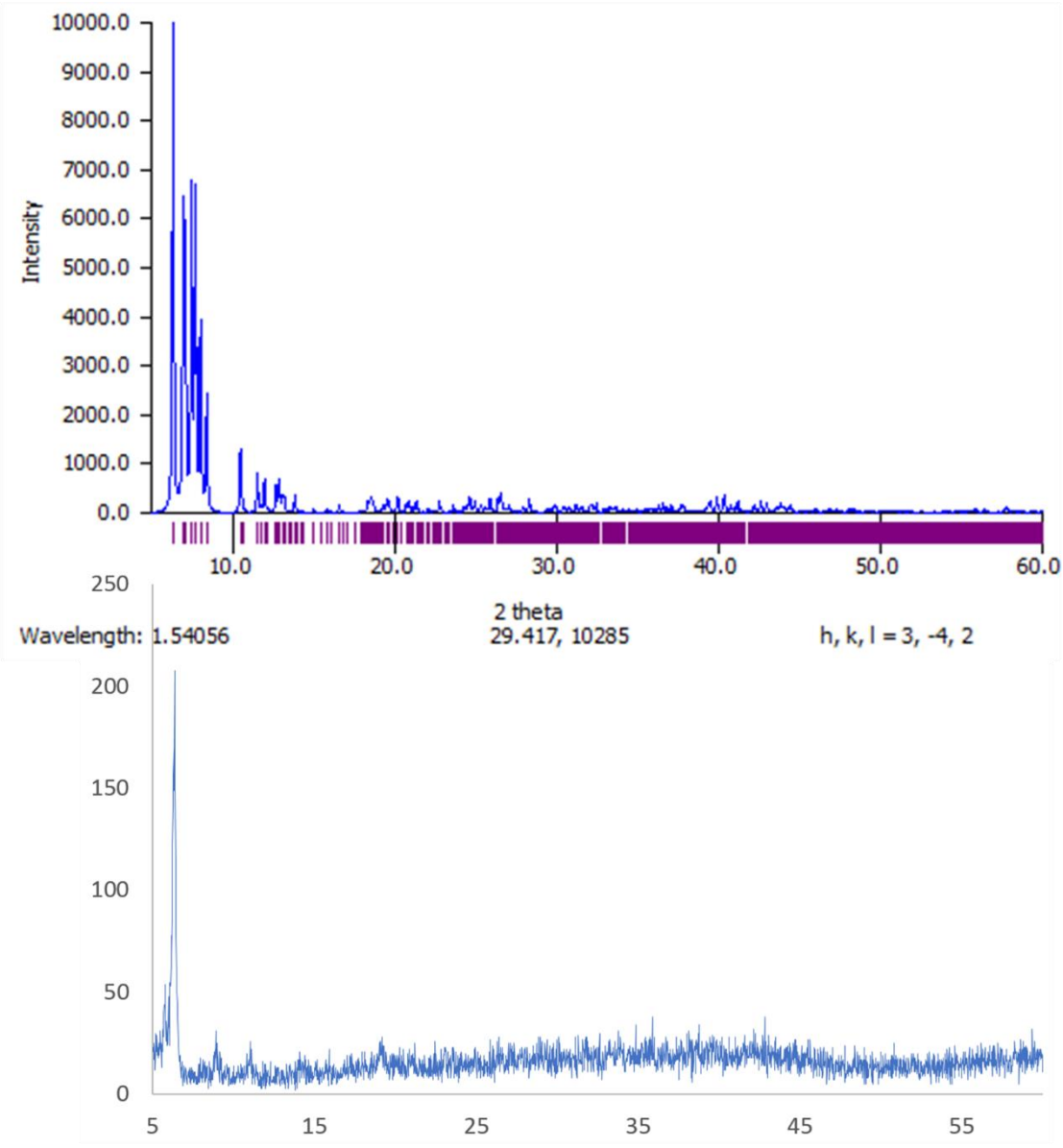

Figure III.2.2 PXRD Pattern (*top*, calculated; *bottom*, experimental) for compound **3**, Mn_{13}-2-Phenyl, $Mn_{13}O_8(O_2CPh\text{-}o\text{-}Ph)_{12}(OEt)_6$

III.2.3 Powder Pattern for Compound 4a, "Mn_3O-2-Methyl" (rod), $Mn_{12}O_{12}(O_2CPh\text{-}o\text{-}Me)_{16}(H_2O)_4$

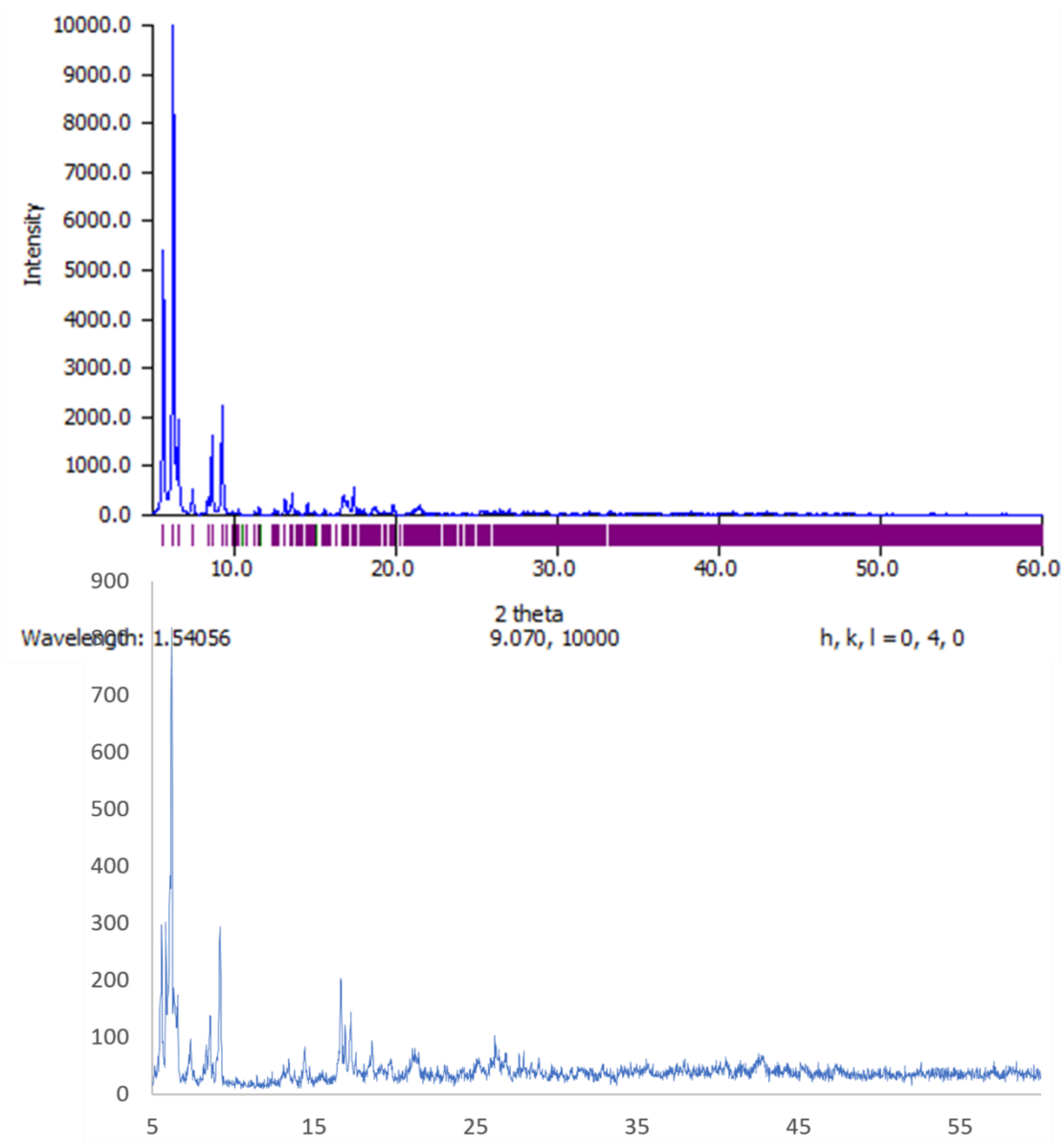

Figure III.2.3 PXRD Pattern (*top*, calculated; *bottom*, experimental) for compound **4a**, "Mn_3O-2-Methyl" (rod), $Mn_{12}O_{12}(O_2CPh\text{-}o\text{-}Me)_{16}(H_2O)_4$

III.3 Powder Pattern Data for Chapter 4 Compounds

III.3.1 Powder Pattern for Compound 1, Benzylammonium Formate

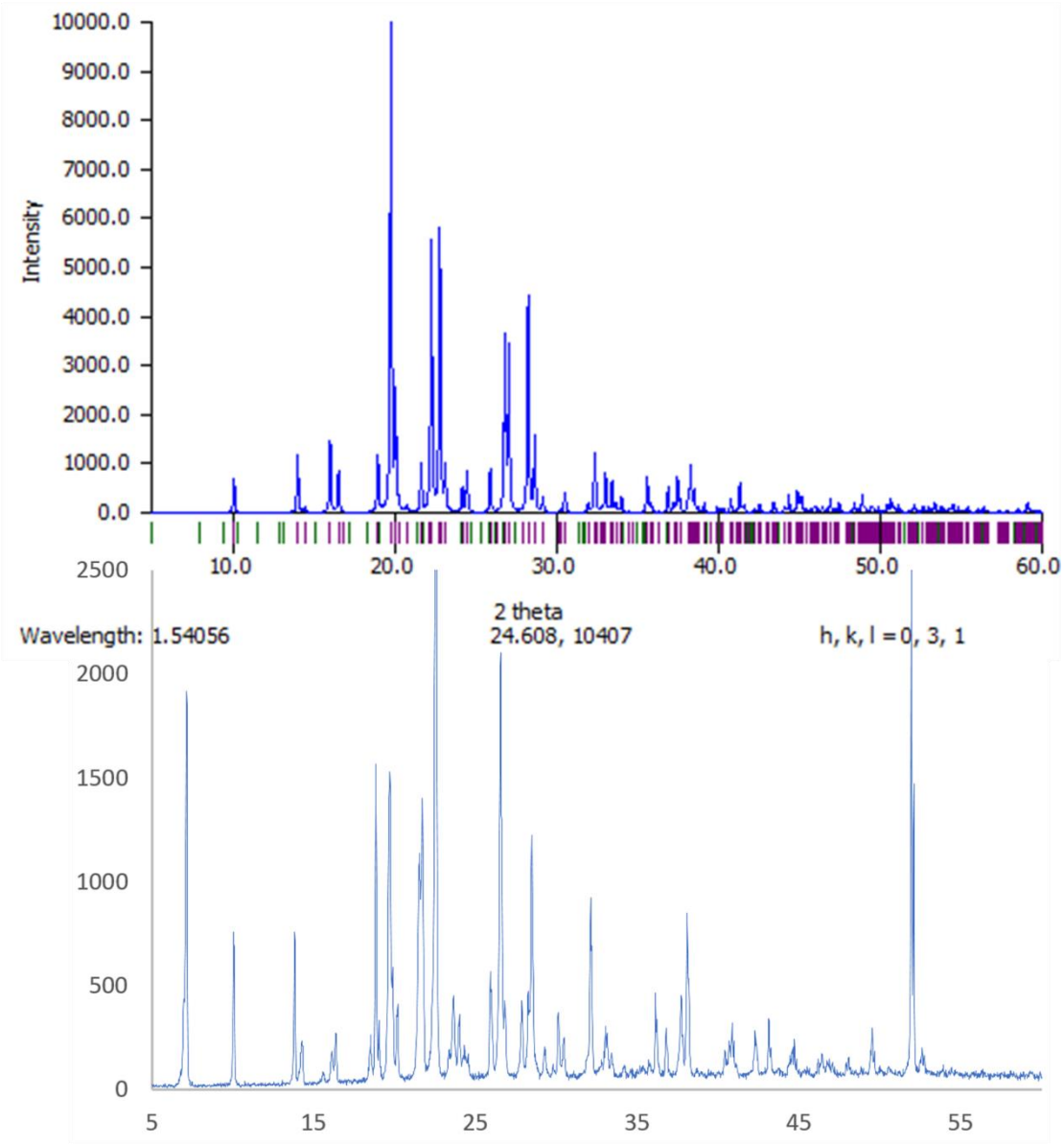

Figure III.3.1 PXRD Pattern (*top*, calculated; *bottom*, experimental) for compound **1**, Benzylammonium Formate

III.3.2 Powder Pattern for Compound 2, 2-Methylbenzylammonium Formate

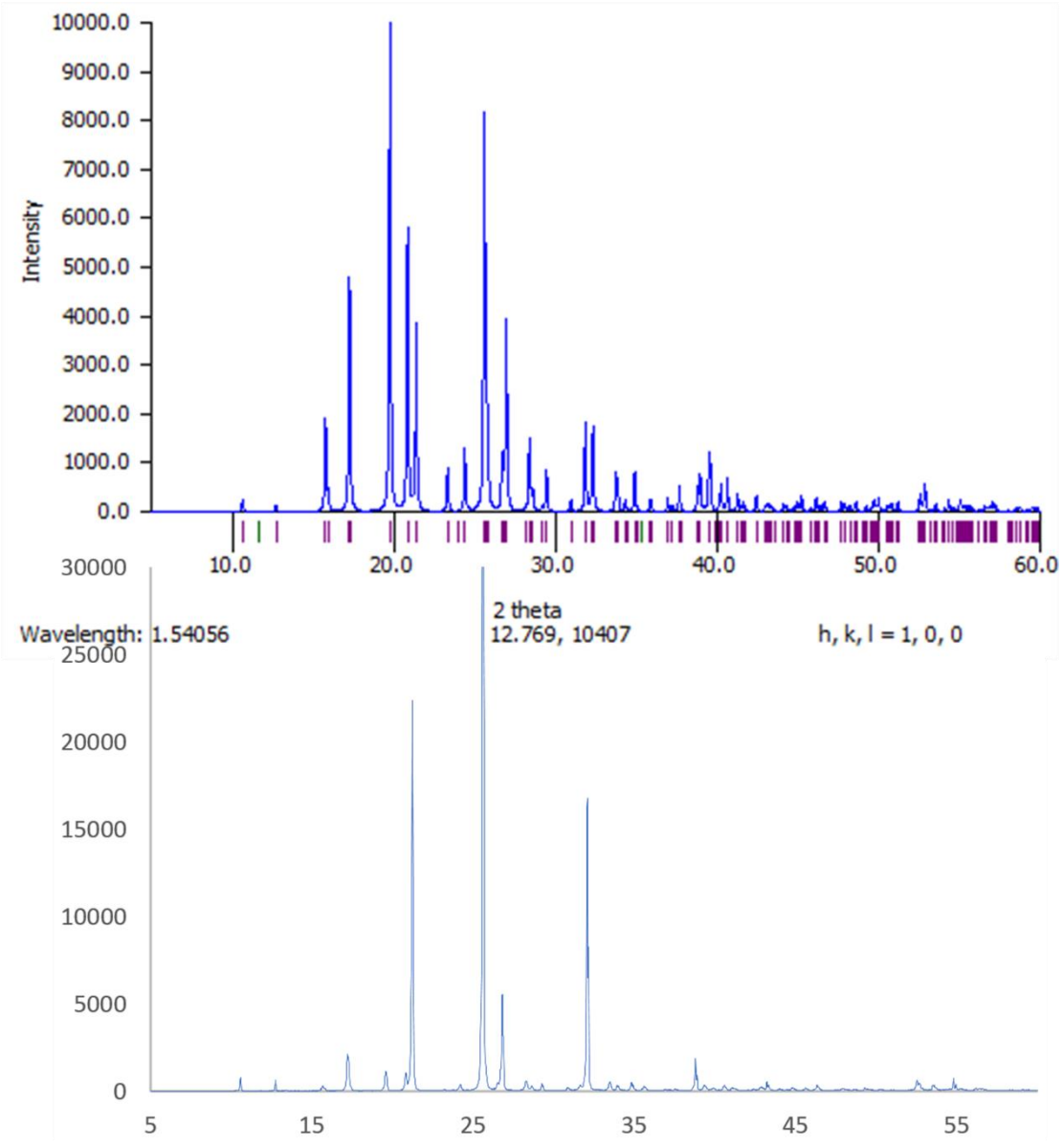

Figure III.3.2 PXRD Pattern (*top*, calculated; *bottom*, experimental) for compound **2**, 2-Methylbenzylammonium Formate

III.3.3 Powder Pattern for Compound 4, 4-Methylbenzylammonium Formate

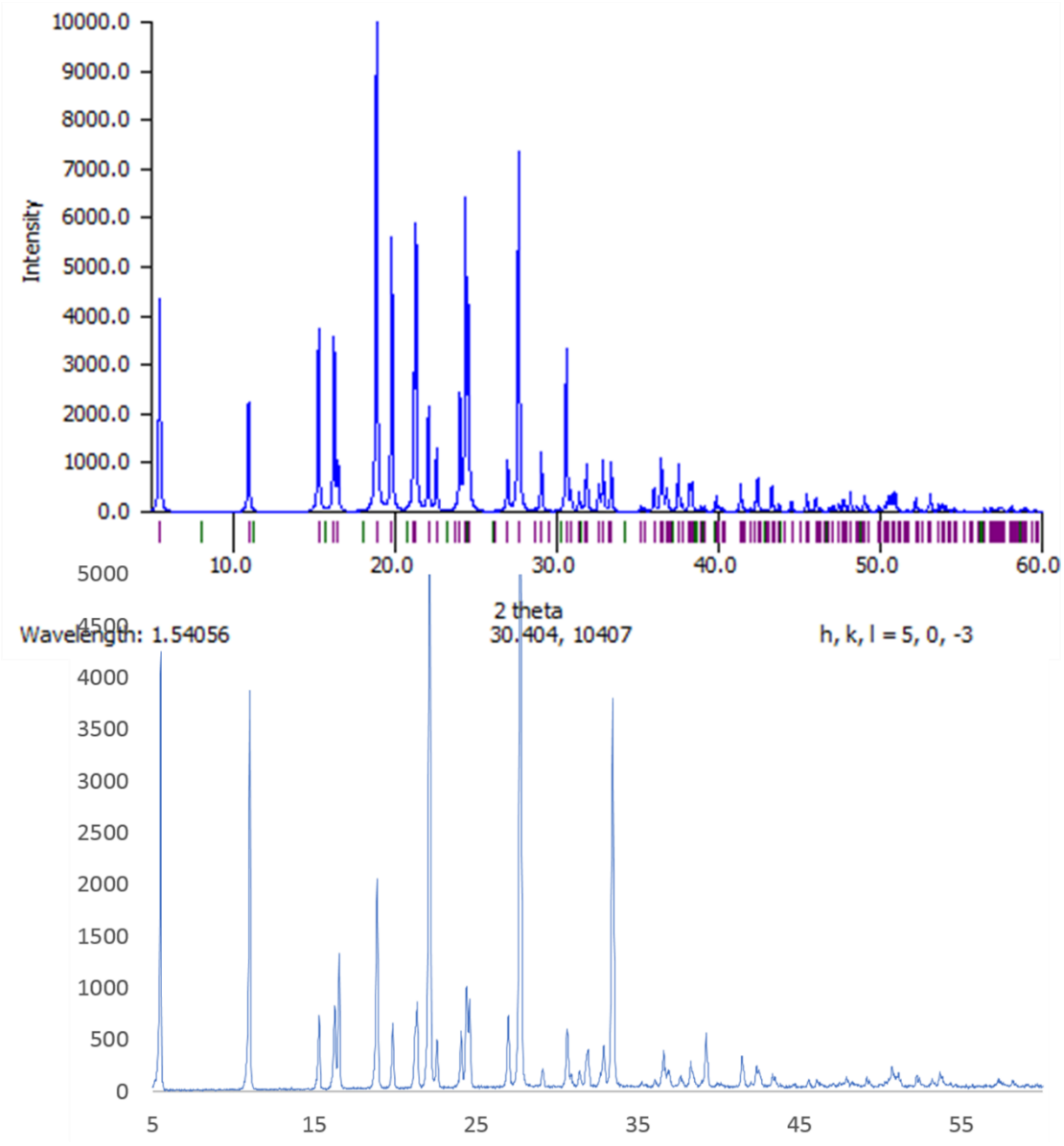

Figure III.3.3 PXRD Pattern (*top*, calculated; *bottom*, experimental) for compound **4**, 4-Methylbenzylammonium Formate

III.3.4 Powder Pattern for Compound 5, 4-(Trifluoro)Methylbenzylammonium Formate

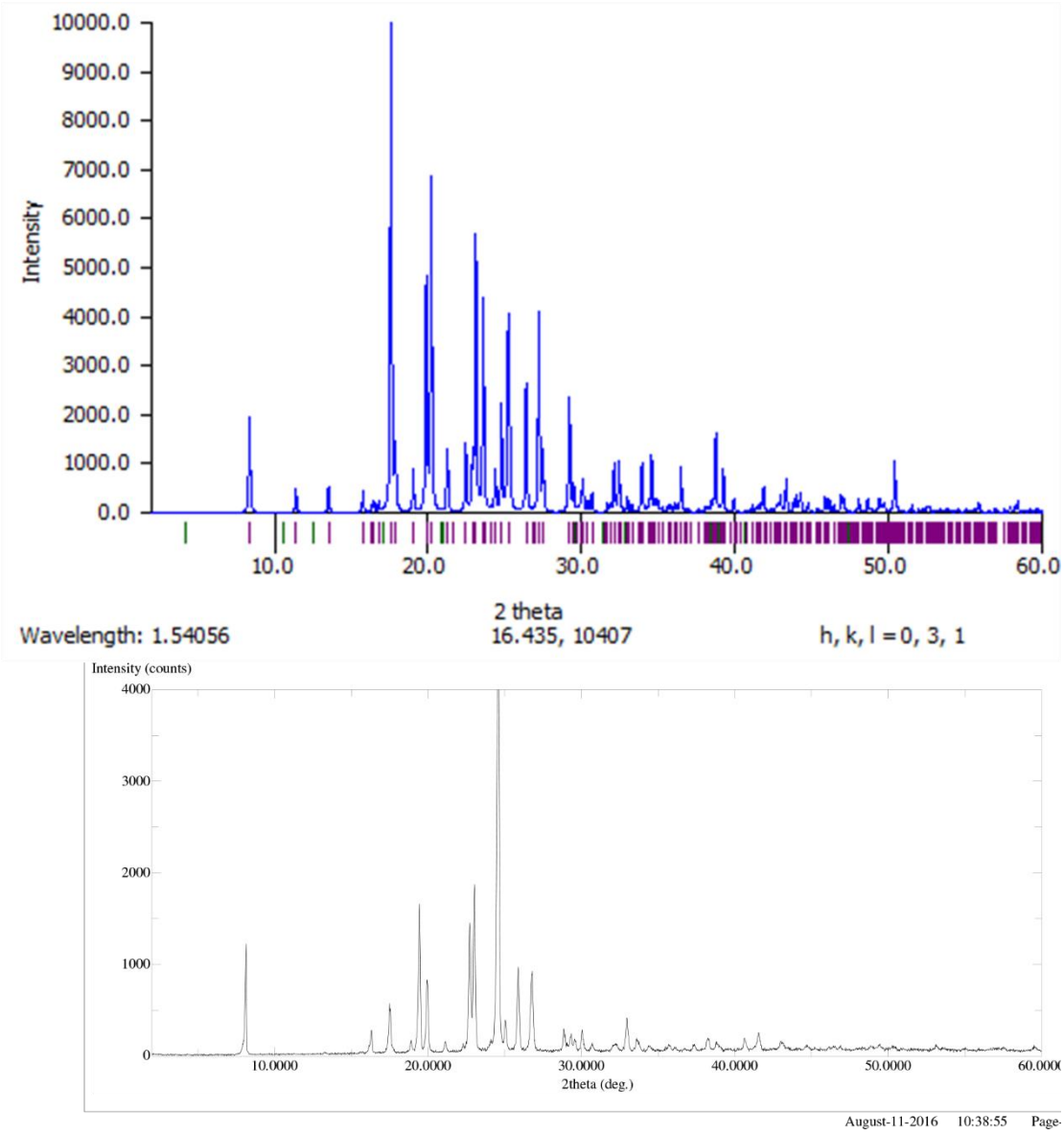

Figure III.3.4 PXRD Pattern (*top*, calculated; *bottom*, experimental) for compound **5**, 4-(Trifluoro)Methylbenzylammonium Formate

III.3.5 Powder Pattern for Compound 7, 4-*Tert*-Butylbenzylammonium Formate

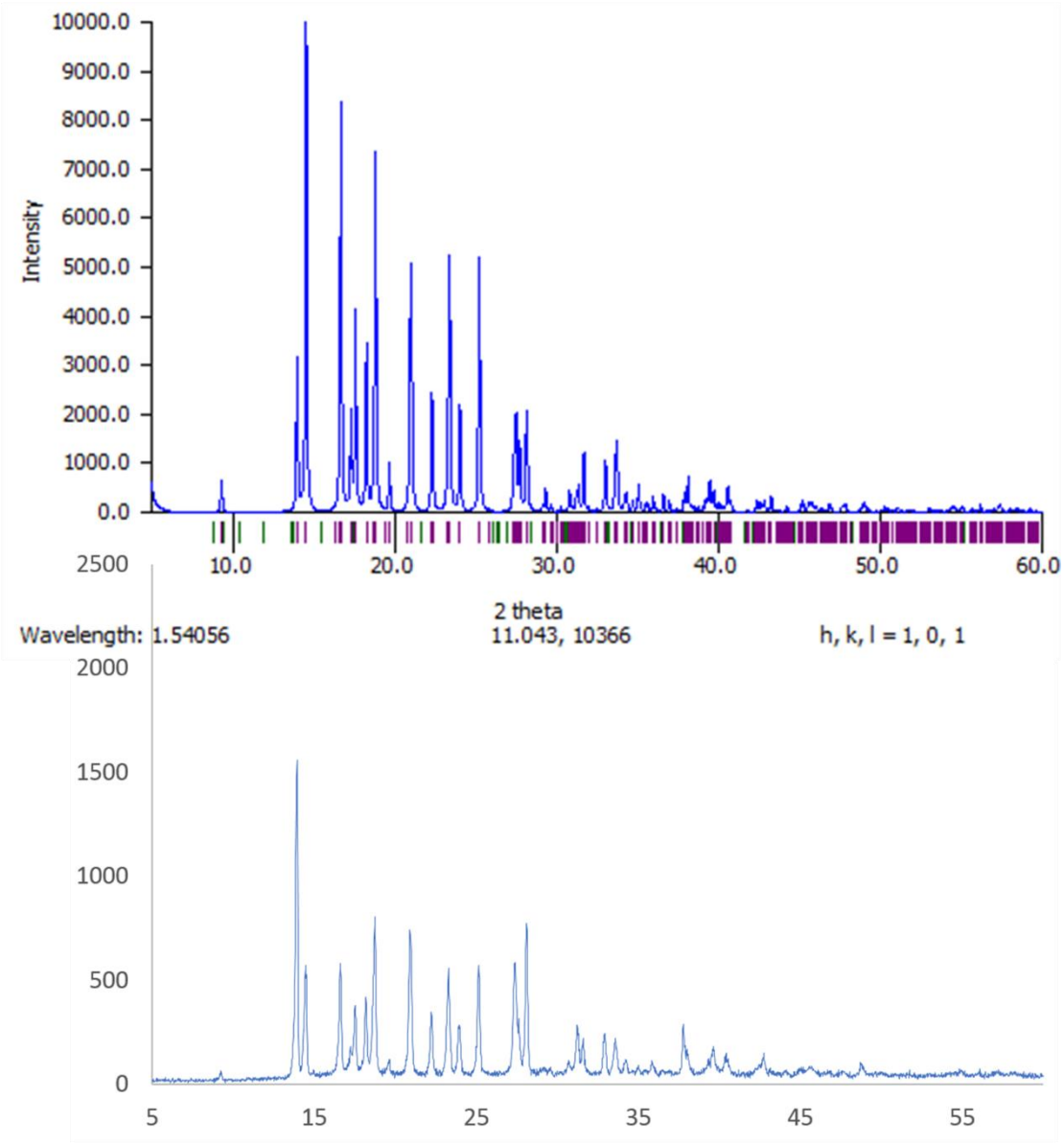

Figure III.3.5 PXRD Pattern (*top*, calculated; *bottom*, experimental) for compound **7**, 4-*Tert*-Butylbenzylammonium Formate

III.3.6 Powder Pattern for Compound 8, 3-Chloronenzylammonium Formate

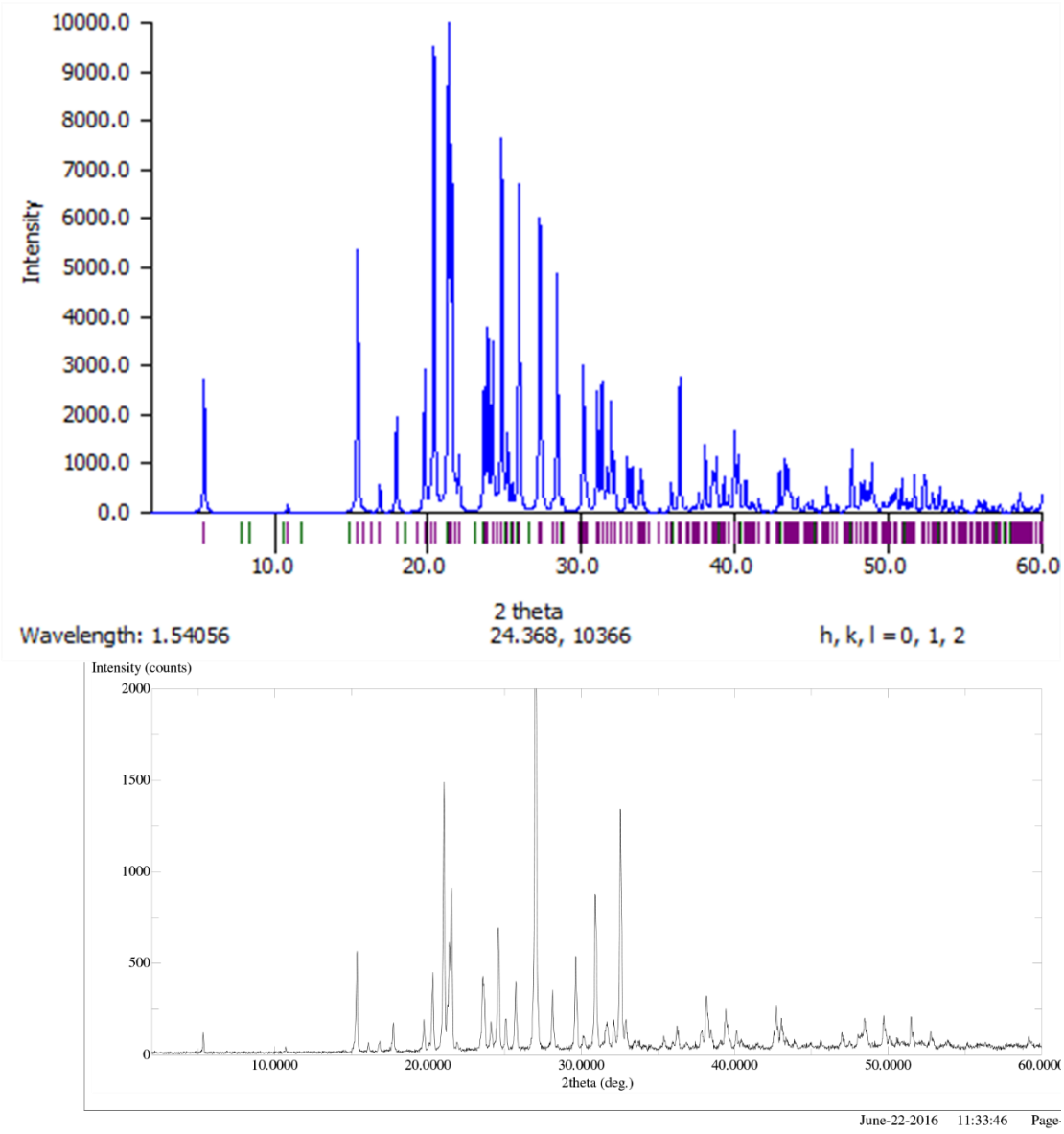

Figure III.3.6 PXRD Pattern (*top*, calculated; *bottom*, experimental) for compound **8**, 3-Chloronenzylammonium Formate

III.3.7 Powder Pattern for Compound 9, 4-Chlorobenzylammonium Formate

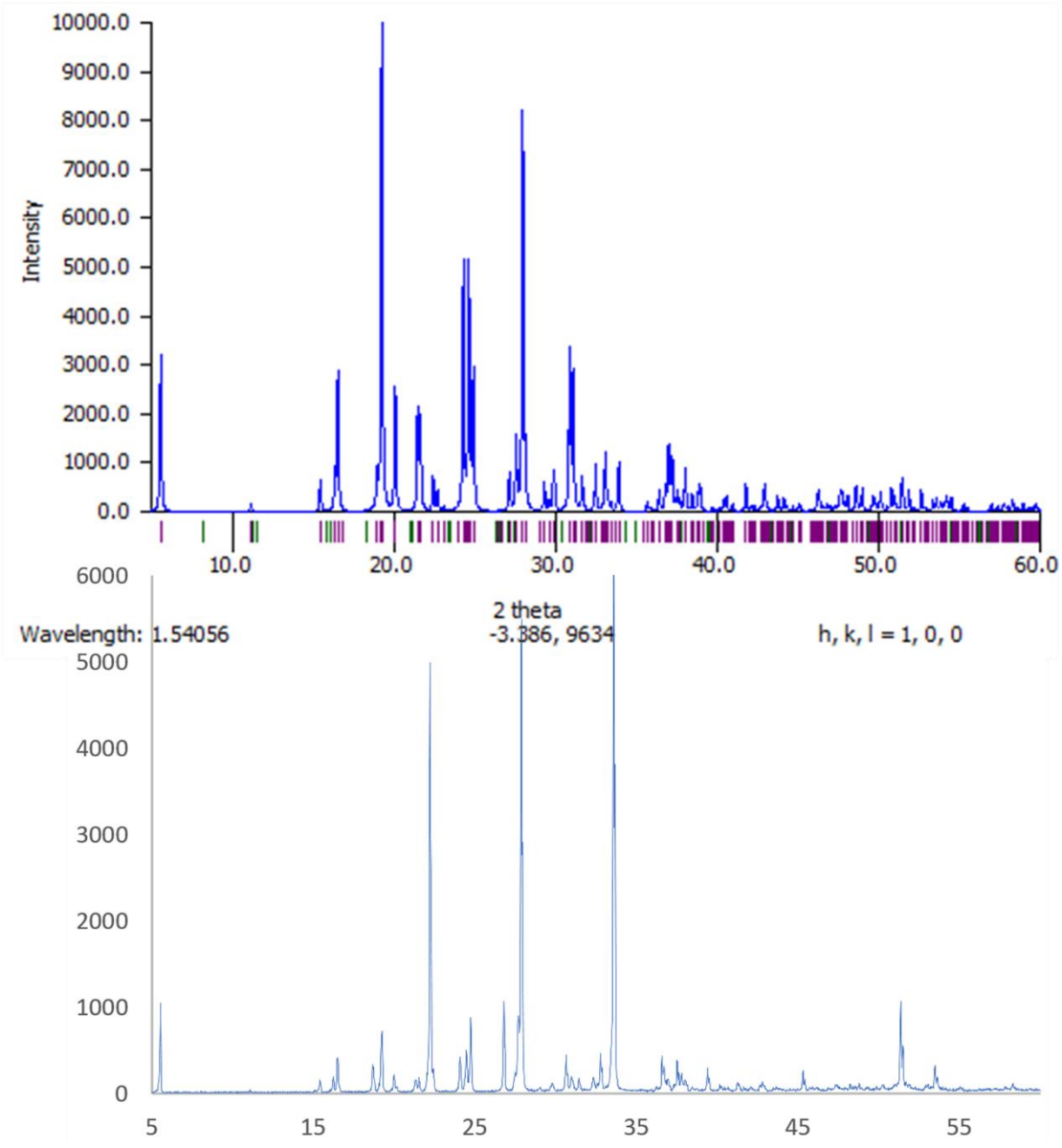

Figure III.3.7 PXRD Pattern (*top*, calculated; *bottom*, experimental) for compound **9**, 4-Chlorobenzylammonium Formate

III.3.8 Powder Pattern for Compound 10, 3,5-Difluorobenzylammonium Formate

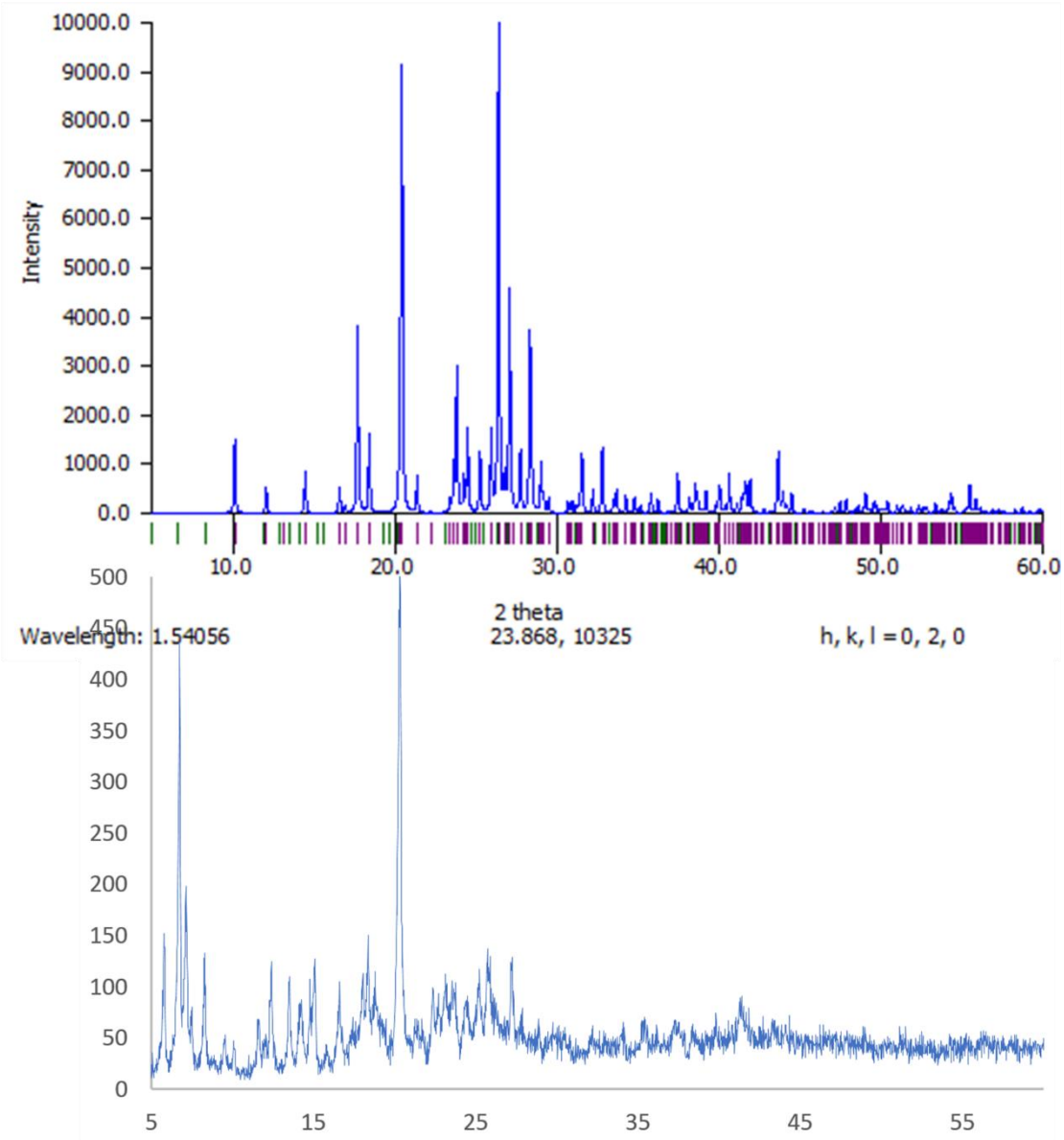

Figure III.3.8 PXRD Pattern (*top*, calculated; *bottom*, experimental) for compound **10**, 3,5-Difluorobenzylammonium Formate

III.3.9 Powder Pattern for Compound 11, 1-(1-Naphthyl)-Benzylammonium Formate

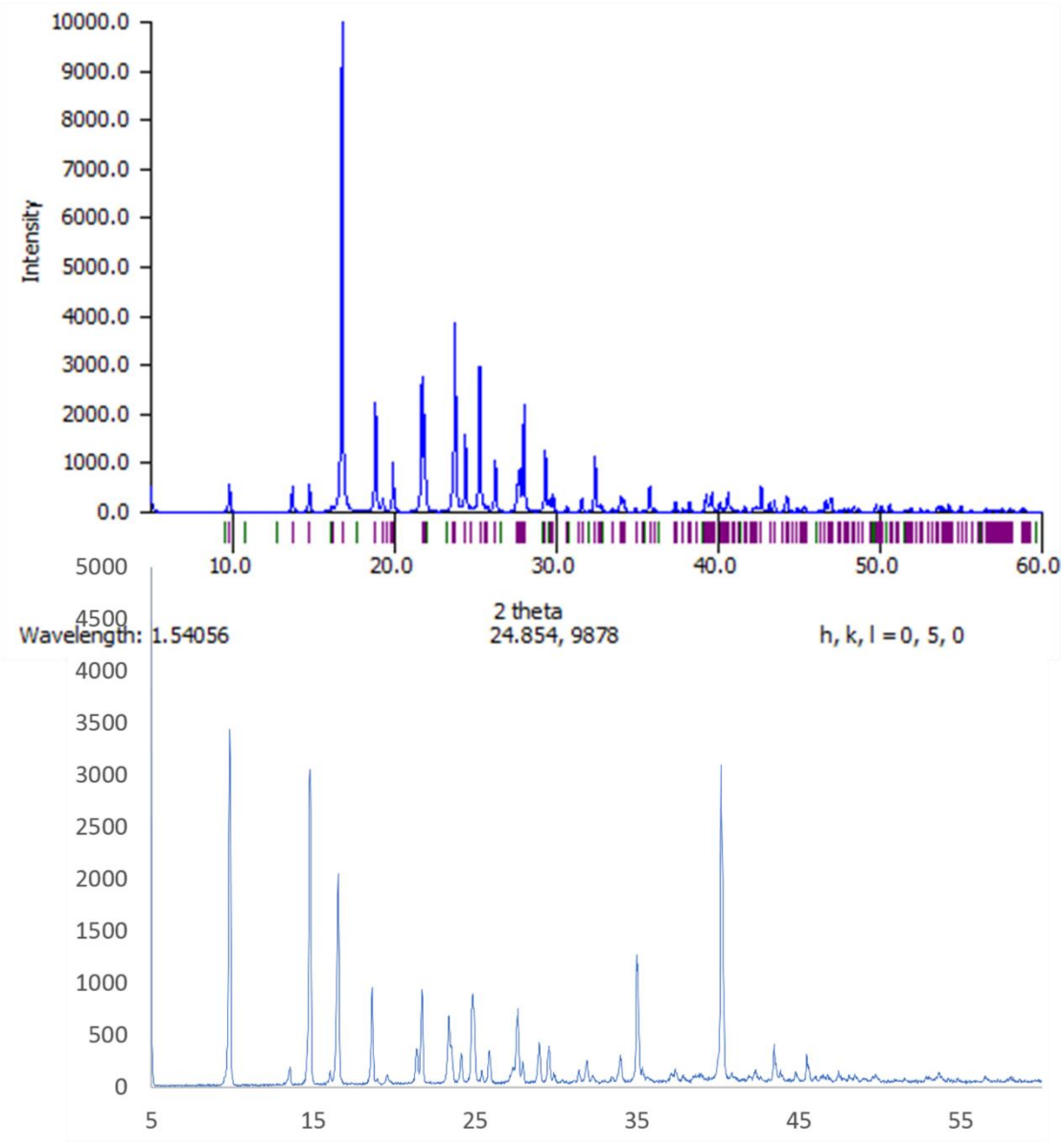

Figure III.3.9 PXRD Pattern (*top*, calculated; *bottom*, experimental) for compound **11**, 1-(1-Naphthyl)-Benzylammonium Formate

III.3.10 Powder Pattern for Compound 12, 4-Aminobenzylammonium Formate

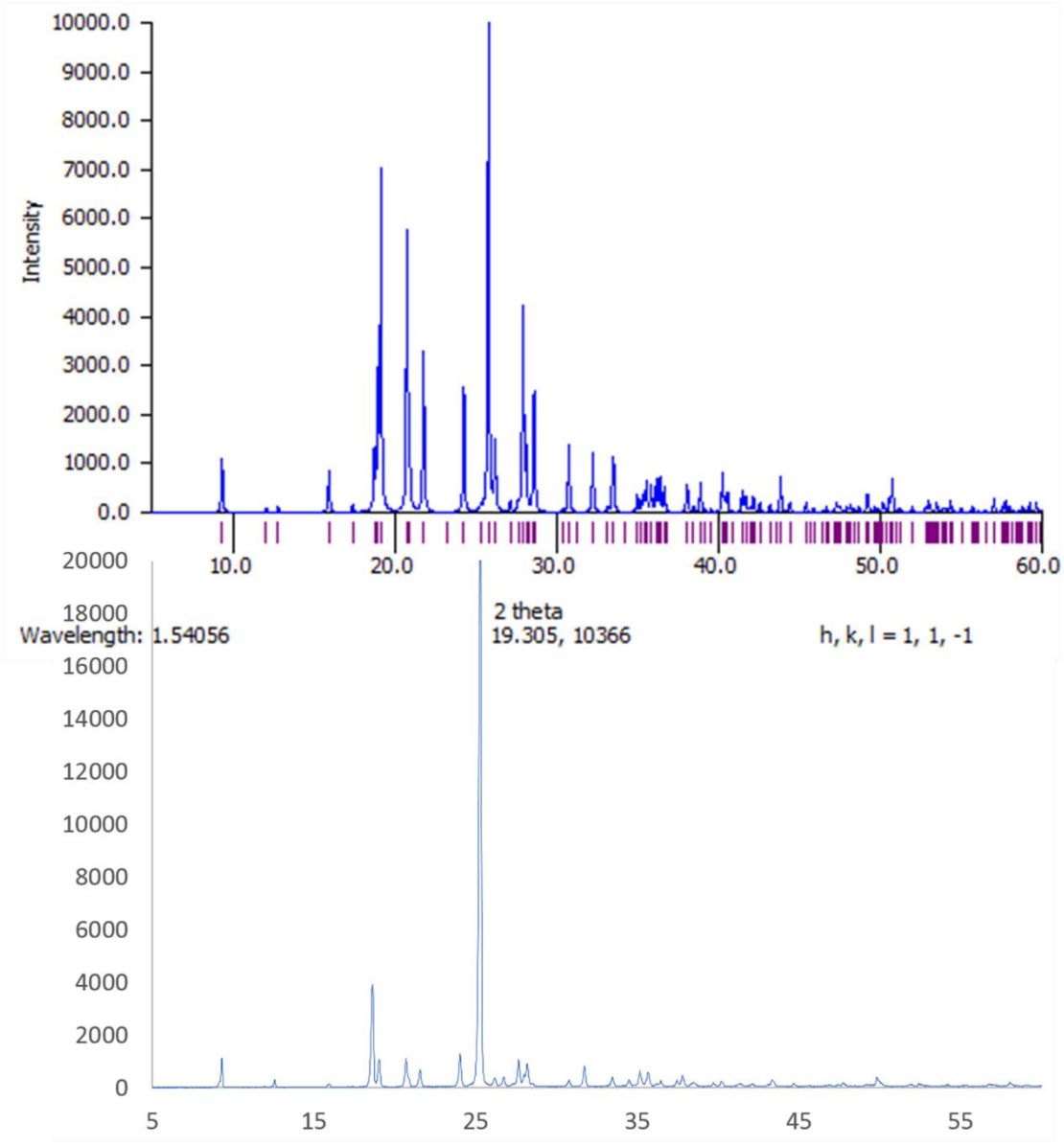

Figure III.3.10 PXRD Pattern (*top*, calculated; *bottom*, experimental) for compound **12**, 4-Aminobenzylammonium Formate

III.3.11 Powder Pattern for Compound 13, Phenethylammonium Formate

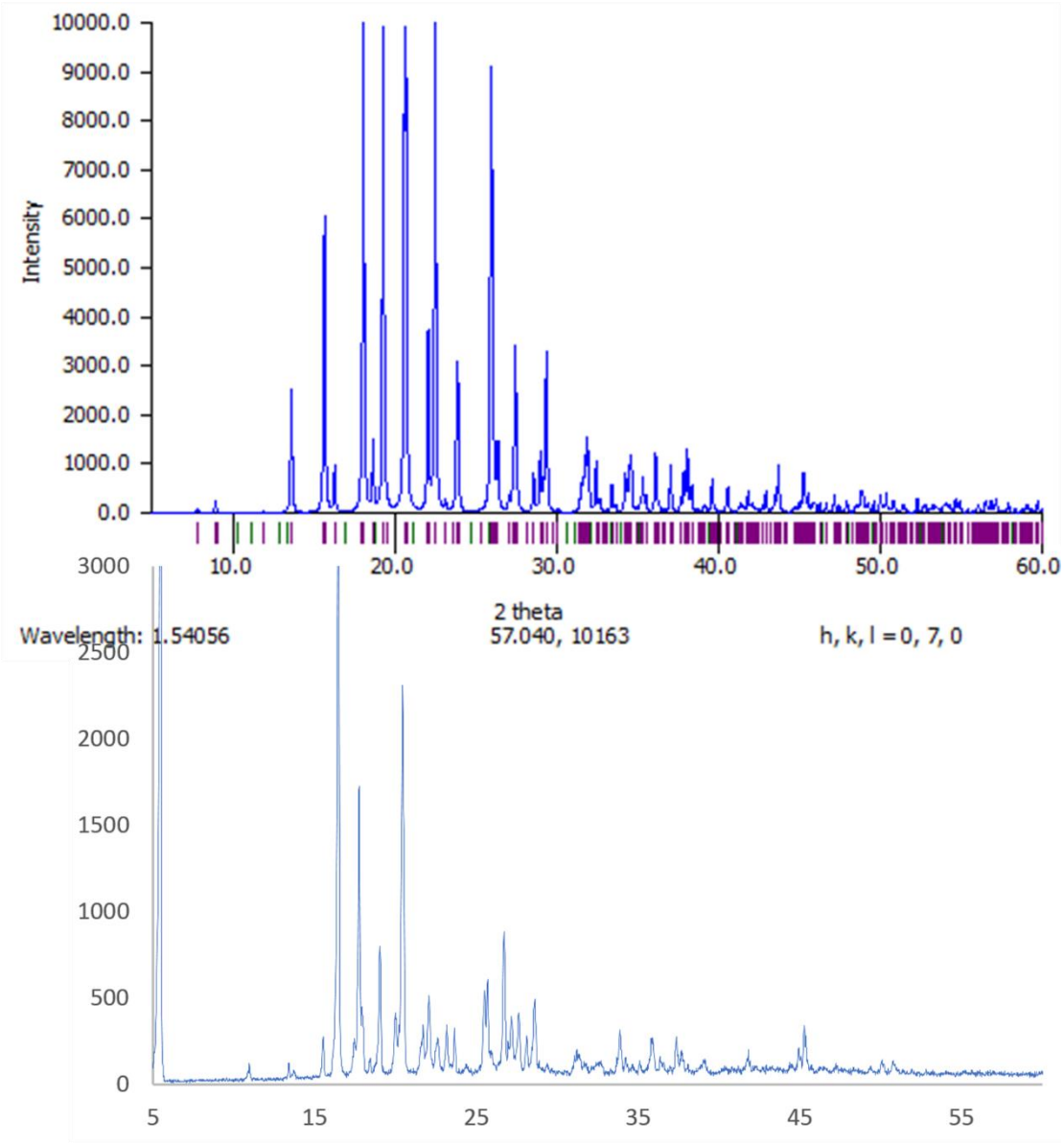

Figure III.3.11 PXRD Pattern (*top*, calculated; *bottom*, experimental) for compound **13**, Phenethylammonium Formate

III.3.12 Powder Pattern for Compound 14, 2-Chlorophenethylammonium Formate

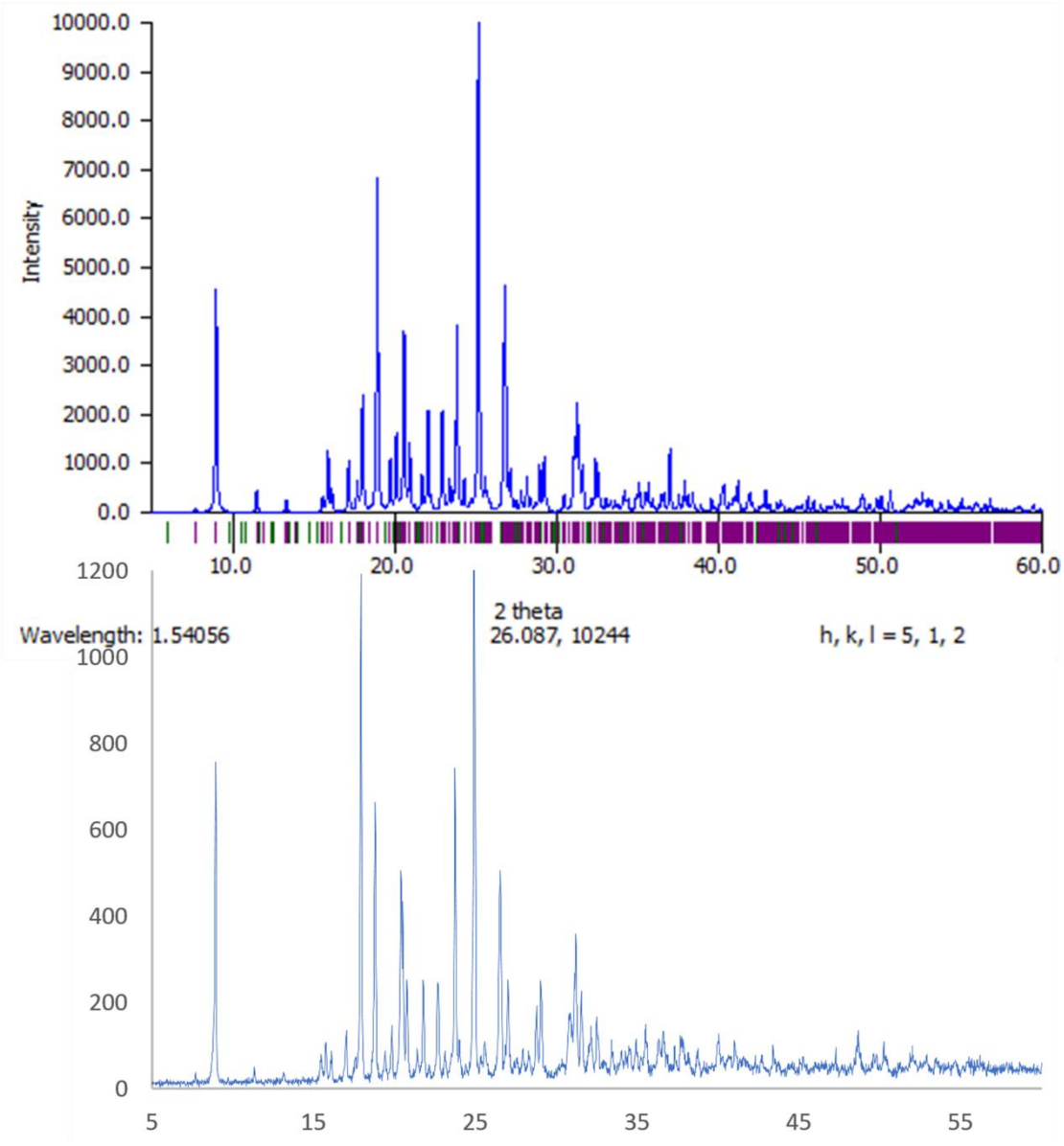

Figure III.3.12 PXRD Pattern (*top*, calculated; *bottom*, experimental) for compound **14**, 2-Chlorophenethylammonium Formate

III.3.13 Powder Pattern for Compound 16, 3-Chlorophenethylammonium Formate

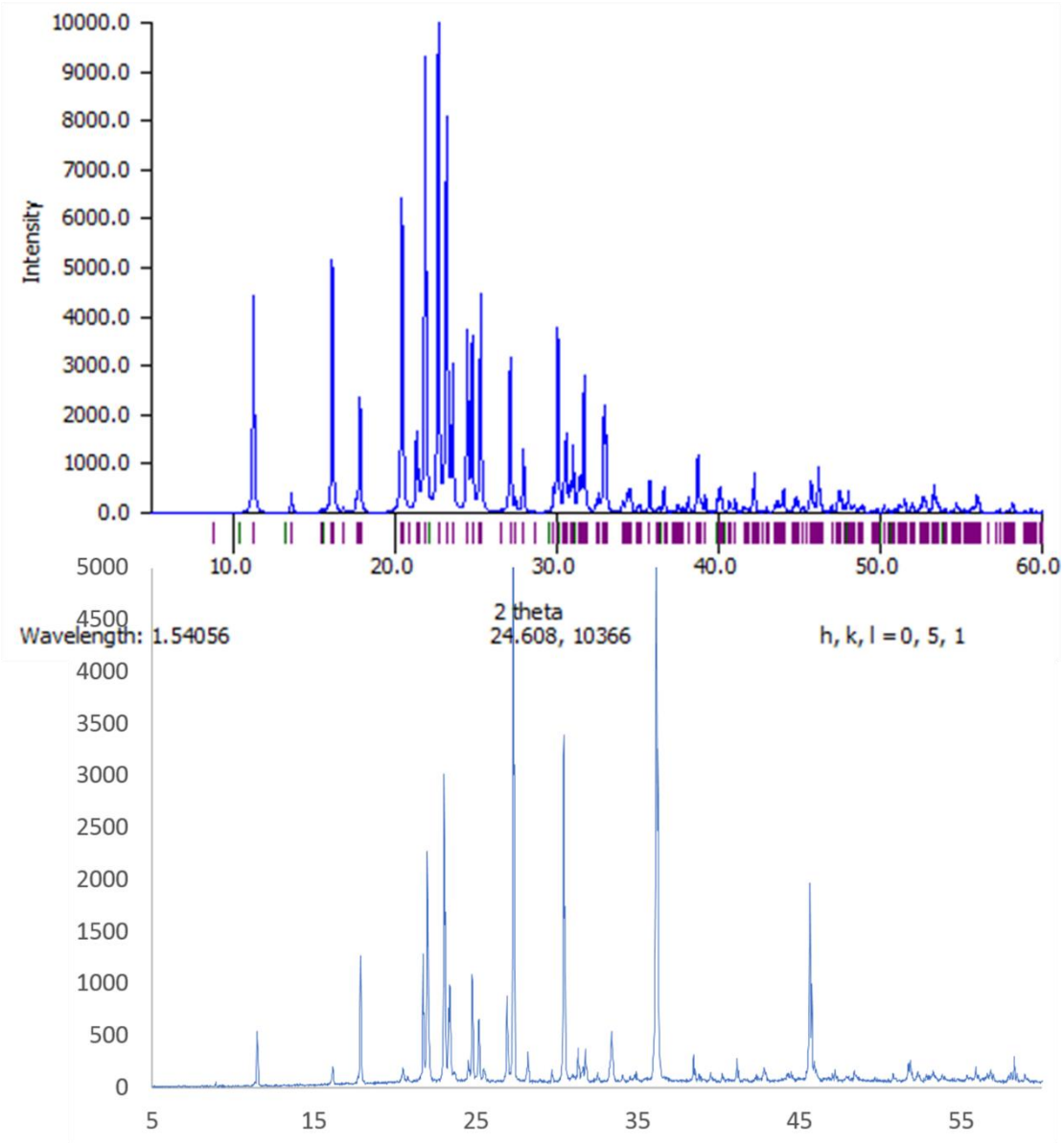

Figure III.3.13 PXRD Pattern (*top*, calculated; *bottom*, experimental) for compound **16**, 3-Chlorophenethylammonium Formate

III.3.14 Powder Pattern for Compound 17, 4-Chlorophenethylammonium Formate

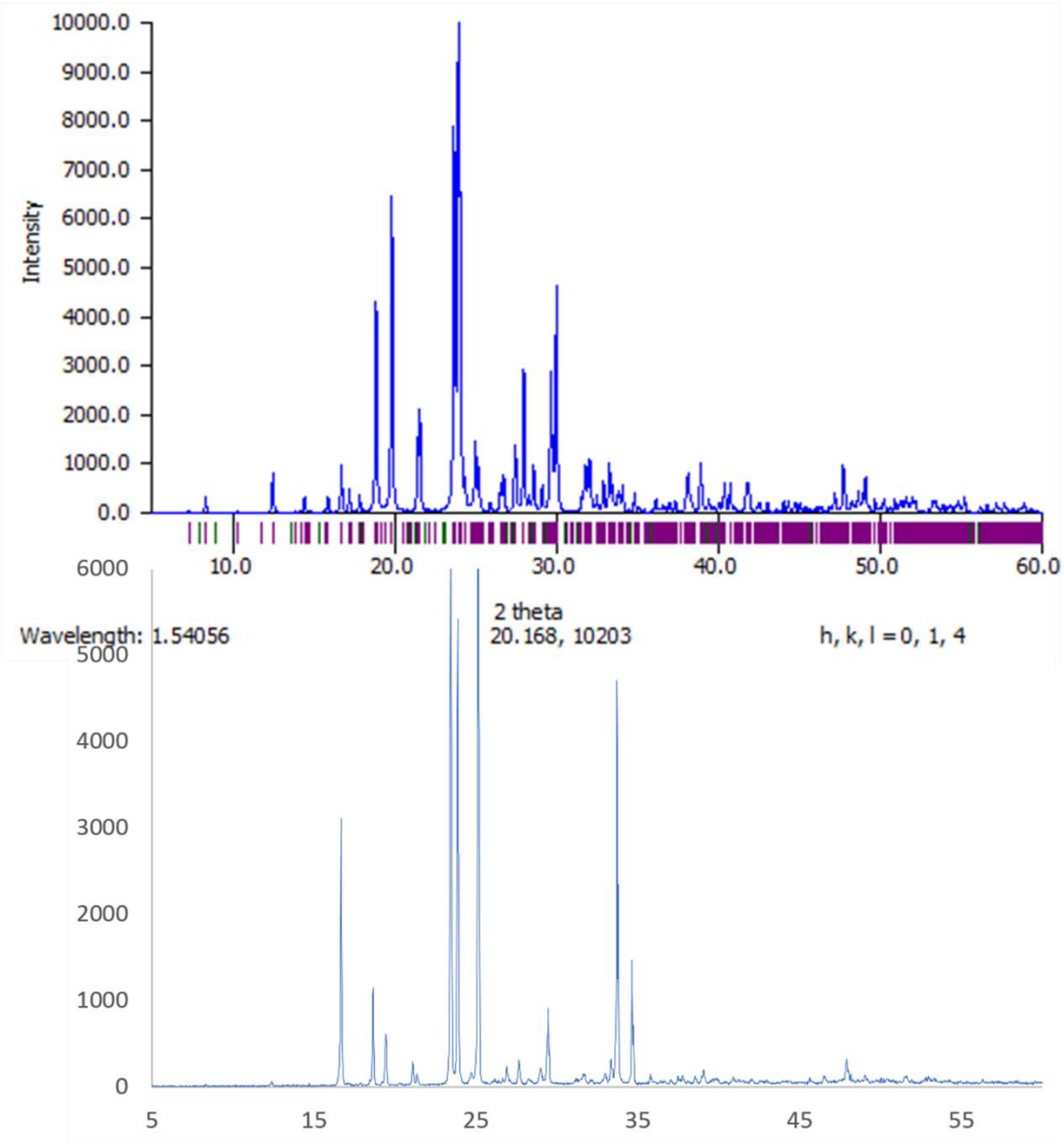

Figure III.3.14 PXRD Pattern (*top*, calculated; *bottom*, experimental) for compound **17**, 4-Chlorophenethylammonium Formate

III.3.15 Powder Pattern for Compound 18, 4-Bromophenethylammonium Formate

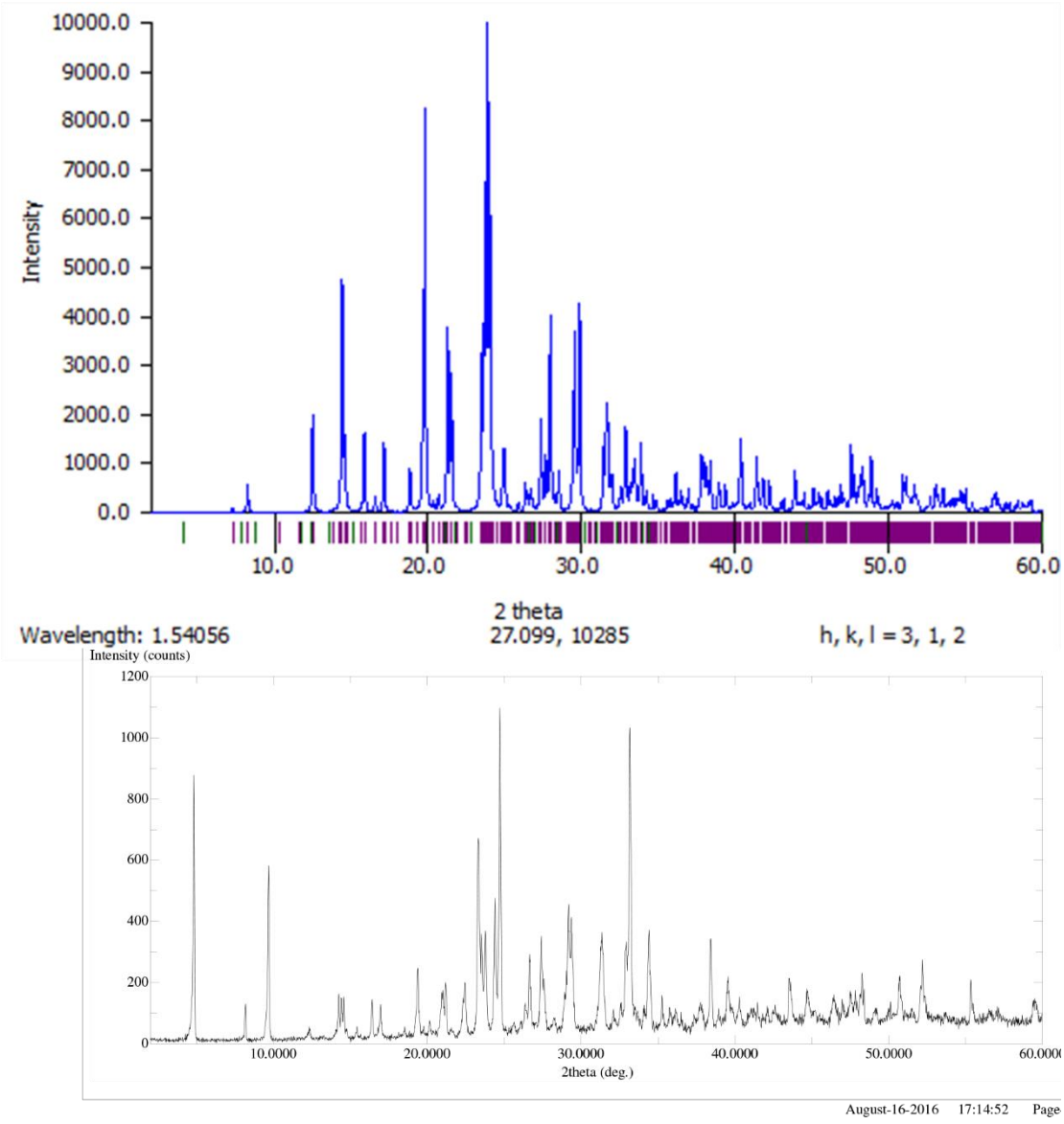

Figure III.3.15 PXRD Pattern (*top*, calculated; *bottom*, experimental) for compound **18**, 4-Bromophenethylammonium Formate

III.3.16 Powder Pattern for Compound 19, 2,4-Dichlorophenethylammonium Formate

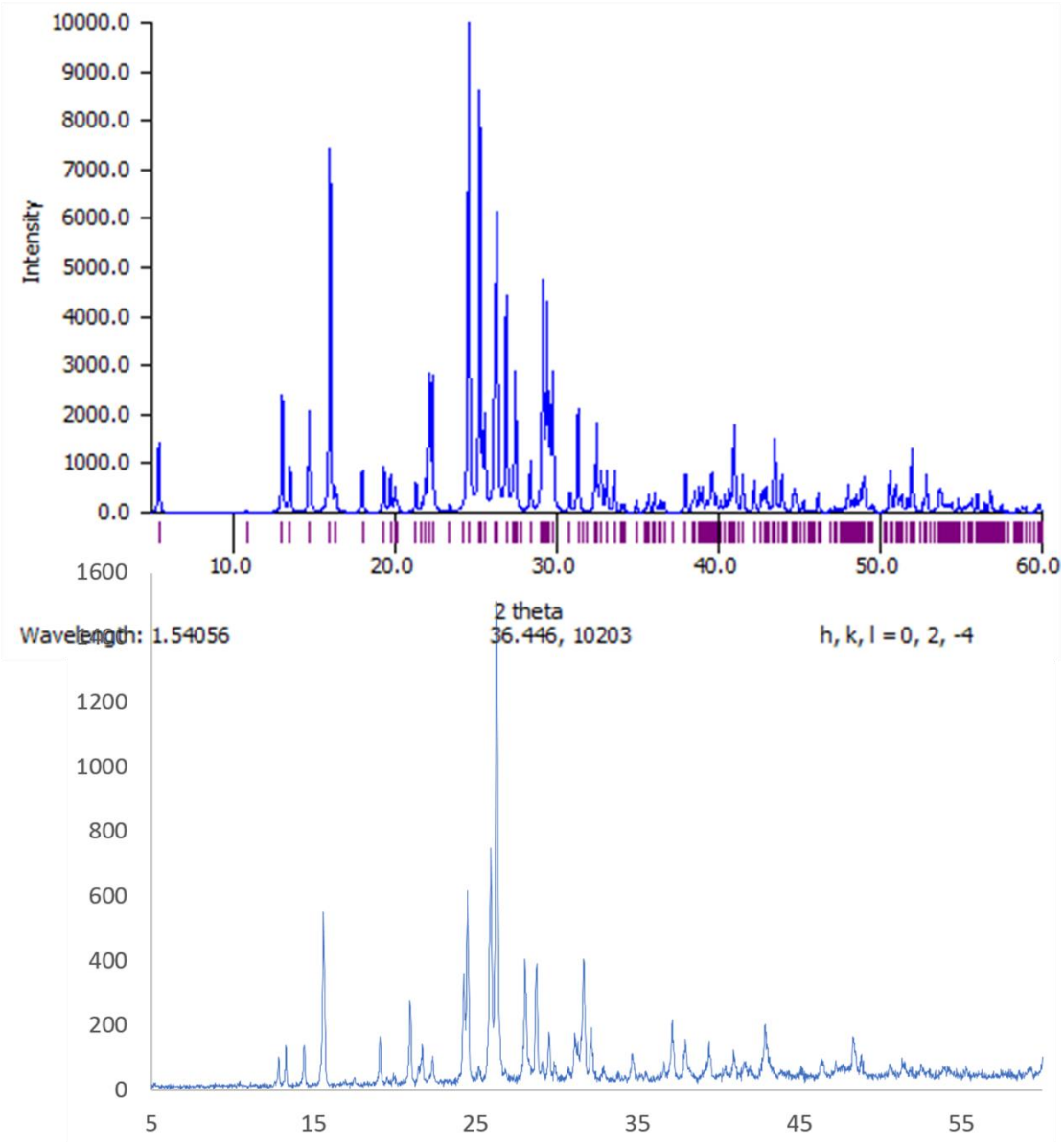

Figure III.3.16 PXRD Pattern (*top*, calculated; *bottom*, experimental) for compound **19**, 2,4-Dichlorophenethylammonium Formate

III.3.17 Powder Pattern for Compound 20, Di-N-Octylammonium Formate

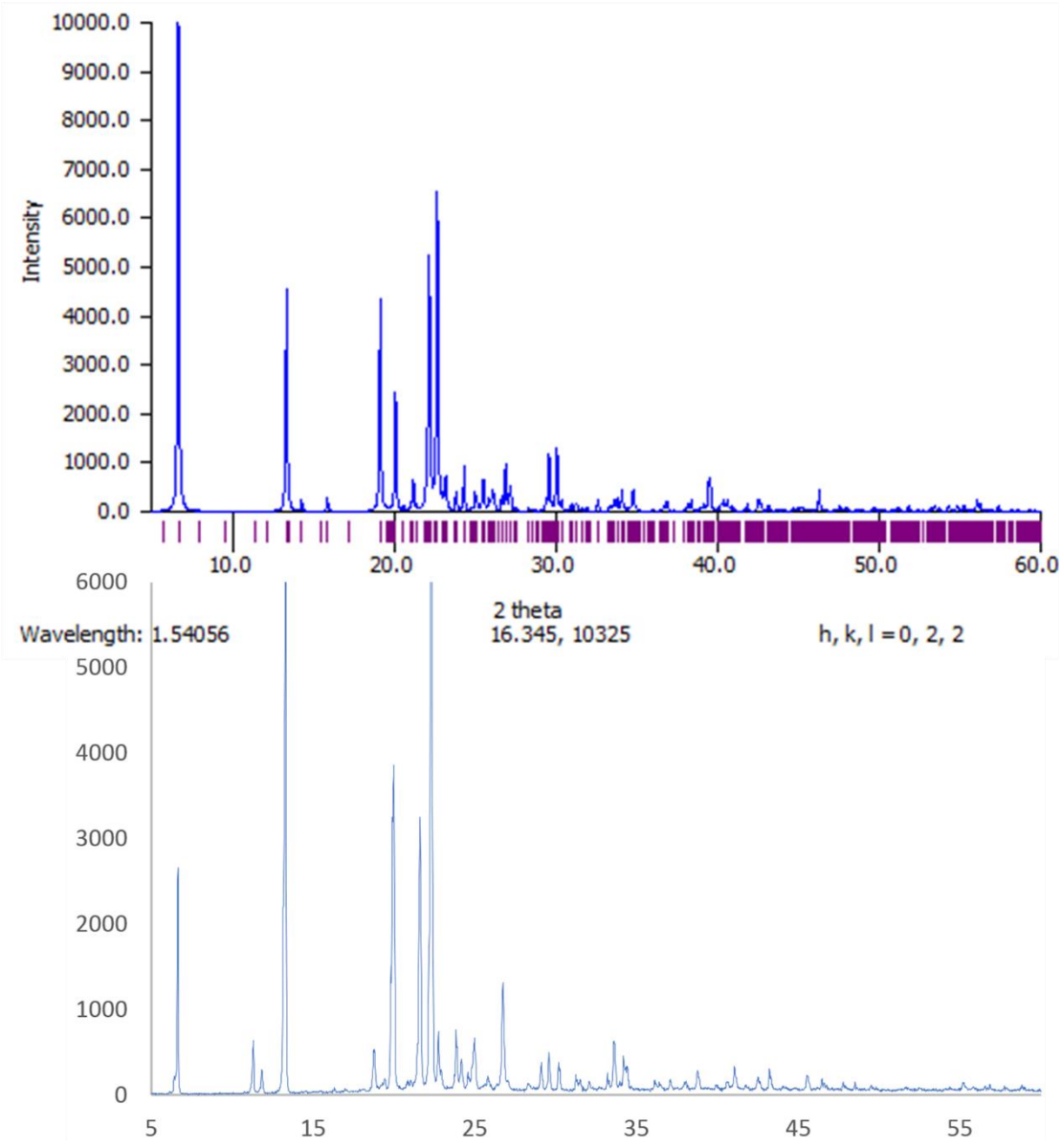

Figure III.3.17 PXRD Pattern (*top*, calculated; *bottom*, experimental) for compound **20**, Di-N-Octylammonium Formate

III.3.18 Powder Pattern for Compound 21, Dicyclohexylammonium Formate

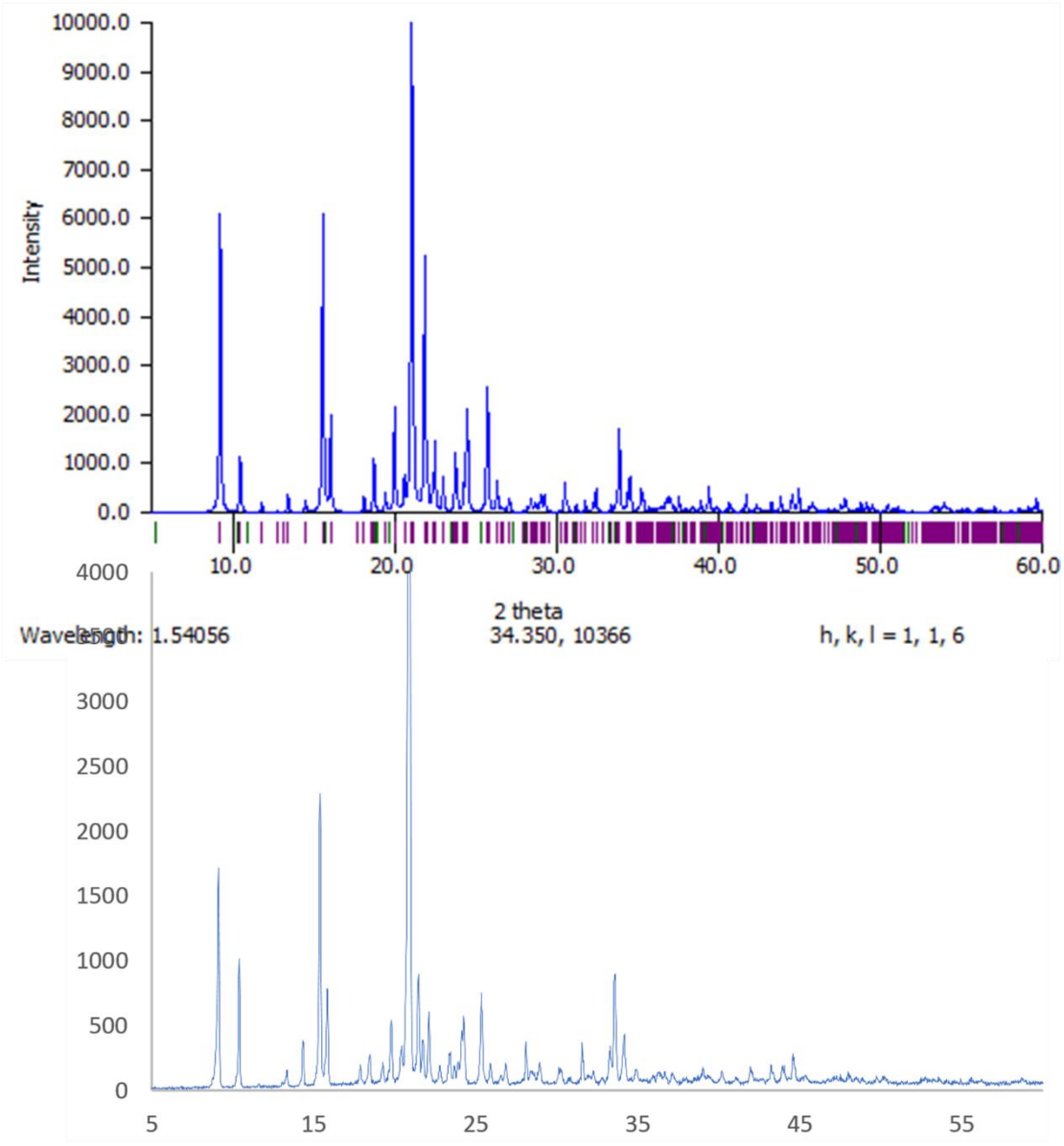

Figure III.3.18 PXRD Pattern (*top*, calculated; *bottom*, experimental) for compound **21**, Dicyclohexylammonium Formate

III.3.19 Powder Pattern for Compound 22, 4-Aminomethylpiperidine Carbamate

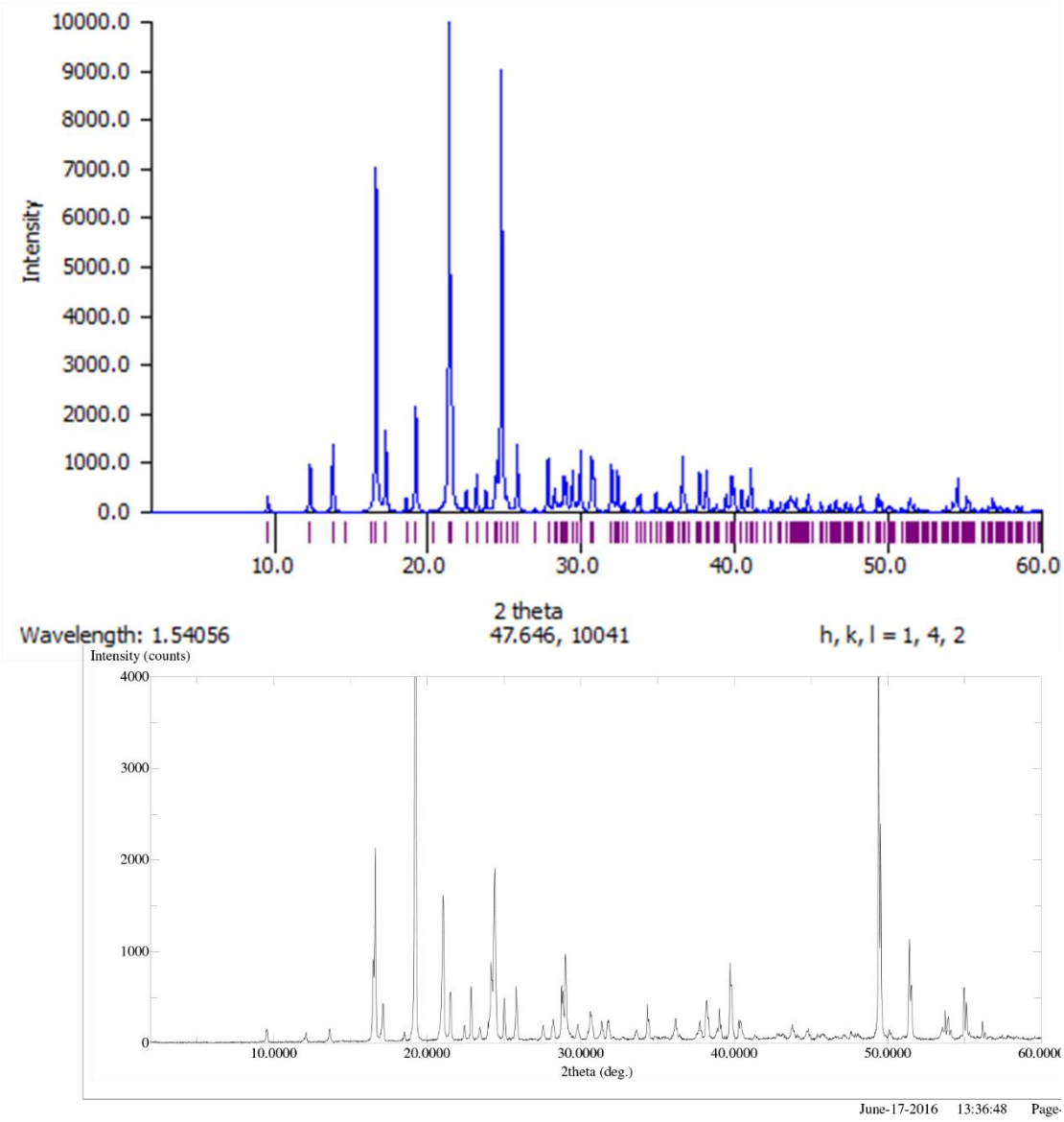

Figure III.3.19 PXRD Pattern (*top*, calculated; *bottom*, experimental) for compound **22**, 4-Aminomethylpiperidine Carbamate

III.3.20 Powder Pattern for Compound 30, *o*-Phenetidine-N-Formamide

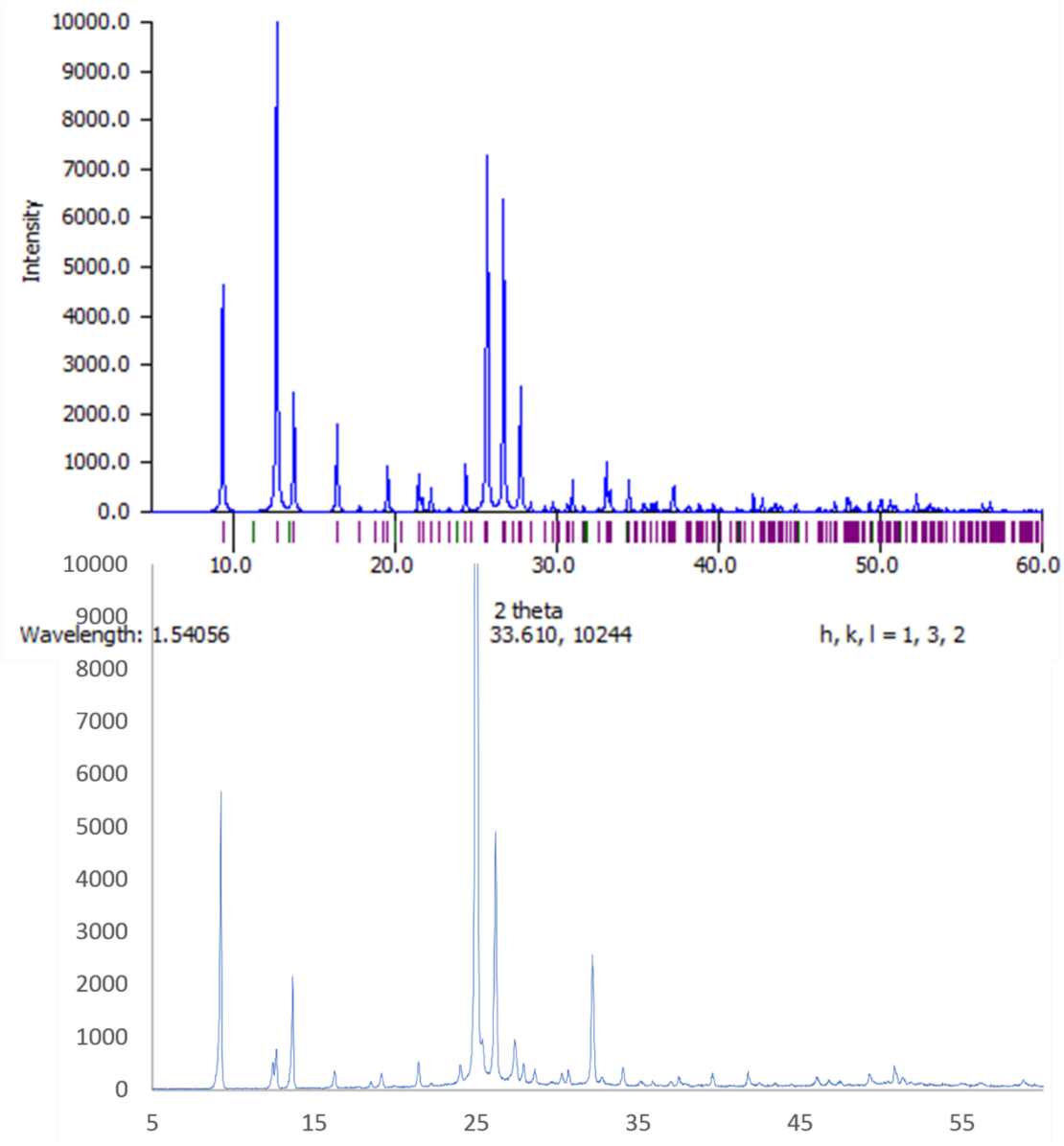

Figure III.3.20 PXRD Pattern (*top*, calculated; *bottom*, experimental) for compound **30**, *o*-Phenetidine-N-Formamide

III.3.21 Powder Pattern for Compound 31, 1-Amino-2-Methylnaphthyene-N-Formamide

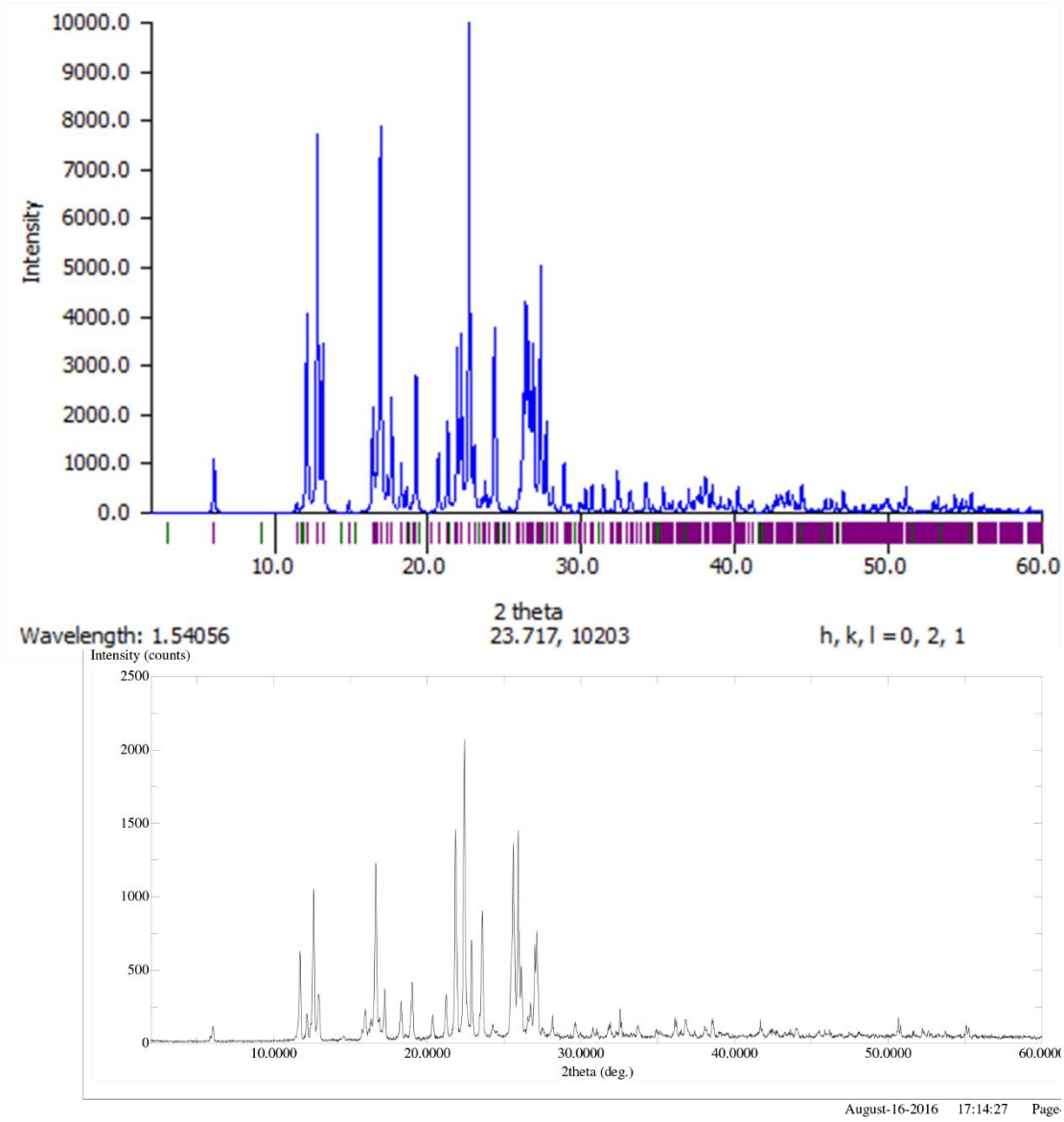

Figure III.3.21 PXRD Pattern (*top*, calculated; *bottom*, experimental) for compound **31**, 1-Amino-2-Methylnaphthyene-N-Formamide

Appendix IV

Thermal Data

All TGA experiments were performed on a Thermal Advantage TGA Q50, and all TGA plots and data were handled with the bundled Universal Analysis Software package. Prior to experimental temperature ramp, each sample is held isothermally for five minutes at room temperature to balance the pan and allow for the evaporation of any remaining solvent on the surface of the crystals. For the experimental procedure, the ground crystalline sample is placed on the platinum TGA pan and scanned from 25 °C to 400 °C, at a rate of 10° C per minute, under constant nitrogen flow.

IV.1 Thermal Data for Chapter 2 Compounds

IV.1.1 Thermal Data for Compound 2, Mn_{12}-2-Me, $Mn_{12}O_{12}(O_2CPh\text{-}o\text{-}Me)_{16}(H_2O)_4$

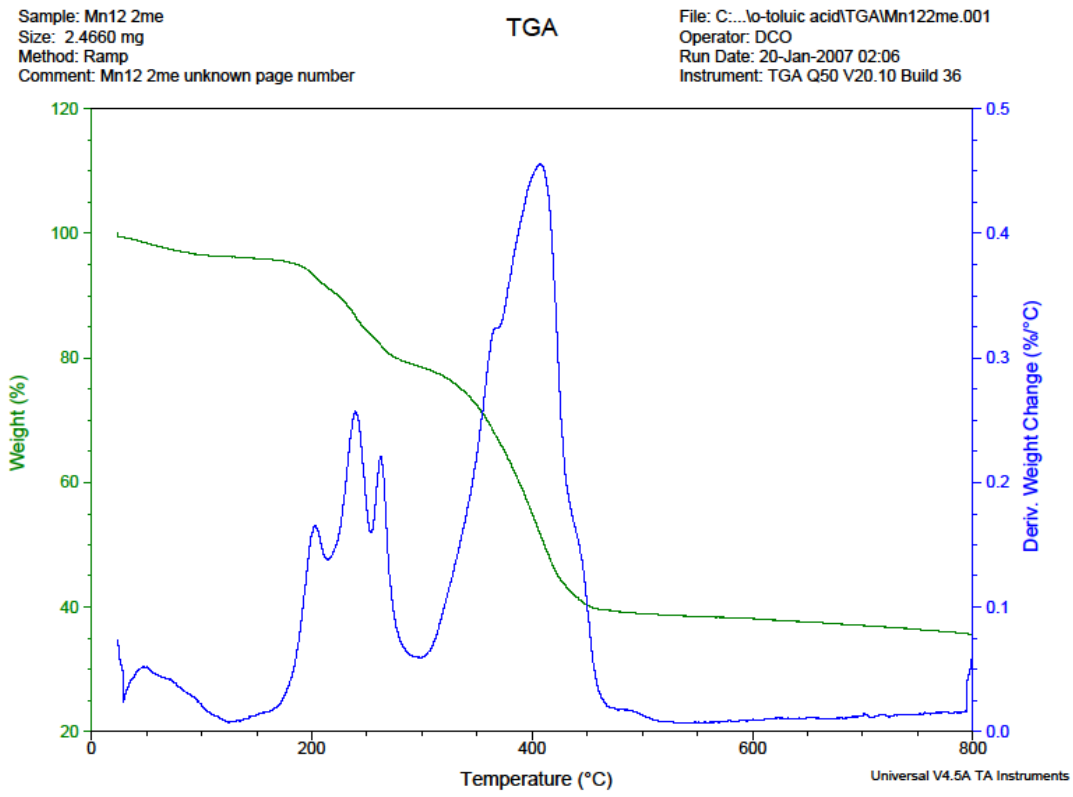

Figure IV.1.1 TGA Plot for Compound **2**, Mn_{12}-2-Me, $Mn_{12}O_{12}(O_2CPh\text{-}o\text{-}Me)_{16}(H_2O)_4$

IV.1.2 Thermal Data for Compound 4, Mn_{12}-2-Ph, $Mn_{12}O_{12}(O_2CPh\text{-}o\text{-}Ph)_{16}(H_2O)_4$

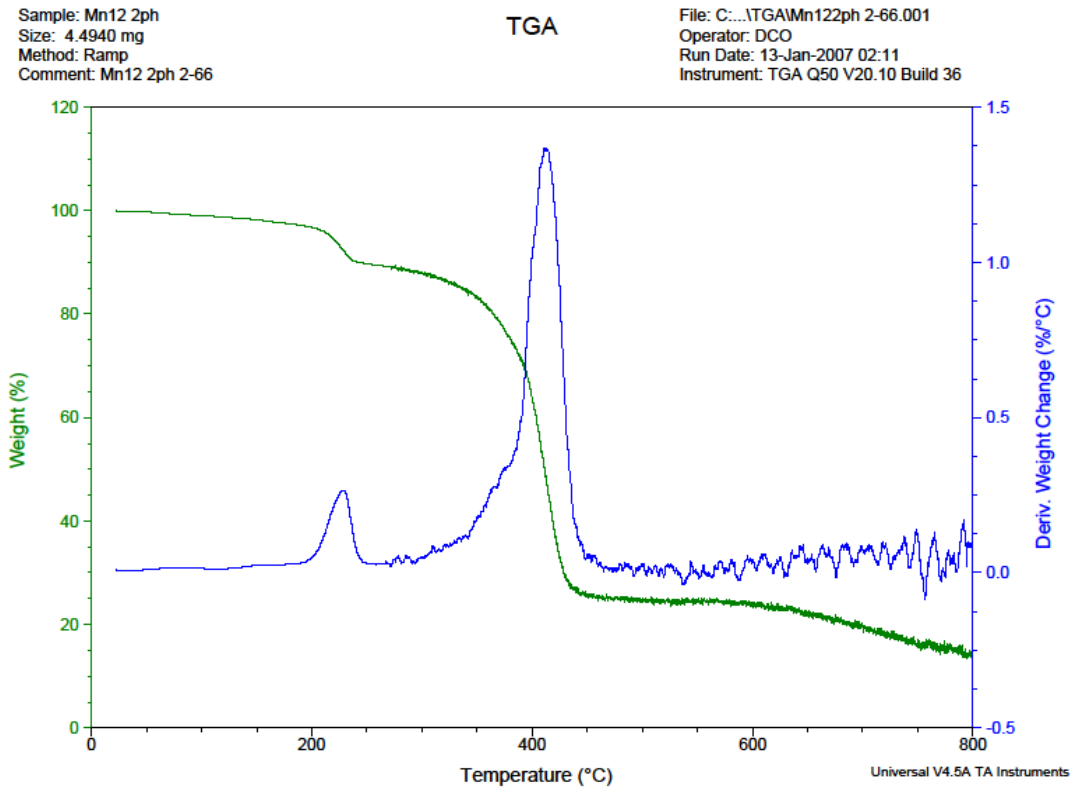

Figure IV.1.2 TGA Plot for Compound **4**, Mn_{12}-2-Ph, $Mn_{12}O_{12}(O_2CPh\text{-}o\text{-}Ph)_{16}(H_2O)_4$

IV.2 Thermal Data for Chapter 3 Compounds

IV.2.1 Thermal Data for Compound 4a, "Mn_3O-2-Methyl" (rod), $Mn_{12}O_{12}(O_2CPh\text{-}o\text{-}Me)_{16}(H_2O)_4$

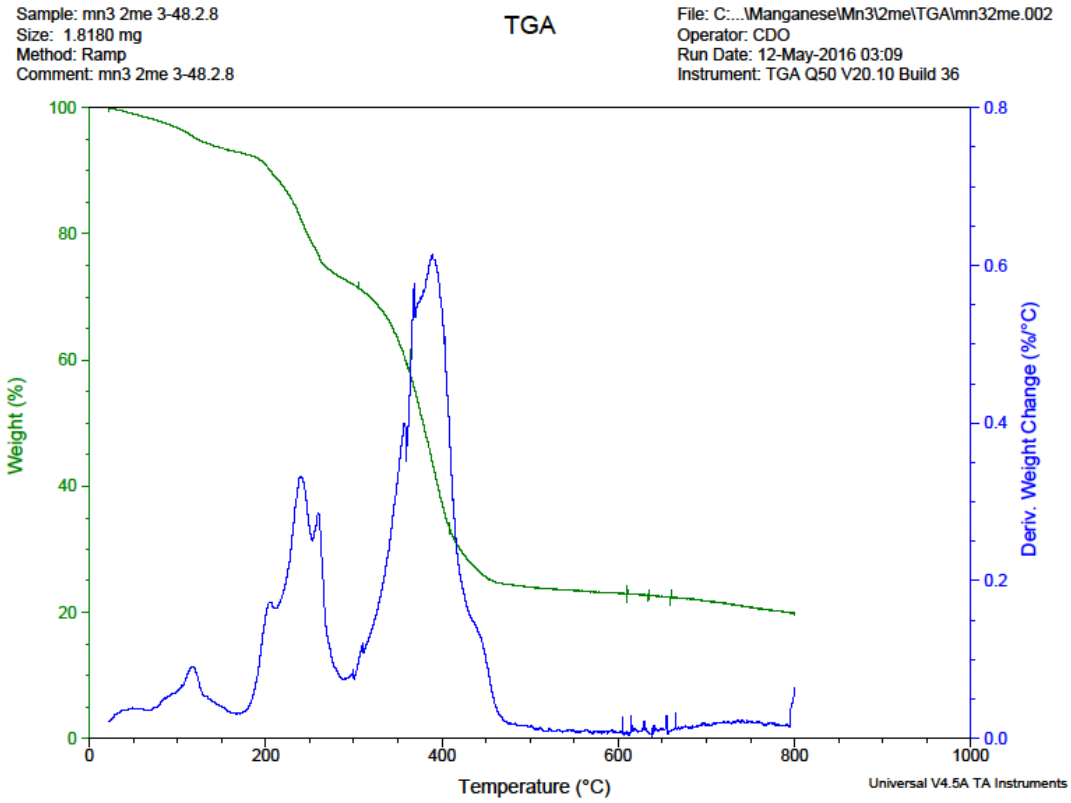

Figure IV.2.1 TGA Plot for Compound **4a**, "Mn_3O-2-Methyl" (rod), $Mn_{12}O_{12}(O_2CPh\text{-}o\text{-}Me)_{16}(H_2O)_4$

IV.3 Thermal Data for Chapter 4 Compounds

IV.3.1 Thermal Data for Compound 1, Benzylammonium Formate

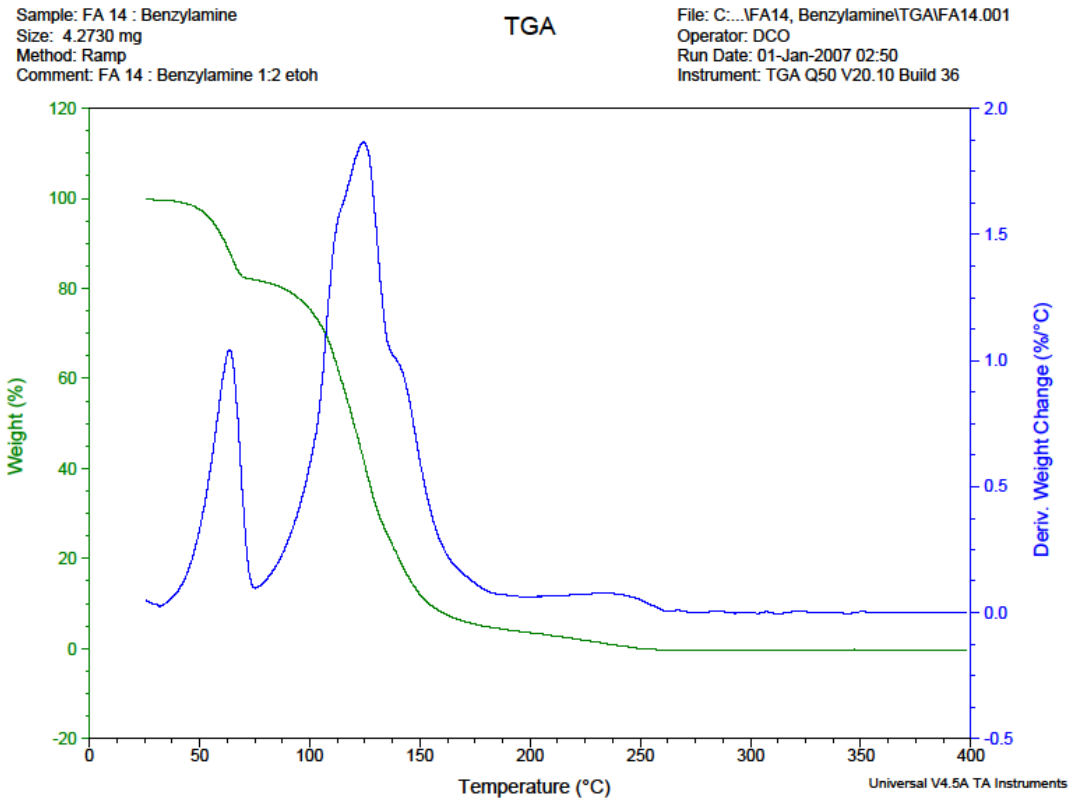

Figure IV.3.1 TGA Plot for Compound **1**, Benzylammonium Formate

IV.3.2 Thermal Data for Compound 2, 2-Methylbenzylammonium Formate

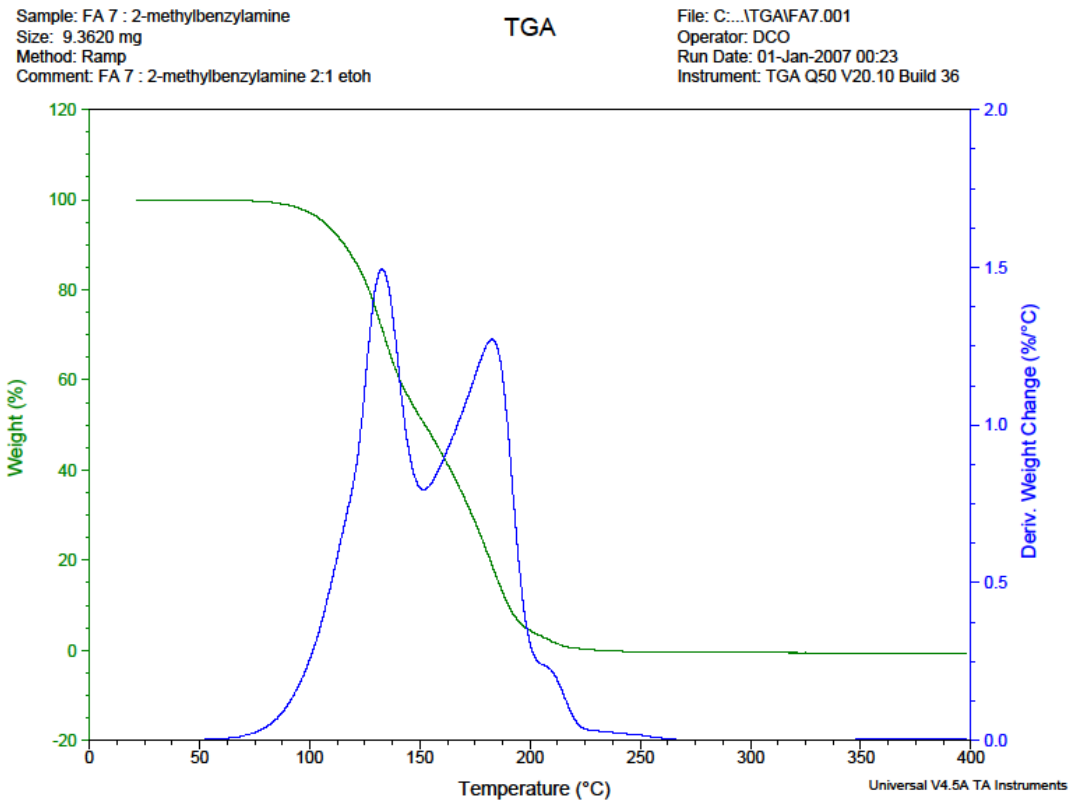

Figure IV.3.2 TGA Plot for Compound **2**, 2-Methylbenzylammonium Formate

IV.3.3 Thermal Data for Compound 4, 4-Methylbenzylammonium Formate

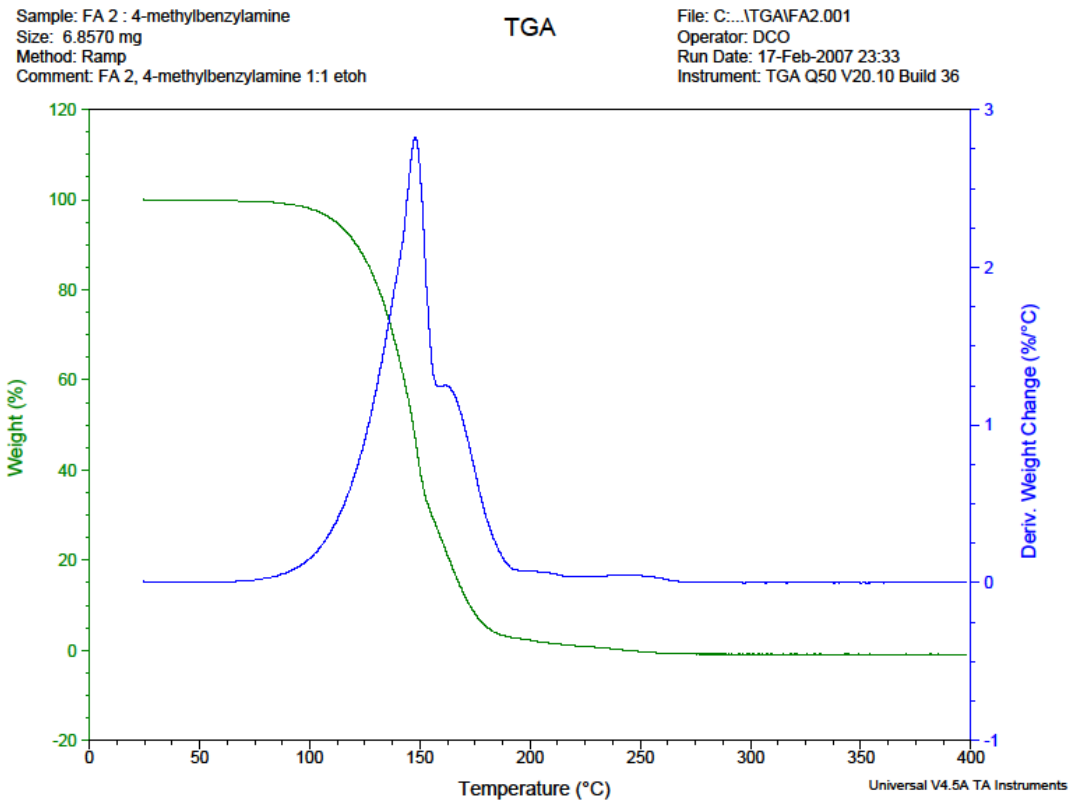

Figure IV.3.3 TGA Plot for Compound **4**, 4-Methylbenzylammonium Formate

IV.3.4 Thermal Data for Compound 7, 4-*Tert*-Butylbenzylammonium Formate

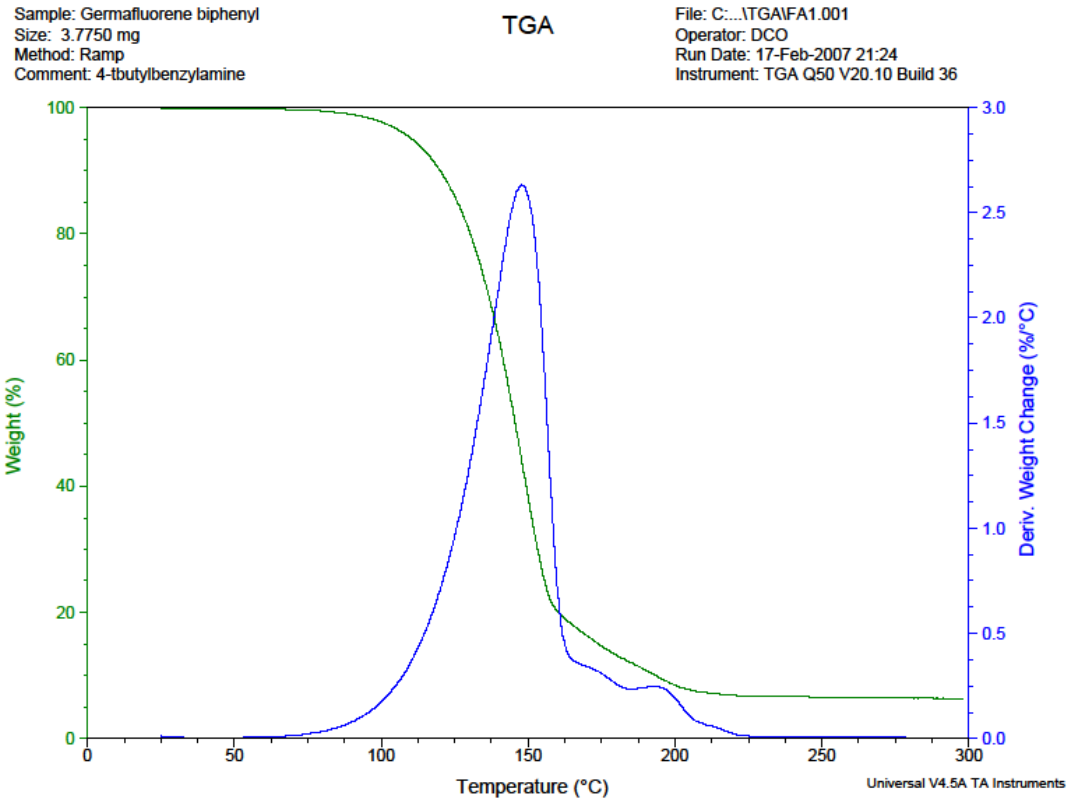

Figure IV.3.4 TGA Plot for Compound **7**, 4-*Tert*-Butylbenzylammonium Formate

IV.3.5 Thermal Data for Compound 8, 3-Chloronenzylammonium Formate

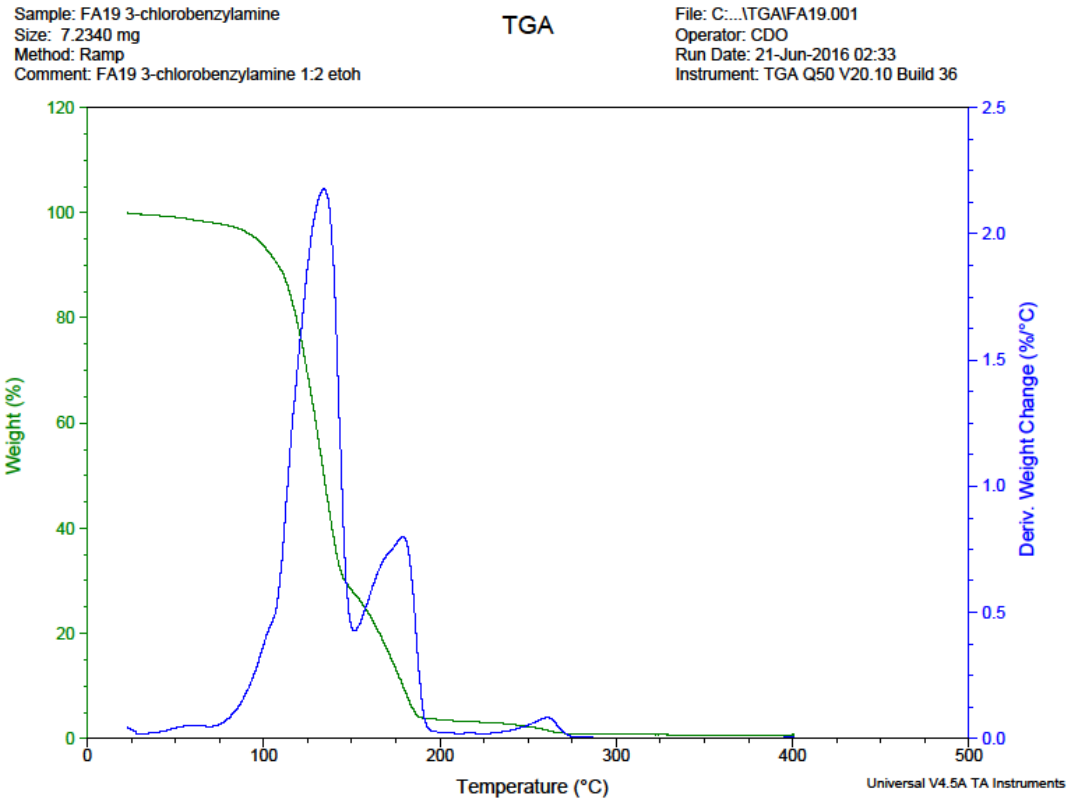

Figure IV.3.5 TGA Plot for Compound **8**, 3-Chloronenzylammonium Formate

IV.3.6 Thermal Data for Compound 9, 4-Chlorobenzylammonium Formate

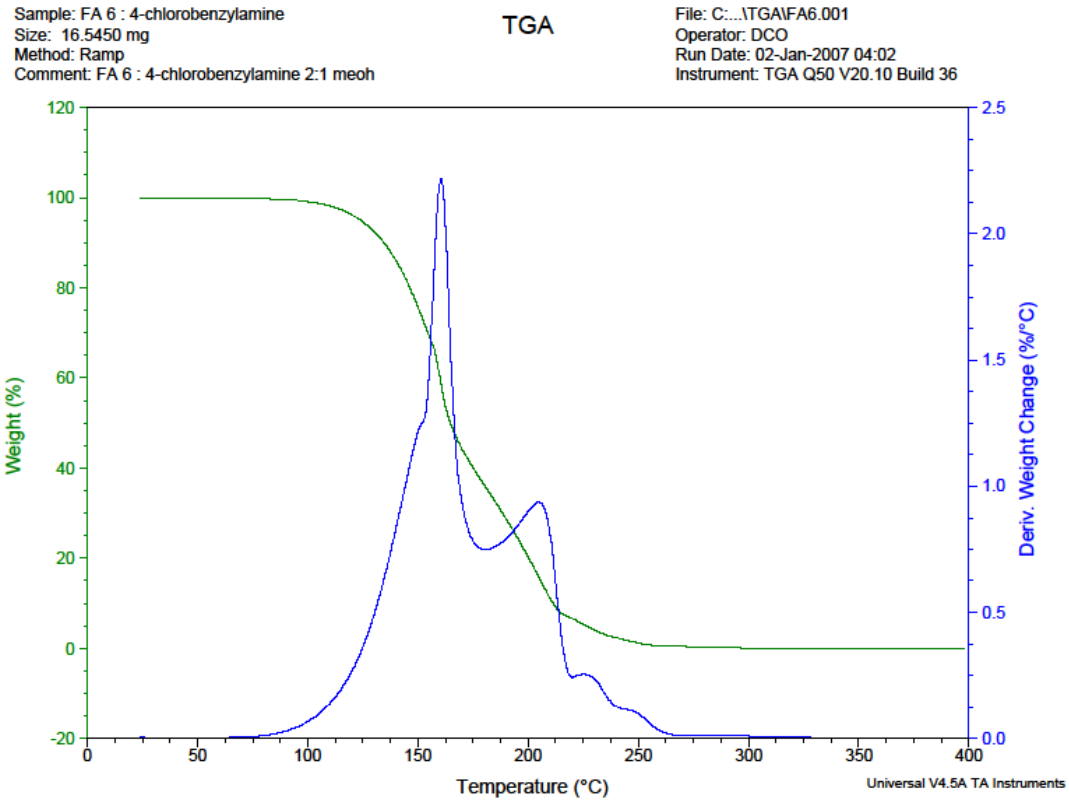

Figure IV.3.6 TGA Plot for Compound **9**, 4-Chlorobenzylammonium Formate

IV.3.7 Thermal Data for Compound 10, 3,5-Difluorobenzylammonium Formate

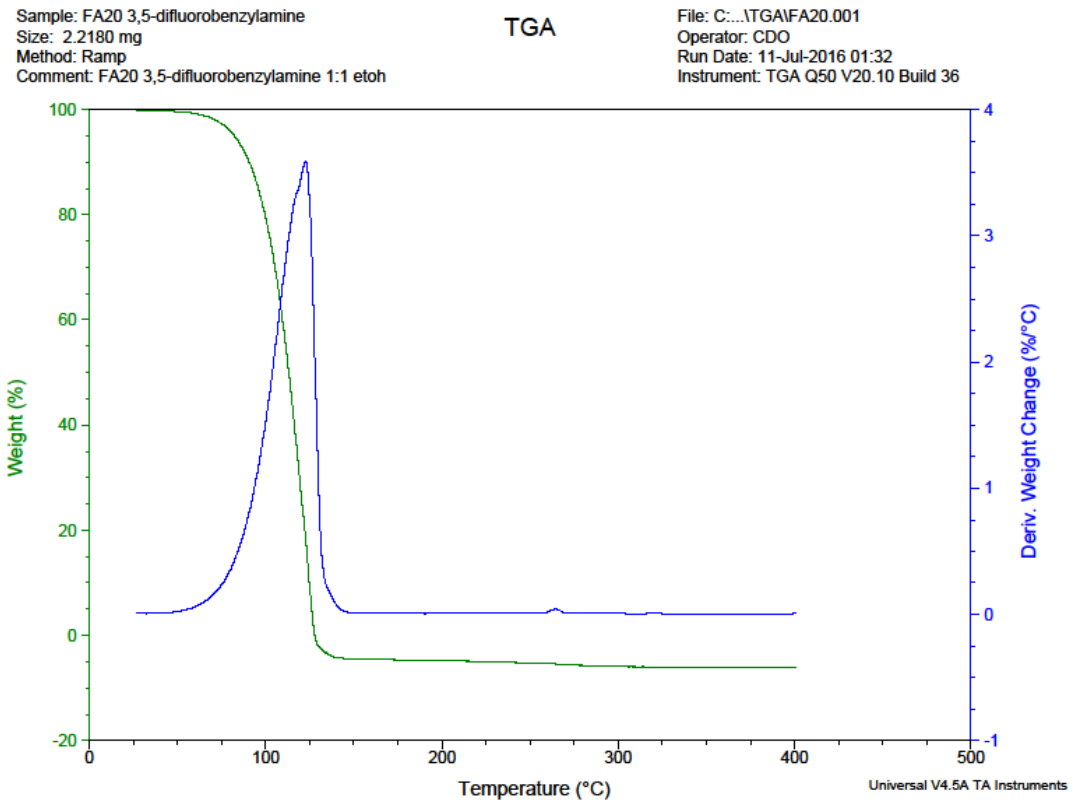

Figure IV.3.7 TGA Plot for Compound **10**, 3,5-Difluorobenzylammonium Formate

IV.3.8 Thermal Data for Compound 11, 1-(1-Naphthyl)-Benzylammonium Formate

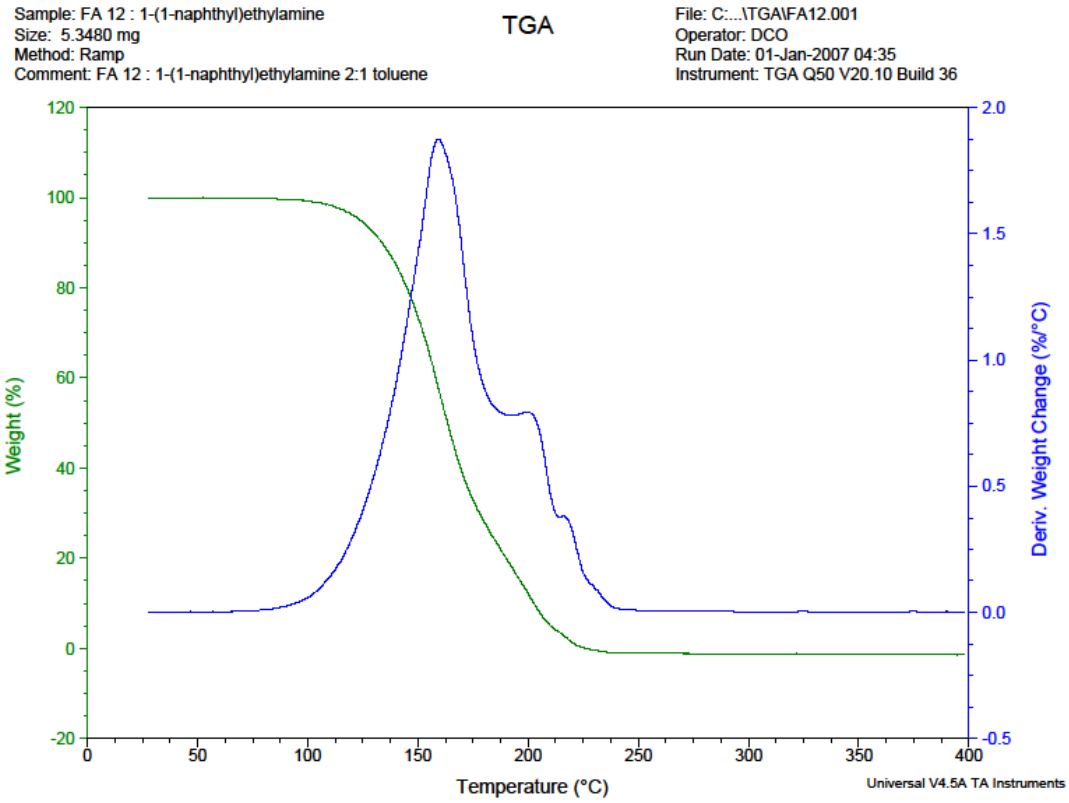

Figure IV.3.8 TGA Plot for Compound **11**, 1-(1-Naphthyl)-Benzylammonium Formate

IV.3.9 Thermal Data for Compound 12, 4-Aminobenzylammonium Formate

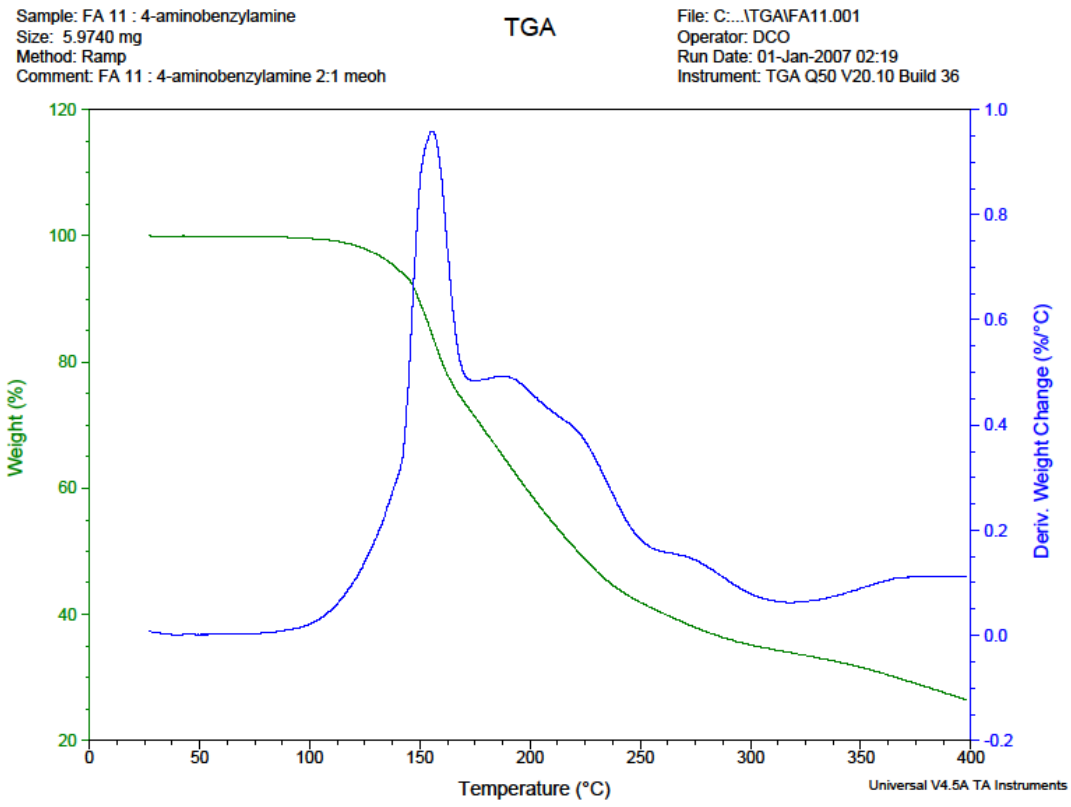

Figure IV.3.9 TGA Plot for Compound **12**, 4-Aminobenzylammonium Formate

IV.3.10 Thermal Data for Compound 13, Phenethylammonium Formate

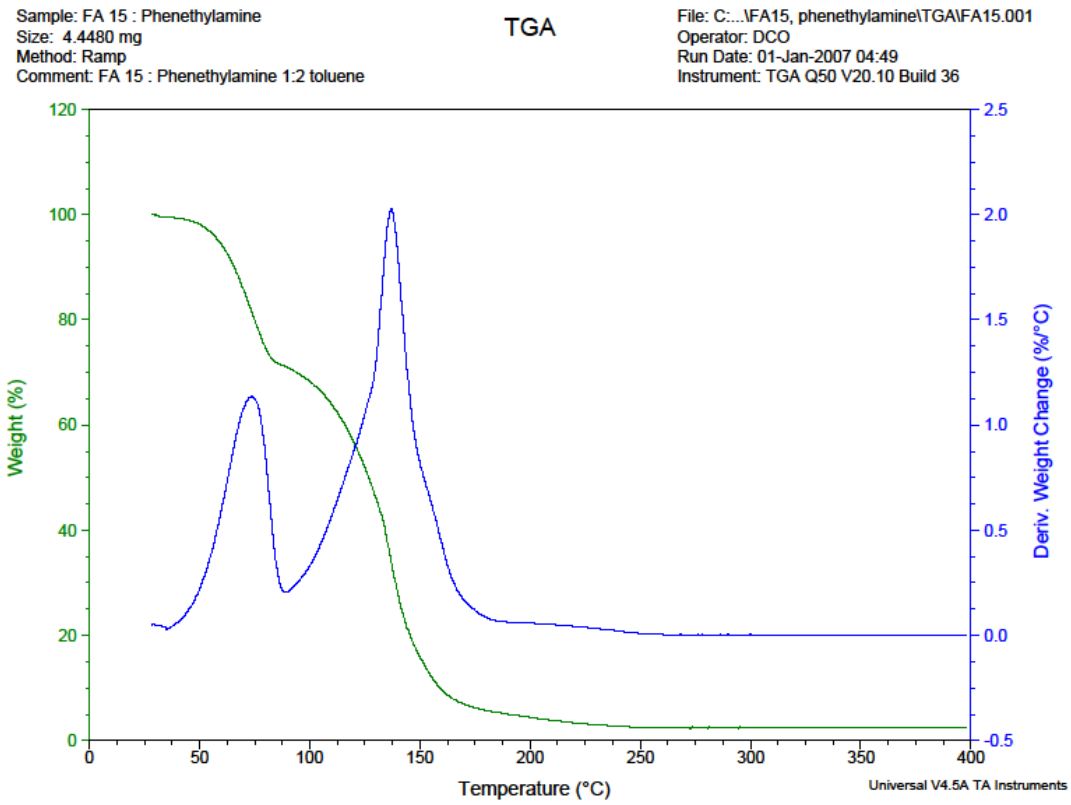

Figure IV.3.10 TGA Plot for Compound **13**, Phenethylammonium Formate

IV.3.11 Thermal Data for Compound 14, 2-Chlorophenethylammonium Formate

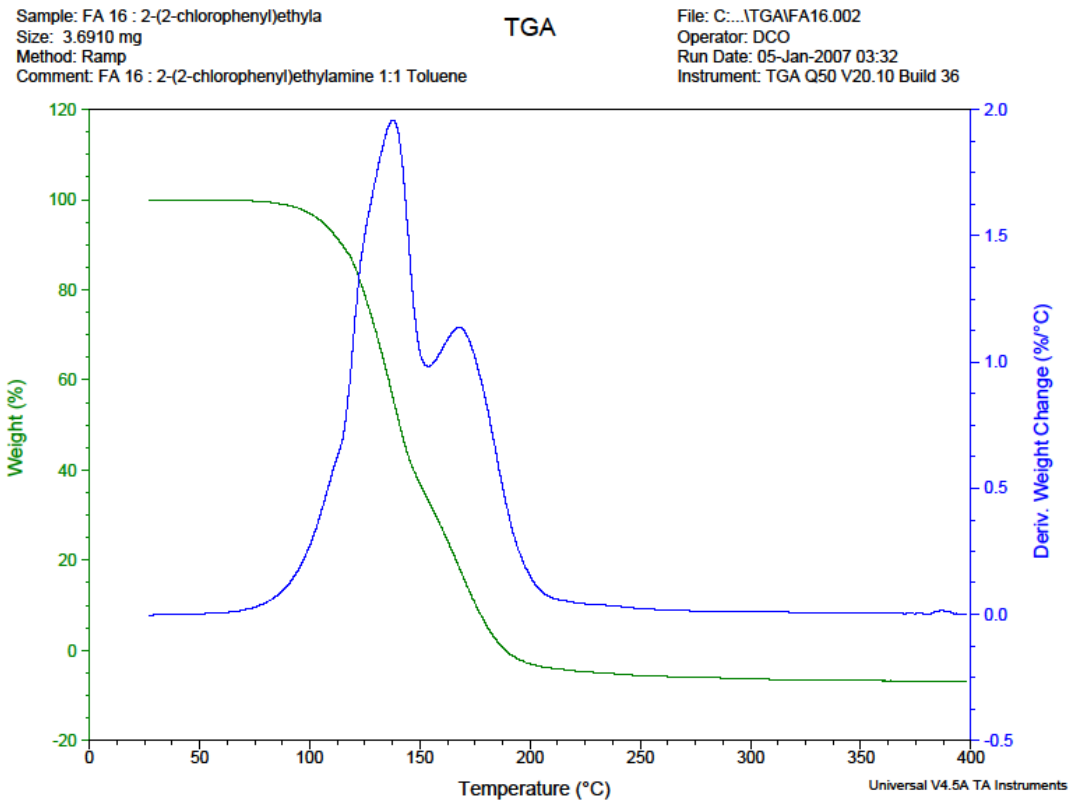

Figure IV.3.11 TGA Plot for Compound **14**, 2-Chlorophenethylammonium Formate

IV.3.12 Thermal Data for Compound 16, 3-Chlorophenethylammonium Formate

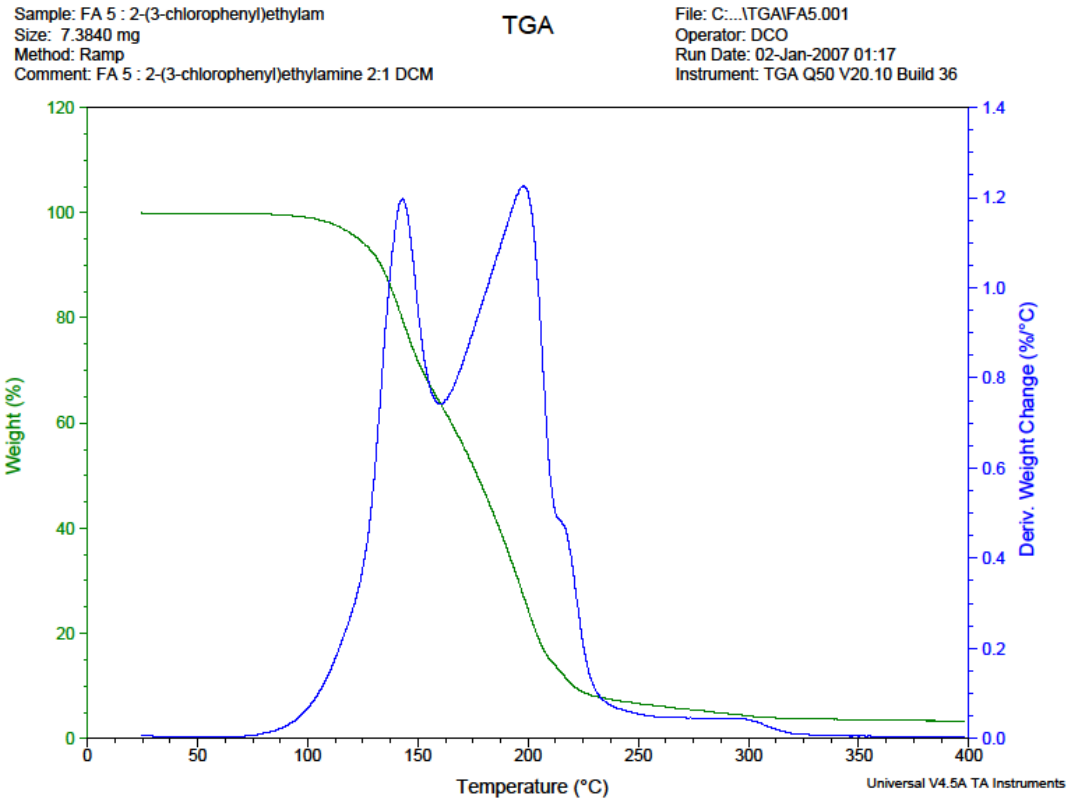

Figure IV.3.12 TGA Plot for Compound **16**, 3-Chlorophenethylammonium Formate

IV.3.13 Thermal Data for Compound 17, 4-Chlorophenethylammonium Formate

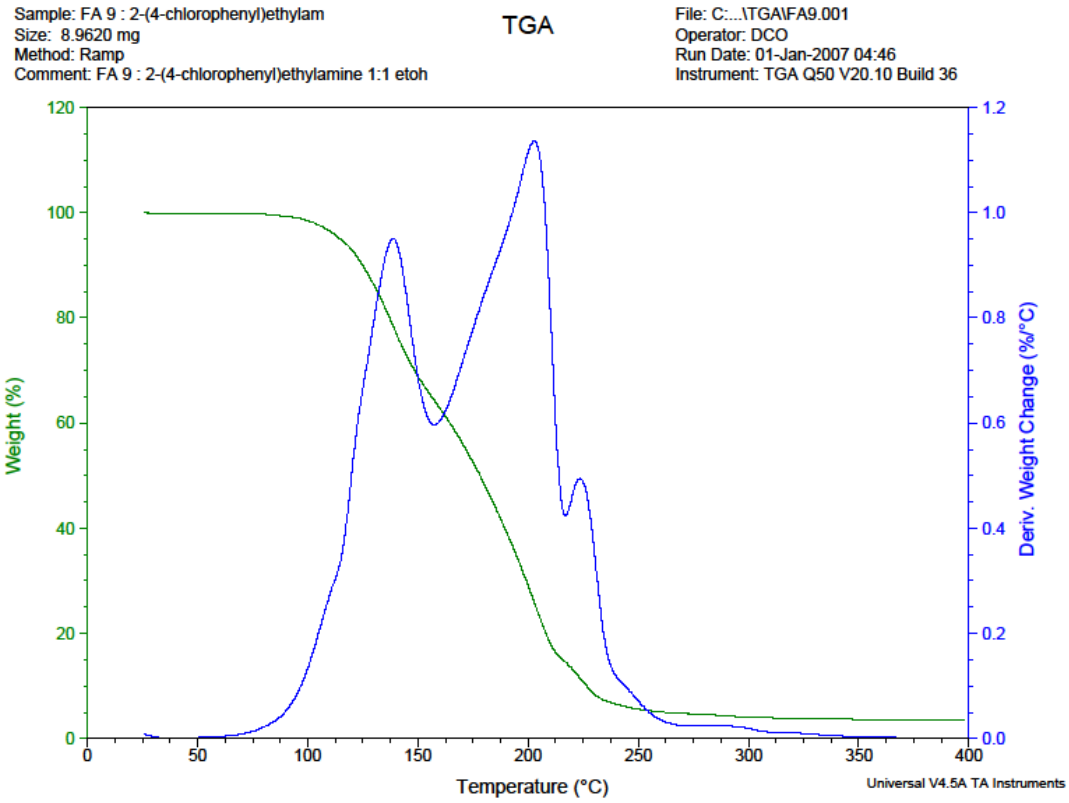

Figure IV.3.13 TGA Plot for Compound **17**, 4-Chlorophenethylammonium Formate

IV.3.14 Thermal Data for Compound 19, 2,4-Dichlorophenethylammonium Formate

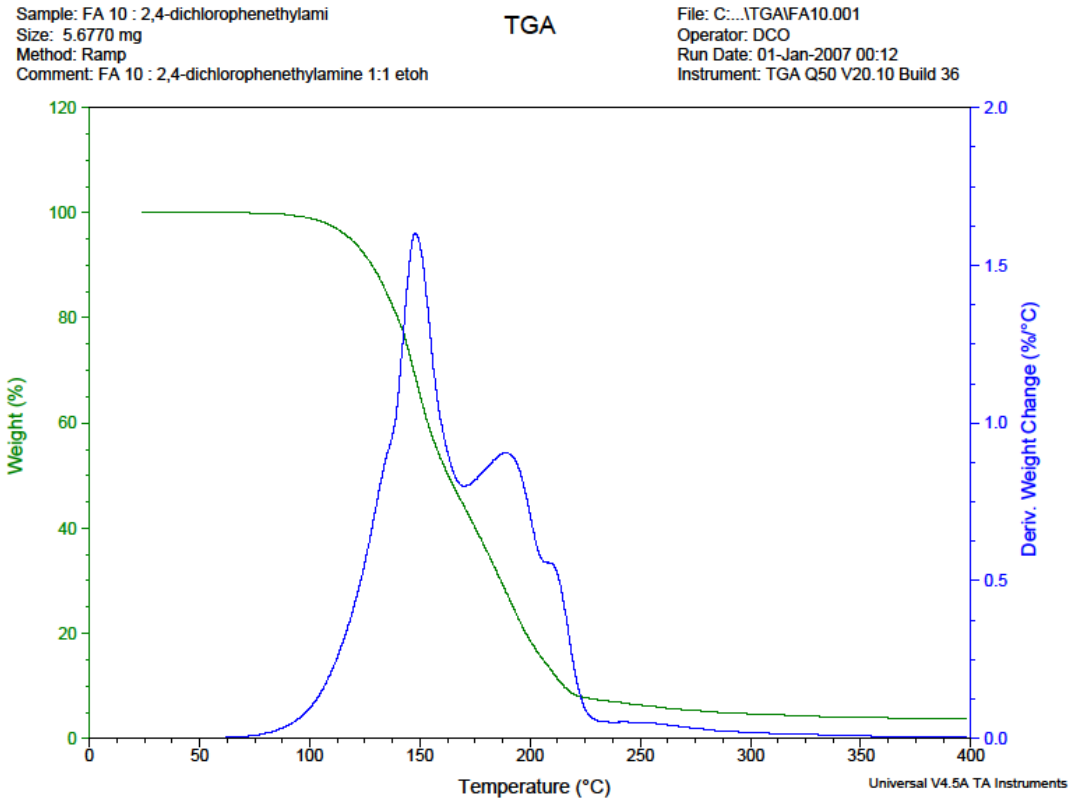

Figure IV.3.14 TGA Plot for Compound **19**, 2,4-Dichlorophenethylammonium Formate

IV.3.15 Thermal Data for Compound 20, Di-N-Octylammonium Formate

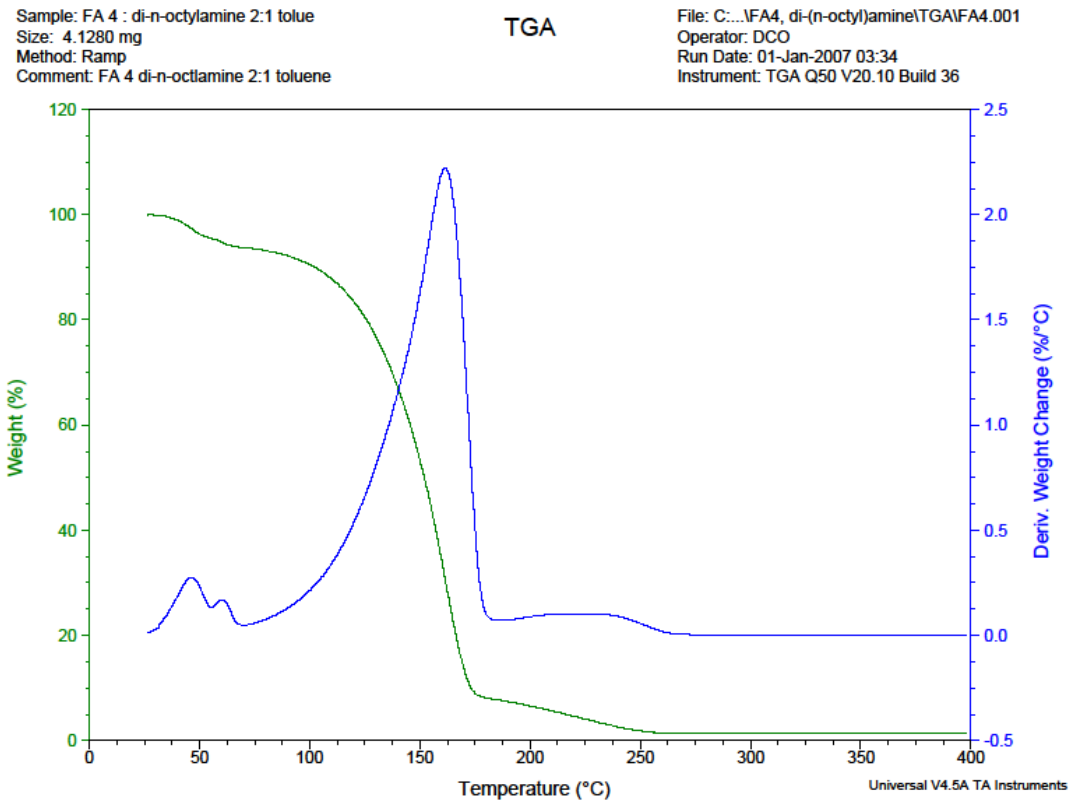

Figure IV.3.15 TGA Plot for Compound **20**, Di-N-Octylammonium Formate

IV.3.16 Thermal Data for Compound 21, Dicyclohexylammonium Formate

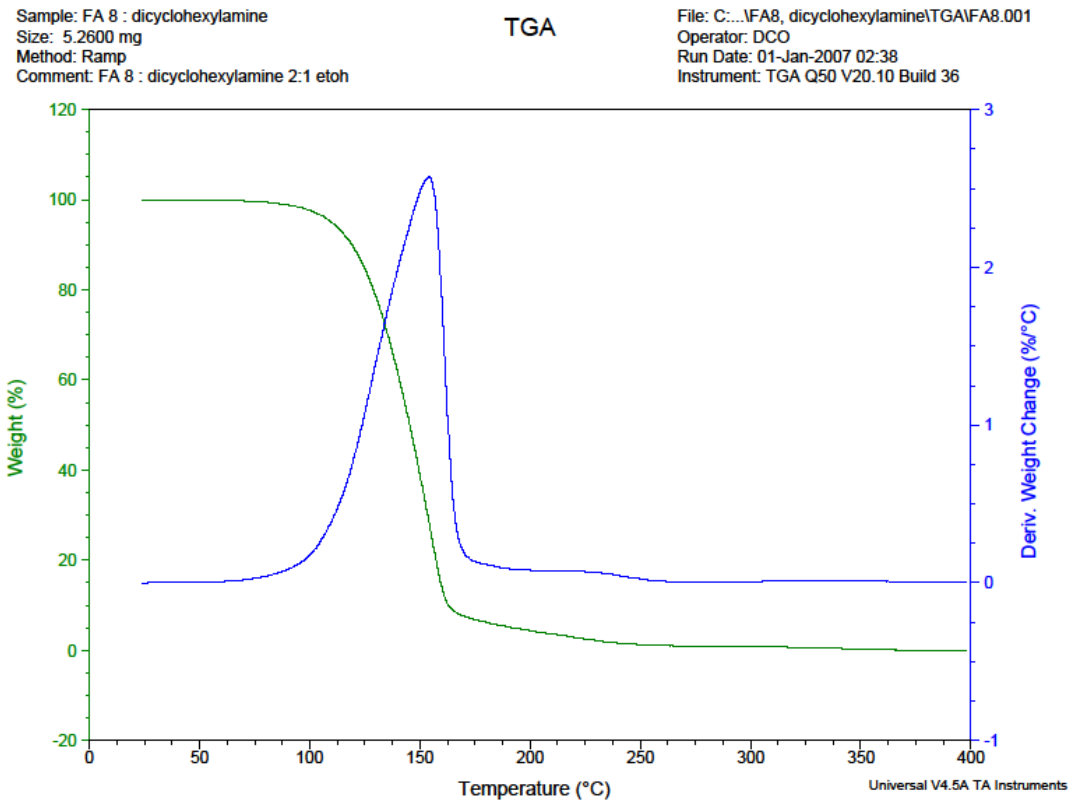

Figure IV.3.16 TGA Plot for Compound **21**, Dicyclohexylammonium Formate

IV.3.17 Thermal Data for Compound 22, 4-Aminomethylpiperidine Carbamate

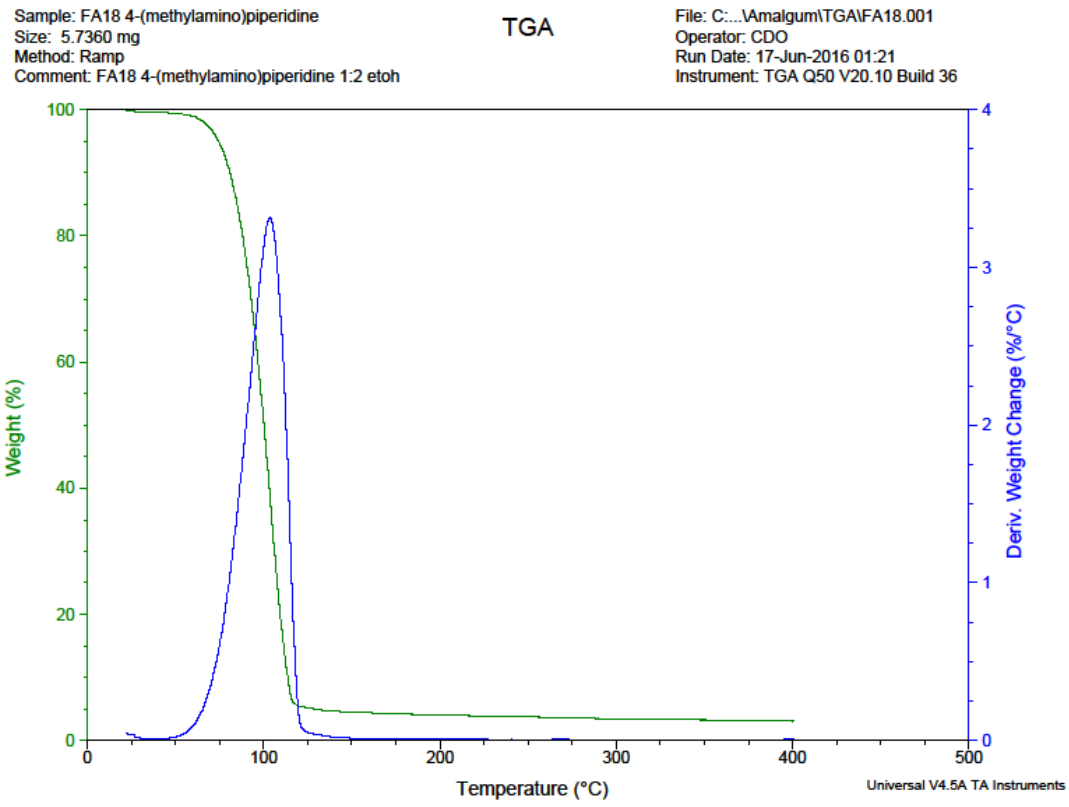

Figure IV.3.17 TGA Plot for Compound **22**, 4-Aminomethylpiperidine Carbamate

IV.3.18 Thermal Data for Compound 30, *o*-Anisidine-N-Formamide

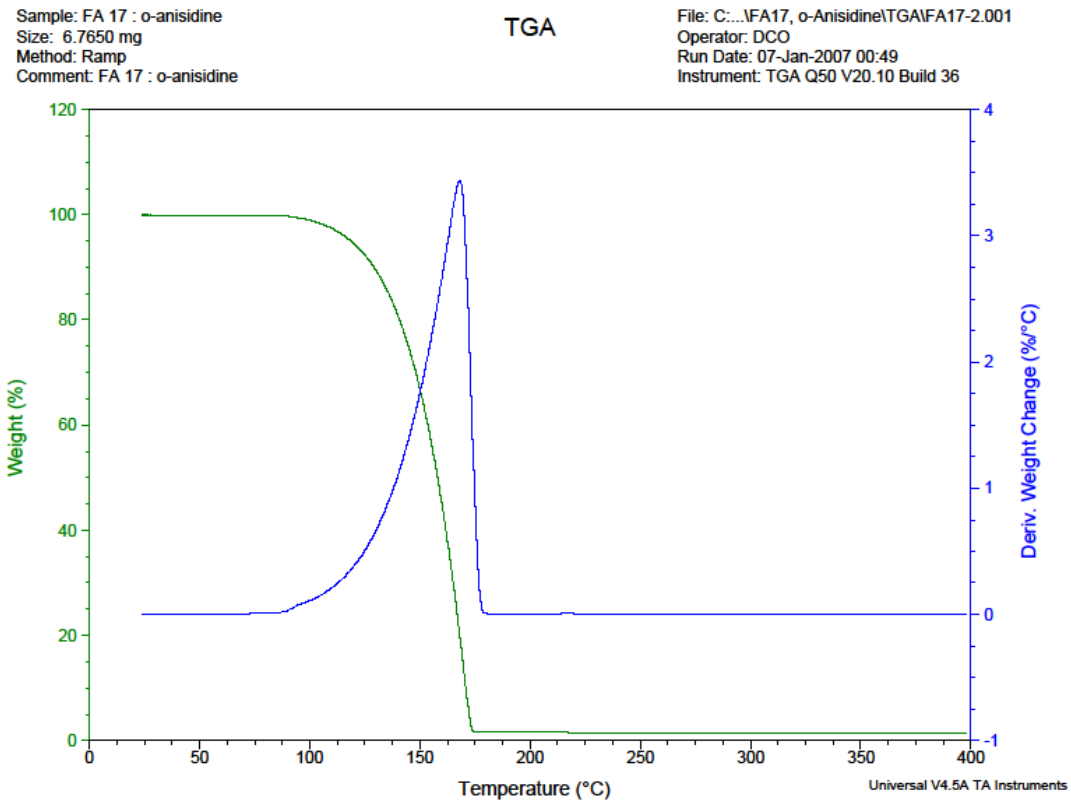

Figure IV.3.18 TGA Plot for Compound **30**, *o*-Anisidine-N-Formamide

Appendix V

Supplemental Compound Characterization

V.1 Supplemental Compound Characterization for Chapter 2

V.1.1 SEM Images of Compounds

SEM experiments and images were with a Jeol JSM-6320F Scanning Electron Microscope. Samples were gold sputtered before analysis. Sample chamber and pump brought to 10^{-7} torr and beam held at 5kV for each image at various magnifications (notated in the figure captions).

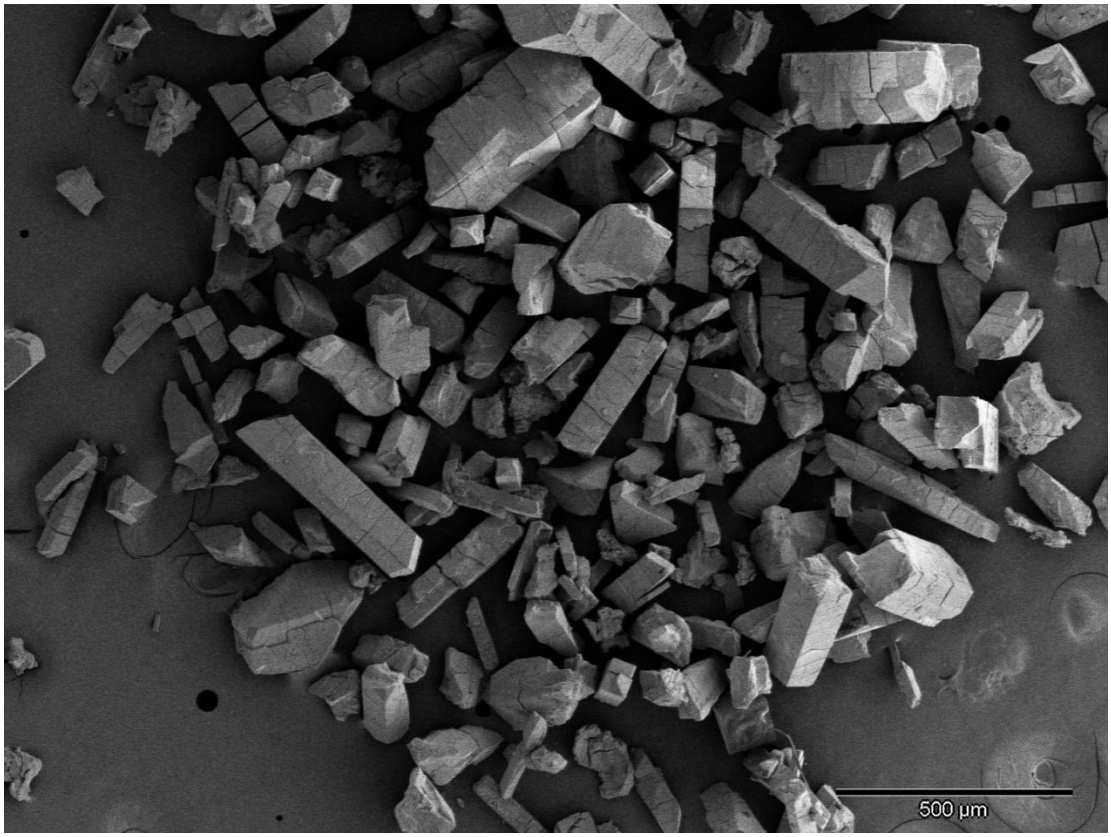

Figure V.1.1.1 SEM image of crystals of **1**. Taken at 5 kV, 50x magnification.

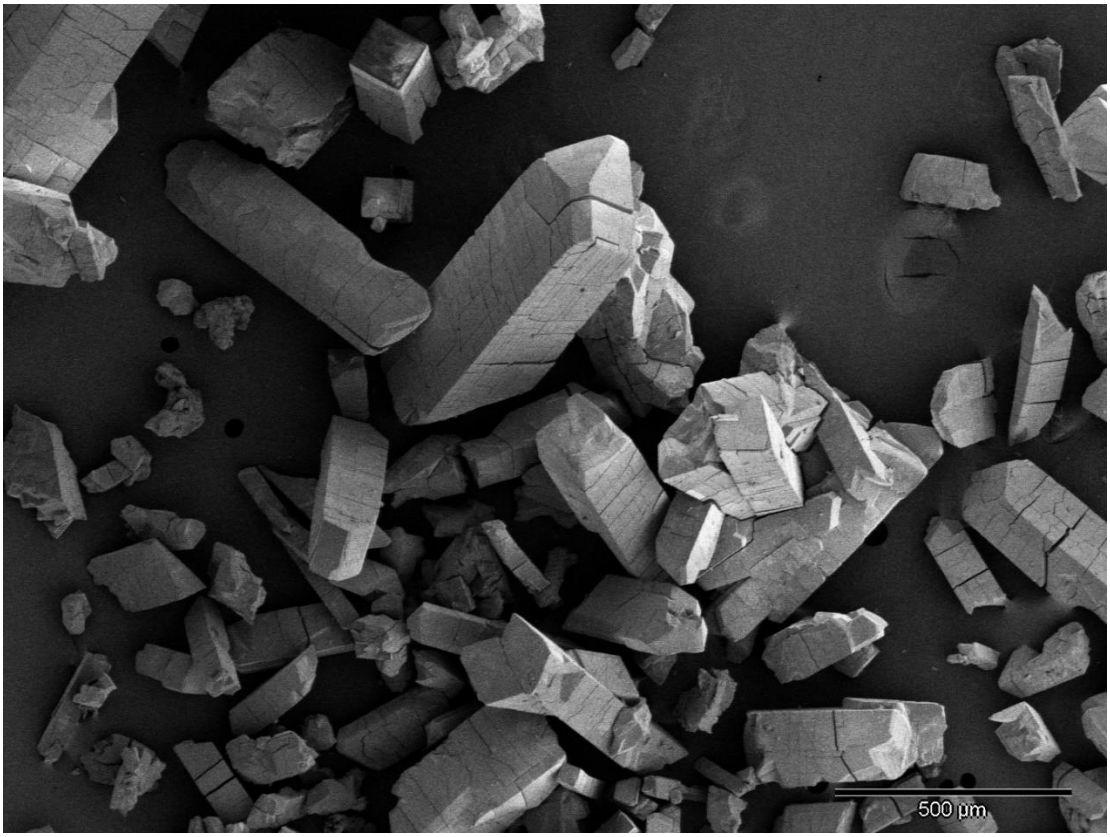

Figure V.1.1.2 SEM image of crystals of **1**. Taken at 5 kV, 50x magnification.

Figure V.1.1.3 SEM image of crystals of **1**. Taken at 5 kV, 100x magnification.

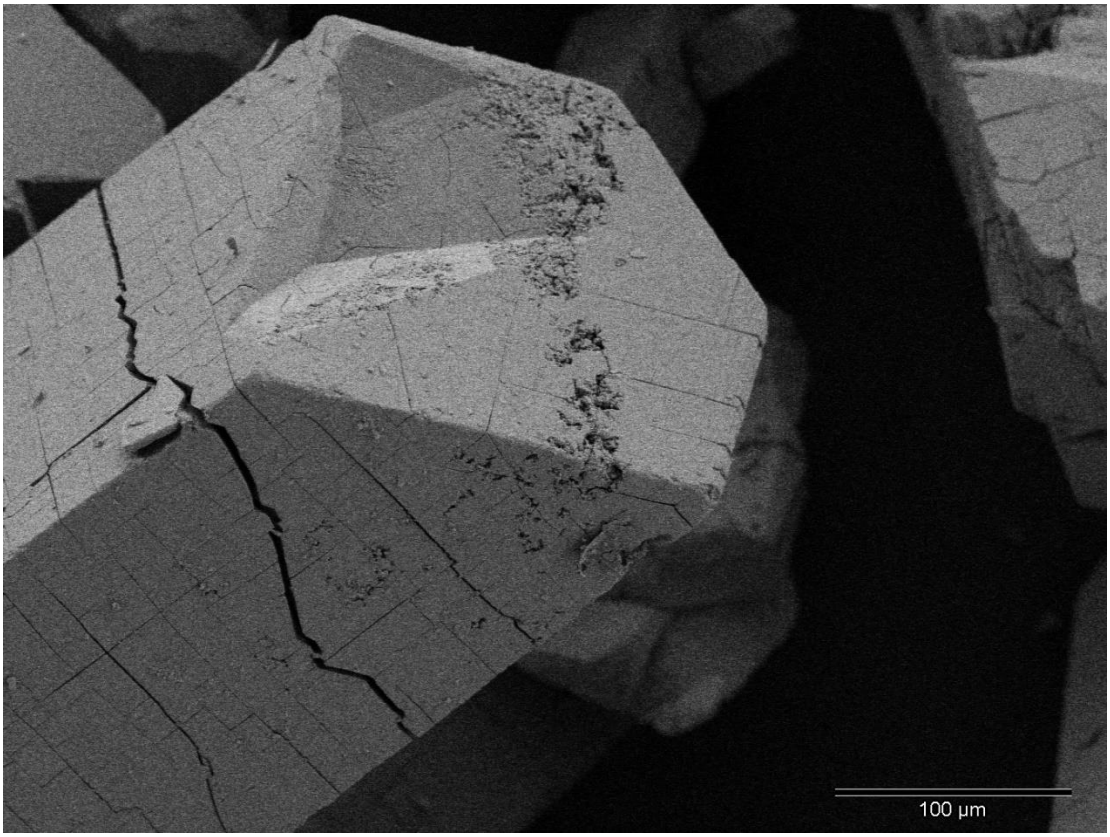

Figure V.1.1.4 SEM image of crystals of **1**. Taken at 5 kV, 250x magnification.

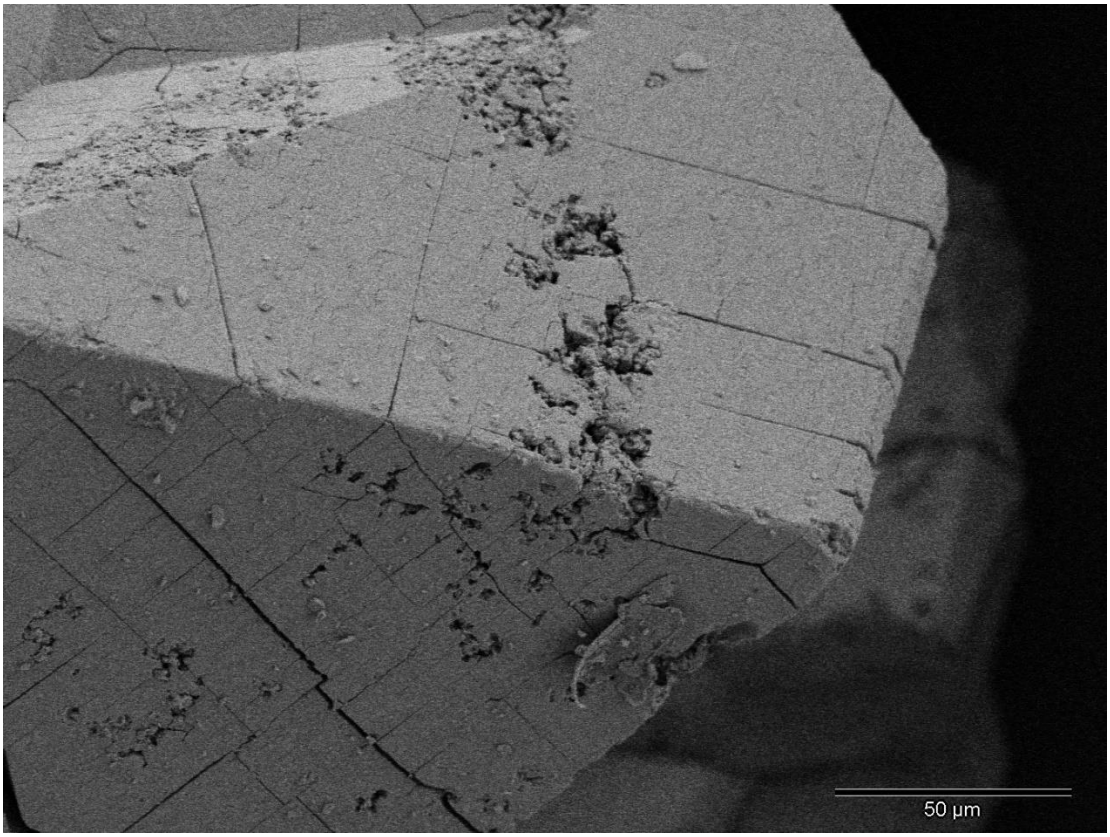

Figure V.1.1.5 SEM image of crystals of **1**. Taken at 5 kV, 500x magnification.

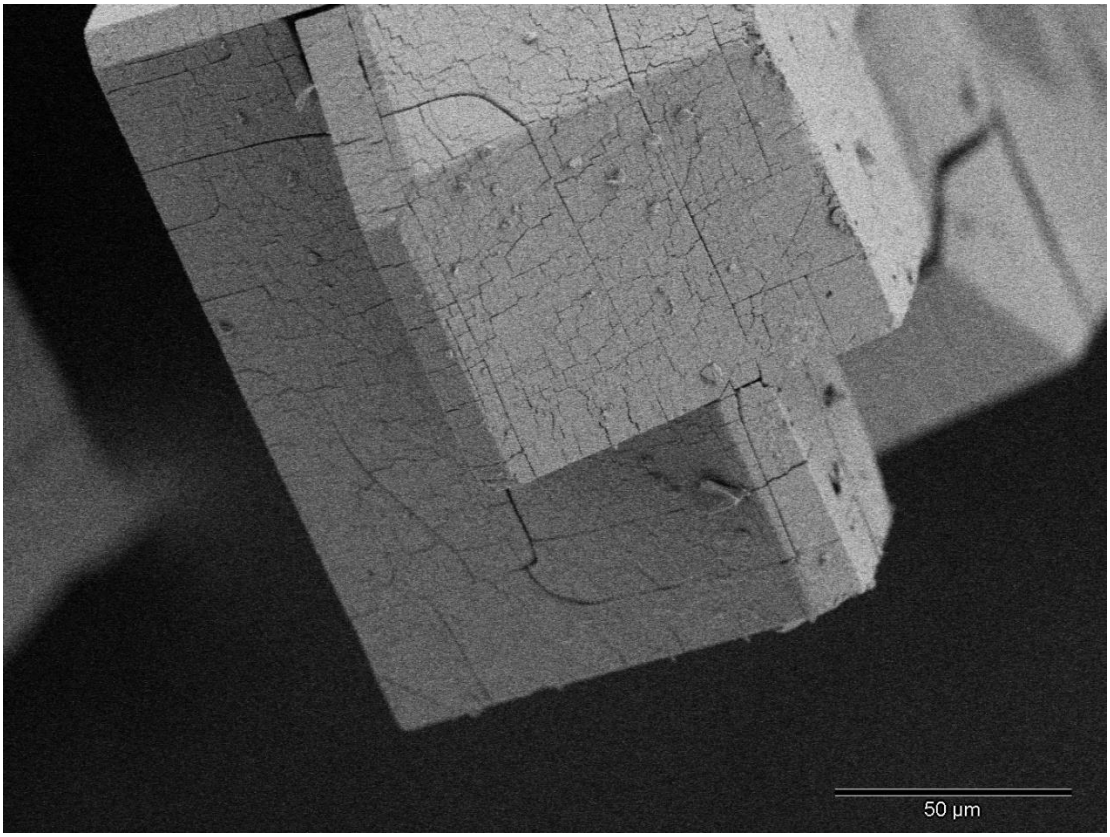

Figure V.1.1.6 SEM image of crystals of **1**. Taken at 5 kV, 500x magnification.

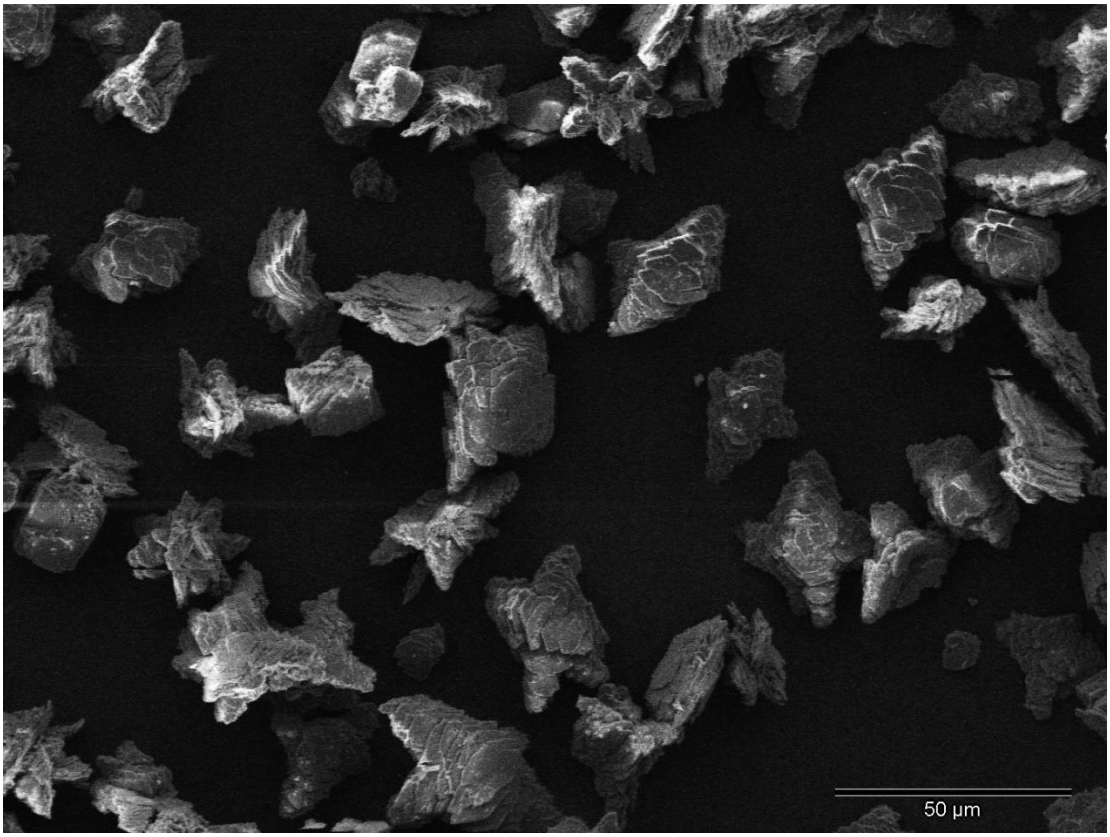

Figure V.1.1.7 SEM image of microcrystals of Mn_{12}-Benzoic Acid. Taken at 5 kV 50x magnification.

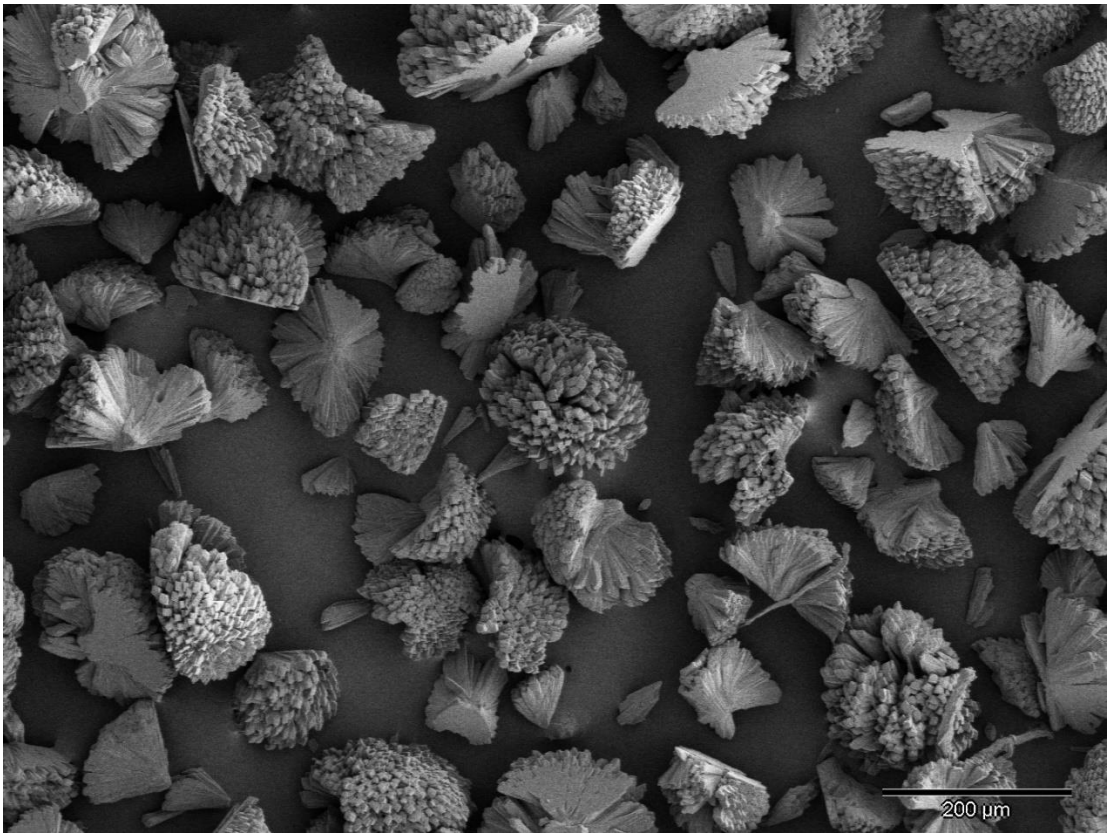

Figure V.1.1.8 SEM image of microcrystals of **4**. Taken at 5 kV, 50x magnification.

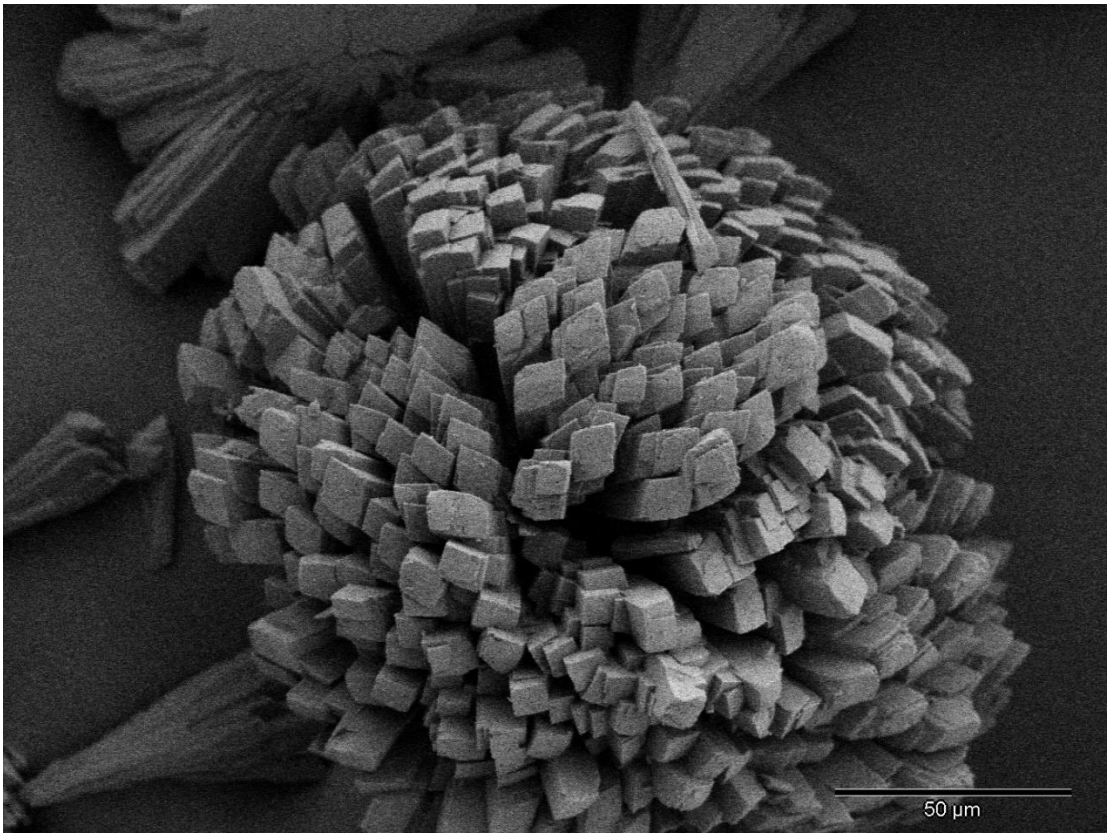

Figure V.1.1.9 SEM image of microcrystals of **4**. Taken at 5 kV, 500x magnification.

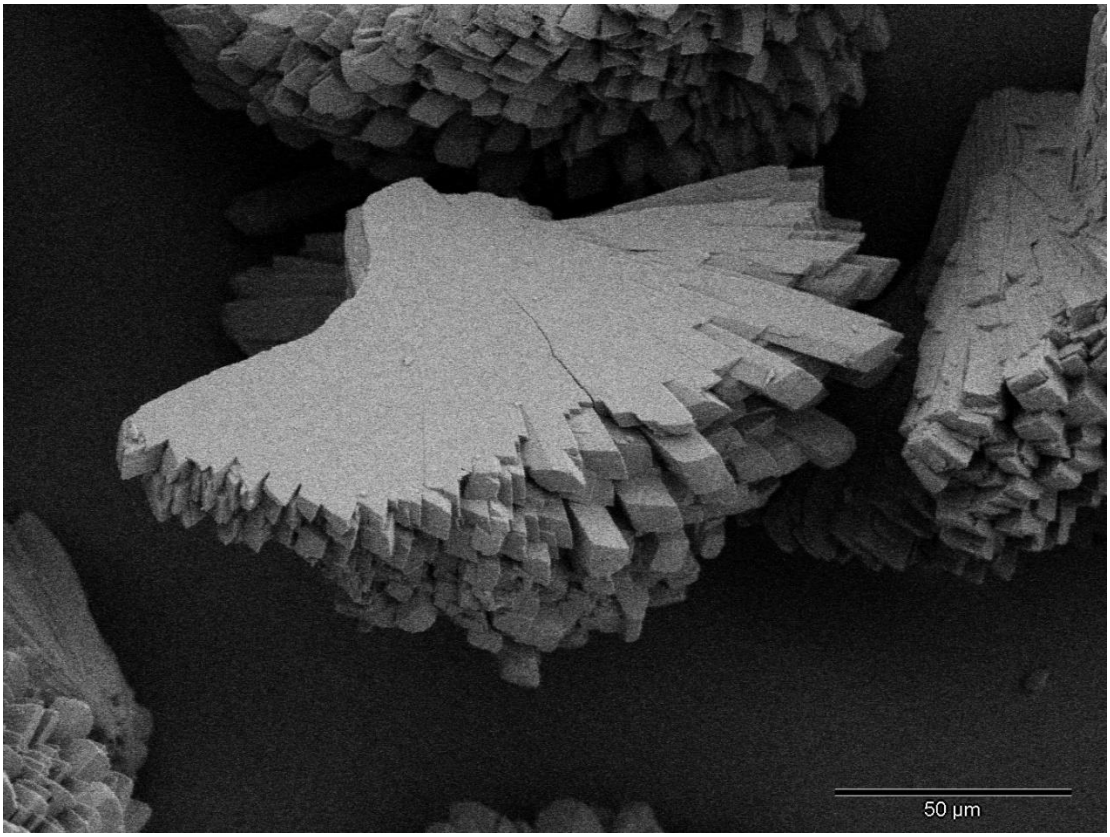

Figure V.1.1.10 SEM image of microcrystals of **4**. Taken at 5 kV, 500x magnification.

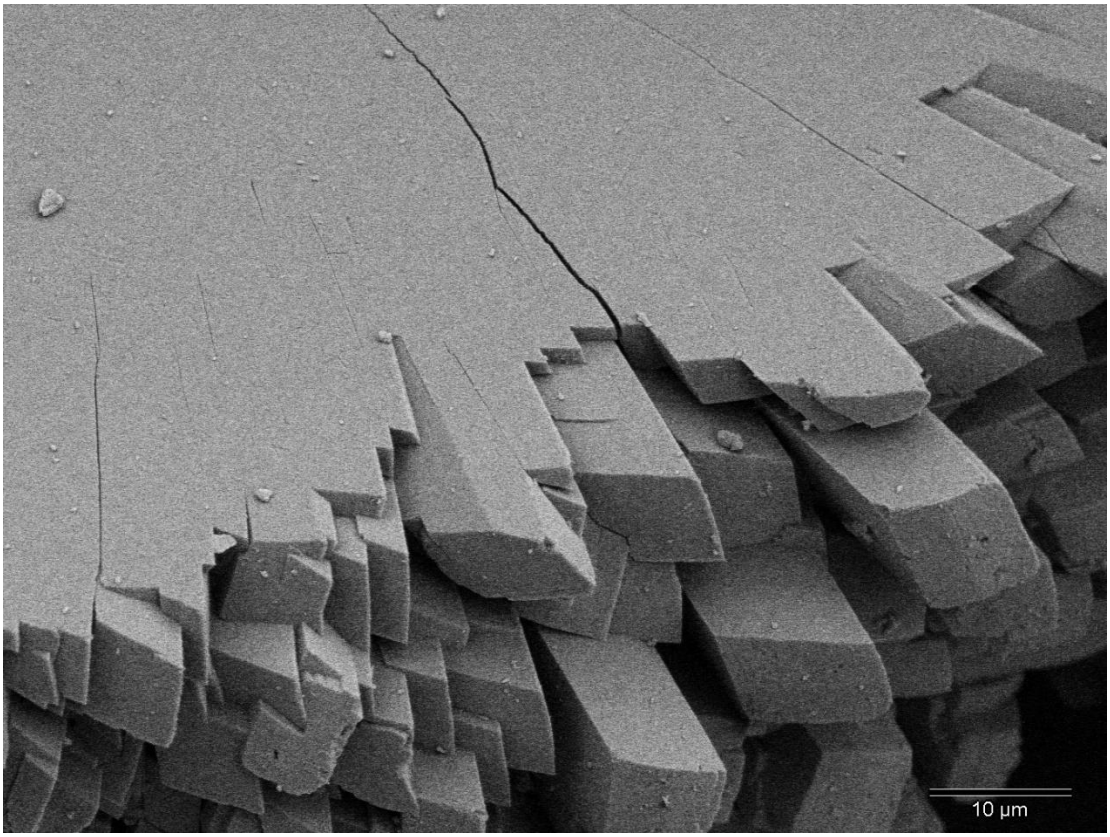

Figure V.1.1.11 SEM image of microcrystals of **4**. Taken at 5 kV, 1500x magnification.

V.1.2 Additional Magnetization Data for Compounds 2 and 4

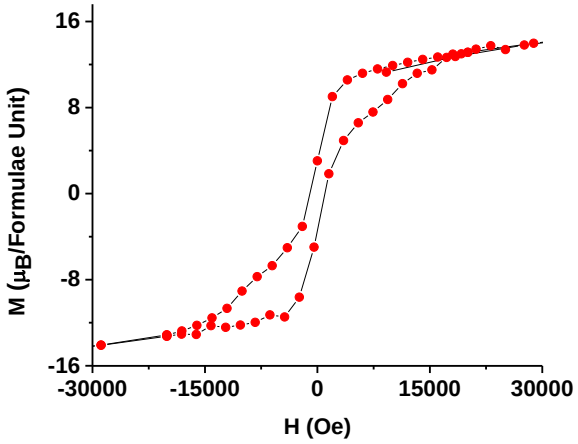

Figure V.1.2.1 Field dependent magnetization of **2** is displayed up to 30 000 G and measured at 1.8 K which shows a slight coercive force and remnant magnetization. The presence of a hysteresis cycle confirms SMM behavior.

The curves of $\chi_M T$ vs T measured under ZFC conditions displayed in **Figure I.1.** go through a broad minimum with decreasing temperatures and slowly increases to a maximum of 59.9 emu·K·mol^{-1} at 7.00 K (μ_{eff} = 21.9), afterward decreasing rapidly below 3 K due to zero field splitting from the applied magnetic field. This behavior indicates ferrimagnetic ordering. The theoretical spin-only value for 8 Mn^{III} (S = 2) and 4 Mn^{IV} (S = 3/2) ions that are magnetically non-interacting yields a μ_{eff} = 21 which is very close to our value of μ_{eff} = 21.9. Near room temperature, at 300 K, the $\chi_M T$ value is 18.6 cm^3 K mol^{-1}, which is significantly lower than the theoretical value 31.5 cm^3 K mol^{-1} indicating anti-ferromagnetic coupling within the cluster. The Field dependent magnetization was measured at 1.8 K with an applied magnetic field of up to 7 T and is displayed in **Figure I.1.**.

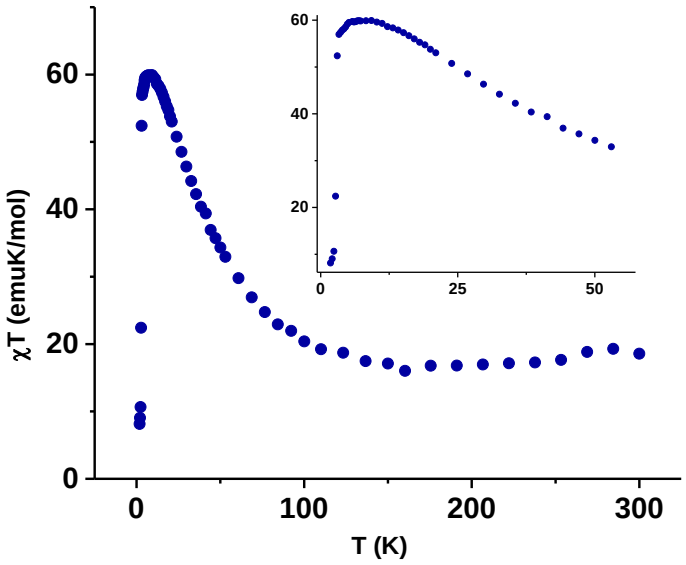

Figure V.1.2.2 Temperature dependent susceptibility for the zero-field-cooled measurement on **4** indicating ferrimagnetic ordering. The inset focuses on the range of 1.8 K to 50 K and shows a maximum at 7.0 K.

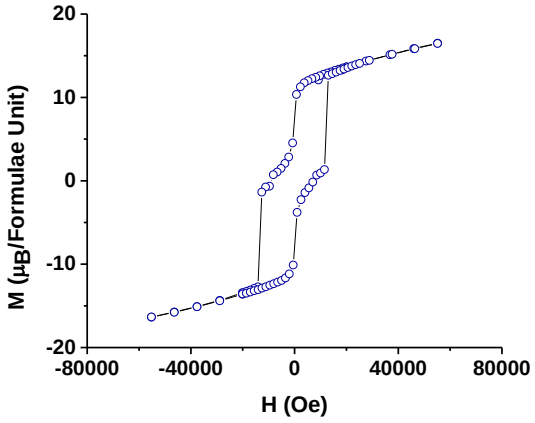

Figure V.1.2.3 Field dependent magnetization of **4** measured up to 7 T at 1.8 K and displaying a coercive force and remnant magnetization.

V.1.3 Solvothermal Methods with Excess Carboxylic Acid

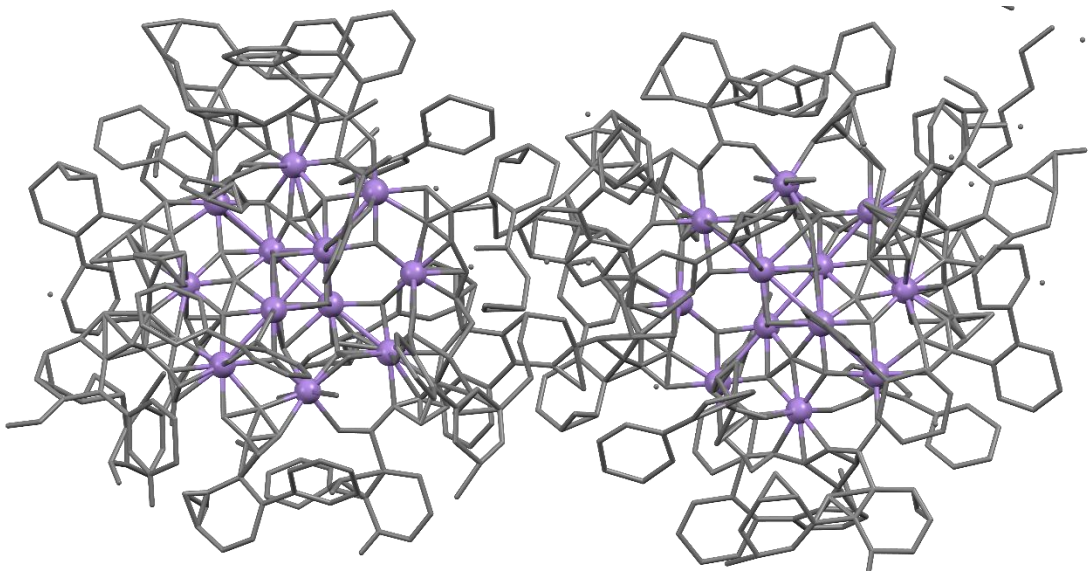

Figure V.1.3.1 Low quality crystal data of solvothermal prep of **4** with excess molar ratio (64:1) carboxylic acid added to Parr Bomb. Results of crystal solution reminiscent of Mn_{12}-type cluster.